सत्यमेव जयते

INDIAN AGRICULTURAL
RESEARCH INSTITUTE, NEW DELHI

I.A.R.I. 6.
GIP NLK—H-3 I.A.R.I.—10-5-55—15,000

PROCEEDINGS

OF THE

ROYAL SOCIETY OF LONDON

SERIES A. MATHEMATICAL AND PHYSICAL SCIENCES

VOL 191

LONDON
Printed and published for the Royal Society
By the Cambridge University Press
Bentley House, N.W.1

3 December 1947

Printed in Great Britain at the University Press, Cambridge
(Brooke Crutchley, University Printer)
and published by the Cambridge University Press
(Cambridge, and Bentley House, London)

Agents for Canada and India: Macmillan

CONTENTS

SERIES A VOLUME 191

No. A 1024. 26 September 1947

PAGE

On interference microscopy. By Sir Thomas Merton, Treas.R.S. 1

Heat transfer at low temperatures between tube walls and gases in turbulent flow. By T. A. Hall and P. H. Tsao 6

The absorption spectra of benzene derivatives in the vacuum ultra-violet. I. By W. C. Price and A. D. Walsh. (Plates 1 to 3) 22

The absorption spectra of benzene derivatives in the vacuum ultra-violet. II. By A. D. Walsh. (Plate 4) 32

The electronic structure of conjugated systems. I. General theory. By C. A. Coulson and H. C. Longuet-Higgins 39

The binding energies of very light nuclei. By H. Fröhlich, Kun Huang and I. N. Sneddon 61

An X-ray study of horse methaemoglobin. I. By J. Boyes-Watson, E. Davidson and M. F. Perutz. (Plates 5 and 6) 83

Quantum electrodynamics and low-energy photons. By C. Jayaratnam Eliezer . 133

No. A 1025. 11 November 1947

Application of quaternions to rotations in hyperbolic space of four dimensions. By A. W. Conway, F.R.S. 137

The formation of hydrogen peroxide in the combustion of hydrogen at low pressures. By Sir Alfred C. Egerton, Sec.R.S. and G. J. Minkoff. (Plate 7) . 145

A general kinetic theory of liquids. IV. Quantum mechanics of fluids. By M. Born, F.R.S. and H. S. Green 168

Interference studies of diamond faces. A crossed fringe technique. By S. Tolansky and W. L. Wilcock. (Plates 8 to 11) 182

On the scattering of fast neutrons by protons. By W. H. Ramsey 195

The initial stages of explosion in nitroglycerine. By M. F. R. Mulcahy and R. G. Vines. (Plates 12 to 15) 210

The propagation of detonation in thin layers of nitroglycerine. By M. F. R. Mulcahy and R. G. Vines. (Plates 16 to 18) 226

An electron-diffraction study of the heating of straight-chain organic films and its application to lubrication. By K. G. Brummage 243

On first order wave equations for elementary particles without subsidiary conditions. By E. Wild 253

No. A 1026. 18 November 1947

PAGE

The ejection of protons from nitrogen on bombardment with α-particles of short range. By F. C. Champion and R. R. Roy. (Plate 19) 269

The theory of combined plastic and elastic deformation with particular reference to a thick tube under internal pressure. By R. Hill, E. H. Lee and S. J. Tupper 278

Discharge currents associated with kite balloons. By R. Davis and W. G. Standring 304

The hodograph transformation in trans-sonic flow. I. Symmetrical channels. By M. J. Lighthill 323

The hodograph transformation in trans-sonic flow. II. Auxiliary theorems on the hypergeometric functions $\psi_n(\tau)$. By M. J. Lighthill 341

The hodograph transformation in trans-sonic flow. III. Flow round a body. By M. J. Lighthill 352

The surface impedance of superconductors and normal metals at high frequencies. I. Resistance of superconducting tin and mercury at 1200 Mcyc./sec. By A. B. Pippard 370

The surface impedance of superconductors and normal metals at high frequencies. II. The anomalous skin effect in normal metals. By A. B. Pippard . . 385

The surface impedance of superconductors and normal metals at high frequencies. III. The relation between impedance and superconducting penetration depth. By A. B. Pippard 399

No. A 1027. 3 December 1947

The Research Laboratories of the General Electric Company. By Sir Clifford C. Paterson, F.R.S. (Plate 20) 417

Attempts to detect the emission of secondary charged particles in the fission of ^{235}U by slow neutrons. By J. M. Cassels, J. Dainty, N. Feather, F.R.S. and L. L. Green 428

A connexion between the criterion of yield and the strain ratio relationship in plastic solids. By Sir Geoffrey Taylor, F.R.S. 441

The method of the hypercircle in function-space for boundary-value problems. By J. L. Synge, F.R.S. 447

Photoelectric measurements of the seasonal variations in daylight at Plymouth, from 1938 to March 1941, compared with the years 1930 to 1937. By W. R. G. Atkins, F.R.S. and M. A. Ellison 467

Progressive lightning. VII. Directly-correlated photographic and electrical studies of lightning from near thunderstorms. By D. J. Malan and B. F. J. Schonland, F.R.S. (Plates 21 and 22) 485

A note on a problem of Mahler. By C. A. Rogers 503

Extensive penetrating cosmic ray showers. By D. Broadbent and L. Jánossy . 517

An investigation, by the method of characteristics, of the lateral expansion of the gases behind a detonating slab of explosive. By R. Hill and D. C. Pack . 524

The interaction of radiation and matter. By P. M. Davidson 542

Index 553

On interference microscopy

BY SIR THOMAS MERTON, TREAS.R S.

(*Received* 19 *February* 1947—*Read* 5 *June* 1947)

Interference microscopy provides a method of increasing the visibility of specimens which are colourless and which differ slightly in refractive index from the surrounding medium by enclosing them between semi-reflecting surfaces, which thus constitute an interferometer. In making observations by this method, it is necessary to use monochromatic light or light of two different wave-lengths, which can be isolated conveniently by the use of a mercury-arc lamp with appropriate filters. This method owes its inception to Frederikse (1933), and has been further developed by the writer in a recent communication (Merton 1947).

When monochromatic light falls normally on a pair of semi-reflecting surfaces which are parallel to one another, the intensity of the light which is transmitted is a function of the separation of the plates and, owing to the effect of multiple reflexions, a curve in which intensity is plotted against separation shows a succession of maxima the width of which, in relation to the minima between them, depends on the reflecting power of the semi-reflecting surfaces. The introduction of a body of different refractive index between the plates is optically equivalent to changing their separation with the result that if the plates are at a distance such that the transmission is a maximum, a small change in refractive index is sufficient to cause a great decrease in the transmission. In such a case the body would be seen as a dark object on a bright background. For other separations of the plates the reverse may occur and the body may be seen bright on a dark background When two radiations (e.g. the green and violet lines of mercury) are used simultaneously it frequently occurs that the object appears in one colour and the background in another.

In the communication referred to (Merton 1947), I have described a technique of making observations by this method and of preparing semi-reflecting surfaces which are well adapted to the purpose. It was found possible to observe intricate detail in certain thin cells, and living bacteria could be clearly seen under a high magnification, but these results could only be obtained in the case of specimens a few microns in thickness.

The reason for this limitation lies in the following considerations. The optical difference of path between successively reflected rays depends not only on the separation of the plates and the refractive index of the medium between them, but also varies directly as the cosine of the angle which the rays make with the normal Thus for any separation of the plates (other than a very small separation) there will be a number of maxima and minima at different angles of incidence, the maxima being at those angles of incidence at which the optical difference of path is equal to an integral number of wave-lengths of the light used is making the observations. If the light has passed through the half-metallized plates in a convergent cone subtending a substantial angle it is evident that unless the separation of the plates is very small the total amount of light transmitted will not vary appreciably with the separation of the plates, the only effect of a change in the separation being that those rays which reach the observer will have passed through the plates at a different series of angles; and the introduction of an object of different refractive index will not give rise to any substantial change in intensity. Unless the specimen is very thin it is necessary to illuminate it with parallel or nearly parallel light. This however would result in an intolerable reduction in the resolving power of the microscope and also a reduction in the intensity of the light which would be so great as to render observation at high magnifications impracticable.

I have obtained good results with specimens up to a few microns in thickness by a compromise which consisted in putting a piece of ground glass on the microscope stage with the ground surface uppermost and with the half-platinized slide and its cover on the ground glass. The image of the mercury lamp after traversing the filter and after reflexion from the mirror of the microscope was brought to a focus on the ground glass by means of a lens of $1\frac{5}{8}$ in. focus working at $f/3{\cdot}1$, the objective being thus illuminated in a manner determined by the polar curve of the ground glass, the greatest intensity being along the optic axis.

It is easy to see exactly what happens by the following procedure. The mercury lamp was brought to a focus on a platinized slide with a platinized cover, which was not quite flat, by means of a condenser of 1 in. focus working at $f/1{\cdot}25$ (N.A. = 0·37). The eyepiece of the microscope was removed and replaced by a viewer which consisted of a convex lens of about 10 in. focus in a brass cell with a very small hole through which the rear lens of the objective could be seen. Under these conditions, the rear lens is seen illuminated by a series of concentric rings (resembling Fabry and Perot rings seen at infinity). When the stage of the microscope is slightly moved, the rings contract or expand as the case may be since the plates are not quite parallel, but the total amount of light which reaches the eye is substantially the same unless the rings are very few in number. The result is that when the viewer is replaced by the eyepiece, no fringes can be seen. What is wanted is an angular filter which will limit transmission to one set of rings only and, if such a filter were available, then on changing the separation of the plates, the rings would assume a new series of angles which the angular filter would reject and the fringes would be visible through the eyepiece.

This suggests the use of two pairs of semi-reflecting plates in series, a device which has been used in other fields for many years. An arrangement which is attractive on theoretical grounds is shown (figure 1). Here the rays from the lamp after traversing the condenser *C* converge through a pair of plane parallel semi-reflecting plates *P* and after being brought to a focus on the semi-reflecting slide and cover *S*, diverge to the objective *O*. The plates *P* would need to be provided with a fine adjustment for altering their separation. Their function would be simply that of an angular filter and if they were set so as to be at the same optical separation as the separation between the slide *S* and its cover, then *S* would transmit precisely at the same angles as *P* and a specimen of different refractive index on the slide would show as sharp a contrast with the background as if the system were illuminated with parallel light. Since the area of the plates *P* which is illuminated is considerable, these plates would need to be of the highest optical perfection and the fine adjustment for altering their separation without disturbing their parallelism would offer considerable, though not insuperable, difficulties.

I have found that the same result can be achieved by a much simpler method which is shown in diagram in figure 2, and which makes use of a series of zone plates. Here the rays from the source pass through the zone plate *Z* and are brought to a focus on the slide *S*, by the condenser *C*. The zone plate is placed at the principal focus of the condenser *C* on the opposite side to the slide. It is thus localized at infinity as seen from the slide and therefore fulfils the function of an angular filter.

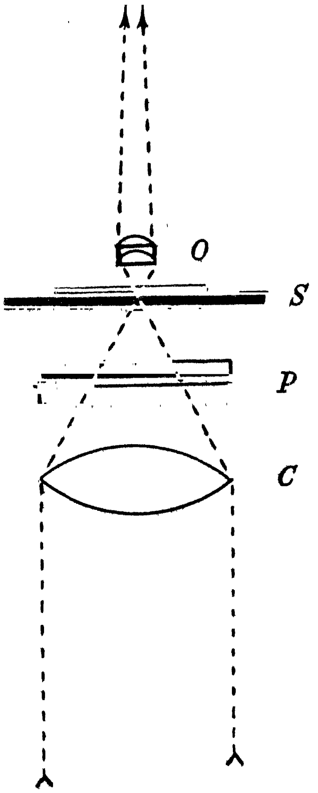

FIGURE 1

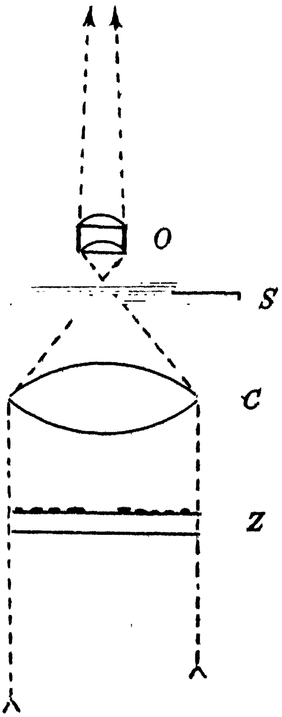

FIGURE 2

The zone plates consist of small plates of glass on which there are annular zones of opaque material with clear annular spaces between them. Plates of glass about 4 in. square were heavily silvered and mounted on a lathe, the transmitting zones being cut out to an accuracy of about 0·001 in. with a gramophone needle attached to a hacksaw blade as a tool. If the order of interference at the centre of a system is N, n the number of a ring reckoned from the centre, f the focal length of the condensing lens, θ the angle subtended by the nth ring and r the radius of the corresponding circle on the zone plate, we have $1-n/N = \cos\theta$ and $r = F\tan\theta$, from which the radii of the zones can be calculated. For a high degree of purity it is necessary that the transmitting zones should be narrow. Good results have been obtained by working out a series of values of r for $n = 0{\cdot}2$, $1{\cdot}0$, $1{\cdot}2$, $2{\cdot}0$, $2{\cdot}2$, etc., and cutting out the silver in the regions corresponding to 0·0 to 0·2, 1·0 to 1·2, etc. The zone plates used in observations were prepared from the silvered glass zone plates by photography on very fine grained photographic plates with the required reduction in scale and slips of glass were cemented on to the photographic zone plates to ensure their permanence. It is found that a plate which has been calculated for a given order of interference is in fact reasonably effective over a number of orders on either side, so that the total number of zone plates which are required is not excessive.

On looking through the viewer it is not difficult to choose a zone plate which matches the rings seen on the rear lens of the objective but the centring of the zone plate calls for a precision which can hardly be effected without some form of mechanical fine adjustment and which increases in difficulty with the number of zones used. I have made zone plates with which clearly defined fringes have been observed up to an order of 140 in mercury green light, which corresponds to a separation of the plates of about 38μ with air and about 29μ when water is used between the plates. There seems no reason why this limit should not be exceeded.

The zone plates which have been described above are designed for specified orders of interference and it is evident that if the microscope is illuminated by two radiations, a zone plate can only function effectively for one of them. My son, Mr C. R. Merton, has succeeded in making zone plates which are effective for two radiations simultaneously, for example the green and violet rays of mercury, the wave-lengths of which happen to be very nearly in the ratio of 5 to 4. Thus, for example, the 60th order of the green ray will be nearly coincident with the 75th order of the violet ray, and the problem is to make a zone plate which will function as a 60th order plate for the green ray and a 75th order plate for the violet ray. Instead of printing the zone plates on fine grain photographic plates, a plate of glass was coated with bichromated gelatine and was exposed to light under the negative of a 60th order zone plate. The plate was developed in hot water, the parts which had not been exposed to light being dissolved, leaving zones of bare glass. The plate was then dyed in eosin which made the gelatine opaque to the green ray whilst transmitting the violet ray. In the same way a bichromated gelatine plate was exposed under the negative of a 75th order zone plate and after development in hot water was dyed in a mixture of auremine and malachite green which absorbs the violet ray and freely transmits the green ray. These two stained gelatine plates were cemented together in register, the result being a two colour zone plate which functioned effectively for both the green and violet rays. Fringes of great purity of colour have been obtained up to the 80th order for the green ray and the 100th for the violet ray by this method. The matching of the two components is of course affected by the dispersion of any liquid between the two half-metallized plates but not to a degree which impairs the usefulness of the method. In using a mercury lamp as a source of light it is desirable to include, in addition to the didymium filter, a gelatine filter lightly stained with methylene blue.

In observing very thin specimens with which the cover can be squeegeed on to the slide, it is practically certain that over considerable regions the surfaces will be sufficiently parallel for the fringes to be broad in comparison with the specimens, but with thicker layers some means must be found to separate the surfaces and at the same time keep them parallel. If a thin rod of glass is heated in a flame and very suddenly drawn out some 4 or 5 ft., there is a length of about 6 in. or more in the centre of the fibre which is usually of remarkably uniform thickness. Such fibres can be drawn to a thickness down to 20μ without much difficulty by hand and two short contiguous pieces from the centre make very effective separators. A convenient arrangement is shown in figure 3. Two strokes *M* are drawn across the slide with a brush dipped in thin mastic varnish and the fibres *G* are quickly laid on the strips of mastic. A small plate of glass is carefully pressed on the fibres to ensure that they are in contact with the slide and the mastic is allowed to dry. Slides prepared in this way will stand a reasonable amount of handling.

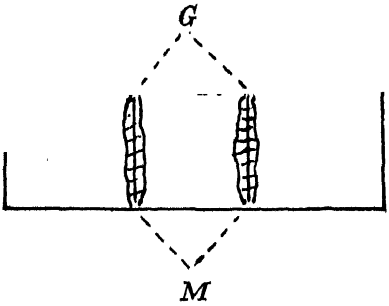

FIGURE 3

Another very simple method of providing distance pieces consists in coating a platinized slide with a layer of cellulose nitrate of the desired thickness leaving a clear space in the middle of the slide. This can be done by pouring a small quantity of a 10 % solution of cellulose nitrate in amyl acetate on one end of the slide and guiding the flow of the liquid with a glass rod so that it is bounded by as straight an edge as possible about half a centimetre from the centre of the slide. The slide is at once placed in a vertical position, so that the excess of solution drains away from the centre and is allowed to dry. The other end of the slide is then treated in the same way. It is important that the slide and its cover should be nearly parallel so that the fringes are broad in relation to the objects observed. Satisfactory results are not obtained if the fringes are too close together.

In making tests use has been made of epithelial cells from the tongue in saliva. These cells are of no special biological interest but familiarity with their appearance made them convenient objects for testing the method. What is seen is in effect a contour map showing optical path differences and it is evident that this contour map must in some measure be distorted when the object is illuminated by oblique rays, unless the separation of the plates is very small. In the case of oblique illumination successively reflected beams will pass through adjacent portions of the object or even outside the object. This effect is somewhat complicated and the extent of the resulting disturbance of the image is difficult to assess, but within certain limits it does not appear to be very important. With a condenser of numerical aperture 0·37 there does not appear to be any conspicuous difference in the structure of the cells when observed between plates with separations varying between 2 and 15μ.

REFERENCES

Frederikse, A. M. 1933 *Acta brev. neerl. Physiol.* **3**, 8.
Merton, T. 1947 *Proc. Roy. Soc.* A, **189**, 309.

Heat transfer at low temperatures between tube walls and gases in turbulent flow

BY T. A. HALL, *Imperial College and Gas Research Board*
AND P. H. TSAO, *Imperial College*

(*Communicated by Sir Alfred Egerton, Sec.R.S.—Received* 4 *December* 1946)

An apparatus was designed on the counter-flow system to study heat transfer between tube walls and gases at low temperatures in a region in which careful measurements had not previously been made.

Oxygen, nitrogen and carbon dioxide were used, covering a temperature range from +45° to −167° C, pressures up to 11 atm., and Reynolds numbers from 3000 to 60,000.

Results were correlated by the use of dimensionless groups and a general equation obtained, independent of the nature of the gas and applicable over the whole range of experiments. With Reynolds numbers evaluated at mean film temperatures, the coefficient in the equation was found to be 5% lower than that obtained from measurements made at normal and high temperatures. This is regarded as justifying the extension of the ordinary equation to low-temperature regions.

Determinations on friction accompanying heat transfer with gases in turbulent flow at low temperatures showed that the effect of heat transfer on the friction factor was small.

NOMENCLATURE

C	constant in Sutherland equation.
D	diameter of tube; equivalent diameter of annulus, i.e. internal diameter of outer tube minus external diameter of inner tube.
F	frictional force per lb. of fluid.

L	length of tube.
T	absolute temperature, ° K.
V	linear velocity of gas, as calculated from mass flow per unit time per unit of cross sectional area, divided by the mean density of the fluid.
c	specific heat of fluid at constant pressure.
f	friction factor, or coefficient of proportionality in pressure drop equation.
g	acceleration due to gravity.
h	coefficient of heat transfer between fluid and surface.
k	thermal conductivity of fluid.
r, s	constants (used as exponents).
α, β	constants.
$\phi(x)$	function of x.
μ	absolute viscosity of fluid.
ρ	absolute density of fluid.
Δp	pressure drop in pipe.

Subscripts

a	refers to annulus.
i	refers to inner tube.
f	refers to properties evaluated at film temperatures. Film temperature is taken as the arithmetic mean of the bulk fluid temperature and the tube-wall temperature.

INTRODUCTION

The transfer of heat by forced convexion at temperatures above atmospheric, between fluids and the walls of tubes or annuli, has been the subject of much work in the past and has resulted in many empirical relationships of limited application.

Seeking a more rational approach to the subject, Nusselt (1909), using the principle of similarity, developed the following general equation between dimensionless groups embodying the variables relating to the flow pattern, the physical constants of the fluid, and the apparatus dimensions:

$$\frac{hD}{k} = \phi\left[\left(\frac{DV\rho}{\mu}\right)\left(\frac{c\mu}{k}\right)\right]$$

or

$$\frac{hD}{k} = \alpha\left(\frac{DV\rho}{\mu}\right)^r\left(\frac{c\mu}{k}\right)^s. \tag{1}$$

The three groups, reading from left to right, are known respectively as the Nusselt, Reynolds and Prandtl numbers. α, r and s are constants. This equation applies only so long as there is no phase change in the fluid.

Fishenden & Saunders (1932), McAdams (1942), Colburn (1933) and others have correlated numerous experimental data on gases and liquids by means of Nusselt's equation, and have shown that the following relationship represents heat transfer behaviour over a wide range of conditions for Reynolds numbers exceeding 2100, using consistent units:

$$\frac{hD}{k} = 0{\cdot}023\left(\frac{DV\rho}{\mu}\right)^{0{\cdot}8}\left(\frac{c\mu}{k}\right)^{\substack{0{\cdot}4\text{ for heating fluids}\\ 0{\cdot}3\text{ for cooling fluids}}} \tag{2}$$

The relationship holds for conditions of reasonably high pressure and temperature, for example, for the results of Kerr (1932) obtained with superheated steam at temperatures up to 427° C and pressures up to 3300 lb./sq.in., and for the results of Ulloch & Badger (1937) on linseed oil and petroleum at temperatures up to 316° C.

The purpose of the present work was to make measurements of heat transfer between a tube wall and gases in turbulent flow in the range of very low temperature (such as would occur in gas liquefaction and separation processes), to determine whether equation (2) would apply, or whether some modification of it would be necessary. The gases used were carbon dioxide, oxygen and nitrogen, and the temperature range covered in the experiments was approximately 0° to −170° C; pressures up to 10 atm. and Reynolds numbers of from 3000 to 60,000 were employed. A few measurements were made using air at ordinary temperatures as a check on the experimental procedure, but these are not described in the text.

Some determinations were made of the pressure drop accompanying heat transfer, to test the validity of Reynolds's analogy in the low-temperature experiments.

APPARATUS

The general arrangement of the apparatus (in diagrammatic form, not to scale) is shown in figure 1. It consists of an experimental counter-current heat exchanger insulated by a vacuum-jacketed copper tube, and fed with cold gas which is produced by boiling the liquid in a spherical steel generator of 7 gal. capacity, lagged with slag wool. Numerous temperature measurements were made upon the gas in the exchanger, and its rate of flow was measured by a flowmeter and a wet-drum meter after warming up in a thermostat. The wet meter had an accuracy of ± 0·5 %, or better. The total pressure of the gas was measured by a Bourdon-type gauge. The cold gas pipe from the generator to the exchanger was heavily lagged with felt.

The experimental counter-current heat exchanger is shown in detail in figure 2. It consists of two concentric tubes, an inner one L, of 0·367 in. mean internal diameter and 0·625 in. mean external diameter, and an outer one M, of 1 in. external diameter and wall thickness 0·064 in. (no. 16 s.w.g.). The thick wall of the inner tube allows room for the embedding of thermocouple elements in a manner described later.

Re-entrant flow gas mixing chambers, H and I, are situated at both ends of both exchanger tubes, providing a region of isothermal flow where accurate gas temperatures could be observed. At all points where metallic contact is undesirable, ebonite bushes or cork washers are inserted. Glands are made tight with ebonite bushes and dry asbestos packing.

Incoming cold gas enters the inner tube mixing chamber via a tube shown at the right-hand end of the drawing. It traverses the inner heat transfer tube and leaves it via the mixing chamber *H*. It then passes through a heater *F*, where its temperature is raised a few degrees, continues via headers *E* and *N* to the outer tube mixing chamber *I*, traverses the outer heat transfer tube *M*, and leaves it via a mixing chamber and the header *O*. In this way two streams of gas of the same mass flow rate are obtained, flowing counter-current, with a temperature head between the streams at all points along the exchanger. The effective length of the exchanger is 9 ft. 3 in., and the overall length 14 ft. 3 in.

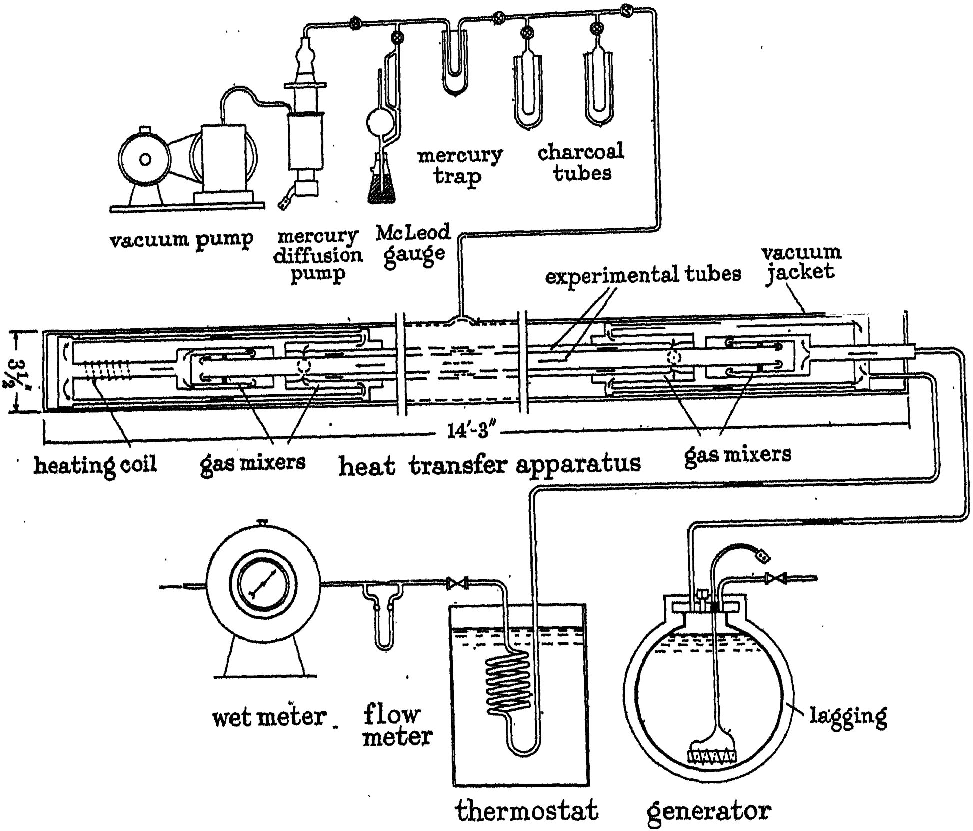

FIGURE 1. General arrangement of the apparatus.

In designing the exchanger, care was taken to arrange all the components in a straight line, and to bring all gas, electric and thermocouple connexions away at one end only so that the unit could be slipped into a vacuum-jacketed tube to minimize the leakage of heat from the surroundings into the system. The vacuum jacket, *K*, consists of two concentric tubes, approximately 14 ft. 3 in. long, of 3½ in. and 2⅞ in. external diameters, joined together at one end (the open end), and both closed (although not joined) at the other end. This design allows free movement of the inner tube on cooling and warming up, while the vacuum is maintained in the annulus between the tubes. This annulus was pumped out continuously during experiments, to a pressure of the order of 10^{-5} mm. of mercury. The tube surfaces of the annulus were polished before assembly, and the insulating capacity of the jacket was extremely good, much better than could have been obtained with any lagging. It was not practicable to render the exchanger adiabatic by means of a jacketing fluid, as the low temperature would have necessitated the consumption of very large quantities of liquid air at prohibitive cost.

The whole of the exchanger and jacket, with the exception of bushes, gland packing, etc., is of copper or brass, all permanent metal joints being made with soft or hard solder. The exchanger was designed for a pressure of 10 atm.

On leaving the exchanger the gas passes through a copper coil immersed in a thermostatically controlled water-bath, to bring it to a standard temperature (20° C) for measurement.

TEMPERATURE MEASUREMENT

(1) *Calibration of thermocouples*

Temperature measurements were by means of thermocouples consisting of no. 33 s.w.g. high-conductivity copper and no. 34 s.w.g. constantan wires, both silk covered. Leads were of no. 33 s.w.g. copper, and junctions were soft-soldered, the standard ones being immersed in tubes of glycerine placed in a Dewar flask containing melting ice. E.m.f.'s were measured by a Tinsley concentric potentiometer having a sensitivity of 2μV.

Ten couples were calibrated against the boiling-points of pure liquid ethylene, oxygen and nitrogen, and the sublimation point of carbon dioxide in pure toluene. In all cases the temperatures were corrected for the divergence of the vapour pressure from 760 mm. of mercury, and for hydrostatic head due to the depth of immersion of the couples. The liquids were stirred by a slow stream of pure gas during the task. All other couples were calibrated directly against boiling oxygen only. Some couples were calibrated for temperatures above atmospheric, by comparison with a standard mercury thermometer in the range between 0° and 100° C.

The calibrations were consistent, and did not vary with time. A precision of ± 0·05° C was obtainable. The curves of e.m.f. versus temperature were compared with those given by Scott (1941) for carefully selected wires tested against a standard resistance thermometer over the range 0° to − 190° C, and were found to differ by about 1 % at the point of greatest divergence. In the range 0° to 100° C the results were compared with values for e.m.f. given in *International Critical Tables* (1926), and a maximum divergence of 2 % was observed.

(2) *Measurement of gas temperatures*

Three sources of error in the measurement of the bulk gas temperatures at the ends of the heat transfer tubes are as follows.

First, the existence of a temperature gradient in the plane normal to the direction of flow. This would probably not be significant with turbulent flow, but in any case

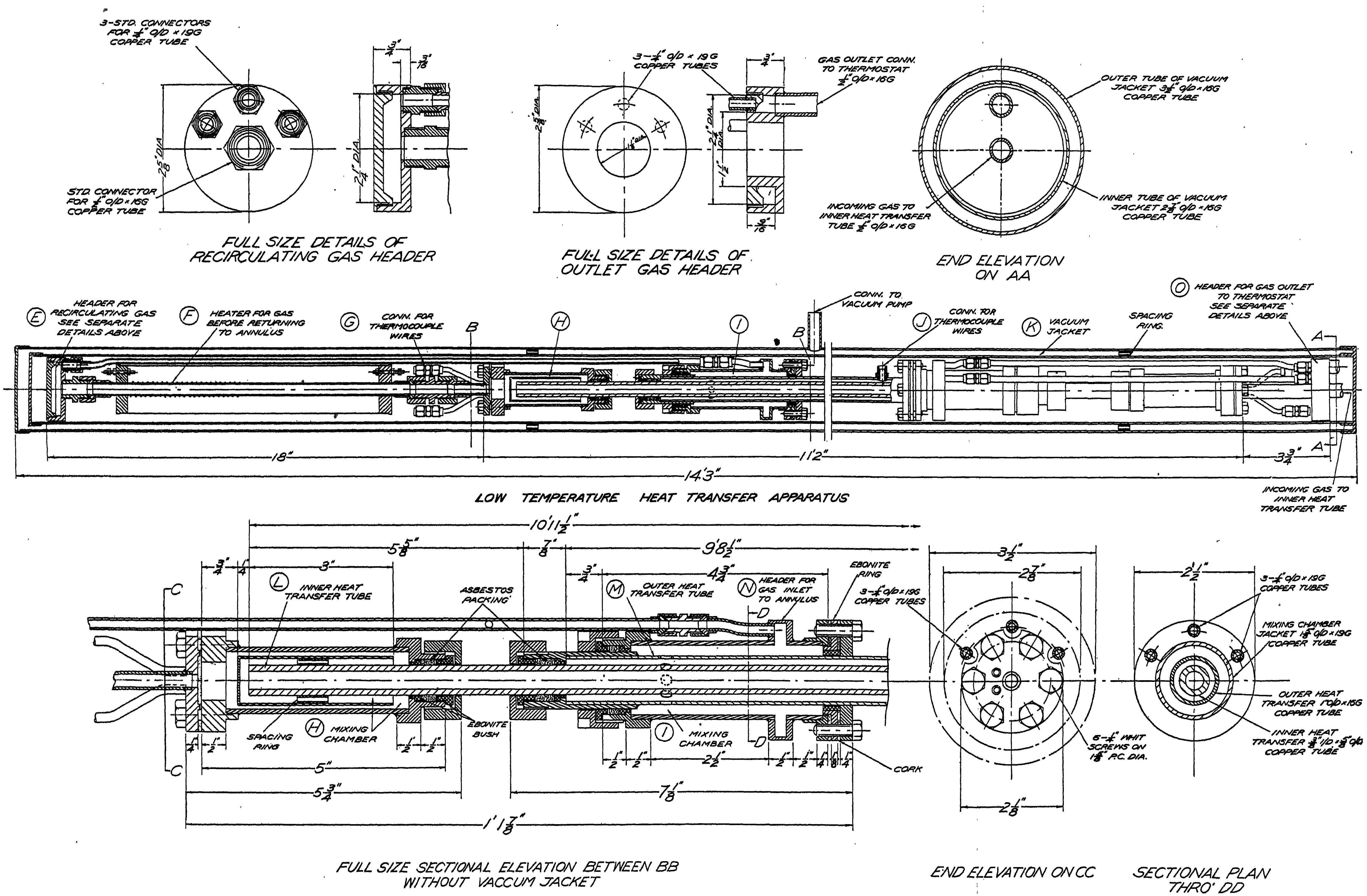
3-STD. CONNECTORS FOR 1/4" O/D × 19G COPPER TUBE
STD. CONNECTOR FOR 1/2" O/D × 16G COPPER TUBE
2 5/8" DIA
2 1/4" DIA
FULL SIZE DETAILS OF RECIRCULATING GAS HEADER
3-1/4" O/D × 19G COPPER TUBES
GAS OUTLET CONN. TO THERMOSTAT 1/2" O/D × 16G
FULL SIZE DETAILS OF OUTLET GAS HEADER
INCOMING GAS TO INNER HEAT TRANSFER TUBE 1/2" O/D × 16G
OUTER TUBE OF VACUUM JACKET 3 1/2" O/D × 16G COPPER TUBE
INNER TUBE OF VACUUM JACKET 2 7/8" O/D × 16G COPPER TUBE
END ELEVATION ON AA
E HEADER FOR RECIRCULATING GAS SEE SEPARATE DETAILS ABOVE
F HEATER FOR GAS BEFORE RETURNING TO ANNULUS
G CONN. FOR THERMOCOUPLE WIRES
H
I
CONN. TO VACUUM PUMP
J CONN. FOR THERMOCOUPLE WIRES
K VACUUM JACKET
SPACING RING.
O HEADER FOR GAS OUTLET TO THERMOSTAT SEE SEPARATE DETAILS ABOVE
A
B
18"
11'2"
3 3/4"
14'3"
INCOMING GAS TO INNER HEAT TRANSFER TUBE
LOW TEMPERATURE HEAT TRANSFER APPARATUS
10'11 1/2"
5 5/8"
7/8"
9'8 1/2"
4 3/4"
3"
L INNER HEAT TRANSFER TUBE
ASBESTOS PACKING
M OUTER HEAT TRANSFER TUBE
N HEADER FOR GAS INLET TO ANNULUS
EBONITE RING
3-1/4" O/D × 19G COPPER TUBES
C
D
SPACING RING
H MIXING CHAMBER
EBONITE BUSH
I MIXING CHAMBER
CORK
5"
5 3/4"
7 1/8"
1'1 7/8"
FULL SIZE SECTIONAL ELEVATION BETWEEN BB WITHOUT VACCUM JACKET
3 1/2"
2 7/8"
2 1/8"
6-1/4" WHIT SCREWS ON 1 5/8" P.C. DIA.
END ELEVATION ON CC
2 1/2"
3-1/4" O/D × 19G COPPER TUBES
MIXING CHAMBER JACKET 1 5/8" O/D × 19G COPPER TUBE
OUTER HEAT TRANSFER 1" O/D × 16G COPPER TUBE
INNER HEAT TRANSFER 3/8" I/D × 5/8" O/D COPPER TUBE
SECTIONAL PLAN THRO' DD

FIGURE 2. Experimental counter-current heat exchanger.

it would be eliminated by the return-flow mixing chambers which, by providing an isothermal length of tube where no heat is gained or lost by the gas, permits a mean bulk temperature to be attained.

Secondly, the radiation of heat between the thermocouple junction and adjacent tube walls. This effect was reduced by surrounding the junction with a close helix formed by a portion of the insulated thermocouple wires. The method of forming the enclosure was to push the junction $\frac{1}{2}$ in. or so into $\frac{1}{16}$ in. external diameter capillary glass tube, and to wind the insulated leads closely round the tube until the junction was passed and was no longer visible. The glass was then withdrawn.

Thirdly, the conduction of heat along the thermocouple wires between the junction and a zone at a different temperature. This effect was reduced by the provisions made for the other two sources of error. In the case of the inner heat transfer tube the wires traversed a long isothermal path in the mixing chambers, and in the case of the outer tube, although the path was not so long, the spiral winding increased it considerably above that of the direct path.

The above remarks apply to the important gas-temperature measurements made at the ends of the heat-transfer tubes. There were additional gas-temperature measurements made along the length of the outer tube to indicate the temperature distribution, when it was not possible to apply all the foregoing precautions, partly because of the impossibility of proper mixing, and partly because the junctions had to be inserted in such a way as to cause the smallest possible disturbance to the flow pattern of the gas.

Temperatures were read to $\pm 5\,\mu$V corresponding to an accuracy of $\pm 0{\cdot}3^\circ$ C. The potentiometer circuit would allow of a greater accuracy than this, but so many temperatures needed observing in a limited time that a balance had to be struck between accuracy and speed of observation. In each inner tube mixing chamber there were three thermocouples, and in each outer tube mixing chamber four. The temperatures measured in each of these always agreed to within $\pm 0{\cdot}3^\circ$ C.

(3) *Measurement of the tube-wall temperatures*

The method of measuring the temperature of the wall of the inner tube, which separates the two gas streams, is that proposed by Hebbard & Badger (1933), with slight modifications (see figure 3). A longitudinal groove $\frac{3}{32}$ in. wide and $\frac{1}{16}$ in. deep was milled in the tube from each end to a little under half-way along. Diametrically opposite the groove, and at points equidistant along its length, were drilled six holes, $\frac{1}{8}$ in. diameter and $\frac{1}{16}$ in. deep (i.e. not perforating the tube). Grooves of the same depth, and $\frac{1}{32}$ in. wide, were then cut round the circumference, linking each hole with the longitudinal groove. Thermocouple junctions were soft-soldered to the bottom of the holes, the wires were led in opposite directions round the tube, and then along the milled groove to the end of the tube. These wires were not insulated with silk, but by a hardened plastic which was put in prior to hardening.

This plastic served the double purpose of insulating the wires and restoring the original surface contour of the tube, so that the flow pattern of the gas over it would not be disturbed. It consisted of thermosetting Bakelite Resin R 1373 (liquid at room temperature) with kaolin added as a filler to give a malleable consistency. The composition found most satisfactory was 42 % by weight of resin, the remainder being kaolin. The mixture was pressed into the grooves, moulded to the tube contour as well as possible, and then hardened in sections at 100° to 120° C from 1 to 1½ hr., in an electrically heated tube of 2½ ft. length. The surface was finally shaped by filing, and polished with fine emery cloth. When the process was finished no discontinuity was visible in the tube surface. This filling was particularly suitable in that it showed no tendency to separate from the metal under thermal stress, even after repeated cooling to temperatures of the order of −190° C followed by rewarming.

The correctness of the temperature measurements was indicated by the existence of a linear relation between wall temperature and distance along the tube.

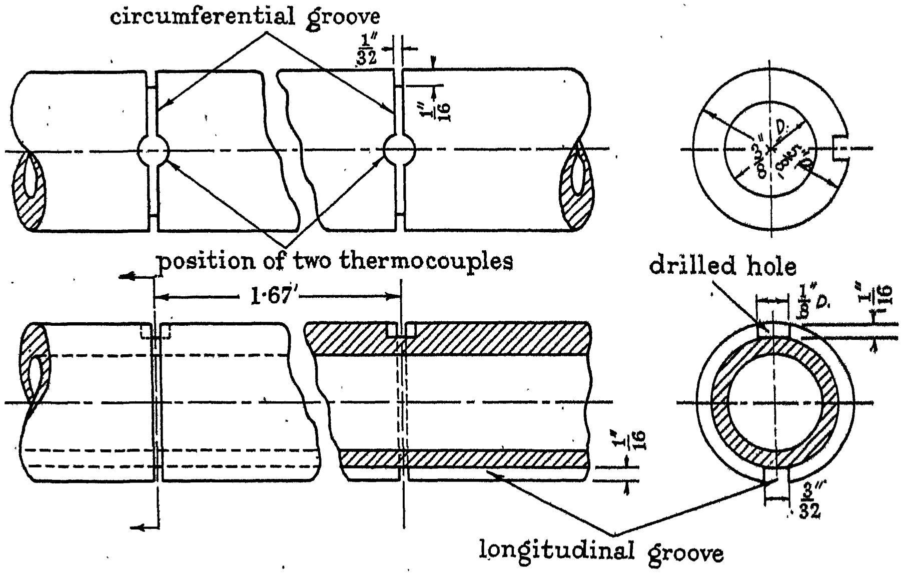

FIGURE 3. Method of installing wall thermocouples.

(4) *The obturation of the thermocouple leads*

It is always a troublesome matter to lead wire connexions through the walls of metal apparatus subject to internal pressure, when electrical contact with the walls must be avoided. In the present case there were upwards of twenty thermocouples to be brought out of the exchanger, while there was insufficient room to provide separate glands for each.

The method adopted is indicated in figure 4. Standard $\frac{3}{16}$ in. brass union bodies were adapted as shown, and either soldered to tubes as at *G*, in figure 2, or soldered direct into the wall of the apparatus. Ebonite cones with holes drilled for four to six wires were first coated with picein wax. The union was then screwed down while a jet of hot air was directed on to it. This procedure resulted in a tight joint easily capable of standing 10 atm. pressure.

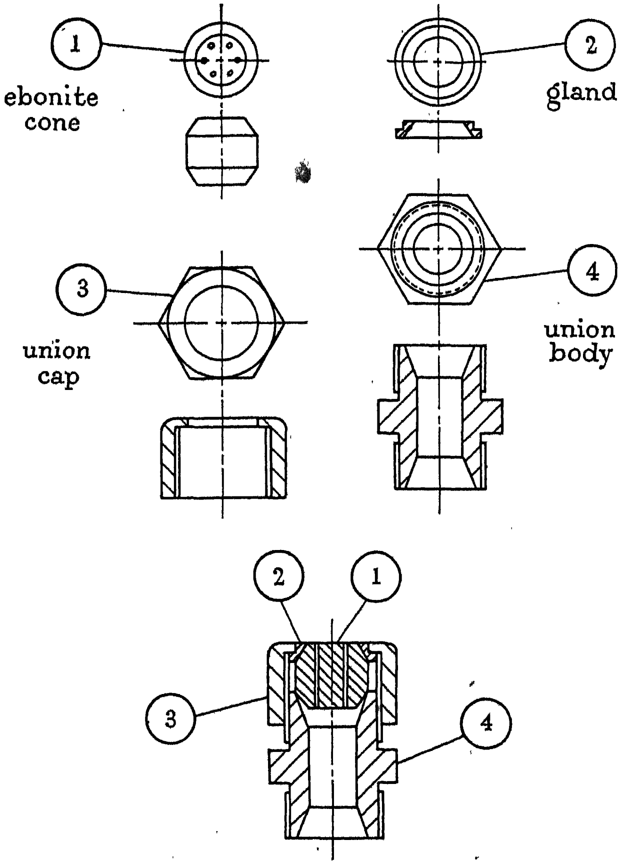

FIGURE 4. Pressure-tight joint for thermocouple leads.

PHYSICAL PROPERTIES OF THE GASES

For the calculation of the Nusselt, Reynolds and Prandtl numbers, data are required on the viscosity, thermal conductivity and specific heat of the gases under the conditions of the experiments. The sources of information were as follows.

(1) *Viscosity*

The values used were those of Johnston & McClosky (1940) which were obtained at pressures varying from 500 to 760 mm. Hg by an oscillating disk method. The reference viscosity was that of air at 296·1° K, taken as $1833{\cdot}0 \times 10^{-7}$ poise. The results were claimed to have an accuracy of 0·3 % at 300° K, and 0·7 to 0·8 % in the most unfavourable cases. Those used in the present experiments are given in table 1.

TABLE 1. VALUES FOR THE VISCOSITIES OF GASES AT ATMOSPHERIC PRESSURE AND LOW TEMPERATURE

oxygen		nitrogen		carbon dioxide	
temp. °K	viscosity × 10^7 poise	temp. °K	viscosity × 10^7 poise	temp. °K	viscosity × 10^7 poise
90·28	692·7	90·17	631·4	197·88	1004·8
118·81	908·6	118·26	816·4	198·00	1005·9
131·29	999·4	130·82	892·4	214·75	1086·1
144·94	1098·6	140·98	954·7	230·17	1161·2
158·46	1185·0	155·56	1041·8	245·08	1232·6
172·56	1288·2	169·40	1122·5	259·76	1302·5
184·61	1374·0	184·72	1210·0	273·13	1365·7
201·49	1483·5	200·16	1298·2	286·59	1431·2
215·17	1573·7	215·75	1380·8	298·44	1487·4
229·94	1664·9	229·88	1453·5	300·32	1496·4
245·13	1759·5	245·19	1531·3	—	—
260·11	1846·9	260·13	1603·0	—	—

(2) *Thermal conductivity*

There is a considerable divergence in the values of the thermal conductivities for air and other gases obtained by various workers, due to the difficulty of eliminating heat transfer by convexion and radiation during the measurements. Moreover, there is very scanty information at temperatures below 0° C. In a critical review of available data at 0° C made by Schmidt (1937), the values selected in an earlier review by Ulsamer (1936) were accepted as being the most reliable. Of these, the ones used in the present experiments are shown in table 2.

TABLE 2. THERMAL CONDUCTIVITIES OF GASES AT 0° C (k_{273})

substance	thermal conductivity × 10^6 g.cal./sec./sq.cm./° C/cm.
air	57·4
oxygen	58·3
nitrogen	57·3
carbon dioxide	34·4

Results obtained by Eucken (1911) on oxygen and nitrogen at temperatures below 0° C were found to comply with the Sutherland equation,

$$k_T = k_{273}\frac{273+C}{T+C}\left(\frac{T}{273}\right)^{\frac{3}{2}}, \tag{3}$$

where T is the absolute temperature, k is the thermal conductivity, C is a constant (144 for oxygen 114 for nitrogen). Equation (3) was used to calculate values of k_T from the values of k_{273} given in table 2. In the case of carbon dioxide, numerical values of the ratio k_T/k_{273} were taken from *International Critical Tables* and used in conjunction with k_{273} from table 2.

The results of these calculations, expressed in different units, are shown in table 3.

TABLE 3. THERMAL CONDUCTIVITIES OF GASES AT LOW TEMPERATURE

	thermal conductivity × 10^5 B.T.U./hr./sq.ft./°F/ft.		
temp. °C	oxygen	nitrogen	carbon dioxide
−191·4	426	449	—
−170·0	551	574	—
−150·0	666	686	—
−130·0	776	793	—
−110·0	883	896	—
− 90·0	900	994	—
− 78·4	—	—	555
− 70·0	1090	1090	—
− 50·0	1180	1180	651
− 30·0	1280	1270	—
− 10·0	1370	1350	—
0	1410	1390	832

Since the gases are not ideal under the conditions of the experiment, it is not strictly correct to assume that viscosity and thermal conductivity are independent of pressure, but in the absence of information on the pressure effect at low temperatures this assumption has been made, and the values shown in tables 1, 2 and 3 are used throughout. If there are changes with pressure they will probably be in the same direction for both quantities, and the error produced in the results (expressed in the form of equation (2)) will be less than the individual errors.

(3) *Specific heat at constant pressure*

There is little experimental data available on the specific heat of the gases at low temperatures and pressures above atmospheric. In the cases of oxygen and nitrogen at 1 to 2 atm. pressure, it was found that experimental values obtained by Scheele & Heuse (1913) were in good agreement with values given by Millar & Sullivan (1928) in their tabulation of the thermodynamic properties of these gases. Moreover, there was no appreciable variation in these values over the whole temperature range covered by the heat-transfer experiments, and it was therefore possible, without appreciable error, to use one value for each gas, namely: for oxygen (1 to 2 atm.) 0·222 B.T.U./lb./° F, for nitrogen (1 to 2 atm.) 0·253 B.T.U./lb./° F.

For oxygen at higher pressures, a separate value was taken for each pressure investigated, from Millar & Sullivan's data (1928). Where an appreciable variation occurred over the temperature range covered by an experiment, an arithmetic mean was taken. There were no experiments on nitrogen at higher pressures.

All experiments on carbon dioxide were carried out in the pressure range 6 to 8·3 atm. (abs.), and using the values for specific heat of Sweigert, Weber & Allen (1946), it was found that no appreciable variation occurred over this pressure range. The value taken was 0·203 B.T.U./lb./° F.

RESULTS OF HEAT-TRANSFER EXPERIMENTS

The temperatures observed in each trial were plotted against distance along the exchanger, as shown in figure 5. It can be shown theoretically that in the absence of heat leakage, and provided that the specific heat of the gas remains constant, the three lines should be straight and parallel. In fact, there is a slight difference in slope between the annulus gas and tube-wall lines, due to heat leakage.

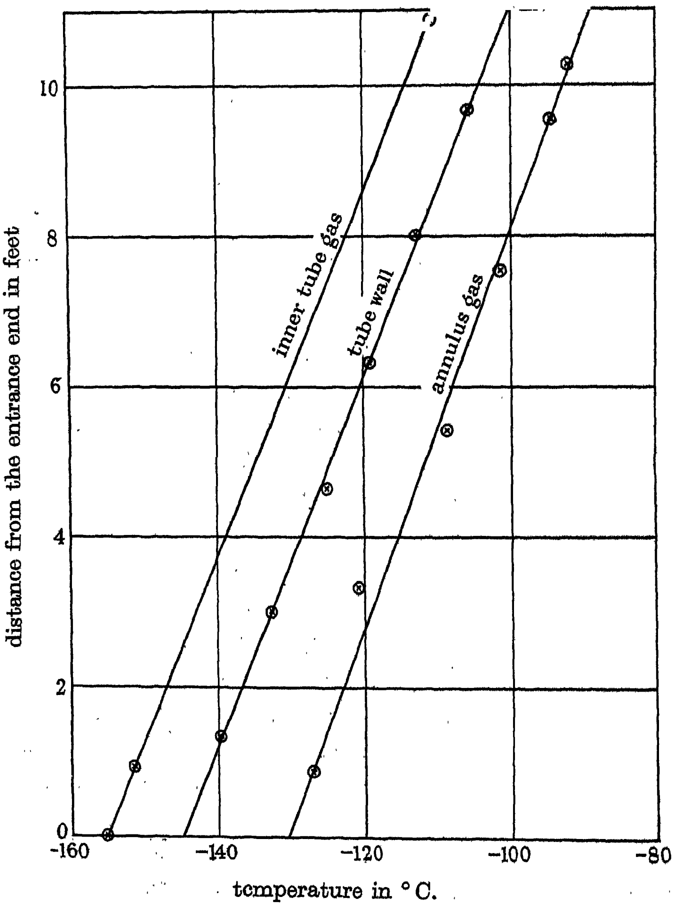

FIGURE 5. Plot of temperature against distance along tube.

The amount of heat gained in the inner tube and lost in the annulus was calculated from the inlet and outlet temperatures of the inner gas stream, and the temperature gradient controlling heat transfer was taken as the arithmetic mean value between points at 1 and 9·25 ft. along the exchanger. Physical properties of the gas were evaluated at mean bulk temperatures or at mean film temperatures, giving slightly different results in each case, as is shown later. The effect of radiation between the concentric tubes was neglected, because it was shown by calculation that heat transfer by this means was of the order of only 0·2 % of the total transfer.

No correction was necessary for temperature drop across the wall of the inner tube, since the temperatures of the surfaces were found by calculation to differ by less than 0·01° C from the measured temperature at the middle of the wall. Results were calculated as heat-transfer coefficients, h_i for the inner tube and h_a for the annulus.

The Prandtl number for gases, $(c\mu/k)$, varies somewhat with the conditions under which the gases are flowing, but when the term is raised to the 0·3 or 0·4 power in equation (2) the variation is so small that a constant value can be assigned to it. Equation (2) then reduces to the form

$$\frac{hD}{k} = \beta\left(\frac{DV\rho}{\mu}\right)^r. \tag{4}$$

In the correlation of results at normal and high temperatures β is usually assigned the value of 0·020, and r is 0·8.

From plots of Nusselt numbers versus Reynolds numbers for each gas, the values of β and r were evaluated and are given in table 4.

TABLE 4. VALUES OF CONSTANTS IN EQUATION (4)

	β		r	
gas	inner tube	annulus	inner tube	annulus
oxygen	0·0205	0·0206	0·791	0·781
nitrogen	0·0225	0·0195	0·776	0·784
carbon dioxide	0·0175	0·0182	0·806	0·800

In figure 6 all the results have been plotted together, and it is seen that good correlation can be obtained irrespective of the nature of the gas even at pressures up to 11 atm. The equation of the best line through all the points is

$$\frac{hD}{k} = 0\cdot0179\left(\frac{DV\rho}{\mu}\right)^{0\cdot8}, \tag{5}$$

in which the value for β is 10·5 % lower than the normal figure of 0·020. If the data for the annulus are excluded as being rather less accurate than those for the inner tube, β becomes 0·184, which is 8 % lower than normal; while if the correlation is made by evaluating the Reynolds numbers at mean film temperatures instead of mean bulk fluid temperatures, β becomes 0·0190, which is only 5 % lower than normal.

The lower values of β may be taken to represent better than the normal value the quantitative relationship between heat and mass flow at lower temperatures, or they may indicate that the chosen values for the thermal conductivities of the gases are a few percent too high. It is considered that further work in this field would best be directed towards the accurate evaluation of the physical properties of gases at low temperatures and elevated pressures.

At a very conservative estimate, the average error to be expected in the determination of heat-transfer coefficients is ± 3·2 %, with the maximum error in a single experiment of 8 %.

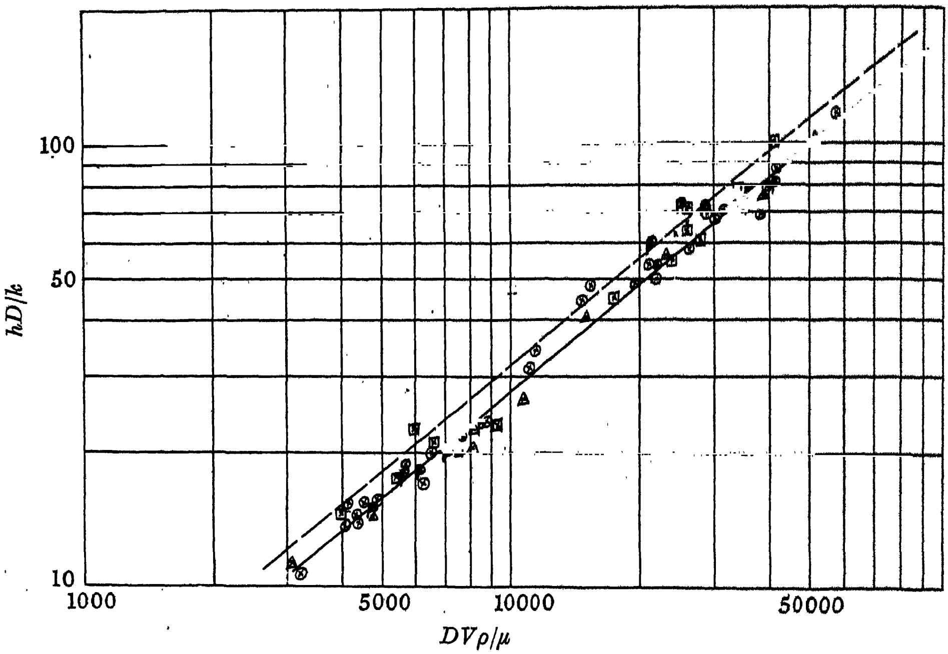

FIGURE 6. Results of heat-transfer experiments on oxygen, nitrogen and carbon dioxide. ---- For ordinary equation $hD/k = 0\cdot020\left(\frac{DV\rho}{\mu}\right)^{0\cdot8}$; —— for three gases. *O*, oxygen; *P*, oxygen under 10 atm.; *Δ*, nitrogen; □, carbon dioxide.

The ranges of the experiments in which the foregoing results were obtained were as follows:

Oxygen:	Reynolds numbers	3000 to 60,000.
	Pressures	1·2 to 11·1 atm. (abs.).
	Temperatures	-159 to 0° C.
Nitrogen:	Reynolds numbers	3000 to 50,000.
	Pressures	1·5 to 1·8 atm. (abs.).
	Temperatures	-167 to $+16°$ C.
Carbon dioxide:	Reynolds numbers	4000 to 40,000.
	Pressures	6·0 to 8·3 atm. (abs.).
	Temperatures	-43 to $+45°$ C.

The results themselves are given in tables 5, 6 and 7. Position of thermocouples (distance in feet from the entrance end of the tube):

	inner gas inlet	inner gas outlet	inner gas	tube wall					
couple number	1, 2, 3	12, 13, 14	17	4	5	6	9	10	11
distance (ft.)	0	10·88	0·93	1·33	3·00	4·67	6·34	8·01	9·68

	annulus gas outlet	annulus gas inlet	annulus gas			
couple number	7*a*, 7*b*, 8*a*, 8*b*	15*a*, 15*b*, 16*a*, 16*b*	18	19	20	21
distance (ft.)	0·86	10·28	3·34	5·43	7·54	9·58

trial number	*W*	*Pa*	1, 2, 3	4	5	6	7*a*, 7*b*, 8*a*, 8*b*	9	10	11	12, 13, 14	15*a*, 15*b*, 16*a*, 16*b*	17	18	19	20	21
1	24·68	0·70	−155·5	−141·0	−136·0	−129·0	−129·5	−124·5	−119·0	−113·5	−117·6	−101·0	−152·0	−124·3	−114·3	−107·0	−102·8
2	17·07	0·70	−152·0	−134·0	−126·5	−117·1	−122·0	−110·1	−102·5	− 93·8	− 98·5	− 77·6	−147·0	−111·5	−100·0	− 89·0	− 81·3
3	19·42	0·70	−155·5	−139·5	−132·5	−124·7	−127·0	−119·0	−112·5	−105·5	−110·5	− 92·0	−151·0	−120·5	−108·2	−101·0	− 94·0
4	19·29	0·70	−149·7	−130·8	−124·8	−116·0	−119·9	−110·0	−103·8	− 96·2	−101·0	− 80·4	−146·5	−110·0	− 98·8	− 89·6	− 83·0
5	14·41	0·70	−144·5	−120·0	−110·0	− 95·5	−104·0	− 84·0	− 70·5	− 61·5	− 68·8	− 42·5	−136·6	− 90·0	− 71·5	− 58·5	− 46·5
6	29·74	0·70	−161·8	−147·5	−142·7	−137·2	−138·0	−132·5	−127·8	−123·0	−127·3	−110·9	−158·5	−132·0	−124·5	−118·8	−113·0
7	14·85	0·70	−151·5	−126·5	−117·2	−103·0	−111·5	− 94·0	− 84·2	− 72·5	− 79·0	− 50·5	−145·0	− 98·0	− 79·3	− 64·0	− 55·2
8	18·63	0·70	−154·1	−119·5	−102·5	− 84·0	− 93·0	− 67·0	− 52·0	− 33·5	− 44·2	+ 1·0	−144·0	− 74·0	− 46·0	− 22·0	− 6·0
9	11·00	0·70	−154·8	−123·1	−113·2	−100·0	−108·0	− 90·0	− 80·0	− 66·5	− 73·0	− 44·9	−138·5	− 94·5	− 75·3	− 60·0	− 50·0
10	15·09	0·70	−149·2	−127·3	−117·7	−105·8	−112·9	− 97·0	− 87·5	− 77·0	− 83·1	− 57·3	−143·0	−101·0	− 83·9	− 71·0	− 61·5
11	22·48	0·65	−158·5	−141·0	−134·5	−126·5	−128·5	−121·0	−115·5	−108·5	−114·0	− 93·6	−155·0	−121·6	−110·0	−101·5	− 96·2
12	15·83	0·65	−149·0	−127·6	−119·5	−108·2	−114·6	−100·0	− 92·4	− 82·0	− 88·1	− 63·4	−143·0	−103·1	− 88·0	− 76·8	− 67·1
13	11·33	0·70	−141·5	−112·1	−101·0	− 83·5	− 96·4	− 71·5	− 61·3	− 46·2	− 50·9	− 20·5	−131·7	− 79·5	− 56·0	− 37·5	− 26·5
14	33·99	0·80	−154·5	−141·0	−135·0	−129·4	−128·5	−124·6	−119·5	−113·5	−118·6	− 99·0	−151·3	−122·0	−113·5	−105·0	−102·5
15	15·09	0·39	−155·0	−128·5	−117·2	−105·1	−110·0	− 94·2	− 81·9	− 70·5	− 77·0	− 47·1	−148·0	− 95·2	− 81·0	− 65·1	− 52·0
16	8·58	0·20	−136·3	−113·5	−103·0	− 91·0	− 99·8	− 80·5	− 68·8	− 60·5	− 62·5	− 42·5	−130·0	− 84·5	− 71·0	− 59·0	− 46·1
17	19·32	4·02	−146·5	−130·0	−124·7	−117·0	−117·3	−111·0	−105·5	− 98·3	−103·2	− 83·5	−142·0	−111·0	− 99·9	− 91·7	− 86·2
18	28·12	10·10	−140·9	−121·4	−115·0	−108·2	−107·4	—	− 94·4	− 88·5	− 96·4	− 91·6	—	− 96·5	− 89·0	− 82·2	—
19	25·04	9·90	−141·9	−118·3	−110·5	−101·8	−100·4	—	− 84·5	− 77·2	− 86·7	− 57·5	—	− 88·0	− 79·5	− 67·5	—
20	13·08	9·00	−145·5	−136·7	—	−131·8	−131·0	−128·9	−125·9	−121·7	−124·4	−110·6	—	−124·1	−119·0	−114·0	−111·3
21	15·93	9·10	−149·5	−137·0	—	−127·3	−129·2	−122·9	−117·3	−111·5	−116·0	− 99·1	—	−118·6	−114·5	−105·0	−100·3

W, mass-flow rate (lb./hr.); *Pa*, gauge pressure of the system (atm.).

Table 6. Heat-transfer data on nitrogen

thermocouple readings in °C

trial number	*W*	*Pa*	1, 2, 3	4	5	6	7*a*, 7*b*, 8*a*, 8*b*	9	10	11	12, 13, 14	15*a*, 15*b*, 16*a*, 16*b*	17	18	19	20	21
1	25·09	0·70	−168·7	−154·4	−149·0	−142·8	−143·0	−139·3	−133·9	−127·0	−133·0	−114·4	−166·3	−137·1	−128·5	−122·9	−116·5
2	18·09	0·63	−164·5	−144·0	−140·0	−130·5	−134·1	−124·6	−118·6	−110·6	−116·4	− 95·0	−160·5	−125·1	−114·5	−104·4	− 97·2
3	13·51	0·65	−155·0	−131·3	−123·0	−110·0	−116·0	−102·1	− 94·0	− 82·5	− 88·1	− 61·0	−150·0	−105·5	− 87·2	− 74·0	− 64·5
4	19·26	0·80	−171·0	−152·6	−148·5	−141·0	−139·0	−135·5	−130·5	−123·5	−129·0	−109·0	−168·0	−133·5	−124·0	−115·5	−111·0
5	21·70	0·55	−164·5	−141·0	−132·5	−124·0	−125·0	−115·8	−108·2	− 99·4	−107·1	− 81·0	−160·0	−115·5	−102·5	− 90·0	− 85·5
6	10·69	0·50	−145·6	−108·2	− 88·2	− 66·2	− 84·1	− 50·4	− 38·0	− 16·0	− 23·8	+ 16·8	−137·0	− 59·5	− 33·0	− 6·0	+ 7·7

Table 7. Heat-transfer data on carbon dioxide

thermocouple readings in °C

trial number	*W*	*Pa*	1, 2, 3	4	5	6	7*a*, 7*b*, 8*a*, 8*b*	9	10	11	12, 13, 14	15*a*, 15*b*, 16*a*, 16*b*	17	18	19	20	21
1	20·57	7·3	−37·5	−27·0	−21·5	−18·5	−20·3	−14·5	−11·3	− 6·4	−10·6	+ 2·3	—	−12·9	−10·0	− 3·4	+ 0·5
2	13·10	5·1	−38·6	−24·5	−17·0	−12·5	−15·5	− 5·8	0	+ 6·2	+ 2·1	+17·2	—	− 5·3	0	+ 9·0	+14·8
3	17·69	6·3	−41·4	−25·0	−18·7	−14·0	−15·8	− 7·5	− 2·5	+ 4·0	− 0·5	+18·0	—	− 5·9	0	+ 8·1	+14·9
4	19·12	5·5	−41·3	−26·5	−19·5	−13·7	−15·5	− 6·9	0	+ 6·6	+ 2·6	+22·0	—	− 4·6	+ 2·3	+12·0	+19·4
5	4·78	5·0	−28·0	−12·4	− 3·3	+ 4·0	− 5·3	+12·9	+21·8	+32·0	+30·0	+45·0	—	+ 8·7	+18·4	+28·4	+42·1
6	29·52	5·0	−46·0	−33·5	−27·5	−23·5	−21·3	−17·3	−12·9	− 7·0	−11·3	+ 6·4	—	−14·0	− 8·5	− 2·0	+ 4·4
7	24·80	5·0	−44·8	−29·0	−21·2	−15·5	−16·5	− 7·5	− 0·5	+ 7·0	+ 0·5	+26·0	—	− 5·5	+ 2·2	+12·8	+22·6

PRESSURE DROP ACCOMPANYING HEAT TRANSFER

A series of experiments was carried out on the measurement of pressure drop in the inner tube, when the gas flowing through it was (*a*) isothermal air at room temperature, (*b*) heating oxygen and (*c*) cooling oxygen. In all cases the friction drop was calculated from the following equation:

$$\frac{dF}{dL} = 2f\frac{V^2}{gD}. \tag{6}$$

Where the flow was non-isothermal, the velocity term V was expressed as a linear function of the length of the tube L, as the velocity term could be expressed in terms of the total volume of the gas, which could be assumed to be directly proportional to the absolute temperature of the gas; there was a linear relationship between the temperature of the gas and the length of the tube. The pressure drop due to friction in this case was obtained from the measured pressure drop corrected for the work of expansion of the gas.

The friction factor, f, is a dimensionless number, whose value depends on the Reynolds number of the fluid, and the relative roughness of the pipe. Values of f were plotted against Reynolds numbers, and in all three cases the results fell about straight lines, whose slopes are shown in figure 7. A line corresponding to the data of Stanton & Pannell (1914) for isothermal air is shown for comparison. It will be seen that there is very little difference in the results for heating and cooling oxygen, and that they differ from those for isothermal air by about 6 %.

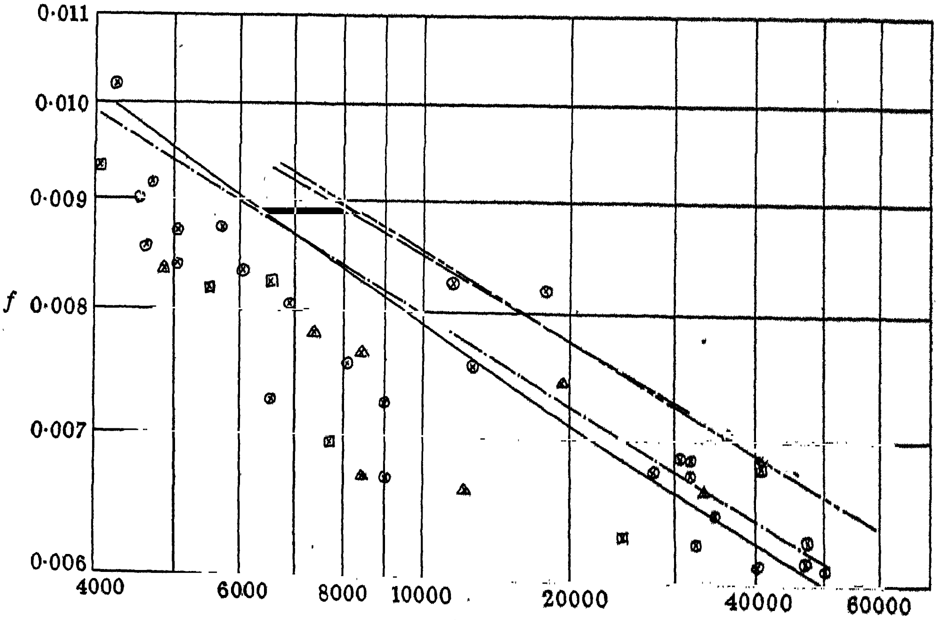

FIGURE 7. Comparison of friction loss experiments. ——— cooling of oxygen gas; —·—isothermal air; ——-— heating of oxygen gas; ——— Stanton & Pannell's data.

In Reynolds's analogy, a comparison is drawn between the transfer of heat from a fluid to a surface and the transfer of momentum, which is manifested as pressure drop in the case of flow in a pipe. The two are related by the equation

$$f = \frac{2h}{c\rho V}. \tag{7}$$

That this is approximately true in the present experiments is shown by the points in figure 7, which show the relation between Reynolds numbers and the group $2h/c\rho V$, calculated from determined values of the heat-transfer coefficients.

The authors wish to thank Professor Sir Alfred Egerton, Sec.R.S., Head of the Department of Chemical Engineering and Applied Chemistry, Imperial College, for his advice and encouragement; Professor O. A. Saunders, Head of the Department of Mechanical Engineering, for helpful discussions during the early part of the work; and Mr A. M. Alger for the construction of most of the apparatus. The Gas Research Board are thanked for providing financial assistance for one of us (T. A. H.), and for their interest in the investigation.

REFERENCES

Colburn 1933 *Trans. Amer. Inst. Chem. Engrs*, **29**, 174.
Eucken 1911 *Phys. Z.* **14**, 324.
Fishenden & Saunders 1932 *The calculation of heat transmission.* London: H.M.S.O.
Hebbard & Badger 1933 *Industr. Engng Chem.* (Anal. ed.), **3**, 359.
Johnston & McClosky 1940 *J. Phys. Chem.* **44**, 1038.
Kerr 1932 *Trans. Amer. Soc. Mech. Engrs*, **54**, 1.
McAdams 1942 *Heat transmission.* New York: McGraw Hill.
Millar & Sullivan 1928 *Tech. Pap. U.S. Bur. Min.* no. 424.
Nusselt 1909 *Z. Ver. dtsch. Ing.* **53**, 1750 and 1809.
Scheele & Heuse 1913 *S.B. preuss. Akad. Wiss.* **44**.
Schmidt 1937 *Phys. in regalmäss. Ber.* **5**, 101.
Scott 1941 *Temperature; its measurement and control in science and industry*, p. 206. New York: Rheinhold.
Sweigert, Weber & Allen 1946 *Industr. Engng Chem.* **38**, 185.
Stanton & Pannell 1914 *Phil. Trans.* A, **214**, 199.
Ulsamer 1936 *Z. Ver. dtsch. Ing.* **80**, 537.
Ulloch & Badger 1937 *Trans. Amer. Inst. Chem. Engrs*, **33**, 417.

The absorption spectra of benzene derivatives in the vacuum ultra-violet. I

By W. C. Price and A. D. Walsh, *Laboratory of Physical Chemistry, University of Cambridge*

(*Communicated by R. G. W. Norrish, F.R.S.—Received* 13 *December* 1946)

[Plates 1 to 3]

New photographs of the far ultra-violet spectrum of benzene are presented. The absorption from 2000 to 1800 A ($\lambda_{\text{max.}}$, c. 1980 A) is regarded not as a part of the much stronger absorption of peak at 1790 A but as due to a separate transition. Sharp bands lying at 1790 A represent the first member of a previously reported Rydberg series.

The spectra of toluene, xylene, monochloro- and *o*-dichlorobenzene, bromobenzene, iodobenzene and pyridine are briefly described, and the shifts relative to benzene are discussed. Two Rydberg series were observed for toluene, converging to a first ionization potential of 8·77 ± 0·05 V.

The spectrum of benzene (Plate 1)

The ultra-violet absorption spectrum of benzene at wave-lengths less than 2100 A may conveniently be divided into three regions. The first of these (plate 1) is a diffuse absorption region of maximum about 1980 A. The absorption (which has $\log \epsilon \sim 4{\cdot}0$ (Morton & Stubbs 1940)) is considerably stronger than that of the well-known 2600 A region ($\log \epsilon \sim 2{\cdot}5$ (Morton & Stubbs 1940)). The second is an extremely strong region of $\lambda_{\text{max.}}$ about 1790 A. So strong is this region that in absorption curves the 1980 A region usually only appears as a weak, long wave-length, 'step out' of the 1790 A peak. The 1790 A peak itself consists of several sharp bands overlaid by a continuous hump of absorption: this continuous background can be well seen on the accompanying plate 1. The third region of absorption lies below 1600 A. Here a series of strong, narrow, bands of the familiar Rydberg type occurs. These have been shown by Price & Wood (1935) to fit into two Rydberg series and to converge to the first ionization potential of 9·19 V (around 1350 A). Beyond 1350 A other strong bands occur which are thought to be the first resonance bands leading to the second ionization potential of benzene: from them the latter can be estimated as 11·7 ± 0·3 V.

Benzene has six π electrons, and of the three orbitals which they usually occupy in pairs, it is known that four electrons (orbitals χ_2 and χ_3) fall in the same energy level, this level being thus doubly degenerate. In terms of the parameter β, which is the resonance integral for the π electrons of the double bond, χ_1 corresponds to an energy level of binding energy -2β and $\chi_{2,3}$ to a level of energy $-\beta$. The normal electronic configuration may thus be written

$$N: \ \chi_1^2, \chi_{2,3}^4.$$

Anti-bonding orbitals χ_4, χ_5, χ_6 correspond to the bonding orbitals χ_1, χ_2, χ_3; χ_4 and χ_5 lying at the same energy level. Mulliken (1939) has shown from the electronic selection rules for a molecule of the high symmetry of benzene that transitions from the ground state to all the possible excited states are forbidden with the exception of that to the $V_1\ {}^1E_{1u}$ state.

Mulliken (1939) has calculated the intensity of this allowed transition. He assigns the transition to the whole of the 2000 to 1600 A region. Although he suggests that a Rydberg transition may possibly overlie the short wave-length part of this region, he is inclined to regard the whole spectrum from 2000 to 1600 A as predominantly non-Rydberg in type and to identify it with the $N \rightarrow V_1\ {}^1E_{1u}$ transition. He points out that the alteration in symmetry in the upper state, according to a theorem of Jahn & Teller (1937), would cause the degenerate state ${}^1E_{1u}$ to split into two non-degenerate states and might lead to a rather slight subdivision of the spectrum into two parts: hence the 1790 and 1980 A regions might arise.

We think it probable, from the separation of the 1790 and 1980 A regions shown by our photographs of the 2000 to 1600 A region, that at least two electronic transitions are concerned here, one being responsible for the strong 1790 A absorption and one for the weaker absorption of maximum around 1980 A. The subsidiary step out is also present in the spectra of toluene, xylene, pyridine, monochlorobenzene and *o*-dichlorobenzene; but it is interesting to note that it is absent in phenyl ethylene, phenyl acetylene, phenyl cyanide and benzaldehyde, that is, whenever a side chain is conjugated with the ring.

The fact that the 1780 A region is probably

$$\chi_1^2\chi_{2,3}^4 \rightarrow \chi_1^2\chi_{2,3}^3\chi_{4,5}$$

in type is indicated by the appearance of a closely similar region in cyclohexene (Price & Tutte 1940): the two π electrons of cyclohexene have binding energy $-\beta$ just as have the benzene $\chi_{2,3}$ electrons.

It is certain that the sharp bands of the 1790 A region represent a Rydberg transition. Reference to the paper of Price & Wood (1935) shows that the system fits their series II resonably well when one remembers the disturbance expected for such a low Rydberg orbital of a large molecule. The calculated and observed frequencies are: $\nu_{\text{obs.}}$ 55,860 cm.$^{-1}$; $\nu_{\text{calc.}}$ 57,547 cm.$^{-1}$. But the strongest grounds for this interpretation are that the sharp 1790 A band has accompanying it vibration frequencies ~700 and 970 cm.$^{-1}$, i.e. a vibrational pattern identical with that accompanying the other members of series II.* There can thus be no reasonable

---

* These frequencies can be found from the measurements of Carr & Stücklen (1938). The relevant figures are

$$\begin{array}{llll} \text{cm.}^{-1} & & & \\ 55860 & & & \\ 56590 & 970 & & 730 \\ 56830 & & & \end{array}$$

The results of Price & Wood show that the 730 cm.$^{-1}$ vibration is reduced to c. 688 cm.$^{-1}$ in the higher Rydberg members, but that the 970 cm.$^{-1}$ vibration maintains its magnitude.

doubt of the association of the sharp 1790 A bands with the Rydberg series II. This assignment is in agreement with the interpretations suggested by Goeppert-Mayer & Sklar (1938) and by Nordheim, Sponer & Teller (1940), though these authors did not give the vibrational evidence.

Nordheim *et al.* (1940) suggest the forbidden transition $N \rightarrow V_1\ {}^1B_{1u}$ for the 1980 A region and identify the sharp 1790 A bands both as the $N \rightarrow V_1\ {}^1E_{1u}$ transition and as the first member of the Rydberg series II of Price & Wood. This contrasts with Mulliken's interpretation of the 1790 A continuous absorption as the allowed $N \rightarrow V$ transition, the sharp bands being Rydberg bands accidentally superimposed upon the continuum. Nordheim *et al.* suggest that the continuous background around the low-pressure 1790 A band is due to another transition, namely, that of a C-H bonding electron to an antibonding repulsive state involving a C-H dissociation. They show that a repulsive state E_u^- can be constructed by superimposing excitation in the different C-H bonds with appropriate phases; and that if one C-H distance (r) is increased, the superimposed amplitudes change until, for great r values, the excitation is localized in that C-H bond which is to be broken.

The explanation is probably not quite so simple as Nordheim *et al.* suggest. If the excitation is simply that of a C-H bonding electron, a similar absorption region might be expected to appear in cyclohexane. However, there is no such region in cyclohexane, and it seems more likely that the primary excitation is that of a π electron to the stable $V_1\ {}^1E_{1u}$ state, but that some of the excitation energy is immediately transferred (e.g. by internal collision) to a C-H bonding electron, exciting it to a repulsive energy curve leading to dissociation of a C-H bond. If this is so, it would explain why the maxima of the $N \rightarrow V_1\ {}^1E_{1u}$ transition and of the 1790 A continuous absorption coincide. We believe that processes of this kind are common in the absorption spectra of polyatomic molecules, e.g. photo-dissociation of R_1R_2 CO into R_1R_2 + CO arises from the initial excitation of the non-bonding oxygen electrons, transfer of the energy by internal collision to the C-C bonding electrons then occurring.

In toluene the continuous absorption becomes stronger relative to the sharp first Rydberg bands. In xylene the Rydberg bands seem to have lost all their intensity to the continuous absorption. This supports the hypothesis put forward in the preceding paragraphs, since increase of alkyl substitution means increased possibilities of C-H dissociation and of collision of the excited π electrons with C-H bonding electrons.

A similar explanation might apply to ethylene. Here the continuous absorption in the longest wave-length region is of about the same order of intensity as the Rydberg bands. With increase of alkyl substitution it becomes more intense than the Rydberg bands. This is explicable on the basis of a C-H dissociation. Since ethane has no corresponding absorption, the primary excitation must be regarded as that of a π electron, switching over into excitation of a C-H bonding electron to a repulsive state as a result of an electron impact process. This explanation modifies to some extent the usual assignment of the first continuous absorption of the ethylenes to a simple $N \rightarrow V$ transition. Of course the spatial distribution of the electron in the V orbital (being to a considerable extent located on the side of the carbon atoms remote from the C=C bonds) is especially favourable to this type of internal electron collision.

The first ionization potential of 9·19 V found by Price & Wood corresponds to the removal of a $\chi_{2,3}$ electron and the second (11·7 V) to the removal of a χ_1 electron. Electron impact values have been given by Hustrulid, Kusch & Tate (1938) for the first and second ionization potentials of benzene: they are $9{\cdot}8 \pm 0{\cdot}1$ and $17{\cdot}2 \pm 1{\cdot}0$ V respectively. The value of 9·8 V is to be compared with the earlier electron impact values of 9·6 V given by Boucher (1922) and 9·5 V given by Friedlander & Kallman (1932). The value 17·2 V can hardly be the *second* ionization potential of benzene—it is much too far above the 9·8 V first limit to correspond to the separation of the χ_1 and $\chi_{2,3}$ levels. The separation of the levels is β, where $\beta \sim 1{\cdot}9$ V. Several other ionization potentials (e.g. of the σ C-C electrons and the C-H electrons) should lie between 9·8 and 17·2 V.

THE SPECTRA OF TOLUENE AND XYLENE (PLATE 1)

The spectrum of toluene is essentially similar to that of benzene except that it is shifted some 3300 cm.$^{-1}$ to long wave-lengths relative to benzene. It is noticeable, however, that the Rydberg bands are much less intense than in benzene: their intensity seems to have passed into the peak of absorption lying at 1830 A in toluene (1790 A in benzene).

The phenomenon is similar to that occurring with the alkyl-substituted ethylenes relative to ethylene, and a possible explanation has been suggested above.

As for benzene, two Rydberg series were found, but owing to the low intensity of the bands the series do not contain as many members as do those found for benzene. Tables 1 and 2 respectively show the accuracy with which the series are represented by the formulae

$$\nu_0^n = 71{,}130 - \frac{R}{(n+0{\cdot}05)^2}, \tag{1}$$

$$\nu_0^n = 71{,}180 - \frac{R}{(n+0{\cdot}50)^2}. \tag{2}$$

The tables show also the shifts of the bands relative to benzene. The two series converge to approximately the same limit: $8{\cdot}77 \pm 0{\cdot}05$ V. This is supported by an electron impact value of $8{\cdot}5 \pm 0{\cdot}5$ V (Groot & Penning 1933). As in the case of benzene, the first peak superimposed upon the strong region of continuous absorption (at 1830 A) is probably the first ($n = 2$) member of series (2). Observed and calculated frequencies for this are 54,640 and 53,622 cm.$^{-1}$ respectively.

The shift of the spectrum to the red and the lowered ionization potential relative to benzene are probably due to three causes: (1) transfer of negative charge from the methyl group into the ring, (2) hyperconjugation, (3) polarizability of the methyl group, i.e. the group acts as a small element of dielectric reducing all electrostatic forces and potentials in its neighbourhood. Some discussion of these factors is given below after our description of the monochlorobenzene spectrum.

The spectrum of xylene (a commercial specimen, presumably a 1 : 4 : 1 mixture of *o* : *m* : *p*) is practically the same as that of toluene, except that it is shifted still further to long wave-lengths relative to benzene and that the Rydberg bands have lost practically all their intensity. The peak of absorption now lies at about 1890 A. From this the first ionization potential of xylene may be estimated as ~ 8·3 V.

TABLES SHOWING THE OBSERVED AND CALCULATED FREQUENCIES OF THE RYDBERG BANDS IN TOLUENE AND THE SHIFTS OF THE BANDS RELATIVE TO BENZENE

TABLE 1

n	$\nu_{\text{obs.}}$	$\nu_{\text{calc.}}$	ν_{benzene}	$\nu_{\text{benzene}}-\nu_{\text{toluene}}$
3	59,679	59,383	—	—
4	64,391	64,440	67,529	3,138
5	66,784	66,827	70,047	3,251
6	68,103	68,132	71,415	3,312
7	68,944	68,922	72,242	3,298
8	69,433	69,436	72,777	3,344

TABLE 2

n	$\nu_{\text{obs.}}$	$\nu_{\text{calc.}}$	ν_{benzene}	$\nu_{\text{benzene}}-\nu_{\text{toluene}}$
3	62,380	62,222	65,716	3,336
4	65,829	65,761	69,273	3,444
5	67,635	67,552	71,025	3,390
6	68,561	68,583	72,035	3,474

THE SPECTRA OF HALOGENOBENZENES (PLATES 2 AND 3)

Monochlorobenzene (plate 2). The spectrum of monochlorobenzene is very similar to that of benzene except that it is shifted to long wave-lengths. As in xylene, the Rydberg bands of benzene do not appear: all their intensity seems to have gone into the peak of absorption which has its maximum at about 1870 A. Bands probably analogous to the benzene 1980 A system occur at about 2150 A on the long wave-length side of this peak; and the usual ultra-violet system around 2600 A can just be seen on the left of the photograph. The 2600 A bands are much weaker than those at 2150 A. From the position of the 1870 A peak the first ionization potential of the π electrons of the benzene ring of monochlorobenzene may be estimated as slightly less than that of toluene (8·77 V). This is to be compared with the analogous case of chloroprene and isoprene, where the ionization potentials have been determined as 8·79 and 8·81 V respectively (Price & Walsh 1940).

There is a strong band in the spectrum at about 1460 A. It seems probable that this is analogous to the 'D' bands of the alkyl halides (Price 1936). The fact that it lies to shorter wave-lengths than in ethyl and propyl chlorides (1465 and 1475 A respectively) indicates that the chlorine atom bears a smaller negative charge in monochlorobenzene than in those alkyl chlorides. Similar bands near 1460 A occur in the spectra of chloroprene (Price & Walsh 1940) and the chloroethylenes (Walsh 1945).

The shift of the monochlorobenzene spectrum to long wave-lengths and the reduction of the first π ionization potential relative to benzene may be considered in relation to several other important and related effects: (1) the CCl distance is shortened relative to the CCl distances found in the alkyl halides (Brockway & Palmer 1937), (2) further substituents are directed mainly into the *o*-*p* positions, (3) substitution reactions are generally slower than those of benzene (Bird & Ingold 1938). All these properties may be discussed in terms of (*a*) an inductive effect, and (*b*) resonance between the forms

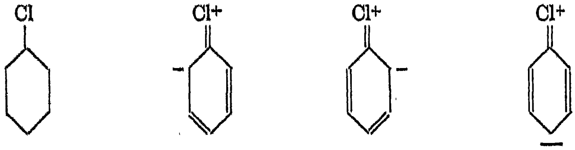

Effect (*b*) may be subdivided into four parts: (I) the actual state of the molecule bears more negative charge upon the ring than would otherwise be the case; (II) the actual state has more double bond CCl character than would otherwise be the case; (III) there is a raising (relative to benzene) of the ground energy level ($\chi_{2,3}$) of the least strongly bound π electrons; and (IV) there is a resonance energy and the actual molecule is more stable than any of the forms shown above.

The shortening of CCl distance has usually been interpreted in terms of effect (*b*) (II), but this is not the only effect at work. Elsewhere (Walsh 1947) we have pointed out that there is an enhanced electro-negativity of a carbon atom on the side remote from the multiple bonds. The latter effect probably plays an important, if not a major, part in shortening the CCl bond.

The long wave-length spectroscopic shift is to be interpreted mainly in terms of effects (*b*) (I) and (*b*) (III). It will also be affected according as the binding of the ϕ-Cl electrons is greater than or less than that of the electrons of $\phi - H$: the greater this binding the less the binding of the ring π electrons, for there exists a balance between the binding of the σ electrons and the polarizability of the π electron (Walsh 1947) on the carbon atom concerned and hence of the molecular π orbital constructed from the constituent atomic $2p_z$ orbitals.

The sign of the ϕ Cl dipole ($\phi^{+}\text{Cl}^{-}$) shows that the long wave-length shift of the ϕ Cl spectrum relative to benzene cannot be due to an inductive effect. In other words, the spectrum provides important evidence that conjugation of the ring π electrons with the chlorine $2p\pi$ electrons is occurring. The resonance effect is not one that occurs solely on the approach of another molecule.

The sign of the dipole means that the inductive effect predominates over effect (*b*) (I), as far as actual magnitude of moments are concerned. We wish, however, to stress that the inductive effect is a short range effect. The decrease in ionization potential of the halogen electrons in CH_3X on passing to $\text{CH}_3.\text{CH}_2X$ is much less than the decrease on passing from HX to CH_3X. We therefore expect the inductive effect to be largely concentrated on the ring C atom nearest to the Cl. There will be a smaller effect on the *o* atoms, but probably very little effect on the *m* and none on the *p* atoms. Relative to saturated compounds, the effect will be exerted through a longer chain of atoms in conjugated molecules because of the higher polarizability of conjugated bonds; but Denbigh (1940) finds the longitudinal polarizability of a $C_{arom.}$-$C_{arom.}$ bond to be 22·5/18·8 times that of a $C_{alip.}$-$C_{alip.}$ bond, i.e. an increase of only 25 %. In any case there will be a continuous decrease (not an alternation) of the effect as we pass farther from the polarizing centre. This decrease means that the postulate of Ri & Eyring (1940) that the inductive effect causes equal charges on all six carbon atoms cannot be correct.

Pauling (1940) describes the inductive effect as resulting from resonance between ionic structures including

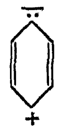

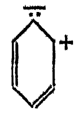

but it seems to us that this formulation confuses the distinction between inductive and resonance effects, neglecting the short-range nature of the former and suggesting an alternating nature.

In comparison with the inductive effect, the resonance effect may be long-range. This means that the orientation property, relating in part to the *p* position, must be explained in terms of the resonance effect. In conjunction with the foregoing, it also means that large changes in ionization potential of conjugated systems cannot be attributed to inductive effects, but may be explained in terms of resonance. A corollary from this is that the reduced ionization potential of toluene relative to benzene must be explained largely in terms of hyperconjugation (see Mulliken 1942), that is, resonance involving the non-localization of the electrons in the CH_3 group, rather than exclusively of inductive effect. We think, in contrast to Pauling (1940), the *o-p* orientation of toluene is to be explained similarly rather than solely in terms of an inductive effect.

The reduced reactivity has probably a more complex explanation than any of the others. A number of factors may be listed which, among others, will affect the reactivity. In the first place, if the substituting agent is a positive ion (e.g. NO_2^+), then the dipole in ϕ Cl will tend to cause collision between the ion and the Cl rather than between the ion and the ring. In the second place, increase in electronic density in the ring will facilitate reaction with a cationoid reagent. The greater the ring electronic density, the easier it is for the transition complex that must precede reaction to form. Thirdly, the greater the number of resonance structures possible in such a complex the greater the ease of reaction. (Such transition state resonance is greatest for the *o-p* positions.) Fourthly, effect (*b*) (IV)—the stabilization due to resonance—will lower the reactivity. Fifthly, reactivity to substituting agents will also be determined by the CH bond strength. Sixthly, the polarizability of the π electrons may be important.

Whether or no a benzene derivative shows increased or reduced reactivity relative to benzene thus depends upon the resultant of a number of effects. Toluene shows enhanced reactivity, probably largely because the hyperconjugation and inductive effects both increase the ring negative charge. Monochlorobenzene shows reduced reactivity, probably partly because of the first of the above factors and because of the inductive and resonance-stabilization effects, offset by the effect (*b*) (I).

o-Dichlorobenzene (plate 2). In *o*-dichlorobenzene the absorption peak at 1790 A in benzene and at 1830 A in monochlorobenzene is at about 1900 A. Accordingly, the first ionization potential of the π electrons of the ring is probably further depressed: it may be estimated as $\sim 8{\cdot}3$ V. The depression is presumably due to resonance to further ionic structures made possible by the extra chlorine atom. The strong band identified in monochlorobenzene as analogous to the alkyl chloride 'D' band here occurs at slightly shorter wave-lengths (1450 A) than in monochlorobenzene.

In monochlorobenzene there is a tendency for the 'step-out' on the long wave-length side of the absorption peak to become more pronounced and to separate from the peak. The most noticeable feature of the *o*-dichlorobenzene spectrum is that this separation has become practically complete, a short region of transparency occurring around 2100 to 1950 A. The maximum of the longer wave-length absorption is at about 2160 A. On the long wave-length side of the maximum one or two very diffuse bands are visible. Similar bands are to be seen in the corresponding regions of benzene and monochlorobenzene. It seems probable that conjugation of a substituent with the benzene ring causes the benzene 2000 A region to move farther to long wave-lengths than the 1790 A (first Rydberg) band, so separating the two transitions. In monochlorobenzene, where the lone pair chlorine electrons conjugate with the benzene-ring electrons, this separation is seen just beginning. In *o*-dichlorobenzene the increased resonance causes the separation to proceed a stage further. In benzaldehyde (Walsh 1946), phenyl cyanide, phenyl ethylene and phenyl acetylene (see following paper), the extra conjugation is such that the two regions are completely separated. The much greater shift of the benzene 1980 A region to long wave-lengths with increasing conjugation (compared with the 1790 and 2600 A regions) should be an important confirmatory clue to the identification of each transition.

In the photograph (plate 2), the usual near ultra-violet absorption can be seen around 2700 A. Very diffuse bands, probably due to the chlorine electrons, can be seen to the short wave-length side of 1350 A.

Monobromo- and monoiodobenzene (plate 3). In monobromo- and monoiodobenzene the absorption is essentially as in monochlorobenzene except that the bands due to the non-bonding $p\pi$ halogen electrons are more prominent than in the monochloro compound, since iodine and bromine absorb at longer wave-lengths than chlorine: this is due to their greater atomic volumes and their consequently greater ease of excitation.

In monoiodobenzene the first region of absorption on our photographs occurs around 2250 A. We think it partly analogous to the benzene 1980 A region, since it seems to bear a resemblance to the system around 2150 A in chlorobenzene. It probably also includes analogues of the so-called 'B' bands of methyl iodide (Price 1936). The second region, around 2050 A, corresponds to the 'C' bands of methyl iodide (Price 1936) and isopropyl iodide (Walsh, unpublished work). The bands around 1700 to 1750 A probably include analogues of the 'D' bands of the alkyl halides. A peak of absorption which is probably analogous to the benzene 1790 A peak occurs at about 1890 A. It is noticeably weaker than the bands at 1700 to 1750 A, and roughly comparable in intensity with the systems around 2250 and 2050 A.

In monobromobenzene the 'B' bands occur between 2000 and 2100 A, the 'C' bands at about 1970 A and the 'D' band is at about 1600 A. The analogue of the benzene 1790 A peak is at about 1870 A: it is rather stronger than the bromine absorption. Comparatively weak absorption around 2120 A possibly corresponds to the benzene 1980 A system.

The spectrum of the π electrons in the benzene ring is thus shifted to long wave-lengths in monobromobenzene and monoiodobenzene relative to monochlorobenzene. This is presumably due to a decreased inductive effect in the two former molecules, this more than compensating for the fact that the resonance effect is greater with chlorine than with bromine than with iodine (Bird & Ingold 1938).

The spectrum of pyridine (Plate 3)

Pyridine gives a spectrum very similar to that of benzene and its simple derivatives, but at rather shorter wave-lengths. There is the usual main peak of absorption (maximum ~ 1700 A), and on the long wave-length side of this there is the usual 'step-out' (2000 to 1800 A). The shift to short wave-lengths relative to benzene supports Pauling's explanation of the fact that pyridine substitutes in the β position (Pauling 1940). The nitrogen atom attracts electrons from the ring, these electrons coming mainly from the α and γ carbon atoms according to the resonance forms

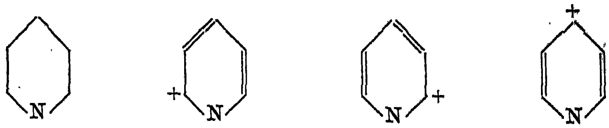

Justification for the partial negative charge on the nitrogen atom lies in the considerable basic character of pyridine, while the short wave-length spectroscopic shift provides evidence of reduced electronic density in the rest of the ring.

From the shift of the main absorption peak relative to benzene, the first ionization potential of the π electrons in pyridine may be estimated as $\sim 0{\cdot}5$ V higher than that of benzene (9·19 V), i.e. $\sim 9{\cdot}7$ V. An electron impact value of $9{\cdot}8 \pm 0{\cdot}2$ V has been given by Hustrulid, Kusch & Tate (1938).

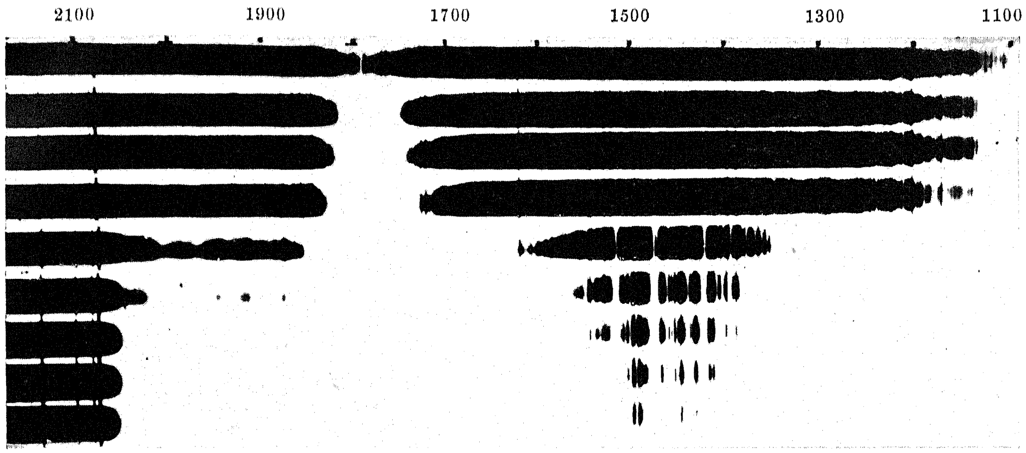

benzene

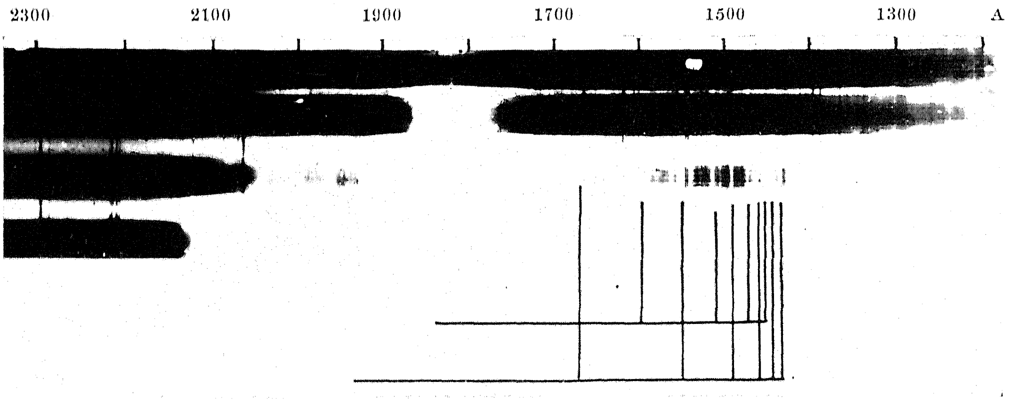

toluene

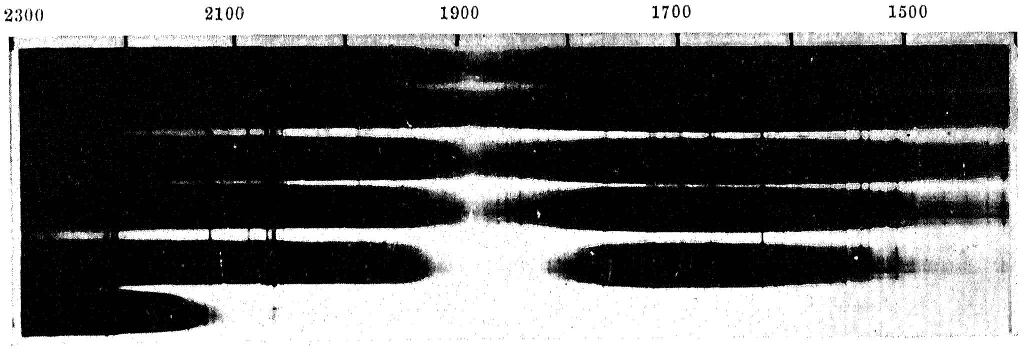

xylene

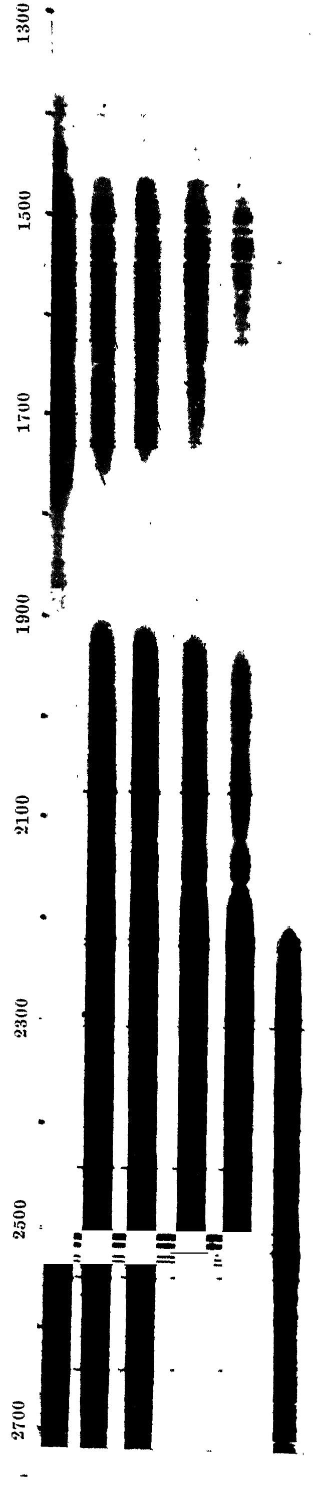

monochlorobenzene

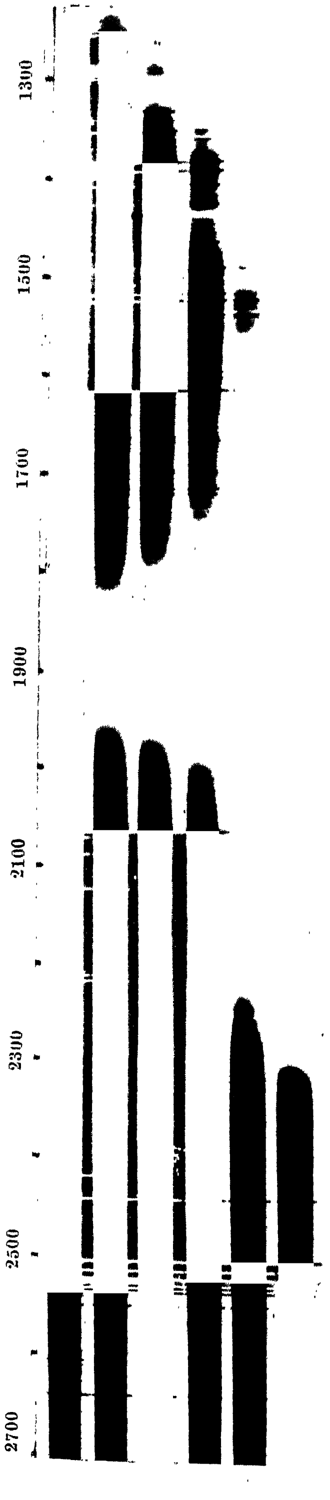

o-dichlorobenzene

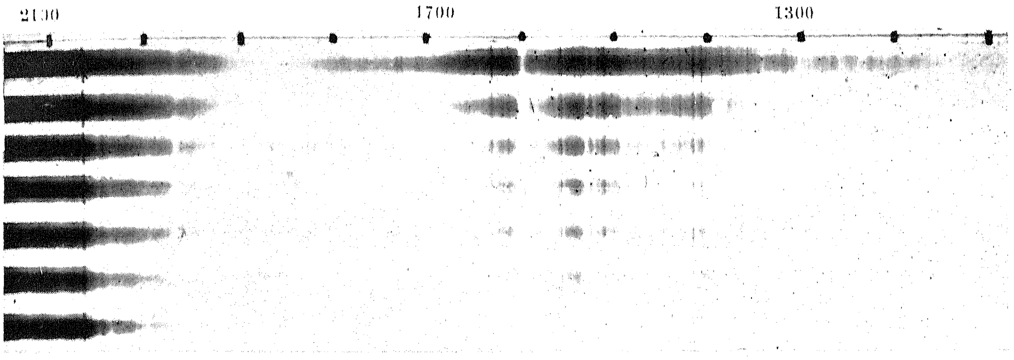

monobromobenzene

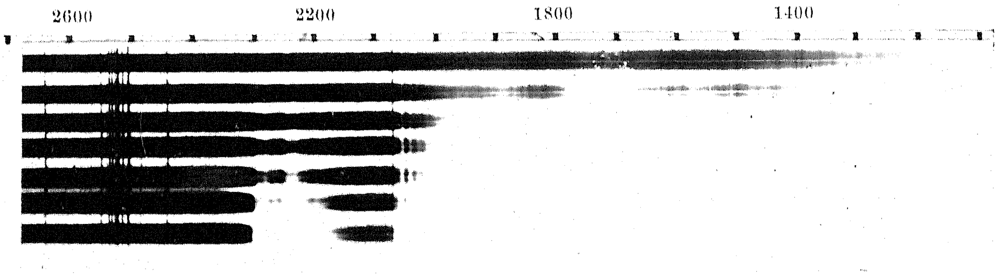

monoiodobenzene

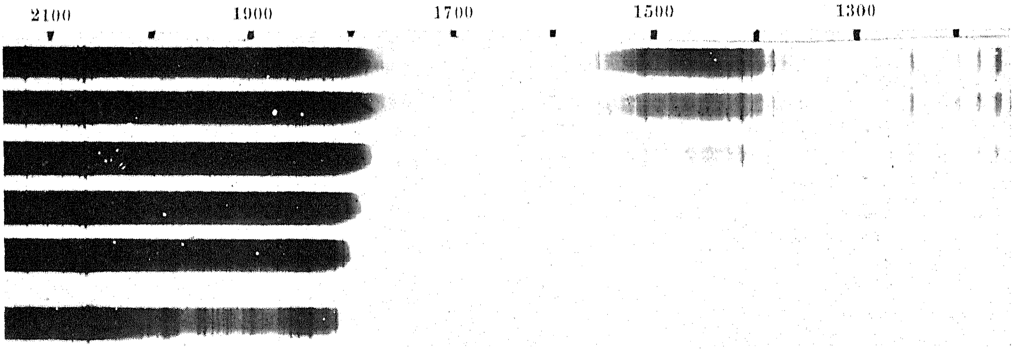

pyridine

The 1700 A peak is to be identified with the allowed $N \rightarrow V$ transition, the upper V state being coupled with a C-H repulsive curve as in benzene. Mulliken (1939) has pointed out that in pyridine the analogues of the benzene forbidden transition $N \rightarrow {}^1B_{2u}$ and $N \rightarrow {}^1B_{1u}$ are no longer forbidden and may be considered as normal $N \rightarrow V$ transitions. In accord with this the near ultra-violet spectrum of pyridine near 2600 A is about thirty times as intense as the otherwise very similar 2600 A region in benzene ($N \rightarrow {}^1B_{2u}$). The 2000 to 1800 A region, however, does not seem to be much stronger than in benzene: but it is difficult to compare the intensities from our photographs.

This work was carried out during 1940–1, and we have to thank the Department of Scientific and Industrial Research for financial assistance during that time.

REFERENCES

Bird & Ingold 1938 *J. Chem. Soc.* p. 918.
Brockway & Palmer 1937 *J. Amer. Chem. Soc.* **59**, 2181.
Boucher 1922 *Phys. Rev.* **19**, 189.
Carr & Stücklen 1938 *J. Chem. Phys.* **6**, 55.
Denbigh 1940 *Trans. Faraday Soc.* **36**, 936.
Friedlander & Kallman 1932 *Z. Phys. Chem.* B, **17**, 265.
Goeppert-Mayer & Sklar 1938 *J. Chem. Phys.* **6**, 645.
Groot & Penning 1933 *Handbuch der Physik.*
Hustrulid, Kusch & Tate 1938 *Phys. Rev.* **54**, 1037.
Jahn & Teller 1937 *Proc. Roy. Soc.* A, **161**, 220.
Morton & Stubbs 1940 *J. Chem. Soc.* p. 1347.
Mulliken 1939 *J. Chem. Phys.* **7**, 20, 353.
Mulliken 1942 *Rev. Mod. Phys.* **14**, 265.
Nordheim, Sponer & Teller 1940 *J. Chem. Phys.* **8**, 455.
Pauling 1940 *The nature of the chemical bond*, pp. 149–150. Cornell.
Price 1936 *J. Chem. Phys.* **4**, 539, 547.
Price & Wood 1935 *J. Chem. Phys.* **3**, 439.
Price & Tutte 1940 *Proc. Roy. Soc.* A, **174**, 207.
Price & Walsh 1940 *Proc. Roy. Soc.* A, **174**, 220.
Ri & Eyring 1940 *J. Chem. Phys.* **8**, 433.
Walsh 1945 *Trans. Faraday Soc.* **41**, 35.
Walsh 1946 *Trans. Faraday Soc.* **42**, 62.
Walsh 1947 *Trans. Faraday Soc.* **43**, 60; *J. Chem. Soc.* (in the Press).

The absorption spectra of benzene derivatives in the vacuum ultra-violet. II

By A. D. Walsh, *Laboratory of Physical Chemistry, University of Cambridge*

(*Communicated by R. G. W. Norrish, F.R.S.—Received* 13 *December* 1946)

[Plate 4]

The far ultra-violet spectra of styrene, α-methyl styrene, phenyl acetylene, phenyl cyanide and phenyl isocyanate are described. Many of the observed regions of absorption are correlated with those of the benzene spectrum. The important fact emerges that, with increasing conjugation of the side chain with the ring, the benzene 1980 A absorption moves much farther to long wave-lengths than do the benzene 2600 and 1790 A absorptions. α-Methyl styrene shows a shift to the violet of certain regions of its spectrum relative to styrene. Phenyl isocyanate has a spectrum much closer to that of benzene than have the other molecules discussed.

The preceding paper has dealt with the far ultra-violet spectra of the simplest monosubstituted benzenes. The present paper describes the spectra of further benzene derivatives, with particular reference to compounds where the side chain is conjugated with the ring.

THE SPECTRUM OF STYRENE (PLATE 4)

The styrene used was a redistilled specimen of b.p. 146° C.

The near ultra-violet absorption of styrene was studied by Ley (1918), who found weak maxima at 2910 and 2820 A and an intense maximum at 2460 A. Ramart-Lucas & Amagat (1932) observed maxima at 2910, 2815 and 2435 A.

The photographs show the shorter wave-length absorption as a strong region extending (at the vapour pressures used) from about 2450 to 2300 A. It consists of two main humps separated by about 1650 cm.$^{-1}$. This is probably a symmetrical C=C valence frequency. The first absorption in hexatriene (Price & Walsh 1946) occurs at closely similar wave-lengths and shows a frequency ~ 1615 cm.$^{-1}$. At high pressures the 2400 A styrene absorption spreads to both long and short wave-lengths, and on the short wave-length side one or two more very diffuse bands become visible.

The most prominent feature of the spectrum occurs below 2000 A in the shape of a peak at about 1950 A, apparently analogous to the benzene 1790 A peak. Its position indicates a lower first ionization potential for the π electrons of the ring, relative to benzene. Like phenyl acetylene, phenyl cyanide and benzaldehyde, the peak has no long wave-length 'step-out'.

A few diffuse bands occur to short wave-lengths of the 1950 A peak. The strongest of these has its maximum at about 1560 A. Below 1400 A strong continuous absorption from the C-C electrons occurs.

The styrene molecule has its eight π electrons arranged in four orbitals of different energy (Penney & Kynch 1938). It seems certain that the 2400 A absorption represents a transition of the $N \rightarrow V_1$ type; perhaps it is analogous to the benzene $N \rightarrow V_1$, transition of $\lambda_{\text{max.}}$ 1980 A, but increased in intensity by the symmetry alteration due to the side chain. It is only a little weaker than the 1950 A peak. The sensitivity of the intensity and position of the 2350 A region to the degree of conjugation of the side-chain π electrons with those of the ring is referred to later in the discussion of the methyl styrene spectrum, as also is the nature of the 1560 A absorption. As regards the 2910 A absorption, McMurry (1941) has suggested that this is analogous to the absorption occurring in benzaldehyde around 2800 A and has identified both as $N \rightarrow V_1$. It is probable that they represent the benzene 2600 A $N \rightarrow V_1$ transition (Walsh 1946*b*). The separation of the 2910 A styrene bands is closely similar to that of the benzene 2600 A bands.

The change of a CH_2 group in styrene for an oxygen atom in benzaldehyde is small compared with the total size of the molecule. We therefore expect—and find—a very considerable resemblance between the styrene and benzaldehyde spectra. Styrene shows absorption from 2900 to 2800 A, benzaldehyde around 2800 A; each has strong absorption around 2350 A; styrene has its most intense peak at 1950 A, benzaldehyde at 1940 A. Benzaldehyde also shows absorption near 3200 A: the absence of such absorption in styrene lends further confidence to the identification of this region as due to a transition of the non-bonding oxygen electrons (McMurry 1941; Walsh 1946*b*).

THE SPECTRUM OF α-METHYL STYRENE (PLATE 4)

The specimen of α-methyl styrene had a boiling-point of 160° C and a vapour pressure of $\sim 0{\cdot}3$ cm. of mercury at room temperature. Ley (1918) found that the compound showed an inflexion in its absorption curve in the region 2900 to 2800 A.

A methyl-substituted compound usually has a spectrum very similar to that of the parent compound but shifted to long wave-lengths. The absorption regions of α-methyl styrene, however, though they resemble the bands of styrene, do not suffer regular shifts. Thus (*a*) the 1950 A peak of styrene is moved to *short* wavelengths and now has a maximum at about 1880 A, (*b*) the 2350 A region is very much reduced in intensity relative to the short wave-length absorption and is also moved to short wave-lengths relative to styrene, (*c*) the absorption at 1560 A in styrene is moved to long wave-lengths (*c.* 1600 A) in α-methyl styrene.

These effects are probably due to the partial suppression of the coupling of the ethylene π electrons with those of the benzene ring. This results in decreased conjugation energy and therefore in a raising of the frequency of the first $N \rightarrow V$ transition and of the first Rydberg band. The fact that the 1560 A region in styrene is moved to long wave-lengths in α-methyl styrene must mean that the region is due to the ethylene group rather than to the benzene ring: it suffers a shift to long wavelengths by reason of the usual inductive and other effects associated with a CH_3

group. The region is presumably analogous to the first ethylene absorption at 1700 A. This means that the spectra of the π electrons of the benzene ring and of the π electrons of the ethylene group are differently affected by the CH_3 group. The phenomenon shows that the π electrons of both the styrene and α-methyl styrene molecules are not completely equivalent: some are localized rather more in the benzene ring and give rise to the 1880 or 1950 A peaks, while others are localized rather more in the ethylene group and give rise to the 1600 or 1560 A absorption.

1, 4 interaction of C atoms is probably slight. The reason for the reduced conjugation in α-methyl styrene can hardly therefore be steric interference between the CH_3 and C_6H_5 groups. 2, 3-Dimethyl-cyclohexadiene-1-3 shows a somewhat similar effect. We are inclined to connect the reduced conjugation with the *s-cis* (for the meaning of this term see Mulliken 1942) nature of these compounds. The repulsion of the electrons in the double bonds of *s-cis* compounds means that there is only slight overlap in the single bond, so that further repulsion by a methyl group might cause a reduction of conjugation more than offsetting the usual inductive effect.

Similar behaviour is found in acetophenone relative to benzaldehyde. Just as styrene strongly resembles benzaldehyde, so does α-methyl styrene resemble acetophenone. The benzaldehyde absorptions at 3280 and 2810 A are shifted to *short* wave-lengths in acetophenone (3205 and 2785 A respectively: Bielecki & Henri 1914), paralleling the effect in styrene and α-methyl styrene.

THE SPECTRUM OF PHENYL ACETYLENE (PLATE 4)

The phenyl acetylene used was a B.D.H. specimen of b.p. 143° C.

The near ultra-violet spectrum has been studied by Macbeth & Stewart (1917) who found an inflexion in the absorption curve in the region 2770 to 2560 A. The photographs show a band system from about 2390 to about 2200 A. The two main bands are separated by 1870 cm.$^{-1}$. This must be a symmetrical valence vibration of the C$\equiv$C bond. Other fainter bands reveal frequency differences of about 780 cm.$^{-1}$ (799 and 755 cm.$^{-1}$) and about 1000 cm.$^{-1}$ (1008 and 1022 cm.$^{-1}$).

Just below 2000 A a diffuse region of absorption appears, with a peak at about 1910 A. It spreads rapidly to short wave-lengths with increasing pressure. About 1650 A a diffuse doublet occurs. This is thought to be analogous to the similar doublet in the divinyl acetylene spectrum (Price & Walsh 1946): the first member lies only 100 cm.$^{-1}$ to short wave-lengths relative to its analogue in divinyl acetylene. A few other faint, diffuse, bands occur at shorter wave-lengths.

The two π_x electrons of the C$\equiv$C bond conjugate with the π electrons of the benzene ring. The two π_y electrons have orbital axes perpendicular to those of the π_x electrons and presumably give rise to the diffuse Rydberg bands below 1650 A as in divinyl acetylene. The position of the 1650 A doublet indicates a very slightly higher π_y ionization potential for phenyl acetylene than for divinyl acetylene.

The conjugation of the side chain with the ring causes somewhat radical alterations in the appearance of the spectrum relative to benzene. The first ionization potential of the π electrons in the ring will presumably be lowered relative to benzene owing to the increased conjugation. In accord with this the 1910 A peak is thought to be analogous to the benzene 1790 A peak and thus shifted to long wave-lengths. Its shift is to be compared with the similar shift in phenyl cyanide, phenyl ethylene and benzaldehyde (Walsh 1946*b*). It is noticeable that it seems to have no long wave-length 'step-out' as in benzene, toluene, xylene, monochlorobenzene, *o*-dichlorobenzene and pyridine. It may be that the band system from 2390 to 2200 A is the analogue of the benzene 2000 A system. Its intensity is reasonable and it is expected that extra conjugation would push it well to longer wave-lengths—perhaps more than the benzene 1790 A (first Rydberg) band is affected, so separating the two transitions. Phenyl ethylene, as already seen, also has an absorption region around 2350 A and this has a resemblance to the first ($N \rightarrow V_1$) absorption in hexatriene: support is thus found for the identification of the phenyl acetylene 2350 A region as $N \rightarrow V_1$ in type. It is most interesting to note how in monochlorobenzene one can see the beginning of the separation of the benzene 1980 and 1790 A regions and follow the increasing divergence through a series of intermediate molecules (such as monochlorobenzene, benzaldehyde and phenyl cyanide) right up to styrene and phenyl acetylene (cf. Walsh 1946*b*).

The extra resonance energy due to the conjugation of the side chain with the ring π electrons is given by Pauling (1940) as a little greater for phenyl acetylene (10 kcal./g.mol.) and phenyl ethylene (7 kcal./g.mol.) than for benzaldehyde (4 kcal./g.mol.) and phenyl cyanide (5 kcal./g.mol.). In accord with this the shift to long wave-lengths of the benzene 1980 A region is rather greater in phenyl acetylene and phenyl ethylene than in the other molecules cited. Also in accord with this, the appearance of the benzene spectrum is more radically altered in passing to phenyl acetylene and phenyl ethylene than to the other molecules listed above.

THE SPECTRUM OF PHENYL CYANIDE (PLATE 4)

The phenyl cyanide was obtained from Messrs B.D.H. and had a boiling-point of 190·7° C.

The most prominent feature of the far ultra-violet spectrum is an absorption peak of maximum at 1900 A, obviously analogous to the benzene peak at 1790 A. There is no 'step-out' on the long wave-length slope of this peak as in benzene. Instead, a strong region of absorption appears from 2240 to about 2090 A: this contains a progression of diffuse, but well marked, bands, the frequencies of which are shown in table 1.

Three prominent frequency differences are involved. They have the approximate magnitudes 1924, 715 and 245 cm.$^{-1}$. That of 1924 cm.$^{-1}$ must be a vibration mainly in the C$\equiv$N bond.

The operation of the inductive and mesomeric effects ought to result in negative charge being taken out of the benzene ring by the meta-directing CN group. These two effects alone would result in a shift of the benzene spectrum to short wave-lengths in phenyl cyanide. The fact that the opposite is the case must be due to the raising of the highest occupied bonding energy level by the conjugation. This effect is also responsible for shifting the $N \rightarrow V$ transition at 1980 A in benzene to longer wave-lengths in phenyl cyanide, thereby separating it from the first Rydberg peak.

TABLE 1. FREQUENCIES OF BANDS IN THE 2240 A SYSTEM OF PHENYL CYANIDE

cm.$^{-1}$			
44648			
		721	
45369			
	241		
45610			
	251	706	1924
45861			
46075			
	256		
46331			
46572			
	223		
46795			
	241	717	
47036			
47289			
	230		
47519			
	281		
47800			
obscured			
48545			
	222		
48767			

The position of the 1900 A peak indicates a first ionization potential for the π electrons of the benzene ring as $\sim 8{\cdot}3$ V.

On the short wave-length side of the 1900 A peak, one or two diffuse bands occur around 1660 A. A frequency difference ~ 680 cm.$^{-1}$ seems to be involved

$$({}_1\Delta_2 = 650\ \text{cm.}^{-1};\quad {}_2\Delta_3 = 705\ \text{cm.}^{-1}).$$

It might have been expected that absorption bands due to the CN group and similar to those in HCN and C_2N_2 would have appeared in the photograph. The CN part of the phenyl cyanide molecule, however, seems to give only continuous absorption. A similar effect has been found for methyl cyanide. This continuous absorption sets in strongly from 1400 A onwards.

THE SPECTRUM OF PHENYL ISOCYANATE (PLATE 4)

The ultra-violet spectrum of phenyl isocyanate starts with a system of sharp bands around 2600 A. These are obviously analogous to the benzene 2600 A bands, though they are somewhat stronger owing to the disturbance of the sixfold symmetry caused by the side chain. The existence of this absorption system has been reported by Woo & Liu (1935). These authors also noted the onset of a continuum of absorption at 2420 A and thence deduced an energy value for the disruption of the ϕ-N bond. The photographs show that there is no particular significance to be attached to the wave-length 2420 A. It so happened that at the pressures used by Woo & Liu the continuum began at that wave-length, but the onset wave-length depends very much upon the pressure used. The continuum is actually due to the spreading at high pressures of an absorption region of maximum at about 1830 A and with a long wave-length 'step-out' (of maximum about 1990 A) analogous to the benzene 1790 A peak and 1980 A 'step-out'.

This close analogy with the benzene spectrum shows that phenyl isocyanate is to be classed with the simpler substituted benzenes: it does not show the large shift of the 'step-out' to long wave-lengths as found in molecules where the side chain is definitely conjugated with the benzene ring. This is somewhat surprising, since the results of Kohlrausch (1931) from Raman data indicate the structure Ph—N=C=O for the phenyl isocyanate molecule. It must be that the double bond between the carbon and oxygen atoms prevents appreciable conjugation of the π electrons of the N=C bond with those of the benzene ring.

Another peculiarity of the phenyl isocyanate molecule is that it does not show the characteristic absorption at 2900 A found in simple ketonic molecules containing the C=O group. In this respect it is similar to the acids R.COOH. It is also to be noted that the frequency characteristic of the ketonic C=O bond does not appear in the Raman spectrum of phenyl isocyanate.

It is thought that these peculiarities of the phenyl isocyanate molecule are connected with a lower polarity in the C=O group than is found in aldehydes and ketones. The CO bond length in methyl isocyanate is 1·18 A, i.e. considerably shorter than the CO lengths in formaldehyde and acetaldehyde (1·21 and 1·22 A respectively) and approaching that of carbon dioxide (1·15 A). Probably the CO length in phenyl isocyanate is close to that in methyl isocyanate, since the spectrum indicates that little conjugation between the side chain and ring is occurring. It has been pointed out elsewhere (Walsh 1946*a*, 1947) that the shorter a CO length the less the ionic character. It is probable therefore that the differences between the phenyl isocyanate spectrum and the spectra of aldehydes and ketones are due to the much lower ionic character of the CO group of the former. In other words, the structure ϕ—N=C=O contributes much more to the normal state of the phenyl isocyanate molecule than such structures as $\phi\text{—}\overset{+}{\mathrm{N}}\equiv\mathrm{C}\text{—}\mathrm{O}^-$ or $\phi\text{—}\mathrm{N}{=}\overset{+}{\mathrm{C}}\text{—}\mathrm{O}^-$. It is to be noted that carbon dioxide similarly does not show the 2900 A absorption and that the ionization potential of HCOOH (also showing no 2900 A absorption) indicates a lowered carbonyl polarity relative to formaldehyde. Herzberg & Kölsch (1933) have found that formamide also has no 2900 A region of absorption. If the conclusion—that ϕ—N=C=O represents the phenyl isocyanate molecule to a fair approximation—is valid, then a parallel between phenyl isocyanate and ketene is expected. The fact that, chemically, such a parallel is strongly marked (the characteristic reactions of both compounds being not those of ketones but additions at the N=C or C=C bond) supports the above conclusions.

A strong diffuse band occurs at 1750 A. Between 1700 and 1600 A a few diffuse bands occur, the frequencies of which are shown in table 2. A difference ~ 550 cm.$^{-1}$ is involved. The first three bands are stronger than those following and are therefore more accurately measured.

TABLE 2. TABLE SHOWING THE FREQUENCIES OF THE PHENYL ISOCYANATE BANDS BETWEEN 1700 AND 1600 A

cm.$^{-1}$	
59675	
	482
60157	
	522
60679	
	562
61241	
	623
61864	
	545
62409	

A few more faint, diffuse, bands occur in the region 1500 to 1400 A. At 1400 A the continuum weakens considerably and thenceforward nothing but continuous absorption is observable.

The author is greatly indebted to Dr H. P. Koch for valuable criticisms.

REFERENCES

Bielecki & Henri 1914 *Ber. dtsch. Chem. Ges.* **47**, 1690.
Herzberg & Kölsch 1933 *Z. Elektrochem.* **39**, 572.
Kohlrausch 1931 *Der Smekal Raman Effekt.* Berlin.
Ley 1918 *Ber. dtsch. Chem. Ges.* **51**, 1808.
Macbeth & Stewart 1917 *J. Chem. Soc.* **111**, 834.
McMurry 1941 *J. Chem. Phys.* **9**, 241.
Mulliken 1942 *Rev. Mod. Phys.* **14**, 265.
Pauling 1940 *The nature of the chemical bond*, pp. 137–139. Cornell.
Penney & Kynch 1938 *Proc. Roy. Soc.* A, **164**, 409.
Price & Walsh 1946 *Proc. Roy. Soc.* A, **185**, 182.
Ramart-Lucas & Amagat 1932 *Bull. Soc. Chim.* **51**, 965.
Walsh 1946*a* *Trans. Faraday Soc.* **42**, 56.
Walsh 1946*b* *Trans. Faraday Soc.* **42**, 62.
Walsh 1947 *Trans. Faraday Soc.* **43**, 158.
Woo & Liu 1935 *J. Chem. Phys.* **3**, 544.

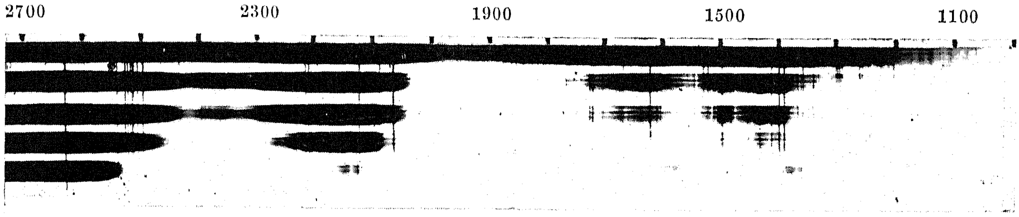

styrene

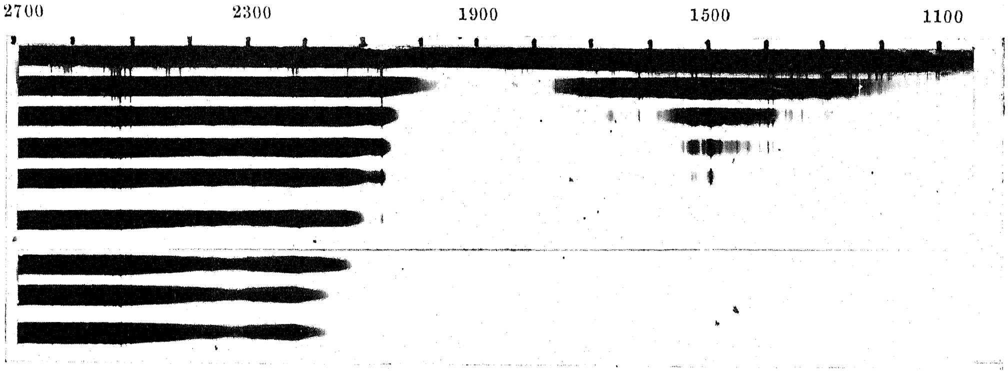

α-methyl styrene

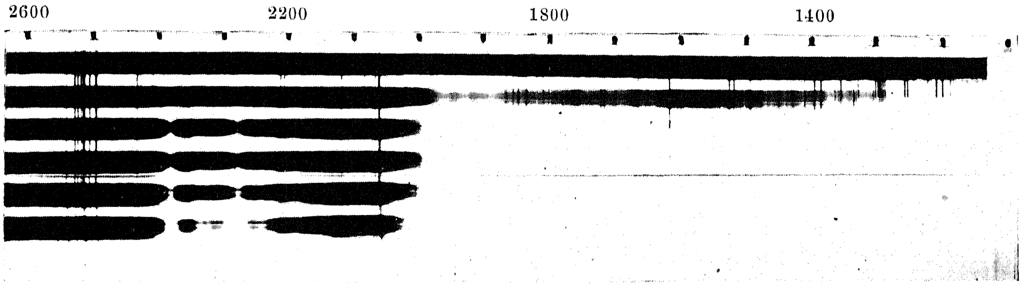

phenyl acetylene

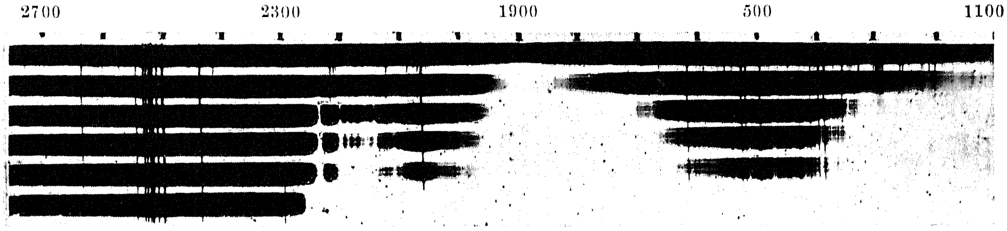

phenyl cyanide

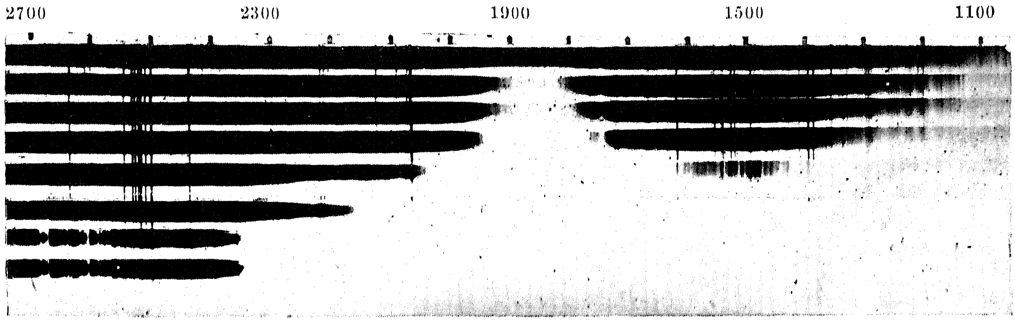

phenyl isocyanate

The electronic structure of conjugated systems

I. General theory

By C. A. Coulson and H. C. Longuet-Higgins

(*Communicated by R. P. Bell, F.R.S.—Received* 2 *January* 1947)

This paper develops the general theory of conjugated systems by the method of molecular orbitals. The electron densities and bond orders appear as first-order derivatives of the energy of the mobile electrons with respect to the energy integrals in the secular equations; and various other relations are established which confirm the appropriateness of the definitions. A set of new quantities are introduced and discussed for the first time, namely, the mutual polarizability of two atoms or two bonds or an atom and a bond, and it is shown that they are important in determining the effect of structural changes on chemical reactivity, and also in calculating force constants and interaction terms for the vibration of bonds. Formulae are derived for the calculation of the total energy, electron densities, bond orders and mutual polarizabilities, and the relation of these quantities to other physical and chemical properties is briefly discussed.

NOTATION

The notation used in this and later papers is summarized below; the numbers in brackets denote the equations in which the quantities are defined mathematically:

n	number of atomic orbitals.	
r, s, t, u	atoms of a conjugated system.	
ϕ_r	the atomic orbital for atom r.	
ψ, ψ_j	any (the jth) molecular orbital.	
c_r, c_{rj}	the coefficient of ϕ_r in ψ, ψ_j.	(1)
n_j	the number of electrons in ψ_j.	
E	the energy of a molecular orbital.	(3)
H	the effective Hamiltonian operator for a π-electron	(3)
H_{rr}	the coulomb integral for ϕ_r.	(5)
$H_{rs} = \beta_{rs}$	the resonance integral between ϕ_r and ϕ_s.	(5)
S_{rs}	the overlap integral between ϕ_r and ϕ_s.	(6)
H_{CC}	the coulomb integral for a carbon atom in benzene.	
α_r	the coulomb term for atom r.	(11)
$\epsilon = E - H_{\mathrm{CC}}$	the binding energy of a mobile electron.	(11)
ϵ_j	the value of ϵ for an electron in ψ_j.	
$\mathscr{E}$	the total binding energy of the mobile electrons.	(26)
q_r	the electron density at atom r.	(9)
p_{rs}	the mobile order of bond rs.	(13)
$\Delta(\epsilon)$	the secular determinant for a conjugated system, regarded as a function of ϵ.	(14)
$\Delta'(\epsilon)$	$= \partial\Delta(\epsilon)/\partial\epsilon$.	

$\Delta_{r,t}$, $\Delta_{rs,tu}$	where $r<s$, $t<u$, denote Δ with rows r (and s) and columns t (and u) struck out.	
$\pi_{r,t}$, $\pi_{rs,tu}$	denote the mutual polarizabilities of atoms r and t and bonds rs and tu.	(46), (49)
$\pi_{rs,t}$, $\pi_{t,rs}$	denote the polarizability of bond rs by atom t and vice versa.	(47), (48)
δ	denotes increment.	
H', c', ψ'	denote increments in H, c, ψ.	

Every determinant occurring in an integral with respect to y is to be taken as a function of iy, the limits of integration, except where otherwise stated, being $-\infty$ to $+\infty$.

INTRODUCTION

Theoretical treatments of unsaturated molecules begin by dividing the electrons into three classes, as follows:

(*a*) those which are not concerned with bond formation—the inner shell electrons;

(*b*) those which are engaged in the formation of σ bonds, i.e. localized bonds having maximum density along the line joining two adjacent atoms;

(*c*) the π-electrons, whose orbitals are antisymmetric with respect to the plane of the σ bonds at any atom. These electrons are variously called π, p_h, mobile, and unsaturation electrons. The part of the molecule in which they move is called a conjugated system.

The inner-shell electrons and σ-electrons are supposed to have their energies and distributions governed solely by the atomic orbital, or pair of orbitals, in which they move; and all effects depending on conjugation of unsaturation electrons, such as resonance energies and variations in bond order and electron density, are ascribed to the π-electrons. This series of papers will be concerned solely with these π-electrons; and it will be supposed, as is customary, that they may be treated quite independently of the underlying framework composed of the nuclei and the other types of electrons (*a*) and (*b*). This implies that the π-electrons are given a wave function of their own, from which their properties may be determined. Very little work has been published on the general theory of these π-electrons, although a large number of papers have appeared describing particular applications in the field of pure hydrocarbons; and a few calculations have been made of the energy, bond orders and electron densities in specific cases where there is one, or at most two, heteroatoms (e.g. quinones (Coulson 1946), Würster's salts (Goeppert-Mayer & McCallum 1942), pyridine, pyrrole and similar systems with one nitrogen atom (Wheland & Pauling 1935; Wheland 1942; Longuet-Higgins & Coulson 1947)). It is our intention in these papers to develop certain aspects of the theory of mobile electrons in a perfectly general way, applicable to hydrocarbons and heterosystems alike. Our first paper will be almost entirely theoretical; later papers will give applications to specific problems.

In calculating the energy and distribution of the π-electrons we here follow the method of molecular orbitals. That is, we express the π-electronic part of the wave function as a simple product, each term of which represents a wave function for a single electron moving in the field of the nuclei and the other electrons. Such a wave function is called a *molecular orbital* (m.o.). (In a molecule in its ground state it can be shown that no great change in the total energy or electron distribution would result from taking, instead, the more accurate antisymmetric determinantal product. Such a procedure would, however, introduce quite unmanageable complexities into our analysis.) The total energy of the π-electrons is thus given by the sum of the energies of the electrons in these m.o.; in the ground state the occupied m.o. are those of lowest energy, each m.o. accommodating two electrons with opposed spins. If there is an odd number of electrons, at least one m.o. must contain only one electron. This implies the existence of an uncompensated spin, so that the molecule will be paramagnetic and behave chemically as a free radical.

In calculating the form of the m.o. one may express them arbitrarily as linear combinations of atomic orbitals (a.o.). If there are n distinct a.o. ϕ_r $(r = 1, 2, \ldots, n)$ out of which the m.o. ψ are constructed, the jth m.o. may be written

$$\psi_j = \sum_{r=1}^{n} c_{rj}\phi_r. \tag{1}$$

The c_{rj} are numerical coefficients to be determined presently. (It is convenient to omit the suffix j from ψ_j and c_{rj} in much of the following discussion, when there is no danger of confusion.) Remember in (1) that out of the n a.o. ϕ_r exactly n m.o. ψ_j can be formed, so that the suffix j ranges from 1 to n. These m.o. are generally labelled in such a way that $j = 1$ is the most binding, i.e. has lowest energy value, and $j = n$ is the most antibonding, i.e. has highest energy value. The whole set of m.o. may, by analogy with the $K, L, \ldots$ shells of atomic structure, be referred to as the π molecular shell, or the mobile shell.

Although no assumption need be made about the precise form of ϕ_r, it is convenient to regard it as the $2pz$ wave function for the rth atom (or $3pz$ for Cl, etc.), since such wave functions are antisymmetric with respect to the plane of the σ bonds and have an axis of symmetry perpendicular to that plane. It should perhaps be mentioned here that the $2pz$ a.o. of covalently attached hydrogen have too great energy to take part appreciably in the formation of these m.o. Hyperconjugation with a methyl group, as recently discussed by Mulliken, Rieke & Brown (1941), is, however, included in the analysis by treating the H_3 group as a single a.o. conjugating with the rest of the molecule.

The coefficients c_r and the energy E of each m.o. are determined by minimizing the latter with respect to the former; that is

$$\partial E/\partial c_r = 0 \quad (r = 1, 2, \ldots, n), \tag{2}$$

where

$$E = \int \psi^* H \psi \, dv \Big/ \int \psi^* \psi \, dv. \tag{3}$$

H is here the effective Hamiltonian operator for each π-electron. The set of conditions (2) leads to the 'secular equations'

$$(H_{rr} - ES_{rr})\, c_r + \sum{}' (H_{rs} - S_{rs}E)\, c_s = 0, \tag{4}$$

where H_{rs} is the matrix component of H in the system ϕ_r, and is defined by

$$H_{rs} = \int \phi_r^* H \phi_s dv \quad \text{and} \quad S_{rs} = \int \phi_r^* \phi_s dv. \tag{5}$$

There is one equation of type (2) for each of the n values of r; and the $'$ after the summation sign denotes that the term with $s = r$ is omitted from the sum. Neglecting overlap between a.o., i.e. putting

$$S_{rs} = 0 \tag{6}$$

for $r \neq s$, and supposing each a.o. to be normalized, so that

$$S_{rr} = 1, \tag{7}$$

then

$$(H_{rr} - E)\, c_r + \sum_s{}' H_{rs} c_s = 0. \tag{8}$$

Now in a given molecule the coulomb integrals H_{rr} will depend upon the density of electrons near atom r. The number of electrons on atom r is defined as

$$q_r = \sum_j n_j c_{jr}^2, \tag{9}$$

where n_j is the number of electrons (either 0, 1 or 2) in the jth m.o. H_{rr} would be expected to depend on q_r. But it will be supposed that in fact H_{rr} depends only on the nature of atom r, e.g. whether it is carbon or nitrogen. There are many cases where this is quite a fair assumption. Thus, Coulson & Rushbrooke (1940) have shown that in hydrocarbons containing no odd-numbered unsaturated rings, the assumption that all the H_{rr} are equal leads to the conclusion that in the ground state all the q_r are equal, and hence also the H_{rr}, so that the hypothesis is at least self-consistent. For other systems in general all the q_r will not be equal (Longuet-Higgins & Coulson 1947), even for the atoms of one kind; in any particular case it might be possible to allow for the variation of H_{rr} with q_r in order to make a truly self-consistent field, but in the general case this is quite impossible and it will be necessary to be content with the approximation that H_{rr} depends solely on the nature of atom r. As it appears that the charges q_r on atoms of one kind do not vary greatly from molecule to molecule, it is unlikely that the assumption introduces greater errors than are already inherent in the whole scheme of calculation.

It will be found best to measure the energy of a m.o. in terms of its difference from H_{CC}, which denotes the coulomb integral for the carbon atom in, say, benzene. The secular equations (8) then become

$$(\alpha_r - \epsilon)\, c_r + \sum_s{}' \beta_{rs} c_s = 0 \quad (r = 1, 2, \ldots, n), \tag{10}$$

where

$$\alpha_r = H_{rr} - H_{\mathrm{CC}}, \quad \epsilon = E - H_{\mathrm{CC}} \quad \text{and} \quad \beta_{rs} = H_{rs}. \tag{11}$$

β_{rs} is often referred to as the 'resonance integral' between the a.o. ϕ_r and ϕ_s; for non-bonded atoms it is very small and may be taken to be zero. For hydrocarbons where the H_{rr} are all equal to H_{CC}, the secular equations are therefore

$$-\epsilon c_r + \sum{}' \beta_{rs} c_s = 0 \quad (r = 1, 2, \ldots, n). \tag{12}$$

It is desirable, in what follows, to have some physical interpretation for the quantities H_{rr} and α_r. According to (8), H_{rr} is the energy of an electron in an orbit for which all the c_s are zero except c_r, i.e. an electron confined to nucleus r. At first sight one would expect this to be equal to the ionization energy of the corresponding atom; but this is not quite so, because (i) the Hamiltonian H involves the field from the other atoms, so that at best H_{rr} would measure the energy of removal of the electron from nucleus r in the presence of the other atoms, and (ii) when one electron is removed there is a considerable reorganization of the remaining electrons (see, for example, the case of methane treated by Coulson (1937), where the actual ionization energy is shown to be about one-quarter of the corresponding H_{rr}). It is not possible at present to calculate this energy with any accuracy. The most, therefore, that can be said with regard to H_{rr} is that if the atom r is particularly electronegative, so that it is difficult to remove its electrons, H_{rr} will have a larger numerical value (its sign is necessarily relative to zero energy at infinity). Thus α_r, which is the difference $H_{rr} - H_{\mathrm{CC}}$, will certainly be closely related to the difference in ionization potential of the two atoms, and it may be regarded as a measure of this difference, since the two will vary in the same way. Nor must α_r be put equal to the difference in electron affinity of the two atoms, though it does seem quite likely that H_{rr} is more intimately related to the electron-affinity scale introduced by Mulliken (1934). In view of the importance which will later be attached to this quantity α_r, it is a pity that no more precise interpretation can be given to it. The matter, however, will not be pursued further just now.

Fortunately, the situation is more satisfactory as regards the other parameter in (10). This is the resonance integral β_{rs}, and, as shown by Lennard-Jones (1937) and others, $2\beta_{rs}$ may be taken as the difference in energy between a pure single and a pure double bond connecting atoms r and s. It is a negative quantity whose magnitude increases along the series C=C, C=N, C=O.

The secular equations (10) determine the energies of the m.o. and the coefficients c_{rj}, from which the numbers of electrons on the different nuclei may be calculated. These numbers q_r have been successfully correlated with the chemical reactivities of different positions in a number of molecules (see, for example, Longuet-Higgins & Coulson 1947). The coefficients may also be used for calculating the mobile orders p_{rs} of unsaturated bonds. For according to the theory developed by Coulson (1939) each of the π-electrons makes a separate contribution, positive or negative, to every one of the bond orders. If r and s are neighbouring atoms, an electron in the jth m.o. (see equation (1)), which is assumed to be real and not complex, makes a contribution $c_{rj}c_{sj}$ to the bond r-s. So the total mobile bond order is

$$p_{rs} = \sum_j n_j c_{rj} c_{sj}. \tag{13}$$

If r and s are not neighbours, the mobile bond order is taken to be zero. Experimental bond lengths and force constants have been successfully correlated with bond orders calculated in this way (Lennard-Jones & Coulson 1939; Gordy 1946).

The exact significance of the overlap integrals S_{rs} occurring in (4) has recently been discussed by Wheland (1941) and by Mulliken, Rieke and Brown (1941), who point out that in practice this overlap is not negligible. However, although its inclusion makes a difference to the calculation of energies, it does not affect the relative values of the coefficients c_{rj}. The secular equations (8), in which overlap is neglected, have therefore been taken as our starting point in the present theory.

GENERAL THEORY

The secular equations for a conjugated system of n atomic orbitals are, by (10),

$$(\alpha_r - \epsilon)\, c_r + \sum_s{}' \beta_{rs} c_s = 0 \quad (r = 1, 2, \ldots, n). \tag{10}$$

α_r and β_{rs} $(= \beta^*_{sr})$ are fixed quantities characteristic of the molecule; ϵ and the coefficients c_r are the unknowns. By choosing a purely real form for every atomic wave function ϕ_r, which is always permitted except when dealing with certain magnetic properties, one ensures that the β_{rs} and the c_r are real also. The condition for consistency of the n equations (10) is that the 'secular determinant' shall vanish, viz. that

$$\Delta(\epsilon) \equiv \begin{matrix} \alpha_1 - \epsilon & \beta_{12} & \beta_{13} \\ \beta_{21} & \alpha_2 - \epsilon & \beta_{23} \\ \beta_{31} & \cdots & \cdots \end{matrix} \qquad 0. \tag{14}$$

In general this equation has n roots ϵ_j $(j = 1, 2, \ldots, n)$. Each of these is substituted back in turn into the secular equations (10) to give the corresponding sets of coefficients $c_{1j}, c_{2j}, \ldots, c_{nj}$, or rather their ratios—their absolute magnitudes are fixed by the normalization condition, viz.

$$c_{1j}^2 + c_{2j}^2 + c_{3j}^2 + \ldots + c_{nj}^2 = 1. \tag{15}$$

Since the matrix of Δ is Hermitean, the ϵ_j are all real, and in most of the succeeding analysis it will be assumed that they are all distinct: this is true in general, and makes the proofs much less cumbersome, while few of the conclusions depend on it (see Appendix 2). It can be proved that if $\epsilon_j \neq \epsilon_k$, then

$$\sum_r c_{rj} c_{rk} = 0. \tag{16}$$

Therefore since all the ϵ_j are different, all the m.o. are orthogonal, and this fact can be combined with (15) in the equation

$$\sum_r c_{rj} c_{rk} = \delta_{jk}. \tag{17}$$

Further, except when the contrary is stated, we shall discuss only molecules in which all the electrons are paired, so that each occupied m.o. contains exactly two electrons. Lastly, the zero of energy can be chosen in such a way that ϵ is negative for each of the occupied m.o. and positive for each of the unoccupied m.o. In the ground state of the molecule the occupied m.o. will be measured from 1 to m, and the unoccupied from $m+1$ to n, so that

$$\epsilon_1 < \epsilon_2 < \ldots < \epsilon_m < 0 < \epsilon_{m+1} < \ldots < \epsilon_n. \tag{18}$$

Total mobile bond orders and π-electron densities

According to the definitions (9) and (13), the total mobile order of a bond r-s is given by

$$p_{rs} = 2\sum_{j=1}^{m} c_{rj}c_{sj}, \tag{19}$$

and the total density of π-electrons around atom r by

$$q_r = 2\sum_{j=1}^{m} c_{rj}^2. \tag{20}$$

In this form both p_{rs} and q_r are given as a sum over the occupied m.o. But we propose to show now how both these quantities may be determined directly from the secular determinant introduced in (14). From this certain important deductions can be made concerning both their absolute magnitudes and their variations with changes in the fundamental parameters α and β.

Now it follows from equation (3) and the definitions of α_r, β_{rs} and ϵ in (11) that for any linear combination of the ϕ_r

$$\epsilon = \left(\sum_r c_r^2\alpha_r + 2\sum_{r<s}\sum c_r c_s \beta_{rs}\right)\Big/\sum_t c_t^2. \tag{21}$$

Therefore $$\delta\epsilon = \sum_r \left\{\frac{c_r^2}{\sum_t c_t^2}\right\}\delta\alpha_r + \sum_{r<s}\sum\left\{\frac{2c_r c_s}{\sum_t c_t^2}\right\}\delta\beta_{rs} + \sum_r \delta c_r \frac{\partial\epsilon}{\delta c_r}.$$

But for a m.o. by (2) and (15)

$$\partial\epsilon/\partial c_r = 0, \quad \sum_t c_t^2 = 1.$$

Therefore $$\delta\epsilon = \sum_r c_r^2\delta\alpha_r + \sum_{r<s}\sum 2c_r c_s \beta_{rs}$$

for any small changes in α_r, β_{rs} and c_r. But for a m.o. ϵ may be obtained in terms of α_r, β_{rs} as a root of the secular determinant, and hence $\left(\frac{\partial\epsilon}{\partial\alpha_r}\right)_{\Delta=0}$ may be written for its variation with α_r. It follows that

$$\left(\frac{\partial\epsilon}{\partial\alpha_r}\right)_{\Delta=0} = c_r^2, \quad \left(\frac{\partial\epsilon}{\partial\beta_{rs}}\right)_{\Delta=0} = 2c_r c_s. \tag{22, 23}$$

Summation of (22) and (23) over the occupied m.o. gives

$$q_r = 2\sum_{j=1}^{m} c_{rj}^2 = 2\sum_{j=1}^{m}\left(\frac{\partial\epsilon_j}{\partial\alpha_r}\right)_{\Delta=0} = \left(\frac{\partial\mathscr{E}}{\partial\alpha_r}\right)_{\Delta=0} \tag{24}$$

and $$p_{rs} = 2\sum_{j=1}^{m} c_{rj}c_{sj} = \sum_{j=1}^{m}\left(\frac{\partial\epsilon_j}{\partial\beta_{rs}}\right)_{\Delta=0} = \frac{1}{2}\left(\frac{\partial\mathscr{E}}{\partial\beta_{rs}}\right)_{\Delta=0}, \tag{25}$$

where $\mathscr{E}$ is the sum of the π-electron energies, i.e.

$$\mathscr{E} = \sum_{j=1}^{m} 2\epsilon_j. \tag{26}$$

Equation (24) suggests that the electron density at a position is closely related to its chemical reactivity, since the approach of a charged reagent will alter the coulomb integral of the position in question, and the resulting changes in $\mathscr{E}$ will be very important in determining the activation energy for reaction. This suggestion is supported by the results of calculations for various particular molecules (Wheland & Pauling 1935; Longuet-Higgins & Coulson 1947). Continuing with the argument, then

$$\left(\frac{\partial \epsilon_j}{\partial \alpha_r}\right)_{\Delta=0} = -\left(\frac{\partial \Delta}{\partial \alpha_r}\right)\Big/\left(\frac{\partial \Delta}{\partial \epsilon}\right), \tag{27}$$

and

$$\left(\frac{\partial \epsilon_j}{\partial \beta_{rs}}\right)_{\Delta=0} = -\left(\frac{\partial \Delta}{\partial \beta_{rs}}\right)\Big/\left(\frac{\partial \Delta}{\partial \epsilon}\right), \tag{28}$$

in which, after differentiation, ϵ is given the value ϵ_j. And

$$\frac{\partial \Delta}{\partial \alpha_r} = \Delta_{r,r}, \quad \frac{\partial \Delta}{\partial \beta_{rs}} = 2(-)^{r+s}\Delta_{r,s}, \tag{29, 30}$$

where $\Delta_{r,r}$ and $\Delta_{r,s}$ are the determinants obtained by striking out from Δ the rth row and rth or sth columns respectively. (The factor 2 arises from the fact that $\beta_{sr} = \beta_{rs}$.) Thus, from equations (24) to (30),

$$q_r = -2\sum_{j=1}^{m} \frac{\Delta_{r,r}(\epsilon_j)}{\Delta'(\epsilon_j)}, \tag{31}$$

$$p_{rs} = (-)^{r+s+1}\, 2\sum_{j=1}^{m} \frac{\Delta_{r,s}(\epsilon_j)}{\Delta'(\epsilon_j)}, \tag{32}$$

where $\Delta'(\epsilon_j)$ denotes $\left[\frac{\partial \Delta(\epsilon)}{\partial \epsilon}\right]_{\epsilon=\epsilon_j}$.

The sums in (31) and (32) can be converted into integrals as follows: Consider the complex integral (33)

$$\frac{1}{2\pi i}\int_{\gamma} \frac{\Delta_{r,s}(z)}{\Delta(z)}\,dz, \tag{33}$$

where the path of integration γ (figure 1) is the imaginary axis from $-\infty i$ to $+\infty i$, and the infinite semicircle to the left of the y-axis. At large distances from the origin the integrand is of order z^{-2}, provided that $r \neq s$. So the integral over the large semicircle vanishes and hence (33) reduces to

$$\frac{1}{2\pi i}\int_{-\infty i}^{\infty i} \frac{\Delta_{r,s}(z)}{\Delta(z)}\,dz. \tag{34}$$

Now by Cauchy's theorem (33) equals the sum of the residues of the integrand at its poles within γ. Clearly, the poles of the function $\Delta_{r,s}/\Delta$ are the roots of $\Delta = 0$, i.e. points on the real axis for which $z = \epsilon_1, \epsilon_2, \ldots, \epsilon_n$. These are all simple poles, since Δ has no repeated roots; therefore the residue at ϵ_j is $\Delta_{r,s}(\epsilon_j)/\Delta'(\epsilon_j)$. Further, by (18) the poles within the contour γ are just those corresponding to the occupied m.o., and those outside correspond to the unoccupied m.o. Therefore (33) equals

$$\sum_{j=1}^{m} \Delta_{r,s}(\epsilon_j)/\Delta'(\epsilon_j).$$

It follows from (32) that

$$\begin{aligned} p_{rs} &= (-)^{r+s+1}\frac{2}{2\pi i}\int_{-\infty i}^{\infty i} \frac{\Delta_{r,s}(z)}{\Delta(z)}\,dz \\ &= (-)^{r+s+1}\frac{1}{\pi}\int_{-\infty}^{\infty} \frac{\Delta_{r,s}(iy)}{\Delta(iy)}\,dy, \end{aligned} \tag{35}$$

which may be written as

$$-\frac{1}{2\pi}\int_{-\infty}^{\infty} \frac{\partial}{\partial \beta_{rs}} \log \Delta(iy)\,dy. \tag{36}$$

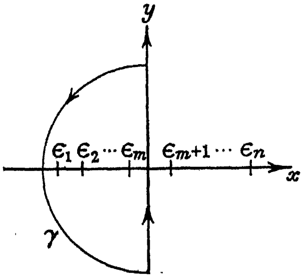
y
$\epsilon_1\ \epsilon_2 \cdots \epsilon_m$
$\epsilon_{m+1} \cdots \epsilon_n$
x
γ

FIGURE 1

A similar expression for q_r may be found by considering the integral

$$\frac{1}{2\pi i}\int_{\gamma} \frac{\Delta_{r,r}(z)}{\Delta(z)}\,dz. \tag{37}$$

At large distances from the origin the integrand tends to $-1/z$. Hence the part of the integral round the infinite semicircle equals $-\frac{1}{2}$. Now the sum of the residues of $\Delta_{r,r}(z)/\Delta(z)$ at its simple poles within γ (there being no poles on γ) equals

$$\sum_{j=1}^{m} \Delta_{r,r}(\epsilon_j)/\Delta'(\epsilon_j).$$

Therefore by Cauchy's theorem

$$\frac{1}{2\pi i}\int_{-\infty i}^{\infty i} \frac{\Delta_{r,r}(z)}{\Delta(z)}\,dz - \tfrac{1}{2} = \sum_{j=1}^{m} \frac{\Delta_{r,r}(\epsilon_j)}{\Delta'(\epsilon_j)}.$$

Therefore by (31)

$$\begin{aligned} q_r &= 1 - \frac{1}{\pi i}\int_{-\infty i}^{\infty i} \frac{\Delta_{r,r}(z)}{\Delta(z)}\,dz \\ &= 1 - \frac{1}{\pi}\int_{-\infty}^{\infty} \frac{\Delta_{r,r}(iy)}{\Delta(iy)}\,dy. \end{aligned} \tag{38}$$

This may also be written

$$q_r = 1 - \frac{1}{\pi}\int_{-\infty}^{\infty} \frac{\partial}{\partial \alpha_r} \log \Delta(iy)\, dy. \tag{39}$$

Provided the integrals are given their principal values, (35) and (38) still represent p_{rs} and q_r in an 'odd molecule' for which

$$\left.\begin{aligned} &\epsilon_j < 0, \quad n_j = 2 \quad (j = 1, 2, \ldots, (m-1)),\\ &\epsilon_m = 0, \quad n_m = 1,\\ &\epsilon_k > 0, \quad n_k = 0 \quad (k = (m+1), \ldots, n).\end{aligned}\right\} \tag{40}$$

The values of α_r can always be adjusted so that $\epsilon = 0$ for the m.o. containing one electron. In this case the integrand in (33) has a pole on γ, at $z = 0$. The contour of integration is therefore modified to γ', which differs from γ in traversing a small semicircle c centred at the origin (figure 2). As before, the integral over γ' equals the sum of the residues at ϵ_1 to ϵ_{m-1}, and the integral over the large semicircle is zero; but the integral over c equals $-\frac{1}{2}$ times the residue at ϵ_m, i.e. at the origin. Therefore the integral over the straight part of the contour equals

$$\frac{1}{2\pi i} P \int_{-\infty i}^{\infty i} \frac{\Delta_{r,s}(z)}{\Delta(z)}\, dz = \sum_{j=1}^{m-1} \frac{\Delta_{r,s}(\epsilon_j)}{\Delta'(\epsilon_j)} + \frac{1}{2}\frac{\Delta_{r,s}(0)}{\Delta'(0)}.$$

But, by analogy with (32), the right-hand side of this is $(-)^{r+s+1}\,\frac{1}{2}p_{rs}$. Therefore

$$p_{rs} = \frac{(-1)^{r+s+1}}{\pi} P \int_{-\infty}^{\infty} \frac{\Delta_{r,s}(iy)}{\Delta(iy)}\, dy. \tag{35a}$$

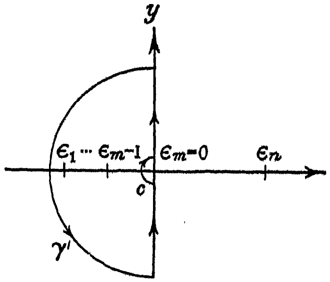

FIGURE 2

A similar argument shows that

$$q_r = 1 - \frac{1}{\pi} P \int_{-\infty}^{\infty} \frac{\Delta_{r,r}(iy)}{\Delta(iy)}\, dy. \tag{38a}$$

A corresponding integral formula for $\mathscr{E}$ may be obtained from the integral

$$\frac{1}{2\pi i}\int_{\gamma} \left\{ z \frac{\Delta'(z)}{\Delta(z)} - n \right\} dz.$$

On account of the fact that (see equation (14))

$$\Delta(z) \doteq (-)^n \left\{ z^n - \left(\sum_r \alpha_r\right) z^{n-1} + \ldots \right\},$$

it follows that the integrand equals $\left(\sum_r \alpha_r\right) z^{-1} + O(z^{-2})$. The contribution from the infinite semicircle is therefore $\frac{1}{2}\sum_r \alpha_r$. But the poles within γ are at ϵ_j $(j = 1, 2, \ldots, m)$, and the residue at ϵ_j is ϵ_j. Therefore

$$\frac{1}{2\pi i}\int_{-\infty i}^{\infty i}\left\{z\frac{\Delta'(z)}{\Delta(z)} - n\right\} dz + \tfrac{1}{2}\sum_r \alpha_r = \sum_{j=1}^{m} \epsilon_j = \tfrac{1}{2}\mathscr{E}.$$

Therefore

$$\mathscr{E} = \sum_r \alpha_r + \frac{1}{\pi}\int_{-\infty}^{\infty}\left\{iy\frac{\Delta'(iy)}{\Delta(iy)} - n\right\} dy. \tag{41}$$

This equation also holds for molecules having an orbital of zero energy containing 0, 1 or 2 electrons, since these contribute nothing to $\mathscr{E}$, nor does the integrand develop a pole at $z = 0$, since $z\Delta'(z)/\Delta(z) = O(1)$. Equation (41) is a generalization of a formula previously obtained (Coulson 1940) for hydrocarbons in which each α_r is zero.

Three integral formulae have now been obtained; before proceeding further it is convenient to list them together:

$$p_{rs} = -\frac{1}{2\pi}\int\frac{\partial}{\partial\beta_{rs}}\log\Delta\, dy = (-)^{r+s+1}\frac{1}{\pi}\int\frac{\Delta_{r,s}}{\Delta} dy, \tag{42}$$

$$q_r = 1 - \frac{1}{\pi}\int\frac{\partial}{\partial\alpha_r}\log\Delta\, dy = 1 - \frac{1}{\pi}\int\frac{\Delta_{r,r}}{\Delta} dy, \tag{43}$$

$$\mathscr{E} = \sum_r \alpha_r + \frac{1}{\pi}\int\left\{y\frac{\partial}{\partial y}\log\Delta - n\right\} dy = \sum_r \alpha_r + \frac{1}{\pi}\int\left\{iy\frac{\Delta'}{\Delta} - n\right\} dy. \tag{44}$$

Here and later every determinant which occurs in an integral is to be taken as *a function of iy, not y*, and the limits of integration, when not given, are $-\infty$ to $+\infty$.

These three formulae, besides certain applications which will be considered later, enable us to calculate in one step the total π-electronic energy, the total mobile charge on a particular nucleus, or the total mobile order of any particular bond, without the need of solving the secular determinant for each of the separate molecular orbitals; and as one of the writers has shown (Coulson 1940) this single integration may often be achieved numerically to a high degree of accuracy without great labour. The mobile charges may be used (e.g. Longuet-Higgins, unpublished work) to estimate the resonance dipole moment, and the active centres for cationoid and anionoid attack; and the bond order, which measures the double-bond character of a bond, will indicate its reactivity as well as its length and force constant.

MUTUAL POLARIZABILITIES OF ATOMS AND BONDS

To some extent the above applications of the theory of molecular orbitals are familiar. But there is another application which has not been widely applied hitherto, and which promises to yield important results. Suppose that by some means one is able to alter the energy integral α_r of one atom to a different value $\alpha_r + \delta\alpha_r$. This may be achieved, for example, by replacing a boundary hydrogen atom by a methyl group or other radical—the effect of alkylation has been much discussed in relation to the change in energy levels, and hence of colour, in certain conjugated dye molecules—or it may be achieved by replacing one group by another with different electron affinity, for example, CH in benzene by N, giving pyridine. But however it arises this change in α_r will cause changes in the charge densities around all the nuclei. In particular, if the change may be treated in first approximation as a perturbation applied to atom r, the change of electron density on atom s is

$$\delta q_s = \frac{\partial q_s}{\partial \alpha_r}\delta\alpha_r = \pi_{s,r}\,\delta\alpha_r, \quad \text{say.} \tag{45}$$

Values of $\pi_{s,r}$ will therefore tell what differences in electron distribution are to be expected between pairs of molecules related in this way. Now according to (24)

$$\pi_{s,r} = \frac{\partial q_s}{\partial \alpha_r} = \frac{\partial^2 \mathscr{E}}{\partial \alpha_r \partial \alpha_s} = \frac{\partial^2 \mathscr{E}}{\partial \alpha_s \partial \alpha_r} = \frac{\partial q_r}{\partial \alpha_s} = \pi_{r,s}, \tag{46}$$

so thus follows the theorem: 'A change in electron affinity at atom r produces the same change in electron density at atom s as a similar change at atom s would produce at atom r.' This symmetry suggests that both $\pi_{s,r}$ and $\pi_{r,s}$ should be referred to as the *mutual polarizability of atoms r and s.*

As has been seen, one would expect the magnitudes and signs of these mutual polarizabilities to be of importance in determining how a substituent will affect the electron density and hence the chemical reactivity at different positions in a conjugated molecule. There is, however, another rather practical use to which these mutual polarizabilities can be put—and the others shortly to be introduced. It arises from the fact that the secular equations are vastly easier to solve for pure hydrocarbons than for systems such as pyridine or indole. Thus for indole it is necessary to solve a determinantal equation of the ninth degree, whereas in the corresponding hydrocarbon (benz-pentadienyl) the secular determinant factorizes into a quartic and a quintic. Once the wave functions have been calculated for the appropriate hydrocarbon, it is possible with little further labour to estimate the charge shifts in the related hetero-molecules, as we hope to do in a later paper.

But when α_r is changed, not only do the electron densities q_s change, so also do the bond orders p_{st}. A polarizability may be introduced, called the bond-atom polarizability $\pi_{st,r}$, to measure this change. In fact

$$\delta p_{st} = \frac{\partial p_{st}}{\partial \alpha_r}\delta\alpha_r = \pi_{st,r}\,\delta\alpha_r, \quad \text{say.} \tag{47}$$

This will be discussed later.

The effects represented by $\pi_{s,r}$ and $\pi_{st,r}$ result from a change in the coulomb energy integral α_r at some atom; and to the extent to which first-order perturbation theory is valid any number of such changes may be superposed at different atoms. But, of course, the effect of changing one of the resonance integrals β_{rs} across a bond r-s could be studied equally well. A particularly important way in which this occurs is during the process of vibration; for as the molecule vibrates, the bond lengths are changing, and hence also the resonance integrals. An alteration in β_{st}, say, will cause a change in electron density at atom r which is measured by the atom-bond polarizability

$$\pi_{r,st} = \frac{\partial q_r}{\partial \beta_{st}}, \tag{48}$$

and a change in the order of bond ru measured by

$$\pi_{ru,st} = \frac{\partial p_{ru}}{\partial \beta_{st}}. \tag{49}$$

Now changes in the charge density—and hence electric moment—as a result of vibration are responsible for the absorption of infra-red light, so that the intensity of absorption in a given vibrational transition is related in part to the coefficients $\pi_{r,st}$. And changes in bond order imply changes in energy, so that cross-terms in the potential energy function for vibrations are closely dependent upon the magnitudes of the quantities $\pi_{ru,st}$. A fuller account of this effect is being given in a later paper.

Relationships similar to (46) may be found for $\pi_{st,r}$ and $\pi_{r,st}$. Thus

$$\pi_{st,r} = \frac{\partial p_{st}}{\partial \alpha_r} = \frac{1}{2}\frac{\partial^2 \mathscr{E}}{\partial \alpha_r \partial \beta_{st}} = \frac{1}{2}\frac{\partial q_r}{\partial \beta_{st}} = \tfrac{1}{2}\pi_{r,st}. \tag{50}$$

This is, the polarizability of a bond by an atom equals half the polarizability of the atom by the bond. Similarly

$$\pi_{rs,tu} = \frac{\partial p_{rs}}{\partial \beta_{tu}} = \frac{1}{2}\frac{\partial^2 \mathscr{E}}{\partial \beta_{tu} \partial \beta_{rs}} = \frac{\partial p_{tu}}{\partial \beta_{rs}} = \pi_{tu,rs}. \tag{51}$$

Here again, therefore, one may speak of the *mutual polarizability of a pair of bonds*.

Integral formulae for $\pi_{r,s}$, $\pi_{rs,t}$ and $\pi_{rs,tu}$ may be obtained by differentiation of the integrals in (42) and (43). Thus

$$\pi_{r,s} = -\frac{1}{\pi}\int \frac{\partial^2}{\partial \alpha_r \partial \alpha_s} \log \Delta \, dy, \tag{52}$$

$$\pi_{rs,t} = -\frac{1}{2\pi}\int \frac{\partial^2}{\partial \alpha_t \partial \beta_{rs}} \log \Delta \, dy, \tag{53}$$

$$\pi_{rs,tu} = -\frac{1}{2\pi}\int \frac{\partial^2}{\partial \beta_{rs} \partial \beta_{tu}} \log \Delta \, dy. \tag{54}$$

More useful relationships are obtained by using the alternative forms of the integrands in (38) and (39), as follows:

$$\begin{aligned}\pi_{r,s} &= -\frac{1}{\pi}\int \frac{\partial}{\partial \alpha_s}\left\{\frac{\Delta_{r,r}}{\Delta}\right\} dy \\ &= -\frac{1}{\pi}\int \frac{\Delta . \Delta_{rs,rs} - \Delta_{r,r}\Delta_{s,s}}{\Delta^2} dy,\end{aligned} \tag{55}$$

where the letters before and after the comma in each suffix denote respectively rows and columns omitted from Δ, and as agreed on p. 49 all the determinants are functions of iy, not y. Thus, for example, $\Delta_{rs,tu}$ means that the rows r and s, together with the columns t and u, have been removed from the determinant Δ. It is also supposed, where necessary in this notation, that $r<s$, $t<u$. If $r>s$, then in order to preserve consistency in the analysis $\Delta_{rs,tu}$ must be interpreted as $-\Delta_{sr,tu}$. But on account of the symmetric nature of Δ, then $\Delta_{r,s}=\Delta_{s,r}$.

Now by Jacobi's formula for the adjugate to a determinant

$$\Delta\,.\,\Delta_{rs,tu}=\Delta_{r,t}\Delta_{s,u}-\Delta_{r,u}\Delta_{s,t}. \tag{56}$$

Putting $t=r$, $u=s$ in (56) and substituting in (55), it follows that

$$\pi_{r,s}=\frac{1}{\pi}\int\left\{\frac{\Delta_{r,s}}{\Delta}\right\}^2 dy. \tag{57}$$

Again, from (42),
$$\pi_{rs,t}=(-)^{r+s+1}\frac{1}{\pi}\int\frac{\partial}{\partial\alpha_t}\left\{\frac{\Delta_{r,s}}{\Delta}\right\}dy$$
$$=(-)^{r+s+1}\frac{1}{\pi}\int\frac{\Delta\,.\,\Delta_{rt,st}-\Delta_{r,s}\Delta_{t,t}}{\Delta^2}dy, \tag{58}$$

assuming for the moment that both r and s are less than t. In view of (56) and the fact that $\Delta_{t,s}=\Delta_{s,t}$, this becomes

$$\pi_{rs,t}=(-)^{r+s}\frac{1}{\pi}\int\frac{\Delta_{r,t}\Delta_{s,t}}{\Delta^2}dy. \tag{59}$$

Finally, from (42),
$$\pi_{rs,tu}=(-)^{r+s+1}\frac{1}{\pi}\int\frac{\partial}{\partial\beta_{tu}}\left\{\frac{\Delta_{r,s}}{\Delta}\right\}dy. \tag{60}$$

But it is easily seen by writing down the form of $\Delta_{r,s}$ that if r and s are each less than t and u, then

$$\frac{\partial\Delta_{r,s}}{\partial\beta_{tu}}=(-)^{t+u}\{\Delta_{rt,su}+\Delta_{ru,st}\}$$

and
$$\frac{\partial\Delta}{\partial\beta_{tu}}=(-)^{t+u}\,2\Delta_{t,u}.$$

So under these conditions it follows from (56) that

$$\pi_{rs,tu}=(-)^{r+s+t+u}\frac{1}{\pi}\int\frac{\Delta_{r,u}\Delta_{s,t}+\Delta_{r,t}\Delta_{s,u}}{\Delta^2}dy. \tag{61}$$

Equations (57), (59) and (61), in which it is understood that all the determinants are functions of iy, have been proved under certain conditions of inequality between the indices r, s, t and u (e.g. $r<t$, $s<u$). It is not difficult to prove, however, that they are actually valid for all relative values of these indices. In particular, (57) holds even if $r=s$, so that the *self-polarizability of atom* r satisfies the equation

$$\pi_{r,r}\left(=\frac{\partial q_r}{\partial\alpha_r}\right)=\frac{1}{\pi}\int\left\{\frac{\Delta_{r,r}}{\Delta}\right\}^2 dy. \tag{62}$$

And (61) is true if $r = t$, $s = u$; so that the *self-polarizability of bond rs* is given by

$$\pi_{rs,rs}\left(=\frac{\partial p_{rs}}{\partial \beta_{rs}}\right) = \frac{1}{\pi}\int \frac{\Delta_{r,r}\Delta_{s,s}+\Delta^2_{r,s}}{\Delta^2}dy. \tag{63}$$

The self-polarizability of an atom measures the change of charge density at the atom when its electron affinity is altered; the self-polarizability of a bond measures the change of mobile order in the bond when its resonance integral is altered.

It is easy to prove that (57), (59) and (61) still hold for an odd molecule with one electron in an m.o. of zero energy, provided one takes the principal values of the integrals. One merely starts from equations (35*a*) and (38*a*) instead of (35) and (38); the reasoning follows exactly similar lines.

FORMULAE FOR POLARIZABILITIES IN TERMS OF THE COEFFICIENTS

Equations (57), (59) and (61) give the three types of polarizability in terms of certain integrals, and for many purposes this is the most convenient form for them. But the m.o. is often known explicitly, and then it is desirable to have equivalent expressions in terms of the coefficients c_{rj} of (1). These alternative expressions for $\pi_{r,s}$, $\pi_{rs,t}$ and $\pi_{rs,tu}$ may be derived by application of ordinary first-order perturbation theory to the secular equations.

Suppose there is a molecule in which the occupied m.o. are $\psi_1, \psi_2, \ldots, \psi_m$ and the unoccupied m.o. are $\psi_{m+1}, \ldots, \psi_n$, built up according to (1) from the component atomic orbitals $\phi_1, \ldots, \phi_n$. Notice what happens to the coefficients, electron densities and bond orders when the coulomb integral α_r is increased by a small amount $\delta\alpha_r$. (An increase in α_r corresponds, of course, to a decrease in electron affinity.) By first-order perturbation theory the perturbed wave functions can be expanded in the form

$$\psi_j+\psi'_j = \psi_j + \sum_{k=1}^{n}{}' \left\{\frac{\int \psi_j H'\psi_k dv}{\epsilon_j-\epsilon_k}\right\}\psi_k,$$

which equals
$$\psi_j + \sum_{k=1}^{n}{}' \frac{c_{rj}c_{rk}\delta\alpha_r}{\epsilon_j-\epsilon_k}\psi_k,$$

since
$$\psi_j = \sum_{s=1}^{n} c_{sj}\phi_s \quad \text{and} \quad \int \phi_r H'\phi_r dv = \delta\alpha_r,$$

all other integrals of this type being zero. So

$$\psi'_j = \delta\alpha_r \sum_{k=1}^{n}{}' \left\{\frac{c_{rj}c_{rk}}{\epsilon_j-\epsilon_k}\sum_{s=1}^{n} c_{sk}\phi_s\right\} = \sum_{s=1}^{n} c'_{sj}\phi_s, \quad \text{say,}$$

where
$$c'_{sj} = \delta\alpha_r c_{rj} \sum_{k=1}^{n}{}' \frac{c_{rk}c_{sk}}{\epsilon_j-\epsilon_k}.$$

Bearing in mind the fact that the occupied orbitals are those for which $1 \leq j \leq m$, the change in electron density at atom s equals may be deduced as

$$\delta q_s = 2\sum_{j=1}^{m} \{(c_{sj}+c'_{sj})^2 - c_{sj}^2\}$$

$$= 4\sum_{j=1}^{m} c_{sj}c'_{sj}$$

since c'_{sj} is small. Thus
$$\delta q_s = 4\delta\alpha_r \sum_{j=1}^{m} \sum_{k=1}^{n}{}' \frac{c_{rj}c_{sj}c_{rk}c_{sk}}{\epsilon_j - \epsilon_k}.$$

From this it follows that

$$\pi_{s,r} = \frac{\partial q_s}{\partial \alpha_r} = 4\sum_{j=1}^{m} \sum_{k=1}^{n}{}' \frac{c_{rj}c_{sj}c_{rk}c_{sk}}{\epsilon_j - \epsilon_k}.$$

But the summand here is antisymmetric in j and k so that $\sum_{j=1}^{m} \sum_{k=1}^{m}{}' = 0$. Therefore

$$\pi_{s,r} = 4\sum_{j=1}^{m} \sum_{k=m+1}^{n} \frac{c_{rj}c_{sj}c_{rk}c_{sk}}{\epsilon_j - \epsilon_k}. \tag{64}$$

In particular the self-polarizability of atom r is

$$\pi_{r,r} = 4\sum_{j=1}^{m} \sum_{k=m+1}^{n} \frac{c_{rj}^2 c_{rk}^2}{\epsilon_j - \epsilon_k}. \tag{64a}$$

Similarly, the change in order of bond st equals

$$\delta p_{st} = 2\sum_{j=1}^{m} \{(c_{sj}+c'_{sj})(c_{tj}+c'_{tj}) - c_{sj}c_{tj}\}$$

$$= 2\sum_{j=1}^{m} (c_{sj}c'_{tj} + c_{tj}c'_{sj})$$

$$= 2\delta\alpha_r \sum_{j=1}^{m} \sum_{k=1}^{n}{}' \frac{c_{rj}c_{rk}(c_{sj}c_{tk} + c_{tj}c_{sk})}{\epsilon_j - \epsilon_k}.$$

Therefore
$$\pi_{st,r} = 2\sum_{j=1}^{m} \sum_{k=m+1}^{n} \frac{c_{rj}c_{rk}(c_{sj}c_{tk} + c_{tj}c_{sk})}{\epsilon_j - \epsilon_k}. \tag{65}$$

Equations (64) and (65) show the effect of changing the coefficient α_r; next note how a change of β_{rs} to $\beta_{rs} + \delta\beta_{rs}$ alters the electron densities and bond orders. As before ψ_j becomes $\psi_j + \psi'_j$, where now

$$\psi'_j = \sum_{k=1}^{n}{}' \left\{ \frac{\int \psi_j H' \psi_k \, dv}{\epsilon_j - \epsilon_k} \right\} \psi_k = \sum_{k=1}^{n}{}' \frac{(c_{rj}c_{sk} + c_{sj}c_{rk})\,\delta\beta_{rs}}{\epsilon_j - \epsilon_k} \psi_k$$

$$= \sum_{t=1}^{n} c'_{tj}\phi_t,$$

where
$$c'_{tj} = \delta\beta_{rs} \sum_{k=1}^{n}{}' \frac{c_{tk}(c_{rj}c_{sk} + c_{sj}c_{rk})}{\epsilon_j - \epsilon_k}.$$

This leads to a change in density on atom t given by

$$\delta q_t = 4\sum_{j=1}^{m} c_{tj}c'_{tj} = 4\delta\beta_{rs}\sum_{j=1}^{m}\sum_{k=1}^{n}{}' \frac{c_{tj}c_{tk}(c_{rj}c_{sk}+c_{sj}c_{rk})}{\epsilon_j-\epsilon_k}.$$

This may be written

$$\pi_{t,rs} = 4\sum_{j=1}^{m}\sum_{k=m+1}^{n} \frac{c_{tj}c_{tk}(c_{rj}c_{sk}+c_{sj}c_{rk})}{\epsilon_j-\epsilon_k}. \tag{66}$$

Comparing this with (65) then $\pi_{t,rs} = 2\pi_{rs,t}$, in agreement with (50). Finally,

$$\begin{aligned}\pi_{tu,rs} &= 2\sum_{j=1}^{m}(c_{tj}c'_{uj}+c_{uj}c'_{tj})/\delta\beta_{rs}\\ &= 2\sum_{j=1}^{m}\sum_{k=m+1}^{n}\frac{(c_{rj}c_{sk}+c_{sj}c_{rk})(c_{tj}c_{uk}+c_{uj}c_{tk})}{\epsilon_j-\epsilon_k}.\end{aligned} \tag{67}$$

Equations (64) to (67) enable one to calculate all the atom and bond polarizabilities in a molecule in terms of the energies and coefficients of its molecular orbitals. These equations are the exact analogues of (57), (59) and (61), and may be verified directly by the evaluation of certain complex integrals. For instance, we may relate (64) to (57) by integrating

$$P\int_{-\infty i}^{\infty i}\int_{-\infty i}^{\infty i}\frac{\Delta_{r,s}(w)\,\Delta_{r,s}(z)}{\Delta(w)\,\Delta(z)\,(w-z)}\,dw\,dz$$

successively with respect to w and z, using Cauchy's residue theorem. It should be noted that equations (64) to (67) do not hold for odd molecules with one electron in a m.o. of zero energy; the necessary modifications are, however, not difficult to make.

An interesting chemical implication of (67) is the following: If there are two conjugated systems initially separate, and they are then joined by a weak bond between atom r of the first and atom s of the second, then to a first approximation, in which only conjugation effects are considered, the order of any other bond tu in either system is unaffected.

To prove this one takes as the basis of the perturbation calculation in (67) the separated conjugated systems. Then each suffix j in a term of (67) will refer to an occupied m.o. in one of the two systems, and each suffix k to an unoccupied m.o. Suppose that j and k refer to the same system. Then either c_{rj} and c_{rk}, or else c_{sj} and c_{sk}, must vanish, since r and s are in different systems; thus the first bracket in (67) is zero. But if j and k refer to different systems, and tu is a bond in one of the systems, either c_{tj} and c_{uj}, or else c_{tk} and c_{uk}, must vanish; and so the second bracket is zero. Hence in all cases every term of (67) is zero and so $\pi_{rs,tu} = 0$, which establishes the theorem. This theorem tells us something about the condition when a reaction between conjugated systems is being initiated. For it shows that (steric conditions permitting) conjugation may begin to take place, with the introduction of resonance forces, without the reacting groups having to be deformed. It is only when the reaction complex is well on the way to being formed that serious changes in bond order occur in the two separate parts.

INEQUALITIES AND IDENTITIES INVOLVING ELECTRON DENSITIES, BOND ORDERS AND ATOM AND BOND POLARIZABILITIES

The electron densities, bond orders and the various polarizabilities have been calculated independently of one another. But there are several identities and inequalities between them that must now be described. These inequalities are useful in understanding certain experimental phenomena, as will be shown; and the identities provide useful checks upon the numerical working at various stages.

(i) The first inequality concerns the electron density q_r; this being a sum of square terms must obviously be positive. But we shall now show that it cannot exceed 2. For this purpose return to equation (17). This shows us that the molecular orbitals ψ_j may be regarded as a set of unit orthogonal vectors in the n-space defined by the unit orthogonal vectors ϕ_r, c_{rj} being the cosine of the angle between ψ_j and the base vector ϕ_r. But the roles of ϕ and ψ may be interchanged, and ϕ_r regarded as a unit vector relative to the set of orthogonal base vectors ψ_j; it follows that $\sum_{j=1}^{n} c_{rj}^2 = 1$, so that $\sum_{j=1}^{m} c_{rj}^2 \leqslant 1$. But $q_r = 2\sum_{j=1}^{m} c_{rj}^2$, and so

$$0 \leqslant q_r \leqslant 2. \tag{68}$$

This inequality gives a simple explanation of the charge shifts in certain conjugated systems. For example, in chlorobenzene there are six π-electrons from the benzene nucleus and two from the Cl atom. If the Cl atom were not conjugated with the ring, it would have exactly two of these electrons. But by (68) conjugation can only reduce this number, so that there is a charge drift into the ring. Our analysis shows that this migration would be expected even though Cl is more electronegative than carbon. In fact, it is only the magnitude of the electron drift, and not its direction, which depends upon the nature of the attached group. The conventional valence-bond description of this phenomenon is that there is resonance between covalent structures of type (*a*) and ionic structures of type (*b*) in which charge has moved from Cl to the less electronegative C. We believe that the present explanation by the method of m.o. is a worth-while supplement to the resonance picture. A similar explanation is behind the drift of electrons away from the electronegative N atom in molecules such as pyrrole and indole (Longuet-Higgins & Coulson 1947).

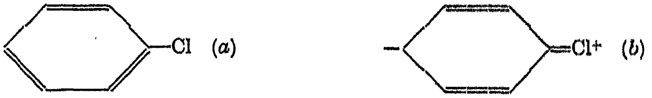

(ii) It is worth noting that there is no condition analogous to (68) requiring p_{rs} to be positive; in fact, generalizing the idea of bond order to apply to atoms which are not actually adjacent to one another, it is easy to show that the bond order between *para* positions in benzene is negative; the implications of this fact are discussed in a later paper.

(iii) By a direct application of Cauchy's inequality it can be proved that the order of a bond is not greater than the geometric mean of the electron densities at the atoms forming the bond. For Cauchy's inequality is that

$$\left\{\sum_{j=1}^{m} c_{rj} c_{sj}\right\}^2 \leqslant \left\{\sum_{j=1}^{m} c_{rj}^2\right\}\left\{\sum_{j=1}^{m} c_{sj}^2\right\}, \tag{69}$$

so that

$$p_{rs}^2 \leqslant q_r q_s. \tag{70}$$

(iv) It follows from (18) and (64*a*) that

$$\pi_{r,r} = 4\sum_{j=1}^{m}\sum_{k=m+1}^{n}\frac{c_{rj}^2 c_{rk}^2}{\epsilon_j - \epsilon_k} < 0. \tag{71}$$

This means that an increase in α_r (i.e. a decrease in the electron affinity of atom r) results in a decrease of electron charge there, as would be expected.

(v) Similarly, from (67) it follows that

$$\pi_{rs,rs} < 0. \tag{72}$$

That is, an increase in the numerical value of β_{rs}—which is actually negative—leads to an increase of bond order, also as expected.

Equation (72) has an important application in the interaction of two conjugated systems. Imagine the systems to be initially isolated, and then to approach so that the atomic orbital ϕ_r of the first overlaps the atomic orbital ϕ_s of the second. Then β_{rs} will decrease steadily from zero, and p_{rs}, which satisfies

$$p_r = \int_0^{\beta_{rs}} \pi_{rs,rs}\, d\beta_{rs}, \tag{73}$$

will therefore increase steadily. But since r and s belong initially to separate systems, p_{rs} is initially zero; its final value must therefore be positive. Hence *the mobile order of a bond between two otherwise disconnected systems must be positive.* Such a bond will later be referred to as a 'chain bond'. This conclusion is of obvious and fundamental importance from the chemical point of view. It explains, for instance, why the single bond connecting two aryl radicals, as in diphenyl or phenylethylene, is always partly double. Conjunction between the two groups across this bond will necessarily increase its bond order, and therefore presumably shorten it and increase its force constant. This conclusion is independent of whatever substituent groups there may be in the two halves, provided always that they do not interfere sterically with one another (as in various diphenyl *o-o′* derivatives).

It is convenient at this point to introduce a few identities:

(vi) In the first place (21) can be used for checking the charge distributions and bond orders. For summation over the occupied m.o. gives the very useful relation

$$\mathscr{E} = \sum_r \alpha_r q_r + 2\sum_{r<s}\sum \beta_{rs} p_{rs}. \tag{74}$$

(vii) Secondly, it follows from (15) and (20) that $\sum_r q_r = 2m$, which is constant and does not depend on the values of α_r and β_{rs}. Hence from the definitions of $\pi_{r,s}$ and $\pi_{r,st}$

$$\sum_r \pi_{r,s} = 0 = \sum_r \pi_{r,st}. \tag{75}$$

(viii) Finally, by differentiating (74) with respect to α_r or β_{tu} and then using (24) and (25), then

$$\sum_s \alpha_s \pi_{s,r} + 2\sum_{s<t}\sum \beta_{st}\pi_{st,r} = 0, \tag{76}$$

$$\sum_s \alpha_s \pi_{s,tu} + 2\sum_{r<s}\sum \beta_{rs}\pi_{rs,tu} = 0. \tag{77}$$

Equations (75) to (77) are useful in checking values of the polarizabilities.

The suitability of the definitions adopted for electron density and bond order is satisfactorily confirmed by the reasonableness of all these results, as judged by qualitative chemical ideas. In following papers of this series we hope to show how the various formulae introduced in this paper may be used to explain and correlate various experimental phenomena.

APPENDIX 1

Integrals involving determinants of the type $\Delta_{r,s}$ occur frequently in the formulae given in this paper, for instance in equations (42), (57), (59) and (61). When they do, it is often convenient or illuminating to expand $\Delta_{r,s}$ by the following theorem:

When the rth row and sth column are struck out from Δ, the secular determinant for a conjugated system, the resulting determinant $\Delta_{r,s}$ equals

$$(-)^{r+s}\Sigma(-)^{l}\beta_{rt}\beta_{tu}\cdots\beta_{vs}\Delta_{rtu\ldots vs,\,rtu\ldots vs}, \tag{78}$$

where atoms $r, t, u, \ldots, v, s$ lie along a continuous non-crossing chain, l is the number of bonds in the chain, and $\Delta_{rtu\ldots vs,\,rtu\ldots vs}$ is the secular determinant for the rest of the molecule (taken equal to unity if $r, t, \ldots, s$ include all the atoms in the molecule), the summation being taken over all such chains.

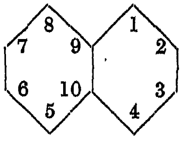

The theorem may be illustrated by the example of $\Delta_{1,6}$ for naphthalene. There are four chains of the specified kind between atoms 1 and 6, namely,

1 9 8 7 6, 1 9 10 5 6, 1 2 3 4 10 5 6 and 1 2 3 4 10 9 8 7 6.

$\Delta_{1,6}$ is therefore expressible as the sum of four terms, of which the second, for example, is $-\beta^4\Delta_{1\,9\,10\,5\,6,\,1\,9\,10\,5\,6}$. Since the corresponding route cuts the molecule in two, the latter determinant is itself the product of the secular determinants for the systems (7 8) and (2 3 4).

First prove that every term of $\Delta_{r,s}$ ($= \Delta_{s,r}$) must contain a factor of the type $\beta_{rt}\beta_{tu}\dots\beta_{vs}$. Expand $\Delta_{s,r}$ in terms of row r. A typical term in the expansion is $\pm\beta_{rt}\Delta_{rs,rt}$, where $t \neq r$. If $t = s$, this is a factor of the required type. If $t \neq s$, expand $\Delta_{rs,rt}$ in terms of row t. A typical term is $\pm\beta_{tu}\Delta_{rst,rtu}$, where $u \neq r$ or t. If $u = s$, we have a factor of the required type; if $u \neq s$, we expand again. It is clear that as this process is continued every new letter introduced must differ from all of $r, t, u, \dots$ so that ultimately the letter s must be reached. When this happens the typical term will be of the form $\pm\beta_{rt}\beta_{tu}\dots\beta_{vs}\Delta_{rtu\dots vs,rtu\dots vs}$. In this the β part will be zero unless $rt, tu, \dots, vs$ are all bonds; therefore there is one such term for each non-crossing chain of bonds from r to s. If atoms $r, t, u, \dots, v, s$ include all the atoms of the system, the factor multiplying the β's will be unity.

Now in the expansion of Δ, the sign of $\beta_{sr}\beta_{rt}\beta_{tu}\dots\beta_{vs}\Delta_{rtu\dots vs,rtu\dots vs}$ is + or − according as the permutation $(rtu\dots vs)$ is even or odd; that is, the sign is $(-)^l$, where l is the number of bonds in the chain $rt, tu, \dots, vs$. But $\Delta_{s,r}$ is $(-1)^{r+s}$ times the coefficients of β_{sr} in the expansion of Δ. It follows that

$$\Delta_{r,s} = \Delta_{s,r} = (-)^{r+s}\Sigma(-)^l\beta_{rt}\beta_{tu}\dots\beta_{vs}\Delta_{rtu\dots vs,rtu\dots vs},$$

the summation being taken over all non-crossing chains of bonds between atoms r and s.

Not only is this result useful in calculations involving $\Delta_{r,s}$, but it also suggests why the effects of a perturbation applied to a conjugated system die away at long distances—a fact which is hardly self-evident from the secular equations, although to be expected on physical grounds. For the highest power of ϵ occurring in $\Delta_{r,s}(\epsilon)$ is ϵ^{n-1-b}, where b is the number of conjugated bonds along the shortest route between atoms r and s. This means that, for example, in equation (57), where $\pi_{r,s}$ is expressed as an integral, the integrand by (78) is of order y^{-2b-2}, so that the integral would be expected to be small for large values of b. This effect is well illustrated by the polyenes, which are discussed in a later paper.

APPENDIX 2

It has been assumed throughout this paper that the roots of Δ are all distinct; this is nearly always true, but it is interesting to inquire how many of the equations depend upon this assumption.

If one applies to a molecule with degenerate energy levels any perturbation H' which separates all the degenerate levels, all the expressions derived for $\mathscr{E}$ and its derivatives will certainly hold for the perturbed molecule. Supposing, as is reasonable, that $\mathscr{E}$ and its derivatives vary continuously with H', their values for the unperturbed molecule will be the limits of the expressions as H' tends to zero, *if such limits exist.*

Now the expressions for $\mathscr{E}$ and its derivatives are of two kinds. An example of the first is (38), viz.

$$q_r = 1 - \frac{1}{\pi}\int_{-\infty}^{\infty}\frac{\Delta_{r,r}(iy)}{\Delta(iy)}dy.$$

Both numerator and denominator in the integrand are continuous functions of H', and the denominator cannot vanish since by hypothesis all the roots of Δ are real and do not include zero. Therefore the limit of the right-hand side as H' tends to zero is obtained simply by putting $H' = 0$ before integrating. Therefore formulae of this type hold for a molecule with multiple-energy levels. An example of the second type of expression is (64), viz.

$$\pi_{s,r} = 4\sum_{j=1}^{m}\sum_{k=m+1}^{n}\frac{c_{rj}c_{sj}c_{rk}c_{sk}}{\epsilon_j-\epsilon_k}.$$

By hypothesis all the occupied m.o. have negative energies and the unoccupied m.o. positive energies, so the denominator cannot vanish; hence the right-hand side tends to a limit as H' tends to zero, the terms c_{rj} becoming the coefficients of the a.o. ϕ_r in the zeroth order m.o. ψ_j appropriate to the perturbation H'.

It is therefore seen that any of the formulae for $\mathscr{E}$ and its derivatives which include the electron densities, bond orders and atom and bond polarizabilities, may be legitimately applied to molecules containing degenerate energy levels, provided the m.o. used as basis are correct zeroth order m.o. for any perturbation whatever which separates all the energies.

REFERENCES

Coulson, C. A. 1937 *Trans. Faraday Soc.* **33**, 388.
Coulson, C. A. 1939 *Proc. Roy. Soc.* A, **169**, 413.
Coulson, C. A. 1940 *Proc. Camb. Phil. Soc.* **36**, 201.
Coulson, C. A. 1946 *Trans. Faraday Soc.* **42**, 106.
Coulson, C. A. & Rushbrooke, G. S. 1940 *Proc. Camb. Phil. Soc.* **36**, 193.
Goeppert-Mayer, M. & McCallum, K. J. 1942 *Rev. Mod. Phys.* **14**, 248.
Gordy, W. 1946 *J. Chem. Phys.* **14**, 305.
Lennard-Jones, J. E. 1937 *Proc. Roy. Soc.* A, **138**, 280.
Lennard-Jones, J. E. & Coulson, C. A. 1939 *Trans. Faraday Soc.* **35**, 811.
Longuet-Higgins, H. C. & Coulson, C. A. 1947 *Trans. Faraday Soc.* **43**, 87.
Mulliken, R. S. 1934 *J. Chem. Phys.* **2**, 782.
Mulliken, R. S., Rieke, C. A. & Brown, W. G. 1941 *J. Amer. Chem. Soc.* **63**, 41.
Wheland, G. W. 1941 *J. Amer. Chem. Soc.* **63**, 2025.
Wheland, G. W. 1942 *J. Amer. Chem. Soc.* **64**, 906.
Wheland, G. W. & Pauling, L. 1935 *J. Amer. Chem. Soc.* **57**, 2091.

The binding energies of very light nuclei

By H. Fröhlich and Kun Huang,
H. H. Wills Physical Laboratory, University of Bristol,
and I. N. Sneddon, *Department of Natural Philosophy, University of Glasgow*

(*Communicated by N. F. Mott, F.R.S.—Received* 20 *January* 1947)

The static interaction of the Møller-Rosenfeld theory is used to calculate approximately the binding energies of the nuclei H^2, H^3, He^3 and He^4. The value of the meson mass and of the two other parameters available in the theory are determined from a comparison with the observed binding energies of the H^3 nucleus and of the singlet and triplet states of the deuteron. The meson mass so determined is between 210 and 220 electron masses which is in fair agreement with cosmic-ray measurements. The binding energy of He^3 calculated from the energy difference $H^3 - He^3$ is also found to be in fair agreement with the observed value.

The theoretical binding energy of He^4 is less than half the observed value, and it is suggested that in this nucleus there exists an additional many-body interaction.

1. Introduction

In the present paper the version of the meson theory, usually known as the Møller-Rosenfeld theory (referred to as M.-R. theory (Møller & Rosenfeld 1940; Rosenfeld 1945, 1947)) will be used to calculate approximately the binding energies of the nuclei H^2, H^3, He^3 and He^4. In this theory a 'static' interaction is separated from the total interaction between nucleons. The purpose of the present calculations is to investigate to what extent this static interaction can account for the observed binding energies.

The M.-R. theory is preferable to other meson theories because in the static approximation it leads to a finite value for the binding energy of the triplet state of the deuteron. Other theories such as the vector theory (Yukawa, Sakata, Kobayasi & Taketani 1938; Fröhlich, Heitler & Kemmer 1938; Bhabha 1938) lead to an infinite value for this binding energy.

The static M.-R. interaction contains three available constants—the mass of the meson and two other constants having the dimensions of charge. These three constants can be determined from a comparison of the calculated values of the binding energies of the triplet and singlet states of the deuteron and that of the hydrogen isotope H^3 with the experimental values. A first check can then be made by comparing the theoretical value of the meson mass with that obtained in cosmic-ray experiments, and by calculating the $H^3 - He^3$ energy difference. The constants thus determined will then be used to calculate the binding energy of He^4.

The influence of the non-static terms (depending on the time derivatives of the co-ordinates describing position, spin and charge of a nucleon) will not be considered. Theoretically this can be justified in the case of the deuteron (Rosenfeld 1945, 1947), although these terms alone are responsible for its quadripole moment. The question of the influence of non-static terms in nuclei containing more than two nucleons is much more complicated than in the case of the deuteron. The following investigations should, therefore, give a semi-empirical estimate of the importance of the non-static terms in these heavier nuclei based on the assumption that the static M.-R. interaction is a correct first approximation. Moreover, the semi-empirical nature of the present investigations is further emphasized by the fact that the convergence of the higher order interactions is in no way assured.

Some of the results of the present paper have already been communicated at the Cambridge conference (Fröhlich, Ramsey & Sneddon 1947), but it seemed desirable to give a full account of the methods used in the calculations, and of the results obtained from them.

2. WAVE EQUATION FOR THE n-NUCLEON PROBLEM

According to the M.-R. theory (Rosenfeld 1945, equation (16)) the 'static' interaction energy between two nucleons is given by

$$U_{12} = (\boldsymbol{\tau}_1 . \boldsymbol{\tau}_2)\,[G^2 + F^2(\boldsymbol{\sigma}_1 . \boldsymbol{\sigma}_2)]\,\frac{e^{-\lambda r_{12}}}{r_{12}}, \tag{1}$$

where r_{12} denotes the distance between the two nucleons, and $\boldsymbol{\sigma}_1$, $\boldsymbol{\sigma}_2$; $\boldsymbol{\tau}_1$, $\boldsymbol{\tau}_2$ are the spin and isotopic spin-vector operators. The constant λ is related to the meson mass m by the equation

$$\lambda = \frac{mc}{\hbar}, \tag{2}$$

and G and F are two constants with the dimensions of an electric charge. They are related to the constants g_i, f_i, appearing in the M.-R. theory and explained in the original paper, by the equations

$$4\pi G^2 = g_1^2 - \frac{m}{M} g_1 g_2, \quad 4\pi F^2 = g_2^2 - \frac{m}{M}\,\frac{2g_1 g_2 - f_1 f_2}{3},$$

where M denotes the mass of the nucleon. The difference between the masses of the neutron and the proton is neglected throughout. Equation (1) may be written in the form

$$U_{12} = \frac{m^2c^2}{M} V_{12}, \tag{3}$$

where V_{12} is defined by the relation

$$V_{12} = (\boldsymbol{\tau}_1 . \boldsymbol{\tau}_2)\,[g^2 + f^2(\boldsymbol{\sigma}_1 . \boldsymbol{\sigma}_2)]\,\frac{e^{-\lambda r_{12}}}{\lambda r_{12}}, \tag{4}$$

the constants f, g being determined from the equations

$$f^2 = \frac{M}{m}\frac{F^2}{\hbar c}, \quad g^2 = \frac{M}{m}\frac{G^2}{\hbar c}. \tag{5}$$

When there are n nucleons present it is assumed that the total interaction is

$$U_n = \sum_{i<j}^{n} U_{ij} = \frac{m^2c^2}{M} \sum_{i<j}^{n} V_{ij}, \tag{6}$$

where U_{ij}, the interaction between the ith and jth nucleon, is defined by a relation similar to equation (1). This assumption neglects all non-static interaction and also the existence of many-body forces which in the M.-R. theory are contained in the non-static terms. The binding energy E_n of a nucleus containing n nucleons is determined from the solution of the Schrödinger equation

$$\left\{\sum_{i=1}^{n} \frac{p_i^2}{2M} - (E_n - U_n)\right\} \Psi_n = 0, \tag{7}$$

where Ψ_n is the wave function which depends on the co-ordinates specifying the positions, spins and isotopic spins of the nucleons. If the co-ordinates of the ith nucleon are denoted by (x_1^i, x_2^i, x_3^i), then, in the usual manner,

$$p_i^2 = -\hbar^2\left(\frac{\partial^2}{\partial x_1^{i2}} + \frac{\partial^2}{\partial x_2^{i2}} + \frac{\partial^2}{\partial x_3^{i2}}\right).$$

If now a change of variable is made so that

$$\lambda(x_1^i, x_2^i, x_3^i) = (x_i, y_i, z_i),$$

then by equation (2)

$$\frac{p_i^2}{2M} = -\frac{m^2c^2}{2M}\left(\frac{\partial^2}{\partial x_i^2} + \frac{\partial^2}{\partial y_i^2} + \frac{\partial^2}{\partial z_i^2}\right) = -\frac{m^2c^2}{2M}\Delta_i. \tag{8}$$

The substitution of these values of U_n, p_i from equations (6) and (8) into the Schrödinger equation (7) leads to the equation

$$(a_n - S_n)\Psi_n = 0, \tag{9}$$

where S_n denotes the operator

$$S_n = -\frac{1}{2}\sum_{i=1}^{n}\Delta_i + \sum_{i<j}^{n} V_{ij}, \tag{10}$$

and a_n is related to the binding energy by the equation

$$a_n = \frac{M}{m^2c^2}E_n. \tag{11}$$

Multiplying equation (9) on the left by Ψ_n^*, the Hermitian conjugate of Ψ_n, and integrating over all the co-ordinates (including spin and isotopic spin co-ordinates), it follows that

$$a_n = \int \Psi_n^* S_n \Psi_n \Big/ \int \Psi_n^* \Psi_n. \tag{12}$$

The integrations go over the space, spin and isotopic spin co-ordinates of all the particles. The space integrations are carried out over a large but finite volume. The energy constant a_n will be determined from this equation by a variational method.

It seemed desirable to use for the three-body calculations the same approximations as have to be used in the case of He^4. A better approximation may be developed in the former case (§ 7). This will be used to check the accuracy of simpler methods developed below.

Assume now that the wave function Ψ_n may be written as a product of the form

$$\Psi_n = \psi_n(\mathbf{r}_1, \dots, \mathbf{r}_n)\,\phi_n(s_1, \dots, s_n;\, t_1, \dots, t_n), \tag{13}$$

where ϕ_n is a function of the spin variables $s_1, s_2, \dots, s_n$ and of the isotopic spin variables $t_1, t_2, \dots, t_n$; $\psi_n(\mathbf{r}_1, \dots, \mathbf{r}_n)$ is a function of the space co-ordinates only but may contain one or more parameters $\alpha, \beta, \dots$.

Except for the deuteron ($n = 2$), where the exact solutions are of the form (13), these wave functions can have only approximate validity. In the exact solutions it is not possible to separate the space co-ordinates from the spin and isotopic spin variables (cf. § 7).

To fulfil the Pauli exclusion principle Ψ_n must be an antisymmetrical function. Then ψ_n can be either symmetrical or antisymmetrical, and hence ϕ_n must be either antisymmetrical or symmetrical. The interaction V_{ij} (which is a symmetrical function) does not lead to transitions between the two types of solutions. In the ground state we expect ψ_n to be symmetrical and thus ϕ_n to be antisymmetrical.

From the symmetry of ψ_n it follows that, integrating over the space co-ordinates,

$$\left(\int \psi_n^* \psi_n\right) I_n = \int \psi_n^* \Delta_1 \psi_n = \int \psi_n^* \Delta_2 \psi_n = \dots \tag{14}$$

and

$$\left(\int \psi_n^* \psi_n\right) J_n = \int \psi_n^* \frac{e^{-r_{12}}}{r_{12}} \psi_n = \int \psi_n^* \frac{e^{-r_{13}}}{r_{13}} \psi_n = \dots. \tag{15}$$

Writing (integrating over all co-ordinates as in (12))

$$b_{ij,n} = \int \phi_n^* (\tau_i \cdot \tau_j)\,[g^2 + f^2(\sigma_i \cdot \sigma_j)]\,\phi_n \Big/ \int \phi_n^* \phi_n \tag{16}$$

and

$$b_n = \sum_{i<j}^{n} b_{ij,n}, \tag{17}$$

equation (12) can be reduced to the form

$$a_n = -\tfrac{1}{2} n I_n + b_n J_n. \tag{18}$$

The energy constant a_n is determined by this equation as a function of the parameters $\alpha, \beta, \dots$ introduced in the function $\psi_n(\mathbf{r}_1, \dots, \mathbf{r}_n)$. The value of a_n is found by minimizing this function with regard to these parameters; the value of the binding energy E_n is then derived from equation (11).

The functions ϕ_n $(s_1 \dots s_n, t_1 \dots t_n)$ are uniquely determined so that the values of the constants b_n are readily found. The calculations are given in Appendix A2; they lead to the results

$$\left.\begin{aligned} b_2({}^1\mathrm{S}) &= g^2 - 3f^2, \qquad & b_2({}^3\mathrm{S}) &= -3g^2 - 3f^2, \\ b_3 &= -3(g^2 + 3f^2), \qquad & b_4 &= -6(g^2 + 3f^2) = 2b_3, \end{aligned}\right\} \tag{19}$$

so that

$$b_2({}^1\mathrm{S}) + b_2({}^3\mathrm{S}) = \tfrac{2}{3} b_3 = \tfrac{1}{3} b_4. \tag{20}$$

^{1}S and ^{3}S refer to the singlet and triplet state of the deuteron respectively.

3. THE DEUTERON

The differential equation satisfied by the radial part of the wave function of the deuteron has been studied in detail by Wilson (1938). By substituting a wave function of the type

$$\psi_2 = e^{-\frac{1}{2}\alpha r_{12}} \tag{21}$$

into equations (14) and (15), making use of the results in equation (18) with $n = 2$ and minimizing a_2 with respect to α, it is easily established that

$$a_2(\alpha) = -\frac{\alpha^2(\alpha-1)}{4(\alpha+3)}, \quad b_2(\alpha) = -\frac{(\alpha+1)^3}{\alpha(\alpha+3)} \tag{22}$$

are the parametric equations of the relation between a_2 and b_2. Wilson compares this solution with that obtained mechanically by solving the Schrödinger equation for ψ_2 by means of the differential analyzer. The results are summarized in the first three columns of table 1. The second column gives the value of b_2, corresponding to the value of a_2 on the left, as determined by the differential analyzer. The third column was constructed by calculating b_2 from equation (22) for the value of α necessary to give the prescribed value of a_2. It will be observed that the two a_2-b_2 curves lie close to each other except in the region of the point $a_2 = 0$. Wilson also computed the a_2-b_2 curve which would arise from assuming instead of (21) a wave function of the form

$$\psi_2 = e^{-\frac{1}{2}\alpha r_{12}} - e^{-\frac{1}{2}\beta r_{12}}$$

containing two parameters α, β, but found that there was no marked improvement on that obtained from the wave function (21).

TABLE 1

	b^2		
a_2	analyzer	Wilson	Hulthén
0·00	−1·70	−2·00	−1·68
−0·25	−2·73	−2·81	−2·77
−0·50	−3·15	−3·23	−3·20
−0·75	−3·48	−3·54	−3·52
−1·00	−3·76	−3·83	−3·82

More recently Hulthén (1942) has employed for the deuteron an approximate wave function of the form

$$\psi_2 = \frac{1}{r_{12}} e^{-\sqrt{(-ME_2)}r_{12}/\hbar\lambda} [1 - e^{-r_{12}} - c(1-e^{-r_{12}})^2], \tag{23}$$

where c is a parameter. The values of b_2 corresponding to the prescribed value of a_2 calculated from equations (14), (15) and (18) are given in the final column of table 1. The agreement with the exact solution obtained from the differential analyzer is very close in this case (cf. figure 1 of Fröhlich *et al.* 1947).

In calculating the binding energy of the deuteron the a_2-b_2 curve obtained by Wilson from the differential analyzer was employed. For the energy $E_2(^1S)$ of the singlet state we use the approximate value

$$E_2(^1S) = 0. \tag{24}$$

Actually $E_2(^1\mathrm{S})$ is of the order of 10^5 eV, which leads to an error of 5 to 10 % in the determination of $b_2(^1\mathrm{S})$. Since, however, $b_2(^3\mathrm{S})$ will be found to have about twice the magnitude of $b_2(^1\mathrm{S})$, the relative error in b_3 and b_4 (cf. equation (20)) will be less than 5 %. The correct value will be used, however, in the calculations of § 7. It follows at once from (24) that $a_2(^1\mathrm{S}) = 0$ and from table 1 that $b_2(^1\mathrm{S}) = -1{\cdot}70$. Substituting from equations (5) and (19)

$$3\frac{F^2}{\hbar c}-\frac{G^2}{\hbar c} = 1{\cdot}70\,\frac{m}{M}. \tag{25}$$

Similarly for the triplet state,

$$E_2(^3\mathrm{S}) = -2{\cdot}19\,\mathrm{MeV},$$

so that

$$a_2(^3\mathrm{S}) = -0{\cdot}0023\left(\frac{M}{m}\right)^2. \tag{26}$$

From this equation a value can be assigned to $a_2(^3\mathrm{S})$ for each value of the meson mass m. If the corresponding value of $b_2(^3\mathrm{S})$ is $-b_2^m$, say, then

$$3\left(\frac{M}{m}\right)\left(\frac{F^2}{\hbar c}+\frac{G^2}{\hbar c}\right) = b_2^m,$$

which by virtue of equation (25) reduces to

$$\frac{F^2}{\hbar c} = \frac{m}{M}\,\frac{b_2^m+5{\cdot}10}{12}. \tag{27}$$

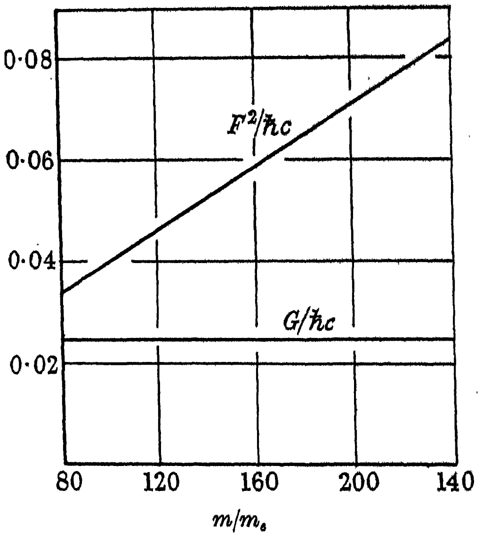

FIGURE 1. Variation in the field constants F^2, G^2 with meson mass m; first approximation.

Taking a set of values of the meson mass m, $a_2(^3\mathrm{S})$ can be calculated from equation (26). From the differential analyzer a_2-b_2 curve the value of b_2^m can be determined and $F^2/\hbar c$, $G^2/\hbar c$ calculated from equations (25) and (27). Thus from the deuteron energies it is possible to draw curves relating F^2 and G^2 to the meson mass m. These curves are shown in figure 1; they consist of two straight lines with equations

$$\frac{G^2}{\hbar c} = 0{\cdot}0246, \quad \frac{F^2}{\hbar c} = 0{\cdot}000306\frac{m}{m_e} + 0{\cdot}0085, \tag{28}$$

m_e denoting the electronic mass.

These values lead to the relation

$$(3F^2 + G^2)/\hbar c = 0{\cdot}000918\frac{m}{m_e} + 0{\cdot}0501, \tag{29}$$

which is equivalent to

$$b_3 = -3(g^2 + 3f^2) = -5{\cdot}067 + 0{\cdot}01503\frac{M}{m}. \tag{30}$$

4. THE HYDROGEN ISOTOPE H^3 (TRITON), FIRST APPROXIMATION

The binding energy of the hydrogen isotope H^3 is approximately determined by the variational method taking for ψ_3 a product of three two-body wave functions of the form

$$\psi_3(1,2,3) = \psi_2(1,2)\,\psi_2(2,3)\,\psi_2(3,1), \tag{31}$$

as has previously been suggested by Wigner (1932) and by Feenberg (1935). For the two-body wave functions $\psi_2(i,j)$ to be inserted into (31) the Wilson approximation

$$\psi_2(i,j) = e^{-\frac{1}{2}\alpha r_{ij}} \tag{32}$$

will be used. It may readily be verified (cf. figure 1 of Fröhlich *et al.* 1947) that the form of the wave function (21) is in satisfactory agreement with that of the function computed on the differential analyzer. Hulthén's wave function (23) is in still closer agreement with the mechanically computed function, but we have used the form (32), for the H^3 wave function because, despite its simplicity, the agreement with the exact function obtained by its use seems to be sufficiently good in view of the other approximations made.* The substitution of (32) into (31) leads to the form

$$\psi_3 = e^{-\frac{1}{2}\alpha(r_{12}+r_{23}+r_{31})} \tag{33}$$

for the wave function of H^3.

Now it follows from the Schrödinger equation for the deuteron that

$$\frac{e^{-r_{12}}}{r_{12}}\psi_2(1,2;\alpha) = \frac{1}{b_2(\alpha)}\left[\Delta_{12}\psi_2(1,2;\alpha) + a_2(\alpha)\,\psi_2(1,2;\alpha)\right], \tag{34}$$

where $a_2(\alpha)$ and $b_2(\alpha)$ are given by equations (22). From equations (15), (31) and (34) it may then readily be deduced that

$$J_3 = \frac{a_2(\alpha)}{b_2(\alpha)} + \frac{1}{b_2(\alpha)}\int \psi_3^* \Delta_{12}\psi_3 \Big/ \int \psi_3^*\psi_3. \tag{35}$$

By direct differentiation one finds

$$\Delta_{12}\psi_2 = \left(\frac{\alpha^2}{4} - \frac{\alpha}{r_{12}}\right)\psi_2. \tag{36}$$

---

* We have also calculated the average value of $1/r_{12}$ using the wave functions (21) and (23) and found agreement within 1 % for a wide range of energies.

If the notation
$$K_1 = \alpha^9 \int \psi_3^* \psi_3 = \int e^{-(r_{12}+r_{23}+r_{31})} \, d1 \; d2 \; d3, \tag{37}$$

$$K_2 = \alpha^8 \int \frac{\psi_3^* \psi_3}{r_{12}} = \int e^{-(r_{12}+r_{23}+r_{31})} \frac{1}{r_{12}} \, d1 \; d2 \; d3 \tag{38}$$

is introduced so that K_1 and K_2 are pure numbers independent of α, then it follows at once from equations (35), (36), (37) and (38) that

$$J_3 = \frac{a_2(\alpha)}{b_2(\alpha)} + \frac{1}{b_2(\alpha)} \left(\frac{\alpha^2}{4} - \frac{\alpha K_2}{K_1} \right). \tag{39}$$

Similarly, it can be shown that

$$\Delta_1 \psi_3 = \left\{ \frac{\alpha^2}{2} - \alpha \left(\frac{1}{r_{12}} + \frac{1}{r_{13}} \right) + \frac{\alpha^2}{2} \frac{(\mathbf{r}_{12} \cdot \mathbf{r}_{13})}{r_{12} r_{13}} \right\} \psi_3;$$

so that using this result and the fact that

$$\int \frac{\psi_3^* \psi_3}{r_{12}} = \int \frac{\psi_3^* \psi_3}{r_{13}},$$

the integral I_3 in equation (14) can be expressed in terms of K_1, K_2 and a third integral

$$K_3 = \alpha^9 \int \frac{\mathbf{r}_{12} \cdot \mathbf{r}_{13}}{r_{12} r_{13}} \psi_3^* \psi_3 = \int \frac{\mathbf{r}_{12} \cdot \mathbf{r}_{13}}{r_{12} r_{13}} e^{-(r_{12}+r_{23}+r_{31})} \, d1 \; d2 \; d3 \tag{40}$$

by the formula
$$I_3 = \alpha^2 \left(\frac{1}{2} - \frac{2K_2}{K_1} + \frac{K_3}{2K_1} \right). \tag{41}$$

In equations (37), (38) and (40) the parameter α has been eliminated under the integrals by replacing $e^{-\alpha r_{ij}}$ by $e^{-r_{ij}}$, and correspondingly $(\alpha r_{ij})^n$ by r_{ij}^n. Integration over the space co-ordinates of the three particles after this transformation has been carried out is indicated by $d1 \; d2 \; d3$.

The elimination of the parameter α from the integral is made possible by the substitution (34). In view of the inaccuracy of ψ_2 this involves an error which in terms of its influence on the binding energy amounts to 10 % as will be shown in § 7. This error is not excessive though it could be avoided in the present case. The reason for maintaining (34) is to make use of the same type of approximation for both H^3 and He^4 calculations. For the latter case the elimination of the parameter from the corresponding integrals is imperative unless one is prepared for numerical work of an amount that was prohibitive for us.

Equation (18) with $n = 3$ and with the aid of equations (39) and (41) now yields the result

$$a_3(\alpha) = -\tfrac{3}{2}\alpha^2 \left(\frac{1}{2} - \frac{2K_2}{K_1} + \frac{K_3}{2K_1} \right) + \frac{b_3}{b_2(\alpha)} \left(a_2(\alpha) + \frac{\alpha^2}{4} - \frac{\alpha K_2}{K_1} \right). \tag{42}$$

The evaluation of the integrals K_1, K_2, K_3 defined by equations (37), (38) and (40) is straightforward (cf. Appendix A 3); it turns out that

$$\frac{K_2}{K_1} = \frac{5}{7}, \quad \frac{K_3}{K_1} = \frac{3}{7}. \tag{43}$$

Equation (42), together with the relations (22) and (43), gives finally

$$a_3(\alpha) = \tfrac{15}{14}\alpha^2 + b_3\frac{\alpha^3(5\alpha+8)}{7(\alpha+1)^3}. \tag{44}$$

The condition $$\frac{\partial a_3}{\partial \alpha} = 0$$

then gives rise to the parametric equations

$$b_3 = -\frac{15(1+\alpha)^4}{\alpha(5\alpha^2+20\alpha+24)}, \tag{45}$$

$$a_3 = -\frac{15\alpha^2(5\alpha-4)(\alpha+2)}{14(5\alpha^2+20\alpha+24)}, \tag{46}$$

for the relation between a_3 and b_3. By assigning a set of values to the parameter α a curve can be drawn to show the relation of a_3 to b_3. Such a curve is shown in figure 2. Now for each value of the meson mass m the value of b_3 can be determined from equation (30), and from figure 2 the corresponding value of a_3 (and hence by equation (11) of E_3) can be found.

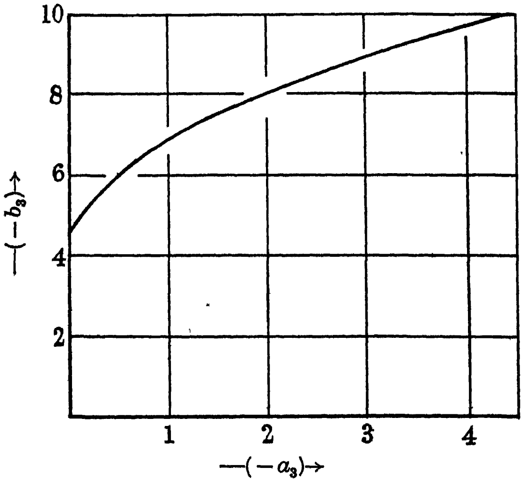

FIGURE 2. Relation between a_3 and b_3 for the H^3 nucleus.

The dependence of the theoretical binding energy E_3 on the value of the meson mass m is shown in table 2.*

TABLE 2

m/m_e	160	180	200	220	240	260	280
$-E_3$(MeV)	6·427	7·044	7·582	8·146	8·741	9·512	10·275

The experimental value of the binding energy of H^3 is (Mattauch & Flügge 1942)

$$E_3 = -8{\cdot}30\,\text{MeV};$$

---

* The variation of E_3 with m is shown graphically in figure 2 of Fröhlich *et al.* (1947).

an interpolation of the values of table 2 shows that this binding energy corresponds to a meson mass $225m_e$. Substituting this value of m in equation (28) leads then to the values

$$m = 225m_e, \quad F^2/\hbar c = 0{\cdot}0774, \quad G^2/\hbar c = 0{\cdot}0246 \tag{47}$$

for the constants involved in the M.-R. interaction formula (1).

More accurate values will be given in § 7.

5. HELIUM (He^4)

As in the case of the H^3-nucleus it is assumed that the wave function of the helium nucleus is the product of two-body wave functions, i.e.

$$\psi_4 = e^{-\frac{1}{2}\alpha(r_{12}+r_{13}+r_{14}+r_{23}+r_{24}+r_{34})}. \tag{48}$$

The analysis proceeds along lines similar to those of the last section, using

$$\Delta_1\psi_4 = \left[\tfrac{3}{4}\alpha^2 - \alpha\left(\frac{1}{r_{12}}+\frac{1}{r_{13}}+\frac{1}{r_{14}}\right)+\frac{\alpha^2}{2}\left(\frac{(\mathbf{r}_{12}\,.\,\mathbf{r}_{13})}{r_{12}r_{13}}+\frac{(\mathbf{r}_{12}\,.\,\mathbf{r}_{14})}{r_{12}r_{14}}+\frac{(\mathbf{r}_{13}\,.\,\mathbf{r}_{14})}{r_{13}r_{14}}\right)\right]\psi_4. \tag{49}$$

If integrals L_1, L_2, L_3 are defined as pure numbers similar to K_1, K_2, K_3, namely, by the equations

$$L_1 = \alpha^{12}\int\psi_4^*\psi_4 = \int e^{-(r_{12}+r_{13}+r_{14}+r_{23}+r_{24}+r_{34})}\,d1\,d2\,d3\,d4, \tag{50a}$$

$$L_2 = \alpha^{11}\int\frac{\psi_4^*\psi_4}{r_{12}} = \int\frac{1}{r_{12}}\,e^{-(r_{12}+r_{13}+r_{14}+r_{23}+r_{24}+r_{34})}\,d1\,d2\,d3\,d4, \tag{50b}$$

$$L_3 = \alpha^{12}\int\frac{(\mathbf{r}_{12}\,.\,\mathbf{r}_{13})}{r_{12}r_{13}}\,\psi_4^*\psi_4 = \int\frac{(\mathbf{r}_{12}\,.\,\mathbf{r}_{13})}{r_{12}r_{13}}\,e^{-(r_{12}+r_{13}+r_{14}+r_{23}+r_{24}+r_{34})}\,d1\,d2\,d3\,d4, \tag{50c}$$

then from the definition (14) and equations (48), (49) and (50) it follows that

$$I_4 = \tfrac{3}{4}\alpha^2 - 3\alpha^2\frac{L_2}{L_1}+\tfrac{3}{2}\alpha^2\frac{L_3}{L_1}. \tag{51}$$

Similarly the formula

$$J_4 = \frac{a_2(\alpha)}{b_2(\alpha)}+\frac{1}{b_2(\alpha)}\left(\frac{\alpha^2}{4}-\alpha^2\frac{L_2}{L_1}\right) \tag{52}$$

can be deduced from the definition (15) and the equations (48), (34) and (50).

Substituting for I_4 and J_4 in equation (18) with $n = 4$ gives

$$a_4(\alpha) = \tfrac{3}{2}\alpha^2\left(4\frac{L_2}{L_1}-2\frac{L_3}{L_1}-1\right)-b_4\left(\frac{\alpha}{\alpha+1}\right)^3\left(1-(\alpha+3)\frac{L_2}{L_1}\right). \tag{53}$$

It does not seem to be possible to evaluate the integrals L_1, L_2, L_3 analytically; their values had therefore to be found numerically (cf. Appendix A 4). They are

$$\frac{L_2}{L_1}=\frac{597}{709}, \quad \frac{L_3}{L_1}=\frac{113}{709}. \tag{54}$$

Substituting from equations (54) into equation (53) gives finally

$$a_4(\alpha) = 3{\cdot}07\alpha^2 + b_4\left(\frac{\alpha}{\alpha+1}\right)^3 (1{\cdot}53 + 0{\cdot}842\alpha). \tag{55}$$

Minimizing this with respect to α leads to the equation

$$b_4 = -\frac{6{\cdot}14(1+\alpha)^4}{\alpha(4{\cdot}59 + 3{\cdot}368\alpha + 0{\cdot}842\alpha^2)}. \tag{56}$$

Equations (55) and (56) yield on the elimination of α the relation between a_4 and b_4 so that it is possible to plot an $a_4 - b_4$ curve similar to the $a_3 - b_3$ curve of figure 2.

Substituting the values (47) of the M.-R. constants into equations (5) and (19) gives

$$b_4 = -12{\cdot}60, \tag{57}$$

which corresponds to a value of $a_4 = -0{\cdot}79$ (with $\alpha \simeq 1{\cdot}13$) which is less than half of the experimental value

$$a_4 = -2{\cdot}0. \tag{58}$$

Because of this discrepancy it might be considered advisable to use the He^4 calculations, instead of H^3, together with the results of the deuteron calculations to determine the values of the constants m, F, G. If this is done it is found that the value of m turns out to be in the region of $500m_e$, a value which is in disagreement with that determined by cosmic-ray measurements.

An alternative interpretation of these results is possible however. The binding energy calculated from equation (55) is the difference between the kinetic and the potential energy, both of which are separately much larger. In fact, it can be shown from the $a_4 - b_4$ curve that the experimental value (58) of a_4 corresponds to a value

$$b_4 = -14{\cdot}74 = -12{\cdot}60 \times 1{\cdot}17, \tag{59}$$

which is only 17 % larger than that given by equation (57) calculated from the M.-R. constants (47). This suggests that the high value of the binding energy of the helium isotope He^4 is due to the existence of a non-static interaction which is about 20 % of the static interaction.

6. THE ENERGY DIFFERENCE $H^3 - He^3$

The energy difference $H^3 - He^4$, which is chiefly* made up of the difference in mass of the proton and neutron and of the Coulomb interaction C of the two protons in the He^3 nucleus, is very small in comparison with the binding energy of the H^3 nucleus. Let the exact masses of the He^3 and H^3 nuclei be denoted by He^3 and H^3, and those of the neutron and proton by N and P. Then when C is expressed in mass units

$$H^3 - He^3 = N - P - C. \tag{60}$$

From the experimental observations of the β-decay of H^3 (cf. Nielsen 1941; O'Neal 1941) it is known that

$$H^3 = He^3 + m_e + T/c^2, \tag{61}$$

---

* There is also a contribution due to the difference in the magnetic interaction between the magnetic moments of the nucleons. This term should be considerably smaller than the Coulomb energy, and will, therefore, be neglected.

where T, the kinetic energy of the emitted β-particle, is less than 15 kV, so that

$$T/c^2 < 0{\cdot}03m_e. \tag{62}$$

Furthermore (Mattauch & Flügge 1942)

$$N - P = 0{\cdot}00137M = 2{\cdot}52m_e. \tag{63}$$

Eliminating the differences $N+P$, $H^3 - He^3$ between equations (60), (61) and (63) leads finally to the formula

$$C = 1{\cdot}52m_e - T/c^2, \tag{64}$$

where T/c^2 satisfies the relation (62).

If the wave function of He^3 is assumed to be the same as that of H^3, the value of C can be calculated from perturbation theory by use of the operators representing the electric charge. The Coulomb interaction is then

$$C = \int \Psi_3^*(C_{12}+C_{23}+C_{31})\,\Psi_3 \Big/ \int \Psi_3^*\Psi_3 = 3\int \Psi_3^* C_{12}\Psi_3/\Psi_3^*\Psi_3,$$

where C_{12} denotes the operator

$$C_{12} = \lambda \frac{e^2}{r_{12}} \frac{1+\tau_z(1)}{2} \frac{1+\tau_z(2)}{2}.$$

Separating the wave function Ψ_3 into space-dependent and spin-dependent factors ψ_3 and ϕ_3 respectively, and noting that for ϕ_3 of the correct form (cf. Appendix A 2),

$$\int \phi_3^*(1+\tau_z(1))\,(1+\tau_z(2))\,\phi_3 = 8, \quad \int \phi_3^*\phi_3 = 6,$$

it can be shown that

$$C = \lambda e^2 \alpha \frac{K_2}{K_1} = \frac{K_2}{K_1}\alpha \frac{e^2}{\hbar c}\frac{m}{m_e} m_e c^2. \tag{65}$$

Now it was shown that $K_1/K_2 = \frac{5}{7}$, $m/m_e = 225$, and the value of α giving the correct value of the binding energy of H^3 is 1·60. Substituting these values into equation (65) gives finally

$$C = 1{\cdot}86m_e c^2. \tag{66}$$

The comparison of the theoretical value (66) and the experimental value (64) does not represent a strong test of the nuclear interaction potential employed in this paper but is a test for the H^3 wave functions. The fact that the two results differ by 20 % only seems to be rather satisfactory.

7. THE TRITON, SECOND APPROXIMATION

To obtain an estimate of the error involved in the above calculations the binding energy of H^3 will be calculated with the variational method, using two parameters α, β instead of one (similar to Brown 1939). Let α_i, β_i be the Pauli spin functions of the ith nucleon, and let ξ_i, η_i be the corresponding isotopic spin functions satisfying

$$\int \alpha_i^2 = \int \beta_i^2 = \int \xi_i^2 = \int \eta_i^2 = 1, \quad \int \alpha_i\beta_i = \int \xi_i\eta_i = 0, \tag{67}$$

where the integrations refer to the spin or the isotopic spin co-ordinates of the ith nucleon. Then the most general H^3 wave function satisfying the Pauli principle must be of the form

$$\Psi_3 = F(1,2,3)\,\xi_1\xi_2\eta_3 + F(3,1,2)\,\xi_1\eta_2\xi_3 + F(2,3,1)\,\eta_1\xi_2\xi_3, \tag{68}$$

where the function $F(1,2,3)$ depends on the space and the spin co-ordinates of the three nucleons, each set indicated by $1, 2, 3$, and

$$F(1,2,3) = -F(2,1,3). \tag{69}$$

Furthermore, to obtain a total spin of $\frac{1}{2}\hbar$ one requires

$$F(1,2,3) = G(1,2,3)\,\alpha_1\alpha_2\beta_3 + H(1,2,3)\,\alpha_1\beta_2\alpha_3 - H(2,1,3)\,\beta_1\alpha_2\alpha_3, \tag{70}$$

where the functions G and H depend on the space co-ordinates only, and satisfy

$$G(1,2,3) = -G(2,1,3). \tag{71}$$

Introducing now Ψ_3 into equation (12), making use of (68) to (71), (10) and (4), and carrying out the integrations over the spin and isotopic spin co-ordinates (cf. (67)), leads to

$$\begin{aligned} a_3 = \Bigg\{\int\Bigg[& -\frac{1}{2}\Big(G^*(1,2,3)\sum_{i=1}^{3}\Delta_i G(1,2,3) + 2H^*(1,2,3)\sum_{i=1}^{3}\Delta_i H(1,2,3)\Big) \\ & + (f^2+g^2)\,G^*(1,2,3)\frac{e^{-r_{12}}}{r_{12}}G(1,2,3) + 2(f^2-g^2)\,G^*(1,2,3)\frac{e^{-r_{23}}}{r_{23}}G(1,2,3) \\ & - 8f^2G^*(1,2,3)\frac{e^{-r_{23}}}{r_{23}}G(1,3,2) - 2(f^2-g^2)\,H^*(1,2,3)\frac{e^{-r_{12}}}{r_{12}}H(1,2,3) \\ & - 2(f^2+g^2)\,H^*(1,2,3)\frac{e^{-r_{13}}}{r_{13}}H(1,2,3) + 2(f^2-g^2)\,H^*(1,2,3)\frac{e^{-r_{23}}}{r_{23}}H(1,2,3) \\ & - 4f^2H^*(1,2,3)\frac{e^{-r_{12}}}{r_{12}}H(2,1,3) - 4(f^2+g^2)\,H^*(1,2,3)\frac{e^{-r_{13}}}{r_{13}}H(3,2,1) \\ & - 8f^2H^*(1,2,3)\frac{e^{-r_{23}}}{r_{23}}H(1,3,2) - 4f^2G^*(1,2,3)\frac{e^{-r_{23}}}{r_{23}}H(1,2,3) \\ & - 4f^2H^*(1,2,3)\frac{e^{-r_{23}}}{r_{23}}G(1,2,3) + 4(f^2-g^2)\,G^*(1,2,3)\frac{e^{-r_{23}}}{r_{23}}H(1,3,2) \\ & + 4(f^2-g^2)\,H^*(1,2,3)\frac{e^{-r_{23}}}{r_{23}}G(1,3,2)\Bigg]\Bigg\}\Bigg/\int[G^*(1,2,3)\,G(1,2,3) \\ & \qquad + 2H^*(1,2,3)\,H1,2,3)], \end{aligned} \tag{72}$$

where the remaining integrations have to be carried out over the space co-ordinates of the three nucleons.

The approximation used in § 4 can now be obtained by putting $G(1,2,3) \equiv 0$ and $H = \psi_3$. To obtain a better approximation put

$$G(1,2,3) \equiv 0, \quad H(1,2,3) = e^{-\frac{1}{2}\alpha(r_{12}+r_{23})-\frac{1}{2}\beta r_{13}} = H(3,2,1). \tag{73}$$

This seems to be a reasonable extension of equation (33) because $H(1,2,3)$ corresponds to the case in which the neutron 1 and the proton 3 have parallel spins and, therefore, attract each other in a similar way as in the ground (triplet) state of H^2. The interaction between 2 and 3 is weaker, corresponding rather to the virtual (singlet) state of H^2, and the interaction between 1 and 2 is of a similar order. One may thus expect the average distance between 1 and 3 to be smaller than the distance of 2 from 1 or 3. The alteration required if $G \neq 0$ is assumed will be estimated below. It may be expected to be small as G corresponds to a state in which the two neutrons repel each other, whereas their interaction with the proton is relatively weak (corresponding to the singlet state of H^2).

Introducing (73) into (72) one finds

$$a_3 = \left\{\int\left[-H(1,2,3)\sum_{i=1}^{3}\Delta_i H(1,2,3) - 6(f^2+g^2)\,H(1,2,3)\frac{e^{-r_{13}}}{r_{13}}H(1,2,3)\right.\right.$$
$$\left.\left.-12f^2 H(1,2,3)\frac{e^{-r_{12}}}{r_{12}}H(2,1,3)\right]\right\}\Big/\int 2H^2(1,2,3), \qquad (74)$$

where the integrations go over the space co-ordinates. They can be carried out in a similar way as the integrals in § 4.

Putting $$\gamma = \alpha/\beta$$
this leads to

$$a_3 = \frac{1}{4}\left\{\beta^2\left[\frac{10}{(1+\gamma)^4}+\frac{4}{\gamma(1+\gamma)^3}+\frac{1}{\gamma^2(1+\gamma)^2}+\frac{1}{\gamma^3(1+\gamma)}\right]\right.$$
$$-6\beta(f^2+g^2)\left[\frac{2}{\gamma(1+\gamma+1/\beta)^4}+\frac{2}{\gamma^2(1+\gamma+1/\beta)^3}+\frac{1}{\gamma^3(1+\gamma+1/\beta)^2}\right]$$
$$-12\beta f^2\left[\frac{2}{((1+\gamma)/2)((1+\gamma)/2+\gamma+1/\beta)^4}+\frac{2}{((1+\gamma)/2)^2((1+\gamma)/2+\gamma+1/\beta)^3}\right.$$
$$\left.\left.+\frac{1}{((1+\gamma)/2)^3((1+\gamma)/2+\gamma+1/\beta)^2}\right]\right\}\Big/\left\{\frac{4}{\gamma(1+\gamma)^5}+\frac{3}{\gamma^2(1+\gamma)^4}+\frac{1}{\gamma^3(1+\gamma)^3}\right\}. \qquad (75)$$

The minimum of a_3 was located by plotting a number of curves corresponding to different values of β with γ as variable parameter in each case. The values of the charge constants are known from (28) and (29) in terms of the meson mass. More accurate values due to Ramsey (1947) were used, however. They are obtained by replacing the energy (24) of the singlet state of H^2 by a more accurate value. The results are shown in table 3. The experimental binding energy $E_3 = -8{\cdot}30$ MeV thus corresponds to the following values for the parameters in the M.-R. interaction (1) (cf. (5)):

$$m = 220m_e, \quad F^2/\hbar c = 0{\cdot}0714, \quad G^2/\hbar c = 0{\cdot}0310. \qquad (76)$$

The meson mass is nearly the same as given in equation (47), but the force constants are somewhat altered. The value of $3F^2+G^2$, which was required for the H^3 and He^4 calculations, differs, however, only very slightly from the previous one, as can be seen by comparing the b_4-values (cf. (20)) of table 3 ($\sim 12{\cdot}3$) with equation (57).

TABLE 3

m/m_e	$-E_3$ (MeV)	$6(f^2+g^2)$	$12f^2$	$-b_4$
200	$-7{\cdot}66$	5·30	7·20	12·50
225	$-8{\cdot}50$	5·08	7·14	12·12
250	$-9{\cdot}60$	4·92	7·11	12·03

The small alteration of the meson mass compared with the first-order calculation is mainly due to a cancellation of the effect of altering the force constants by the effect of a more accurate calculation. Actually, using the same values for the constant as in § 4, i.e. those given by equation (47), one obtains $-E_3 = 9{\cdot}6\,\text{MeV}$. Most of the difference is, however, not due to the introduction of a second parameter, but to the previous use of equation (34) with a not quite accurate wave function ψ_2. To show this the previous wave function (33) was used to calculate $-E_3$ with the same values (47) for the parameters as before but without introducing (34). The result is 9·2 MeV. Thus the introduction of a second parameter improves the energy by only about 4 %. The values of the two parameters are $\alpha = 1{\cdot}47$, $\beta = 1{\cdot}84$. With the one parametric wave function (33) one finds $\alpha = 1{\cdot}6$.

To estimate the influence of the function $G(1, 2, 3)$ in (70) it was assumed that

$$G = A(r_{13}-r_{23})\,e^{-\frac{1}{2}\alpha(r_{12}+r_{23}+r_{31})}$$

and

$$H = e^{-\frac{1}{2}\alpha(r_{12}+r_{23}+r_{31})}, \tag{77}$$

where A and α are two parameters. The calculations can be carried out in a similar way as before. They show that the inclusion of the function G leads to an energy level which is about 3 % lower than that obtained by putting $A = 0$. Considering this as an additional decrease to the 4 % obtained by using the wave functions (73) leads to a meson mass of $212m_e$. It is, however, not certain that these two decreases do not overlap. The conclusion, therefore, must be that the meson mass is between 210 and $220m_e$.

The use of the wave functions (73) also leads to a slight decrease of the Coulomb energy (cf. (66)) to the value

$$C = 1{\cdot}77m_e c^2. \tag{78}$$

8. CONCLUSIONS

In the calculations outlined in the preceding sections the only exact ones are those for the deuteron obtained by Wilson by means of the differential analyzer. Approximate methods have had to be used in the calculations for H^3 and He^4, and for the latter the question of estimating the error in the energy value obtained is one of great difficulty. To obtain a coherent view it seemed desirable to use the same method of calculation for both H^3 and He^4. Such a method is mainly restricted by the difficulties of the four-body problem. It was possible, however, to improve the H^3 calculations (§ 7) and to show that in this case at least the method employed is sufficiently accurate to draw certain conclusions.

This will now be done on the assumption that the calculations are sufficiently accurate; subsequently the influence of the inaccuracies will be considered. The calculation of the binding energy of the deuteron and the H^3 nucleus with the M.-R. interaction has led to a value for the meson mass between $m = 210m_e$ and $m = 220m_e$ (§ 7). This is in fair agreement with the meson mass $m \sim 200m_e$ which (according to private communication by Dr Jánossy and Dr J. G. Wilson) is found to agree with all reliable cosmic-ray measurements. The calculated Coulomb energy of the He^3 nucleus is about 10 to 20 % higher than that deduced from experiment, which may also be considered as satisfactory agreement. Furthermore, in the paper by Fröhlich *et al.* (1947) (cf. also Ramsey 1947), it is shown that with the values of the constants of the M.-R. theory used in the present paper fair agreement between theoretical and experimental angular distribution of neutron-proton scattering is obtained, although it should be remembered that the present accuracy of the experiments (cf. Occhialini & Powell 1947) does not allow a detailed comparison.

It would thus seem that the M.-R. interaction (1) with the values (76) for the constants is a good '*static*' approximation to the interaction between two nucleons. Using this interaction (cf. § 5) the binding energy for He^4 was found to be less than half of the observed value. The correct value can be obtained, however, by increasing the interaction energy (1) by about 20 %, i.e. by a relatively small amount (because the binding energy is only about one-fifth of the absolute value of the potential energy). If the constants of the M.-R. theory are chosen in such a way that the He^4 (and not the H^3) binding energy is in agreement with experiment, the value $m \sim 500m_e$ would follow for the meson mass which is in disagreement with cosmic-ray data. It thus seems to follow that in He^4 an additional interaction is required which amounts to about 20 % of the static interaction, and which is of minor importance for H^3 or H^2. This would require the existence of many-body forces which in He^4 would be of much greater importance than in H^3. Such a many-body interaction has been discussed by various authors (e.g. Jánossy 1939; Primakoff & Holstein 1939). In the M.-R. theory such an interaction would be contained in the non-static terms. The conclusion to be drawn is thus that the static M.-R. interaction is a fair first approximation to the total interaction and accounts for the binding energies of H^2, H^3 and He^3. For He^4 the non-static terms become more important and should amount to about 20 % of the static terms* in order to reconcile the result of our calculation with the experimental value.

Consider now the influence of the inaccuracies of the calculations on these conclusions.

Approximate methods were introduced at two occasions:

(i) instead of solving the wave equations exactly a variational method was used; and

(ii) the integrations were simplified by using the substitution (34) with wave functions ψ_2 which are not quite accurate.

---

* Qualitatively it should be expected that the relative importance of many-body forces increases with the number of nucleons; for four nucleons, for instance, there are four three-body links, and one four-body link as compared with one three-body link in the case of three nucleons.

Both approximations lead to binding energies which are too small. For H^3 the error involved has been estimated in § 7, giving 10 % for approximation (ii). To estimate the error due to (i) more general wave functions of the correct symmetry were introduced, leading to an energy decrease of less than 7 % compared with the one-parametric wave functions. It seems that the error due to (i) should be of the same order.*

This indicates that the value for the meson mass given above is an upper limit, but that the actual (theoretical) value† (which would be obtained from an exact solution of the H^3 problem) is unlikely to be much lower than $200m_e$.

No corresponding estimate can be made for the He^4 calculations because of the difficulties involved in carrying out the relevant integrals. The mere introduction of the improved values (76) of the parameters does not lead to an appreciable change in a_4. To obtain the experimental result for the binding energy the relative errors in the He^4 calculations would have to be many times larger than for H^3. This seems to be unlikely. In fact, in view of the high symmetry of the He^4 nucleus one might expect the ψ_4-wave functions (48) to be even better than the ψ_3-wave functions (33). The main error would thus be due to the use of approximation (ii), involving equation (34). To estimate this error the integral $\int \frac{1}{r_{12}} e^{-\alpha(r_{12}+r_{23}+r_{13}+r_{14}+r_{24})}$ was calculated by direct integration and by the use of equation (34). The ratio of the latter to the former was found to be 0·92 for $\alpha = 1{\cdot}1$. The actual integrals required have a further factor $e^{-\alpha r_{34}}$ under the integral which prevents the possibility of direct integration. It may be hoped, however, that this factor does not essentially change the ratio. Using 0·92 for the ratio would bring the binding energy from $a_4 = -0{\cdot}79$ to $a_4 = -1{\cdot}2$, which is still considerably lower than the experimental value $a_4 = -2{\cdot}0$. The conclusion about the necessity of many-body forces in He^4 should, therefore, still hold, although the quantitative estimate of 20 % cannot be maintained.

The main conclusion, therefore, seems to be that the calculations of the present paper on the basis of the M.-R. theory do not lead to any disagreement with experiments on H^2, H^3 and He^3. They suggest that the binding energies of H^2, H^3 and He^3 but not that of He^4 can be accounted for by the static interaction; they also indicate the existence of many-body forces which would be of importance for He^4, and for heavier nuclei.‡ A more quantitative comparison was impossible in view of the difficulties of the four-body problem. The most suitable way to obtain a better view on the validity of the M.-R. theory would probably be to increase the accuracy as well as the range of experiments on neutron-proton and proton-proton scattering, and to attempt to obtain more accurate experimental values for the meson mass.

---

* It must be admitted, however, that the error might be larger because the general form of the wave functions may be rather important. Thus spatial wave functions, which are much simpler than those used by us, can be obtained by putting $\psi_n = \prod_{s=1}^{n} \chi(r_s)$, χ being a one-particle wave function. In this way the correlation between nucleons is entirely neglected, and the binding energies obtained are much smaller than those found with the wave functions (21), (33) and (48), as shown in Appendix A 1 and in figure 3. These simpler wave functions become, however, increasingly better the heavier the nucleus to which they are applied.

† Brown (1939) finds a similar value, although he does not use the M.-R. interaction.

‡ Similar conclusions have also been reached by Svartholm (1945) except for the sign.

The authors wish to express their gratitude to Dr J. C. P. Miller and to Dr H. O. Hartley for their help in connexion with the He^4 integrals which were carried out by the Scientific Computing Service (Director: Dr L. J. Comrie), and to the Grants Committee of the Royal Society for a grant covering the expenses of the computations.

APPENDIX

A 1. *Solution of n-nucleon problem by means of one-body wave functions*

If it is assumed that the spatial wave function can be written as a product of one-body wave functions of the form

$$\psi(\mathbf{r}_1 \dots \mathbf{r}_n) = \left(\frac{\alpha^3}{8\pi}\right)^n \exp\left(-\frac{\alpha}{2}\sum_{i=1}^{n} r_i\right),$$

then
$$I_n = \left\{\frac{\alpha^2}{4}\int e^{-\alpha r}\, r^2\, dr\, d\Omega - \alpha\int e^{-\alpha r}\, r\, dr\, d\Omega\right\}\Big/\int e^{-\alpha r}\, r^2\, dr\, d\Omega = -\frac{\alpha^2}{4}$$

and
$$J_n = \left(\frac{\alpha^3}{8\pi}\right)^2 \int e^{-\alpha r_1} r_1^2\, dr_1\, d\Omega_1 \int e^{-\alpha r_2 - r_{12}} \frac{r_2^2}{r_{12}}\, dr_2\, d\Omega_2.$$

Now the function

$$\Phi(\xi, \eta, \zeta) = (1+\xi^2+\eta^2+\zeta^2)^{-1} = (1+\rho^2)^{-1}$$

is the Fourier transform of the function

$$\phi(x, y, z) = \frac{1}{(2\pi)^{\frac{3}{2}}}\int \frac{e^{i(\boldsymbol{\rho}\cdot\mathbf{r})}}{1+\rho^2}\rho^2\, d\rho\, d\Omega = \left(\frac{\pi}{2}\right)^{\frac{1}{2}} \frac{e^{-r}}{r},$$

and similarly
$$\Theta(\xi, \eta, \zeta) = (\alpha^2+\rho^2)^{-2}$$

is the Fourier transform of
$$\theta(x, y, z) = \left(\frac{\pi}{2}\right)^{\frac{1}{2}} \frac{e^{-\alpha r}}{2\alpha}.$$

Then by application of the resultant theorem (Bochner 1932)

$$\int \Theta(\boldsymbol{\rho})\, \Phi(\boldsymbol{\rho})\, e^{-i(\boldsymbol{\rho}\cdot\mathbf{r})}\, d\boldsymbol{\rho} = \int \theta(\mathbf{r}')\, \phi(\mathbf{r}-\mathbf{r}')\, d\mathbf{r}',$$

it follows that

$$\int e^{-r_{12}-\alpha r_2} \frac{r_2^2}{r_{12}}\, dr_2\, d\Omega_2 = \frac{4\alpha}{\pi}\int \frac{e^{-i(\boldsymbol{\rho}\cdot\mathbf{r}_1)}}{(\rho^2+1)\,(\rho^2+\alpha^2)^2}\rho^2\, d\rho\, d\Omega$$

$$= \frac{4\pi}{r_1(1-\alpha^2)^2}\{[(1-\alpha^2)\, r_1 - 2\alpha]\, e^{-\alpha r_1} + 2\alpha e^{-r_1}\},$$

so that finally
$$J_n = \frac{\alpha^3(1+4\alpha+5\alpha^2)}{16(1+\alpha)^4}.$$

Substituting for I_n, J_n in equation (18)

$$a_n = \frac{n\alpha^2}{8} + b_n \frac{\alpha^3(1+4\alpha+5\alpha^2)}{16(1+\alpha)^4}, \tag{79}$$

so that

$$b_n = -\frac{4n(1+\alpha)^5}{\alpha(3+15\alpha+25\alpha^2+5\alpha^3)}, \tag{80}$$

as a result of differentiating with respect to α and setting $\partial a_n/\partial\alpha = 0$. Equations (79) and (80) are the parametric equations of the curve relating a_n to b_n.

If the quantities $\beta_n = 8b_n/n$, $\epsilon_n = 8a_n/n$ are introduced equations (79) and (80) may be written in the form

$$\epsilon_n = \alpha^2 - 2\alpha f(\alpha)/f'(\alpha), \quad \beta_n = -2\alpha/f'(\alpha), \tag{81}$$

where

$$f(\alpha) = \frac{\alpha^3(1+4\alpha+5\alpha^2)}{16(1+\alpha)^4}. \tag{82}$$

The ϵ_n–β_n curve defined by equations (81) and (82) is drawn in figure 3. The values of ϵ_n and β_n given by the two-body wave functions can also be calculated; the curves corresponding to $n = 2, 3, 4$ are also shown in figure 3. If the curve given by (81) were a good approximation these curves would all coincide.

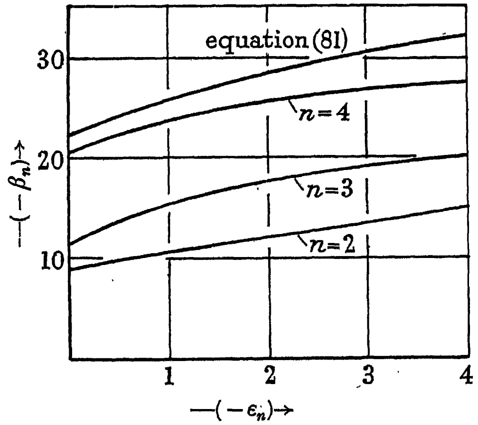

FIGURE 3. Comparison of solutions obtained by using one-body and two-body wave functions.

A 2. *Calculation of the spin integrals*

(*a*) *Deuteron* H^2

For the triplet state,

$$\phi_2(^3S) = \alpha_1\alpha_2(\xi_1\eta_2 - \eta_1\xi_2),$$

where the functions (ξ, η) refer to the isotopic spin and (α, β) to the spin.

For the singlet state

$$\phi_2(^1S) = (\alpha_1\beta_2 - \beta_1\alpha_2)(\xi_1\eta_2 + \eta_1\xi_2).$$

In both cases the calculation of b_2 is simple.

(*b*) *Hydrogen isotope* H^3

In this case

$$\phi_3 = \begin{vmatrix} \alpha_1\xi_1 & \alpha_1\eta_1 & \beta_1\xi_1 \\ \alpha_2\xi_2 & \alpha_2\eta_2 & \beta_2\xi_2 \\ \alpha_3\xi_3 & \alpha_3\eta_3 & \beta_3\xi_3 \end{vmatrix}.$$

The calculation of b_3 follows in a straightforward way from the expansion of this determinant.

(*c*) *Helium*, He^4

For the helium isotope He^4 the spin- and isotopic spin-dependent part of the wave function is the fourth-order determinant

$$\phi_4 = \begin{vmatrix} \alpha_1\xi_1 & \alpha_1\eta_1 & \beta_1\xi_1 & \beta_1\eta_1 \\ \alpha_2\xi_2 & \alpha_2\eta_2 & \beta_2\xi_2 & \beta_2\eta_2 \\ \alpha_3\xi_3 & \alpha_3\eta_3 & \beta_3\xi_3 & \beta_3\eta_3 \\ \alpha_4\xi_4 & \alpha_4\eta_4 & \beta_4\xi_4 & \beta_4\eta_4 \end{vmatrix},$$

which may be expanded according to the rule

$$\phi_4 = \sum_{i,k} (-1)^{i+k+1} (ik)\{ik\},$$

where the (ik) and $\{ik\}$ are second-order determinants, (ik) consisting of elements of the first and second rows and ith and kth columns, e.g.

$$(13) = \begin{vmatrix} \alpha_1\xi_1 & \beta_1\xi_1 \\ \alpha_2\xi_2 & \beta_2\xi_2 \end{vmatrix} = \xi_1\xi_2 \begin{vmatrix} \alpha_1 & \beta_1 \\ \alpha_2 & \beta_2 \end{vmatrix},$$

and $\{ik\}$ consisting of elements of the third and fourth rows but *neither* the ith *nor* the kth column, e.g.

$$\{13\} = \begin{vmatrix} \alpha_3\eta_3 & \beta_3\eta_3 \\ \alpha_4\eta_4 & \beta_4\eta_4 \end{vmatrix} = \eta_3\eta_4 \begin{vmatrix} \alpha_3 & \beta_3 \\ \alpha_4 & \beta_4 \end{vmatrix}.$$

All the (ik)'s and $\{ik\}$'s are normalized to 2; thus

$$\int (13)^2 \, d1\, d2 = \int \xi_1^2\xi_2^2(\alpha_1^2\beta_2^2 - 2\alpha_1\alpha_2\beta_1\beta_2 + \alpha_2^2\beta_1^2)\, d1\, d2 = 2$$

and similarly

$$\int \{13\}^2 \, d3\, d4 = 2.$$

Now

$$\int \phi_4^*(\boldsymbol{\sigma}_1.\boldsymbol{\sigma}_2)\phi_4 \, d1\, d2\, d3\, d4 = \int \sum_{\substack{i,k\\r,s}} (-1)^{i+k+r+s} (ik)\{ik\}(\boldsymbol{\sigma}_1.\boldsymbol{\sigma}_2)(rs)\{rs\}\, d1\, d2\, d3\, d4$$

$$= 2\sum_{i,k} \int (ik)(\boldsymbol{\sigma}_1.\boldsymbol{\sigma}_2)(ik)\, d1\, d2.$$

Similarly,

$$\int \phi_4^*(\boldsymbol{\sigma}_1.\boldsymbol{\sigma}_2)(\boldsymbol{\tau}_1.\boldsymbol{\tau}_2)\phi_4 \, d1\, d2\, d3\, d4 = 2\sum_{i,k} \int (ik)(\boldsymbol{\sigma}_1.\boldsymbol{\sigma}_2)(\boldsymbol{\tau}_1.\boldsymbol{\tau}_2)(ik)\, d1\, d2.$$

Now the application of the operator $(\boldsymbol{\sigma}_1 . \boldsymbol{\sigma}_2)$ to the six quantities (12), (34), (13), (24), $\frac{1}{2}[(14)+(23)]$, $\frac{1}{2}[(14)-(23)]$ is equivalent to multiplication by $+1$ for the first two and the last and by -3 for the remainder. The result of the operation $(\boldsymbol{\sigma}_1 . \boldsymbol{\sigma}_2)(\boldsymbol{\tau}_1 . \boldsymbol{\tau}_2)$ on all six is that of multiplying by -3. Hence

$$\int \phi_4^*(\boldsymbol{\sigma}_1 . \boldsymbol{\sigma}_2)\phi_4 = -24, \quad \int \phi_4^*(\boldsymbol{\sigma}_1 . \boldsymbol{\sigma}_2)(\boldsymbol{\tau}_1 . \boldsymbol{\tau}_2)\phi_4 = -72.$$

But
$$\int \phi_4^* \phi_4 = 24.$$

Thus
$$\sum_{i<j} \int \phi_4^*(\boldsymbol{\sigma}_i . \boldsymbol{\sigma}_j)\phi_4 \Big/ \int \phi_4^* \phi_4 = -6,$$

$$\sum_{i<j} \int \phi_4^*(\boldsymbol{\sigma}_i . \boldsymbol{\sigma}_j)(\boldsymbol{\tau}_i . \boldsymbol{\tau}_j)\phi_4 \Big/ \int \phi_4^* \phi_4 = -18,$$

giving finally
$$b_4 = -6(g^2 + 3f^2).$$

A 3. *Evaluation of the* H³ *integrals*

The evaluation of the integrals involved in the calculations of the binding energy of H³ is simple. It is of advantage to take the three distances r_{12}, r_{23}, r_{31} as independent co-ordinates, and integrate over the relative distances only. This leaves the integration over the position in space of the triangle 1–2–3. This integration need not be carried out, as it leads to the same multiplicative factor for all the integrals. Furthermore, following Hylleras, introduce elliptic co-ordinates

$$s = r_{12} + r_{23}, \quad t = r_{12} - r_{23}, \quad u = r_{13}.$$

The volume element is then given by

$$d\tau = \pi^2 u(s^2 - t^2)\, ds\, dt\, du,$$

and the limits are
$$-u \leqslant t \leqslant u, \quad 0 \leqslant u \leqslant s < \infty.$$

With this substitution all integrals can be carried out quickly and in an elementary way.

A 4. *The* He⁴ *integrals*

We found it impossible to integrate analytically the integrals L_1, L_2 and L_3 defined by equations (50). We found, however, that following a suggestion by Coulson (1937) the angular part of the integrations can be carried out, and thus the integrals can be reduced to a quickly converging series of triple integrals. To take L_1 (equation (50a)) as an example denote the vectors $\mathbf{r}_{12}$, $\mathbf{r}_{13}$ and $\mathbf{r}_{14}$ by $\mathbf{r}$, $\mathbf{s}$ and $\mathbf{t}$ respectively. Also let θ, Φ and Ω be the angles between $(\mathbf{r}, \mathbf{s})$, $(\mathbf{r}, \mathbf{t})$ and $(\mathbf{s}, \mathbf{t})$ respectively, and ϕ the azimuth around the $\mathbf{r}$-axis. Then according to Watson (1922)

$$e^{-r_{23}} = e^{-|\mathbf{r}-\mathbf{s}|} = \sum_{n=0}^{\infty} \frac{2n+1}{\sqrt{rs}} P_n(\cos\theta)\, p_n(r, s),$$

where the P_n are Legendre polynomials, and the $p_n(r,s)$ can be expressed in terms of products of Bessel functions. Similar expressions hold for $e^{-r_{24}}$ and $e^{-r_{34}}$. Thus

$$e^{-(r_{12}+r_{13}+r_{14}+r_{23}+r_{24}+r_{34})} = \frac{e^{-(r+s+t)}}{rst} \sum_{n=0}^{\infty} \sum_{m=0}^{\infty} \sum_{q=0}^{\infty} (2n+1)$$
$$\times (2m+1)(2q+1) P_n(\cos\theta) P_m(\cos\Phi) P_q(\cos\Omega) p_n(r,s) p_m(s,t) p_q(t,r).$$

Now $\cos\Omega = \cos\theta\cos\Phi - \sin\theta\sin\Phi\cos\phi$. Thus using the addition theorem for Legendre polynomials

$$\int_0^{2\pi} P_q(\cos\Omega)\,d\phi = 2\pi P_q(\cos\theta) P_q(\cos\Phi).$$

Next the integration over θ and Φ can be carried out. In view of the orthogonality of the P_n this reduces the triple sum into a single one, and one obtains

$$8\pi \frac{e^{-(r+s+t)}}{rst} \sum_{n=0}^{\infty} (2n+1) p_n(r,s) p_n(s,t) p_n(t,r).$$

There remain now the integrations over r, s and t which still require a great amount of computing.

To carry out the integrals (50) the Scientific Computing Service Ltd. was approached who put Dr H. O. Hartley in charge. Dr J. C. P. Miller, University of Liverpool, devised the methods to be used for the computations. The above sum was found to converge rapidly, and it was found sufficient to use the first three terms ($n = 0$, $n = 1$, $n = 2$). For all three integrals, the second term is less than 10 % of the first one.

REFERENCES

Amaldi, Bocciarelli, Feretti & Trabacchi 1942 *Naturwissenschaften*, **30**, 352; *Ric. Sci.* **13**, 502.
Bhabha 1938 *Proc. Roy. Soc.* A, **166**, 501.
Bochner 1932 *Vorlesungen über Fouriersche Integrale*. Leipzig: Akad. Verlag.
Brown 1939 *Phys. Rev.* **56**, 1107.
Coulson 1937 *Proc. Camb. Phil. Soc.* **33**, 104.
Feenberg 1935 *Phys. Rev.* **47**, 850; **48**, 906.
Fröhlich, Heitler & Kemmer 1938 *Proc. Roy. Soc.* A, **166**, 154.
Fröhlich, Ramsey & Sneddon 1947 *Proc. Phys. Soc.* (in the Press).
Hulthén 1942 *Ark. Mat. Astr. Fys.* **28**, no. 5.
Janossy 1939 *Proc. Camb. Phil. Soc.* **35**, 616.
Mattauch & Flügge 1942 *Kernphysikalische Tabellen*. Berlin:
Møller & Rosenfeld 1940 *K. Danske Vidensk. Selskab. mat.-fys. Medd.* **17**, no. 8.
Nielsen 1941 *Phys. Rev.* **60**, 160.
Occhialini & Powell 1947 *Proc. Phys. Soc.* (in the Press).
O'Neal 1941 *Phys. Rev.* **60**, 359.
Primakoff & Holstein 1939 *Phys. Rev.* **55**, 1218.
Ramsey 1947 *Proc. Roy. Soc.* A (in the Press).
Rosenfeld 1945 *K. Danske Vidensk. Selskab. mat.-fys. Medd.* **23**, no. 13.
Rosenfeld 1947 *Proc. Phys. Soc.* (in the Press).
Svartholm 1945 Thesis, Lund.
Watson 1922 *Theory of Bessel functions*, p. 366. Camb. Univ. Press.
Wigner 1932 *Phys. Rev.* **43**, 252.
Wilson 1938 *Proc. Camb. Phil. Soc.* **34**, 365.
Yukawa, Sakata, Kobayasi & Taketani 1938 *Proc. Phys. Math. Soc. Japan*, **20**, 319, 720.

An X-ray study of horse methaemoglobin. I

BY JOY BOYES-WATSON, EDNA DAVIDSON AND M. F. PERUTZ

Cavendish Laboratory and Molteno Institute, University of Cambridge

(*Communicated by Sir Lawrence Bragg, F.R.S.—Received* 3 *February* 1947)

[Plates 5 and 6]

The paper describes a detailed study of horse methaemoglobin by single crystal X-ray diffraction methods. The results give information on the arrangement of the molecules in the crystal, their shape and dimensions, and certain features of their internal structure.

Horse methaemoglobin crystallizes in the monoclinic space group $C2$ with two molecules of weight 66,700 per unit cell. In addition, the wet crystals contain liquid of crystallization which fills 52·4% of the unit cell volume. Deliberate variations in the amount and composition of the liquid of crystallization, and the study of the effects of such variations on the X-ray diffraction pattern, form the basis of the entire analysis.

The composition of the liquid of crystallization can be varied by allowing heavy ions to diffuse into the crystals. This increases the scattering contribution of the liquid relative to that of the protein molecules and renders it possible to distinguish the one from the other. The method is analogous to that of isomorphous replacement commonly used in X-ray analysis. It yielded valuable information on the shape and character of the haemoglobin molecules and also led to the determination of the phase angles of certain reflexions.

The amount of liquid of crystallization was varied by swelling and shrinkage of the crystals. This involves stepwise, reversible transitions between different well-defined lattices, each being stable in a particular environment of the crystal. The lattice changes were utilized in two different ways: the first involved comparison of Patterson projections at different stages of swelling and shrinkage, and the second an attempt to trace the molecular scattering curve as a function of the diffraction angle.

The results of the analysis can be summarized as follows. The methaemoglobin molecules resemble cylinders of an average height of 34 A and a diameter of 57 A. In the crystal these cylinders form close-packed layers which alternate with layers of liquid of crystallization. The layers of haemoglobin molecules themselves do not swell or shrink, either in thickness or in area, except on complete drying, and lattice changes merely involve a shearing of the haemoglobin layers relative to each other, combined with changes in the thickness of the liquid layer. Thus the molecules do not seem to be penetrated by the liquid of crystallization, and their structure is unaffected by swelling and shrinkage of the crystal.

Space-group symmetry requires that each molecule consists of two chemically and structurally identical halves. Evidence concerning the internal structure of the molecules comes both from two-dimensional Patterson projections and one-dimensional Fourier projections. The former indicate that interatomic vectors of 9 to 11 A occur frequently in many directions, and the latter show four prominent concentrations of scattering matter just under 9 A apart along a line normal to the layers of haemoglobin molecules. No structural interpretation of these features is as yet attempted.

The liquid of crystallization consists of two distinct components: water 'bound' to the protein and not available as solvent to diffusing ions, and 'free' water in dynamic equilibrium with the suspension medium. An estimate of the 'frictional ratio' based on the molecular shape and hydration found in this analysis is in good agreement with the frictional ratio calculated from the sedimentation constant.

1. INTRODUCTION

(*a*) *Background and scope of research*

The molecular structure of the crystalline proteins is one of the major unsolved problems in biology to-day. During the last 25 years the recognition of their ubiquity and paramount importance in plant and animal metabolism has set in motion a vast volume of research into the functions and properties of proteins. Numerous biological, chemical and physical methods have been applied to their study and have led to the gradual emergence of a coherent picture of *protein constitution*. The striking advances which have been made in the methods of amino-acid analysis have led to the determination of almost complete balance sheets of the amino-acid composition of certain proteins (Chibnall 1945), and are beginning to yield information on the number of separate polypeptide chains of which protein molecules are composed, on the sequence of amino-acid residues within these chains, and on the types of chemical linkages between them (Synge 1943; Sanger 1945). Knowledge of *protein structure*, on the other hand, has so far been confined to protein fibres, where Astbury has shown polypeptide chains to follow certain structural patterns whose geometry is independent of the detailed amino-acid composition (see Astbury 1940, 1942). Among the crystalline proteins no such structural classes have as yet emerged. It is known that the molecules of crystalline proteins do not consist of single polypeptide chains coiled up in random fashion, but are probably composed of one or several chains of definite length and configuration, linked together to form particles of definite shape and dimensions, with a characteristic pattern of active side chains facing the solvent; though we can infer that such definite features exist we do not know what they are, and we possess only partial and indirect information regarding the molecular shape and dimensions.

Since the structure of the crystalline proteins is unknown, their classification has to be based on differences in solubility and isoelectric points. In many cases this classification has lost its meaning and should be replaced by a rational one based upon structural types. Thus there is need both for detailed investigations of the structure of individual crystalline proteins and for comparative studies of the structural characteristics of different types or groups of proteins. Perhaps the most powerful method for studying the molecular structure of intact proteins is single-crystal X-ray analysis. The present investigation is an attempt to derive the maximum information that this method can provide from a study of the crystal structure of horse methaemoglobin. This substance was chosen because it is available in large quantities, is stable and easy to crystallize, and contains only two molecules in a face-centred monoclinic unit cell. The research was begun in 1938. As the work was continued with various interruptions due to the war, short accounts of progress were published from time to time (Bernal, Fankuchen & Perutz 1938; Perutz 1939*a*, 1942*a* and *b*; Boyes-Watson & Perutz 1943). The results reported there have been substantially confirmed, with one exception, which will be discussed in § 4 (*a*) below.

The results of X-ray analyses of other proteins have recently been reviewed both by Crowfoot (1941) and by Fankuchen (1945) and need not be described here. A general account is also given by Cohn & Edsall (1943).

(*b*) *The argument*

The task of analysing the crystal structure of haemoglobin is of a complexity much greater than anything previously attempted in X-ray crystallography. In the presentation of what is admittedly a very limited advance towards the solution of this problem, the logical sequence of the argument tends to become lost among a mass of essential detail. For this reason an outline of the main points of the argument is given below.

(§ 4 (*b*), p. 92.) Determination of the unit-cell dimensions and space group of horse methaemoglobin crystals shows that there are two molecules of weight 66,700 in a face-centred monoclinic unit cell. The symmetry properties of the space group ($C2$) require that each molecule consists of two structurally and chemically identical halves. All structure amplitudes in this space group are complex with the exception of the $h0l$'s, i.e. the reflexions from lattice planes parallel to the b-axis. This means that an analysis of the structure in projection along the b-axis is less difficult than in other projections, since in this case the phase factors are reduced to signs of the amplitudes (i.e. the phase angles are 0 and π).

(§ 4 (*c*), p. 94.) In normal wet crystals only 47·6 % of the unit-cell volume is occupied by the haemoglobin molecules and the remainder consists of liquid. It is most important to know the composition or at least the density of this liquid, because such knowledge opens the way to finding the signs of some of the structure amplitudes. The density of the *liquid of crystallization*, as it was decided to call it, was calculated from the density of the wet crystals and their cell dimensions. The wet-crystal densities were found to vary as a function of the composition of the suspension medium even when the unit cell dimensions remained constant, thus proving that ions can diffuse through the crystals. The concentration of these ions, on the other hand, is always lower in the liquid of crystallization than in the suspension medium, which implies that the crystals contain a surplus of water. The presence of this surplus is attributed to protein hydration, i.e. water of solvation which is 'bound' to the polar groups of the protein molecules and which is therefore not available as solvent to the diffusing ions. The presence and the exact location of this 'bound' water come to play an important part in the X-ray analysis.

(§ 5 (*b*), p. 97.) One of the first steps of the analysis concerns the question whether the haemoglobin molecules themselves are sponge-like and take up the liquid or whether the liquid merely fills the spaces between them. This was investigated by what might in effect be called 'staining' the liquid of crystallization, i.e. by allowing heavy ions to diffuse into the crystal for the purpose of changing the scattering contribution of the liquid relative to that of the protein. It was found that the presence of heavy ions had a far more powerful influence on the intensities of the lowest order reflexions than on those of the higher orders, which gives a first indication that the bulk of the liquid lies between the molecules rather than within them.

(§ 5 (*c*), p. 101.) Experiments on swelling and shrinkage of the crystals confirm this conclusion and provide one of the most valuable clues about the structure, because they show the presence of alternate layers of protein and liquid parallel to the plane containing the a- and b-axes (henceforth called *the layer plane*). The protein layers themselves do not swell or shrink, except on complete drying, and lattice changes merely involve a shearing of the protein layers relative to each other, combined with changes in the layer spacing. Patterson projections indicate that the number of liquid layers per unit cell cannot be greater than two and is more likely to be one.

(§ 6, p. 106.) At this stage in the analysis it is useful to examine the likely shape and external dimensions of the haemoglobin molecules. Two arguments are used for this purpose, one based on considerations of packing in the *dry* crystals and the other on intensity changes produced by the introduction of heavy ions into the *wet* crystals. Both methods indicate that the protein layers consist of close-packed cylindrical molecules of approximately 57 A diameter with the cylinder axes normal to the layer plane. In the dry crystals the height of the cylinders is estimated as 34 A; in the wet crystals it must be either 34 or 17 A, depending on whether there are one or two liquid layers per unit cell. The liquid of crystallization fills the gaps between successive layers of cylinders and also the interstices between neighbouring cylinders within each layer. (See figure 13, p. 123).

(§ 7 (*a*), p. 111.) This information makes it possible to calculate curves for the electron-density distribution in the unit cell, projected on a line normal to the layer plane, on the basis of three simplified models. These models merely take account of the average electron density in the protein and liquid layers, respectively, and of their approximate thickness, without involving any assumptions as to the precise dimensions of the molecules or their internal structure. The first curve is calculated on the assumption that there is only one liquid layer per unit cell, and the other two curves on the assumption of two liquid layers. Introduction of heavy ions helps to distinguish between the three alternative models, by showing that the intensity changes among the reflexions from the layer plane (the $00l$ reflexions) are not compatible with the existence of more than one liquid layer per unit cell.

The further steps in the analysis are mainly concerned with the calculation of one-dimensional Fourier projections which should give a view of the electron-density distribution in the unit cell, projected on to a line normal to the layer plane. The determination of the signs of the $00l$ reflexions, needed for this purpose, is done by three partly independent methods which are referred to as the isomorphous exchange, the nodal point and the layer structure method. These will now be outlined in turn.

(§ 7 (*b*), p. 115.) The isomorphous exchange method consists in finding the signs of the amplitudes of the $00l$ reflexions by calculating the phase contributions of heavy ions introduced into the liquid and comparing them with the observed intensity changes. This can only be done provided the concentration of the ions and the boundaries of the regions which they occupy are at least approximately known. Although the density of the liquid of crystallization is known and the boundaries of the liquid regions are given by the shape and dimensions of the protein molecules, there remains a choice between two alternatives, each leading to entirely different results.

(§ 7 (*a*), p. 111.) When calculating the density at any point in the liquid layer it may either be assumed that the 'bound water' is uniformly distributed throughout the liquid of crystallization, in which case the concentration of solute ions *throughout* the liquid of crystallization would be much *lower* than in the suspension medium, as shown by its lower density. Alternatively, it may be assumed that the 'bound water' is directly attached to the protein molecules and that the concentration of solute ions in the remaining liquid (the 'free' liquid of crystallization available to diffusing ions) is *the same* as in the suspension medium. Since the 'bound' water would occupy a considerable amount of space, the second assumption, if valid, would also reduce the size of the regions through which solute ions can diffuse, and thus alter the dimensions of the liquid regions whose phase contribution it is desired to calculate. Fortunately, there is an obvious reversal of phase of the 001 reflexion at a certain salt concentration from which it can be shown to follow that the electron density in the 'free' liquid of crystallization must be the same as in the suspension medium, thus deciding in favour of the second assumption. At this point the way is clear for calculating the phase contributions of the heavy ions, and the signs of some of the 00*l* reflexions can be found, though not with complete certainty in every case.

(§ 7 (*c*), p. 117.) The nodal point method is an attempt to trace the curve of the molecular structure amplitude (the amplitude of the wave scattered by a single haemoglobin molecule at different angles) along a line normal to the layer plane. This curve itself cannot be found by direct experiment, but an outline of the square of the curve can be obtained by plotting the intensities of the 00*l* reflexions at different stages of swelling and shrinkage against the sine of the diffraction angle. The points where this intensity curve touches the abscissa should coincide with the 'nodal points' where the amplitude curve crosses the abscissa and changes sign. This method does not give the absolute signs, but it helps to find the relation between the signs of different reflexions, and thereby confirms and amplifies the information that can be derived from the isomorphous exchange method.

(§ 7 (*d*), p. 119.) The layer-structure method is an attempt to find the signs by trial and error. On the evidence of the Patterson projections it is thought that each protein layer contains secondary layers of scattering matter which are parallel to the layer plane and spaced 9 A apart. Assuming that the presence of the secondary layers determines the signs of the 00*l* reflexions, these signs are calculated for structures containing any number of layers between two and five, and it is shown that only a model with four layers gives a sign for the 002 reflexion which agrees with previously established evidence. This model gives the same distribution of signs as found by the combination of the other two methods.

(§ 7 (*e*), p. 120.) The three methods for finding the signs of the 00*l* reflexions are independent of each other only to a limited extent and none is entirely free from ambiguities. Yet the fact that, where the three methods are independent, they give consistent results, helps to establish confidence in the Fourier projections to which the usual, rigorous test of comparison between observed and calculated structure amplitudes cannot be applied. With the calculation of the one-dimensional Fourier projections the present analysis ends. Its implications are discussed in §§ 8 and 9, pp. 122 to 128.

2. PREPARATION OF CRYSTALS

Horse methaemoglobin solutions were prepared by the method of Keilin & Hartree (1935). The protein was crystallized in simple diffusion cells by dialysis of 10 ml. 1 % methaemoglobin solution against 30 to 40 ml. concentrated salt solution. Diffusion took place through cellophane membranes. Initially, great difficulties were encountered in preparing crops of sufficiently perfect crystals reproducibly. Attempts were made, therefore, to discover the factors influencing crystal size, habit and twinning. In series of experiments, temperature, rate of diffusion, protein and salt concentration, presence of colloidal impurities or dust particles and pH of the precipitating solution were tested as possible factors influencing growth, but none except pH and a factor which, for lack of a more precise definition, may be called the state of the protein had a decisive influence. The optimum pH for crystallization was found to be 7·2 to 7·3. At this hydrogen-ion concentration half-saturation with ammonium sulphate is sufficient to effect complete precipitation of the protein. As a rule, solutions made up of 2 parts $4\text{M-}(NH_4)_2SO_4$ + 1 part $2\text{M-}(NH_4)_2HPO_4$ were used for precipitating the protein. Alternatively, a solution containing $3\text{M-}K_2HPO_4 + 1\text{M-}HCl$ was employed. Dr E. F. Hartree devised another method for growing the crystals which was to prove of decisive importance in the X-ray analysis. Making use of the low solubility of methaemoglobin in the absence of salt he electrodialyzed a concentrated solution of methaemoglobin against tap water and produced an excellent crop of large single crystals after some 24 hr. The very concentrated solutions of methaemoglobin needed for this method can be obtained by oxidizing a mush of oxyhaemoglobin crystals with a few drops of saturated potassium ferricyanide solution. The linear dimensions of single crystals in a good crop vary from 0·1 to 1·5 mm.

3. CRYSTAL OPTICS AND THE ORIENTATION OF THE HAEM GROUPS

Methaemoglobin crystallizes in a monoclinic and an orthorhombic form which seem to be isomorphous with the α- and β-oxyhaemoglobin crystals described by Reichert & Brown (1909). The orthorhombic modification was only observed once, as part of a crop obtained by electrodialysis against tap water. These crystals exhibited low birefringence and pleochroism; they were metastable and dissolved before much work could be done on them. Their unit-cell dimensions and space group are described in the next section.

The monoclinic crystals proved remarkably stable and sometimes kept for years. They form plates parallel to (001) whose thickness diminishes visibly on drying. The only other faces developed are of the {110} type. The wet crystals show strong birefringence and pleochroism; dried crystals are always cracked and opaque, and their optics hard to observe. The wet crystals are exceedingly soft. They are also permeable to ions, a property which can be demonstrated in a variety of ways. For instance, if a drop of sodium azide solution is added to the suspension medium of acid methaemoglobin crystals on a slide, a colour change can be observed to proceed from the surface towards the centre of the crystals. If the change is followed with a microspectroscope, the absorption spectrum is seen to change from that of acid methaemoglobin to that of its addition compound azide-methaemoglobin. Similarly, the change from acid to alkaline methaemoglobin can be followed in the interior of the crystals by watching the changing absorption spectrum.

Since the two haemoglobin molecules in the monoclinic unit cell have the same orientation (as shown in the next section) and the distances between neighbouring molecules are much larger than the interatomic distances within them, it can reasonably be assumed that the optical anisotropy of the methaemoglobin crystals represents the intrinsic optical anisotropy of the molecules themselves, though a certain amount of form birefringence, due to the shape of the 'liquid regions' in the crystals, must be expected to contribute. The birefringence of the salt-free crystals was determined by cutting appropriate sections with a razor blade and measuring the path differences with a Berek compensator. The crystals are optically positive: $\alpha \wedge a = 16^\circ$, $\beta \| b$ and $\gamma \wedge c = 5^\circ$, $n_\gamma - n_\alpha = 0{\cdot}0070$ and $2V = 68^\circ$. This birefringence is an average for the wave-lengths transmitted by acid methaemoglobin, which include part of the red and yellow regions of the spectrum. During careful drying, the orientation of the optic axes remains unchanged with respect to the *a*-axis, whereas the angle β increases noticeably.

The pleochroism of the crystals has been described elsewhere (Perutz 1939 *a* and *b*) and will only be summarized in the light of recent additional evidence. It would be more appropriate to call it dichroism of the negative uni-axial type with equally strong absorption along β and γ, and weak absorption along α. All the absorption bands of the haemoglobin spectrum seem to be equally affected, no matter whether the crystals are in acid or alkaline medium, or whether they are transformed into azidemethaemoglobin. It was also shown that the dichroic properties of the crystals remain unchanged even if the methaemoglobin inside the crystals is split into globin and haemin. When interpreting those observations, it was assumed that maximum absorption took place when the electric vector of the incident light was parallel to the plane of the haemin molecule, and on the basis of this assumption it was concluded that all the haem groups in the unit cell are approximately parallel to each other and are oriented normal to α. (See figure 12, p. 123).

That assumption has since been verified by a preliminary optical and X-ray study of crystalline haemin itself (Perutz & Rogers, unpublished 1945), which showed that in haemin crystals the flat molecules are arranged in parallel stacks. When viewed in polarized light with the electric vector parallel to the plane of the haemin molecules, the crystals appear opaque; they are transparent and pale yellow if the electric vector is normal to that plane, exactly as expected. Thus the *orientation* of the haem groups with respect to the optic axes in methaemoglobin crystals seems certain, though their *position* in the unit cell has yet to be determined.

4. UNIT-CELL DIMENSIONS AND SPACE GROUP

(a) *Experimental technique*

For the purpose of taking X-ray pictures, wet haemoglobin crystals are mounted as follows. Capillaries of either borosilicate glass or quartz are prepared, with a wall thickness of 0·01 to 0·02 mm., a bore of about 1 mm. and a length of about 30 mm. A single protein crystal is isolated on a slide with the help of a dissecting needle and drawn into the capillary with a drop of mother liquor. A firm cotton thread, made by twisting cotton-wool between the fingers, is now introduced half-way into the capillary and the liquid drawn off very gently through the thread, leaving the crystal behind. The thread is now withdrawn and the liquid re-introduced into both ends of the capillary, if necessary with the help of a hypodermic syringe, but leaving the crystal itself clear. After this operation the ends of the capillary are sealed with picein (figure 1). This method of mounting has the advantage of keeping the crystal in equilibrium with its former suspension medium and yet avoids it actually being suspended in liquid; without this precaution it is difficult to keep crystals stationary during exposures.

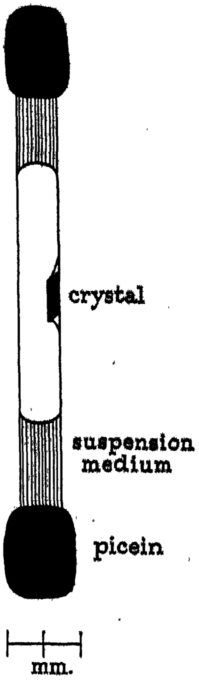

FIGURE 1. Wet protein crystal mounted for X-ray diffraction work.

The capillary is mounted on an X-ray goniometer in the usual way, and oscillation photographs are taken at specimen-to-film distances ranging from 5 to 10 cm. A typical series of oscillation photographs is shown in figures 14 to 19, plate 5. The

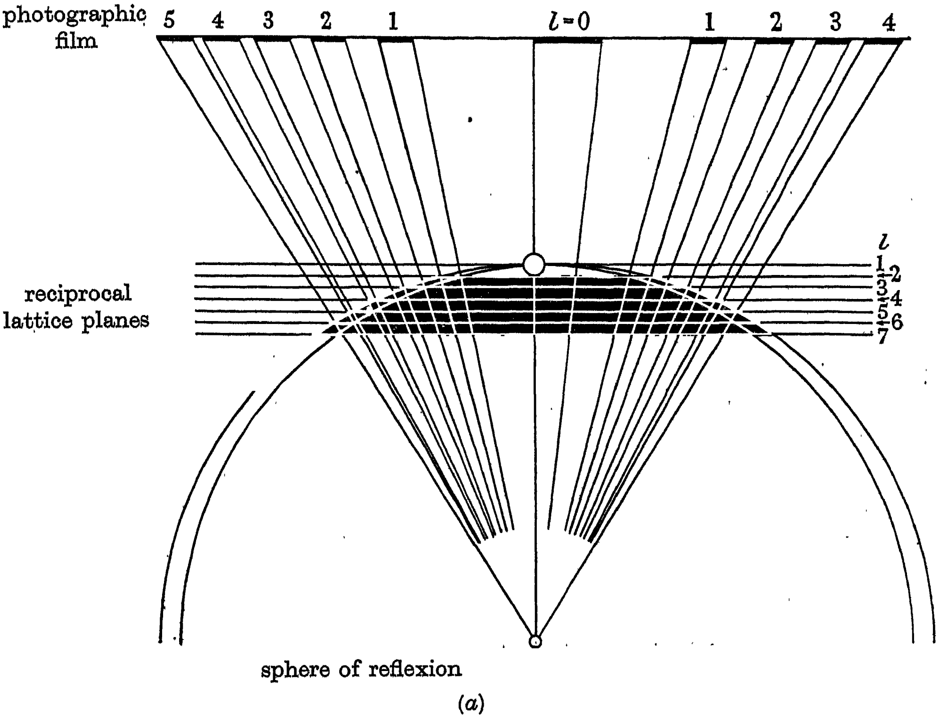

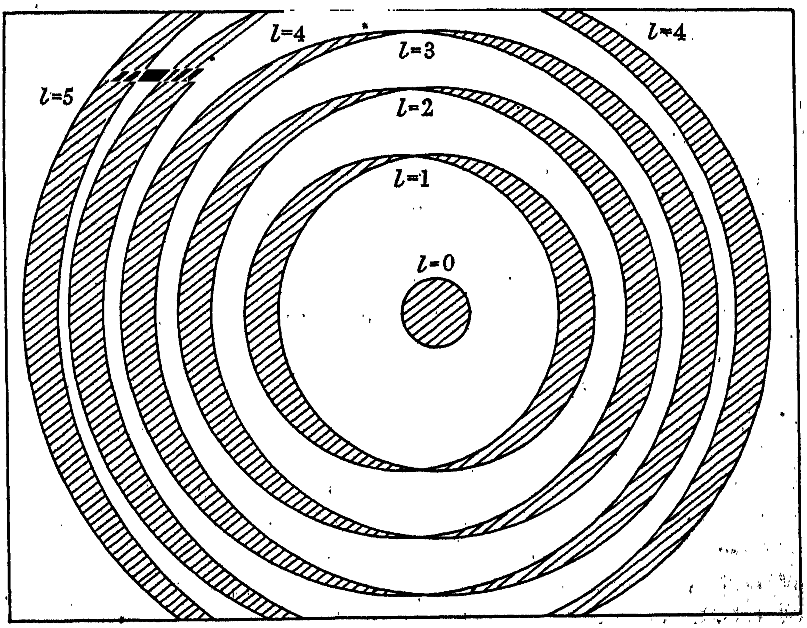

FIGURE 2. Reciprocal lattice planes of horse methaemoglobin and sphere of reflexion, illustrating the arrangement of reflexions on oscillation photographs in the form of concentric annular regions. (Cu $K\alpha$-radiation, 3° oscillation.)

reflexions occur in a series of concentric annular regions whose origin is explained in figure 2. Each ring on the photograph represents part of a reciprocal lattice plane intersecting the sphere of reflexion. Reciprocal lattice planes passing through the origin give rise to rings which pass through the centre of the photograph. On plate 5 that central ring has the index $l = 0$, and the reflexions on it can be indexed simply by counting from the centre. Systematic absences are often obvious from mere inspection of the pictures.

When measuring cell dimensions, errors due to absorption are not easily avoided. It is always advisable to plot spacing against $\sin\theta$, but even so the best accuracy that could be attained did not exceed 1/300, due to the fading out of the reflexions beyond $\sin\theta/\lambda = 0{\cdot}19$. In the absence of a suitable moving-film camera, all records of intensities had to be made on series of oscillation photographs. In order to register the $hk0$ reflexions, for example, three series of six oscillation pictures were taken about [100], [110] and [010] (figures 14 to 19, plate 5, show one such series).

Satisfactory dried crystals are difficult to prepare, because rapid shrinkage and crystallization of salt between mosaic blocks of crystalline protein tends to disrupt the crystals and to destroy most of the diffraction pattern. The best dried specimens were finally obtained by immersing salt-free wet crystals in pure xylene which is hygroscopic and absorbs the intracrystalline water very gradually, without itself penetrating the crystals. Air-scattering often obscured the feeble pattern of the dried crystals; this has now been eliminated by placing the X-ray goniometer in a vacuum tank (Perutz & Rogers 1946).

(*b*) *Cell dimensions*

The cell dimensions of the monoclinic and orthorhombic modifications of horse methaemoglobin, both in the wet and in the dried state, are given in table 1. The cell dimensions of the wet monoclinic crystals are independent of the medium in which the crystals are grown (see § 2), nor do they vary in crystals prepared from the blood of different horses. Their swelling in different suspension media will be described below.

The unit-cell dimensions of dried crystals vary according to the method of drying. Table 1 shows four different sets of cell dimensions, three obtained by drying in air and the fourth by drying in xylene. Evidently the haemoglobin molecules can pack together in a variety of ways, giving loose or closely packed structures according to the rate of drying, presence of salt and other factors. The last row of figures shows that these factors also affect the degree of order in the crystal, leading to a variation in the observed minimum spacing between 7 and 13 A. In no case is the degree of order in the dried crystals as good as in the wet.

Crystals dried from 25 % alcohol were used for determining the number of molecules in the unit cell. Their density, measured by flotation in toluene-bromobenzene mixtures, was 1·270 and their water content 7·4 %, giving a net protein weight of

Table 1. Unit-cell dimensions of normal wet and of dried crystals

All measurements are in Ångström units. The unit-cell numbers in this table and in table 3 were chosen so as to conform with the numbers on figure 6 of a previous paper (Perutz 1947).

symmetry ...	monoclinic					orthorhombic	
unit-cell number ...	5	9	2	1	10	11	12
description	normal wet	dried rapidly from $(NH_4)_2SO_4$ solution	dried slowly from $(NH_4)_2SO_4$ solution	dried from 25 % alcohol	salt-free crystals dried in xylene	wet	air-dried
a	109	102	104	102	107	122	95
b	63·2	56	63·2	51·4	60	82·4	72
c	54·4	49	54·1	47	53·2	63·7	61
$c \sin \beta$	50·7	36	36·5	36	32	—	—
β	111°	134°	137·5°	130°	143°	—	—
cell volume	349,000	206,000	242,000	189,000	204,000	2 × 320,000	2 × 208,000
minimum spacing observed	2·5	13	8	13	7·5	3	9

Table 2. Crystal composition in different suspension media

suspension medium	density of medium at 18° C	D (crystal density)	d_{li} (apparent density of liquid of crystallization)	composition of suspension medium	apparent composition of liquid of crystallization	w ('bound' water in g./g. protein)	electron density of suspension medium in electrons/A^3
A	1·0	1·160	1·0	tap-water	tap-water	—	0·33
B	1·186	1·218	1·118	2·5 M-$(NH_4)_2SO_4$ + 0·4 M-$(NH_4)_2HPO_4$	1·5 M-$(NH_4)_2SO_4$ + 0·2 M-$(NH_4)_2HPO_4$	0·3	0·39
C	1·309	1·274	1·210	2·4 M-K_2HPO_4 + 0·8 M-HCl	1·6 M-K_2HPO_4 + 0·5 M-HCl	0·25	0·43
D	1·410	1·355	1·368	3·3 M-K_2HPO_4 + 1·1 M-HCl	2·9 M-K_2HPO_4 + 1 M-HCl	0·1	0·45

Table 3. Change of unit-cell dimensions on swelling and shrinkage

$a = 109$ A and $b = 63·2$ A in all unit cells listed here.

unit-cell number ...	3	4	5	6	7
description	intermediate shrinkage stages		normal wet	expanded in dilute $(NH_4)_2SO_4$ solution, unneutralized	expanded in acid media below pH 5·5
c	53·5	51·4	54·4	55·4	54·6
$c \sin \beta$	42·3	46·1	50·7	54·9	54·4
β	127·5°	116°	111°	98°	84·5°
cell volume	292,000	318,000	349,000	378,000	375,000
volume % liquid in unit cell	43·1	47·8	52·4	56·0	55·8

2 × 66,700 (± 3500).* (Ammonium sulphate had been removed by washing with 25 % alcohol at 0° C.) There are thus two molecules in the monoclinic unit cell.

If a similar density and water content are assumed for the dried orthorhombic crystals, it is found that they contain four molecules in the unit cell. It is interesting to note that the orthorhombic crystals, although found in the same crop with monoclinic ones, contain considerably less liquid per molecule than the latter, indicating that the amount of liquid is partly determined by the mode of packing of the protein molecules.

(c) *Composition, swelling and shrinkage*

The composition and swelling properties of protein crystals have been described in detail elsewhere (Perutz 1947). Though they form an important part of this study and are essential for the analysis which follows, space does not permit to give more than a summary here.

The permeability of wet methaemoglobin crystals to ions makes it possible to vary the composition of the liquid of crystallization within wide limits, while keeping the unit-cell dimensions unchanged. The converse experiment of keeping the composition of the liquid constant and varying the cell dimensions is more difficult. It succeeded, at least to a certain extent, in the case of swelling, but not of shrinkage experiments.

Table 2 shows an example of changes in the composition of the liquid of crystallization in the normal wet cell (number 5). (The four suspension media are those in which records of reflexions from complete zones were taken and later used for the work described in §§ 5, 6 and 7.) The pH of the salt solutions in each of the media was close to 7.

The figures given in table 2 were derived as follows. The crystal densities (D) were measured by the method of McMeekin & Warner (1942), as described by Perutz (1947). The apparent densities of the liquids of crystallization were calculated from the formula

$$d_{li} = \frac{VD - nM}{V - nMv_p}, \tag{1}$$

where d_{li} = apparent density of the liquid of crystallization, V = unit-cell volume in A^3, n = number of haemoglobin molecules per unit cell, M = molecular weight of haemoglobin in 10^{-24} g., D = crystal density, and v_p = partial specific volume of the anhydrous protein in solution. The apparent composition of the liquid of crystallization was derived from its density, on the assumption that the proportions of different ions inside the crystal are the same as in the suspension medium. The reasons for referring to the density and composition as apparent will become clear in the sequel. It is seen that the apparent density of the liquid of crystallization is considerably lower than that of the suspension medium, a fact which can readily be accounted for by the presence of 'bound water'.

---

* 66,700 is the best obtainable value for the molecular weight of horse haemoglobin, derived from analysis of its iron content on the assumption that there are four iron atoms per molecule. It is probably more accurate than the value of 68,000 often quoted in the literature and has been used in all our calculations. The close agreement between the unit-cell molecular weight and that derived from chemical analysis is purely fortuitous, since the error in the dry unit-cell volume may be as much as 5 % owing to the poor quality of the diffraction pattern.

'Bound water' is defined as water attached to the protein molecules and not available as solvent to the diffusing ions. It is calculated from the formula

$$w = \frac{v - v_m}{v_{H_2O} - v_m}\left(\frac{VD}{nM} - 1\right), \qquad (2)$$

where w means 'bound water' in g./g. protein, $v = 1/d_{li}$, v_{H_2O} is the specific volume of water, and v_m that of the suspension medium. This formula implies the existence of two distinct components in the liquid of crystallization, one of which is 'bound water' not available as solvent to the mobile ions and the other 'free liquid' through which ions can diffuse, and where the salt concentration is therefore the same as in the suspension medium. This division of the liquid of crystallization into two components may appear artificial, and as no more than a useful hypothesis, making protein hydration a well-defined and measurable quantity. On the other hand, it will be shown in the sequel that this hypothesis accounts for certain X-ray results which could not otherwise be interpreted and which lend considerable support to its validity (see § 7 (*a*)). In neutral ammonium sulphate solutions $w = 0{\cdot}3$ ($\pm\, 0{\cdot}03$) at all salt concentrations; the highly concentrated potassium phosphate solution of medium D is the only one where this value is significantly altered. This dehydrating effect, indicated by the reduction of w to 0·1, is accompanied by a considerable deterioration in the X-ray diffraction pictures.

The changes in cell dimensions which were observed during swelling and shrinkage are listed in table 3. Crystals were made to swell by suspending them in certain media such as unneutralized ammonium sulphate solutions of concentration $< 2{\cdot}6$ M (unit cell number 6) or $> 3{\cdot}2$ M (unit cell number 7). Unit cell number 7 was also observed in ammonium sulphate solutions buffered to pH $< 5{\cdot}5$. Shrinkage of the crystals was produced by piercing the capillary in which they were mounted (figure 1) and allowing the suspension medium (medium B) to dry up gradually. The medium had to reach supersaturation before any shrinkage could be observed.

With the exception of unit cell number 3 which was only observed once, all the lattice changes listed in table 3 proved to be both reproducible and reversible. Despite extensive search no unit-cell dimensions intermediate between those listed have been discovered, which indicates that swelling and shrinkage proceeds in discrete steps which form transitions between different stable lattices. As long as complete drying of the crystals is avoided, the only cell dimensions affected by swelling and shrinkage are c and β, the latter changing from 127·5° in unit cell number 3 to 84·5° in unit cell number 7. The fact that a and b remain constant is of great importance in the later analysis.

Figures 21 to 25, plate 6, are reproductions of a series of oscillation photographs taken in identical crystal settings at all stages of swelling and shrinkage listed in table 3. Figure 20 gives a diffraction picture from a completely dry crystal. The pictures show that short of complete drying the unit-cell dimensions can be altered over extraordinarily wide limits without causing the diffraction pattern to deteriorate very appreciably.

(*d*) *Space groups*

All photographs from monoclinic methaemoglobin crystals show hkl to be absent if $h+k$ is odd, no matter what the state of swelling or shrinkage happens to be. $I'_{hkl} = I'_{h\bar{k}l}$ on all photographs. Thus the possible space groups are $C2$, Cm and $C2/m$. In fact, both Cm and $C2/m$ can be excluded on account of the optic activity of haemoglobin in solution.* The space group $C2$ has four general positions. As there are only two haemoglobin molecules per unit cell, they must occupy special positions on the diad axes and must themselves possess twofold symmetry.

The orthorhombic crystals show the absences characteristic for the space group $P2_12_12_1$, which has four general positions. It is interesting that in this modification there are four haemoglobin molecules per cell, and therefore each must lie in a general position. Since it is unlikely that the same molecules possess different symmetries in the two polymorphous modifications, this result suggests that the crystal structure often does not reveal the full symmetry of protein molecules. This would be consistent with the low symmetry of the crystal structures observed in the case of many highly symmetrical organic compounds (e.g. coronene, Robertson 1945), where the full molecular symmetry rarely reveals itself in the form of space-group symmetry.

5. THE DIFFRACTION PATTERN

(*a*) *General characteristics; Patterson projections of normal unit cell*

The diffraction pattern of wet haemoglobin crystals extends to a spacing of 2·5 A, but indexing was not, as a rule, carried beyond a spacing of 2·8 A, since only isolated weak reflexions occur beyond this range. Even so the limiting sphere contains 62,700 reciprocal lattice points which symmetry reduces to 7840 reflexions relevant for analysis. Not counting the hydrogens each haemoglobin molecule contains approximately 5000 atoms; since the molecules lie on diad axes the number of independent parameters is therefore roughly 7500. If the amplitudes as well as the phase factors of the reflexions could be found, the data contained in the diffraction pattern should therefore suffice to determine the positions of all the atoms in the unit cell, though hardly with any accuracy. The structure amplitudes of all but the $h0l$ reflexions are complex, yet even if they were real the determination of their signs would at present be a hopeless task. Thus the only method capable of translating the wealth of information which the diffraction pattern contains into a form which could give information on the molecular structure of the protein is the Patterson-Fourier synthesis. *A priori*, even this holds out little prospect of success, since the theoretical number of vector peaks in the unit cell is of the order of 10^8.

---

* Mirror planes cannot exist in crystals containing only one optical isomer of an optically active compound.

Yet if the protein molecule possesses internal regularity, certain interatomic vectors should recur throughout the molecule, and, moreover, larger scattering masses corresponding to the backbones of polypeptide chains, say, should repeat at regular intervals. Thus the occurrence of pronounced maxima in vector density is not as unlikely as it appears at first sight. There should be little overlapping of inter- and intramolecular peaks, because the distance of separation of the molecules in the wet crystal is large compared to the prominent interatomic vectors to be expected within each molecule.

It was decided, in the first place, to calculate Patterson-Fourier projections along the three principal crystal axes for unit cell number 5 and suspension medium B (see tables 1 and 2, p. 93). Relative intensities were recorded on series of oscillation photographs, estimated visually and corrected by the usual factors. The Patterson projections are seen in figure 3*a*, *b* and *c*. Not only do they show very distinct maxima, but these maxima are distributed with a certain regularity, particularly in the *b* projection, a feature which was first pointed out by Crowfoot (1941). If a mesh of 9 × 9 A × 78° is super-imposed on the *b* projection such that one set of lines is parallel to the *a*-axis and the other is inclined at 9° to the *c*-axis, the majority of the prominent peaks coincide with the corners of the mesh. Similarly, the peaks in the *a* projection lie on lines parallel to *b* and spaced 9 A apart. The most prominent features of the *c* projection are two rings of peaks at distances of 10 to 11 and 20 to 22 A from the origin. Thus all projections indicate a spacing of scattering masses at 9 to 11 A apart, though the peak system in the *b* projection can be distinguished with greater clarity than in the other two, where the introduction of an artificial plane of symmetry normal to the *b*-axis tends to complicate matters. This meagre information is all that can be obtained from Patterson projections of the wet crystals without changing either the composition of the suspension medium or the unit-cell dimensions.

(*b*) *The effect of changes in the liquid of crystallization*

It has been mentioned that the scattering contribution of the liquid of crystallization can be altered relative to that of the protein by allowing heavy ions to diffuse into the crystal, and that by this method a distinction can be made between the sponge-like and the rigid models of protein structure. The distinction, which at this stage is purely qualitative, rests on the following argument: The general character of the X-ray diffraction pattern shows that the protein molecules in the wet crystals possess a highly ordered structure. Supposing the molecules imbibed liquid and ions could diffuse through them, these ions would have to pass through channels occupying definite positions in the unit cell. If there were many such channels passing through the molecules, the presence or absence of heavy ions in them would completely alter the electron density distribution in the unit cell and change profoundly the intensity distribution in the whole diffraction pattern. On the other hand, if the liquid merely filled the spaces between rigid protein molecules which are themselves impenetrable to liquid, the introduction of heavy ions would change

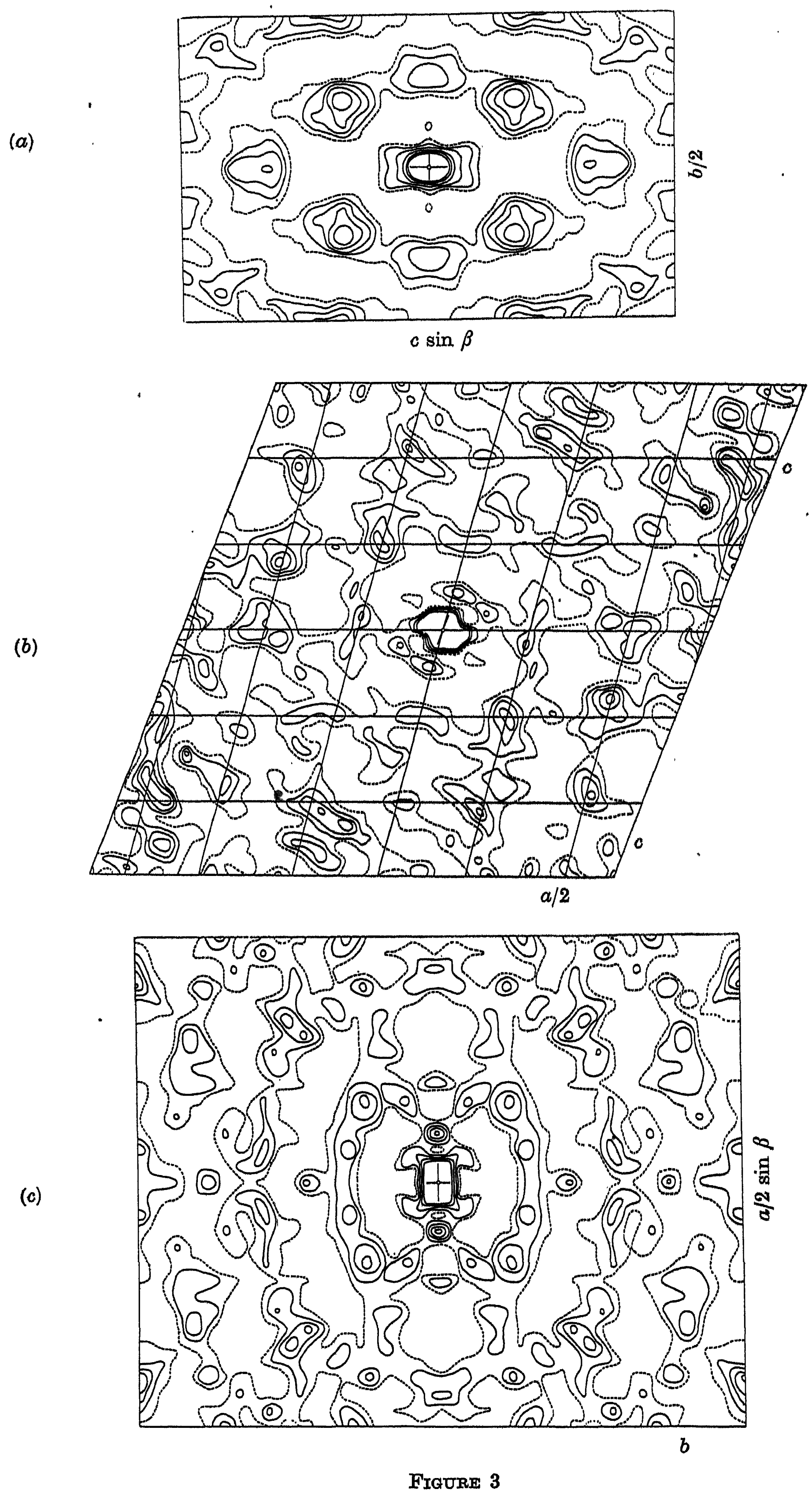

FIGURE 3

the electron density of broad regions in the unit cell without altering the distribution of scattering masses *within* the protein molecules. This would result in intensity changes among the lower order reflexions, but would have little influence on the distribution of intensities of the diffraction-pattern as a whole.

Complete records of the *h*0*l* reflexions were made for unit cell number 5 in suspension media A, B, C and D. Records of the *hk*0 and 0*kl* reflexions were confined to reflexions above 10 A spacing, since the *F*'s in both these zones are complex, and little interpretable information could be derived from the higher orders.

The general distribution of relative intensities in the *h*0*l* and *hk*0 reciprocal lattice planes seemed to be so little affected by the different suspension media that the calculation of Patterson projections in each case appeared unnecessary, since the close similarity of corresponding projections in different media was a foregone conclusion. An example of the intensity changes that occur is shown in table 4, giving the relative intensities of the *h*0*l* reflexions in tap water and ammonium sulphate solution. The relative contribution of the liquid is seen to be powerful at the smallest glancing angles and to diminish gradually as the glancing angle increases. Among the low order reflexions, the change in the intensity of 001 is outstanding, while 200 and $\overline{2}01$ are little affected, though their spacing is practically the same as that of 001. Among the higher order reflexions it is often difficult to distinguish real changes in intensity from errors in their estimation, particularly if the reflexions are weak, but there are some cases such as $\overline{6}.0.10$, $\overline{26}.0.7$, 20.0.1 where the observed changes are well beyond the limit of error.* On the other hand, the agreement among the majority of strong high-order reflexions is remarkably good (e.g. $\overline{10}.0.12$, $\overline{14}.0.12$, 2.0.12, $\overline{30}.0.4$). Among the *hk*0 reflexions 110 is the only one which is powerfully affected by the density of the liquid, while 200 and 020 show little change.

It is seen that the presence of heavy ions has a far more powerful effect on the intensities of the lowest order reflexions than on any of the higher order ones. This speaks strongly in favour of the view that the protein molecules are rigid and impenetrable to liquid rather than sponge-like. It is interesting that some reflexions such as 001 and 110 are particularly sensitive to changes in the liquid of crystallization, while other reflexions of similar spacings are hardly altered. This kind of information was found to be of great value for locating the positions of the 'liquid regions' in the unit cell.

---

* The limits of error are about 20 to 25 % for medium and high intensities, and 30 to 40 % for low ones.

Legend to Figure 3

FIGURE 3. Patterson-Fourier projections along the three principal crystal axes. The dashed lines indicate arbitrary zero levels; contours are drawn at arbitrary intervals and negative contours are omitted. The origins are at the centres of the projections and are marked by crosses (unit cell number 5; 1 cm. = 7 A). These projections were calculated by Dr D. P. Riley.

Table 4. Relative intensities of $h0l$ reflexions of normal wet crystals in medium B (black figures) and medium A (italics). Unit cell number 5

←—h +h→

+l	34	32	30	28	26	24	22	20	18	16	14	12	10	8	6	4	2	0	2	4	6	8	10	12	14	16	18	20	22	24	26	28	30	32	34	
0	—	—	—	—	—	—	—	—	—	—	—	—	—	—	—	—	—	—	6 *5*	11 *24*	— *9*	3 *5*	42 *25*	13 *11*	—	8 *9*	—	8 *6*	6 *5*	—	19 *8*	—	11 *13*	—	—	0
1	—	—	6	8 *14*	—	14 *9*	5 *6*	—	—	—	—	51 *43*	—	3	5	8	—	10 *95*	5 *3*	3 *11*	22 *16*	16 *8*	37 *23*	—	18 *8*	10 *6*	5 *5*	22 *12*	19 *16*	6 *5*	6 *9*	—	—	—	—	1
2	—	—	—	—	—	14 *16*	—	—	—	14 *12*	5 *11*	10 *10*	3	16 *13*	46 *53*	2 *6*	13 *25*	10 *34*	3 *4*	19 *36*	— *5*	3	14 *4*	— *1*	5 *3*	3 *13*	—	—	— *5*	—	— *6*	—	—	—	—	2
3	—	—	—	—	21 *13*	—	10 *6*	11 *7*	6	—	50 *48*	5 *6*	10 *9*	—	10 *14*	2 *5*	3 *1*	2 *7*	13 *16*	19 *19*	14 *11*	3 *6*	— *3*	5 *6*	5 *2*	11 *12*	—	8 *4*	—	—	4 *5*	—	—	—	—	3
4	3 *5*	—	14 *12*	—	6	—	5 *8*	—	10 *7*	5 *8*	—	38 *29*	—	14 *11*	16 *13*	8 *2*	6 *12*	5	11 *13*	6 *11*	14 *6*	—	10 *8*	5 *8*	6 *9*	21 *15*	—	8 *7*	—	—	— *5*	—	—	—	—	4
5	8 *5*	—	6	—	14 *15*	—	14 *11*	3	3	—	—	10 *13*	2	8 *14*	— *6*	26 *24*	16 *16*	21 *23*	35 *40*	—	32 *28*	—	—	29 *19*	—	—	5	— *4*	6	—	2 *7*	—	—	—	—	5
6	—	2	6 *11*	—	—	6 *7*	8 *6*	3 *4*	6 *7*	3 *3*	14 *14*	13 *13*	2	5 *7*	8	— *6*	—	46 *46*	—	10 *6*	10 *20*	—	11 *12*	—	5 *5*	—	—	—	— *4*	—	— *5*	—	—	—	—	6
7	—	5	5	—	34 *20*	—	18 *20*	5 *3*	11 *3*	34 *26*	—	29 *30*	2	—	38 *35*	—	—	11 *17*	—	3 *5*	13 *13*	3 *6*	18 *10*	14 *11*	—	5 *6*	—	—	6 *6*	—	—	—	—	—	—	7
8	—	—	—	—	—	— *9*	5 *4*	3	—	16 *18*	—	10 *9*	2	2	5 *7*	8 *4*	—	— *5*	— *8*	14 *9*	18 *17*	5 *6*	10 *15*	16 *13*	—	2	—	—	3 *4*	—	—	—	—	—	—	8
9	10 *4*	—	—	—	13 *7*	11 *9*	— *9*	26 *13*	13 *12*	— *5*	11 *9*	—	3	2	—	3 *6*	—	6 *5*	3 *5*	—	11	— *4*	— *7*	3 *4*	—	—	—	—	—	—	—	—	—	—	—	9
10	—	—	6	— *7*	3	5	6	5	32 *26*	—	6 *6*	—	—	—	19 *34*	3 *5*	—	6 *8*	—	8	10 *7*	19 *16*	— *3*	5 *11*	—	—	—	—	—	—	—	—	—	—	—	10
11	—	—	6 *5*	—	8	3	6 *7*	16 *14*	10 *8*	10 *5*	3 *5*	3	10 *7*	— *6*	10 *18*	11 *8*	3	3 *7*	8 *9*	18 *7*	— *7*	19 *19*	42 *31*	—	3 *6*	3	13	—	—	—	—	—	—	—	—	11
12	—	3 *6*	—	—	—	—	—	—	6	21 *22*	57 *50*	—	40 *40*	—	6 *11*	—	3 *7*	8 *12*	24 *28*	—	— *7*	—	—	—	3	3	—	—	—	—	—	—	—	—	—	12
13	—	3 *2*	—	—	—	13 *10*	3	10 *5*	21 *15*	8 *10*	—	—	6	22 *21*	—	5	8 *7*	—	8 *13*	—	—	5	—	—	—	—	—	—	—	—	—	—	—	—	—	13
14	—	3 *4*	—	—	5	5	6 *10*	5	3 *7*	14 *14*	8 *14*	3	5 *7*	—	—	—	—	—	8 *8*	—	—	5 *7*	—	—	—	—	—	—	—	—	—	—	—	—	—	14
15	—	—	—	—	5	2	—	—	5	5	5	5 *6*	— *4*	—	29 *20*	6 *11*	—	—	—	8 *7*	—	—	3	—	—	—	—	—	—	—	—	—	—	—	—	15
16	—	—	—	—	—	3	13 *7*	6 *5*	—	2 *5*	2	—	—	— *5*	10 *7*	5 *7*	—	8 *5*	—	3	3	—	—	—	—	—	—	—	—	—	—	—	—	—	—	16
17	—	—	—	—	—	— *4*	—	3 *4*	—	—	2	—	5	—	—	3 *5*	—	10 *8*	—	—	—	—	—	—	—	—	—	—	—	—	—	—	—	—	—	17
18	—	—	—	—	—	—	—	—	—	2	3	—	3	—	—	—	—	—	—	—	—	—	—	—	—	—	—	—	—	—	—	—	—	—	—	18

(c) *The effects of swelling and shrinkage*

Considerably more information on the distribution of the liquid in the unit cell can be obtained from the diffraction pattern of crystals at different states of swelling and shrinkage. The sharpness of the reflexions on photographs of shrunk and swollen crystals, together with the fact that swelling and shrinkage are reversible, show that the ordered structure of the protein molecules is at any rate not *destroyed* by these lattice changes. It remained to be seen, however, to what extent this structure is *altered*, i.e. whether swelling and shrinkage are wholly or partly intramolecular processes or whether they merely affect the distances between structurally rigid molecules. Since the angle β is the unit-cell parameter which shows the greatest changes, it was thought that the Patterson projections along the b-axis should be the most likely to provide information on this point.

Records of the $h0l$ reflexions were therefore made for each of the five states of swelling and shrinkage listed in table 3 and Patterson projections were calculated. It was found that superposition of any pair of the five projections with the a-axes in parallel brings most of the major peaks into coincidence, and that this is the only orientation of two projections relative to each other where such coincidence can be observed. Figure 4 shows the five projections printed in different colours and superimposed as six pairs, such that in each pair the origins at the centre of the diagram coincide and the a-axes are parallel to the horizontal base-line. The similarity of the peak distribution in the different pairs is striking. If the superposition is continued over several adjoining unit cells, the coincidence of peaks can be seen to continue indefinitely in the x direction (the direction of the base-line), but deteriorates in the direction normal to x beyond 20 A from the base-line. This deterioration could be seen well on a diagram shown elsewhere by one of us (Perutz 1942*a*, figure 3).

From these findings several important conclusions can be drawn. The Patterson projections show that the molecules do not change their orientation with respect to the a, b plane during swelling and shrinkage, whatever the angle β. This is also indicated by the constancy of the angle between the optic axes and the a-axis, mentioned in § 3. Since neither a nor b are altered by swelling and shrinkage, this implies that coherent, rigid layers of protein extend throughout the a, b plane. During swelling and shrinkage these layers must be sheared relative to each other, due to the change in β, and their distance apart must be altered by the change in the c spacing. This, in turn, must be due to changes in the thickness of layers of liquid of crystallization which are sandwiched between the protein layers. Figure 5*a* (p. 104) illustrates the lattice changes undergone by a single unit cell.

The next problem concerns the number of such liquid layers per unit cell and the thickness of the protein layers themselves. An estimate of the *minimum* thickness of the protein layers can be made from extent of the regions in which vector peaks in different Patterson projections can be brought to coincidence. If two corresponding peaks at different shrinkage stages coincide and are similar in shape, it is highly probable that they correspond to interatomic distances *within* any one protein layer. In that case the thickness of the protein layers cannot be smaller than the distance of such a peak from the horizontal base-line in figure 4 (pp. 130 to 132). Superposition of figures 4*c* and *d*, say, shows that peaks as far as 18 to 20 A from the base-line still satisfy this condition, so that the individual protein layers should reach at least this thickness. Beyond 20 A from the base-line the correspondence of different projections deteriorates, until finally the majority of peaks in different projections no longer overlap. This does not mean that the thickness of the protein layers cannot exceed 20 A, but merely implies that vectors between atoms in *neighbouring* protein layers (intermolecular vectors) become prominent beyond 20 A.

The *maximum* thickness of the layers cannot exceed the *c* spacing in the dried crystals, i.e. 32 to 36 A, which implies that not more than two layers of 18 A thickness could be accommodated in the unit cell (if there are two layers per unit cell, their thickness must be the same on account of the diad axis). In fact, coincidence of peaks up to 20 A from the base-line makes it appear more probable that there is only one layer of protein per unit cell, of a thickness approximately equal to that of the *c* spacing in the dried crystals; this will be borne out by the further analysis described in § 7 below.

To summarize the evidence of swelling and shrinkage experiments, it has been shown that there are rigid layers of protein extending through the crystal parallel to the *a*, *b* plane, and that the thickness of these layers cannot be less than 18 nor greater than 36 A. In the first case there would be two layers of protein and two layers of liquid of crystallization per unit cell, in the second case there would only be one of each. It will be convenient to postpone a decision on this point until after the consideration of molecular shape in § 6.

(*d*) *The Fourier transform of the molecule*

Consider a crystal consisting of molecules which all have the same orientation with respect to the axes and whose distance of separation is large compared to the interatomic distances within each molecule. Hettich (1935), Ewald (1935) and Knott (1940) have shown that the amplitude of the wave scattered from one individual molecule at different angles can be represented by what is called the Fourier transform of that molecule. This transform gives a continuous distribution of amplitude T in reciprocal space defined by the equation

$$T_{XYZ} = \sum_n f_n \exp\left[2\pi i(Xx+Yy+Zz)\right], \tag{3}$$

where X, Y and Z are the co-ordinates of any point in reciprocal space, f_n is the atomic structure factor of the nth atom and x, y and z are the co-ordinates of that atom in the unit cell. The structure amplitude F_{hkl} of any reflexion will be determined by the value of T_{XYZ} at the point in reciprocal space having the co-ordinates $X = ha^*$, $Y = kb^*$, $Z = lc^*$; a^*, b^* and c^* being the dimensions of the reciprocal unit cell.

Supposing it is desired to find the distribution of T_{XYZ} from the experimentally determined intensities I_{hkl}, all that can normally be measured is the value of T^2 at isolated points where $X = ha^*$, $Y = kb^*$ and $Z = lc^*$; it is not possible, therefore, to trace the continuous distribution of T^2, let alone of T. If, however, the lattice could be made to swell and shrink so that a^*, b^* and c^* became variable quantities, the number of points where T^2 could be measured would be greatly increased and it may become possible, in the ideal case where swelling and shrinkage is continuous, to trace the distribution of T^2 as a function of X, Y and Z throughout reciprocal space.

As long as T is complex this would still not allow one to calculate the atomic co-ordinates. If T is real, on the other hand, the distribution of T^2 would show nodal lines where $T^2 = 0$ and where the amplitude T changes sign. Thus the relative signs of all F_{hkl}'s would be determined by their co-ordinates in reciprocal space and the atomic parameters could be found with the help of a Fourier summation.

The case of haemoglobin is in several respects ideal for applying this method. All the molecules have the same orientation relative to the crystal axes. Moreover, the indications are that the intensities of the great majority of reflexions are determined by the internal structure of the individual molecules rather than the positions of the molecules relative to each other. There are however certain limitations. In the first place F is real only when $Y = 0$. Even in this plane I_{h0l} can be measured only along a series of parallel and equidistant lines, but not between the lines. The reason is this: As the crystal swells by the moving apart of parallel layers, the reciprocal lattice will contract by the moving together of points along parallel lines which are normal to the layer plane (figure 5*a*). Since the layers are parallel to the *a*-axis, the reciprocal lattice points will move along lines of constant X and only their Z co-ordinates will change. Finally, only the relative intensities of the $h0l$ reflexions have been determined, so that no absolute values of T^2 could be found. This in itself is no serious obstacle, but it introduces the difficulty of the relative scaling of F'^2 values measured at different stages of swelling and shrinkage and with different crystals.

Despite these limitations, an attempt to trace the distribution of T^2 in the plane $Y = 0$ was considered worth while and a three-dimensional diagram was constructed, superimposing the reciprocal lattice planes a^*, c^* at different stages of swelling and shrinkage with their c^* axes in parallel, and using wires of different length to indicate the values of F'^2. Figure 5 shows only two lines of constant X from this diagram as an example, since reproduction of the complete diagram in two dimensions is difficult. As expected, the diagram shows definite regions in reciprocal space where F'^2 is high and others where it is low, independent of the state of swelling or shrinkage. Passing along any line of constant X, stretches of the T^2 curve can clearly be recognized. A complete tracing of the T^2 curve is unfortunately prevented by the combination of several factors. First, it is generally impossible to judge whether T changes sign in passing from one line of constant X to the next. Secondly, there are long stretches of low intensity where it is impossible to keep track of the curve even along lines of constant X. Finally, changes in the salt concentration of the liquid which inevitably accompany shrinkage tend to produce additional intensity changes which obscure part of the picture.

It was decided that the method might help nevertheless in determining the signs of the F's. Figure 5 shows certain reflexions to be part of a single peak of T^2 which clearly means that they all have the same sign. Therefore, if the sign of one of those reflexions could be found by an independent method, the signs of all the other reflexions within that peak would become known. Thus the three-dimensional diagram, though not sufficient by itself to trace the Fourier transform of the haemoglobin molecule, might be of considerable help if used in conjunction with other methods.

(e) *The dried crystals*

Most dried crystals give such poor diffraction patterns that the information to be derived from them is negligible. The best patterns were obtained from salt-free crystals slowly dried in xylene (unit cell number 10) where the $h0l$ reflexions show an interesting disorder effect. While the first four orders of $00l$ are perfectly sharp, many of the $h0l$ reflexions tend to be drawn out into streaks parallel to c^* (figure 20, plate 6). The explanation of the effect is to be sought in the shearing of the protein layers during shrinkage which produces a disordered translation of the protein layers parallel to a, but does not impair the regularity of the c spacing. As expected, the $hk0$ reflexions show no disorder effects and they extend to a spacing of 7 A.

Mosaic structure is extreme in all dried crystals, so that any given reflexion appears over a wide range of angular positions, and its intensity varies according

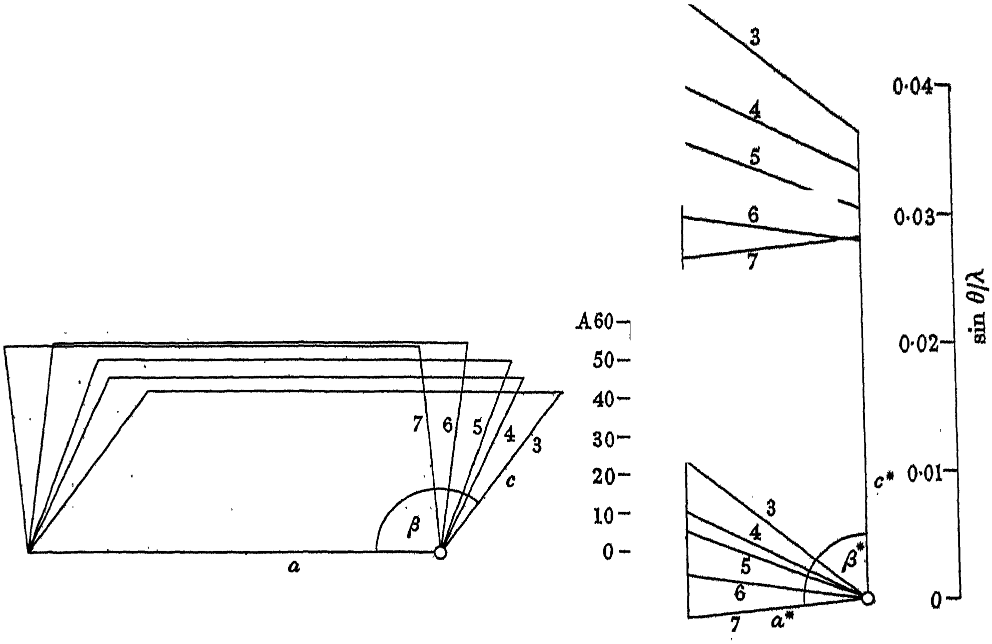

FIGURE 5a. Swelling and shrinkage of real unit cell (left) and reciprocal unit cell (right) viewed in projection along the b- and b^*-axes. The numbers refer to the unit-cell numbers of table 3, p. 93.

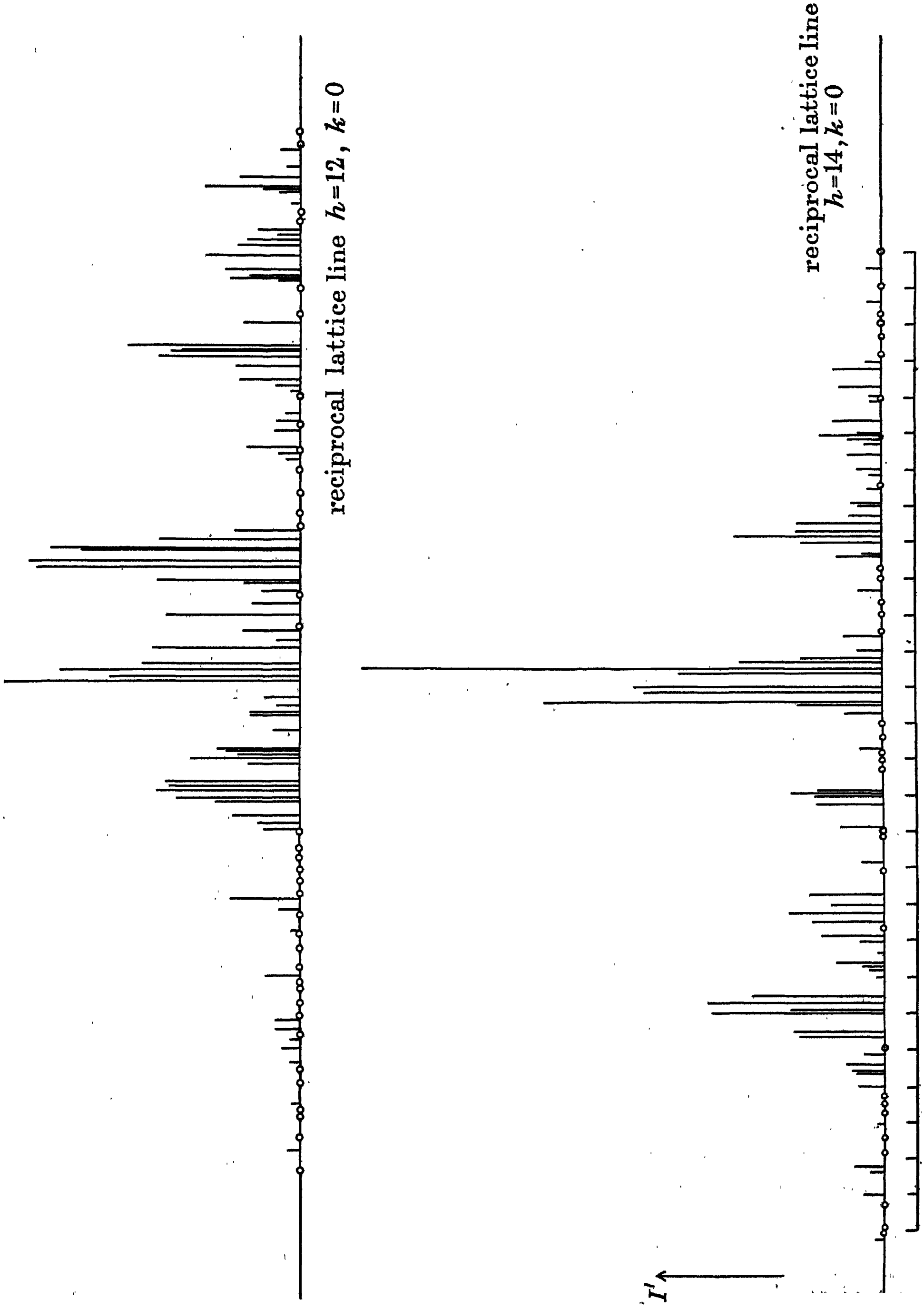

FIGURE 5*b*. Plot of intensities of $h0l$ reflexions along lines of constant h. The diagram includes intensities from unit cells numbers 3 to 7. 1 scale division = c^* of unit cell No. 5 ($\sin\theta/\lambda = 0{\cdot}0304$).

to the range of oscillation. Thus estimates of intensities tend to be somewhat arbitrary.

The data presented in the foregoing pages have shown how the diffraction pattern is affected by changes in the dimensions and composition of the unit cell. For further analysis certain features of the pattern will now be examined in closer detail.

6. The shape of the molecule

(a) *Previous estimates*

An estimate of the shape and external dimensions of the methaemoglobin molecule was made some time ago on the basis of the lattice changes observed during shrinkage (Perutz 1942*a*). It was argued that the length of the molecule should be equal to *b*, since *b* remains unchanged during slow shrinkage. It was further suggested that the molecule resembles a cylinder with an elliptical base whose major axis is equal to *b* (63 A) and whose minor axis is slightly smaller than $a/2$ (48 A), while the height of the cylinder is equal to the *c* spacing in the air-dried crystals, i.e. 36 A.

The argument regarding the length of *b* has since been rendered untenable by the discovery that the intensity of 110 is powerfully affected by changes in the density of the liquid while that of 200 remains practically unaltered (see § 5 (*b*)). On the basis of the model which had been proposed one would expect exactly the opposite effect. This contradiction led to a reconsideration of the problem of molecular shape and to certain modifications in the dimensions originally proposed.

(b) *Estimates based on considerations of packing*

The packing of the molecules in the dried crystal is pseudo-rhombohedral, as shown by figure 6. The molecules in any one layer form an almost perfect hexagonal pattern, and the molecules in the two succeeding layers come to lie fairly closely at the centres of the triangles formed by the lattice points of the first layer. Four of the rhombohedral faces are also prominent crystal faces. Nevertheless, it can be shown that neither spheres nor oblate spheroids can be fitted into the cell, because spheres would have to have a diameter $d = 2\sqrt[3]{(3M/4\pi N\rho)} = 54{\cdot}5$ A,* and would require a minimum *c* spacing of $0{\cdot}82d = 45$ A, whereas the observed spacings were 32 to 36 A. If the molecules were oblate ellipsoids of revolution whose axis is normal to the *a*, *b* plane, their maximum diameter in that plane could not exceed the distance between neighbouring molecules in the dried crystals, i.e. 58 A. Therefore their diameter along the axis of revolution would have to be at least

$$3M/[(58)^2 N\rho\pi] = 48{\cdot}5\ \text{A},$$

which would require a *c* spacing >40 A, which is still greater than the observed *c* spacings. Since the packing of the molecules strongly suggests that they are circular in projection on the *a*, *b* plane, the only alternative which remains is to regard them as *cylinders* with slightly convex top and bottom surfaces, to account for their pseudorhombohedral packing. If the height of the cylinders (h) is of the same order as the c spacing in the dried crystals, i.e. 34 A, their diameter should be

---

* ρ designates the true density of the protein, estimated at 1·30.

$$2\sqrt{\frac{M}{\pi h N \rho}} = 2\sqrt{(85{,}000/34\pi)} = 56\,\text{A}.$$

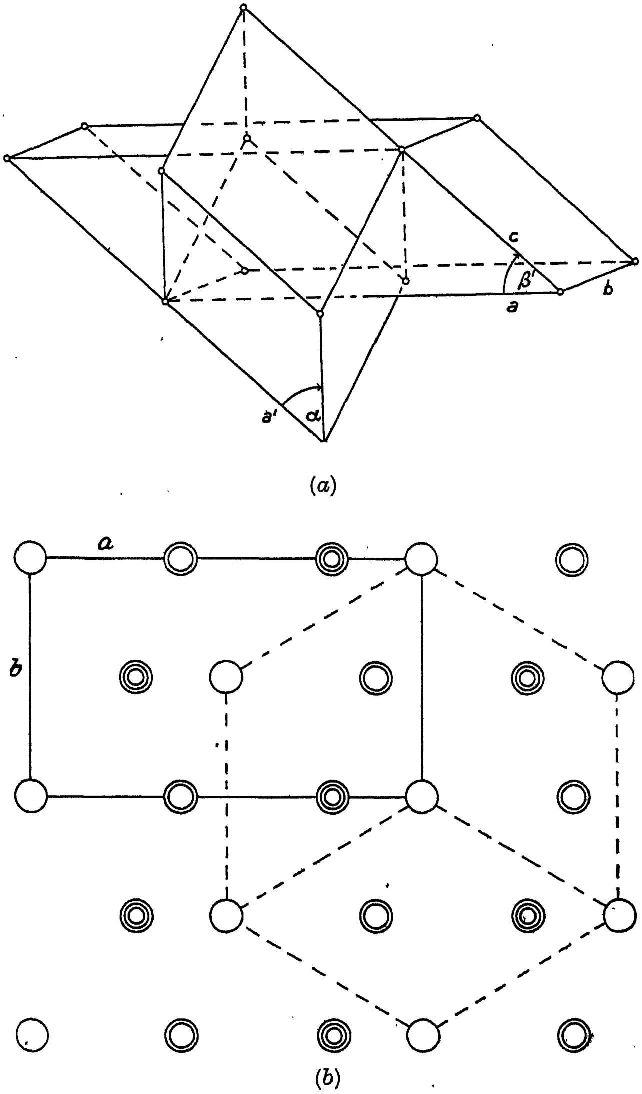

FIGURE 6. (*a*) Unit cell of air-dried crystal (table 1, number 2) showing pseudo-rhombohedral nature of the lattice. (*b*) Same structure projected on to the *a*, *b* plane, showing the extent of deviation from true rhombohedral packing. The full lines indicate the monoclinic unit cell and the dashed lines three pseudo-hexagonal cells. Each circle represents a lattice point. ○, 1st layer. ◎, 2nd layer. ⦾, 3rd layer.

There is another reason why spherical or ellipsoidal shapes are improbable. Close-packed spheres fill only 73 % of the volume of a cubic or hexagonal unit cell, while the haemoglobin molecules fill between 84 and 92 % of the unit-cell volume. Perfect close-packed cylinders would fill 90·7 %.

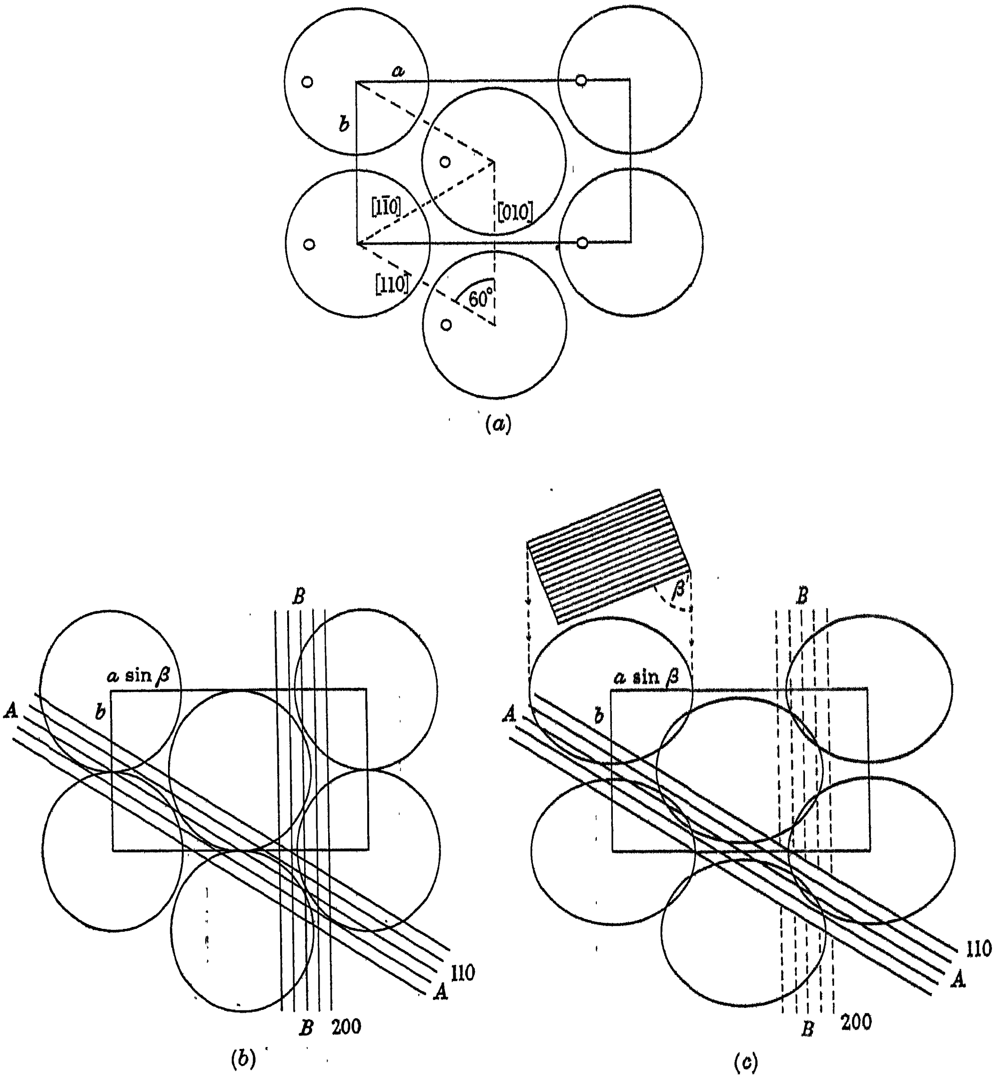

(a)

(b)

(c)

FIGURE 7. (a) Normal wet unit cell (number 5) projected on to the a, b plane. The large circles indicate lattice points in the plane of the paper and the small ones lattice points in the first layer underneath. (b) Same unit cell projected along the c-axis. The ellipses are projections of the molecules according to our old model. The shaded areas indicate the regions between the molecules where the scattering power of the liquid would influence the relative intensities of the 110 and 200 reflexions. (c) Same as (b) but with projections of molecules according to the revised model. The figure at the top left shows how one of the circular cylinders projects as an ellipse.

(c) *Estimates based on scattering contribution of liquid*

The unit-cell dimensions of the wet crystals confirm the impression that the haemoglobin molecules are approximately circular when viewed in projection on the a, b plane, since [010], [110/2] and [110/2] form a perfect equilateral triangle (figure 7a). For the purpose of estimating the diameter of the molecules the initial assumption was made that the curved surface of each cylinder is surrounded by a monomolecular shell of 'bound' water 3 A thick and that the shells of neighbouring cylinder surfaces touch. (The justification for assuming such shells of 'bound' water cannot be demonstrated at this stage, but will become clear in the further course of the analysis.) On the basis of this assumption, the diameter of the dry cylinders would be $b/2-6 = 57$ A, which agrees with the estimate based upon considerations of packing in the dried crystals. The height of the cylinders can be obtained from the diameter and the molecular volume:

$$h = M/(N\rho\, 28{\cdot}5^2\pi) = 33{\cdot}5\ \text{A},$$

which is in good agreement with the previous estimate of 34 A.

More detailed information about the possible shape of the molecules can be obtained by considering the intensity changes produced among the $hk0$ reflexions by the introduction of heavy ions into the liquid. The shape and dimensions of the 'liquid regions' will, of course, be determined by the shape and dimensions of the haemoglobin molecules, and have to be such that a change in the density of the liquid affects the intensity of 110 more powerfully than that of 200. (See § 5b, p. 99.)

A method has to be found, therefore, whereby the scattering contribution of the 'liquid regions' to different reflexions can be calculated without having to make any assumptions about the internal structure of the haemoglobin molecules themselves. This was done as follows. Suppose $R(x, y)$ is the electron density at any point in the unit cell projected along the c-axis. $R(x, y)$ will be a two-dimensional periodic function. The amplitude of any reflexion having the indices h and k will be given by the Fourier transform T_{hk} of this function:

$$T_{hk} = \int_0^a \int_0^b R(x, y) \exp\left[2\pi i\left(\frac{hx}{a\sin\beta} + \frac{ky}{b}\right)\right] dx\, dy. \tag{4}$$

This integral can be solved graphically for any distribution of R with the help of the Fourier analysis method of Ross (1943) using Beevers-Lipson strips (Beevers & Lipson 1936). Each of the unit-cell edges is divided into 60 parts and the value of $R(m/60, n/60)$ calculated for each of the 3600 co-ordinates m and n. If the projection has a centre of symmetry T_{hk} will be given by the double Fourier sum

$$T_{hk} = 2\sum_{m=0}^{29}\sum_{n=0}^{29} R(m, n) \cos 2\pi(hm + kn). \tag{5}$$

In the present case R need only be worked out for one-eighth of the unit cell and T_{hk} can be calculated very quickly and easily.

In order to work out the scattering contribution of heavy ions introduced into the liquid, a certain outline of the protein molecules has to be assumed. The electron density inside the protein molecule can be assigned any arbitrary constant value, while the electron density in the liquid region has to be raised from an initial value R_1 in medium A, say, to another value R_2 in medium B. The function T_{hk}, corresponding to the change in amplitude of any given reflexion, can then be evaluated with the help of the Fourier summation given in equation (2). The results are expressed as $\Delta T^2/\Delta\rho_{li}$, the calculated intensity change for a given change in the electron density of the liquid. The calculation was done for three different arrangements in the unit cell: (1) Elliptical cylinders having the dimensions $a = 31{\cdot}6$, $b = 24$ and $h = 36$ A. These are the dimensions estimated by Perutz (1942*a*). (2) Circular cylinders having the dimensions $r = 28{\cdot}5$ and $h = 34$ A (the dimensions derived above). (3) Circular cylinders having the dimensions $r = 31{\cdot}6$ and $h = 40$ A (the same as (2), but covered with a monomolecular shell of water 3 A thick).

The results for these three arrangements are as follows:

index of reflexion	200	110
(1) $\Delta T^2/\Delta\rho_{li}$ for elliptical cylinders (figure 7*b*)	9·4	1
(2) $\Delta T^2/\Delta\rho_{li}$ for circular cylinders (figure 7*c*)	1	1·5
(3) $\Delta T^2/\Delta\rho_{li}$ for circular cylinders (hydrated)	1	19·5
observed intensity changes .	small	large

Thus only for hydrated circular cylinders are the calculated intensity changes in qualitative accord with the observed ones.

Figures 7*b* and *c* illustrate the two types of cylinders as seen in projection along the *c*-axis, the first showing the elliptical cylinders and the second the circular ones. The regions between the molecules which contain most of the liquid and which determine the strength of the intensity changes are shown as shaded areas (*AA* and *BB*). Figure 7*c* clearly shows that a projection of circular cylinders gives the appearance of continuous ribbons of molecules extending in the [110] and [110] directions, thus giving intense 110 reflexions, while in figure 7*b* the neighbouring molecules are well separated.

The conclusions reached here agree with all the important facts so far discovered.* It is now obvious why the molecules cannot rotate about *b* during swelling and shrinkage, since the cylinders would get in each other's way. It is also clear that coherence between the cylinders in any one layer will be stronger than between cylinders in neighbouring layers. It still remains to be shown whether the molecules in the wet crystals are really cylinders 34 A high or whether they consist of two cylinders 17 A high and separated by liquid. This will be discussed in the next section.

Molecular shapes other than those discussed here, such as rectangular prisms, ellipsoids elongated along *a* or assemblies of smaller units separated by liquid, have also been considered, but were found to be incompatible with the data just described. At the same time it should be emphasized that the very nature of those data—requirements of packing and intensities of low-order reflexions—do not allow one to distinguish more than a 'fuzzy outline' of the molecules. They could not distinguish between cylinders with a circular base and hexagonal or octagonal prisms, or close-packed assemblies of a number of smaller cylinders or prisms. Their meaning is rather that the whole molecule, viewed under a microscope of insufficient magnification to resolve any details, appears as a circular cylinder.

---

* The value of $b = 51$ A in the crystals dried from 25 % alcohol is too small for a cylinder diameter of 57 A. The photographs from these crystals, however, are exceedingly poor, and it is doubtful whether the layered structure of the crystals or the dimensions of the molecules themselves remained intact after drying in alcohol. It is the only case where a value of *b* below 56 A was observed.

7. ONE-DIMENSIONAL FOURIER PROJECTIONS

(*a*) *Preliminary calculations: the number of liquid layers per unit cell and the position of the 'bound water'*

The information on the shape of the molecule derived in the preceding section simplifies the task of deciding whether there are one or two liquid layers per unit cell. The distinction between these two possibilities is now made by comparing the intensity changes of 001 and 002 on transition from medium A to medium B with the changes calculated for three simplified electron-density distributions. For calculating these distributions it is necessary to know the approximate thickness of the protein layers and the volume of liquid *within* them, i.e. the volume between the curved surfaces of the cylinders. No other data will be required.

Consider the electron-density distribution in the unit cell projected on to a line normal to the layer plane. The length of the line will be $c\sin\beta$. This projection can be divided into regions of average electron density R_{li} and R_p, where R_{li} is the projected electron density in the liquid layers and R_p the projected electron density of the protein layers, both expressed in electrons/A. Since only the effects of *changes in the density of the liquid* have to be considered, the precise electron-density distribution in the protein layers is immaterial, and only the average electron densities in the protein and liquid layers have to be calculated. It is important to realize, though, that any change in the composition of the liquid will affect the electron densities of both the liquid and the protein regions, since part of the liquid of crystallization is within the protein layers, i.e. between the curved surfaces of the cylinders. Thus in the projection

$$R_{li} = \rho_{li}ab \tag{6}$$

and

$$R_p = \frac{ab\left(\Sigma\epsilon - \overset{li}{\Sigma}\epsilon\right)}{V - V_{li}}, \tag{7}$$

where ρ_{li} is the electron density of the liquid in electrons/A^3, a and b are the unit-cell dimensions of the wet crystal, $\Sigma\epsilon$ is the total number of electrons per unit cell, $\overset{li}{\Sigma}\epsilon$ the number of electrons in the liquid layer, V the unit-cell volume and V_{li} the volume of the liquid layer.

Figure 8 shows the three possible distributions of protein and liquid layers, the first curve containing only one liquid layer per cell and the others two. The thickness of the liquid layers in the three curves was derived as follows. If there is but one liquid layer per unit cell the thickness of the protein layer will be 34 A, and that of the liquid layer $c \sin\beta - 34 = 16{\cdot}7$ A (figure 8*a*). If there are two liquid layers of unequal thickness, neither can be thinner than 2·7 A, the diameter of a water molecule. The presence of pure water layers, however, is immaterial for the purpose of this argument, since their density would not be changed when ammonium sulphate is introduced into the crystal. If two protein layers are to be separated sufficiently for sulphate ions to diffuse into the space between them, the liquid layer must be thicker than the diameter of a sulphate ion, i.e. 5·7 A. If one liquid layer is to be 5·7 A thick, the other must be $16{\cdot}7 - 5{\cdot}7 = 11$ A thick (figure 8*b*). If the width of the first liquid layer is to be enlarged, the position is soon reached when the thicknesses of the two liquid layers become equal, and this was chosen as the third alternative (figure 8*c*).

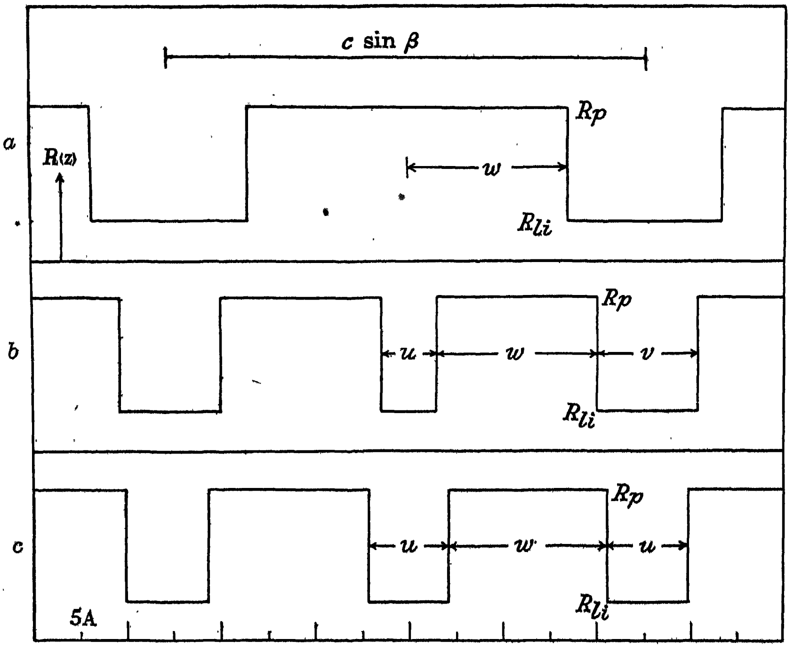

FIGURE 8. Diagrammatic representation of three possible electron density distributions in the unit cell. R_p, mean electron density in the protein region; R_{li}, mean electron density in the liquid regions; *w*, half-thickness of protein region; *u* and *v*, thickness of liquid regions.

It remains to be shown how a change in the density of the liquid would affect the relative intensities of 001 and 002 on the basis of each of the three curves. This can be calculated from the Fourier transforms which are derived from the equation

$$T_l = \int_{\pi}^{-\pi} R(z) \cos\left(2\pi l \frac{z\,dz}{c \sin\beta}\right), \tag{8}$$

where T_l is the structure amplitude of the lth reflexion and R the projected electron density at any point z. Solution of this integral for the three curves leads to the following equations:*

$$T_l = \frac{c\sin\beta}{\pi l}(R_p - R_{li})\sin\left(2\pi l\frac{w}{c\sin\beta}\right), \tag{8a}$$

$$T_l = -\frac{c\sin\beta}{\pi l}(R_p - R_{li})\left[\sin\left(\pi l\frac{u}{c\sin\beta}\right) + (-1)^l\sin\left(\pi l\frac{v}{c\sin\beta}\right)\right], \tag{8b}$$

$$T_l = -\frac{2c\sin\beta}{\pi l}(R_p - R_{li})\sin\left(\pi l\frac{u}{c\sin\beta}\right)\cos^2\tfrac{1}{2}\pi l. \tag{8c}$$

R_p and R_{li} are the projected electron density in the protein and liquid regions respectively; u, v and w are the thicknesses of the liquid and protein regions, as shown in figure 8. Evaluation of the three equations shows that a change in the density of the liquid of crystallization would affect the relative intensities of 001 and 002 in the following way:

curve (*a*)	$\Delta I'_{001}:\Delta I'_{002} = 3{\cdot}3:1$,
curve (*b*)	$\Delta I'_{001}:\Delta I'_{002} = 1:9{\cdot}5$,
curve (*c*)	$\Delta I'_{001} = 0$; $\Delta I'_{002} =$ strong,
observed changes	$\Delta I'_{001}:\Delta I'_{002} = 3{\cdot}5:1$.

The results can now be compared with the observed intensity changes.

A list of the relative intensities of the first seven orders of $00l$ in four different suspension media is given in table 5. This shows that in medium A the intensities of 001 and 002 are 95 and 34 respectively, while in medium B they are both 10. Thus $\Delta I'_{001} = 85$ and $\Delta I'_{002} = 24$; $\Delta I'_{001}:\Delta I'_{002} = 3{\cdot}5:1$, compared to a ratio of $3{\cdot}3:1$ calculated on the basis of model (*a*). The experimental results are obviously incompatible with models (*b*) and (*c*) and in agreement with model (*a*). This proves that there can only be one layer of liquid per unit cell, and hence the thickness of the protein layers must be 34 A, no matter whether the crystals are wet or dry.

TABLE 5. RELATIVE INTENSITIES OF $00l$ REFLEXIONS IN DIFFERENT SUSPENSION MEDIA

index	I' in medium A	I' in medium B	I' in medium C	I' in medium D
001	95	10	17	28
002	34	10	0	0
003	7	2	10	0
004	0	5	20	6
005	23	21	16	32
006	46	46	46	45
007	17	11	11	19

The composition of the suspension media is given in table 2, p. 93.

---

* The Fourier transforms were formulated with the help of Dr N. Kemmer.

There is, of course, the possibility mentioned above that a pure-water layer is sandwiched within the protein layers; this is part of the question of protein hydration which will now be considered.

For finding the signs of the F_{00l}'s by the isomorphous exchange method it is necessary to know the thickness of that part of the liquid layer whose electron density is changed by the presence of heavy ions. Thus, knowing the total thickness of the liquid layer is not enough, and it becomes necessary to find the boundaries between the 'free' water which is available as solvent to diffusing ions, and the 'bound' water which is not. Seeing that the division of the liquid into 'bound' and 'free' is so far purely hypothetical, it will first be considered whether the X-ray data offer any support for the reality of its existence.

The existence of 'bound' water is inferred from the fact that the concentration of mobile ions in the liquid of crystallization is always lower than in the suspension medium, so that the crystals contain a surplus of water whose amount is largely independent of salt concentration. It is possible to make two extreme assumptions about the location of that surplus water. The first of these disregards all hypotheses about protein hydration and assumes that the surplus water is uniformly distributed throughout the liquid of crystallization. As there is in this case no division between 'bound' and 'free' water the concentration of mobile ions will be uniform right up to the surface of the protein molecules, i.e. the *whole* liquid layer will change its density when heavy ions diffuse into the crystal and, furthermore, the electron density of the liquid layers will have to be calculated from the *apparent* composition of the liquid of crystallization (table 2, column 6, p. 93).

The second assumption involves a division into 'bound' and 'free' water, the former being directly attached to the protein, the latter available to diffusing ions and in dynamic equilibrium with the suspension medium; the composition of the 'free' liquid in this case will be the same as that of the suspension medium (table 2, column 5). Moreover, for calculating the phase contribution of the heavy ions the total thickness of the liquid layer (16·7 A) will have to be reduced by the ratio of 'free' water to total water (0·52/0·82)* which gives 10·6 A as the thickness of the layer through which ions can diffuse.

There are thus two extreme hypotheses to be considered: one is a structure containing alternate layers of protein and salt solution of thickness 34 and 16·7 A respectively, the salt concentration throughout the liquid layer being uniform and lower than in the suspension medium (hypothesis 1); the other structure consisting of alternate layers of *hydrated protein* and 'free' liquid of thickness 40·1 and 10·6 A respectively, the salt concentration in the 'free' liquid being the same as in the suspension medium (hypothesis 2).

It is reasonable to expect that the intensity of 001 which may be called a predominantly intermolecular reflexion will chiefly depend on the differences between the mean electron densities of the protein and liquid layers, and will not be very sensitive to the detailed electron-density distribution within either of these layers.

* These figures represent g. H_2O/g. protein and are taken from the data of Perutz (1947).

It should be possible, therefore, to distinguish between the two hypotheses by calculating the differences between the mean electron densities of the protein and liquid layers for different suspension media on the basis of each hypothesis and comparing these values with the observed intensity changes of the 001 reflexion. This comparison is shown in table 6. The second column contains the differences in the mean electron densities derived from formulae (6) and (7) (p. 111), R_{li} being calculated from the apparent composition of the liquid of crystallization and V_{li} being taken as the total volume of the liquid layer. In the third column R_{li} is calculated from the composition of the suspension medium, and V_{li} is taken as the volume of the 'free' liquid layer.

TABLE 6

medium	hypothesis 1 $R_p - R_{li}$; bound water uniformly distributed in liquid of crystallization	hypothesis 2 $R_p - R_{li}$; bound water separate and attached to protein	I'_{00l} (observed)
A	+500	+430	95
B	+300	+120	10
C	+230	−100	17
D	+ 20	−130	28

Thus, if the 'bound water' were uniformly distributed, table 6 shows that the intensity of 001 should gradually diminish to zero on passing from medium A to D, in accordance with the reduction in the difference between the mean electron densities of the protein and liquid regions (see equation (8*a*)). If the 'bound' water is separate, on the other hand, the amplitude of 001 should diminish in passing from medium A to B, it should reach zero half-way between B and C, and it should increase again with reversed sign between C and D. It is obvious that the observed intensities which decrease from A to B and increase again between C and D are compatible with the second assumption, but not with the first. This proves that there exists a real division of the liquid of crystallization into two components.

To summarize the evidence of the foregoing pages, it has been shown that there is only one layer of protein and one layer of liquid per unit cell. The protein layer is hydrated and has a total thickness of 40·1 A, including the 'bound' water. The thickness of the layer through which mobile ions are free to diffuse is 10·6 A in the normal wet crystal. This information opens the way for finding the signs of the F_{00l}'s by the isomorphous exchange method. No assumptions need be made about the location of the 'bound' water, i.e. whether it is on the surface of the protein molecules or in the interior.

(*b*) *Phase determination by the isomorphous exchange method*

One method commonly used in crystal-structure analysis for finding the signs of structure amplitudes is the exchange of light atoms for heavier ones in an isomorphous series of compounds. In order to apply the method it is generally necessary to know the absolute F's, the number of atoms that are being replaced and their position in the unit cell. The method can be adapted to protein crystals by introducing heavy atoms into the liquid of crystallization, so that the scattering contribution of the liquid can be distinguished from that of the protein itself. Of the three requirements for applying the method, only two have been met so far: The number of atoms that are being replaced have been found by means of the density measurements described in § 4 (*c*) and the boundaries of the regions through which the heavy atoms can diffuse have been determined, at least to a first approximation with the help of the argument just outlined. On the other hand, owing to lack of suitable apparatus, it has not yet been possible to determine the absolute F's with sufficient certainty. Instead of using absolute F's, the relative intensities of the $h0l$ reflexions in different liquids were brought to approximately the same scale by comparison of corresponding high-order reflexions to which the liquid does not seem to make a large contribution. An example of this method of scaling is shown in table 4, p. 100; in media A and B it probably leads to correct scaling of the intensities to within ± 15 %. In medium C, the X-ray pictures are much poorer and the scaling of the F's is probably not accurate to more than ± 30 %. Measurements taken in medium D will not be used, because the pictures are too poor to give reliable intensity readings and also because reduced hydration alters the thickness of the 'free' liquid layer. It was decided, therefore, that in media A, B and C the relative scaling of the intensities should be sufficiently accurate to apply the isomorphous exchange method without knowing the absolute F's, while medium D is unsuitable for this purpose.

So far, the determination of signs by the isomorphous exchange method has been confined to the $00l$ reflexions. The heavy ions introduced into the crystal were represented as a layer 10·6 A thick, parallel to the a, b plane and centred at $z = 1/2$. The phase contribution of this layer was calculated with the help of a Fourier transform of an electron density distribution curve similar to figure 8*a*, p. 112, only with the thickness of the protein and liquid layers changed to 40·1 and 10·6 A respectively. The Fourier transform is given by

$$T'_l = -\int_{\pi}^{-\pi} R(z)\cos\left(2\pi l\frac{z\,dz}{c\sin\beta}\right) = -\frac{k}{l}\sin\left(2\pi l\frac{w}{c\sin\beta}\right), \tag{9}$$

where $w = 40{\cdot}1/2$ and k is an arbitrary constant. The negative sign is due to the choice of origin half-way between the liquid layers. The values of T' for the first seven orders of $00l$ are listed in table 7, together with the observed F' values in media A, B and C.

The signs can now be found by the usual argument. For example, let $|F_A|$, $|F_B|$ and $|F_C|$ represent the relative amplitudes of the 002 reflexion in the three media. In this case $|F_A| > |F_B|$, and $|F_C| = 0$; T' is positive. Since $|F_{002}|$ is reduced by a positive phase contribution from the heavy ions the sign of F_{002} must be negative.

Similar arguments were used to determine the signs of the other reflexions. The signs found for the three series of $00l$ reflexions are listed in table 7. The signs of the first four orders can be determined with a considerable degree of certainty. Even if the scaling of the three series were in error by 50 % and the thickness of the 'free' liquid layer were anywhere between 12·7 and 0·7 A, the signs would still be the same. The sign of 005, on the other hand, is uncertain, both on account of the intensity changes in different liquids being smaller than the errors of scaling, and also because a decrease in the thickness of the liquid layer by 0·8 A would reverse the sign of T'. The sign of 006 is indeterminate, because it was chosen as the basis of the scale, while that of 007 is reasonably certain. The table also shows that the values of T', to be consistent with the observed intensity changes, should fall off more steeply with increasing θ than they actually do on the basis of our model. This merely indicates that the boundary between the liquid and protein layers is not as sharp as for the sake of simplicity it was assumed to be.

TABLE 7. DETERMINATION OF SIGNS OF F'_{00l} BY THE ISOMORPHOUS EXCHANGE METHOD

index	scattering contribution of salt T'	$\lvert F'\rvert$ in medium A	$\lvert F'\rvert$ in medium B	$\lvert F'\rvert$ in medium C
001	−66	98 (+)	32 (+)	41 (−)
002	+50	58 (−)	32 (−)	0
003	−31	26 (+)	14 (+)	32 (−)
004	+12	0	22 (+)	45 (+)
005	+ 4	48 (?)	46 (?)	40 (?)
006	−13	68 (?)	68 (?)	68 (?)
007	+15	41 (−)	33 (−)	33 (−)

$|F'| = \sqrt{I'}$ of table 4.

(*c*) *Phase determination by the 'nodal point' method*

This is an attempt to plot the molecular Fourier transform along the Z-axis (see § 5 (*d*), p. 102) and to discover the 'nodal points' where it changes sign. The outline of the T^2 curve was obtained by plotting the relative intensities of the $00l$ reflexions at different states of swelling and shrinkage against $\sin\theta/\lambda$. The points where this T^2 curve touches the abscissa should be the 'nodal points' where the T curve crosses it.

Table 8 gives a list of the relative intensities of the $00l$ reflexions at four different states of swelling and shrinkage. The scaling of the intensities in different sets was done, as in the case of table 5, by bringing the relative intensities of the higher order $h0l$ reflexions at corresponding points in the reciprocal lattice to values of the same order. Figure 9*a* shows a plot of I'_{00l} against $\sin\theta/\lambda$. There seem to be four distinct points where the I' curve reaches the abscissa. If the sign of F_{001} is taken as positive, in accordance with the findings outlined in the preceding section, the resulting F curve would take the shape indicated in figure 9*b*. The distribution of signs derived from this curve agrees with the one deduced by the isomorphous exchange method. In addition, the curve indicates that the signs of 005 and 006 which had been left

TABLE 8. RELATIVE INTENSITIES OF 00l REFLEXIONS AT FOUR DIFFERENT STATES OF SWELLING

index	cell number 3 ($c \sin \beta = 42{\cdot}3$)	cell number 4 ($c \sin \beta = 46{\cdot}1$)	cell number 5 ($c \sin \beta = 50{\cdot}7$)	cell number 7 ($c \sin \beta = 54{\cdot}4$)
001	3	4	10	5
002	0	6	10	7
003	17	21	2	0
004	17	11	5	20
005	45	11	21	24
006	0	32	46	28
007	4	0	17	16

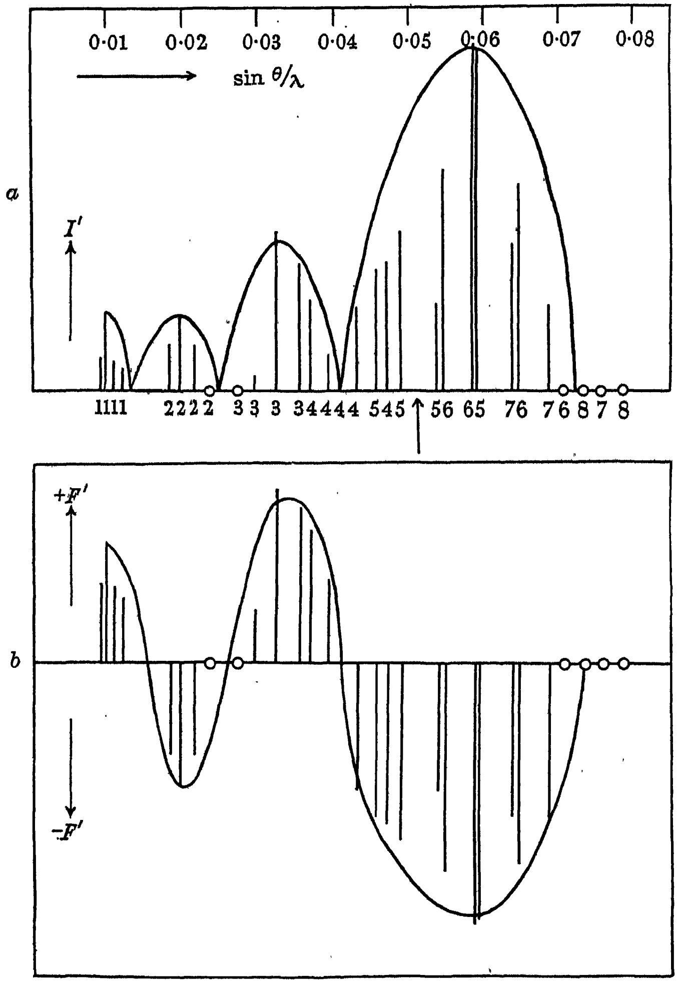

FIGURE 9. (*a*) Relative intensities of 00l reflexions at different states of swelling plotted against sin θ/λ. The numbers on the abscissa indicate the order of reflexion (the figure includes data from unit cells numbers 3, 4, 5 and 7). (*b*) Tentative plot of the molecular structure factor curve.

indeterminate are negative. There remains a slight doubt about this, though, on account of a small gap between 005 and 006 (indicated by an arrow in figure 9*a*), where the possibility of another phase change is not entirely excluded; if it occurred 006 would be positive. On the other hand, the curve shows that 006 and 007 have the same sign; since the isomorphous exchange method indicated that 007 is negative, this would make 006 negative as well and confirm the deduction made above.

(*d*) *Distribution of phases on the basis of assumed layer structures*

The peaks in the two-dimensional Patterson projections along the *a*- and *b*-axes tend to be concentrated in layers which are parallel to the *a*, *b* plane and are spaced 9 A apart. One-dimensional Patterson projections perpendicular to the *a*, *b* plane all show very pronounced peaks at 9 A from the origin and slightly smaller (but still prominent) peaks at about 18 A (figure 10).

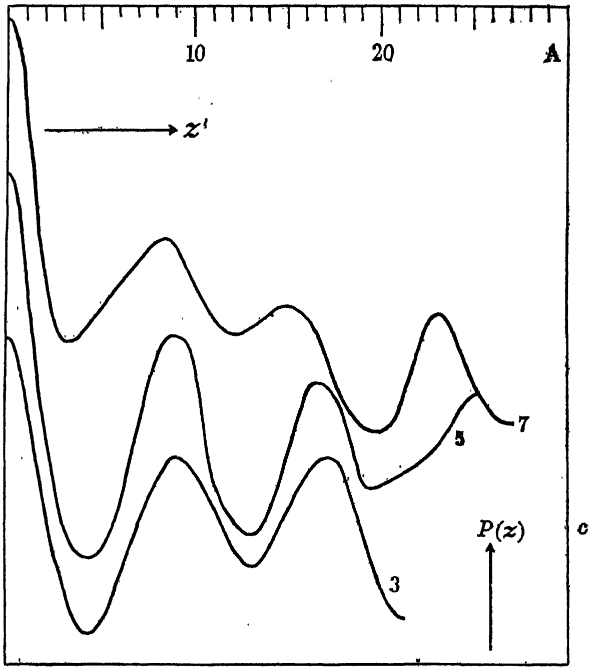

FIGURE 10. Patterson-Fourier projections on a line normal to the *c* plane (z') at three different states of swelling (unit cells numbers 3, 5 and 7).

If the assumption is made that the layers of peaks in the Patterson projections are due to the concentration of scattering matter in two or more layers within the protein molecule, it is reasonable to suppose that such concentrations will determine the signs of the F_{00l}'s, particularly if there is no salt in the liquid of crystallization. An attempt was made, therefore, to calculate the *F*'s on the basis of four simple models, consisting of scattering points of equal weight spaced 9 A apart along a line normal to the *a*, *b* plane in unit cell number 5. The number of such points was varied from two in the first model to five in the fourth model, five being the maximum number that could be accommodated in the unit cell. The F's were calculated from the formula

$$F_l = \sum_n L_n \cos\left(2\pi l \frac{z}{c \sin\beta}\right), \tag{10}$$

where L_n is the (arbitrary) structure factor of the nth layer having the co-ordinate $z/c \sin\beta$. Table 9 gives the F's deduced on the basis of these four models, together with the observed F's and their signs as determined by the previous two methods. The observed F's are those for the normal wet unit cell in salt-free suspension medium and are taken from table 7, column 3.

TABLE 9. STRUCTURE FACTORS CALCULATED ON THE BASIS OF ASSUMED LAYER STRUCTURES (UNIT CELL NUMBER 5)

index	$F'_{\text{calc.}}$ for two layers	$F'_{\text{calc.}}$ for three layers	$F'_{\text{calc.}}$ for four layers	$F'_{\text{calc.}}$ for five layers	$F'_{\text{obs.}}$ medium A
001	+84	+148	+ 71	+ 90	98 (+)
002	+43	+ 41	− 54	+ 16	58 (−)
003	−13	+ 2	+ 18	+ 95	26 (+)
004	−64	+ 75	+ 28	− 13	0
005	−95	+175	−143	+190	48 (−)
006	−98	+193	−179	+270	68 (−)
007	−73	+106	− 9	+ 7	41 (−)

The most direct way of distinguishing between the four possibilities is this: the sign of 002 has been proved to be negative beyond any reasonable doubt, and it can be argued, therefore, that any structure which gives a positive sign of 002 must be wrong. It is seen that the only structure leading to a negative sign of 002 is one containing four layers of scattering matter. On the basis of this model, the signs of all the F's are the same as those determined by the previous two methods, a result which allows one to conclude with some confidence that those signs are correct.

(e) *Results*

By the methods described in the preceding pages, the signs of the F_{00l}'s were determined for unit cell number 5 in media A, B and C, and for unit cells numbers 3, 4, 6, 7 and 10. The three methods employed are independent of each other only to a limited extent; where they are, each confirms the signs deduced by either of the two others. The isomorphous exchange method gives the signs of the first four orders of 00l with a high degree of certainty, but leaves the signs of 005 and 006 in doubt. The nodal-point method by itself gives no information about the absolute signs, and evidence of the isomorphous exchange method has to be used to determine the sign of 001. Once this is done the nodal-point method confirms the signs of the first four orders calculated by the isomorphous exchange method, and, in addition, it gives strong evidence in favour of 005, 006 and 007 (of unit cell number 5) all being negative. In the layer structure method, three of four possible structures are rejected because they give a sign of 002 opposite to that derived by the isomorphous exchange method. The fourth structure leads to the same distribution of signs as the combination of the other two methods. Only in unit cell number 5 were the signs of the first seven orders of $00l$ determined by three different methods; the signs of the F's for unit cells numbers 3, 4, 6, 7 and 10 are derived from the nodal-point method alone, and no independent checks have as yet been applied.

One-dimensional Fourier projections on to a line normal to the a, b plane were calculated with the F_{00l}'s as coefficients of the terms. The results of the Fourier summations are shown in figure 11. Curves a, b and c show the effects of changes in the composition of the suspension medium for unit cell number 5. There are four main peaks spaced slightly less than 9 A apart, apparently representing the protein molecule; these peaks are largely unaffected by the density of the liquid. On each side of those peaks is a region obviously representing the liquid of crystallization where the electron density varies between a very low value in medium A (tap water), and a value exceeding the density of the protein in medium C (potassium phosphate solution).

Figure 11 d to g show the effects of swelling and shrinkage. Again the position of the electron density peaks in the protein part of the curve show little change, while

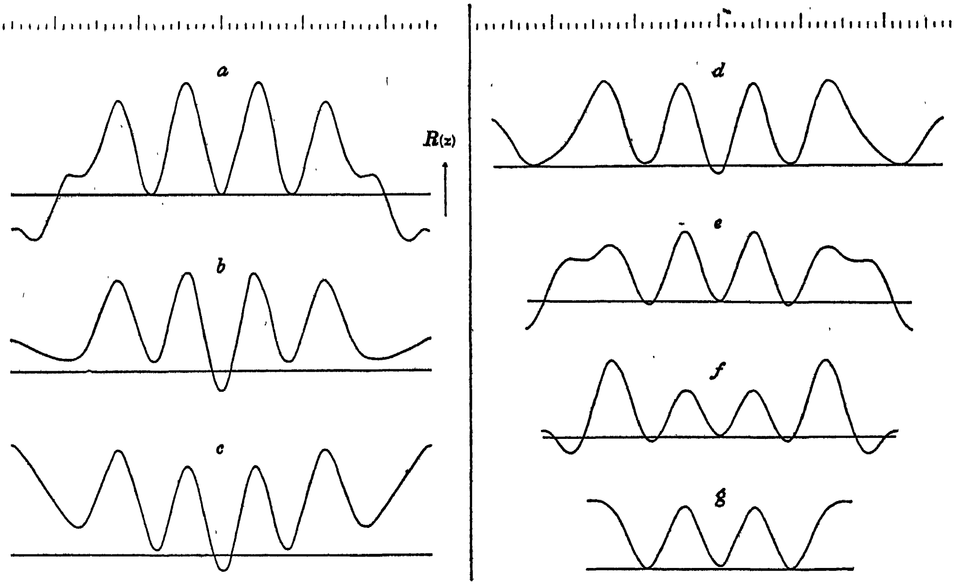

FIGURE 11. Fourier projections of relative electron densities on z'. The base lines are drawn at arbitrary levels. The scale shows Angstrom units.

figure	unit cell number	suspension medium
(a)	5	A
(b)	5	B
(c)	5	C
(d)	7	3·2M-$(NH_4)_2SO_4$
(e)	4	supersaturated $(NH_4)_2SO_4$
(f)	3	supersaturated $(NH_4)_2SO_4$
(g)	10	dried in xylene

both the width and the density of the liquid region vary between wide limits. The bulges on the outside of the protein molecule in figure 11*e* are surprising and seem to indicate an adsorption of the salt on to the surface of the protein molecule. The liquid of crystallization in this case (the first shrinkage stage) consists of supersaturated ammonium sulphate solution. In figure 11*f*, corresponding to the second shrinkage stage, the protein part of the curve looks least like any of the others, but it must be remembered that this projection had to be calculated with only four terms. The same applies to figure 11*g*, which was calculated on the basis of the intensity data collected from a crystal dried in xylene, i.e. the X-ray picture shown in figure 20, plate 6.

The curves give a picture of a rigid molecule whose structure is unaffected either by the amount of liquid in the crystal or by the composition of that liquid. The thickness of the molecule can be estimated as 32 to 36 A, which agrees with the value of 34 A deduced in § 6. The meaning of the four concentrations of scattering matter indicated by the curves will be discussed below.

It might be argued that the picture of the electron-density distribution provided by the one-dimensional syntheses is misleading, since the Fourier summations contain only the first seven terms, while the X-ray pattern in the normal wet crystal (medium B) contains seventeen orders of $00l$. Of the last ten orders, however, four reflexions are absent, one is very weak and five have weak to medium strength. The phases of these can at present not be assessed, but whatever they are, the contribution from those five reflexions would not be strong enough to alter the main outline of the Fourier projections. Their effect would be rather to superimpose a fine structure on the curves shown in figure 11.

8. CONCLUSIONS

Molecular shape and packing

The methaemoglobin molecule appears to be a cylindrical disk of an average height of 34 A with a slightly convex circular base of 57 A diameter (figure 12). This is merely a simplified, diagrammatic picture, giving as it were the fuzzy outline of the molecule, whose surface could not possibly be as smooth as this drawing suggests. Most probably groups of different length protrude from the surface, so that the exact thickness in any particular direction will not be known until the structure of the protein has been completely determined.

The arrangement of the molecules in the normal wet crystal is fairly clear. The cylindrical protein molecules form close-packed layers parallel to the *a*, *b* plane (figure 13). The liquid of crystallization fills both the interstices between neighbouring cylinders in any one layer and the spaces between successive layers of cylinders. Crudely, the crystals can be pictured as consisting of alternate layers of haemoglobin molecules and of liquid of crystallization.

Swelling and shrinkage

Swelling and shrinkage involve stepwise, reversible transitions between different, well-defined lattices, each being stable in a particular environment of the crystal.

So long as complete drying of the crystals is avoided, swelling and shrinkage merely alter the thickness of the liquid layers without having any effect on the area or thickness of the layers of haemoglobin molecules. These molecules themselves do not seem to be penetrated by the liquid of crystallization, and their structure is unaffected by swelling and shrinkage of the crystal.

The unit-cell dimensions of dried crystals vary considerably according to the method of drying. In slowly dried crystals the individual layers of haemoglobin molecules only shrink in area by a small amount; not more, in fact, than would be

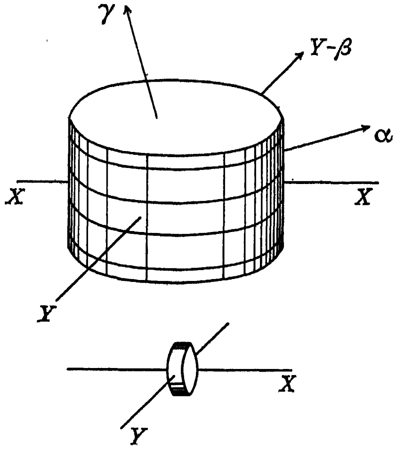

FIGURE 12. Diagrammatic model of haemoglobin molecule, showing its orientation with respect to the crystal axes. *Y* is the diad axis. The small disk underneath represents a haem group drawn on the same scale and in its correct orientation with respect to the crystal axes. The four lines on the cylinder surface indicate the positions of the concentrations of scattering matter deduced from the Fourier projections. The directions of the principal refractive indices are indicated by arrows.

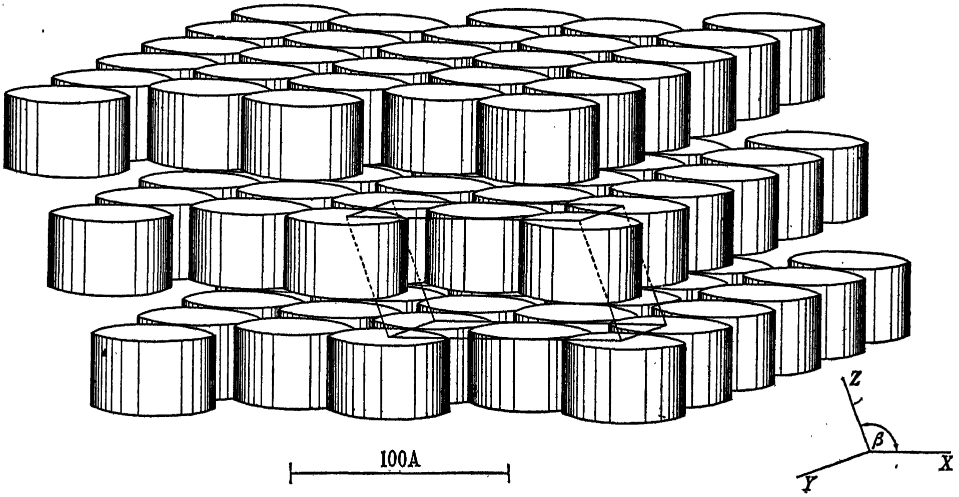

FIGURE 13. Packing of haemoglobin molecules in the crystal structure, showing layers of close-packed molecules separated by liquid. One unit cell is shown in the foreground on the right.

required for removing one layer of water molecules from around each cylinder. On drying by whatever method, the haemoglobin molecules tend to pack in pseudo-rhombohedral fashion, with any molecule in one layer coming to lie above the centre of a triangle formed by three molecules in the preceding layer.

Molecular structure

Space-group symmetry requires that each haemoglobin molecule consists of two chemically and structurally identical halves. The relative position of these two components in the unit cell cannot yet be distinguished. Evidence concerning the internal structure of the haemoglobin molecule comes both from two-dimensional Patterson projections and from one-dimensional Fourier projections. The former indicate that interatomic distances of 9 to 11 A occur frequently in several directions, while the latter show four prominent concentrations of scattering matter slightly less than 9 A apart along a line normal to the a, b plane. In figure 12 these concentrations are indicated by four horizontal lines around the surface of the cylinder. It is tempting to suggest that the concentrations of scattering matter actually correspond to four layers of polypeptide chains within each haemoglobin molecule, but there is too little evidence so far to support this view.

One of the most interesting questions concerns the positions of the four haem groups. Their *orientation* with respect to the crystal axes has been found from the optical dichroism of the crystals and is shown in figure 12. Apart from indirect evidence indicating the haem groups to lie on the surface of the haemoglobin molecules, no information about their *position* has emerged from this study.

Protein hydration and the liquid of crystallization

In the normal wet crystals the liquid of crystallization occupies 52·4 % of the unit-cell volume. In salt-free crystals this amounts to a water content of 0·82 g./g. protein. This intracrystalline water appears to consist of two distinct components: water 'bound' to the protein and not available as solvent to the diffusing ions, and 'free' water through which mobile ions can diffuse. In neutral ammonium sulphate solutions, the amount of 'bound' water was found to be approximately 0·3 g./g. protein over a wide range of salt concentrations, from which it may be deduced that 63 % of the total water $\left(\frac{0{\cdot}82-0{\cdot}3}{0{\cdot}82}\right)$ contained in salt-free crystals is available as solvent to mobile ions.

There are strong indications that the 'bound' water is on the surface of the protein molecules rather than in their interior, which suggests that they might be surrounded by a shell of solvent molecules similar to that of smaller solvated ions. This view is supported by calculations which show that the quantity of water required to cover each haemoglobin molecule with a single layer of water molecules is 0·28 g./g. protein, in good agreement with the observed value of 0·3. Nevertheless, this picture is probably oversimplified, because the density of electrostatic charges is not likely to be the same over the whole surface of the haemoglobin molecules, nor is the surface likely to be smooth.

9. DISCUSSION

(*a*) *Molecular symmetry*

It is sometimes asked whether the symmetry shown by X-ray photographs of proteins may not be spurious, whether certain symmetry elements would not, in fact, disappear if reflexions could be observed at sufficiently high angles or whether the symmetry might be due to some kind of statistical twinning. As regards the first argument it can now be stated that the entire diffraction pattern from wet methaemoglobin crystal has been analyzed down to spacings of 2·8 A, and that no case was observed where $I_{hkl} \neq I_{h\bar{k}l}$. The validity of the second argument cannot be tested by X-ray methods, but physico-chemical evidence speaks in favour of the twofold symmetry of the 66,700 unit. The molecular weight of horse haemoglobin in urea solution is only 34,000 (Wu & Yang 1932). Tiselius & Gross (1934) and Gutfreund (1946, unpublished) also found evidence that horse haemoglobin splits in dilute solution and in the presence of 1 M-ammonium sulphate. Wu & Yang state that sheep haemoglobin in urea solution does not split into halves, and it is interesting that Kendrew recently found sheep methaemoglobin to crystallize in the same space group as horse methaemoglobin, but with twice the number of molecules per unit cell (Kendrew 1946, unpublished). It is unlikely, therefore, that the diad axis in horse methaemoglobin gives a false picture of the symmetry of the molecule, though it is important to bear in mind that the scattering contribution from one individual amino-acid residue is insignificant compared with that of the molecule as a whole, so that small differences in the composition of the two halves need not necessarily have a measurable effect on the relative intensities of the X-ray reflexions.

(*b*) *Intramolecular structure*

We have refrained, so far, from offering any detailed interpretation of the one-dimensional Fourier synthesis or of the Patterson projections. Such interpretation is comparatively easy in the light of current ideas of polypeptide chain structure; the present difficulty is that almost any model based on a folded polypeptide chain structure agrees with the main features of the X-ray data. In view of the four prominent peaks on the one-dimensional Fourier projections it is tempting to propose a four-layered structure with the backbones of the polypeptide chains in the plane of the layers and the side chains protruding above and below, but the X-ray data do not prove its correctness, they are merely compatible with it. Surprisingly, the crystals are optically positive and the direction of the *greatest* refractive index is almost normal to the *a*, *b* plane (see figure 12). This might be attributed to the effect of the side chains which should run normal to the *a*, *b* plane, but in general one would expect a layer structure to be optically negative with the direction of the *smallest* refractive index normal to the layer plane.

The results described in this paper do not represent the limit of information which X-ray analysis can give. An extension of the Patterson synthesis to three dimensions is under way and should provide more clues regarding the internal structure of the molecule. With the help of absolute intensities whose measurement has recently come within the realm of possibility the derivation of a two-dimensional Fourier projection along the *b*-axis should also become feasible. Some revealing modifications in the crystal structure might also be brought about by chemical reactions inside the crystal leading to partial denaturation.

(c) *Molecular shape and the frictional ratio*

Attempts have been made to derive the shape of the haemoglobin molecule from its frictional ratio, as calculated from sedimentation and diffusion constants. Assuming the molecule to be an elongated ellipsoid of revolution, and hydration to be negligible, Polson (1939*b*) and Neurath (1939) suggested that the haemoglobin molecule has an axial ratio of 5 : 1. This result has been criticized by Oncley (1941), who showed that hydration and deviation from the spherical shape have complementary effects on the dissymmetry constant. Quite apart from the more detailed results of the X-ray analysis it would be impossible to fit a molecule of the shape proposed by Polson and Neurath into the unit cell.

It is of interest to compute the frictional ratio of haemoglobin on the basis of the X-ray data, treating the cylindrical molecule as an oblate spheroid with an axial ratio $34/57 = 0{\cdot}59$ (i.e. height/diameter of the cylinder) and a hydration of 0·3 g./g. protein. According to Oncley's chart (1941) this should have a frictional ratio $f/f_0 = 1{\cdot}15$. The observed frictional ratios given in the literature vary from 1·10 (Polson 1939*a*) to 1·24 (Tiselius & Gross 1934) and 1·28 (Anson & Northrop 1937). In view of these discrepancies Gutfreund (1946, unpublished) made a very careful determination of the sedimentation constant of horse methaemoglobin in a series of runs on a Svedberg oil-turbine ultra-centrifuge. In 0·5 to 0·9 % solutions he obtained an average sedimentation constant of $4{\cdot}6 \times 10^{-13}$, which, for a molecular weight of 66,700, gives a frictional ratio of $f/f_0 = 1{\cdot}13$ ($\pm 0{\cdot}02$). The agreement between this value and the one calculated on the basis of the X-ray data (1·15) is surprisingly good, and is an indication that the hydration of the protein in solution is the same as in the crystals.

Crowfoot (1941) in her review of X-ray work on protein crystals quotes the molecular dimensions of haemoglobin given in Perutz's thesis (1939*b*), where he showed that a triaxial ellipsoid with $x = 22$, $y = 24$, $z = 37{\cdot}6$ A was likely to fit into the unit cell of the dried crystals. These dimensions are, of course, superseded by the present analysis; they were calculated purely from considerations of packing, before the effects of swelling and shrinkage and of the presence of heavy ions in the liquid of crystallization had been discovered. Some preliminary investigations on the effect of caesium chloride in the suspension medium were actually reported in the thesis, but in these experiments insufficient attention had been paid to the recording of the lowest order reflexion which, as is now known, are the ones most strikingly affected by the presence of heavy ions.

(d) *Disorder effects in dried crystals*

Most of the X-ray diffraction pattern of horse methaemoglobin crystals disappears on drying, however carefully that process is carried out. The question arises, therefore, whether complete as opposed to partial drying of the crystals actually has a destructive influence on the molecular architecture of the protein itself. On the evidence of horse methaemoglobin crystals alone this seems not unlikely, except that there is no other evidence of denaturation on drying, i.e. dried crystals can be dissolved and recrystallized. The evidence of other crystalline proteins indicates that the degree of disorder may be merely a function of the amount of shrinkage in the crystals. Wet human CO-haemoglobin crystals, for instance, contain only 41·4 volume % of liquid, as opposed to 52·4% in horse methaemoglobin. When the crystals are dried without taking any special precautions, the pattern still extends to spacings of 6 A, as compared to 13 A in rapidly dried horse haemoglobin. Wet sheep methaemoglobin crystals, on the other hand, contain 56 volume % of liquid, with the result that the pattern obtained from rapidly dried crystals is too poor even to measure the cell dimensions. All these data go to show that shrinkage of the crystals introduces a degree of intermolecular disorder which may chiefly depend on the amount of liquid in the wet unit cell. It would be interesting to know why such great variations in the liquid content of different protein crystals exist. It must be partially a question of packing, as shown by the different cell volumes of orthorhombic and monoclinic horse haemoglobins (table 1). There may be other factors, such as the proportion of polar side chains in different proteins and the extent to which the polar groups are in contact with the surrounding liquid.

(*e*) *Structural similarities of different proteins*

The general character of the X-ray pattern seems to be the same in all wet protein crystals studied so far. The pattern usually extends to spacings of 2 to 3 A, even in crystalline viruses with unit-cell dimensions of the order to 300 A (Crowfoot & Schmidt 1945). Strong intensities appear at spacings of the order of 10 and 4·5 A and give rise to distinctive systems of peaks on the vector diagrams. There is no doubt that these vector peaks must have a similar origin to Astbury's well-known backbone and side-chain reflexions on protein fibre photographs, but the multiplicity of the vector peaks has so far prevented any unambiguous interpretation. The rigidity of the intramolecular vector peak system and its independence of the cell dimensions were first discovered by Crowfoot & Riley in crystalline insulin (Crowfoot & Riley 1939); lactoglobulin also shows it, though less markedly on account of the more complex intermolecular structure (Riley 1942). The shape of the insulin molecule may actually be similar to that of horse haemoglobin and approximate to a cylinder 30 A high with a hexagonal base 43 A across (Crowfoot 1941). Moreover, insulin crystals show positive birefringence of the same order of magnitude as haemoglobin (in insulin $n_\varepsilon - n_\omega = 0{\cdot}007$; in methaemoglobin $n_\gamma - n_\alpha = 0{\cdot}007$) and in both cases the direction of the highest refractive index coincides approximately with the cylinder axis of the molecule.

Apart from these general similarities which point to the existence of certain common features among the proteins investigated so far, one can perceive a bewildering variety of different structures. As far as the unit-cell dimensions and space groups are concerned, a survey of the available data reveals no sign of the emergence of certain structural types. This may partly be due to differences in intermolecular packing which may obscure common features of the intramolecular architecture.

The relationship between different haemoglobin derivatives of the same species emerges more clearly. Though oxy- and carboxyhaemoglobin were usually obtained in the orthorhombic form described elsewhere (Perutz 1942*b*), this form is closely related to the orthorhombic modification of methaemoglobin described in § 4 (*b*), p. 92. The monoclinic variety of oxy- and carboxyhaemoglobin described by Reichert & Brown (1909) seems to be isomorphous with the monoclinic modification of methaemoglobin studied here. Azide methaemoglobin has the same unit-cell dimensions and intensity distribution as methaemoglobin. Thus methaemoglobin and its compounds, and oxy- and carboxyhaemoglobin seem to have closely related if not identical crystal structures. Reduced haemoglobin, on the other hand, crystallizes in the rhombohedral system and possibly has a molecular structure differing from both methaemoglobin and oxyhaemoglobin (Haurowitz 1938; Perutz, unpublished data). There are no measurable differences of structure between haemoglobins from different individuals of the same species.

The authors wish to thank Sir Lawrence Bragg for contributing many vital suggestions to this work, which would never have been carried to the present stage without his active encouragement and interest; and Professor D. Keilin, who gave us much valuable help on the biochemical side of the problem. The work was begun originally under the direction of Professor J. D. Bernal, to whom we are grateful for his continued interest and much stimulating discussion and criticism. We also benefited from discussion with Dr D. Crowfoot, Dr H. Lipson and Dr A. J. C. Wilson. We should like to acknowledge the help of Dr D. P. Riley, who calculated three of the Patterson projections; Dr Christian Finbak, who calculated one projection; Mrs A. C. Horton, who kindly helped us with the preparation of additional Fourier strips; and Mr James Buchanan, who also did some computing work for us. We are grateful to the Rockefeller Foundation for their generosity in financing this research and for helping us over some difficult periods.

REFERENCES

Anson, M. L. & Northrop, J. H. 1937 *J. Gen. Physiol.* **20**, 575.
Astbury, W. T. 1940 *J. Soc. Leath. Tr. Chem.* **24**, 69.
Astbury, W. T. 1942 *J. Chem. Soc.* p. 337.
Beevers, C. A. & Lipson, H. 1936 *Proc. Phys. Soc.* **48**, 772.
Bernal, J. D., Fankuchen, I. & Perutz, M. F. 1938 *Nature*, **141**, 523.
Boyes-Watson, J. & Perutz, M. F. 1943 *Nature*, **151**, 714.
Chibnall, A. C. 1945 *J. Soc. Leath. Tr. Chem.* **30**, 1.
Cohn, E. J. & Edsall, J. T. 1943 *Proteins, amino-acids and peptides.* New York: Reinhold Publ. Corp.
Crowfoot, D. 1938 *Proc. Roy. Soc.* A, **164**, 580.
Crowfoot, D. 1941 *Chem. Rev.* **28**, 215.

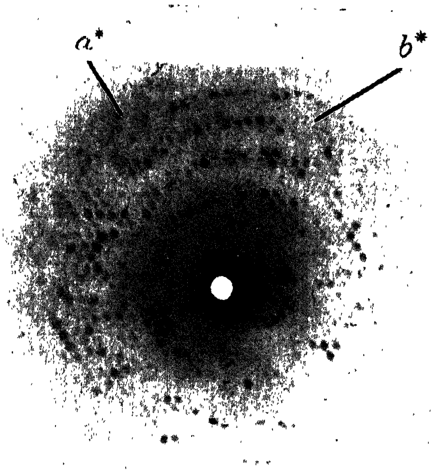

14

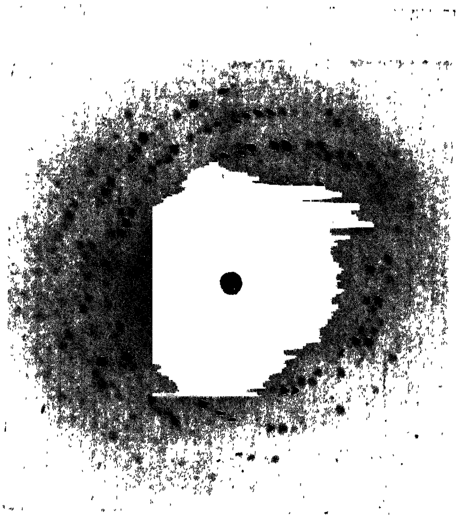

15

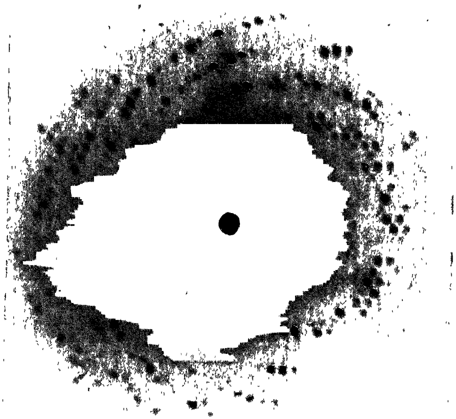

16

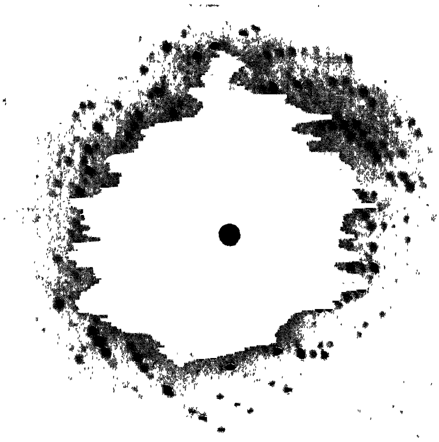

17

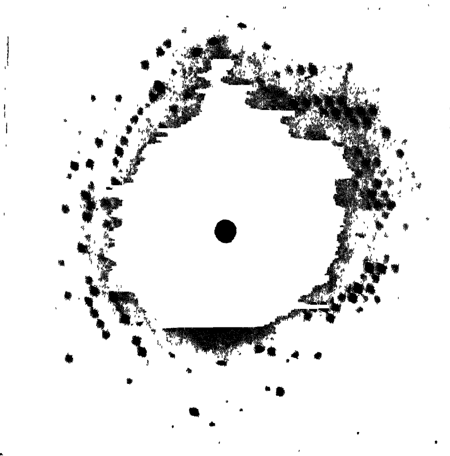

18

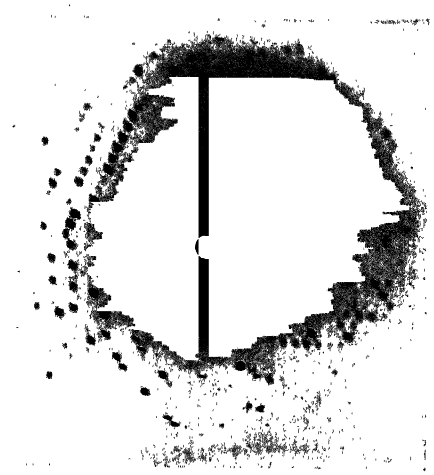

19

20

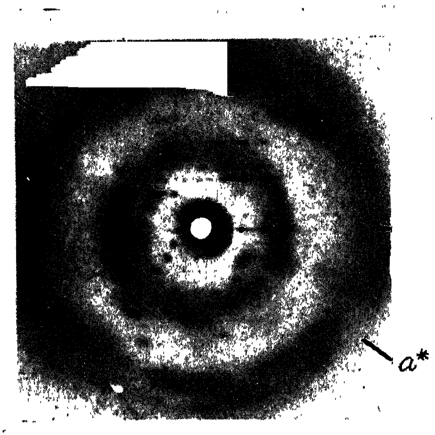

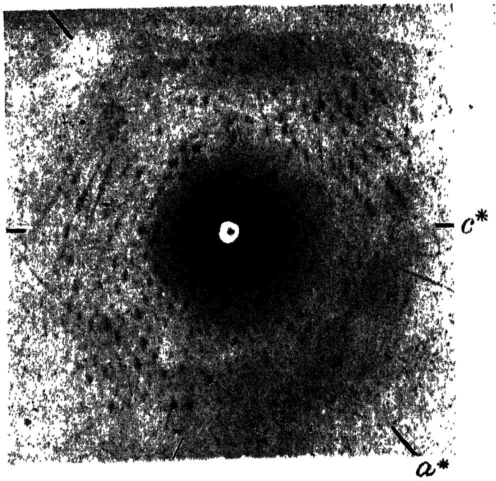

21

22

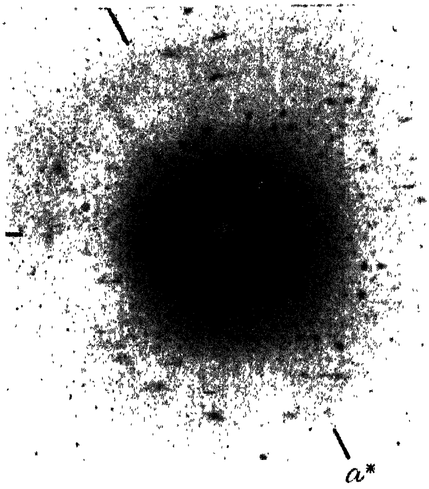

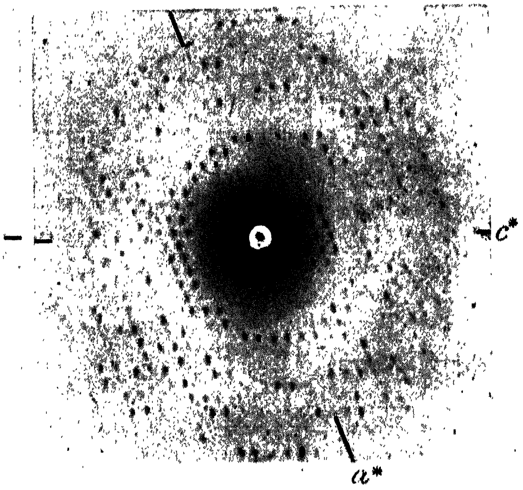

23

24

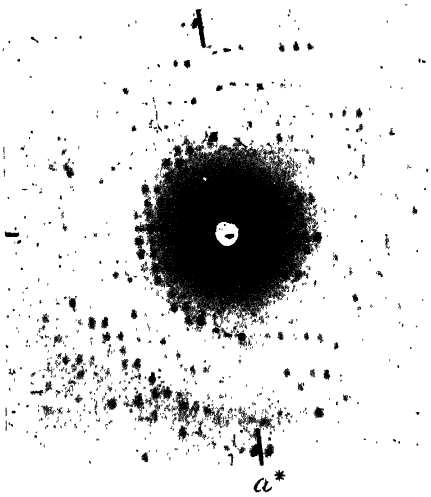

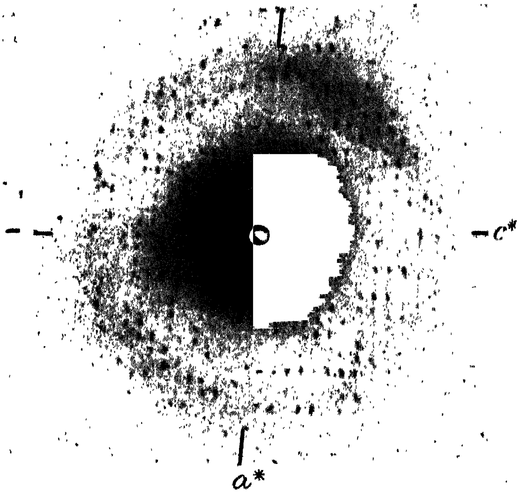

25

Crowfoot, D. & Riley, D. P. 1939 *Nature*, **144**, 1011.
Crowfoot, D. & Schmidt, G. M. J. 1945 *Nature*, **155**, 504.
Ewald, P. P. 1935 *Z. Kristallogr.* **90**, 493.
Fankuchen, I. 1940–1 *J. Gen. Physiol.* **24**, 315.
Fankuchen, I. 1945 *Ann. Rev. Biochem.* **14**, 213.
Haurowitz, F. 1938 *Hoppe-Seyl. Z.* **254**, 266.
Hettich, A. 1935 *Z. Kristallogr.* **90**, 483.
Keilin, D. & Hartree, E. F. 1935 *Proc. Roy. Soc.* B, **117**, 1.
Knott, G. 1940 *Proc. Phys. Soc.* **52**, 229.
McMeekin, T. L. & Warner, R. C. 1942 *J. Amer. Chem. Soc.* **64**, 2393.
Neurath, H. 1939 *J. Amer. Chem. Soc.* **61**, 1841.
Oncley, J. L. 1941 *Ann. N.Y. Acad. Sci.* **41**, 121.
Perutz, M. F. 1939*a* *Nature*, **143**, 731.
Perutz, M. F. 1939*b* Ph.D. Thesis, Cambridge.
Perutz, M. F. 1942*a* *Nature*, **149**, 491.
Perutz, M. F. 1942*b* *Nature*, **150**, 324.
Perutz, M. F. 1947 *Trans. Faraday Soc.* A discussion on swelling and shrinkage. (In the Press.)
Perutz, M. F. & Rogers, G. L. 1946 *J. Sci. Instrum.* **23**, 217.
Polson, A. 1939*a* *Kolloidzschr.* **87**, 149.
Polson, A. 1939*b* *Kolloidzschr.* **88**, 51.
Reichert, E. T. & Brown, A. P. 1909 *The crystallography of the haemoglobins.* Carnegie Institute of Washington.
Riley, D. P. 1942 The crystal structure of some proteins. Ph.D. Thesis, Oxford.
Ross, M. A. S. 1943 *Nature*, **152**, 302.
Robertson, J. M. 1945 *J. Chem. Soc.* p. 607.
Sanger, F. 1945 *Biochem. J.* **39**, 507.
Synge, R. L. M. 1943 *Chem. Rev.* **32**, 135.
Tiselius, A. & Gross, D. 1934 *Kolloidzschr.* **66**, 11.
Wu, H. & Yang, E. 1932 *Chinese J. Physiol.* **6**, 51.

Description of Plates 5 and 6

Plate 5

Figures 14 to 19. Oscillation photographs of wet horse methaemoglobin crystal taken on flat films at 5 cm. distance from the specimen with filtered Cu radiation. Oscillation about [110]; beam parallel [001] at 0° in figure 14. Oscillation from 0 to 5° in figure 14, from 4·5 to 7° in figure 15, 6·5 to 9° in figure 16, etc.

Plate 6

Figures 20 to 25. 5° oscillation photographs of horse methaemoglobin crystals at six different states of swelling. In each case the crystal was oscillated about [100] and the beam was parallel to [010] at one end of the oscillation. The photographs correspond to unit cells numbers 10, 3, 4, 5, 6 and 7 respectively. Film distance 6 cm. The c^* axis is horizontal in all photographs; the direction of a^* varies according to the angle β, as indicated. The dark haloes near the centre of the photographs are due to air scattering. Their intensity is much exaggerated by the reproductions.

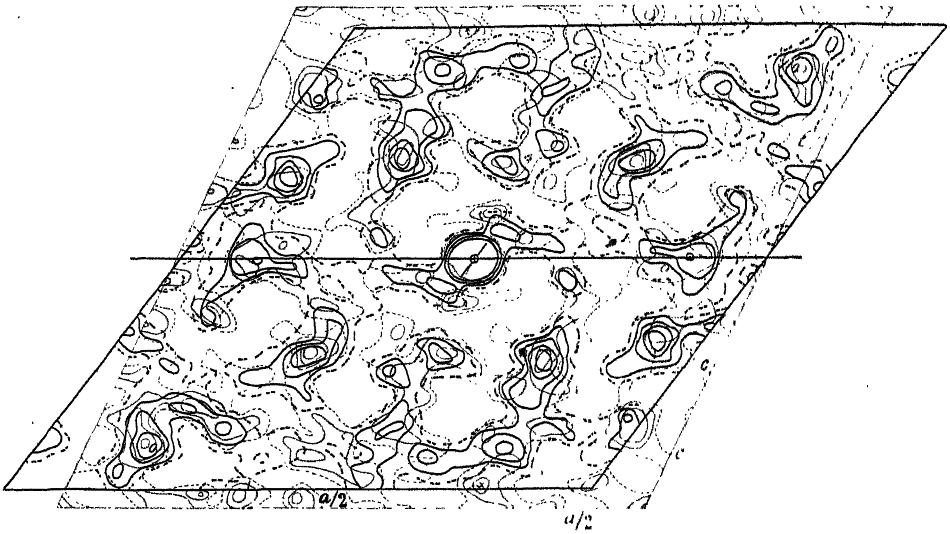

FIGURE 4*a* and *b*

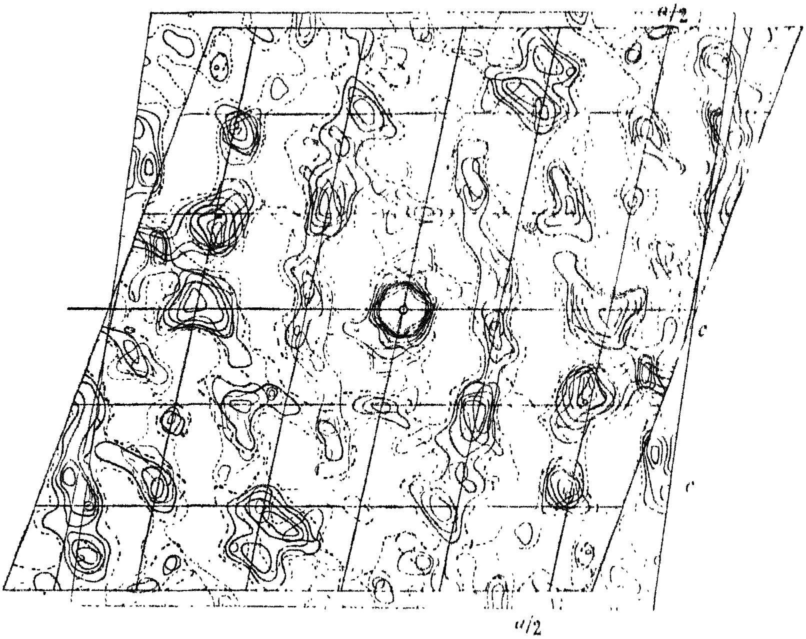

FIGURE 4*c* and *d*

FIGURE 4. Patterson-Fourier projections along the *b*-axis at different states of swelling. For cell dimensions see table 3. Figure 4*a* (black) corresponds to unit cell number 3, *b* (red) to number 4, *c* (green) to number 5, *d* (blue) to number 6 and *e* (orange) to number 7. Figure 4*c* is the same as figure 3*b* except for the application of a temperature factor of $e^{-60\sin^2\theta/\lambda^2}$. Projection 4*e* was calculated by Dr Christian Finbak. 1 cm. = 7 A.

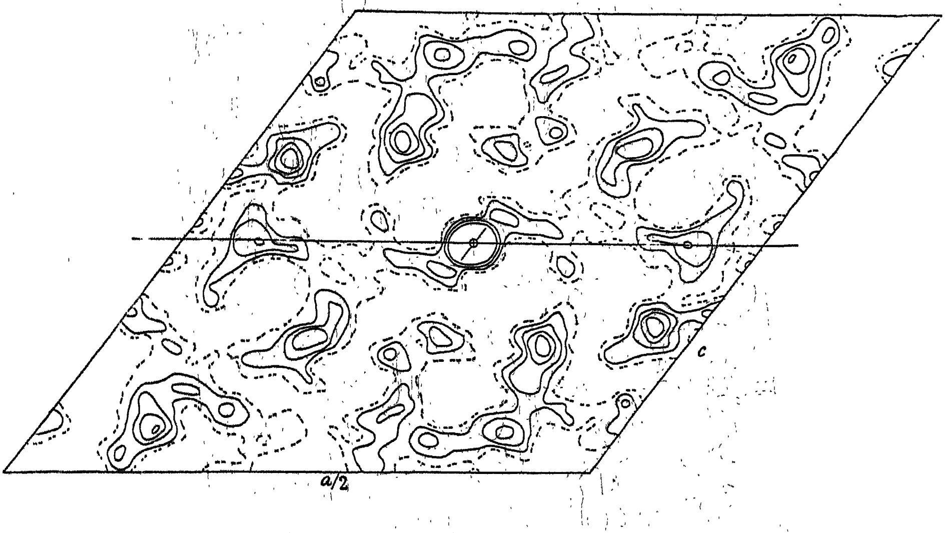

FIGURE 4*a* and *e*

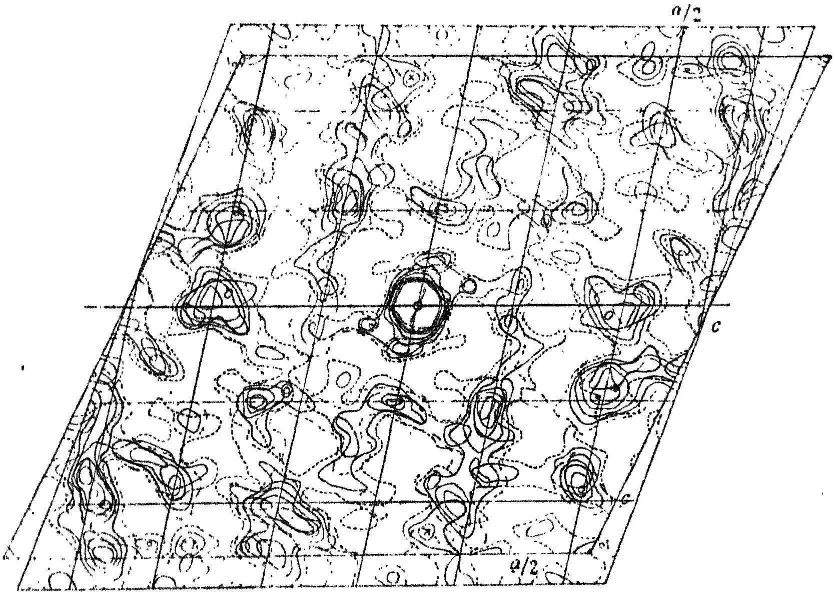

FIGURE 4*b* and *c*

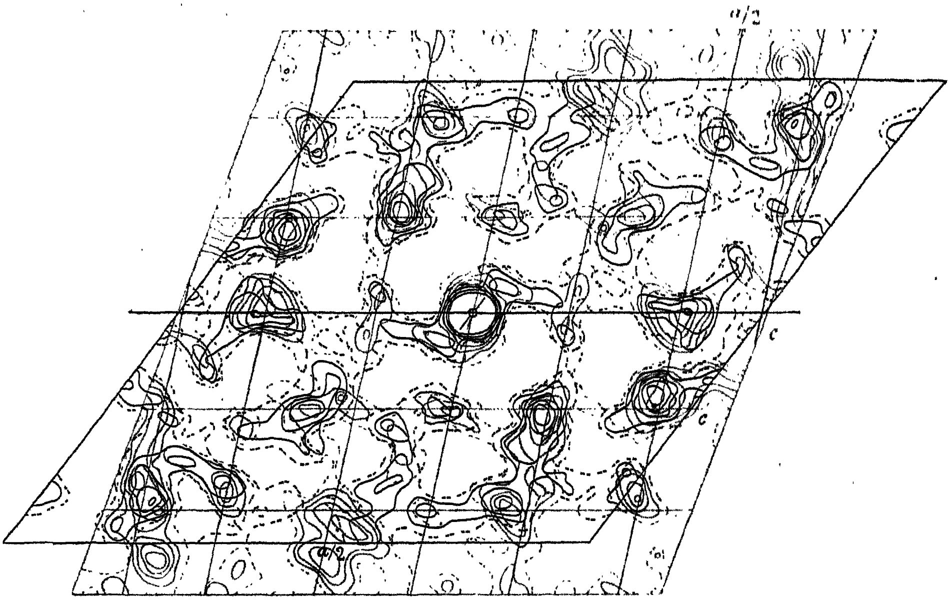

FIGURE 4*a* and *c*

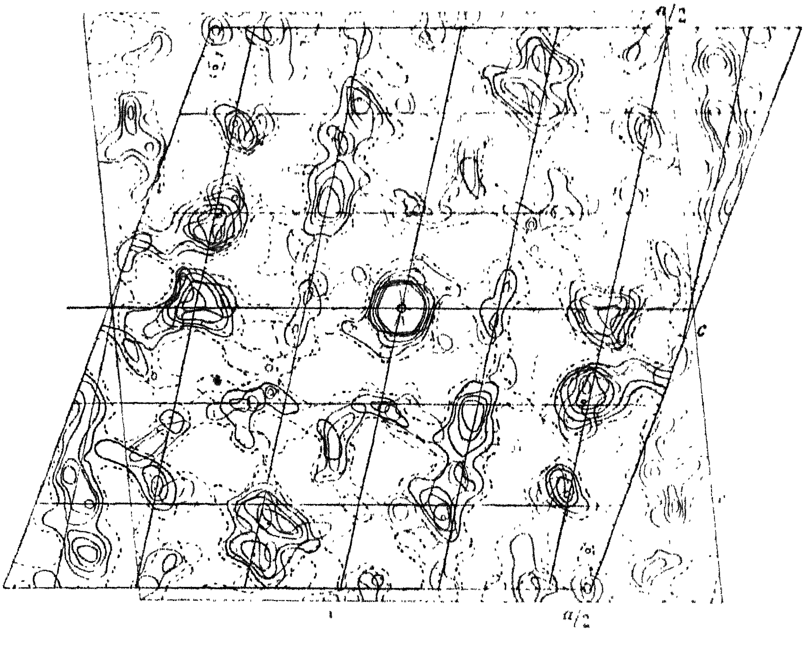

FIGURE 4*c* and *e*

Quantum electrodynamics and low-energy photons

By C. Jayaratnam Eliezer, *Christ's College, University of Cambridge*

(*Communicated by P. A. M. Dirac, F.R.S.—Received* 11 *March* 1947)

The probability of certain transition processes involving low-energy photons is investigated on the basis of Dirac's recent method of field quantization. It is shown that the treatment using an expansion in powers of $e^2/\hbar c$ is inconsistent, as it leads to an infinite value for the probability, when one integrates over a low-energy photon.

1. Introduction

In some recent papers Dirac (1939, 1942) has given a formulation of quantum electrodynamics which eliminates the usual divergent integrals that arise when the wave equation that describes the interaction of an electron and an electromagnetic field is solved by expressing the wave function as an expansion in ascending powers of $e^2/\hbar c$, the fine-structure constant. This elimination of infinities is brought about by the use of the λ-limiting process which is employed to express the classical equations of motion in Hamiltonian form, and the introduction of negative-energy photons in the physical interpretation of the quantum-mechanical representation. Further, one also takes as the physical solutions only those which correspond to outgoing waves of the electron (Eliezer 1946*a*).

The existence of these finite solutions makes it now possible to investigate exactly processes involving any number of photons. I have considered recently (Eliezer 1946*b*) a scattering process in which three photons take part. It was shown that the probability of a photon dividing into two photons in the presence of an electron could be large if one of the emitted photons is of small frequency. This result could be generalized to any number of photons, and the conclusion be drawn that the probability of multiple emission could be large, provided some of the emitted photons are of small frequency. A natural inference would be that quantum electrodynamics does not disallow the possibility of photon showers in which a large number of photons are simultaneously emitted, a phenomenon which seems to be in evidence in cosmic-ray experiments.

The next stage of the calculations is to integrate the probability over the directions and frequencies of the emitted photons of small frequency, this integrated probability being the one of physical interest in such processes. One would expect that even though the number of low-frequency photons may be infinite, the total energy emitted should be finite and small, and the scattering cross-section also should be finite and comparatively smaller than that for the simple Compton scattering. But the calculations which are given below show that this is not the case. The present theory does not give a finite value for the cross-section. Thus, in the three-photons process in which an incident photon is scattered into two photons, it is found that the scattering cross-section increases without limit as one of the emitted photons approaches the frequency and direction corresponding to the simple Compton scattering. In this way it appears that the present treatment using the expansion in powers of $e^2/\hbar c$ requires modification before it can be used to give a consistent account of processes involving low-energy photons. The same conclusion has been arrived at by Pauli (1946), who considers the emission of a light quantum by a bound electron.

2. The transition probability

Take units such that c, the velocity of light, is unity, and $\hbar$, Planck's constant divided by 2π, is also unity. Let $\mathbf{1}$ denote the direction of propagation, k_0 the frequency and I the intensity of the k photon beam, with similar meanings for $\mathbf{1}'$, k_0', I' and $\mathbf{1}''$, k_0'', I''. The method of calculating the probability is briefly recapitulated. Starting with an electron which is initially at rest, solve the wave equation by expanding in ascending powers of e, the charge of the electron, thus obtaining $e^3\psi_{3,3}$ as the appropriate wave function for a process in which three photons take part. Then determine the density of electrons, which is given by the diagonal sum of the matrix $e^6\psi_{3,3}\phi_{3,3}$, and divide by the initial density of electrons. Assuming that one of the beams of photons, k'' say, to be not sharply monochromatic, replace I'' by $k_0''^3 dk_0''/2\pi$ and integrate over its frequency range, obtaining a transition probability which is proportional to the time. From this expression the probability per unit time of a triple emission process in which the k'' photon is spontaneously emitted and the k and k' photons stimulated is deduced. It is seen that such a process can take place only when the photons satisfy a certain relation

$$(m-k_0-k_0'-k_0'')^2-m^2-(\mathbf{k}+\mathbf{k}'+\mathbf{k}'')^2 = 0,$$

which condition is seen to express the conservation of energy and momentum in the process.

The probability of an incident photon k dividing into two photons k' and k'' is then obtained by changing k_0 to $-k_0$ and by replacing I' by $k_0'^3/2\pi$. The conservation requirement gives the relation

$$m(k_0-k_0'-k_0'') = k_0k_0'(1-\mathbf{1}.\mathbf{1}')+k_0k_0''(1-\mathbf{1}.\mathbf{1}'')-k_0'k_0''(1-\mathbf{1}'.\mathbf{1}''). \tag{1}$$

After summing the probability expression over the directions of polarization of the emitted photons and averaging over the incident photon, an expression is obtained of the form

$$P = \frac{\pi^4 e^6 k_0' k_0''^2 I}{4m^2 k_0^2 \gamma_{k'-k}}\left[\frac{\lambda_1}{\gamma^2_{k'+k''}}+\frac{\lambda_1'}{\gamma^2_{k''-k}}+\frac{\lambda_1''}{\gamma^2_{k'-k}}+\frac{\lambda_2}{\gamma_{k'-k}\gamma_{k''-k}}+\frac{\lambda_2'}{\gamma_{k'-k}\gamma_{k'+k''}}+\frac{\lambda_2''}{\gamma_{k''-k}\gamma_{k'+k''}}\right], \tag{2}$$

as the probability per unit time per unit solid angle of direction of k' photon about $\mathbf{1}'$, and k'' photon about $\mathbf{1}''$, and per unit frequency range of the k' photon. The notation

$$\gamma_a \equiv (m-a_0)^2-\mathbf{a}^2-m^2$$

has been used, where $(a_0, \mathbf{a})$ is a four-vector. The λ's have been calculated but are not reproduced here owing to their lengthy expressions. They are homogeneous expressions of the third degree in m, k_0, k_0' and k_0''. In this notation, the conservation requirement (1) is equivalent to $\gamma_{k'+k''-k} = 0$.

3. INTEGRATION OVER LOW-FREQUENCY PHOTON

The expression (2) gives the probability per unit solid angle of direction of k'' photon about $\mathbf{1}''$, and therefore by integrating (2) over the directions of emission of k'' photon, the total probability of the emission of the k' photon is obtained for all possible k'' photons. For a given direction $\mathbf{1}''$, the corresponding frequency k_0'' is given by the equation (1), which may be written as

$$2k_0'' = \frac{\gamma_{k'-k}}{m + k_0 - k_0' - (\mathbf{k} - \mathbf{k}').\mathbf{1}''}. \tag{3}$$

Therefore this value of k_0'' is substituted in P, and

$$\int P \, d\Omega''$$

is evaluated, where $d\Omega''$ is the elemental solid angle about the direction $\mathbf{1}''$. Taking the direction $\mathbf{k}-\mathbf{k}'$ for the polar axis, and denoting by θ the angle between $\mathbf{k}-\mathbf{k}'$ and $\mathbf{1}''$, one obtains

$$\int P \, d\Omega'' = \int_0^\pi P \, 2\pi \sin\theta \, d\theta.$$

The integration with respect to θ is seen to be straightforward. The crucial question is whether the integrated probability value remains finite for all possible k' photons. For given direction $\mathbf{1}'$, the corresponding frequency k_0' should lie between zero and ν, where

$$\nu = mk_0/\{m + k_0(1 - \mathbf{1}.\mathbf{1}')\}. \tag{4}$$

The extreme values zero and ν are excluded but may be approached close enough to any desired extent. The difficulty arises when k_0' tends to ν. It is seen that as k_0' approaches ν, $\gamma_{k'-k}$ tends to zero, and

$$P = \pi^4 e^6 k_0' k_0''^2 I \lambda_1''/4m^2 k_0^2 \gamma_{k'-k}^3, \tag{5}$$

approximately, retaining only the terms of the highest order. λ_1'' has been calculated in a previous paper (Eliezer 1946*b*) and is

$$\begin{aligned}\lambda_1'' = {} & 16(k_0 - k_0' - k_0'')\,[\{2k_0^2 + 2k_0'^2 - k_0 k_0'(1 + 2\zeta - \zeta^2)\}\,(1-\zeta) + m(2m + k_0 - k_0') \\ & \times (1+\zeta^2) - \zeta\gamma_{k'-k}] + 8(\mathbf{k} - \mathbf{k}' - \mathbf{k}''.\mathbf{1}'')\,[\gamma_{k'-k}(1+\zeta)\,(1 + \mathbf{1}'.\mathbf{1}'') - 4(\mathbf{k} - \mathbf{k}'.\mathbf{1}'') \\ & \times \{(k_0 - k_0')\,(1-\zeta) + m(1+\zeta^2)\}] + 32m(1-\zeta)\,\{k_0^2 + k_0'^2 - k_0 k_0'(1-\zeta^2)\},\end{aligned} \tag{6}$$

where $\mathbf{1}.\mathbf{1}' \equiv \zeta$. Neglecting terms which vanish with $\gamma_{k'-k}$, and making further simplifications, one obtains

$$\lambda_1'' = 32[m(1+\zeta^2) + (k_0 - k_0')\,(1-\zeta)]\,[(\mathbf{k} - \mathbf{k}')^2 - (\mathbf{k} - \mathbf{k}'.\mathbf{1}'')^2]. \tag{7}$$

Writing $m+k_0-k_0'=E$, $|\mathbf{k}-\mathbf{k}'|=K$, then $k_0''=\frac{1}{2}\gamma_{k'-k}/(E-K\cos\theta)$. Since $E^2-K^2=m^2+\gamma_{k'-k}>0$, therefore $E-K\cos\theta$ does not vanish for any value of θ, and hence no difficulties arise in the integration with respect to θ. Thus

$$\int P\,d\Omega''=\frac{4\pi^5e^6k_0'\,I}{m^2k_0^2}[m(1+\zeta^2)+(k_0-k_0')(1-\zeta)]\frac{1}{\gamma_{k'-k}}\int_0^\pi\frac{(1-\cos^2\theta)\sin\theta\,d\theta}{(\cos\theta-E/K)^2}. \tag{8}$$

Hence, unless the integral in (8) is of the order $\gamma_{k'-k}$, the total probability would not remain finite as $\gamma_{k'-k}$ tends to zero. This integral is

$$\int_{-1}^{1}\frac{1-\omega^2}{(\omega-E/K)^2}d\omega=\frac{2E}{K}\log\frac{E+K}{E-K}-4,$$

which does not vanish with $\gamma_{k'-k}$. Therefore the probability per unit time per unit frequency range of the k' photon and per unit solid angle about $\mathbf{l}'$, integrated over all k'' photons, is approximately

$$\frac{8\pi^5e^6k_0'\,I}{m^2k_0^2}[m(1+\mathbf{l}.\mathbf{l}')^2+(k_0-k_0')(1-\mathbf{l}.\mathbf{l}')]$$
$$\times\left[\frac{m+k_0-k_0'}{|\mathbf{k}-\mathbf{k}'|}\log\frac{m+k_0-k_0'+|\mathbf{k}-\mathbf{k}'|}{m+k_0-k_0'-|\mathbf{k}-\mathbf{k}'|}-2\right]\frac{1}{\gamma_{k'-k}}$$

which increases without limit as $\gamma_{k'-k}$ approaches zero, that is, as k_0' approaches ν.

It is thus apparent that Dirac's method of field quantization does not remove the difficulty of 'the infra-red catastrophe' of the older theories. Therefore in dealing with processes involving low-energy photons, one has for the present to give up the expansion in powers of $e^2/\hbar c$, and make use of some approximate treatment such as by Bloch & Nordsieck (1937), where there is closer analogy with the classical theory of radiating electrons.

The author records his warmest thanks to Professor P. A. M. Dirac and Professor W. Pauli for their interest in this work, and the Royal Commissioners for the Exhibition of 1851 for a senior studentship.

REFERENCES

Bloch & Nordsieck 1937 *Phys. Rev.* **52**, 54.
Dirac 1939 *Ann. Inst. Poincaré*, **9**, 13.
Dirac 1942 *Proc. Roy. Soc.* A, **180**, 1.
Eliezer 1946*a* *Proc. Roy. Soc.* A, **187**, 197.
Eliezer 1946*b* *Proc. Roy. Soc.* A, **187**, 210.
Pauli 1946 *Helv. Phys. Acta*, **19**, 234.

Application of quaternions to rotations in hyperbolic space of four dimensions

By A. W. Conway, F.R.S.

(*Received* 13 *December* 1946)

The application of quaternions to flat 4-space was first made in two papers, which have largely escaped notice, by Stringham (1901) and Hathaway (1902). The Lorentz transformation in special relativity is a simple type of rotation in hyperbolic space, and for early applications reference can be made to Silberstein (1924). Recent papers are by Weiss (1941), Dirac (1945) and Gormley (1947). The latter paper treats of a very general type of homographic transformation.

In flat 4-space a general rotation can be made up of two planar rotations in orthogonal planes, and these component rotations are commutative. In hyperbolic space a general rotation is made up of two planar rotations in planes which are reciprocal with respect to the hypercone, $t^2 = x^2+y^2+z^2$. Of the two planes one cuts the hypercone in real 4-vectors and the rotation in this plane is hyperbolic, the rotation in the other plane is circular. The rotations are commutative. A second type of transformation which has some of the properties of a rotation is also considered.

Notation

A 4-vector is represented by a quaternion $q = t+\alpha x+\beta y+\gamma z$ ($\beta\gamma = -\gamma\beta = \alpha$; $\alpha^2 = -1$, etc.). C_3 is the hypercone $Sq^2 = 0$, i.e. $t^2-x^2-y^2-z^2 = 0$. The 4-space $t^2 > x^2+y^2+z^2 > 0$ will be called the inside of the hypercone. The outside will have $x^2+y^2+z^2 > t^2$.

Two 4-vectors q_r, q_s are reciprocal with respect to C_3 if $Sq_rq_s = 0$, i.e.

$$t_rt_s = x_rx_s+y_ry_s+z_rz_s.$$

From this $t_r^2t_s^2 < (x_r^2+y_r^2+z_r^2)(x_s^2+y_s^2+z_s^2)$. Therefore of two reciprocal 4-vectors one must be inside or both outside C_3.

Hamilton's function $(q_1q_2q_3q_4)$ is the 4-volume given by the determinant $|x_ry_rz_rt_r|$. From this we get

$$(q_1q_2q_3q_4)^2 = -Sq_1^2Sq_2^2Sq_3^2Sq_4^2, \tag{1}$$

if q_r ($r = 1, 2, 3, 4$) are reciprocal 4-vectors. We can normalize the tetrad q_r by putting $Sq_r^2 = \pm 1$. Hence only one of the tetrads can be inside C_3, and so for a normal reciprocal tetrad

$$Sq_1^2 = -Sq_2^2 = -Sq_3^2 = -Sq_4^2; \quad Sq_rq_s = 0 \quad (r \neq s),$$

any q can be expressed in the form

$$q = q_1Sqq_1-q_2Sqq_2-q_3Sqq_3-q_4Sqq_4. \tag{2}$$

From (1) we see that $(q_1q_2q_3q_4) = \pm 1$, so that there are two kinds of normal reciprocal tetrads. We shall speak of tetrads as like or unlike; 3-vectors will be denoted by greek letters. (α, β, γ); (ξ, η, ζ); (λ, μ, ν); (σ, τ, υ), will denote triads of mutually perpendicular vectors, and in all cases we shall take them as right-handed, i.e. $\alpha\beta\gamma = \xi\eta\zeta = \lambda\mu\nu = -1$. ρ will denote any vector, i.e. $q = t+\rho$.

Generally a, b, p, q, r will denote quaternions.

The rotation function f

If q_1, q_2, q_3, q_4 and q_1', q_2', q_3', q_4' are two like tetrads, a linear function of q is given by

$$f(q) = q_1' Sqq_1 - q_2' Sqq_2 - q_3' Sqq_3 - q_4' Sqq_4,$$

and its quaternion conjugate by

$$f_c(q) = q_1 Sqq_1' - q_2 Sqq_2' - q_3 Sqq_3' - q_4 Sqq_4'.$$

From these and the properties of the tetrads $f_c f(q) = 1$.

If we form the invariant n of f, i.e.

$$\begin{aligned} n &= (fq_1fq_2fq_3fq_4)/(q_1q_2q_3q_4) \\ &= (q_1'q_2'q_3'q_4')/(q_1q_2q_3q_4) = 1 \end{aligned}$$

because the tetrads are like. We then define the rotation function f by the equations

$$ff_c = 1; \quad n = 1.$$

(The function $ff_c = 1$; $n = -1$ will be considered briefly in the last section.) We have then for any two quaternions

$$Sfpfq = Spf_cfq = Spq.$$

Axes and latent roots of f

f satisfies a symbolic quartic

$$f^4 - n'''f^3 + n''f^2 - n'f + n = 0. \tag{3}$$

f_c satisfies the same quartic and $f_c = f^{-1}$, and so (3) is the same quartic as

$$f^4 - n^{-1}n'f^3 + n^{-1}n''f^2 - n^{-1}n''' + n^{-1} = 0,$$

so that $n^2 = 1$, and for f we have taken the positive value $+1$ and we get $n' = n'''$ and the quartic breaks up into the quadratics

$$f^2 - 2z_1f + 1 = 0, \quad f^2 - 2z_2f + 1 = 0. \tag{4}$$

The latent roots x_r satisfy the same equations.

Let a_r be the axes of f, then $\quad f(a_r) = x_r a_r.$ (5)

It may first be noted that $\quad Sa_r^2 = Sfa_rfa_r = x_r^2 Sa_r^2.$

If we suppose that none of the roots x_r is ± 1 then

$$Sa_r^2 = 0, \tag{6}$$

i.e. all the axes are on C_3.

From (5) $$a_r = f_c f a_r = x_r f_c a_r,\quad f_c a_r = x_r^{-1} a_r,$$
and so from (5) $$(f+f_c)\,a_r = (x_r + x_r^{-1})\,a_r.$$

$f+f_c$ is a self-conjugate linear function, and so its latent roots are real. Thus f has latent roots x_1, x_1^{-1}, x_3, x_3^{-1} in which $x_1+x_1^{-1}$, $x_3+x_3^{-1}$ are real, the corresponding axes being a_1, a_2, a_3, a_4.

If x_r, x_s are two roots which are not reciprocals, i.e. $x_r x_s \neq 1$,

$$Sa_r a_s = Sfa_r fa_s = x_r x_s Sa_r a_s,$$
therefore $$Sa_r a_s = 0,$$
i.e. any 4-vector in the plane $\{a_1 a_2\}$ is reciprocal to any 4-vector in the plane $\{a_3 a_4\}$. In each plane we can get an infinite number of reciprocal pairs of 4-vectors and two such pairs will make a reciprocal tetrad, and so out of each two pairs only one will be inside C_3 and thus one plane will meet C_3 in real 4-vectors and the other in imaginary. Suppose that $\{a_1 a_2\}$ meet it in real lines, then x_1 and x_1^{-1} are real, x_3 and x_3^{-1} are imaginary.

Writing $$b_1 = l_1 a_1 + l_2 a_2,\quad b_2 = l_1 a_1 - l_2 a_2,$$
we get $$Sb_1 b_2 = 0,\quad Sb_1^2 = -Sb_2^2 = l_1 l_2 Sa_2 a_2.$$
We will suppose that $l_1 l_2 Sa_2 a_2$ is positive, and so we can choose $l_1 l_2$ such that
$$Sb_1^2 = -Sb_2^2 = 1.$$
We can further choose l_1, l_2 such that $l_1 a_1 - l_2 a_2$ is a vector σ and it is a unit vector because $-Sb_2^2 = -S\sigma^2 = 1$. b_1 is of the form $l+m\nu$, and if we take $\nu^2 = -1$ we get for $Sb_1^2 = 1$, $l^2 - m^2 = 1$. Also since $Sb_1 b_2 = 0$ we have $S\sigma\nu = 0$.

The equations $$fa_1 = x_1 a_1,\quad fa_2 = x_1^{-1} a_2$$
become $$fb_1 = b_1 \cosh u + b_2 \sinh u,\quad fb_2 = b_1 \sinh u + b_2 \cosh u, \tag{7}$$
where $$x_1 = e^u.$$

In the same way for the imaginary roots putting $x_3 = e^{iv}$, we get
$$f(b_3) = b_3 \cos v - b_4 \sin v,\quad f(b_4) = b_3 \sin v + b_4 \cos v.$$
Here b_4 is a vector τ and since
$$Sb_4 b_3 = 0,\quad Sb_4 b_2 = 0,\quad Sb_4 b_1 = 0,$$
b_3 must be of the form $m + l\nu$ and σ, τ, ν are a triad of unit vectors.

Any q can be expressed in the form
$$q = b_1 Sb_1 q - b_2 Sb_2 q - b_3 Sb_3 q - b_4 Sb_4 q,$$
and finally
$$f(q) = (b_1 \cosh u + b_2 \sinh u)\, Sb_1 q - (b_1 \sinh u + b_2 \cosh u)\, Sb_2 q$$
$$- (b_3 \cos v - b_4 \sin v)\, Sb_3 q - (b_3 \sin v + b_4 \cos v)\, Sb_4 q,$$
where $$b_1 = l + m\nu,\quad b_2 = \sigma,\quad b_3 = m + l\nu,\quad b_4 = \tau \quad\text{and}\quad l^2 - m^2 = 1. \tag{8}$$

Properties of f

All functions f constitute a group. For if we take any functions to this type $f', f'', f'' \dots f^{(n)}$, the conjugate of the function $f'f'' \dots f^{(n)}$ is $f_c^{(n)} \dots f_c'' f_c'$, and as $f_c^{(r)} f^{(r)} = 1$ we get the fact that the product of any number of such functions is another of the same type. Again, the invariant of $f'f'' \dots f^{(n)}$ is the product of the invariants of the constituent functions, and as each of these is positive unity the complete product is the same, and lastly the multiplication of the functions is clearly associative.

Any two functions f', f'' are commutative if they have the same axes. This is obvious from the equations $f'a = x'a$, $f''a = x''a$, ... The reciprocal is also true. This includes the case of equal roots in any of the functions concerned, and all such functions constitute a subgroup. Another subgroup consists of functions which all possess fixed planes, all of which pass through a common 4-vector. Thus let $f^{(r)}q = q$, where q is in the plane

$$\{q_1^{(r)} q_2^{(r)}\} \quad (r = 1, 2, \dots).$$

Then

$$f^{(s)} f^{(r)} q = f^{(s)} q = q.$$

This is a generalization of the 'conical' rotator $r(\ )r^{-1}$, the fixed plane of which contains the scalar axis $q = 1$ and ν_r the vector part of r, and all such planes $\{1, \nu_r\}$ have in common the scalar axis 1.

The conjugate function f_c obviously can be obtained from (8) by putting $-u$ for u and $-v$ for v, and we get two formulae which we shall require:

$$\left.\begin{aligned} \tfrac{1}{2}(f+f_c) &= (b_1 Sb_1 q - b_2 Sb_2 q)\cosh u - (b_3 Sb_3 q + b_4 Sb_4 q)\cos v, \\ \tfrac{1}{2}(f-f_c) &= (b_2 Sb_1 q - b_1 Sb_2 q)\sinh u + (b_4 Sb_3 q - b_3 Sb_4 q)\sin v. \end{aligned}\right\} \qquad (9)$$

If we put

$$f' = (b_1 \cosh u + b_2 \sinh u)\, Sb_1 q - (b_1 \sinh u + b_2 \cosh u)\, Sb_2 q - b_3 Sb_3 q - b_4 Sb_4 q,$$

and $$f'' = b_1 Sb_1 q - b_2 Sb_2 q - (b_3 \cos v - b_4 \sin v)\, Sb_3 q - (b_3 \sin v + b_4 \cos v)\, Sb_4 q,$$

we see that f' has a fixed plane $\{b_1, b_2\}$, and a plane $\{b_3 b_4\}$ having a hyperbolic rotation, f'' has a fixed plane $\{b_3 b_4\}$ and a plane $\{b_1 b_2\}$ containing a circular rotation, and it is clear that

$$f'f'' = f''f' = f,$$

the planes $\{b_1 b_2\}$, $\{b_3 b_4\}$ being reciprocal, which is the analogue in hyperbolic space of Jordan's theory in flat space of four dimensions that any rotation can be made up of two planar rotations in perpendicular planes.

Second expression for f

If we proceed directly to find f, we get a very different expression from (8) but closer to the forms used in the theory of special relativity. Every function f has the form

$$f(q) = f(t+\rho) = (c + s\xi)t + s' S\lambda\rho + \phi\rho,$$

where c, s, s' are scalars, ξ, λ unit vectors and $\phi\rho$ a linear vector function of ρ. The conjugate function f_c is given by

$$f_c(q) = (c+s'\lambda)\,t+sS\xi\rho+\phi_c\rho,$$

and the equation $f_c f = 1$ gives

$$c^2-s^2 = 1, \quad s\phi_c\xi+cs'\lambda = 0, \quad \phi_c\phi\rho+s'^2\lambda S\lambda\rho = \rho,$$

and we get one solution which has its invariant n equal to 1

$$f(t+\rho) = (c+s\xi)\,t-(s+c\xi)\,S\lambda\rho-\eta S\mu\rho-\zeta Sr\rho, \tag{10}$$

where (ξ,η,ζ) and (λ,μ,ν) are triads of mutually perpendicular vectors and

$$\xi\eta\zeta = \lambda\mu\nu = -1.$$

If $\qquad r(\lambda,\mu,\nu)\,r^{-1} = \xi,\eta,\zeta, \quad -(\eta S\mu\rho+\zeta S\nu\rho) = r(\rho+\lambda S\lambda\rho)\,r^{-1},$

so that $\qquad f(t+\rho) = (c+s\xi)\,t-(s+c\xi)\,S\lambda\rho+r(\rho+\lambda S\lambda\rho)\,r^{-1}. \qquad (11)$

The constants of f are thus c, ξ, λ, and r, where $r\lambda r^{-1} = \xi$.

We have $\qquad (\xi+\lambda)\,\lambda(\xi+\lambda)^{-1} = \xi$

and further $\qquad (\cos\tfrac{1}{2}\psi+\xi\sin\tfrac{1}{2}\psi)\,\xi(\cos\tfrac{1}{2}\psi+\xi\sin\tfrac{1}{2}\psi)^{-1} = \xi,$

and so we can put $\qquad r = (\cos\tfrac{1}{2}\psi+\xi\sin\tfrac{1}{2}\psi)\,(\xi+\lambda). \qquad (12)$

It may be seen that if θ is the angle between ξ and λ, ψ is the supplement of the sum of the other Eulerian angles which fix the position of λ, μ, ν with respect to ξ, η, ζ.

Thus f is completely specified by

$$c,\ \psi,\ \xi,\ \lambda. \tag{13}$$

To form the latent quartic for f, the simplest method is to form the invariant for the function $fq-xq$, putting in turn $q = 1,\lambda,\mu,\nu$. For the quartic

$$x^4-n'''x^3+n''x^2-n'x+1 = 0,$$

we get $\qquad n' = n''' = 4\cos^2\tfrac{1}{2}\theta(s_1^2+\sin^2\tfrac{1}{2}\psi),$

$$n'' = -8\cos^2\tfrac{1}{2}\theta(\sin^2\tfrac{1}{2}\psi+s_1^2)+16c_1^2\cos^2\tfrac{1}{2}\theta\sin^2\tfrac{1}{2}\psi-2,$$

where $\qquad c = c_1^2+s_1^2, \quad s = 2c_1s_1.$

Factorizing the quartic into the form

$$(x^2-2z_1x+1)\,(x^2-2z_2x+1) = 0,$$

we get $\qquad z_1+z_2 = 2\cos^2\tfrac{1}{2}\theta(\sin^2\tfrac{1}{2}\psi+s_1^2),$

$$4z_1z_2 = n''-2 = -8\cos^2\tfrac{1}{2}\theta(\sin^2\tfrac{1}{2}\psi+s_1^2)-4+16c_1^2\cos^2\tfrac{1}{2}\theta\sin^2\tfrac{1}{2}\psi,$$

from which

$$\begin{aligned}(z_1-z_2)^2 &= 4\{\cos^2\tfrac{1}{2}\theta(\sin^2\tfrac{1}{2}\psi+s_1^2)+1\}^2-16c_1^2\cos^2\tfrac{1}{2}\theta\sin^2\tfrac{1}{2}\psi\\ &= 4\{c_1^2\cos^2\tfrac{1}{2}\theta\sin^2\tfrac{1}{2}\psi+1+s_1^2\cos^2\tfrac{1}{2}\theta\cos^2\tfrac{1}{2}\psi\}^2-16c_1^2\cos^2\tfrac{1}{2}\theta\sin^2\tfrac{1}{2}\psi,\end{aligned}$$

which is positive, so that z_1, z_2 are real. We also get

$$(1-z_1^2)(1-z_2^2) = -s^2\cos^4\tfrac{1}{2}\theta\sin^2\psi, \tag{14}$$

so that one of the roots $z_1 > 1$ (say) and the other < 1, and therefore we can put $z_1 = \cosh u$, $z_2 = \cos v$, which agrees with the previous section.

If $\psi = \pi$ we get two planar rotations

$$u = 0, \quad \cos v = -(1-2c_1^2\cos^2\tfrac{1}{2}\theta),$$

and $$v = 0, \quad \cosh u = 2c_1^2\cos^2\tfrac{1}{2}\theta - 1.$$

In the former case $$\sin v = 2c_1\cos\tfrac{1}{2}\theta(1-c_1^2\cos^2\tfrac{1}{2}\theta)^{\frac{1}{2}},$$

and in the second case $$\sinh u = 2c_1\cos\tfrac{1}{2}\theta(c_1^2\cos^2\tfrac{1}{2}\theta-1)^{\frac{1}{2}},$$

so that the conditions are

$$c_1^2\cos^2\tfrac{1}{2}\theta < 1 \quad\text{and}\quad c_1^2\cos^2\tfrac{1}{2}\theta > 1$$

respectively. The characteristic constants are in the two cases

$$c, \quad \xi, \quad \lambda, \quad \pi.$$

Relations between the constants of the two forms of f

The expression (8) for f comprises the constants l, m and the triad σ, τ, v with the quantities u, v, in all equivalent to six independent quantities. The expression (11) contains the constants c, s, ξ, λ, r equivalent to six independent quantities. The comparison can be simplified by taking the values of $f(1) \pm f_c(1)$ for each expression. From $f(1) = c+s\xi$ and $f_c(1) = c-s\lambda$ and the equations (9) we get

$$l^2\cosh u - m^2\cos v = c, \tag{15}$$

$$vlm(\cosh u - \cos v) = \tfrac{1}{2}s(\xi-\lambda), \tag{16}$$

$$\sigma l\sinh u + \tau m\sin v = \tfrac{1}{2}s(\xi+\lambda), \tag{17}$$

which, along with the expressions for $\cosh u$ and $\cos v$ from the quartic, give the necessary relations.

As an example let us take the case of the two functions f' with constants $(c', \xi', \lambda', \pi)$, in which, with θ' the angle between ξ', λ', we have $c_1'^2\cos^2\frac{1}{2}\theta' < 1$ and f'' with constants $(c'', \xi'', \lambda'', \pi)$ in which, with θ'' the angle between ξ'', λ'', we have $c_1''^2\cos^2\frac{1}{2}\theta'' > 1$. For f' we have $u = 0$ and the equations

$$l^2 - m^2\cos v = c', \quad vlm(1-\cos v) = \tfrac{1}{2}s'(\xi'-\lambda'), \quad \tau m\sin v = \tfrac{1}{2}s'(\xi'+\lambda').$$

From the quartic $$\cos v = -(1-2c_1'^2\cos^2\tfrac{1}{2}\theta')$$

and we find $$l^2 = \frac{c_1'^2\sin^2\frac{1}{2}\theta'}{1-c_1'^2\cos^2\frac{1}{2}\theta'}, \quad m^2 = \frac{s_1'^2}{1-c_1'^2\cos^2\frac{1}{2}\theta'},$$

$$v = (\xi'-\lambda')/2\sin\tfrac{1}{2}\theta', \quad \tau = (\xi'+\lambda')/2\cos\tfrac{1}{2}\theta', \quad \sigma = \tau v = -V\xi'\lambda'/\sin\theta'.$$

For the function f'',

$$l^2 = \frac{s_1''^2}{c_1''^2\cos^2\tfrac{1}{2}\theta''-1}, \quad m^2 = \frac{c_1''^2\sin^2\tfrac{1}{2}\theta''}{c_1''^2\cos^2\tfrac{1}{2}\theta''-1}, \quad \upsilon = (\xi''-\lambda'')/2\sin\tfrac{1}{2}\theta'',$$

$$\sigma = (\xi''+\lambda'')/2\cos\tfrac{1}{2}\theta'', \quad \tau = \upsilon\sigma = V\xi''\lambda''/\sin\theta''.$$

These functions f' and f'' make $f'f'' = f''f'$.

Monomial form of f

From *any* function fq we can form a function $Vfq+iSfq$ which we can denote by $F(it+\rho)$. Conversely we have

$$VF(it+\rho)-iSF(it+\rho) = f(t+\rho) = fq.$$

From the rotation function f in the form

$$fq = (c+s\xi)\,t-(s+c\xi)\,S\lambda\rho-\eta S\mu\rho-\zeta S\nu\rho,$$

we get

$$F(it+\rho) = (c-is\xi)\,(it-\xi S\lambda\rho)-\eta S\mu-\zeta S\nu\rho$$

$$c-is\xi = (c_1-is_1\xi)\,(c_1-is_1\xi)$$

and

$$(c_1-is_1\xi)\,(\eta,\zeta)\,(c_1-is_1\xi) = (c_1-is_1\xi)\,(c_1+is_1\xi)\,(\eta,\zeta)$$
$$= \eta,\zeta,$$

and hence

$$F(it+\rho) = (c_1-is_1\xi)\,(it-\xi S\lambda\rho-\eta S\mu\rho-\zeta S\nu\rho)\,(c_1-is_1\xi)$$
$$= (c_1-is_1\xi)\,r(it+\rho)\,r^{-1}(c_1-is_1\xi)$$
$$= r(c_1-is_1\lambda)\,(it+\rho)\,(c_1-is_1\xi)\,r^{-1},$$

where

$$r(\lambda,\mu,\nu)\,r^{-1} = (\xi,\eta,\zeta).$$

We can use this function to get the results of the previous section. Let a, b be two quaternions. The equation

$$aqb = q$$

has solutions provided that

$$Sa = Sb \quad\text{and}\quad |a| = |b| = 1.$$

If we take the function f' we have

$$r' = \xi'(\xi'+\lambda')/2\cos\tfrac{1}{2}\theta', \quad ((12)\text{ and } |\nu'| = 1)$$

and for the prefactor in the case of $F(it+\rho)$ we get

$$-c_1'(1-S\xi'\lambda')+c_1'V\xi'\lambda'+is_1'(\xi'+\lambda') = a,$$

and the post factor

$$-c_1'(1-S\xi'\lambda')-c_1'V\xi'\lambda'+is_1'(\xi'+\lambda') = b.$$

Here $\quad Sa = Sb \quad$ and $\quad |a| = |c_1'-is_1'\xi|\,|\xi'|\,|\xi'+\lambda'|/2\cos\tfrac{1}{2}\theta' = 1,$

and we get $\quad Va-Vb = V\xi'\lambda' \quad$ dropping a real factor, and $$Va(Va-Vb) = -c_1' \sin\tfrac{1}{2}\theta' + \frac{is_1'(\xi'-\lambda')}{2\sin\frac{1}{2}\theta'}$$

dropping a real factor, $2\sin\frac{1}{2}\theta'$ and so the axes of f' corresponding to equal roots are

$$V\xi'\lambda', \quad c_1'\sin\tfrac{1}{2}\theta' + s_1'(\xi'-\lambda')/2\sin\tfrac{1}{2}\theta',$$

or σ, $l+mv$ as in the last section.

The secondary rotation function

The other form of function, say f_0, makes

$$Sf_0q_rf_0q_s = Sq_rq_s$$

but has its invariant $=-1$.

The symbolic quartic (3) with $n=-1$ now gives $n'''=-n'$ and $n''=0$. The actual quartic is

$$f_0^4 - n'''(f_0^3 - f) - 1 = 0,$$

which factorizes into $$(f_0^2-1)(f_0^2+2z_1f_0+1) = 0,$$

where $$z_1 = 4\cos^2\tfrac{1}{2}\theta(\sin^2\tfrac{1}{2}\psi + s'^2) - 2c,$$

and the latent roots are 1, -1, x, x^{-1}, where x may be real or imaginary.

To find the axes for the root -1 we have

$$(c+s\xi)t + (s+c\xi)S\lambda\rho + \eta S\mu\rho + \zeta S\nu\rho = -t-\rho.$$

From the scalar part $t = -\dfrac{s_1}{c_1}S\lambda\rho$ and this gives for the rest $-r\rho r^{-1} = -\rho$, so that

$$\rho = Vr = \cos\tfrac{1}{2}\psi(\xi+\lambda) + \sin\tfrac{1}{2}\psi V\xi\lambda$$

and the axis a_1 is $$\cos\tfrac{1}{2}\psi\left\{\frac{s_1}{c_1}(1+\cos\theta) + \xi + \lambda\right\} + \sin\tfrac{1}{2}\psi V\xi\lambda.$$

The axis for the root $+1$, a_2, must be reciprocal to a_1 for

$$Sa_1a_2 = Sf_0a_1f_0a_2 = -Sa_1a_2,$$

therefore $$Sa_1a_2 = 0.$$

The scalar part is easily found to be $-\dfrac{c_1}{s_1}S\lambda\rho$, and we get

$$a_2 = \sin\tfrac{1}{2}\psi\left\{\frac{c_1}{s_1}(1+\cos\theta) + \xi + \lambda\right\} - \cos\tfrac{1}{2}\psi V\xi\lambda.$$

The other axes are complicated in expression but must give a circular or hyperbolic rotation in a reciprocal plane.

If we put this function in the monomial form we get

$$\begin{aligned} Vf_0q - ciSf_0q &= (c_1-is_1\xi)r(t-\rho)r^{-1}(c_1-is_1\xi) \\ &= r(c_1-is_1\lambda)(t-\rho)(c_1-is\lambda_1)r^{-1}, \end{aligned}$$

so that really consists of (1) a reflexion in the scalar axis $t+\rho \to t-\rho$, (2) a rotation $(c_1-is_1\lambda)(\quad)(c_1-is_1\lambda)$ of Lorentz type, and (3) a 'conical' rotation.

REFERENCES

Dirac, P. M. 1945 *Proc. R. Irish. Acad.* A, **50**, 261.
Gormley, P. 1947 *Proc. R. Irish Acad.* A, **51**, 6.
Hathaway, A. S. 1902 *Trans. Amer. Math. Soc.* **3**, 46.
Jordan 1875 *Bull. Soc. Math. Fr.* **3**, 103.
Silberstein, L. 1924 *Theory of relativity*, 2nd ed. London: Macmillan and Co. Ltd.
Stringham, J. 1901 *Trans. Amer. Math. Soc.* **2**, 183.
Weiss, P. 1941 *Proc. R. Irish Acad.* A, **46**, 129.

The formation of hydrogen peroxide in the combustion of hydrogen at low pressures

BY SIR ALFRED C. EGERTON, SEC.R.S. AND G. J. MINKOFF

(*Received* 20 *February* 1947)

[Plate 7]

Hydrogen peroxide has been obtained in appreciable concentrations when a flame of hydrogen and oxygen burning at pressures of 3 to 4 cm. mercury was directed against a surface cooled to −180° C (*c.* 5 to 10 %), and when an oxy-hydrogen mixture was exploded by the action of a spark, in glass or aluminium vessels *c.* 2 × 15 cm., cooled in liquid air, the products were shown to contain up to 30 % hydrogen peroxide (*w/v*), depending on the conditions.

The conditions controlling the formation of hydrogen peroxide in such explosions have been investigated more fully than was done by previous authors. It was found that as the overall gas pressure was decreased the yield of peroxide passed through a maximum value. The effects were also investigated of varying the dimensions of the vessels, the gas composition, the external temperature, and other factors.

A series of experiments was carried out in order to ascertain whether the hydrogen peroxide was formed in the gas phase or only on the walls. In these experiments, the ultra-violet absorption spectrum of the explosion region was studied. It was found that a considerable quantity of hydrogen peroxide was present in the gas phase, even when the walls of the reaction tube were not cooled.

The results are discussed in the light of modern views regarding the combination of hydrogen and oxygen. It would appear that the peroxide is formed by two mechanisms; one of these consists of recombination of hydroxyl radicals on the cold walls, the other involves the formation of an excited HO_2 radical, and its subsequent reaction with a hydrogen molecule to give a hydrogen atom and a molecule of excited hydrogen peroxide, which then decomposes unless it is stabilized and frozen on the walls. No other explanation has been found to account for all the observed facts, and at the same time not to contradict established mechanisms for the hydrogen oxygen reaction.

1. INTRODUCTION

At the British Association meeting in Johannesburg in 1929, one of the authors (A.C.E.) reported the results of some experiments on the ignition of hydrogen at low pressures. The apparatus which had been used for these experiments consisted of a 1 in. transparent silica tube, inserted in a furnace; into the silica tube projected two concentric tubes to introduce the oxygen and hydrogen, the pressure being maintained at the required value by the regulation of a vacuum pump. The flash on ignition was observed through the end of the tube and the temperature determined by thermocouples in the gas stream. The ignition was thus effected by a method similar to that used by H. B. Dixon, but adapted for measurements at low pressures. Figure 1 gives a typical set of the results obtained. As the pressure decreased ignition occurred at lower temperatures. It was noted at the time that traces of hydrogen peroxide were detectable in the condensed water.

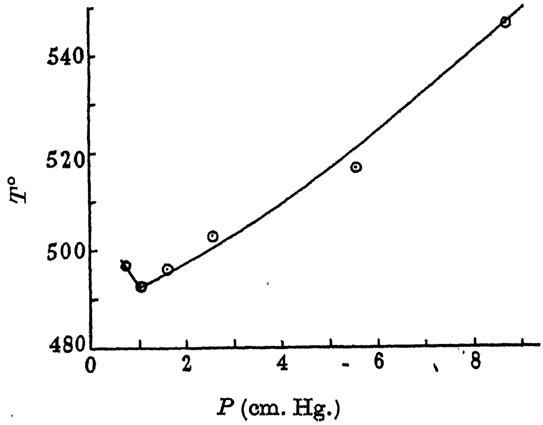

FIGURE 1. Ignition temperatures of hydrogen.

The experiments were only of a preliminary kind and were discontinued, because so much work was being done about that time (particularly by Hinshelwood and his collaborators) on the low-pressure ignition of hydrogen and oxygen which greatly advanced the knowledge of the mechanism of the hydrogen-oxygen reaction, and has culminated in a precise interpretation of the observed phenomena (Hinshelwood, 1946).

Pease (1930) has investigated the thermal reaction of hydrogen and oxygen at atmospheric pressure, and determined the amount of hydrogen peroxide formed. He found that when the reaction products were passed from the reaction tube (at 540° C) into a vessel cooled at − 79° C, concentrations of up to 4 % hydrogen peroxide were obtained. In further experiments, spherical pyrex vessels, 4·3 cm. in diameter, were filled with a hydrogen-oxygen mixture containing 95 % hydrogen and heated for a short time, then rapidly cooled to − 79° C. The products contained up to 25 % hydrogen peroxide. Pease, however, found under these conditions that no peroxide was formed at low pressures.

Poljakow and his co-workers (1934 and onwards) published a series of papers on the production of hydrogen peroxide during low-pressure explosions of hydrogen and oxygen. In general, the gas mixture was exploded by a spark, at pressures below 15 cm. mercury, in a small vessel immersed in liquid air; in some experiments, catalysis over platinum was used, leading to smaller yields of peroxide. A maximum yield of 13 % was obtained at 6 cm. pressure in an enamelled tube. Increase of tube diameter decreased the yield of peroxide; a maximum value of the yield was also found as the tube length was increased. Increase in the external temperature led to a smaller concentration of peroxide in the product. In one set of experiments, a platinum gauze surrounded the spark gap; the explosion products contained no peroxide. These experiments led the authors to conclude that the peroxide is formed on the cold surface from the recombination of hydroxyl radicals. The authors gave no information as to the method of estimating the reaction products. It was found during the present research that, though the determination of c. 10^{-5} g. peroxide was easily accomplished, the simultaneous determination of c. 10^{-4} g. water was not easy to obtain with accuracy. It is therefore possible that the percentage values of hydrogen peroxide quoted by Poljakow may have been on the low side.

It is well known that hydrogen peroxide is the main product of the photochemical oxidation of hydrogen both in the sensitized and the unsensitized reactions (Kistiakowsky 1930; Cario & Franck 1922; Frankenberger & Klinkhardt 1931; Bates *et al.* 1933, 1935; Napravnik & Smith 1940). The reaction in general proceeds through the formation of the radical HO_2, the reaction of this radical with hydrogen giving hydrogen peroxide and a hydrogen atom, i.e.

$$HO_2 + H_2 \rightarrow H_2O_2 + H.$$

In the mercury-sensitized reaction, the chain initiation is due to hydrogen atoms,

$$H_2 + Hg^* \rightarrow 2H + Hg, \quad H + O_2 \rightarrow HO_2,$$

while in the unsensitized reaction, oxygen atoms are formed:

$$O_2 + h\nu \rightarrow 2O, \quad H_2 + O \rightarrow HO + H, \quad M + H + O_2 \rightarrow HO_2 + M.$$

Hydroxyl radicals may also react together, in three-body collisions (for instance, on the walls), to give hydrogen peroxide. Reactions of oxygen atoms and of hydroxyls, leading to the formation of water, are envisaged, together with the above mechanisms, by Napravnik & Smith (1940).

Another set of conditions in which hydrogen peroxide has been found is connected with experiments involving electric discharges through water vapour. It had been noticed that when the products of such discharges were cooled to − 183° C hydrogen peroxide was formed. Campbell & Rodebush (1936) showed that hydrogen peroxide is only formed appreciably on surfaces cooled to liquid-air temperature. Geib (1934) found that atomic hydrogen only reacted with oxygen to give peroxide on a surface at temperatures well below − 80° C. Campbell, Rodebush & Wende (1937) showed that the radicals H and OH react in traps at − 80° C to give mainly gaseous products, and at − 180° C to give c. 50 % peroxide. Frost & Oldenberg (1936) agree with these conclusions; they have also carried out ultra-violet absorption experiments which indicate that the hydrogen peroxide is not formed in the gas phase. All this evidence indicates that hydroxyl radicals recombine on surfaces cooled to − 180° C, yielding hydrogen peroxide.

The thermal reaction of hydrogen and oxygen has been very closely studied (Hinshelwood 1946; Lewis & von Elbe 1942). The theory accounting for the observed facts may now be said to be in a high state of development. The theory allows for the production of hydrogen peroxide in the gas phase, in the slow thermal reaction, via $HO_2 + H_2 + M \rightarrow H_2O_2 + H + M$, under the conditions which held in the experiments of Pease (Lewis & von Elbe 1942, p. 376). In the low-pressure explosion region, the behaviour at the limits is fully accounted for without the formation of any H_2O_2; in fact, unlike in the photochemical oxidation, it would not be expected to be sufficiently stable at the temperature of explosion to exist as such.

With this estimate of the knowledge about the production of hydrogen peroxide in the combustion of hydrogen, the ignition experiments, to which reference was made at the commencement of the Introduction, and the experiments of Poljakow seemed well worth further study. The significant result of the investigation to be described is that under certain conditions in the low-pressure thermal explosion of hydrogen and oxygen, more than 30 % of the condensate can consist of hydrogen peroxide.

2. EXPERIMENTAL

The various sections of the experimental work will be described separately.

(a) *Flame experiments*

The apparatus which had been used for the experiments made in 1928–9 still existed and was adapted to produce hydrogen peroxide continuously by heating a stream of hydrogen, by means of a tungsten heating coil, to such a temperature that on mixing with oxygen ignition would occur, the products being rapidly cooled by impinging on the bottom of the silica tube, which was immersed in liquid air (see figure 2). The results obtained for the quantity of H_2O_2 in the water condensed are summarized in table 1. The H_2O_2 was estimated iodometrically by back titration with thiosulphate.

TABLE 1

total pressure (cm. Hg)	$H_2:O_2$	total rate of flow (c.c./min.)	% H_2O_2 in the water condensed
4	1:1	1500	0·8
4	1:1	1500	0·8
4	1:1	1500	0·6
4	1:1	1500	1·5
4	1:1	1500	1·0
3	1:1	800	10·0
3	1:2	800	6·0
3	2:1	800	6·0
3	1:1	800	6·0

In the following experiments at 3 cm. pressure, hydrogen and oxygen were supplied at the rate of 200 to 300 c.c./min. (measured at atmospheric pressure). The rate of formation of product was *c.* 0·8 g. in 10 min. The lower part of the outer tube was now made of aluminium instead of silica. The aluminium tube was no improvement over the silica tube; the last two results showed that the flame must be chilled within 1·5 cm. of the jet if the efficiency is not to be reduced. When air was used instead of oxygen, the mixture refused to burn.

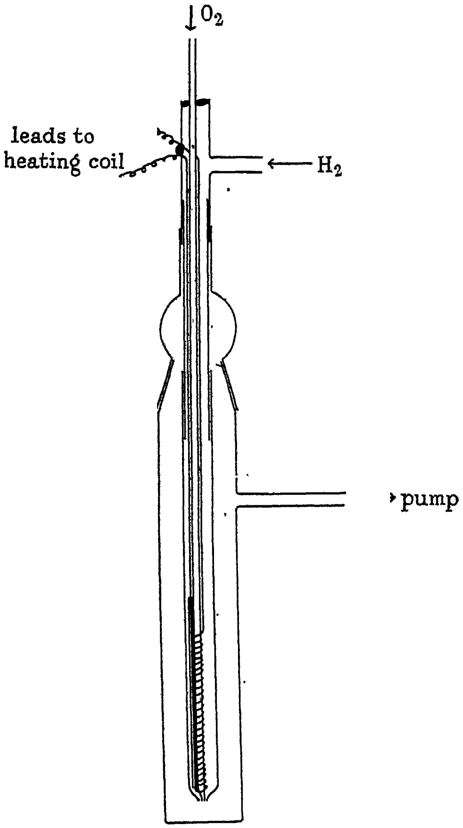

FIGURE 2. Silica combustion vessel.

TABLE 2. EFFECT OF DISTANCE OF JET FROM COOLED SURFACE

distance of jet from cooled surface (cm.)	cooling agent	lining	yield % H_2O_2/H_2O
1·3	liq. O_2	Al	4·0
1·3	liq. O_2	Al	4·5
1·3	liq. O_2	Al	5·0
4·0	liq. O_2	Al	2·0
0·3	liq. O_2	Al	5·0

The effect of lining the internal surface on the yield was next investigated (table 3). A surface treated with potassium chloride decreased the yield of peroxide. The effect of boric acid, or of boron oxide, was equivalent to that of silica. This agrees with observations of Lewis & von Elbe (1942, p. 370) regarding the kinetic course of the reaction in lined vessels.

TABLE 3

distance of jet from cooled surface (cm.)	cooling agent	lining	yield % H_2O_2/H_2O
1·3	liq. O_2	KCl	2·5
1·3	liq. O_2	KCl	1·0
1·3	liq. O_2	H_3BO_3	3·0
1·3	liq. O_2	H_3BO_3	5·5
1·3	liq. O_2	H_3BO_3	4·5
1·3	liq. O_2	B_2O_3	7·0

All attempts to condense the products by cooling at the temperature of ice or of cold water failed. Anhydrous calcium chloride was used as a lining, and water as a cooling agent; after reaction, the calcium chloride was washed out and tested for peroxide, with negative results.

There were considerable difficulties in these experiments in maintaining the tungsten heating coil in good condition. It was therefore decided to maintain a spark to ignite the gases as they entered and mixed in the tube. The first experiments in the new apparatus designed on such lines did not give a yield of peroxide more than about 1 %, so it was decided to investigate the conditions necessary to obtain a higher yield.

(b) *Production of hydrogen peroxide in thermal explosions induced by spark at low pressures*

(i) *Preliminary experiments*

Preliminary experiments were made in a steel pressure vessel of 10 cm. length, 1·3 cm. diameter, but, although considerable attack of the steel occurred, no appreciable hydrogen peroxide was formed, even when a glass or aluminium liner was used; on repeating the experiments and cooling the vessel in liquid air, a good yield of hydrogen peroxide was obtained (for results see table 4). The weight of water is that theoretically expected assuming all the hydrogen is oxidized.

TABLE 4

total pressure (cm. Hg)	H_2/O_2	% H_2O_2*	total pressure (cm. Hg)	H_2/O_2	% H_2O_2*
4	1·5	30	4	2·5	20
5	1·5	11	6	2·5	12
6	1·5	5	8	2·5	5
11	1·5	0·4	10	2·5	2
			12	2·5	0·6

* Calculated as $\dfrac{\text{wt.}\,H_2O_2}{\text{wt.}\,H_2O\text{ theoretically expected}} \times 100$.

The hydrogen peroxide was estimated colorimetrically with the titanous chloride reagent. The optimum pressure was about 4 cm.; below this pressure no ignition occurred. Ignition also depended on the potential across the spark gap and the size of the gap.

These results indicated that it was possible to obtain a considerably greater yield of peroxide in the explosion of hydrogen and oxygen at low pressures than Poljakow had obtained.

(ii) *Experiments in pyrex vessels; single explosions*

The mixture was let into a pyrex tube 13 to 14 cm. long, 1·4 cm. diameter, completely immersed in liquid air. The apparatus was similar to that shown in figure 5, but without the mixing tube and the exit tube. The pressure was adjusted to the required value. The mixture consisted of 1·5 parts hydrogen and 1 part oxygen. After explosion, the tube was allowed to warm up to room temperature, and the contents rinsed with distilled water into a 10 c.c. graduated flask, and then determined colorimetrically in a Klett colorimeter by comparison with standard solutions of H_2O_2 using the titanous chloride reagent.

The results are expressed as

$$\frac{\text{g. } H_2O_2 \text{ formed}}{\text{g. } H_2O \text{ formed assuming } 100\ \% \text{ formation of } H_2O} \times 100.$$

The weight of water was calculated as follows:

$$\text{Vol. of gas} = 18 \text{ c.c. at } 4 \text{ cm. pressure.}$$
$$\text{Vol. at } 76 \text{ cm. pressure} = 18 \times \tfrac{4}{76} \text{ c.c.}$$

Assuming complete formation of water,

$$\begin{array}{ccccc} 3H_2 & + & 2O_2 & \rightarrow 3H_2O & + \tfrac{1}{2}O_2, \\ 3\text{ mol.} & & 2\text{ mol.} & 3\text{ mol.} & \end{array}$$

5 parts of gas lead to 3 of water; since the reaction is probably not 100 % complete, the factor used was $\frac{1}{2}$; the weight of water expected is then

$$18 \times \tfrac{4}{76} \times \tfrac{18}{22400} \times \tfrac{1}{2} = 3{\cdot}80 \times 10^{-4} \text{ g.}$$

The gases did not reach the temperature of liquid air before being exploded, as they were only in the vessel a short time before sparking. The pressures in the vessel were measured in liquid air and in air, and the maximum ratio was 1·66 to 1. Thus, the weight of water expected should not be more than $1{\cdot}66 \times 3{\cdot}80 = 6{\cdot}3 \times 10^{-4}$ g. Using this value, the true yield of peroxide estimated is not less than the figure given. Table 5 shows the variation in yield with pressure and composition of the gas mixture.

In later experiments, the pressure changes during reaction were observed using a butyl phthallate differential manometer. Results were rather erratic and seemed to indicate that reaction was complete only to the extent of 60 to 90 %. Results were calculated, however, on the assumption that the reaction was 100 % complete. The estimate of H_2O_2 formed may therefore be considerably lower than the true value. The weight of peroxide formed, however, seemed reasonably consistent.

TABLE 5

pressure (cm. Hg)	H_2/O_2	% yield Pt electrodes	 Ni electrodes
2	1·0	2?	1? (difficult to detect)
3	1·0	11	—
4	1·0	4	3
6	1·0	0·8	0·8
2	2·0	0?	0?
3	2·0	16	9
4	2·0	16	17
5	2·0	5	6
8	2·0	—	0
3	2·5	19	—
4	2·5	20	—
4	2·5	20	—
5	2·5	12	—
6·5	2·5	6·2	—
8	2·5	3·5	—

The above experiments, and those carried out to investigate the effect of argon and of nitrogen, are summarized in figures 3 and 4.

The 'dead-space' in the reaction vessel consisted of 1·0 c.c. in the side-arm through which the gas mixture was introduced; this gas was exploded.

Blank experiments with a spark in oxygen showed that any ozone formed was insufficient to affect the $TiCl_3$ reagent. At first experiments were carried out using platinum electrodes, 1 to 2 mm. long. After the tube had been once cleaned with nitric acid, the yield rose in successive experiments to a steady value, 8, 12 and 15 %; on further cleaning 7, 8·5 %; the electrodes were then cut off short and filed flush with the glass, and yields of 22, 27 and 27 % were then obtained.

(iii) *Experiments in pyrex vessels; successive explosions*

The mixed gases were next introduced and exploded in succession without removal of the tube from the surrounding liquid air. After a given number of explosions had taken place the tube was removed and the yield of peroxide in the contents determined as before. Interposed between such sets of multiple explosions, the effect of a single explosion would be determined. The tubes were cleaned out with water and acetone between such experiments.

number of explosions	yield	number of explosions	yield
1	27	10	12
50	12	1	25
1	28	3	18
1	28	2	16
24	10		

These results indicated that the film of deposited water reduced the yield of subsequent explosions. In order to eliminate the deposit of platinum which formed on the walls, nickel electrodes were used, and the tube was cleaned with hydrofluoric

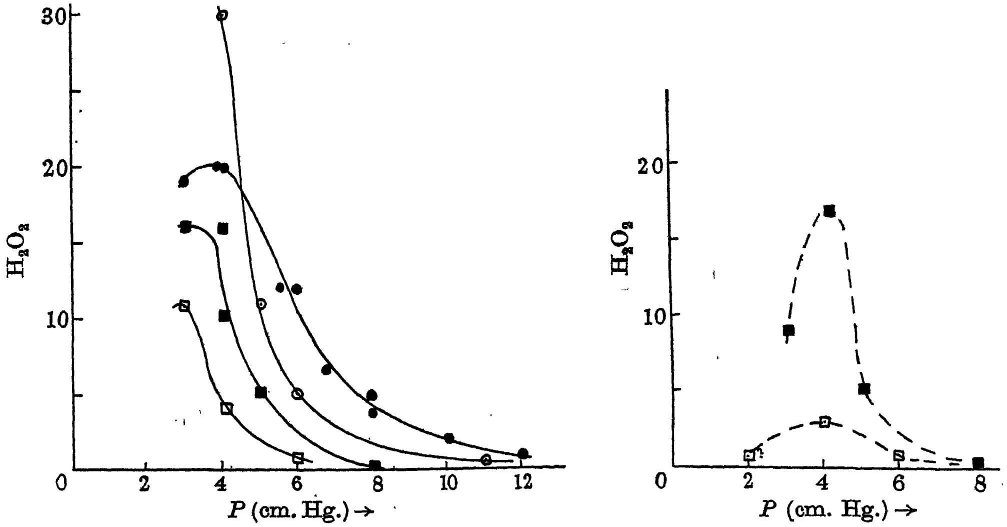

a *b*

FIGURE 3. Single explosions. *a*, Pt electrodes; *b*, Ni electrodes; H_2/O_2 = -□- 1·0, -○- 1·5; -■-2·0 and -●- 2·5.

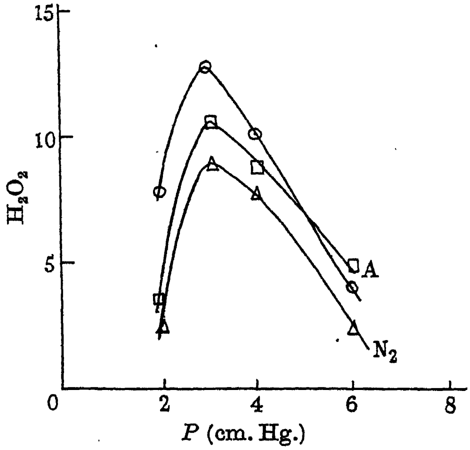

FIGURE 4. Effect of inert gases on single explosions. -○- 1·7 $H_2/1\ O_2$, -□- 1·7 $H_2/1\ O_2 + 5\%$ A., -△- 1·7 $H_2/1\ O_2 + 5\%\ N_2$.

acid. Nickel electrodes led to a steady yield of 18 %, while with platinum the yield rose from 18 to 25 % and then gradually decreased, in single explosions.

Successive explosions were once more investigated. The experimental technique was modified as follows: after the first explosion, the discharge from a Tesla coil was applied to the exterior of the reaction tube while the latter was being evacuated. This process being repeated after each explosion, it was found that, using nickel electrodes, the yield remained steady at 20 % for as many as ten successive explosions. With platinum electrodes, the yield fell off much more slowly than previously. In view of conclusions reached later, the effect of the discharge was probably to break up the film of ice on the walls of the tube.

(iv) *Flow experiments using spark ignition*

In the earlier experiments by a flow method which have been quoted, the gases burned at a jet, directed against a surface cooled in liquid air, but the products contained only 5 % peroxide. Since the flow method has the advantage of providing enough water for the concentration of peroxide to be determined directly by a titration method, the method was further investigated in the light of the information obtained and described in §§ (ii) and (iii).

The hydrogen and oxygen, from cylinders, passed through flowmeters and liquid-air traps into a mixing-tube, and thence into the reaction tube. This was similar to that used in the experiments described in §§ (ii) and (iii), except that an exit tube was provided about an inch above the bottom. The most satisfactory electrodes were eventually found to be of thin carbon wire, though fine tungsten wire was used in a number of experiments. The apparatus is shown in figure 5.

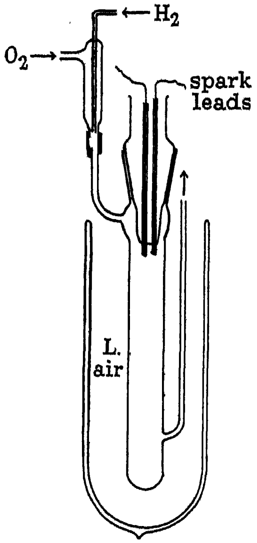

FIGURE 5. Continuous-flow apparatus.

The procedure was as follows. The apparatus was evacuated by a Hyvac pump. With the pump still running, the flow first of one gas, then of the other, was adjusted to pass through the apparatus, and out through the pump, at the partial pressures required. A spark was then passed continuously across the electrodes; the energy for the spark was derived from a medium-size induction coil; the potential was sufficient to cross a gap of about 3 in. in air. The gases exploded as frequently as the required pressure was built up, and in fact appeared to burn almost continuously. After a given time, the reaction tube was removed and the frozen product melted; the concentration of peroxide was then determined by titration with acid potassium permanganate.

After some preliminary, apparently erratic, results, it was realized that for given conditions the concentration of peroxide depended on the amount of product which had been frozen on the walls. That this effect was due to thermal insulation by the ice film was confirmed by an experiment in which a known volume of water was spread over the walls and frozen before explosions were carried out; the decrease in yield of peroxide was then in very close agreement with that calculated on the basis of this hypothesis. This fact made it necessary to obtain curves relating yield of peroxide to volume of product formed whenever the effects of various factors were being investigated. The factors investigated were as follows:

(1) *Nature of the electrodes:*

Conditions:	Overall pressure	5 cm. mercury
	Hydrogen/oxygen	1·6/1.
	Tube diameter	1·4 cm.
	Tube length	14 cm.

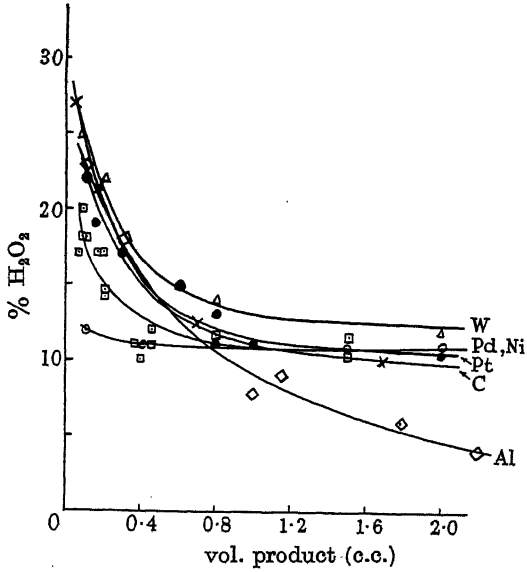

FIGURE 6. Effect of electrodes, –●– Pt, –○– Ni, –△– W, –□– Pd, –◇– Al, –×– C.

The experimental results show that with platinum, tungsten and carbon electrodes the rate of decrease of peroxide yield with increasing volume of product was similar. In spite of this, with aluminium electrodes (which are believed not to sputter) the yield decreased somewhat more rapidly. Palladium produced a rapid decrease in the yield of peroxide, after which the product was of almost constant composition. Nickel electrodes were associated with a decrease in yield so rapid as to be almost unobservable, followed again by a product containing 11 % peroxide. In all cases except that of aluminium, the product obtained when over 2 c.c. had been produced contained approximately 11 % peroxide. The initial yield appeared to have been between 30 and 35 %.

A comparison of these results with the relative tendencies of the metals to sputter (Waran 1931)

Al, 0, Mg, 1, Ni, 11, Pt, 44, Pd, 100,

shows that indiscriminate gas-phase destruction of peroxide by hot metal particles is not the chief controlling factor.

(2) *Effect of tube diameter:*

Conditions:	Overall pressure	5 cm. mercury
	Hydrogen/oxygen	1·6/1.
	Electrodes	Tungsten

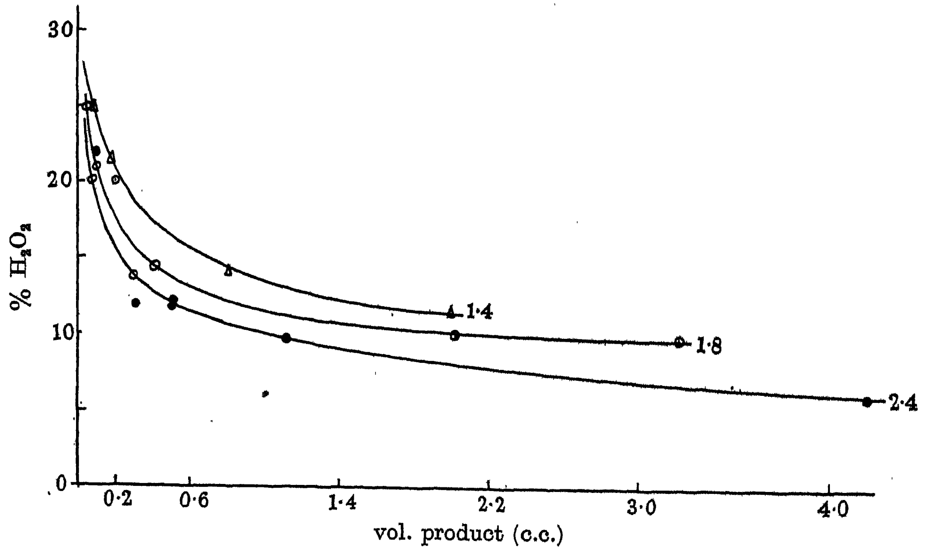

FIGURE 7. Effect of tube diameter. –△– 1·4 cm. diam., 14 cm. long; –○– 1·8 cm. diam., 9 cm. long; –●– 2·4 cm. diam., 5 cm. long.

(*a*) Tube length 14 cm. An increase in the tube diameter led to a product which reached a steady concentration of 15 % peroxide.

(*b*) In order to have strictly comparable conditions (viz. equal rates of flow of gas), tubes of different diameters were constructed with equal volumes. The results showed that increasing diameter reduces the concentration of peroxide in the product. This observation is in accordance with that of Poljakow, in his experiments under static conditions.

(3) *Effect of tube length*:

Conditions:	Overall pressure	5 cm. mercury
	Hydrogen/oxygen	1·6/1.
	Electrodes	Tungsten
	Diameter	2·4 cm.

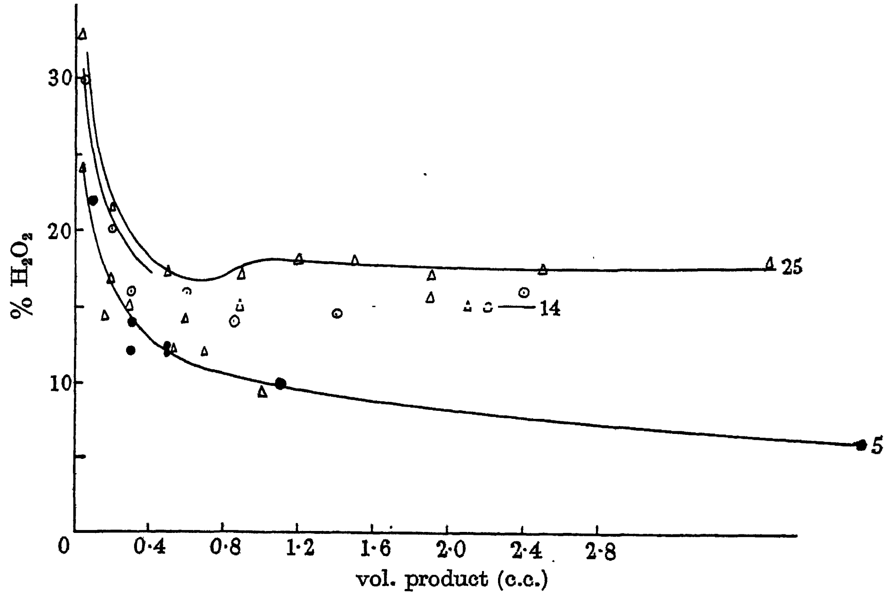

FIGURE 8. Effect of tube length. –●– 5 cm., –○– 14 cm., –△– 25 cm.

It was found that increasing the length of the tube increased the concentration of peroxide in the final product. With the longest tube used (25 cm.), erratic results were obtained for small volumes of product. This may be due to irregular deposition of product on the large wall surface available, until a fairly thick film has been built up.

(4) *Effect of pressure*:

Conditions:	Hydrogen/oxygen	1·6/1.
	Electrodes	Tungsten
	Tube	2·4 × 14 cm.

Variation of pressure showed that the maximum yields of peroxide were obtained with pressures of 4, 5 and 6 cm. mercury. The influence of pressure was less marked than in the static experiments, probably because here the pressure was less even, owing to the intermittent explosions.

(5) *Effect of hydrogen/oxygen ratio.* A brief investigation showed that results were unaffected when the ratio of hydrogen to oxygen was greater than 1·6; below this value, the yield decreased rapidly.

(6) *Effect of surface.* A reaction tube 1·4 × 14 cm. lined with cellophane gave results identical with those obtained with a glass surface. An aluminium tube was also found to give similar results.

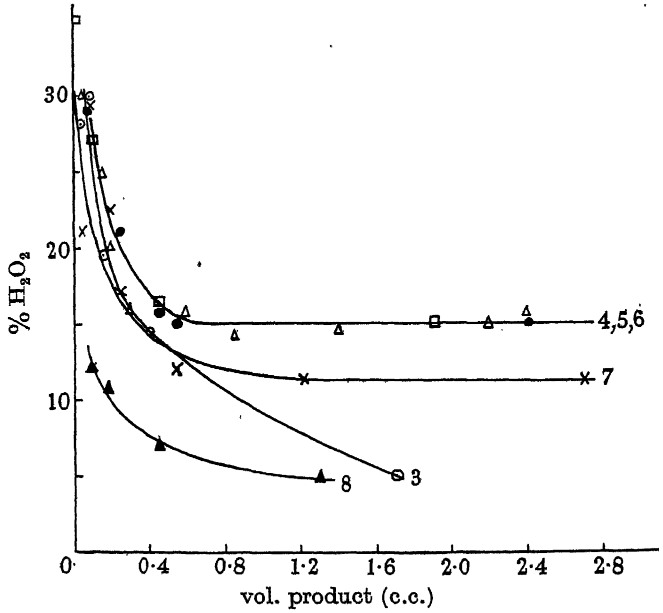

FIGURE 9. Effect of pressure. –○– 3 cm. Hg, –●– 4 cm. Hg, –△– 5 cm. Hg, –□– 6 cm. Hg, –×– 7 cm. Hg, –▲– 8 cm. Hg.

(7) *Effect of external temperature.* An experiment was carried out with a reaction tube 2·4 × 14 cm. under conditions which led to a yield of 15 % when the walls were cooled to *c.* −180° C; in this experiment, however, the walls were cooled to −79° C, and a yield of 6 % was obtained. In another experiment the tube surrounding the electrodes was enclosed in a water-jacket; the products then passed downwards into the bottom of the tube, which was cooled in liquid air. The yield obtained was only 2 %.

(v) *Summary of evidence that hydrogen peroxide is formed in the combustion of hydrogen at low pressures*

The experiments described in the preceding sections have shown that hydrogen peroxide is formed in the low-pressure explosion of hydrogen with oxygen, when the reaction vessel is cooled to −183° C. The yield of peroxide is maximum for a critical value of the gas pressure, and is decreased by the presence of excess oxygen, or of nitrogen, or, to a lesser extent, of argon. The yield of peroxide is also decreased by increasing vessel diameter, and by increased external temperature; the film of product formed on the wall of the reaction vessel also reduces the amount of peroxide isolated.

Frost, Linnett & Raynor (1945) have published work which supports the view that the low-pressure hydrogen-oxygen explosion initiated by sparking does not differ appreciably from the low-pressure explosion to which the considerations of Lewis & von Elbe, and of Hinshelwood (1946) apply. Experiments have been carried out in the course of the work being described which show that the formation of peroxide was due to the explosion and not to the spark (see also p. 160): the continuous-flow apparatus was modified so that the explosive mixture entered by what was previously the exit tube; after passing through the reaction chamber, the gas encountered a spark situated away from the reaction chamber; explosion was then propagated back through the incoming gas, before the latter could come into contact with the spark. The yield of peroxide was unaffected. The product appeared to be frozen in a uniform deposit.

(c) *Seat of formation of hydrogen peroxide*

The hydrogen peroxide might be formed from the recombination of hydroxyl radicals at the surface, their extra energy being removed by rapid cooling and the H_2O_2 remaining stable. It is also conceivable that the action is not exclusively at the surface, for example, that HO_2 reacts with hydrogen to give hydrogen peroxide in the gas phase, and that the peroxide exists long enough to reach the surface before decomposition takes place.

This third section of the experimental work was designed to find out whether the hydrogen peroxide existed in the gas phase during the explosion. A beam of ultraviolet light was passed through the tube during the explosion, and the absorption by the hydrogen peroxide formed was measured in a narrow region of wave-lengths.

Hydrogen peroxide absorbs continuously below 2800 A. Its presence could therefore be detected by the decrease in intensity of a beam of ultra-violet light passing through the reaction region. The mercury line at 2537 A was selected, as it could be easily isolated, and since its intensity would not be affected by anything else present in the reaction (except possibly ozone: see below).

A low pressure mercury lamp was used as a source. The radiation was very strong at 2537 A. The remaining light was filtered off by means of a Christiansen filter (Gaydon & Minkoff 1946). Using an iron arc, it was shown that a band of only 20 to 30 A was transmitted.

Measurement of the light intensity with a photocell was attempted, but was found, for various reasons, to be impracticable. The photocell was consequently replaced by a plateholder, on which a number of photographs of the beam could be taken. Ilford 'Zenith' plates were used; the intensities of the photographs were compared using a Hilger microphotometer. The experimental arrangement is shown in figure 10.

The light from the lamp was itself directly photographed both before and after nearly each experiment in which the light had been photographed while it passed through the explosion. Emission from the flame was investigated to ensure that no light at 2537 A came from it; this was every time confirmed. There was a certain irregularity in the results obtained owing to the precise number of separate explosions in a given time being indeterminate. These results are shown in table 6. The first four results in the table show clearly that absorption does take place. Results 2A′ (1) and (2), in which light passed through the gases which were being sparked, although they were not exploding, indicate that the absorption was connected with the explosion. In the next four experiments explosions were taking place in the presence of excess hydrogen, to destroy any ozone formed (by the spark or otherwise); they, and 3B (1), indicate that absorption was not due to ozone. In other experiments the spark was passed across water vapour at a pressure of *c.* 1 mm., but no absorption occurred. These observations support the conclusion that some peroxide is formed in the gas phase during the explosion.

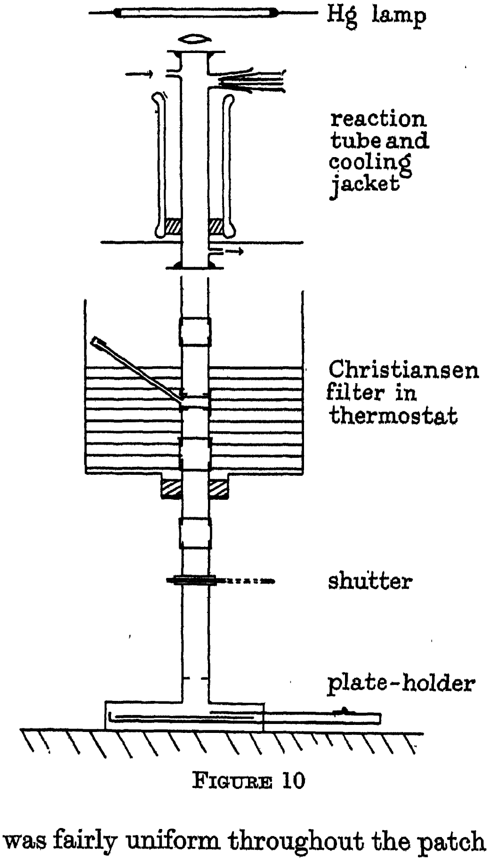
Hg lamp
reaction tube and cooling jacket
Christiansen filter in thermostat
shutter
plate-holder

FIGURE 10

As the absorption was fairly uniform throughout the patch of light falling on the plate, particularly when the alinement was good, there is indication that the hydrogen peroxide was certainly not formed exclusively on the walls. If the peroxide were only formed on the sudden cooling, for instance, of OH radicals at the walls cooled by liquid air, a higher concentration might be expected round the periphery, if there were any absorption at all. The results are contrary to this expectation. Therefore another mechanism involving gas-phase formation must enter.

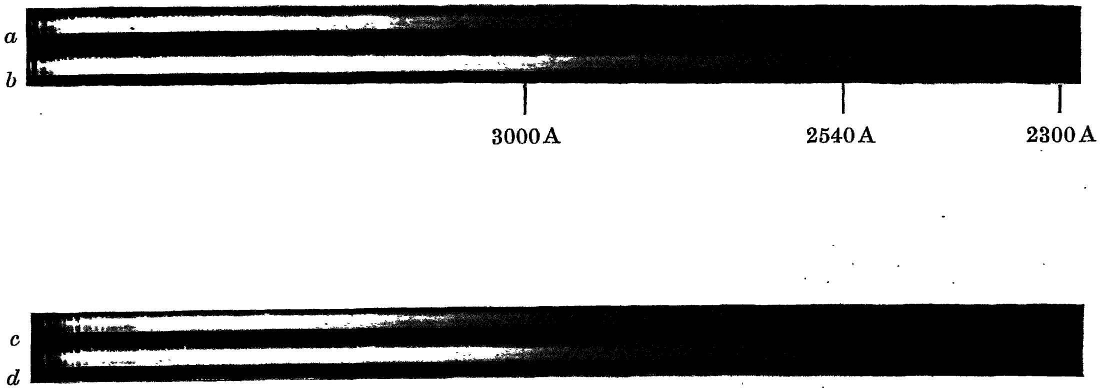

Figure 11. *a*, *c*, hydrogen discharge spectra viewed through explosion region, showing absorption beyond *c*. 2800 A. *b*, *d*, hydrogen discharge spectra viewed direct.

In order to obtain some idea of the concentration of peroxide present in the gas phase, parallel experiments were carried out in which the light absorption was measured with hydrogen peroxide vapour passing through the reaction tube under controlled conditions. Such experiments indicated that the average partial pressure of hydrogen peroxide during reaction was of the order of 3 to 4 mm. mercury. Calculations based on the data of Dawsey, Rice & Urey (1929) also indicated that the amount of 'peroxide' was commensurable with that actually isolated. These estimates are, of course, very approximate.

TABLE 6

exp.	H_2/O_2	pressure (cm.)	% extinction	
1A	1·0	5·1	83	
1B	1·0	5·1	76	
2A	1·0	5·1	89	
2B	1·0	5·1	61	
2A′ (1)	3·3	5·1	7	very few explosions
2A′ (2)	3·3	5·1	14	very few explosions
2B′ (1)	2·1	5·1	62	
2B′ (2)	2·1	5·1	27	few explosions
3A (1)	2·6	6·3	52	yield of peroxide generally smaller
3A (2)	2·6	6·3	53	
3B (1)	O_2 only	2	*c.* 10	i.e. negligible
3B (2)	H_2 only	4	*c.* 0	
3A′ (1)	1·6	5·1	66	reaction tube not cooled
3A′ (2)	1·6	5·1	30	

Instead of measuring the absorption of a monochromatic beam of ultra-violet light, the next series of experiments were made by measuring the absorption throughout the ultra-violet spectrum (3000 to 2100 A). Since the background provided by an iron arc was not entirely satisfactory, a 'special' hydrogen discharge tube giving a continuous spectrum was used. The spectroscope was a Hilger (medium) quartz spectroscope, and the photographic plates were again Ilford 'Zenith'. The intensities of blackening were measured with the same microphotometer, and a calibration curve was drawn relating the blackening of the plate to the amount of light which had fallen on the plate.

In one set of experiments it was shown that no light was absorbed when it passed through either hydrogen or oxygen in the tube, even though the spark was switched on. In all other experiments the explosions studied were of mixtures in which the partial pressures were 1·8 cm. oxygen and 3·3 cm. hydrogen respectively. Photographs of the light from the discharge tube passing through the explosion region were bracketed with photographs of the light passing through the tube with no explosion taking place; this was intended to provide evidence that the windows of the tube had not become at all opaque. Both time of exposure and slit width were varied in different experiments. The percentage light transmitted at particular wave-lengths was calculated for a large number of experiments, and mean values derived. This was necessary in order to compensate to some extent the irregularities due to spasmodic explosions. Two specimen pairs are shown in figure 11, plate 7. In table 7 the mean values of $\log_e I_0/I$ are compared with values derived from the data of Dawsey, Rice & Urey. It is seen that absorption increases steadily towards the ultra-violet without significant interruptions. Nevertheless, the rate of increase of absorption with decreasing wave-length observed was not as great as that indicated by the figures of the above authors. This is consistent with the following reasoning: in the periods between explosions, when no light is absorbed in the tube, more light falls on the plate at all wave-lengths than would be the case if hydrogen peroxide were absorbing; therefore, the decrease in intensity of blackening due to peroxide will be most masked where the overall intensity is least, i.e. towards shorter wave length.

TABLE 7. $\text{Log}_e I_0/I$

wave-length	3130	3000	2800	2700	2537	2400	2300	2200	2100
experimental values	0·32	0·36	0·52	0·69	0·64	0·69	0·87	0·82	1·24
D., R. & U.	0·04	0·05	0·12	0·20	0·45	0·75	1·1	1·45	1·65

The absorption of light by ozone has been shown by Fowler & Strutt (1917) to have a maximum value in the region of 2500 A, and to be small before c. 2200 A. These features are clearly not observed in the results here recorded, proving that if ozone is present under these conditions, its concentration is much smaller than that of hydrogen peroxide.

The possibility that the absorption was due to small particles of vapour (i.e. a fog) has been considered. Such particles, if present, would absorb all wave-lengths; in fact, absorption in the whole spectrum was observed in one or two experiments (which have not been made use of in the calculation of transmission coefficients), but not in any others. This shows that when fine particles were present in the gas phase, they could be detected by the decrease in intensity of the visible region of the spectrum, and that they were not responsible for the normal absorption in the ultra-violet.

It may thus be taken as proved that hydrogen peroxide is, indeed, formed in the gas phase during the low-pressure explosion of hydrogen with oxygen, and that this is so even when the walls of the reaction vessel are not cooled. The order of magnitude of the concentration of this peroxide in the gas phase may be very roughly estimated to be 10 %.

3. DISCUSSION

In the experimental work which has been described, three features are of special importance. In the first place, it is found that as the total pressure is increased, so the concentration of hydrogen peroxide in the product passes through a maximum value, and eventually becomes negligible. Secondly, there is the observation that as an increasing thickness of ice is built up on the walls, so the concentration of hydrogen peroxide in the product decreases from 30 to 35 % to a steady value of 10 to 15 %, which is approximately independent of the thickness of the ice film. Finally, there is the observation that the explosion region absorbs continuously in the ultra-violet in a manner which indicates the presence of a considerable quantity of peroxide in the gas phase; this happens whether the walls are cooled to − 180° C or are not cooled at all, although in the latter instance, the peroxide cannot be detected appreciably in the products.

The effect of the ice film is clearly due to its insulating properties. The thermal conductivity of the wall decreases as the film thickens, hence decreasing the rate of heat transfer through the walls. This means that the freezing-out of hydroxyl radicals (with subsequent formation of H_2O_2) becomes less efficient, since at temperatures much above − 180° C it is well known that hydroxyls do not react on the cold surface to give H_2O_2 (Rodebush 1937). It can thus be deduced that the part of the products which is formed in smaller amount as more overall products are formed (i.e. while the concentration of hydrogen peroxide falls from 30 to 15 %) is probably due to the mechanism

$$\mathrm{OH}+\mathrm{OH}+\text{wall}\rightarrow \mathrm{H_2O_2}+\text{wall}. \tag{1}$$

The remaining hydrogen peroxide formed (i.e. 10 to 15 % of the product) is presumably that whose presence has been detected in the gas phase, and has been formed in a gas-phase reaction.

Hydrogen peroxide is indeed postulated as an intermediary in the reaction schemes proposed by Lewis & von Elbe (1942), and by Hinshelwood (1946), but its role is then to continue chains in the so-called slow, thermal reaction, at pressures above the second limit. H atoms, which are chain-carriers in the low-pressure explosion, are removed by three-body collisions with oxygen

$$\mathrm{O_2}+\mathrm{H}+M\rightarrow \mathrm{HO_2}+M, \tag{2}$$

whence the product HO_2 is either destroyed (later) at the surface as

$$2\mathrm{HO_2}+\text{wall}\rightarrow \mathrm{H_2O_2}+\mathrm{O_2}, \tag{3}$$

or else it reacts with hydrogen to give hydrogen peroxide as

$$\mathrm{HO_2}+\mathrm{H_2}\rightarrow \mathrm{H_2O_2}+\mathrm{H}; \tag{4}$$

or to give water, as

$$\mathrm{HO_2}+\mathrm{H_2}\rightarrow \mathrm{H_2O}+\mathrm{OH}, \tag{4a}$$

it can also destroy H_2O_2 by the reaction

$$\mathrm{HO_2}+\mathrm{H_2O_2}\rightarrow 2\mathrm{H_2O}+\mathrm{O_2}+\mathrm{H}. \tag{5}$$

(The isolation of H_2O_2 from the slow thermal reaction has been confirmed by Pease 1930). It is specified, nevertheless, that the gas-phase reactions 4, 4*a* and 5 only become important beyond the upper limit of the low-pressure explosion. Even if these reactions were more important than the above authors assume, they would not explain the phenomena described in this communication (even apart from their effect on the explosion limits), because they follow on three-body collisions forming HO_2 (2), which would be expected to be favoured by increasing pressure, unlike the bimolecular reactions leading to the formation of water, e.g.

$$H_2 + OH \rightarrow H_2O + H. \tag{6}$$

This, however, does not agree with the experimentally observed decrease in yield of H_2O_2 with increasing pressure.

No other mechanisms are mentioned in the papers referred to above, which lead to the formation of H_2O_2 in the gas phase. The mechanism for the formation of water in the low pressure explosion, as shown below, is of no direct help. The scheme is

$$H + O_2 \rightarrow OH + O, \tag{7}$$

$$H_2 + O \rightarrow OH + H, \tag{8}$$

$$H_2 + OH \rightarrow H_2O + H, \tag{6}$$

together with suitable chain-breaking reactions.

The work of Geib & Harteck (1932) seems at first sight to have a direct bearing on the present discussion. These authors mixed hydrogen atoms (from a discharge) with a stream of oxygen, at a pressure of 0·5 mm., in a vessel cooled to low temperatures. The product contained a high percentage of H_2O_2, which reached 100 % when the external temperature was $-252°$ C (liquid hydrogen). The formation of the peroxide is due to the formation of HO_2, first,

$$O_2 + H + M \rightarrow HO_2 + M, \tag{2}$$

and its subsequent reaction with an H atom,

$$HO_2 + H + M \rightarrow H_2O_2 + M. \tag{9}$$

The authors point out that as these reactions involve very little, if any, activation energy, they are much more probable under these conditions than the alternative bimolecular exchange reactions of the type

$$H + O_2 \rightarrow OH + O, \tag{7}$$

which require much more energy of activation. Nevertheless, this mechanism cannot be applied directly to the conditions of the low-pressure explosion, partly because reaction (7) would be favoured by the comparatively high temperature of the explosion, and partly because the mechanism does not account for the decreasing yield of H_2O_2 with increasing pressure.

The only way which seems to remain of explaining the formation of H_2O_2 under the conditions of the low-pressure explosion is based on a modification of a mechanism which was proposed by Kassel & Storch (1935) to account for the low-pressure explosion. It was assumed that HO_2 was formed in an activated form by direct association of H and O_2

$$H + O_2 \rightarrow HO_2^*, \tag{10}$$

and that it then reacted with hydrogen to give an H atom and two hydroxyls

$$HO_2^* + H_2 \rightarrow 2OH + H. \tag{11}$$

It had to be assumed that reaction (11) was much more rapid than was deactivation of the excited HO_2 by further collisions. Lewis & von Elbe (1942) point out that this mechanism could function concurrently with that described above, and that it would satisfy their derived rate expressions. Kassel (1937), however, repudiated these steps in the reaction-chain mechanism, becoming convinced that the formation of HO_2 only occurred in three-body collisions. Kassel quotes the work of Cook & Bates (1935), Bodenstein & Schenk (1933), and Farkas & Sachsse (1934) as proof of this. The argument is invalid, however, for the purpose of the present discussion, because all these authors worked at comparatively high pressures.

It is quite possible that the formation of HO_2 by two-body collisions is not always highly improbable. It is now generally accepted that in most simple reactions, the reactants come together for a short period of time, to form what is usually termed the transition state complex (Glasstone, Laidler & Eyring 1941). This complex represents a state of high potential energy; it possesses all degrees of freedom except that of translational energy in the co-ordinate of decomposition. For any reaction of H with O_2 the transition state can be formally represented by the formula HO_2. When some of its energy of formation has been removed it has an appreciable existence as an entity. This has been shown by approximate calculations (e.g. Rosen 1933), and by the number of reaction mechanisms in which it is an integral link. It has always been assumed that if some energy is not removed, decomposition to $OH + O$ will occur before other reactions can take place. This is not necessarily true. If the number of collisions with other molecules is suitable it should be possible for the energy in the newly formed bond to be shared, for a short period of time, with the vibrational and rotational degrees of freedom. The HO_2 radical should thus have a short but definite lifetime in the excited state; this will be referred to as HO_2^*.

That part of the mechanism which involves interaction of a hydrogen atom with an oxygen molecule can now be regarded as follows. The first entity formed, as explained above, is the activated complex HO_2^*; below a certain pressure the number of collisions will be so small that most HO_2^* will disintegrate into OH and O before any third body encounters it. At a higher pressure, so long as there is a high enough concentration of hydrogen molecules, collisions may occur with the HO_2^*. The excess energy associated with the latter will generally be sufficient for the reaction

$$HO_2^* + H_2 \rightarrow H_2O_2 + H \qquad (12)$$

to be frequent. The excess energy will be removed partly by the H atom as translational energy, and partly by the peroxide. It is known from the experiments described previously that the peroxide exists long enough for its absorption spectrum to be recorded, even if the walls are not cooled. It follows, therefore, that the energy of formation of the peroxide does not immediately pass into the HO—OH bond, causing rupture of the molecule; it must therefore be distributed amongst the vibrational and rotational degrees of freedom for a short period of time. After this, if the energy is not removed on the cold walls, the hydrogen peroxide decomposes, most probably into two hydroxyls. Collisions with oxygen molecules, or other molecules which can take up energy, will result in stabilization of HO_2^*, and hence in a decrease in the amount of peroxide formed by this mechanism; this effect is especially noticed when excess oxygen is present.

As the pressure is further increased, so the number of actual three-body collisions will become greater, resulting in the formation of a higher proportion of stabilized HO_2 radicals, and hence of a smaller concentration of peroxide.

The effect of introducing nitrogen, which can take up rotational and vibrational energy, is similar to that of oxygen, namely, to lead to a decrease in yield. Small quantities of argon, which can take up translational energy only, decrease the yield of peroxide less than does nitrogen, as is to be expected.

It should be emphasized that the mechanism postulated above for the formation of peroxide is only of importance within the low-pressure explosion range, but operates very infrequently at the pressures in the neighbourhood of the actual lower and upper explosion limits. This means that the rate—and limit—expressions calculated by the above authors (Lewis & von Elbe 1942; Hinshelwood 1946), remain unaffected.

The fact that the branched-chain reaction

$$H+O_2 \rightarrow OH+O \tag{7}$$

has been replaced to some extent by the reaction summarized as

$$H+O_2+H_2 \rightarrow H_2O_2+H,$$

in which the reaction chain is continued without branching, is not of great importance, for the following reasons. First, O atoms resulting from the decomposition of H_2O_2, or from some other source, will still give rise to the branched-chain reaction (8)

$$H_2+O \rightarrow OH+H.$$

Then, under normal conditions, when the walls are not cooled, the peroxide decomposes into two hydroxyls, giving rise to a branched chain, as shown by Kassel & Storch (1935). Finally, there is the argument of Semenov (1929), discussed by Hinshelwood & Williamson (1934), that in such a reaction the excess translational energy removed by the hydrogen atoms would be sufficient to break up some hydrogen molecules into atoms, i.e. to increase the number of chain-carriers.

The mechanism also accounts for most of the other observations made in the course of the present investigation. The effect of increased tube diameter is to increase the time for the peroxide to reach the walls, and thus reduces the probability of the peroxide being stabilized; similarly, the wall reactions involving hydroxyls are made less probable. The effect of tube length may perhaps be explained if it is supposed that the longer the tube the smaller is the effect of reflexion of the hot zone from the ends of the tube, leading to less destruction of the peroxide in the gas phase before the peroxide reaches the walls. The only factor which has not been elucidated is that relating the yield to the metal used in the electrodes; no relation appears to exist between the yields with different metals and any properties of these metals. It is possible that the spark produces small quantities of silica, silicates and oxides of metals, which tend to catalyse the decomposition of the peroxide. In fact, some of the peroxide produced has on occasion been noticeably turbid and prone to decomposition. As impurities have a very specific action on the decomposition of hydrogen peroxide, the effects obtained using different metals as electrodes are not surprising.

It should be pointed out that the hydrogen peroxide is formed in an excited state, whence the excess energy has to be rapidly removed, unlike that formed in the ordinary thermal or photochemical oxidations of hydrogen, but that the peroxide appears to be perfectly normal once it has been frozen out and melted. This observation differs from that of Geib & Harteck (1932); these authors stated that the peroxide which they obtained from the reaction of hydrogen atoms with oxygen at low temperatures possessed unusual properties.

This work leads to the conclusion that even in exceedingly rapid explosion processes, the mechanism is one which is essentially related to the process of peroxidation. Peroxides are not necessarily formed, but removal of excess energy immediately allows the peroxide to be formed. The experiments are being continued, and it is interesting that at low pressures methane explosions have been found also to provide peroxides, but in this case not hydrogen peroxide.

The authors wish to record their thanks to Radiation Ltd. for the provision of the Radiation Fellowship tenable at the Department of Chemical Technology at the Imperial College, which one of them held (G.J.M.), during this work; also to the Admiralty (Department of Scientific Research) for support of the work and to the General Electric Co. for the gift of the low-frequency mercury lamp. They wish particularly to thank Dr A. G. Gaydon for his helpful advice in the spectroscopic work and in its interpretation.

REFERENCES

Bates & Cook 1935 *J. Amer. Chem. Soc.* **57**, 1775.
Bates & Lavin 1933 *J. Amer. Chem. Soc.* **55**, 81.
Bates & Salley 1933 *J. Amer. Chem. Soc.* **55**, 110.
Bodenstein & Schenk 1933 *Z. phys. Chem.* B, **20**, 420.
Campbell & Rodebush 1936 *J. Chem. Phys.* **4**, 293.
Campbell, Rodebush & Wende 1937 *J. Amer. Chem. Soc.* **59**, 1924.
Cario & Franck 1922 *Z. Phys., Lpz.* **11**, 161.
Dawsey, Rice & Urey 1929 *J. Amer. Chem. Soc.* **51**, 1371.
Farkas & Sachsse 1934 *Z. phys. Chem.* B, **27**, 111.
Fowler & Strutt 1917 *Proc. Roy. Soc.* A, **93**, 577.
Frankenberger & Klinkhardt 1931 *Trans. Faraday Soc.* **27**, 431.
Frost & Oldenberg 1936 *J. Chem. Phys.* **4**, 642.
Frost, Linnett & Raynor 1945 *Trans. Faraday Soc.* **41**, 487.
Gaydon & Minkoff 1946 *Nature*, **158**, 788.
Geib 1934 *Z. phys. Chem.* A, **170**, 1.
Geib 1936 *J. Chem. Phys.* **4**, 391.
Geib & Harteck 1932 *Ber. dtsch. chem. Ges.* **65**, 1551.
Glasstone, Laidler & Eyring 1941 *Theory of rate processes.* McGraw Hill.
Hinshelwood 1946 *Proc. Roy. Soc.* A, **188**, 1.

Hinshelwood & Williamson 1934 *The reaction between hydrogen and oxygen*, p. 46.
Kassel & Storch 1935 *J. Amer. Chem. Soc.* **57**, 672.
Kassel 1937 *Chem. Rev.* **21**, 331.
Kistiakowsky 1930 *J. Amer. Chem. Soc.* **52**, 1868.
Lewis & von Elbe 1942 *J. Chem. Phys.* **10**, 366.
Napravnik & Smith 1940 *J. Amer. Chem. Soc.* **62**, 385.
Pease 1930 *J. Amer. Chem. Soc.* **52**, 5106.
Pease 1931 *J. Amer. Chem. Soc.* **53**, 3188.
Poljakow *et al.* 1934*a* *C.R. Acad. Sci. U.R.S.S.* **4**, 454.
Poljakow *et al.* 1934*b* *Acta Phys. Chem. U.R.S.S.* **1**, 551.
Poljakow *et al.* 1934*c* *Acta Phys. Chem. U.R.S.S.* **1**, 821.
Poljakow *et al.* 1935 *Acta Phys. Chem. U.R.S.S.* **2**, 397.
Poljakow *et al.* 1938 *Acta Phys. Chem. U.R.S.S.* **9**, 517.
Poljakow *et al.* 1939*a* *Acta Phys. Chem. U.R.S.S.* **10**, 441.
Poljakow *et al.* 1939*b* *Acta Phys. Chem. U.R.S.S.* **11**, 453.
Rodebush 1937 *J. Amer. Chem. Soc.* **59**, 1924.
Rosen 1933 *J. Chem. Phys.* **1**, 319.
Semenov 1929 *Z. phys. Chem.* B, **2**, 169.
Waran 1931 *Phil. Mag.* (7), **11**, 397.

A general kinetic theory of liquids
IV. Quantum mechanics of fluids

BY M. BORN, F.R.S.,* AND H. S. GREEN

(*Received* 7 *March* 1947—*Read* 26 *June* 1947)

In this paper the classical theory of liquids developed in the first three parts of this series is translated into the quantum formalism. After the fundamental equations have been reformulated, it is shown that in the classical limit $\hbar = 0$, they go over into the corresponding classical equations. A quantized proof of the Boltzmann distribution law is given which is simpler and more direct than that of the Darwin-Fowler method. Then the equation of state is derived in a form which exhibits clearly the deviations from the classical law at very low temperatures.

An approximate method of solution of the fundamental equations is developed in a form suitable for practical application. Finally, the quantum equations of motion and energy transport are obtained, and it is shown that they are formally identical with the classical 'hydrodynamical equations'. This enables a discussion of the viscosity and thermal conductivity of quantum liquids to be given which exposes clearly the alternative explanations of the abnormal properties of liquid He II.

1. INTRODUCTION

In the first three parts of this series the theory of liquids was treated with the help of classical mechanics. In the present paper we propose to apply instead quantum mechanics. This is necessary because there are physical phenomena which indicate quantum effects, namely, the superfluidity of He II, and the superconductivity of certain metals; further, it seems very likely that atomic nuclei must be treated as droplets of a very dense liquid consisting of neutrons and protons. Superfluidity is the simplest case, in so far as only one kind of particle is involved; the main phenomenon consists in an abnormally small viscosity. We shall develop the theory in this paper far enough to be able to discuss the possible explanations of this effect. Superconductivity is more involved, as it presents a diffusion problem concerning two kinds of particles, the mobile electrons and the almost fixed ions. The rigorous theory of diffusion in liquids is complicated; the classical treatment is now in preparation. The case of diffusing electrons is still more difficult, as the Coulomb forces between them and the ions do not have a short range. Therefore we have to postpone this problem.

---

* I have signed this paper, as it is part of the programme with which we started this series. My contribution consists of some general suggestions, such as the use of the density matrix as the proper tool, and many critical remarks. The work itself is due to Mr Green.—M. BORN.

The main result of the present paper is that the hydrodynamico-thermal equations are not changed by the introduction of quantum mechanics, but only their interpretation in terms of microscopic phenomena and therefore the values of the physical constants in terms of atomic data. This result is at variance with the only previous attempt to develop a quantum hydrodynamics, namely that made by Landau (1941). Landau transcribes the hydrodynamical equations themselves into operator equations; the meaning of these is obscure, and Landau himself does not make any real application of them, apart from a very general contention that the vortex motion is quantized (in 'rotons'), and has therefore discrete lowest states of rotation. Landau's results concerning the behaviour of He II have nothing to do with his general quantum theory of fluids, but are based on the idea of rotons and some other independent assumptions. We do not think that he has solved the problem of superfluidity. We believe, on the other hand, that our paper contains the correct basis for an explanation, and we shall discuss the different possibilities, while postponing the solution itself to the following publication.

2. The quantum formalism

According to the general principles of quantum mechanics, it is impossible to measure simultaneously the position and velocity of a molecule; so that the classical theory of the early parts of this series is invalidated by the assumption that it is possible to define a function $f_q(t, \mathbf{x}^{(1)} \dots \mathbf{x}^{(q)}, \boldsymbol{\xi}^{(1)} \dots \boldsymbol{\xi}^{(q)})$, which determines the probability of a group of molecules having simultaneous positions and velocities. Thus the theory of parts I to III must be re-examined in the light of quantum theory to ascertain its range of validity.

The transition from classical to quantum theory is effected by replacing every function $\alpha_q(t, \mathbf{x}^{(1)} \dots \mathbf{x}^{(q)}, \boldsymbol{\xi}^{(1)} \dots \boldsymbol{\xi}^{(q)})$ of co-ordinates and velocities by a corresponding operator represented by the 'matrix' $\alpha_q(t, \mathbf{x}^{(1)} \dots \mathbf{x}^{(q)}, \mathbf{x}^{(1)\prime} \dots \mathbf{x}^{(q)\prime})$, often abbreviated to $\alpha_q(\mathbf{x}, \mathbf{x}')$ or α_q. The sum $(\alpha_q + \beta_q)$ and the product $\alpha_q \beta_q$ of two operators α_q and β_q are operators defined by the matrix equations

$$\left.\begin{aligned} (\alpha_q + \beta_q)(\mathbf{x}, \mathbf{x}') &= \alpha_q(\mathbf{x}, \mathbf{x}') + \beta_q(\mathbf{x}, \mathbf{x}'), \\ \alpha_q \beta_q(\mathbf{x}, \mathbf{x}') &= \int^{(q)}\!\!\dots\!\int \alpha_q(\mathbf{x}, \mathbf{x}'')\, \beta_q(\mathbf{x}'', \mathbf{x}') \prod_{i=1}^{q} d\mathbf{x}^{(i)\prime\prime}. \end{aligned}\right\} \tag{2·1}$$

The operators corresponding to the position vector $\mathbf{x}^{(i)}$ and the momentum vector $\mathbf{p}^{(i)} = m\boldsymbol{\xi}^{(i)}$ of the molecule (i) are represented by the matrices

$$\left.\begin{aligned} \mathbf{x}^{(i)}(\mathbf{x},\mathbf{x}') &= \mathbf{x}^{(i)} \prod_{j=1}^{q} \delta(\mathbf{x}^{(j)} - \mathbf{x}^{(j)\prime}), \\ \mathbf{p}^{(i)}(\mathbf{x},\mathbf{x}') &= -\iota\hbar \frac{\partial}{\partial \mathbf{x}^{(i)}} \prod_{j=1}^{q} \delta(\mathbf{x}^{(j)} - \mathbf{x}^{(j)\prime}). \end{aligned}\right\} \tag{2·2}$$

With the aid of (2·1) the operator $\alpha_q(\mathbf{x},\mathbf{x}')$ corresponding to any function $\alpha_q(\mathbf{x},\boldsymbol{\xi})$ of the positions and velocities of the molecules can be constructed. As special cases, one has for a function $\gamma_q(\mathbf{x})$ of positions alone,

$$\left.\begin{aligned} \gamma_q(\mathbf{x},\mathbf{x}') &= \gamma_q(\mathbf{x}) \prod_{j=1}^{q} \delta(\mathbf{x}^{(j)} - \mathbf{x}^{(j)\prime}), \\ (\mathbf{p}^{(i)}\gamma_q)(\mathbf{x},\mathbf{x}') &= -\iota\hbar \frac{\partial \gamma_q(\mathbf{x})}{\partial \mathbf{x}^{(i)}} \prod_{j=1}^{q} \delta(\mathbf{x}^{(j)} - \mathbf{x}^{(j)\prime}). \end{aligned}\right\} \tag{2·3}$$

The trace of an operator α_q will be denoted by $\chi_q(\alpha_q)$, and is defined by

$$\chi_q(\alpha_q) = \iint \alpha_q(\mathbf{x},\mathbf{x}')\, \delta(\mathbf{x}^{(q)} - \mathbf{x}^{(q)\prime})\, d\mathbf{x}^{(q)} d\mathbf{x}^{(q)\prime}; \tag{2·4}$$

for $q > 1$ it is an operator of the type α_{q-1}, and must be distinguished from the 'complete trace' $X(\alpha_q)$, defined by

$$X(\alpha_q) = \chi_1[\chi_2\{\cdots \chi_q(\alpha_q)\}], \tag{2·5}$$

which is a c-number. $\chi_q(\alpha_q)$ is the quantum analogue of the classical expression $\iint \alpha_q(\mathbf{x},\boldsymbol{\xi})\, d\mathbf{x}^{(q)} d\boldsymbol{\xi}^{(q)}$; by comparison with (2·4) it is seen that the classical operation $\int d\boldsymbol{\xi}^{(q)}$ is replaced by $\int d\mathbf{x}^{(q)\prime}\, \delta(\mathbf{x}^{(q)} - \mathbf{x}^{(q)\prime})$ in the quantum theory.

It is clear from what has been said that the classical distribution function $f_q(\mathbf{x},\boldsymbol{\xi})$ is replaced by an Hermitian matrix operator $\rho_q(\mathbf{x},\mathbf{x}')$. ρ_q is normalized according to the relation

$$\chi_{q+1}(\rho_{q+1}) = (N-q)\,\rho_q, \tag{2·6}$$

which corresponds to $\iint f_{q+1} d\mathbf{x}^{(q+1)} d\boldsymbol{\xi}^{(q+1)} = (N-q) f_q$

[(2·4) of part I] in the classical theory. The formula

$$\int \overset{(q)}{\cdots} \int f_q \prod_{i=1}^{q} d\boldsymbol{\xi}^{(i)} = n_q$$

[(2·1) of part I] now reads

$$\int \overset{(q)}{\cdots} \int \rho_q \prod_{i=1}^{q} \delta(\mathbf{x}^{(i)} - \mathbf{x}^{(i)\prime})\, d\mathbf{x}^{(i)\prime} = n_q,$$

or

$$\rho_q(\mathbf{x},\mathbf{x}) = n_q(\mathbf{x}), \tag{2·7}$$

expressing the important property of the matrix $\rho_q(\mathbf{x},\mathbf{x}')$, that its diagonal element is the number-density function. It will now be clear that ρ_q is the density matrix introduced into quantum mechanics by von Neumann (1932) and Dirac (1935), the equilibrium properties of which have been carefully examined by Husimi (1940).

To formulate the equation satisfied by ρ_q, consider first the operator ρ_N. Like f_N, this may be given an arbitrary initial value, subject only to the normalizing condition and the Hermitian property; its subsequent variation is then given by the Heisenberg equation

$$\frac{\partial \rho_N}{\partial t} = [W_N, \rho_N], \tag{2·8}$$

where W_N is the Hamiltonian operator for the system of N molecules, and, in conformity with Dirac's notation, $[\alpha,\beta]$ means simply $-\iota(\alpha\beta-\beta\alpha)/\hbar$. The Hamiltonian W_q for a system of q molecules is given by

$$W_q = \frac{1}{2m}\sum_{i=1}^{q}\mathbf{p}^{(i)2} + \frac{1}{2}\sum_{i,j=1}^{q}\phi^{(ij)} + \sum_{i=1}^{q}\psi^{(i)}, \tag{2·9}$$

where $\psi^{(i)}$ is the potential energy at $\mathbf{x}^{(i)}$ due to the external forces, which are assumed to constitute a conservative system, so that $\boldsymbol{P}^{(i)} = -\partial\psi^{(i)}/\partial\mathbf{x}^{(i)}$.

Taking the trace of (2·8), one obtains

$$\frac{\partial \rho_{N-1}}{\partial t} = [W_{N-1}, \rho_{N-1}] + \sum_{i=1}^{N}\chi_N[\phi^{(iN)}, \rho_N], \tag{2·10}$$

since $\chi_N[\mathbf{p}^{(N)2}, \rho_N]$ is reducible to

$$-\int\frac{\partial}{\partial\mathbf{x}^{(N)}}\int(\mathbf{p}^{(N)}\rho_N + \rho_N\mathbf{p}^{(N)})\,(\mathbf{x},\mathbf{x}')\,\delta(\mathbf{x}^{(N)}-\mathbf{x}^{(N)\prime})\,d\mathbf{x}^{(N)\prime}\,d\mathbf{x}^{(N)},$$

which in turn may be transformed to a vanishing surface integral. Repeating this operation indefinitely, and cancelling the factor $(N-q)!$ which appears, one obtains

$$\frac{\partial \rho_q}{\partial t} = [W_q, \rho_q] + \sum_{i=1}^{q}\chi_{q+1}[\phi^{(iq+1)}, \rho_{q+1}]. \tag{2·11}$$

Now, the well-known classical analogue of $[\alpha_q, \beta_q]$ is the 'Poisson bracket'

$$\sum_{i=1}^{q}\left(\frac{\partial\alpha_q}{\partial\mathbf{x}^{(i)}}\cdot\frac{\partial\beta_q}{\partial\mathbf{p}^{(i)}} - \frac{\partial\alpha_q}{\partial\mathbf{p}^{(i)}}\cdot\frac{\partial\beta_q}{\partial\mathbf{x}^{(i)}}\right),$$

so that $[W_q, \rho_q]$ becomes

$$\sum_{i=1}^{q}\left\{\frac{1}{m}\left(\sum_{j=1}^{q}\frac{\partial\phi^{(ij)}}{\partial\mathbf{x}^{(i)}} - \boldsymbol{P}^{(i)}\right)\cdot\frac{\partial f_q}{\partial\boldsymbol{\xi}^{(i)}} - \boldsymbol{\xi}^{(i)}\cdot\frac{\partial f_q}{\partial\mathbf{x}^{(i)}}\right\}$$

and $\chi_{q+1}[\phi^{(iq+1)}, \rho_{q+1}]$ becomes

$$\frac{1}{m}\iint\frac{\partial\phi^{(iq+1)}}{\partial\mathbf{x}^{(i)}}\cdot\frac{\partial f_{q+1}}{\partial\boldsymbol{\xi}^{(i)}}\,d\mathbf{x}^{(q+1)}\,d\boldsymbol{\xi}^{(q+1)}$$

in the transition to classical theory. Thus (2·11) goes over into the classical form

$$\frac{\partial f_q}{\partial t} + \sum_{i=1}^{q}\left\{\boldsymbol{\xi}^{(i)}\cdot\frac{\partial f_q}{\partial\mathbf{x}^{(i)}} + \frac{1}{m}\left(\boldsymbol{P}^{(i)} - \sum_{j=1}^{q}\frac{\partial\phi^{(ij)}}{\partial\mathbf{x}^{(i)}}\right)\frac{\partial f_q}{\partial\boldsymbol{\xi}^{(i)}}\right\} = \frac{1}{m}\iint\frac{\partial\phi^{(iq+1)}}{\partial\mathbf{x}^{(i)}}\cdot\frac{\partial f_{q+1}}{\partial\boldsymbol{\xi}^{(i)}}\,d\mathbf{x}^{(q+1)}\,d\boldsymbol{\xi}^{(q+1)}$$

in the limit $\hbar \to 0$, and it may be inferred that in the region of high temperatures, where the number of energy states is so large that one may substitute a continuous spectrum without error (thus effectively writing $\hbar = 0$), the classical theory will not give rise to any appreciable error.

3. THEORY OF THERMODYNAMIC EQUILIBRIUM

In order to calculate the density matrix ρ_N by means of the equation (2·8), it must first be specified at an initial time t_0. For this purpose it is necessary to choose any commuting set of operators $\lambda^{(r)}$ $(r = 1, \ldots, 3N)$, and to specify the probability $a_N(l) = a_N(l^{(1)} \ldots l^{(3N)})$ that at time t_0 the molecular assembly is in the state l in which the $\lambda^{(r)}$ have the simultaneous eigenvalues $l^{(r)}$. Let $\psi_N(l, \mathbf{x})$ be the corresponding normalized eigenfunction, satisfying

$$\lambda^{(r)}\psi_N(l,\mathbf{x}) = l^{(r)}\psi_N(l,\mathbf{x}). \tag{3·1}$$

Then at time t_0, ρ_N is given by (cf. Dirac 1935)

$$\rho_N = N! \sum_l a_N(l)\, \psi_N(l,\mathbf{x})\, \psi_N^*(l,\mathbf{x}'). \tag{3·2}$$

One possible set of λ is that set of independent operators which commute with the Hamiltonian energy W_N, and are therefore constants of the motion; it is convenient, however, to choose the λ in a slightly different way, as follows. Suppose the fluid is divided into a number of parts containing $q_1, q_2, \ldots, q_w$ molecules $(q_1 + q_2 + \ldots + q_w = N)$ in such a way that the interaction between molecules in different parts is very weak; then the λ are chosen to be the $\lambda_1, \lambda_2, \ldots, \lambda_w$ which commute with $W_{q_1}, W_{q_2}, \ldots, W_{q_w}$ respectively. Write

$$W_N = W_{q_1} + W_{q_2} + \ldots + W_{q_w} + V \tag{3·3}$$

so that V is very small. Let E_N be the eigenvalue of $W_{q_1} + W_{q_2} + \ldots + W_{q_w}$, which is a function of the λ. Then, in the l-representation, (2·8) reads

$$i\hbar \frac{\partial \rho_N}{\partial t}(l,l') = (E_N - E'_N)\,\rho_N(l,l') + \sum_{l''} \{V(l,l'')\,\rho_N(l'',l') - \rho_N(l,l'')\,V(l'',l')\}, \tag{3·4}$$

where, according to (3·2), at time t_0,

$$\rho_N(l,l') = a_N(l)\,\delta_{ll'}. \tag{3·5}$$

The condition for the equilibrium between the various parts of the fluid is expressed by the vanishing of the last term in (3·4), or

$$V(l,l')\{a_N(l') - a_N(l)\} = 0. \tag{3·6}$$

It is not difficult to show further that starting from any initial state the fluid will approach asymptotically a state in which (3·6) is satisfied, apart from small random fluctuations; a detailed discussion of the H-theorem, of which this is a special case, is being given by the authors elsewhere.

(3·6) means that in equilibrium $a_N(l)$ will have the same value for all states l between which transitions are not forbidden by the vanishing of the matrix elements $V(l, l')$.

In general, however, the only transitions thus forbidden will be those from one energy state to another, which violate the principle of conservation of energy. Thus, in equilibrium,

$$a_N(l) = a(E_N), \tag{3·7}$$

though in certain circumstances, namely, when motion in a certain direction or rotation about a given axis is entirely uninhibited, the momentum and angular momentum must be included among the 'absolute' constants of the motion, and $a_N(l)$ will depend also on these.

Now let $a_{q_1}(l_1)$ be the probability that the first group of q_1 molecules is in the eigenstate l_1 at time t_0, etc. Then, since the different groups are virtually independent of one another,

$$a(E_N) = a_{q_1}(l_1)\, a_{q_2}(l_2) \dots a_{q_w}(l_w); \tag{3·8}$$

also

$$E_N = E_1 + E_2 + \dots + E_w \tag{3·9}$$

where $E_1, E_2, \dots$ are the eigenvalues of $W_{q_1}, W_{q_2}, \dots$ and depend only on the $l_1, l_2, \dots$ respectively. It follows rigorously from (3·8) and (3·9) that

$$\left.\begin{aligned} a(E_N) &= e^{-(\alpha+\beta E_N)}, \\ a_{q_1}(E_1) &= e^{-(\alpha_1+\beta E_1)}, \text{ etc.,} \end{aligned}\right\} \tag{3·10}$$

where $\alpha = \alpha_1 + \alpha_2 + \dots + \alpha_w$. As is well known, (3·10) summarizes the whole of statistical thermodynamics. It is unnecessary to give here the argument, stated concisely by Schrödinger (1946), by which β is identified with $(kT)^{-1}$, where T is the thermodynamic temperature, and the entropy expressed in the form

$$S = -k \sum_l a_N(l) \log a_N(l) = -\frac{k}{N!} X(\rho_N \log \rho_N). \tag{3·11}$$

The internal energy U is given by

$$U = \sum_l a_N(l)\, E_N = \frac{1}{N!} X(\rho_N W_N), \tag{3·12}$$

and the free energy $A = U - TS$ by

$$e^{-A/kT} = \frac{1}{N!} \sum_l e^{-E_N/kT} = \frac{1}{N!} X(e^{-W_N/kT}). \tag{3·13}$$

The constant α in (3·10) is determined by the condition $\sum_l a_N(l) = 1$ in the form $e^{\alpha} = N!\, e^{-A/kT}$, and it follows that ρ_N may be expressed in the operator form

$$\rho_N = e^{(A-W_N)/kT}. \tag{3·14}$$

Using (2·6), one obtains

$$(N-q)!\, \rho_q = \chi_{q+1}[\chi_{q+2}\{\cdots \chi_N(e^{(A-W_N)/kT})\}]. \tag{3·15}$$

To calculate the thermodynamic pressure p from (3·13) with the aid of the formula $p = -\partial A/\partial V$, it is convenient to assume that $\psi^{(i)}$ vanishes. Writing $\sigma_N = e^{-W_N/kT}$, and $\mathbf{x}^{(i)} = b\boldsymbol{\theta}^{(i)}$, where $b^3 = V$, one has

$$X(\sigma_N) = b^{3N} \int^{(N)}\!\!\dots\!\int \sigma_N(b\boldsymbol{\theta}, b\boldsymbol{\theta}) \prod_{i=1}^{N} d\boldsymbol{\theta}^{(i)}, \tag{3·16}$$

so that
$$\frac{1}{3b^2}\frac{\partial X(\sigma_N)}{\partial b} = \frac{N}{V}X(\sigma_N) + \frac{1}{3V}\int^{(N)}\!\!\cdots\!\int \sum_{i=1}^{N} \mathbf{x}^{(i)}.\frac{\partial}{\partial \mathbf{x}^{(i)}}\sigma_N(\mathbf{x},\mathbf{x}) \prod_{j=1}^{N} d\mathbf{x}^{(j)},$$

or
$$\frac{\partial X(\sigma_N)}{\partial V} = \frac{1}{3V}\int^{(N)}\!\!\cdots\!\int \sum_{i=1}^{N} \frac{\partial}{\partial \mathbf{x}^{(i)}}.\{\mathbf{x}^{(i)}\sigma_N(\mathbf{x},\mathbf{x})\} \prod_{j=1}^{N} d\mathbf{x}^{(j)}. \tag{3·17}$$

This expression can be simplified in two ways. First, writing (3·13) in the form $N!\,e^{-A/kT} = X(\sigma_N)$, and making use of (3·14) and (2·6), one obtains

$$\begin{aligned} p &= \frac{kTe^{A/kT}}{N!}\frac{\partial X(\sigma_N)}{\partial V} \\ &= n_1 kT + \frac{kT}{6V(N-1)}\iint\left(\mathbf{x}^{(1)}.\frac{\partial}{\partial \mathbf{x}^{(1)}} + \mathbf{x}^{(2)}.\frac{\partial}{\partial \mathbf{x}^{(2)}}\right)\rho_2(\mathbf{x},\mathbf{x})\,d\mathbf{x}^{(1)}d\mathbf{x}^{(2)} \\ &= n_1 kT + \frac{kT}{6V(N-1)}\iint r n_2'(r)\,d\mathbf{x}^{(1)}d\mathbf{x}^{(2)}, \end{aligned} \tag{3·18}$$

where $\mathbf{r} = \mathbf{x}^{(2)} - \mathbf{x}^{(1)}$. Because of the classical equation

$$\frac{\partial n_2}{\partial \mathbf{x}^{(i)}} + \frac{n_2}{kT}\frac{\partial \phi}{\partial \mathbf{x}^{(i)}} + \int \frac{n_3}{kT}\frac{\partial \phi^{(i3)}}{\partial \mathbf{x}^{(i)}}\,d\mathbf{x}^{(3)} = 0,$$

this reduces classically to the formula

$$p = n_1 kT - \frac{1}{6}\int n_2(r)\,\phi'(r)\,r\,d\mathbf{r}.$$

Next, the integrand of (3·17) may be written in the form

$$\frac{\iota}{\hbar}\sum_{i=1}^{N}(\mathbf{p}^{(i)}.\mathbf{x}^{(i)}\sigma_N - \sigma_N\mathbf{p}^{(i)}.\mathbf{x}^{(i)})\,(\mathbf{x},\mathbf{x});$$

to evaluate this expression one may make use of the lemma that if μ and ν are any two operators, and $f(\nu)$ is any power series in ν, then

$$\begin{aligned} \mu f(\nu) - f(\nu)\mu &= f'(\nu)\frac{\mu_1}{1!} + f''(\nu)\frac{\mu_2}{2!} + f'''(\nu)\frac{\mu_3}{3!} + \dots \\ &= \frac{\mu_1}{1!}f'(\nu) - \frac{\mu_2}{2!}f''(\nu) + \frac{\mu_3}{3!}f'''(\nu) + \dots \\ &= \frac{1}{1!}\{\mu_1 f'(\nu)\} + \frac{1}{3!}\{\mu_3 f'''(\nu)\} + \dots - \tfrac{1}{2}\iota\hbar\left\{\frac{1}{2!}\,[\mu_2, f''(\nu)] + \frac{1}{4!}\,[\mu_4, f^{(\mathrm{iv})}(\nu)] + \dots\right\}, \end{aligned} \tag{3·19}$$

where $\{\alpha\beta\}$ stands for $\frac{1}{2}(\alpha\beta + \beta\alpha)$, $\mu_1 = \mu\nu - \nu\mu$ and $\mu_{k+1} = \mu_k\nu - \nu\mu_k$ $(k = 1, 2, \dots)$. This is easily proved by induction for $f(\nu) = \nu^n$, after which the generalization is trivial. Putting $\nu = W_N$, $\mu = \sum_{i=1}^{N}\mathbf{p}^{(i)}.\mathbf{x}^{(i)}$, and $f(\nu) = e^{-\nu/kT} = \sigma_N$, one obtains, for the integrand in (3·17), the expression

$$-\frac{\iota}{\hbar}\left[\frac{(kT)^{-1}}{1!}\{\mu_1\sigma_N\} + \frac{(kT)^{-3}}{3!}\{\mu_3\sigma_N\} + \dots\right] + \frac{1}{2}\left\{\frac{(kT)^{-2}}{2!}[\mu_2, \sigma_N] + \frac{(kT)^{-4}}{4!}[\mu_4, \sigma_N] + \dots\right\}.$$

The terms involving μ_{2k} vanish on insertion in (3·16), but terms in μ_{2k-1} survive, giving a power series in $(\hbar/kT)^2$, effectively, for the pressure. Since

$$\mu_1 = \iota\hbar \sum_{i=1}^{N} \left\{ \frac{1}{m} \mathbf{p}^{(i)2} - \frac{1}{2} \sum_{j=1}^{N} r^{(ij)} \phi'^{(ij)} \right\}, \tag{3·20}$$

the first term alone gives

$$p_1 = n_1 k T_1 - \frac{1}{6} \int n_2(r)\, r\phi'(r)\, d\mathbf{r}, \tag{3·21}$$

where T_1 is defined by

$$\tfrac{3}{2} N k T_1 = \chi_1 \left(\frac{1}{2m} \mathbf{p}^{(1)2} \rho_1 \right) \tag{3·22}$$

in terms of the mean kinetic energy of the molecules. This T_1 is in quantum theory quite distinct from the thermodynamic temperature T which appears in (3·18). Quite apart from this, the neglect of squares and higher powers of $\hbar/kT$ shows that (3·21) is only an approximation valid for high temperatures.

In view of this deviation from the classical formula which occurs under quantum conditions at low temperatures, it is worth noting the physical meaning of the thermodynamic pressure, namely the force per unit area on the wall of the vessel as measured, for example, by the work done on a movable piston. It does not follow in quantum mechanics that this will be the same as the diagonal elements p_1 of the pressure tensor p_1 which appears in the equation of motion

$$m n_1 \frac{d}{dt} \mathbf{u}_1 + \frac{\partial}{\partial \mathbf{x}} . \mathsf{p}_1 = 0$$

and it will be seen from the calculations of § 5 that the two quantities are indeed different, inasmuch as p_1 is given *exactly* by the equation (3·21) in equilibrium. Thus in quantum mechanical fluids the situation is that both pressure and temperature may be defined either thermodynamically or in terms of dynamical properties, but the definitions will not be equivalent. In problems where equilibrium obtains, the thermodynamic definitions have the obvious advantage of describing what is actually measured; but in non-equilibrium problems the dynamical quantities may play an important role. Thus in the process of thermal conduction, the energy flux is proportional to the gradient of the 'dynamical' temperature, and it is the pressure tensor, as defined in § 5, which plays an important part in the phenomenon of viscosity. These considerations may help to elucidate some of the puzzling properties of liquid He II.

4. THE BEHAVIOUR OF MOLECULAR CLUSTERS

The exact equilibrium theory of the previous section is quite unsuited to the practical investigation of the properties of condensed systems. For this purpose the study of the density matrices of small clusters of molecules is quite sufficient, since all macroscopic quantities can be obtained in terms of ρ_1 and ρ_2. In this section the equation (2·11) will therefore be examined with small values of q; it may be written in the form

$$\iota\hbar\frac{\partial\rho_q}{\partial t} = W_q\rho_q - \rho_q W_q + V_q\rho_q - \rho_q V_q^\dagger, \tag{4·1}$$

where

$$V_q = \sum_{i=1}^{q}\chi_{q+1}(\phi^{(iq+1)}\rho_{q+1})\,\rho_q^{-1}, \tag{4·2}$$

and $V_q^\dagger$ denotes the Hermitian conjugate, which is generally different from V_q, though both quantities correspond classically to the average potential energy of the cluster of q molecules due to the other molecules. As in § 3, one may take an l-representation in which W_q is diagonal with eigenvalue E_q, when, after writing

$$\left.\begin{aligned}\rho_q(l,l') &= \bar\rho_q(l,l')\,e^{\iota(E_q-E_q')t/\hbar},\\ V_q(l,l') &= \bar V_q(l,l')\,e^{\iota(E_q-E_q')t/\hbar},\end{aligned}\right\} \tag{4·3}$$

(4·1) takes the form

$$\iota\hbar\frac{\partial\bar\rho_q}{\partial t} = \bar V_q\bar\rho_q - \bar\rho_q\bar V_q^\dagger. \tag{4·4}$$

If $t-t_0$ is small, this equation may be solved by writing

$$\bar\rho_q = \rho(0)+\rho(1)+\rho(2)+\ldots, \tag{4·5}$$

where $\rho(0)$ is the value at time t_0, so that

$$\iota\hbar\frac{\partial}{\partial t}\rho(s+1) = \bar V_q\rho(s) - \rho(s)\bar V_q^\dagger. \tag{4·6}$$

If $a(l)$ is the probability of finding the cluster of q molecules in the state l at time t_0, one may take $\rho(0) = a(l)\,\delta_{ll'}$; also, if

$$U = \int_{t_0}^{t}\bar V_q\,dt;\quad \bar V_q = \dot U, \tag{4·7}$$

one finds

$$\left.\begin{aligned}\iota\hbar\rho(1) &= U\rho(0) - \rho(0)\,U^\dagger,\\ -\hbar^2\rho(2) &= \int_{t_0}^{t}(\dot U U\rho(0) + \rho(0)\,U^\dagger\dot U^\dagger)\,dt - U\rho(0)\,U^\dagger.\end{aligned}\right\} \tag{4·8}$$

Taking the diagonal elements of these equations, it becomes clear that the probability $p_{l'l}$ of a transition from the state l' to the state l in the small time $t-t_0$ is $\frac{1}{\hbar^2}\,|\,U(l,l')\,|^2$, but that this is generally different from $p_{ll'}$, since V_q is not Hermitian. The condition for equilibrium is now

$$a(l)\,P_l = \sum_{l'}a(l')\,p_{l'l}, \tag{4·9}$$

where

$$P_l = \sum_{l'}\int_{t_0}^{t}\{\dot U(l,l')\,U(l'l) + U^\dagger(l,l')\,\dot U^\dagger(l'l)\}\,dt. \tag{4·10}$$

Whether one has equilibrium or not, if there is to be no increase in the sum of the probabilities of the occupation of all states, one must have

$$\sum_l a(l)\,P_l = \sum_{ll'}a(l')\,p_{l'l}, \tag{4·11}$$

and it follows from this, since the $a(l)$ are arbitrary, that

$$P_l = \sum_{l'} p_{ll'}. \tag{4·12}$$

(4·9), together with the normalizing condition $\sum_l a(l) = 1$, suffices to determine the equilibrium values of the $a(l)$ when V_q is regarded as known. The calculation of V_q, however, requires a knowledge of $\rho_{q+1}\rho_q^{-1}$, and although certain properties of this matrix are known, for example,

$$\chi_{q+1}(\rho_{q+1}\rho_q^{-1}) = N - q, \tag{4·13}$$

its exact evaluation is as difficult as that of ρ_q. As in the classical theory, therefore, it is necessary to make some approximative assumption to render the problem in a tractable form. Probably the simplest assumption to make is that V_q is approximately Hermitian, which amounts to replacing the field of the other molecules by a corresponding conservative field imposed from outside; this procedure is similar to Hartree's method of the self-consistent field. Then, as was seen in § 3, the precise form of V_q is unimportant, and only its vanishing elements must be known. In equilibrium, these will include those which represent transitions from one energy state to another; and we find that this condition, together with (4·13), makes the problem quite determinate.

5. QUANTUM HYDRODYNAMICS

From the fundamental equation (2·11), the hydrodynamical equations will now be derived in a manner corresponding to the classical theory of part III. For this purpose, the quantum definitions of the number density function n_q, the mean velocity $\mathbf{u}_q^{(i)}$, and the generalized temperature $T_q^{(i)}$, relating to a cluster of molecules whose positions are known, are first required. The definitions ought to conform to the condition that in passing from classical to quantum theory, the operation $\int d\xi^{(i)}$ becomes $\int d\mathbf{x}^{(i)'}\,\delta(\mathbf{x}^{(i)} - \mathbf{x}^{(i)'})$, and a product $\alpha\beta$ is replaced by $\{\alpha\beta\} = \frac{1}{2}(\alpha\beta + \beta\alpha)$, which is Hermitian when α and β are Hermitian. Then, in agreement with (2·7), $n_q(\mathbf{x}) = \rho_q(\mathbf{x},\mathbf{x})$, and

$$mn_q\mathbf{u}_q^{(i)}(\mathbf{x}) = \{\rho_q\mathbf{p}^{(i)}\}(\mathbf{x},\mathbf{x}), \tag{5·1}$$

whilst

$$3mn_q kT_q^{(i)}(\mathbf{x}) = \{\{\rho_q\mathbf{v}_q^{(i)}\}.\mathbf{v}_q^{(i)}\}, \tag{5·2}$$

where $\mathbf{v}_q^{(i)}$ is defined by

$$\mathbf{v}_q^{(i)}(\mathbf{x},\mathbf{x}') = \frac{1}{m}\mathbf{p}^{(i)}(\mathbf{x},\mathbf{x}') - \mathbf{u}_q^{(i)}(\mathbf{x})\,\delta(\mathbf{x}-\mathbf{x}'). \tag{5·3}$$

Since

$$\begin{aligned}(\mathbf{p}^{(i)2}\rho_q - \rho_q\mathbf{p}^{(i)2})(\mathbf{x},\mathbf{x}') &= -\hbar^2\left(\frac{\partial^2}{\partial\mathbf{x}^{(i)2}} - \frac{\partial^2}{\partial\mathbf{x}^{(i)'2}}\right)\rho_q(\mathbf{x},\mathbf{x}')\\ &= -\iota\hbar\left(\frac{\partial}{\partial\mathbf{x}^{(i)}} + \frac{\partial}{\partial\mathbf{x}^{(i)'}}\right).(\mathbf{p}^{(i)}\rho_q + \rho_q\mathbf{p}^{(i)})(\mathbf{x},\mathbf{x}'),\end{aligned} \tag{5·4}$$

one may write (2·11) in the form

$$\iota\hbar\frac{\partial}{\partial t}\rho_q(\mathbf{x},\mathbf{x}')+\frac{\iota\hbar}{m}\sum_{i=1}^{q}\left(\frac{\partial}{\partial\mathbf{x}^{(i)}}+\frac{\partial}{\partial\mathbf{x}^{(i)\prime}}\right)\cdot\{\rho_q\mathbf{p}^{(i)}\}(\mathbf{x},\mathbf{x}')$$
$$=\frac{1}{2}\sum_{i,j=1}^{q}(\phi^{(ij)}-\phi^{(ij)\prime})\,\rho_q(\mathbf{x},\mathbf{x}')+\sum_{i=1}^{q}(\psi^{(i)}-\psi^{(i)\prime})\,\rho_q(\mathbf{x},\mathbf{x}')$$
$$+\sum_{i=1}^{q}\iint(\phi^{(iq+1)}-\phi^{(iq+1)\prime})\,\rho_{q+1}(\mathbf{x},\mathbf{x}')\,\delta(\mathbf{x}^{(q+1)}-\mathbf{x}^{(q+1)\prime})\,d\mathbf{x}^{(q+1)}d\mathbf{x}^{(q+1)\prime}. \quad (5·5)$$

On writing $\mathbf{x}=\mathbf{x}'$ in this equation, all terms on the right-hand side vanish, and one has

$$\frac{\partial n_q}{\partial t}+\sum_{i=1}^{q}\frac{\partial}{\partial\mathbf{x}^{(i)}}\cdot(n_q\mathbf{u}_q^{(i)})=0, \quad (5·6)$$

which is the quantum expression of the equation of continuity, and its generalization for $q>1$.

Next, multiplying (5·4) before and after by $\mathbf{p}^{(i)}$, and taking half the sum, one obtains

$$\iota\hbar\frac{\partial}{\partial t}\{\rho_q\mathbf{p}^{(i)}\}(\mathbf{x},\mathbf{x}')+\frac{\iota\hbar}{m}\sum_{j=1}^{q}\left(\frac{\partial}{\partial\mathbf{x}^{(j)}}+\frac{\partial}{\partial\mathbf{x}^{(j)\prime}}\right)\cdot\{\{\rho_q\mathbf{p}^{(j)}\}\mathbf{p}^{(i)}\}(\mathbf{x},\mathbf{x}')$$
$$=\frac{1}{2}\sum_{j,k=1}^{q}(\phi^{(jk)}-\phi^{(jk)\prime})\{\rho_q\mathbf{p}^{(i)}\}(\mathbf{x},\mathbf{x}')-\frac{\iota\hbar}{2}\sum_{j=1}^{q}\left(\frac{\partial\phi^{(ij)}}{\partial\mathbf{x}^{(i)}}+\frac{\partial\phi^{(ij)\prime}}{\partial\mathbf{x}^{(i)\prime}}\right)\rho_q(\mathbf{x},\mathbf{x}')$$
$$+\sum_{j=1}^{q}(\psi^{(j)}-\psi^{(j)\prime})\{\rho_q\mathbf{p}^{(i)}\}(\mathbf{x},\mathbf{x}')+\frac{\iota\hbar}{2}(\mathbf{p}^{(i)}+\mathbf{p}^{(i)\prime})\,\rho_q(\mathbf{x},\mathbf{x}')$$
$$+\sum_{j=1}^{q}\iint(\phi^{(jq+1)}-\phi^{(jq+1)\prime})\{\rho_{q+1}\mathbf{p}^{(i)}\}(\mathbf{x},\mathbf{x}')\,\delta(\mathbf{x}^{(q+1)}-\mathbf{x}^{(q+1)\prime})\,d\mathbf{x}^{(q+1)}d\mathbf{x}^{(q+1)\prime}$$
$$-\frac{\iota\hbar}{2}\iint\left(\frac{\partial\phi^{(iq+1)}}{\partial\mathbf{x}^{(i)}}+\frac{\partial\phi^{(iq+1)\prime}}{\partial\mathbf{x}^{(i)\prime}}\right)\rho_{q+1}(\mathbf{x},\mathbf{x}')\,\delta(\mathbf{x}^{(q+1)}-\mathbf{x}^{(q+1)\prime})\,d\mathbf{x}^{(q+1)}d\mathbf{x}^{(q+1)\prime}. \quad (5·7)$$

Again writing $\mathbf{x}=\mathbf{x}'$, one has

$$\frac{\partial}{\partial t}(n_q\mathbf{u}_q^{(i)})+\sum_{j=1}^{q}\frac{\partial}{\partial\mathbf{x}^{(j)}}\cdot\{\{\rho_q\mathbf{p}^{(j)}\}\mathbf{p}^{(i)}\}(\mathbf{x},\mathbf{x}')=n_q\eta_q^{(i)}, \quad (5·8)$$

where
$$m\eta_q^{(i)}=-\sum_{j=1}^{q}\frac{\partial\phi^{(ij)}}{\partial\mathbf{x}^{(i)}}+\mathbf{p}^{(i)}-\int\frac{\partial\phi^{(iq+1)}}{\partial\mathbf{x}^{(i)}}\frac{n_{q+1}}{n_q}\,d\mathbf{x}^{(q+1)}. \quad (5·9)$$

As in the case of the corresponding classical equation [(2·6) of part III], (5·8) is easily transformed to

$$mn_q\frac{d}{dt}\mathbf{u}_q^{(i)}+\sum_{j=1}^{q}\frac{\partial}{\partial\mathbf{x}^{(j)}}\cdot\mathsf{k}_q^{(ji)}=mn_q\eta_q^{(i)}, \quad (5·10)$$

where $\frac{d}{dt}$ means $\frac{\partial}{\partial t}+\sum_{i=1}^{q}\mathbf{u}_q^{(i)}\cdot\frac{\partial}{\partial\mathbf{x}^{(i)}}$, and

$$\mathsf{k}_q^{(ji)}=m\{\{\rho_q\mathbf{v}_q^{(j)}\}\mathbf{v}_q^{(i)}\}(\mathbf{x},\mathbf{x}). \quad (5·11)$$

Equation (5·10) is the quantum equation of motion, differing only from the classical equation by the definition in atomistic terms of those quantities which classically involve the velocities.

To obtain the corresponding equation for $T_q^{(i)}$, take the scalar product of (5·6) with $\mathbf{p}^{(i)}$ before and after, and half the sum of the resulting expressions, afterwards putting $\mathbf{x} = \mathbf{x}'$. The result is

$$\frac{\partial}{\partial t}(3n_q kT_q^{(i)} + mn_q \mathbf{u}_q^{(i)2}) + \frac{1}{m^2}\sum_{j=1}^{q} \frac{\partial}{\partial \mathbf{x}^{(j)}} \cdot \{\{\{\rho_q \mathbf{p}^{(j)}\} p^{(i)}\} \cdot \mathbf{p}^{(i)}\}(\mathbf{x}, \mathbf{x}')$$

$$= -2\sum_{j=1}^{q} n_q \frac{\partial \phi^{(ij)}}{\partial \mathbf{x}^{(i)}} \cdot \mathbf{u}_q^{(i)} + 2n_q \mathbf{p}^{(i)} \cdot \mathbf{u}_q^{(i)} - 2\int n_{q+1} \frac{\partial \phi^{(iq+1)}}{\partial \mathbf{x}^{(i)}} \cdot \mathbf{u}_{q+1}^{(i)}\, d\mathbf{x}^{(q+1)}. \quad (5{\cdot}12)$$

This is also readily transformed to

$$\tfrac{3}{2} n_q k \frac{dT_q^{(i)}}{dt} + \sum_{j=1}^{q} \left\{ \frac{\partial}{\partial \mathbf{x}^{(j)}} \cdot \mathbf{m}_q^{(ji)} + \left(\mathsf{k}_q^{(ji)} \cdot \frac{\partial}{\partial \mathbf{x}^{(j)}} \right) \cdot \mathbf{u}_q^{(i)} \right\}$$

$$= -\int n_{q+1} \frac{\partial \phi^{(iq+1)}}{\partial \mathbf{x}^{(i)}} \cdot (\mathbf{u}_{q+1}^{(i)} - \mathbf{u}_q^{(i)})\, d\mathbf{x}^{(q+1)}, \quad (5{\cdot}13)$$

where

$$\mathbf{m}_q^{(ji)} = \tfrac{1}{2} m \{\{\{\rho_q \mathbf{v}_q^{(j)}\} \mathbf{v}_q^{(i)}\} \cdot \mathbf{v}_q^{(i)}\}(\mathbf{x}, \mathbf{x}). \quad (5{\cdot}14)$$

(5·13) differs from the classical equation of energy transport only in the atomistic definition of quantities which classically involve the velocities.

At first it is rather surprising to find that quantum mechanics involves no change of the equations of continuity, motion, and energy transport from those obtained through the classical theory, but reflexion shows that this must be so: the macroscopic, visible changes of a fluid in motion give no indication of the existence of quantum phenomena. This is true even in the case of liquid He II, where the abnormal viscosity, thermal conductivity, etc., in no way conflict with the macroscopic description of matter, though they lead one to suspect that quantum phenomena are responsible. This may indeed be the case, since the evaluation of n_q, $\mathbf{u}_q^{(i)}$, $T_q^{(i)}$, etc., from the atomistic standpoint is quite different in the quantum formalism from the classical procedure, and one therefore expects quantum complications at low temperatures.

6. DISCUSSION

The fact that we have been able, in the last section, to derive hydrodynamical equations, identical in form with those resulting from the classical theory of part III, has far-reaching consequences. One conclusion which may be drawn immediately is that the theory of viscosity and thermal conductivity developed from these hydrodynamical equations in part III can be taken over into the quantum theory unchanged, provided one interprets the classical temperature and pressure as the 'dynamical' temperature and pressure of quantum theory. The formulae for the pressure tensor and thermal flux are unaltered, and so, therefore, are those for the coefficients of viscosity and thermal conduction. This enables us without further analysis to examine the possible causes of the abnormal values found experimentally for these constants in liquid He II.

First consider the expression for the viscosity, namely

$$\mu = \frac{1}{30}\int \nu(r)\phi'(r)r^3\,d\mathbf{r} - \tfrac{1}{15}m\int \phi_2(v)\,v^4\,d\mathbf{v}, \tag{6·1}$$

where $\phi_2(v)\,\mathbf{v}\,.\,\mathbf{b}\,.\,\mathbf{v}$ is the distortion of the velocity (momentum) distribution function by the motion, and $\nu(r)\,\mathbf{r}\,.\,\mathbf{b}\,.\,\mathbf{r}$ the corresponding distortion of the radial distribution function, $\mathbf{b}$ representing the symmetrical non-divergent part of the velocity gradient tensor. It is clear that an abnormally small value of μ can arise at low temperatures from three main causes. In the first place, it is possible that the second, or 'kinetic' term, which is usually positive but entirely negligible for the liquid phase, by becoming negative and of appreciable magnitude, might annul the first, or 'potential' term, which usually has a considerable positive value. This has to be considered because under quantum conditions there is no longer any obvious reason why $\phi_2(v)$ should be negative; but in view of the entirely different nature of the two terms, the likelihood of their cancelling in this way over any substantial range of temperature is small enough to be dismissed.

We therefore turn to the alternative hypothesis, that both terms appearing in (6·1) are very small for He II. That the kinetic term should be small is quite acceptable: there is no positive reason to suppose that the ordinary formula of the kinetic theory of gases does not describe its behaviour quite well, even down to the lowest temperatures. The potential term, which contains the force on one molecule due to others at distance r in the integrand, may almost vanish for two distinct reasons. In the first place, the function $\nu(r)$ may almost vanish around the minimum of potential between the two molecules. In principle, this can be decided on theoretical grounds; one of the authors has undertaken the calculation of $\nu(r)$ for the helium atom, and his results so far appear to confirm this hypothesis in a remarkable way. It should, however, be possible to decide this point also experimentally by the study of the scattering of X-rays by He II; the experiments of Keesom & Taconis (1938) and Reekie (1940) indicate that the assumption is correct; yet it is desirable that this important experimental determination of the structure of He II should be effected with the highest possible accuracy.

A third and obvious way of accounting for the smallness of the potential term in (6·1) is by supposing that the interaction between the molecules represented by the potential function $\phi(r)$ breaks down at low temperatures. This question is beyond the scope of the methods developed in our theory of liquids, and must, if it appears to be useful, be treated by the investigation of the means of interaction between the elementary particles.

It appears that nearly all the properties of He II can be explained in terms of its low viscosity. For example, the apparently high thermal conductivity is caused by the transference of energy by the visible motion of the liquid, and the true thermal conductivity is thereby completely masked. For this reason we believe that our formula for the thermal conductivity corresponding to (6·1) has no great interest in the application to He II. The driving force for the convexion currents transporting heat is, as was pointed out at the end of § 3, not the hydrostatic pressure, but the dynamical pressure, which differs from it at low temperatures. From this standpoint, some strange features of the behaviour of He II become less puzzling. These questions, and the problem of the discontinuity between the normal and superfluid states, may be discussed in a subsequent paper.

Some previous attempts to explain the abnormal properties of He II have been based on the application of Bose-Einstein statistics to the molecular assembly; these are not successful because they omit to take into consideration the interaction between the molecules. It is worth examining, however, how far the present theory is in accord with the new statistics. For Bose-Einstein statistics the density matrices ρ_q are unchanged for any permutation of either the $\mathbf{x}^{(1)}, \mathbf{x}^{(2)}, \ldots$ or the $\mathbf{x}^{(1)\prime}, \mathbf{x}^{(2)\prime}, \ldots$ while for Fermi-Dirac statistics ρ_q changes sign for odd permutations of either of these two sets, In both events ρ_q remains unaltered if both the $\mathbf{x}^{(1)}, \mathbf{x}^{(2)}, \ldots$ and the $\mathbf{x}^{(1)\prime}, \mathbf{x}^{(2)\prime}, \ldots$ are subjected to the same permutation. The general conclusion seems to be that Bose-Einstein statistics do not play a very important part, even at low temperatures, in determining the properties of a fluid; this conclusion was reached also by Kahn (1938). Much more important than this effect of 'second quantization' is that of the low temperatures themselves on the occupation of the lowest energy states not forbidden by the exclusion principle.

REFERENCES

Born, M. & Green, H. S. 1946 *Proc. Roy. Soc.* A, **188**, 10.
Born, M. & Green, H. S. 1947 *Proc. Roy. Soc.* A. **190**, 455–474,
Dirac, P. A. M. 1935 *The principles of quantum mechanics.* Oxford Univ. Press.
Husimi, K. 1940 *Proc. Phys.-Math. Soc. Japan*, Ser. 3, **22**, 264.
Kahn, B. 1938 Dissertation. Utrecht.
Keesom, W. H. & Taconis, K. W. 1939 *Physica*, **5**, 270.
Landau, L. 1941 *J. Phys.* **5**, 71.
v. Neumann, J. 1932 *Math. Grundl. d. Quantenmechanik*, Ch. 4. Springer: Berlin.
Reekie, J. 1940 *Proc. Camb. Phil. Soc.* **36**, 236.
Schrödinger, E. 1946 *Statistical thermodynamics.* Cambridge Univ. Press.

Interference studies of diamond faces. A crossed fringe technique

By S. Tolansky, *University of London* and
W. L. Wilcock, *University of Manchester*

(*Communicated by P. M. S. Blackett, F.R.S.—Received* 6 *February* 1947—
Read 5 *June* 1947)

[Plates 8 to 11]

Precision multiple-beam interference methods are applied to the study of the topography of octahedral faces of three diamonds. A new crossed fringe technique of high sensitivity is described. Evidence is adduced to support the view that the curvature of diamond faces and the occurrence of triangular pits are to be attributed to growth and not to solution. The observations thus settle a long-standing controversy. Irregular depressions which are observed are attributed to a solution mechanism.

New features associated with the triangular growth pits are described and interpreted.

A crystal surface with regions showing an abnormally high degree of optical plane uniformity is described.

The surface of a polished diamond is described.

INTRODUCTION

There exists an extensive literature dealing with the morphology and topography of diamond crystal surfaces. Comprehensive reviews have been published by Fersmann & Goldsmidt (1911), Mohr (1924) and Williams (1932). Only goniometric and microscopic studies have, however, been considered by these workers. An attempt has also been made by Kayser (1944) to examine diamond surfaces by interference methods. He used *two-beam* interferometry only; consequently little that was new was discovered, and no effective contribution was made.

We have applied a number of distinct precision *multiple-beam* interference techniques to the examination of the octahedron faces of three diamonds, with results which throw light both on the mechanism of diamond growth and on some old controversies. Thus it has long been known that the faces of diamond crystals are frequently curved, often considerably so. Fersmann & Goldsmidt attributed this to a solution mechanism, whilst Williams advocated growth as the responsible agent. Further, the octahedron faces frequently exhibit sharply defined equilateral triangular pits with quite straight edges. Of these Miers (1902) cautiously stated that they are supposed to be etch pits. Fersmann & Goldsmidt also considered that solution can be their origin. Mohr's geometrical analysis of the crystal growth appeared to indicate that such pits may arise during growth, whilst Williams strongly advocated growth as the cause, although offering no very convincing evidence for his theory. As will appear later, our observations throw light on both of these controversies. The experiments reported here have been made on three 'portrait' stones (A, B, C) specially selected for the purpose from the stocks held by the Research Laboratory of the Diamond Trading Company. These stones are natural octahedra in which one pair of opposite parallel octahedral faces is exceptionally developed with the result that the crystal is effectively a natural 'plane parallel' plate and as such is admirably suited for interferometric studies. Stone A, of 0·314 carats, is from Angola; stones B and C, of 0·353 and 0·262 carats respectively, are from Sierra Leone.

EXPERIMENTAL

The multiple-beam techniques employed have already been described (Tolansky 1945 *a*, *b*). They have been improved in one important respect which will be discussed later. The crystal to be studied is cleaned and a suitable silver film deposited on it by evaporation *in vacuo*. It is matched against a silvered optical flat. It has been shown elsewhere (Tolansky 1945 *c*, 1946) that the three most important factors affecting the fringe definition are: (1) high reflecting power together with low absorption, (2) the separation between the interference surfaces must not exceed a few light waves, (3) attention must be paid to securing a parallel beam of light. These three conditions were satisfied. In particular, the employment of a plane parallel plate crystal made it easy to collimate the light beams correctly. The optical flats used were specially prepared by Hilger who selected a glass likely to have the smoothest optical surface. The flats are disks accurately worked to $\lambda/40$ over more than half an inch diameter. Locally the perfection of figure far exceeds this accuracy. The fringes invariably exhibit a fine grain structure, and this represents residual polish marks on the flat. These polish marks will be discussed again later, and evidence will be given showing that over local areas of the order of 1 sq.mm. the flats are true to much better than $\lambda/250$, i.e. better than 20 A, indeed, probably 10 A.

The crystal and flat were often demounted and put together again, the crystal being matched each time against a different area of the flat. No noticeable major differences in the interference pattern were detected, showing that the topography reported is attributable to the crystal only.

The crystal-flat combination was mounted on the stage of a microscope with camera attachment, magnifications up to × 100 being available.

The microscope was used for studies with (*a*) multiple-beam Fizeau fringes, (*b*) fringes of equal chromatic order (Tolansky 1945 *c*). The Fizeau fringe studies will first be discussed. For these the source used was a high-pressure mercury arc (somewhat under-run). It can be shown that if the two silvered surfaces are sufficiently close together, a source line-width of several angstroms can be tolerated, with no impairment in definition. The green line or green-plus-yellow lines could be isolated by filters. The transmission quality of the silver is so good that fringe photographs at × 20 are obtainable in a matter of seconds with both types of fringes. Fringes in all cases were studied in transmission only.

CROSSED FRINGE TECHNIQUE

A powerful modification of multiple-beam Fizeau fringes has been developed for these topographical studies and will be described here as the 'crossed fringe' technique. A preliminary note describing this procedure has already been published (Tolansky & Wilcock 1946). This consists in photographing successively superposed on the same plate two, or even three, independent systems of fringes.

(1) The first set consists of the normal high-definition, narrow, multiple-beam Fizeau fringes, using either the green line or green-yellow group, obtained by setting a small wedge angle between flat and crystal. Such a fringe pattern for crystal A is shown in figure 7*a*, plate 8. In this G, G' are adjacent green fringes, with the yellow doublet between. Attention is drawn to the excellence of the fringe definition, which we have not surpassed in any previous interferometric studies with Fizeau fringes. It can be shown that the multiple-beam Fizeau fringe shape is given closely enough by the well-known Airy sum formula $I = I_{\text{max.}}/(1 + F\sin^2 \frac{1}{2}\delta)$, in which the intensity I is given in terms of the intensity maximum $I_{\text{max.}}$. In this expression $F = 4R/(1-R)^2$, where R is the reflecting coefficient, $\delta = 4\pi t/\lambda$, λ is the wave-length and t the separation between surfaces. This holds closely enough if $t = 0{\cdot}01$ mm. (see Tolansky 1946). For these fringes a value of R approaching 0·94 has been used making $F = 1044$. This is a measure of fringe sharpness, since the half-width of the fringes can be shown to be $\omega = 2/\pi F^{\frac{1}{2}}$. For $R = 0{\cdot}94$ then $\omega = \frac{1}{51}$. As a setting on a fringe can be made with an error not exceeding one-tenth of this width, the setting error is of the order of 5 A at most. This fringe pattern reveals a great deal of structural detail, yet before a comprehensive topographical interpretation is possible it is clear that a large number of such photographs would be required to build up a picture of the surface; for the meaning of the various irregularities cannot be deduced from one or even from several such pictures. In this connexion the 'crossing' method to be described leads to a great saving in labour, considerably simplifies interpretation and reveals unsuspected relationships in detail.

(2) The second superposed set of fringes is obtained by reducing the wedge angle until the two surfaces are as near parallel as is possible. Residual angles remain due to the topographical pattern on the crystal. The filters are removed and the resulting high-dispersion complex pattern exhibits a complete picture of the crystal surface, revealing with high contrast a wealth of structural detail, not observable by ordinary micrographic methods. A separate picture of crystal A taken by this method is shown in figure 7*b*, plate 8. It is emphasized that this is an interference pattern, and one of high sensitivity. A detailed treatment of the properties of these fringes is being given elsewhere, a brief résumé only being given here.

Monochromatic Fizeau fringes between parallel plates lead to a uniform tint of intensity determined by the separation of the plates, in accordance with the Airy formula. A change in separation produces a change in intensity, and it is clear from figure 1 that maximum sensitivity occurs if t is selected such that approximately half the peak intensity is in the field of view. Supposing a change in tint intensity of 10 % is recognizable, then we have the following. In figure 1 the intensity I at the half-intensity is $I = \frac{1}{2}I_{\text{max.}}$. Thus

$$\frac{I_{\text{max.}}}{2} = \frac{I_{\text{max.}}}{1+F\sin^2\frac{1}{2}\delta}.$$

From which

$$\sin^2\tfrac{1}{2}\delta = \frac{1}{F}.$$

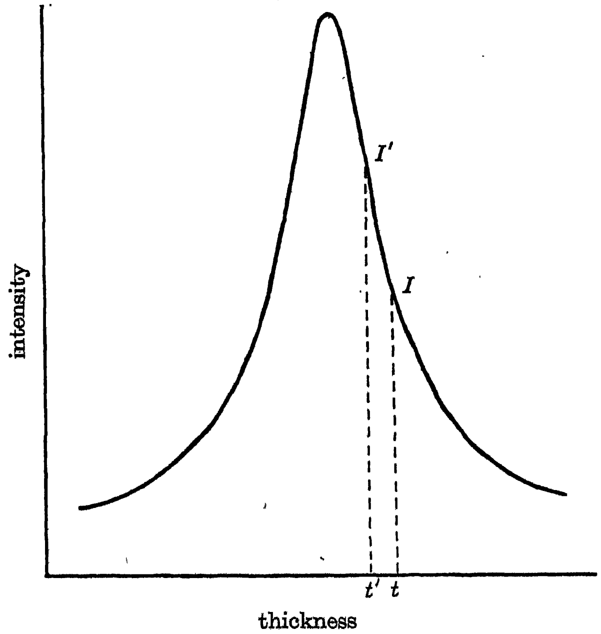

Figure 1

As F is large (exceeding 1000), $\sin\frac{1}{2}\delta$ can be replaced by $\frac{1}{2}\delta$ giving $\delta = 2/F^{\frac{1}{2}}$. This value δ represents the change in phase on descending from the maximum to the half-value. Suppose now that a 10 % change in intensity is produced by a change in the thickness t to a new value t', corresponding to a new value δ' (where $\delta' = 4\pi t'/\lambda$) then

$$0{\cdot}55\,I_{\text{max.}} = \frac{I_{\text{max.}}}{1+F\sin^2\frac{1}{2}\delta'},$$

giving

$$\delta' = \frac{6}{\sqrt{11}F^{\frac{1}{2}}},$$

from which

$$t'-t = \frac{\lambda}{4\pi F^{\frac{1}{2}}}\left(2-\frac{6}{\sqrt{11}}\right),$$

which is, closely, $\lambda/66F^{\frac{1}{2}}$. For $R = 0{\cdot}94$, $F = 1044$ making $t'-t = \lambda/2126$, i.e. approximately 2·5 A.

Clearly the tint change method is of delicate sensitivity.

As was pointed out (Tolansky & Wilcock 1946), such an interference picture reveals submicroscopic detail, enhancing contrast; for small transparent features of but a few angstroms in height (depth) are invisible to the microscope, yet are revealed by these fringes. In effect the interference picture is such that the arrangement can justly be called a 'phase-difference microscope' of the most delicate sensitivity.

Yet the interference picture as it stands cannot be interpreted, for there is no indication either of direction or of overlapping of orders. Further, for exact numerical work, microphotometer density determinations would be required in general.

(3) The result of 'crossing' the previous two fringe types is shown in figure 8*a*, plate 8, and this shows clearly the power of the method. The various twists and turns of the narrow fringes of the type shown in figure 7*a*, can be interpreted at sight, and conversely numerical data become readily available for the vivid topographical features of figure 7*b*.

A further more striking combination is shown by the triple crossed fringes of figure 8*b*, plate 8. Here the high-dispersion fringes have superposed on them *two* independent sets of narrow wedge fringes, roughly at right angles to each other, this arrangement being obtained by suitable adjustment of wedge angles. This picture is so complete that a large number of the interesting features can be numerically evaluated from this one photograph. The gain in ease of interpretation and the saving in labour is clearly considerable.

The crossed fringes are used first to examine the whole crystal surface, and from such a survey individual features have been selected for study by the fringes of equal chromatic order. As pointed out in previous publications these high-precision white-light fringes are particularly suited to revealing and interpreting local features even if only of molecular dimensions.

A detailed discussion of the whole of the complex topography revealed for each crystal is not being given and only those isolated features which throw light on fundamental growth processes will be considered in detail.

TOPOGRAPHY OF CRYSTAL A (ANGOLA STONE)

Growth sheets

The general topographical features are revealed by the crossed Fizeau fringes of figures 8*a*, *b*. For purpose of reference to different regions the schematic diagram of figure 2 will be used. The stone dimensions are 0·47 × 0·32 cm. Region A is a curved plateau, the highest position on the surface, and has a radius of curvature of some 3 m. The B, C regions almost certainly represent successive growth sheets, of the type observed by Bunn & Emmett (1946) on growing crystals. The scale and nature of these growth sheets are indicated by figure 3, which is a contour diagram of a line section from X through B, C, etc., to Y. The whole complex of sheets is encompassed within a height of about a light wave. Considering a traverse at right angles to XY, namely, in the direction PQ, the region D is quite flat, whilst the

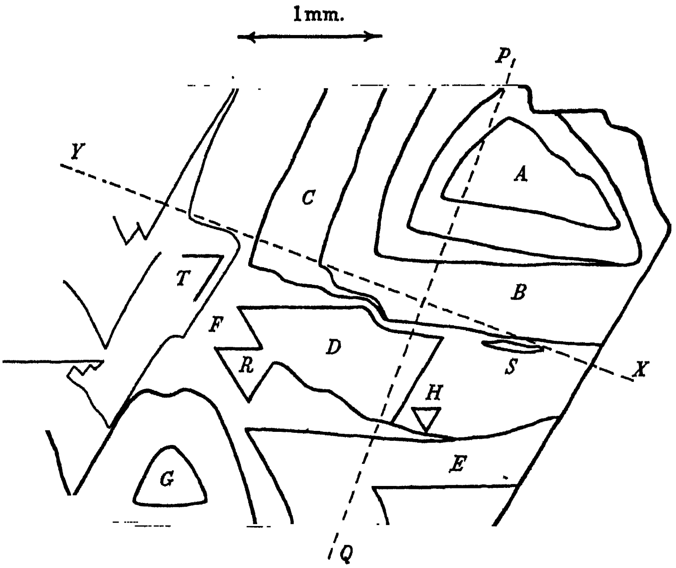

FIGURE 2

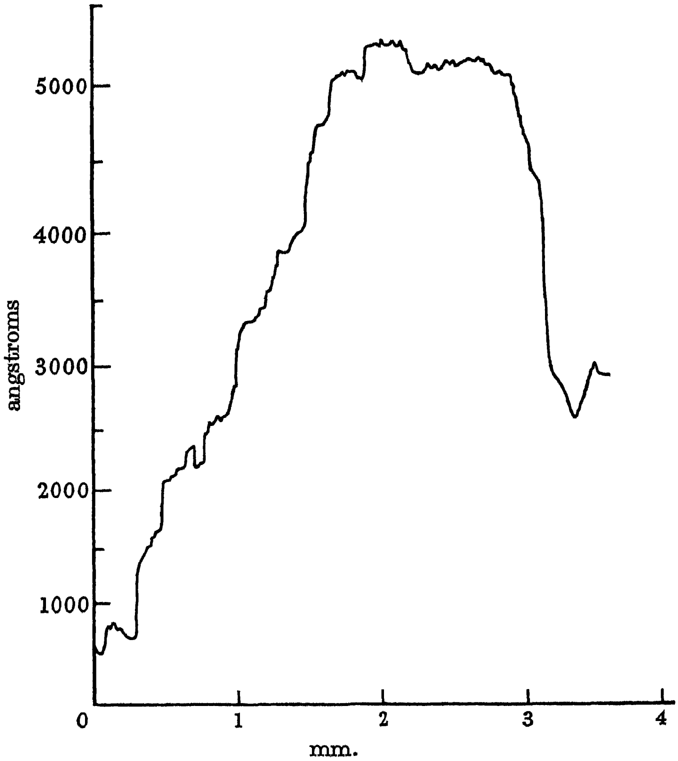

FIGURE 3

region E shows a group of growth sheets descending down to a hollow. Figure 9, plate 9, shows fringes of equal chromatic order which refer to a line section in the direction XY. These high-dispersion fringes show in a very clear manner the variations in contour across the crystal. (The figures in plate 8 are at right angles to figure 2.)

It seems clear from the fringes that the stepped pyramidal growth sheets can easily lead to the formation of effectively curved surfaces. Curvature is particularly marked at F and G. To account for the orientations of the growth sheets it is only necessary to postulate that growth takes place by means of sheets, or wave fronts, advancing in three possible directions inclined at 60° to each other. That this is undoubtedly the case will be shown later in the discussion of the triangular pit features.

Whilst some growth sheets are almost truly plane, others are distinctly convex, a typical example of the latter being shown in figure 10, plate 9. This region, F in the diagram, is shown with double-crossed fringes. In this the central dark triangular region is a high area and is curved (convex) with quite a large radius of curvature (60 cm.). This is adjacent to a plane area on one side. There seems no reason to suppose that any solution process has taken place, particularly in view of the strict rectilinearity of the boundary edges. Furthermore, it is quite unreasonable to suppose that solution could attack the upper region and yet fail to attack an adjacent lower region when the difference in height is merely 200 A. It is concluded therefore that the curvatures of the faces arise during growth.

Triangular pits

A characteristic feature shown by a large number of diamond surfaces is the appearance of oriented rectilinear pit depressions having the shape of equilateral triangles. As already stated there has been some controversy, extending over many years, as to the origin of these pits. Two views have been held, namely, (1) that they are due to solution or etching, (2) that they are due to growth. It is shown below that a typical triangular pit is due to growth only.

The triangle under discussion is that shown at H in figure 2 and is clearly recognizable in figure 11, plate 9 which is an enlargement, the base of the triangle actually being $\frac{1}{5}$ mm. in length.

The green fringe J (figure 11) proceeds over a fairly extensive plane area until it reaches the ridge KL, the height of which is 400 A. The fringe *through* the triangle is, however, a strict linear continuation of the fringe J within the limits of error of observation ($\pm$ 5 A). From this it follows that the triangle represents a pit, with its base at the level of the considerable outer region. It appears that one must attribute the formation of this pit to growth. It is only necessary to suppose that the ridge area below KL has grown by sheets advancing in plane waves inclined at 60° to each other. If these growth sheets arrest and fail to complete, the result is the formation of an equilateral pit depression as shown, with its base at the same level as the outer region.

In this specific case one cannot invoke etching as a possible explanation, for it is entirely improbable that any hypothetical etching could go on just to the exact level of the distantly removed outer region and then cease. Furthermore, evidence will be adduced later which seems to indicate that any etching processes which occur on a diamond face do not produce rectilinear markings but irregular hollows. It is therefore concluded that the characteristic rectilinear triangular pit markings on diamond faces are a growth phenomenon. This view is not based only on this single example, for other evidence supporting this view can readily be obtained from the crossed fringes. For example, the *R* region in figure 2 shows the process of growth pit formation arrested in a partially completed state on a larger scale.

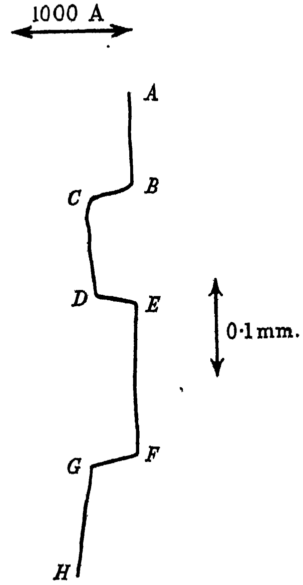

Figure 4

Further light is thrown on the mechanism of the pit formation by fringes of equal chromatic order taken across the ridge and pit of figure 11. These are shown in figure 12, plate 9, and reproduced schematically in figure 4. *AB* refers to the plane area above the ridge, which begins at *C*. The ridge region *CD* is not parallel to *AB*, but drops down slightly until the pit is reached. *EF* is the base of the pit and this appears to be very nearly plane, with an indication of a slight convexity. On rising at *FG* from the pit, the ridge surface is again not parallel to the base of the pit or to *AB*, since *GH* rises quite clearly. The co-linearity of *AB* and *EF* is strikingly demonstrated by these fringes and shows convincingly that the base of the pit is at the same level as the extensive outer region and is in fact to be identified with it.

It may be noted in figure 11, that the ridge region *H* (of figure 2) is steeply curved near its edge, and, in fact, one can regard the large area *D* (of figure 2) as an extensive pit with the growth regions *H*, *F*, *ABC* converging on it. It is of interest that the edge of *H* exhibits the identical stepped curvature shown on a smaller scale by the triangular pit feature.

Solution regions

There exist on this crystal face a number of distinctive irregularly shaped depressions which may be due either to surface occluded matter preventing crystal growth, or alternatively to a true solution action. That the 'blue ground' in which diamonds are found has a solvent action has long been known. As previously indicated an extensive solution mechanism has already been proposed to account both for the triangular pits and for the face curvature, a view which is rejected here. Yet the few highly irregular depressions, of which two are described below (*S* and *T* in figure 2) are strikingly different from the many ordered rectilinear growth features already described. It seems reasonable to suggest that they are due to a solution process.

The two features to be described are illustrated in figures 13*a*, *b*, 14*a*, *b*, plates 9 and 10. Figures 13*a*, *b* are shown with crossed Fizeau fringes; figures 14*a*, *b* show a section of each taken with fringes of equal chromatic order. These latter fringes show particularly in a very striking manner how totally different are these irregular depressions from the typical growth pit rectilinear fringes of figure 12.

Figures 14*a* and *b* have been taken under very high dispersion conditions, the two interfering surfaces being three light waves apart at $\lambda = 6500$ A. Fringe definition is particularly good when account is taken of the high dispersion. These plates reveal the power of the fringes of equal chromatic order in a distinctive manner.

It is to be noted that these solution regions are relatively small and are not connected with the general curvature of the faces; again, they all lie along a 'fault' which is almost a straight line joining S and T, and skirting the growth sheets B and C.

Since the evidence from crystal A (and also from crystal B) seems to point strongly to the association of rectilinear *edges* with growth, there may be grounds for supposing that edges showing marked curvature parallel to the surface have been affected by solution localized close to the edge itself. A further point to be noted is that only the 'high' regions show marked curvature, whilst the 'valleys' are relatively flat. The possibility of weathering and abrasion being responsible must not therefore be overlooked. It is hoped in the future to undertake a more thorough examination of the question of solution by submitting diamond surfaces to solvent action either of hot nitrates or hot 'blue ground'.

The fine structure of the fringes

All these fringe types, namely, the uniform tint high-dispersion fringes, the sharp Fizeau fringes and the fringes of equal chromatic order, exhibit characteristic fine structures. In the high-dispersion fringes the various areas show a mottled background. When definition is at its best both the sharp Fizeau fringes and the fringes of equal chromatic order exhibit a dotted broken appearance. This is only clearly seen when the interfering surfaces are very close together (less than ten light waves; the reason for this has been discussed elsewhere).

This fine structure is in all cases due to defects on the optical flats used and is not a characteristic of the diamond. This is proved by figure 21, plate 11. The flats used were made of borosilicate glass and were specially selected by Hilger as likely to have a smooth surface with high local uniformity. A number of similar flats were available. A pair were silvered and brought into close contact. The combined surface contour was examined by means of fringes of equal chromatic order, figure 21 representing a section of about 1 mm. in length. The characteristic fine structure can be clearly seen, and this, indeed, is virtually identical with that visible on the pictures taken with the diamond-flat combination. This structure undoubtedly represents polish scratch marks on the glass. These scratches appear to vary from

$\frac{1}{100}$ to $\frac{1}{200}$ mm. in width, but some are narrower and are observed only as diffraction patches. No estimate of their depth can be made, for the scratches do not appear to have specular reflexion and are simply characterized by complete absence of light within the scratch regions. Specular and non-specular regions appear to be approximately of equal width.

It is clear that random distributions of scratch markings can lead to the mottled patterns shown by the high-dispersion fringes. The same mottling appears on other crystals examined with the same flats.

A feature of considerable importance to these observations is the high degree of local plane uniformity revealed by figure 21. In these fringes there is only one very small region where the deviation from the plane is as much as $\lambda/300$, the average local deviation being less than $\lambda/400$. This local uniformity shows that considerable reliance can be placed upon the interpretation of detail in the crystal fringe patterns.

In addition to the spurious fine structure just considered, a number of the smaller triangular features (some with a base of only 0·04 mm.) show within their boundaries distinct regular diffraction patterns of spots. These indicate internal detail which the microscope is failing to resolve, due in part possibly to the employment of parallel incident light, and in part to the inherent closeness of the pattern on the crystal.

TOPOGRAPHY OF CRYSTAL B (SIERRA LEONE STONE)

The second crystal examined has revealed further novel topographical growth features not formerly recorded in the extensive literature on the diamond. This is attributable to the delicate sensitivity of the multiple-beam method of investigation. The surface area is 0·57 × 0·34 cm.

Crossed fringes are shown in figure 15, plate 10. The surface is not plane, the fringes indicating the presence of three vicinal faces coming to a point and forming a tetrahedron as shown in figure 5. The angles between the vicinal faces are quite small; for example, one is 0·9 min. of arc (which is on the limit of resolution with the goniometer). On each of the vicinal faces are a number of the characteristic triangular growth pits. The *majority* of the triangles have a sharply defined striation as a continuation of one of their sides, three typical examples being illustrated in figure 5. The orientation of these striations with respect to the edges of the octahedron face depends on which vicinal face the triangle occupies and is always parallel to the common edge of the vicinal and octahedron faces. Thus whilst the orientation of the triangles depends on the primary crystal symmetry, the striations are related to the vicinal symmetry and are therefore growth phenomena.

The significance of the oriented projections is made clear by figure 16, plate 10, which is an enlarged section. The striations clearly represent marked discontinuities, indeed, sharp-edged shelves. But it can be seen also that the shelves are plane below the striae but curved in the regions occupied by the pits. The dispersion is considerable, so that the effects are highly magnified.

A more detailed study of the nature of these shelves has been carried through with the aid of both high-dispersion Fizeau fringes and fringes of equal chromatic order. Figure 17, plate 10, was taken with high-dispersion Fizeau fringes, set in the region of great sensitivity. From these it can be seen that the basal projecting streaks are sharply defined below the triangles, but fade away on the upper line of demarcation. The observations with the fringes of equal chromatic order were difficult owing to the small extension of the features investigated. (Many of the triangles are less than 0·1 mm. across.) A triangular pit was selected as shown in figure 6, and the fringes of equal chromatic order observed over two sections *AA'* and *BB'* on either side of a basal striation. These are respectively the upper and lower fringe patterns of figure 18, plate 10. The *A* fringe shows that the surface is plane here. The *B* fringe shows marked curvature, as the pit is approached (the fringe *within* the pit is faintly visible on the original; the pit is about 1500 A deep).

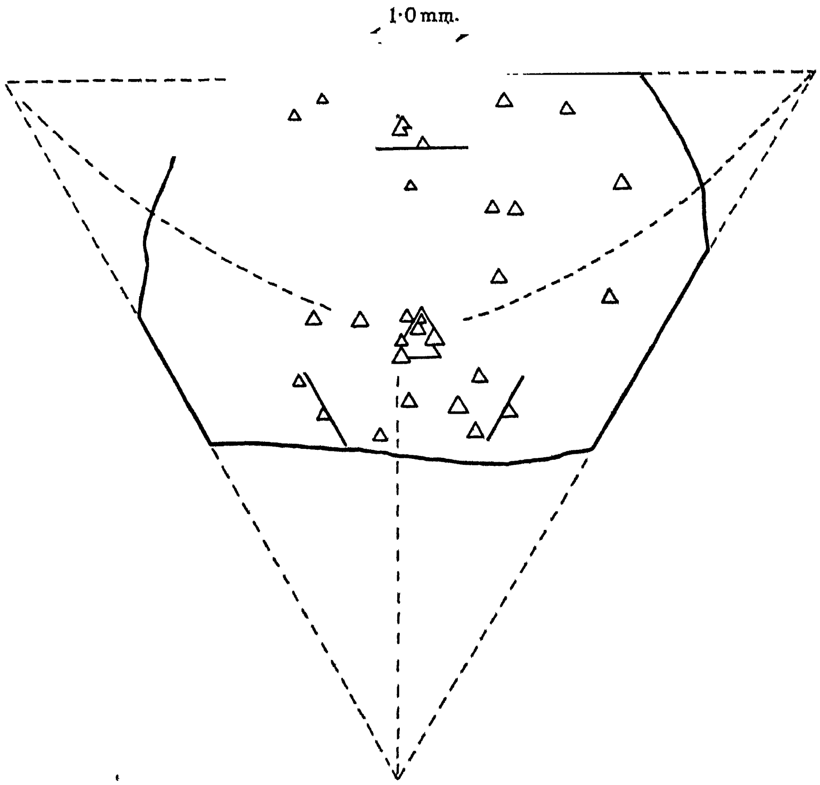

FIGURE 5

The high-dispersion Fizeau fringes of figure 17, were secured with optimum conditions for very high sensitivity, and this shows in a very clear manner a further characteristic feature of the basal striations. It shows how the shelf is strictly plane below the striation, but above this line the surface curves down

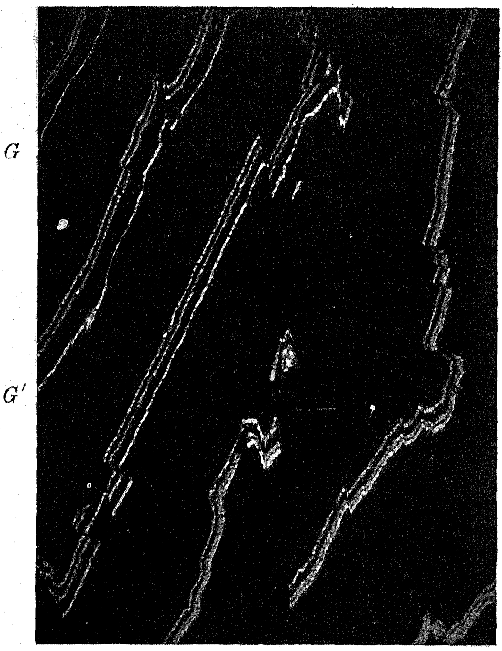

7*a*

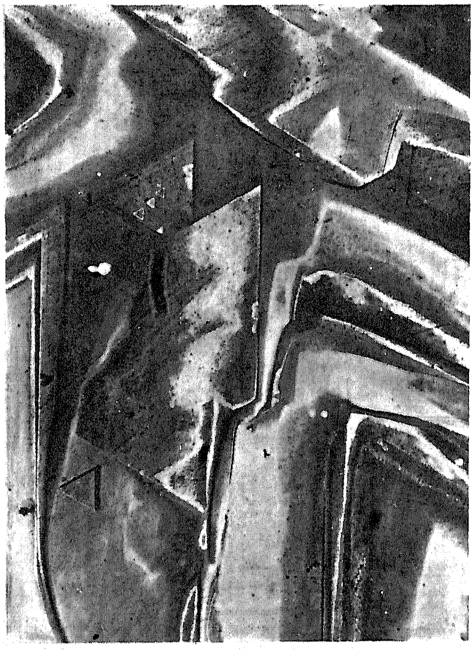

7*b*

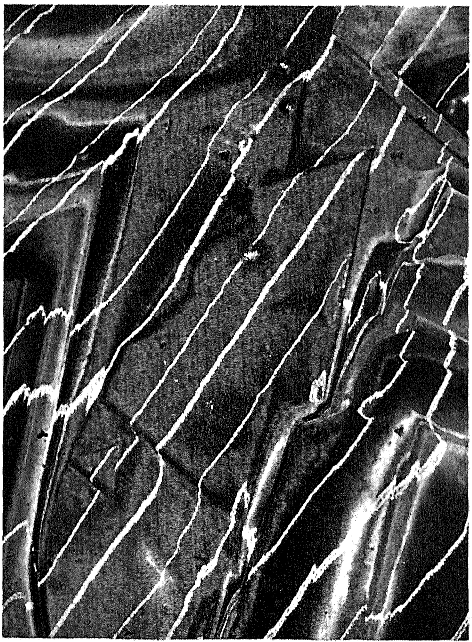

8*a*

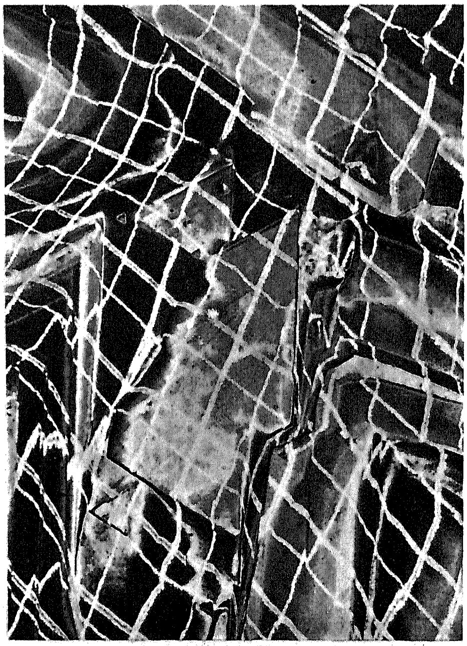

8*b*

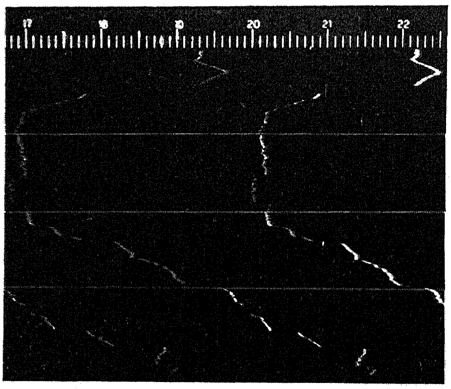

9

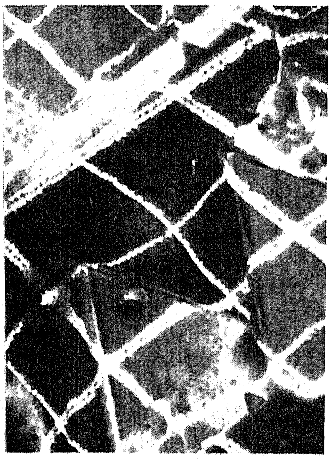

10

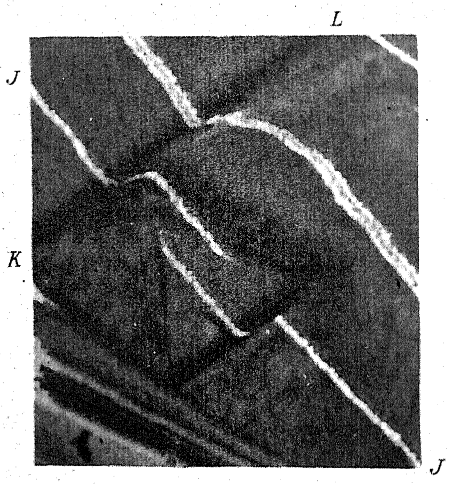

11

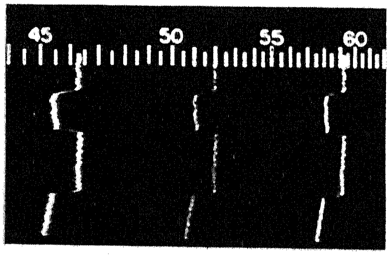

12

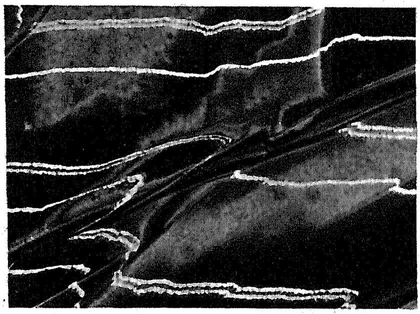

13*a*

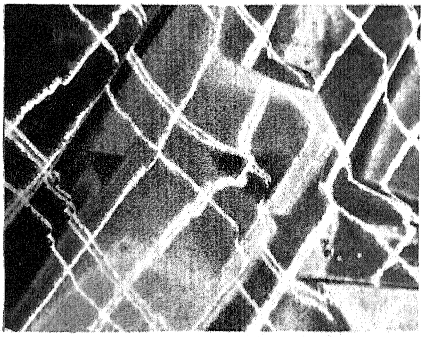

13*b*

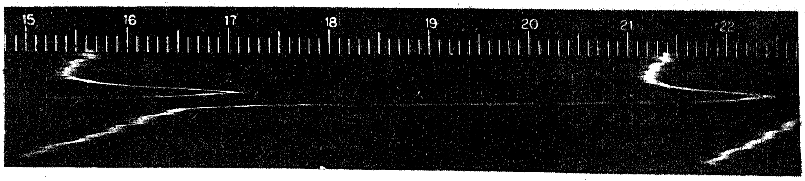

14*a*

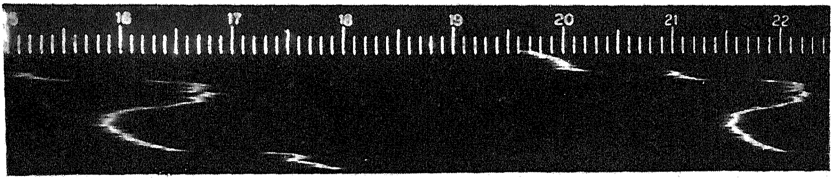

14*b*

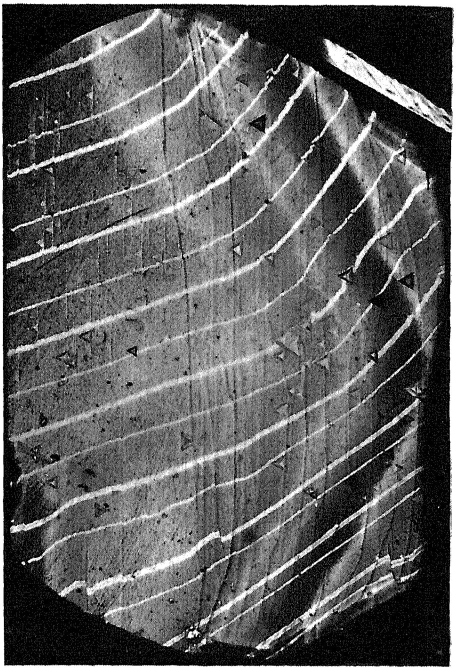

15

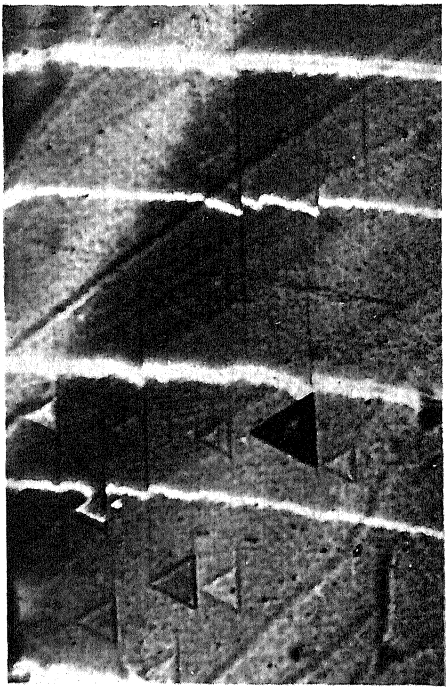

16

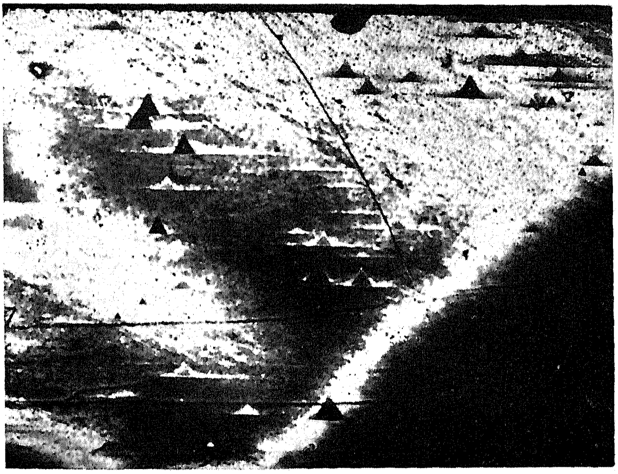

17

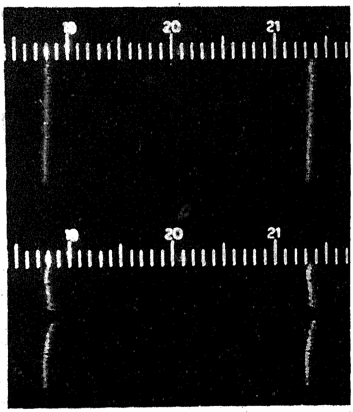

18

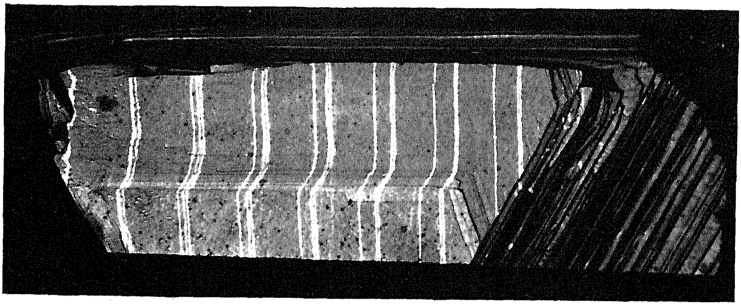

19

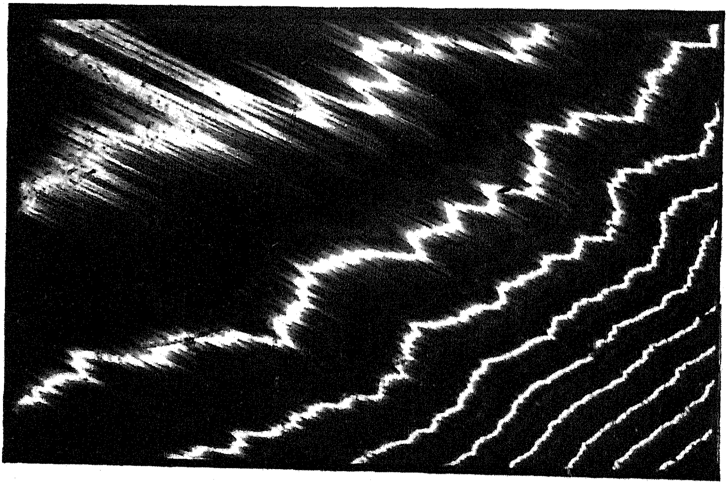

20

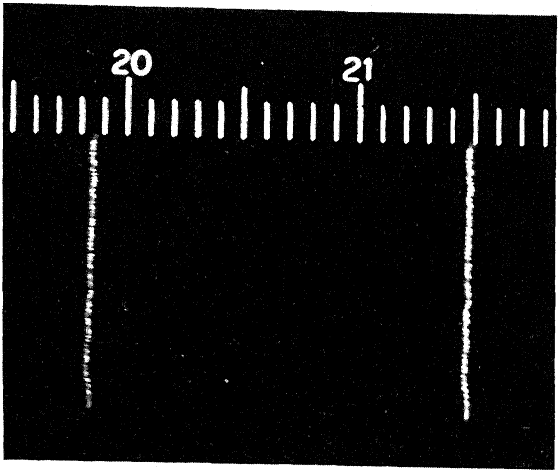

21

towards the hollow of the pit. Furthermore, the manner in which this curvature fades away along the extension of the basal projection is clearly rendered.

It would seem that the growth sheets spreading out from some point stop abruptly forming the striae, and incompletion from other directions leads to both the shelving and triangular pits.

It is emphasized that only the high sensitivity of the multiple-beam technique renders such features visible.

Although all the triangular markings have not been studied in detail, every one so far examined is a pit and not an elevation. On this particular crystal some only of the triangular pits have a flat bottom. Many are true symmetrical tetrahedra. Many more are truncated tetrahedra, i.e. the sides are tetrahedral, but these do not complete to the apex, truncating to give a flat base. These structures can be easily recognized on the photographs.

The depths of the pits vary from a few angstrom units to about a light wave (say 5000 A). In a few cases a large triangular pit exhibits smaller pits within its boundaries.

Topography of crystal C (Sierra Leone)

The third crystal examined has very few features on its surface (size 0·49 × 0·17 cm.). Crossed Fizeau fringes are shown in figure 19, plate 11. The surface, which is seen to consist of three distinct regions divided by steps, is characterized by two main features. The first is the absence of growth triangles; yet there is still some indication of growth having taken place in three directions, mutually inclined at 60°, as was the case in the two previous crystals.

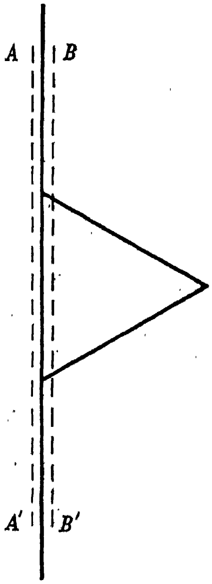

Figure 6

The second, and perhaps the most striking characteristic of this crystal, is the remarkable optical uniformity of the two major areas shown by the crossed fringes For, leaving out the intermediate steps, these areas are optically flat planes, flat to within a striking perfection. This degree of flatness is noteworthy and has not yet been observed over so extensive an area on any of the limited number of crystal faces hitherto examined (quartz, selenite, calcite, baryta, mica). It affords strong evidence that this crystal surface has not been subjected to any solution process.

The mottling in the high-dispersion crossed fringes has the secondary origin already discussed and is due to the glass flat.

Polished diamond stone

As an appendix to this investigation on natural diamond surfaces, a brief report is included on the examination of the topography of the face of a polished diamond which was available.

This diamond was supplied by The Diamond Trading Co. as a small optical flat of dimensions 0·30 × 0·21 cm. The Fizeau fringes are shown in figure 20, plate 11. The surface exhibits cylindrical curvature, and apart from this has local errors of the order of $\frac{1}{4}\lambda$. As a flat it is of poor grade. The only feature of interest lies in the fairly deep parallel scratches due to polishing which are best seen in the region of high dispersion.

We wish to thank Dr P. Grodzinski of the Research Laboratory of The Diamond Trading Co., both for the loan of the diamonds and for supplying mounts to hold them; and also for copies of the publications by Mohr and by Fersmann & Goldschmidt. This research was made possible with the help of a Department of Scientific and Industrial Research grant to W. L. Wilcock.

REFERENCES

Bunn & Emmett 1946 *Nature*, **158**, 164.
Fersmann & Goldsmidt 1911 *The Diamond*. Heidleberg: Winter.
Kayser 1944 *Industr. Diamond Rev.* 4 Jan.
Miers 1902 *Mineralogy*. London: Macmillan.
Mohr 1924 *Abh. Heidelberg Akad. Math.-naturw.* **12**, 1.
Tolansky 1945*a* *Proc. Roy. Soc.* A, **184**, 41.
Tolansky 1945*b* *Proc. Roy. Soc.* A, **184**, 51.
Tolansky 1945*c* *J. Sci. Instrum.* **22**, 161.
Tolansky 1946 *Proc. Phys. Soc.* **58**, 663.
Tolansky & Wilcock 1946 *Nature*, **157**, 583.
Williams 1932 *The genesis of the diamond*. London: Benn.

On the scattering of fast neutrons by protons

By W. H. Ramsey, *H. H. Wills Physical Laboratory, University of Bristol*

(*Communicated by N. F. Mott, F.R.S.—Received* 8 *February* 1947)

The features of the scattering of fast neutrons by protons are calculated using the Møller-Rosenfeld version of the meson theory of nuclear forces. The experimental results of Occhialini & Powell are used to check the predicted angular distribution of the scattered particles and to determine the mass of the meson; the meson mass indicated is about 215 electronic masses, which agrees with the mass of cosmic ray mesons. The total scattering cross-section predicted by the theory agrees with the empirical results.

Introduction

A detailed knowledge of the interaction between the neutron and the proton is of great importance for the theory of nuclear forces. As the deuteron has only one stable state, no very far-reaching conclusions about the interaction can be drawn from the discrete spectrum. The main attention must, therefore, be directed to the careful investigation of the scattering of neutrons by protons. Measurements yield a total cross-section for scattering and an angular distribution of the scattered particles which are characteristic of the energy of the incident neutrons.

In the present paper the version of the meson theory of nuclear forces, usually known as the Møller-Rosenfeld theory, will be used to make detailed theoretical predictions about the scattering cross-section and its dependence on the angle of scattering and on the energy of the incident particles. This theory contains three adjustable parameters, two of which will be chosen so that the energies of the stable and virtual states of the deuteron are given correctly; the third parameter is the mass of the meson. The experimental results of Occhialini & Powell (1947) will be used to check the predicted angular distribution of the scattered neutrons and to determine the mass of the meson.

Interest in the scattering of fast neutrons by protons was increased as a result of experiments by Amaldi, Bocciarelli, Ferretti & Trabacchi (1942) which suggested that the scattering is predominantly forward. Hulthén (1943, 1944*a*) has shown that this is at variance with meson theories which are symmetrical as regards electric charge, including the Møller-Rosenfeld theory, and that important modifications of present ideas on the nature of nuclear forces would have to be made if the conclusions of these experiments were to be confirmed by later investigators. It is therefore important that neutron-proton scattering should be further investigated experimentally and the results viewed in the light of current meson theories.

Some of the results of this investigation have already been published by Fröhlich, Ramsey & Sneddon (1947) in connexion with the Physical Society Conference at Cambridge.

INTERACTION BETWEEN NUCLEONS

The version of meson theory due to Møller & Rosenfeld (1940), which involves electrically charged and neutral mesons in a symmetrical way, will be used to describe the interaction between two nucleons. The objections to theories which do not allow both charged and neutral mesons are well known. Theories postulating charged mesons only cannot account for the equality, or approximate equality, of neutron-proton and proton-proton forces. On the other hand, theories postulating neutral mesons only cannot lead to the saturation property of nuclear forces exhibited by heavy nuclei, nor can the mesons be identified with the charged particles found in cosmic radiation. The Møller-Rosenfeld theory is the most consistent and least ambiguous of all the symmetrical theories; in the static approximation no arbitrary 'cutting off' of the interaction is required to avoid divergencies arising from terms of the dipole-dipole type. Fröhlich, Huang & Sneddon (1947) have used this theory with some success to calculate the binding energies of the lightest nuclei, and Rozental (1941, 1945) has shown that a satisfactory description of β-disintegration can be based on it. It has also been shown by Hulthén (1943) that the non-static part of the interaction in this theory can account for the observed value and sign of the quadrupole moment of the deuteron.

The static part of the interaction between two nucleons is given by

$$V = \frac{G}{r} e^{-\lambda r}, \tag{1a}$$

$$G = (\boldsymbol{\tau}_1, \boldsymbol{\tau}_2)\{g^2 + f^2(\boldsymbol{\sigma}_1, \boldsymbol{\sigma}_2)\}, \tag{1b}$$

where r is the distance between the nucleons and where $\boldsymbol{\sigma}_i$, $\boldsymbol{\tau}_i$ are the usual vector operators associated with the spin and isotopic spin respectively of nucleon i. The length λ^{-1}, which measures the range of the force, is related to the meson mass m by the equation

$$\lambda = mc/\hbar. \tag{2}$$

The quantities f and g are universal constants with the dimensions of an electric charge. Rosenfeld (1945) has shown that part of the non-static interaction in the original paper by Møller & Rosenfeld (1940) is of the same mathematical form as the static interaction and can be included in it by merely altering the values of the charge constants. The charges f and g appearing in equation (1b) are connected with the charges f_i and g_i appearing in the paper by Møller & Rosenfeld (1940) by the equations

$$4\pi g^2 = g_1^2 - \frac{m}{M} g_1 g_2,$$

$$4\pi f^2 = g_2^2 - \frac{m}{M} \frac{2g_1 g_2 - f_1 f_2}{3},$$

where M denotes the mass of a nucleon (the difference in the masses of the neutron and proton is neglected throughout this paper). The remaining part of the non-static interaction is comparatively small and will be neglected; the work of Hulthén (*1943, 1944a*) *shows that this is justified at the energies considered.*

The value of the operator G defined by equation (1*b*) depends only on the symmetry properties of the wave function describing the two nucleons. The operator $(\boldsymbol{\sigma}_1, \boldsymbol{\sigma}_2)$ has the value $+1$ or -3 according as the wave function is symmetrical or antisymmetrical in the spin variables; the value of the operator $(\boldsymbol{\tau}_1, \boldsymbol{\tau}_2)$ is determined analogously. Consider the wave function representing the two nucleons in the system of co-ordinates in which the centre of mass is at rest; suppose that the spatial part of this wave function is of the form

$$\psi_l(\mathbf{r}) = \frac{1}{r} R_l(r)\, Y_l^m(\theta, \phi), \tag{3}$$

where $Y_l^m(\theta,\phi)$ is the usual surface harmonic. All the relevant symmetry properties of the complete wave function are determined if the value of l is specified and if it is indicated whether the state is a singlet or a triplet. The symmetry with respect to the isotopic spin variables is then determined by the fact that the complete wave function must be antisymmetrical with respect to the interchange of the two nucleons, in accordance with the Pauli principle. The eigenvalues of the operator G in the different states are given in table 1 for the neutron-proton interaction.

TABLE 1. STATIC INTERACTION CONSTANTS

	l even	l odd
singlet	$\mathrm{G} = -(3f^2 - g^2)$	$\mathrm{G} = 3(3f^2 - g^2)$
triplet	$\mathrm{G} = -3(f^2 + g^2)$	$\mathrm{G} = (f^2 + g^2)$

As $f^2 \sim 0{\cdot}07\hbar c$ and $g^2 \sim 0{\cdot}03\hbar c$ (see table 3) it follows that, in the Møller-Rosenfeld theory, the interaction for states with odd values of l is strongly repulsive if the spins of the neutron and proton form a singlet, and only weakly repulsive if they form a triplet. For neutrons of low energy (say below 5 MeV), the anisotropy in the scattering is mainly due to the P-states; as the interaction is repulsive for these states, the intensity of the scattered wave is greater in the backward direction than in the forward direction in the system of co-ordinates in which the centre of mass is at rest. The higher orders (D, F, G, etc.) become more important as the energy of the incident neutrons is increased; nevertheless, the feature of backward scattering remains if the Møller-Rosenfeld description of nuclear forces is correct.

The set of interaction constants given in table 1 is characteristic of the Møller-Rosenfeld theory. Other theories give different sets of constants; for example, in the case of 'ordinary' forces the interaction is not influenced by the quantum state of the particles, and in the mixed neutral meson theory the interaction depends on the spin state but not on the value of l. The set of constants given in table 1 is even more characteristic of the theory than is the radial dependence of equation (1*a*), and should be, if possible, tested directly by experiment.

It will be assumed that the wave function which describes the behaviour of the particles satisfies a Schrödinger wave equation. The difficulties of setting up and solving a relativistic wave equation which can be applied to nuclear particles are very great, and it does not seem necessary to take this course. The kinetic energy of an 18 MeV neutron is only 0·02 Mc^2, and so the relativistic correction at this energy will be very small. Moreover, it would be inconsistent to use a relativistic wave equation and to neglect the non-static terms in the interaction.

For a wave function of the form given in equation (3) the problem reduces to one of finding the appropriate solution of the differential equation

$$\left[\frac{\hbar^2}{M}\left(\frac{d^2}{dr^2}-\frac{l(l+1)}{r^2}\right)+E-\frac{G}{r}e^{-\lambda r}\right]R_l(r)=0. \tag{4}$$

It is convenient to introduce the dimensionless quantities

$$x=\lambda r,\quad \mu=m/M,\quad a=E/\mu^2Mc^2,\quad b=-G/\mu\hbar c, \tag{5}$$

so that equation (4) takes the form

$$\mathbf{L}R_l(r)\equiv\left[\frac{d^2}{dx^2}-\frac{l(l+1)}{x^2}+a+b\frac{1}{x}e^{-x}\right]R_l(x)=0. \tag{4a}$$

THE DEUTERON

The ground state of the deuteron is a ^3S state which, according to Wiedenbeck & Marhoefer (1945), has a binding energy of 2·185 ± 0·006 MeV. A virtual ^1S state also is known from the scattering of very slow neutrons by protons. Hanstein (1941) found a cross-section of $21\pm1\times10^{-24}$ cm.^{2} for the scattering of neutrons of energy 1 eV by protons; this corresponds to an energy of about 0·06 MeV for the virtual state, the precise value depending on the meson mass assumed. For a fixed value of λ these experimental results have been used to determine the charge constants f and g appearing in the interaction (1); this leaves the range of the force or the meson mass as the only undetermined parameter.

Hulthén (1944*b*, 1945) has shown that, for the ground state, satisfactory results can be obtained using a wave function of the form

$$R_0(x)=(1-e^{-x})(1+\beta e^{-x})e^{-\sqrt{(-a)}x}, \tag{6}$$

and that for S waves of the continuous spectrum a suitable wave function is

$$R_0(x)=\cos\eta_0\sin x\sqrt{a}+(1-e^{-x})(1+\beta e^{-x})\sin\eta_0\cos x\sqrt{a}, \tag{7}$$

where the phase shift η_0 is related to the energy parameter a in such a way as to give the observed cross-section for the scattering of slow neutrons; in equation (7) only $a\sim0$ is of interest. In each case the parameter β is to be determined by a variation of the integral

$$\bar{L}=\int_0^\infty R_0(x)\,\mathbf{L}R_0(x)\,dx,$$

where $\mathbf{L}$ is the operator defined by equation (4*a*) with $l=0$. The value of the constant b is then given by the relation

$$\bar{L}=0.$$

The results of these calculations are given in table 2. In table 3 the charge constants are shown as a function of the mass of the meson (m_e denotes the mass of the electron).

TABLE 2

	^{3}S state		^{1}S state	
meson mass	β	b	β	b
$200m_e$	0·5889	2·65	0·4587	1·52
$225m_e$	0·5841	2·54	0·4663	1·53
$250m_e$	0·5801	2·46	0·4726	1·55

TABLE 3. STATIC CHARGE CONSTANTS

meson mass	$f^2/\hbar c$	$g^2/\hbar c$
$200m_e$	0·0653	0·0309
$225m_e$	0·0729	0·0310
$250m_e$	0·0806	0·0310

DETERMINATION OF PHASE SHIFTS AND APPLICATION OF BORN APPROXIMATION

Calculation of the scattering to be expected involves finding the solution (4a) which vanishes at the origin and which has the asymptotic form

$$R_l(x) \sim \sin(x\sqrt{a} - \tfrac{1}{2}l\pi + \eta_l),$$

where η_l is the phase shift introduced by the interaction between the nucleons. The characteristics of the scattering are completely determined by the phase shifts η_l (cf. Mott & Massey 1933). In equations (4) and (5) the energy of the incident neutrons in the laboratory system of co-ordinates is $2E$.

The simplest procedure to determine the phase shifts is to use the following approximation:

$$\begin{aligned}\eta_l &= b\,\tfrac{1}{2}\pi\int_0^\infty e^{-x}\{J_{l+\frac{1}{2}}(x\sqrt{a})\}^2\,dx \\ &= \frac{b}{2\sqrt{a}}\,Q_l\left(1+\frac{1}{2a}\right),\end{aligned} \tag{8}$$

where $Q_n(z)$ is the Legendre function of the second kind of order n (cf. Mott & Massey 1933; Watson 1944). If formula (8) is used throughout and if only first powers of the phase shifts are retained in the expression for the amplitude of the scattered wave, the scattering is given by the Born approximation (cf. equations (11)). Equation (8) is sufficiently accurate only for large values of l. For the values of a and b considered the phase shifts given by equation (8) were wrong by 2 to 7 % in the case of ^{3}P, ^{3}D and ^{1}D states, and by 32 to 37 % in the case of ^{1}P states. The phase shifts for S states were underestimated by as much as 60 %. This approximation consistently overestimates the phase shifts for the states in which the interaction is repulsive, and it consistently underestimates the phase shifts for the states in which the interaction is attractive; the net result is a serious exaggeration of the anisotropy of the scattering.

A much better approximation has been developed by Pais (1946). A suitable solution of equation (4a) when there is no interaction between the nucleons is

$$R_l(x) = \sqrt{(\tfrac{1}{2}\pi x\sqrt{a})}\,J_{l+\frac{1}{2}}(x\sqrt{a}).$$

Pais takes the effect of the interaction between the nucleons into account by using a solution of the type

$$R_l(x) = \sqrt{(\tfrac{1}{2}\pi x\sqrt{a})}\,J_{l+\Delta+\frac{1}{2}}(x\sqrt{a}), \quad \eta_l = -\tfrac{1}{2}\pi\Delta,$$

where Δ is to be determined from equation (4a) by the relation

$$\int_0^\infty R_l(x)\,\mathrm{L}R_l(x)\,dx = 0.$$

This leads directly to Pais's formula

$$\frac{2l+\Delta+1}{2l+2\Delta+1}\Delta = -\frac{b}{\pi\sqrt{a}}Q_{l+\Delta}\left(1+\frac{1}{2a}\right), \tag{9}$$

where $Q_n(z)$ is again a Legendre function of the second kind. This formula may be expected to give very accurate results provided that the interaction between the nucleons is small compared with the centrifugal term $l(l+1)/x^2$. It breaks down completely in the case of S states, and it is not sufficiently accurate in the case of ^{1}P states. Table 4 compares the results of Pais's formula with those found by numerical integration.* Pais's formula gives phase shifts wrong by 7 to 10 % in these cases. Nevertheless, the improvement over the Born formula (8) can be gauged from the fact that the corresponding errors with that approximation were 32 to 37 %.

TABLE 4. PHASE SHIFTS OF ^{1}P STATES

		phase shift	
a	b	numerical integration	Pais's formula
0·64	−5·09	−0·307	−0·328
0·595	−5·09	−0·293	−0·3145
0·47	−5·12	−0·251	−0·272
0·38	−5·13	−0·215	−0·236
0·32	−5·12	−0·188	−0·206

---

* The numerical integrations were carried out for charge constants corresponding to the virtual ^{1}S state of the deuteron having zero energy (cf. Fröhlich, Ramsey & Sneddon 1947). For the purpose of assessing the accuracy of Pais's formula the results of the actual numerical integrations have been given in table 4.

Phase shifts found by numerical integration have been modified to correspond to the charge constants given in table 3 on the assumption that the phase shift can be expressed as a power series in b:

$$\eta = c_1 b + c_2 b^2 + c_3 b^3,$$

where c_1, c_2 and c_3 are constants and c_1 corresponds to the Born formula (8). The error introduced by this alteration should be very small.

The phase shifts of all S and ^{1}P states were found by a step-by-step numerical integration. Hulthén (1943) has pointed out that the accuracy of a numerical integration can be estimated from the identity

$$\sin\eta_l = b\,\tfrac{1}{2}\pi\int_0^\infty (\tfrac{1}{2}\pi x\sqrt{a})^{-\frac{1}{2}}\, e^{-x} J_{l+\frac{1}{2}}(x\sqrt{a})\, R_l(x)\, dx,$$

by using the value of $R_l(x)$ found by the numerical integration. This was done for the third and fifth cases of table 4, and the values $-0{\cdot}2513$ and $-0{\cdot}1877$ respectively were found for the phase shifts; these differ by less than 1 % from the results of numerical integration.

The phase shifts found in the various cases considered are given in table 5; these refer to the values of the charge constants given in table 3. The method used to derive each value is indicated; numerical integration, the Pais approximation (9) and the Born formula (8) are denoted by (*N*), (*P*) and (*B*) respectively.

TABLE 5. PHASE SHIFTS

energy ...	18·05 MeV	13·25 MeV	13·25 MeV	13·25 MeV	9·02 MeV
meson mass ...	$225m_e$	$200m_e$	$225m_e$	$250m_e$	$225m_e$
^{1}S	0·859 (*N*)	0·868 (*N*)	0·910 (*N*)	0·956 (*N*)	0·965 (*N*)
^{1}P	−0·282 (*N*)	−0·267 (*N*)	−0·229 (*N*)	−0·198 (*N*)	−0·172 (*N*)
^{1}D	0·0315 (*P*)	0·0288 (*P*)	0·0216 (*P*)	0·0163 (*P*)	0·0125 (*P*)
^{1}F	−0·0240 (*P*)	−0·0210 (*P*)	−0·0140 (*P*)	−0·00931 (*P*)	−0·00641 (*P*)
^{1}G	0·00215 (*B*)	0·00187 (*B*)	0·00108 (*B*)	0·00063 (*B*)	0·00039 (*B*)
^{1}H	−0·00125 (*B*)	−0·00151 (*B*)	−0·00076 (*B*)	−0·00039 (*B*)	−0·00022 (*B*)
^{3}S	1·578 (*N*)	1·684 (*N*)	1·694 (*N*)	1·711 (*N*)	1·835 (*N*)
^{3}P	−0·0664 (*P*)	−0·0655 (*P*)	−0·0543 (*P*)	−0·0449 (*P*)	−0·0404 (*P*)
^{3}D	0·0533 (*P*)	0·0508 (*P*)	0·0362 (*P*)	0·0262 (*P*)	0·0209 (*P*)
^{3}F	−0·00450 (*P*)	−0·00412 (*P*)	−0·00261 (*B*)	−0·00166 (*B*)	−0·00119 (*B*)
^{3}G	0·0036 (*B*)	0·00327 (*B*)	0·00179 (*B*)	0·00101 (*B*)	0·00064 (*B*)
^{3}H	−0·00023 (*B*)	−0·00029 (*B*)	−0·00014 (*B*)	−0·00007 (*B*)	−0·00004 (*B*)

As an alternative to the treatment by the phase-shift method, the Born approximation may be used to calculate the features of the scattering. Using the system of co-ordinates in which the centre of mass is at rest, the Schrödinger equation appropriate to the problem is

$$(\nabla^2 + k^2)\,\Psi = \frac{M}{\hbar^2}\,\mathrm{V}\Psi, \quad k^2 = \frac{ME}{\hbar^2}, \tag{10}$$

where Ψ is the complete wave function representing the behaviour of the nucleons, $2E$ is the energy of the incident neutrons and V is the interaction operator (1). The singlet and triplet states form two non-combining sets and so may be treated separately. In the Born approximation it is assumed that the wave function Ψ on the right-hand side of equation (10) may be replaced by the corresponding solution of the free equation. This procedure is justified only if the total cross-section for scattering is small. If the beam of neutrons is incident in the z-direction, in the case of the singlet states the right-hand side of equation (10) becomes in this approximation

$$\frac{M}{\hbar^2}\mathrm{V}\Psi \simeq \frac{M}{\hbar^2}\mathrm{V}\{\mathrm{S}_A \cos kz + i\mathrm{S}_S \sin kz\}$$

$$= -\frac{M}{\hbar^2}(3f^2-g^2)\frac{1}{r}e^{-\lambda r}\{\mathrm{S}_A \cos kz - 3i\mathrm{S}_S \sin kz\}, \qquad (10a)$$

making use of the eigenvalues of the operator V given in table 1; here S_S, S_A respectively are symmetrical and antisymmetrical partial wave functions depending only on the spin and isotopic spin variables. Inserting (10a) into equation (10), multiplying by $(\mathrm{S}_A^* + \mathrm{S}_S^*)$ and summing over the spin and isotopic spin variables, the equation reduces to

$$(\nabla^2 + k^2)\,\psi(\mathbf{r}) = -\frac{M}{\hbar^2}(3f^2-g^2)\{\cos kz - 3i \sin kz\}\frac{1}{r}e^{-\lambda r},$$

where $\psi(\mathbf{r})$ is the spatial part of the wave function Ψ. This equation can be solved by the standard method (cf. Mott & Massey 1933). The treatment of the triplet states is similar. This calculation gives the following amplitudes of the scattered waves at angle θ:

$$\left.\begin{aligned} F_S(\theta) &= -\frac{M}{\hbar^2}(3f^2-g^2)\left\{\frac{1}{\lambda^2+4k^2\sin^2\frac{1}{2}\theta} - \frac{2}{\lambda^2+4k^2\cos^2\frac{1}{2}\theta}\right\}, \\ F_T(\theta) &= \frac{M}{\hbar^2}(f^2+g^2)\left\{\frac{1}{\lambda^2+4k^2\sin^2\frac{1}{2}\theta} + \frac{2}{\lambda^2+4k^2\cos^2\frac{1}{2}\theta}\right\}, \end{aligned}\right\} \qquad (11)$$

where $F_S(\theta)$, $F_T(\theta)$ refer to the singlet and triplet states respectively. The cross-section for scattering through an angle θ in the centre of mass system of co-ordinates is

$$I(\theta) = \tfrac{1}{4}\,|F_S(\theta)|^2 + \tfrac{3}{4}\,|F_T(\theta)|^2.$$

ANGULAR DISTRIBUTION AND TOTAL CROSS-SECTION

In this section the results of the calculations by the phase-shift method will be presented and compared with the available experimental material.

Throughout the calculations six orders (that is, S, P, D, F, G and H states) have been taken into account. Fröhlich, Ramsey & Sneddon (1947) have pointed out the necessity of this in calculating the angular distribution of the scattered neutrons; figure 3 of that paper, which shows the contribution of the different orders in the case of 13½ MeV neutrons and a meson mass of $200m_e$, clearly demonstrates the importance of the states with large angular momenta. This state of affairs is exaggerated in the 18·05 MeV case considered here. The higher orders, on the other hand, contribute little to the total cross-section; 92 % of the total cross-section for the scattering of 18·05 MeV neutrons is due to the S-states and the predominance is even more pronounced at lower energies.

The cross-section $I(\theta)$ for scattering through an angle θ in the system of co-ordinates in which the centre of mass is at rest, and the total cross-section for scattering can be derived from the phase shifts given in table 5 by a standard procedure (cf. Mott & Massey 1933). The angular distribution of the scattered wave is the most characteristic feature of the scattering and its analysis is the most powerful method of testing a theory of nuclear forces by experiments on scattering. All meson theories which involve electrically charged and electrically neutral mesons in a symmetrical way lead to a distribution of scattered neutrons which is predominantly backward, that is, $I(\pi) > I(0)$. On the other hand, meson theories postulating neutral mesons only lead to scattering predominantly forward, that is $I(0) > I(\pi)$. Theories which allow only charged mesons lead to an angular distribution even more predominantly backward than do the symmetrical theories. It is therefore of the greatest importance that the scattering cross-section $I(\theta)$ be found accurately experimentally over the entire range $0 \leqslant \theta \leqslant \pi$, and compared with the predictions of the various contending theories. However, the experimental material at present available is not sufficient to allow so detailed a test, and attempts (e.g. Amaldi *et al.* 1942) have been made to assign a number which measures the departure of the distribution from isotropy. The usual measure γ, which will be referred to as the anisotropy ratio, is defined by the relation

$$\gamma = \frac{I(\pi)}{I(\frac{1}{2}\pi)}. \tag{12}$$

In the next section it will be shown that this ratio is not the most characteristic index which can be associated with the angular distribution; a more suitable number ρ, which will be referred to as the asymmetry ratio, is defined by

$$\rho = \frac{I(\pi)}{I(0)}. \tag{13}$$

TABLE 6. CHARACTERISTICS OF SCATTERING

energy (MeV)	meson mass	anisotropy ratio	asymmetry ratio	total cross-section (cm.^{2})
18·05	$225m_e$	1·90	1·69	$5{\cdot}61 \times 10^{-25}$
13·25	$200m_e$	1·70	1·59	$7{\cdot}53 \times 10^{-25}$
13·25	$225m_e$	1·45	1·41	$7{\cdot}43 \times 10^{-25}$
13·25	$250m_e$	1·29	1·29	$7{\cdot}37 \times 10^{-25}$
9·02	$225m_e$	1·17	1·19	$10{\cdot}34 \times 10^{-25}$

The results of the calculations are summarized in table 6 and in figures 1 to 4. In figures 1 and 2 the calculated angular distributions for the scattering of 9·02 and 13·25 MeV neutrons are compared with the experimental values found by Occhialini & Powell (1947) for 9·2 and 13·4 MeV neutrons respectively. These workers, who used a photographic method to detect the recoil protons, did not measure absolute cross-sections, and in each case their values have been normalized to correspond to the theoretical total cross-section for a meson mass of $225m_e$; this procedure is justified, as the theory gives the total cross-section correctly (see figure 3). In figures 1 and 2 only the more recent observations which were made under refined conditions have been included. The standard error associated with each empirical value allows only for the statistical fluctuation in the number of tracks, and not for any systematic error in the method; there are, in all, 2562 tracks for the 9·2 MeV case and 415 for the 13·4 MeV case. Provided that there is no large systematic error which has been overlooked by the investigators, these experiments leave little doubt that the anisotropy ratio is greater than unity; there is less than one chance in a thousand that these experimental values are a fluctuation of an angular distribution which has an anisotropy ratio less than unity. It is apparent from table 6 and from figure 2

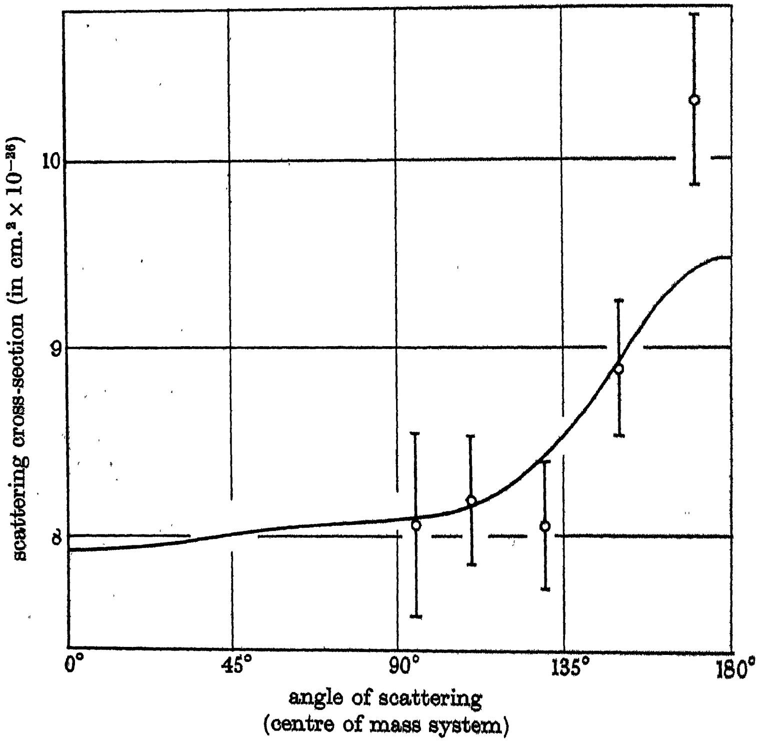

FIGURE 1. The calculated variation of the scattering cross-section for 9·02 MeV neutrons with the angle of scattering in the case of a meson mass of 225m_e. The experimental results shown are those of Occhialini & Powell (1947) for the scattering of 9·2 MeV neutrons by protons.

that the anisotropy ratio γ varies rapidly with the meson mass; if the quantity $(\gamma-1)$ were known within 10 % for the scattering of 13·25 MeV neutrons, the uncertainty in the meson mass which must be used in the theory would be about 3 %. The meson mass which is indicated by the experiments of Occhialini & Powell is $211 \pm 10m_e$ in the 9·2 MeV case and $250 \pm 30m_e$ in the 13·4 MeV case, or, taking both sets of observations together, $215 \pm 10m_e$; the standard errors again take only statistical fluctuations into account. These are in good agreement with the value 210 to $220m_e$ found by Fröhlich, Huang & Sneddon (1947) from the binding energies of the lightest nuclei, and also with the mass of the mesons found in cosmic radiation which is about $200m_e$. However, these experimental results fall far short of the detailed test to which the theory should be subjected, especially in the case of the higher energy, and they cannot be reconciled with the experiments of Amaldi *et al.* (1942), who obtained an anisotropy ratio less than unity using a counter technique to detect the recoil protons. This discrepancy emphasizes the need for further work on the scattering of fast neutrons by protons by both the photographic and counter methods.

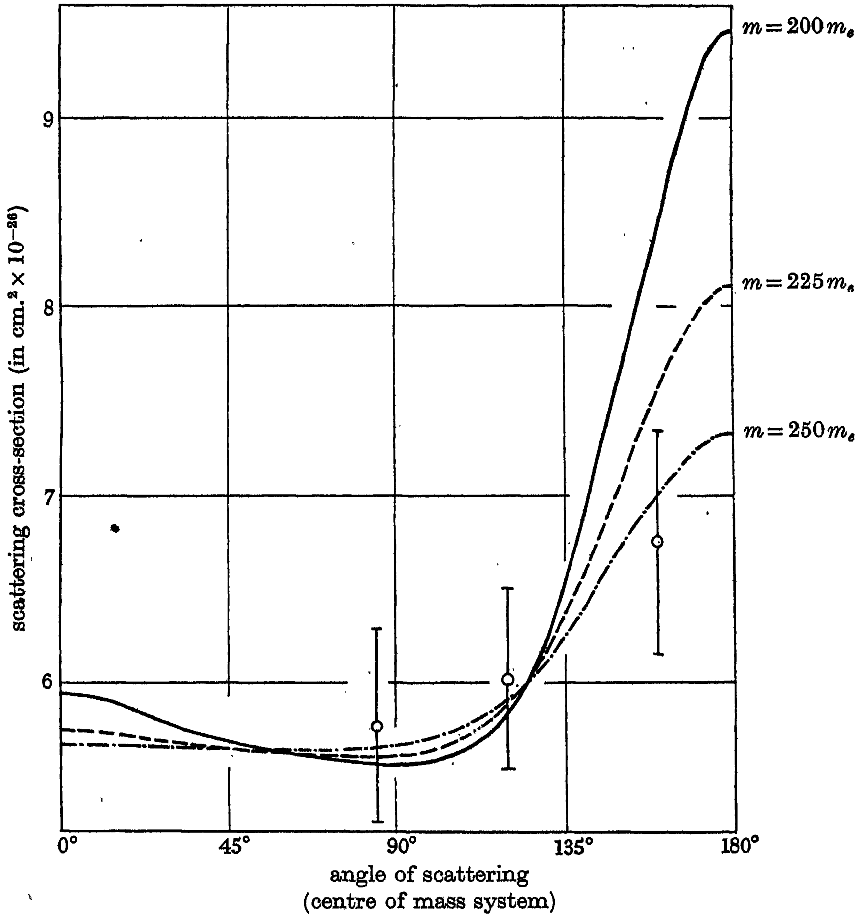

FIGURE 2. The calculated variation of the scattering cross-section for 13·25 MeV neutrons with the angle of scattering for meson masses of 200, 225 and 250 electronic masses. The experimental results shown are those of Occhialini & Powell (1947) for the scattering of 13·4 MeV neutrons by protons.

Figure 3 shows the dependence of the total cross-section for scattering on the energy of the incident neutrons for a meson mass of $225m_e$. The cross-sections determined experimentally by various workers are also shown, together with the errors estimated by the investigators. The agreement is fairly good and constitutes a test of the theory. From the values given in table 6 for 13·25 MeV neutrons it can be seen that the total cross-section, unlike the angular distribution, is highly insensitive to the meson mass assumed; decreasing the meson mass by 20 % increases the total cross-section by only 2 %. Thus, if the theory gave a wrong value for the total cross-section it would not be possible to rectify this by altering the assumed mass of the meson. Also, it does not follow that a theory whose arbitrary constants have been adjusted to give the states of the deuteron correctly will also give the total cross-section correctly; Rarita & Schwinger (1941) have shown that their neutral theory gives total cross-sections wrong by 50 % in the 15 MeV region under these conditions. However, the agreement indicated in figure 3 is not as decisive as might appear. The variation of the total cross-section with energy is dominated by the usual reciprocal of the energy term, and so if the total cross-section agrees with experiment at one energy it will agree with experiment over a wide range of energies. The test therefore effectively consists in comparing one number predicted by theory with the empirical value; nevertheless, this is as good a test of the theory as, say, comparing the calculated with the observed binding energy of the α-particle.

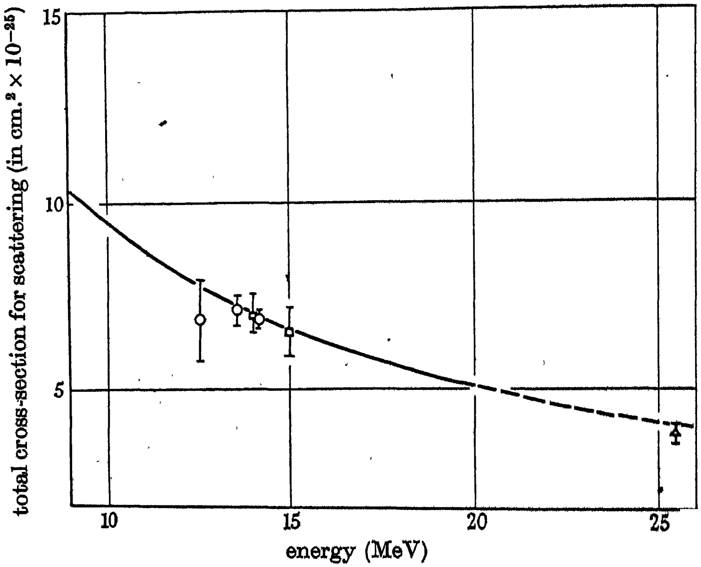

FIGURE 3. The calculated variation of the total cross-section for scattering with energy in the case of a meson mass of $225m_e$. The empirical values are due to the following workers: ○ Ageno *et al* (1943); □ Salent & Ramsey (1940); △ Sherr (1945).

SCATTERING OF VERY HIGH ENERGY NEUTRONS BY PROTONS

At medium and high energies the total cross-section for scattering is approximately inversely proportional to the energy. Hence the Born approximation may be used to survey the characteristics of the scattering at energies much greater than those considered in the preceding section. Hulthén (1943) has shown that this approximation also gives the characteristics of the scattering qualitatively even at medium energies (10 to 20 MeV), though not much weight can be placed on its quantitative predictions in this region; for example, for the scattering of 18·05 MeV neutrons and for a meson mass of $225 m_e$, formulae (11) lead to an anisotropy ratio of 4·3 compared with the actual value of 1·90 as given by the phase-shift method.

From formulae (11) the following expressions are obtained for the anisotropy ratio γ and the asymmetry ratio ρ in the Born approximation:

$$\left.\begin{aligned} \gamma &= \left(\frac{1+2a}{1+4a}\right)^2 \frac{(3f^2-g^2)^2(1+8a)^2+3(f^2+g^2)^2(3+8a)^2}{(3f^2-g^2)^2+27(f^2+g^2)^2}, \\ \rho &= \frac{(3f^2-g^2)^2(1+8a)^2+3(f^2+g^2)^2(3+8a)^2}{(3f^2-g^2)^2(1-4a)^2+3(f^2+g^2)^2(3+4a)^2}, \end{aligned}\right\} \tag{14}$$

where the parameter a, defined by relations (5), is proportional to the energy of the incident neutrons. For very large energies the anisotropy ratio tends to infinity as the square of the energy and the asymmetry ratio has the asymptotic value $+4$. The behaviour of these ratios as a function of the energy is shown in figure 4 in the case of a meson mass of $225 m_e$. In the region below 20 MeV the curves have been constructed from the results of the phase-shift calculations; the broken curves are extrapolations which exhibit the general features of relations (14). To a good approximation these ratios depend on the mass of the meson through the parameter a only; if the energy scale is altered by a factor $(225 m_e/m)^2$ the curves will be approximately true for a meson mass m.

To study the significance of the ratios (14), let G_S, G_T be the values of the operator G of equation (1 a) for the singlet and triplet states respectively when l is even, and let the corresponding values for odd l be $(1+\lambda_S)\,G_S$ and $(1+\lambda_T)\,G_T$. The factors

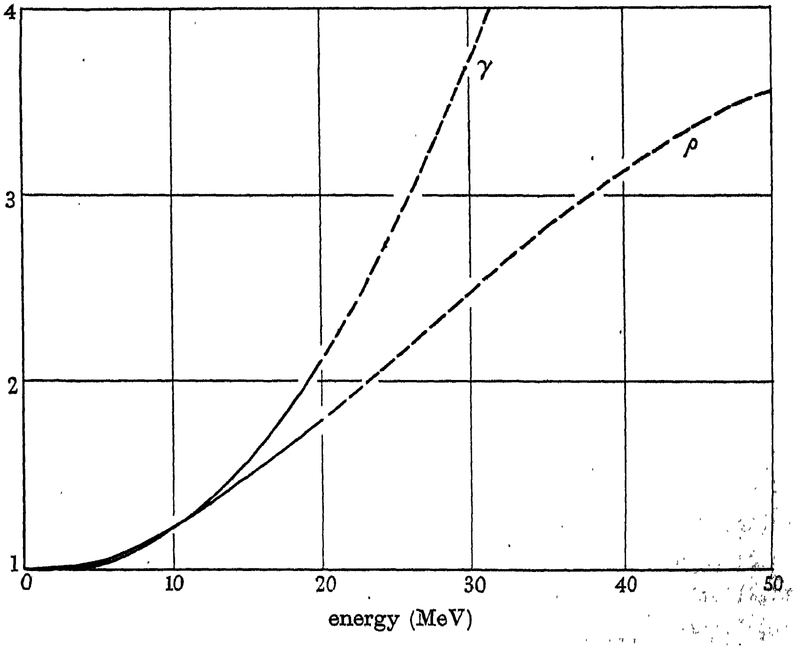

FIGURE 4. The variation of the anisotropy ratio γ and the asymmetry ratio ρ with energy.

λ_S and λ_T and the difference $(G_T - G_S)$ measure the departure of the nuclear forces from 'ordinary' forces which do not depend on the quantum state of the particles. In this notation the anisotropy and asymmetry ratios are

$$\left.\begin{aligned} \gamma &= \left(\frac{1+2a}{1+4a}\right)^2 \frac{G_S^2(1-2\lambda_S a)^2 + 3G_T^2(1-2\lambda_T a)^2}{G_S^2 + 3G_T^2}, \\ \rho &= \frac{G_S^2(1-2\lambda_S a)^2 + 3G_T^2(1-2\lambda_T a)^2}{G_S^2\{1+2(2+\lambda_S)\,a\}^2 + 3G_T^2\{1+2(2+\lambda_T)\,a\}^2}. \end{aligned}\right\}. \tag{15}$$

Thus the anisotropy ratio γ tends to a finite limit as the energy increases only if $\lambda_S = \lambda_T = 0$, and then the limit is $+\frac{1}{4}$; 'ordinary' forces and the mixed neutral meson theory of Møller & Rosenfeld (1940) are included in this case. In all other cases γ tends to infinity as the square of the energy. It will be noted that a large anisotropy ratio does not imply that the scattering is predominantly backward; at large energies γ tends to infinity as the energy increases irrespective of the signs of λ_S and λ_T. A large anisotropy ratio does imply a departure from 'ordinary' forces in that either λ_S or λ_T is not zero. A number characteristic of the theory can be introduced, namely,

$$\left(\frac{\gamma}{a^2}\right)_\infty = \frac{\lambda_S^2 G_S^2 + 3\lambda_T^2 G_T^2}{G_S^2 + 3G_T^2}, \tag{16}$$

where $(\gamma/a^2)_\infty$ denotes the limiting value of (γ/a^2) as the energy tends to infinity. This limiting ratio involves the mass of the meson or the range of the forces directly through the parameter a, and indirectly through the interaction constants G_S and G_T if these have been chosen to give the states of the deuteron correctly.

As the energy tends to infinity, the asymmetry ratio ρ tends to a limit which is characteristic of the theory on hand:

$$\rho_\infty = \frac{\lambda_S^2 G_S^2 + 3\lambda_T^2 G_T^2}{(2+\lambda_S)^2 G_S^2 + 3(2+\lambda_T)^2 G_T^2}.$$

In the most important cases this ratio reduces to a number which depends neither on the range of the force nor on the interaction constants G_S and G_T, but only on the factors λ_S and λ_T. In the symmetrical theory of Møller & Rosenfeld, which is the one treated in detail in this paper, $\lambda_S = -4$ and $\lambda_T = -\frac{4}{3}$, and so $\rho_\infty = +4$. For 'ordinary' forces and for the mixed neutral meson theory λ_S and λ_T are zero, and so ρ_∞ vanishes. For the mixed charged theory ρ_∞ is infinite as $\lambda_S = \lambda_T = -2$. In these (and other) special cases ρ_∞ does not depend on the range of the force; in fact, it does not involve the form of the radial dependence of the interaction at all. In other cases ρ_∞ involves the range of the force only through the interaction constants G_S and G_T if these have been chosen to give the states of the deuteron correctly. Hence this limiting ratio may be used to test the eigenvalues of the operator G which are given in table 1 without referring to any specific form of radial dependence of the interaction. A fairly good indication of the value of ρ_∞ would be given by the scattering of 50 MeV neutrons, provided that the effect of the non-static interaction proves to be small at this energy. The second relation which is necessary to determine both

λ_S and λ_T can be obtained from equation (16) or from proton-proton scattering, but this will refer to a specific meson mass. Having established the set of eigenvalues of the operator G, the radial dependence of the interaction can be investigated by a detailed study of the cross-section for scattering as a function of both the angle of scattering and the energy.

Note added in proof (*June* 1947). Laughlin & Kruger (1947) have investigated the scattering of 12 to 13 MeV neutrons by protons using a high pressure cloud chamber. The results indicate scattering of the 'backward' type which is in agreement with repulsive P states as in the Møller-Rosenfeld theory. Best agreement with theory is obtained if a meson mass of $265 m_e$ is used; in view of the large statistical uncertainties and the possible systematic errors in the experimental methods, this is in satisfactory agreement with the estimates of the meson mass based on the results of the experiments of Occhialini & Powell (1947). It should also be pointed out that recent experiments on proton-proton scattering by Wilson (1947) indicate that the interaction is weakly repulsive in the ^3P state, which is in accord with the Møller-Rosenfeld theory.

In conclusion, the writer would like to express his thanks to Dr H. Fröhlich for acquainting him with the problem and for the many valuable suggestions given; he would also like to thank Professor N. F. Mott and Dr L. Hulthén for profitable discussions and Miss M. J. Lyttleton for assistance with computations.

REFERENCES

Ageno, Amaldi, Bocciarelli & Trabacchi 1943 *Naturwissenschaften*, **31**, 231; *Nuovo Cim.* **1**, no. 3.
Amaldi, Bocciarelli, Ferretti & Trabacchi 1942 *Naturwissenschaften*, **30**, 582.
Fröhlich, Huang & Sneddon 1947 *Proc. Roy. Soc.* A, **191**, 61.
Fröhlich, Ramsey & Sneddon 1947 *Proc. Phys. Soc.* (in the press).
Hanstein 1941 *Phys. Rev.* **59**, 489.
Hulthén 1943 *Ark. Mat. Astr. Fys.* **29** A, no. 33; **30** A, no. 9.
Hulthén 1944*a* *Ark. Mat. Astr. Fys.* **31** A, no. 15.
Hulthén 1944*b* *K. fysiogr. Sällsk. Lund. Förh.* **14**, no. 21.
Hulthén 1945 *K. fysiogr. Sällsk. Lund. Förh.* **15**, no. 22.
Laughlin & Kruger 1947 *Phys. Rev.* **71**, 736.
Møller & Rosenfeld 1940 *K. Danske Vidensk. Selsk. mat.-fys. Meddel.* **17**, no. 8.
Mott & Massey 1933 *The theory of atomic collisions*. Oxford Univ. Press.
Occhialini & Powell 1947 *Proc. Phys. Soc.* (in the press).
Pais 1946 *Proc. Camb. Phil. Soc.* **42**, 45.
Rarita & Schwinger 1941 *Phys. Rev.* **59**, 556.
Rosenfeld 1945 *K. Dansk. Vidensk. Selsk. mat.-fys. Meddel.* **23**, no. 13.
Rozental 1941 *K. Dansk. Vidensk. Selsk. mat.-fys. Meddel.* **18**, no. 7.
Rozental 1945 *K. Dansk. Vidensk. Selsk. mat.-fys. Meddel.* **23**, no. 11.
Salant & Ramsey 1940 *Phys. Rev.* **57**, 1075.
Sherr 1945 *Phys. Rev.* **68**, 240.
Watson 1944 *Theory of Bessel functions*, p. 389. Camb. Univ. Press.
Wiedenbeck & Marhoefer 1945 *Phys. Rev.* **67**, 54.
Wilson 1947 *Phys. Rev.* **71**, 384.

The initial stages of explosion in nitroglycerine

By M. F. R. Mulcahy and R. G. Vines

Council for Scientific and Industrial Research, Section of Tribophysics, University of Melbourne

(*Communicated by Sir David Rivett, F.R.S.—Received* 11 *February* 1947
—*Read* 8 *May* 1947)

[Plates 12 to 15]

The sequence of events which occurs in a thin confined film of nitroglycerine, after an explosion is initiated by a condenser spark, has been examined by means of a rotating drum camera. It has been found that in a very thin film (< 0·01 mm. thick) the explosion begins as a gentle process which is propagated through the nitroglycerine film at 400 m./sec. After continuing for about 0·5 cm. this process is transformed suddenly to a more violent type of explosion which is propagated at 2000 m./sec. The explosion reproduces in miniature several of the well-known effects characteristic of the setting up of the detonation wave in gaseous mixtures.

When explosion is initiated in the same manner in a thicker film, the 400 m./sec. type of propagation is not set up immediately but is preceded by a very much faster process ($\nless$ 5000 m./sec.), which after propagating for a few millimetres is transformed into the normal 400 m./sec. process. Subsequent to this transformation the propagation continues exactly as in the very thin films.

It is suggested that, under conditions of impact initiation, the propagation of the explosion through the film of nitroglycerine between the hammer and the anvil takes place in a manner closely similar to that which obtains after initiation by spark.

Introduction

The experimental study of explosive substances usually centres about two phenomena: the *initiation* of explosion under the influence of some external agency, e.g. mechanical shock, or heat, and the *propagation* of the explosion through the mass of the explosive. The conditions for initiation of the explosion by mechanical shock are frequently examined by means of falling weight impact experiments. The explosive in small quantity is put on an anvil and the energy (or velocity) of impact necessary for initiation of the explosion measured. On the other hand, most work on the propagation of the explosion has been concerned with the measurement of the velocity of propagation through an extended mass of explosive (see, for example, Laffitte 1925; Jones 1928).

It is of interest to examine the conditions of propagation of the explosion in that part of the explosive immediately adjacent to the point where the initiation has been effected. In an earlier investigation (Bowden, Eirich, Ferguson & Yoffe 1943*a*; Bowden, Eirich, Mulcahy, Vines & Yoffe 1943*b*; Bowden, Mulcahy, Vines & Yoffe 1947*a*) the conditions for initiation of explosion in thin layers of nitroglycerine and other liquid explosives have been described. Examination of the blast marks left on hammer and anvil after the explosion, and of the light effects observed when the explosion was initiated on a photographic plate, indicated that the propagation of the explosion in the thin film of liquid between hammer and anvil took place in two or more successive stages, and that a complex series of events occurred before the final stage of explosion was set up. Furthermore, it was shown that this behaviour was not peculiar to the method of initiation but occurred whether the explosion was initiated by impact, electric spark, or rapid heating.

In the experiments described in this paper a rotating drum camera has been used to examine the initial stages of propagation in thin films of nitroglycerine immediately adjacent to the point of initiation. The results obtained confirm the conclusions arrived at from the earlier experiments, and enable considerable resolution and clarification of the successive events which occur between initiation and the later stages of propagation of the explosion.

THE EXPLOSION PATTERN

When a thin film of nitroglycerine is spread on a flat metal anvil and explosion initiated by the impact of a flat metal fall-hammer, a characteristic blast pattern remains imprinted on the surfaces of hammer and anvil. This blast pattern, which is particularly well defined when polished brass surfaces are used, has been described in some detail previously (Bowden *et al.* 1943 *a, b*). A brief recapitulation of its most characteristic features is given below.

Figure 1, plate 12, is a typical example of the blast pattern obtained on a brass hammer (diameter 1·8 cm.).* It will be observed that the surface of the hammer is sharply divided into two regions: one (A) in which the brass has been deformed very little by the explosion and the other (B) in which the damage to the surface has been severe. The relative proportions of the surface covered by each of the regions and their positions relative to each other vary from one explosion to another, but the basic features are retained in each case. The reason for the differences observed has been made clear by the result of experiments in which the condition of the nitroglycerine film at the moment of impact was simulated by confining a very thin layer of nitroglycerine between two stationary horizontal brass disks. The explosion was initiated at the centre of the disks by the passage of a condenser spark. Figure 2,† plate 12, shows the type of blast pattern invariably obtained on the surfaces of the brass disks. The general features of this pattern closely resemble those of figure 1, except that in the case of the spark-initiated explosion the 'unmarked' region A is central and the boundary of the 'heavily blasted' region B roughly symmetrically disposed about the central point of initiation. It is clear, therefore, that the variation in the relative positions of the regions A and B in the impact experiments is due to differing positions of the point of initiation which may occur at any point within the area of the surface.* Presumably in the example given in figure 1 the initiation took place at about the point J.

---

* A mirror image of the pattern is found on the anvil.

† The photographs shown in figures 2, 3, 4, 5, plates 12 and 13 were obtained during the period of the investigation when the authors were working in collaboration with Dr F. P. Bowden, Dr F. R. Eirich and Mr A. Yoffe (cf. Bowden *et al.* 1943 *b*).

The explosion patterns indicate that the explosion proceeds outward from the point of initiation by two successive, different modes of propagation, and that the first explosion process, which follows immediately after initiation, is a relatively gentle one. In fact, it is so gentle that even a mica surface is practically undamaged by it. The second stage (region B) is much more violent; it causes considerable deformation of the surface in the form of numerous small pits in the metal. These indentations appear to arrange themselves in irregular chains many of which radiate out from the boundary of the unmarked region (see figure 1).

The sharp boundary between regions A and B indicates an abrupt transition from the gentle type of propagation to the more violent. Figure 3, plate 12, is an enlarged photograph of a portion of the boundary and shows particularly well the interesting features frequently found to be associated with the sudden transformation of the first explosion process. In this experiment the surface was well polished before the impact. Within the unmarked area the explosion has removed the polished Beilby layer except for a narrow band (PP) immediately before the transition to the stage of heavy blasting. This is apparent from the fact that in the inner part of region A the original lapping marks have become visible. Along the inner edge of the band the brass has been indented by a number of radially disposed grooves† (GG).

The band is again apparent if the surface has been lead plated before the experiment (figure 4*a*, *b*, plate 12). In both these figures the area A of the first stage is covered by a series of characteristic lines radiating out from the centre (the point of initiation) and separated from the area of heavy blasting, B, by a band of untouched lead. (In figure 4*b* a portion of the band has been obliterated by a subsequent retrograde process.)

When explosion occurs on a photographic plate‡ (figures 5*a*, *b*, *c*, plate 13), or on a transparent anvil at the focus of a camera lens (figure 10*a*, plate 14), a pattern of light effects is observed which corresponds closely to the blast pattern. It will be seen that a dark band PP, corresponding to the band of unaffected metal on the lead and brass surfaces, separates an inner region (A) from the outer zone (B) in which the photographic emulsion is usually damaged (figure 5). The dark band is shown well in figures 5*b* and *c*,* which were obtained from impact experiments, and in figure 10*a* in which the initiation was by spark. In figure 5*a* it is partly obscured by cracks in the plate originating from the region B.

---

* Experiments (Bowden *et al.* 1943*b*) have shown that the observed *size* of the unmarked region A in the impact experiments is determined not only by the position of the point of initiation relative to the edge of the hammer but probably also by the thickness of the explosive film at the instant of initiation. Explosion patterns corresponding to more than one point of initiation have also been observed quite frequently.

† When the initiation is brought about by a spark the grooves (GG) very rarely appear.

‡ The photographic plate was attached rigidly, emulsion side upwards to the surface of a flat anvil. The explosive was distributed (usually as a number of droplets) on a thin piece of mica resting on the emulsion and struck with a flat brass surface.

Explosion patterns, such as those shown in the preceding pictures, have been obtained in a variety of ways: by high-energy impact on a thin continuous film of explosive, by impact on a number of droplets and on nitroglycerine films in which air bubbles were present, and by spark initiation. The evidence points to the conclusion that the explosion, irrespective of the method of initiation, spreads out for a short distance (0·5 to 1 cm.) as a relatively gentle process until it undergoes a sudden conversion to a second more violent type of propagation.† At the point where the transformation occurs the patterns show that separating the two stages is a narrow band (width 0·5 to 1 mm.), which appears on the photographic plate as a dark space and on lead and brass surfaces as a band of unaffected metal.

ROTATING DRUM CAMERA TRACES OF THE EXPLOSION

The relative intensities of the mechanical effects associated with the first and second stages of propagation indicate that these two successive stages are considerably different in nature. It might therefore be expected that they would be propagated at different velocities. Earlier experiments with a rotating drum camera (Bowden *et al.* 1947*b*) have indicated that when explosion is initiated by impact on a film of nitroglycerine containing entrapped air spaces the explosion beneath the hammer is first propagated at a velocity of about 400 m./sec. This velocity is maintained for about 0·5 cm. from the point of initiation, after which the explosion passes over to a considerably higher rate of propagation (> 1000 m./sec.). The distance from the point of initiation at which the transformation to the higher velocity occurs was found to correspond roughly to the radius of the unmarked region shown in the blast pattern on the surface of the hammer. On the other hand, with other methods of initiation, an initial slow rate of propagation was not detected and no obvious discontinuity in the propagation velocity was observed. However, this latter result must now be revised in the light of results obtained with improved apparatus.

A rotating drum camera capable of better optical resolution and greater film speed has been set up. The results obtained have revealed a number of interesting phenomena which have not previously been detected.

EXPERIMENTAL

The machine used was a Fraser High Speed Drum Camera (Bone & Fraser 1929), specially adapted for the present investigation. In so far as the point of initiation cannot conveniently be predetermined when explosion is produced by impact, initiation was brought about in every experiment by the passage of a condenser discharge spark.* The apparatus is represented diagrammatically in figure 6.

---

* In figure 5*c* there are a number of independent points of initiation from each of which the luminous radii characteristic of the first stage process emanate. Each of the first stage regions so formed is separated from the next by a dark line which merges with the band PP and becomes indistinguishable from it.

† The second stage process may be caused to propagate any desired distance merely by initiating the explosion in a sufficiently extended and confined film of explosive.

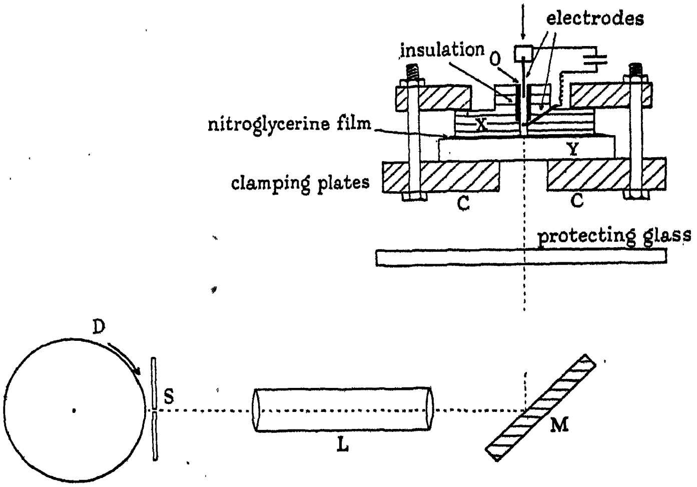

FIGURE 6

The explosive was spread as a thin film† between the upper brass confining surface X and a block of laminated glass Y which rested upon two flat rectangular steel slabs CC. The explosion was initiated by the passage of a spark between an electrode in the brass block X and a falling electrode which moved down the insulated spark hole O, the hole O being filled with the explosive. The light from the explosion passed through the narrow space between the two steel slabs and was deflected by a highly reflecting mirror M through the lens system L of the camera, finally coming to a focus on the film carried on the rotating drum D. Close to the drum was a metal sheet containing a linear slit S, of width $\frac{1}{2}$ mm., placed at right angles to the direction of movement of the film (see figure 6).

The spark hole was so clamped above the supporting steel plates that its image fell upon the film; it was thereby possible to follow the entire course of the explosion, along the line of the slit, as it spread out from the point of initiation. Since the slit was at right angles to the direction of movement of the film, the traces were compounded of the velocities of propagation of the explosion and rotation of the drum. The angle from the horizontal of a trace at any point is therefore a measure of the speed of propagation of the explosion at that point.

The film (Kodak Verichrome) was glued to the surface of the drum and for each experiment was hypersensitized with ammonia vapour. The drum was rotated at speeds up to 15,000 r.p.m., though most experiments were made at 10,000 r.p.m., corresponding to a film velocity of about 150 m./sec. The speed of rotation could be read continuously from a quadrature tachometer coupled directly to the shaft of the drum.

---

* 250V, 12μF.

† The thickness of the film of explosive could be controlled by the use of metal spacing pieces. In these experiments the film thickness was varied from $<0{\cdot}01$ mm. to $0{\cdot}15$ mm.

RESULTS

Typical photographs are shown in figures 7 *a*, *b*,* plate 13. Initiation has occurred at the point J,† from which the explosion propagates in both directions for a distance JP with a velocity of about 400 m./sec.‡ as measured from the slope of the trace. In each photograph there is at P a marked discontinuity in the propagation velocity. Comparison of measurements of the horizontal length JP on the film with the extent of the unmarked region in the corresponding blast patterns has shown that the discontinuity corresponds in position to the point of transition in the blast patterns from the first to the second stage of the explosion.

There is, furthermore, at P a small gap between the two portions B and A of the explosion trace. Within this gap there are no luminous effects visible. It corresponds undoubtedly to the bands of unaffected metal in the explosion patterns (PP in figures 1, 3, 4 and 5).

Beyond P the inclination of the trace is much smaller. This corresponds to a velocity of propagation of about 2000 m./sec.‡ This portion of the trace (B) corresponds to the region of heavy blasting in the explosion patterns.

The characteristics of the traces which are of outstanding interest are those associated with the transition from the first to the second stages of the explosion. It may be seen from the figures (see, for example, figure 7 *a*) that the second stage actually begins from a point in the nitroglycerine film about 1 mm. ahead of the explosion front of the first stage. The dark space P in the explosion traces results from the fact that the first stage either never reaches this point or does so at a time subsequent to the initiation of the second stage. Again it will be observed (figure 7 *b*) that a luminous process (R) originates at the dark space and proceeds *back* at high velocity (roughly 1000 m./sec.) through the combustion products left in the wake of the explosion front of the first stage. These features are common to all the explosion traces, although they may not appear clearly in the photographs since in the printing of the negatives much detail is invariably lost. The various stages in the explosion traces are represented diagrammatically in figure 12, plate 15, and correlated with an actual explosion pattern on brass.

The photographs obtained with the drum camera immediately suggest a comparison with the well-known phenomena associated with the propagation of explosions in mixtures of combustible gases. This point will be elaborated in the discussion.

---

* Since it has proved very difficult to reproduce adequately the details of the negatives, the prints in figures 7 *b* and 10 *b* have been retouched.

† There may be a prolonged burning within the spark hole before propagation begins (cf. figure 8 *b*). In fact it is possible that this may be a characteristic of every explosion, but the localized burning may take place above the stationary electrode being obscured by it and consequently failing to appear on the film.

‡ See next section.

The velocities of propagation of the two stages

The velocity of the explosion can be calculated from the angle of inclination of the trace on the film and the speed of rotation of the drum. However, because of the short length over which the explosion is propagated in these experiments, the angles can only be measured roughly, and considerable scatter has therefore been obtained in the results. The average value for the propagation velocity of the first stage obtained from nine of the clearest photographs (17 measurements*) has been found to be 420 m./sec. ± about 15 %. This agrees with the value of approximately 400 m./sec. previously obtained (Bowden *et al.* 1947*b*) from the impact experiments mentioned above. The average of thirteen measurements made on seven of the 'best' pictures has yielded 1900 m./sec. ± about 15 % for the velocity of the second stage.† The velocity of the 'retonation wave' (R) has been estimated from several pictures to be in the region of 1000 m./sec.

Within the limits of error indicated above, increase in the thickness of the film from < 0·01 to 0·15 mm. produced no change in any of the three observed velocities.

It seems probable that the velocity of propagation of the second stage process, 2000 m./sec., corresponds to that of the so-called 'low' velocity detonation which is obtained when a tube of nitroglycerine is initiated with a weak detonator. Chariton & Ratner (1943) find that when the nitroglycerine is confined in a glass tube of less than 2 mm. bore the low-velocity detonation is the stable one even when a powerful detonator is used. They give 1800 m./sec. for the low-velocity detonation in tubes of 2 mm. bore. In a wider tube with a powerful detonator the 'high' velocity detonation (~7500 m./sec.) is almost always set up.

The propagation in thicker films

In the experiments just described (e.g. figures 7*a*,*b*, plate 13) the explosion occurred in films of nitroglycerine < 0·01 mm. thick. In order to ascertain whether there is any variation in the velocities of propagation with increasing thickness of the explosive film, a number of experiments were carried out with films up to 0·15 mm. thick. Although no appreciable change in the velocity of either stage was observed, the results proved most interesting.

Figures 8*a*,*b*, plate 13, are typical traces obtained from explosions in films 0·08 mm. thick. It may be seen that in these cases the 400 m./sec. first stage propagation is not set up immediately on initiation, but is preceded by a phenomenon which was not observed in traces obtained from films < 0·01 mm. thick.

---

* Because of the propagation in two directions two measurements of the velocity can (usually) be made on each photograph.

† In a preliminary communication (Vines & Mulcahy 1946) a value of 1800 m./sec. ± about 5 % was erroneously given for this velocity. This value was based on these and other experiments to be reported later, and should have read 1800 m./sec. ± about 15 %.

The spark has initiated an explosion of very much higher velocity which subsequently (at the point Z) is transformed to the normal 400 m./sec. process. However, the traces of this new phenomenon present a number of puzzling features, and since the present experimental arrangement is unable to achieve the high speed necessary for closer examination it is not possible to estimate its velocity beyond ascribing to it a lower limit of about 5000 m./sec.

It will be observed in figures 8*a*, *b* that the transition from the 400 m./sec. propagation to the 2000 m./sec. second stage occurs exactly as in the thinner films; the 'auto-initiation' of the 2000 m./sec. stage, i.e. its inception at a point ahead of the approaching explosion front of the first stage, and the retrograde process originating near this point, may be seen clearly.

The blast patterns impressed on the brass surface in these circumstances are also interesting (figure 9, plate 13). As reported in previous papers, the unmarked region is enlarged with increased film thickness, and beyond it the region of heavy blasting appears as usual. Within the 'unmarked' area, however, a ring Z may be noticed about the spark hole corresponding in position to the point at which the normal 400 m./sec. process first appears. The area enclosed by this ring is quite considerably depressed, and the brass shows signs of extensive recrystallization over the whole confining surface as a result of the deformation. It is clear, therefore, that in thick films there are two distinct processes occurring before the final stage of the explosion is set up. The possible nature of these processes will be discussed later.

Experiments with plastic supports

A few experiments were carried out in which a block of transparent 'Perspex', covered by a thin sheet of mica, was substituted for the glass block Y in figure 6. Under these conditions it was found that the high-velocity initial process was set up even in the thinnest films. Figure 10*b*, plate 14, is a camera trace obtained in such an experiment, and it may be seen that in this case the initial process was followed by a period of the 400 m./sec. propagation after which an 'auto-initiation' took place at P. However, the 2000 m./sec. process was not permanently set up—as is always the case under these conditions—and after the 'auto-initiation' the velocity of propagation continuously decreased. Figure 10*c*, plate 14, shows the blast pattern obtained in a similar experiment. The innermost region corresponding to the high-velocity process can be seen clearly but apart from a narrow depressed ring (B) at the beginning, there is very little deformation corresponding to the final stage of the explosion (C in figures 10*b*, *c*).

In these experiments the extent of each of the various stages of the explosion varied erratically. In the still photograph in figure 10*a* the initial high-velocity process was almost absent (it is not visible in figure 10*a*). On the other hand, in the explosion of which figure 11*a*, plate 14, is the rotating drum photograph, and figure 11*b*, plate 14, the blast pattern, the high-velocity explosion was propagated for a centimetre. Figure 11*a* illustrates clearly the very high velocity characteristic of the initial process. Figure 11*b* is especially interesting, since it shows that though the deformation resulting from the initial process is severe it is *uniform*, i.e. the surface is evenly depressed within the boundary Z. This is in marked contrast to the non-uniform pit marking type of deformation characteristic of the 2000 m./sec. propagation, a trace of which can be seen at B (cf. figure 2, plate 12). It will be observed also that in figure 10*b* the period of illumination after the passage of the explosion through the nitroglycerine is longer than when glass supports are used (cf. figures 7, 8, plate 13). This effect is undoubtedly mainly due to the fact that the glass blocks are quickly pulverized, and rendered opaque by the explosion, whereas the Perspex is shattered into relatively large pieces which remain transparent after the explosion (cf. figure 10*a*).

The initiation of the 2000 *m./sec. stage*

The drum camera traces indicate that the 2000 m./sec. stage of the explosion begins ahead of the explosion front of the 400 m./sec. stage. However, the possibility must be considered that this may be only an apparent effect occasioned by the experimental arrangement. In the experiments described the explosion expands radially from the point of initiation, but the slit limits observation to events occurring along a single diameter of the explosive film. It is therefore not impossible, *a priori*, that in any particular experiment the 2000 m./sec. process is not 'auto-initiated' but arises in the explosion front at some point invisible to the camera. The apparent 'auto-initiation' shown in the trace could then be attributed to the 2000 m./sec. process crossing the slit at a point ahead of the more slowly travelling 400 m./sec. explosion front. If this explanation is correct, the dark space P in the traces will not be found to extend continuously around the entire circle of the explosion front, or, more precisely, it will not extend on either side of an arbitrarily chosen point for a distance around the circumference of greater than five (i.e. 2000/400) times its width at that point. On the other hand, continuity of the dark space would indicate that the 'auto-initiation' of the 2000 m./sec. stage is a real and not an apparent effect.

A considerable number of 'still' photographs of the whole explosion have been taken with a plate camera, and though the pictures are frequently obscured by secondary effects, the evidence is strongly in favour of the essential continuity of the dark space (see, for example, figure 10*a*, plate 14). This result has been confirmed by photographs obtained on the rotating drum after the same manner as the velocity traces, except that the steel slabs CC (figure 6) were replaced by a single slab containing a window, and the slit S was removed so that the whole explosion was registered on the film. This arrangement takes a photograph very similar to a 'still' photograph, but, as a consequence of the movement of the film, the leading half of the picture is less obscured by effects occurring subsequent to the explosion. Figure 15, plate 15, is such a photograph. PP is the dark space. It will be seen that in the upper half of the picture it is clearly defined and is continuous over at least half of its circumference.* This is strong evidence against the alternative explanation of the 'auto-initiation' phenomenon given above. It seems clear, therefore, that the 2000 m./sec. stage is, in fact, initiated at a point in the nitroglycerine film ahead of the front of the 400 m./sec. process as indicated by the drum camera traces.

Other explosives

It has been reported previously that when nitroglycol and other liquid explosives (molten T.N.T., tetryl, picric acid) are exploded by impact between flat surfaces, the blast patterns which result are remarkably similar to those obtained with nitroglycerine (Bowden *et al.* 1943*b*). Similar behaviour has also been found for molten P.E.T.N. and hexogen, and mixtures of tetranitromethane and toluene (Vines 1944) and for methyl nitrate. For example, a pattern from a tetranitromethane/toluene mixture initiated by a spark is shown in figure 16, plate 15, in which the central unmarked area and surrounding zone of surface deformation are clearly visible. It is possible, therefore, that the first stages of the propagation in all these liquid explosives are essentially similar to those which occur in nitroglycerine. Preliminary experiments with methyl nitrate and nitroglycol on the rotating drum camera have afforded some support for this hypothesis, since the traces obtained from these two substances are closely similar to those given by nitroglycerine.

It is interesting to compare the behaviour of nitroglycerine with that of solid primary explosives. It is known that when certain primary explosives, notably mercury fulminate, are initiated by contact with a flame, detonation does not begin instantly but is preceded by a period of combustion or deflagration ('Anlauf'). Patry & Laffitte (1931) have studied this phenomenon with a rotating drum camera (cf. also Muraour (1942)). They find that when a train of mercury fulminate of appropriate dimensions is ignited in the open air, the explosion begins first as a relatively slow deflagration (~ 20 m./sec.) which, after a distance of propagation of a few centimetres, is abruptly succeeded by detonation (~ 2000 m./sec.). Furthermore, a retrograde wave of high velocity is sent back through the combustion products from the point where the detonation begins. There is an obvious analogy between this result and the behaviour of thin films of nitroglycerine, though the velocity of propagation of the first stage in the mercury fulminate experiments is about twenty times lower than that found in our experiments with nitroglycerine.

In view of this similarity of behaviour, it is perhaps not surprising that we have found that when mercury fulminate is spread as a thin layer of powder between two metal disks and initiated at the centre by a spark, the deformation of the surfaces of the disks by the explosion does not begin at the point of initiation, but on the circumference of a rough circle a few millimetres from it; i.e. the blast pattern resembles (though not exactly) figure 2. On the other hand, when the mercury fulminate is replaced by lead azide, which is known not to give the initial period of deflagration but detonates immediately on heating, the deformation of the surfaces begins at the point of initiation: there is no central 'untouched' region (Vines 1944).

---

* Some of the negatives of these photographs show the presence of faintly luminous streaks which cross the dark space at one or two points. The origin of the streaks is obscure, but their presence does not invalidate the conclusion that the dark space is continous since it is apparent that they traverse an already existing band of darkness.

DISCUSSION

The analogy with gaseous explosions

Reference has been made in a previous section of this paper to the similarity between the order of events which occur in the nitroglycerine film and that peculiar to the setting up of detonation in a gaseous mixture. The work of Mallard & Le Chatelier (1883), Dixon (1903) and many others has shown that the propagation of combustion along a tube filled with a combustible gaseous mixture normally begins as a relatively slow movement which, after continuing along the tube for some distance, is suddenly interrupted by the inception of the 'detonation wave'. Thereafter, the explosion proceeds by a much faster and more violent process of constant velocity.

Figure 14, plate 15, a rotating drum photograph obtained by Dixon (1903) of such an explosion, has been reproduced for comparison with our photographs of the explosion in nitroglycerine. The scales of the two phenomena are, of course, quite different; Dixon's photograph represents a process occurring in a tube about 1 cm. in diameter and about 1 m. long, whereas figures 7*a*, *b*, record events taking place in a film of nitroglycerine $< 0\cdot01$ mm. thick and about (twice) 2 cm. in length.

The most characteristic feature of the initiation of the detonation wave in gases is that it begins suddenly, throwing back a strongly luminous fast-moving compression wave (the 'retonation' wave) through the burnt gases. In Dixon's photograph shown in figure 14 the initial flame enters the picture near the top left-hand corner, and the transformation to detonation occurs in the centre ('*r*' is the retonation wave). According to a number of investigators (Le Chatelier 1900; Campbell & Woodhead 1926; Egerton & Gates 1927; Bone & Fraser 1929) the detonation wave commonly commences from a point a few centimetres ahead of the advancing front of the initial flame, i.e. the initiation of the wave is something of a spontaneous explosion occurring in the gas ahead of the flame. Figure 13, plate 15, is a very striking high-speed photograph of the inception of detonation in a 1·3 cm. tube of carbon monoxide/oxygen mixture taken by Bone, Fraser & Wheeler (1935). The flame enters the picture at high speed at the top right-hand corner; when it has reached about one-quarter the distance across the picture, detonation is spontaneously set up in the gas ahead of it and proceeds at higher velocity out of the picture; ('*r*' is the retonation wave).

It is clear that there is a very close analogy between the effects observed in gaseous explosions and those shown by our drum camera photographs to occur (on a much smaller scale) in a thin film of nitroglycerine. In both cases the explosion begins as a relatively gentle and slow-moving process, which, after some distance of propagation, is transformed abruptly to the faster and more violent detonation. The spontaneous initiation of detonation ahead of the first stage explosion front, with the consequent dark space between the first stage and the detonation wave in the moving film photographs, is another common phenomenon —compare the parts of figures 7, 8 and 12, marked P with the photograph of Bone *et al.*, figure 13.* Again, the high-velocity retrograde phenomenon (R in figures 7, 8 and 12) which originates near the point of inception of detonation in the film of nitroglycerine, is analogous to the retonation wave in gaseous systems (*r* in figures 13 and 14). The general aspect of the phenomena occurring after the initiation of explosion in a very thin film of nitroglycerine (and probably other liquid or molten explosives) may be considered a replica in miniature of an explosion in a combustible gaseous mixture.

The first stage (400 *m./sec.*) *process, and the transition to the second stage* (2000 *m./sec.*)

Considerable interest attaches to the question of the mechanism of propagation of the first stage (400 m./sec.) process and to the cause of its sudden transition to detonation. In gaseous explosions the first stage (flame) type of propagation takes place mainly by conduction of heat; the temperature of each successive layer of unburnt gas is raised to the 'ignition point' by heat transmitted to it by conduction (and convection) from the combustion of the preceding layer. On the other hand, in the detonation wave each successive layer is heated to its ignition point (at least in part) by adiabatic compression due to the passage through it of an intense shock wave. In view of the similarity between gas-phase explosions and the behaviour of nitroglycerine, it is not unlikely that the propagation of the first stage of the explosion in nitroglycerine is conditioned by the transfer of heat from the zone of 'combustion' to the next layer of undecomposed explosive ahead, though the details of the propagation mechanism must be somewhat more complex than in the case of flame propagation, since with nitroglycerine the explosion products are gaseous, but the undecomposed explosive is initially in the liquid state.

It has been suggested, on the evidence of the blast patterns and stationary light photographs, that the first stage process consists of a deflagration occurring in the vapour phase, and that in the second stage, the explosion is propagated through the liquid phase (Bowden *et al.* 1943*b*). It was assumed that a pocket of vapour forms about the first nucleus of decomposition at the point of initiation; vigorous combustion takes place within the vapour, the heat evolved in the reaction evaporating more explosive from the surrounding film. The zone of combustion was visualized as being separated from the liquid phase by a narrow layer of vapour in which the explosive, newly evaporated, is heated to its ignition temperature. Thus the liquid surface, continually evaporated by conduction from the combustion zone, recedes and is followed by the layer of cool vapour, and finally by the combustion zone itself. The rate of propagation of the explosion is therefore dependent on the transfer of heat from the gaseous explosion front to the undecomposed liquid ahead of it. It was suggested further that the transition to the second stage of the propagation results from the initiation of the explosion in the liquid phase by the impact on the liquid surface of a shock wave passing across the layer of cool vapour, or by sudden heating of the liquid by increased radiation from the explosion front.

---

* It will be observed that in figures 7 and 8 the initiation of detonation occurs at a distance of 0·5 to 1 mm. ahead of the explosion front, whereas in the gaseous explosion (figure 13) the auto-ignition takes place 6·4 cm. ahead of the flame.

At first sight the experimental results reported in this paper appear to give some support to this hypothesis. The considerable difference between the propagation velocities of the two stages, as well as their different mechanical intensities, points to a basic difference in the mechanisms. It is clear that the initiation of the second stage does, in fact, occur spontaneously at a point ahead of the first stage explosion front, and there is evidence that the point of auto-initiation is separated from the advancing first stage explosion front by a relatively cool space, since the retonation wave, which presumably is a shock wave sent back at the moment of initiation of detonation, is visible only in the hot gaseous products in the wake of the first stage process. If, therefore, it be assumed (as seems probable) that the second stage is a liquid phase process, then the dark space (P) in the photographs could be identified with the preheating layer of cool vapour ahead of the explosion front at the moment of the initiation of the second stage.

However, in spite of the general compatibility of the explosion traces with this mechanism, the value of 400 m./sec. found for the velocity of propagation renders it untenable, at least in the form outlined above. A simple calculation shows that the recession of the surface of the liquid by evaporation at 400 m./sec. would involve an impossibly high value for the thermal conductivity of the layer of vapour. Belajev (1938) has proposed a similar mechanism for the deflagration type of propagation common to high explosives, and has provided evidence for it in the cases of nitroglycol and (less directly) a number of other substances (Belajev & Jusephovich 1940; Belajev & Samburskaya 1941). The deflagration process investigated by Belajev is, however, normally propagated through the explosive at a velocity of less than 1 mm./sec. and even if the deflagration occurred under pressures corresponding to the detonation pressure (which is certainly greater than the pressure acting during the first stage process of our experiments) it is improbable that its propagation velocity would be greater than a few metres/sec. (cf. Schmidt 1938). Furthermore it is improbable that absorption of radiation from the combustion zone transmitted across the vapour screen could supply the heat of vaporization, since the heat required per square centimetre to account for a velocity of 400 m./sec. is many orders of magnitude greater than the total energy radiated from a black body at a temperature of 4000° C.

The rotating drum photographs provide no evidence as to the cause of the sudden inception of the second stage. In gaseous explosions this is occasioned by the presence of shock waves which break through the flame front from behind and travel ahead of it (Bone *et al.* 1935; Payman 1928). The possibility of detecting such shock waves in our experiments is remote, and the question of their existence must therefore remain open, though it would not be expected that their influence would be so critical in view of the fact that the medium is liquid. On the other hand it does not appear that the inception of detonation is preceded by increased luminosity of the first stage explosion front as postulated previously.

However, the photographs suggest that the initiation of the second stage occurs at a phase boundary (or at least at some other discontinuity) since after initiation, the second stage process is propagated in the forward direction only. If it were initially set up at a point within the liquid (or other) phase it would also be propagated in the backward direction until it reached the first stage explosion front (in the manner of gaseous explosions, e.g. figure 13). On the contrary, in the photographs there is a dark space between the point of inception of the second stage and the first stage explosion front.

Though it is clear that the high velocity of propagation necessitates abandoning the mechanism of the first stage process involving evaporation of the liquid, no plausible alternative hypothesis has been found so far, which will explain satisfactorily the nature of the dark space and the 'auto-initiation' of the second stage process.*

The propagation in thicker films

It has been shown that in thicker films of nitroglycerine, the explosion begins at a very high velocity ($\nless$ 5000 m./sec.), which is maintained for a few millimetres and then falls abruptly to 400 m./sec. It is well known that nitroglycerine has two characteristic velocities of detonation—the 'high' velocity of about 8000 m./sec. which is normally set up by powerful initiation, and the 'low' velocity of about 1800 m./sec. which is set up by weaker initiators. It is possible that, under the conditions of the experiments with the thicker films, the high velocity detonation, or a type of propagation approaching it, is initially set up. This conclusion is supported by the fact that the phenomenon is accompanied by a violent mechanical effect on the confining surfaces. The appearance of the phenomenon in thicker films is probably occasioned by lower heat loss to the confining surfaces at the beginning of propagation.

---

* Although there is no direct evidence to support it, an alternative hypothesis which eliminates the difficulty may be tentatively suggested: It is perhaps possible that the reaction involved in the first stage process occurs in two steps: (1) a non-actinic decomposition reaction giving active intermediate products or radicals, which then (2) after a short time lag react together in the gas phase emitting light and supplying the heat (or radiation) necessary to initiate the decomposition reaction in the next layer ahead. Such a hypothesis as this would 'explain' the phenomena of the explosion traces quite as well as the evaporation mechanism, without necessarily involving a very low velocity of propagation.

It is interesting that the explosion in the thicker films, which begins at a high rate of detonation, passes through a period of the 400 m./sec. type of propagation before reaching the stable velocity of 2000 m./sec. It is possible that the explosion begins in every case at high velocity, but in very thin films is immediately damped down to the 400 m./sec. process.

Propagation after initiation by impact

Under most conditions of impact the initiation of the explosion in nitroglycerine is brought about by the adiabatic compression of tiny air spaces entrapped in the liquid during the impact (Bowden *et al.* 1947*a*). The fact that the general aspect of the blast patterns and stationary photographs obtained from impact experiments is identical with that of patterns obtained by spark initiation is strong evidence that the sequence of events after impact initiation is similar to that observed in the rotating drum camera photographs obtained with initiation by spark. Experiments previously reported have shown that when initiation is effected in a very thin film by adiabatic compression of air spaces the explosion begins at about 400 m./sec. (Bowden *et al.* 1947*b*). The question arises, however, as to whether in a thicker film the explosion begins as the normal first stage 400 m./sec. process, or as a process of higher velocity. It is probable that, under these conditions the explosion does, in fact, commence at 400 m./sec. But whatever its initial velocity may be, it is clear, in view of the similarity of the blast patterns to those obtained in spark experiments, that the explosion rapidly assumes the 400 m./sec. type of propagation, after which the 2000 m./sec. detonation is set up in the normal manner.

The work described in this paper was carried out as part of the research programme of the Section of Tribophysics, of the Council for Scientific and Industrial Research, Australia. The authors wish to thank Mr R. E. Summers, Assistant Superintendent, Munitions Supply Laboratories, for the loan of the Fraser Camera, and Messrs I.C.I.A.N.Z. and Dr A. E. Finn for kindly supplying the explosive. Our thanks are due to Dr S. H. Bastow and Dr D. Tabor for their helpful suggestions and to Professor E. J. Hartung for laboratory facilities in the Chemistry Department of the University of Melbourne.

REFERENCES

Belajev, A. F. 1938 *Acta Physicochim. U.R.S.S.* 8, 763.
Belajev, A. F. 1941 *Acta Physicochim. U.R.S.S.* 14, 523.
Belajev, A. F. & Jusephovich, N. 1940 *C.R. Acad. Sci. U.R.S.S.* 27, 131.
Belajev, A. F. & Samburskaya, E. 1941 *C.R. Acad. Sci. U.R.S.S.* 30, 632.
Bone, W. A. & Fraser, R. P. 1929 *Phil. Trans.* A, 228, 197.
Bone, W. A., Fraser, R. P. & Wheeler, W. H. 1935 *Phil. Trans.* A, 235, 29.
Bowden, F. P., Eirich, F., Ferguson, A. E. & Yoffe, A. 1943*a* *Bull. Coun. Sci. Industr. Res., Aust.*, no. 167.
Bowden, F. P., Eirich, F., Mulcahy, M. F. R., Vines, R. G. & Yoffe, A. 1943*b* *Bull. Coun. Sci. Industr. Res., Aust.*, no. 173.

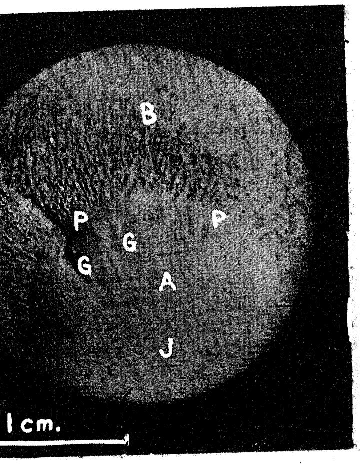

1

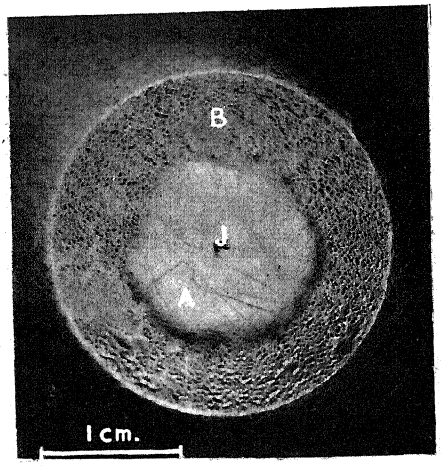

2

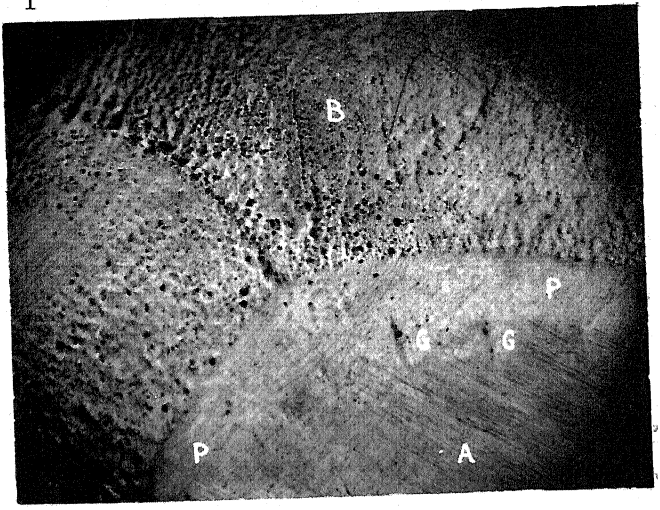

3

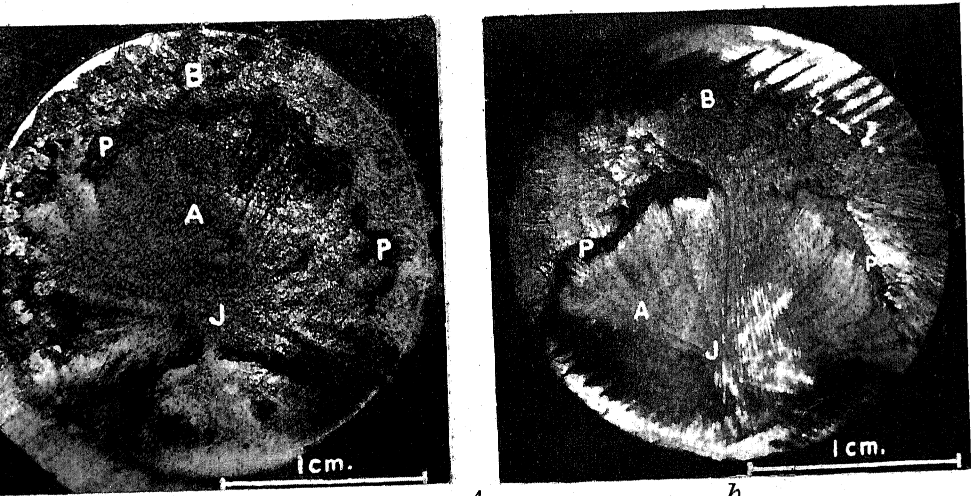

a 4 *b*

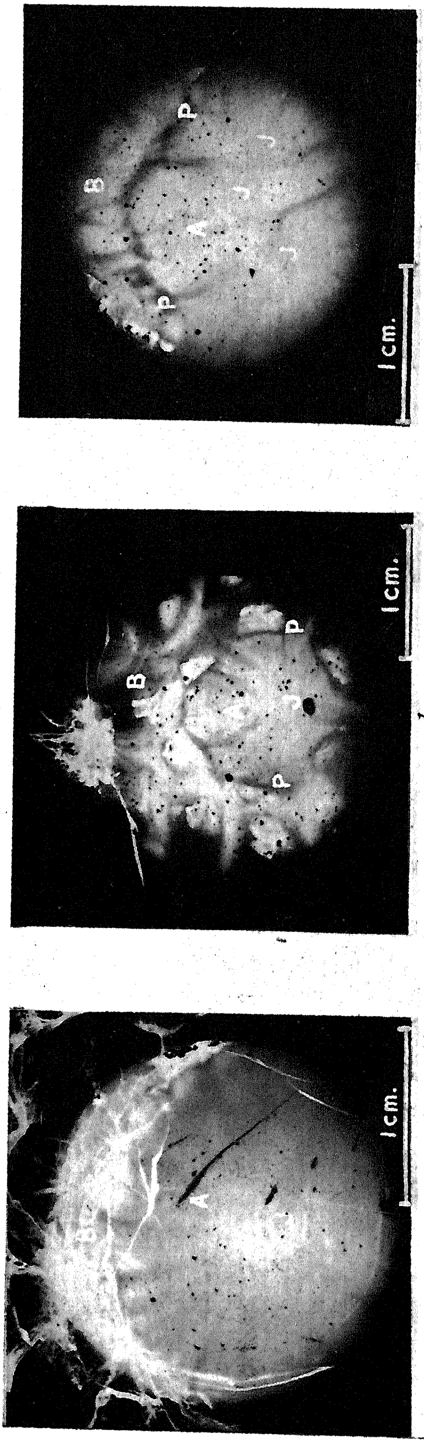

a *b* *c*
5

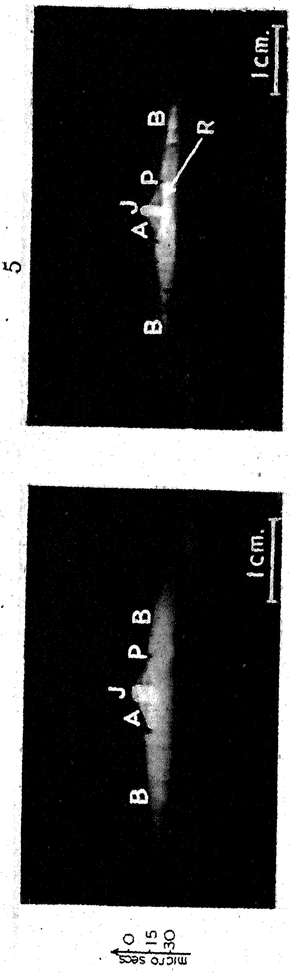

a *b*
7

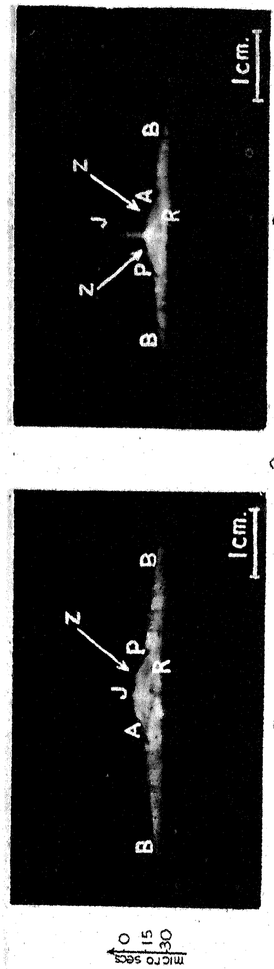

a *b*
8

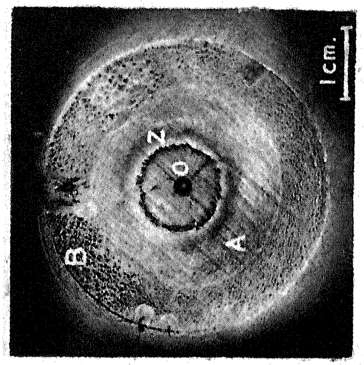

9

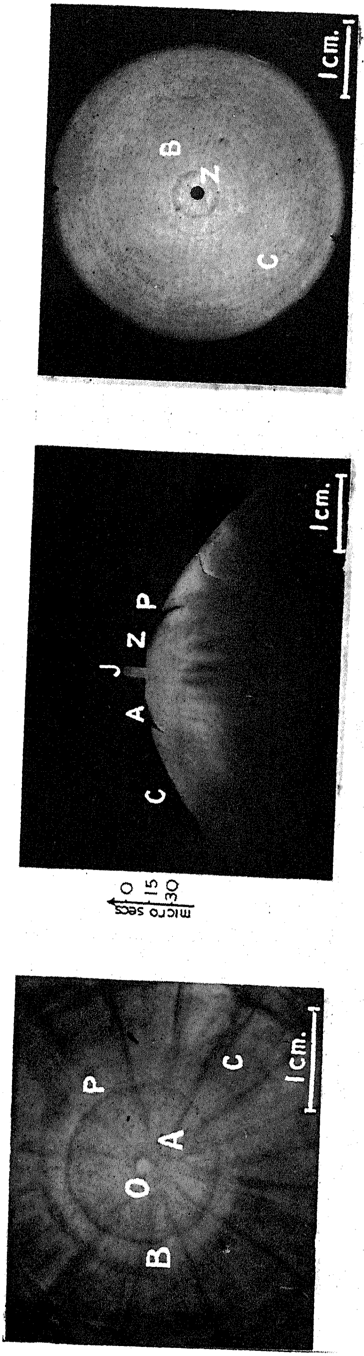
P
O
A
B
C
1cm.
micro secs
0
15
30
C
A
J
Z
P
1cm.
B
Z
C
1cm.

a

b

c

10

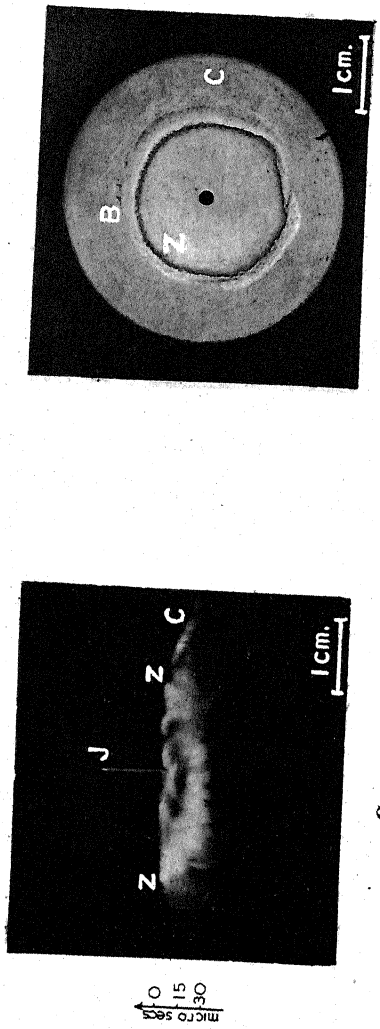
Z
J
Z
C
1cm.
micro secs
0
15
30
B
Z
C
1cm.

a

b

11

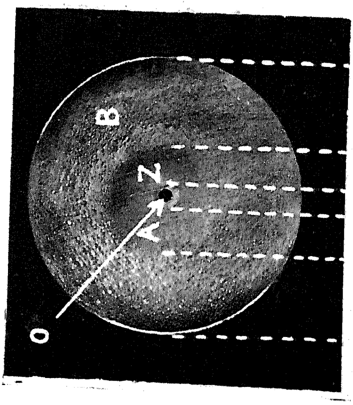

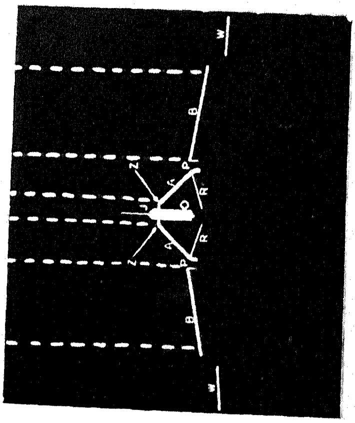

12

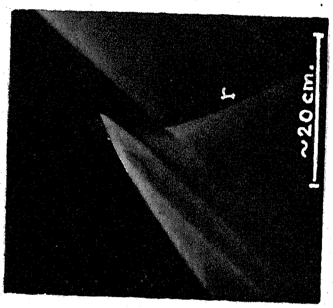

13

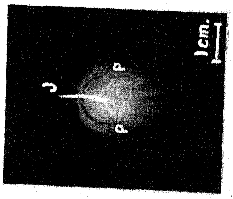

15

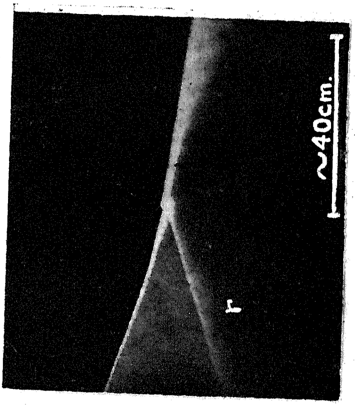

14

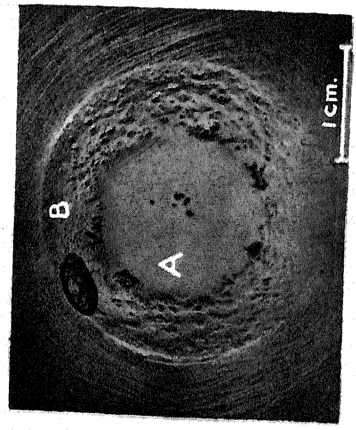

16

Bowden, F. P., Mulcahy, M. F. R., Vines, R. G. & Yoffe, A. 1947*a* *Proc. Roy. Soc.* A, **188**, 291.
Bowden, F. P., Mulcahy, M. F. R., Vines, R. G. & Yoffe, A. 1947*b* *Proc. Roy. Soc.* A, **188**, 311.
Campbell, C. & Woodhead, D. W. 1926 *J. Chem. Soc.* p. 3010.
Chariton, J. B. & Ratner, S. B. 1943 *C.R. Acad. Sci. U.R.S.S.* **41**, 293.
Le Chatelier, H. 1900 *C.R. Acad. Sci., Paris*, **130**, 1755.
Dixon, H. B. 1903 *Phil. Trans.* A, **200**, 315.
Egerton, A. & Gates, S. F. 1927 *Proc. Roy. Soc.* A, **114**, 137.
Jones, F. 1928 *Proc. Roy. Soc.* A, **120**, 603.
Laffitte, P. 1925 *Ann. Phys., Paris*, **4**, 587.
Mallard & Le Chatelier 1883 See Bone, W. A. & Townend, D. T. A. (1927). *Flame and combustion in gases.* Longmans.
Muraour, H. 1942 *Chim. et Industr.* **47**, 162.
Patry, M. & Laffitte, P. 1931 *C.R. Acad. Sci., Paris*, **193**, 171, 1339.
Payman, W. 1928 *Proc. Roy. Soc.* A, **120**, 90.
Schmidt, A. 1938 *Z. ges. Schiess-u. Sprengstoffw.* **33**, 121.
Vines, R. G. 1944 Unpublished thesis.
Vines, R. G. & Mulcahy, M. F. R. 1946 *Nature*, **157**, 626.

DESCRIPTION OF PLATES 12 TO 15

PLATE 12

FIGURE 1. Explosion pattern produced by impact on a number of nitroglycerine droplets.

FIGURE 2. Pattern produced by explosion in a thin film of nitroglycerine. Initiation by spark.

FIGURE 3. Enlarged photograph showing features associated with the transition from the first to the second stage of the explosion.

FIGURE 4. Patterns on lead plated surfaces produced by impact on nitroglycerine droplets.

PLATE 13

FIGURE 5. Light patterns on photographic plates. *a*, initiation by impact on a thin film of nitroglycerine containing air bubbles; *b*, *c*, initiation by impact on nitroglycerine droplets.

FIGURE 7. Drum camera traces of explosions in very thin films of nitroglycerine. (The arrow indicates the direction of motion of the drum.)

FIGURE 8. Camera traces of explosions in thicker nitroglycerine films.

FIGURE 9. Explosion pattern produced by sparking in a thicker film of nitroglycerine. (The ring of raised metal immediately outside Z, is due to the crumpling of the surface.)

PLATE 14

FIGURE 10. Explosions on a plastic support. *a*, light photograph; *b*, drum camera trace; *c*, explosion pattern on brass. (The radial lines in figure 10*a* are due to the cracking of the support.)

FIGURE 11. Explosion on plastic support. *a*, drum camera trace; *b*, corresponding explosion pattern.

PLATE 15

FIGURE 12. Diagrammatic representation of an explosion trace and correlation with an actual blast pattern. (W is a shock wave in the atmosphere.)

FIGURE 13. Explosion in a gaseous mixture. Drum camera trace obtained by Dixon (1903).

FIGURE 14. Rotating mirror camera trace of explosion in a carbon monoxide, oxygen mixture (Bone *et al.* 1935).

FIGURE 15. Explosion photograph on drum camera (see text).

FIGURE 16. Tetranitromethane-toluene spark pattern. (The dark hole (upper left) is due to a fault in the brass.)

The propagation of detonation in thin layers of nitroglycerine

By M. F. R. Mulcahy and R. G. Vines

Council for Scientific and Industrial Research, Section of Tribophysics, University of Melbourne

(*Communicated by Sir David Rivett, F.R.S.—Received* 11 *February* 1947 —*Read* 8 *May* 1947)

[Plates 16 to 18]

An investigation has been made on the propagation of the low-velocity detonation through layers of nitroglycerine 0·01 to 0·75 mm. thick. By the rotating drum photographic method the detonation velocity was found to be 1800 ± 200 m./sec. The forward and backward movement of the decomposition products behind the detonation front has been recorded and the velocities measured approximately.

Evidence has been collected which shows that the detonation does not proceed through the explosive as a uniform wave, but is essentially a discontinuous process involving a non-uniform distribution of intensity across the breadth of the detonation front.

Supplementary evidence to that reported previously (Vines & Mulcahy 1946; Mulcahy & Vines 1947) is given of the analogy between the phenomena associated with the setting up of the low-velocity detonation in nitroglycerine and those characteristic of the initiation of detonation in gaseous systems.

INTRODUCTION

The previous paper has described a high-speed photographic study of the first stages of explosion in thin layers of nitroglycerine. It was shown that a complex series of events occurs within the first 1 to 2 cm. of propagation of the explosion (Mulcahy & Vines 1947). In very thin layers the explosion begins at the comparatively low rate of about 400 m./sec., and then, after propagating for about 1 cm. at this velocity, suddenly accelerates to about 2000 m./sec. This faster type of propagation is mechanically more violent than the initial process. In thicker layers the explosion begins at very high velocity ($\nless$ 5000 m./sec.), within about 1 cm. falls suddenly to 400 m./sec., and then accelerates abruptly to about 2000 m./sec., as in the thinner layers. It was shown also that the inception of the 2000 m./sec. explosion takes place 'spontaneously' at a point in the nitroglycerine layer ahead of the explosion front of the 400 m./sec. process, and that simultaneously a luminous process ('retonation wave') is sent back towards the point of initiation through the decomposition products remaining from the 400 m./sec. stage of the explosion.

This paper describes a more detailed examination of the 2000 m./sec. propagation process and of certain characteristic effects found to be associated with it. It has been found that the process once established, maintains a strictly constant velocity except, in certain circumstances, over a short distance close to the point where it begins. A more accurate value for the propagation velocity has been obtained, viz. 1800 ± 200 m./sec.; this velocity corresponds to that of the well-known 'low-velocity' detonation of nitroglycerine, with which the process is therefore presumably identical.

The movement of the luminous gaseous products left in the wake of the explosion front ('Schwaden') has been recorded photographically. The photographs obtained are remarkably similar to those published by other workers, recording the behaviour of the Schwaden subsequent to the passage of the detonation wave in gaseous explosions (described by Jost 1939). A knowledge of the behaviour of the Schwaden has been valuable in interpreting the characteristic pattern of fine lines which remain 'scratched' on a smooth lead-plated metal surface after a thin confined layer of nitroglycerine, in contact with it, has been detonated.

Photographs obtained provide further evidence of 'structure' in the detonation process, which appears to be propagated as a series of small localized explosions in the liquid of the order of 0·5 mm. apart (cf. Bowden, Eirich, Ferguson & Yoffe 1943*a*; Bowden, Eirich, Mulcahy, Vines & Yoffe 1943*b*). The constant velocity of 1800 m./sec. is therefore very probably an overall or average velocity.

The experiments have incidentally provided further illustration of the phenomena associated with the beginning of the explosion which have been described in detail elsewhere (Vines & Mulcahy 1946; Mulcahy & Vines 1947).

THE PROPAGATION OF DETONATION THROUGH THIN LAYERS OF NITROGLYCERINE

(1) *Blast patterns on brass surfaces*

When explosion is initiated at the centre of a thin layer of nitroglycerine confined sandwich fashion between two flat brass disks, a characteristic blast pattern is imprinted on the confining surfaces. The two distinct regions of surface damage remaining after the explosion have been described in detail in earlier papers (Bowden *et al.* 1943*a*, *b*; Mulcahy & Vines 1947). When explosion is initiated at the end of a continuous layer of nitroglycerine confined in the same fashion between a metal block and a narrow long brass strip, the two regions of surface damage may again be observed.*

Figure 1*a*, plate 16, shows such a strip, 8 cm. long and 2 cm. in width. An explosion adjacent to the end A served to fire the confined layer† which was 0·1 mm. thick in this case. At A there is a small area which is almost unmarked by the explosion and beyond it (beginning at b) the region of heavy-surface deformation, B, appears. The deformation consists of a multitude of tiny pits, approximately 0·5 mm. apart, impressed in the metal, and extends without a break to the far end of the strip. The discontinuous nature of the deformation is seen more clearly in figure 10, plate 18, which is a magnified photograph of a portion of the surface.

---

* Actually the deformation may be observed on any metal surface, but is most clearly visible on brass which is soft enough to be marked distinctly, and sufficiently hard not to be damaged too badly.

† See p. 229 for the details of this method of initiation.

(2) *Patterns on lead-plated surfaces*

By lead plating the brass strip beneath which the layer of nitroglycerine is confined, a further interesting explosion pattern is obtained (cf. Bowden *et al.* 1943*b*). After an explosion such a lead-plated surface is found to be covered entirely by a large number of fine and gradually divergent 'scratches' which appear to originate from a point near the remote end of the strip, and to be directed back towards the end where initiation was effected. Such a pattern may be seen in figure 1*b*, plate 16. The explosion was initiated at J, and O is the apparent origin of the marks at the far end of the strip.

It is found that the nature of the pattern is unaltered by the width and shape of the strip. This may be seen from figure 1*c*, which shows the marks on a strip 4 cm. wide. Again, if the layer of explosive is confined beneath a flat strip of circular shape, the marks are similar but follow the curve of the strip. Figure 1*d* is a photograph of a pattern produced in an experiment where the explosion was initiated at the centre of a strip; in this case two separate series of scratches may be seen originating at both ends.

By dissolving away the film of lead the normal explosion pattern on the underlying brass surface becomes apparent; for example, if the lead coating on the strip shown in figure 1*b* were removed, the brass pattern beneath would be found to be similar to that in figure 1*a*. Close examination of the disposition of the scratches and of the underlying pit markings has revealed no connexion between them, i.e. the scratches seem to be produced independently of, and subsequently to, the formation of the pit markings.

A magnified photograph of a part of a lead surface similar to figure 1*b*, taken at about the centre of its length, is given in figure 7, plate 18. This central section is representative of the 'typical' disposition of the scratches uninfluenced by the special conditions which obtain at the two ends of the strip. By taking a small element of the length of such photographs and measuring the angles of orientation of individual scratches, it is found that there is a linear relationship between the angle of orientation and the distance of the scratch from the centre of the strip. This angle increases from zero at the centre to about 60° at the two edges, apparently irrespective of the width of the strip, since with strips 1·25 to 4 cm. wide the angle is roughly the same.

It may be observed at this stage that, since the scratch-mark pattern is superimposed upon, and apparently independent of the underlying deformation, it follows that it is produced by a process which occurs subsequently to the passage of the detonation through the explosive.

(3) *Rotating drum camera traces*

The high-speed photographic technique used previously (p. 213) to examine the initial stages of the explosion has been applied to more extended layers of nitroglycerine. The objects of the experiments were to obtain a more accurate value for the velocity of the stage of the explosion responsible for the pressure marks on brass surfaces; to ascertain whether there is any appreciable dependence of this velocity on the thickness of the layer of explosive; and to obtain more data on the fundamental nature of the explosive process and of its effects on brass and lead-plated surfaces.

Experimental

The same machine was used as in the previous investigation, but the experimental arrangement was somewhat modified. The apparatus is represented diagrammatically in figure 2. The layer of nitroglycerine* was confined between a brass strip A, similar to those described in the previous section, and a thick slab of laminated glass Y. By means of three stiff compression springs the strip and slab were clamped tightly (clamping device not shown) to the two flat steel plates CC which supported the arrangement.

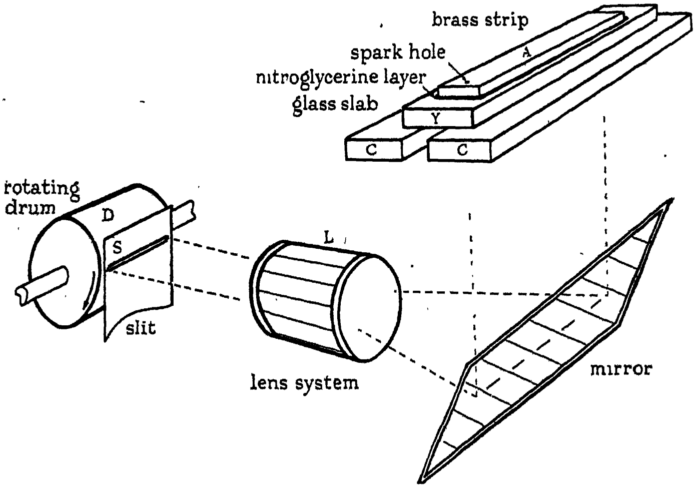

FIGURE 2

By means of a lens system L, the light from the explosion beneath the strip was brought to a focus upon the rotating drum D, which carried the film. Adjacent to the drum was a narrow linear slit S, at right angles to the direction of motion of the film. The position of the strip was so arranged that only the light from the explosion at its centre could be transmitted through the slit to the film. In this way it was possible to follow the entire course of the explosion from the point of initiation to the far end of the strip.

The explosion was initiated either by impact or by condenser spark. For impact initiation a number of droplets of nitroglycerine were distributed upon the glass slab Y close to one end of the brass strip, and struck with a flat metal striker.†

---

* The thickness of the layer could be varied by inserting small metal spacing pieces of known thickness between the brass strip and the glass slab.

† See Bowden *et al.* (1943*b*, 1947*a*) for this method of initiation.

The explosion so produced fired the confined layer. In the experiments in which initiation was effected by means of a condenser spark (250 V, 12 μF), the arrangement was similar to that described previously (Mulcahy & Vines 1947).

The velocity of propagation

Figures 3*a*, *b*, plate 17, are typical* traces obtained with this apparatus.

The propagation velocity of the explosion at any point along the length of a nitroglycerine layer can be calculated from the angle of inclination of the trace to the horizontal at that point. In figure 3*a* propagation of the explosion (in both directions) has begun at the characteristic initial velocity of about 400 m./sec. At P the second stage of the explosion (detonation)† began suddenly. As has been described fully previously (Vines & Mulcahy 1946; Mulcahy & Vines 1947), detonation begins at a point in the nitroglycerine layer a little ahead of the advancing explosion front. In this case a gap of 3 mm. separated the explosion front of the 400 m./sec. process from the point where detonation began. In the experiment of figure 3*b* the explosion first spread from the point of initiation with extreme rapidity ($\nless$ 5000 m./sec.) for a short distance JZ, but at Z this first process changed abruptly to the 400 m./sec. process, which ultimately, at the point P, gave way to detonation in the normal fashion. (The 'auto-ignition' phenomenon is also seen clearly.) It has been suggested that the initial, very rapid process usually observed with thicker layers (Mulcahy & Vines 1947) corresponds to the 'high velocity' ($\sim$ 8000 m./sec.) detonation of nitroglycerine which should be expected to be unstable under these conditions of experiment (cf. Chariton & Ratner 1943).

It will be seen from figures 3*a* and *b* that, except for a brief period PQ following its inception (when the speed is abnormally fast), the detonation is propagated with constant velocity, since the slope of each trace is uniform over the length QQ′.

Figure 5*a*, plate 17 is a trace obtained with a thinner layer (0·1 mm.).‡ The point of initiation is not shown. The explosion enters the photograph at 400 m./sec., detonation begins at P and immediately assumes its constant velocity of propagation. (It may be noted that this photograph shows the retonation wave (R) clearly.)

---

* In these experiments initiation was brought about by the passage of a spark at the point J. The thickness of the nitroglycerine layer was in both cases 0·5 mm. With layers of this thickness it is difficult, in setting up the apparatus, to avoid the inclusion of a small air bubble in the bottom of the spark hole. Such a bubble was present in both the experiments shown. Apparently this results in the complete (figure 3*a*) or partial (figure 3*b*) suppression of the period of very high-speed propagation which normally occurs at the beginning of the explosion in thick layers.

† For the sake of brevity this stage of the propagation, which is that responsible for the deformation marks on brass surfaces (figure 1*a*) has been referred to as 'detonation'. It will be shown later that the velocity of this process is the same as that of the propagation mechanism commonly described as the 'low velocity' detonation of nitroglycerine.

‡ In this experiment the lower confining surface was not a glass slab but an alternative arrangement described on p. 233.

From these and other traces the propagation velocity of the detonation could be calculated with some improvement in accuracy on the previous measurements made on shorter lengths of explosive. Values for the velocity calculated from a number of traces are given in table 1. Column 2 gives the method of initiation, viz. condenser spark, impact on droplets, or cavity impact.† Column 3 indicates

TABLE 1. VELOCITY OF DETONATION IN THIN LAYERS OF NITROGLYCERINE

thickness of nitroglycerine layer	method of initiation	lower confining surface	velocity (m./sec.)
touching* (*c.* 0·01 mm.)	spark	glass	1700 1700 1800 1840 1900
	cavity impact	glass	1860
	impact on droplets	glass	1770 1900
	impact on droplets	'perspex slit'	1900 1900 2000 2000 2000
0·1 mm.	spark	glass	1760 1820
	cavity impact	glass	1900
	impact on droplets	glass	1860 1860 1900
	impact on droplets	'perspex slit'	1840 1860 1880 1900 1900 1900 1900 1900 1900 2000
0·5 mm.	spark	glass	1700 1720
	impact on droplets	glass	1600 1650
	impact on droplets	'perspex slit'	1760
0·75 mm.	spark	glass	1650

* Under conditions of 'touching' thickness the layer is confined between the surfaces without spacing pieces interposed; it is estimated that the overall thickness of the layer is $\ngtr$ 0·01 mm. (Bowden *et al.* 1943*b*).

† For the method of initiation by cavity impact see Bowden *et al.* (1943*a*, *b*; 1947*a*).

the type of lower confining surface, viz. glass or the 'perspex slit' described on p. 233.

It will be seen from table 1 that the values obtained are within the range 1650 to 2000 m./sec. The experimental error of each measurement has been estimated to be ± about 10 %: consequently the most probable value for the detonation velocity is 1800 m./sec. Table 1 also shows that, within the limits of experimental error, the detonation velocity is independent of the method of initiation of the explosion and of the thickness of the layer of explosive in the range $\not> 0{\cdot}01$ to 0·75 mm. It is possible that the performance of a statistically adequate number of experiments with different layer thicknesses would reduce the probable error, and consequently might reveal some variation in velocity. In fact it appears probable from the results that the velocity with the perspex slit support is a little higher than when a glass support is used. Again in the thickest layers the velocity may possibly be somewhat lower. However, as a new camera with considerably greater writing speed is at present in the course of construction, it is not considered worth while at this stage to follow up this point.

The value of 1800 m./sec. agrees with that of 1800 ± 200 m./sec. found by Chariton & Ratner (1943) for the velocity of the 'low velocity' detonation of nitroglycerine in glass tubes of 2 to 2·5 mm. diameter. It seems clear therefore, that as suggested in the preceding paper, the process responsible for the deformation of the brass surfaces in our experiments is, in fact, the low velocity detonation. It may be noted that it follows from our results that the low velocity detonation is capable of stable propagation in a layer of nitroglycerine 0·01 mm. thick.

The initial velocity of detonation

As indicated above, the traces (figures 3*a*, *b*) shows that detonation begins ($P \rightarrow Q$) at a velocity rather higher than the stable speed eventually attained ($Q \rightarrow Q'$). This effect is most apparent in the experiments with thicker layers. It is notable that under these conditions the surface deformation characteristic of the detonation process (i.e. the pit markings in figure 1*a*), is quite considerably reduced on the brass strips up to the point where the process begins to propagate at the constant velocity.

The beginning of detonation at high velocity has a parallel in the setting up of detonation in gaseous explosions: when gaseous combustion passes from the flame type of propagation to detonation, the detonation wave begins at an unstable high velocity which in a short distance of travel falls to the stable velocity of propagation (cf. Bone & Fraser 1931).

Events subsequent to the passage of the detonation wave

The rotating drum camera traces just described give no information regarding events occurring at any appreciable time subsequent to the passage of the detonation wave through the explosive layer. The reason for this is clear. After an experiment, the slab of laminated glass which supported the nitroglycerine is found to be completely shattered and quite opaque. The thickness of the explosion traces (e.g. figures 3*a*, *b*) indicates that, allowing for the width of the slit, each element of glass becomes opaque within 10×10^{-6} sec. after the passage of the detonation wave over it. If, as has been inferred previously, the pattern of 'scratch' markings on a lead-plated surface is caused by a process occurring after the detonation has passed through the liquid, little or nothing of this process will be seen in the explosion photographs when the nitroglycerine is supported by a glass slab, because of the shattering of the glass. If any subsequent luminous processes are to be observed, it is necessary to support the explosive by a substance which remains transparent after the detonation has passed over it.

Slabs of transparent plastic ('perspex' and cellulose acetate) were tried in place of glass, but under these conditions it was not found possible to set up stable detonation in the explosive, presumably because of the lower rigidity of the plastic support (cf. Mulcahy & Vines 1947).

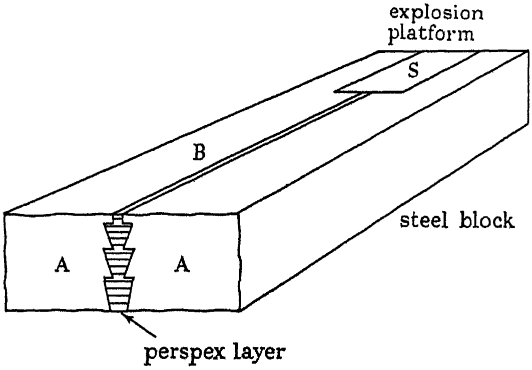

FIGURE 4

The difficulty was overcome by a modification of a device used in previous experiments (Bowden *et al.* 1947*b*), viz. by clamping a small sheet of perspex between two steel blocks as shown in figure 4. The blocks AA were heated in boiling water and then squeezed together so that a thin layer of perspex, B, was moulded to fit the space between them. The apparatus was so constructed that a solid steel platform S was left at each end of the perspex, and narrow grooves in the steel blocks kept the perspex rigidly in place. The upper and lower surfaces of the composite slab were ground and polished so that the two surfaces of the perspex inlay were rendered completely flat, level with the steel surfaces, and transparent. The width of the perspex at the upper surface was 1 mm. This steel-and-perspex slab was substituted for the original glass support. Otherwise the apparatus was the same as previously described, except that the slit adjacent to the camera drum was removed since this new arrangement itself provided a slit adjacent to the explosive. A new piece of perspex was inserted and the whole slab ground and polished for each experiment.* The explosion was initiated by impact on a number of nitroglycerine droplets distributed on the steel platform S.

With the rigidity of the support improved in this way, it was possible to detonate the explosive layer, and although the perspex was often considerably damaged, it still remained reasonably transparent after the explosion. Figures 5*a*, *b*, plate 17, are examples of the photographs obtained. It is at once evident that the products of detonation remain luminous for an appreciable time after the passage of detonation through the explosive. This time can easily be computed from the photographs and (allowing for the width of the slit) normally amounts to $\sim 30 \times 10^{-6}$ sec. The duration of the luminosity can also be measured by causing the explosion to propagate diametrically across the slit instead of along it. Figure 9, plate 18, is a photograph obtained in this way. The detonation front first became visible to the camera at A, and passed across the slit out of view, but the products remained luminous while the film moved through the distance AB. The total period of luminosity is the time equivalent of the distance AB minus the width of the slit, i.e. 30×10^{-6} sec. Further discussion of figure 9 will be given later.

Photographs such as figures 5*a*, *b* also record the *motion* of the luminous hot gases left immediately behind the detonation wave ('Schwaden'). Unfortunately it is extremely difficult to obtain prints which are capable of showing the fine details of the negatives when reproduced, and figure 5*b* has been chosen from the point of view of possibility of reproduction, rather than because it shows typical behaviour. Figure 5*b* shows that the Schwaden, possibly after barely perceptible motion forward, move backwards from the detonation zone. In most of the photographs obtained, the Schwaden are seen to move at first forward in the direction of the detonation wave, with a velocity of the order of 200 to 400 m./sec., come to a standstill, and then move backwards at about 400 to 800 m./sec. Though it has not yet been possible to obtain detonation photographs which show up this behaviour on reproduction, it is seen much more clearly in photographs obtained when stable detonation was not set up.† Figures 6*a*, *b*, *c*, plate 17, are such photographs.‡

The photographs immediately suggest comparison with those obtained by Dixon, Bone & Fraser, and others in their work on the propagation of detonation in combustible gas mixtures (described by Jost 1939). They have shown that subsequent to the passage of the detonation wave through such mixtures, the hot gases which are left behind the detonation front move rapidly after it, their velocity gradually decreasing until they come to a standstill, after which their

---

[*] Owing to the fact that nitroglycerine is absorbed by perspex it was found necessary to initiate the explosion immediately after setting up the apparatus. The nitroglycerine could be separated from the perspex by a thin sheet of mica but in these circumstances stable detonation is not set up (see § 4).

[†] See § 4.

[‡] In the explosion in figure 6*c*, initiation took place at both ends of the strip. In all photographs similar to figures 6*a*, *b*, and *c* the period of luminosity is rather more protracted than when full detonation is set up.

movement is reversed and they travel rather more slowly in the opposite direction. The velocity of the forward movement of the Schwaden has in certain cases been measured by Lewis & Friauf (1930) and found by them to agree reasonably well with that predicted by the hydrodynamic theory of detonation. Figure 8, plate 18, a photograph of the detonation wave in an acetylene-oxygen mixture taken from a paper by Bone & Fraser (1931), shows the phenomenon well and is included for comparison with figures 5, 6, plate 17. The similarity is obvious though the difference in scale should be noted: figure 8 represents the passage of the gaseous detonation through 1 m. whereas, for example, figure 5*b* represents a 9 cm. length of nitroglycerine. It seems, therefore, that the hot decomposition products left in the wake of the detonation wave passing through our nitroglycerine layers behave in substantially the same fashion as the Schwaden in a gaseous detonation.

The movement of the Schwaden provides an explanation for the 'scratch' mark pattern on a lead surface. The previous speculation (Bowden *et al.* 1943*b*), that the marks are caused by an extra explosion process which sweeps back from the far end of the layer through the products of detonation, is rendered less probable in the light of the experiments just described. Such a process should be expected to be luminous but no sign of it appears in the photographs taken with the perspex slit, though it remains fairly transparent after the explosion. On the other hand, if the marks are considered to be scratched on the lead surface by the backward flowing Schwaden, the pattern becomes immediately intelligible (see discussion).

(4) *The discontinuous nature of the explosive propagation*

The pit markings characteristic of the detonation process (figure 10, plate 18) indicate that it is essentially discontinuous, and it has been suggested that they are impressed in the surface by a succession of powerful, localized explosions occurring irregularly about 0·5 mm. apart. The camera traces also show variations in luminous intensity along their length which are ascribable to this phenomenon. These are difficult to reproduce from the negatives but may be seen faintly in figures 3, 5, plate 17.* The streaked appearance of the Schwaden in the explosion traces and the discrete nature of the 'scratch' marks are also indicative of 'structure' in the detonation front (though here the possibility that both are due to moving particles within the hot gases cannot be ruled out (see § 5).

In photographs such as figure 9, plate 18, the line of first appearance of light (AA) is a snap-shot of the (curved) detonation front. Examination of the negatives reveals that this line is finely serrated, i.e. the luminosity of the detonation front is not uniform across its width but is made up of a number of bright spots separated by spaces of lower luminosity. This is clear evidence of structure in the detonation front. It is reasonable to identify the bright spots with the pits which the detonation produces in the surface over which it passes. When stable detonation is not

* The resolution of our apparatus is insufficient to detect any possible changes in slope which might indicate alternation between high and low velocity, corresponding to the more and less deformed elements of the surface.

set up* the camera traces show that the explosion proceeds in a more markedly discontinuous fashion. Figures 6*a*, *b*, *c* are traces of such explosions. It will be observed in figure 6*b* that the luminosity of the explosion is intermittent and that the velocity of propagation varies in an irregular manner.† In fact, it appears that propagation took place as an explosion which alternately flared up and then died out. The effect is shown again in figure 6*c*: the Schwaden appear as luminous bands separated by dark spaces. The presence of the dark spaces in the photographs is of some interest since it indicates that each of the intermittent explosions is 'spontaneously' initiated ahead of the one preceding it. The phenomenon is reminiscent of the auto-initiation of detonation which normally occurs in front of the 400 m./sec. explosion.

DISCUSSION

(5) *Interpretation of the 'scratch' mark pattern*

As indicated in § 2, the scratch marks are made on the lead surface at some time after the detonation has passed over it, but no subsequent explosion or disturbance propagated through the detonation products has been detected, which could be considered to have produced them. It is reasonable, therefore, to attribute the pattern to the movement of the Schwaden behind the detonation zone. As they emerge from the detonation zone, the Schwaden move forward with a velocity of ~ 200 m./sec. but, as a result of cooling and expansion, a region of low pressure is created behind the detonation zone and their motion is reversed.‡ The Schwaden will also expand sideways towards the low-pressure region at the sides of the strip; the motion of the gases at any time will therefore be compounded of their sideways and forward or backward movement. If it be assumed that each individual scratch is caused by a small element of volume of the backward moving Schwaden, this explains in a general way the increasing obliquity of the scratches from the centre (maximum pressure) to the edges (low pressure).§ Again the apparent 'origin' of the scratches, O in figures 1*b*, *c*, *d*, may be ascribed to a reversal of the normal direction of flow resulting from the establishment of a pressure gradient in the direction of propagation after the detonation has terminated at the end of the explosive layer.

---

* This usually occurs when the explosive layer is held between the strip and a piece of (transparent) mica resting on the perspex slit.

† The overall velocity was in this case 1000 m./sec. for the first 4 cm. and 1350 m./sec. for the final 6 cm.

‡ According to the theoretical work of Becker (1922) and Langweiler (1938), a rarefaction wave may be expected to follow the detonation wave (see also Jost 1939, p. 203). There is some evidence of this in our across-the-slit photographs in which a temporary diminution of luminous intensity in the region behind the detonation front may sometimes be observed.

§ It may be noted that photographs similar to figure 8 show no sign of sideways expansion (except at the edges): it seems not unlikely that the scratch marks observed are made after the Schwaden become non-luminous.

Though it seems fairly clear from the foregoing discussion that the 'scratch' marking is associated with the flow of the Schwaden, the actual cause of the discrete nature of the scratches is more obscure. It is possible that they are caused by particles of lead dragged across the surface, or by small droplets of undecomposed explosive entrained in the Schwaden.* On the other hand it seems not unlikely that the discrete 'scratches' result from local regions of high pressure within the moving Schwaden which are a consequence of the discontinuous nature of the detonation process.

(6) *The low-velocity detonation*

The close similarity between the phenomena characteristic of the setting up of the 1800 m./sec. detonation in nitroglycerine and those observed in gaseous explosions has been pointed out in the previous paper. The work described here has revealed at least two further points of similarity, viz. the forward and backward movement of the Schwaden and, in the thicker layers, the beginning of the detonation at an abnormally high velocity.

The evidence indicates strongly that the 1800 m./sec. detonation of nitroglycerine (and similar liquid explosives) is not propagated as a homogeneous wave front but proceeds as, or is accompanied by, a discontinuous series of localized explosions (see also below). In this connexion it is of interest to observe that the work of Bone, Fraser & Wheeler (1935) has shown that the propagation of gaseous detonation in many cases—the so-called spinning detonations (Campbell & Woodhead 1926; Campbell & Finch 1928; Bone & Fraser 1929)—involves a continuous series of regularly occurring, discrete explosions. It is perhaps possible to see the behaviour of nitroglycerine as analogous to this. Furthermore, Bone *et al.* (1935) have observed that, in its initial high velocity phase, a gaseous detonation proceeds uniformly, the intermittent explosions only appearing just before the stable velocity is reached: as noted previously the initial high-velocity phase of the detonation in nitroglycerine is accompanied by a considerable reduction in the number of pit marks impressed in the metal surface.

The fact that nitroglycerine can detonate at either the 'high' velocity (7700 m./sec. (Lawrence 1944)) or the 'low', roughly sonic, velocity ($\sim$ 1800 m./sec.) has been known for some time. Recently Chariton & Ratner (1943) and Ratner (1944) have shown that liquid nitroglycol and methyl nitrate behave similarly. No satisfactory explanation of the phenomenon has yet been found. Dserschkowitsch & Andreev (1930) have attributed the two velocities of nitroglycerine to two different isomers, but as Ratner has pointed out, this explanation cannot reasonably apply to methyl nitrate. The value for the detonation velocity of nitroglycerine predicted by the hydrodynamic theory corresponds to the 'high' velocity (Lawrence 1944). It follows that it is the 'low' velocity which is the exceptional one, and therefore in need of a special explanation. It is probably significant that the existence of a low velocity seems to be confined to liquid explosives,* all solid explosives including solid nitroglycerine (Dserschkowitsch & Andreev 1930), having but one (high) rate of detonation.

---

* The full energy of the explosive cannot be released in the low velocity detonation wave.

While sufficient data are not yet available to provide a mechanism for the low-velocity detonation, it is clear that the discontinuous nature of the propagation, as revealed in the pressure marks and photographs, is an important (and hitherto unsuspected) factor. It is significant that when an explosion in nitroglycerine is propagated at a rate approaching that of the high velocity, the deformation of the confining surfaces though more severe than that from the low-velocity detonation, is quite uniform (Mulcahy & Vines 1947, figure 11*b*, plate 14). This is in contrast to the pitting characteristic of the 1800 m./sec. process.

It can be shown that the pressure involved in the production of the pit marks is $\nless$ 60,000 atmospheres.† In view of this high value the possibility arises that the low-velocity detonation may consist of small periods of high-velocity detonation (7700 m./sec.)—during which the pit markings are produced—alternating with the 400 m./sec. type of propagation in such a fashion that the average velocity of propagation is 1800 m./sec. Actually when the total extents of the depressed and undepressed parts are measured over a length of surface (e.g. from figure 10, plate 18) the average ratio between the two comes out at about 1 : 5 which is roughly the expected value. However, no great reliance can be placed on this agreement since in making the measurement it is difficult to estimate the precise extent of each pit. Nevertheless, irrespective of whether the velocities of the two processes be 7700 and 400 m./sec., it may reasonably be assumed that the detonation velocity observed is an average of the velocities corresponding to two different explosion mechanisms.‡

The evidence available hardly allows inference of the mechanism by which the discontinuities in the propagation occur. However, the following qualitative scheme may be tentatively suggested: The propagation of the explosion may be assumed to be maintained by the impinging of the molecules of the decomposition products on the surface of the undecomposed explosive ahead (cf. Schmidt 1938), the products resulting mainly from a combustive type of reaction analogous to the 400 m./sec. process. However, because of inhomogeneities in the initiation of the reaction along the width of the explosion front, or perhaps as the result of a disturbance propagated ahead of the explosion, the hot gases are able to proceed deeper into the liquid in some places than in others. Consequently, small elements of liquid may become partly surrounded by hot gases and detonate *in situ*. This will produce local high-pressure regions within the surrounding combustion, and the inhomogeneity of the propagation will be maintained.

---

* Or those containing a liquid explosive such as blasting gelatine.

† See Appendix.

‡ It is to be observed that after detonation has occurred in a thin layer of finely crystalline mercury fulminate or lead azide confined in the same manner as the nitroglycerine layers, the confining surfaces are covered with pits in a similar fashion; each pit presumably corresponds to the detonation of an individual crystal in contact with the surface (Vines, 1944).

In view of the essentially discontinuous nature of the propagation it is surprising that the 'overall' velocity should be so uniform; it appears that, whatever their nature, there must be some degree of regularity in the occurrence of the discontinuities. The mechanism suggested above provides no explanation for this, except in so far as it is possible that the liquid may be in some (unknown) way 'prepared' for reaction by an invisible shock wave which travels at constant velocity ahead of the explosion front (cf. Bone *et al.* 1935) and determines the rate of propagation.

The work described in this paper was carried out as part of the research programme of the Section of Tribophysics of the Council for Scientific and Industrial Research, Australia. The authors gratefully acknowledge the helpful criticism of Dr S. H. Bastow and Dr J. S. Anderson. Our thanks are due to Professor E. J. Hartung for laboratory facilities in the Chemistry Department of the University of Melbourne, and to Mr M. E. Hargreaves for his assistance in various metallurgical investigations associated with the work.

APPENDIX

The impulsive pressure exerted by the detonation

It was of interest to attempt an estimation of the impulsive pressure involved in the production of the pits in a metal surface by the detonation. This was done by exploding layers of nitroglycerine confined between steel strips of increasing hardness. As the hardness of the metal is increased the pits become less distinct, until beyond a hardness of about 600 (Vickers) they are no longer observed.* Since the explosion is just incapable of causing deformation of a surface of this hardness, the (dynamic) flow pressure of the metal must correspond roughly to the explosive pressure exerted. A static hardness of 600 (Vickers) is equivalent to 60,000 atmospheres. As the apparent hardness increases, in general, with decreasing duration of application of the pressure, it is clear that the value of 60,000 atmospheres represents the lowest possible value for the impulsive pressure.

It is interesting to compare this value with that which might be expected if the detonation were propagated through the explosive as a uniform wave front. The total pressure effect of a detonation wave is the sum of the hydrostatic pressure in the wave front, and the impulse due to the motion of the Schwaden. This has been shown by Becker (1922) to be given by the expression

$$i = P\frac{\sigma_1}{\sigma_2}, \tag{1}$$

---

* Metallurgical examination of the steel strips has shown that the hardness of the surface layers is not appreciably altered by the explosion, when the strips remain unmarked.

where P is the hydrostatic pressure in the wave front (the 'detonation pressure'), σ_1 the specific volume of the explosive, and σ_2 that of the Schwaden in the wave front. From this it is easily shown that

$$i = P\frac{D}{D-W}, \tag{2}$$

where D is the detonation velocity and W the velocity of forward movement of the Schwaden behind the detonation front.

Furthermore it may be shown that

$$P = \rho D W, \tag{3}$$

and consequently

$$i = \rho\frac{D^2 W}{D-W}, \tag{4}$$

where ρ is the density of the explosive (1·6 for nitroglycerine).

Thus from values of ρ, D and W, it is possible to calculate the total pressure from equation (4).

On substituting in equation (4) the value of 200 m./sec. obtained for W (§ 3), a value of 6500 atmospheres is obtained for the total pressure. The values corresponding to $W = 300$ and 400 m./sec. are 10,000 and 14,500 atmospheres respectively. It is clear therefore that, on the basis of the value for the Schwaden velocity obtained from the photographs the pressure expected from a uniform detonation wave is in the region of 10,000 atmospheres. This figure is considerably lower than the measured value of $\nless 60{,}000$ atmospheres for the pressure involved in the production of the pit marks.*

The value of 200 to 400 m./sec. obtained for W is very rough because of the difficulty of measuring it from the photographs. However, that this is a reasonable value may be seen from the following considerations. The Schwaden velocity W of an explosive may be calculated from physical and thermochemical data and the hydrodynamic theory of detonation (Schmidt 1936; Roth 1940). (The corresponding value of P may be calculated from equation (3).) Table 2 gives values of W calculated by various authors, together with the corresponding values of D, for liquids, and for solid explosives in the region of their maximum charge density.

It will be seen from table 2 that the calculated value of the Schwaden velocity is about 1/7 to 1/8 that of the detonation velocity. The value of 200 to 400 m./sec. for the Schwaden velocity of the low-velocity detonation of nitroglycerine is therefore compatible with the general behaviour. This affords indirect supporting evidence for the measured value of the Schwaden velocity and therefore for the figure of $\sim 10{,}000$ atmospheres for the calculated total impulsive pressure.† The high pressure involved in the pit marking, together with the absence of any substantial variation in the detonation velocity when the thickness of the layer is varied by a factor of 50 or more renders it improbable that the discontinuous nature of the propagation is merely a consequence of the thinness of the layer of explosive, since if this were so the pressure would not be greater than the calculated pressure, and the velocity would be expected to rise with increasing thickness of the layer.

---

* Even if the Schwaden velocity were half the detonation velocity, which appears most unlikely from the photographs, the calculated value for the total pressure would be only 51,000 atmospheres.

† Strictly speaking, equation (1) gives the pressure in the direction of propagation. It is probable that the pressure on the confining surfaces is between this value and the hydrostatic pressure, i.e. lower than 10,000 atmospheres.

TABLE 2

explosive	charge density g./c.c.	detonation velocity (measured) *D* m./sec.	Schwaden velocity (calculated) *W* m./sec.	*D*/*W*	author
nitroglycerine	1·59	7700	930*	8·3	Lawrence (1944)
tetranitromethane (T.N.M.)	1·64	6400	735	8·7	Roth (1941)
T.N.M. nitrobenzene 90/10	1·58	7100	930	7·6	Roth (1941)
T.N.M. nitrobenzene 50/50	1·37	7050	1085	6·5	Roth (1941)
T.N.M. nitrobenzene 30/70	1·3	5800	842	6·9	Roth (1941)
T.N.T.	1·59	6900	893	7·7	Schmidt (1936)
			855	8·1	Langweiler (1938)
P.E.T.N.	1·6	7900	1090	7·4	Schmidt (1936)
tetryl	1·6	7470	1000	7·5	Schmidt (1936)
picric acid	1·63	7210	940	7·7	Schmidt (1936)

* Calculated from *P* by means of equation 3.

It seems, therefore, that the detonation zone contains numerous local regions of considerably higher pressure than that expected from a uniform wave of the same velocity. The value of the impulsive pressure of the high-velocity detonation obtained from equation (2) is 134,000 atmospheres. It is not improbable that the process responsible for the pit markings is actually the high-velocity detonation.

REFERENCES

Becker, R. 1922 *Z. Phys., Lpz.*, **8**, 321.
Bone, W. A. & Fraser, R. P. 1929 *Phil. Trans.* A, **228**, 197.
Bone, W. A. & Fraser, R. P. 1931 *Phil. Trans.* A, **230**, 363.
Bone, W. A., Fraser, R. P. & Wheeler, W. H. 1935 *Phil. Trans.* A, **235**, 29.
Bowden, F. P., Eirich, F., Ferguson, A. E. & Yoffe, A. 1943*a* *Bull. Coun. Sci. Industr. Res., Aust.*, no. 167.
Bowden, F. P., Eirich, F., Mulcahy, M. F. R., Vines, R. G. & Yoffe, A. 1943*b* *Bull. Coun. Sci. Industr. Res., Aust.*, no. 173.
Bowden, F. P., Mulcahy, M. F. R., Vines, R. G. & Yoffe, A. 1947*a* *Proc. Roy. Soc.* A, **188**, 291.
Bowden, F. P., Mulcahy, M. F. R., Vines, R. G. & Yoffe, A. 1947*b* *Proc. Roy. Soc.* A, **188**, 311.
Campbell, C. & Finch, A. C. 1928 *J. Chem. Soc.* p. 2094.
Campbell, C. & Woodhead, D. W. 1926 *J. Chem. Soc.* p. 3010.
Chariton, J. B. & Ratner, S. B. 1943 *C.R. Acad. Sci. U.R.S.S.* **41**, 293.
Dserschkowitsch, A. A. & Andreev, K. K. 1930 *Z. ges. Schiess- u. Sprengstoffw.* **25**, 353, 400.
Jost, W. 1939 *Explosions- und Verbrennungsvorgänge in Gasen.* Berlin: Springer.
Langweiler, H. 1938 *Z. techn. Phys.* **19**, 271.

Lawrence, R. W. 1944 *Geophysics*, **9**, 1.
Lewis, B. & Friauf, J. B. 1930 *J. Amer. Chem. Soc.* **52**, 3905.
Mulcahy, M. F. R. & Vines, R. G. 1947 *Proc. Roy. Soc.* A, **191**, 210.
Ratner, S. B. 1944 *C.R. Acad. Sci. U.R.S.S.* **42**, 265.
Roth, J. F. 1940 *Z. ges. Schiess- u. Sprengstoffw.* **35**, 198, 220, 243.
Roth, J. F. 1941 *Z. ges. Schiess- u. Sprengstoffw.* **36**, 4, 28, 52.
Schmidt, A. 1936 *Z. ges. Schiess- u. Sprengstoffw.* **31**, 8, 37.
Schmidt, A. 1938 *Z. ges. Schiess- u. Sprengstoffw.* **33**, 121.
Vines, R. G. 1944 Unpublished thesis.
Vines, R. G. & Mulcahy, M. F. R. 1946 *Nature*, **157**, 626.

DESCRIPTION OF PLATES 16 TO 18

PLATE 16

FIGURE 1. Patterns produced on metal strips by explosions in thin layers of nitroglycerine. *a*, the pit markings on a brass surface; *b*, *c* and *d*, the 'scratches' on lead-plated surfaces.

PLATE 17

Drum camera traces of explosions in thin layers of nitroglycerine. (The arrow indicates the direction of motion of the film.)

FIGURE 3. With glass support. Initiation by spark.

FIGURE 5. With 'perspex slit' support. (Point of initiation not visible.)

FIGURE 6. With 'perspex slit' and thin mica sheets. (In these experiments stable detonation was not set up.)

PLATE 18

FIGURE 7. Enlarged photograph of the 'scratches' on a lead-plated surface after explosion.

FIGURE 8. Explosion in an acetylene, oxygen mixture. Camera trace obtained by Bone & Fraser (1931).

FIGURE 9. 'Across the slit' photograph obtained with rotating drum camera. The dark vertical lines are due to the cracking of the perspex.

FIGURE 10. Enlarged photograph of the pit markings on a brass surface after explosion.

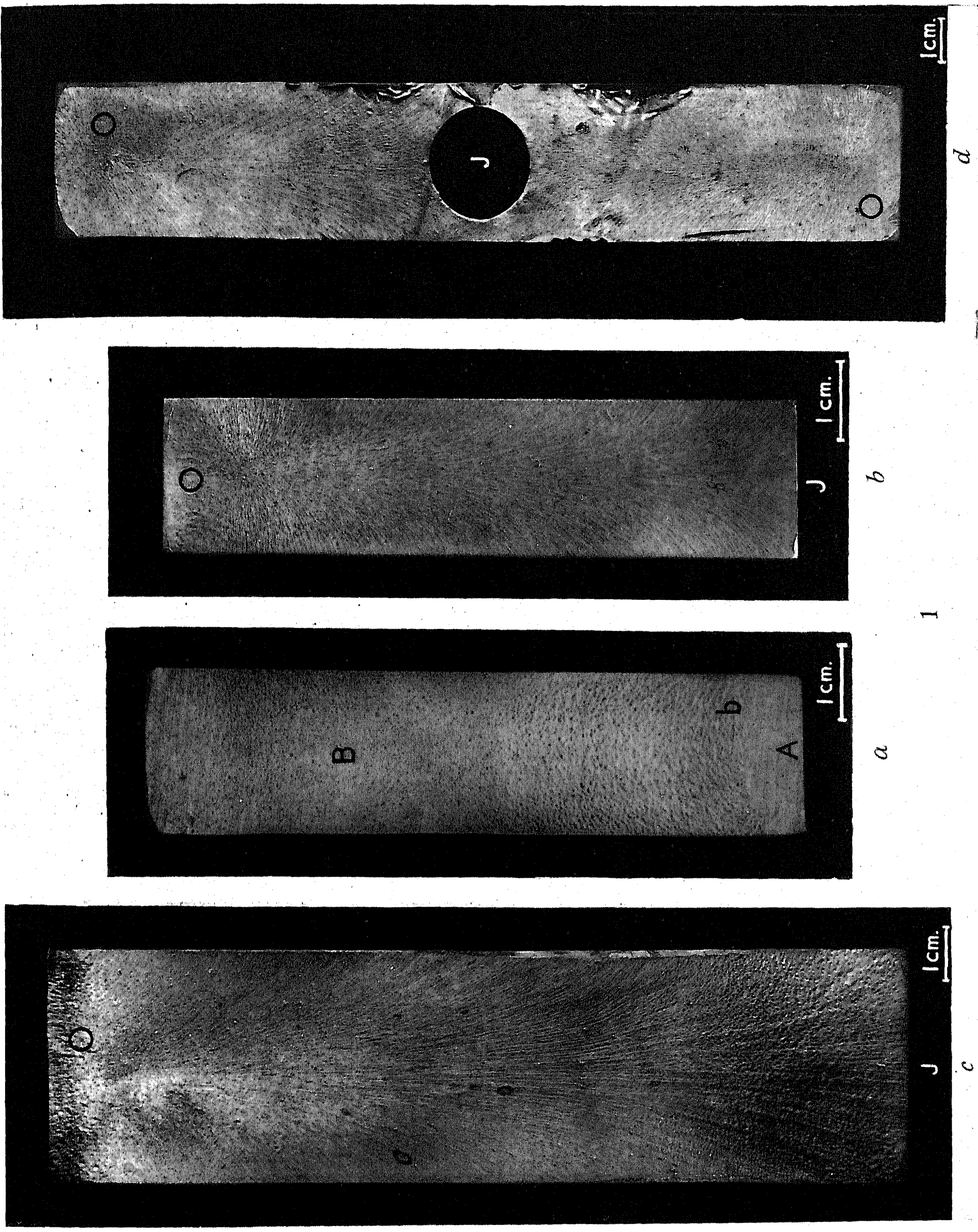

1

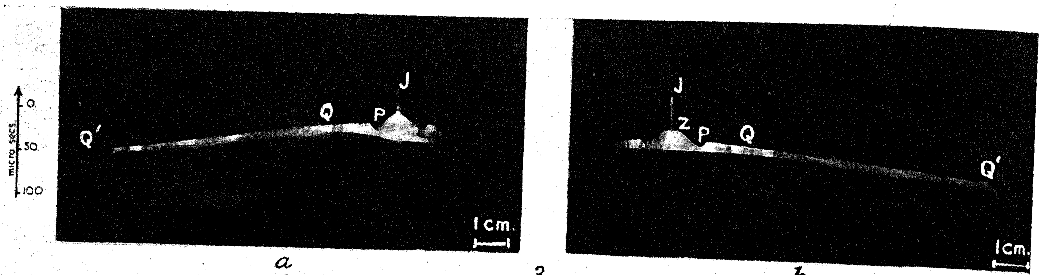
micro secs
0
50
100
Q′
Q
P
J
1 cm.
J
Z
P
Q
Q′
1 cm.

a 3 *b*

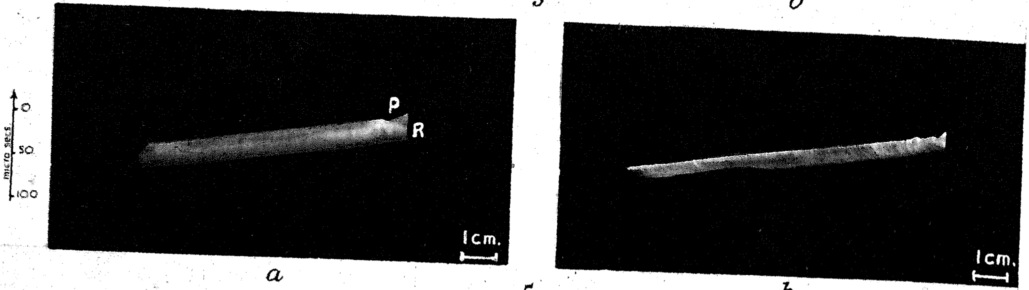
micro secs
0
50
100
P
R
1 cm.
1 cm.

a 5 *b*

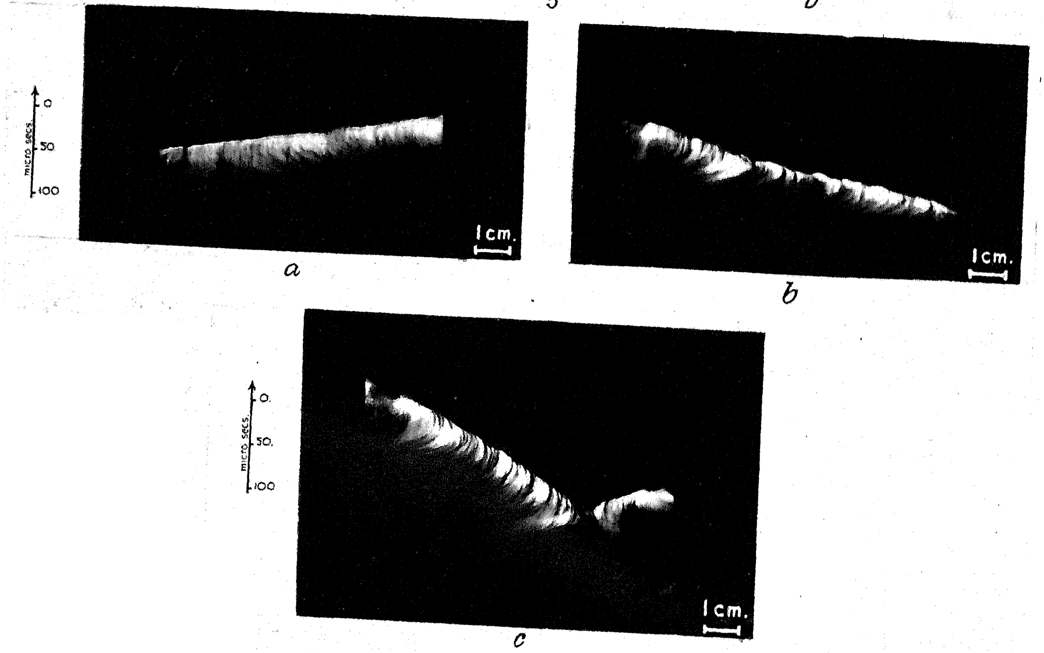
micro secs
0
50
100
1 cm.
1 cm.
micro secs
0.
50.
100
1 cm.

a *b*

c

6

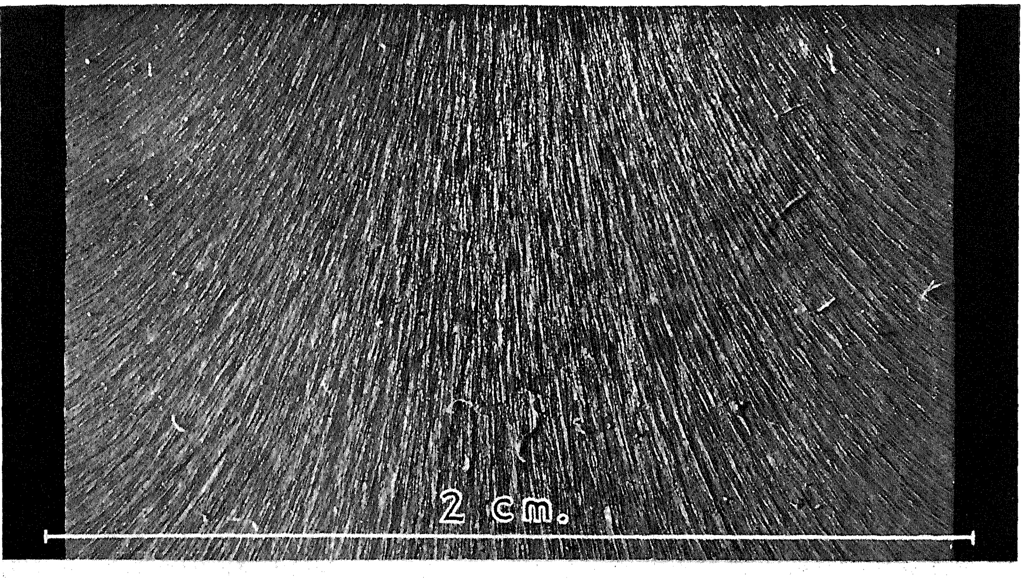

7

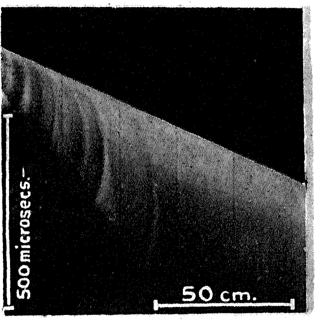

8

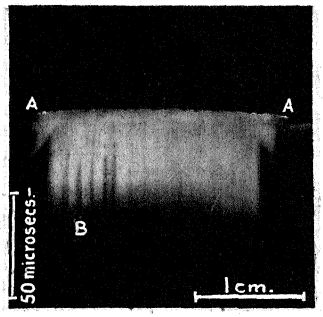

9

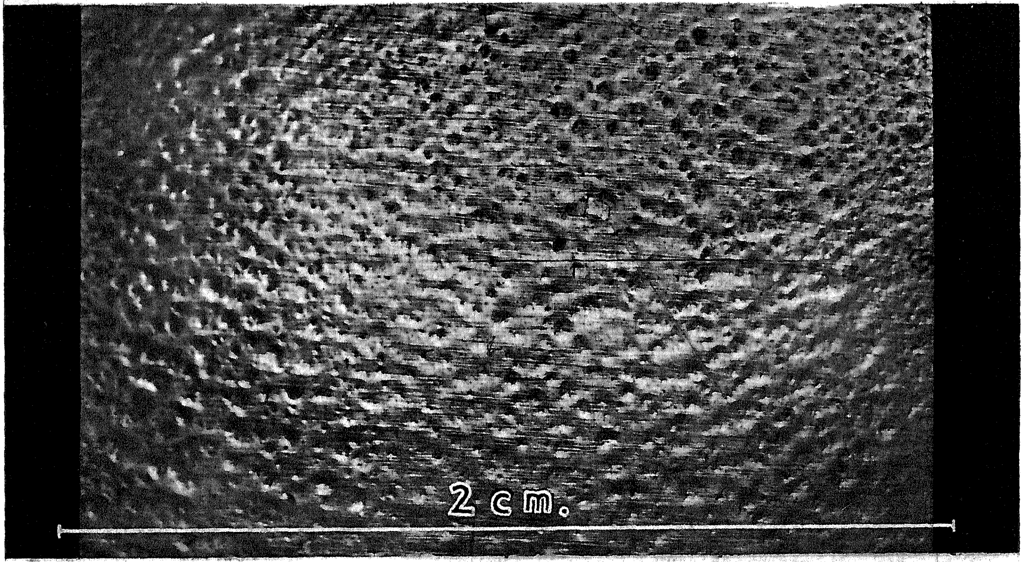

10

An electron-diffraction study of the heating of straight-chain organic films and its application to lubrication

By K. G. Brummage

(*Communicated by Sir Frank Smith, F.R.S.—Received* 6 *March* 1947)

Thin films of normal paraffins, fatty acids and esters have been examined by electron diffraction during heating upon a variety of metal surfaces. In all cases the films lost their orderly condensed structure at a comparatively low temperature, leaving expanded films of individual molecules.

The disorientation temperatures observed depended upon the chemical composition and thickness of the films, and upon the substrate metal. Evidence has been obtained of the formation of metallic soaps when fatty acid films are deposited upon reactive surfaces such as copper, cadmium and mild steel. Close agreement has been found between disorientation temperatures and the temperatures of friction discontinuities measured by other workers using Bowden-Leben type friction apparatus.

Introduction

In work described in a previous paper (Brummage 1947), electron-diffraction technique was used to investigate the effect of heat upon thin films of normal paraffins deposited on stainless steel and copper. As a result, it was postulated that at comparatively low temperatures the paraffin films lost their orderly structure, or, to use the terms applied to monolayers upon water, they changed from a condensed to an expanded state.

Similar studies have now been made of films of normal paraffins, fatty acids and esters upon polished surfaces of aluminium, cadmium, copper, nickel, silver, mild steel and stainless steel.

It was felt that the results of these experiments should bear some relationship to the frictional behaviour of the same lubricant-metal combinations, and a comparison has therefore been made between the electron-diffraction measurements and friction data obtained by various workers using Bowden-Leben type apparatus.

Apparatus

The electron-diffraction camera and the heated reflexion fittings were the same as those used in the earlier work on normal paraffins.

Materials and specimen preparation

The metals employed as substrates were of at least 99 % purity, except in the cases of mild and stainless steel. The substances deposited upon them were mostly synthesized in the laboratories of the Anglo-Iranian Oil Company at Sunbury-on-Thames, and special care was taken to ensure that they were of high purity. They are listed in table 1 together with their melting-points, as measured at Sunbury.

The substrate surfaces were metallographically polished, and films for reflexion purposes were formed on them either by the Langmuir-Blodgett method, using monolayers deposited on water, or by direct deposition upon the metal from isohexane, as previously described (Brummage 1947). No differences were observed in the disorientation temperatures of similar specimens prepared by the two techniques. The second method was used to much the greater extent, owing to its simplicity and speed.

TABLE 1. THE FILM MATERIALS EMPLOYED

substance	m.p. (° C)	substance	m.p. (° C)
n-tetratriacontane ($C_{34}H_{70}$)	72	palmitic acid ($C_{16}H_{32}O_2$)	64
n-triacontane ($C_{30}H_{62}$)	65	cetyl palmitate ($C_{16}H_{31}O_2C_{16}H_{33}$)	54
n-tetracosane ($C_{24}H_{50}$)	50	ethyl stearate ($C_{18}H_{35}O_2C_2H_5$)	33
behenic acid ($C_{22}H_{44}O_2$)	78	methyl stearate ($C_{18}H_{35}O_2CH_3$)	38
stearic acid ($C_{18}H_{36}O_2$)	72		

EXPERIMENTAL RESULTS

The substances chiefly studied were normal tetratriacontane, stearic acid, methyl stearate and ethyl stearate. Films of these materials all gave diffraction patterns of the layer-line type, indicating the presence of crystals orientated so that the long axes of the molecules were normal to the surface. When such a film was heated, the bright parts of the pattern gradually became diffuse, and eventually disappeared, leaving an apparently blank screen. On allowing the specimen to cool, the diffraction pattern returned, showing that the change was due simply to disorientation, and not to volatilization.

The disorientation temperatures are plotted in figures 1 to 7 as functions of film thickness, in numbers of monolayers, for each compound upon each substrate. In all cases the curves have the same shape; the disorientation temperature was lowest for the monolayer and increased with thickness to a steady value which remained constant for films up to 100 molecular layers in thickness.

Disorientation was always well defined using tetratriacontane, but with the more diffuse patterns from stearic acid and the stearates disorientation was more difficult to detect, especially in thin films. The data given include all the readings obtained, the error in general being about ± 2° C. However, with some thinner stearic acid and stearate films the error is probably ± 5° C, or even more. Some of the curves are absent or incomplete because the patterns were in those cases too faint and diffuse to allow a fade point to be distinguished.

CORRELATION OF RESULTS WITH FRICTION DATA

In order to study the role of the disorientation temperature in lubrication, measurements are required of the coefficient of friction between sliding lubricated surfaces as a function of temperature. A considerable amount of such data has been published in recent years as a result of work with friction apparatus of the type

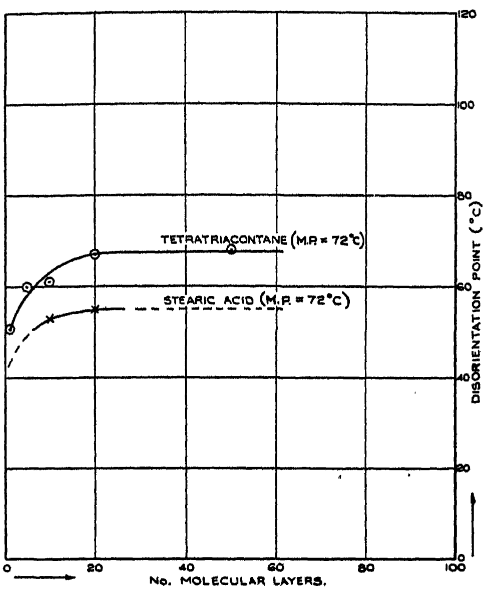

FIGURE 1. Disorientation points of films on aluminium.

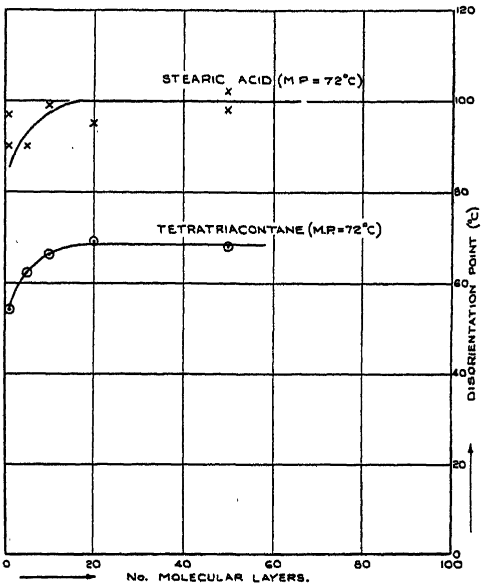

FIGURE 2. Disorientation points of films on cadmium.

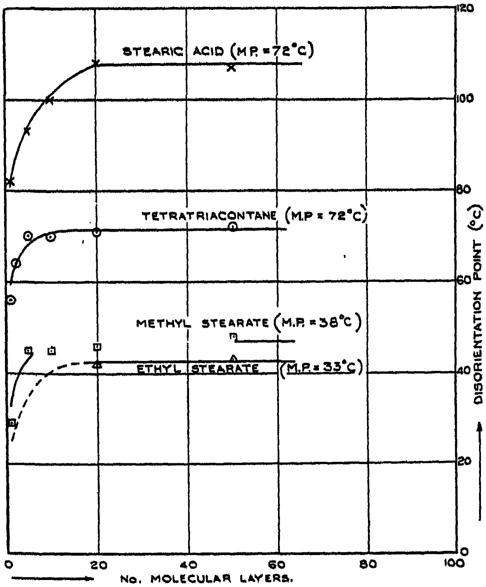

FIGURE 3. Disorientation points of films on copper.

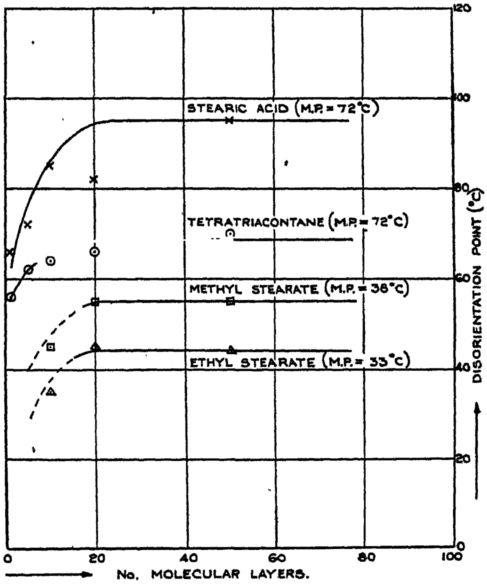

FIGURE 4. Disorientation points of films on nickel.

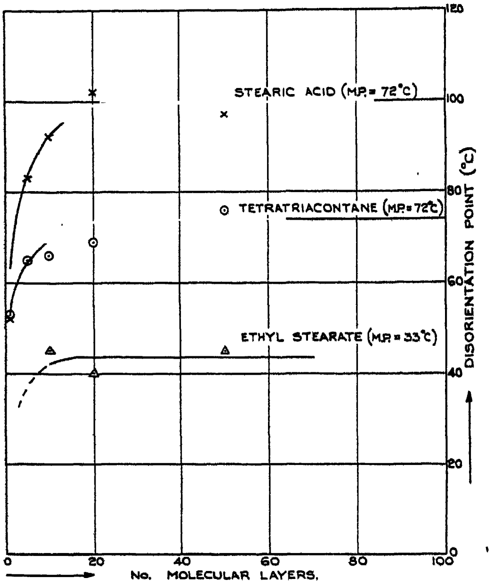

FIGURE 5. Disorientation points of films on silver.

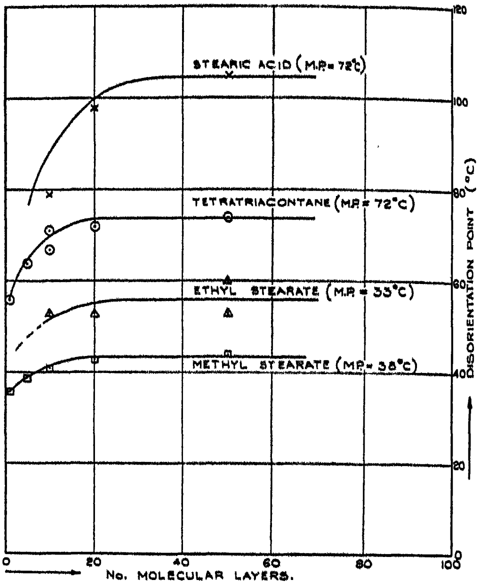

FIGURE 6. Disorientation points of films on mild steel.

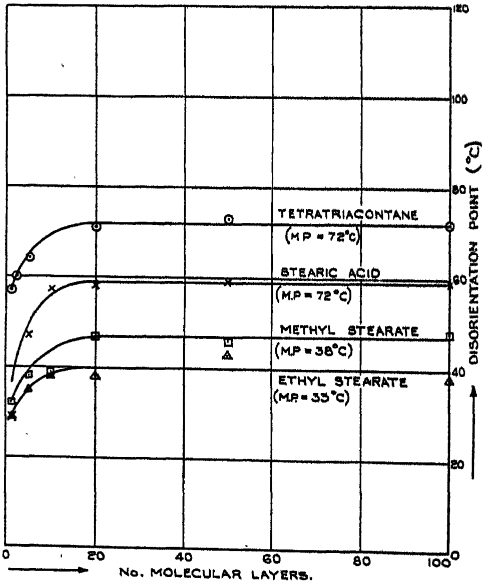

FIGURE 7. Disorientation points of films on stainless steel.

described by Bowden & Leben (1939). This apparatus is particularly suitable because the sliding speed is very low, so that frictional heating is small, and the measured temperature of the sliding members approximates closely to the actual general surface temperature, which is that determining the type of lubricant film. High temperatures occur at points of metallic contact where the film has broken down, but the number and frequency of such contacts is a minimum at low speeds.

The deflexion of the slider in the Bowden-Leben apparatus is a measure of the coefficient of friction. With some lubricants this deflexion is steady, but with others the slider reaches a maximum deflexion and then slips back. The process is repeated indefinitely, giving rise to the phenomenon known as 'stick-slip'. For experiments upon the effect of heat on the coefficient of friction measured by this type of apparatus, the flat moving plate is electrically heated and its temperature measured by a thermocouple. It is found that as the temperature goes up the type of sliding changes from smooth to stick-slip at a definite temperature, known generally as the transition temperature, and that this change is reversed when the surfaces cool below the transition point. In addition, a discontinuity is often observed in the smooth friction operative at lower temperatures, at which the friction suddenly increases, and this change is also reversible on cooling. It is generally assumed that the transition point corresponds to the desorption of the lubricant film, and Frewing (1943) has suggested that the lower temperature discontinuity is due to expansion of the lubricant film. If this is so, then this discontinuity should correlate with the disorientation points shown in figures 1 to 7.

Frictional data have been collected from the papers and reports of Frewing (1943), Hughes & Whittingham (1942), Greenhill (1945), Greenhill & Gregory (1945) and Ballantyne (1945). Only experiments where both sliding surfaces were of the same material have been considered; data for mild steel and stainless steel in the presence of stearic acid have been omitted because of the wide discrepancies between different workers. For example, Hughes & Whittingham give the transition point for a thick film of stearic acid on stainless steel as 98° C, while Greenhill & Gregory give 200° C. These discrepancies may be due to the fact that the substrate metals are not pure materials.

The collected data relevant to the present experiments from the above papers are given in table 2, together with the disorientation points of the films, as obtained from the curves of figures 1 to 7. The number of molecular layers given is the total number deposited between the surfaces.

The bracketed figures give the sources of the friction observations, and the papers to which they refer are listed at the foot of the table.

It is apparent from table 2 that the disorientation temperatures measured by electron diffraction correspond with the discontinuity in smooth friction observed on the Bowden-Leben type of apparatus; this confirms Frewing's (1943) suggestion that this change of friction is due to a change of lubricant film structure from a condensed to an expanded state.

Where no figures are given in table 2 for the smooth friction discontinuity temperature, no data were available in the literature. In some cases this was probably because the change in friction was too small to be recorded. In others, notably stearic acid on nickel and silver, transition occurred approximately at the melting-point, while disorientation was not observed until a considerably higher temperature was reached. No smooth friction discontinuity could therefore be expected. The significance of these high disorientation temperatures is considered in the following discussion.

TABLE 2. FRICTION DATA AND DISORIENTATION POINTS

lubricant	surface	number of molecular layers	transition point (° C)	discon-tinuity (° C)	disori-entation point (° C)
tetratriacontane	any metal	excess	72 (1, 4)	—	68–74
stearic acid	cadmium	3	—	90 (3)	90
		excess	120 (3)	95 (4)	100
	copper	3	—	90 (3)	90
		excess	150 (4)	108 (4)	108
	nickel	excess	75 (4)	—	95
	silver	7	68 (3)	—	88
		13	70 (3)	—	95
		excess	70 (3)	—	100
		excess	77 (4)	—	100
methyl stearate	mild steel	excess	95 (1)	—	44
	stainless steel	2	50 (1)	25 (1)	35
		excess	90 (1)	—	47
ethyl stearate	copper	excess	34 (3)	—	41
	mild steel	excess	200 (2)	—	56
	stainless steel	2	60 (1)	30 (1)	31
		excess	88 (1)	—	40

References: (1) Frewing (1943); (2) Greenhill (1945); (3) Greenhill & Gregory (1945); (4) Ballantyne (1945).

DISCUSSION OF RESULTS

Whilst the previous section has established a connexion between electron-diffraction and friction measurements, it has thrown little light upon the factors determining the disorientation temperatures observed, nor upon their dependence on film thickness. Table 3 summarizes the general position by giving the disorientation points of thick films on each metal, the bulk melting-points of the film constituents, and those of the stearates of the substrate metals, where these are known.

TABLE 3. THICK FILM DISORIENTATION TEMPERATURES (° C)

	film				
metal	tetratria-contane	stearic acid	methyl stearate	ethyl stearate	m.p. of metal stearate
aluminium	68	55	—	—	—
cadmium	68	100	—	—	—
copper	72	108	47	43	115–120
nickel	69	95	55	44	80–86
silver	74	100	—	44	205
mild steel	74	105	44	56	—
stainless steel	72	59	47	40	—
melting-point	72	72	38	33	—

At the disorientation temperature the surface structure changes, in general, from crystals to individual molecules, the surface behaviour of which will depend upon their constitution. Hence, disorientation temperatures should be connected with melting-points, any differences being due to surface influence.

Figure 8 shows typical graphs of $(T_D - T_M)$ plotted against the number of carbon atoms in the molecule, T_M being the melting-point and T_D the disorientation temperature of a thick film. The materials used to obtain the points shown were those given in table 1; the data employed in drawing the graphs are shown in table 4.

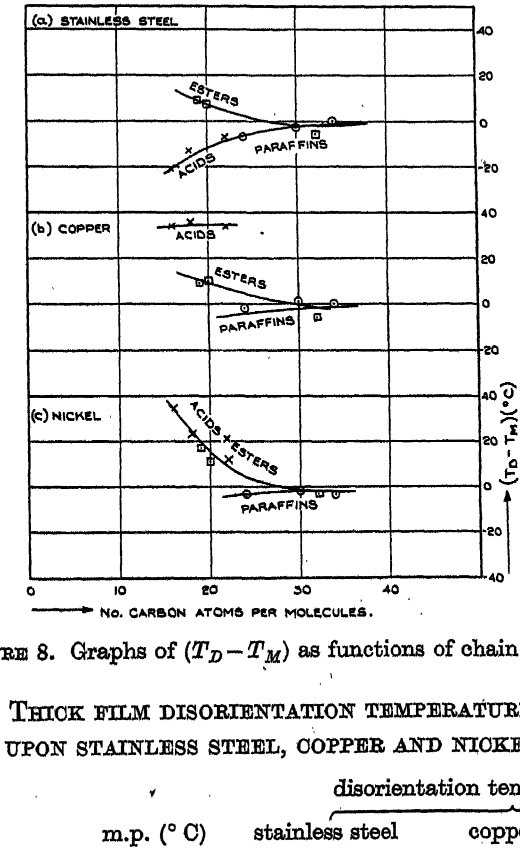

Figure 8. Graphs of $(T_D - T_M)$ as functions of chain length.

Table 4. Thick film disorientation temperatures of films upon stainless steel, copper and nickel

film material	m.p. (° C)	disorientation temperature (° C)		
		stainless steel	copper	nickel
tetratriacontane	72	72	72	69
triacontane	65	62	66	63
tetracosane	50	43	48	47
behenic acid	78	71	112	90
stearic acid	72	59	108	95
palmitic acid	64	43	98	98
cetyl palmitate	54	48	48	51
ethyl stearate	33	40	43	44
methyl stearate	38	47	47	55

The surfaces studied could be divided into three groups depending upon the values of $(T_D - T_M)$ for films deposited on them. The first group comprised stainless steel and aluminium, and was characterized by the fact that points due to fatty acids and paraffins lay on the same curve (see figure 8 (*a*)), whilst esters with short 'alcohol' chains lay on a second line tending to the paraffin-acid line as the 'alcohol' chain increased in length (*vide* cetyl palmitate, with 32 carbon atoms).

The second group consisted of copper, cadmium and mild steel, and the $(T_D - T_M)$ curves for copper are given in figure 8 (*b*). They are generally similar to figure 8 (*a*) except that the fatty acid points form a separate curve with $(T_D - T_M)$ equal to about 35, that is, the fatty acid disorientation temperatures are about 35° C above their melting-points on these metals.

The remaining metals examined, namely, nickel and silver, gave $(T_D - T_M)$ curves of the type shown in figure 8 (*c*), with the fatty acid points lying on the curve previously occupied only by ester points.

It will be noticed in figure 8 that normal paraffin and ester results vary little from one surface to another, the grouping being entirely due to differences in fatty acid behaviour. It is known that fatty acids form soaps upon suitable surfaces, with melting-points much higher than the free acids, and Bowden, Gregory & Tabor (1945) give the order of decreasing tendency to form soaps as: zinc, cadmium, copper, magnesium, iron, chromium, platinum, nickel, aluminium, silver.

They observed negligible reaction with lauric acid for platinum and the metals following it. Comparison of this list with the groups into which the metals examined have been divided makes it clear that the high disorientation temperatures on copper, cadmium and mild steel were due to soap formation. The melting-point of the copper soap is 115 to 120° C, so that the disorientation temperature of the stearate film lies below its melting-point; the behaviour of soap films is therefore similar to that of paraffin films. Hence, the surfaces may be divided into two general groups, namely,

group 1	group 2
aluminium	nickel
cadmium (soap)	silver
copper (soap)	
mild steel (soap)	
stainless steel	

In the first group, fatty acids or soaps exhibit similar disorientation behaviour to paraffins, and in the second they are similar to esters.

It is evident that disorientation is related to melting, and also that different metals influence the disorientation temperature by altering this relationship. The reason for the different behaviours of paraffin and ester crystals is not known, nor is the reason why fatty acids sometimes resemble esters and sometimes paraffins. It may be that the carboxyl groups are adjacent to the surface in the former case, and the ends of the long paraffinic chains in the other.

Two types of bonding can be visualized between organic molecules and solid surfaces:

(1) Simple cohesive or adsorptive forces such as those normally operative between molecules in a solid.

(2) Attachment of a chemical nature, which should be possible when the molecules contain carboxyl groups, the carboxyl groups then being adjacent to the surface.

Both these types of attachment are possible in dealing with individual molecules, that is, in expanded films, but when the molecules are grouped into crystals the bonding is in all probability cohesive, except, possibly, with fatty acids. In the case of acids, the carboxyl group is at one end of the molecule in the crystal, and can therefore lie adjacent to the surface, whereas in ester crystals it lies between the 'acid' and 'alcohol' chains, which are believed to be in line. These chains must therefore prevent any contact between the carboxyl group and the surface.

Consideration of the $(T_D - T_M)$ curves has shown that the behaviour of fatty acid films is not radically different from that of ester or paraffin films; hence, as with the latter materials, it is probable that the fatty acid crystals are cohesively attached to the substrate in a surface film.

Several conclusions worthy of note may be deduced from table 2:

(1) In most cases the transition temperature at which smooth sliding gives way to stick-slip motion in the Bowden-Leben apparatus is considerably above the disorientation temperature, indicating that adsorption of the individual molecules to the surface does occur above the disorientation point.

(2) With normal paraffins, the attachment of the molecules to the surface must be cohesive. The films of these materials become expanded near the melting-point and transition occurs at the melting-point.

(3) If transition at the melting-point is accepted as a criterion of a cohesively held expanded film, it follows that where the transition temperatures lie above both disorientation temperatures and melting-points, the expanded films are chemically adsorbed.

(4) In a few cases, notably stearic acid on nickel and silver, transition occurs at the melting-point, while disorientation is not observed until a higher temperature is reached. It is most probable that the adsorption is cohesive in nature and apparently sufficient to maintain a condensed film in the electron diffraction camera. It breaks down, however, under shear.

The reason for the dependence of disorientation temperature upon film thickness is not clear. The existence of the effect is confirmed by the excellent agreement in table 2 between friction discontinuities and disorientation points in very thin films. The same factors must be operative as in thick films, with the additional complication of changes in physical properties of crystals when only a few molecules thick.

SUMMARY

1. It has been demonstrated that disorientation at a characteristic temperature is quite general in thin films of normal paraffins, fatty acids and esters deposited on metals.

2. The results show that the disorientation temperature is invariably lowest for a monolayer quantity deposited on a given surface and increases with thickness to

a steady characteristic value, which may be above or below the melting-point of the material constituting the film.

3. The high disorientation temperatures of fatty acids deposited on cadmium, copper and mild steel are due to the formation of soap films.

4. The difference between the thick-film disorientation temperature and the melting-point of a given substance depends on its molecular weight and upon its nature, that is, whether it is a paraffin, a fatty acid, or an ester.

5. The metals studied may be divided into two groups, depending upon the thick film disorientation temperatures of fatty acids (or their soaps) deposited upon them. In the first, comprising aluminium, cadmium, copper, mild steel and stainless steel, the fatty acids or soaps become disorientated in thick films at temperatures below their melting-points, like the paraffins. Upon nickel and silver, however, their disorientation temperatures are above their melting-points, as with esters.

6. The measured disorientation temperatures correlate well with the discontinuity in smooth friction often observed in Bowden-Leben friction apparatus. It is thus confirmed that this discontinuity corresponds to the change of the lubricant film structure from a condensed to an expanded state.

7. The reasons for the dependence of disorientation temperature upon film thickness, and of thick-film disorientation temperature upon film constitution and substrate metal are unknown.

The writer wishes to thank the Chairman of the Anglo-Iranian Oil Company for permission to publish this paper, and for providing facilities for the work. He is also most grateful to Professor G. I. Finch, F.R.S., for his helpful discussions of the results and for his continued interest, and to Mrs H. M. Cooke, who carried out a high proportion of the experimental work.

References

Ballantyne 1945 *Lubrication and friction report*, no. 51, C.S.I.R. (Aust.).
Bowden, Gregory & Tabor 1945 *Nature*, **156**, 97.
Bowden & Leben 1939 *Proc. Roy. Soc.* A, **169**, 371.
Brummage 1947 *Proc. Roy. Soc.* A, **188**, 414.
Frewing 1943 *Proc. Roy. Soc.* A, **181**, 23.
Greenhill 1945 *Lubrication and friction report*, no. 47, C.S.I.R. (Aust.).
Greenhill & Gregory 1945 *Lubrication and friction report*, no. 48, C.S.I.R. (Aust.).
Hughes & Whittingham 1942 *Trans. Faraday Soc.* 38, 9.

On first order wave equations for elementary particles without subsidiary conditions

By E. Wild, *Trinity College, Cambridge*

(*Communicated by P. A. M. Dirac, F.R.S.—Received* 20 *March* 1947)

The possibility of extending the application of the formalism used for the electron and meson fields, as developed from the equation

$$\partial_k \beta^k \psi = i\kappa\psi$$

to other types of field, is investigated. It is shown that, subject to the conditions that (1) the equations must contain no subsidiary conditions, (2) either the total energy must be positive definite, or it must be possible to quantize the equations according to Fermi statistics without using an indefinite metric in Hilbert space, no such extension is possible.

1. Introduction

In setting up field equations which, on quantization, describe elementary particles of non-zero rest mass, three general methods have been used. One can start from a vector or a spinor field, which is required to satisfy a simple differential equation; from an invariant Lagrangian function, bi-linear or quadratic in the field components and their derivatives; or from the homogeneous first-order equation

$$\beta^k \frac{\partial\psi}{\partial x^k} = i\kappa\psi,$$

where the β^k are hyper-complex numbers on which certain restrictions must be placed to ensure the Lorentz invariance of the system, and κ is a real number.

Dirac (1936) and Fierz (1939) have investigated the application of the first method to particles of spin greater than one-half. The equations studied by them contain, in addition to the equations of motion which determine the development of the field from given initial conditions, subsidiary conditions which reduce the number of degrees of freedom. These subsidiary conditions cannot be obtained as quantum mechanical equations of motion, but have to be arbitrarily imposed in the quantized theory. Removal of the subsidiary conditions gives rise to indefinite total charge, in the case of half-integral spin, and to indefinite total energy in the case of integral spin.

Fierz & Pauli (1939) have shown that these equations can be derived from a Lagrangian function. The method adopted is to introduce auxiliary field functions, and to determine the coefficients in the Lagrangian so that the auxiliary fields vanish, and the subsidiary conditions are fulfilled, as a consequence of the variational equations. This means, however, that the equations of motion of the auxiliary fields cannot be obtained as quantum mechanical equations, and the number of degrees of freedom is less than the number of field components.

One form of the Dirac equation for the electron is of the type given for the third method. Kemmer (1939) has shown that the equations for mesons of spins zero and one can also be put in this form. In both cases the representation of the β^k can be chosen so that some of the components of ψ (which we shall call the redundant components) are defined explicitly in terms of the spatial derivatives of the others (the essential components), and the time derivatives of the essential components are given explicitly in terms of all the components and their spatial derivatives. The redundant components can thus be eliminated, and the whole of the equations of motion obtained as quantum equations. In the Dirac equation there are no redundant components.

The presence of subsidiary conditions is not important in the theory of fields without interaction, but when interactions with other fields are introduced it is essential that they be so chosen that they do not increase the number of degrees of freedom. Fierz & Pauli (1939) have shown that neglect of this condition leads to singularities in the solutions for weak interaction. It is, therefore, of interest to consider the extension of the third type of formalism to particles of higher spin, with the restriction that the equations shall not contain implicit subsidiary conditions.

Bhabha (1945) has investigated such an extension with the restriction (which holds in the electron and meson equations) that the infinitesimal operators of the representation of the Lorentz group contained in the algebra generated by the β^k should be given by

$$I_{kl} = \beta_k \beta_l - \beta_l \beta_k.$$

The results are of considerable interest in that some of the equations so obtained describe 'composite' particles which have states of different spin and rest mass, but which, in the state of lowest rest mass, have spin one-half. It is suggested that the proton and neutron might be described by one of these equations.

The equations, however, are such that the total energy and the total charge are both indefinite in all cases except the Dirac and the meson equations, and it is therefore impossible to obtain physically significant results from them by quantization by the usual methods. Bhabha has proposed quantization according to Fermi-Dirac statistics, using an indefinite metric in Hilbert space to overcome this difficulty, but the general interpretation of such a formalism is somewhat uncertain. The purpose of the present paper is to investigate the possibility of extending the formalism of the meson and Dirac equations to particles of higher spin, without recourse to this device.

The general formalism in which we are interested is set out in § 3 in order to delimit clearly the field of inquiry. The rest of the paper is concerned with defining the permissible forms of the matrices used in the theory, and with the discussion of the results.

2. NOTATION

We use the four-vector notation with real x^0 co-ordinate:

$$x^0 = ct.$$

Small Latin letters from the middle of the alphabet will be used for vector indices. Such indices are raised and lowered by the metric tensors g^{ik} and g_{ik}, with

$$g^{00} = g_{00} = 1, \quad g^{ik} = g_{ik} = -\delta_{ik} \quad (\text{for } i \neq 0).$$

Small Greek letters will be used for spinor indices. They are raised and lowered by the metric forms $\epsilon^{\alpha\beta}$ and $\epsilon_{\alpha\beta}$:

$$\epsilon_{12} = \epsilon^{21} = -\epsilon_{21} = -\epsilon^{12} = 1, \quad \epsilon^{\alpha\beta} = \epsilon_{\alpha\beta} = 0 \quad (\text{for } \beta = \alpha).$$

The summation convention is extended to apply to a repeated index which appears once as a dotted and once as an undotted index:

$$v^{\alpha}u^{\dot{\alpha}} = v^1u^{\dot{1}} + v^2u^{\dot{2}}.$$

Small Latin letters from the end of the alphabet will be used as indices for general purposes and also sometimes as matrix suffixes. The Dirac bracket notation will also be used occasionally for component submatrices of the matrices under discussion.

The symbol $-$ denotes complex conjugate of a number, and Hermitian conjugate of a quantum mechanical operator. $\sim$ denotes the transpose of a matrix, and $*$ denotes Hermitian conjugate of a matrix defined by

$$\psi^* = \tilde{\bar{\psi}}.$$

3. THE FIELD EQUATIONS AND QUANTIZATION

We consider a set of functions of space-time, denoted by the single column matrix ψ, which satisfy the equations

$$\partial_k \beta^k \psi = i\kappa\psi, \tag{1}$$

where $\partial_k = \partial/\partial x^k$ and the β^k are linear operators on ψ with constant coefficients.

To ensure Lorentz invariance of the equations, we assume that, for each Lorentz transformation

$$x^i \to a^i_{.k} x^k,$$

there exists a transformation of ψ

$$\psi \to U\psi, \quad \beta^k \to U\beta^k U^{-1},$$

such that

$$a^i_{.k} U\beta^k U^{-1} = \beta^i. \tag{2}$$

We assume also the existence of a matrix A, which has the properties

$$U^*A = AU^{-1}, \tag{3a}$$

$$A\beta^k = \beta^{k*}A, \tag{3b}$$

where U is the transformation defined in (2).

All the equations (1), (2) and (3) are unaltered by the change of basis

$$\psi \to S\psi, \quad \beta^k \to S\beta^k S^{-1}, \quad U \to SUS^{-1}, \quad A \to S^{-1*}AS^{-1}.$$

It is important that the metric form A transforms differently from the linear operators of the system except in unitary transformations.

If such a matrix A exists, then A^* also satisfies (3). We can, therefore, without loss of generality, choose A to be Hermitian. This we shall do.

With these assumptions we can define a stream-vector and a momentum-energy tensor for the field ψ by

$$s^k = \psi^* A\beta^k\psi, \tag{4}$$

$$T_i^{\cdot k} = \frac{1}{2i}\{\psi^* A\beta^k \partial_i\psi - (\partial_i\psi^*) A\beta^k\psi\}. \tag{5}$$

It follows from $(3a)$ and (2) that these quantities have the correct transformation properties, and from $(3b)$ and (1) that they obey the conservation laws

$$\partial_k s^k = 0 \quad \text{and} \quad \partial_k T_i^{\cdot k} = 0.$$

The quantization of the equations is now straightforward. We take as the Hamiltonian for the system

$$H = \iiint \mathscr{H}\, dV,$$

where

$$\mathscr{H} = -\frac{c}{2i}\sum_{k=1}^{3}\{\psi^* A\beta^k \partial_k\psi - (\partial_k\psi^*) A\beta^k\psi\} + c\kappa\psi^* A\psi. \tag{6}$$

Consider a representation of the β^k in which $A\beta^0$ (which is Hermitian by virtue of $(3b)$ and our choice of A) is diagonal, with diagonal elements, say, λ_r. Those equations of the set

$$\partial_k A\beta^k\psi = i\kappa A\psi \tag{7}$$

which correspond to zero values of λ_r constitute a set of inhomogeneous equations for the corresponding components of ψ which contain no time derivatives. If the equations can be solved, the solutions can be taken as definitions of these components, which are then redundant in the sense used in § 1.

The commutation rules

$$\left.\begin{aligned} \overline{\psi}_r(\mathbf{x},t)\,\psi_s(\mathbf{x}',t) - \psi_s(\mathbf{x}',t)\,\overline{\psi}_r(\mathbf{x},t) &= -\frac{1}{\lambda_r}\delta_{rs}\delta(\mathbf{x}-\mathbf{x}'), \\ \psi_r(\mathbf{x},t)\,\psi_s(\mathbf{x}',t) - \psi_s(\mathbf{x}',t)\,\psi_r(\mathbf{x},t) &= 0, \end{aligned}\right\} \tag{8a}$$

or

$$\left.\begin{aligned} \overline{\psi}_r(\mathbf{x},t)\,\psi_s(\mathbf{x}',t) + \psi_s(\mathbf{x}',t)\,\overline{\psi}_r(\mathbf{x},t) &= \frac{1}{\lambda_r}\delta_{rs}\delta(\mathbf{x}-\mathbf{x}'), \\ \psi_r(\mathbf{x},t)\,\psi_s(\mathbf{x}',t) + \psi_s(\mathbf{x}',t)\,\psi_r(\mathbf{x},t) &= 0, \end{aligned}\right\} \tag{8b}$$

($\mathbf{x}$ is the vector with components x^1, x^2, x^3) for values of r and s such that $\lambda_r \neq 0$, $\lambda_s \neq 0$, together with the quantum-mechanical equations of motion

$$\frac{1}{i}\frac{\partial\psi_r}{\partial t} = \psi_r H - H\psi_r \tag{9}$$

give the remaining equations of (7). But it will be shown in § 5 that in the cases with which we are concerned, A can be chosen to be non-degenerate, so that (1) follows from (7). The quantized theory is thus fully equivalent to the classical theory.

The commutation rules (8) can be written in matrix form

$$A\beta^0[\psi, \psi^*]A\beta^0 = \delta(\mathbf{x}-\mathbf{x}')A\beta^0, \tag{8c}$$

where $[\psi, \psi^*]$ is the matrix defined by

$$[\psi, \psi^*]_{rs} = \psi_r(\mathbf{x}, t)\,\overline{\psi}_s(\mathbf{x}', t) - \overline{\psi}_s(\mathbf{x}', t)\,\psi_r(\mathbf{x}, t).$$

In this form the commutation relations are invariant to change of basis.

To complete the theory it is necessary to establish the Lorentz invariance of the commutation relations. We do not consider this problem here.

It may happen that the equations for the redundant components are not in general consistent, and that the condition for consistency imposes restrictions on the permissible solutions for the essential components. This is one way in which implicit subsidiary conditions may arise. It will be shown in § 6 that this situation does not arise if β^0 satisfies a certain reality condition.†

The commutation relations (8a) are always consistent, since the eigenvalues of $A\beta^0$ are real, but the use of them gives indefinite total energy in the quantized theory unless the total energy in the classical theory is positive definite. The use of commutation relations (8b) makes it possible to use the well-known subtraction formalism to get positive definite energy in the quantized theory from a classical theory with indefinite energy, but these relations are self-consistent only if all the non-zero eigenvalues of $A\beta^0$ are positive. If, as a consequence of implicit subsidiary conditions, the components of ψ which correspond to negative eigenvalues of $A\beta^0$ are necessarily zero, it may still be possible to quantize according to Fermi statistics (8b), but corresponding subsidiary conditions must still be imposed in the quantized theory.

Pauli (1941) has shown that fields of half-integral spin always give indefinite energy, and that for integral spin quantization according to Fermi statistics is always inconsistent. We have to consider, therefore, only the eigenvalues of $A\beta^0$ for half-integral spin, and the sign of the total energy for integral spin.

4. CHOICE OF REPRESENTATION

In order to investigate further the matrices β^0 and A, we shall define the representation more precisely.

The conditions for Lorentz invariance (2), show that the components of ψ form the basis of a representation of the Lorentz group. We choose the representation of the β^k so that this representation of the Lorentz group is the direct sum of its irreducible constituents, all equivalent constituents are equal, and the representation of the rotation group contained therein is unitary.

---

† It can, in fact, be shown by similar methods that subsidiary conditions arise only if β^0 cannot be brought to diagonal form.

Further: Each irreducible representation $L'(k,l)$ of the complete Lorentz group with $k \neq l$ is to be the direct sum of two irreducible representations $L(k,l)$ and $L(l,k)$ of the proper Lorentz group. $L(k,l)$ is to be the direct product of $L(k,0)$ and $L(0,l)$, and the representative of the reflexion operator, T, defined by

$$T \text{ corresponds to } x^0 \to x^0, \quad x^i \to -x^i \quad (\text{for } i = 1, 2 \text{ or } 3)$$

is to be

$$\left.\begin{array}{l} \psi(k,l) \to a\psi(l,k), \quad \psi(l,k) \to a\psi(k,l) \quad (\text{for } k \neq l), \\ \psi_{rs}(k,k) \to b\psi_{sr}(k,k). \end{array}\right\} \tag{10}$$

In the second line of (10), the first suffix refers to the representation $L(k,0)$, and the second to $L(0,k)$. b may have the value $+$ or -1, and a the value 1 or i for $k+l$ half-integral, 1 for $k+l$ integral.

(In this representation the basis of $L(k,0)$ is a set of linear combinations of the independent components of a symmetrical spinor $a_{\alpha_1 \ldots \alpha_{2k}}$ and that of $L(0,k)$ the same set of linear combinations of the components of a symmetrical spinor $a^{\dot{\alpha}_1 \ldots \dot{\alpha}_{2k}}$).

The infinitesimal operators of a representation of the Lorentz group, I_{ik}, are defined by the correspondence

$$x^i \to x^i + \epsilon^i_{.k} x^k \text{ is represented by } (1 + \tfrac{1}{2}\epsilon^i_{.k} I_i^{k})$$
$$(\epsilon \text{ infinitesimal}, \ \epsilon_{ik} = -\epsilon_{ki}, \quad I_{ik} = -I_{ki}).$$

In the representation we have chosen I_{0k} is Hermitian, and I_{ik} skew-Hermitian $(k, i \neq 0)$.

For the validity of equations (2) and ($3a$) it is necessary and sufficient that the corresponding equations for the infinitesimal operators and for T should be true.

We shall restrict the choice of representation still further in § 5. The representation so defined will be called the standard representation.

5. THE METRIC FORM A

Equations ($3a$) give for I_{ik} the relations

$$AI_{0k} = -I_{0k}A, \quad AI_{ik} = I_{ik}A \quad (i, k \neq 0). \tag{11}$$

We also have from (10) and from the well-known properties of the Lorentz group

$$\left.\begin{array}{l} TI_{0k} = -I_{0k}T, \quad TI_{ik} = I_{ik}T \quad (i, k \neq 0), \\ TA = AT, \end{array}\right\} \tag{12}$$

We label the irreducible representations of the Lorentz group which occur in the representation of the β^k r, s, etc.; (11) and (12) give for the component of A which couples two such representations (suspending the summation convention)

$$A_{rs}(I_{0k})_s = -(I_{0k})_r A_{rs}$$
$$= T_r (I_{0k})_r T_r^{-1} A_{rs},$$

therefore

$$\left.\begin{array}{ll} & T_r^{-1} A_{rs} (I_{0k})_s = (I_{0k})_r T_r^{-1} A_{rs}; \\ \text{similarly} & T_r^{-1} A_{rs} (I_{ik})_s = (I_{ik})_r T_r^{-1} A_{rs} \quad (i, k \neq 0) \\ \text{and} & T_r^{-1} A_{rs} T_s = T_r T_r^{-1} A_{rs}. \end{array}\right\} \tag{13}$$

By a well-known theorem it follows from (13) that $T_r^{-1}A_{rs}$ is zero (and therefore A_{rs} is zero) unless the representations r and s are equivalent, in which case (since equivalent representations are equal) it is a multiple of the unit matrix.

$T^{-1}A$ can therefore be brought to diagonal form by a unitary transformation which does not affect the representation of the Lorentz group, and when this is done, A is of the form

$$A_{rs} = \lambda_r T_r \delta_{rs}. \tag{14}$$

By the further non-unitary transformation

$$\psi_r \rightarrow \sqrt{(|\lambda_r|)}\,\psi_r \quad (\text{for } \lambda_r \neq 0),$$

all the constants in (14) can be made equal to $+1$, 0, or -1 (or $\pm i$ for double-valued representations with $T^2 = -1$). (It is obvious that in an irreducible system of equations such as (1) only components with the same sign of T^2 occur. This possibility does not affect the subsequent arguments, and it will not be referred to again.)

If some λ, λ_r say, is zero, then, since $A\beta^k$ is Hermitian, for all s such that λ_s is not zero we must have $\beta^k_{sr} = 0$. The β algebra, therefore, is reducible (though not necessarily completely reducible). The equations for the components ψ_s do not contain ψ_r, and ψ_r does not enter in the momentum-energy tensor or the stream vector. The equations (1), therefore, are equivalent to those obtained from them by leaving out those equations which contain ψ_r, and A may be assumed to be non-degenerate.

We have also $A^2 = 1$, and (3b) gives also $A\beta^{k*} = \beta^k A$. From (2) T commutes with β^0, so that $T^{-1}A$ commutes with $\beta^{0*}+\beta^0$, and anti-commutes with $\beta^{0*}-\beta^0$. We have therefore (since $T^{-1}A$ is diagonal)

$$(\beta^0{}_{st})^* = (\beta^{0*})_{ts} \quad \text{or} \quad (\beta^0{}_{st})^* = -(\beta^{0*})_{ts}, \tag{15}$$

according as $T_s^{-1}A_s$ and $T_r^{-1}A_r$ have the same or opposite signs.

6. THE FORM OF β^k

In this section we need to make use of the matrices $u^\alpha(k)$, $v^\alpha(k)$, introduced by Dirac (1936), and further studied by Fierz (1939). The relevant properties of these matrices are

$u^\alpha(k)$ is a rectangular matrix with $2k+1$ rows and $2k$ columns,

$v^\alpha(k)$ is a rectangular matrix with $2k$ rows and $2k+1$ columns,

The matrices
$$S = (2k+1)^{-\frac{1}{2}}\begin{pmatrix} u_1(k+\frac{1}{2}) & u_2(k+\frac{1}{2}) \\ v_1(k) & v_2(k) \end{pmatrix},$$

$$S^{-1} = (2k+1)^{-\frac{1}{2}}\begin{pmatrix} v^1(k+\frac{1}{2}) & u^1(k) \\ v^2(k+\frac{1}{2}) & u^2(k) \end{pmatrix}(-1)^{2k+1},$$

define a transformation which reduces the representation $D(\frac{1}{2}) \times D(k)$ of the rotation group into the direct sum of its irreducible constituents $D(k+\frac{1}{2})$ and $D(k-\frac{1}{2})$:

$$\left.\begin{aligned} v_\alpha(\tfrac{1}{2})\, u^\beta(\tfrac{1}{2}) &= \delta^\beta_\alpha, \\ v^\alpha(k)\, u_\beta(k) + u^\alpha(k-\tfrac{1}{2})\, v_\beta(k-\tfrac{1}{2}) &= 2k\delta^\alpha_\beta(-1)^{2k}, \\ u^\alpha(k)\, v_\alpha(k) = 2k(-1)^{2k+1}, \quad v_\alpha(k)\, u^\alpha(k) &= (2k+1)(-1)^{2k+1}, \\ u^\alpha(k)\, u_\alpha(k-\tfrac{1}{2}) = v^\alpha(k)\, v_\alpha(k+\tfrac{1}{2}) &= 0. \end{aligned}\right\} \tag{16}$$

From the $u(k)$ and $v(k)$ we can form the single-column matrices P, and the single-row matrices R:

$$P^{\alpha_t}(k) = P^{\alpha_1\alpha_2\cdots\alpha_{2k}}(k) = u^{\alpha_1}(k)\, u^{\alpha_2}(k-\tfrac{1}{2}) \ldots u^{\alpha_{2k}}(\tfrac{1}{2}),$$
$$R^{\alpha_t}(k) = R^{\alpha_1\alpha_2\cdots\alpha_{2k}}(k) = v^{\alpha_1}(\tfrac{1}{2})\, v^{\alpha_2}(1) \ldots v^{\alpha_{2k}}(k),$$

which are symmetrical in all spinor indices, and which satisfy the relations

$$\left.\begin{aligned} P^{\alpha_t}(k) \times R_{\alpha_t}(k) = P^{\alpha_t}(k)\, R_{\alpha_t}(k) &= (2k)!\,(-1)^{k(2k-1)}, \\ R_{\alpha_t}(k)\, P^{\beta_r}(k) &= \{\Sigma(\mathrm{Perm}\,\alpha_t)\, \delta^{\beta_1}_{\alpha_1}\delta^{\beta_2}_{\alpha_2}\ldots\}\,(-1)^{k(2k-1)}. \end{aligned}\right\} \tag{17}\dagger$$

(In (16) and (17) the unit matrix of appropriate rank is to be understood as a factor on the right-hand side where necessary. We shall not in general mention such factors explicitly.)

The above relations were given by Fierz.

We introduce also the matrices Q:

$$\begin{aligned} Q^{\alpha_t}(j,l,k) &= Q^{\alpha_1\cdots\alpha_{2l}}(j,l,k) \\ &= v^{\alpha_1}(j+\tfrac{1}{2}) \ldots v^{\alpha_s}(j+\tfrac{1}{2}s)\, u^{\alpha_{s+1}}(j+\tfrac{1}{2}s) \ldots u^{\alpha_{2l}}(k+\tfrac{1}{2}), \end{aligned}$$

where $s = k+l-j$, $k+l \geqslant j$, $j+l \geqslant k$.

$Q^{\alpha_t}(j,l,k)$ is symmetrical in the indices $\alpha_1 \ldots \alpha_s$ and in the indices $\alpha_{s+1} \ldots \alpha_{2l}$. It will be shown in the Appendix that

$$\begin{aligned} &\Sigma(\mathrm{Perm}\,\alpha_t)\, Q^{\alpha_r}(j,l,k)\, Q_{\alpha_t}(k,l,j') \\ &\qquad = (-1)^{l(4k+2l-1)} \frac{(k+l-j)!\,(j+l-k)!\,(k+l+j+1)!}{(2j+1)\,(k+j-l)!}\, \delta_{jj'} \end{aligned} \tag{18}$$

$$Q^{\alpha_t}(j,k,0)\, Q_{\alpha_t}(0,k,j') = (-1)^{\{j\}} \frac{(k+j+1)!\,(k-j)!}{(2j+1)}\, \delta_{jj'} \tag{19}$$

($\{j\}$ means the integral part of j.)

(In (18) and (19) we use the convention that, when the representative index α appears in two places with different subscripts, say α_r and α_t, then the indices represented by α_t are an arbitrary permutation of those represented by α_r, and contraction over repeated indices is implied. The sum $\Sigma(\mathrm{Perm}\,\alpha_t)$ then extends over all such permutations. When the representative index has the same subscript in

---

† The sign factor in (17) is not given in the paper by Fierz.

both places, the indices represented by it are to have the same order in both places, and contraction is again implied.)

To return to the discussion of the β^k, equations (2) give, for the infinitesimal operators I_{kl}, the well-known relations

$$\beta^i I^{kl} - I^{kl}\beta^i = g^{ik}\beta^l - g^{il}\beta^k. \tag{20}$$

First we note that (20) defines β^k in terms of β^0 and I^{0k} $(k \neq 0)$. From (20) and (11) we have

$$A\beta^k = A\beta^0 I^{0k} + I^{0k} A\beta^0,$$

so that, in a representation in which $A\beta^0$ is diagonal, $(A\beta^k)_{rs} = 0$, where r and s refer to a row and a column for which $A\beta^0$ has the eigenvalue zero. If now β^0 is Hermitian in the standard representation, A and β^0 can be brought simultaneously to diagonal form by a unitary transformation (since in this representation A commutes with β^0). When this is done, equations (7) define the redundant components of ψ explicitly in terms of the space derivatives of the essential components, so that no subsidiary conditions arise from the elimination of the redundant components.

Bhabha (1945) has shown that from (20) it follows that the spinor components of the β^k must be of the form

$$\left.\begin{aligned}
\langle (k,l)_r \,|\, \beta^{\alpha\dot\beta} \,|\, (k-\tfrac{1}{2}, l+\tfrac{1}{2})_s\rangle &= c_{rs} u^{\alpha}(k) \times v^{\dot\beta}(l+\tfrac{1}{2}),\\
\langle (k,l)_r \,|\, \beta^{\alpha\dot\beta} \,|\, (k+\tfrac{1}{2}, l-\tfrac{1}{2})_s\rangle &= c_{rs} v^{\alpha}(k+\tfrac{1}{2}) \times u^{\dot\beta}(l),\\
\langle (k,l)_r \,|\, \beta^{\alpha\dot\beta} \,|\, (k-\tfrac{1}{2}, l-\tfrac{1}{2})_s\rangle &= c_{rs} u^{\alpha}(k) \times u^{\dot\beta}(l),\\
\langle (k,l)_r \,|\, \beta^{\alpha\dot\beta} \,|\, (k+\tfrac{1}{2}, l+\tfrac{1}{2})_s\rangle &= c_{rs} v^{\alpha}(k+\tfrac{1}{2}) \times v^{\dot\beta}(l+\tfrac{1}{2}),\\
\langle (k,l)_r \,|\, \beta^{\alpha\dot\beta} \,|\, (k',l')_s\rangle &= 0 \quad \text{unless} \quad k' = k \pm \tfrac{1}{2} \quad \text{and} \quad l' = l \pm \tfrac{1}{2};
\end{aligned}\right\} \tag{21}$$

here $(k,l)_r$ denotes an irreducible representation of the proper Lorentz group, and c_{rs} is an arbitrary complex number.

For consistency with the standard representation, we must choose the representation of the $u(k)$ and $v(k)$ in such a way that

$$\left.\begin{aligned}
u^{\alpha}(k) = u_{\dot\alpha}(k), \quad v^{\alpha}(k) = v_{\dot\alpha}(k),\\
\{u^{\alpha}(k)\}^* = (-1)^{2k+1} v_{\alpha}(k).
\end{aligned}\right\} \tag{22}$$

The first line of (22) ensures the consistency of the representation of T, and the second line that of the unitary property of the representation of the rotation group.

If r, t and s, u denote two pairs of inequivalent irreducible representations of the proper Lorentz group, such that r goes into t and s into u by reflexion, it follows directly from (22) and from the fact that T commutes with β^0, that we must have $c_{rs} = -c_{tu}$. The corresponding relations for coupling to a representation (k,k) are given at the end of this section.

From (22) and (15) it follows that $c_{rs} = \pm \bar{c}_{sr}(-1)^{2(k+l)}$, according as $T_r^{-1}A_r$ and $T_s^{-1}A^s$ have the same or opposite signs.

This completes the investigation of the form of A and β^k in the standard representation. To study the sign of the eigenvalues of $A\beta^0$, and the sign of the total energy, we transform to a representation in which the representation of the rotation group contained in each irreducible representation of the proper Lorentz group is the direct sum of its irreducible constituents, equivalent representations again being equal. In this representation, since A and β^0 both commute with I_{kl} $(k, l \neq 0)$, these matrices have no components which couple inequivalent representations of the rotation group, and a component which couples equivalent representations is a multiple of the unit matrix.

The transformation is given by

$$\beta^k \to S\beta^k S^{-1}, \quad A \to SAS^{-1},$$

with S defined by (for $k \geqslant l$)

$$\left.\begin{aligned} \langle j_r \mid S \mid (k,l)_s\rangle &= N(j,l,k)\, Q^{\alpha_t}(j,l,k) \times R^{\dot{\alpha}_t}(l)\, \delta_{rs}, \\ \langle (k,l)_r \mid S^{-1} \mid j_s\rangle &= (-1)^{4l(k+l)} N(j,l,k)\, Q_{\alpha_t}(k,l,j) \times P_{\dot{\alpha}_t}(l)\, \delta_{rs}, \\ N(j,l,k) &= \sqrt{\frac{(2j+1)\,(k+j-l)!}{(k+l-j)!\,(j+l-k)!\,(k+l+j+1)!}}. \end{aligned}\right\} \tag{23}$$

For $l > k$ we interchange l and k and interchange dotted and undotted indices in the definitions, and multiply by $(-1)^{2k}$.

It follows from (17), (18) and (22) that S and S^{-1} so defined are, in fact, reciprocal, and from (22) that the transformation is unitary. It is also obvious from the *raison d'être* of the $u(k)$ and $v(k)$ that the transformation gives the required reduction. We do not prove this formally, since we use only the fact that the transformation brings A and β^0 to the required form. This we now prove.

For the (j, j') component of the interchange operator in the representation (k, l) of the complete Lorentz group we have (omitting the normalizing factors $N(j, l, k)$ except in the final result)

for $k \neq l$:

$$\begin{aligned} &(-1)^{4l(k+l)+2l}\, Q^{\alpha_r}(j,l,k)\, Q_{\beta_t}(k,l,j') \times R^{\dot{\alpha}_r}(l)\, P_{\beta_t}(l) \\ &= (-1)^{4l(k+l)+2l}\, Q^{\alpha_r}(j,l,k)\, Q_{\beta_t}(k,l,j') \times R_{\alpha_r}(l)\, P^{\beta_t}(l) \\ &= (-1)^{l(4k+2l-1)}\, \Sigma(\text{Perm}\,\alpha_t)\, Q^{\alpha_r}(j,l,k)\, Q_{\alpha_t}(k,l,j') \\ &= \delta_{jj'}; \end{aligned} \tag{24a}$$

for $k = l$:

$$\begin{aligned} &(-1)^{8k}\, Q^{\alpha_r}(j,k,k)\, P_{\beta_t}(k) \times R^{\dot{\alpha}_r}(k)\, Q_{\beta_t}(k,k,j') \\ &= (-1)^{2k}\, Q^{\alpha_r}(j,k,k)\, P^{\beta_t}(k) \times R_{\alpha_r}(k)\, Q_{\beta_t}(k,k,j') \\ &= (-1)^{2k}\, Q^{\alpha_s}(j,2k,0)\, Q_{\alpha_s}(0,2k,j') \\ &= (-1)^{2k+j}\, \delta_{jj'}. \end{aligned} \tag{24b}$$

(In (24*a*) the component couples two inequivalent irreducible representations of the proper Lorentz group. In (24*b*) it is a multiple of part of the unit matrix of a single such representation.)

For the (j, j') component of the component of β^0 which couples the representations r $(= L(k,l))$ and s $(= L(k',l'))$ of the proper Lorentz group we have (again omitting normalizing factors except in the final results)

for $k = k' + \frac{1}{2}$, $l = l' + \frac{1}{2}$, $k \geqslant l$:

$$\begin{aligned}
&(-1)^{(4l-2)(k+l-1)}\sigma^0_{\sigma\dagger}\,c_{rs}\,Q^{\alpha_t}(j,l,k)\,u^{\sigma}(k)\,Q_{\beta_u}(k-\tfrac{1}{2},l-\tfrac{1}{2},j')\times R^{\dot{\alpha}_t}(l)\,u^{\dagger}(l)\,P_{\beta_u}(l-\tfrac{1}{2})\\
&= (-1)^{(2l-1)(2k+2l-1)}\,c_{rs}\,Q^{\alpha_t\sigma}(j,l+\tfrac{1}{2},k-\tfrac{1}{2})\,Q_{\beta_u}(k-\tfrac{1}{2},l-\tfrac{1}{2},j')\,R_{\alpha_t}(l)\,P^{\cdot\beta_u}_{\sigma}(l)\\
&= (-1)^{(2l-1)(2k+l-1)}\,c_{rs}\{\Sigma(\mathrm{Perm}\,\alpha_t)\,\delta^{\beta_1}_{\alpha_1}\ldots\delta^{\beta_{2l-1}}_{\alpha_{2l-1}}\,\epsilon_{\sigma\alpha_{2l}}\}\\
&\qquad\qquad\qquad\qquad\times Q^{\alpha_t\sigma}(j,l+\tfrac{1}{2},k-\tfrac{1}{2})\,Q_{\beta_u}(k-\tfrac{1}{2},l-\tfrac{1}{2},j')\\
&= (-1)^{2l(2k+l)+k-j}(k+l+j+1)\,(k+l-j)\,c_{rs}\\
&\qquad\qquad\qquad\qquad\times\Sigma(\mathrm{Perm}\,\alpha_t)\,Q^{\alpha_u}(j,l-\tfrac{1}{2},k-\tfrac{1}{2})\,Q_{\alpha_t}(k-\tfrac{1}{2},l-\tfrac{1}{2},j')\\
&= (-1)^{k+l+j}\,c_{rs}\sqrt{[(k+l+j+1)\,(k+l-j)]}\,\delta_{jj'};
\end{aligned}\tag{24c}$$

for $k = k' + \frac{1}{2}$, $l = l' - \frac{1}{2}$, $k > l + \frac{1}{2}$:

$$\begin{aligned}
&(-1)^{(4l+2)(k+l)}\sigma^0_{\sigma\dagger}\,c_{rs}\,Q^{\alpha_t}(j,l,k)\,u^{\sigma}(k)\,Q_{\beta_u}(k-\tfrac{1}{2},l+\tfrac{1}{2},j')\times R^{\dot{\alpha}_t}(l)\,v^{\dagger}(l+\tfrac{1}{2})\,P_{\beta_u}(l+\tfrac{1}{2})\\
&= (-1)^{(2l+1)(2k+l-1)}\,c_{rs}\,Q^{\alpha_t\sigma}(j,l+\tfrac{1}{2},k-\tfrac{1}{2})\,Q_{\beta_u}(k-\tfrac{1}{2},l+\tfrac{1}{2},j')\,R_{\alpha_t\sigma}(l+\tfrac{1}{2})\,P^{\beta_u}(l+\tfrac{1}{2})\\
&= (-1)^{(2l+1)(2k+l-1)}\,c_{rs}\,\Sigma(\mathrm{Perm}\,\alpha_t)\,Q^{\alpha_u}(j,l+\tfrac{1}{2},k-\tfrac{1}{2})\,Q_{\alpha_t}(k-\tfrac{1}{2},l+\tfrac{1}{2},j')\\
&= c_{rs}\sqrt{[(k+j-l)\,(j+l-k+1)]}\,\delta_{jj'};
\end{aligned}\tag{24d}$$

for the coupling $(k+\frac{1}{2},k)$ to $(k,k+\frac{1}{2})$:

$$\begin{aligned}
&\sigma^0_{\sigma\dagger}\,c_{rs}\,Q^{\alpha_t}(j,k,k+\tfrac{1}{2})\,u^{\sigma}(k+\tfrac{1}{2})\,P_{\beta_u}(k)\times R^{\dot{\alpha}_t}(k)\,v^{\dagger}(k+\tfrac{1}{2})\,Q_{\beta_u}(k+\tfrac{1}{2},k-\tfrac{1}{2},j')\\
&= -c_{rs}\,Q^{\alpha_t\sigma\beta_u}(j,2k+\tfrac{1}{2},0)\,Q_{\alpha_t\sigma\beta_u}(0,2k+\tfrac{1}{2},j')\\
&= (-1)^{\{j\}+1}\,c_{rs}(j+\tfrac{1}{2})\,\delta_{jj'};
\end{aligned}\tag{24e}$$

for the coupling (k,k) to $(k-\frac{1}{2},k+\frac{1}{2})$:

$$\begin{aligned}
&(-1)^{2k-1}\sigma^0_{\sigma\dagger}\,c_{rs}\,Q^{\alpha_t}(j,k,k)\,u^{\sigma}(k)\,P_{\beta_u}(k-\tfrac{1}{2})\times R^{\dot{\alpha}_t}(k)\,v^{\dagger}(k+\tfrac{1}{2})\,Q_{\beta_u}(k+\tfrac{1}{2},k-\tfrac{1}{2},j')\\
&= (-1)^{2k-1}\,c_{rs}\,Q^{\alpha_t\sigma\beta_u}(j,2k,0)\,Q_{\alpha_t\sigma\beta_u}(0,2k,j')\\
&= (-1)^{2k-1+j}\,c_{rs}\sqrt{[j(j+1)]}\,\delta_{jj'}.
\end{aligned}\tag{24f}$$

The coupling components for all other values of k and l can be obtained from the results given in (24*c*–*f*) by the use of (22). The component of $(k',l')\ldots(k,l)$ is $(-1)^{2k+2l}$ times that of $(k,l)\ldots(k',l')$. The component of $(l,k)\ldots(l',k')$ is -1 times that of $(k,l)\ldots(k',l')$ except when $k = l$ or $k' = l'$. The exceptional case is given by (24*f*), which corresponds on reflexion to the inverse of (24*d*) for $k' = l'$.

These last relations, together with those given earlier in this section between associated values of c_{rs}, give the correct commutation relations of β^0 with T and A. By use of (24) we can add to the relations between associated values of c_{rs}:

In all representations $r = L'(k,k)$ of the complete Lorentz group T must have the same sign for any one representation (say $D(0)$) of the rotation group; and if $s = L(k+\frac{1}{2},k-\frac{1}{2})$ and $t = L(k-\frac{1}{2},k+\frac{1}{2})$ are representations of the proper Lorentz which go into each other by reflexion and are coupled to r, then $c_{sr} = \mp(-1)^{2k} c_{tr}$ according as this sign is positive or negative.

The points in (24) which are of importance in the rest of the discussion are the dependence of sign on j in (24b) and (24e), and the fact that no (j, j) components in the range

$$k+l \geqslant j \geqslant |k-l|, \quad k'+l' \geqslant j \geqslant |k'-l'|$$

are zero.

It is convenient now to consider the cases of integral and half-integral spin separately.

7. HALF-INTEGRAL SPIN

We wish to find the forms of β^0 which give eigenvalues of $A\beta^0$ of one sign only. The β algebra may contain any representation $L'(k, l)$ of the complete Lorentz group such that $k+l$ is half-integral.

Suppose first that a representation $L'(k, l)$ with $k \neq l+\frac{1}{2}$, or a representation $L'(k+\frac{1}{2}, k)$ in which the two constituents $L(k+\frac{1}{2}, k)$ and $L(k, k+\frac{1}{2})$ are not coupled in β^0, is included. Then, in the standard representation, multiplication on the left by A interchanges the rows corresponding to the two constituents $L(k, l)$ and $L(l, k)$, and the corresponding diagonal elements of $A\beta^0$ are zero. $A\beta^0$, therefore, is a Hermitian matrix with zero diagonal elements at the intersection of some non-zero rows and columns. From this, by considering the (unitary) transformation which brings it from diagonal form to the form considered, it can easily be shown that $A\beta^0$ must have eigenvalues of both signs.

Suppose, then, that only representations $L'(k+\frac{1}{2}, k)$ in which the two constituents are coupled in β^0 occur. Then, if in any case $k \neq 0$, after the transformation (23) the diagonal elements of $A\beta^0$ arising from this coupling which correspond to representations $D(j+\frac{1}{2})$ of the rotation group with j even and j odd are of opposite sign (from (24)). $A\beta^0$, therefore, is a Hermitian matrix with diagonal elements of both signs, and it follows in the same way as above that it has eigenvalues of both signs.

The only permissible representation, therefore, is $L'(\frac{1}{2}, 0)$. It is obvious that a system in which this representation occurs more than once is reducible. If it occurs once only, the β^0 are determined to within a numerical factor by the considerations of § 6, and the equation so determined is the Dirac equation.

Our conclusion, then, is that the only irreducible equation for half-integral spin which satisfies our conditions is the Dirac equation. It should be noted that the reflexion operator is not completely determined by these considerations ($T^2 = \pm 1$).

8. INTEGRAL SPIN

For integral spin the condition to be satisfied is that the total energy must be positive. The β algebra may contain any representation $L'(k, l)$ of the complete Lorentz group such that $k+l$ is integral.

We consider first the case in which β^0 is Hermitian in the standard representation. In this case A commutes with β^0, and A and β^0 can be brought simultaneously to diagonal form by a unitary transformation from the standard representation.

Now for each eigenvalue $\lambda_r \neq 0$ of β^0, there is a solution of the field equations (1)

$$\psi_s = \text{const.} \exp\left(\frac{i\kappa ct}{\lambda_r}\right) \delta_{rs},$$

for which, if A and β^0 are both in diagonal form, the total energy has the same sign as the corresponding eigenvalue of A. Thus, for the total energy to be always positive, it is necessary that the eigenvalues of β^0 which correspond to negative eigenvalues of A should be zero. Since all the eigenvalues of A are $+1$ or -1 this implies

$$A\beta^0 = \beta^0. \tag{25}$$

But this relation is invariant to unitary transformations, and therefore, in the present case, must hold also in the standard representation.

Consider, then, a representation $L'(k', l')$ of the complete Lorentz group with $k' \neq l'$ contained in the β algebra. In the standard representation, multiplication on the left by A interchanges the rows which correspond to the two constituent representations of the proper Lorentz group, and (25) can be satisfied only for components of β^0 which couple both these constituents to the same representation of the proper Lorentz group. Inspection of the list of permissible couplings (21) shows that this representation must be of the type $L(k, k)$.

The only permissible couplings, then, are of the type $L'(k,k) \ldots L'(k', l')$. (24*b*) now shows that (25) is not satisfied unless the couplings are such that, after the transformation (23) they have a non-zero component in only one representation of the rotation group. This reduces the possibilities to $L'(\frac{1}{2}, \frac{1}{2}) \ldots L'(1, 0)$ and $L'(\frac{1}{2}, \frac{1}{2}) \ldots L'(0, 0)$, which may not occur together.

For each type it follows, as in the case of half-integral spin, that only one irreducible equation arises. These equations are respectively those for mesons of spin one and spin nought.

If β^0 is not Hermitian in the standard representation, assume first that it can be brought to diagonal form, and has real eigenvalues. Then, in the representation in which it is diagonal, it is Hermitian and therefore commutes with A. A and β^0 can again be brought simultaneously to diagonal form in such a way that the eigenvalues of A are $+1$ and -1, and for positive definite total energy (25) must hold. On transforming back to the standard representation, we have the relation

$$A\beta^0 = S^* S \beta^0, \tag{26}$$

where S is the matrix of the transformation.

$S^* S$ is a positive definite matrix, and (26) therefore implies that for any column, say the rth, of β^0 and $A\beta^0$, $(\beta^0_r)^* (A\beta^0)_r$ is greater than 0. Now in the standard representation as transformed by (23), those components of a column of β^0 and of the same column of $A\beta^0$ which correspond to a coupling $L'(k, l) \ldots L'(k', l')$ with $k \neq l$, $k' \neq l'$ are orthogonal; and those which correspond to $L'(k, k) \ldots L'(k', l')$ give opposite signs in representations of the rotation group $D(j)$ with j odd and j even. This again excludes all couplings except $L'(\frac{1}{2}, \frac{1}{2}) \ldots L'(1, 0)$ and $L'(\frac{1}{2}, \frac{1}{2}) \ldots L'(0, 0)$.

This time, however, these cases are excluded by the fact that the inverse couplings give opposite signs of $(\beta_r^0)^* (A\beta^0)_r$.

If β^0 can be brought to diagonal form but has complex eigenvalues, it can be shown that these must occur in conjugate pairs, and that the contribution to the energy density of the spatially constant solutions corresponding to such a pair, say r and s, is

$$\bar{\psi}_r \psi_s + \bar{\psi}_s \psi_r.$$

The sign of this contribution can be changed by changing the sign of ψ_r, and the total energy may therefore be negative.

Finally, if β^0 cannot be brought to diagonal form, the number of independent spatially constant solutions of equations (1) is less than the number of components whose time derivatives appear in the equations. It can, in fact, be shown by considering a representation in which β^0 is in the 'canonical form' for non-Hermitian matrices ($\beta^0_{rs} = 0$ unless $s = r$ or $r+1$, etc.) that the number of such solutions is less than the number of non-zero eigenvalues of $A\beta^0$. The equations therefore contain subsidiary conditions.

The conclusion for integral spin, then, is that the only irreducible equations which satisfy our conditions are the meson equations.

Appendix

We have to evaluate the expression

$$Q^{\alpha_r}(j, l, k)\, Q_{\alpha_t}(k, l, j'), \tag{A 1}$$

where the indices α_t are an arbitrary permutation of the indices α_r, and the summation convention is implied.

The expression is unaltered by permutation of v indices among themselves and of u indices among themselves. We therefore arrange them in the order

$$v^{\alpha_1}(j+\tfrac{1}{2}) \dots v^{\alpha_r}(j+\tfrac{1}{2}r)\, v^{\beta_1}\left(j+\frac{r+1}{2}\right) \dots v^{\beta_t}(j+\tfrac{1}{2}s)\, u^{\gamma_1}(j+\tfrac{1}{2}s) \dots$$
$$\times u^{\gamma_{t'}}\left(k+\frac{u+1}{2}\right) u^{\delta_1}(k+\tfrac{1}{2}u) \dots u^{\delta_u}(k+\tfrac{1}{2})\, v_{\delta_u}(k+\tfrac{1}{2}) \dots v_{\delta_1}(k+\tfrac{1}{2}u)\, v_{\beta_1}\left(k+\frac{u+1}{2}\right) \dots$$
$$\times v_{\beta_t}(j'+\tfrac{1}{2}s')\, u_{\gamma_1}(j'+\tfrac{1}{2}s') \dots u_{\gamma_{t'}}\left(j'+\frac{r+1}{2}\right) u_{\alpha_r}(j'+\tfrac{1}{2}r) \dots u_{\alpha_1}(j'+\tfrac{1}{2}),$$

where

$$s = k+l-j, \quad s' = k+l-j', \quad t = s-r = 2l-s'-u, \quad t' = s'-r = 2l-s-u.$$

r, u is the number of indices which occur as v, u indices in $Q^{\alpha_r}(j, l, k)$ and as u, v indices in $Q_{\alpha_t}(k, l, j')$.

(1) We can now remove the matrices with indices δ by the use of (16), replacing them by the factor

$$(-1)^{\frac{1}{2}u(4k+u+3)} \frac{(2k+u)!}{(2k)!}. \tag{A 2}$$

(2) We now interchange the factors $v^{\beta_t}(j+\frac{1}{2}s)$ and $u^{\gamma_1}(j+\frac{1}{2}s)$ in $Q^{\alpha_r}(j,l,k)$ by (16) giving

$$(-1)^{2j+s}(2j+s)\,\epsilon^{\gamma_1\beta_t}-u^{\beta_t}(j+\tfrac{1}{2}s-\tfrac{1}{2})\,v^{\gamma_1}(j+\tfrac{1}{2}s-\tfrac{1}{2}).$$

With the term $\epsilon^{\gamma_1\beta_t}$ we remove the factor $v_{\beta_t}(j'+\frac{1}{2}s')\,u_{\gamma_1}(j'+\frac{1}{2}s')$ from $Q_{\alpha_t}(k,l,j')$, giving the further factor

$$(-1)^{2j'+s'}(2j'+s'+1).$$

The factor $v^{\gamma_1}(j+\frac{1}{2}s-\frac{1}{2})$ can be moved to the right, giving a change of sign at each interchange with a u, since the $\epsilon^{\gamma_v\gamma_w}$ term arising from the interchange applied to $u_{\gamma_v}(\ldots)\,u_{\gamma_w}(\ldots)$ gives zero. Finally, the contracted products $v^{\gamma}(j'+\frac{1}{2}s')\,u_{\gamma}(j'+\frac{1}{2}s')$ and $u^{\beta}(k+\frac{1}{2}u)\,v_{\beta}(k+\frac{1}{2}u)$ can be calculated, giving a factor

$$(-1)^{2k+u+1+2j'+s'}(2j'+s'+1)\,(2k+u).$$

Thus the result of each half of this operation is to remove one β and one γ index from each half of the original expression, the corresponding matrix factors being replaced by a numerical factor.

We repeat this process until all the β or all the γ indices are removed. If $t'\neq t$ the resulting expression contains a factor $u^{\gamma}(x+\frac{1}{2})\,u_{\gamma}(x)$ or $v^{\beta}(x)\,v_{\beta}(x+\frac{1}{2})$, and is therefore zero by (16). Thus $Q^{\alpha_r}(j,l,k)\,Q_{\alpha_t}(k,l,j')=0$ unless $t'=t$, i.e. $s'=s$, i.e. $j'=j$.

If $j'=j$, the factor arising from the elimination of the first β and γ indices is $(2j+s+1)\,(t)$.

The factor arising from the removal of all β and γ indices is thus

$$\frac{(2j+s+1)!\,(t)!}{(2j+1+s-t)!}. \tag{A3}$$

(3) The remaining expression containing only indices α can now be evaluated by (16) giving

$$(-1)^{\frac{1}{2}r(4j+r+1)}\frac{(2j+r+1)!}{(2j+1)!}. \tag{A4}$$

Collecting the factors (A2), (A3) and (A4) and expressing them in terms of k, l, j and t as independent variables, we have

$$Q(j,l,k;t)=(-1)^{l(4k+2l-1)+t}\frac{(k+l+j+1)!\,(k+l+j-t)!\,t!}{(2j+1)!\,(2k)!},$$

where $Q(j,l,k;t)$ is (A1) with the indicated order of indices.

We have then

$$\begin{aligned}Q^{\alpha_t}(j,k,0)\,Q_{\alpha_t}(0,k,j')&=Q(j,k,0;k-j)\,\delta_{jj'}\\&=(-1)^{2k^2-j}\frac{(k+j+1)!\,(k-j)!}{(2j+1)}\,\delta_{jj'},\end{aligned} \tag{19}$$

$$\begin{aligned}&\Sigma(\mathrm{Perm}\,\alpha_t)\,Q^{\alpha_r}(j,l,k)\,Q_{\alpha_t}(k,l,j')\\&\quad=\sum_t\frac{\{(k+l-j)!\}^2\{(j+l-k)!\}^2}{(k+l-j-t)!\,t!(j+l-k-t)!\,t!}\,Q(j,l,k;t)\,\delta_{jj'}\\&\quad=(-1)^{l(4k+2l-1)}\frac{\{(k+l-j)!\}^2\{(j+l-k)!\}^2\,(k+l+j+1)!}{(2j+1)!\,(2k)!}\,\delta_{jj'}\\&\qquad\times\sum_{t=0}^{\min\substack{k+l-j\\j+l-k}}(-1)^t\frac{(k+l+j-t)!}{(k+l-j-t)!\,(j+l-k-t)!\,t!}.\end{aligned}$$

To evaluate this series, we note that it is symmetrical in j and k. We take $j \geqslant k$, and put $k+l-j = s$. Then, denoting the series by $S(j,l,s)$, we have

$$S(j,l,s) = \sum_{t=0}^{s} (-1)^t \frac{(2j+s-t)!}{(2l-s-t)!\,(s-t)!\,t!};$$

therefore

$$\begin{aligned} &S(j+\tfrac{1}{2}, l-\tfrac{1}{2}, s-1) - S(j, l-1, s-1) \\ &\quad = \sum_{t=0}^{s-1} (-1)^t \frac{(2j+s-t)!}{(2l-s-t)!\,(s-t-1)!\,t!} + \sum_{t=1}^{s} (-1)^t \frac{(2j+s-t)!}{(2l-s-t)!\,(s-t)!\,(t-1)!} \\ &\quad = s\sum_{t=0}^{s} (-1)^t \frac{(2j+s-t)!}{(2l-s-t)!\,(s-t)!\,t!} \end{aligned}$$

(by addition of corresponding terms).

We thus have the recurrence relation

$$S(j,l,s+1) = \frac{1}{s+1}\{S(j+\tfrac{1}{2}, l-\tfrac{1}{2}, s) - S(j, l-1, s)\}. \tag{A 5}$$

It can be seen by inspection that the formula

$$S(j,l,s) = \frac{(2j-2l+2s)!\,(2j)!}{(2j-2l+s)!\,(2l-s)!\,s!}$$

holds for $s = 0$ and all j and l. With the help of the recurrence relation (A 5) it follows easily by induction that the formula is true generally.

Thus, using this result in the above formula and expressing it in terms of j, l and k, we have the final result

$$\begin{aligned} &\Sigma(\mathrm{Perm}\,\alpha_t)\, Q^{\alpha_r}(j,l,k)\, Q_{\alpha_t}(k,l,j') \\ &\qquad = (-1)^{l(4k+2l-1)} \frac{(k+l-j)!\,(j+l-k)!\,(k+l+j+1)!}{(2j+1)\,(j+k-l)!}\,\delta_{jj'}. \end{aligned} \tag{18}$$

REFERENCES

Bhabha, H. J. 1945 *Rev. Mod. Phys.* **17**, 200.
Dirac, P. A. M. 1936 *Proc. Roy. Soc.* A, **155**, 447.
Fierz, M. 1939 *Helv. Phys. Acta*, **12**, 3.
Fierz, M. & Pauli, W. 1939 *Proc. Roy. Soc.* A, **173**, 211.
Kemmer, N. 1939 *Proc. Roy. Soc.* A, **173**, 91.
Pauli, W. 1941 *Phys. Rev.* **58**, 716.

The ejection of protons from nitrogen on bombardment with α-particles of short range

By F. C. Champion and R. R. Roy

(*Communicated by J. T. Randall, F.R.S.—Received* 5 *February* 1947)

[Plate 19]

Using the expansion-chamber method, ninety proton tracks are obtained from 850 photographs showing the disintegration of nitrogen under bombardment by slow α-particles. The number of disintegrations decreases as the energy of the α-particles is reduced, but the photographs show disintegrations occurring for energies less than 1·7 MeV. The angular distribution is approximately isotropic for the protons ejected by α-particles of energy less than 3 MeV, but there is a marked preponderance at about 90° for the protons ejected by α-particles of range about 2 cm. in air at N.T.P. Typical photographs are reproduced.

Introduction

The ejection of protons as a result of the disintegration of nitrogen under bombardment by α-particles of about 7 cm. range in air at N.T.P. was the first example of artificial disintegration (Rutherford 1919). The scintillation method of detection was used in these early experiments (Rutherford & Chadwick 1922), and it was shown that the number of protons ejected decreased rapidly as the range of the incident α-particles was reduced. Using the expansion-chamber method (Blackett 1925; Blackett & Lees 1932), the reaction N^{14} (α, p) O^{17} was found to occur. In three instances, however, out of a total of thirteen disintegrations, the α-particle responsible for the disintegration had a range of somewhat less than 3 cm.

By electrical counting methods (Steudel 1932; Pollard 1933) it was next shown that protons were produced when the range of the α-particles was as low as 2·2 cm. Such slow α-particles were assumed to enter the nucleus by a resonance process. These results were later confirmed and extended (Stegmann 1935) when two close resonance levels corresponding to $R_\alpha = 2{\cdot}2$ and $R_\alpha = 2{\cdot}6$ cm. were established.

In the present work we have shown that the expansion method reveals that disintegration is produced by α-particles of much lower ranges. The main aim of the investigation, however, was to form an estimate of the numbers of protons ejected at various angles with respect to the initial direction of the α-particle.

Experimental details

The expansion chamber was about 13 cm. in diameter and 1 cm. high. The success of the experiment depended essentially upon the use of an intense source of α-particles, canalized by a system of slits so as to produce an almost parallel beam of α-particles of narrow breadth. Rather more than 80 % of the α-particles are situated in a beam which changes in width from 2 mm. at the beginning to 10 mm. at the end in a total length of about 30 mm. The broader appearance shown in the photographs is due to the presence of a mass of unresolved tracks of α-particles scattered by elastic collisions with nitrogen nuclei, accompanied by a certain amount of ionic diffusion. The source consisted of polonium deposited electrolytically upon a piece of platinum foil; it was situated inside a cylinder which was closed at the end except for a slot 2 mm. wide. The arrangement was introduced into the expansion chamber through a side window, and it was inserted at such a distance that the α-ray tracks were formed centrally in the chamber which was filled with nitrogen gas from a gas cylinder. Because of the intense ionization, very heavy condensation occurred, and it was necessary to make some dozen small subsidiary expansions to clear the chamber between each main expansion. Standard methods of expansion, illumination and stereoscopic photography were used.

RESULTS

In 850 photographs, ninety proton tracks were obtained. The results, as found without corrections except for the reduction of the remaining range R_α to air equivalent at N.T.P., are shown in figure 1, where the ordinate θ is the angle of ejection of the protons in laboratory co-ordinates and the abscissa represents the corresponding value of R_α. Sample photographs are reproduced in figure 4, plate 19.

DISCUSSION OF RESULTS

Perhaps the most striking characteristic of the distribution exhibited in figure 1 is the small number of protons which are ejected in the forward and backward directions, that is, between $\theta = 0$ to 30° and 150 to 180°. A simple direct count reveals that over 80 % are ejected in the angular range $\theta = 30°$ to $\theta = 150°$. Another prominent feature is the large number of points around a value of $R_\alpha = 2$ cm. for which θ lies between 80 and 100°, indicating a marked preference at this energy for ejection at about 90°. It is interesting to recall that both the disintegration protons recorded by Blackett & Lees for α-particles of this energy were ejected at just such angles. A more detailed analysis of figure 1 indicates further points of interest, some of which can be made with certainty, while others are only probabilities based on prevailing theoretical views of nuclear disintegration.

(a) *The distribution at* $\theta = 90°$

First, between $\theta = 80°$ and $\theta = 100°$, the error δR_α due to the finite thickness of the beam is very small. It may therefore be concluded that the values of R_α and θ as shown in figure 1 are truly representative of the facts. In figure 2*a* is shown the variation of yield with change in R_α. No disintegrations are observed until $R_\alpha = 0{\cdot}8$ cm. At this range protons begin to be found. Between $R_\alpha = 1{\cdot}0$ and 1·4 cm. only one disintegration occurred. At greater ranges the number increased again, reaching a second maximum at about $R_\alpha = 2{\cdot}1$ cm. Beyond this range the number falls rapidly.

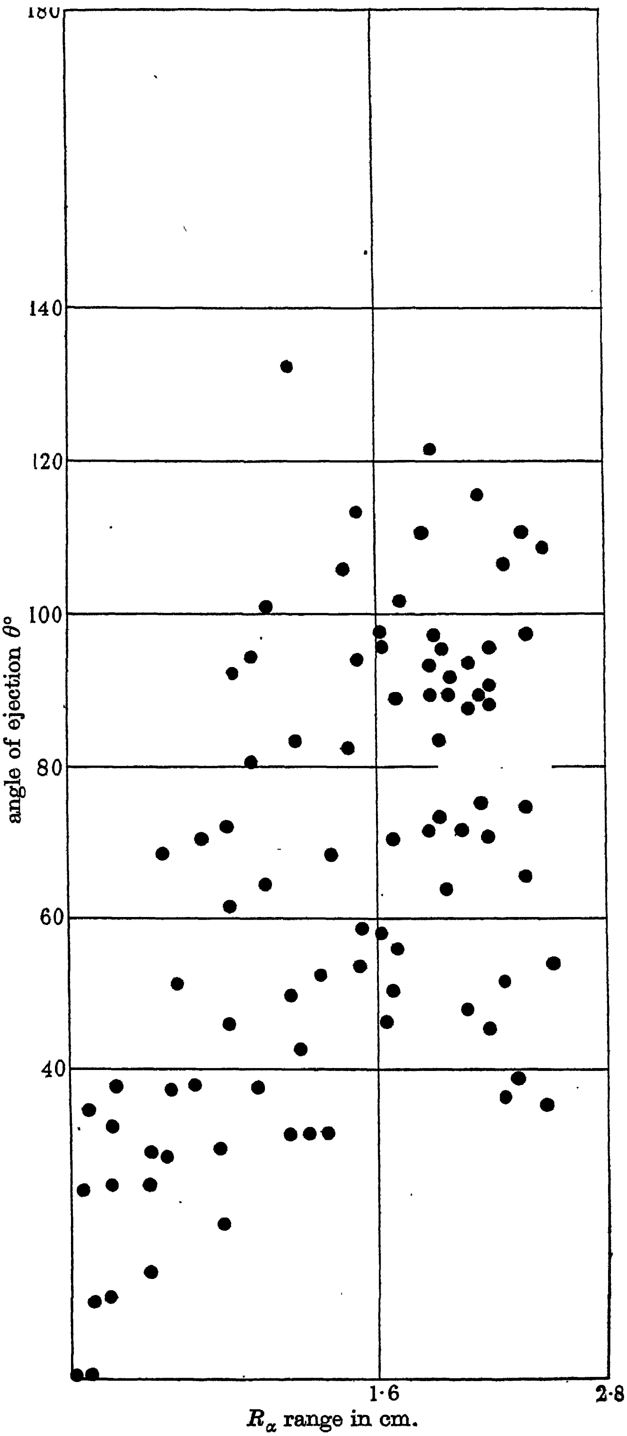
180
140
120
100
80
60
40
angle of ejection $\theta°$
1·6
2·8
R_α range in cm.

FIGURE 1

The existence of a resonance level at $R_\alpha = 2{\cdot}2$ cm. has already been established by other workers. In particular, Stegmann pointed out that if disintegration occurred for $R_\alpha < 2{\cdot}1$ cm. it must be of quite low intensity. There cannot be any doubt that our photographs show disintegrations occurring at much lower range than this. The distribution shown in figure 2*a* suggests strongly the existence of a resonance level in the neighbourhood of $R_\alpha = 0{\cdot}9$ cm., and this is substantiated by consideration of the combined distribution at $\theta = 70°$ and $\theta = 110°$ as shown in figure 2*b*. The distribution for the total angular range $\theta = 60°$ to $\theta = 120°$ is shown in figure 2*c*.

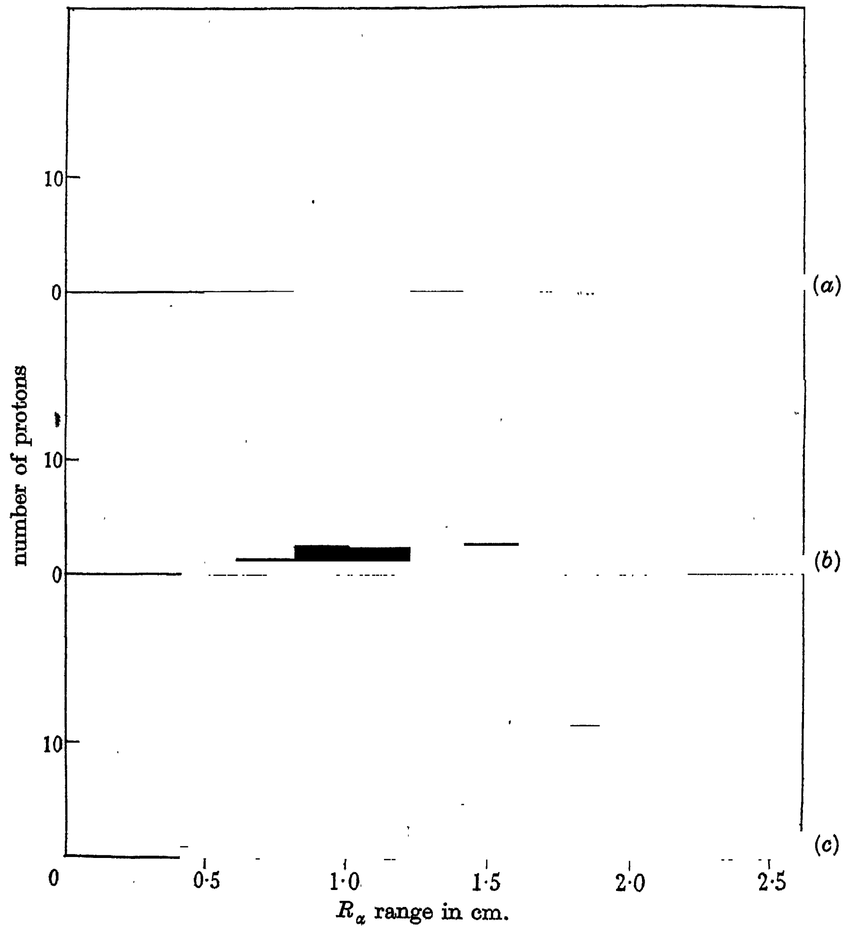

FIGURE 2. *a*, $\theta = 90°$; *b*, $\theta = 70$ and $110°$; *c*, $\theta = 60$ to $120°$.

There is, however, no essential disagreement with Stegmann's results, either in the position or in the intensity of the resonance levels. First with regard to position we cannot guarantee our absolute range to within 10 %, and we therefore identify our resonance level at 2·1 cm. with that found by Stegmann at 2·2 cm. Both finite thickness of the polonium deposit and possible foreign matter on the source surface could reduce the effective range of the α-particles by this amount. As for intensity, Stegmann's observations were made largely in the region of 90° where the relative reduction in intensity proceeding from the 2·2 cm. level to lower levels is most marked. Our numbers are so small that statistical fluctuations alone would prevent much reliance being placed on quantitative estimates. To this must be added the uncertainty in θ which could amount to $\pm 5°$. Then, for example, the proton recorded in the 1 cm. group as having $\theta = 82°$ might possibly have $\theta < 80°$; such an alteration would reduce our estimated relative intensity by 30 %.

Referring to figure 2*c*, the resonance group at 2·1 cm. is too broad and too asymmetrical to be attributed to a single level. Stegmann has shown that two definite levels occur at $R_\alpha = 2{\cdot}2$ and 2·6 cm. respectively. We interpret the breadth of the larger group in figure 2*c* to imply the existence of at least one and possibly two or three levels between $R_\alpha = 1{\cdot}4$ and 2·1 cm. Until more data are available, however, not much importance can be attached to particular figures for these levels intermediate between those at 0·9 and 2·1 cm. respectively.

(*b*) *The distribution between* $\theta = 80$ *to* 60° *and* 100 *to* 120°

Since the possible error δR_α becomes progressively larger at other angles of ejection of the proton, being proportional to $b \cot \theta$, where b is the breadth of the beam, the interpretation of our results becomes more uncertain at angles other than 90°. The information which has been obtained under the unambiguous conditions of $\theta = 90°$ acts as a valuable guide to the behaviour under less favourable conditions. The inference already made that resonance levels, if they exist at all between $R_\alpha = 1{\cdot}1$ and 1·4 cm., must be of quite low intensity, allows us to assign a considerable number of protons to the 1 cm. group for small values of R_α. One cannot, of course, rule out the possibility that some of these may correspond to even lower energy levels where $R_\alpha < 0{\cdot}9$ cm. However, the number of protons ejected from such possible levels is presumably not large, for existing nuclear theory suggests that the separation of the energy levels becomes progressively greater at lower energies, and consequently the energy of the α-particle responsible for the disintegration would be very small indeed. The large thickness of the potential barrier for such small values of E_α would be likely to make the probability of penetration of the nucleus by the α-particle a rare process.

First, note that once again there are practically no disintegrations between $R_\alpha = 1{\cdot}1$ and 1·4 cm., thus confirming the view already expressed that there are no resonance levels of appreciable intensity in this region. The most significant point is that the number of protons in the lower groups remains independent of the angle between 60 and 120°, while the number in the 2·1 cm. group falls by about 50 % as θ is increased or decreased by 30° from 90°.

(*c*) *Angular distribution for other values of* θ

The above behaviour is maintained broadly speaking as one proceeds to other angular ranges down to $\theta = 30°$ and up to $\theta = 150°$, and it is therefore concluded that the marked peak at 90° is characteristic of the highest energy group only. Below 30° one cannot distinguish for all values of R_α between *projected* protons due to elastic impact of the α-particles with the possible hydrogen contamination in the chamber, and *ejected* protons formed in genuine disintegrations. With water and alcohol vapour present some of these protons at $\theta < 30°$ may arise from elastic collisions.

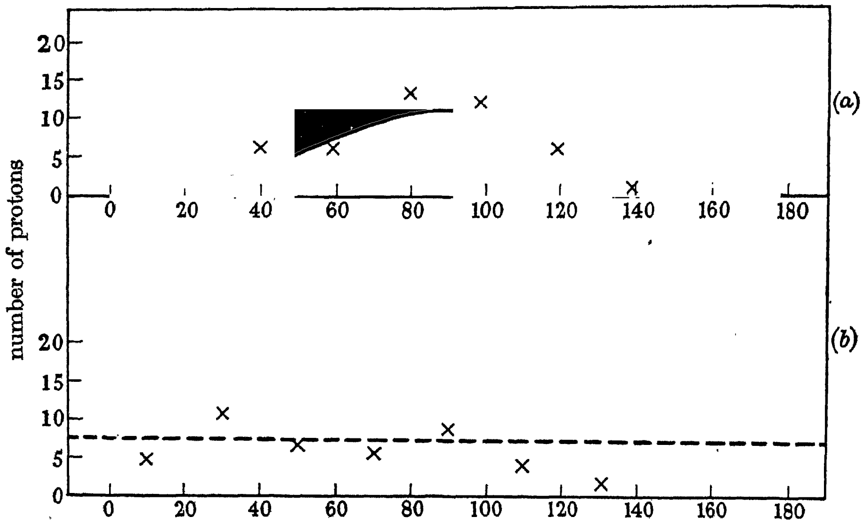

FIGURE 3

In figure 3*b* is shown the angular distribution obtained for the protons ejected by α-particles with R_α up to 1·6 cm., while figure 3*a* refers to those with $R_\alpha = 2{\cdot}1$ cm. The essential point revealed is that whereas the distribution for the 2·1 cm. group shows a very marked preference for $\theta \simeq 90°$, with the other groups the distribution is uniform within the rather large statistical error. The inference would appear to be that for the lower groups the disintegration is of an *S* type while for the 2·1 cm. group it is of some other type. We might expect the latter, if it is of the *P* type, to be proportional to $\sin^2\theta$, provided that certain assumptions are made about the angular momentum of the resonance level of the compound nucleus F_9^{18}. This expression is shown in the full line in figure 3*a*; the agreement is fairly satisfactory, but the experimental distribution suggests on the whole a rather sharper peak. The apparent too rapid falling away at the largest angles is probably instrumental, for the range of the protons at $\theta > 130°$ would be short before they impinged on the slit system. However, had there been an appreciable number of these occurrences, some of the protons of such artificially short range would have been observed, whereas in practice none was found.

(*d*) *The energy balance*

In all cases the range of the protons exceeded the confines of the expansion chamber. This meant that the range of the proton $R_p > 5$ cm., corresponding to a proton energy $E_p > 1{\cdot}6$ MeV. The limitation on the range measurement was unfortunate but unavoidable, since the chamber was originally designed for another purpose. It is, however, fortunate that the protons ejected are not of very short range, otherwise the separation of genuine disintegrations from projected protons due to possible hydrogen contamination would have been difficult. The energies of the two main groups of α-particles responsible for the disintegrations and with $R_\alpha = 0{\cdot}9$ and $2{\cdot}1$ cm. respectively, are about $1{\cdot}7$ and $3{\cdot}5$ MeV. Hence, taking into account also the energy of recoil of the nucleus, all that can be inferred is that the values of the energy balance Q are greater than $-0{\cdot}1$ and $-1{\cdot}9$ MeV respectively. These values are consistent with those found by other workers.

Unless either the ranges of the ejected protons and the recoil nuclei, or else the Q values, are known, the transformation of the angular distribution of the protons from laboratory co-ordinates to co-ordinates moving with the centre of mass of the system cannot be effected. We have, however, calculated the corrected distribution on the assumption that $Q = -1{\cdot}0$ MeV. The effect is to increase θ at 90° by about 10 % and by a proportionately lesser amount at larger and smaller angles. This merely improves the symmetry of our distribution shown in figure 3*a* and makes no appreciable difference to our conclusions.

(*e*) *The absolute intensity of the disintegration process*

The shutter arrangement which admitted the α-particles was such that every disintegration which occurred during the sensitive period of the expansion chamber was recorded. Proton tracks which formed before the supersaturation was sufficiently high to cause condensation would show appreciable breadth due to the diffusion of the ions from their points of origin. Inspection of the tracks showed that this occurred in a few per cent of the cases. From observations on diffusion breadth as a function of the age of the tracks and from work on the sensitive period of expansion chambers of various sizes (Blackett 1934; Williams 1939), the effective time during which the proton tracks would be recorded is estimated as about $\frac{1}{50}$ sec. The strength of the polonium source was approximately 3 millicuries. Taking into account also the solid angle subtended by the slit at the source, the number of α-particles entering the chamber per second was estimated as 10^7. The solid angle in which the disintegrations were recorded was determined from the depth of the light beam and the diameter of the chamber to be about unity. Since ninety disintegrations were found in 850 expansions, the total probability of disintegration when nitrogen is bombarded with α-particles of energy less than $3{\cdot}5$ MeV is found to be about one in two million. This value is too approximate to be regarded as very much better than expressing an order of magnitude.

(*f*) *General conclusions*

It does not seem that any complete theoretical calculation has yet been made of the precise angular distribution to be expected for the disintegration protons in the present experiment. In broadest outline, our results show, however, that when the uncorrected data shown in figure 1 are corrected for (*a*) possible contamination protons and large probable error in R_α for $\theta < 30°$, (*b*) the artificial reduction in the number of protons recorded for $\theta > 150°$ due to the experimental arrangement of the slit system, and (*c*) the transformation of the distribution from laboratory co-ordinates to co-ordinates moving with the centre of mass of the system, then, irrespective of the energy of the incident α-particles, the angular distribution of the ejected protons is symmetrical in the forward and backward directions, about a plane at 90° to the direction of the incident α-particles. Such an angular distribution is to be expected for all energies of the incident α-particles, provided one is concerned with resonance disintegrations operating on the type of nuclear model suggested by Bohr. While, however, Bohr's liquid-drop model may account for this very general feature of the angular distribution, and while it may be best suited to account for the wide range of experimental observations concerning the behaviour of heavy nuclei, particularly as regards interaction with neutrons, for light nuclei some degree of substructure is probably present. The well-known fact that disintegration of nitrogen with the emission of protons occurs at much lower energies of the incident α-particles than are necessary for the disintegration with neutron emission, suggests that the protons are closer to the nuclear surface than the neutrons. Without postulating any precise arrangement it therefore appears that when an α-particle strikes the nucleus it will in general first impinge on a proton.

If the α-particle impinged centrally on the nucleus, the struck proton would have to traverse the nucleus in order to escape. In doing so it would, if not very fast, communicate all its energy to the other nuclear particles. The compound nucleus would therefore exist for an appreciable time, and when final disintegration occurred the direction of ejection of the protons would be expected to be approximately isotropic. This is in agreement with the angular distribution found for the disintegrations produced by α-particles at the lowest energies.

Those α-particles which impinged off-centre on the nucleus would communicate angular momentum to it. For a semi-rigid nucleus if the speed of rotation, the energy communicated to the struck proton and the force with which this proton is bound to the remainder of the nucleus, are just of the right relationship, one may imagine that the proton does not leave the nucleus until the latter has rotated through an appreciable angle. To explain the angular distribution for the 2·1 cm. group, the most probable value of this angle of rotation would have to be about 90°. Like all classical nuclear models, the above constitutes only a working approach to the problem, and it appears that ultimately the distribution should be accounted for on the general principles of quantum mechanics (Myers 1938).

We are particularly grateful to Dr Pincherle of King's College, London, for discussion on theoretical aspects of the work, and to Dr Brode of the Cavendish Laboratory, Cambridge, for information on the preparation of polonium sources.

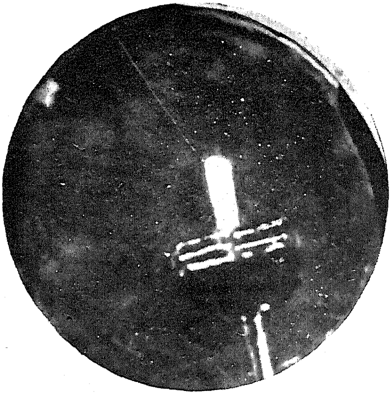

FIGURE 4

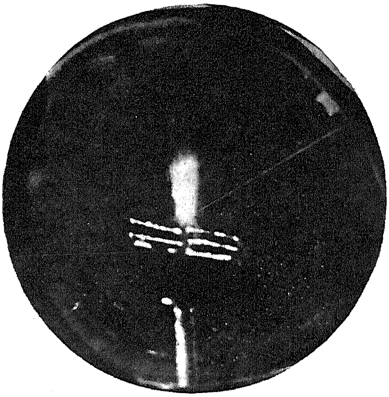

FIGURE 5

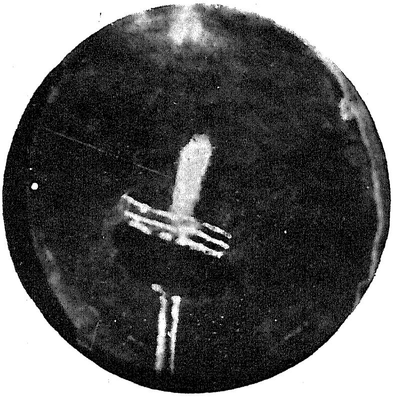

FIGURE 6

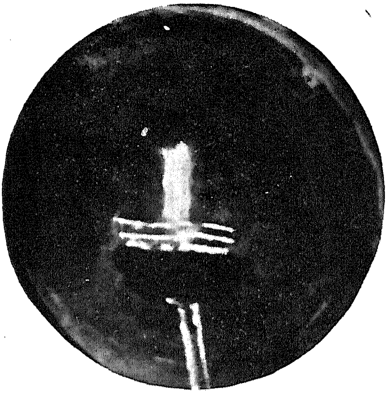

FIGURE 7

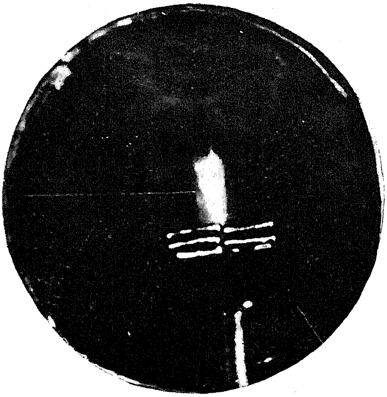

FIGURE 8

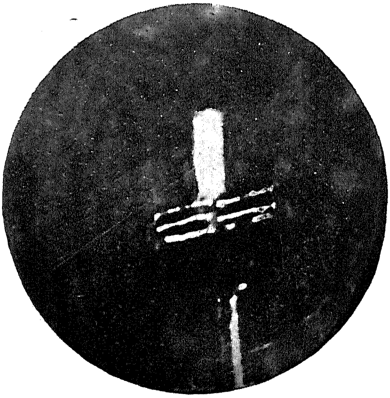

FIGURE 9

REFERENCES

Blackett 1925 *Proc. Roy. Soc.* A, **107**, 349.
Blackett 1934 *Proc. Roy. Soc.* A, **146**, 281.
Blackett & Lees 1932 *Proc. Roy. Soc.* A, **136**, 325.
Myers 1938 *Phys. Rev.* **54**, 361.
Pollard 1933 *Proc. Roy. Soc.* A, **141**, 375.
Rutherford 1919 *Phil. Mag.* **37**, 581.
Rutherford & Chadwick 1922 *Phil. Mag.* **44**, 417.
Stegmann 1935 *Z. Phys.* **95**, 72.
Steudel 1932 *Z. Phys.* **77**, 139.
Williams 1939 *Proc. Roy. Soc.* A, **172**, 194.

DESCRIPTION OF PLATE 19

Certain features are common to all the photographs. At the bottom is the source-holder, and in front of this is the slit system. The beam of α-particles is shown as the dense column of condensation emerging from the slit system; it is situated centrally in the expansion chamber. In all cases the ejected proton travels beyond the confines of the chamber. The magnification varies between about 0·5 and 0·75.

FIGURE 4. A proton track is ejected at about 25° to the incident beam of α-particles by one of the α-particles of short remaining range. The possible error δR_α is large, and either the 0·9 cm. or one of the intermediate groups might be the cause of the disintegration.

FIGURE 5. In this disintegration $\theta = 60°$ and the transmutation is clearly due to the 2·1 cm group. The track is inclined to a horizontal plane, for while it begins quite sharply, by the time it reaches the edge of the chamber it has apparently become broadened because of the finite depth of focus of the camera lens.

FIGURE 6. Here $\theta = 85°$ and $R_\alpha = 1·65$ cm.

FIGURE 7. $R_\alpha = 0·5$ cm. and $\theta = 68°$. This has been assigned to the $R_\alpha = 0·9$ cm. group, but it is quite possible that it is an example of disintegration at a still lower energy group.

FIGURE 8. $\theta = 90°$, $R_\alpha = 1·6$ cm.

FIGURE 9. $\theta = 133°$. The stereoscopic pair of photographs gives the mean value of $R_\alpha = 1·2$ cm. with a maximum error of ± 0·3 cm.

The theory of combined plastic and elastic deformation with particular reference to a thick tube under internal pressure

By R. Hill, E. H. Lee and S. J. Tupper

(*Communicated by Sir Geoffrey Taylor, F.R.S.—Received* 5 *March* 1947)

In certain problems of plastic flow, for example, a thick tube expanded by internal pressure, it is important to consider changes in the elastic strain of material which is flowing plastically in order to deduce the correct stress distribution and deformation. The usual plastic theory which neglects elastic strains in the plastic region may lead to considerable errors in certain cases.

In this paper we review the theory of the deformation of a material under combined stresses which involves both elastic and plastic components of strain. The relationship between stress and strain is represented on a plane diagram, the reduced stress-strain diagram, which facilitates discrimination between the elastic and plastic components of strain and aids considerably the solution of certain problems. The diagram can also be used to express the relationships governing the dissipation of energy during plastic flow under combined stresses.

The theory is applied to the deformation of a long thick tube under internal pressure with zero longitudinal extension. The solution is compared with that based on the usual theory which neglects elastic strains in the plastic region, revealing an error which reaches a maximum of over 60 % in the longitudinal stress distribution. The significance of the differences between the two solutions is discussed in detail.

1. INTRODUCTION

When a metal is deformed under continuously increasing stress, it is first strained elastically, the relationship between stress and strain under combined stress being expressed by the familiar equations of the theory of elasticity. With increasing stress the material may be overstrained and permanent plastic flow will occur. The total strain under load is then a combination of an elastic and a plastic component. With release of stress the elastic component disappears and the material is left with the permanent plastic strain.

In many applications, the plastic strain is very much larger than the elastic component, and it is permissible to neglect the latter in analyzing the deformation. In some cases, however, the amount of deformation in the plastic region is constrained by a surrounding boundary of elastic material, and the total strain throughout is limited to be of the order of elastic strains. The analysis of such problems must take into account both the elastic and the plastic components of strain in the plastic region. In such cases, application of the usual theory valid for large plastic strains will lead to erroneous stress distributions.

When a long, thick tube is subjected to increasing internal pressure, the material adjacent to the hole is first overstrained, and a plastic region spreads through the tube until all the material has been deformed plastically. At an intermediate pressure the plastic elastic boundary is a cylindrical surface co-axial with the tube, and the plastic deformation is constrained by the elastic material surrounding it. In these circumstances, a correct analysis of the stress distribution must take account of the elastic strains in the plastic region.

The usual analysis of this problem (Nadai 1931) assumes incompressible deformation in the plastic region, where the dilatation is, in fact, of the same order as all the strain components. Such an assumption is only permissible when the plastic component of strain, which involves no volume change, is large compared with elastic strains. The resulting solution for a thick tube introduces a fictitious discontinuity in the longitudinal stress at the plastic-elastic boundary which is a direct result of allowing for components of elastic strain in the elastic region, and equating them to zero in the adjacent plastic region.

A correct analysis overcoming this inconsistency was suggested in 1943 by G. I. Taylor in some unpublished work. In the present paper, the general theory of deformation considering both the elastic and plastic components of strain is reviewed, and a method of geometrical representation of stress and strain is described which leads to a comparatively simple formulation of the type of analysis suggested by Taylor. The problem of a thick tube with zero longitudinal strain subjected to internal pressure is solved numerically and compared with the solution which neglects elastic strains in the plastic region. The new solution approaches the inelastic-plastic case when the plastic component of strain predominates during continued expansion after the whole tube has been overstrained. The inelastic-plastic solution is, however, considerably in error earlier in the deformation while part of the tube is elastic.

2. DEFORMATION UNDER COMBINED STRESS

We will first consider the general relationships governing combined elastic-plastic deformation in an isotropic solid. As large plastic deformations are possible we shall formulate relationships in terms of natural strain components and true stresses. An increment of natural strain is determined by the extension of an element of material divided by its length at that stage in the deformation, and differs from nominal strain in which extension is expressed as a percentage of the original unstrained length of the element. Similarly, true stress refers to force per unit stressed area of the material. We shall assume that the elastic constants are unchanged by plastic flow. This means that during unloading the linear relationship between true stress and natural strain is identical with that for the undeformed material; this assumption is not strictly accurate because of the formation of a hysteresis loop; but the initial gradient of the unloading curve in a tension test has been shown by Howard & Smith (1925) to obey this law.

The assumption of a linear true stress-natural strain curve in the elastic region means that the load extension relationship will not be exactly linear. However, because of the small strain increments involved, no practical difficulties arise and the elastic constants are unchanged. The difference between true and nominal stress-strain curves only becomes significant at strains considerably greater than yield-point strain.

For simplicity we will first analyze uniform longitudinal strain in a tension test. Let an increase in stress $d\sigma$ produce a natural strain increment $d\epsilon$. The work done per unit volume of strained material is $\sigma d\epsilon$, of which a part is recoverable elastic-strain energy and part irrecoverable plastic work. The former can be determined from the stress increment and the elastic constants, and is equal to

$$dW_e = \sigma \frac{d\sigma}{E}, \tag{2·1}$$

where E is Young's modulus. Thus, the irrecoverable plastic work is given by the difference

$$dW_p = \sigma\left(d\epsilon - \frac{d\sigma}{E}\right). \tag{2·2}$$

This equation suggests a definition for the increment of plastic strain which will correspond to the energy absorbed in plastic deformation

$$d\epsilon_p = d\epsilon - \frac{d\sigma}{E}. \tag{2·3}$$

This definition agrees with the increment of natural strain of the unloaded test piece obtained by measuring extensions after removing the load; for if L is the loaded specimen length corresponding to the length L_0 when the load is removed, the unloading line on the stress-strain diagram gives

$$\text{elastic strain} = \log \frac{L}{L_0} = \frac{\sigma}{E}.$$

Differentiating, we have

$$\frac{dL}{L} - \frac{dL_0}{L_0} = \frac{d\sigma}{E}, \tag{2·4}$$

showing that the increment of plastic strain defined in equation (2·3) is, in fact, the natural strain increment of the unloaded bar dL_0/L_0.

Deformation under combined stresses can be treated in a similar manner, the components of a plastic natural strain increment in Cartesian co-ordinates being given by

$$\left.\begin{aligned}
d\epsilon_{px} &= d\epsilon_x - \frac{d\sigma_x - \nu(d\sigma_y + d\sigma_z)}{E}, & d\gamma_{pxy} &= d\gamma_{xy} - \frac{d\tau_{xy}}{G},\\
d\epsilon_{py} &= d\epsilon_y - \frac{d\sigma_y - \nu(d\sigma_z + d\sigma_x)}{E}, & d\gamma_{pyz} &= d\gamma_{yz} - \frac{d\tau_{yz}}{G},\\
d\epsilon_{pz} &= d\epsilon_z - \frac{d\sigma_z - \nu(d\sigma_x + d\sigma_y)}{E}, & d\gamma_{pzx} &= d\gamma_{zx} - \frac{d\tau_{zx}}{G},
\end{aligned}\right\} \tag{2·5}$$

where ν is Poisson's ratio, and G the modulus of rigidity or shear distortion. As before, the plastic strain defined here is the strain increment of the unloaded element.

Under combined principal stresses $\sigma_1, \sigma_2, \sigma_3$ which produce plastic flow, a plastic-strain increment with principal values $d\epsilon_{p_1}, d\epsilon_{p_2}, d\epsilon_{p_3}$ is found experimentally

(Taylor & Quinney 1931; Baildon 1943) to be approximately governed by the viscous-flow relationship, applied to plastic flow by Levy and von Mises,

$$\frac{d\epsilon_{p_1}-d\epsilon_{p_2}}{\sigma_1-\sigma_2}=\frac{d\epsilon_{p_2}-d\epsilon_{p_3}}{\sigma_2-\sigma_3}=\frac{d\epsilon_{p_3}-d\epsilon_{p_1}}{\sigma_3-\sigma_1}. \tag{2·6}$$

This is combined with zero volume change

$$d\epsilon_{p_1}+d\epsilon_{p_2}+d\epsilon_{p_3}=0. \tag{2·7}$$

(2·6) is equivalent to the statement that the Mohr's circle diagrams of stress- and plastic-strain increment are similar.

Taylor & Quinney (1931) also found that the principal axes of plastic-strain increment and stress coincide.

(2·6) and (2·7) can now be combined to give, in Cartesian co-ordinates,

$$\left.\begin{aligned} d\epsilon_{px}&=\frac{d\lambda}{2G}(\sigma_x-\sigma), & d\gamma_{pxy}&=\frac{d\lambda}{G}\tau_{xy},\\ d\epsilon_{px}&=\frac{d\lambda}{2G}(\sigma_y-\sigma), & d\gamma_{pyz}&=\frac{d\lambda}{G}\tau_{yz},\\ d\epsilon_{pz}&=\frac{d\lambda}{2G}(\sigma_z-\sigma), & d\gamma_{pzx}&=\frac{d\lambda}{G}\tau_{zx},\end{aligned}\right\} \tag{2·8}$$

where $3\sigma=\sigma_x+\sigma_y+\sigma_z$.

$d\lambda$ is a non-dimensional parameter introduced to express the development of the plastic flow. If the material work hardens, $d\lambda$ is a function of the stress increment. For zero work hardening $d\lambda$ has sometimes been identified with an element of time during which an increment of plastic flow develops, but this introduces an unnecessary restriction on λ; time need not be introduced until the dynamics of the process are considered.

In considering combined plastic and elastic deformation, it is convenient to follow Reuss (1930) in segregating the components of strain involving dilatation and shear distortion. The relationship between stress and strain in the elastic region is then expressed in terms of the shear modulus G, and the compressibility K, instead of the more usual pairs of elastic constants. Using rectangular Cartesian co-ordinates, we have for elastic deformation

$$\left.\begin{aligned} \epsilon_{ex}-\epsilon_e&=\frac{1}{2G}(\sigma_x-\sigma), & \gamma_{exy}&=\frac{1}{G}\tau_{xy},\\ \epsilon_{ey}-\epsilon_e&=\frac{1}{2G}(\sigma_y-\sigma), & \gamma_{eyz}&=\frac{1}{G}\tau_{yz},\\ \epsilon_{ez}-\epsilon_e&=\frac{1}{2G}(\sigma_z-\sigma), & \gamma_{ezx}&=\frac{1}{G}\tau_{zx},\end{aligned}\right\} \tag{2·9}$$

$$\epsilon_e=\frac{\sigma}{3K}, \tag{2·10}$$

where $\epsilon_e=\tfrac{1}{3}(\epsilon_{ex}+\epsilon_{ey}+\epsilon_{ez})$ and $\sigma=\tfrac{1}{3}(\sigma_x+\sigma_y+\sigma_z)$.

The relations (2·9) determine the shearing distortion which is expressed in terms of the modulus of rigidity only. (2·10) represents the volume change which is expressed in terms of the compressibility modulus.

A combination of equations (2·9) and (2·10) will give the usual elastic relationships in terms of, say, Young's modulus and Poisson's ratio.

Combining the elastic and plastic components of strain according to equations (2·5), and using the form of equations (2·8, 2·9, 2·10) for the separate parts, an increment of total strain satisfies the equations

$$\left.\begin{aligned} 2G\,d(\epsilon_x-\epsilon) &= d(\sigma_x-\sigma)+d\lambda(\sigma_x-\sigma), & G\,d\gamma_{xy} &= d\tau_{xy}+d\lambda\,\tau_{xy},\\ 2G\,d(\epsilon_y-\epsilon) &= d(\sigma_y-\sigma)+d\lambda(\sigma_y-\sigma), & G\,d\gamma_{yz} &= d\tau_{yz}+d\lambda\,\tau_{yz},\\ 2G\,d(\epsilon_z-\epsilon) &= d(\sigma_z-\sigma)+d\lambda(\sigma_z-\sigma), & G\,d\gamma_{zx} &= d\tau_{zx}+d\lambda\,\tau_{zx},\end{aligned}\right\} \tag{2·11}$$

$$d\epsilon = \frac{d\sigma}{3K}. \tag{2·12}$$

A non-zero $d\lambda$ is only possible if the combined stresses satisfy the criterion for plastic flow. If the stresses acting fall below the plastic limit, only elastic changes in strain occur, $d\lambda = 0$, and equations (2·11) are merely a differential form of equations (2·9).

We must now consider the relationship between the stress components in order to maintain continued plastic flow. Our immediate interest is in small strains, so that it will be permissible to neglect work hardening, and the limit for continued plastic flow under varying combined stresses will be the same as the limit for the initiation of plastic flow.

The most satisfactory criterion, due to von Mises, is that during plastic flow the elastic shear-strain energy remains constant, and we have

$$(\sigma_y-\sigma_z)^2+(\sigma_z-\sigma_x)^2+(\sigma_x-\sigma_y)^2+6(\tau_{xy}^2+\tau_{yz}^2+\tau_{zx}^2) = 2Y^2, \tag{2·13}$$

where Y is the yield stress in tension. Mohr's criterion of flow at a constant value of the maximum shear stress also provides a good approximation. This limit is represented by

$$\sigma_{\text{max.}}-\sigma_{\text{min.}} = Y, \tag{2·14}$$

where $\sigma_{\text{max.}}$ and $\sigma_{\text{min.}}$ are the greatest and least principal stresses.

Either of these limits governs possible stress variations for non-zero $d\lambda$ in equations (2·11).

If the principal stress directions remain fixed in the element, it is convenient to refer to axes parallel to these directions, and the following simplified relations result by writing $\tau_{xy} = \tau_{yz} = \tau_{zx} = 0$ in the previous formulae:

$$\left.\begin{aligned} 2G\,d(\epsilon_1-\epsilon) &= d(\sigma_1-\sigma)+d\lambda(\sigma_1-\sigma),\\ 2G\,d(\epsilon_2-\epsilon) &= d(\sigma_2-\sigma)+d\lambda(\sigma_2-\sigma),\\ 2G\,d(\epsilon_3-\epsilon) &= d(\sigma_3-\sigma)+d\lambda(\sigma_3-\sigma),\end{aligned}\right\} \tag{2·11a}$$

$$d\epsilon = d\sigma/3K, \tag{2·12a}$$

$$(\sigma_2-\sigma_3)^2+(\sigma_3-\sigma_1)^2+(\sigma_1-\sigma_2)^2 = 2Y^2. \tag{2·13a}$$

These relationships can be conveniently illustrated in a plane diagram, which facilitates the solution of some particular problems (figure 1).

Figure 1 shows the representation of a state of combined stress using σ_1, σ_2 and σ_3 as space co-ordinates. The vector from the origin to $(\sigma_1, \sigma_2, \sigma_3)$ can be combined from the two components: $(\sigma_1-\sigma, \sigma_2-\sigma, \sigma_3-\sigma)$ lying in the plane $\sigma_1+\sigma_2+\sigma_3 = 0$, and a component (σ, σ, σ) normal to this plane. Plastic properties are, in general, insensitive to the hydrostatic component of stress σ, and the particular relations we are considering (equations (2·8), (2·11), (2·13)) are independent of σ. We need, therefore, use only the component of the stress vector in the plane $\sigma_1+\sigma_2+\sigma_3 = 0$ in considering plastic properties, the other component being responsible for the elastic change in volume only. This simplification can be achieved by considering the projection of the stress diagram of figure 1 on to the plane $\sigma_1+\sigma_2+\sigma_3 = 0$ as shown in figure 2, thus, in effect, representing the reduced stress vector

$$(\sigma_1-\sigma,\ \sigma_2-\sigma,\ \sigma_3-\sigma).$$

The stress axes σ_1, σ_2, σ_3 project into the axes σ_1', σ_2', σ_3' at 120° to each other. It is convenient to increase the scale of the projection by the factor $\surd(3/2)$, so that the reduced stress components $\sigma_1-\sigma$, $\sigma_2-\sigma$, $\sigma_3-\sigma$ are measured directly along the axes σ_1', σ_2', σ_3'. This method of representing stress has been discussed by Geiringer & Prager (1934).

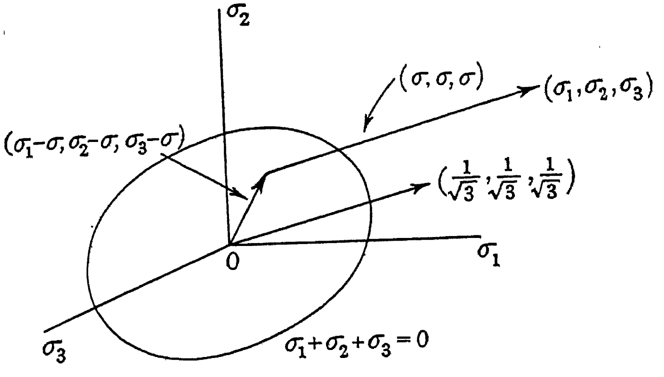
σ_2
(σ, σ, σ)
$(\sigma_1, \sigma_2, \sigma_3)$
$(\sigma_1-\sigma, \sigma_2-\sigma, \sigma_3-\sigma)$
$\left(\frac{1}{\sqrt{3}}, \frac{1}{\sqrt{3}}, \frac{1}{\sqrt{3}}\right)$
0
σ_1
σ_3
$\sigma_1+\sigma_2+\sigma_3=0$

FIGURE 1. Representation of combined stress using the principal stresses as co-ordinates.

The state of combined stress corresponding to a point P in figure 2 is determined by a simple geometrical construction. OMX is drawn perpendicular and PM parallel to σ_2'. N divides PM in the ratio 2 : 1 and NQ is drawn parallel to σ_3'.

Then $PN = 2MN = NR$ and $OQ = QR$. Hence, $OQ+NP-NQ = 0$, so that OQ, NP and NQ, with due regard to sign, are the reduced stress components σ_1', σ_2', σ_3', satisfying the equation

$$\sigma_1'+\sigma_2'+\sigma_3' = 0.$$

The stress criterion for plastic flow determines a closed curve, the 'flow-limit curve', in the reduced stress diagram. For zero work hardening one flow-limit curve exists for all states of strain, the stress point remaining on this curve during an increment of plastic strain.

When considering the stress history of a particular element it is convenient to associate $\sigma_1, \sigma_2, \sigma_3$ with particular directions in the body even though the relative magnitudes of these stresses vary. It would be possible to choose these directions so that for any particular increment of flow $\sigma_1 \geqslant \sigma_2 \geqslant \sigma_3$, and only the sector between σ_1' and $-\sigma_3'$ would be used in figure 2. All possible combined stress conditions could be represented in this limited region of the diagram, but it might be necessary to interchange axes in the body when treating a particular problem as opposed to discussing general stress-strain relationships. We will therefore use the whole field to retain this additional freedom for handling particular problems.

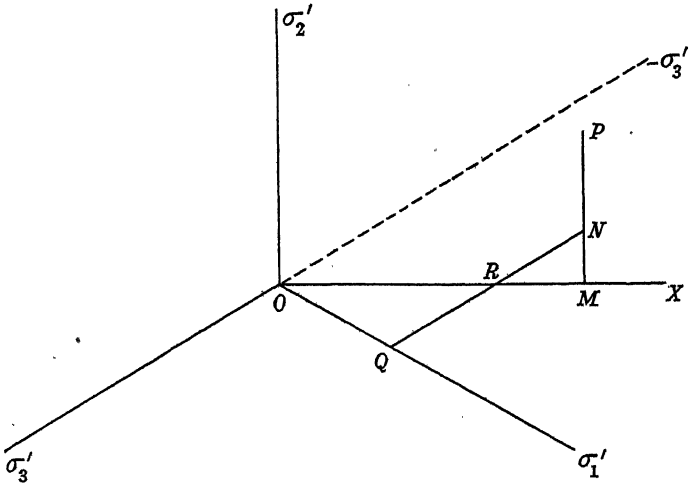

FIGURE 2. The reduced stress-plane diagram for representing combined stresses.

The reduced strain increments $d\epsilon_1', d\epsilon_2', d\epsilon_3'$ equal respectively to $d\epsilon_1 - d\epsilon$, $d\epsilon_2 - d\epsilon$, $d\epsilon_3 - d\epsilon$, can be represented in the same diagram by plotting $2G\,d\epsilon_1'$, $2G\,d\epsilon_2'$, $2G\,d\epsilon_3'$. Since we are assuming here that the principal axes of stress and strain increment in the same element do not change their directions during the flow, it is possible to give the integrals $\int d\epsilon_1$, $\int d\epsilon_2$, $\int d\epsilon_3$ (starting from zero strain) a simple physical interpretation. If ΔL, $(\Delta L)_0$ are the strained and unstrained lengths of the element in one of the principal directions, then $\int d\epsilon$ in that direction is equal to $\log[\Delta L/(\Delta L)_0]$, and it is then legitimate to speak of the vector OQ, components $2G\int d\epsilon_i'$ $(i = 1, 2, 3)$, as representing the total reduced natural strain of the element at any moment. In the elastic region the stress and strain points coincide according to equations (2·9).

When, however, the principal axes of strain increment rotate during the flow, although it is still possible to plot the principal values $d\epsilon_i'$ in the diagram, the integrals

$\int d\epsilon_i'$ no longer have much physical significance, nor is there any one-one relationship between Q and the final state of strain.

Suppose P_1 in figure 3 represents the combined stress and Q_1 the strain at any stage. During further flow the stress point changes along the flow-limit curve to P_2 and the resulting strain increment is Q_1Q_2, determined by equations (2·11*a*). $Q_1Q' \equiv P_1P_2$ represents the increment in elastic strain. $Q'Q_2$, the plastic-strain increment, is parallel to the stress vector OP_1. The magnitude of the increment of plastic strain $Q'Q_2$ depends on the constraint to flow supplied by the surrounding material.

When stress release occurs, the stress point moves from the flow-limit curve towards the origin, and an increment of elastic strain only appears.

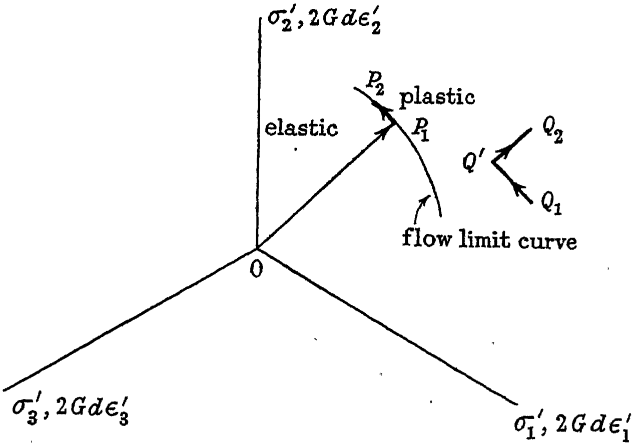
$\sigma_2', 2G\,d\epsilon_2'$
P_2
plastic
elastic
P_1
Q_2
Q'
Q_1
flow limit curve
0
$\sigma_3', 2G\,d\epsilon_3'$
$\sigma_1', 2G\,d\epsilon_1'$

FIGURE 3. The reduced stress-strain diagram for representing deformation under combined stresses.

The stress and strain history of an element of material can be represented on the type of diagram shown in figure 3. If flow occurs at constant stress, what has been called free-flow follows, and the strain point moves parallel to the constant-stress vector.

3. DEFORMATION WITH VON MISES'S YIELD LIMIT

Von Mises's flow-stress criterion of constant elastic shear-strain energy is given in equation (2·13*a*). In the three-dimensional stress diagram of figure 1 it is represented by a circular cylindrical surface normal to the plane $\sigma_1+\sigma_2+\sigma_3 = 0$ with its axis passing through the origin. It therefore projects into a circle on the plane diagram of figure 2 as shown in figure 4.

The tensile flow stress is given by the reduced stress $(\frac{2}{3}Y, -\frac{1}{3}Y, -\frac{1}{3}Y)$, which determines the radius of the flow-limit circle to be Y.

With this form of yield-limit curve, an increment of stress for continued plastic flow, being tangential to the limit curve, is normal to the plastic-strain increment. This, combined with the stress vector of constant radius, leads to a simple mechanical representation of the relationship between stress and strain.

In figure 5, Q_1 represents the strain in an element under the combined stress P_1. The strain changes to Q_2 under the stress change P_1P_2. We consider an inextensible string Q_1O_1' of length Y lying parallel to OP_1 attached to the strain point Q_1 and having a heavy particle at O'. As the strain point Q_1 moves, the particle O_1' is dragged after it such that $O_1'Q_1$ remains parallel to OP_1; that is, $O_1'Q_1$ represents the stress or elastic component of strain, and O_1' the permanent strain throughout the motion.

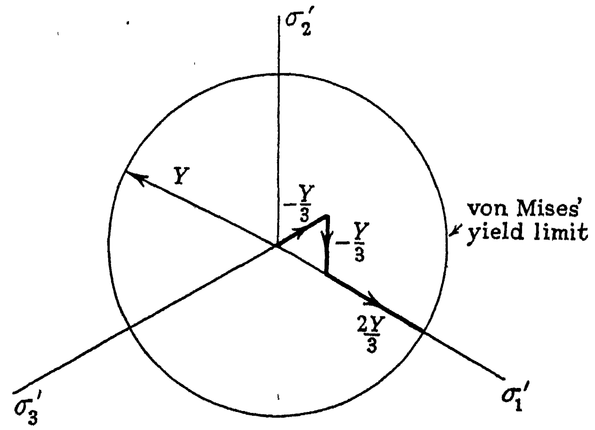

FIGURE 4. The reduced stress diagram showing von Mises's yield-limit criterion.

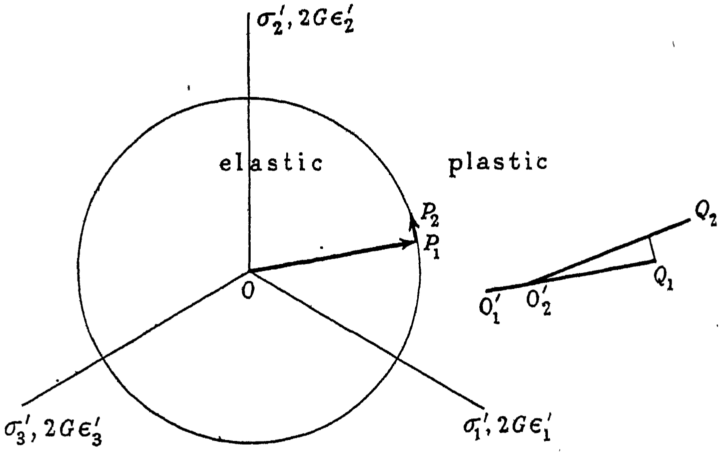
$\sigma_2', 2G\epsilon_2'$
elastic
plastic
P_2
P_1
O
Q_2
Q_1
O_1'
O_2'
$\sigma_3', 2G\epsilon_3'$
$\sigma_1', 2G\epsilon_1'$

FIGURE 5. The reduced stress-strain diagram representing deformation with von Mises's yield-limit criterion.

A pure plastic-strain increment involves motion of Q_1 along $O_1'Q_1$ and so produces no change in stress. A purely elastic-strain increment for a stress change along the flow-limit curve involves rotation of $O_1'Q_1$ equal to the rotation of the stress vector.

If the stresses fall below the yield limit the string becomes slack and O_1' remains fixed, representing the permanent plastic strain.

This model is similar to that suggested by Prager (1944) for combined torsion and tension in a thin tube.

4. DEFORMATION WITH MOHR'S YIELD LIMIT

Mohr's flow criterion of constant maximum shear stress is expressed in equation (2·14). It is represented by a regular hexagonal prism inscribed in the von Mises cylinder in the three-dimensional stress diagram of figure 2, which projects into a hexagon on the reduced stress diagram, figure 6.

The hexagon is inscribed in the von Mises circle discussed in the last section, and each side corresponds to a different maximum and minimum principal stress as indicated in figure 6.

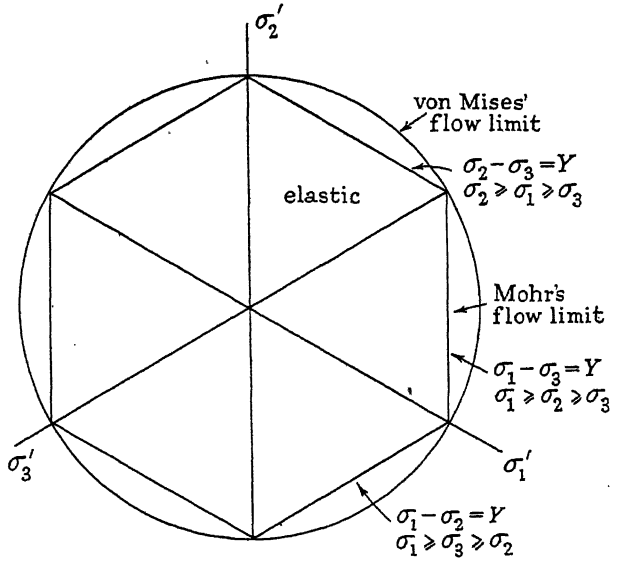
σ_2'
von Mises' flow limit
$\sigma_2-\sigma_3=Y$
$\sigma_2 \geqslant \sigma_1 \geqslant \sigma_3$
elastic
Mohr's flow limit
$\sigma_1-\sigma_3=Y$
$\sigma_1 \geqslant \sigma_2 \geqslant \sigma_3$
σ_3'
σ_1'
$\sigma_1-\sigma_2=Y$
$\sigma_1 \geqslant \sigma_3 \geqslant \sigma_2$

FIGURE 6. Reduced stress diagram showing Mohr's flow limit.

The corresponding relationship between stress and strain is demonstrated in figure 7.

The stress system causing flow is represented by P_1, for which

$$\sigma_1-\sigma_3 = Y,$$

and σ_2 is the intermediate stress. During a change in stress P_1P_2, the strain increment is represented by Q_1Q_2, Q_1Q', the elastic-strain increment, being equal to P_1P_2, and $Q'Q_2$, the plastic-strain increment, parallel to OP_1.

This relationship between deformation and stress does not appear as fundamentally simple as that described in the previous section for the von Mises flow limit. The significance of this difference is discussed in the following section.

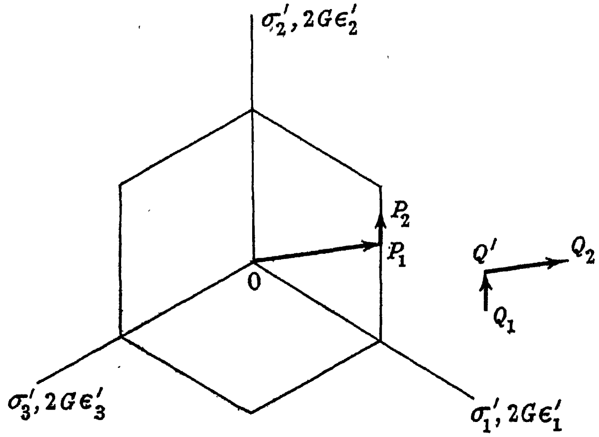
$\sigma_2', 2G\epsilon_2'$
P_2
P_1
0
Q'
Q_2
Q_1
$\sigma_3', 2G\epsilon_3'$
$\sigma_1', 2G\epsilon_1'$

Figure 7. The reduced stress-strain diagram representing deformation with Mohr's yield-limit criterion.

5. ENERGY RELATIONSHIPS DURING FREE PLASTIC FLOW

Free flow was defined in § 2 as flow under constant stress. The elastic component of strain remains constant, and we are therefore concerned only with plastic-strain increments.

The dissipation of energy in these circumstances was discussed in 1943 in unpublished work by G. I. Taylor. The reduced stress-strain diagrams described in the previous sections of the present paper facilitate the general discussion of this problem, and clarify the significance of the stress-deformation relationships already described.

Consider the reduced stress-strain diagram in figure 8. We shall assume the strain increment Q_1Q_2 to be developed under the constant flow-limit stress OP, the former restriction that these vectors are parallel being discarded. The energy dissipated during this flow may be expressed as the scalar product of the stress and strain vectors

$$dW = \sigma_1' d\epsilon_1' + \sigma_2' d\epsilon_2' + \sigma_3' d\epsilon_3',$$

since the elastic-strain energy remains constant.

If we consider the strain increment Q_1Q_2 as given, and consider the energy dissipated, assuming that this strain increment corresponds to different positions of P on the flow-limit curve, the variation of dW will be determined by the variation of the component of OP on the given direction Q_1Q_2. If the flow-limit curve is always concave towards the origin, dW is zero when OP is perpendicular to Q_1Q_2, and reaches a maximum value when the normal at P is parallel to Q_1Q_2 and in the same sense. If we therefore postulate a condition of maximum energy dissipation for a given strain increment, any particular flow-limit curve determines a flow criterion and vice versa.

Taylor introduced the concept of a stationary energy dissipation condition in the work mentioned above. The criterion of maximum energy dissipation is in line with other force-displacement associations such as friction, hydrostatic compression, where the force and resulting deformation are associated to produce maximum energy absorption. Minimum energy relations are associated with equilibrium problems when the stress-deformation relations are already assumed.

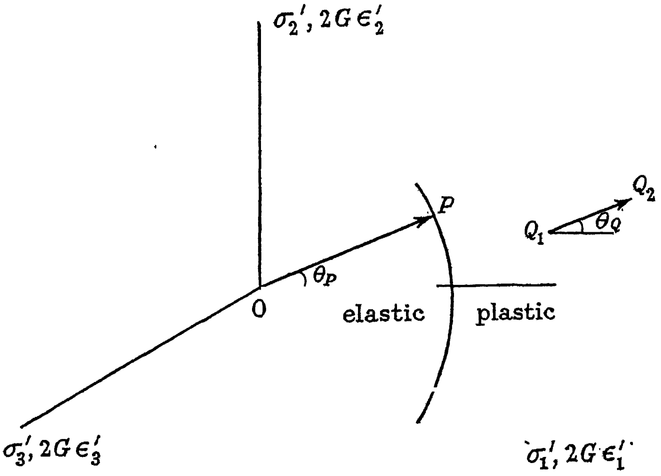
$\sigma_2', 2G\epsilon_2'$
P
Q_2
Q_1
θ_Q
θ_P
O
elastic
plastic
$\sigma_3', 2G\epsilon_3'$
$\sigma_1', 2G\epsilon_1'$

FIGURE 8. The reduced stress-strain diagram representing general flow conditions.

Assuming von Mises's flow-limit relationship, P lies on a circle centre the origin, OP is the normal to the flow-limit curve, and Q_1Q_2 parallel to OP satisfies the maximum energy dissipation condition. This relationship between Q_1Q_2 and OP is, in fact, that expressed in equations (2·11), which have been used throughout the previous sections.

Assuming the Mohr flow criterion, if the strain increment Q_1Q_2 is chosen arbitrarily, the energy dissipated will vary linearly along each side of the flow hexagon, and will reach a maximum value at one of the vertices, where a discontinuity in gradient occurs. The maximum energy criterion will therefore determine a flow stress vector corresponding to a vertex of the hexagon, and the same stress vector will correspond to a range of strain increment directions. If, however, Q_1Q_2 is normal to a side of the flow hexagon, the energy dissipated will be constant as the stress point varies along that side of the hexagon and will fall off along the adjacent sides. The maximum energy dissipation criterion therefore determines a strain increment normal to a side of the flow-limit hexagon for stress points on that side, and an intermediate range of strain increments for stress vectors to the vertices of the hexagon.

Q_1Q_2 will not, in general, be parallel to OP, so that deformation satisfying equation (2·11) combined with Mohr's criterion will not satisfy the maximum energy dissipation condition.

If, in this case, we take Q_1Q_2 according to the maximum energy hypothesis instead of using equation (2·11), the deformation Q_1Q_2 represents pure shear in the plane of maximum shear stress, with zero strain in the direction of the intermediate principal stress. For a stress vector to a vertex of the hexagon, two principal stress differences reach the maximum value, two principal stresses are equal, and an infinity of planes touching a cone are all subject to the maximum shear stress. The corresponding strain increment is pure shear on one of these planes. Though this would seem to be a rational deduction from a maximum shear stress flow limit, it is not in accordance with experiment.

These considerations suggest that the von Mises's criterion combined with the viscous-flow plastic deformation law (equation (2·11)) is the most satisfactory combination. Mohr's flow limit is an adequate approximation for a flow-stress criterion, but experiments show that the deformation law of equation (2·11) should be retained, rather than the physically more rational associated pure shearing deformation.

A common means of relating the stress and strain vectors, OP and Q_1Q_2 in figure 8, has been by means of Lode's parameters μ and ν:

$$\mu = \frac{2\sigma_2' - \sigma_1' - \sigma_3'}{\sigma_1' - \sigma_3'}, \quad \nu = \frac{2d\epsilon_2' - d\epsilon_1' - d\epsilon_3'}{d\epsilon_1' - d\epsilon_3'}.$$

These are related to the vectors in figure 8 by the relations

$$\mu = \sqrt{3}\tan\theta_P, \quad \nu = \sqrt{3}\tan\theta_Q.$$

For an isotropic solid the yield-limit relationship and that between θ_P and θ_Q must be symmetrical about the axes 1, 2, 3. This specifies $\theta_P = \theta_Q$ for $\theta = \frac{1}{6}(2n+1)\pi$, where n is an integer, positive or negative.

If reversal of stress merely reverses strain conditions, symmetry about the origin must also obtain and $\theta_P = \theta_Q$ for $\theta = \frac{1}{6}n\pi$.

These relations express the usual conditions $\mu = \nu = 0, \pm 1$.

For a given relationship between μ and ν, that is, between θ_P and θ_Q, use of the maximum energy dissipation criterion determines the direction of the tangent to the flow-limit curve for each θ_P, for then Q_1Q_2 is parallel to the normal at P. In this way the flow-limit curve is determined if one point on it is given.

For a given flow-limit curve, the maximum energy criterion determines the direction of Q_1Q_2 as that of the normal at the corresponding value of stress.

6. APPLICATION TO THE STRESS DISTRIBUTION IN A LONG THICK TUBE WITH INTERNAL PRESSURE

We shall consider the stress distribution and deformation while part of the tube is elastic, and also when the plastic region has spread throughout the section. If von Mises's flow criterion is assumed, the unknown distribution of longitudinal stress across the section may influence the determination of the radial and circumferential stresses, which introduces complications. If Mohr's criterion is used, however, the stresses in planes normal to the axis can be treated independently of the longitudinal stress. The theory of combined plastic-elastic deformation, dealt with in previous sections, can then be used to determine the complete stress distribution and the deformation as the flow develops with increasing pressure. At all stages in the deformation, this solution depends on the strain history of the material in plastic flow, a requirement that has not been included in earlier solutions.

This solution, based on Mohr's hypothesis, can be easily applied to satisfy von Mises's flow condition throughout the flow to within 3 % in the particular case we consider later. This extension is possible, since only a limited sector of the reduced stress diagram is used and the tangent to the von Mises's circle is a satisfactory approximation for the circle in this restricted region. This tangent criterion is equivalent to Mohr's criterion with flow stress $2Y/\surd 3$.

We shall treat the problem in which the longitudinal restraint takes the form of zero longitudinal strain. Using cylindrical co-ordinates r, θ, z, considerations of symmetry make σ_r, σ_θ, σ_z principal stresses. We shall assume $\sigma_\theta \geqslant \sigma_z \geqslant \sigma_r$, which can be verified in the final solution, so that Mohr's flow-limit criterion becomes

$$\sigma_\theta - \sigma_r = Y. \qquad (2\cdot 14b)$$

The section of the tube is shown in figure 9 when the plastic region has spread to a radius c. We are considering small deformations so that the boundary conditions at the surfaces during the flow are determined by $r = a$ and $r = b$, the radii of the unstrained tube.

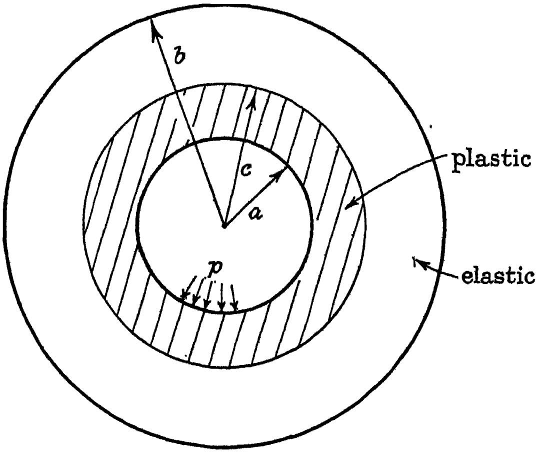

FIGURE 9. Section of the tube when partially plastic.

In the elastic region we have the usual Lamé solution

$$\sigma_r = A - \frac{B}{r^2}, \quad \sigma_\theta = A + \frac{B}{r^2}, \qquad (6\cdot 1)$$

where A and B are constants.

We have the boundary conditions

$$r = b, \quad \sigma_r = 0; \quad r = c, \quad \sigma_\theta - \sigma_r = Y, \tag{6·2}$$

since the material at radius c is about to become plastic. These determine

$$\sigma_r = \frac{Yc^2}{2}\left(\frac{1}{b^2}-\frac{1}{r^2}\right), \quad \sigma_\theta = \frac{Yc^2}{2}\left(\frac{1}{b^2}+\frac{1}{r^2}\right) \tag{6·3}$$

in the elastic region.

In the plastic region, equilibrium in the radial direction demands that

$$r\frac{d\sigma_r}{dr} = \sigma_\theta - \sigma_r = Y, \tag{6·4}$$

with boundary conditions

$$r = c, \quad (\sigma_r)_{\text{plastic}} = (\sigma_r)_{\text{elastic}}; \quad r = a, \quad \sigma_r = -p. \tag{6·5}$$

These conditions determine

$$\sigma_r = Y\log\frac{r}{a} - p, \quad \sigma_\theta = Y\left(\log\frac{r}{a}+1\right) - p, \tag{6·6}$$

and the relationship

$$p = Y\left\{\log\frac{c}{a}+\frac{1}{2}\left(1-\frac{c^2}{b^2}\right)\right\}. \tag{6·7}$$

Thus, for given a, b, Y and p, c is determined by equation (6·7). The condition $c = a$ determines the pressure at the initiation of plastic flow at $r = a$, and $c = b$ determines the pressure when the whole tube is in plastic flow. So far this analysis agrees with earlier solutions (Nadai 1931).

The additional condition $\epsilon_z = 0$ directly determines σ_z and the radial displacement, u, in the elastic region, but the history of the deformation must be analyzed to obtain σ_z and u in the plastic region.

The reduced stress-strain diagram described in § 4 facilitates the analysis of the development of flow. For the sake of completeness, we will first consider how the stresses and strain distributions are represented while the tube is still elastic throughout.

The reduced stresses, determined from the equations (6·1) with boundary conditions

$$\sigma_r = -p, \quad r = a, \quad \sigma_r = 0, \quad r = b,$$

are

$$\left.\begin{aligned} \sigma'_\theta &= \sigma_\theta - \sigma = \frac{pb^2}{b^2-a^2}\left(\alpha+\frac{a^2}{r^2}\right), \\ \sigma'_z &= \sigma_z - \sigma = \frac{pb^2}{b^2-a^2}(-2\alpha), \\ \sigma'_r &= \sigma_r - \sigma = \frac{pb^2}{b^2-a^2}\left(\alpha-\frac{a^2}{r^2}\right), \end{aligned}\right\} \tag{6·8}$$

where $\alpha = \frac{1-2\nu}{3}\frac{a^2}{b^2}$ and ν is Poisson's ratio.

Figure 10 shows the representation of these reduced stresses on the reduced stress-strain diagram.

The terms containing α are seen to represent a constant vector $\frac{3pb^2\alpha}{b^2-a^2}$ along $-\sigma'_z$, the terms involving r adding a perpendicular vector of magnitude proportional to $1/r^2$.

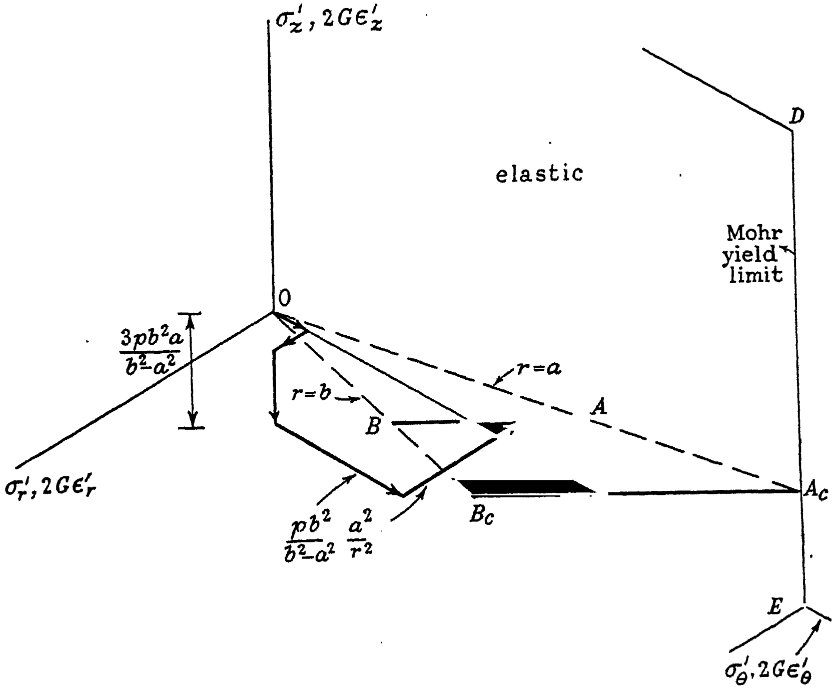
$\sigma'_z, 2G\epsilon'_z$
elastic
D
Mohr yield limit
0
$\frac{3pb^2a}{b^2-a^2}$
$r=a$
$r=b$
A
B
A_c
B_c
$\frac{pb^2}{b^2-a^2}\frac{a^2}{r^2}$
$\sigma'_r, 2G\epsilon'_r$
E
$\sigma'_\theta, 2G\epsilon'_\theta$

FIGURE 10. The stress and strain variation while the tube is still elastic.

The combined stress condition throughout the tube is represented by the line AB. Since elastic strains only exist this line also represents the strain in the tube as discussed in § 2. If u is the radial displacement, which is assumed small, nominal strains may be used, giving

$$\epsilon_\theta = \frac{u}{r}, \quad \epsilon_z = 0, \quad \epsilon_r = \frac{du}{dr}.$$

The reduced strains are therefore

$$\epsilon'_\theta = \frac{2}{3}\frac{u}{r} - \frac{1}{3}\frac{du}{dr}, \quad \epsilon'_z = -\frac{1}{3}\left(\frac{u}{r}+\frac{du}{dr}\right), \quad \epsilon'_r = \frac{2}{3}\frac{du}{dr} - \frac{1}{3}\frac{u}{r}.$$

In this way AB determines the radial displacement of each element in the tube.

With increasing pressure the stress vectors increase proportionately, until A reaches the yield-limit line DE. The stress and strains throughout the tube are then given by points on A_cB_c, and further increase in pressure will cause plastic flow to spread from the inside of the tube.

The reduced stresses at the initiation of plastic flow are

$$\sigma'_\theta = \frac{Y}{2}\left(\alpha+\frac{a^2}{r^2}\right), \quad \sigma'_z = -\frac{Y}{2}2\alpha, \quad \sigma'_r = \frac{Y}{2}\left(\alpha-\frac{a^2}{r^2}\right). \tag{6·9}$$

As yet stress and strain points in figure 10 have been coincident for all elements of the tube, but, as plastic flow develops, the strain points corresponding to material in plastic flow will move to the right of DE, while the corresponding stress points remain on DE, as discussed in § 2.

The condition in the elastic region of figure 9, however, can be immediately represented in figure 10. For any given value of c, the stresses and strains in the elastic region are completely determined by equations (6·3) and the zero longitudinal strain condition. The reduced stresses are

$$\sigma'_\theta = \frac{Y}{2}\left(\alpha\frac{c^2}{a^2}+\frac{c^2}{r^2}\right), \quad \sigma'_z = -\frac{Y}{2}2\alpha\frac{c^2}{a^2}, \quad \sigma'_r = \frac{Y}{2}\left(\alpha\frac{c^2}{a^2}-\frac{c^2}{r^2}\right). \tag{6·10}$$

Figure 11 shows the corresponding reduced stress-strain diagram.

The form of equations (6·10) shows that for varying c, points corresponding to constant r lie on radii through the origin.

B_cA_c, also shown in figure 10, gives the conditions at the initiation of plastic flow when $c = a$. $B'A'$ represents an intermediate condition, and A'' the last shell of elastic material, $c = b$, before the whole tube becomes plastic.

The vectors indicated in figure 11 show how the components expressed in equations (6·10) combine to specify a point on $B'A'$.

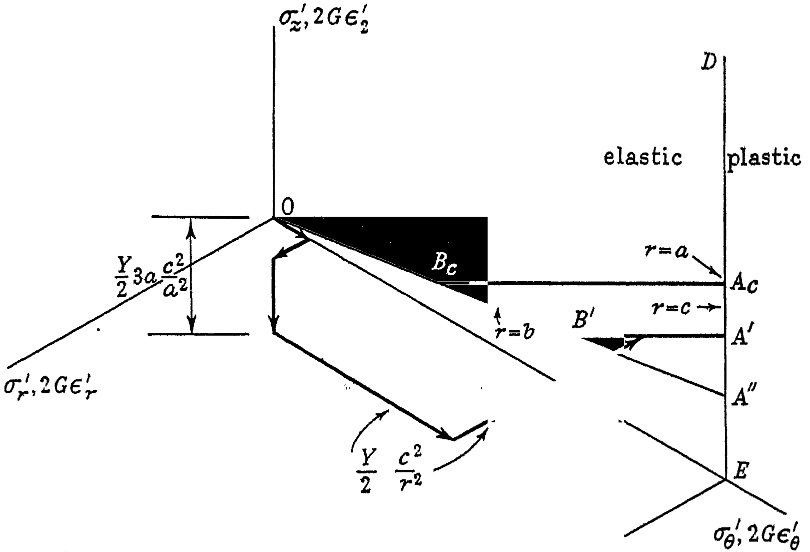

FIGURE 11. The stress and strain variation in the elastic part of a partially plastic tube.

Figure 11 expresses the stress and strain distribution for $c \leqslant r \leqslant b$, $a \leqslant c \leqslant b$. We require to extend the lines of constant c (which specify conditions at a particular stage in the flow) into the region where $a \leqslant r < c$ to the right of DE. These curves, each point of which corresponds to a particular value of r, will express the deformation throughout the tube.

It is convenient to use axes x, y shown in figure 12. During plastic flow, two points are required to specify the stress and deformation of a particular element. Their co-ordinates are x_s, y_s and x_e, y_e respectively.

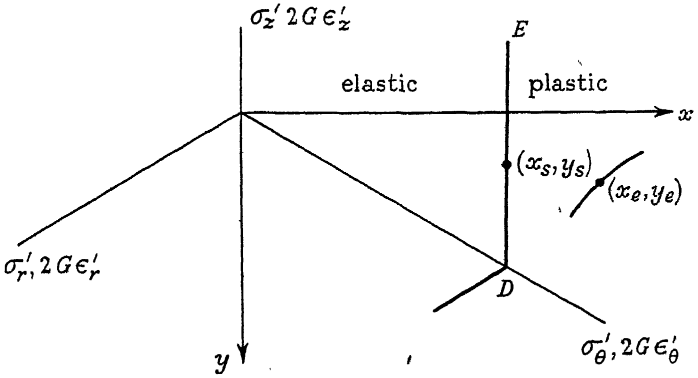
$\sigma_z'\ 2G\epsilon_z'$
E
elastic
plastic
x
(x_s, y_s)
(x_e, y_e)
$\sigma_r', 2G\epsilon_r'$
D
y
$\sigma_\theta', 2G\epsilon_\theta'$

FIGURE 12. Axes used for the plastic solution.

Expressing these in terms of the stresses and displacement, according to the geometry of the diagram discussed in § 2, we have

$$x_s = \frac{\sqrt{3}}{2}(\sigma_\theta - \sigma_r), \qquad y_s = \frac{\sigma_\theta + \sigma_r}{2} - \sigma_z, \tag{6·11}$$

$$x_e = \sqrt{3}\,G\left(\frac{u}{r} - \frac{\partial u}{\partial r}\right), \quad y_e = G\left(\frac{u}{r} + \frac{\partial u}{\partial r}\right). \tag{6·12}$$

As previously discussed, this diagram can, in general, only represent shear properties, but for our particular problem the volumetric strain, $(u/r + \partial u/\partial r)$, is expressed as y_e/G. The compressibility equation (2·12) then determines the relationship

$$Y\left(\log\frac{r^2}{c^2} + \frac{c^2}{b^2}\right) + \sigma_z = \frac{3K}{G}\,y_e, \tag{6·13}$$

using equations (6·6), (6·7) for the stress components. This equation determines σ_z in the plastic region for given y_e and c.

Eliminating u between (6·12) gives

$$\left\{\frac{\partial y_e}{\partial r}\right\}_c + \frac{1}{\sqrt{3}}\left\{\frac{\partial x_e}{\partial r}\right\}_c + \frac{2}{\sqrt{3}}\frac{x_e}{r} = 0. \tag{6·14}$$

This is valid for constant c, that is for a particular stage in the flow.

We now make use of the stress-strain relationship during plastic flow discussed in § 4. For any element of the tube at a particular stage in the deformation (given c), the next increment of flow corresponding to dc is determined, according to figure 7, by the equation

$$dy_e = dy_s + \frac{y_s}{x_s}\,dx_e. \tag{6·15}$$

This becomes
$$\left\{\frac{\partial y_e}{\partial c}\right\}_r = \left\{\frac{\partial y_s}{\partial c}\right\}_r + \frac{2}{\sqrt{3}}\frac{y_s}{Y}\left\{\frac{\partial x_e}{\partial c}\right\}_r. \qquad (6\cdot16)$$

The determination of the deformation of the tube until it becomes plastic throughout requires the solution of the simultaneous partial differential equations (6·14) and (6·16) with y_e, x_e as dependent variables, and r, c as independent variables. y_s can be expressed in terms of the variables by the second of equations (6·11), giving
$$y_s = 3Y\left\{\log\frac{r}{c} + \frac{1}{2}\frac{c^2}{b^2}\right\} - \frac{3K}{G}y_e. \qquad (6\cdot17)$$

Conditions on the plastic-elastic boundary $r = c$ are known from the solution of the elastic region, and the solution in the shaded region ABC shown in figure 13 is required.

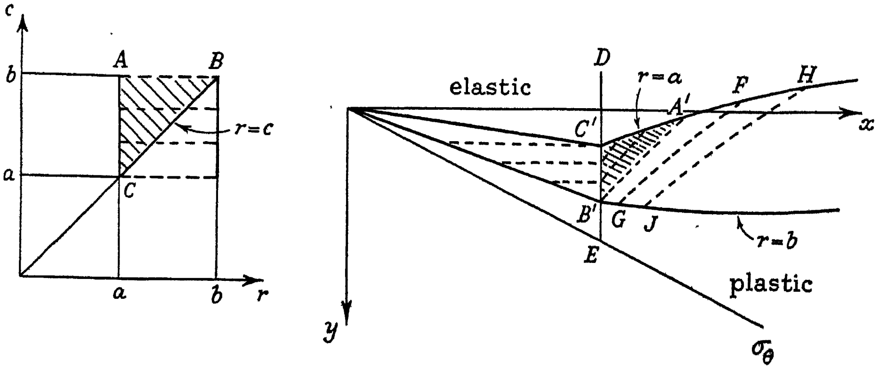

FIGURE 13. Regions covered in the solution of equations (6·14) and (6·16).

The equations are hyperbolic in form with characteristics r = constant and c = constant, so that the solution in the region ABC can be built up numerically along characteristics from the known conditions on BC. The x, y field on the right of figure 13 shows the resulting type of solution, the details of which are discussed in the following section. $A'B'C'$ corresponds to ABC, and lines of constant c, representing particular stages in the flow, are shown dotted in each diagram.

After the whole tube has become plastic, continued flow occurs under the constant pressure $Y\log b/a$. The values of σ_r and σ_θ for each element remain constant also, so that the strain history of each element develops independently of the rest of the tube. The strain trajectory for a particular value of r can be obtained directly from (6·16) and (6·17).

Thus (6·17) becomes
$$y_s = 3Y\left\{\log\frac{r}{b} + \frac{1}{2}\right\} - \frac{3K}{G}y_e. \qquad (6\cdot18)$$

Substituting this in (6·16)
$$dy_e\left(1 + \frac{3K}{G}\right) = 2\sqrt{3}\left\{\left(\log\frac{r}{b} + \frac{1}{2}\right) - \frac{K}{G}\frac{y_e}{Y}\right\}dx_e.$$

On integration

$$x_e = x_{e0} + Y\frac{(G/K+3)}{2\sqrt{3}}\log\left\{\frac{G/K(\log r/b+\frac{1}{2})-y_{e0}/Y}{G/K(\log r/b+\frac{1}{2})-y_e/Y}\right\}, \tag{6·19}$$

where (x_{e0}, y_{e0}) is the strain point when $c = b$ for the particular value of r, and is known from the last stage of the characteristic solution. In figure 13, $A'FH$ and $B'GJ$ are the strain trajectories for $r = a$ and $r = b$.

The stresses σ_r, σ_θ for an element r are obtained by substituting $c = b$ in (6·6) and (6·7):

$$\sigma_r = Y\log\frac{r}{b}, \quad \sigma_\theta = Y\left(\log\frac{r}{b}+1\right). \tag{6·20}$$

The displacement u is found in terms of (x_e, y_e) from (6·12):

$$\frac{2Gu}{r} = \frac{x_e}{\sqrt{3}}+y_e. \tag{6·21}$$

The compressibility equation (2·12) with (6·12) determines σ_z as

$$\sigma_z = \frac{3K}{G}y_e - Y\left(2\log\frac{r}{b}+1\right), \tag{6·22}$$

which is formally the same as substituting $c = b$ in (6·13).

Now that the tube is completely plastic the variable c no longer represents the development of the flow so that it is convenient to introduce a new variable u_b, the displacement of the exterior of the tube. This method has the advantage that u_b is easily measured in practice. It must be remembered that u/a must still be restricted to be small in the physical problem. We can obtain points on the trajectory $r = b$ (6·19) corresponding to required values of u_b from (6·21). Integration of (6·14) from these boundary points then gives the strain distributions throughout the tube at particular stages in the flow, represented by the dotted curves GF, JH in figure 13.

7. The finite difference solution for the plastic flow

For convenience, we divide all co-ordinates in the x, y plane by the yield-stress Y, so that the dependent variables are non-dimensional.

The solution involves integrating equations (6·14) and (6·16) along the characteristics c = constant and r = constant. Values of the dependent variables x_e, y_e are known on BC in figure 13, and integration over increasing c and decreasing r covers the region ABC.

The step by step triangulation is shown in figure 14.

At some stage in the procedure the point r, c representing the deformation of an element at stage c in the flow, and the point $r+dr$, $c+\Delta c$ have been determined. The next step is to determine the point r, $c+\Delta c$. When the corresponding x_e and y_e have been determined, the displacement, stress and strain are given by the formulae deduced in the previous section. The increments dx_e, dy_e, dy_s in figure 14 are known; Δx_e, Δy_e, Δy_s are to be determined.

Expressing equation (6·14) in finite differences for the increment $r+dr$, r on the characteristic $c+\Delta c$, we have

$$\Delta y_e = dy_e + \frac{1}{\sqrt{3}}\left(1+\frac{dr}{r+\frac{1}{2}dr}\right)dx_e + \frac{2}{\sqrt{3}}x_e\frac{dr}{r+\frac{1}{2}dr} - \frac{1}{\sqrt{3}}\left(1-\frac{dr}{r+\frac{1}{2}dr}\right)\Delta x_e. \tag{7·1}$$

Equation (6·16) for the interval c, $c+\Delta c$ on the characteristic r becomes

$$\Delta y_e\left\{1+\frac{3K}{G}+\frac{\sqrt{3}K}{G}\Delta x_e\right\} = 3\left\{\frac{2c+\Delta c}{2b^2}\Delta c - \log\frac{c+\Delta c}{c}\right\}\left(1+\frac{\Delta x_e}{\sqrt{3}}\right)+\frac{2}{\sqrt{3}}y_s(r,c)\,\Delta x_e. \tag{7·2}$$

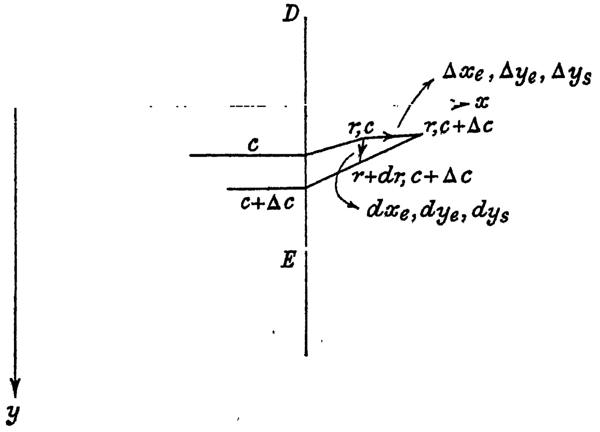

FIGURE 14. Finite difference procedure in the x, y plane.

Substituting Δy_e from (7·1) into (7·2) gives a quadratic for Δx_e, from which Δy_e, Δy_s and $\Delta\hat{zz}$ follow at once.

This procedure was found to be sufficiently convergent taking increments of 0·1 in r and c for $a = 1$, $b = 2$. A simple check is provided by evaluating the integral form of equation (6·14) along lines of constant c

$$y_e + \frac{1}{\sqrt{3}}x_e + \frac{2}{\sqrt{3}}\int^r x_e\, d(\log r) = \text{constant}. \tag{7·3}$$

8. DISCUSSION OF NUMERICAL RESULTS OBTAINED FOR THE PARTICULAR CASE $b = 2a$

The solution for $b = 2a$ has been solved numerically. Throughout, r and c are expressed non-dimensionally in units of a. Poisson's ratio ν is taken to be 0·3, other elastic constants are not required for expressing results in non-dimensional units. The corresponding value of

$$3K/G = 2(1+\nu)/(1-2\nu) = 6·5.$$

Figure 15 shows the resulting reduced strain diagram of the form described in figure 13, but with an enlarged y scale. DE is the Mohr flow-limit boundary. The full curves represent the strain trajectories for constant r, which give the strain history of particular elements. The broken curves represent the stress and strain distribution at successive stages in the flow. KC' represents the condition just before the initiation of plastic flow at the inside of the tube. The plastic region has spread throughout the tube at $B'A'$, and GF and JH represent successive stages in the continued flow at constant internal pressure.

The distribution of the longitudinal stress σ_z as the flow develops is shown by the full lines in figure 16. Particular points are denoted by the letters used in figure 15: $C'K$ represents the initiation of plastic flow, $A'B'$ flow throughout the tube, etc. The marked increase in the longitudinal stress towards the outside of the tube with continued complete plastic flow is significant.

The full line in figure 17 shows the variation of the total longitudinal force required to produce the constraint of zero longitudinal extension. It increases by a considerable amount during the continued flow after the tube has become completely plastic.

Figure 15 shows that only a narrow band along the x-axis is required to represent the deformation throughout the thick tube which we have been considering. This necessitated magnification of the ordinates in figure 15. The stress ordinate y_s is even more restricted as shown in figure 18, which depicts the variation in y_s for particular elements throughout the flow. In each case y_s reaches a maximum at the initiation of plastic flow, thereafter approaching zero as the deformation increases.

In these circumstances it is evident that, using the von Mises's flow-limit circle, only a restricted arc near the x-axis would be required. Replacing this arc by the vertical tangent would introduce only a small error in the combined stresses required to produce flow, and the analysis would be identical with that already carried out for Mohr's limit, Y being replaced by $2Y/\sqrt{3}$. For the problem considered, the error in flow stress is less than 3 % and this occurs only during the initial increment of plastic flow for each element.

The above analysis can therefore be interpreted as the solution for a flow-limit criterion which is a close approximation to von Mises's shear-strain energy criterion. In view of experimental results (Taylor & Quinney 1931; Baildon 1943) and the discussion in § 5, von Mises's criterion is the most satisfactory, so that our solution, although developed on the basis of the Mohr theory, should be considered as a close approximation to the solution according to von Mises's criteria.

9. COMPARISON WITH THE INELASTIC-PLASTIC SOLUTION

Although the longitudinal constraint considered in the solution discussed in the previous section does not represent auto-frettage practice, comparison with the corresponding inelastic-plastic solution will give an indication of the error involved in making this usual assumption.

Nadai (1931) neglects all elastic strain in the plastic region, so that

$$\sigma_z = \sigma = \tfrac{1}{2}(\sigma_r + \sigma_\theta)$$

(i.e. $y_s = 0$) from the condition $\epsilon_z = 0$ (2·8), and $y_e = 0$ from (2·7) which in this case stipulates incompressible flow. Von Mises's flow criterion reduces to $\sigma_\theta - \sigma_r = 2Y/\sqrt{3}$. Thus the solution in the plastic region obtained above by following the history of the flow of each element is replaced by $y_e = y_s = 0$. In the elastic region, Nadai's solution agrees with our solution.

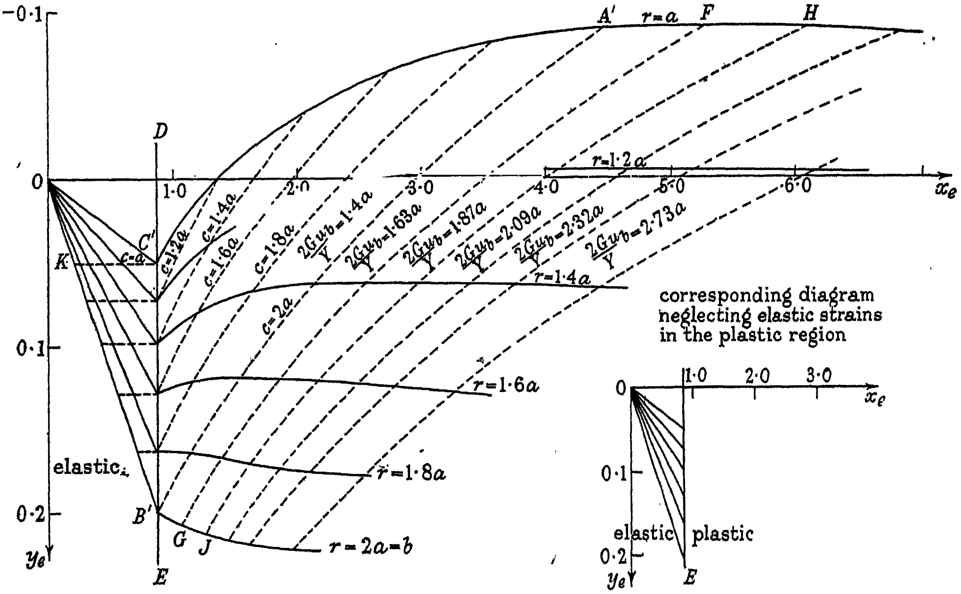

Figure 15. The reduced strain diagram with enlarged ordinate scale for a thick tube with internal pressure. —— Particular element, r constant. – – – – Particular stage in the flow, c or u_b constant.

The lower figure in figure 15 shows the corresponding reduced strain diagram. In the plastic region, to the right of DE, all points lie on the x-axis. It should, perhaps, be pointed out that the difference between the types of solution in figure 15 is over-emphasized by the change in the scale of the ordinate. The distribution of longitudinal stress over the cross-section obtained from the inelastic-plastic solution is represented by the broken lines in figure 16. This distribution is derived at once for each value of c from the relationship

$$\sigma_z = \frac{\sigma_r + \sigma_\theta}{2}.$$

The stress in the elastic region agrees with our complete solution, but, instead of the continuous stress distribution, neglect of the elastic strains in the plastic region involves a discontinuity in σ_z at the plastic-elastic boundary. The difference between the two solutions becomes more marked as c increases. At the moment when the tube becomes plastic throughout, σ_z at $r = b$ is $0{\cdot}5Y$ according to the inelastic-plastic solution, instead of $0{\cdot}3Y$, an error of over 60 %.

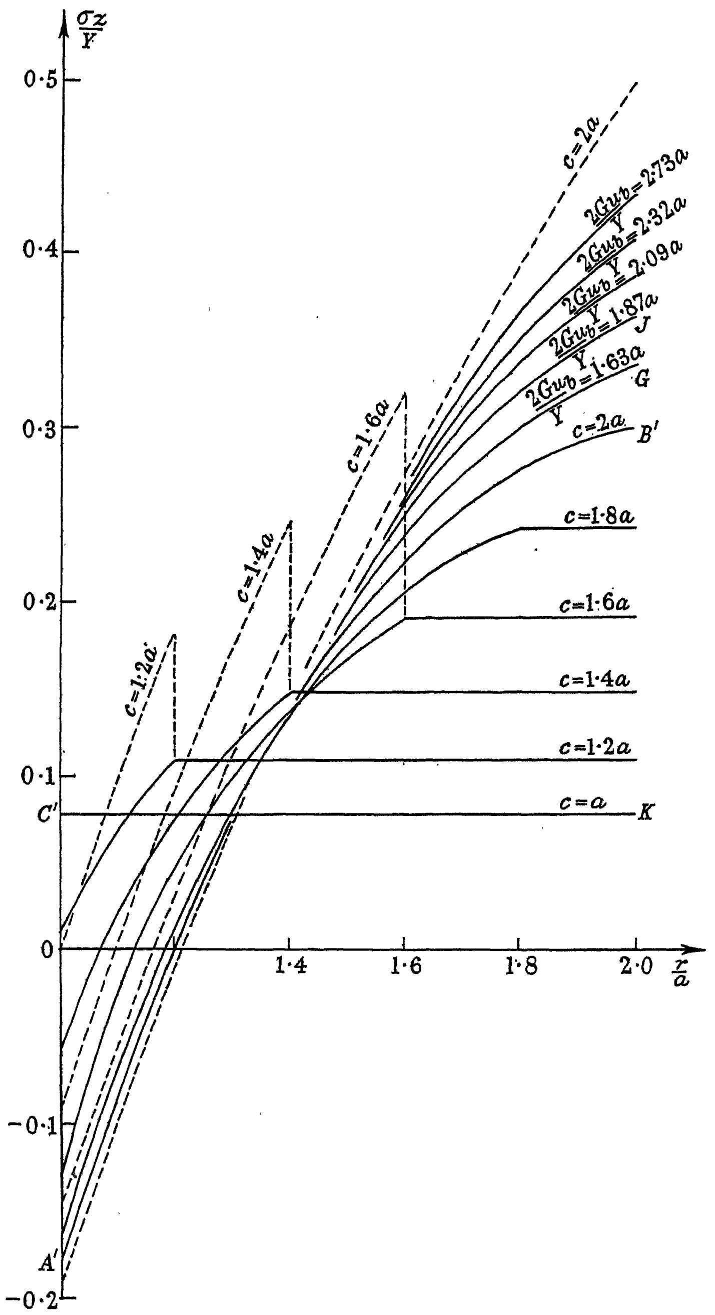

FIGURE 16. Distribution of longitudinal stress over the section at various stages in the flow. —— Complete solution. – – – – Neglecting elastic strains in the plastic region.

When the whole tube is in plastic flow, the inelastic-plastic solution determines a distribution of σ_z, which is not affected by continued flow. For the correct solution, however, the stress distribution is modified as flow continues and approaches the inelastic-plastic solution with increasing deformation. Thus, if we take x_e large in (6·19), $y_e/Y \to G/K(\log r/b + \frac{1}{2})$, which with (6·18) determines that $y_s \to 0$ and $\sigma_z \to \frac{1}{2}(\sigma_r + \sigma_\theta)$. This limit seems physically reasonable, for as the flow develops, the plastic component of strain predominates and the assumptions involved in the inelastic-plastic solution become justified. The error in the earlier part of the expansion, however, when part of the tube is still elastic, may be considerable. It is interesting to observe that the elements near the inside of the tube, which deform plastically at an earlier stage, settle down sooner to close agreement with the inelastic-plastic stress distribution.

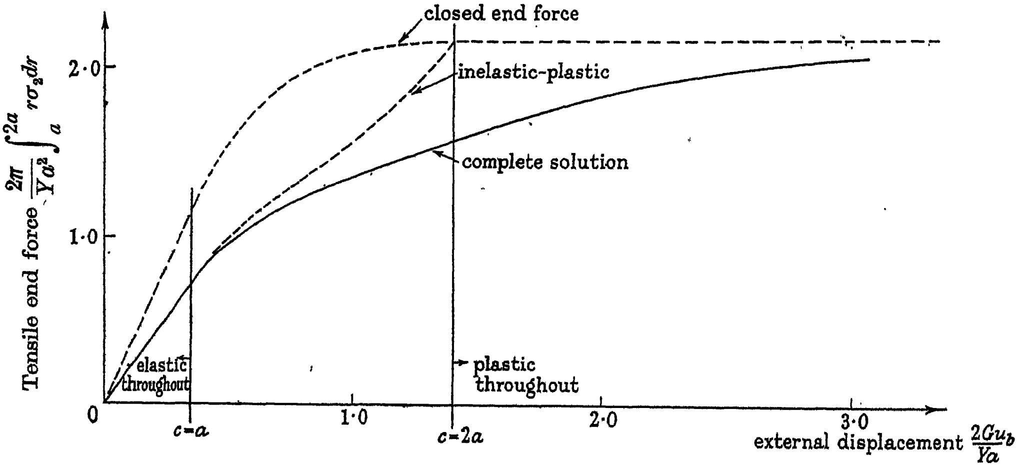

FIGURE 17. Variation of end force required to produce zero longitudinal strain as the flow develops.

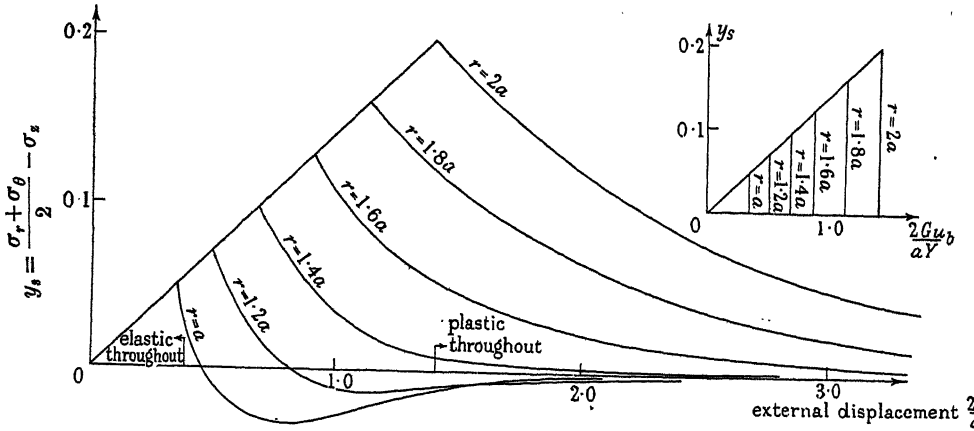

FIGURE 18. Variation of y_s for particular elements as the flow proceeds. The stage of flow is represented by the external deformation.

Figure 17 shows the total longitudinal force over the end of the tube determined from the incompressible plastic solution, compared with the correct variation. The inelastic-plastic value reaches a maximum value when the whole tube becomes plastic and remains constant with increasing deformation. The complete solution approaches this same maximum as the deformation continues.

The inset diagram in figure 18 shows the variation of y_s for the inelastic-plastic solution. y_s is zero in the plastic region compared with the gradual approach to zero deduced from the complete solution.

10. CONCLUSIONS

The analysis of the deformation of a thick tube subjected to internal pressure has shown that while plastic flow is constrained by surrounding elastic material, the correct stress distribution can only be obtained by considering the elastic part of the total strain in the material flowing plastically. In the particular case considered an error of over 60 % resulted in the determination of the longitudinal stress on the assumption of zero elastic strain in the plastic region.

The problem treated involved the constraint of zero longitudinal strain. The curve of closed end force in figure 17 shows how much the conditions differ from a closed-end condition. It is seen that with a closed ended tube the longitudinal force is greater than that required for zero longitudinal strain, indicating some longitudinal extension. The flow at constant pressure, when the tube is plastic throughout, involves the same end force as the constant inelastic-plastic distribution of σ_z which is the limit approached by the complete solution. This obtains for all ratios of $b:a$, so that the problem we have considered is not far removed from the expansion of a closed ended tube, and the differences between types of solution will be similar in both cases. The problem of a closed ended tube could be treated, using a similar method, but the determination of the increment of longitudinal strain corresponding to each increment of internal pressure would be an added complication.

We wish to acknowledge the influence which Sir Geoffrey Taylor, F.R.S., has had on the initiation of this investigation through his, as yet unpublished, work mentioned in paragraphs 1 and 5. We also express our thanks to the Chief Scientific Officer, Ministry of Supply, for permission to publish this paper.

REFERENCES

Baildon, E. 1943 *Aut. Res. Comm.* Feb.
Geiringer, H. & Prager, W. 1934 *Ergebn. Exakt. Naturw.* **13**, 310.
Howard, J. V. & Smith, S. L. 1925 *Proc. Roy. Soc.* A, **107**, 113.
Nadai, A. 1931 *Plasticity*, p. 196.
Prager, W. 1944 *J. Appl. Phys.* **15**, 65.
Reuss, A. 1930 *Z. angew. Math. Mech.* **10**, 266.
Taylor, G. I. & Quinney, H. 1931 *Phil. Trans.* A, **230**, 323.

Discharge currents associated with kite balloons

By R. Davis, M.Sc. and W. G. Standring, M.A.

National Physical Laboratory

(*Communicated by Sir Charles Darwin, F.R.S.—Received* 7 *March* 1947)

Observations of electric currents flowing in the flying cables of barrage balloons were made during an investigation of the problem of protecting balloons in thundery weather. It was found that charges of the order of coulombs are transferred between balloon cable and air by currents ranging from milliamperes to kiloamperes. The observations give some indications of the distribution of charges in clouds.

1. INTRODUCTION

Kites have been associated with the study of atmospheric electricity since the days of Franklin, and the risks involved in handling them in thundery weather have been appreciated since Richmann was killed when repeating Franklin's experiments. During the period 1939 to 1945, kite balloons were used for defence purposes on a large scale, and an investigation of the problems of protecting balloons and crews was begun in 1937. At this time the belief was held that many balloons had been destroyed through the agency of 'brush discharge', and laboratory experiments in which wet balloon fabrics were set on fire by the passage of a current of the order of 1 mA/cm. width supported the view. The investigation therefore included measurements down to low values of the current flowing in the balloon cable in order to study the relation between atmospheric conditions, balloon current, and risk of destruction or damage.

Measurements were made at the Balloon Development Establishment, Cardington, with indicating instruments, cathode-ray oscillographs, and magnetic indicators, and in operational balloon barrages with magnetic indicators. The data obtained from widely scattered barrages indicated that destruction of balloons by brush discharge, if existent, was of minor importance, and that in the large majority of cases damage or destruction could be attributed to lightning strokes involving currents of hundreds of amperes rather than fractions of an ampere.

Some degree of protection against lightning strokes was attempted by mounting a spike 3 m. long above the nose of the balloon. Comparative magnetic indicator measurements suggested that this protection reduced losses through lightning by a factor of 3 or 4. The highest recorded stroke current survived by a protected balloon was 30,000 amp. Complete protection against lightning strokes could not be hoped for, as two occasions are known on which the flying cable was 'demetallized'—the vaporization of the steel occurring so quickly that the hemp core was not scorched.

The investigation was carried out as an urgent service requirement with the equipment available, and not as a scientific experiment. In particular, the balloons in barrages were of necessity flown entirely according to operational requirements. Although the information obtained was adequate for the object in view, more oscillographic equipment would be very desirable for a comprehensive study of discharge currents. The current measurements, nevertheless, appear to be worth recording as a contribution to the study of atmospheric electricity.

The equipment used is described in appendix 1. The data on cable currents are given in some detail in § 2, and discussed in § 3.

2. CABLE CURRENT OBSERVATIONS

The measured currents can be roughly classified as small sustained currents or large transient currents. The former were measured with a microammeter or a recording milliammeter, and the latter with cathode-ray oscillographs. Two oscillographs were used, a drum oscillograph giving a record lasting 15 min. of all currents sufficient to cause the deflexion of the focused spot outside a small mask (Lutkin 1937) and a single sweep oscillograph giving a record lasting for a predetermined time up to a maximum of about 10 msec. In addition to these instruments magnetic indicators were used for measuring peak values of currents in the range 500 to 60,000 amp. The equipment is described in detail in appendix 1.

It is convenient to describe the results under the headings of the measuring instruments used to obtain them. The measured values quoted refer to the current flowing down the cable. If the current is due to a cloud charge the charge in the cloud will be of the same polarity as the current flowing down the cable.

2·1. *Measurements by microammeter*

Fine weather unidirectional currents were less than 100 μA in value and sensibly stable. Examples of measurements made during balloon ascents and descents (at a rate of about 60 m./min.) are given in figure 1. Measured points were within 5 μA of the lines drawn, and there was no appreciable difference between observations during ascent and descent. Curves 1 and 2 were obtained in calm weather at Lakenheath, curves 3 and 4 in strong winds at Cardington. For curves 1, 2 and 3 the sky was less than 2/10 cloud, for curve 4 there was 10/10 cloud. During the flight to which curve 2 refers a length of 450 m. of light steel cable was trailing from the top of the flying cable during the ascent, but 300 m. of this were removed before the descent with inappreciable effect on the discharge current.

Measurements of the vertical electric field at the ground surface 50 m. to windward of the balloon winch were made on the occasions to which curves 3 and 4 refer. The observations relating to curve 3 were about 125 V/m. before the ascent, 95 V/m. with the balloon at its highest point, and 105 V/m. after the descent. The corresponding figures relating to curve 4 were 35, 70 and 100 V/m. These readings suggest that on these occasions the field measurements with the balloon up were not greatly influenced by the effects of the balloon cable charge and any accumulated space charge. These effects are considered in appendices 2 and 3.

In general, all measuring apparatus was housed in a transportable hut near the balloon winch. Simultaneous measurements of the vertical electric field at this position, and of the current in the flying cable of a balloon flying at 900 m. in fine weather with less than 1/10 cloud, are given in figure 2. The observations are differentiated according to wind speed, and for each voltage gradient and wind speed the upper and lower limits of current observations are shown. There is no close correlation between current and voltage gradient; some of the fields are negative though all the currents are positive, but the possibility of higher currents does appear greater with stronger fields and also with higher wind speeds. The negative field observations and the effect of wind speed on current are believed to be due to

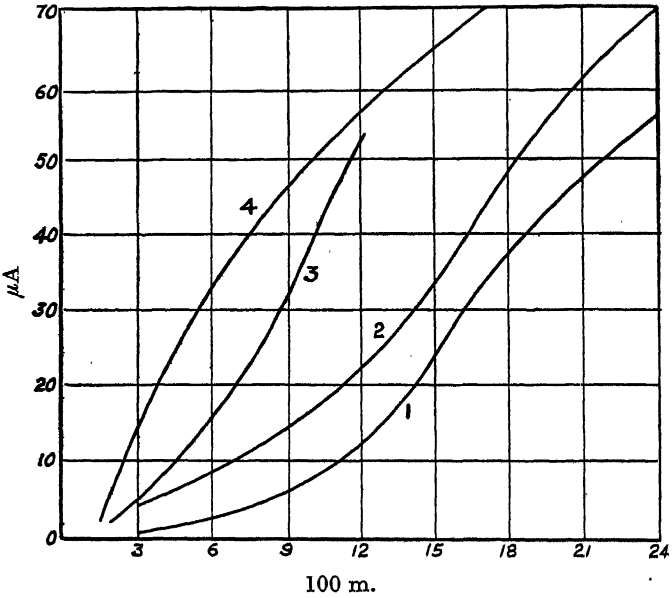

Figure 1. Variation of flying cable current with height of balloon.

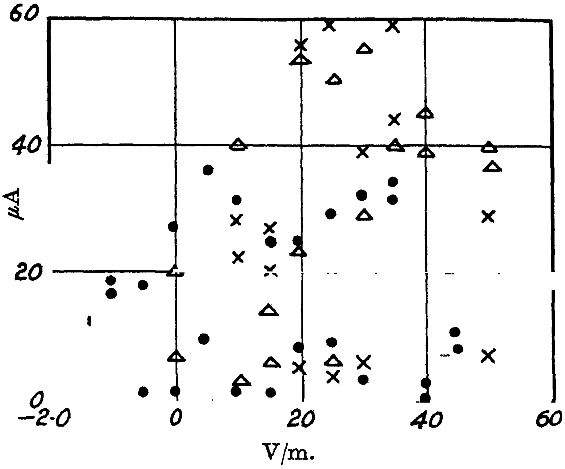

Figure 2. Fine-weather observations of discharge current and vertical electric field near foot of balloon cable. Height of balloon, 900 m. Wind speed: ● < 15 km./hr., × 15 to 30 km./hr., △ > 30 km./hr.

accumulated space charge. It is shown in appendix 3 that this space charge can have a considerable effect on the gradient at ground level. It will also have a limiting effect on discharges especially at low wind speeds.

In thundery weather the balloon at Cardington was usually flown at 600 m. The voltage gradient near the winch was measured with a Kohlhorster-type voltmeter, and a shadow photograph was obtained on a film in fine weather, but on the approach of a charged cloud the reading became very variable, and a record was not obtained.

2·2. *Measurements by recording milliammeter*

Various features of the milliammeter records are illustrated in figures 3, 4 and 5, where the records have been redrawn to suitable scales. The deflexion of the instrument was kept within the recording limits by the use of a variable shunt.

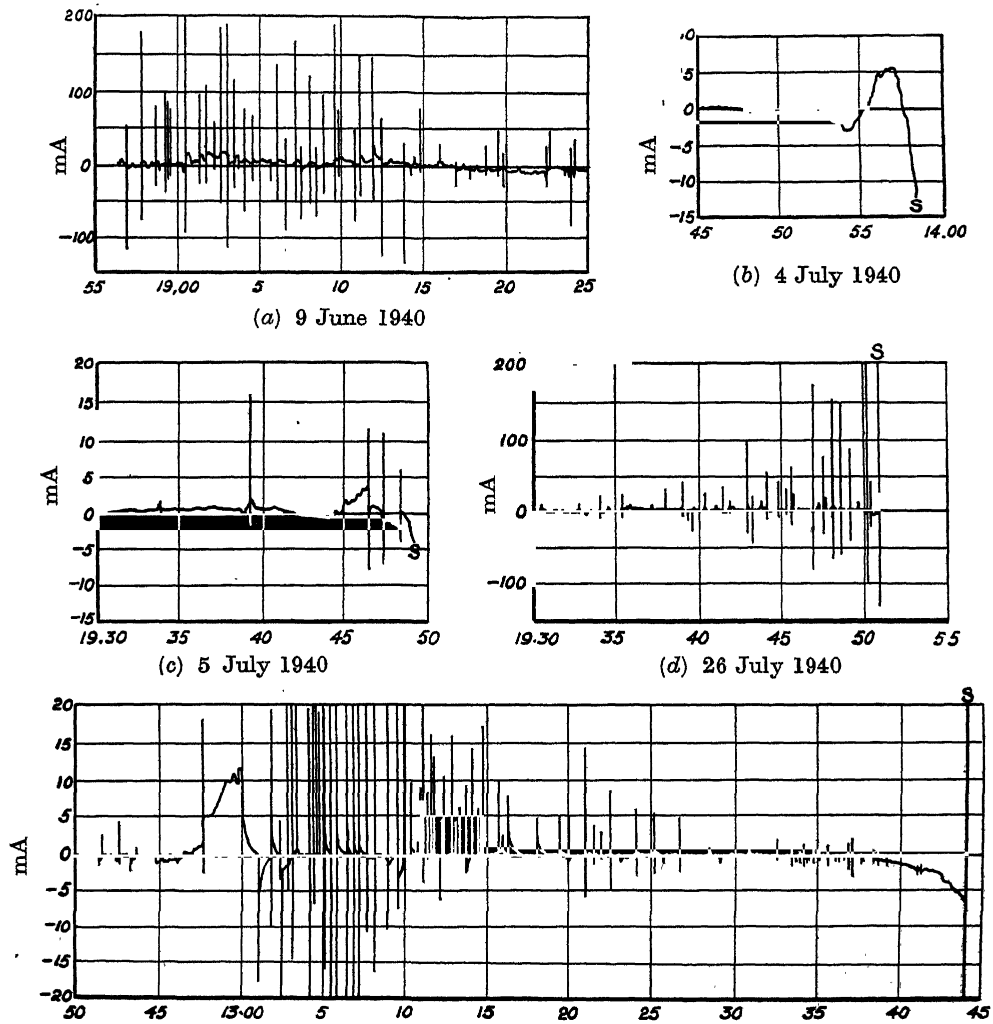

(*a*) 9 June 1940

(*b*) 4 July 1940

(*c*) 5 July 1940

(*d*) 26 July 1940

(*e*) 10 July 1940

Figure 3. Recorded currents preceding strokes to balloon.

Figure 3 shows current variations preceding strokes to the balloon. Each record was terminated by a lightning stroke to the balloon, as indicated by the letter S, except on one occasion (figure 3*a*) when the instrument was out of action 2 min. before the first stroke which was followed by four more within an hour. On most occasions kicks were produced on the milliammeter record by transient currents other than lightning strokes to the balloon—for example, figures 3*a* and 3*d* show nearly full-scale kicks with a 100 to 1 shunt on the milliammeter—but on one day (figure 3*b*) no kicks at all were recorded, and no other strokes were heard or seen. Transient activity in figures 3*c* and 3*d* is greatest immediately before the first stroke, but in figures 3*a* and 3*e* it is very much less then than a quarter or half an hour earlier. Most of the milliammeter kicks were not associated with any visible or audible evidence of a lightning stroke. More sustained currents of the order of milliamperes flowing for minutes involved charges of the order of a coulomb.

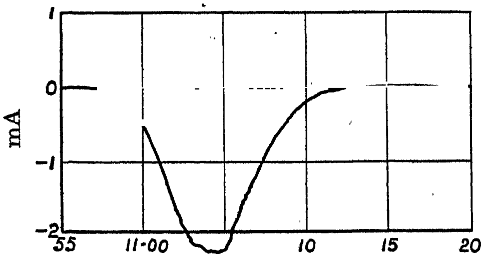

(*a*) 7 July 1940

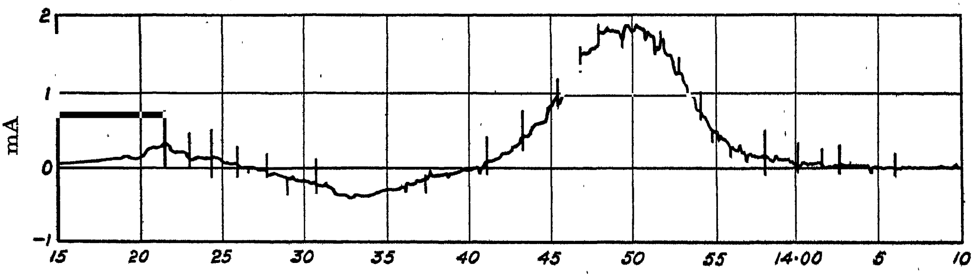

(*b*) 11 July 1940

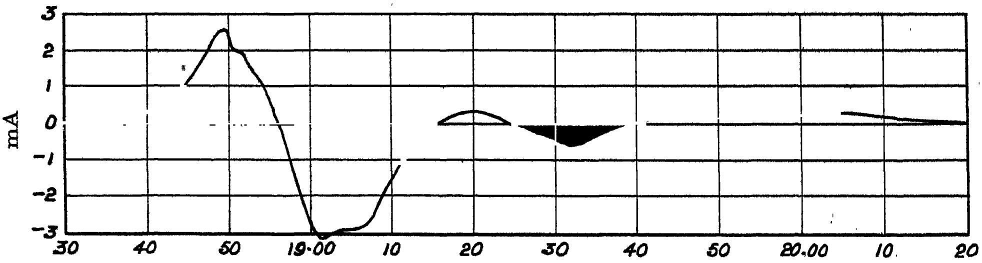

(*c*) 16 July 1940

Figure 4. Discharges of coulombs on days without thunder. (*a*) and (*b*) under cumulo-nimbus without rain, (*c*) under nimbo-stratus with continuous rain.

Figure 4 records measurements, also involving coulombs, on days when no lightning was seen and no thunder heard except for a distant rumble at 17.30 hr. on 11 July 1940. Figure 4*a* showing the passage of 1½ coulombs, and figure 4*b* showing the passage of a similar quantity of opposite polarity, refer to observations under cumulo-nimbus clouds from which no rain was falling. The record in figure 4*c* was obtained in continuous rain under what was believed to be low-lying layer cloud, and indicates the passage of 1 coulomb of one polarity followed by 2 coulombs of the other, although nimbo-stratus is not normally associated with the generation of electricity.

Records obtained on two days when there appeared to be considerable lightning activity, although the balloon was not struck, are given in figure 5. Figure 5*a* refers to the passage overhead of a cumulo-nimbus cloud from which a stroke to ground was observed during the approach of the cloud (corresponding to the kick in the record at 19.25 hr.). The anticipated stroke to the balloon did not occur, but the recorded current indicates the passage to earth of 1½ coulombs positive, followed by 4½ negative, 3 positive, and 1 negative; from 19.36 to 19.56 hr. it was raining—from 19.49 to 19.54 hr. very heavily. Figure 5*b* indicates another large quantity, 4½ coulombs positive followed by 1 coulomb negative—during this period rain started at 14.31 hr. This record also shows a number of kicks of which that at 13.52 hr. when thunder was heard is smaller than some of the succeeding kicks when it was not heard. Figure 5*c* follows on figure 5*b*. During the passage of about 1 coulomb between 15.50 and 16.25 hr. rain was falling from 15.53 to 15.58 hr., from 16.11 to 16.12 hr. and from 16.15½ hr. onwards, becoming heavy at 16.29 hr.

2·3. *Drum-oscillograph measurements*

Two records from the drum oscillograph are reproduced in figure 8, but the drum oscillograms on the whole are not suitable for photographic reproduction—for example, the record redrawn in figure 6*a* occupied 37 cm. in the abscissal and only 2 mm. in the ordinate direction.

Figure 8*a* was obtained by applying to the oscillograph the voltage across a non-linear resistance in series with the cable. The stroke current rose to 150 amp. negative in about 14 msec., and then was erratic for a few milliseconds with maxima about 600 amp. The resistance was then damaged and no further trace was obtained on the oscillograph, but magnetic indicators showed that the current rose to at least 1600 amp. positive. In figure 8*b* the current scale is linear, and the record is believed to be complete—the passage of this current was not noted as a 'lightning stroke'.

Four lightning stroke records are redrawn in figure 6. Except for the lower limit of recordable current due to the mask it is believed that *a*, *c* and *d* are complete records. Figure 6*b* refers to a stroke which subsequently damaged the measuring resistance and produced magnetic indicator observations of 60,000 amp. of opposite polarity. The charges indicated by these oscillograms range from 4 to 16 coulombs. In figure 6*a* two alternating time scales are used in order to show the shape of the current bursts—the current exceeded 300 amp. for the whole period of 45 msec.

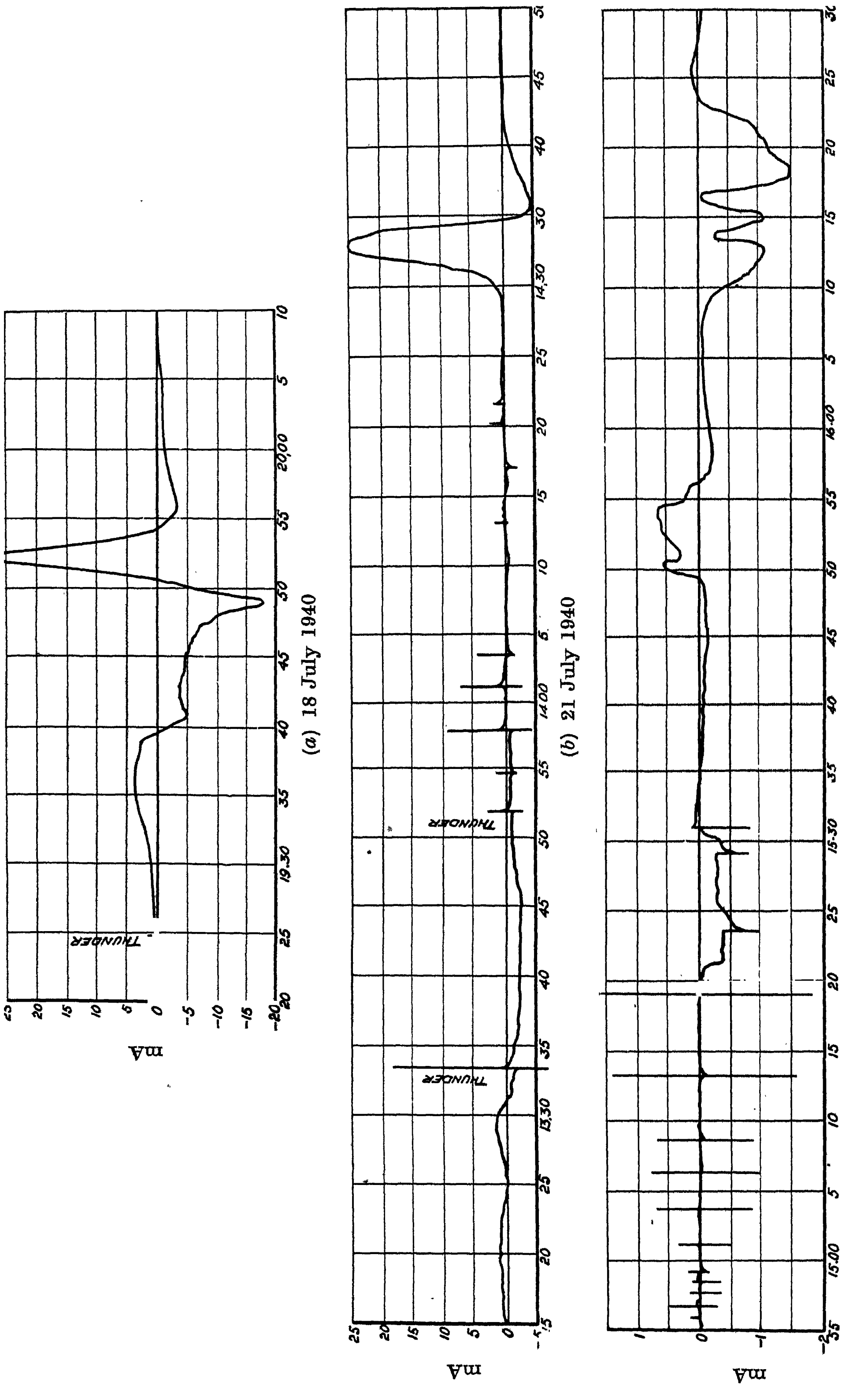

(*a*) 18 July 1940

(*b*) 21 July 1940

(*c*) 21 July 1940

FIGURE 5. Discharges of coulombs without strokes to balloon.

Records of four other strokes were obtained in which resolution is insufficient for delineation of wave shape. One shows during a period of 60 msec., four negative current surges of maximum value from 50 to 150 amp. and duration from 50 μsec. to 1 msec. The same stroke also produced a record of 25,000 amp. negative on the other oscillograph (figure 7*g*) and gave magnetic indicator readings of 40,000 amp. positive. In another stroke a current of 6000 amp. dropped to 3500 amp., each step lasting about 90 μsec. (quantity 1 coulomb). In a third a current of 2000 amp. lasting for about 20 μsec. was followed after 20 msec. by one of 3000 amp. lasting about 60 μsec. (quantity $\frac{1}{5}$ coulomb). In the fourth there were nine surges of current having maximum values from 3500 to 6500 amp. lasting for periods from 10 to 100 μsec. with intervals from $1\frac{1}{2}$ to 19 msec. (mean 11 msec.) involving a total quantity of about $2\frac{1}{2}$ coulombs.

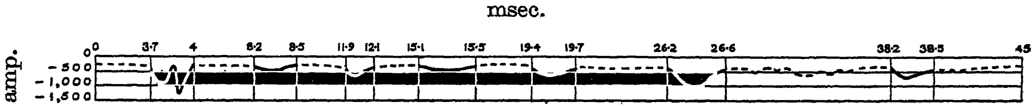

(*a*) 1300 amp.; 16 coulombs; ratio of time scales for full and dotted lines 10/1; 15.46 hr. 5 July 1940

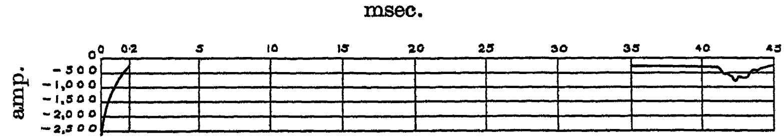

(*b*) 2600 amp.; 4 coulombs; 15.54 hr. 5 July 1940

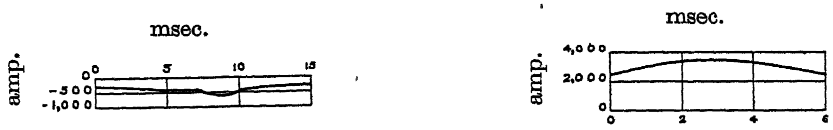

(*c*) 600 amp.; 6 coulombs; 15.50 hr. 5 July 1940

(*d*) 3500 amp.; 15 coulombs; 20.16 hr. 26 July 1940

FIGURE 6. Lightning stroke records on drum oscillograph. Minimum current recordable with 0·085 ohm shunt, 300 amp. (*a*, *b*, *c*), with 0·01 ohm, 2500 amp. (*d*).

As the drum only traverses 0·01 mm./rev., the measured intervals between different parts of one stroke may be in error by multiples of 0·12 sec.

Records were also obtained during storms of a number of smaller currents, between 20 and 200 amp., not associated with observed lightning strokes. These currents could be roughly divided into two types—unidirectional and oscillatory. The frequency of the oscillatory type was of the order of the natural frequency of the balloon cable, and these currents are believed to occur during a readjustment of charge on the balloon cable corresponding to a sudden change in the electric field; they persisted from 0·5 to 2 msec. The unidirectional currents lasted from 0·5 to

50 msec. and involved quantities up to 1 coulomb. They are believed to be discharges from the balloon or cable into the air, although not apparent to visual observers. The unidirectional currents preponderated when the storm cloud was overhead.

2·4. *Single-sweep oscillograph measurements*

Seven lightning strokes recorded on the single-sweep oscillograph are illustrated in figure 7. In order to show all the detail discernible in the originals the records have been redrawn. A photographic reproduction of the record illustrated in figure 7*g*

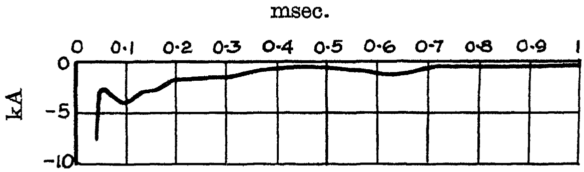

(*a*) 1¼ coulombs; 20.11 hr. 26 July 1940

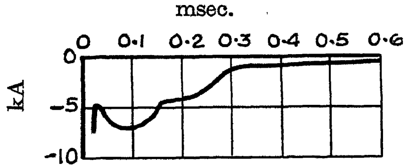

(*b*) 1½ coulombs; 20.07 hr. 26 July 1940

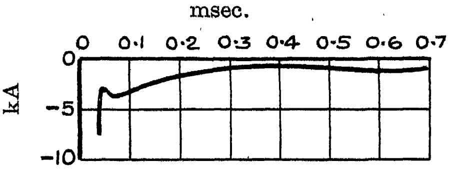

(*c*) 1 coulomb; 20.14 hr. 26 July 1940

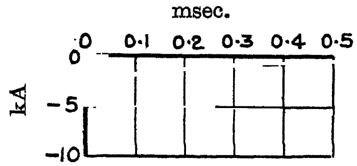

(*d*) ½ coulomb; 19.58 hr. 26 July 1940

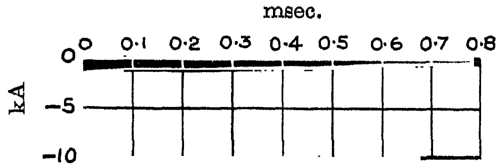

(*e*) ½ coulomb; 20.18 hr. 26 July 1940

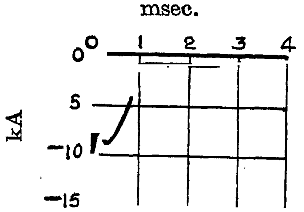

(*f*) 11 coulombs; 17.28 hr. 10 July 1940

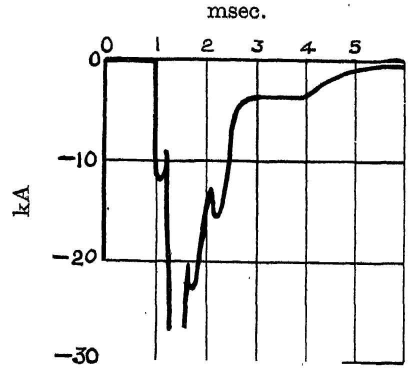

(*g*) 30 coulombs; 14.01 hr. 10 July 1940

FIGURE 7. Lightning stroke oscillograms with limited time sweep.

is given in figure 8*c*. For this stroke magnetic indicator measurements were also obtained and indicated a current of opposite polarity of 40,000 amp.

Observations in fine weather with greater sensitivity indicated the presence of oscillatory currents with occasional peaks up to 30 mamp. (balloon height 900 m.). The two main frequencies observed, 200 and 78 kc./sec., were ascribed to the influence of radio-transmitting stations at Droitwich and Rugby.

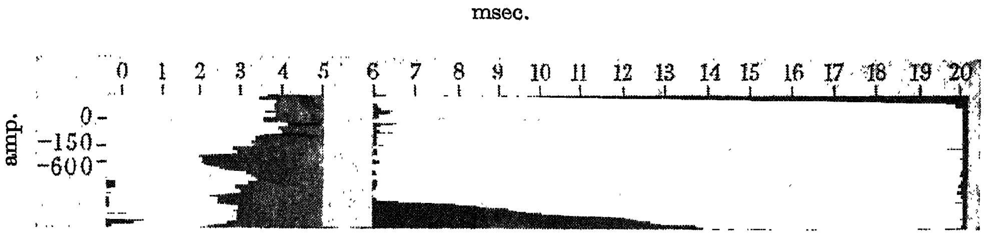

(*a*) Rise of current at beginning of stroke 13.58 hr. 4 July 1940

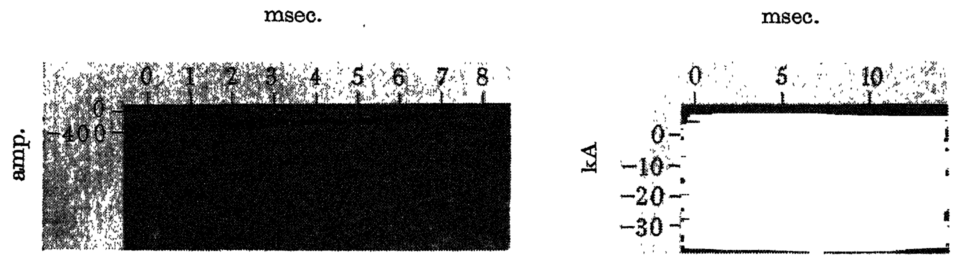

(*b*) Record obtained without aural or visual notice of a stroke 13.47 hr. 10 July 1940

(*c*) Stroke redrawn in Fig. 7 (*g*)

FIGURE 8. Reproductions (*a*) and (*b*) of drum oscillograms, (*c*) of single-sweep oscillograms.

2·5. *Magnetic-indicator measurements*

Barrage balloons were fitted with magnetic indicators in order to ascertain whether destruction in thundery weather was due to brush discharge or to lightning stroke. Indicators were salved from 135 unprotected balloons which were damaged or destroyed. One current was greater than 60,000 amp. and the balloon cable was vaporized. On fifteen occasions the indicator remanences were inconsistent with the passage of a unidirectional current. In all but fourteen cases the indicators showed that currents greater than 500 amp. were involved, and in six of these fourteen cases the balloon was observed to be struck.

When protection of barrage balloons against lightning strokes was attempted magnetic indicators were fitted to the protected balloons for examination after thunderstorms. Current indications greater than 500 amp. were obtained on sixty-five occasions.

The current observations on both protected and unprotected balloons are given in table 1.

A majority (about two-thirds) of the strokes to unprotected balloons were of negative polarity, but there were equal numbers of positive and negative currents above 20,000 amp. The number of high current strokes is too small to draw a definite conclusion, but the observations suggest that the proportion of positive to negative is greater at the higher current values. Negative strokes to protected balloons were in a minority (about two-fifths). It is probable that many of the protected balloons were struck more than once, in which case only the highest currents would be recorded. These results reinforce the suggestion that the proportion of positive to negative currents is greater for high than for low currents.

TABLE 1. MAGNETIC-INDICATOR CURRENT MEASUREMENTS

	number of unprotected balloons damaged or destroyed		number of recorded strokes to protected balloons	
indicated current (amp.)	by positive currents	by negative currents	positive	negative
> 60,000	1	0	1	0
> 40,000	1	0	2	1
> 30,000	2	1	2	2
> 20,000	4	4	3	4
> 10,000	5	16	5	7
> 2,000	6	30	19	19
> 500	41	80	39	26
< 500	14			

3. CHARACTERISTICS OF DISCHARGE CURRENTS

3·1. *Effect of flying cable charge on the measurements*

In a vertical electric field E the potential at a height x is Ex. An earthed conductor, such as a balloon cable, must carry a charge of opposite polarity which neutralizes this potential on all points of the conductor. If the charge on the cable of radius r and height h be Kx per unit length at height x, then the potential of the cable at a height a due to this charge is

$$K\int_{-h}^{h}\frac{x\,dx}{\sqrt{[(x-a)^2+r^2]}}$$

$$= K\left[\sqrt{[(h-a)^2+r^2]}-\sqrt{[(h+a)^2+r^2]}+a\log\left(\frac{h-a+\sqrt{[(h-a)^2+r^2]}}{\sqrt{[(h+a)^2+r^2]}-(h+a)}\right)\right]$$

$$= Ka\left(\log\frac{4h^2}{r^2}-2\right) \text{ approximately}$$

except near the top of the cable. A charge of $-\frac{Ex}{\log(4h^2/r^2)-2}$ per unit length at height x will therefore maintain the cable approximately at earth potential in a field E. The total charge on the cable is $\int_0^h Kx\,dx = \frac{1}{2}Kh^2$.

When the field changes the corresponding change in cable charge involves a current which is included in cable-current measurements. The extensive investigations of Wormell (1939) indicated that a field change in the neighbourhood of a lightning stroke of 50,000 V/m. is extremely rare. The cable charge corresponding to this field for a balloon flying at 600 m. (the height at which the balloon was flown at Cardington in thundery weather) is approximately 0·05 coulomb, and the balloon charge considering the balloon as a conductor would be about 0·02 coulomb. It follows that in thundery weather observations indicating the passage of quantities greater than 0·1 coulomb involve the transference of electric charge between cable and air. In fine weather with small field changes the corresponding quantity is proportionately smaller.

3·2. *Origin and range of discharge currents*

Adopting the criterion described in the preceding paragraph it can be seen from the data in §§ 2·1 to 2·4 that electric charges are transferred between balloon cable and air by currents ranging from a few microamperes persisting for hours to tens of thousands of amperes flowing for a millisecond or less. The higher currents are in general of shorter duration and less frequent occurrence.

The contribution to these currents provided by the ions ordinarily present in the air can be estimated from data obtained by different observers which are in general agreement (Schonland 1932). Over land the number of ion pairs produced per second is about 10, and their average life as small ions with a mobility of about 1·5 cm./sec./V/cm. varies from 10 to 60 sec.

If the cable had a uniform density of charge the gradient at a distance r would be say g/r. The velocity of ions would be $1{\cdot}5g/r$ so that the time ions take to reach the cable from a distance R would be $R^2/3g$. Taking the life of an ion as 60 sec., ions could reach the cable from a distance $R = \surd(180g)$. From the formula in § 3·1 the mean gradient at the cable surface in a field of 1 V/cm. for a height of 900 m. (the usual balloon height in fine weather during the measurements) and a cable diameter of 5 mm. is 15 kV/cm., so that at a distance r the mean field is $\frac{15}{4}r$ kV/cm., and the mean value of R is about 8 m. The total number of small ions which can reach the cable per second is therefore about 2×10^{12} and the corresponding current $0{\cdot}3\,\mu$A. The current would be proportional to the field and to the square of the balloon height. The contribution of large slow ions would be small in comparison and would not develop for some time. It appears that most of the currents illustrated in figures 1 and 2 cannot be obtained from the ions normally present in the air.

At the extreme top of the cable the charge density assumed in § 3·1 gives only half the required effect on the voltage. The charge density at the top will therefore be more than twice that assumed, and the gradient at the cable surface will be more than 60 kV/cm. in a field of 1 V/cm. In moving from the cable surface (gradient 60 kV/cm.) to a distance 2·5 mm. away (gradient 30 kV/cm.), one electron would generate an avalanche of about 10^{10}, and if the field were increased 25 % the number of electrons in the avalanche would be about 10^{22}. Photons would also be produced and liberate more electrons at the cable surface, and it is clear that in the higher field sufficient ions would be generated by collision to provide currents of the order measured, though sufficient data are not available for calculating the currents (the agreement between laboratory and field 'corona constants' inferred by Bruce (1944) is not considered valid).* In fields of 1 V/cm. and below the mechanism is less certain, although since the cable is stranded, and terminated by thinner stranded rigging wires, which may have some sharp points projecting at their end splices, local stresses may be considerably greater than the value quoted.

It is concluded that all the currents measured, except the lowest of the fine-weather currents, originate in a process of ionization by collision at the balloon cable, ions of one polarity carrying their charge to the cable, ions of the other polarity forming an outward moving-space charge. The polarity of the outward moving-space charge is the same as that of the cable, and the current may be most simply described as a 'discharge' current of this polarity. With currents of high value, including those recognized as lightning strokes, electric breakdown of the air is not confined to the vicinity of the cable, but the currents observed must have started by ionization at the cable, and there seems no reason for regarding the discharges as changing in nature at any particular current value over the range from tens of microamperes through milliamperes and amperes to kiloamperes.

3·3. *Current in a 'lightning stroke'*

The description 'lightning stroke' may be taken to refer to a discharge during which a flash is seen or a noise varying from a long thunder roll to a faint crack is heard. It seems probable that the brightness of a flash is mainly dependent on the maximum current. During the measurements at Cardington several oscillograph observations were obtained of discharges carrying about 100 amp. which were not apparent to visual or aural observers. A few oscillograph observations of less than 1000 amp. corresponded to discharges which were heard and seen and described as 'strokes'. In § 2·5 reference is made to six occasions on which, although a balloon was observed to be struck, magnetic indicators gave no evidence that a current of 500 amp. or more had passed. It seems probable, therefore, that the lower limit of discharge currents which are observed as lightning strokes is in the neighbourhood of 500 amp. There seems, however, no justification for drawing a distinction in kind at this or any other particular point in the current range, and discussion will not be limited to discharges which would be called 'lightning strokes'.

Other characteristics of 'strokes' illustrated by the observations are that one stroke may last 90 msec. and consist of a fairly steady 'continuing' current plus a number of surges, the current may exceed 300 amp. for 45 msec., the surges may be not much greater in magnitude than the 'continuing' current, and a stroke in which the first surge is negative may include a larger positive surge.

---

* The line constant quoted was obtained from experiments in a cylinder of one size. Almy (1901) obtained a constant varying inversely as the cube of the cylinder diameter. The point constants quoted relate the current to the voltage between electrodes.

Some consideration of the current required to vaporize the flying cable may be of interest. It is estimated that the cable will vaporize if a current I amp. flows for a time $8 \times 10^6/I^2$ sec. A current of 50 kA would require a duration of 3·2 msec. and involve a charge of 160 coulombs, a current of 100 kA a duration of 0·8 msec. and a charge of 80 coulombs, and a current of 200 kA a duration of 200 μsec. and a charge of 40 coulombs. For a charge of 60 coulombs, which appears to be very exceptional (Wormell 1939), the current required would be between 100 and 200 kA for some hundreds of microseconds. The maximum current might be considerably more than the average and possibly greater than 200 kA.

3·4. *Location of cloud charges*

The general picture of charge distribution in thunderclouds derived by Simpson & Robinson (1941) from potential gradient measurements by free balloon soundings consists mainly of an upper positive charge and a lower negative charge in a region where the temperature is below the freezing-point, and usually, if not always, a smaller positive charge below the negative at a temperature above the freezing-point. Under the low positive charge they observed positively charged rain and concluded that this charge was produced by the breaking-drop mechanism.

The discharge currents from kite balloons (flying at a height of 600 m. in thundery weather) provide some evidence for amplifying the description of the possible distribution of the lower charges. The milliammeter records in figures 4 and 5 show positive currents (involving coulombs) of limited duration, the origin of which would be difficult to explain in the absence of a low positive charge of some coulombs. Rapid fluctuations of discharge current suggest that space or cloud charges may be very local and not much higher than 600 m. (balloon height). For example, figure 5*c* shows between 16.13 and 16.18 hr. four large relative changes in current magnitude. The wind speed was about 16 km./hr. so that each change corresponds to a cloud movement of about 300 m. A similar phenomenon is shown in figure 5*a*—between 19.49 and 19.52 hr. the current changed from maximum negative to maximum positive, while the cloud in a wind of 8 km./hr. moved not much more than 300 m. The probable explanation of these fluctuations seems to be that charges in or below clouds may vary from a maximum of one polarity to zero or a maximum of opposite polarity in distances of the order of 300 m., and that such charges may come within a comparable distance of a balloon flying at 600 m., i.e. the local charges may be less than 1 km. above ground.

The magnetic-indicator measurements give a higher proportion of positive to negative lightning currents than had previously been observed, and also indicate a greater proportion of high magnitudes in positive than in negative currents. The maximum current in a stroke with an upward leader probably depends on the concentration of charge tapped in the cloud. A relatively small, low, concentrated charge which would not produce a stroke to ground might easily excite a leader from a kite balloon at 600 m. It appears reasonable to conclude that a number of strokes to kite balloons may be from low positive cloud charges, and that the charge density in the low positive charge is greater than in the negative portion of the cloud.

The positive currents in figures 5*a*, *b* and *c* and 4*c* were accompanied by rain, as would be expected if the positive cloud charge were formed by the breaking-drop mechanism, but no rain fell during the period referred to in figure 4*b*. The number of kicks in figure 4*b*, however, suggest that the cloud was actively generating electricity, and possibly the upward air currents were so strong that water drops were unable to descend as rain.

3·5. *Mechanism of discharges*

In discharges carrying only milliamperes the quantity of electricity involved may come within the range of charges hitherto associated with lighting strokes. Examples have been given of discharges in unsettled weather involving quantities of the order of a coulomb varying from currents of the order of 10 mA flowing for a minute or two (figures 3, 5) to currents of the order of 1000 amp. flowing for a millisecond (figure 7). All these currents are presumably caused by space charges mainly located and generated in clouds, and the quantity of electricity released must be related to the magnitude and distribution of the charge in the cloud. The discharge is more likely to take the form of a high current flowing for a short time or a low current flowing for a long time, according as the cloud charge is concentrated or distributed. If the velocity of the upward moving charge is low it may reduce the propagating field at the cable and cut off the discharge, which, however, may recommence as the released charge moves farther away from the balloon. It seems probable that the many discharges of 10 to 100 amp., and perhaps the 400 amp. discharge illustrated in figure 8*b*, are instances of this condition, where the charge from the cable does not actually reach the cloud charge.

All initial upward discharges of either polarity presumably start because the field at the earthed electrode is sufficient to cause ionization by electron collision. The stronger the field the longer is the avalanche path of electrons before they are checked by positive space charge, the greater the field due to the positive ions left behind, and the greater the probability of streamer formation and rapid propagation by the mechanisms envisaged by Loeb & Meek (1941). Simultaneous measurements of the various quantities involved are required before satisfactory correlation of field, discharge current, and width, luminosity, and rate of propagation of discharge channel can be expected.

By photographic observations, Schonland, Malan & Collens (1935) demonstrated that a discharge from cloud to ground in open country starts from the cloud, and that its arrival at the ground is followed by a sudden increase of illumination (implying a sudden increase of current) propagated rapidly upwards, the two processes being called leader stroke and return stroke—the initial leader stroke being usually stepped. In observations on fifty-three strokes, all negative, to the Empire State Building, McEachron (1938) identified thirty-six as having initial stepped upward leaders, two as having non-stepped upward initial leaders, and two as having non-stepped downward initial leaders, the remainder being unidentifiable. With upward leaders he found no return stroke, attributing this to the lack of charge immediately available when the leader reached the poorly conducting cloud, in contrast to that which could be drawn from the relatively highly conducting ground.

In the experiments with a balloon flying at 600 m. it would be expected that the effect of conductor height would be greater than with the Empire State Building (375 m.), and that the proportion of strokes initiated by upward leaders would be still higher. Only five of the thirteen oscillograms in figures 6, 7 and 8 (6*a*, *c*, *d*, and 8*a*, *b*) suggest, from the absence of a sudden increase in current, initiation by upward leaders. It is possible that in the other cases the initial leader currents were too small to be recorded, and photographic evidence is probably indispensable in studying leader processes. In four of the five cases mentioned as suggesting upward leaders the recorded currents flowing down the cable were negative, i.e. the balloon cable was the positive electrode. For the currents of the order of 10 to 100 amp. recorded on the drum oscillograph the balloon cable was also the positive electrode in the majority of cases, but in some the negative. These currents should probably also be regarded as upward leaders. While it seems advisable to maintain the convention of describing the polarity of a stroke by the polarity of the charge brought to earth, it appears desirable when speaking of a leader stroke to describe it by the polarity of the point of origin. In this sense the observations suggest that upward leaders of both polarities are to be expected from a kite balloon, though the majority are likely to be positive.

3·6. *Influence of height of earthed electrode on magnitude of lightning currents*

A balloon cable 600 m. long short-circuits an appreciable fraction of the gap between cloud and ground, and strokes to the balloon may occur from cloud charges which are too small or too widely distributed to produce strokes to open ground. The presence of a balloon should thus increase the total number of strokes, and it seems probable that the currents in the additional strokes due to the balloon will be relatively low in magnitude.

In controlled laboratory experiments on discharges between points, Allibone & Meek (1938) found maximum luminosity at the meeting point of upward and downward leaders and concluded that the 'main stroke' originated here. Presumably the effect is due to the meeting and neutralization of charges of opposite polarity contained in the two leader channels. If maximum luminosity corresponds to maximum current, and if maximum current occurs during the neutralization of the charge in the leader stroke channel, then in the case of a stroke in which a downward leader nearly reaches the ground the current is a maximum there. A stroke to a balloon, however, probably involves an upward leader of appreciable length, and the maximum current, occurring where the charge in the upward leader is neutralized on reaching the cloud or a downward leader carrying an opposite charge, will not appear at the ground. The current at the earthed electrode would in such cases only be the upward leader stroke current until a conducting channel is established between cloud and balloon. The maximum current in the balloon cable would thereafter depend on the magnitude and concentration of the remaining cloud charge.

Strokes to a kite balloon flying at 600 m. are thus not likely to be typical of strokes to open ground but will probably contain a greater proportion of low currents, as well as a greater proportion of upward leaders.

Conclusions

In thundery weather electric charges of the order of coulombs may be transferred between the atmosphere and the flying cable of a kite balloon by currents ranging from milliamperes flowing for minutes to kiloamperes flowing for milliseconds.

If the current in a discharge exceeds 500 amp. an observer would probably recognize the discharge, aurally or visually, as a 'lightning stroke'.

Charge centres of opposite polarity may exist within 300 m. of each other and within 1 km. of the ground.

The proportion of positive to negative discharges appears to be greater at the higher current values.

The low positive charge centres in thunderclouds are probably more concentrated than the negative.

A kite balloon affords very suitable means for observing, in a suitable locality, a large number of strokes in a reasonable time. The strokes to a balloon will probably not be typical of strokes to ground, but they should contain more upward leaders of both polarities, giving opportunity for the study of leader mechanism.

In further study of lightning discharges it is desirable to make simultaneous observations of field and current and of luminosity and speed of propagation of discharge channel. Oscillographs recording current should preferably record continuously and not require to be 'tripped' by a surge, should cover a very wide current range and include a slow speed oscillograph.

The work described was carried out by the Electricity Division of the National Physical Laboratory, on behalf of the Air Ministry and the Ministry of Aircraft Production, by whose permission this paper is published. The authors desire to acknowledge the assistance rendered by Mr Bateman and the staff of the Balloon Development Establishment in the investigation at Cardington, and also the co-operation of R.A.F. personnel in obtaining the data on operational balloons.

Appendix 1. Measuring instruments and technique

During current measurements the winch from which the balloon was flown was insulated from the ground by its rubber tyres and the balloon current flowed to earth through indicating instruments and through resistances suitable for providing deflexion voltages for cathode ray oscillograph plates.

The indicating instruments consisted of a d.c. mirror galvanometer with a sensitivity of 2 cm./μA, and a d.c. milliammeter with a sensitivity of 2¼ cm./mA giving a continuous ink record on a paper roll. Suitable shunts were used when necessary to reduce the sensitivity of these instruments.

A non-linear ceramic resistor was first used for the oscillographs but this was damaged by an early stroke, and subsequent measurements were made with non-inductive metal resistors.

Two 5 kV sealed off cathode ray oscillographs were used for recording transient currents. One was maintained at full brightness but the undeflected spot was covered by a mask. This oscillograph gave a continuous record of deflexions beyond the mask on a drum camera 1 m. in circumference rotating at 500 r.p.m. and traversing 7·5 cm. in 15 min. (Lutkin 1937). The sensitivity of the drum record was 43 V/mm. in the ordinate direction and 0·12 msec./mm. in the time direction. The width of the unrecorded band was ± 0·6 mm. The other oscillograph was 'tripped' by the transient and the trace was photographed on a roll film, the time sweep being 10 msec. or less. The record was 50 mm. long in the time direction, and the ordinate sensitivity was 17 V/mm.

An earth connexion of 2 ohms resistance was obtained by laying some copper cable in a wet ditch; the possibility of any other earth connexion was avoided. The oscillograph resistances mentioned were located at the earth terminal, and connexion to the instruments in a light-tight hut 10 m. away was made by pairs of concentric conductors.

The magnetic indicators consisted of steel strips 5 cm. long in waterproof containers. Two indicators were supported at right angles to the flying cable at distances of 10 and 20 cm. Before issue they were demagnetized in a slowly reduced alternating field to a remanence of less than 1·7 Maxwells. From the remanent magnetism of the indicators an estimate could be made of the current which had flowed in the cable over a range from 500 to 60,000 amp. The unidirectional cable currents required to produce the remanences observed in the two indicators were obtained by calibration. If the two measurements agreed within the limits of experimental error, the simplest interpretation is that a unidirectional current of the indicated value flowed in the conductor. Disagreement indicated that the stroke was not unidirectional, or that more than one stroke of different polarities had occurred. In such cases the lowest value of initial current, followed by the appropriate reversed current, to give the measured remanence could be found by calibration. There seems, however, no justification for assuming that the simplest explanation for the measured remanence is necessarily the correct one—for example, both indicators may be left practically demagnetized after the passage of a large current followed by a suitable reversed current. The most reliable use of magnetic indicator readings, therefore, seems to be to take the unidirectional current corresponding to the indicator remanence as a lower limit for the conductor current.

APPENDIX 2. EFFECT OF CABLE CHARGE ON VOLTAGE GRADIENT AT GROUND LEVEL

The gradient at ground level due to the charge on a vertical cable of height h, in a field E, at a distance d from the cable, is

$$-\frac{E}{\log(4h^2/r^2)-2}\int_{-b}^{b}\frac{x^2\,dx}{(x^2\times d^2)^{\frac{3}{2}}}=-\frac{2E}{\log(4h^2/r^2)-2}\left(\log\left(\frac{h+\sqrt{(h^2+d^2)}}{d}\right)-\frac{h}{\sqrt{(h^2+d^2)}}\right).$$

For a height of 600 m. the effect is to reduce the gradient near the cable foot by 0·23, 0·18 and 0·12E at distances of 0·05, 0·1 and 0·2h. Thus the presence of the cable does not alter the order of magnitude of the gradient at the ground even at 30 m. from the cable. The greater part of the cable was usually more than 30 m. to leeward of the observation hut.

APPENDIX 3. EFFECT OF DISCHARGE ON VERTICAL FIELD AT GROUND LEVEL

The discharge is not confined to one point of the cable, but the distribution is unknown and the order of the effect can be calculated by assuming a concentrated discharge. In fields in which the discharge current is steady, ion velocities will be negligible in comparison with wind velocities, so that the space charge generated will drift approximately horizontally to leeward.

If the discharge current is I at a height h, and the wind velocity is v, the vertical field at the ground at a distance d to windward of the cable due to the space charge, neglecting recombination, is

$$2\int_{0}^{\infty}\frac{Ih\,dx}{v[h^2+(x+d)^2]^{\frac{3}{2}}}=\frac{2I}{vh}\left(1-\frac{d}{\sqrt{(d^2+h^2)}}\right).$$

At a distance $d = 0{\cdot}1h$ the effect is 0·9 of the effect at the cable foot.

If $I = 50\,\mu$A, $v = 40$ km./hr., and $h = 600$ m. the effect on the vertical gradient at the ground near the foot of the cable is a reduction of about 130 V/m. For a wind velocity of 8 km./hr. the effect would be 650 V/m. It seems probable that the field observations given in figure 2 are subject to this effect, but to an extent diminished by recombination. Knowledge of ion concentration, etc., is insufficient to estimate the rate of recombination.

The space charge will also decrease the field at the cable and so have a limiting effect on the discharge, an effect which will decrease as the wind velocity increases.

REFERENCES

Allibone, T. E. & Meek, J. M. 1938 *Proc. Roy. Soc.* A, **166**, 104.
Almy, J. E. 1901 *Amer. J. Sci.* **12**, 175.
Bruce, C. E. R. 1944 *Proc. Roy. Soc.* A, **183**, 228.
Loeb, L. B. & Meek, J. M. 1941 *The mechanism of the electric spark.* Stanford Univ. Press.
Lutkin, F. E. 1937 *J. Sci. Instrum.* **14**, 209.
McEachron, K. B. 1938 *Elect. Engr.* **57**, 493.
Schonland, B. F. J. 1932 *Atmospheric electricity.* London: Methuen.
Schonland, B. F. J., Malan, D. G. & Collens, H. C. 1935 *Proc. Roy. Soc.* A, **152**, 595.
Simpson, Sir George & Robinson, G. D. 1941 *Proc. Roy. Soc.* A, **177**, 281.
Wormell, T. W. 1939 *Phil. Trans.* A, **238**, 249.

The hodograph transformation in trans-sonic flow. I. Symmetrical channels

By M. J. Lighthill

(*Communicated by S. Goldstein, F.R.S.—Received* 19 *September* 1946)

1. Introduction

It seems likely that any general theory of compressible flow applicable to problems with regions both of sub- and supersonic flow (such problems have been called 'trans-sonic') must be based on the 'hodograph transformation' (due originally to Molenbroek 1890 and Chaplygin 1904). This is because in the hodograph plane, in which the independent variables are the magnitude and direction of the velocity, the equations of motion are linear; while in the physical plane they are not even approximately linear for trans-sonic problems.

But the hodograph transformation presents difficulties quite apart from those of applying suitable boundary conditions. It has in fact singularities, notably near the sonic speed and the velocity at infinity. This fact considerably elaborates its use. In the present paper a study is initiated of the application of the hodograph transformation to trans-sonic problems by considering the steady plane adiabatic flow of a gas in symmetrical channels in which the velocity rises from zero at infinity on the left to a supersonic value at infinity on the right; this is a problem easier to begin on than those with a body inside the field of flow, which are known in practice to involve shock-waves and hence regions of non-adiabatic flow.

It is found that in part of the hodograph plane the potential and stream function are three-valued functions, though one-valued in the remainder. The two parts are divided by a curve independent of channel shape, and all the streamlines touch this curve in the hodograph plane. The three-valued region is entirely supersonic, and the dividing curve is a singularity of the transformation.

This and other properties of the transformation are investigated in detail here, together with the problem of deducing a channel shape from a given axial velocity distribution. Certain important qualitative results are first established by expansion in series in the physical plane; this method of presentation has been adopted because the results obtained, so far as they go, carry more complete conviction and give greater physical comprehension of affairs than corresponding investigations in the elusive hodograph plane.

Channels of the type under review are actually used in 'two-dimensional' supersonic wind-tunnels of the 'induced-flow' type. The practical requirements are that they should be short and that the velocity should increase steadily on every streamline; shock-waves and large boundary-layer growth should both be absent in such a tunnel, because on both the curved and the flat walls the velocity gradient is everywhere positive. The conclusions of the theory are applied to the design of such a channel in the Appendix.

2. 'PHYSICAL PLANE' THEORY

All the velocities are scaled down so that the maximum velocity (attained at zero pressure) is unity. Bernoulli's equation then becomes

$$\tfrac{1}{2}w^2+\frac{p_0}{\rho_0^\gamma}\frac{\gamma}{\gamma-1}\rho^{\gamma-1}=\tfrac{1}{2}, \quad \text{or} \quad \rho=\rho_0(1-w^2)^{1/(\gamma-1)}, \tag{1}$$

where w is the velocity, ρ the density, γ the adiabatic index, and p_0 and ρ_0 the pressure and density at a stagnation point. The equation of motion for the potential ϕ can be written

$$(\phi_{xx}+\phi_{yy})(1-\phi_x^2-\phi_y^2)=\frac{2}{\gamma-1}(\phi_x^2\phi_{xx}+2\phi_x\phi_y\phi_{xy}+\phi_y^2\phi_{yy}), \tag{2}$$

suffices denoting partial derivatives.

For flow symmetrical about the x-axis ϕ may be assumed expansible in a series $\phi(x,y)=f_0(x)+y^2f_1(x)+y^4f_2(x)+\dots$. (This expansion has of course been used by many authors.) The equation of motion becomes

$$\begin{aligned}&[f_0''+y^2f_1''+\dots+2f_1+12y^2f_2+\dots][1-f_0'^2-2y^2f_0'f_1'-4y^2f_1^2+\dots]\\&\quad=\frac{2}{\gamma-1}[(f_0'^2+2y^2f_0'f_1'+\dots)(f_0''+y^2f_1''+\dots)+8f_0'f_1f_1'y^2+\dots+8f_1^3y^2+\dots],\end{aligned} \tag{3}$$

whence, equating coefficients of powers of y,

$$(1-f_0'^2)(f_0''+2f_1)=\frac{2}{\gamma-1}f_0'^2f_0'', \tag{4}$$

$$\begin{aligned}&(1-f_0'^2)(f_1''+12f_2)-(2f_0'f_1'+4f_1^2)(f_0''+2f_1)\\&\quad=\frac{2}{\gamma-1}[f_0'^2f_1''+2f_0'f_1'f_0''+8f_0'f_1f_1'+8f_1^3],\end{aligned} \tag{5}$$

……………………………

of which the nth equation contains f_n on the left-hand side with coefficient $2n(2n-1)(1-f_0'^2)$, and nowhere else contains any f of suffix as large as n. It follows that the equations enable us to determine each f_n uniquely when f_0 is given; and that, in any range of x in which f_0 and all its derivatives are bounded and continuous and the upper bound of f_0' is less than unity, each f_n and all its derivatives are also bounded (*quâ* function of x) and continuous. (It is noticed that to give $f_0(x)$ is to give the axial velocity distribution, $f_0'(x)$.)

In this section it is proposed to concentrate on the behaviour of the flow near the sonic line, where the singularities in the hodograph transformation arise. An approximate equation for the sonic line is obtained as follows. For the sonic speed we have $w^2 = dp/d\rho = (p_0\rho_0^{-\gamma})\gamma\rho^{\gamma-1}$. Hence from (1) $w^2 = (\gamma-1)/(\gamma+1)$. But

$$\phi_x^2+\phi_y^2 = (\gamma-1)/(\gamma+1)$$

implies $$f_0'^2+2y^2f_0'f_1'+4y^2f_1^2+O(y^4) = (\gamma-1)/(\gamma+1).$$

Hence $f_0'^2 \doteqdot (\gamma-1)/(\gamma+1)+O(y^2)$. But from (4)

$$f_1 = f_0''\left(\frac{\gamma+1}{\gamma-1}f_0'^2-1\right)\Big/2(1-f_0'^2). \tag{6}$$

Hence $f_1 = O(y^2)$ on the sonic line and

$$y^2 = (2f_0'f_1')^{-1}\left(\frac{\gamma-1}{\gamma+1}-f_0'^2\right)+O(y^4). \tag{7}$$

Here f_1' could be replaced (neglecting $f_0'^2-(\gamma-1)/(\gamma+1)$ without loss of accuracy) by $(\gamma+1)f_0'f_0''^2/(\gamma-1)(1-f_0'^2)$, a positive number. It follows that (near the axis at any rate) the sonic line is concave to the oncoming flow.

Next consider θ, the direction of motion at any point. Since

$$\begin{aligned}\tan\theta = \phi_y/\phi_x &= (2yf_1+4y^3f_2+\dots)/(f_0'+y^2f_1'+\dots)\\ &= (2yf_1+4y^3f_2+\dots)(f_0'^{-1}-y^2f_1'f_0'^{-2}+\dots),\end{aligned}$$

it and hence θ also can be expressed as a series of odd powers of y whose coefficients are finite in any range in which f_0' is never 0 or 1. The first two terms in the series for θ are

$$\theta = 2yf_1f_0'^{-1}+y^3(4f_2f_0'^{-1}-2f_1f_1'f_0'^{-2}-\tfrac{8}{3}f_1^3f_0'^{-3})+O(y^5). \tag{8}$$

Observing that (5) can be written

$$f_2 = \frac{(\gamma+1)}{6(\gamma-1)}\frac{f_0'f_1'f_0''}{1-f_0'^2}+O\left(\frac{\gamma-1}{\gamma+1}-f_0'^2\right), \tag{9}$$

it is deduced that the curve $\theta = 0$, $y \neq 0$ has approximate equation

$$y^2 = -f_1/2f_2+O(y^4), \quad \text{or} \quad y^2 = 3(2f_0'f_1')^{-1}\left(\frac{\gamma-1}{\gamma+1}-f_0'^2\right)+O(y^4). \tag{10}$$

This curve is therefore, like the sonic line, concave (near the axis) to the oncoming flow, but has a radius of curvature at the axis three times as great. Thus it touches the sonic line on the supersonic side. It follows from this that, for velocities just supersonic, the stream function ψ is a many-valued function of θ for constant speed; for in particular the value $\theta = 0$ is taken three times, on the axis and at two symmetrically placed points on the curve (10). To investigate this relation further use is made of the defining equation for the stream function,

$$\psi_y = \frac{\rho}{\rho_0}\phi_x = (1-\phi_x^2-\phi_y^2)^{1/(\gamma-1)}\phi_x = (1-f_0'^2+\dots)^{1/(\gamma-1)}(f_0'+\dots), \tag{11}$$

which equals a series of even powers of y with finite coefficients whose first term is $(1-f_0'^2)^{1/(\gamma-1)}f_0'$, to deduce that ψ is a series of odd powers of y beginning

$$(1-f_0'^2)^{1/(\gamma-1)}f_0'y+\ldots.$$

Now for constant speed $\tau^{\frac{1}{2}}$ we have

$$\tau=\phi_x^2+\phi_y^2=f_0'^2+2y^2f_0'f_1'+4y^2f_1^2+\ldots, \tag{12}$$

which can be inverted as
$$y^2=\frac{\tau-f_0'^2}{2f_0'f_1'}+O(\delta^2), \tag{13}$$

if τ and $f_0'^2$ are both restricted to lie within δ of $(\gamma-1)/(\gamma+1)$. Hence

$$\begin{aligned}\theta&=\frac{2yf_1+4y^3f_2}{f_0'}+O(\delta^{\frac{5}{2}})\\&=2\left(\frac{\tau-f_0'^2}{2f_0'f_1'}\right)^{\frac{1}{2}}\frac{\dfrac{\gamma+1}{\gamma-1}f_0'^2-1}{2(1-f_0'^2)f_0'}f_0''+4\left(\frac{\tau-f_0'^2}{2f_0'f_1'}\right)^{\frac{3}{2}}\frac{\gamma+1}{6(\gamma-1)}\frac{f_1'f_0''}{1-f_0'^2}+O(\delta^{\frac{5}{2}})\\&=\left(\frac{\tau-f_0'^2}{2f_0'f_1'}\right)^{\frac{1}{2}}\left[\frac{\dfrac{\gamma+1}{\gamma-1}f_0'^2-1+\dfrac{\gamma+1}{3(\gamma-1)}(\tau-f_0'^2)}{f_0'(1-f_0'^2)}\right]f_0''+O(\delta^{\frac{5}{2}})\\&=A\left(\tfrac{2}{3}f_0'^2+\tfrac{1}{3}\tau-\frac{\gamma-1}{\gamma+1}\right)\sqrt{(\tau-f_0'^2)}+O(\delta^{\frac{5}{2}}),\end{aligned} \tag{14}$$

where A depends only on γ. But $\psi=B\sqrt{(\tau-f_0'^2)}+O(\delta^{\frac{3}{2}})$, where B depends only on γ and the value of f_0'' at the sonic point. Hence

$$\theta=A\frac{\psi}{B}\left(\tau-\frac{\gamma-1}{\gamma+1}-\frac{2}{3}\frac{\psi^2}{B^2}\right)+O(\delta^{\frac{5}{2}}). \tag{15}$$

This exhibits the three-valued nature of ψ (as a function of θ for constant $\tau=w^2$). It has a branch-point when $\partial\theta/\partial\psi=0$, i.e. when

$$\tau=\frac{\gamma-1}{\gamma+1}+2\frac{\psi^2}{B^2},\quad \text{i.e. when}\quad \tau=2f_0'^2-\frac{\gamma-1}{\gamma+1}. \tag{16}$$

For such a branch-point we have from (13) and (16)

$$y^2=-(2f_0'f_1')^{-1}\left(\frac{\gamma-1}{\gamma+1}-f_0'^2\right)+O(y^4), \tag{17}$$

which is therefore the approximate equation of the line of branch-points. It is identical with (7) except in sign, showing that the line of branch-points (where in the hodograph plane $\psi_\theta=\infty$) touches the sonic line on the supersonic side and has equal but opposite radius of curvature at the axis.

From these investigations it is now possible to draw (see figure 1) the shape of things near the sonic point of the axis; in particular the curves of constant τ and θ. On the line of branch-points the directions of constant τ and of constant θ coincide (since $\partial\theta/\partial\psi = 0$ for constant τ), so the curves of the two systems touch. This is illustrated in figure 1. It is seen that the transformation $(x, y) \rightarrow (\tau, \theta)$ is simple on the left and triple on the right, the dividing line coming somewhere between the sonic line and the line $\theta = 0$, $y \neq 0$. (This dividing line is the locus of points for which (τ, θ) is the same as at some point on the line of branch-points the other side of the axis.)

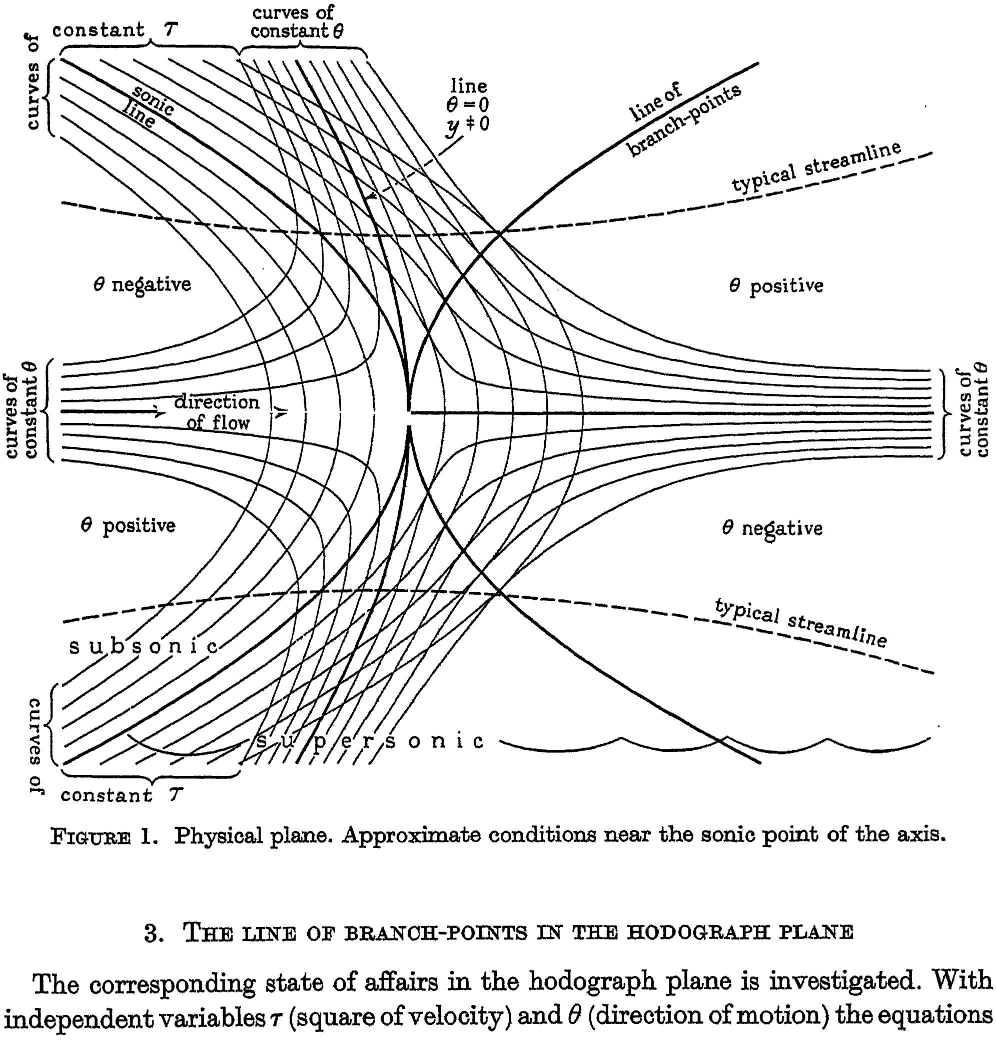

FIGURE 1. Physical plane. Approximate conditions near the sonic point of the axis.

3. THE LINE OF BRANCH-POINTS IN THE HODOGRAPH PLANE

The corresponding state of affairs in the hodograph plane is investigated. With independent variables τ (square of velocity) and θ (direction of motion) the equations of motion can be written

$$P\phi_\tau = \psi_\theta, \quad Q\psi_\tau = \phi_\theta, \tag{18}$$

where P, Q are functions of τ only:

$$P(\tau) = \frac{2(\gamma-1)\tau}{(\gamma+1)\tau-(\gamma-1)}(1-\tau)^{\gamma/(\gamma-1)}, \quad Q(\tau) = 2\tau(1-\tau)^{-1/(\gamma-1)}. \tag{19}$$

These 'hodograph equations' are of course linear, as pointed out in § 1. Now $d\phi/d\tau$ along a streamline is always finite if (as is required) the velocity increases steadily along each streamline. $d\phi/d\tau$ is

$$\phi_\tau - \phi_\theta \frac{\psi_\tau}{\psi_\theta} = \psi_\theta\left(\frac{1}{P} - Q\frac{\psi_\tau^2}{\psi_\theta^2}\right). \tag{20}$$

Hence, on the line of branch-points where ψ_θ is infinite, the contents of the brackets in (20) are zero and

$$\frac{\psi_\tau}{\psi_\theta} = (PQ)^{-\frac{1}{2}} = \pm\frac{1}{2\tau}\sqrt{\frac{(\gamma+1)\tau-(\gamma-1)}{(\gamma-1)(1-\tau)}}. \tag{21}$$

But $\psi_\tau/\psi_\theta = -(d\theta/d\tau)_{\psi\,\text{constant}}$. Choose now (in the physical plane) temporary Cartesian axes with origin at any point on the line of branch-points and x-axis tangent to a line of constant τ (and hence also to a line of constant θ). Then $\partial\theta/\partial x = \partial\tau/\partial x = 0$ at the origin. Suppose $\partial\theta/\partial y = a$, $\partial\tau/\partial y = b$. Then along the line $y = mx$ we have

$$\frac{d\theta}{d\tau} = \frac{\partial\theta/\partial x + m\,\partial\theta/\partial y}{\partial\tau/\partial x + m\,\partial\tau/\partial y} = \frac{a}{b}, \tag{22}$$

a number independent of m. Thus $d\theta/d\tau$ is the same along any curve through the point not touching the line of constant τ. In particular it is the same along the line of branch-points as along a streamline. Hence at every point along the line of branch-points

$$\frac{d\theta}{d\tau} = \pm\frac{1}{2\tau}\sqrt{\frac{(\gamma+1)\tau-(\gamma-1)}{(\gamma-1)(1-\tau)}}. \tag{23}$$

But the line of branch-points goes through $\tau = (\gamma-1)/(\gamma+1)$, $\theta = 0$. Hence it is

$$\begin{aligned}\theta &= \pm\int_{\frac{\gamma-1}{\gamma+1}}^{\tau}\sqrt{\left(\frac{(\gamma+1)\tau-(\gamma-1)}{(\gamma-1)(1-\tau)}\right)}\frac{d\tau}{2\tau}\\ &= \pm\left[\sqrt{\left(\frac{\gamma+1}{\gamma-1}\right)}\tan^{-1}\sqrt{\left(\frac{(\gamma+1)\tau-(\gamma-1)}{(\gamma+1)(1-\tau)}\right)} - \tan^{-1}\sqrt{\left(\frac{(\gamma+1)\tau-(\gamma-1)}{(\gamma-1)(1-\tau)}\right)}\right];\end{aligned} \tag{24}$$

a fixed curve in the hodograph plane. (It is, in fact, in the language of the general theory of hyperbolic differential equations, a 'characteristic' curve for the equation of motion (which is hyperbolic in the supersonic region): it is the characteristic of both 'systems' through the sonic point of the axis.)

The shape of the curve is shown in figure 2 (it is cusped at the sonic point). The rough shape of a typical system of streamlines is also shown. Each streamline, though it cuts the line of branch-points in the physical plane (figure 1) must *touch* it in the hodograph plane since, for constant τ, θ is stationary as a function of ψ on this line. It is seen that this line divides (in the hodograph plane) the simple and multiple regions, though quite a different line did so in the physical plane. The correspondence between figures 1 and 2 should be carefully studied.

It will make for clarity to define explicitly the three branches of ψ (in the multiple region) as follows:

(i) $\psi^{+}(\tau,\theta)$ is the value of ψ on the streamline through (τ,θ) which has come up (see figure 2) from below the τ-axis and cut the line of branch-points once before reaching the point.

(ii) $\psi^-(\tau, \theta)$ is defined as in (i) with 'above' for 'below'. In fact

$$\psi^-(\tau, \theta) = -\psi^+(\tau, -\theta).$$

(iii) $\psi^0(\tau, \theta)$ is the value of ψ on the streamline through (τ, θ) which has already touched (as well as cut) the line of branch-points before reaching the point.

In the physical plane (figure 1) ψ^+ and ψ^- are values taken between the sonic line and the line of branch-points, while ψ^0, an odd function of θ, is the value taken on the right of the line of branch-points (and in particular on the axis of the channel).

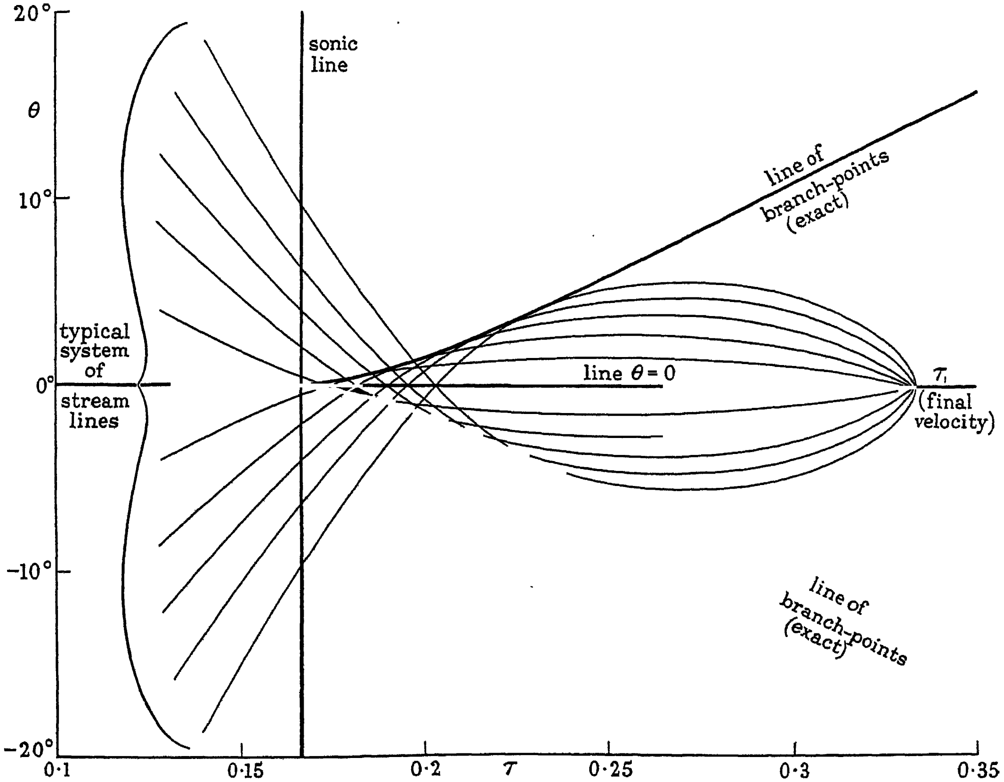

FIGURE 2. Hodograph plane. Line of branch-points and streamlines.

Let (24) be written as $\theta = \pm t$ where t is a positive function of τ satisfying $dt/d\tau = (PQ)^{-\frac{1}{2}}$. The function $\Psi(\tau, \theta) = \psi^+(\tau, \theta) - \psi^0(\tau, \theta)$ is the difference between two branches of ψ which separate at the branch-point $\theta = t$, and so it can be expressed as a series of odd powers of $(t-\theta)^{\frac{1}{2}}$ near $\theta = t$. Certain facts can be found about the coefficients in this series which, though they are not used in what follows, seem worth recording as likely to be of use some day.

Eliminating ϕ from equations (18) we have as equation for ψ

$$PQ\psi_{\tau\tau} + PQ_\tau \psi_\tau - \psi_{\theta\theta} = 0, \tag{25}$$

so that, with t instead of τ as independent variable,

$$PQ(\psi_t t_{\tau\tau} + \psi_{tt} t_\tau^2) + PQ_\tau \psi_t t_\tau - \psi_{\theta\theta} = 0 \tag{26}$$

or

$$\psi_{tt} + S(t)\,\psi_t - \psi_{\theta\theta} = 0, \tag{27}$$

where

$$S(t) = \tfrac{1}{2}(PQ)^{\frac{1}{2}}\,(Q_\tau Q^{-1} - P_\tau P^{-1}). \tag{28}$$

In writing the equation of motion in this form we follow Professor Temple. If now $\Psi(\tau, \theta)$, which satisfies the equation of motion by its definition, has the series form $\sum_{n=0}^{\infty} (t-\theta)^{n+\frac{1}{2}} g_n(t)$ we have

$$\sum_{n=0}^{\infty} (g_n''(t)\,(t-\theta)^{n+\frac{1}{2}} + 2g_n'(t)\,(n+\tfrac{1}{2})\,(t-\theta)^{n-\frac{1}{2}}) + S(t) \sum_{n=0}^{\infty} (g_n'(t)\,(t-\theta)^{n+\frac{1}{2}} + g_n(t)\,(n+\tfrac{1}{2})\,(t-\theta)^{n-\frac{1}{2}}) = 0; \tag{29}$$

and hence, equating coefficients of $(t-\theta)^{n-\frac{1}{2}}$,

$$\left.\begin{array}{c} 2g_0'(t) + S(t)\,g_0(t) = 0, \\ \cdots\cdots\cdots\cdots\cdots\cdots\cdots\cdots \\ (2n+1)\,[g_n'(t) + \tfrac{1}{2}S(t)\,g_n(t)] = -g_{n-1}''(t) - S(t)\,g_{n-1}'(t). \\ \cdots\cdots\cdots\cdots\cdots\cdots\cdots\cdots \end{array}\right\} \tag{30}$$

The first of these gives

$$\log g_0(t) = -\frac{1}{2}\int \tfrac{1}{2}(PQ)^{\frac{1}{2}}\,(Q_\tau Q^{-1} - P_\tau P^{-1})\,dt + \text{constant}, \tag{31}$$

or, since $dt/d\tau = (PQ)^{-\frac{1}{2}}$,

$$g_0(\tau) = C_0\left(\frac{P}{Q}\right)^{\frac{1}{4}}, \tag{32}$$

where C_0 is arbitrary. Thus

$$\Psi(\tau, \theta) \sim C_0(P(\tau)/Q(\tau))^{\frac{1}{4}}\,(t-\theta)^{\frac{1}{2}}$$

as $\theta \to t$, a fact of some interest. The $(n+1)$th of equations (30) gives

$$\frac{g_n'(t)}{g_0(t)} - \frac{g_n(t)\,g_0'(t)}{g_0^2(t)} = -\frac{1}{2n+1}\left[\frac{g_{n-1}''(t)}{g_0(t)} - 2\frac{g_{n-1}'(t)\,g_0'(t)}{g_0^2(t)}\right], \tag{33}$$

whence, with τ as independent variable,

$$\frac{g_n(\tau)}{g_0(\tau)} = -\frac{1}{2n+1}\int g_0(\tau)\,d\left(\frac{g_{n-1}'(\tau)}{g_0^2(\tau)}\sqrt{(PQ)}\right) + \text{constant}. \tag{34}$$

If we put $G_0(\tau) = (P(\tau)/Q(\tau))^{\frac{1}{4}}$ and define $G_n(\tau)$ successively by

$$G_n(\tau) = \frac{G_0(\tau)}{2n+1}\int_\tau^{\tau_1} G_0(\tau)\,d(Q(\tau)\,G_{n-1}'(\tau)) \tag{35}$$

we can deduce from (34)—but omit the details as we do not use the result again—

$$\Psi(\tau, \theta) = C_0 G(\tau, \theta) + C_1\int_\theta^t G(\tau, \theta_1)\,d\theta_1 + C_2\int_\theta^t d\theta_1\int_{\theta_1}^t G(\tau, \theta_2)\,d\theta_2 + \ldots, \tag{36}$$

where $G(\tau,\theta) = \sum_{n=0}^{\infty} G_n(t)\,(t-\theta)^{n+\frac{1}{2}}$ and $C_0, C_1, \ldots$ are arbitrary constants. An equivalent expression is

$$\Psi(\tau,\theta) = C_0\,G(\tau,\theta) + \int_{\theta}^{t} G(\tau,\theta_1)\,f(\theta_1-\theta)\,d\theta_1, \tag{37}$$

where f is an arbitrary function.

4. The stream function as independent variable

One more result is required from 'physical plane' theory. This is that the incipient series (15) for θ in terms of ψ (τ constant) can be continued without encountering coefficients which become infinite near the sonic speed (or anywhere else except perhaps at $\tau = 0$). We require in fact the finiteness of $(\partial^n\theta/\partial\psi^n)_{\tau\,\text{constant}}$. To show this we observe that the functions

$$A = -\frac{\partial\tau/\partial y}{\dfrac{\partial(\tau,\psi)}{\partial(x,y)}}, \quad B = \frac{\partial\tau/\partial x}{\dfrac{\partial(\tau,\psi)}{\partial(x,y)}} \tag{38}$$

are, together with all their derivatives, finite everywhere on the axis (except as $x \to -\infty$), since the Jacobian

$$\frac{\partial\tau}{\partial x}\frac{\partial\psi}{\partial y} - \frac{\partial\tau}{\partial y}\frac{\partial\psi}{\partial x} = \frac{\partial\tau}{\partial x}\frac{\rho}{\rho_0}\tau^{\frac{1}{2}} \tag{39}$$

does not vanish (for $\tau > 0$) if the velocity increases steadily on the axis. Hence

$$\left[\left(\frac{\partial^n\theta}{\partial\psi^n}\right)_{\tau\,\text{constant}}\right]_{\psi=0} = \left[\left(A\frac{\partial}{\partial x} + B\frac{\partial}{\partial y}\right)^n \theta\right]_{y=0} \tag{40}$$

is finite for $\tau > 0$.

It has been assumed throughout that the velocity increases steadily on every streamline, and the expansion in series in the physical plane shows that if this is true on the axis it is true at any rate in some region including the axis and other streamlines. In designing a channel it is advisable to start from such an axial velocity distribution and work outwards to a pair of streamlines as far out as possible for which the velocity is still increasing.

Beyond this limit θ is no longer a single-valued function of ψ, τ. The expansion in series whose existence was shown above can therefore no longer converge; and the relation between planes becomes rather more complicated than that illustrated in figures 1 and 2. This region is not studied here, as it must in any case be excluded from our tunnels.

It should be observed that when a pair of streamlines is fixed upon as walls for the tunnel, so that ψ is bounded, not all the points on the supersonic side of the line of branch-points are triple. This region is then divided into four by the two bounding streamlines; in one of the four subregions the representation (of physical on hodograph plane) is triple, in two of them double, and in one simple. There remains a region further to the right with no representation in the physical plane. This point also is illustrated in figure 2.

5. GENERAL 'HODOGRAPH PLANE' THEORY

Equation (25), written in full, becomes

$$\psi_{\theta\theta}=\frac{4(\gamma-1)\tau}{(\gamma+1)\tau-(\gamma-1)}\left[\tau(1-\tau)\psi_{\tau\tau}+\left(1+\frac{2-\gamma}{\gamma-1}\tau\right)\psi_{\tau}\right], \tag{41}$$

which is used rather than the corresponding equation for ϕ largely because it is simpler. The general solution of (41), regular at $\tau = 0$ and odd in θ, is (as Chaplygin pointed out in his original paper, 1904)

$$\psi(\tau,\theta)=A_0\theta+\sum_1^\infty A_n\psi_n(\tau)\sin n\theta, \tag{42}$$

where the ψ_n are hypergeometric functions:

$$\psi_n(\tau)=\tau^{\frac{1}{2}n}F(a_n,b_n;n+1;\tau),\quad a_n+b_n=n-\frac{1}{\gamma-1},\quad a_nb_n=-\frac{n(n+1)}{2(\gamma-1)}. \tag{43}$$

These functions are bounded and continuous in the whole range (0, 1) of values which τ can take.

(Of course it can be said immediately, knowing that ψ is many-valued, that no series (42) can represent it throughout the channel. It is doubtless true that the channel could be divided into a finite number of sections in each of which some expansion of the form (42) holds, provided that the second solution of the hypergeometric equation may occur in some of the sections. But this is temporarily neglected.)

On the axis we may write $\phi_\tau = \phi_x x_\tau = \tau^{\frac{1}{2}} dx/d\tau$ (regarding $x(\tau)$ in the last expression as the inverse function of the axial velocity distribution $\tau(x)$). Hence by (18)

$$(\psi_\theta)_{\psi=0}=\frac{2(\gamma-1)\tau^{\frac{3}{2}}}{(\gamma+1)\tau-(\gamma-1)}(1-\tau)^{\gamma/(\gamma-1)}\frac{dx}{d\tau}. \tag{44}$$

To obtain steadily increasing axial velocity from 0 at $x = -\infty$ to τ_1 (some supersonic value) at $x = +\infty$ we must therefore have (on the axis)

$$\left.\begin{array}{llll}\psi_\theta<0 & \text{for}\quad 0<\tau<\dfrac{\gamma-1}{\gamma+1}, & \psi_\theta=\infty & \text{at}\quad \tau=\dfrac{\gamma-1}{\gamma+1},\\[2ex] \psi_\theta>0 & \text{for}\quad \dfrac{\gamma-1}{\gamma+1}<\tau<\tau_1, & \psi_\theta=\infty & \text{at}\quad \tau=\tau_1.\end{array}\right\} \tag{45}$$

Since $(\psi_\theta)_{\psi=0}$ depends uniquely on the axial velocity distribution, we can deduce (from the arguments following equation (5)) that given any form for $(\psi_\theta)_{\psi=0}$ satisfying (45) we can obtain a unique solution of the equations of motion: and (41) shows how this comes about, since it gives, on differentiating $(2n-1)$ times and putting $\theta = 0$,

$$(\psi_{\theta^{2n+1}})_{\psi=0} = \frac{4(\gamma-1)\tau}{(\gamma+1)\tau-(\gamma-1)}\left\{\tau(1-\tau)\frac{d^2}{d\tau^2}[(\psi_{\theta^{2n-1}})_{\psi=0}] + \left(1+\frac{2-\gamma}{\gamma-1}\tau\right)\frac{d}{d\tau}[(\psi_{\theta^{2n-1}})_{\psi=0}]\right\}, \tag{46}$$

which, together with $$\psi(\tau,\theta) = \sum_{n=0}^{\infty}\frac{\theta^{2n+1}}{(2n+1)!}(\psi_{\theta^{2n+1}})_{\psi=0}, \tag{47}$$

determines ψ, at any rate in the region in which (47) converges. (In the above the suffix $\psi = 0$ not $\theta = 0$ has been written because, as was seen in § 2, the former implies the latter but not vice versa.)

If $(\psi_\theta)_{\psi=0}$ were never infinite the problem could be solved to any desired degree of accuracy by approximating to $(\psi_\theta)_{\psi=0}$ with a finite sum $A_0+\sum_1^m nA_n\psi_n(\tau)$; then $A_0\theta+\sum_1^m A_n\psi_n(\tau)\sin n\theta$ would give the correct form for the stream-function. As it is ψ must be divided into three parts

(i) a part singular at the sonic speed defined by

$$(\psi_\theta)_{\psi=0} = \frac{K_1}{\tau-(\gamma-1)/(\gamma+1)} \quad (K_1>0); \tag{48}$$

(ii) a part singular at $\tau = \tau_1$ defined by

$$(\psi_\theta)_{\psi=0} = \frac{K_2}{\tau_1-\tau} \quad (K_2>0); \tag{49}$$

and (iii) a part for which $(\psi_\theta)_{\psi=0}$ is bounded and continuous in $0\leqslant\tau\leqslant\tau_1$ and therefore approximable by a finite sum $A_0+\sum_1^m nA_n\psi_n(\tau)$; the ψ for this part being $A_0\theta+\sum_1^m A_n\psi_n(\tau)\sin n\theta$.

Thus if the ψ's can be found corresponding to (48) and (49)—e.g. by a method based on (46) and (47)—the general problem of determining the flow from the axial velocity distribution can be solved to any given degree of approximation.

But before this is accomplished in §§ 6 and 7 some further remarks on the above dissection are essential, for ψ is a three-valued function in part of the plane, while the ψ of (iii) is single-valued. It follows that any two functions built up as in (i), (ii) and (iii) with the same K_1 and K_2 differ by a single-valued function. Thus the $\Psi(\tau,\theta)$ (§ 3) for any two such functions—being the difference between two branches in each case—must be the same. Now it would be a mistake to draw any general conclusions from this, for these reasons. A general value of $(\psi_\theta)_{\psi=0}$, even with the terms (48) and (49) subtracted from it, leads as can be seen from (46) to higher derivatives of ψ becoming infinite (with the factor outside the square brackets) at the sonic point of the axis—and this in general means branch-points and many-valuedness. For any finite sum as in (iii), however, the term in square brackets in (46) vanishes at the sonic speed and all the derivatives of ψ are finite there. Thus it can be seen that however closely we may approximate to $(\psi_\theta)_{\psi=0}$ by a finite sum as in (iii)—and approximation to $(\psi_\theta)_{\psi=0}$ means in effect, by (44), approximation to the acceleration on the axis—the expression

$$\tau(1-\tau)\frac{d^2}{d\tau^2}[(\psi_\theta)_{\psi=0}]+\left(1+\frac{2-\gamma}{\gamma-1}\tau\right)\frac{d}{d\tau}[(\psi_\theta)_{\psi=0}] \tag{50}$$

remains zero at $\tau=(\gamma-1)/(\gamma+1)$, so that no approach at all is made to its real value there. Thus in particular the second derivative of the acceleration may be given quite incorrectly at the sonic point. If an attempt were made to approximate simultaneously to all the derivatives of $(\psi_\theta)_{\psi=0}$—as can theoretically be done—one would arrive at a many-valued function in part (iii). But of course from the physical requirements it is quite sufficient to approximate closely to the acceleration without worrying about its derivatives.

If one spoke of equating the $(\psi_\theta)_{\psi=0}$ of (iii) to an infinite series $A_0+\sum_1^\infty nA_n\psi_n(\tau)$ —instead of approximating to it with a finite sum—one would certainly find in general that the series could not be differentiated twice with respect to τ and remain convergent near the sonic speed, else the expression (50) would vanish there whatever function we had started with. The expression approximable by a finite sum in (iii) is therefore preferable, together with the proviso that it will be satisfactory if the acceleration is approximated without its higher derivative being so.

To strike a practical note, the approximation discussed above will be greatly facilitated by the tabulations, in a subsequent part of this work, of a wide range of the $\psi_n(\tau)$.

6. CONSTRUCTION OF THE SINGULAR SOLUTIONS

Two singular solutions of the equation of motion are now constructed, corresponding to the values (48) and (49) for $(\psi_\theta)_{\psi=0}$. We write $\eta=(\gamma+1)\tau/(\gamma-1)-1$, $\eta_1=(\gamma+1)\tau_1/(\gamma-1)-1$, and henceforth assume $\gamma=1{\cdot}4$, its value for a diatomic gas. The equation (46) becomes

$$\psi_{\theta^{2m+1}}=\frac{1}{3}\left[(10\eta^{-1}+18+6\eta-2\eta^2)\frac{d^2}{d\eta^2}\psi_{\theta^{2m-1}}+(15\eta^{-1}+18+3\eta)\frac{d}{d\eta}\psi_{\theta^{2m-1}}\right], \tag{51}$$

leaving the suffices $\psi=0$ to be understood.

Assuming
$$\psi_{\theta^{2m+1}}=3^{-m}\left[\sum_{n=1}^{\infty}a_{m,n}\eta^{-n}+\sum_{n=1}^{\infty}b_{m,n}\eta_1^n(\eta_1-\eta)^{-n}\right], \tag{52}$$

recurrence formulae are deduced for the a's and b's. In fact if η^{-n} is inserted for $\psi_{\theta^{2m-1}}$ on the right of (51) we get

$$\frac{1}{3}\left[(10\eta^{-1}+18+6\eta-2\eta^2)\frac{n(n+1)}{\eta^{n+2}}-(15\eta^{-1}+18+3\eta)\frac{n}{\eta^{n+1}}\right], \tag{53}$$

whereas if $(\eta_1-\eta)^{-n}$ is inserted we get

$$\begin{aligned}\frac{1}{3}\Big[&(10\eta^{-1}+18+6\eta-2\eta^2)\frac{n(n+1)}{(\eta_1-\eta)^{n+2}}+(15\eta^{-1}+18+3\eta)\frac{n}{(\eta_1-\eta)^{n+1}}\Big]\\ &=\frac{1}{3}\Big[n(n+1)\Big\{10\left(\frac{\eta_1^{-n-2}}{\eta}+\frac{\eta_1^{-n-2}}{\eta_1-\eta}+\ldots+\frac{\eta_1^{-1}}{(\eta_1-\eta)^{n+2}}\right)\\ &\quad+\frac{18+6\eta_1-2\eta_1^2}{(\eta_1-\eta)^{n+2}}+\frac{4\eta_1-6}{(\eta_1-\eta)^{n+1}}-\frac{2}{(\eta_1-\eta)^{n}}\Big\}\\ &\quad+n\Big\{15\left(\frac{\eta_1^{-n-1}}{\eta}+\frac{\eta_1^{-n-1}}{\eta_1-\eta}+\ldots+\frac{\eta_1^{-1}}{(\eta_1-\eta)^{n+1}}\right)+\frac{18+3\eta_1}{(\eta_1-\eta)^{n+1}}-\frac{3}{(\eta_1-\eta)^{n}}\Big\}\Big]. \end{aligned}\tag{54}$$

Hence the recurrence formulae for the a's and b's are

(i) for $n>1$,

$$\begin{aligned}a_{m+1,n}&=-n(2n+5)\,a_{m,n}+6(n-1)(n-3)\,a_{m,n-1}\\ &\qquad+3(n-2)(6n-11)\,a_{m,n-2}+10(n-2)(n-3)\,a_{m,n-3};\end{aligned}\tag{55}$$

(ii) for $n=1$, $a_{m+1,1}=-7a_{m,1}+\sum\limits_{r=1}^{\infty}\left[\frac{10r(r+1)}{\eta_1^2}+\frac{15r}{\eta_1}\right]b_{m,r}$;

(iii) for all n,

$$\begin{aligned}b_{m+1,n}&=(n-2)(n-1)(18\eta_1^{-2}+6\eta_1^{-1}-2)\,b_{m,n-2}\\ &\quad+(n-1)\,n\,(-6\eta_1^{-1}+4)\,b_{m,n-1}-n(n+1)\,.\,2b_{m,n}+(n-1)(18\eta_1^{-1}+3)\,b_{m,n-1}\\ &\quad-n\,.\,3b_{m,n}+10\eta_1^{-3}[(n-2)(n-1)\,b_{m,n-2}+(n-1)\,nb_{m,n-1}+\ldots]\\ &\quad+15\eta_1^{-2}[(n-1)\,b_{m,n-1}+nb_{m,n}+\ldots].\end{aligned}$$

Actually $a_{m,n}$ is non-zero only for $1\leqslant n\leqslant 3m+1$ and $b_{m,n}$ for $1\leqslant n\leqslant 2m+1$ so that the series in (ii) and (iii) are always finite.

In the ensuing calculations η_1 is taken as 1. This corresponds to $\tau_1=\frac{1}{3}$ and a 'working-section Mach number' of $(5/2)^{\frac{1}{2}}=1{\cdot}58$. (This is actually about the maximum Mach number which seems to be obtainable with tunnels of the 'induced flow' type.)

Three tables are needed (i) that produced by $\psi_\theta=\eta^{-1}$ (including only $a_{m,n}$'s); (ii) and (iii) the $a_{m,n}$'s and $b_{m,n}$'s produced by $\psi_\theta=(\eta_1-\eta)^{-1}$.

(i) is independent of η_1 and is obtained by applying (55) under the conditions $a_{0,1}=1$, $a_{0,n}=0$ for $n>1$.

(ii) and (iii) with our choice of η_1 satisfy the recurrence formulae:

$$\left.\begin{aligned}&\text{(ii)}\ \ a_{m+1,1}=-7a_{m,1}+5\sum_{r=1}^{\infty}r(2r+5)\,b_{m,r},\quad a_{0,1}=0\quad\text{(with (55))},\\ &\text{(iii)}\ \ b_{m+1,n}=32(n-2)(n-1)\,b_{m,n-2}+4(n-1)(2n+9)\,b_{m,n-1}\\ &\qquad+4n(2n+5)\,b_{m,n}+5\sum_{r=n+1}^{\infty}r(2r+5)\,b_{m,r},\quad b_{0,1}=1,\quad b_{0,n}=0\quad(n>1).\end{aligned}\right\}.\tag{56}$$

The tables for $m = 0$ to 3 (so that the neglected terms in (47) are $O(\theta^9)$) are as follows:

	$m=0$	$m=1$	$m=2$	$m=3$
		(i) $a_{m,n}$ from $\psi_\theta=\eta^{-1}$		
$n=1$	1	−7	49	−343
$n=2$		−6	150	−2,994
$n=3$		21	−840	28,749
$n=4$		20	−1,270	63,600
$n=5$			4,191	−509,925
$n=6$			8,520	−973,650
$n=7$			4,000	2,389,695
$n=8$				7,771,620
$n=9$				7,190,400
$n=10$				2,240,000
		(ii) $a_{m,n}$ from $\psi_\theta=(1-\eta)^{-1}$		
$n=1$		35	15,975	19,793,015
$n=2$			−210	−92,070
$n=3$			735	311,220
$n=4$			700	279,950
$n=5$				146,685
$n=6$				298,200
$n=7$				140,000
		(iii) $b_{m,n}$ from $\psi_\theta=(1-\eta)^{-1}$		
$n=1$	1	28	16,024	19,792,672
$n=2$		52	15,760	19,893,568
$n=3$		64	16,480	20,298,496
$n=4$			23,040	20,396,160
$n=5$			24,576	20,705,280
$n=6$				25,067,520
$n=7$				23,592,960

Write

$$\left.\begin{aligned} P^{(0)}_m(\eta) &= \sum_{n=1}^{3m+1} a_{m,n}\eta^{-n} \quad \text{from (i);} \\ P^{(\eta_1)}_m(\eta) &= \sum_{n=1}^{3m-2} a_{m,n}\eta^{-n} + \sum_{n=1}^{2m+1} b_{m,n}\eta_1^n(\eta_1-\eta)^{-n} \quad \text{from (ii) and (iii).} \end{aligned}\right\} \tag{57}$$

The eight functions $P^{(0)}_m$, $P^{(1)}_m$ $(m = 0, 1, 2, 3)$ and their derivatives are tabulated in the Appendix. (The fact that each $P^{(\,)}_m$ vanishes at $\eta = -1$ affords a simple check on the accuracy of the above tables.)

$$\psi^{(\,)} = \sum_{m=0}^{\infty} \frac{\theta^{2m+1}}{(2m+1)!} 3^{-m} P^{(\,)}_m = \theta P^{(\,)}_0 + \frac{\theta^3}{18} P^{(\,)}_1 + \frac{\theta^5}{1080} P^{(\,)}_2 + \frac{\theta^7}{136{,}080} P^{(\,)}_3 + \dots \tag{58}$$

is a solution of the hodograph equations for each set of P's.

7. APPLICATION OF THE SINGULAR SOLUTIONS

A linear combination of $\psi^{(0)}$, $\psi^{(\eta_1)}$ and any finite sum $A_0\theta + \sum_1^m A_n\psi_n(\tau)\sin n\theta$ will represent the flow in a channel with τ rising steadily on the axis from 0 to τ_1, provided that condition (45) holds. Whatever combination is taken we may write ψ as

$$\psi = \theta Q_0 + \theta^3 Q_1 + \theta^5 Q_2 + \theta^7 Q_3 + \dots \tag{59}$$

(replacing each sine by its series form), where each Q_n is $O(\eta^{-3n-1})$ as $\eta \to 0$. This series can converge only in some region of the form $|\theta^2\eta^{-3}| <$ constant. (Indeed if each Q_n is replaced by the part proportional to η^{-3n-1} a series of hypergeometric type convergent for $|\theta^2\eta^{-3}| < 2/15$ is obtained.) Such a region is bounded in the physical plane by two curves each symmetrical about the axis, touching at the sonic point and facing in opposite directions. The excluded region contains part of every streamline except the axis. In particular it includes all the region in which the values ψ^+ and ψ^- of the stream function are taken, since (59) is a one-valued function and must represent $\psi^0(\tau, \theta)$ when it converges.,

How are we to find the relation between ψ, τ and θ when (59) diverges? The answer is, by inverting the series. The inverted series is

$$\theta = R_0\psi + R_1\psi^3 + R_2\psi^5 + R_3\psi^7 + \dots, \tag{60}$$

where

$$\left.\begin{aligned} R_0 &= Q_0^{-1}, \quad R_1 = -Q_1 Q_0^{-4}, \quad R_2 = (3Q_1^2 - Q_0 Q_2)\, Q_0^{-7}, \\ R_3 &= (-12Q_1^3 + 8Q_0 Q_1 Q_2 - Q_0^2 Q_3)\, Q_0^{-10}, \text{ etc.} \end{aligned}\right\} \tag{61}$$

From the fact that $Q_n = O(\eta^{-3n-1})$ as $\eta \to 0$, we could only deduce that $R_n = O(\eta^{-n+1})$. But we have already shown (in § 4) that $R_n = O(1)$: thus the coefficients of $\eta_1^{-1}, \dots, \eta_1^{-n+1}$ in R_n must vanish when calculated, as is in fact found to occur; and the series (60) is convergent for $|\psi| <$ constant, uniformly in τ in any range $\tau \geqslant \tau_0 > 0$, in particular near $\tau = (\gamma - 1)/(\gamma + 1)$.

Equation (60) is used to deduce the shape of a channel $|\psi| = K$, K being chosen small enough to ensure that the number of terms taken (in this case four) represents θ with sufficient accuracy in the whole range—except possibly near $\tau = 0$ where the original series (59) must be used.

To obtain the shape equation (20) is used in the form with independent variables ψ, τ:

$$\left(\frac{\partial\phi}{\partial\tau}\right)_{\psi=K} = \frac{1}{\theta_\psi}\left(\frac{1}{P} - Q\theta_\tau^2\right). \tag{62}$$

θ_ψ is easily obtained from (60): for θ_τ we require the derivatives of the R_n (at any rate in the region in which (59) diverges—elsewhere it may be calculated as $-\psi_\tau/\psi_\theta$ from (59)): these are most easily found by calculating successively the coefficients of (i) θ^{2n} in ψ_θ^{-1}, (ii) θ^{2n+1} in $-\psi_\tau\psi_\theta^{-1} = \theta_\tau$, (iii) ψ^{2n+1} in θ_τ, the last named by replacing θ by (60) in (ii). Finally the co-ordinates of points on the streamline are obtained by numerically integrating the equation

$$dx + i\,dy = \tau^{-\frac{1}{2}} e^{i\theta} \left(\frac{\partial\phi}{\partial\tau}\right)_{\psi=K} d\tau. \tag{63}$$

On the sonic line the Q_n are infinite and equations (61) require the analytical expressions for the Q_n, the values of R_n and R_n' being the coefficients of 1 and $\eta/6$ respectively. If $(\psi_\theta)_{\psi=0} = \eta^{-1} + a + b\eta + c\eta^2 + \dots$ near $\eta = 0$ we have there (derivatives being with respect to τ)

$$\left.\begin{aligned} &R_0 = 0, \quad R_1 = -\tfrac{10}{9}, \quad R_2 = -\tfrac{1}{9} - \tfrac{100}{27}a, \quad R_3 = 1{\cdot}50661 - 0{\cdot}98765a - 16{\cdot}4609a^2, \\ &R_0' = 6, \quad R_1' = -7 + \tfrac{80}{3}a, \quad R_2' = -\tfrac{727}{60} - \tfrac{128}{3}a + \tfrac{1400}{9}a^2 - \tfrac{200}{9}b. \end{aligned}\right\} \tag{64}$$

On the line of branch-points $\theta_\psi = 0$ and the coefficient of θ_ψ^{-1} in (62) is also zero: the true value is obtained by taking the limit of the expression required along a line $\tau =$ constant, giving

$$\left(\frac{\partial\phi}{\partial\tau}\right)_{\psi=K} = -\frac{2Q\theta_\tau\theta_{\tau\psi}}{\theta_{\psi\psi}}, \tag{65}$$

the derivatives in this expression being all obtainable in terms of R_n and R'_n.

At $\tau = \tau_1$, the $dy/d\tau$ given by (63) contains the ratio of two zeros ($\sin\theta$ and θ_ψ). Its actual value is given by hydraulic theory since at infinity the flow is uniform. On $\psi = K$ at infinity

$$y\rho\rho_0^{-1}w = y(1-\tau)^{1/(\gamma-1)}\tau^{\frac{1}{2}} = K, \tag{66}$$

so

$$\left(\frac{dy}{d\tau}\right)_{\tau=\tau_1} = K\left[\frac{1}{2}+\left(\frac{1}{\gamma-1}-\frac{1}{2}\right)\tau_1\right](1-\tau_1)^{(\gamma-2)/(\gamma-1)}\tau_1^{-\frac{1}{2}}. \tag{67}$$

8. CONCLUSION

Thus it has been shown in detail how the problem of obtaining the channel shape from the axial velocity distribution may be solved. The calculations have been found to be not prohibitively long if four terms in the series are taken, so that ψ^9 is neglected. The corresponding method based on the 'physical plane' expansions of § 2 is only practicable if y^5 (sive ψ^5) is neglected.

Finally attention is drawn to the qualitative ideas which may find application to other trans-sonic problems. These are the essential relationship between planes embodied in figures 1 and 2; and the idea of doing the main body of the work in the hodograph plane and then finally *inverting* to obtain results in the regions of non-convergence which may occur near the sonic line—the independent variables after inversion being, for example, ψ, τ, but possibly others still.

APPENDIX

Here the practicality of the foregoing theory is demonstrated by using it to design a channel shape with a given value of $(\psi_\theta)_{\psi=0}$, i.e. with a given velocity distribution along the axis.

This velocity distribution must asymptote fairly rapidly at both ends of the channel. If for example $\tau \sim ae^{bx}$ as $x \to -\infty$, then $d\tau/dx \sim b\tau$ and so by (44)

$$\psi_\theta \sim -\frac{2}{b}\tau^{\frac{1}{2}} \quad \text{as } \tau \to 0. \tag{68}$$

In the same way if $\tau_1 - \tau \sim ce^{-dx}$ as $x \to +\infty$, then $d\tau/dx \sim -d(\tau-\tau_1)$ and so

$$\psi_\theta \sim \frac{\text{constant}}{\tau_1-\tau} \quad \text{as } \tau \to \tau_1. \tag{69}$$

The expression $\psi = K_0\psi^{(0)} + K_1\psi^{(1)} + A_0\theta + \sum_1^\infty A_n\psi_n(\tau)\sin n\theta$ will satisfy these conditions if K_1 is positive, A_1 negative, and $-K_0 + (1+\eta_1)^{-1}K_1 + A_0 = 0$. (Here the facts that, at $\tau = 0$, $P_0^{(0)} = -1$, $P_0^{(\eta_1)} = (1+\eta_1)^{-1}$, and $\psi_n(\tau) \sim \tau^{\frac{1}{2}n}$ have been used.)

In the channel designed below, $\eta_1 = 1$, $A_0 = 0$, $K_0 = 1$ (so that $K_1 = 2$), $A_1 = -7$, and $A_n = 0$ for $n > 1$ have been taken. Thus

$$\psi(\tau, \theta) = \psi^{(0)}(\tau, \theta) + 2\psi^{(1)}(\tau, \theta) - 7\psi_1(\tau) \sin \theta. \tag{70}$$

(This also satisfies conditions (45).) The value $A_1 = -7$ was chosen to make the rate at which the velocity asymptotes at the two ends of the channel approximately equal. Further A_n's were omitted for the sake of simplicity in a first test of the method.

For the ψ of (70) the Q_m (see (59)) will have the form

$$Q_m = \frac{3^{-m}}{(2m+1)!}(P_m^{(0)} + 2P_m^{(1)}) - 7\psi_1 \frac{(-1)^m}{(2m+1)!}. \tag{71}$$

In table 1 the fundamental functions $P_m^{(0)}(\eta)$, $P_m^{(1)}(\eta)$ and $\psi_1(\tau)$ have been tabulated, with their derivatives, dividing the range $0 \leqslant \tau \leqslant \frac{1}{3}$ into twelve for this purpose. The P's were obtained from (57) and ψ_1 from the hypergeometric series. The functions in this table are of general use. The functions relating to the particular choice of stream-function (70) are tabulated in table 2. First we have $Q_m(\tau)$ and $Q'_m(\tau)$. Then the $R_m(\tau)$ are calculated by means of (61); and for certain values near the sonic speed (where the series in powers of θ diverge and cannot be used) the $R'_m(\tau)$ are calculated by the process indicated in the passage following equation (62).

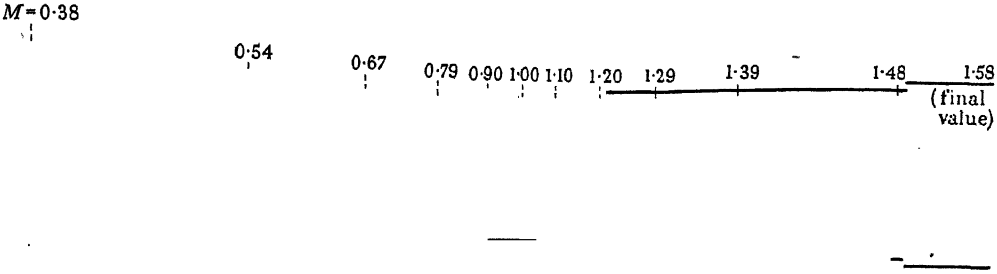

FIGURE 3. Channel-shape designed in the Appendix with distribution of Mach number along the wall.

$\psi = \pm 0{\cdot}2$ are taken as walls; there is every indication that four terms of the series (60) give θ fairly accurately for this value. This series gives also θ_ψ, and θ_τ in the region in which the $R'_m(\tau)$ have been calculated. Elsewhere it is possible (and quicker) to use the series (59) to obtain ψ_τ (θ having already been calculated) and then to get θ_τ as $-\psi_\tau/\psi_\theta$.

The values of $dx/d\tau$ and $dy/d\tau$ on $\psi = 0{\cdot}2$ are now obtained from (62) and (63), using (65) and (67) in certain special cases. The use of (65) needs slight elaboration. At $36\tau = 7$ in this case θ_ψ is very small and (62) would be inaccurate. Expression (65)

TABLE 1. THE FUNDAMENTAL FUNCTIONS $P_m^{(0)}$, $P_m^{(1)}$ AND ψ_1, WITH THEIR DERIVATIVES

36τ	0	1	2	3	4	5	6	7	8	9	10	11	12
$P_0^{(0)}(\eta)$	−1	−1·2	−1·5	−2	−3	−6	∞	6	3	2	1·5	1·2	1
$P_1^{(0)}(\eta)$	0	4·944	27·375	142	1020	21210	∞	30198	2112	450	148·125	60·72	28
$P_2^{(0)}(\eta)$	0	−345·44	−6451·41	−113930	−3·634320$_6$	−7·562835$_8$	∞	1·548021$_9$	1·585344$_7$	1·165050$_6$	188363·9	46391·66	14800
$P_3^{(0)}(\eta)$	0	62295·4	4·094983$_6$	2·507093$_8$	3·592292$_{10}$	7·532456$_{13}$	∞	2·215799$_{14}$	3·291865$_{11}$	8·193264$_9$	6·310501$_8$	8·895030$_7$	1·819715$_7$
$P_0^{(1)}(\eta)$	0·5	$0{\cdot}\dot{5}\dot{4}$	0·6	$0{\cdot}\dot{6}$	0·75	$0{\cdot}\dot{8}5714\dot{2}$	1	1·2	1·5	2	3	6	∞
$P_1^{(1)}(\eta)$	0	−0·871	−3·156	−9·259	−27·75	−107·492	∞	429·072	480	846	2332·5	15906	∞
$P_2^{(1)}(\eta)$	0	39·16	372·82	2887·5	38506·5	704529	∞	1·333579$_6$	540960	1·430190$_6$	8·502594$_6$	2·252076$_8$	∞
$P_3^{(1)}(\eta)$	0	−4167	−133887	−3·105911$_6$	−1·167955$_8$	−2·616241$_{10}$	∞	5·513064$_{10}$	1·740927$_9$	5·982561$_9$	7·738083$_{10}$	7·966753$_{12}$	∞
$P_0^{(0)\prime}(\eta)$	−1	−1·44	−2·25	−4	−9	−36	∞	−36	−9	−4	−2·25	−1·44	−1
$P_1^{(0)\prime}(\eta)$	12	57·7728	263·8125	1484	14076	538092	∞	−700884	−24156	−3444	−870·1875	−298·8864	−124
$P_2^{(0)\prime}(\eta)$	−144	−6761·312	−107783·3	−2·085796$_6$	−8·820742$_7$	−3·373277$_{10}$	∞	−6·227455$_{10}$	−3·093536$_8$	−1·485220$_7$	−1·779522$_6$	−348861	−92824
$P_3^{(0)\prime}(\eta)$	1548	1·741273$_6$	9·795687$_7$	6·580823$_9$	1·249955$_{12}$	4·810619$_{15}$	∞	−1·269254$_{16}$	−9·095526$_{12}$	−1·473553$_{11}$	−8·361603$_9$	−9·321043$_8$	−1·579572$_8$
$P_0^{(1)\prime}(\eta)$	0·25	0·2975207	0·36	$0{\cdot}\dot{4}$	0·5625	0·7346939	1	1·44	2·25	4	9	36	∞
$P_1^{(1)\prime}(\eta)$	−3	−8·196326	−22·3228	−58·81482	−194·625	−1066·870	∞	−641·8368	1071	3876	18533·25	272253·6	∞
$P_2^{(1)\prime}(\eta)$	36	610·1939	4622·272	36211·08	428374·2	1·839898$_7$	∞	−2·433856$_7$	1·500804$_6$	1·173532$_7$	1·169073$_8$	6·521151$_9$	∞
$P_3^{(1)\prime}(\eta)$	−432	−106363·1	−2·509400$_6$	6·085830$_7$	−4·107208$_9$	−1·172385$_{12}$	∞	−2·189719$_{12}$	−2·310023$_9$	7·148333$_{10}$	1·513849$_{12}$	3·250463$_{14}$	∞
$\psi_1(\tau)$	0	0·16096	0·21979	0·25985	0·28991	0·31239	0·33013	0·34394	0·35460	0·36265	0·36855	0·37263	0·37515
$\psi_1'(\tau)$	∞	2·69472	1·70115	1·22782	0·93174	0·72175	0·56243	0·43639	0·33360	0·24898	0·17778	0·11728	0·06582

Figures in suffix following a number indicate the power of ten by which that number is to be multiplied.

TABLE 2. FUNCTIONS APPERTAINING TO THE PARTICULAR CHANNEL DISCUSSED IN THE APPENDIX

36τ	0	1	2	3	4	5	6	7	8	9	10	11	12
$Q_0(\tau)$	0	−1·23581	−1·83853	−2·48562	−3·52937	−6·47244	∞	5·99242	3·51780	3·46145	4·92015	10·59159	∞
$Q_1(\tau)$	0	0·36568	1·42659	7·16327	53·92156	1166·754	∞	1725·743	171·0804	119·4231	267·8258	1771·141	∞
$Q_2(\tau)$	0	−0·25670	−5·29594	−100·1587	−3303·820	−698957·8	∞	1435822	15680·09	3727·229	15827·34	417094·0	∞
$Q_3(\tau)$	0	0·52113	28·12500	1796·719	262267·1	5·535297$_8$	∞	1·629116$_9$	2·444653$_6$	148136·3	1·141922$_6$	1·170899$_8$	∞
$Q_0'(\tau)$	∞	−23·9328	−21·0880	−27·2614	−53·7722	−212·2359	∞	−201·7747	−29·3352	22·2571	93·2555	422·5390	∞
$Q_1'(\tau)$	∞	16·9372	86·6478	456·8892	4563·374	178653·6	∞	−234055·4	−7337·611	1436·290	12065·64	181402·9	∞
$Q_2'(\tau)$	∞	−30·9401	−547·5369	−11185·48	−485281·4	−1·871998$_8$	∞	−3·462402$_8$	−1·701956$_6$	47880·18	1·289084$_6$	7·245530$_7$	∞
$Q_3'(\tau)$	∞	67·4000	4097·801	284793·0	5·475048$_7$	2·120051$_{11}$	∞	−5·598290$_{11}$	−4·012410$_8$	−193505·2	1·331277$_8$	2·866365$_{10}$	∞
$R_0(\tau)$	∞	−0·809186	−0·543913	−0·402314	−0·283337	−0·154501	0	0·166877	0·284269	0·288896	0·203246	0·094414	0
$R_1(\tau)$	∞	−0·15678	−0·12486	−0·18766	−0·34751	−0·66482	−1·11111	−1·33834	−1·11716	−0·83187	−0·45702	−0·14074	0
$R_2(\tau)$	∞	−0·01907	0·05114	0·16209	0·43067	0·92468	1·04041	1·19117	4·89703	4·70523	1·96735	0·33392	0
$R_3(\tau)$	∞	−0·05472	−0·04257	−0·13827	−0·39442	−0·16867	0·22249	−23·24910	−51·15613	−40·04022	−11·06993	−0·96878	0
$R_0'(\tau)$	—	—	—	—	4·31682	5·06620	6	5·61904	2·37054	—	—	—	—
$R_1'(\tau)$	—	—	—	—	−8·21662	−14·59774	−15·80344	1·25707	10·65051	—	—	—	—
$R_2'(\tau)$	—	—	—	—	14·76087	17·47443	−13·67728	68·1737	123·1315	—	—	—	—
$R_3'(\tau)$	—	—	—	—	−0·09094	62·8815	c. −330	−1437·189	−339·271	—	—	—	—
$\theta\ (\psi=0{\cdot}2)$	−∞	−0·16310	−0·10977	−0·08191	−0·05931	−0·03593	−0·00855	0·02275	0·04883	0·05212	0·03748	0·01785	0
$\theta_\psi\ (\psi=0{\cdot}2)$	−∞	−0·8282	−0·5585	−0·4236	−0·3218	−0·2270	−0·1251	0·0054	0·1665	0·2088	0·1592	0·0798	0
$\theta_\tau\ (\psi=0{\cdot}2)$	∞	3·175	1·233	0·854	0·802	0·903	1·065	1·137	0·594	−0·288	−0·675	−0·696	—
$dx/d\tau$	∞	122·62	56·82	34·38	22·86	15·84	11·68	11·27	19·28	25·34	37·80	94·06	∞
$dy/d\tau$	−∞	−20·17	−6·26	−2·82	−1·36	−0·58	−0·10	0·26	0·94	1·32	1·42	1·67	2·15
x	−∞	−5·264	−2·918	−1·689	−0·906	−0·378	0	0·287	0·704	1·341	2·171	3·854	∞
y	∞	1·312	0·981	0·861	0·806	0·780	0·771	0·773	0·789	0·822	0·859	0·903	0·955

Figures in suffix following a number indicate the power of ten by which that number is to be multiplied.

is calculated for the values $36\tau = 6, 7, 8$ and hence by interpolation for the value of τ for which $\theta_\psi = 0$. This then is the value of $(\partial\phi/\partial\tau)_{\psi=K}$ for *this* value of τ, which must then be corrected to get the value at $36\tau = 7$ by use of the known values at $36\tau = 6$ and 8.

The integration now proceeds by normal methods, starting from a value of y at $\tau = \tau_1$ given by (66). x, y having been obtained as functions of the parameter τ, the shape can be drawn out as in figure 3.

REFERENCES

Chaplygin, S. A. 1904 *Ann. Sci. Mosc. Imp. Univ. Math. Phys. Sect.*, **21**, 1.
Molenbroek, P. 1890 *Arch. Math. Phys.* **9**, 157.

The hodograph transformation in trans-sonic flow. II. Auxiliary theorems on the hypergeometric functions $\psi_n(\tau)$

BY M. J. LIGHTHILL

(*Communicated by S. Goldstein, F.R.S.—Received* 17 *March* 1947)

1. INTRODUCTION

The applications of the theorems of this paper will be found in subsequent parts of this work. The author does not lay claim to originality for all of them,† but believes that no connected account of the properties of $\psi_n(\tau)$ as function of n in the complex plane has previously been given.

The differential equation for the stream function in compressible flow is written, as in part I, in the form

$$PQ\psi_{\tau\tau} + PQ_\tau\psi_\tau - \psi_{\theta\theta} = 0, \tag{1}$$

where

$$P(\tau) = \frac{2(\gamma-1)\tau}{(\gamma+1)\tau-(\gamma-1)}(1-\tau)^{\gamma/(\gamma-1)}, \quad Q(\tau) = \frac{2\tau}{(1-\tau)^{1/(\gamma-1)}}. \tag{2}$$

For supersonic flow the alternative form

$$\psi_{tt} + S(t)\,\psi_t - \psi_{\theta\theta} = 0 \tag{3}$$

was found, where

$$\left.\begin{aligned} dt/d\tau &= (PQ)^{-\frac{1}{2}}, \\ t &= \sqrt{\frac{\gamma+1}{\gamma-1}}\tan^{-1}\sqrt{\frac{(\gamma+1)\tau-(\gamma-1)}{(\gamma+1)(1-\tau)}} - \tan^{-1}\sqrt{\frac{(\gamma+1)\tau-(\gamma-1)}{(\gamma-1)(1-\tau)}}, \\ S(t) &= \tfrac{1}{2}(PQ)^{\frac{1}{2}}(Q_\tau Q^{-1} - P_\tau P^{-1}) \\ &= \frac{2(\gamma+1)}{(\gamma-1)^2}\tau^2(1-\tau)^{-\frac{1}{2}}\left(\frac{\gamma+1}{\gamma-1}\tau-1\right)^{-\frac{3}{2}}. \end{aligned}\right\} \tag{4}$$

---

† His attention has been drawn to an unpublished work of G. Guderley which gives the asymptotic formulae for real n, with valuable information concerning the numerical magnitude of the error term.

For subsonic flow the similar form

$$\psi_{ss}+\psi_{\theta\theta} = T(s)\,\psi_s \tag{5}$$

is used, where

$$\left.\begin{aligned} ds/d\tau &= (-PQ)^{-\frac{1}{2}},\\ s &= \sigma+\sqrt{\frac{\gamma+1}{\gamma-1}}\tanh^{-1}\sqrt{\frac{(\gamma-1)-(\gamma+1)\tau}{(\gamma+1)(1-\tau)}}-\tanh^{-1}\sqrt{\frac{(\gamma-1)-(\gamma+1)\tau}{(\gamma-1)(1-\tau)}},\\ \sigma &= -\sqrt{\frac{\gamma+1}{\gamma-1}}\tanh^{-1}\sqrt{\frac{\gamma-1}{\gamma+1}}+\tfrac{1}{2}\log\,[2(\gamma-1)],\\ T(s) &= -\tfrac{1}{2}(-PQ)^{\frac{1}{2}}\,(Q_\tau Q^{-1}-P_\tau P^{-1})\\ &= \frac{2(\gamma+1)}{(\gamma-1)^2}\tau^2\,(1-\tau)^{-\frac{1}{2}}\left(1-\frac{\gamma+1}{\gamma-1}\tau\right)^{-\frac{3}{2}}. \end{aligned}\right\} \tag{6}$$

The object of the insertion of the constant σ is to cause τ to be asymptotically e^{2s} as $\tau \to 0$ and $s \to -\infty$. σ is the value of s at $\tau = (\gamma-1)/(\gamma+1)$, the sonic speed; comparison of (4) and (6) suggests the relation $s = \sigma \pm it$; it is preferable not to use this owing to obvious difficulties of deciding on the sign to be taken in any particular case.

LEMMA 1. Both τ and T are analytic functions of e^{2s} in the region $|e^{2s}| < e^{2\sigma}$.

Proof. By (6), $e^{2s} = \tau+\ldots$ is an analytic function of τ in any domain excluding $\tau = (\gamma-1)/(\gamma+1)$ and $\tau = 1$; its derivative is not zero in such a domain; and at neither of the singular points can $|e^{2s}|$ be less than $e^{2\sigma}$. Hence, by the inversion theorem, τ is an analytic function of e^{2s} in the region $|e^{2s}| < e^{2\sigma}$. As τ is never 1 or $(\gamma-1)/(\gamma+1)$ in the region, T also must be analytic.

2. $\psi_n(\tau)$ AND ITS POLES

$\psi_n(\tau)$ is defined† by the equations

$$\left.\begin{aligned} \psi_n(\tau) &= \tau^{\frac{1}{2}n}\,F(a_n, b_n; n+1; \tau),\\ a_n+b_n &= n-(\gamma-1)^{-1}, \quad a_n b_n = -n(n+1)/2(\gamma-1),\\ a_n, b_n &= \tfrac{1}{2}[n-(\gamma-1)^{-1} \pm \sqrt{\{(\gamma+1)\,n^2/(\gamma-1)+(\gamma-1)^{-2}\}}], \end{aligned}\right\} \tag{7}$$

as in part I. (One distinguishes between a_n and b_n when n is real by the convention $a_n \geqslant b_n$.) When n is not a negative integer, $\psi_n(\tau)$ is an analytic function of τ except at $\tau = 0, 1$, one-valued if cuts are made from both these points to infinity. As a function of n (in the complex plane) for given τ with $0<\tau<1$, $\psi_n(\tau)$ is analytic except possibly at the negative integers. For then

$$\psi_n(\tau) = \tau^{\frac{1}{2}n}\sum_0^\infty \frac{a_n b_n(a_n b_n+a_n+b_n+1)\ldots\{a_n b_n+(r-1)\,(a_n+b_n)+(r-1)^2\}}{(n+1)\,(n+2)\ldots(n+r)\,r!}\tau^r, \tag{8}$$

---

† When n is not a negative integer. For negative integers $\leqslant -2$ ψ_n is undefined: for $n=-1$, then $\psi_{-1}(\tau) = \lim\limits_{n\to -1} \psi_n(\tau) = \tau^{-\frac{1}{2}}+(2\gamma-2)^{-1}\psi_1(\tau)$. Actually it can be shown (since $a_1 = 1$) that $\psi_1(\tau) = (\gamma-1)\,\{1-(1-\tau)^{\gamma/(\gamma-1)}\}/\gamma\sqrt{\tau}$. Note also that $\psi_0(\tau) = 1$.

which is the sum of a uniformly convergent series of functions of n analytic except at the negative integers. To show that $n = -m$ is a pole of $\psi_n(\tau)$, and to find its residue there one can write

$$\begin{aligned}\lim_{n\to -m}(n+m)\,\psi_n(\tau) &= \tau^{-\frac{1}{2}m}\sum_{r=m}^{\infty}\frac{a_{-m}(a_{-m}+1)\ldots(a_{-m}+r-1)\,b_{-m}(b_{-m}+1)\ldots(b_m+r-1)}{(-m+1)(-m+2)\ldots(-2)(-1).1.2.\ldots.(-m+r)\,r!}\tau^r\\ &= \frac{a_{-m}(a_{-m}+1)\ldots(a_{-m}+m-1)\,b_{-m}(b_{-m}+1)\ldots(b_{-m}+m-1)}{(-1)^{m-1}(m-1)!\,m!}\\ &\quad\times\tau^{\frac{1}{2}m}\sum_{s=0}^{\infty}\frac{(a_{-m}+m)(a_{-m}+m+1)\ldots(a_{-m}+m+s-1)(b_{-m}+m)(b_{-m}+m+1)\ldots(b_{-m}+m+s-1)}{(m+1)(m+2)\ldots(m+s)\,s!}\tau^s.\end{aligned} \tag{9}$$

But it is easily seen that $a_{-m} = a_m - m$, $b_{-m} = b_m - m$. Hence the second line of equation (9) is simply $\psi_m(\tau)$, and the first, which depends only on m and γ, can be written $-mC_m$, where

$$C_m = \frac{\Gamma(a_m)\,\Gamma(m+1-b_m)}{\Gamma(a_m-m)\,\Gamma(1-b_m)\,(m!)^2} \tag{10}$$

$$= \frac{(a_m-1)(a_m-2)\ldots(a_m-m)(1-b_m)(2-b_m)\ldots(m-b_m)}{(m!)^2}. \tag{11}$$

The latter form shows that C_m is positive if $a_m > m$ and $b_m < 1$. When $\gamma > 1$ this is true for all $m \geqslant 2$. C_1, however, is always zero since $a_1 = 1$, and there is no pole at $n = -1$. When $\gamma = -1$, all the C_m are zero: this is what causes the simplicity of the 'Kármán-Tsien' approximation in compressible flow. When $\gamma = +1$ all results have to be greatly modified (though the final conclusions are not qualitatively changed); the hypergeometric functions become confluent in this case. It is assumed that $\gamma > 1$ in future. On this assumption one can deduce from (10), with the asymptotic formula for the gamma function and the expressions (7) for a_m, b_m, that as $m \to \infty$,

$$C_m = \frac{1}{2\pi m}e^{-2\sigma m}\left(1+O\left(\frac{1}{m}\right)\right), \tag{12}$$

where σ is as in (6). These results are summed up in

THEOREM 1. If $0 < \tau \leqslant 1$, $\psi_n(\tau)$ is an analytic function of n except at $n = -2, -3, -4, \ldots$, where it has simple poles, its residue at $n = -m$ being $-mC_m\psi_m(\tau)$, where C_m (given by (11)) is positive and $\sim (2\pi m)^{-1}e^{-2\sigma m}$ as $m \to \infty$.

3. ASYMPTOTIC FORMULAE FOR SUBSONIC τ

$\psi_n(\tau)$ is the unique function for which $\psi_n(\tau)\,e^{in\theta}$ satisfies (1) and $\tau^{-\frac{1}{2}n}\psi_n(\tau)$ is analytic at $\tau = 0$ and equal to unity there. Hence, translating to the variable s and using lemma 1, ψ_n is the unique function satisfying

$$\frac{d^2\psi_n}{ds^2} - n^2\psi_n = T(s)\frac{d\psi_n}{ds}, \tag{13}$$

for which $e^{-ns}\psi_n$ is an analytic function of e^{2s} for $|e^{2s}| < e^{2\sigma}$ and is unity at $s = -\infty$.

Put
$$\left.\begin{aligned} V(\tau) &= (-P/Q)^{\frac{1}{2}} = \exp\left\{\frac{1}{2}\int_{-\infty}^{s} T(s_1)\,ds_1\right\}, \\ dV/ds &= \tfrac{1}{2}TV \quad \text{and} \quad V(0) = 1, \end{aligned}\right\} \tag{14}$$
so that

and write
$$\psi_n(\tau) = e^{ns}V(\tau)\,W_n(s).$$

$V(\tau)$ is by lemma 1 analytic and not zero for $|e^{2s}| < e^{2\sigma}$, so $W_n(s)$ is analytic for $|e^{2s}| < e^{2\sigma}$ and equal to unity when $s = -\infty$. Hence $W_n(s) = \sum_0^\infty d_{n,r}e^{2rs}$ for $|e^{2s}| < e^{2\sigma}$, where $d_{n,0} = 1$. The equation for W_n is found from (13) to be

$$\frac{d^2W_n}{ds^2} + 2n\frac{dW_n}{ds} = [\tfrac{1}{4}T^2(s) - \tfrac{1}{2}T'(s)]\,W_n(s). \tag{15}$$

By lemma 1 one can write

$$\tfrac{1}{4}T^2(s) - \tfrac{1}{2}T'(s) = \sum_2^\infty t_r e^{2rs} \quad \text{for} \quad |e^{2s}| < e^{2\sigma}.$$

Hence in this region (15) becomes

$$\sum_0^\infty d_{n,r}\,.\,4r^2e^{2rs} + 2n\sum_0^\infty d_{n,r}\,.\,2re^{2rs} = \sum_2^\infty t_r e^{2rs}\sum_0^\infty d_{n,r}e^{2rs}, \tag{16}$$

and one can write
$$4r(n+r)\,d_{n,r} = \sum_{m=0}^{r-2} t_{r-m}d_{n,m}. \tag{17}$$

Now let σ_1, σ_2, σ_3 be any numbers satisfying $\sigma_1 < \sigma_2 < \sigma_3 < \sigma$. Then $\sum_2^\infty t_r e^{2r\sigma_3}$ converges, so its terms are bounded and one can write $|t_r| < Ae^{-2r\sigma_3}$.

Lemma 2. If $m > 0$, and $|n| > AC/\delta$, where $C = 1/(e^{2(\sigma_3-\sigma_2)} - 1)$, and n is restricted to lie at a distance $> \delta$ from any negative integer (where $0 < \delta < 1$), then

$$d_{n,m}| < \frac{A}{\delta|n|}e^{-2m\sigma_2}.$$

Proof. Assume it true for $m = 1, 2, \ldots, r-1$. Then by (17)

$$\begin{aligned} |4r(n+r)\,d_{n,r}| &< Ae^{-2r\sigma_3} + \sum_{m=1}^{r-2}\frac{A}{\delta|n|}e^{-2m\sigma_2}Ae^{-2(r-m)\sigma_3} \\ &= Ae^{-2r\sigma_3} + \frac{A^2e^{-2r\sigma_3}}{\delta|n|}\sum_{m=1}^{r-2}e^{2m(\sigma_3-\sigma_2)} \\ &< Ae^{-2r\sigma_3} + \frac{A^2}{\delta|n|}e^{-2r\sigma_3}\,.\,Ce^{2r(\sigma_3-\sigma_2)}. \end{aligned} \tag{18}$$

Now $|4r(n+r)| > 2|n|\delta$, for when $|r| > |\tfrac{1}{2}n|$ it is $> 4|\tfrac{1}{2}n|\delta$, and when $|r| < |\tfrac{1}{2}n|$ it is $> 4|\tfrac{1}{2}n|$. Hence

$$|d_{n,r}| < Ae^{-2r\sigma_2}\left(1 + \frac{AC}{\delta|n|}\right)\frac{1}{2\delta|n|} < \frac{Ae^{-2r\sigma_2}}{\delta|n|} \tag{19}$$

if $|n| > AC/\delta$. Hence the result is true for $m = r$. But for $m = 1$, $d_{n,m} = 0$, so the result is true and the lemma follows.

It is deduced that, for $s \leqslant \sigma_1$, under the restrictions of lemma 2,

$$|W_n(s) - 1| \leqslant \sum_1^\infty |d_{n,r}| e^{2r\sigma_1}$$

$$< \frac{A}{\delta |n|} \cdot \frac{1}{1 - e^{2(\sigma_1 - \sigma_2)}}, \tag{20}$$

and hence

THEOREM 2. If $\delta > 0$ and $\sigma_1 < \sigma$, then $W_n(s) \to 1$, i.e. $\psi_n(\tau) \sim e^{ns} V(\tau)$, uniformly for $s \leqslant \sigma_1$ and for n in the whole complex plane with circles of radius δ round each negative integer excluded, as $|n| \to \infty$.

Consider now the function

$$\Delta(n, \tau) = \frac{e^{-ns}\psi_n(\tau) - 1}{n} - \sum_2^\infty \frac{C_m e^{ms} \psi_m(\tau)}{n + m}. \tag{21}$$

When n is not a negative integer and $0 \leqslant \tau < (\gamma - 1)/(\gamma + 1)$, i.e. $s < \sigma$, the series converges, since $C_m e^{ms} \psi_m(\tau) \sim (2\pi m)^{-1} V(\tau) e^{2m(s-\sigma)}$ as $m \to \infty$ by theorems 1 and 2. The series has the same poles as $(e^{-ns}\psi_n(\tau) - 1)/n$ and the same residue at each pole. Hence $\Delta(n, \tau)$ is an integral function of n. Also when n is at a distance $> \delta$ from every negative integer†

$$\left| \sum_2^\infty \frac{C_m e^{ms} \psi_m(\tau)}{n + m} \right| \leqslant \sum_{m < \frac{1}{2}|n|} \frac{C_m e^{ms} \psi_m(\tau)}{\frac{1}{2}|n|} + \sum_{\frac{1}{2}|n| \leqslant m} \frac{C_m e^{ms} \psi_m(\tau)}{\delta}, \tag{22}$$

which tends to zero as $|n| \to \infty$ if $0 \leqslant \tau < (\gamma - 1)(\gamma + 1)$, since by theorems 1 and 2 the series $\sum_2^\infty C_m e^{ms} \psi_m(\tau)$ then converges.

Hence taking $\delta < \frac{1}{2}$ and writing $\Delta_m = \max |\Delta(n, \tau)|$ on $|n| = m + \frac{1}{2}$ for positive integral m, a circular contour which passes outside all the small circles, then $\Delta_m \to 0$ as $m \to \infty$. But by the maximum modulus theorem, since $\Delta(n, \tau)$ is an integral function, $|\Delta(n, \tau)| < \Delta_m$ when $|n| < m$. Hence $\Delta(n, \tau)$ is identically zero for all $s < \sigma$, i.e. for $0 \leqslant \tau < (\gamma - 1)/(\gamma + 1)$, and we deduce

THEOREM 3. For $0 \leqslant \tau < (\gamma - 1)/(\gamma + 1)$ and all complex n,

$$\psi_n(\tau) = e^{ns}\left(1 + n \sum_{m=2}^\infty \frac{C_m e^{ms} \psi_m(\tau)}{n + m}\right); \tag{23}$$

and so, when $\Re(n) > 0$,

$$\psi_n(\tau) = n \int_{-\infty}^{s} e^{ns_1} L(\tau, s_1)\, ds_1, \tag{24}$$

where
$$L(\tau, s_1) = 1 + \sum_{m=2}^\infty C_m e^{ms_1} \psi_m(\tau). \tag{25}$$

---

† The $\psi_m(\tau)$ occurring in (22) are positive, as will be seen in § 6, lemma 4.

This theorem, which expresses $\psi_n(\tau)$ for any complex n in terms of the $\psi_m(\tau)$ with m a positive integer, is an important special case of a general result fundamental in the physical theory, as will be seen in part III. Meanwhile two corollaries are deduced:

COR. 1.
$$V(\tau) = 1 + \sum_{m=2}^{\infty} C_m e^{ms}\psi_m(\tau). \tag{26}$$

(Proof by letting $|n| \to \infty$ in (23) and using Theorem 2.)

COR. 2. The asymptotic series for $\psi_n(\tau)$, holding uniformly under the conditions of theorem 2, is
$$\psi_n(\tau) \sim e^{ns}\left[L(\tau, s_1) - \frac{1}{n}\frac{\partial L}{\partial s_1} + \frac{1}{n^2}\frac{\partial^2 L}{\partial s_1^2} - \dots\right]_{s_1=s}. \tag{27}$$

Proof. By (23), since
$$n/(n+m) = 1-(m/n)+\dots+(-m/n)^r+(-m)^{r+1}n^{-r}/(n+m)$$

and since
$$\partial^r L/\partial s_1^r = \sum_{m=1}^{\infty} m^r C_m e^{ms_1}\psi_m(\tau),$$

then
$$e^{-ns}\psi_n(\tau) = \left[L(\tau, s_1) - \frac{1}{n}\frac{\partial L}{\partial s_1} + \dots + \left(-\frac{1}{n}\right)^r \frac{\partial^r L}{\partial s_1^r}\right]_{s_1=s} + n^{-r}\sum_{m=2}^{\infty}\frac{(-m)^{r+1}}{n+m}C_m e^{ms}\psi_m(\tau). \tag{28}$$

The remainder is less in modulus than a constant times
$$|n|^{-r}\sum_{m=1}^{\infty} m^r e^{2m(\sigma_1-\sigma)} \tag{29}$$

when $s \leqslant \sigma_1 < \sigma$ and $|n+m| > \delta$ for all m. This remainder term satisfies the conditions for an asymptotic series.

4. ASYMPTOTIC FORMULAE FOR SUPERSONIC τ

For $(\gamma-1)/(\gamma+1) \leqslant \tau \leqslant 1$, $\psi_n(\tau)$ satisfies, by (3),
$$\frac{d^2\psi_n}{dt^2} + S(t)\frac{d\psi_n}{dt} + n^2\psi_n = 0. \tag{30}$$

Also
$$|V(\tau)| = (P/Q)^{\frac{1}{4}}, \quad d|V|/dt = -\tfrac{1}{2}S|V|. \tag{31}$$

Putting
$$\psi_n(\tau) = |V(\tau)|e^{int}X_n(\tau),$$

the equation for X_n is
$$\frac{d^2X_n}{dt^2} + 2in\frac{dX_n}{dt} = [\tfrac{1}{4}S^2(t) + \tfrac{1}{2}S'(t)]X_n. \tag{32}$$

If the solution of (32) is expanded in an asymptotic series
$$f(n)\left(a_0(t) + \frac{1}{n}a_1(t) + \frac{1}{n^2}a_2(t) + \dots\right), \tag{33}$$

the a_n's must satisfy
$$\left.\begin{aligned} a_0'(t) &= 0, \\ 2ia_{r+1}'(t) &= [\tfrac{1}{4}S^2(t) + \tfrac{1}{2}S'(t)]a_r(t) - a_r''(t). \end{aligned}\right\} \tag{34}$$

The foregoing reasoning holds also with $-i$ written for i throughout. It is deduced that any solution of (30) must have an asymptotic value of the form

$$|V(\tau)|\,(f(n)\,e^{int}+g(n)\,e^{-int})\left\{1+O\left(\frac{1}{|n|}\right)\right\}. \tag{35}$$

Since $\frac{1}{4}S^2(t)+\frac{1}{2}S'(t)$ is regular in the range $0<t<t_1=[\sqrt{\{(\gamma+1)/(\gamma-1)\}}-1]\,\frac{1}{2}\pi$, which (see (4)) corresponds to the range $(\gamma-1)/(\gamma+1)<\tau<1$, the O-term in (35) is uniform in any interval interior to this one. But one must look more precisely into conditions at the ends of the interval. Near $t=t_1$ (4) gives† that $1-\tau\asymp(t_1-t)^2$ so that $S(t)\asymp(1-\tau)^{-\frac{1}{2}}\asymp(t_1-t)^{-1}$ and $\frac{1}{4}S^2(t)+\frac{1}{2}S'(t)\asymp(t_1-t)^{-2}$. Integration of equations (34) then yields $a_r(t)\asymp(t_1-t)^{-r}$ for each r. Hence the O-term in (35) has the form $O(1/|n|(t_1-t))$ near $t=t_1$, or $O(1/|n|\sqrt{(1-\tau)})$. Near $t=0$ (4) gives that $\tau-(\gamma-1)/(\gamma+1)\asymp t^{\frac{2}{3}}$ and so $S(t)\asymp[\tau-(\gamma-1)/(\gamma+1)]^{-\frac{3}{2}}\asymp t^{-1}$. From this one deduces as before that $O(1/nt)=O[1/n(\tau-(\gamma-1)/(\gamma+1))^{\frac{3}{2}}]$ is the correct error term in (35) near $t=0$. Slightly altering (35) and inserting correct error terms then, in $(\gamma-1)/(\gamma+1)<\tau<1$,

$$\psi_n(\tau)=|V(\tau)|\,\{F(n)\cos nt+G(n)\sin nt\}\left\{1+O\left(\frac{1}{|n|\sqrt{(1-\tau)}}\right)\right.$$
$$\left.+O\left(\frac{1}{|n|\,(\tau-(\gamma-1)/(\gamma+1))^{\frac{3}{2}}}\right)\right\}. \tag{36}$$

The process by which $F(n)$ and $G(n)$ are found is rather elaborate. Two methods have been used: in the first the value of $\psi_n(1-R/n^2)$ is compared for large fixed R and $n\to\infty$ given by (36) and by the formula of Whittaker & Watson (1935), in the latter replacing the gamma functions by their asymptotic forms and the hypergeometric function of R/n^2 by Bessel functions to which they approximate, these in turn being then replaced by asymptotic forms; in the second method, which can be applied to asymptotic formulae for the fundamental solutions of any equation of mixed type,‡ the equation is transformed to one differing by a term of lower order from that resulting from the simplest possible equation of mixed type

$$\partial^2\psi/\partial x^2=x\partial^2\psi/\partial\theta^2,$$

of which the solution in Bessel functions of order $\pm\frac{1}{3}$ is known. In this latter method the asymptotic form for supersonic τ is deduced from the known form for subsonic τ. Both methods give the same results, which are different in different ranges of $\arg n$. Considerations of space make it necessary to omit the proofs and the results are stated as

THEOREM 4. When $|\arg n|\leqslant\pi-\delta$ and $(\gamma-1)/(\gamma+1)<\tau<1$ then, uniformly as $|n|\to\infty$,

$$\psi_n(\tau)=2\,|V(\tau)|\,e^{n\sigma}\left[\sin(nt+\tfrac{1}{4}\pi)+O\left(\frac{e^{t\,|\mathfrak{I}(n)|}}{|n|\sqrt{(1-\tau)}}\right)\right.$$
$$\left.+O\left(\frac{e^{t\,|\mathfrak{I}(n)|}}{|n|\,(\tau-(\gamma-1)/(\gamma+1))^{\frac{3}{2}}}\right)\right]; \tag{37}$$

---

† '$f\asymp g$' is used to mean '$f\sim Ag$ for some A'.

‡ A brilliant discussion of the general theory is given by R. E. Langer (1931).

When $|\arg(-n)| \leqslant \pi-\delta$ and $(\gamma-1)/(\gamma+1)<\tau<1$ then, uniformly as $|n| \to \infty$,

$$\psi_n(\tau) = |V(\tau)|\, e^{n\sigma}\Big[\sin(nt+\tfrac{1}{4}\pi) - \cot n\pi \cos(nt+\tfrac{1}{4}\pi) + O\left(\frac{e^{t|\mathfrak{I}(n)|}(1+|\cot n\pi|)}{|n|\sqrt{(1-\tau)}}\right) + O\left(\frac{e^{t|\mathfrak{I}(n)|}(1+|\cot n\pi|)}{|n|(\tau-(\gamma-1)/(\gamma+1))^{\frac{3}{2}}}\right)\Big]. \tag{38}$$

The two formulae are consistent in the region where they overlap since there $|\mathfrak{I}(n)|$ is large and so $\cot n\pi$ is effectively $-i \operatorname{sgn} \mathfrak{I}(n)$ and $\cos(nt+\frac{1}{4}\pi)$ is effectively $-i[\operatorname{sgn}\mathfrak{I}(n)]\sin(nt+\frac{1}{4}\pi)$. While in theorem 4 it is shown how error terms can be accurately specified the work will often be shortened (with slight loss of accuracy) elsewhere and in part III by use of the sign $\sim$ of asymptotic equality.

Theorems 2 and 4 give the asymptotic behaviour of $\psi_n(\tau)$ as $|n| \to \infty$ for each τ except $(\gamma-1)/(\gamma+1)$. This omission is remedied by

Theorem 5. When $|\arg n| \leqslant \pi-\delta$,

$$\psi_n\left(\frac{\gamma-1}{\gamma+1}\right) \sim k e^{n\sigma} n^{\frac{1}{6}}, \tag{39}$$

where $k = 2^{(2\gamma-1)/(2\gamma-2)}(\gamma+1)^{-(\gamma+2)/(6\gamma-6)}\pi^{\frac{1}{2}}3^{-\frac{5}{6}}[\Gamma(\frac{2}{3})]^{-1}$. When $|\arg(-n)| \leqslant \pi-\delta$, however,

$$\psi_n\left(\frac{\gamma-1}{\gamma+1}\right) \sim k e^{n\sigma}(-n)^{\frac{1}{6}}\frac{\sin(\pi n-\frac{1}{6}\pi)}{\sin \pi n}. \tag{40}$$

This is obtained by use of the Bessel functions of order $\pm\frac{1}{3}$. These also make it possible to get an asymptotic formula for $\psi_n(\tau)$ valid uniformly in any region $|n|\,|\tau-(\gamma-1)/(\gamma+1)|^{\frac{3}{2}} \leqslant$ constant. These asymptotic values are themselves Bessel functions of order $\pm\frac{1}{3}$, and the result can be used in exactly the region where theorems 2 and 4 fail. But as these results are not needed in future parts, further reference to them will be omitted. The change-over from e^{ns} to $2e^{n\sigma}\sin(nt+\frac{1}{4}\pi)$ in the asymptotic form, with $ke^{n\sigma}n^{\frac{1}{6}}$ as the intermediate value, is a general property of partial differential equations of mixed type.

5. THE SECOND SOLUTION WHEN n IS AN INTEGER

The equation for $\psi_n(\tau)$,

$$\Delta_n(\psi_n) \equiv PQ\frac{d^2\psi_n}{d\tau^2} + PQ_\tau\frac{d\psi_n}{d\tau} + n^2\psi_n = 0, \tag{41}$$

has $\psi_n(\tau)$ and $\psi_{-n}(\tau)$ as fundamental solution except when n is an integer other than ± 1. When $n=0$ the solutions are 1 and $\int Q^{-1}d\tau$. When n is an integer $m \geqslant 2$, the solutions are $\psi_m(\tau)$ and

$$\psi_m^*(\tau) = \lim_{n \to -m}\left(\psi_n(\tau) - \frac{{}^nC_m\,\psi_{-n}(\tau)}{n+m}\right). \tag{42}$$

For Δ_m operating on the expression in brackets gives

$$(m^2-n^2)\left[\psi_n(\tau)-\frac{nC_m\psi_{-n}(\tau)}{n+m}\right], \tag{43}$$

and as $n \to -m$ this tends to zero by theorem 1. (42) can also be written

$$\lim_{n\to -m}\left(\psi_n(\tau)-\frac{nC_m\psi_m(\tau)}{n+m}\right)-mC_m\frac{d\psi_m(\tau)}{dm}, \tag{44}$$

and for subsonic τ this is, by theorem 3,

$$\left[e^{-ms}\left(1+\left(\sum_0^{m-1}+\sum_{m+1}^{\infty}\right)m\frac{C_r e^{rs}\psi_r(\tau)}{m-r}\right)\right]$$
$$+\left[-mC_m s\psi_m(\tau)-mC_m e^{ms}\left(s+\sum_1^{\infty}\frac{sm(m+r)+r}{(m+r)^2}C_r e^{rs}\psi_r(\tau)\right)\right]. \tag{45}$$

As $m \to \infty$ it is easy to show that the terms in square brackets in (45) are asymptotic respectively to $e^{-ms}V(\tau)$ and to $(-sV(\tau)/\pi)\,e^{m(s-2\sigma)}$ so that, for $\tau<(\gamma-1)/(\gamma+1)$, $\psi_m^*(\tau) \sim e^{-ms}V(\tau)$.

For supersonic τ,

$$\psi_m^*(\tau) \sim \lim_{n\to -m}\Bigg[\,|\,V\,|\,e^{n\sigma}(\sin(nt+\tfrac{1}{4}\pi)-\cot n\pi\cos(nt+\tfrac{1}{4}\pi))$$
$$-\frac{e^{-2m\sigma}n}{2\pi m(n+m)}2\,|\,V\,|\,e^{-n\sigma}\cos(nt+\tfrac{1}{4}\pi)\Bigg]$$
$$=|\,V\,|\,e^{-m\sigma}\cos(mt+\tfrac{1}{4}\pi)-|\,V\,|\sin(mt+\tfrac{1}{4}\pi)\lim_{n\to -m}\left(\frac{e^{-n\sigma}+\dfrac{n}{m}e^{-(2m+n)\sigma}}{\pi(n+m)}\right)$$
$$\sim |\,V(\tau)\,|\,e^{-m\sigma}\left(\cos(mt+\tfrac{1}{4}\pi)-\frac{2\sigma}{\pi}\sin(mt+\tfrac{1}{4}\pi)\right). \tag{46}$$

Summing up in

THEOREM 6. When m is an integer $\geqslant 2$, a second fundamental solution of the equation for $\psi_m(\tau)$ is

$$\psi_m^*(\tau)=\lim_{n\to -m}(\psi_n(\tau)-nC_m\psi_{-n}(\tau)/(n+m)).$$

For $0<\tau<(\gamma-1)/(\gamma+1)$,

$$\psi_m^*(\tau)\sim e^{-ms}V(\tau) \quad \text{as} \quad m\to\infty;$$

for $(\gamma-1)/(\gamma+1)<\tau<1$,

$$\psi_m^*(\tau)\sim |\,V(\tau)\,|\,e^{-m\sigma}.(\cos(mt+\tfrac{1}{4}\pi)-(2\sigma/\pi)\sin(mt+\tfrac{1}{4}\pi)).$$

6. THE ZEROS OF $\psi_n(\tau)$

LEMMA 3. If m is an integer $\geqslant 2$, then for every $\tau>0$, $\psi_n(\tau)=0$ for some n with either $m\leqslant n\leqslant m+1$ or $-(m+1)<n<-m$.

Proof. Assume $\psi_n(\tau)\neq 0$ for $m\leqslant n\leqslant m+1$. Then $\psi_m(\tau)$ and $\psi_{m+1}(\tau)$ have the same sign. Hence (theorem 1) the residues at $-m$ and $-(m+1)$ have the same sign, so

ψ_n has opposite signs at a point just greater than $-(m+1)$ and one just less than $-m$: hence there is a zero in between, which proves the lemma.

LEMMA 4. For $n \geqslant 1$ and $0 < \tau \leqslant (\gamma-1)/(\gamma+1)$, then $\psi_n(\tau) > 0$.

Proof. If $v = \tau^{\frac{1}{2}}(1-\tau)^{-1/2(\gamma-1)}\psi_n(\tau)$, the equation for v can be written

$$\frac{d^2v}{d\tau^2} = v\left[\frac{(n^2-1)((\gamma-1)-(\gamma+1)\tau)}{4(\gamma-1)\tau^2(1-\tau)} + \frac{2\gamma-1}{4(\gamma-1)^2(1-\tau)^2}\right], \tag{47}$$

which under the conditions of the lemma shows that v and $d^2v/d\tau^2$ have the same sign. But $v = 0$ when $\tau = 0$ and, for small enough τ, $v > 0$: hence v curves upward from the start and so must continue to do so while $v^{-1}d^2v/d\tau^2$ is positive: this proves the lemma.

It is known that $\psi_{-1}(\tau) = \tau^{-\frac{1}{2}} + (2\gamma-2)^{-1}\psi_1(\tau) > 0$ for $0 < \tau \leqslant (\gamma-1)/(\gamma+1)$. Also $\psi_{-2+\delta}(\tau) \sim -2\delta^{-1}C_2\psi_2(\tau) < 0$ for small enough δ. Hence, when

$$0 < \tau \leqslant (\gamma-1)/(\gamma+1),$$

there is a zero of $\psi_n(\tau)$ between $n = -1$ and $n = -2$. Also by lemmas 3 and 4 combined there is one between every other pair of consecutive negative integers. But, by following $\log\psi_n(\tau)$ round a contour on which $|n|$ is large and $|n+m| > \delta$ for all positive integers m, it is seen by theorem 2 that one must return to the original value (since the possible error term $O(|n|^{-1}) < 2\pi$ for $|n|$ large enough). Hence the number of poles inside such a contour must equal the number of zeros. If it cuts the negative real axis once, between $-m$ and $-(m+1)$, there are exactly $(m-1)$ poles inside it, and at least $(m-1)$ zeros counting only one between each pair of consecutive negative integers and none between $-m$ and $-(m+1)$. Hence (i) there is exactly one zero between each pair of consecutive negative integers, (ii) there are no other zeros in the whole complex n-plane, (iii) however small δ is, the zero between $-m$ and $-(m+1)$ is within a distance δ of $-(m+1)$ if m is large enough. Summing up in

THEOREM 7. When $0 < \tau \leqslant (\gamma-1)/(\gamma+1)$, all the zeros of $\psi_n(\tau)$ as function of n in the complex plane are simple, and they can be arranged in a sequence $z_2, z_3, z_4, \ldots$, where, for each m, $-m < z_m < -(m-1)$, and $|z_m+m| \to 0$ as $m \to \infty$.

We find an asymptotic form for z_m+m. By theorem 2,

$$|\psi_n(\tau) - e^{ns}V(\tau) + mC_m\psi_m(\tau)/(n+m)| < Ae^{ns}/|n|$$

when $\tau \leqslant \tau_1 < (\gamma-1)/(\gamma+1)$ and $|n+m| = \frac{1}{2}$ (say), and hence also (by theorem 1 and the maximum modulus theorem) within $|n+m| = \frac{1}{2}$. Hence

$$0 = \psi_{z_m}(\tau) = e^{sz_m}V(\tau) - e^{-2\sigma m}e^{sm}V(\tau)(1+O(m^{-1}))/2\pi(z_m+m) + O(e^{-ms}/m).$$

Hence

$$z_m+m = (2\pi)^{-1}e^{(s-2\sigma)m-sz_m}(1+O(m^{-1})) = (2\pi)^{-1}e^{2(s-\sigma)m}(1+O(m^{-1})).$$

Calculate also the order of $(d\psi_n(\tau)/dn)_{n=z_m}$. In $|n+m| \leqslant \frac{1}{2}$

$$d\psi_n/dn = se^{ns}V(\tau) + mC_m\psi_m(\tau)/(n+m)^2 + O(se^{ns}|n|^{-1}),$$

and for $n = z_m$ this is asymptotic to $2\pi V(\tau)\, e^{(2\sigma-3s)m}$. Thus

THEOREM 8.
$$z_m + m \sim \frac{1}{2\pi} e^{2(s-\sigma)m}, \tag{48}$$

and
$$\left(\frac{d\psi_n(\tau)}{dn}\right)_{n=z_m} \sim 2\pi V(\tau)\, e^{(2\sigma-3s)m}, \tag{49}$$

uniformly in $0 < \tau \leqslant \tau_1 < (\gamma-1)/(\gamma+1)$.

Results on the zeros for supersonic τ are not needed: it is merely remarked that for large $|n|$ they are given approximately by the zeros of the trigonometrical functions in theorem 4, and so are both positive and negative.

7. APPENDIX

The author actually discovered the important theorem 3 by an elaborate process of inversion from an integral equation, which, though it is not used in subsequent parts, is of sufficient interest to state.

THEOREM 9. When $0 < \tau < (\gamma-1)/(\gamma+1)$ and $\Re(n) > 0$, then

$$\frac{d\psi_n}{ds} = n e^{ns} + \int_{-\infty}^{s} T(s_1) \cosh n(s-s_1) \frac{d\psi_n}{ds_1} ds_1. \tag{50}$$

The proof by differentiation that if ψ_n satisfies (50) then it satisfies (13), and that such a ψ_n has the correct form at $s = -\infty$, is easy, after which only a simple existence theorem for a solution of (50) is necessary to complete it. Discovery was by expansion of $\psi_n(\tau)$ in powers of e^s and examination of the coefficients.

REFERENCES

Langer, R. E. 1931 *Trans. Amer. Math. Soc.* **33**, 23.
Whittaker, E. T. & Watson, G. N. 1935 *Modern analysis*, § 14.53. Cambridge Univ. Press.

The hodograph transformation in trans-sonic flow. III. Flow round a body

By M. J. Lighthill

(*Communicated by S. Goldstein, F.R.S.—Received* 17 *March* 1947)

1. Introduction

As was remarked in part I, § 1, the hodograph transformation offers one of the most hopeful approaches to trans-sonic flow problems. But it is ill adapted for solving exactly the problem of flow past a contour of given shape. Boundary conditions more remote from this ideal one are necessary, chosen to give, past a contour approximating to the one desired, a flow exactly solving the equations of motion. Thus in part I (Symmetrical Channels) the velocity distribution along the axis was stipulated. In the problem of flow round a body, uniform and subsonic at infinity but possibly supersonic in certain regions, it is convenient to construct a flow such as will reduce to the incompressible flow round a body of approximately the same shape when the Mach number tends to zero. Some previous writers have sought to do this by expanding in series in different parts of the incompressible hodograph plane (at least four distinct expansions being necessary to cover the plane) and then modifying each series to allow for compressibility. While each modified series satisfied the equations of motion, they were not analytic continuations of each other, so their combination corresponded to no physical possibility.

These statements on previous writers' work are proved in the Appendix. In § 2 a solution valid over the whole subsonic region of the physical plane is given. This solution is given in terms of integrals in the physical plane for the incompressible flow and can therefore be used when only data of the most numerical kind are available concerning this flow (to which the solution reduces when the Mach number tends to zero). In § 4 it is shown how, when an analytic series (of a very general type) is available in the incompressible flow, the solution can be continued into the supersonic region. The solution contains an arbitrary function: so the different possible determinations of this function lead to an infinity of solutions of the compressible flow problem, all tending to the given incompressible flow as the Mach number tends to zero. It is shown that when circulation is absent all these solutions give a possible physical picture: the natural consequence is to take the simplest one, which particular solution is discussed in § 5. In § 6 it is seen that when circulation is present, however, all the solutions but one give a physical plane which does not close up behind the body. The single solution which gives a physically sensible result in this case is determined and its properties are investigated in § 6. The results of part II on the fundamental functions $\psi_n(\tau)$ are used throughout the work.

Mention must be made of the work of Bergman (1945), who treats the same problem. The present method however seems to us simpler and more general; in that of Bergman (which does not use the $\psi_n(\tau)$) the order of magnitude of functions involved is uncertain, with accompanying difficulties about convergence especially in the supersonic region; further it gives no practical method of treating flow with circulation. A recent paper by Tsien & Kuo (1946) is discussed in the Appendix.

As in part I the singularities in the hodograph transformation must be carefully investigated. Here one has incompressible theory as a guide. In the hodograph plane in incompressible flow round a body the potential and stream-function are (at least) two-valued functions—the hodograph plane may be said to be a Riemann surface of (at least) two sheets. When circulation is absent a branch-point where two values divide is the point corresponding to the point at infinity in the physical plane. When it is present, however, this branch-point corresponds to a finite point in the physical plane, while to the point at infinity corresponds a point (on one sheet only) which is another singularity of the potential and stream-function (the former suffering a fixed increase each time the point is encircled).

For compressible flow it may be expected (and will be proved) that all this will remain true in the subsonic region, since there branch-points must be isolated (it was proved in part I, § 3, that a *line* of branch-points must be a characteristic and hence supersonic). In the supersonic region two difficulties may arise. First a line of branch-points as in part I: but this appears to be absent in most problems of flow round a body. Secondly a 'limit line' where the streamlines turn back on themselves (occurring without any sign of a singularity in the hodograph plane). All possible forms of singularity in the hodograph transformation have been investigated by Craggs (unpublished): all the non-trivial ones are mentioned above. He shows that the limit lines must themselves be cusped, that the cusp is the point on them at which the speed is lowest but that even there it must exceed the sonic speed. The streamline through the cusp is regular, while all those on one side of it pass over the first branch of the limit line, turn back at the second, turn back again on reaching the first once more and then proceed regularly. Shen Yuan, in a London Ph.D. thesis, has found limit lines of this form occurring (his solutions for high and low speeds do not join up—see above—but each is locally possible): it appears that the solutions first reach physical impossibility when the cusped limit line penetrates from the inside the surface of the body. (At the Mach number for which this happens the shock-wave may be expected first to appear.) Discussion of the incidence of limit lines in the solutions proposed below is postponed.

2. DEDUCTION OF COMPRESSIBLE FROM INCOMPRESSIBLE FIELD OF FLOW

If an incompressible field of flow round a body has complex potential $w(z)$ being an analytic function outside the body (with possibly a real period, the circulation, as the body is encircled), and if $dw/dz = \zeta = qe^{-i\theta}$ is the complex velocity, and near a certain stagnation point (where $\zeta = 0$)

$$w = \sum_{n=0}^{\infty} c_n \zeta^n = \sum_{n=0}^{\infty} c_n q^n e^{-in\theta}, \tag{1}$$

and the velocity at infinity is taken as unity; under these circumstances several authors have taken for the corresponding compressible flow (with ψ_n as in equation (7) of part II)

$$\psi = \Im \sum_{n=0}^{\infty} c_n \psi_n(\tau) \,[\psi_n(\tau_0)]^{-1} e^{-in\theta}, \tag{2}$$

where $\tau = q^2/q_{\max}^2$ ($q_{\max}$ the 'maximum velocity', taken as unity in part I) and τ_0 is the value of τ at infinity. The object of the factor $[\psi_n(\tau_0)]^{-1}$ is to make (2) tend to the imaginary part of (1) as $q_{\max} \to \infty$, and to cause the singularity of (2) at $\tau = \tau_0$ to resemble that of (1) at $q = 1$.

This factor $[\psi_n(\tau_0)]^{-1}$ is, however, unsatisfactory: the results of using it are indicated in the Appendix. A general factor $f(n, \tau_0)$ is substituted for it, giving

$$\psi = \Im \sum_{n=0}^{\infty} c_n \psi_n(\tau) f(n, \tau_0)\, e^{-in\theta}. \tag{3}$$

f is assumed to satisfy the following conditions when $0 < \tau_0 < (\gamma - 1)/(\gamma + 1)$:

(i) $f(n, \tau_0)$ is analytic as a function of n in the whole complex plane except possibly at certain real poles (not non-positive integers) at each of which its residue is real.

(ii) If s_0 is the value of s (part II, equation (6)) at $\tau = \tau_0$, then there is a function $A(\tau_0)$ and a sequence of closed contours L_r, whose distance from the origin (which each encircles once) tends to infinity as $r \to \infty$ and whose distance from any pole of $f(n, \tau_0)$ or of $\psi_n(\tau)$ is always greater than $\delta > 0$, such that the maximum of

$$|\, f(n, \tau_0)\, e^{ns_0} - A(\tau_0) \,|$$

on L_r tends to zero as $r \to \infty$.

(iii) $f(n, \tau_0) \sim \tau_0^{-\frac{1}{2}n}$ as $\tau_0 \to 0$, uniformly for all n at a distance $\delta > 0$ from any pole of $f(n, \tau_0)$ for $\tau_0 < \delta$.

More roughly (ii) states that, for large n, $f(n, \tau_0) \sim A e^{-ns_0}$; since $\psi_n(\tau) \sim V e^{ns}$ this ensures parallel behaviour between (3) and (1) near $\tau = \tau_0$ and $q = 1$ respectively; (iii) states that (3) tends to the imaginary part of (1) as $q_{\max} \to \infty$.

The consequences of (3) will be investigated, in particular its continuation over the whole plane. It will be found that any $f(n, \tau_0)$ satisfying the above conditions gives a possible solution when circulation is absent: therefore the simplest value

$$f(n, \tau_0) = e^{-ns_0}$$

will be chosen in this case. When circulation is present, however, it will be found that only one $f(n, \tau_0)$ gives a possible solution (see § 6).

Two results are now proved (equations (6) and (7)) which reduce to theorem 3 (with Cor. 1) of part II when $f(n, \tau_0) = e^{-ns_0}$, and have completely analogous proofs. Consider as a function of n (with τ and τ_0 subsonic)

$$J_1(n, \tau, \tau_0) = \frac{1}{n}\left(\psi_n(\tau)\, f(n, \tau_0)\, e^{n(s_0 - s)} - f(0, \tau_0)\right). \tag{4}$$

By theorem 2 of part II and condition (ii) on f, the maximum modulus of J_1 on L_r tends to zero as $r \to \infty$. If the poles of $\psi_n(\tau) f(n, \tau_0)$ are at $n = p_1, p_2, \ldots$ and the residue of $n^{-1}\psi_n(\tau)\,f(n,\tau_0)$ at $n=p_m$ is r_m then by theorem 1 of part II and condition (i) on f all the p_m and r_m are real. Also either $r_m/\psi_{p_m}(\tau)$ or $r_m/\psi_{-p_m}(\tau)$ is independent of τ. For if p_m is a pole of $\psi_n(\tau)$ then $r_m = C_{-p_m}\psi_{-p_m}(\tau)\,f(p_m,\tau_0)$ by theorem 1 of part II: while, if it is a pole of $f(n,\tau_0)$ at which the latter has residue R, then $r_m = p_m^{-1}\psi_{p_m}(\tau)\,R$.

Consider now
$$J_2(n,\tau,\tau_0) = \sum_{m=1}^{\infty} \frac{r_m e^{p_m(s_0-s)}}{n-p_m}. \tag{5}$$

If $\sum\limits_{m=1}^{\infty} r_m e^{p_m(s_0-s)}$ converges absolutely, then J_2 is an analytic function of n except at poles $n=p_1,p_2,\ldots$; its principal part at each pole is that of J_1; and, if $|n|\to\infty$ in such a manner as to remain at distance $>\delta$ from each p_m then $J_2\to 0$. Hence J_1-J_2 is an integral function whose maximum modulus on L_r tends to zero as $r\to\infty$: therefore $J_1=J_2$. Hence
$$\psi_n(\tau)\,f(n,\tau_0) = f(0,\tau_0)\,e^{n(s-s_0)} + n\sum_{m=1}^{\infty} r_m \frac{e^{(n-p_m)(s-s_0)}}{n-p_m}, \tag{6}$$
and also, since
$$A(\tau_0)\,V(\tau) = \lim_{|n|\to\infty} \psi_n(\tau)\,f(n,\tau_0)\,e^{n(s_0-s)},$$
$$A(\tau_0)\,V(\tau) = f(0,\tau_0) + \sum_{m=1}^{\infty} r_m e^{p_m(s_0-s)}. \tag{7}$$

It is now shown how from (6) and (7) the continuation of (3) over the whole subsonic region can be found: here we proceed formally as the validity of the answer can be verified independently. Equation (3) when τ is subsonic can be written, using (6), as
$$\begin{aligned}\psi &= \Im\left[f(0,\tau_0)\sum_{n=0}^{\infty} c_n e^{n(s-s_0-i\theta)} + \sum_{m=1}^{\infty} r_m e^{-ip_m\theta} \sum_{n=0}^{\infty} nc_n \frac{e^{(n-p_m)(s-s_0-i\theta)}}{n-p_m}\right]\\ &= \Im\left[f(0,\tau_0)\,w(e^{s-s_0-i\theta}) + \sum_{m=1}^{\infty} r_m e^{-ip_m\theta}\left\{\int_{\zeta_0}^{e^{s-s_0-i\theta}} \sum_{n=1}^{\infty} nc_n \zeta^{n-p_m-1}\,d\zeta + \sum_{n=1}^{\infty} nc_n \frac{\zeta_0^{n-p_m}}{n-p_m}\right\}\right]\\ &= \Im\left[f(0,\tau_0)\,w(e^{s-s_0-i\theta}) + \sum_{m=1}^{\infty} r_m e^{-ip_m\theta}\left\{\int_{\zeta_0}^{e^{s-s_0-i\theta}} \zeta^{-p_m}\,dw(\zeta) + g_m\right\}\right].\end{aligned} \tag{8}$$

Now p_m depends on m and τ_0 only, since the poles of $\psi_n(\tau)$ as function of n are independent of τ. g_m therefore depends only on m, τ_0 and ζ_0. r_m is a multiple of $\psi_{p_m}(\tau)$ or $\psi_{-p_m}(\tau)$. Hence the series $\sum\limits_{1}^{\infty} g_m r_m e^{-ip_m\theta}$ is independently a solution of the equation of the motion: hence (8) without it, or
$$\psi = g\left[f(0,\tau_0)\,w(e^{s-s_0-i\theta}) + \sum_{m=1}^{\infty} r_m e^{-ip_m\theta}\int_{\zeta_0}^{e^{s-s_0-i\theta}} \zeta^{-p_m}\,dw(\zeta)\right], \tag{9}$$
is a solution of the equation of motion.

(9) is fundamental in this paper. It exists for all subsonic τ for which it converges: we will always choose $f(n,\tau_0)$ so that it converges for all subsonic τ. It can be shown by formal differentiation that (9) satisfies the equation of motion (1) of part II, using only that r_m is a multiple of $\psi_{\pm p_m}(\tau)$ and that (7) holds with A independent

of τ. This we regard as the real basis of (9). For example (9) is deduced from an equation (3) which implies that $f(n, \tau_0)$ is finite for positive integral n. However (9) will still be a solution if $f(n, \tau_0)$ has poles at the positive integers, i.e. if some of the p_m are positive integers. In fact f was not required to be finite for positive integral n either in conditions (i) to (iii) or in the proof of (6) and (7): hence the proof of (9) by formal differentiation holds. (Of course, when any $p_m \geqslant 1$, ζ_0 must be taken $\neq 0$ in (9) to secure convergence of the integrals.)

Now
$$\int_{\zeta_0}^{e^{s-s_0-i\theta}} \zeta^{-p_m}\, dw(\zeta) = \int_{\zeta_0}^{e^{s-s_0-i\theta}} \zeta^{-p_m+1}\, dz(\zeta), \tag{10}$$

since $dw/dz = \zeta$. $z(\zeta)$ is a regular function of ζ on the Riemann surface (referred to in § 1) which represents the hodograph plane in the incompressible flow. This surface is called R: it has at least two sheets, which divide when circulation is absent at the point corresponding to the point at infinity. (For under these circumstances $\zeta = 1 + O(|z|^{-2})$ as $|z| \to \infty$.) Now (if $z = z_0$ corresponds to $\zeta = \zeta_0$)

$$Y_m(z) = \int_{z_0}^{z} \zeta^{-p_m+1}\, dz \tag{11}$$

is a regular function of z in the whole z-plane[†] when circulation is absent (for the same reason). (When circulation k is present, then Y_m increases by $(1-p_m)\,k$ as the body is encircled once in the positive direction.) Since $z(\zeta)$ is regular on R and $Y_m(z)$ is regular in the whole z-plane,

$$Z_m(\zeta) = Y_m(z(\zeta)) \tag{12}$$

is regular on R.

But the integral in (9) can be written $Z_m(e^{s-s_0-i\theta})$. Hence (9) is one-valued, when circulation is absent, on the Riemann surface for (τ, θ) defined by the condition that $e^{s-s_0-i\theta}$ lies on R. This Riemann surface, which we call R^*, *is* the hodograph plane for the compressible flow. (So far we have defined its subsonic portion only, but we will give the name R^* to the whole surface as continued by methods given below, § 4, beyond the sonic line: the subsonic portion will be denoted henceforth by SR^*.) SR^* must have singularities corresponding to all those of R with $|\zeta| < e^{\sigma-s_0}$ (σ is the value of s on the sonic line; part II, equation (6)): in particular a branch-point at $\tau = \tau_0$, $\theta = 0$.

3. Passage to the physical plane

Write now $p_0 = 0$, $r_0 = f(0, \tau_0)$, so that (9) can be written as a sum from 0 to ∞ without being changed by more than a constant. Taking the imaginary part we have

$$\psi = \sum_{m=0}^{\infty} r_m \int q_1^{-p_m}(-\sin p_m(\theta-\theta_1)\, d\Phi_1 + \cos p_m(\theta-\theta_1)\, d\Psi_1). \tag{13}$$

[†] Outside the body; but the remark is true for *part* of the 'flow' continued inside the body. We are interested only in the region $|\zeta| < e^{\sigma-s_0}$: if all regions with $|\zeta| \geqslant e^{\sigma-s_0}$ (these include all the singularities of ζ) are joined by cuts to form a continuum the remark is true outside this continuum.

Here we have put $w = \Phi + i\Psi$ for the incompressible flow and q for the magnitude, θ for the direction, of the velocity (so that $\zeta = qe^{-i\theta}$); suffix unity refers to the variable of integration, the limits being from the point (Φ_0, Ψ_0) where $\zeta = \zeta_0$ to the point (Φ, Ψ); the τ implicit in r_m is defined by the equation $e^{s-s_0} = q$ (using the one-one relation between s, τ—part II, equation (6)—which holds in the subsonic range). Viewed in this way the relation $\zeta = e^{s-s_0-i\theta}$ is a *transformation* from the incompressible to the compressible flow plane: (13) then gives the transformed value of Ψ and we will find below (equation (20)) the transformed value of z. The reader should notice that θ is the same in both flows.

(13) is an advantageous form of solution compared with series forms like (3), quite apart from its extended range of validity, since it enables ψ to be computed even if data of only the most numerical kind are available concerning the incompressible flow. The lower limit of integration should be taken on the body (in the incompressible flow): for a point on the body in the compressible flow the corresponding incompressible point will be close to the body and (13) becomes an integral along the body (Ψ constant) plus a short integral with Φ constant.

A similar expression is derived for the co-ordinates of the physical plane for the compressible flow. If these are $\mathfrak{X}$, $\mathfrak{Y}$, and $\mathfrak{X} + i\mathfrak{Y} = \mathfrak{Z}$, then

$$\mathfrak{Z}_\theta = \frac{Qe^{i\theta}}{q_{\max}\tau^{\frac{1}{2}}}\left(\psi_\tau + \frac{i}{2\tau}\psi_\theta\right), \quad \mathfrak{Z}_\tau = \frac{Qe^{i\theta}}{q_{\max}\tau^{\frac{1}{2}}}\left(\frac{\psi_\theta}{PQ} + \frac{i}{2\tau}\psi_\tau\right), \tag{14}$$

as can be found by inverting the expressions for ψ_τ, ϕ_τ in terms of $\mathfrak{X}_\tau$, $\mathfrak{Y}_\tau$ and for ψ_θ, ϕ_θ in terms of $\mathfrak{X}_\theta$, $\mathfrak{Y}_\theta$ and using equations (1) and (18) of part I.

In future the velocity at infinity (in the compressible flow) is taken as unity; since it is $q_{\max}\tau_0^{\frac{1}{2}}$, this means that $q_{\max} = \tau_0^{-\frac{1}{2}}$. (13) and (14) then give for $\mathfrak{Z}_\theta$ (writing r'_m for $dr_m/d\tau$)

$$\begin{aligned}\mathfrak{Z}_\theta = Q(\tau_0/\tau)^{\frac{1}{2}}\, e^{i\theta}\Bigg\{ & \sum_{m=0}^{\infty} r'_m \int q_1^{-p_m}(-\sin p_m(\theta-\theta_1)\, d\Phi_1 + \cos p_m(\theta-\theta_1)\, d\Psi_1) \\ & + \sum_{m=0}^{\infty} r_m q^{-p_m}\frac{\partial \Psi}{\partial \tau} + \frac{i}{2\tau}\sum_{m=0}^{\infty} r_m p_m \int q_1^{-p_m}(-\sin p_m(\theta-\theta_1)\, d\Phi_1 - \cos p_m(\theta-\theta_1)\, d\Psi_1) \\ & + \frac{i}{2\tau}\sum_{m=0}^{\infty} r_m q^{-p_m}\frac{\partial \Psi}{\partial \theta}\Bigg\}. \end{aligned} \tag{15}$$

Since $q = e^{s-s_0}$, the coefficient of $\Psi_\tau + i\Psi_\theta/2\tau$ is, by (7) (with this new notation $r_0 = f(0, \tau_0)$, $p_0 = 0$), $A(\tau_0)\, V(\tau)$. Now use the fact that

$$\begin{aligned} & \frac{\partial}{\partial\theta}\left\{e^{i\theta}\int q_1^{-p_m}\left[\frac{e^{-ip_m(\theta-\theta_1)}}{2(p_m-1)}(d\Phi_1 + i\,d\Psi_1) + \frac{e^{ip_m(\theta-\theta_1)}}{2(p_m+1)}(d\Phi_1 - i\,d\Psi_1)\right]\right\} \\ & \quad = \int q_1^{-p_m}\left[-\frac{i}{2}e^{i\theta-ip_m(\theta-\theta_1)}(d\Phi_1 + i\,d\Psi_1) + \frac{i}{2}e^{i\theta+ip_m(\theta-\theta_1)}(d\Phi_1 - i\,d\Psi_1)\right] \\ & \qquad + e^{i\theta}q^{-p_m}\left(\frac{1}{2(p_m-1)}\frac{\partial(\Phi+i\Psi)}{\partial\theta} + \frac{1}{2(p_m+1)}\frac{\partial(\Phi-i\Psi)}{\partial\theta}\right), \end{aligned} \tag{16}$$

and a similar result with $d\Psi$ for $d\Phi$ and $-d\Phi$ for $d\Psi$, to deduce that

$$\begin{aligned}\mathfrak{Z} = Q(\tau_0/\tau)^{\frac{1}{2}}\Bigg[&\sum_{m=0}^{\infty} r'_m e^{i\theta}\int q_1^{-p_m}\left\{\frac{e^{-ip_m(\theta-\theta_1)}}{2(p_m-1)}(d\Phi_1+id\Psi_1)+\frac{e^{ip_m(\theta-\theta_1)}}{2(p_m+1)}(d\Phi_1-id\Psi_1)\right\}\\ &+\frac{i}{2\tau}\sum_{m=0}^{\infty} r_m p_m e^{i\theta}\int q_1^{-p_m}\left\{\frac{e^{-ip_m(\theta-\theta_1)}}{2(p_m-1)}(-i)\,(d\Phi_1+id\Psi_1)+\frac{e^{ip_m(\theta-\theta_1)}}{2(p_m+1)}i(d\Phi_1-id\Psi_1)\right\}\\ &+\int e^{i\theta}\left\{A(\tau_0)\,V(\tau)\left(\Psi_\tau+\frac{i}{2\tau}\Psi_0\right)-\sum_{m=0}^{\infty} r'_m q^{-p_m}\left(\frac{\Phi_\theta+i\Psi_\theta}{2(p_m-1)}+\frac{\Phi_\theta-i\Psi_\theta}{2(p_m+1)}\right)\right.\\ &\left.-\frac{i}{2\tau}\sum_{m=0}^{\infty} r_m p_m q^{-p_m}\left((-i)\,\frac{\Phi_\theta+i\Psi_\theta}{2(p_m-1)}+i\,\frac{\Phi_\theta-i\Psi_\theta}{2(p_m+1)}\right)\right\}d\theta\Bigg].\end{aligned} \tag{17}$$

Now
$$\Psi_\tau = \frac{\partial\Psi}{\partial\log q}\frac{ds}{d\tau} = \Phi_\theta\frac{ds}{d\tau}.$$

Also
$$\int(\Phi_\theta+i\Psi_\theta)\,e^{i\theta}\,d\theta = q\int q^{-1}e^{i\theta}\,d(\Phi+i\Psi) = q\int\zeta^{-1}\,dw = qz$$

(taking $z = 0$ at our lower limit of integration), while

$$\int(\Phi_\theta-i\Psi_\theta)\,e^{i\theta}\,d\theta = q^{-1}\int qe^{i\theta}\,d(\Phi-i\Psi) = q^{-1}\int\bar{\zeta}\,d\bar{w} = q^{-1}\int\overline{\zeta^2\,dz}.$$

Hence

$$\begin{aligned}\mathfrak{Z} = Q(\tau_0/\tau)^{\frac{1}{2}}\Bigg[&\sum_{m=0}^{\infty}\left(r'_m+\frac{r_m p_m}{2\tau}\right)\frac{e^{i(1-p_m)\theta}}{2(p_m-1)}\int\zeta^{1-p_m}\,dz\\ &+\sum_{m=0}^{\infty}\left(r'_m-\frac{r_m p_m}{2\tau}\right)\frac{e^{i(1+p_m)\theta}}{2(p_m+1)}\int\overline{\zeta^{1-p_m}\,dz}+A(\tau_0)\,V(\tau)\frac{ds}{d\tau}\frac{1}{2}\left(e^{s-s_0}z+e^{s_0-s}\int\overline{\zeta^2\,dz}\right)\\ &+\frac{i}{2\tau}A(\tau_0)\,V(\tau)\frac{1}{2i}\left(e^{s-s_0}z-e^{s_0-s}\int\overline{\zeta^2\,dz}\right)\\ &-\sum_{m=0}^{\infty} r'_m e^{p_m(s_0-s)}\left(\frac{1}{2(p_m-1)}e^{s-s_0}z+\frac{1}{2(p_m+1)}e^{s_0-s}\int\overline{\zeta^2\,dz}\right)\\ &-\frac{i}{2\tau}\sum_{m=0}^{\infty} r_m p_m e^{p_m(s_0-s)}\left(\frac{-i}{2(p_m-1)}e^{s-s_0}z+\frac{i}{2(p_m+1)}e^{s_0-s}\int\overline{\zeta^2\,dz}\right)\Bigg],\end{aligned} \tag{18}$$

plus an arbitrary function of τ. Collecting the coefficients of z and $\int\overline{\zeta^2\,dz}$, the former is $Q(\tau_0/\tau)^{\frac{1}{2}}$ times

$$\tfrac{1}{2}AV\frac{ds}{d\tau}e^{s-s_0}+\frac{1}{4\tau}AVe^{s-s_0}-\sum_{m=0}^{\infty}\left(r'_m+\frac{r_m p_m}{2\tau}\right)\frac{e^{(1-p_m)(s-s_0)}}{2(p_m-1)}. \tag{19}$$

Using (6) for $n = 1$, both by itself and differentiated with respect to τ, and using (7), (19) is reduced to $\tfrac{1}{2}f(1,\tau_0)\,(\psi'_1(\tau)+\tfrac{1}{2}\tau^{-1}\psi_1(\tau))$. Similarly the coefficient of $\int\overline{\zeta^2\,dz}$ in (18) is found to be $Q(\tau_0/\tau)^{\frac{1}{2}}$ times $-\tfrac{1}{2}f(-1,\tau_0)\,(\psi'_{-1}(\tau)+\tfrac{1}{2}\tau^{-1}\psi_{-1}(\tau))$. By a footnote to equation (7) in part II

$$\psi'_{-1}(\tau)+\tfrac{1}{2}\tau^{-1}\psi_{-1}(\tau) = (2\gamma-2)^{-1}\,(\psi'_1(\tau)+\tfrac{1}{2}\tau^{-1}\psi_1(\tau)) = \tau^{\frac{1}{2}}/(\gamma-1)\,Q.$$

Hence finally

$$\mathfrak{Z} = \tau_0^{\frac{1}{2}} f(1,\tau_0)\, z - \frac{\tau_0^{\frac{1}{2}} f(-1,\tau_0)}{2\gamma-2} \int \overline{\zeta^2 dz} + Q(\tau_0/\tau)^{\frac{1}{2}}$$
$$\times \left[\sum_{m=0}^{\infty} \left(r'_m + \frac{r_m p_m}{2\tau} \right) \frac{e^{i(1-p_m)\theta}}{2(p_m-1)} \int \zeta^{1-p_m} dz + \sum_{m=0}^{\infty} \left(r'_m - \frac{r_m p_m}{2\tau} \right) \frac{e^{i(1+p_m)\theta}}{2(p_m+1)} \int \overline{\zeta^{1-p_m} dz} \right]. \tag{20}$$

Equation (20) has been proved to within an arbitrary function of τ. But a parallel investigation shows that (20) satisfies the second of equations (14) as well as the first, so it must be true to within an arbitrary constant, which can be neglected. It is noticed at once that all the integrals in (20) are one-valued when circulation is absent: hence the flow closes up behind the body. The reader is reminded that the lower limit in the integrals of (20), as in all those left indefinite in this paper, is the point $\zeta = \zeta_0$, $z = 0$, which can be chosen arbitrarily in the incompressible plane.

It is now observed that in the above investigation it has been tacitly assumed that none of the p_m are ± 1. The assumption (i) on $f(n,\tau_0)$ (together with theorem 1 of part II) excludes the value -1 for a p_m, but it will be necessary to consider a $f(n,\tau_0)$ with a pole at $n = +1$. When this is so we take $p_1 = 1$. The changes that have to be made in the work of this section are as follows:

(i) In (16), on the left-hand side, replace $\dfrac{e^{i\theta - ip_1(\theta-\theta_1)}}{2(p_1-1)}$ by $-\frac{1}{2} i\theta e^{i\theta_1}$; on the right-hand side replace $e^{i\theta} q^{-p_1} \dfrac{1}{2(p_1-1)} \dfrac{\partial(\Phi + i\Psi)}{\partial\theta}$ by $-\frac{1}{2} i\theta e^{i\theta} q^{-1} \dfrac{\partial(\Phi+i\Psi)}{\partial\theta}$.

(ii) In (17) replace as in (i).

(iii) Use in addition to those integrals calculated between (17) and (18) the result

$$\begin{aligned} \int i\theta(\Phi_\theta + i\Psi_\theta)\, e^{i\theta} d\theta &= \log q \int (\Phi_\theta + i\Psi_\theta)\, e^{i\theta} d\theta - \int (\log q - i\theta)\,(\Phi_\theta + i\Psi_\theta)\, e^{i\theta} d\theta \\ &= qz \log q - q \int \log \zeta . \zeta^{-1} dw \\ &= qz \log q - q \int \log \zeta\, dz. \end{aligned}$$

(iv) In (18) replace $e^{i(1-p_1)\theta}/2(p_1-1)$ by $-\frac{1}{2} i\theta$. Replace $e^{s-s_0} z/2(p_1-1)$ by

$$-\frac{1}{2}\left((s-s_0)\, e^{s-s_0} z - e^{s-s_0} \int \log \zeta\, dz \right).$$

(v) The coefficient of z in (18) is now $Q(\tau_0/\tau)^{\frac{1}{2}}$ times

$$\tfrac{1}{2} AV \frac{ds}{d\tau} e^{s-s_0} + \frac{1}{4\tau} AV e^{s-s_0} - \sum_{m=2}^{\infty} \left(r'_m + \frac{r_m p_m}{2\tau} \right) \frac{e^{(1-p_m)(s-s_0)}}{2(p_m-1)} + \left(r'_1 + \frac{r_1}{2\tau} \right) \tfrac{1}{2}(s-s_0). \tag{21}$$

This is found, using (6) and (7), to be

$$\lim_{n\to 1} \left[\frac{1}{2} \left(\psi'_n(\tau)\, f(n,\tau_0) - \frac{n r'_1}{n-1} \right) + \frac{1}{4\tau} \left(\psi_n(\tau)\, f(n,\tau_0) - \frac{r_1}{n-1} \right) \right]. \tag{22}$$

(vi) There is in addition a term in $\int \log \zeta \, dz$ with coefficient $Q(\tau_0/\tau)^{\frac{1}{2}}$ times $-\frac{1}{2}(r_1' + \frac{1}{2}\tau^{-1} r_1)$.

The conclusion is that under these circumstances (20) must be rewritten

$$\begin{aligned}\mathfrak{Z} = Q(\tau_0/\tau)^{\frac{1}{2}} \Bigg[& z \lim_{n\to 1} \left[\frac{1}{2}\left(\psi_n'(\tau) f(n,\tau_0) - \frac{n r_1'}{n-1}\right) + \frac{1}{4\tau}\left(\psi_n(\tau) f(n,\tau_0) - \frac{r_1}{n-1}\right)\right] \\ & - \frac{\tau^{\frac{1}{2}} f(-1,\tau_0)}{2(\gamma-1)\,Q} \int \overline{\zeta^2 \, dz} - \tfrac{1}{2}(r_1' + \tfrac{1}{2}\tau^{-1} r_1)\left(\int \log \zeta \, dz + i\theta z\right) \\ & + \sum_{m=2}^{\infty}\left(r_m' + \frac{r_m p_m}{2\tau}\right)\frac{e^{i(1-p_m)\theta}}{2(p_m-1)}\int \zeta^{1-p_m}\, dz + \sum_{m=0}^{\infty}\left(r_m' - \frac{r_m p_m}{2\tau}\right)\frac{e^{i(1+p_m)\theta}}{2(p_m+1)}\int \overline{\zeta^{1-p_m}\, dz}\Bigg]. \end{aligned} \tag{23}$$

The term $\int \log \zeta \, dz$ is one-valued, like the other integrals involved, in the absence of circulation. When circulation k is present it increases by k as the body is encircled once in the positive direction.

4. Expansions in series

It is of some importance to ascertain the form taken by (9) when $w(\zeta)$ is given as a series $\Sigma d_n \zeta^n$, the range of n including positive, negative, integral and fractional terms in general (such a series will be spoken of henceforth as a 'generalized Laurent expansion'). When $e^{s-s_0-i\theta}$ is inside the domain where the series converges, (9) can be written

$$\psi = \Im \sum_{m=0}^{\infty} r_m e^{-ip_m\theta}\left(\int_{\zeta_0}^{\zeta_1} \zeta^{-p_m}\, dw(\zeta) + \int_{\zeta_1}^{e^{s-s_0-i\theta}} \zeta^{-p_m}\, \Sigma n d_n \zeta^{n-1}\, d\zeta\right), \tag{24}$$

if ζ_1 is some arbitrarily chosen point of the domain. Hence

$$\psi = \Im \sum_{m=0}^{\infty} r_m e^{-ip_m\theta}\left[\int_{\zeta_0}^{\zeta_1} \zeta^{-p_m}\, dw(\zeta) + \Sigma' \frac{n d_n}{n-p_m}\left(e^{(n-p_m)(s-s_0-i\theta)} - \zeta_1^{n-p_m}\right)\right], \tag{25}$$

where Σ' signifies that the term $n = p_m$ if it occurs is to be replaced by

$$n d_n (s - s_0 - i\theta - \log \zeta_1).$$

Equation (25) can be written as

$$\psi = \Im \sum_{m=0}^{\infty} r_m e^{-ip_m\theta}\left(e_m + \Sigma' \frac{n d_n}{n-p_m} e^{(n-p_m)(s-s_0-i\theta)}\right), \tag{26}$$

where e_m includes all the terms involving ζ_1, so that Σ' now signifies that the term $n = p_m$ is to be replaced by $n d_n (s - s_0 - i\theta)$. (26) in turn is

$$\Im \sum_{m=0}^{\infty} e_m r_m e^{-ip_m\theta} + \Im \Sigma d_n e^{-in\theta} n \sum_{m=0}^{\infty}{}' \frac{r_m e^{(n-p_m)(s-s_0)}}{n-p_m}, \tag{27}$$

with $\sum_{m=0}^{\infty}{}'$ signifying that the term $p_m = n$ if it occurs is to be replaced by $r_m(s - s_0 - i\theta)$. Clearly the first series in (27) must be independent of the particular choice of ζ_1, since the second series and ψ are equally so. The 'nth term' of the second series, when the term $p_m = n$ does not occur, is $d_n \psi_n(\tau) f(n, \tau_0)\, e^{-in\theta}$, by (6). When it does occur, say when $p_q = n$, we have

$$n \sum_{m=0}^{\infty}{}' \frac{r_m e^{(n-p_m)(s-s_0)}}{n-p_m} = \lim_{n\to p_q} \left(\psi_n(\tau) f(n, \tau_0) - n \frac{r_q e^{(n-p_q)(s-s_0)}}{n-p_q} \right) + p_q r_q (s - s_0 - i\theta)$$

$$= Q_q(\tau, \tau_0, \theta), \tag{28}$$

say. Hence

$$\psi = \Im \sum_{m=0}^{\infty} e_m r_m e^{-ip_m\theta} + \Im \sum_{n \neq p_q} d_n \psi_n(\tau) f(n, \tau_0)\, e^{-in\theta} + \Im \sum_{q=0}^{\infty} d_{p_q} Q_q(\tau, \tau_0, \theta)\, e^{-ip_q\theta}. \tag{29}$$

When none of the n's is a p_q the 'natural' series arising from $w = \Sigma d_n \zeta^n$ would be $\Im \Sigma d_n \psi_n(\tau) f(n, \tau_0)\, e^{-in\theta}$. But (29) shows that even in this case the true value of ψ contains the additional term $\Im \sum_{m=0}^{\infty} e_m r_m e^{-ip_m\theta}$. It is this term which has been neglected by previous writers, who have used the 'natural' series only (in each part of the plane).

If the series $w = \Sigma d_n \zeta^n$ is absolutely convergent in a region containing part of the line $|\zeta| = e^{\sigma - s_0}$ which corresponds to the sonic line, then the series

$$\sum_{n \neq p_q} d_n \psi_n(\tau) f(n, \tau_0)\, e^{-in\theta} \tag{30}$$

is majorized by $\Sigma |d_n| e^{n\sigma - ns_0 + o(n)}$ when τ is supersonic, by theorems 4 and 5 of part II and condition (ii) on f. Thus (30) converges for all supersonic τ (as well as some subsonic τ). The convergence of the other two series in (29) will depend on the choice of f, but it will be seen (§§ 5 and 6) that for the f actually chosen both are also convergent for all supersonic τ.

It is now seen that when a generalized Laurent expansion exists and is absolutely convergent in a region containing part of the line $|\zeta| = e^{\sigma - s_0}$, then the solution (9) can be continued into the supersonic region, and ψ is regular in the whole supersonic region. Thus 'branch lines' such as were found in part I cannot occur: the only singularities possible when ψ is regular in the hodograph plane are 'limit lines' (see § 1).

The region of validity of (29) will be the whole area which can be joined, to the part of SR^* corresponding to the region where $\Sigma d_n \zeta^n$ converges, by paths wholly supersonic. If there are two supersonic regions it may therefore be necessary to use two expansions.

5. THE CASE $f(n, \tau_0) = e^{-ns_0}$

We have seen that when circulation is absent any $f(n, \tau_0)$ satisfying conditions (i), (ii) and (iii) gives a possible solution, tending to the given incompressible solution when $q_{\max} \to \infty$. Hence in this case the simplest f satisfying these conditions should be taken, namely $f(n, \tau_0) = e^{-ns_0}$. The poles of $\psi_n(\tau) f(n, \tau_0)$ are then simply those of $\psi_n(\tau)$, i.e. $n = -2, -3, -4, \ldots$ (theorem 1 of part II) so $p_m = -m$ can be written if it is arranged that the term $m = 1$ shall be omitted by taking $r_1 = 0$. The residue r_m of $n^{-1}\psi_n(\tau) f(n, \tau_0)$ at $n = -m$ is $C_m \psi_m(\tau)\, e^{ms_0}$ by the same theorem. Hence (9) becomes

$$\psi = \mathfrak{J}\left[w(e^{s-s_0-i\theta}) + \sum_{m=2}^{\infty} C_m \psi_m(\tau)\, e^{m(s_0+i\theta)} \int_{\zeta_0}^{e^{s-s_0-i\theta}} \zeta^m\, dw(\zeta)\right]$$

$$= \mathfrak{J} \sum_{m=0}^{\infty} C_m \psi_m(\tau)\, e^{m(s_0+i\theta)} \int_{\zeta_0}^{e^{s-s_0-i\theta}} \zeta^m\, dw(\zeta), \tag{31}$$

with the convention $C_0 = 1$, $C_1 = 0$.

Since $C_m \sim (2\pi m)^{-1} e^{-2\sigma m}$ and $\psi_m \sim V e^{ms}$ (theorems 1 and 2 of part II) as $m \to \infty$, (31) will converge if the integral, $Z_m(e^{s-s_0-i\theta})$ in the notation of § 2, is $O(K^m)$ where $K < e^{2\sigma-s-s_0}$. But if l is a path joining ζ_0 and $e^{s-s_0-i\theta}$ (on the Riemann surface R) and K is the maximum of $|\zeta|$ thereon, then

$$|Z_m(e^{s-s_0-i\theta})| = \left|\int_l \zeta^{m+1}\, dz\right| \leqslant K^{m+1} l. \tag{32}$$

Hence (31) converges for all points (τ, θ) in SR^*, such that the point $e^{s-s_0-i\theta}$ can be joined to ζ_0 by a path in R on which $\max|\zeta| < e^{2\sigma-s-s_0}$. Two alternative *sufficient* conditions for this to be true for all points in SR are

(i) Every point in the incompressible field of flow can be reached by a line from the point at infinity such that the maximum velocity on the line is at one end or the other.

(ii) The subsonic region (in the compressible flow field) is connected.

For if (i) holds one can take $K \leqslant \max(|\zeta_0|, e^{\delta}, e^{s-s_0})$ for any $\delta > 0$. If $s < \sigma$ and $|\zeta_0| < e^{\sigma-s_0}$ all three can be made less than $e^{2\sigma-s-s_0}$. Alternatively if (ii) holds one can take $K < e^{\sigma-s_0}$ since any point in SR^* can be joined to ζ_0 by paths in SR^*. This again is less than $e^{2\sigma-s-s_0}$ if $s < \sigma$.

In practical cases it is believed that the whole of SR^* would satisfy the condition. In any case (31) converges in the part of SR^* which can be reached by paths in SR^* from the point corresponding to ζ_0.

The form of $\mathfrak{Z}$ in this case is deduced from (20). This becomes

$$\mathfrak{Z} = \tau_0^{\frac{1}{2}} e^{-s_0} z - \frac{\tau_0^{\frac{1}{2}} e^{s_0}}{2\gamma-2} \int \overline{\zeta^2\, dz} + Q(\tau_0/\tau)^{\frac{1}{2}}$$

$$\times \left[\sum_{m=2}^{\infty} C_m e^{ms_0} \left(\psi'_m(\tau) - \frac{m}{2\tau}\psi_m(\tau)\right) \frac{e^{i(1+m)\theta}}{-2(m+1)} \int \zeta^{m+1}\, dz\right.$$

$$\left. + \sum_{m=2}^{\infty} C_m e^{ms_0} \left(\psi'_m(\tau) + \frac{m}{2\tau}\psi_m(\tau)\right) \frac{e^{i(1-m)\theta}}{-2(m-1)} \int \overline{\zeta^{m+1}\, dz}\right] \tag{33}$$

$$= Q(\tau_0/\tau)^{\frac{1}{2}} \left[\sum_{-1}^{\infty} C_m \left(\psi'_m(\tau) - \frac{m}{2\tau}\psi_m(\tau)\right) \frac{e^{ms_0+i(m+1)\theta}}{-2(m+1)} \int \zeta^{m+1}\, dz\right.$$

$$\left. + \sum_{1}^{\infty} C_m \left(\psi'_m(\tau) + \frac{m}{2\tau}\psi_m(\tau)\right) \frac{e^{ms_0+i(1-m)\theta}}{-2(m-1)} \int \overline{\zeta^{m+1}\, dz}\right], \tag{34}$$

under the convention that though C_1 and C_{-1} are zero, $C_m/(m+1)$ for $m = -1$ is to be interpreted as $-(2\gamma-2)$ and $C_m/(m-1)$ for $m = 1$ as $(2\gamma-2)^{-1}$. (34) is simply a more elegant way of writing (33): in making the transformation we have used the footnote to equation (7) of part II.

It should be observed that when $\gamma = -1$ the case considered in the present section becomes the Kármán-Tsien approximation. For then (as was observed in part II) all the C_m $(m > 0)$ are zero. Hence (31) becomes $\psi = \Psi$ and (33) contains only the terms in z and $\int \overline{\zeta^2 dz}$: this agrees with the Kármán-Tsien theory and the coefficients of the last two expressions also agree, as does the relation $q = e^{s-s_0}$. The additional terms in (31) and (33)—involving the C_m—may be regarded as correction terms to the Kármán-Tsien theory.

With the $f(n, \tau_0)$ of this section equation (28) becomes

$$Q_q(\tau, \tau_0, \theta) = \lim_{n\to -q}\left(\psi_n(\tau)\,e^{-ns_0} - nC_q e^{qs_0}\psi_q(\tau)\frac{e^{(n+q)(s-s_0)}}{n+q}\right) - qC_q e^{qs_0}\psi_q(\tau)\,(s-s_0-i\theta)$$

$$= e^{qs_0}\left[\psi_q^*(\tau) + qC_q\left(\psi_q(\tau)\,(s_0+i\theta) + \frac{d}{dq}\psi_q(\tau)\right)\right], \tag{35}$$

using (42) or (44) of part II. Hence (29) becomes

$$\psi = \mathfrak{J}\sum_{n=0}^{\infty} e_m C_m \psi_m(\tau)\,e^{m(s_0+i\theta)} + \mathfrak{J}\sum_{n\neq -q} d_n \psi_n(\tau)\,e^{-n(s_0+i\theta)}$$

$$+\mathfrak{J}\sum_{q=2}^{\infty} d_{-q}\left[\psi_q^*(\tau)\,e^{q(s_0+i\theta)} + qC_q\frac{d}{dq}\left(\psi_q(\tau)\,e^{q(s_0+i\theta)}\right)\right]. \tag{36}$$

The last series has been written so as to evince that it satisfies the equation of motion.

Now the first series in (36) will converge everywhere if $e_m = O(K^m)$ where $K < e^{\sigma - s_0}$ (for $C_m \sim (2\pi m)^{-1}\,e^{-2\sigma m}$, $\psi_m = O(e^{\sigma m + o(m)})$ as $m \to \infty$). Since

$$|\,e_m\,| = \left|\int_{\zeta_0}^{\zeta_1}\zeta^m\,dw - \Sigma'\frac{nd_n}{n+m}\zeta_1^{n+m}\right| \leqslant \left|\int_{\zeta_0}^{\zeta_1}\zeta^m\,dw\right| + |\,\zeta_1\,|^m\,|\,\Sigma' nd_n\zeta_1^n|, \tag{37}$$

this condition holds if $|\,\zeta_1\,| < e^{\sigma-s_0}$ and there is a path from ζ_0 to ζ_1 with $|\,\zeta\,| < e^{\sigma-s_0}$ everywhere on it. Thus, if the region of convergence of $\Sigma d_n\zeta^n$ contains any such point, the first series in (36) converges. The convergence of the second series has already been dealt with in § 4, and that of the third depends on identical conditions with that of the second since the term in square brackets is shown by theorems 4, 5 and 6 of part II to be of essentially the same magnitude as $e^{q(s_0-\sigma)}$. The remarks of § 4 on continuation into the supersonic region therefore hold good under these circumstances.

6. Flow with circulation

The form of $f(n, \tau_0)$ necessary to make these solutions possible when there is a circulation, say k, round the body is now investigated. Both ψ and $\mathfrak{Z}$ must be one-valued functions. Now $\int \zeta^{1-p_m}\,dz$ increases by $(1-p_m)\,k$ if the body is encircled once in the positive direction, since for ζ near unity $\zeta^{1-p_m} = 1+(1-p_m)(\zeta-1)+O(|\zeta-1|^2)$. Hence, if the body is encircled starting from (τ, θ) and returning thereto, (9) increases by

$$-k\sum_{m=1}^{\infty}(1-p_m)\,r_m\sin p_m\theta. \tag{38}$$

This is identically zero only if, to each p_m except possibly $p_m = 1$, there is a $p_{m'}$ with $p_{m'} = -p_m$ and

$$r_{m'} = \frac{1-p_m}{1+p_m}r_m. \tag{39}$$

Since r_m is proportional to $\psi_{-p_m}(\tau)$ if p_m is a pole of ψ_n and to $\psi_{p_m}(\tau)$ if p_m is a pole of $f(n, \tau_0)$, one of p_m and $p_{m'}$ must be a pole of $\psi_n(\tau)$ and the other a pole of $f(n, \tau_0)$. Hence the poles of $f(n, \tau_0)$ must be at $n = 2, 3, 4, \ldots$, with $n = 1$ as the only other possibility. Now the residue of $n^{-1}\psi_n(\tau)\,f(n, \tau_0)$ at $n = -m$ (for $m \geqslant 2$) is

$$C_m\psi_m(\tau)\,f(-m, \tau_0).$$

Hence by (39) that at $n = m$ for $m \geqslant 2$ must be

$$\frac{1+m}{1-m}C_m\psi_m(\tau)\,f(-m, \tau_0), \tag{40}$$

so that the residue of $f(n, \tau_0)$ at $n = m$ is

$$m\frac{1+m}{1-m}C_m\,f(-m, \tau_0). \tag{41}$$

Now observe successively:

(i) $\psi_{-n}(\tau_0)$ satisfies (41) with 1 for $(1+m)/(1-m)$: so does any derivative of $\psi_{-n}(\tau_0)$ with respect to τ_0.

(ii) Correcting this it is found that $\psi_{-n}(\tau_0)/(1-n)$ satisfies (41). Its pole at $n = 1$ is allowable. It satisfies (i) of § 2 (the conditions on $f(n, \tau_0)$) but not (ii) since

$$\psi_{-n}(\tau_0)\,e^{ns_0}/(1-n) = O(|n|^{-1}) \quad \text{as } |n| \to \infty,$$

and not (iii) since

$$\psi_{-n}(\tau_0)/(1-n) \sim \tau_0^{-\frac{1}{2}n}/(1-n) \quad \text{as } \tau_0 \to 0.$$

(iii) Similarly $\psi'_{-n}(\tau_0)/(1-n)$ satisfies (41). It also satisfies (ii) as well as (i) of § 2 (with $A(\tau_0) = V(\tau_0)\,ds_0/d\tau_0$): while as $\tau_0 \to 0$ it is asymptotic to $-\frac{1}{2}n\tau_0^{-\frac{1}{2}n-1}/(1-n)$.

(iv) Hence $[\psi_{-n}(\tau_0)+f(\tau_0)\,\psi'_{-n}(\tau_0)]/(1-n)$ satisfies (41) and (i), (ii) of § 2 for any $f(\tau_0)$. It satisfies (iii) if and only if $f(\tau_0) \sim 2\tau_0$ as $\tau_0 \to 0$.

Taking then $f(n, \tau_0) = [\psi_{-n}(\tau_0)+f(\tau_0)\,\psi'_{-n}(\tau_0)]/(1-n)$ where $f(\tau_0) \sim 2\tau_0$ as $\tau_0 \to 0$, we must now impose the condition that $\mathfrak{Z}$ be one-valued. $\mathfrak{Z}$ is given by (23) since $f(n, \tau_0)$ has a pole at $n = 1$. The period of (23), as the body is encircled once in the positive direction, is

$$\begin{aligned} Q(\tau_0/\tau)^{\frac{1}{2}}\,k\Bigg\{-\frac{\tau^{\frac{1}{2}}}{(\gamma-1)\,Q}f(-1, \tau_0)+\sum_{m=2}^{\infty}\Bigg[\left(r'_m+\frac{r_m p_m}{2\tau}\right)\frac{e^{i(1-p_m)\theta}}{-2} \\ +\left(r'_m-\frac{r_m p_m}{2\tau}\right)\frac{e^{i(1+p_m)\theta}}{2}\,\frac{1-p_m}{1+p_m}\Bigg]-\frac{1}{2}\left(r'_1+\frac{r_1}{2\tau}\right)\Bigg\}. \end{aligned} \tag{42}$$

The $\sum_{m=2}^{\infty}$ in (42) vanishes by virtue of (39). It is deduced that the flow closes up if and only if

$$r_1' + \frac{r_1}{2\tau} + \frac{2\tau^{\frac{1}{2}}}{(\gamma-1)\,Q}\, f(-1, \tau_0) = 0. \tag{43}$$

(It should be noticed that if a value of $f(n, \tau_0)$ had been taken without a pole at $n = 1$, the condition would be $f(-1, \tau_0) = 0$, which is incompatible with the requirement that $f(n, \tau_0) \sim \tau_0^{-\frac{1}{2}n}$ as $\tau_0 \to 0$.)

Now $f(-1, \tau_0) = \frac{1}{2}(\psi_1(\tau_0) + f(\tau_0)\,\psi_1'(\tau_0))$; and r_1, the residue of $n^{-1}\psi_n(\tau)\,f(n, \tau_0)$ at $n = 1$, is $-\psi_1(\tau)\,(\psi_{-1}(\tau_0) + f(\tau_0)\,\psi_{-1}'(\tau_0))$. Hence (43) becomes

$$\psi_{-1}(\tau_0) + f(\tau_0)\,\psi_{-1}'(\tau_0) = \frac{1}{2(\gamma-1)}\,(\psi_1(\tau_0) + f(\tau_0)\,\psi_1'(\tau_0)), \tag{44}$$

(the terms in τ cancelling out). By the footnote to equation (7) in part II, (44) will be equivalent to $\tau_0^{-\frac{1}{2}} + f(\tau_0)\,d(\tau_0^{-\frac{1}{2}})/d\tau_0 = 0$, i.e. to $f(\tau_0) = 2\tau_0$. It is observed that this value satisfies the condition $f(\tau_0) \sim 2\tau_0$ as $\tau_0 \to 0$ that was imposed on $f(\tau_0)$.

Hence, when circulation is present, in order to make the flow close up behind the body, we should take

$$f(n, \tau_0) = \frac{\psi_{-n}(\tau_0) + 2\tau_0\,\psi_{-n}'(\tau_0)}{1-n}. \tag{45}$$

The expressions for ψ and $\mathfrak{z}$ with this value of $f(n, \tau_0)$ are now obtained. The poles of $\psi_n(\tau)\,f(n, \tau_0)$ are:

(i) At $n = -m$ $(m = 2, 3, 4, \ldots)$. Here the residue to $n^{-1}\psi_n(\tau)\,f(n, \tau_0)$ is

$$C_m\,\psi_m(\tau)\,[\psi_m(\tau_0) + 2\tau_0\,\psi_m'(\tau_0)]/(1+m).$$

(ii) At $n = m$ $(m = 2, 3, 4, \ldots)$. Here the residue of $n^{-1}\psi_n(\tau)\,f(n, \tau_0)$ is

$$C_m\,\psi_m(\tau)\,[\psi_m(\tau_0) + 2\tau_0\,\psi_m'(\tau_0)]/(1-m).$$

(iii) At $n = 1$. Here the residue is $-\psi_1(\tau)\,(\psi_{-1}(\tau_0) + 2\tau_0\,\psi_{-1}'(\tau_0))$.

Hence (9) becomes

$$\begin{aligned}\psi = \mathfrak{J}\Big\{ & w - \psi_1(\tau)\,[\psi_{-1}(\tau_0) + 2\tau_0\,\psi_{-1}'(\tau_0)]\,e^{-i\theta}z \\ & + \sum_{m=2}^{\infty} C_m\,\psi_m(\tau)\,[\psi_m(\tau_0) + 2\tau_0\,\psi_m'(\tau_0)]\left[\frac{e^{im\theta}}{m+1}\int \zeta^{m+1}\,dz - \frac{e^{-im\theta}}{m-1}\int \zeta^{-m+1}\,dz\right]\Big\}.\end{aligned} \tag{46}$$

It is observed that, if for $2\tau_0$ some $f(\tau_0)$ which did not asymptote to $2\tau_0$ as $\tau_0 \to 0$ were substituted, ψ would not tend to its imcompressible value as $q_{\max} \to \infty$. (The series $\sum_{m=2}^{\infty}$ in (46) tends to 0, but the second term would not do so under the circumstances contemplated, since $\psi_1(\tau) \sim \tau^{\frac{1}{2}}$, $\psi_{-1}(\tau_0) \sim \tau_0^{-\frac{1}{2}}$.)

To find what (23) becomes we need

$$\begin{aligned} Q(\tau_0/\tau)^{\frac{1}{2}} \lim_{n\to 1}\Bigg[& \frac{1}{2}\left\{\psi_n'(\tau)\,\frac{\psi_{-n}(\tau_0) + 2\tau_0\,\psi_{-n}'(\tau_0)}{1-n} + \frac{n\psi_1'(\tau)}{n-1}\,(\psi_{-1}(\tau_0) + 2\tau_0\,\psi_{-1}'(\tau_0))\right\} \\ & + \frac{1}{4\tau}\left\{\psi_n(\tau)\,\frac{\psi_{-n}(\tau_0) + 2\tau_0\,\psi_{-n}'(\tau_0)}{1-n} + \frac{\psi_1(\tau)}{n-1}\,(\psi_{-1}(\tau_0) + 2\tau_0\,\psi_{-1}'(\tau_0))\right\}\Bigg]. \end{aligned} \tag{47}$$

An investigation (too long to be inserted here), based on the hypergeometric series for $\psi_n(\tau)$, gives (47) in a form adapted for computation as

$$F(\tau,\tau_0) = 1+\frac{1}{2\gamma}(1-(1-\tau_0)^{\gamma/(\gamma-1)})+\frac{\tau_0(1-\tau_0)^{1/(\gamma-1)}}{\gamma-1}$$
$$\times\left[\tfrac{1}{2}\log\frac{\tau_0}{\tau}-1+\left(1+\frac{1}{2\gamma}\right)\int_0^{\tau_0}\frac{(1-x)^{-\gamma/(\gamma-1)}-1}{x}dx+\frac{1}{2\gamma}\int_0^{\tau}\frac{(1-x)^{-\gamma/(\gamma-1)}-1}{x}dx\right]. \tag{48}$$

Professor Goldstein has shown the author how the same result may be obtained from the differential equation for $\psi_n(\tau)$. Equation (23) now becomes

$$\mathfrak{z} = F(\tau,\tau_0)\,z+\frac{\tau_0(1-\tau_0)^{1/(\gamma-1)}}{\gamma-1}\Bigg[\int\log\zeta\,dz+i\theta z$$
$$-\frac{1}{2}\int\overline{\zeta^2dz}-\frac{\tau+(\gamma-1)(1-(1-\tau)^{-1/(\gamma-1)})}{2\gamma\tau}\bar{z}e^{2i\theta}\Bigg]+Q(\tau_0/\tau)^{\frac{1}{2}}\sum_{m=2}^{\infty}C_m(\psi_m(\tau_0)+2\tau_0\psi_m'(\tau_0))$$
$$\times\left\{\left(\psi_m'(\tau)-\frac{m}{2\tau}\psi_m(\tau)\right)\frac{e^{i(m+1)\theta}}{2(m+1)}\left(-\int\frac{\zeta^{m+1}}{m+1}dz+\int\overline{\frac{\zeta^{1-m}}{1-m}dz}\right)\right.$$
$$\left.+\left(\psi_m'(\tau)+\frac{m}{2\tau}\psi_m(\tau)\right)\frac{e^{i(1-m)\theta}}{2(1-m)}\left(-\int\frac{\zeta^{1-m}}{1-m}dz+\int\overline{\frac{\zeta^{m+1}}{m+1}dz}\right)\right\}. \tag{49}$$

Equation (49) has been arranged so as to make it apparent that $\mathfrak{z}$ is a one-valued function.

The convergence of the series in (46) and (49) must now be investigated. The similar investigation in § 5 is followed closely. Clearly each will converge if both

$$\int_{\zeta_0}^{e^{s-s_0-i\theta}}\zeta^{-m}\,dz \quad\text{and}\quad \int_{\zeta_0}^{e^{s-s_0-i\theta}}\zeta^{m}\,dz \tag{50}$$

are $O(K^m)$ as $m\to\infty$, where $K<e^{2\sigma-s-s_0}$, i.e. if a path in R joining ζ_0 to $e^{s-s_0-i\theta}$ exists with $e^{-(2\sigma-s-s_0)}<|\zeta|<e^{2\sigma-s-s_0}$ on it. If ζ_0 is suitably chosen this will be true for all points in SR^* under condition (i) of § 5. For then

$$\min(|\zeta_0|,\, e^{-\delta},\, e^{s-s_0})<|\zeta|<\max(|\zeta_0|,\, e^{\delta},\, e^{s-s_0})$$

on some such path, so if $e^{-(\sigma-s_0)}<|\zeta_0|<e^{\sigma-s_0}$ the above condition holds.

The form of the results of § 4 when (45) holds can similarly be investigated and results similar to those of § 5 found. For brevity's sake they are omitted, remarking only that even a simple series for w like (3) has a compressible counterpart involving the $Q_q(\tau,\tau_0,\theta)$ of (28) and hence terms like $\psi_n^*(\tau_0)$.

To find the magnitude of the circulation an expression is needed for ϕ. Using equations (18) of part I it is possible to show that the ϕ corresponding to the ψ of (9) is

$$\phi = \Re\left[f(0,\tau_0)\,w(e^{s-s_0-i\theta})+Q(\tau)\sum_{m=1}^{\infty}r_m'\frac{e^{-ip_m\theta}}{p_m}\int_{\zeta_0}^{e^{s-s_0-i\theta}}\zeta^{-p_m}\,dw(\zeta)\right]. \tag{51}$$

Hence the circulation is easily deduced to be $kf(0,\tau_0)$ which in this case is simply k.

Since, on a simple linear perturbation theory, the quantity

$$\frac{\text{circulation}}{\text{(velocity at infinity) (aerofoil chord)}} \tag{52}$$

is found to vary as $(1-m^2)^{-\frac{1}{2}}$, the above result indicates that the aerofoil given by the formulae of this paper will contract as the main stream Mach number increases. This fact alone need not be disturbing, as the flows past similar figures are similar.

If the circulation in the incompressible flow has been chosen to satisfy the Joukowski condition of zero velocity at a corner (the trailing edge), this will continue to be satisfied in the compressible flow. For stagnation-points must correspond: and the corner must correspond to a corner in the compressible flow (with the same angle in fact), since near any stagnation-point the right-hand side of equation (49) can be written as a linear function of z plus terms of smaller order than the distance from the stagnation-point (the effects of those terms in (49) whose appearance seems to contradict this statement actually cancel one another out). Similarly at a cusp in the incompressible flow plane at which the velocity is finite $\mathfrak{z}$ is a linear function of z and $\bar{z}$ plus terms of smaller order, so that a cusp appears also in the compressible flow plane and the velocity is also finite. Thus both types of Joukowski condition are preserved by the transformation.

7. CONCLUDING REMARKS

A very general solution has been given of the problem of finding a subsonic flow round a body which reduces, when the Mach number becomes zero, to a given incompressible flow. Since this solution is valid everywhere the error made by some writers of using series in different parts of the plane which are not analytic continuations of one another is avoided. The only functions needed in this solution are a few auxiliary ones and the $\psi_m(\tau)$ and $\psi'_m(\tau)$ for positive integral m. Tables of all these (the latter for $m = 1, 2, \ldots, 15$) will be published shortly. In the series in equations (31), (34), (46) and (49) the mth term is of order M^{2m} (M the main stream Mach number) as $M \to 0$. If each is terminated at the mth term the result will be true to this order. Every case of our general solution is valid when circulation is absent, so the simplest has been singled out in § 5. When circulation is present one solution was found to the problem in § 6, which made it appear likely that it is the only solution.[†] If it was desired to treat the same body with and without circulation it would of course be advisable to use the method of § 6 for both problems.

For a partially supersonic flow, however, this solution is not nearly so complete. Where the subsonic solution requires only the velocity field near the body to calculate its integrals, some sort of series expansion is needed in the supersonic region before it is possible to proceed. More precisely a 'generalized Laurent expansion' in the incompressible flow of w in terms of ζ is needed. Such a one might be obtained for flow past a circle, an ellipse, a Rankine oval, a symmetrical Joukowski aerofoil, a polygon. For a general aerofoil it would be very difficult to obtain. Further, the results are more complicated than in the subsonic region and need the use of additional functions to those mentioned above. Finally there is always the hidden danger of limit lines (see § 1) occurring. It is hoped to get over some of these difficulties in the future but it is believed that others may prove inherent. A serious difficulty is the complexity of theorem 4 of part II (the asymptotic formula for $\psi_n(\tau)$ with τ supersonic) compared with theorem 2 (τ subsonic).

[†] Except, of course, those obtainable by replacing the w therein by any function $w(z, \tau_0)$ tending to the original $w(z)$ as $\tau_0 \to 0$.

APPENDIX

Here the case $f(n, \tau_0) = [\psi_n(\tau_0)]^{-1}$ which is of historical interest is briefly considered. By theorems 1 and 7 of part II the poles of $\psi_n(\tau)/\psi_n(\tau_0)$ as function of n are the points z_m ($m = 2, 3, \ldots$), where $\psi_{z_m}(\tau_0) = 0$ and $-m < z_m < -(m-1)$. The residue of $n^{-1}\psi_n(\tau)/\psi_n(\tau_0)$ at $n = z_m$ is

$$r_m = \frac{\psi_{z_m}(\tau)}{z_m[d\psi_n(\tau_0)/dn]_{n=z_m}}. \tag{53}$$

The results of §§ 2 to 4 hold with this value for r_m and z_m for p_m. The series involved can be shown to converge by the results of theorem 8. Now if $z = 0$ is a stagnation-point (so that $\zeta_0 = 0$), equation (9) corresponds to equation (2) since all the g_m in (8) are then zero. But if there is an expansion $w = \Sigma d_n \zeta^n$ anywhere else in the plane (it may be assumed none of the n's is a z_m), the continuation of (2)—via (9)—is given by (29), which becomes

$$\psi = \Im \sum_{m=0}^{\infty} e_m \frac{\psi_{z_m}(\tau)\, e^{-iz_m\theta}}{z_m[d\psi_n(\tau_0)/dn]_{n=z_m}} + \Im\, \Sigma d_n \frac{\psi_n(\tau)}{\psi_n(\tau_0)} e^{-in\theta}. \tag{54}$$

Some authors have used the latter series only. The difference vanishes when $\tau = \tau_0$ (often the boundary between regions of convergence of different series) since $\psi_{z_m}(\tau) = 0$ when $\tau = \tau_0$: this fact has encouraged belief in the validity of the process. That the difference can become quite large, however (even on approximate theories), is an easy deduction from theorem 8. In no simple example do all the e_m vanish: indeed it is doubtful whether this is theoretically possible.

As a practical method (used correctly) this particular form of $f(n, \tau_0)$ is obviously unsatisfactory owing to the complexity of the r_m.

In a paper entitled 'Two-dimensional irrotational mixed subsonic and supersonic flow of a compressible fluid and the upper critical Mach number' (Tsien & Kuo 1946), however, this form of $f(n, \tau_0)$ is used. They take the series (2) near some stagnation-point and give methods of continuing it past (i) a branch-point of degree two, (ii) a logarithmic singularity. These consist in assuming a series for ψ on the other side of the singularity and determining the coefficients by the condition that ψ and

$\partial\psi/\partial\tau$ are continuous at the transition line. The results obtained are naturally complicated. They 'simplify' them by replacing all series $\Sigma c_n \psi_n(\tau)$ by

$$\Sigma c_n \psi_n^{(as)}(\tau) + \Sigma c_n(\psi_n(\tau) - \psi_n^{(as)}(\tau))$$

where $\psi_n^{(as)}$ is the appropriate asymptotic form of ψ_n. The first series can be written simply. The second converges more rapidly by a factor n^{-1} (but not when τ is near $(\gamma-1)/(\gamma+1)$). This factor is not a great improvement; but the second series should be small for τ near τ_0, and for $\tau \ll (\gamma-1)/(\gamma+1)$. However, the authors propose using it near $\tau = (\gamma-1)/(\gamma+1)$, in particular for values just supersonic where it is valueless.

The authors do not state that it is necessary to continue more than once round a branch-point, i.e. that even for a body symmetrical about two axes the 'natural' series cannot be taken near both stagnation-points. In their worked example (flow past an elliptic cylinder, for which a Laurent series of the type considered in § 4 holds) they adopt a different procedure from their theoretical one, using the 'natural' series for large τ and making a drastic approximation for the small τ for which the series does not converge. The work is still very complicated and conditions in the physical plane are not worked out. Contrary to a statement in their introduction, the method must fail when circulation is present as the results of § 6 prove.

The paper includes valuable tables and an interesting approximation to the conditions for appearance of a limit line.

REFERENCES

Bergman, S. 1945 *N.A.C.A. Tech. Note*, no. 972.
Tsien, Hsue-Shue & Kuo, Yung-Huai 1946 *N.A.C.A. Tech. Note*, no. 995.

The surface impedance of superconductors and normal metals at high frequencies

I. Resistance of superconducting tin and mercury at 1200 Mcyc./sec.

By A. B. Pippard, *Fellow of Clare College, Cambridge, Royal Society Mond Laboratory*

(*Communicated by Sir Lawrence Bragg, F.R.S.—Received* 1 *April* 1947)

This paper is the first in a series in which the behaviour of the electrical impedance of metals at low temperatures and very high frequencies will be considered from experimental and theoretical standpoints. The technique of resonator measurements at 1200 Mcyc./sec. is described in detail, and experimental curves are given showing the variation with temperature of the r.f. resistivities of superconducting tin and mercury. In contrast to the behaviour of superconductors in static fields, a finite resistance is present at all temperatures, tending as the absolute zero is approached to a very low value, which is probably zero for mercury but not for tin. The experimental results are in good agreement with London's measurements on tin by a different method. The latter's observation, that the r.f. resistance of normal tin above the transition point is much greater than that predicted from the classical skin-effect theory, is confirmed, and a similar, though less marked, effect is found also for mercury.

Introduction

In a series of measurements on the heat generated when a tin ellipsoid was placed in a high-frequency alternating magnetic field, London (1940) was able to show that at a frequency of 1500 Mcyc./sec. there was not a complete absence of resistance in the superconducting state. As the temperature was lowered through the transition point (3·71° K) there was a rapid fall of resistance, but not to zero as occurs in d.c. measurements. With further lowering of temperature the resistance continued to fall, apparently tending towards zero at the absolute zero of temperature. The experiments described in the present paper were designed to employ some of the recent advances in radio technique, arising directly from the wartime development of Radar, in order to obtain more accurate data than was possible at the time of London's work. A detailed investigation has been carried out at frequencies around 1200 Mcyc./sec., corresponding to a free-space wave-length of 25 cm., of the resistance of tin and mercury in the superconducting state. These two materials are the most interesting at present, since they have been more extensively studied than any other superconductors, on account of their convenient transition temperatures for use with liquid helium.

Description of apparatus

(*a*) *Method*

The measurement of resistance is carried out by determining the frequency band width of a resonator, in which the main conductors are made of the metal under investigation. The resonator is excited by means of an oscillator the frequency of which may be varied, and the amplitude of the excitation is measured by extracting from the resonator a proportion of the energy, which is then rectified to give a d.c. reading on a galvanometer. With this arrangement a measurable galvanometer deflexion is obtained only when the frequency of the oscillator is near the natural frequency, ω_0, of the resonator. The frequency band width is defined in the usual way as the difference $\Delta\omega$, between those two frequencies, $\omega_0 \pm \frac{1}{2}\Delta\omega$, at which the energy of excitation, i.e. the square of the field strength in the resonator, is equal to one-half the maximum excitation, which occurs at the natural frequency ω_0. With this definition, the quotient $\omega_0/\Delta\omega$ is the selectivity, Q, of the resonator. A discussion of the factors which determine the value of Q will be postponed, but roughly speaking it may be said to be inversely proportional to the total resistance of the resonator circuit.

(*b*) *Resonator*

The design of the resonator is unconventional from the point of view of normal engineering practice, being dictated by a number of considerations peculiar to this particular problem. Owing to the extremely small resistance of the superconducting metal, it is essential to use a resonator which would have a very low selectivity at room temperature, since otherwise the band width at low temperatures would become too narrow for accurate measurements to be made. On account of the great difference between the resistance in the superconducting and normal states it is desirable to be able to alter the coupling between the resonator and the external circuits during an experiment, in order to keep the excitation at resonance roughly constant in going from one temperature to another. Finally, since extremely pure materials must be used (of which details will be given later), it would be inadvisable to have any metallic contacts between the specimen and the rest of the resonator, which might lead to contamination. These various requirements are met by the design shown diagrammatically in figure 1. The specimen A is in the form of a narrow loop of wire attached to a distrene rod, and may be considered to be a section of twin transmission line, open-circuited at the bottom and short-circuited at the top, so that it resonates when it is approximately a quarter wave-length long, with the node and antinode of current at the bottom and top respectively. It is surrounded by a sheath B which serves the dual function of eliminating power loss by radiation and of excluding liquid helium from the resonator. Two coaxial transmission lines CC', terminating in identical loops DD' at opposite ends of a diameter, couple the resonator to the oscillator and detector. The whole resonator is mounted in a Dewar vessel which may be filled with liquid helium; the german silver tube E, through which the specimen is inserted, is open to the helium vapour above the liquid level, so that there is always sufficient vapour inside the resonator to ensure thermal contact between the specimen and the liquid bath. The distrene specimen-holder is mounted on a rod which comes out of the Dewar vessel through a vacuum-tight rubber washer, so that the height and orientation of the specimen, and hence the coupling to the external circuits, may be varied at will during an experiment.

(c) *Specimens*

In a number of experiments with tin specimens, wires of diameter between 0·07 and 2 mm. were used. The thicker wires were made by casting tin into thin-walled glass tubes, which were afterwards cracked and removed piecemeal. The bare wires were then annealed *in vacuo* for several hours at about 200° C and were mounted on the distrene specimen-holders as shown in figure 1, one or more spacers of distrene being used to maintain rigidity and constancy of separation. The thinner wires were too weak to be self-supporting, and were therefore cast into thin-walled capillary tubes of fused silica, which had been previously bent into the required U-shape, and which served to give the specimens rigidity. It was found that glass was unsuitable for this purpose, since the power losses in glass proved to be very much greater than the losses due to resistance in the specimen. Even silica and distrene, as will be seen later, are none too good from this point of view, although they are among the best known dielectrics, with power factors as small as 10^{-4}.

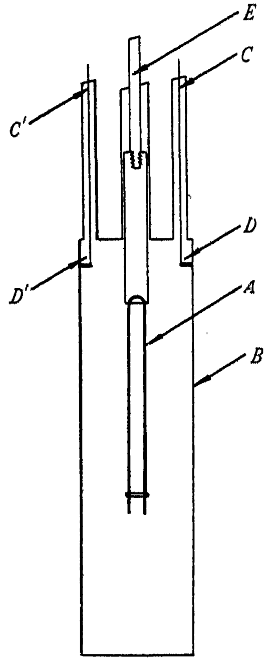

FIGURE 1. Diagram of resonator.

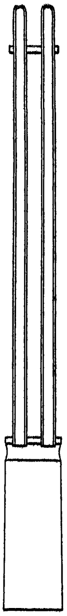

FIGURE 2. Mercury specimen.

The mercury specimens of all diameters were necessarily enclosed in tubes, and silica was again used. The large contraction of mercury on freezing makes it difficult to freeze a simple bent tube without rupturing the thread, so a slight modification of the design was introduced, as shown in figure 2. The straight silica tubes were slightly tapered to allow longitudinal motion of the mercury during freezing, and were sealed by means of distrene cement into the specimen-holder, through which a hole was drilled transversely to connect the two limbs. After filling with mercury, the ends of the transverse hole were sealed with cement.

(*d*) *Oscillator*

The oscillator was a commercial article, designed and constructed by the General Electric Co., in which a special triode (CV 90) is mounted directly in a coaxial cavity of variable length, so that frequencies between 1100 and 1250 Mcyc./sec. may be generated. A fine frequency control, which took the form of a 6 B.A. brass screw projecting into the cavity, enabled the frequency to be adjusted within very fine limits. In a series of tests made with a differential wavemeter which will be described later, it was found that successive settings of the screw were reproducible within $\frac{1}{4}^\circ$ of revolution, and that the backlash could be reduced to well below this limit. At the setting of the fine control at which this test was made, $\frac{1}{4}^\circ$ of revolution of the screw corresponded to a frequency change of 2 parts in 10^7, i.e. 240 cyc./sec. The filament and high-tension (240 V) supplies were from batteries, so that there was no danger of short-period voltage ripple with the resulting frequency modulation. When the oscillator had been running for about 2 hr. it settled down to a very constant frequency drift rate of about 60 cyc./sec./min., which was not fast enough to disturb the measurements.

Power from the oscillator was fed through a long piece of flexible coaxial cable to the input coupling loop of the resonator, the connexion being made through a plug and socket (designed and supplied by G.E.C.) at the top of the Dewar flask. The cable produced an attenuation of 25 db., so that even if total reflexion occurred at the resonator end of the cable, the power reflected back into the oscillator would amount to only 10^{-5} of the outgoing power. In this way, the behaviour of the oscillator was rendered effectively independent of the impedance presented by the resonator, and there was no danger that the resonator would pull the frequency of the oscillator or cause any change in its power output.

(*e*) *Detector*

The output coupling loop of the resonator was connected through a similar plug and socket and a length of cable, attenuating 12 db., to a coaxial cavity in which was mounted a crystal rectifier, and the rectified current was passed through a sensitive galvanometer. For r.f. power inputs into the rectifier up to 1 μW, the rectified current was accurately proportional to the power, and was equal to about $\frac{1}{2}\,\mu\mathrm{A}/\mu\mathrm{W}$. Most of the measurements were carried out with a galvanometer current of 0·07 μA at the peak of the resonance curve, corresponding to 0·14 μW input into the detector, or about 2 μW output from the resonator (allowing for the cable attenuation). Under these conditions the maximum rate of power dissipation in the resonator was only a few microwatts, which was found to produce no observable heating of the specimen, even at temperatures just below the transition point, where a rise in temperature of 0·001° C would have been appreciable, owing to the extremely rapid variation of resistance with temperature. Similarly, the magnetic field of the current was never sufficient to cause any noticeable disturbance of the sharpness of the transition, since it did not exceed 0·2 gauss at the transition point and was usually less. As the temperature was lowered, the field increased as a result of the higher selectivity of the resonator, but at no point was it more than a very small fraction of the critical field.

(*f*) *Wavemeters*

Two wavemeters were used in the experiment, a direct wavemeter for measuring ω_0 with an accuracy of about 0·1 %, and a differential wavemeter for calibrating the fine tuning control of the oscillator. The direct wavemeter consisted of a coaxial cavity of variable length, as described by Shawe & Burrell (1947), but since the accurate measurement of the band width of a resonator whose Q is 10^5 involves the accurate determination of a frequency change of one part in 10^5, it is not practicable to use a direct wavemeter for calibrating the oscillator. Instead, the heterodyne principle was used to obtain the differential frequency calibration. The crystal detector described in the last paragraph was fitted with two r.f. input leads, and provision was also made for supplying a lower frequency oscillation to the crystal, so that in all there were three different frequencies fed into the detector: (1) the output of the 1200 Mcyc./sec. oscillator which was to be calibrated, (2) the output of a similar oscillator whose frequency was kept constant, (3) a relatively strong signal (about 1 V) at 100 kcyc./sec. The rectified output was amplified and passed into headphones; as the fine tuning control of oscillator (1) was turned, a number of settings were observed at which an audio-frequency note was heard, which by careful adjustment could be brought to a frequency below the audible limit. This note may be considered as being due to the beating of a harmonic of oscillator (3) with the difference tone of oscillators (1) and (2), so that by recording those settings, of which about fifty were observable, where the frequency fell below the audible limit, a series of calibration points was obtained at equal intervals of 100 kcyc./sec., the accuracy of setting being at least as good as 0·2 % of the difference between two successive points.

(*g*) *Measuring technique*

The necessary measurements to obtain a value of Q at any given temperature were very straightforward, and occupied only a few minutes, so that it was possible with a single filling of liquid helium to measure at twenty or more different temperatures between 4·2° and 1·7° K, the lowest temperature attainable with the small-capacity vacuum pump employed. The temperature of the helium bath was varied in the usual way by controlling the vapour pressure, which was used as a measure of the temperature; the values throughout this paper have been calculated from the Leiden 1932 scale (Keesom 1932). At each temperature the coupling between the specimen and the external circuits was adjusted until a suitable fraction of the power was transmitted at resonance. This fraction, t^2, the square of the voltage transmission coefficient, was measured by recording: (*a*) the galvanometer reading at resonance, and (*b*) the galvanometer reading with the oscillator and detector cables connected directly, leaving the resonator out of circuit. The reading (*b*) gives a measure of the power incident on the resonator, and the ratio of (*a*) to (*b*) defines

t^2, which is always less than unity. With the resonator connected back into circuit, readings were then taken of the settings of the fine-tuning control at which the power transmission was one-half of the peak value. The difference of these readings, reduced to a frequency difference $\Delta\omega$ by means of the differential frequency calibration, gave the value of the band width. In most of the experiments, the diameter of the specimen was arranged so that the band width when the metal was in the normal state lay between 200 and 1000 kcyc./sec., corresponding to Q values of a few thousand. Such specimens in the superconducting state attained Q values of several hundred thousand, the highest recorded being $5 \cdot 7 \times 10^5$ for a tin wire of diameter 1·2 mm. With such high selectivities it was most important to keep the helium pressure very constant during a band-width determination, since a variation of only 0·1 mm. Hg produced a noticeable change in the dielectric constant of the vapour, and hence in the resonant frequency. It was also found necessary to tie the two limbs of the specimen firmly together with distrene spacers, since a rough calculation showed that a variation in spacing of only 1 μ would cause the resonant frequency to change by an amount comparable to the band width. Neglect of this precaution led to serious errors in some of the preliminary experiments, since minute vibrations of the specimen produced an apparent broadening of the resonant peak.

The theory of resonance in lumped L.C. circuits shows that Q, as defined above, is equal to $\omega L/R$, where L is the inductance and R the resistance of the circuit. In a similar manner the Q of a transmission line or cavity resonator may be equated to an equivalent inductance (representing the stored energy for a given value of the current flowing on the conductors) divided by the effective resistance (representing the rate of dissipation of power). If the only source of power dissipation were the resistive losses in the conductors, the value of $\Delta\omega$ would be directly proportional to the r.f. skin resistivity of the material, which is the quantity to be measured. In fact, however, there are a number of other sources of power loss, which may be regarded as resistances in series with the resistance of the conductors, and which would limit Q to a finite value even if the conductors were to be perfect. It has already been pointed out that radiation losses were eliminated by surrounding the specimen with a cylindrical sheath, but this in its turn becomes a source of power loss, since currents are induced on its inside surface. These currents, however, are small, and the area of the surface is large, so that the current density is very small; by lining the cavity with (superconducting) lead foil the sheath loss can be made entirely negligible ($< 1\,\%$ of the lowest specimen loss). The presence of dielectrics in the cavity can hardly be avoided for the tin specimens, much less for mercury, and the losses so introduced are by no means unimportant. Indeed, even with the minimum amounts of such good dielectrics as distrene and silica, the dielectric losses are comparable with, or even greater than, the conductor loss at the lowest temperatures. The elimination of this source of error will be discussed in detail later.

Finally, the very act of coupling the resonator to external circuits introduces extraneous power losses, which may, however, be allowed for with considerable accuracy, owing to a particularly elegant property of the type of resonator used here.

It follows from a very general analysis of the transmission line or cavity resonator (though not for the L.C. circuit except in special circumstances) that if the input and output loops are equally coupled to the resonant element, i.e. if the system is symmetrical, the selectivity Q and the voltage transmission coefficient t as defined above are related by the linear equation $Q/Q_0+t=1$, in which Q_0 is the ideal Q of the system for $t=0$, that is, uninfluenced by the coupling loops. It is Q_0 which is required in the experiment, since this depends only on the conductor and dielectric losses in the resonator itself.

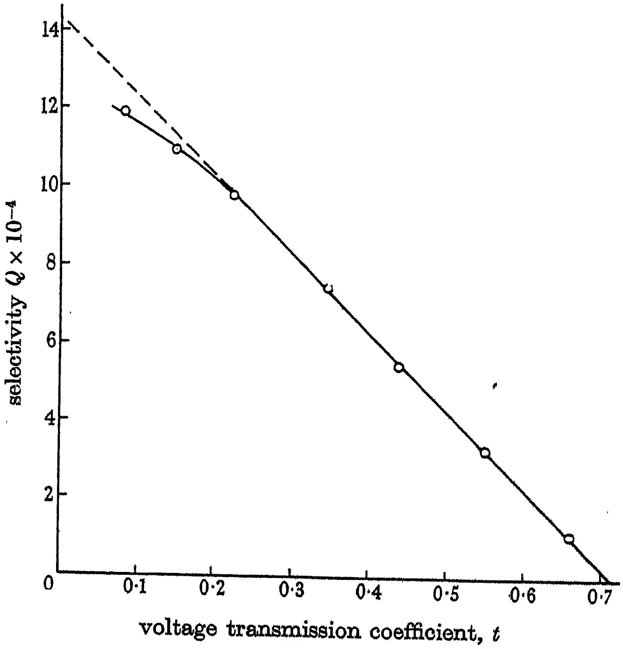

FIGURE 3. Relation between Q and t.

In view of the importance of this relation, experiments were performed to check its validity. For a large cylindrical copper resonator, operating in the H_{01} mode, and coupled at opposite ends of a diameter by means of loops whose projection into the cavity could be varied, the linear relation held accurately over the whole range of measurement, from $t=0·03$ to $t=1·00$. For the resonator of figure 1 departures from the law were observed, which fortunately were of such a nature as not to cause any serious trouble. As can be seen from figure 3, which was taken with a superconducting tin specimen at a temperature of 2·1° K, there are two departures from the simple law stated above. First, the curve cuts the t-axis at a value 0·71, not unity as expected. The reason for this is that there is appreciable attenuation in the coaxial lines connecting the resonator to the top of the Dewar flask, so that the measured transmission coefficient is the product of t and the attenuation factor of the lines. This does not invalidate the law, but merely introduces a constant scaling factor into the abscissae, since the attenuation factor does not vary appreciably over the temperature range used. The second departure, viz. the sudden breakdown of the linear relation below $t = 0{\cdot}2$, is due to direct coupling between the loops, even in the absence of a specimen. It may be shown that there is no linear term in the effect produced by direct coupling, so that extrapolation of the straight portion of the curve to $t = 0$ will give the correct value of Q_0. The curve shown in figure 3 gives an exaggerated idea of the importance of the effect, since it was taken at a frequency, avoided in all future measurements, at which for some unexplained reason the direct coupling between the loops exhibited a sharp maximum. At other frequencies, no departures from the straight line were observed for values of t above 0·1.

Whenever absolute values of the skin resistivity of a specimen were required, Q_0 was estimated by measuring Q for various values of t, and extrapolating to zero. For most of the work, however, only relative values of the resistivity at different temperatures were required, and for these a less elaborate technique was possible. By arranging the coupling at each temperature so that a constant value of t (usually 0·15) was maintained, the measured value of Q bore always a constant relation to Q_0; for instance in the case quoted, if 0·15 is the measured value of t, the real value is $0{\cdot}15/0{\cdot}71$, i.e. 0·21, and Q/Q_0 is always equal to $1 - 0{\cdot}21$ or 0·79. In the tables and curves to be given below, the resistivity at any temperature will be expressed as a fraction or percentage of the resistivity of the normal metal just above the transition point, and the factor 0·79 will disappear.

It is not feasible, in view of the difficulty of computing the geometrical factors involved in a resonator of the present design, to make an accurate estimate of R_n directly from the corresponding value of Q_0. It is also inadmissible to use the simple theory of the skin effect to calculate R_n from the measured d.c. conductivity, since, as was observed by London (1940) there is a pronounced discrepancy between the value so calculated and that actually observed. An experimental and theoretical treatment of this effect, which will be presented in a later paper, has established beyond doubt the correctness of London's hypothesis that it is due to the long mean free path of the conduction electrons, and reasons will be given for supposing that tin at the temperature of liquid nitrogen and mercury at the temperature of liquid hydrogen exhibit no anomalous behaviour. It is therefore permissible to calculate the skin resistivities of tin and mercury at these temperatures from the values of conductivity given in the tables (Onnes & Tuyn 1929), and hence to estimate the resistivities at the transition point from measurements of the change of Q_0 of a specimen in cooling from the higher temperature to the transition temperature, since Q_0 is inversely proportional to the resistivity.

(*h*) *Errors*

Every attempt was made to eliminate systematic errors from the determinations, such as would have been produced by incomplete decoupling of the oscillator from the resonator, reflexions in the transmission lines, frequency modulation of the oscillator, etc. The 100 kcyc./sec. oscillator which was used as a standard in the differential wavemeter was periodically checked against a crystal oscillator. As a result of these precautions, it is unlikely that there are any systematic errors exceeding 1 %. Repeated measurements of the same quantity showed that for Q values up to 10,000 the probable error of a single determination of the band width was less than 1 %; for the higher Q values the accuracy decreased, being about 5 % for values above 200,000, although under particularly favourable conditions (see e.g. figure 3) highly consistent results were obtained.

RESULTS

(a) *Tin*

The data for tin given in this section have been derived by combining the results of measurements on six specimens, whose characteristics are set out in table 1. Two samples of tin were used, Hilger H.S. 10,000 and Johnson Matthey number 12,966, both of great purity, but nevertheless exhibiting small differences in behaviour. Direct current measurements on the resistance show that on cooling from 0° C to 4·2° K the Hilger sample increases in conductivity by a factor 1600, while the corresponding factor for the Johnson Matthey sample is 5000. The superconducting transition point is slightly different also for the two samples, being 3·705° K for the former and 3·712° K for the latter. If, however, a constant increment of 0·007° K be added to all temperature readings for the Hilger specimens, the shapes of the r.f. resistivity curves are found to be in close agreement for all specimens.* Seventy reliable points were used in constructing the curve shown in figure 4, the main deviation of a single point from the curve in any region being not greater than 1·5 % of the mean value. To avoid obscuring the diagram only the measured values for Sn 7 are shown. Table 2 gives values of $100R/R_n$ as a function of temperature, interpolated from the original graph of figure 4.

Apart from the general shape of the curve, which is in good agreement with London's experimental values, in spite of the difference in frequency (1500 instead of 1200 Mcyc./sec.), there are two points of more particular interest, viz. the initial slope of the transition and the limiting value of R/R_n at very low temperatures. Examination of the first point is made difficult by the inevitable rounding off of the transition even for d.c. measurements. Consequently it is not possible to decide with any certainty whether the initial slope in an ideal specimen would be vertical or inclined at a finite angle to the vertical. It is to be expected on general grounds that the gradient will not be quite vertical, especially if the theory of London (1940)

* Between 3·71 and 3·56° K the curve for Sn 12 departs from the mean curve by, at most, 5 % of the normal resistivity R_n, but is in close agreement below this temperature. Sn 11, which was a very thin wire, also departs, though not so much, in this temperature range. It is possible that these departures are due to freezing in of the earth's magnetic field, with the consequent production of small inclusions of normal metal on the surface. This effect was not observed with Sn 7, whose superconductivity could be destroyed and restored by switching on and off a magnetic field, without producing any permanent change in the resistivity. The divergent points of Sn 11 and 12 have been neglected in combining the results for all specimens.

be accepted, since this would imply the transition at the critical temperature of a finite proportion of the electrons into the superconducting state, which would be at variance with the characteristic behaviour of transitions of the second order. This argument derives some support from the experimental results of figure 5, which

TABLE 1. DESCRIPTION OF TIN SPECIMENS

specimen	material	diameter (mm.)	resonant frequency (Mcyc./sec.)	method of construction
Sn 6	Hilger	0·57	1227	silica tube with distrene spacers
Sn 7	Hilger	0·20	1219	
Sn 9	Johnson Matthey	0·50	1192	
Sn 11	Johnson Matthey	0·07	1195	silica tube with silica spacers and supports
Sn 12	Johnson Matthey	0·72	1197	open wires with distrene spacers
Sn 14	Johnson Matthey	0·40	1165	

TABLE 2. SMOOTHED VALUES OF RESISTIVITY OF TIN

temperature (° K)	$100R/R_n$	temperature (° K)	$100R/R_n$	temperature (° K)	$100R/R_n$
3·712	100	3·6725	30	3·366	3·0
3·709	90	3·6515	20	3·150	2·0
3·7055	80	3·633	15	2·91	1·5
3·702	70	3·598	10	2·67	1·2
3·6975	60	3·573	8	2·37	1·0
3·6915	50	3·530	6	2·12	0·9
3·6835	40	3·455	4	1·83	0·8

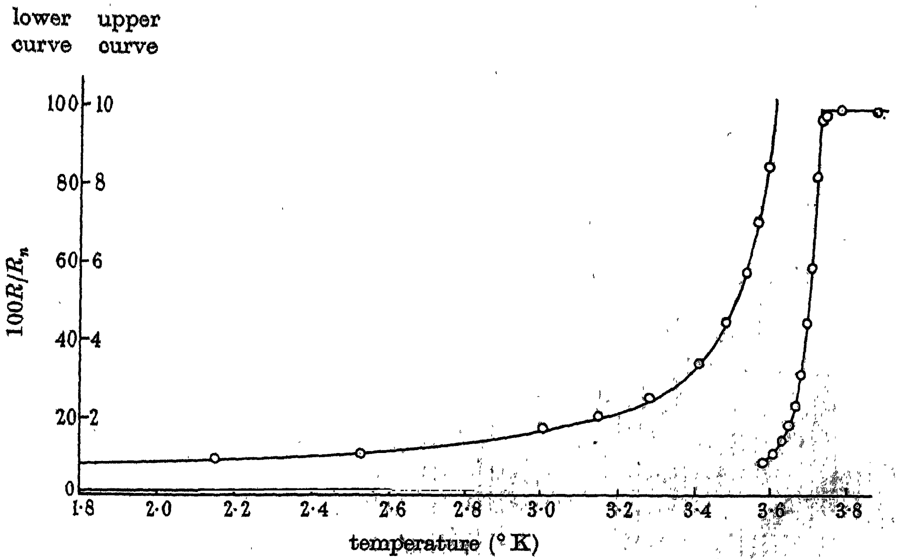

FIGURE 4. Resistivity of superconducting tin at 1200 Mc./sec. The upper curve is drawn on ten times the vertical scale of the lower curve.

shows the transition curves of the same specimen (Sn 14) as measured with r.f. and d.c. It appears probable from this diagram that the initial slope is not quite so great in the r.f. measurements, but it is not possible to make any reliable estimate from such an experiment of the ideal behaviour at the critical temperature.

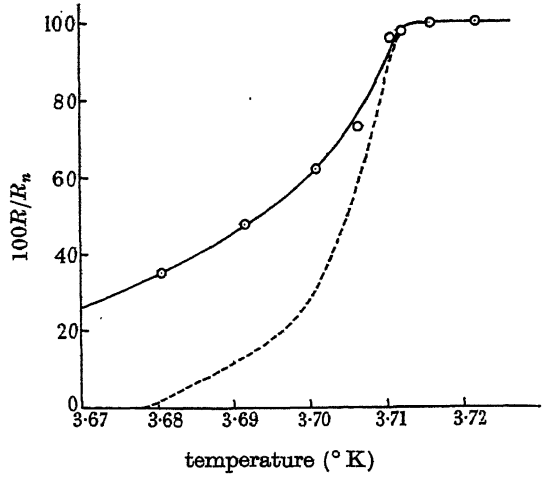

FIGURE 5. Transition curve of tin, measured by d.c. and r.f. — r.f. - - - d.c.

The limiting value of R/R_n at low temperatures, which is assumed by London to be zero, is very difficult to fix precisely because of inevitable extraneous power losses in the cavity arising from the presence of imperfect dielectrics. Three attempts were made, by different methods, to estimate this limit, but the results are not in very close agreement with one another, probably because they all rely on the assumption that two specimens of the same dielectric have exactly the same power factor. While this assumption is probably true for pure substances exhibiting high dielectric loss, it is very likely that good dielectrics, whose loss is due to some unexplained small imperfections in structure, will show widely varying power factors depending on the precise constitution of the material. In the first attempt two specimens (Sn 6 and Sn 7) were constructed having different diameters of wire, but with the proportion of silica to free space made as nearly equal as possible. These specimens, if the conductors were perfect, should have had the same band width, since it would be determined solely by the extraneous losses. If these losses are expressed as an effective limiting width W_d of the resonance peak, the band width of Sn 6 at any temperature is expressible as $W_6 + W_d$, where W_6 is the ideal width due to conductor losses above. Similarly the band width of Sn 7 is expressible as $W_7 + W_d$. Since the variations of W_6 and W_7 with temperature are expected to be identical, apart from a constant scaling factor which arises from the different sizes of the specimens, it ought to be possible to find a quantity W_d which, when subtracted from the measured widths, leaves the curves for Sn 6 and 7 bearing a constant ratio to one another at all temperatures. The relevant results of the experiment are tabulated in table 3, from which it may be deduced that $W_d = 0{\cdot}0520$. When all the data on the specimens had been corrected by subtracting W_d and expressing each corrected value as a ratio R/R_n, the two curves were found to be in excellent agreement with one another. This experiment enabled the value of R/R_n at 2·12° K to be estimated at 0·78 %.

TABLE 3. DATA FOR SN 6 AND SN 7

Sn 6: band width at 3·74° K (in units of 100 kcyc./sec.) = 3·39
band width at 2·12° K (in units of 100 kcyc./sec.) = 0·0778

Sn 7: band width at 3·74° K (in units of 100 kcyc./sec.) = 11·16
band width at 2·12° K (in units of 100 kcyc./sec.) = 0·138

The second estimate of R/R_n at 2·12° K involved two measurements of Sn 12, a bare tin wire, each time with a different number of distrene spacers connecting the two limbs. The loss introduced by each spacer was assumed to be proportional to its volume and to the mean value of E^2 at that point, so that it was possible to calculate the presumed behaviour of the specimen in the absence of any spacers. The results of this measurement were in only fair agreement among themselves, but they suggest that R/R_n at 2·12° K lies between 0·7 and 1·1 %.

The final attempt to determine this ratio involved the use of both tin and mercury specimens, the advantage of the latter being that its resistance drops by a very large factor between 4·2 and 2·1° K, so that at the lower temperature it approximates to a perfect conductor. Two specimens (Sn 11 and Hg 15) were made from silica capillaries drawn from the same piece of tubing, and were mounted on distrene specimen-holders in as nearly identical a manner as possible. The band widths in the normal state and at 2·1° K are shown in table 4. Clearly if the dielectric losses of the two specimens are identical, at least 0·112, the difference between Hg 15 and Sn 11 at 2·1° K, is due to the conductor losses in the tin, so that R/R_n at 2·1° K is not less than 0·80 %. An upper limit of 1·5 % is fixed by the results for Sn 11 alone.

TABLE 4. DATA FOR SN 11 AND HG 15

Sn 11: band width at 3·74° K (in units of 100 kcyc./sec.) = 13·98
band width at 2·1° K (in units of 100 kcyc./sec.) = 0·210

Hg 15: band width at 4·20° K (in units of 100 kcyc./sec.) = 32·8
band width at 2·1° K (in units of 100 kcyc./sec.) = 0·098

Considering these three sets of measurements together, probably the most significant fact is that they all give a positive value for the ratio in the neighbourhood of 1 %. If the real value were much smaller than this, it is likely that the inevitable uncertainties of the methods would have resulted in a wider spread of results, or even in an apparently negative value. In correlating the results for six specimens, which were shown in table 2, a value of 0·90 % was taken for R/R_n at 2·1° K, and appropriate quantities were subtracted from the measured band widths of each specimen to bring them into coincidence at this temperature. It should be realized that even if this value is found eventually to be in error, the figures in the table may be corrected to the new value merely by subtracting the same quantity from each and scaling up to $R_n = 100$.

To determine the absolute value of the normal skin resistivity, two methods were used. A specimen of Hilger tin was measured at 3·8° K, and a similar specimen of copper was measured at room temperature. The inverse ratio of the Q values was taken to be the ratio of the resistivities of the two specimens, and from these measurements it was deduced that tin at 3·8° K has the same skin resistivity as a metal of conductivity $\sigma = 2{\cdot}06 \times 10^7$ ohm^{-1}cm.$^{-1} \pm 5$ %, obeying the simple theory of the skin effect. It is important to point out that the quantity which is actually measured is the skin resistivity, and that the reduction of this to a value of bulk conductivity is merely a convenient way of presenting the result, which has no real physical significance on account of the anomalous behaviour of normal metals at low temperatures. The skin resistivity of the Johnson Matthey sample was measured by the method outlined above, by determining the band width of the same specimen at 3·8° K and at the temperature of liquid nitrogen, where the anomalous behaviour is not exhibited. The apparent conductivity of this sample at 3·8° K was found to be $2{\cdot}10 \times 10^7$ ohm^{-1}cm.$^{-1} \pm 1$ %. London (1940) records a value of $2{\cdot}06 \times 10^7 \pm 15$ %, so that all three determinations are in strikingly good agreement. Taking the figure $2{\cdot}10 \times 10^7$ as correct, the skin resistivity R_n at 3·8° K and 1200 Mcyc./sec. may be deduced to be $1{\cdot}50 \times 10^{-3}$ ohm; as pointed out above, this value is not affected by the anomalous behaviour of tin, since it is the quantity which is directly measured.

(b) *Mercury*

As was mentioned in connexion with the results for tin, the value of R/R_n for mercury at 2·1° K is very much smaller than the corresponding factor for tin. The best estimate is that obtained incidentally from the results on Sn 11 and Hg 15 shown in table 4, from which it may be seen that it is certainly less than 0·30 %. Taking the value 0·90 % for tin, and using this to determine the band width due to dielectric loss, the most probable value for mercury is seen to be 0·04 %. The temperature variation of R/R_n, shown in figure 6 and table 5, has been constructed from the results for two specimens of Hilger 10,673 mercury, Hg 4 and Hg 15, of which only the points for Hg 4 are shown in the figure. The transition temperature was 4·152° K, which is somewhat lower than the usually accepted figure. As in the case of tin, the dielectric losses have been allowed for by subtracting a constant quantity from the measured widths to bring R/R_n at 2·1° K to the estimated value of 0·04 %.

The anomalous behaviour shown by normal tin is also exhibited, though to a lesser degree, by mercury. The skin resistivity at 4·2° K was deduced from measurements of the same specimen at 4·2 and at 20° K at which temperature mercury is found to show no anomaly. In this manner R_n was found to be $2{\cdot}34 \times 10^{-3}$ ohm. A classical metal would have this skin resistivity if its bulk conductivity were

$8{\cdot}75 \times 10^6\,\text{ohm}^{-1}\,\text{cm.}^{-1}$, which is less than the observed conductivity (Onnes & Tuyn 1929) by a factor 2·31. This represents a smaller departure from classical theory than is shown by tin, for which the corresponding factor is 23.

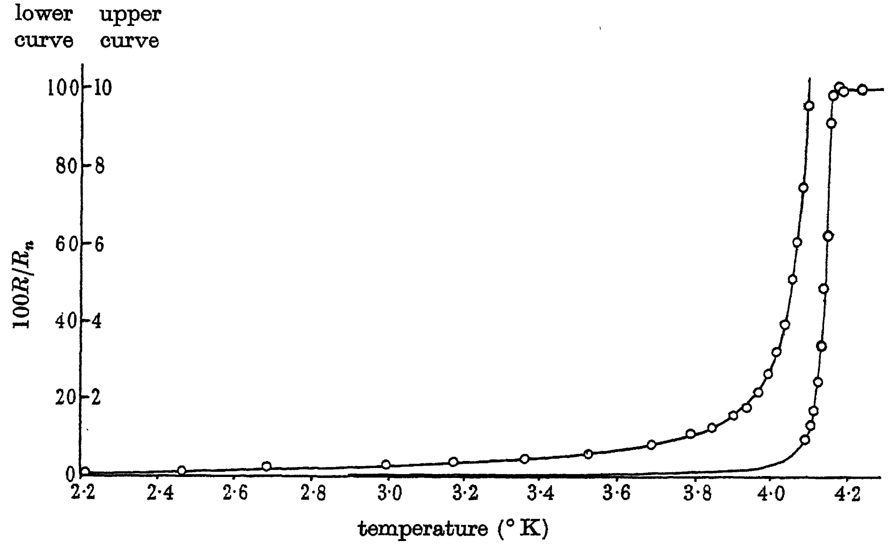

FIGURE 6. Resistivity of superconducting mercury at 1200 Mcyc./sec. The upper curve is drawn on ten times the vertical scale of the lower curve.

TABLE 5. SMOOTHED VALUES OF RESISTIVITY OF MERCURY

temperature (° K)	$100R/R_n$	temperature (° K)	$100R/R_n$	temperature (° K)	$100R/R_n$
4·1525	100	4·092	10	3·775	1·0
4·1475	80	4·082	8	3·625	0·7
4·141	60	4·062	6	3·44	0·5
4·132	40	4·037	4	3·29	0·4
4·126	30	4·010	3	3·09	0·3
4·116	20	3·956	2	2·84	0·2
4·108	15	3·895	1·5	2·50	0·1
				2·20	0·05

DISCUSSION

A theory of the r.f. resistivity of superconductors, relating it to the penetration depth λ of a static magnetic field, has been given by London (1940), and applied by him to his measurements on tin. As it stands, the theory contains a number of assumptions concerning the coexistence of 'resistive' and 'superconducting' electrons, which must be regarded as working hypotheses requiring justification either by experiment or by a detailed theory of superconductivity such as has not yet been given. There is also another assumption as to the behaviour of resistive electrons in such an assembly which appears to be at variance with the experimental results on normal metals, in so far as there is a notable discrepancy between the measured skin resistivity and that predicted by skin effect theory from the d.c. conductivity. This phenomenon makes it doubtful whether the theory developed by London is in fact the correct development of the initial assumptions. A series of measurements have been made, and will be described in a later paper, which demonstrate the salient features of this effect, and an attempt has been made to give a quantitative theoretical explanation. Until this theory has been presented, and extended to cover London's model of a superconductor, there is no advantage to be gained in discussing the interpretation of the results given here. A full discussion, therefore, will be postponed until the end of this series of papers, where the correlation of data on the r.f. resistivity with the known facts concerning the temperature dependence of the penetration depth will be considered.

One point, however, may be made without any detailed theory. If London's hypothesis is correct, the behaviour of R/R_n at low temperatures is important, since it indicates whether all the resistive electrons vanish at the absolute zero. It is most unlikely that the curves for tin can be extrapolated back to reach a zero value at 0° K, so that it must be concluded either that all the electrons do not become superconducting at 0° K, or that there is some other mechanism (e.g. photo-effect having a threshold frequency less than 1200 Mcyc./sec.) which causes energy dissipation. On the other hand, the resistivity of mercury reaches a very low value at 2° K, and there is no evidence that it does not actually become zero at 0° K.

REFERENCES

London, H. 1940 *Proc. Roy. Soc.* A, **176**, 522.
Keesom, W. H. 1932 *Leid. Comm. Supp.* **71***d*.
Shawe, L. W. & Burrell, C. M. 1947 *J. Inst. Elect. Engrs* (in the Press).
Onnes, H. Kamerlingh & Tuyn, W. 1929 *Int. Crit. Tables*, **6**, 124.

The surface impedance of superconductors and normal metals at high frequencies

II. The anomalous skin effect in normal metals

By A. B. Pippard, *Fellow of Clare College, Cambridge, Royal Society Mond Laboratory*

(*Communicated by Sir Lawrence Bragg, F.R.S.—Received* 1 *April* 1947)

Measurements on the skin conductivity of the normal metals silver, gold, and tin show that at low temperatures the skin conductivity tends to become independent of the d.c. conductivity, which is at variance with the predictions of classical skin effect theory. Following a suggestion of H. London that this anomalous behaviour is due to the mean free path of the electrons becoming much greater than the skin depth, an attempt is made to calculate the effect for a semi-classical model of a metal. Although a rigorous solution has not been found, it is shown that the model predicts constancy of skin conductivity when the mean free path becomes very long. Moreover, there is reason to suppose that under these conditions only a small proportion of the conduction electrons contribute effectively to the high-frequency current, and an exact solution is given for a model based on this concept, which also predicts that the skin conductivity should be independent of the d.c. conductivity.

A simple dimensional argument may be applied to enable values of the mean free path in copper, gold, aluminium and tin, relative to the value in silver, to be deduced from the experimental results. These values are not in good agreement with theoretical estimates by Mott and Jones. The behaviour of mercury is different from that of the other metals investigated, in that the skin conductivity does not tend to a constant value. It is suggested that the theory based on a crude classical model is inapplicable to a metal such as mercury, in which the anomalous skin effect appears at such temperatures that the ideal resistance is still many times greater than the residual resistance.

Introduction

The anomalous resistivity of metallic conductors at high frequencies and very low temperatures appears to have been observed first by London (1940), who attributed it to the long mean free path of the electrons. At low temperatures, owing to the increased conductivity, the depth of penetration of the high-frequency field into the metal decreases, while the mean free path increases, so that it may become very many times as large as the skin depth. The experimental observation was confirmed by the present writer during measurements on the high-frequency resistance of superconducting tin and mercury, described in the first paper of this series (p. 370, referred to in future as I), and it seemed desirable to investigate the matter in greater detail, not only on account of its intrinsic interest and the light it might throw on the behaviour of electrons in normal metals, but also because an understanding of its nature is probably essential to a rigorous theory of the resistive effects observed in superconductors at high frequencies. The results presented in this paper do not amount to more than a preliminary survey of the problem, but at any rate some of the principal features of the phenomenon have been demonstrated, sufficient to allow a qualitative understanding of the mechanism, and the part played by the mean free path.

All the measurements to be discussed here were made at frequencies within a narrow band around 1200 Mcyc./sec., and, with the exception of the preliminary investigations, with the same type of resonator and the same technique as was described in I. In particular, the linear relation between Q, the selectivity of the resonator, and t, the voltage transmission coefficient, was used in all the measurements to eliminate the resistive effect of the coupling between the resonator and the external circuits. The band width so determined was governed only by the resistivity of the specimen and dielectric losses in the resonator; the latter, however, amounted to only a small fraction of the resistive loss, and could be allowed for accurately. The metals investigated were copper, silver, gold, aluminium, tin and mercury, in the form of wires of diameters ranging from 1 to 2 mm. In order to vary the specific conductivity of the specimens, the measurements were carried out at several different temperatures, produced by liquid nitrogen (77° K), hydrogen (14 to 20° K) and helium (2·0 to 4·2° K), as well as at room temperature. For each specimen except mercury the d.c. resistance was measured at room temperature and at 4·2° K, and the resistance at intermediate temperatures was calculated from the data of Onnes & Tuyn (1929), assuming the validity of Matthiessen's rule. The d.c. conductivity of mercury was measured with a specimen from the same sample of Hilger mercury, not with the specimen actually used in the r.f. experiment.

EXPERIMENTAL RESULTS

(a) *Effect of surface roughness*

Preliminary measurements were made in order to ascertain whether at room temperature, where the mean free path in all metals is very much less than the skin depth at 1200 Mcyc./sec., the measured skin resistance is in agreement with the predictions of electromagnetic theory. From Maxwell's equations and the conductivity equation $\mathbf{J} = \sigma\mathbf{E}$ it may be shown that the skin depth is given by the expression $\delta = 1/\sqrt{(2\pi\omega\sigma)}$ cm., if σ is expressed in e.m.u., and that the surface resistivity is $\sqrt{(2\pi\omega/\sigma)}$ e.m.u.

Since the resonator described in I is not suitable for absolute measurements, on account of the difficulty of computing the theoretical Q-value for such a shape with materials of known conductivity, a coaxial resonator was constructed in which the specimen was a straight wire approximately $\frac{1}{2}\lambda$ long forming the inner conductor. The outer conductor was a much longer copper tube of 5 cm. diameter, and the specimen was supported axially within it on two thin discs of polythene, whose dielectric loss was quite negligible. The resonator was coupled to the oscillator and detector by two coaxial cables whose inner conductors projected into the interior of the resonator. The theoretical Q-value of such a resonator, constructed from materials of known conductivity, is given in standard works (see e.g. Jackson (1945)), and will not be discussed further here. The specimen was a piece of commercial 16 s.w.g. copper wire, and measurements were made of the Q_0 of the resonator and the d.c. conductivity of the material at room temperature. It was found that the measured value of Q_0 was 5 % lower than the theoretical prediction. The specimen was then heated in a gas flame and plunged while still red hot into alcohol, so that a very clean matt surface was formed, and the Q_0 was found to have decreased by a further 30 %. This result agrees qualitatively with many (unpublished) observations during the war that the attenuation factor of silver-plated waveguides at frequencies around 10,000 Mcyc./sec. might be as much as twice the theoretical value unless the silver was highly polished after deposition. Further experiments with copper wires showed that the smooth surface of a drawn wire enables the skin resistivity to approach most nearly to the theoretical value, and that any attempt to clean the surface by polishing with even the finest emery causes deterioration. The most likely explanation of these effects lies in the fact that the skin depth is extremely small ($\sim 10^{-4}$ cm.) so that scarcely visible scratches and irregularities force the currents to traverse a longer path than is apparent, with a corresponding increase in resistive loss. As a result of these investigations, all the specimens used were left in the state of high surface polish in which they were prepared. It was assumed that the effect of surface irregularities was to increase the r.f. resistance by a constant proportion independent of temperature, which in any case probably did not exceed 5 %. The results quoted are therefore believed to represent the true skin resistivity corresponding to the properties of the bulk material.

(*b*) *Variations of skin resistivity with temperature*

It was pointed out in I that, when due allowance has been made for extraneous power losses in the resonator, the ideal selectivity Q_0 is inversely proportional to the skin resistivity R of the material. It is this resistivity which is actually measured, since the reactive part of the skin impedance Z plays an altogether negligible role in determining Q_0. It is convenient in presentation to use the reciprocal of R, which is of course proportional to Q_0, and this will be referred to as the skin conductivity and denoted by Σ. Now although Σ is proportional to Q_0, it is not practicable, as pointed out above, to calculate the constant of proportionality, on account of the geometrical factors involved. It is possible, however, to estimate the constant of proportionality experimentally by making use of the fact that the classical theory of the skin effect is valid at a sufficiently high temperature. This means that Σ may be calculated at such a temperature from the d.c. conductivity, and correlated with the corresponding value of Q_0 for the resonator. This method of measuring and using a constant proportionality factor incidentally assumes implicitly that any effect of surface irregularities is constant at all temperatures. The method was used at room temperature for copper, silver, gold and aluminium, but it was found to be more convenient to apply it to tin and mercury at lower temperatures, on account of the poor conductivity of these metals at room temperature. Since, however, rough estimates of the mean free path in tin at 77° K and in mercury at 20° K indicated that it was still much smaller than the skin depth, it was concluded that no error would result from determining the proportionality factors at these temperatures. This conclusion is borne out by the consistency of the results obtained.

The specimens of silver and gold were supplied by Heraeus, and were stated to be 99·99 % pure. Two specimens of silver were used, one in the hard-drawn state as supplied, and the other annealed *in vacuo* for a few minutes at dull red heat. The residual resistance of the former was 0·026 times the room temperature resistance, while the corresponding factor for the latter was 0·0033. The tin and mercury specimens were from the same samples as were used in I. In order to measure the normal skin conductivity of mercury below 4·2° K a magnetic field was applied to destroy superconductivity. By observations on the conductivity in fields much larger than those required for this purpose, it was verified that there was no appreciable magneto-resistance effect which would destroy the validity of these observations. The specimens of copper and aluminium had rather large values of the residual resistance, and did not give a sufficiently wide range of conductivities to be worth including in figure 1. They are therefore omitted from consideration at the moment, though they will be discussed at a later stage. Details of the specimens and temperatures will be found in table 1.

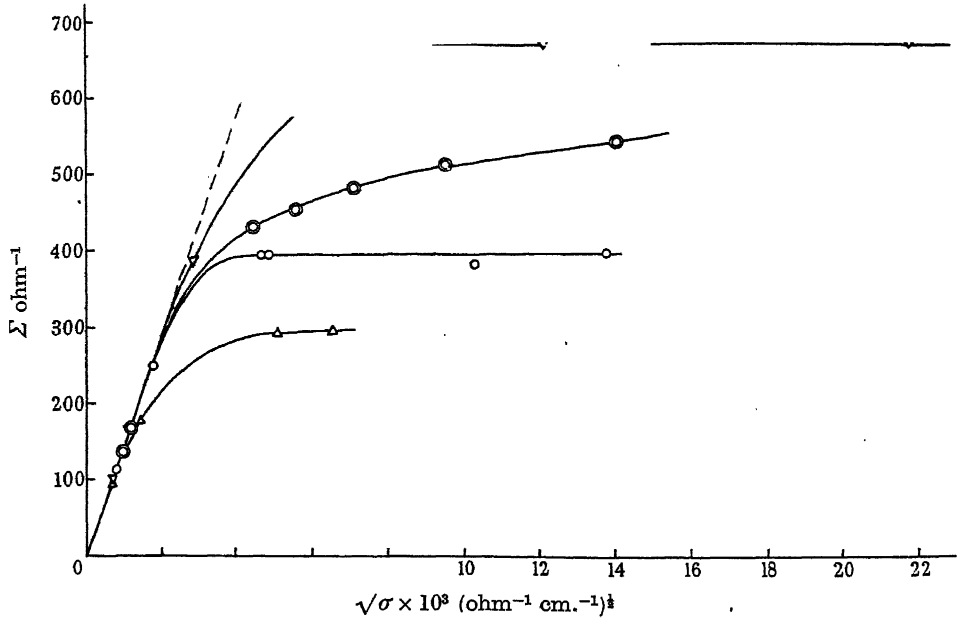

FIGURE 1. Surface conductivity of ○ silver, △ gold, ▽ tin and ◎ mercury at 1200 Mcyc./sec.

In figure 1, Σ is shown plotted against $\sqrt{\sigma}$ for silver, gold, tin and mercury. If the behaviour were consistent with the classical skin effect theory, all the points would lie on the same straight line through the origin. The anomalous behaviour is shown by the characteristic way in which the curves depart rather sharply from the expected straight line and tend, except for mercury, to become parallel to the axis of $\sqrt{\sigma}$, thus bringing to light the remarkable phenomenon that the r.f. skin conductivity is practically independent of σ when the mean free path of the electrons is sufficiently long.

TABLE 1. D.C. AND R.F. CONDUCTIVITIES OF NORMAL METALS

material	resonant frequency (Mcyc./sec.)	temperature (° K)	σ ($\times 10^6$ ohm^{-1} cm.$^{-1}$)	Σ (ohm^{-1})
silver (unannealed)	1250	290	0·625	113·5
		77	3·14	254
		20·4	21·9	396
		4·2	24·0	397
silver (annealed)	1230	290	0·625	113·5
		77	3·22	250
		20·4	106	384
		4·2	190	399
gold	1190	290	0·414	94
		77	1·99	178
		20·4	26·2	294
		4·2	44·5	298
tin Sn A (Hilger)	1220	4·2	150	672
tin Sn B (Johnson Matthey)	1180	77	0·475	102
		20·4	8·80	389
		4·2	480	678
mercury	1160	20·37	0·761	129
		18·17	0·896	137
		13·99	1·35	168
		4·22	20·2	432
		3·716	31·4	455
		3·212	51·7	482
		2·700	91·8	514
		2·137	198	542
copper	1170	290	0·56	110
		77	5·02	281
		20·4	82·0	468
		14·2	86·8	476
		4·2	90·8	484
aluminium	1160	290	0·34	86
		77	3·77	293
		20·4	48·1	582
		14·2	58·2	586
		4·2	62·0	595

THEORY

In this section an attempt will be made to develop London's (1940) tentative explanation of the anomaly as being due to the long mean free path of the electrons. The method of attack is most clearly seen by considering the classical theory of the skin effect. Let the surface of the conductor, of which we consider a semi-infinite slab, be a plane, normal to the X-axis, and let the electric and magnetic fields be parallel to the Y and Z-axes respectively. Then if the displacement current be neglected, we may write Maxwell's equations in electromagnetic units for this problem:

$$\frac{\partial E}{\partial x} = i\omega H, \quad \frac{\partial H}{\partial x} = 4\pi J,$$

in which E, H and J are written for E_y, H_z and J_y, and ω is the angular frequency of the oscillation. These equations may be combined with the conductivity equation $J = \sigma E$ to eliminate J and H, giving an equation for the electric field

$$\frac{\partial^2 E}{\partial x^2} = 4\pi i\omega\sigma E,$$

which has as its solution
$$E = E_0 e^{\pm k_0 x}, \tag{1}$$

in which $k_0^2 = 4\pi i\omega\sigma$. This treatment of the skin effect is valid so long as the conductivity equation is applicable. It is well known that a modification must be introduced at such high frequencies that the period of oscillation is comparable to the relaxation time, τ, of the electrons, but so far as can be judged from theoretical estimates of τ, the anomalous skin conductivity appears at such values of σ that relaxation effects are entirely negligible ($\omega\tau \ll 1$), and even at the highest values of σ it is probably safe to neglect relaxation. It is likely, however, that an increase of frequency by a factor of ten would bring the problem into the region of relaxation effects.

The nature of the invalidity of the conductivity equation which concerns us here arises from the implicit assumption that the current density at any point is dependent solely on the value of the electric field at that point. Clearly if the mean free path of the electrons is comparable with the depth of penetration of the field, an electron during one free path will be moving through regions of varying field, and the drift velocity which it acquires will be related to the field strength at all points along its path. This means that the equation $J = \sigma E$, in which σ is a constant for all parts of the metal, must be replaced by the more general equation $J = f(E, x)$. The equation for the electric field now becomes

$$\frac{\partial^2 E}{\partial x^2} = 4\pi i\omega f(E, x). \tag{2}$$

The problem before us is the calculation of the function f and the solution of equation (2). It is necessary to choose some model of the metal, and in the following argument a semi-classical model will be used, which should at worst give a qualitative explanation of the experimental facts. The conduction electrons, n per unit volume, will be assumed to move isotropically with the same velocity V in the absence of an electric field, and to acquire an additional drift velocity from the applied electric field. The effects of the associated magnetic field will be neglected, for although it will cause a disturbance to the directions of motion of the electrons, the current density resulting from such a disturbance will be zero (cf. van Leeuwen's theorem). The free paths of the electrons will be assumed to be terminated by collision with a lattice ion, without persistence of drift velocity, and the probability of a path of length between r and $r + dr$ will be taken as $\mu e^{-\mu r} dr$, in which μ is written for the reciprocal of the mean free path l. Using this model it is not difficult to calculate by kinetic methods the drift current density produced at any point by the presence of an arbitrary field distribution. Since we shall be concerned with phenomena occurring at the surface of the metal, it is necessary to make an additional assumption concerning the behaviour of an electron after collision with the lattice ions at the surface. It will be assumed that there is a probability $(1-p)$ that collision with the surface terminates a free path. That is to say, a fraction p of electrons are reflected specularly from the surface, with retention of drift velocity, while the rest are scattered diffusely with loss of drift velocity; p may thus be called the 'drift reflexion coefficient' of the surface. It may be included formally in the calculation by replacing the bounded metal slab by an infinite metal, in which the field in the region above the surface is an image of the field below the surface, of the same sign but reduced in magnitude to a fraction p of the field below.

Before treating the model outlined in the last paragraph, which presents considerable mathematical difficulties, it is convenient to consider a still further simplified model for which an exact solution is possible, and which will yield some useful qualitative information. We shall assume that the electrons are constrained to move all in one direction, or rather that their velocities may take only such directions as lie on the surface of a cone of semi-angle θ, having its axis normal to the surface; they may, however, acquire drift velocity in the direction of the electric field, which will be lost on collision with the lattice, so that the direction of motion will revert to its former value θ. Let the electric field in the metal be $E = E(x)\,e^{i\omega t}$. If $\omega\tau \ll 1$, the field may be considered as stationary for the purpose of calculating the current, and the time-variable factor $e^{i\omega t}$ may be omitted. The calculation of the current density $J(x)$ at a point P distant x below the surface now follows the lines of the elementary methods used in the kinetic theory of gases, in so far as the history of each electron is followed from the time of its last collision to the moment when it reaches the point P, and its contribution to the current density at P is thus calculated. The process is extended by integrating over all space, to give the result

$$J(x) = f(E,x) = \tfrac{1}{2}\mu_1^2\sigma\left\{\int_0^\infty e^{-\mu_1 v}\,dv\int_x^{x+v} E(u)\,du + \int_0^x e^{-\mu_1 v}\,dv\int_{x-v}^{x} E(u)\,du \right.$$
$$\left. + \int_x^\infty e^{-\mu_1 v}\,dv\left[\int_0^x E(u)\,du + p\int_0^{v-x} E(u)\,du\right]\right\}, \qquad (3)$$

in which σ is written for the bulk conductivity $ne^2/\mu mV$, and μ_1 for $\mu/\cos\theta$, the reciprocal of the projected length of the mean free path along the normal to the surface. The first term of (3) represents the contribution to the current density by those electrons coming up to P from the body of the metal, the second term the contribution of those which collided last between P and the surface, and then moved downwards in the direction of P, and the third term is the contribution from the 'image field', i.e. those electrons which have reached P from the surface without any intervening collisions. If we put $\mu_1 = \infty$, by putting either $\mu = \infty$ or $\theta = \frac{1}{2}\pi$, equation (3) may be integrated immediately to give $J(x) = \sigma E(x)$, the classical conductivity equation, which is therefore obeyed by all electrons whose projected mean free path $l\cos\theta$ is much smaller than the skin depth; in particular, the classical equation always holds for electrons moving parallel to the surface.

In order to solve for E, it is necessary to substitute (3) in equation (2). When this has been done it is found after substitution and evaluation of the integrals that a solution is possible in the form

$$E = E_0(e^{-k_1x} + ae^{-k_2x}), \tag{4}$$

in which k_1^2 and k_2^2 are the solutions of the quadratic equation

$$\frac{\mu_1^2}{\mu_1^2 - k^2} = \frac{k^2}{k_0^2}, \tag{5}$$

k_0^2 being written for $4\pi i\omega\sigma$ as in the classical case, and

$$a = -\frac{\mu_1^2 - k_2^2}{\mu_1^2 - k_1^2} \frac{(1+p)\,k_1 + (1-p)\,\mu_1}{(1+p)\,k_2 + (1-p)\,\mu_1}. \tag{6}$$

Now equation (5) has four solutions for k, of which only two have positive real parts; since the electric field must vanish at infinity it is these two solutions which are taken as k_1 and k_2. In the limiting case of short free paths, i.e. $\mu_1 \to \infty$, the solution becomes identical with the classical solution as expected. At the other extreme, as $\mu_1 \to 0$, equation (5) reduces to

$$k^4 = -\mu_1^2 k_0^2.$$

Bearing in mind that μ_1, k_0 and $k_{1,2}$ are reciprocals of quantities whose order of magnitude is the mean free path, the classical skin depth, and the actual skin depth respectively, we see that the actual skin depth is of the order of the geometric mean between the classical skin depth and the mean free path. The field therefore penetrates to a much smaller distance than a single mean free path, and this, as we shall see later, has an important bearing on the part played by the reflexion coefficient p.

The skin impedance Z, defined by $E(0)\Big/\int_0^\infty J\,dx$, is readily shown to be equal to

$$-\frac{4\pi i\omega E(0)}{(\partial E/\partial x)_{x=0}};$$

for the field of equation (4), $Z = \dfrac{4\pi i\omega(1+a)}{k_1 + ak_2}$. A rough estimate of Z when the mean free path is very long may be obtained by putting $k_1 = k_2 = \sqrt{|\mu_1 k_0|}$. For any given metal, in which the number and velocity of the electrons remains constant while the temperature is changed, μ_1 is inversely proportional to the conductivity, and k_0 is proportional to the square root of the conductivity. Therefore

$$Z \propto 1/\sqrt{|\mu_1 k_0|} \propto \sqrt[4]{\sigma}, \quad \text{or} \quad \Sigma \propto \sigma^{-\frac{1}{4}}.$$

This means that in the 'linear' metal considered, the skin conductivity actually falls as the bulk conductivity rises, when the mean free path is sufficiently great. This is an exaggerated picture of the experimental facts, as would be expected from the nature of the model. For the fall in Σ only begins when the projected mean free path $l\cos\theta$ is greater than the skin depth; if the electrons were moving isotropically, there would always be a fraction for which $l\cos\theta$ was less than the skin depth, and which would therefore behave according to the classical conductivity equation. It is therefore to be expected that the isotropic model will give a result somewhere in between the predictions of classical theory and this 'linear' model.

Now it has been pointed out before that the skin depth in the limiting case of long free paths becomes much smaller than l. This can only mean that electrons which come from within the body of the metal and return there after reflexion from the surface without colliding with the lattice near the surface cannot carry any drift velocity back with them, for otherwise there would be a finite current density in regions where the field is substantially zero. This conclusion may be verified by calculating $\int_0^\infty E\,dx$, which is proportional to the drift velocity acquired by an electron in moving from the surface into the body of the metal:

$$\int_0^\infty E\,dx = E_0\left(\frac{1}{k_1}+\frac{a}{k_2}\right),$$

from equation (4). But if $k \gg \mu_1$, a is equal to $-k_2/k_1$ from (6), and therefore $\int_0^\infty E\,dx$ vanishes. It follows from this result that any electron which reaches the surface after having collided last in the field-free region reaches it without any drift velocity, so that it is immaterial whether the surface be perfectly reflecting or not. In fact, the precise nature of the surface plays very little part in determining the skin conductivity when the mean free path is very long, in contrast to the apparently similar phenomenon of the low d.c. conductivity of thin films, studied by Lovell (1936), where the reflexion coefficient of the surface is the only important factor. This result is made clearer by an exact computation of Σ from equations (5) and (6) for a particular case. Suppose, for example, that the mean free path is 1000 times as great as the classical skin depth; the conductivity Σ is found to be 12 times less than the classical value $\sqrt{(\sigma/2\pi\omega)}$ when $p=1$ (perfectly reflecting surface), and 12·5 times less when $p=0$ (diffuse surface). Thus the nature of the surface, while not entirely negligible, is of comparatively minor importance relative to the main controlling factor, the mean free path.

In extending the theory to take into account the isotropic distribution of electronic velocities, the equation $J=f(E,x)$ may be set up in a similar manner to that outlined for the linear model, with the difference now that the integration must include all directions of motion. On substituting in equation (2) the equation for E takes the form

$$\frac{\partial^2 E}{\partial x^2} = 2\pi i\omega\mu\sigma\left\{\int_0^\infty \frac{e^{-\mu v}}{v}dv\int_x^{x+v}E(u)\,du+\int_0^x \frac{e^{-\mu v}}{v}dv\int_{x-v}^x E(u)\,du\right.$$
$$\left.+\int_x^\infty \frac{e^{-\mu v}}{v}dv\left[\int_0^x E(u)\,du+p\int_0^{v-x}E(u)\,du\right]\right\}, \qquad (7)$$

in which each term has the same significance as the corresponding term in equation (3). Equation (7) in fact only differs from equation (3) by containing v in the denominator of each integral, but this small difference is sufficient to render equation (7) exceedingly intractable. No solution in finite terms has yet been found, but it is possible, by attacking the problem from a slightly different angle, to deduce a certain amount of information about the nature of the solution.

It was seen that the 'linear' model, in which the electrons were confined to one direction of motion θ, was capable of a solution in the form of the sum of two exponential terms. By setting up an equation analogous to equation (3) for a model in which the electrons are confined to N discrete directions $\theta_1 \ldots \theta_N$, it is found that a solution is possible consisting of the sum of $N+1$ exponential terms. It should therefore be expected that as N tends to infinity, and the model becomes identical with the isotropic model, the solution of (7) might be expressed as

$$E = E_0 \sum_1^\infty a_j e^{-k_j x}. \tag{8}$$

Moreover, by considering the N-directional model, equations may be derived which define the coefficients a_j and the exponents k_j of each of the $N+1$ terms of the solution. As N tends to infinity the equation for k_j becomes

$$k_j^3 = \tfrac{1}{2}\mu k_0^2 \log \frac{\mu + k_j}{\mu - k_j}, \tag{9}$$

which has an infinity of complex solutions, and is analogous to equation (5). The equation defining a_j, analogous to equation 6, is

$$\sum_1^\infty a_j \phi(k_j, \theta) = 0 \tag{10}$$

for all values of θ, in which

$$\phi(k_j, \theta) = \cos\theta \frac{(1+p) k_j \cos\theta + (1-p)\mu}{\mu^2 - k_j^2 \cos^2\theta}. \tag{11}$$

Now although it is possible to solve equation (9) by numerical means, equation (10) has as yet defied solution. Certain results, however, may be deduced without a complete solution. In the limit of very long mean free paths, μ becomes negligible in comparison with k_j, so that equation (9) reduces to $k_j^3 = \frac{1}{2}\log(-1)\,.\,\mu k_0^2$. Since μ is inversely, and k_0^2 directly, proportional to σ, we see that for long free paths each k_j becomes a numerical constant times the quantity $\sqrt[3]{(\mu k_0^2)}$, which is independent of conductivity. Thus the penetration depth, and hence presumably the skin impedance, tend to a constant value, in agreement with experiment.

Further, since equation (10) is true for all values of θ, we may put $\cos\theta = 1$ and consider the case when μ is negligible in comparison with k_j. Then equation (10) reduces to $\sum_1^\infty a_j/k_j = 0$, which means that, as for the linear model, $\int_0^\infty E\,dx$ vanishes; hence, by the same argument, the reflexion coefficient p plays only a small role when the mean free path is much greater than the skin depth.

The vanishing of $\int_0^\infty E\,dx$ implies that the only electrons which are effective in the conduction process when the free path is long are those which suffer collisions in the surface layer containing the electric field. Now those electrons which move normal to the surface have a relatively small chance of colliding in the surface layer compared with those moving at a glancing angle to the surface, and this suggests a possible approximate treatment of the problem. Let us neglect all those electrons which have a small probability of collision in the surface layer, and consider only those whose directions of motion make an angle with the surface of less than $\sin^{-1}(\beta\delta/l)$. Here δ is the skin depth, as yet undetermined, and β is a numerical constant whose value would be expected to be of the order of, but probably not less than, unity. The electrons which we regard as effective in the conduction process are those which can traverse a whole mean free path within a distance $\beta\delta$ from the surface, and which are therefore acted upon by the field at all times, and have a high probability of collision in the surface layer. Now in order to simplify the calculation it is convenient to make one more assumption, namely that we may regard all these electrons as obeying the classical conductivity equation. We saw in the treatment of the 'linear' model that the significant parameter in determining the behaviour of the electrons was μ_1 (i.e. $1/l\cos\theta$). If μ_1 is much greater than k, the classical equation is certainly valid, but here we propose to use it for the case when μ_1 is of the order of k. An exact computation of the linear model for the case $\mu_1 = k$ leads to the result that instead of the skin impedance having the classical value $Z_{\text{Cl}} = \sqrt{\left(\frac{2\pi\omega}{\sigma}\right)}(1+i)$, it takes the value

$$Z = \sqrt{\left(\frac{2\pi\omega}{\sigma}\right)}(1{\cdot}09+1{\cdot}52i).$$

It may be concluded, therefore, that so far as the resistive part of Z is concerned, the assumption will not invalidate the procedure. We may expect, however, that the value deduced for the reactive part will be rather low.

With this assumption then, the calculation of Z follows exactly the lines of the classical calculation, except that in place of σ we must write $\beta\delta\sigma/l$, since $\beta\delta/l$ is the fraction of electrons considered as effective. The field is then given by

$$E = E_0 e^{-kx}, \quad \text{where} \quad k^2 = \frac{4\pi i\omega\beta\delta\sigma}{l}.$$

Now the skin depth is the reciprocal of the real part of k, and we must equate this to δ, i.e.

$$\delta = \sqrt{\frac{l}{2\pi\omega\beta\delta\sigma}},$$

i.e.

$$\delta^3 = \frac{l}{2\pi\omega\beta\sigma} = \frac{mV}{2\pi\omega\beta ne^2}, \quad \text{since} \quad \sigma = \frac{ne^2 l}{mV}.$$

The skin depth δ is thus independent of the conductivity. The skin impedance is given by the same formula as in the classical case, $Z = 4\pi i\omega/k$, since the field is expressed by a single exponential term. Therefore

$$\begin{aligned} Z &= 2\pi\omega\delta(1+i), \\ &= (1+i)\sqrt[3]{\frac{4\pi^2\omega^2 mV}{\beta ne^2}}, \end{aligned} \tag{12}$$

which is also independent of σ, in accordance with the experimental results.

Now the validity of this argument depends on the mean free path being very much greater than the skin depth. In order to verify that this condition is in fact obeyed in the experiments consider the points for unannealed silver, which lie just at the beginning of the flat region of Σ in figure 1. A theoretical estimate for the mean free path in silver at room temperature of $1\cdot 14\times 10^{-5}$ cm. has been given by Mott & Jones (1936). Since the unannealed specimen increased in conductivity by a factor of 38 in cooling to 4° K, we may put l at this temperature equal to $4\cdot 4\times 10^{-4}$ cm. Now from the above theory it follows that $\delta = 1/2\pi\omega\Sigma$, so that δ may be estimated from the experimental results as $5\cdot 2\times 10^{-5}$ cm., which is 8·5 times less than the mean free path. It appears, therefore, that the above theory gives a qualitative picture for the process so long as l is more than 8 times the skin depth.

A further check on the theory may be obtained by using the estimates by Mott & Jones of the mean free path in silver and gold in order to calculate β, which we have seen should have a value rather greater than unity. If we write Σ_∞ for the limiting value of the skin conductivity for long mean free paths, we see from equation (12) that $\beta = (4\pi^2\omega^2 l/\sigma)\,\Sigma_\infty^3$. Substituting the theoretical estimates of l/σ and the measured values of ω and Σ_∞, we arrive at the conclusion that $\beta = 2\cdot 46$ for silver and 0·96 for gold. Without considering for the moment the difference in these two values we may note that the estimated β is of the expected order of magnitude, which suggests that the concept of the 'ineffectiveness' of the majority of the electrons does represent a reasonable qualitative picture of the effect.

If the isotropic model be taken to give a fair approximation to a real metal, a considerable amount of information may be deduced by purely dimensional arguments. We have seen that the surface reflexion coefficient plays a relatively small part, so that if this is neglected, the skin conductivity may be considered as depending on only two quantities, the classical value of the skin depth δ_{Cl}, and the mean free path l, since these two define the independent parameters of the model. We shall now introduce a new quantity D, called the discrepancy factor, which is the ratio of the skin conductivity predicted by classical theory from σ, to the measured skin conductivity. Since D is dimensionless, it must bear a functional relationship to the other dimensionless quantities of the problem, of which there is only one, l/δ_{Cl}, if p be neglected. We may therefore write

$$D = F(l/\delta_{\text{Cl}}).$$

Now σ is given by $\dfrac{ne^2 l}{mV}$, and δ_{Cl} is $1/\surd(2\pi\omega\sigma)$, so that l/δ_{Cl} may be expressed as $\dfrac{\surd(2\pi)\,mV}{ne^2}\surd(\omega\sigma^3)$. This means that if D be plotted against $\log\surd(\omega\sigma^3)$, each metal should give the same shape of curve, but the position of each curve along the axis of $\log\surd(\omega\sigma^3)$ will be different. In fact, if the curve for a metal has to be displaced a distance α in order to coincide with the curve for another metal, then antilog α is a measure of the ratio of the quantity mV/ne^2, i.e. l/σ, for these two metals. In figure 2 these functions are plotted for silver, gold, tin, copper and aluminium, the points for each metal being displaced so that they fit the curve for silver as nearly as possible.

The values so obtained of l/σ relative to silver are shown in table 2. Apart from a certain amount of scatter for the points with low values of D, the values can be fitted to a single curve within the experimental error. So far no results are available for frequencies other than 1200 Mcyc./sec., so that the plotted points do not constitute a complete verification of the functional relationship.

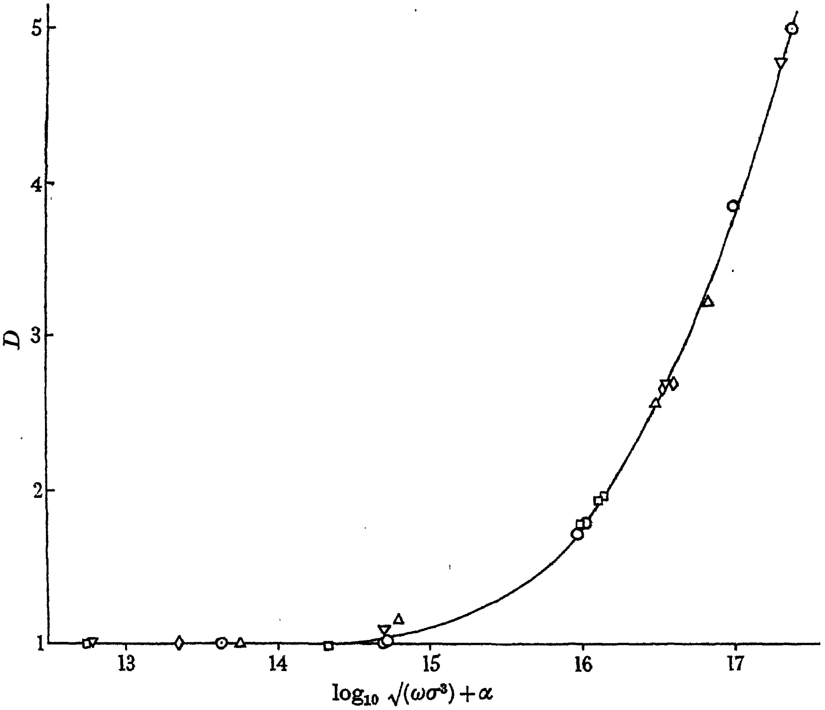

FIGURE 2. Discrepancy factor for ○ silver, △ gold, ▽ tin, ◇ copper and □ aluminium.

TABLE 2. COMPARISON OF EXPERIMENTAL AND THEORETICAL ESTIMATES OF l/σ

material	l/σ relative to silver (experimental)	l/σ (theoretical Mott & Jones)
gold	2·56	1·00
copper	0·50	0·79
tin	0·217	—
aluminium	0·33	—

DISCUSSION

The comparison of theory and experiment leaves no doubt that London's hypothesis of the origin of anomalous resistivity in the long mean free path of the electrons is substantially correct, and that the concept of the 'ineffectiveness' of the majority of the conduction electrons gives a qualitative picture of the process. There are, however, notable discrepancies in the detailed application of the theory. The values of l/σ, for instance, deduced experimentally are not in agreement with the theoretical predictions of Mott & Jones, as can be seen by comparing the second and third columns of table 2. The disagreement in the case of gold is, of course, simply another way of stating that the values deduced above for β are different for silver and gold. Now the values given by Mott & Jones were calculated on the assumption that the electrons in copper, silver, and gold may be treated as a free electron gas, and that the effective number of electrons is one per atom. If this assumption is valid, there is no reason why the dimensional argument outlined above should not apply, for it does not depend on any special model, but only on the supposition that the electrical properties are completely defined by the conductivity and the mean free path; a free electron gas obeying Fermi statistics is so defined. The fact that the theoretical predictions are not in detailed agreement with experiment indicates that this model of the monovalent metals is oversimplified.

The experimental values of l/σ for aluminium and tin are strikingly low. Unfortunately no theoretical estimate seems to have been made with which to compare the results. If we take tin as the extreme example, and substitute numerical values, we find that the value of $n_{\text{eff.}}/V$ (where $n_{\text{eff.}}$ is the effective number of electrons per atom) is about 7 times as great as in silver. Since it is not likely that $n_{\text{eff.}}$ is much greater than 1, the conclusion seems to be that the electronic velocity in tin is much lower than in silver. Let us assume that it is in fact 7 times less than in silver. Then for a given value of the bulk conductivity the relaxation time τ in tin will be 7 times greater than in silver. Using Mott & Jones' estimate of $40{\cdot}9 \times 10^{-15}$ sec. for the relaxation time in silver at room temperature, we arrive at a value of $2{\cdot}1 \times 10^{-10}$ sec. for the tin sample of highest conductivity. The value of $\omega\tau$ for this sample would thus be 1·6 if the above assumptions are correct. Now the experimental results indicate that there is no change in Σ when the conductivity is increased by a factor of 3 (see table 1, data on Sn A and Sn B at 4·2° K), and it is therefore improbable that there are any appreciable relaxation effects. We must conclude that $\omega\tau < 1$, and that the electronic velocity is greater than the assumed value. This in its turn indicates that $n_{\text{eff.}}$ for tin is greater than one. On the other hand, the assumption that the same model is applicable to both silver and tin is open to considerable suspicion, so that it would be unwise to regard the results for tin as anything more than a qualitative indication of the electronic behaviour. Experiments at, say, ten times the frequency would probably help in making a reliable estimate of the relaxation time.

Finally, we must consider the results for mercury, which are not in agreement with the general behaviour of the other metals investigated, in that Σ does not tend to a constant value as σ is increased. It is perhaps significant that of the metals investigated, mercury was the only one for which a number of experimental points were obtained in the region where the anomalous behaviour is well-marked, but where the greater part of the resistance was ideal, not residual, resistance. The evidence on which the conclusion was based that Σ tends to a constant value was obtained with two specimens of tin and two of silver with different residual resistances. It is well-known that the quantum treatment of conductivity at temperatures much lower than the characteristic Debye temperature involves concepts which are far removed from the semi-classical assumptions of the model used here, and it is very probable that the theory based on such a crude model is inapplicable except as a rough guide to the main features of the anomaly. In this connexion it is interesting to note that the two specimens of silver gave the same value of Σ at 4·2° K, where the whole of the resistance was residual, but that the value of Σ for the annealed specimen at 20° K was rather lower than for the unannealed specimen, although σ was much greater. A final decision, however, on this point must wait until more experimental evidence is available.

REFERENCES

Jackson, W. 1945 *High frequency transmission lines*. London: Methuen.
London, H. 1940 *Proc. Roy. Soc.* A, **176**, 522.
Lovell, A. C. B. 1936 *Proc. Roy. Soc.* A, **157**, 311.
Mott, N. F. & Jones, H. 1936 *Properties of metals and alloys*, p. 268. Oxford Univ. Press.
Onnes, H. Kamerlingh & Tuyn, W. 1929 *Int. Crit. Tables*, **6**, 124.

The surface impedance of superconductors and normal metals at high frequencies

III. The relation between impedance and superconducting penetration depth

BY A. B. PIPPARD, *Fellow of Clare College, Cambridge,*
Royal Society Mond Laboratory

(*Communicated by Sir Lawrence Bragg, F.R.S.—Received* 1 *April* 1947)

The theory developed in II is extended to cover the case of a superconductor, and a formula is derived relating the r.f. resistivity to the superconducting penetration depth and other parameters of the metal. It is shown how the penetration depth may be deduced directly from measurements of the skin reactance, and a method of measuring reactance is described, based essentially on the variation of the velocity of propagation along a transmission line due to the reactance of the conductors. For technical reasons it is not convenient to measure the reactance absolutely, but a simple extension of the technique described in I enables the change in reactance to be accurately measured when superconductivity is destroyed by a magnetic field. The method has been applied to mercury and tin. In the former case the results are in agreement with Shoenberg's direct measurements, and confirm that the penetration depth at 0° K is of the order of 7×10^{-6} cm.

The theory developed at the beginning of the paper is used to deduce the variation of penetration depth with temperature from the resistivity measurements of I, and it is shown that agreement with other determinations and with the reactance measurements is fairly good, but not perfect. Some of the assumptions used in developing the theory are critically discussed, and a qualitative account is given to show how Heisenberg's theory of superconductivity offers an explanation of some of the salient features of superconductivity and in particular indicates the relation between superconducting and normal electrons.

INTRODUCTION

In the first two papers of this series, which will be referred to as I and II (pp. 370 and 385), results were presented of measurements on the surface resistivity of superconductors and normal metals at low temperatures and at frequencies around 1200 Mcyc./sec. It was shown in II how the deviations from classical skin effect theory exhibited by normal metals when the free path of the conduction electrons was longer than the skin depth could be approximately described by an 'ineffectiveness concept'; this treatment of the problem, which was justified theoretically, assumed that only those electrons were effective in the conduction process which moved at glancing angles to the surface. In the present paper the concept will be applied to H. London's (1940) model of a superconductor to derive expressions for the surface resistivity and reactance in terms of the penetration depth λ and other parameters. The reactance is found to be very closely related to λ, and this fact suggested an experimental method of studying the variation of λ with temperature with considerable accuracy. Before, however, considering the experimental determination of the surface reactance, expressions will be derived relating the impedance to the penetration depth. It will then be possible to attempt a correlation of the resistivity measurements of I, the reactance measurements of the present paper, and determinations of λ by other workers.

THEORY

The assumptions underlying London's model of a superconductor may be stated briefly thus: the conduction electrons are supposed to exhibit two different modes of behaviour, a certain fraction, depending on the temperature, behaving in accordance with the phenomenological theory of superconductivity developed by F. & H. London (1935), and the rest exhibiting the ordinary resistive properties of the normal state. In the presence of an electric field, the superconducting electrons contribute an amount $\mathbf{J}_s$ to the current density given by $i\omega\mathbf{J}_s = \mathbf{E}/4\pi\lambda^2$ (in e.m.u.), where λ is the penetration depth of a static magnetic field. It was assumed by London that the contribution of the normal electrons to the current density could be represented by $\mathbf{J}_n = \sigma\mathbf{E}$, the classical conductivity equation; he observed however that the resistivity of normal tin was higher than expected from the d.c. conductivity, and attempted an empirical correction for this anomalous skin effect by using for σ not the measured d.c. conductivity, but the conductivity deduced from the r.f. resistivity assuming the classical skin effect theory to be valid. It is the aim of the present theory to use the ineffectiveness concept to determine the contribution by the normal electrons to the current, since a rigorous solution of the problem involves the same mathematical difficulties as were encountered in II.

In the treatment of the normal metal by the ineffectiveness concept, it was assumed that only those electrons whose directions of motion made an angle less than $\sin^{-1}\beta\delta_n/l$ with the surface were effective, δ_n being the skin depth, l the mean free path, and β a numerical constant of the order of unity. Thus the effective conductivity is not σ but $\beta\delta_n\sigma/l$. The natural extension of this concept to superconductors is to define a skin depth in the superconductor δ_s, the distance in which the field drops by a factor e, and to take $\beta\delta_s\sigma/l$ as the effective conductivity. It will be shown that so long as the penetration depth λ is much smaller than the normal skin depth δ_n, δ_s and λ are very nearly equal; in general, however, δ_s is less than λ.

Let us now suppose that the transition of some electrons into the superconducting state alters the normal conductivity by a factor f_n, so that $f_n\sigma$ is the d.c. conductivity which the metal would have if only the normal electrons were present. Then the effective conductivity will be given by $\sigma' = f_n\beta\delta_s\sigma/l$, and an equation may be constructed for the current density,

$$i\omega\mathbf{J} = i\omega(\mathbf{J}_s+\mathbf{J}_n) = \left(\frac{1}{4\pi\lambda^2}+i\omega\sigma'\right)\mathbf{E}. \tag{1}$$

We shall calculate the field distribution for a plane surface normal to the X-axis, taking the Y and Z axes for the directions of E and H respectively. Under these conditions Maxwell's equations become, in e.m.u.,

$$\frac{\partial E}{\partial x} = i\omega H \quad \text{and} \quad \frac{\partial H}{\partial x} = 4\pi J.$$

Combining these equations with (1), we arrive at an equation defining the electric field,

$$\frac{\partial^2 E}{\partial x^2} = \left(\frac{1}{\lambda^2}+4\pi i\omega\sigma'\right)E.$$

Therefore

$$E = E_0 e^{-kx},$$

where

$$k = \frac{1}{\lambda}\{\sqrt{[\tfrac{1}{2}(m+1)]}+i\sqrt{[\tfrac{1}{2}(m-1)]}\}, \tag{2}$$

$$m = \sqrt{\left(1+\frac{4\lambda^4}{\delta^4}\right)}, \tag{3}$$

$$\delta = 1/\sqrt{(2\pi\omega\sigma')}. \tag{4}$$

So far the theory is formally identical with London's, apart from a trivial difference in the definition of δ, but there is an important difference in that σ' is not simply $f_n\sigma$, as assumed by London, but is an implicit function of the solution of (2), since by the ineffectiveness concept the effective conductivity is dependent on the skin depth.

To determine σ', we put δ_s equal to the reciprocal of the real part of k, i.e.

$$\delta_s = \lambda/\sqrt{[\tfrac{1}{2}(m+1)]}. \tag{5}$$

Since $m \to 1$ when $\lambda \ll \delta$, we see that δ_s tends to become equal to λ under these conditions, i.e. at temperatures well below the transition temperature, as stated above. Now from the definition of σ', it is clearly related to the effective conductivity σ'_n in the normal state by the equation $\sigma'/\sigma'_n = f_n\delta_s/\delta_n$. Also σ' and δ are related by equation (4), and σ'_n and δ_n by a similar equation, so that we may write

$$\frac{\delta^2}{\delta_n^2} = \frac{\delta_n}{f_n\delta_s},$$

i.e. substituting from (5) and rearranging, $\delta^2 = \frac{\delta_n^3}{f_n \lambda}\sqrt{[\frac{1}{2}(m+1)]}$. δ may now be eliminated by using equation (3), so that we arrive at an equation defining m,

$$(m+1)(m^2-1) = b, \tag{6}$$

where $b = 8f_n^2\lambda^6/\delta_n^6$, and is a function of temperature.

We may now deduce the surface impedance of the superconductor, which is defined as $Z = \frac{E(0)}{\int_0^\infty J\,dx}$, i.e.

$$Z = \frac{4\pi i\omega}{k} = \frac{4\pi i\omega\lambda}{m}\left(\sqrt{[\tfrac{1}{2}(m+1)]} - i\sqrt{[\tfrac{1}{2}(m-1)]}\right)$$

from (2). Thus

$$\left.\begin{aligned} &\text{the skin resistivity } R = \frac{4\pi\omega\lambda}{m}\sqrt{[\tfrac{1}{2}(m-1)]}, \\ \text{and}\quad &\text{the skin reactance } X = \frac{4\pi\omega\lambda}{m}\sqrt{[\tfrac{1}{2}(m+1)]}. \end{aligned}\right\} \tag{7}$$

We shall evaluate these two quantities separately, since they require different treatment.

(*a*) *The skin resistivity*, R

The resistivity in the normal state, R_n, was shown in II to be equal to $2\pi\omega\delta_n$. Let us put $r = R/R_n$; then from (7),

$$r = \frac{2\lambda}{m\delta_n}\sqrt{[\tfrac{1}{2}(m-1)]}. \tag{8}$$

Combining this equation with (6) to eliminate m, and putting $\xi = 2\lambda^2/\delta_n^2 r^2$, we arrive after a certain amount of algebra at an equation defining ξ, and hence r,

$$b\xi^3 - 2(2+b)\,\xi^2 - (4+3b)\,\xi - (1+b^2) = 0. \tag{9}$$

The exact solution of this equation is too complicated to be of practical use, but for all temperatures except in the region of the transition point the last term is small compared with the others, and may be neglected.

The remaining terms then factorize, to give

$$\xi = \frac{4+3b}{b}. \tag{10}$$

The other solution is negative and does not correspond to any physical case. The error involved in neglecting the last term of (9) may be shown to be less than 2 % for values of r up to 0·5. In the interpretation of the experimental results, presented in I, it will be found that (10) is quite good enough, since r is less than 0·5 except within 0·02° of the critical temperature.

Substituting for ξ and b in (10), we obtain an explicit equation for the skin resistivity,

$$r = R/R_n = \frac{2(\lambda/\delta_n)^4 f_n}{[1+6f_n^2(\lambda/\delta_n)^6]^{\frac{1}{2}}}. \tag{11}$$

Equation (11) is the fundamental equation for the problem, based on the minimum assumptions. Before proceeding further we shall discuss these assumptions, in order to obtain a clear picture of the conditions under which the equation may be regarded as valid.

The basic postulate of the theory is that the state of the electrons in a superconductor may be regarded as being equivalent to the coexistence of two kinds of electrons, superconducting and normal. This assumption is strongly supported by thermal conductivity measurements (de Haas & Rademakers 1940), as well as by the fact that the superconducting transition is of the second kind, so that the electronic state just below the critical temperature must be very similar to that above it. It is also postulated that the superconducting and normal electrons react independently to the applied field; there is no direct evidence for this, but it is a very reasonable assumption in view of the fact that a static magnetic field excites a steady supercurrent, which would not occur if the normal electrons were coupled in any way to the superconducting electrons.

The other postulates concern the behaviour of the two kinds of electrons. The equations of F. and H. London (1935) have been assumed to govern the superconducting electrons, and the ineffectiveness concept to govern the normal electrons. It appears at first sight as if there is a logical inconsistency in this procedure, especially if we adopt a rigidly classical point of view, and regard the superconducting electrons simply as non-resistive electrons having infinite mean free paths. For if the ineffectiveness concept is justified when the mean free path is long compared with the skin depth, it ought surely to be applied to the superconducting electrons. The solution of this apparent paradox lies in the conditions under which the theory of normal electrons was treated in II. It was assumed there that the relaxation time was short compared with the period of the oscillating field, so that the problem could be regarded as quasistatic. Under these conditions it is permissible to neglect, at least to a first approximation, the influence of the magnetic field on the electron trajectories, since a static magnetic field induces no currents, although it curves the trajectories. Now the relaxation time of the superconducting electrons is infinite, so that this assumption does not apply to them. In fact, from the classical point of view, the supercurrent may be regarded as a 'transient phenomenon of infinite duration', the electrons never reaching equilibrium with the applied field. A more exact development of this idea shows that electrons with infinite mean free paths do indeed behave according to the London equations.

The time is not yet ripe for a discussion whether the London equations represent the super-current precisely. Experimental observations by Appleyard, Bristow, London & Misener (1939) and by Shoenberg (1940) suggest that slight deviations may occur, but as it is not improbable that there are factors involved in the behaviour of films and colloids which were neglected in their calculations, this evidence must be regarded with caution. Heisenberg's recent (unpublished) theory of superconductivity implies that the equations may be exact only for low current densities, but since the details of the theory have not been worked out yet, and in any case the experiments described in I were performed with current densities much smaller than the critical values, the assumption that the London equations are exact in this context is consistent with Heisenberg's theory.

The assumption most open to objection is that which concerns the ineffectiveness concept for normal electrons. It was shown in II that this concept gives a reasonably good description of the behaviour of normal metals, especially when the resistance is entirely residual, but in extending the theory to cover the case of superconductors it has been assumed that the parameter β is the same for both states. It is certain that the value of β will depend on the exact field distribution near the surface of the metal, and that it will therefore be different for a superconductor and a normal metal, but it is not possible to make an estimate of the variation of β without a rigorous solution of the problem, which as we stated before has not been accomplished yet. The possible variation of β may be included in equation (11) by multiplying f_n by a new quantity γ. The expected behaviour of γ is that it should take a constant value near, but not equal to, unity, in that range of temperatures for which r is less than (say) 5 % and that in the small temperature range within which r rises to 100 % γ should alter continuously to the value unity. For the moment, however, we shall ignore this factor.

Returning now to equation (11), we see that it involves r, λ, and δ_n which are all essentially measurable quantities, and f_n which has not yet been measured directly.

Let us put $f_s = (\lambda_0/\lambda)^2$, where λ_0 is the penetration depth at 0° K; then H. London's (1940) interpretation of f_s was that it represents the fraction of the conduction electrons which have become superconducting. f_n was interpreted as the fraction of normal electrons, so that from this point of view it seems reasonable to put $f_n + f_s = 1$. It should be remembered, however, that this is not the only possible interpretation of f_n and f_s, and that this relation between them is an assumption additional to those already discussed.

Putting $f_n = 1 - (\lambda_0/\lambda)^2$, equation (11) becomes

$$r = \frac{2\rho^2\alpha(\alpha-1)}{[1+6\rho^3\alpha(\alpha-1)^2]^{\frac{1}{2}}} \tag{12}$$

in which $\alpha = (\lambda/\lambda_0)^2, \quad \rho = (\lambda_0/\delta_n)^2.$

We shall use equation (12) eventually in interpreting the resistance measurements of I, but first we shall evaluate the skin reactance X, and show how it may be used to give independent information about λ.

(b) *The skin reactance X*

According to equation (7),

$$X = \frac{4\pi\omega\lambda}{m}\sqrt{[\tfrac{1}{2}(m+1)]}.$$

At temperatures well below the transition point, m is very nearly equal to 1, and $X = 4\pi\omega\lambda$, the value which would obtain at all temperatures if only the superconducting electrons were present. Let us now introduce and evaluate a new variable

$x = \frac{1}{m}\sqrt{[\frac{1}{2}(m+1)]}$, which represents the correction factor to be applied to allow for the presence of the normal electrons. It will be found that x is only appreciably different from unity in a small temperature range close to the transition point, so that no serious error will be introduced by putting $f_n = 1$ when evaluating the correction factor. The simplest way of evaluating x is to express it graphically as a function of r, by taking some value of λ/δ_n in equation (11) to calculate r, and by using these values of λ/δ_n and r to compute m and hence x from equation (8). The result of this calculation is shown in figure 1, from which it can be seen that X differs from $4\pi\omega\lambda$ by less than 5 % for all values of r less than 0·2. For the frequency of 1200 Mcyc./sec. used in these experiments, r is greater than 0·2 only in the temperature range within 0·05° K of the critical temperature, so that the correction factor is negligible over practically the whole of the range of measurement. The graph has not been extended beyond $r = 0{\cdot}5$, since above this value the approximations used in deriving equation (11) cease to be sufficiently accurate.

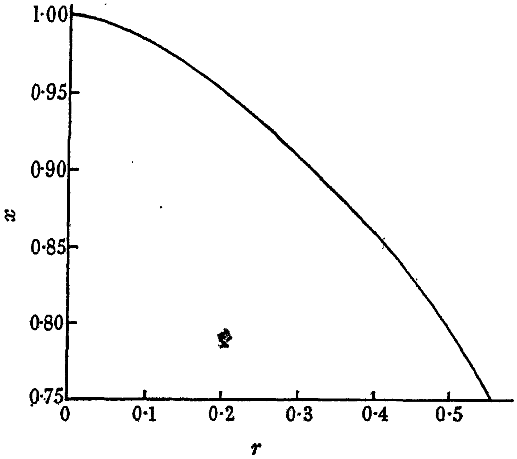

FIGURE 1. Correction factor for inductive skin depth.

It is clear that the simple relation between skin reactance and penetration depth gives a possible experimental method for determining λ, and that except near the critical temperature the value so determined will not depend on any particular theory of the behaviour of the normal electrons, since so long as $X = 4\pi\omega\lambda$, the only theoretical assumption is of the validity of the London equations. This method has been used to supplement existing data on the penetration depth, and the results of such reactance measurements on tin and mercury will be described before considering the correlation between penetration depth and resistivity.

MEASUREMENTS OF SKIN REACTANCE

The principle of the method of measuring skin reactance is based on the well-known property of high-frequency transmission lines that the velocity of a wave along the line is not quite the same as the velocity of an unbounded plane wave in the medium surrounding the line, on account of the intrinsic reactance of the conductors. It is a general theorem for transmission systems of uniform cross-section operating in the normal mode (i.e. not waveguides), that the capacity and external inductance between the lines are related by the equation $L_{\text{ext.}} C = \epsilon/c^2$, where ϵ is the dielectric constant of the medium. If $L_{\text{ext.}}$ were the only inductance of the system, i.e. if the skin impedance of the conductors were zero, the velocity of propagation of a wave on the line would be exactly given by

$$v = 1/\surd(L_{\text{ext.}} C) = c/\surd\epsilon,$$

the velocity of an unbounded plane wave in a medium of dielectric constant ϵ. However, the internal inductance, $L_{\text{int.}}$, of the conductors must be added to $L_{\text{ext.}}$, so that the velocity of propagation is in fact given by

$$v' = v(1 - L_{\text{int.}}/2L_{\text{ext.}}). \tag{13}$$

The internal inductance is directly proportional to the skin reactance for a given transmission line, as we shall see later, so that X may be calculated from the velocity of propagation. In general we may write $v - v' = BX$, where B is a constant which may be calculated from the dimensions of the transmission line.

In principle it should be possible to make an absolute determination of X by measuring the velocity of propagation absolutely. However, for ordinary transmission lines the difference between v' and v is only a few parts in ten thousand if the reactance is due to the penetration of magnetic field into a superconductor. An absolute determination of X would therefore require as elaborate an experimental arrangement as is used for the best determinations of the velocity of light. This, though not entirely impracticable, is inconvenient, but fortunately it is a much more straightforward matter to measure changes in X. Consider, for example, a resonator of the design used in I; this will resonate when the wavelength of a wave on the lines bears some numerical relationship to the dimensions of the resonator. Since a change in velocity involves a change in wavelength for a given frequency, it immediately follows that the resonant frequency depends on the velocity according to the equation $\Delta\omega_0/\omega_0 = \Delta v/v$, and that therefore a change in skin reactance may be observed as a change in resonant frequency. The technique of measuring large values of Q as described in I is essentially a technique of measuring accurately small frequency changes, and the methods of I may be taken over without modification to the present problem. There are two possible ways of determining changes in X; the simplest in principle would be to observe the variation of resonant frequency as the specimen is cooled from above its transition temperature down to the lowest temperatures attainable. This would then give the variation of X over the whole temperature range. There are, however, practical difficulties involved in this method which make it inconvenient, notably the difficulty of stabilizing the frequency of the oscillator over a long period within 1 part in 10^6, and the fact that the dielectric constant of helium vapour is by no means negligible and would have to be kept constant as the temperature changed. It was therefore decided to use the fact that superconductivity may be destroyed with a magnetic field, so that the difference between the reactances of the superconducting and the normal metal may be measured at any temperature.

The experimental determination consisted then of a measurement of the resonant frequency of a superconducting resonator of the type described in I, after which a magnetic field was applied to destroy superconductivity and the resonant frequency was again measured. To guard against frequency drift and the possibility that frozen-in magnetic field might cause serious errors, the resonant frequency was determined once more for the specimen in zero field. The resonant frequencies were of course recorded merely as settings of the fine-tuning control of the oscillator, and the difference in setting for the superconducting and normal states was reduced to a frequency difference by means of the differential wavemeter described in I. The position of the maximum resonator response was found by 'bracketing', that is, by recording the two oscillator settings at which the response had the same, non-maximum, value. Careful experiments showed that the resonance peak was accurately symmetrical, and that the determined peak position was independent of the response-level at which the bracketing was performed. During a set of readings, the helium pressure was maintained constant within 1/20 mm. Hg to minimize variations of dielectric constant.

We must now evaluate the proportionality factor between $\Delta\omega_0$ and X, and this is most simply treated by considering a parallel strip transmission line of unit width, and spacing d, in which the current is evenly distributed across the width of the strip. The external inductance per unit length of such a system is given by $L_{\text{ext.}} = 4\pi d$, and to this must be added twice the internal inductance per unit length, since there are two conductors. We have therefore that $L = L_{\text{ext.}} + L_{\text{int.}} = 4\pi d + 2X/\omega$, since $X = \omega L_{\text{int.}}$. Now L is the same as the external inductance of a strip transmission line of separation d' given by $4\pi d' = 4\pi d + 2X/\omega$. The presence of the skin reactance may therefore be introduced formally in calculating the inductance by shifting each conductor back through a distance $\delta' = X/4\pi\omega$. δ' is clearly the effective depth of penetration of current into the conductor, and it will be referred to as the 'inductive skin depth'. In calculating the capacity between the lines we must leave the conductors in their undisplaced positions, since the charge is carried wholly on the surface, both in normal conductors and superconductors (see London 1936).

Considering now the screened parallel wire transmission line used in the measurements, we may apply the idea of an inductive skin depth to evaluate the velocity of propagation. In such a line the current is not evenly distributed over the surfaces of the conductors, but since the line is operating in a normal mode, the current and fields bear a constant proportion to one another at all points on the surface. The contribution of any element of the surface to the internal inductance is then proportional to the magnitude of the surface current density at that point, and without considering the problem in any greater detail we may allow for the skin reactance by reducing the radius of each conductor by an amount δ' when calculating the external inductance. This procedure automatically takes account of the variations of current over the surface of the conductors. Expressed mathematically, if $L_{\text{ext.}} = L(a, b, s)$

where a is the radius of the wires, b the separation of their axes and s the radius of the screen, we may write

$$L_{\text{int.}} = -\left(\frac{\partial L}{\partial a}\right)_{b,s} \delta'.$$

Therefore, from (13), $$\frac{v'-v}{v} = +\frac{\delta'}{2L}\left(\frac{\partial L}{\partial a}\right)_{b,s}.$$

If when a magnetic field is applied to destroy superconductivity, δ' changes by an amount $\Delta\delta'$, the change in resonant frequency is given by

$$\frac{\Delta\omega_0}{\omega_0} = \frac{\Delta v'}{v} = \frac{\Delta\delta'}{2L}\left(\frac{\partial L}{\partial a}\right)_{b,s}. \tag{14}$$

For the transmission line under consideration, an exact formula for L is very complicated. However, a sufficiently precise approximation has been given by Breisig (1924),

$$L = A\cosh^{-1}\left\{\frac{1}{x}\frac{1-y^2(1-x^2)}{1+y^2(1-x^2)}\right\},$$

where $x = 2a/b$, $y = b/2s$, and A is a constant whose value need not concern us. Substituting in equation (14), and neglecting all terms in y of higher order than y^2, we have

$$\frac{\Delta\omega_0}{\omega_0} = \frac{1-2x^2y^2}{x\sqrt{(1-x^2)}\cosh^{-1}\left\{\frac{1}{x}\frac{1-y^2(1-x^2)}{1+y^2(1-x^2)}\right\}}\frac{\Delta\delta'}{b}. \tag{15}$$

In the resonator used in these experiments the diameter of the screen, $2s = 2{\cdot}6$ cm., and the spacing of the conductors $b \sim 0{\cdot}3$ cm. Putting $y = 0{\cdot}116$ in (15), a numerical calculation shows that the first part of the expression on the right-hand side has a very flat minimum at $x = 0{\cdot}442$, at which (15) becomes,

$$\frac{\Delta\omega_0}{\omega_0} = 1{\cdot}761\frac{\Delta\delta'}{b}. \tag{16}$$

Although from the point of view of accurate measurements this minimum is the least convenient working point, since a given change of skin depth produces here the smallest change in resonant frequency, such a disadvantage is altogether outweighed by the advantages of working at a turning-point, where, provided the spacing b is constant along the line, small variations in the diameter of the wires do not affect the value of the numerical constant. The wires were therefore chosen so that x took a value near 0·442. The change in resonant frequency could be determined with an accuracy of 1 kcyc./sec., so that from (16) the measurement of $\Delta\delta'$ was subject to an error of approximately $\pm 0{\cdot}17 \times 10^{-6}$ cm., which is less than 1 % of the largest measured values of $\Delta\delta'$.

We have seen that the inductive skin depth and the skin reactance are related by the equation $X = 4\pi\omega\delta'$. In certain special cases δ' may be simply related to some characteristic parameter which has the dimensions of a length. For example, in a superconductor well below the transition temperature X was shown to be equal to

$4\pi\omega\lambda$, in accordance with the London equations, so that δ' and λ are equal. In general for a superconductor, $X = 4\pi\omega x\lambda$, so that $\delta' = x\lambda$, where x is the function plotted in figure 1. For a normal metal obeying the classical skin effect equations, $X = R = 2\pi\omega\delta$, where δ is the resistive skin depth $1/\surd(2\pi\omega\sigma)$; the inductive skin depth here is thus equal to one-half of the resistive skin depth. It would be very useful to know the connexion between δ and δ' for the general case of a normal metal, for which the classical theory does not hold, as discussed in II, for it would then be possible from the measurements of $\Delta\delta'$ to calculate the superconducting penetration depth absolutely. It was shown in II that the qualitative picture of the anomalous skin effect based on the ineffectiveness concept leads to equations similar to the classical equations, except that σ must be replaced by another real quantity. This means that for this case too δ' should equal $\delta/2$. It was pointed out there, however, that there is reason to suppose the reactive part of the skin impedance to be underestimated in this treatment, and this prediction is borne out in practice, as will be seen when the results of the measurements are discussed.

Measurements were made on specimens of mercury and tin, which will be considered separately. The mercury specimen was of the design illustrated in figure 2 of I, having two slightly tapering silica tubes of mean diameter 0·123 mm. whose axes were accurately parallel and 0·37 cm. apart. The measured values of $\Delta\delta'$ as a function of temperature are shown as curve 1 in figure 2. It is not possible to compare this directly with determinations by Shoenberg (1940) and Désirant & Shoenberg (1947) of the superconducting penetration depth λ, since the skin resistivity and hence presumably the skin reactance of normal mercury vary with temperature between 4·2 and 2·0° K. However, assuming Shoenberg's curve for λ to be correct, it is possible to deduce the inductive skin depth δ_n' in normal mercury as a function of temperature. Curve 2 in figure 2 is taken from Shoenberg's data, assuming the value of λ at 2·2° K to be $7{\cdot}5 \times 10^{-6}$ cm., which is consistent with his measurements. Now Shoenberg measured λ directly, while, as was pointed out above, the present measurements are of $x\lambda$, where x is the function plotted in figure 1. This correction factor x has been applied in constructing curve 2; the dotted line is Shoenberg's curve, from which it can be seen how very small is the correction which takes account of the presence of the normal electrons. Curve 2, in fact, is what one would expect to observe in an absolute measurement of the inductive skin depth δ_s' at 1200 Mcyc./sec., if such an experiment were feasible. Curve 3 is the sum of curves 1 and 2, and represents therefore the normal inductive skin depth δ_n'. Curve 4 shows the resistive skin depth in normal mercury, calculated from the data in II on the basis of the formulae developed there by use of the ineffectiveness concept, from which it may be seen that the ratio of δ_n' to δ_n is greater than the value $\frac{1}{2}$ predicted by classical theory and by the simplified theory of II, as was mentioned above. As the temperature is lowered the reactance decreases more slowly than the resistivity, the ratio δ_n'/δ_n being 0·74 at 4° K and 0·81 at 2·2° K. Without a much more comprehensive theory of normal metals than is at present available it is impossible to say whether these results indicate good agreement between the various methods of determining the penetration depth in the superconductor, but at any rate the similarity in shape of curves 3 and 4 is encouraging evidence of the consistency of the measurements. By assuming various values of $\lambda_{2\cdot 2^\circ \mathrm{K}}$ in constructing curves similar to curve 2, in order to see how this would affect the smoothness of curve 3, it was concluded that $\lambda_{2\cdot 2^\circ \mathrm{K}}$ almost certainly lies between 7 and 8×10^{-6} cm., in good agreement with the estimate of Désirant & Shoenberg (1947).

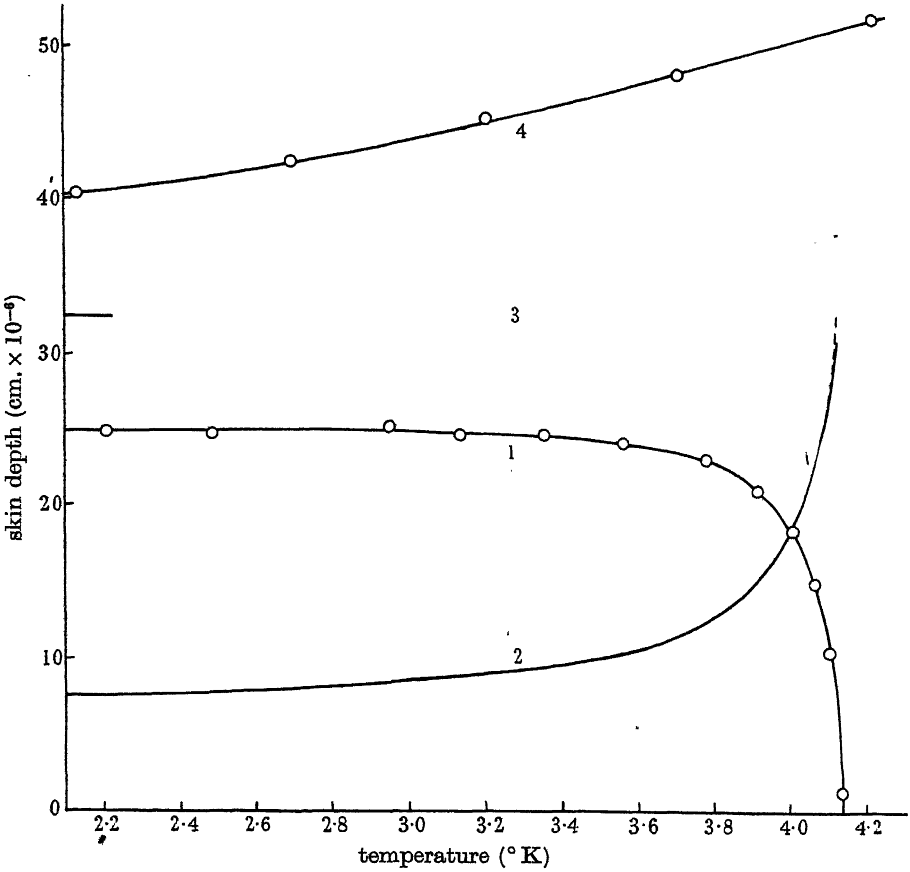

FIGURE 2. Skin depths in mercury.

The measurements on tin were made with a wire of mean diameter 0·147 cm. bent into a loop of mean spacing 0·314 cm. The tin was from the same Johnson-Matthey sample as was used in I. The interpretation of the results for $\Delta\delta'$ is less troublesome than with mercury, since throughout the temperature range the d.c. conductivity of the specimen was constant. It may safely be assumed therefore that δ'_n was constant, and the values of $\Delta\delta'$ represent directly the variation of δ'_s with temperature. The results are shown in figure 3, in which the full curve includes the correction factor x to allow for the normal electrons. Since these results represent the first direct measurements on the penetration depth in tin, values of $(\lambda - \lambda_{2\cdot 3^\circ})$ are also given in table 1, which has been constructed from the full curve of figure 3, and which therefore contains the correction factor x.

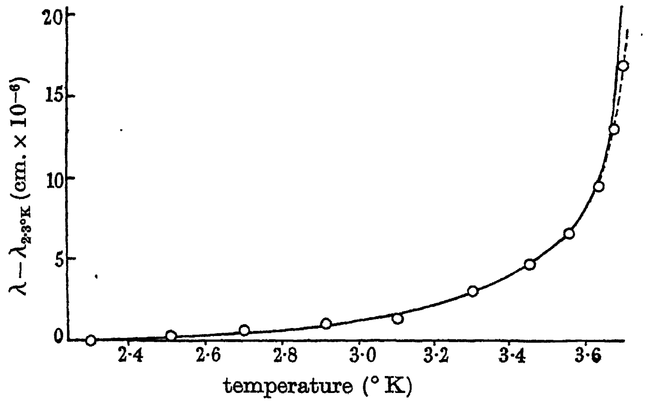

FIGURE 3. Penetration depth in tin.
- - - Measured values, — corrected for effect of normal electrons.

TABLE 1. $(\lambda - \lambda_{2\cdot 3^\circ})$ FOR TIN

T (° K)	$\lambda - \lambda_{2\cdot 3^\circ}$ (× 10^{-6} cm.)	T (° K)	$\lambda - \lambda_{2\cdot 3^\circ}$ (× 10^{-6} cm.)
2·3	0·0	3·3	2·8
2·5	0·2	3·4	4·0
2·7	0·5	3·5	5·6
2·9	0·9	3·6	8·4
3·0	1·1	3·65	12·0
3·1	1·5	3·68	19
3·2	2·1	3·71	∞

CORRELATION OF RESISTIVITY AND PENETRATION DEPTH

The foregoing measurements on the skin reactance serve as a satisfactory check on the accuracy of Shoenberg's (1940) curve for the penetration depth in mercury, and also enable λ_0 to be estimated as $7\cdot 1 \times 10^{-6}$ cm. This value of λ_0 may be used in applying equation (12) to the experimental measurements of the resistivity which were presented in I, to deduce the variation of λ with temperature. A comparison of curves for the penetration depth derived from the resistivity and by the direct method of Shoenberg would enable the validity of the assumptions used in deriving (12) to be tested. It is unfortunate from this point of view that the behaviour of normal mercury does not agree with the theoretical treatment in II, in that the skin resistivity does not tend to a constant value as the mean free path increases. It is therefore difficult to decide on the value to be given to δ_n in equation (12). The most reasonable way of overcoming this obstacle is to assume that the ineffectiveness concept is correct when applied at any given temperature to determine the difference in effective conductivity between the normal and superconducting states, but that there is some inexactness in the theory which prevents it from describing the true behaviour of the normal metal as the temperature is altered. If this is so, the variation of δ_n may be allowed for simply by inserting the appropriate value at each temperature, so that ρ becomes now a function of temperature. The penetration depth may now be calculated directly from r, to give the curve shown in figure 4. Shoenberg's curve is also shown for comparison, as well as the curve calculated from the resistivity data using London's (1940) formula. It is clear from these curves that equation (12) gives a qualitative description of the process, and the agreement is best at temperatures near the transition point, while London's equation diverges at higher temperatures but is better than equation (12) around 2° K. The most probable explanation of the disagreement between theory and experiment lies in the neglect of the factor γ in extending the ineffectiveness concept to cover superconductors. It should, however, be borne in mind that the assumption $f_n + f_s = 1$, which was used in deriving equation (12) from equation (11), cannot be justified without a detailed theory of superconductivity.

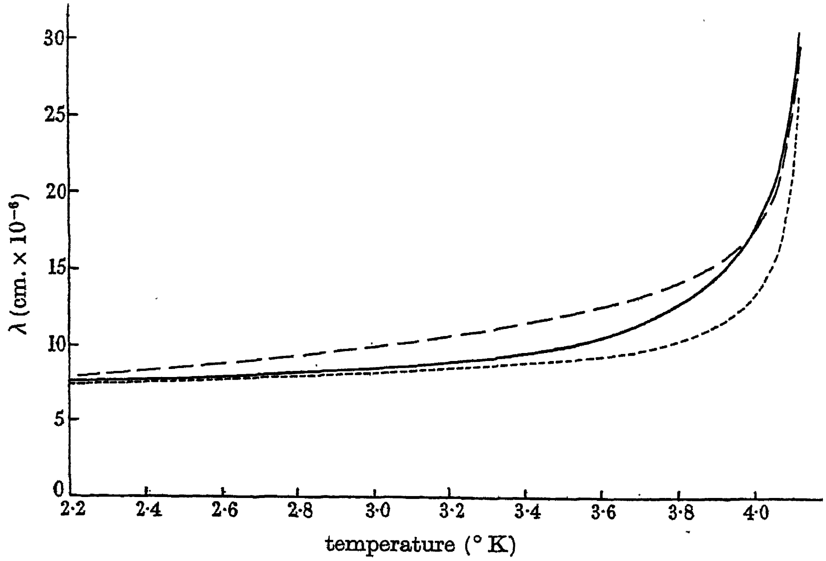

FIGURE 4. Penetration depth in mercury estimated from r.f. resistivity. —— Shoenberg's (1940) measurements, – – – from resistivity, using theory in text, - - - - from resistivity, using London's (1940) theory.

The foundations of such a theory have recently been laid by Heisenberg (unpublished), and it is interesting to speculate on the interpretation of the quantities f_n and f_s in this theory. Heisenberg has shown how the Coulomb interaction between the conduction electrons may lead at low temperatures to a thermodynamically more favourable state in which the electrons at the top of the Fermi distribution are formed into wave-packets which may be propagated through the metal without resistance, and may therefore be regarded as superconducting electrons. It seems likely that as the absolute zero is approached more and more electrons will undergo this 'condensation', but that even at 0° K not all the conduction electrons will be superconducting. This does not mean, however, that the normal conductivity will persist at all temperatures, since the condensed wave-packets must occupy regions at the surface of the electron distribution in phase space, and render these regions inaccessible to the uncondensed normal electrons through the operation of Pauli's Exclusion Principle.

Let us suppose that a fraction f_0 of the conduction electrons forms into wave-packets at the absolute zero, and a fraction f_1 at any other temperature T; moreover let us assume that the form of the wave-packets is independent of temperature; then it seems very probable that the change of penetration depth between 0 and T° K will be given by exactly the same expression as if the electrons were classical electrons, i.e.

$$\left(\frac{\lambda_0}{\lambda}\right)^2 = \frac{f_1}{f_0} = f_s,$$

by the definition of f_s above. In applying similar qualitative considerations to the normal electrons it is necessary to postulate that at the absolute zero the wave-packets are distributed over the whole surface of the Fermi distribution, so that the normal electrons are prevented from making any transitions to higher states. This postulate ensures that the normal conductivity will vanish at 0° K, as evidenced by the vanishing of the r.f. resistivity of mercury. It also provides an explanation for the absence of a linear term in the specific heat of superconducting tin (Keesom & van Laer (1938)). It is now natural to interpret f_s as the fraction of the surface in phase space which is covered by wave-packets and therefore inaccessible to the normal electrons. The normal conductivity will thus be reduced to a value $(1-f_s)$ as great as its value in the normal state, and we arrive by this argument at the expression $f_n+f_s = 1$, which was used above to derive equation (12).

One incidental advantage of this theory, compared with former theories, is that it makes possible a qualitative explanation of the experimental result that λ_0 is several times larger than would be expected if all the electrons became superconducting, although it must be pointed out that the value of $f_0 \sim 0{\cdot}05$ electrons per atom, deduced by Appleyard *et al.* (1939) from their estimate of λ_0 in mercury, is much greater than the value of 10^{-4} envisaged by Heisenberg, who considers the condensation to affect only the electrons at the very top of the Fermi distribution. This value of 10^{-4} is, however, not based on any precise calculation, and it seems not unlikely that a development of the theory to include the interactions between electrons occupying lower energy levels, such as has not yet been given and would be of extreme mathematical complexity, would show that the stable state at the absolute zero is one in which a much larger proportion of the conduction electrons condense into wave-packets. If this is so, the theory gives a rather satisfactory picture of the mechanism of superconductivity, and explains qualitatively how the sum of f_n and f_s may still be unity while neither quantity represents the actual proportion of electrons in each state.

The correlation of the penetration depth and resistivity measurements in tin is rendered uncertain by the absence of any value for λ_0, as well as by the experimental evidence that the resistivity does not tend to zero as the absolute zero is approached. Since the measurements of Keesom & van Laer (1938) show that superconducting tin contains no linear term in its specific heat, the evidence is very strong that f_n tends to zero at low temperatures. If this is so, the finite value of r must be due to some other effect, and it will be assumed that this effect (whether real or due to experimental uncertainties) is constant with changing temperature, and may be allowed for by subtracting 0·55 from all the figures in table 2 of I. In performing the correlation of r with λ using equation (12), several different values of λ_0 were assumed, and for each value a curve showing the variation of λ with temperature was calculated from the resistivity data. The best agreement with the curve of figure 3 was obtained when $\lambda_0 = 7{\cdot}5 \times 10^{-6}$ cm., and the results of the calculation are shown in figure 5. The agreement is much better than for mercury, where more data was available, and it may be largely fortuitous, depending on the appropriate choice for λ_0. It would therefore be unwise to regard this agreement as confirming the theory until the assumed value of λ_0 can be checked by an absolute measurement.

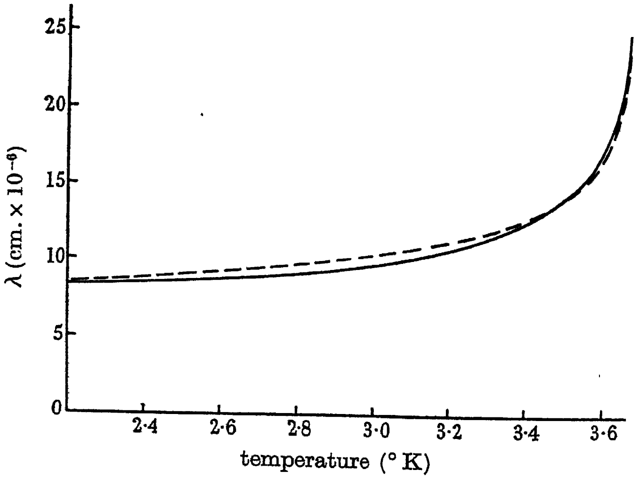

FIGURE 5. Penetration depth in tin, estimated from r.f. resistivity and reactance. —— From reactance, - - - from resistivity.

I should like to express my gratitude to Dr D. Shoenberg for his continual interest and helpful advice throughout these experiments, and to Mr E. R. Andrew for his measurements of all the d.c. conductivities mentioned in these papers. I have also benefited greatly from many discussions of the theory with Mr E. H. Sondheimer and Mr R. B. Dingle. My thanks are due to the Chief Superintendent, R.R.D.E., Malvern, for the loan of apparatus.

The greater part of this work was carried out during the tenure of a Stokes Studentship at Pembroke College, Cambridge.

REFERENCES

Appleyard, E. T. S., Bristow, J. R., London, H. & Misener, A. D. 1939 *Proc. Roy. Soc.* A, **172**, 540.

Breisig, F. 1924 *Theoretische Telegraphie*, 2nd ed. p. 68. Braunschweig.

Désirant, M. & Shoenberg, D. 1947 *Nature*, **159**, 201.

de Haas, W. J. & Rademakers, A. 1940 *Physica*, **7**, 992.

Keesom, W. H. & van Laer, P. H. 1938 *Physica*, **5**, 193.

London, F. & London, H. 1935 *Proc. Roy. Soc.* A, **149**, 71.

London, H. 1936 *Proc. Roy. Soc.* A, **155**, 102.

London, H. 1940 *Proc. Roy. Soc.* A, **176**, 522.

Shoenberg, D. 1940 *Proc. Roy. Soc.* A, **175**, 49.

The Research Laboratories of the General Electric Company

BY SIR CLIFFORD C. PATERSON, F.R.S., *Director of the Laboratories*

(*Lecture delivered* 1 *May* 1947—*Received* 6 *May* 1947)

[PLATE 20]

The lecturer introduced his subject by showing lantern slides illustrating the buildings of the laboratories; also certain processes and tests in progress in various departments.

I am glad of this opportunity to indicate the objectives and the *modus operandi* of the laboratories of which I have been Director since their foundation in 1919. Such a study may raise, I hope, in the minds of some of us, the question of what should be the objectives of research when attached to productive industry—remembering that the rate at which efficient and ordered manufacturing industry can digest new diets of innovations and novel products is inevitably limited, much more limited I think than is usually appreciated by those who are not themselves engaged in productive industry.

The staff engaged at these laboratories now totals rather over 1000. As the establishment is entirely self-contained, that number has to include all essential service personnel in addition to the professional scientific and engineering staffs. These latter number about 250. Physicists and engineers predominate in numbers over the chemists, metallurgists and glass technologists. There are also some 100 young men who are going through their professional training with us in science and in research, and working for B.Sc. degrees or Higher National Certificate qualifications on a part-time basis. Whilst they are passing through this stage they constitute our junior technical staff, to merge in time (or most of them) into the fully qualified research staff. There are, among the total number, 160 skilled craftsmen of all trades who are as much 'on the staff' (with equal staff status) as the professional personnel. We started in 1919 with a staff of about thirty and have grown to these numbers at a fairly even rate over 27 years.

OBJECTIVES OF THE RESEARCH LABORATORIES

Now as to our objects. I would like to dwell upon these, for it was the subject of no little discussion at the start, and I am glad to say there was then no difference of opinion, nor has there been since.

The laboratories have had three main functions.

(*a*) The first and most important is to give scientific service to the factories and departments of the Company.

(*b*) Secondly, from the intimate experience so gained with these factories and departments, to draw inspiration to formulate and carry out such longer-term researches as in the opinion of the laboratory staff will ultimately benefit their industry.

(c) Thirdly, to join in any outside activities in which an industrial scientific staff can help the professional life of the community.

The essential fact I would like you to note is that (i) the starting-point for the grouping of the research work within the laboratories, (ii) the number of men devoted to any field of work, and (iii) especially the organizational link with factories and departments of the company we serve, are based upon the requirement of giving them scientific service in all the ways in which an up-to-date laboratory can help them.

One of these ways (covered by the second objective) is of course to watch all trends and prosecute a certain number of long-term researches which seem likely to lead to outstanding additions to knowledge or drastic changes in technology. This latter function is of course very important, but it is not in fact the primary one for which our laboratories exist.

I believe this is of interest because it seems to be a reversal of the more usual set up. Under this an industrial research laboratory is designed to keep all its thoughts and intentions upon investigations which will lead to new processes and products. The giving of scientific service to existing industry is hardly part of the design: it becomes an incidental duty which is regarded as tending to interfere with its principal and more fundamental functions.

At first sight this difference of objective may appear doctrinaire, but in fact it vitally affects the structure and outlook of the scientific side of the electrical industry so far as my Company's part of it is concerned. I think I can also establish that the scientific approach to an industry, through an intimate knowledge of its existing products and processes, forms the most effective of all vantage points from which to get inspiration for the right sort of long-term as well as short-term researches. There are always so many investigations which can be attempted—so many temptations to unnecessary and ineffective experiment—that the choice of what to do can be a difficult matter unless dictated by first-hand intimate knowledge of the manufacture in question, in all its aspects.

In the days when it was necessary to commend to industrialists the importance of scientific research, I used to reckon that the expensive things they were persuaded not to undertake, went a long way to meeting the cost of my establishment. That is I know a common experience with many of us, but we sometimes forget it in assessing our contribution to industry.

Before I explain by examples how this works out I must just indicate the scope of the factory production units and the like which we exist to serve.

THE GENERAL ELECTRIC COMPANY

The total personnel in the General Electric Company is about 50,000. It was about half this size when we started, but its main units already existed then. Its motto has been 'everything electrical' so you will expect a wide scope of effort.

The factories we were to serve were autonomous establishments widely separated geographically:

A steam turbine and heavy mechanical engineering works at Erith.

An electric cable works at Southampton.

Electrical Engineering Works for heavy rotating machinery, transformers, switchgear and rectifiers, as well as light electrical engineering plant, at Witton, Birmingham.

Electric lamps, radio valves and glass, London.

Measuring instruments and apparatus at Salford and Birmingham.

Telephone and radio works at Coventry.

Electro-medical works in London.

Electrical appliances (household and industrial) at Birmingham.

Carbon and battery works, Birmingham.

Central Sales Department in London with Sales Branches in most large cities.

A number of smaller factories for subsidiary products.

It might have been a baffling matter in 1919 to know how to begin, had it not been for the definite principle of approach which I have indicated plus the urgent request from the management to concentrate attention first on electric lamps and their utilization.

FACTORY COLLABORATION

So you see us starting as a group of industrially raw but enthusiastic scientists approaching a factory staff who had long experience and were justly proud of their production skills and achievements. This was an inflammable situation in which success depended as much on a study of human nature as upon grasping the technical nature of the problems and upon learning the processes.

The problem of welding two such staffs into what is in effect a single team is in my view the essence of successful industrial research and does much to determine the form of the internal organization of the laboratory. It is a battle which is never finally won and the price of its continuance is eternal vigilance.

I have dwelt on this because the same battle has to be fought in every factory with which we collaborate. Almost invariably it falls to the lot of the laboratories to lay siege to the good-will of the factory production staffs at all levels. It is indeed an essential and most beneficial part of the training of the laboratory staff to do so—and ultimately to learn that it must not be one of their objectives to show the factory managements how clever their research people are.

STAFF STRUCTURE

So, in the internal structure of the Laboratories there must be a distinct group of workers with a group leader for each factory or each important section of a factory (or technical Department) of the Company. There are thirty-four of such laboratory groups, the membership of which varies from say three to twenty qualified people each. With us the individuals in the groups are mostly physicists, engineers and chemists.

We have in addition the following strong service groups which are at everyone's disposition: analytical chemists, metallurgists, X-ray workers and spectroscopists, mechanical engineers, glass technologists, and statisticians.

These, who constitute about 10 % of the scientific staff, are at the service of any of the groups working with the factories, and join in their specific researches as required.

The whole set-up is flexible and somewhat informal—partly because there is no apostolic succession of conferred authority or status or staff grades of seniority. Some thirty of the most respected members of the scientific staff are designated Leading Staff. That is the only discrimination in staff status. But the leadership referred to in this case is intellectual and also a matter of character. It is not administrative. Whilst therefore it carries its inevitable moral responsibility it bears no conferred authority. Group Leaders are not necessarily members of the Leading Staff—nor are members of the Leading Staff necessarily Group Leaders.

I must not pursue further the subject of internal staff organization—which, however, I myself find of absorbing interest. I only bring it into this description of the place in order to indicate how we manage to have some thirty-four separate groups nominally responsible to the Director.

The guidance of the work of any group under its group leader is much assisted by the attendance of its members at regular meetings with their opposite numbers from the factory (or technical department) which the group serves. At these meetings the status of products and processes is discussed from the technical and marketing standpoints. These meetings are interlocking and advisory in their character and have no authority actually to direct development or research.

This structure of interlocking meetings was a matter of gradual growth. It derives its standing from the recognition and support of the Chairman and Managing Directors of the Company—an important proviso.

PUBLICATION

From the beginning, publication of the scientific aspects of the work of the laboratories has been pressed. Papers are nominally communications from the scientific staff as a whole, under the authorship of the individuals who have been mainly responsible for the experimental work. The technical aspects of the work are also published where they are likely to be of general interest, but the publication of the technical 'know-how' of processes is as a rule reserved.

It follows that, if a competitor has a well-staffed research establishment of his own, he will be able to derive assistance from studying our scientific publications, and we his; but if he is one of those who merely seeks to trade on other people's work, by cadging information so that he can set up manufacture on empirical lines but making no contribution to knowledge himself, we try not to help him.

There have so far been some 100 major publications to the learned societies, and there is no impediment to joint authorship with staff from outside research establishments.

The policy lying behind this is not merely a philanthropic one. It brings of course its own rewards, one of which is that no research staff can be healthy if it works under a ban on reasonable publication.

TRY-OUT UNITS

As the practical outcome of much of the work must show itself in better or cheaper products for the market, the test of every new development to this end ultimately lies in the making of something. It is necessary therefore for some of the groups to have nucleus production facilities with personnel whom they have trained in the particular skills required (after learning them themselves). These units are located within the laboratories in close proximity to those research workers who guide them and use them.

It has sometimes been a hard battle to persuade a factory production staff that amateurs (particularly scientific ones) can make any useful contributions by trying to produce articles themselves. I think this battle was finally won during the war. In 1940 it was obvious that there was no one ready or able to make the many types of radio valve developed for centimetric radar and the like. So we greatly intensified our amateur efforts. We called our little groups pre-production units and expanded them to the utmost till the number of their personnel reached 700. There were many tears and much perspiration, but we mastered the production problems of each new type of valve as it emerged from the research stage, and by the end of the war had made in the laboratory 360,000 valves of forty-eight types at a cost of 1½ million pounds.

I think the factor which is often overlooked is the very great educative influence which the effort required actually to produce articles has on a scientific staff. The mere making of an article or demonstration of a process can be a relatively small matter compared with putting it into efficient and uniform production whether by unskilled, and maybe unsympathetic, human effort or by skilled and complicated mechanical agencies.

In industry uniformity is a gauge of quality; but the achievement of uniformity presents major problems where every operation has a Gaussian distribution of variability, the causes of which must be found and defined, and where hundreds of such operations and components go to the make-up of the product. Herein lies one of the largest single sources of the research problems which force themselves upon the attention of such a laboratory as ours.

As you will imagine, the solution of many of them requires prolonged research, using the best available resources in the way of equipment. They constantly lead to most interesting investigations, which I hope I may now exemplify.

Example 1. *Glass and refractories*

Glass

Take, as my first example, the field of glass. We first met glass in the making of bulbs for electric lamps. These bulbs are delivered from the glass factory to the lamp factory as open ended envelopes which are then assembled with the other components on somewhat intricate machines. These melt or soften the glass at the right points by means of gas flames. Each bulb follows the previous one through the automatic machine at the shortest possible time interval needed for the melting of the glass and its manipulation. There is no chance of hand control. The timing of the operational sequences of the machine is remorselessly uniform. Thus the amount of heat applied, and the behaviour of the glass under the heat must be very uniform indeed or chaos results.

By skill in empirical operation the factory were managing to use as few as 125 bulbs for 100 good lamps. Was there anything we as research men ought to do to reduce the wastage? We undertook of course a comprehensive study of the influence of the various constituents of the glass on its viscosity over the required temperature range. It was a long road involving continuous work and study in the glass factory. In the end we reached an efficiency of 104 bulbs for 100 good lamps.

The softening point is only one factor in glass quality. The coefficient of expansion is another—ensuring that it shall seal on to other glasses without strain or with the designed amount of strain either in tension or compression. Then there are the wetting properties when sealing to metals and alloys—also the electrical conductivity where the design of the lamp requires that parts of the glass must operate at relatively high temperatures. Over the past 25 years the study of these things has led to the design of glasses for electronic devices which respond to very exacting demands, and without which the devices would not be practicable.

The composition of glasses may involve eight constituents, each having its influence upon the characteristics.

Refractories

It is well known, however, that the art of making good glass is wrapped up with the art of making good refractories in which to melt the glass: molten glass is chemically one of the most active materials—it will attack most things. Therefore, if uniform glass of known characteristics is needed, a grasp of the science and art of refractory manufacture is essential.

The problems of refractories are always with us for they are stimulated by the constant urge to produce special glasses, which are uniform and not subject to disastrous wastage. May I give one example from the work of my colleague Dr Partridge?

By X-ray and other studies we are finding that fire-clay refractory materials consist of crystals of mullite and silica set in a glassy matrix. It would seem clear that their properties at high temperatures must be influenced by the viscosity of this glassy cement. Indeed we find that the behaviour of all kinds of refractory materials at high temperatures can be understood more readily by considering them from this point of view.

Figure 1, plate 20, shows a large fire-clay crucible run at a temperature of over 1400° C. It collapses like this through weakness after a short life under the fluid pressure of the molten glass inside. Curve A in figure 2 shows the result of high temperature creep tests on this refractory and confirms its weakness.

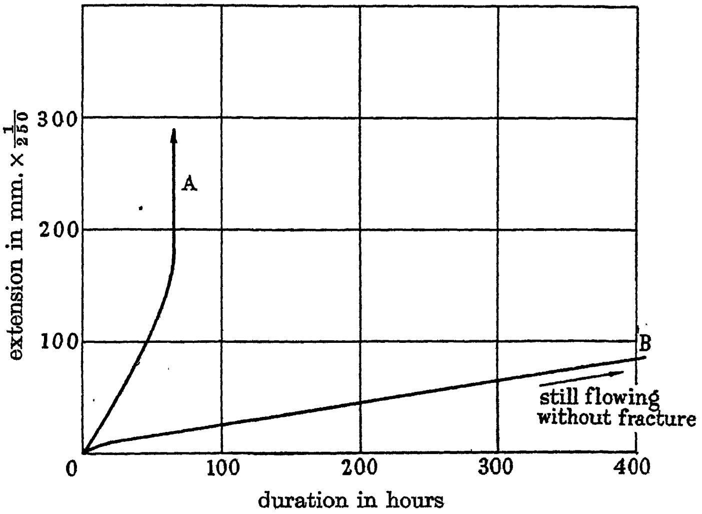

Figure 2. High temperatures creep tests of pot clays.

We have found that the eutectic mixture (i.e. the mixture of lowest melting-point) in the silica-alumina system is actually a glass. This is significant because this eutectic mixture is present in all fire-clay refractories.

When pure it is a very good glass and was the basis of a special glass we developed during the war for seals in silica valves; its melting-point was about 2000° C.

Unfortunately other oxides present in the fire-clay, such as alkalis, iron oxide and magnesia, combine with this matrix glass to render it more fusible and mobile. Guided by this a search for other clays has yielded a refractory whose creep characteristics are represented by curve B of figure 2 and the pot which results is shown in figure 3, plate 20, after a long life. Incidentally, the average life of the pots is now increased three times.

Following the same line of investigation, figure 4, plate 20, shows a photograph of the inside wall of a glass tank which has been operating for many months with 80 tons of molten glass. A tank costs thousands of pounds to put out of action and rebuild. You can see the general corrosion which has been going on. Observe especially the row of white blocks about 12 in. high on the left side of the picture. Refractory blocks of this shape originally extended along to the right-hand side—but here they have been simply eaten away and have gone into the glass and contaminated it. The blocks on the left were made from the new purer refractory, which contained less of the glassy phase. These have now been generally adopted and the tank life has been lengthened greatly as a result.

It is not practical politics to make well-intentioned guess-work changes in the design and materials of these great tanks. The loss of too much money is involved in a bad shot. Anyway, if anyone makes a mistake it must not be the scientist. Therefore all the resources of the research laboratory must be invoked to establish the soundness of a proposed change before making it, and the technical staff of the factory also have to be persuaded by our arguments. Investigations to this end usually take years before practical trial is made, and even then the results cannot be established for another two years or so.

Opal glass

Opal glass is used to diffuse the light from electric lamps and to obscure the intensely bright filament. The opacity was an empirical matter resulting from the precipitation of some constituent from clear glass as it cooled from the molten state.

Measurements showed that the diffusing power and the loss of light by absorption varied greatly in different opal glasses. There was much argument about the nature of the precipitated particles which caused the scattering of the light. X-ray powder photographs showed us that they were, in fact, minute particles of calcium or sodium fluoride, or both. The particles are normally spherical but occasional brittleness of the glass was found to be associated with the development of sharp angular crystals. Another important result emerged from a mathematical investigation. This showed that, consistent with satisfactory diffusion, the size of the particles was critical for low absorption.

These studies of the fundamentals enabled a more efficient opal glass to be made and, more important, enabled consistent results to be achieved in the glass works. All that was 15 or 20 years ago.

One research of course often suggests another in some surprisingly different field. Thus, in 1940, when the practicability of centimetric radar was under active discussion, Ryde (remembering his earlier work on opal glasses) developed the analogous theory of the absorption and scattering of very short radio waves by rain and similar meteorological phenomena. This was followed by detailed numerical predictions of the attenuation and the magnitude of the radar echoes to be expected at different wave-lengths in the centimetre band. These provided much needed information at a critical time when actual measurements of the effects were out of the question. So much for my examples from glass.

Example 2. *Filament lamps*

One of the research objectives stimulated by intimacy with the processes of lamp manufacture was the improvement of the efficiency of the lamp as a light giver. This could be effected by many details of (*a*) tungsten wire processing, (*b*) filament coiling, (*c*) gas-filling and (*d*) glass making. The immediate incentive to improved

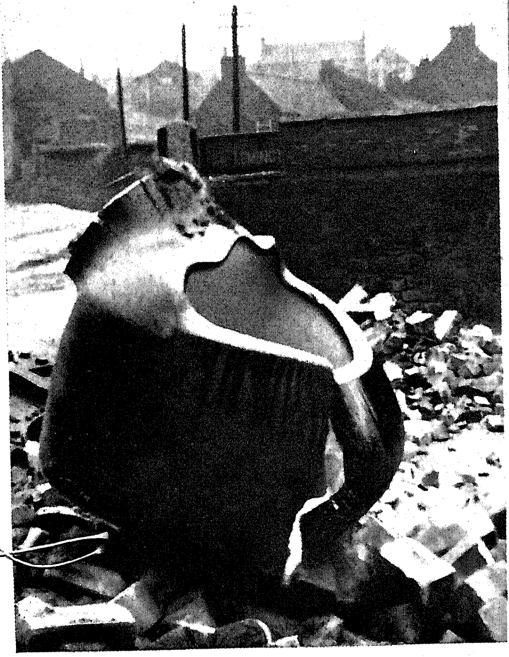

FIGURE 1

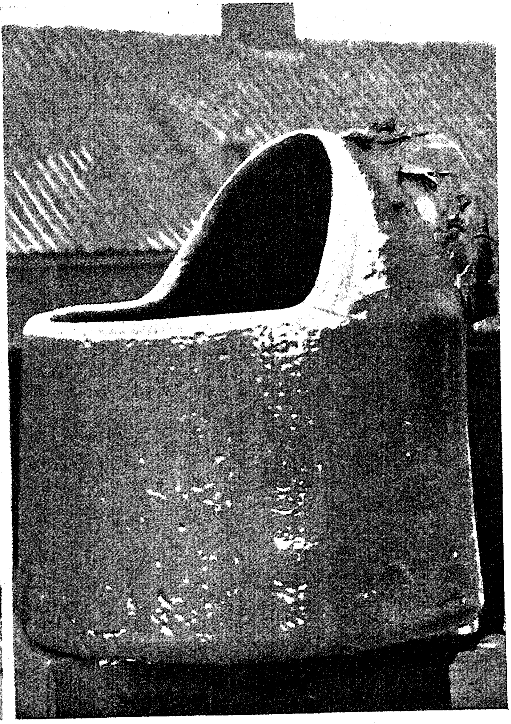

FIGURE 3

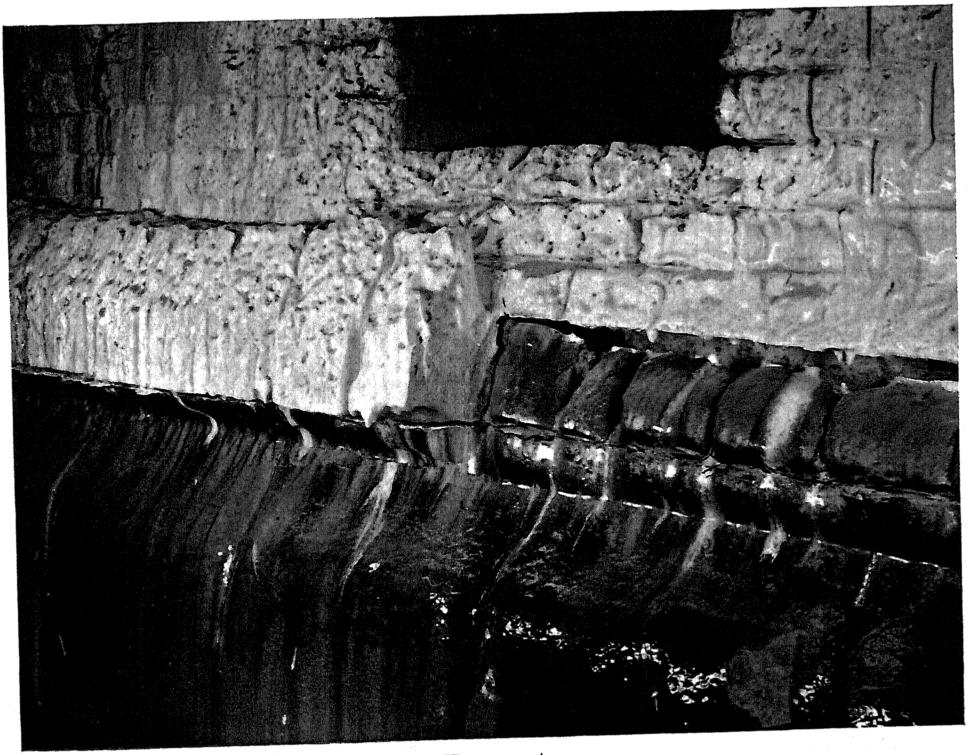

FIGURE 4

efficiency was the normal competition on the market for lamp quality and ability to show more economical use of the electricity for which the user paid.

It is interesting to look for a moment at what this means now from the national standpoint. Electric lighting in this country uses some 4000 million units of electricity per annum. Every 10 % of electricity saved in getting from the lamp the light we want, means in the end a saving of some quarter of a million tons of coal per annum, together with the incidental saving of generating plant.

Example 3. *Discharge lamps*

We worked for a number of years on the above lines during which the average filament lamp efficiency was increased some 25 %. It was clear, however, that little further worth-while gain in efficiency of filament lamps was likely.

A study was therefore taken in hand by a special group (also under J. W. Ryde) of the possibility of the electric discharge in gases and vapours being made to yield useful light. This turned out to be a fortunate inspiration which resulted firstly in the high pressure mercury lamp for street lighting, then the mains voltage luminescent tubular lamp for internal lighting, besides various types of compact source high intensity lamps for projection. As these lamps have now three times the efficiency of filament lamps, when they become generally adopted we shall be able to enjoy the same amount of light in our buildings for one-third the amount of electricity consumed. This was a really fine gain, of which the country has yet to reap the harvest. It means a potential saving of nearly 2 million tons of coal per annum. In terms of electrical generating plant it can mean (assuming a 10 % lighting load factor) the saving of something like three large generating stations of one million kilowatts output each, or say five stations of the present size of Battersea.

These revolutions are but vaguely appreciated because they materialize over a number of years and also because of the natural inclination of the public to employ some, at least, of the advantages presented to them in having more light rather than in using less electricity.

I have no time to mention any of the many interesting problems we met—and still meet—in this field of fluorescent lighting. I refer to it because of course it is an example of a complete break away from existing practice and takes its place in the second of the objectives I mentioned at the outset. Nevertheless, I would insist that even a break-away product like this needs to be evolved from the beginning by people who have an intimate acquaintance with the appropriate manufacturing procedures and materials.

THE THERMIONIC VALVE

I was tempted to take some examples from the extensive field of the development of the radio valve, which has been another of our major subjects of scientific study and development ever since its industrial birth during the first world war. This product indeed rests on the giving of scientific service through intimate association with its manufacturing arts—and affords a wealth of evidence of the theme I am trying to develop. But time and space will hardly permit of further examples of this kind.

PROJECT RESEARCH

There are some categories of equipment manufacture which are assisted best when the associated research group bases its work on projects rather than on scientific service. This applies, for instance, to telecommunications, both radio and line telephony. Thus, the project for distributing television over the country by radio links on centimetric wave-lengths involves some interesting wide wave-band transmission and reception problems. Another is the use of radar techniques for injecting pulses into circuit networks; these pulses probe the electrical characteristics of the circuits and cause them, as it were, to write their own signatures in cathode-ray tube traces.

Some of the war-time projects of this kind, which our groups undertook, made history, for in the first half of 1940 they produced the first centimetric radar and made the first practical cavity magnetrons, the principle of which had just been demonstrated by Randall and Boot. This was followed by the evolution of the radar project known as Oboe, with the leadership and co-operation of T.R.E.

User or Operational Research is in an intermediate category. It formed the basis, for instance, of our investigations into street lighting, where it was found that visibility on the road depended upon making the road as light as possible and objects upon it as dark as possible—a principle which resulted in a radical change in the design of luminaires for street lighting and their location on the roads.

QUALITY APPRAISEMENT AND CONTROL

Whether research is based upon the giving of scientific service or upon the study of new projects, or whether some entire break away in product or process is in hand (wherever there is manufacture) there is always the problem of statistical appraisement of the quality of the manufactured product followed by the introduction of some system of quality control.

This has been proved, by the experience of ourselves and others, to be the key to efficient and intelligent production. We find that it is best introduced to the factory at the craftsman (or charge hand) level (not at the managerial level) by scientific men who, as I have explained, are prepared to immerse themselves in the factory regime.

The practical principles of this quality control are simple—almost childish—but the psychology is often baffling. In our experience the secret of success is to work through the intelligent engineer in the factory and to instil into him the very small but essential amount of statistical technique. The ineffective way is usually to work through trained statisticians, and to expect them to assimilate sufficient knowledge of the processes concerned to ensure a sound practical result—unless of course a statistician can be found who is also an engineer with a gift for immersing himself in factory problems and who has patience to concentrate upon the application of quite simple statistical procedures.

Factory men of the right enthusiasms and psychology are difficult to find. Without the constant encouragement and guidance of the practical statisticians on our research staff, we find this powerful weapon of progress tends to rust and lose its effectiveness.

CONCLUSION

I could touch upon other fields of the work, for instance, (*a*) hard stones like diamond and sapphire and their handling, (*b*) crystal growing, (*c*) powders and the techniques for handling them, (*d*) heating for buildings and for industrial processes, (*e*) household appliances, including cooking, (*f*) carbon, (*g*) insulating materials, (*h*) X-ray and other electro-medical equipment, (*i*) steam and gas turbines, (*j*) heavy electrical equipment. They are very diverse, but the procedures for handling them follow closely the lines I have already sketched.

There is one group of activities which differs somewhat from these in character. We put the resources of the laboratories at the disposal of Government Departments by accepting research or development contracts for investigations for which our particular skills are suited. Probably one-fifth of the research resources I mentioned earlier are occupied in this way.

As you see, I have not attempted in this talk to give a review of the work we are doing, but rather of the way our laboratories have learnt from their experience to go about the work. I have done this not merely in order to describe the establishment, but in the hope that you will allow me to point out a consideration of general importance, the factor of efficiency in the use of scientific facilities in industry.

I sometimes feel we have the idea that we have only to do research and get explanations and knowledge of certain things and the rest follows naturally. If we do not get explanations and knowledge of exactly the right things, and if we produce that knowledge in other than a favourable psychological atmosphere, things just do not happen, or only just happen, in the industry we are trying to serve, notwithstanding all our imposing and praiseworthy treatises and reports, some of which are good of course, but how many?

An extreme case may be that of a detached research laboratory which merely publishes its reports and leaves industry to do all the thinking about whether the results can be made of use for practical purposes. How much of the whole amount of such effort really gets into an industry in a form in which it brings about advances which pay a technical dividend depends naturally upon the level which that industry has reached. But it is I fear, usually a small proportion, say 10 or perhaps 15 %. Even so, that is useful.

A stage higher in effectiveness may be the research establishment which, having done a piece of research, works hard to demonstrate the practicability of the results. What proportion of the total man-power effort of that establishment will have been effective in producing a technical dividend in manufacturing industry? Shall we say 20 or perhaps 30 %?

I contend that when scientific manpower is being employed in the manner I have been trying to indicate in this talk, its efforts have as a rule a maximum of effectiveness in producing technical progress within industry. The stimulating reaction on most research workers of being in contact with the actual application of their work constitutes one aspect of this picture. Another is the progressing of the investigations from their early stages in co-operation with the actual individuals who must implement them and make them serviceable.

I feel we need to foster the conception of the effectiveness and non-effectiveness of industrial research according to the kind of chance and help we give it to fructify, and it is to this end that I commend to you some of the considerations I have been discussing. I hope I have indicated some of the criteria which, as I see it, can give us a sense of values in regard to efficiency in the employment of scientific resources in production industry.

I do not want to hold up my laboratories as an example to be followed. Nearly every research establishment in industry has a unique problem in organization. But laboratories like those I have been describing do, I hope, serve to exemplify certain principles which are worth examination.

Attempts to detect the emission of secondary charged particles in the fission of ^{235}U by slow neutrons

By J. M. Cassels, J. Dainty, N. Feather, F.R.S. and L. L. Green

(*Received* 3 *March* 1947)

INTRODUCTION

If light charged particles (protons, α-particles, etc.) are emitted during fission, it should be possible to establish this fact by a simple coincidence experiment.

Suppose two detectors are arranged so that they can both 'see' a thin film of uranium oxide. Let one of the detectors register the entry of fission fragments only, say at the rate of F (sec.$^{-1}$). Let the other detector register not only fission fragments (unless they are excluded by an interposed absorber) but also light charged particles (protons, α-particles, etc.) with energies within certain limits. Suppose that the rate of registration in the second detector is P (sec.$^{-1}$), that the mean efficiency for the detection of a light charged particle emitted from the uranium film is ϵ, and that the average number of light charged particles liberated per fission is η. Then the coincidence rate, C (sec.$^{-1}$), between the two detectors, is given by

$$C = 2PF\tau + \eta\epsilon F \quad (\eta\epsilon \ll 1),$$

where τ (sec.) is the resolving time of the coincidence circuit, and thus

$$C/F = 2P\tau + \eta\epsilon, \tag{1}$$

a linear relation between C/F and P, from which $\eta\epsilon$ can be obtained, and thus η determined, if ϵ is known. For this determination ϵ was calculated from the mean solid angle subtended by the charged particle detector at the uranium film, assuming no angular correlation between fission fragments and charged particles.

Obviously the correct value of $\eta\epsilon$ will be found from equation (1) only if no true coincidences are missed. This can happen in two ways. First, true coincidences will be missed if the mean time interval between the emission of the charged particles and the expulsion of the fission fragments is not considerably smaller than the resolving time of the coincidence circuit (τ). However, except perhaps for the hypothetical negative proton (Broda, Feather & Wilkinson 1947), it is not to be expected, on theoretical grounds, that secondary charged particles are likely to be emitted which are significantly delayed. It was therefore assumed that no true coincidences could be missed in this way. Secondly, the coincidence resolving time may be so small that, even if there is 'simultaneous' emission of fission fragments and charged particles, coincidences may be missed because of the finite and variable time of rise of the detector pulses, or because of time delays in the detectors. This point will be clearer after a consideration of the problems of coincidence counting with proportional counters and ionization chambers. Obviously, to increase the resolving time uncritically is no easy solution, since as shown by (1) an increase in the chance coincidence rate must eventually result without further gain in 'genuine' coincidences.

COINCIDENCE COUNTING

The problem of counting coincidences between the pulses from two Geiger counters is relatively simple. All the pulses entering the amplifiers are approximately of a uniform size and shape, and the signal-to-noise ratio is very high, usually a thousand or more. This means that the amplifiers can be very simple; no pulse-shaping circuits are necessary (although perhaps desirable), and, because all the pulses have the same size and shape, there is no fear of missing coincidences due to the finite rising time of the counter pulses. With very high single rates of counting, however, some difficulties closely akin to those associated with heavy particle coincidence counting begin to appear.

Conditions are very different with proportional counter and ionization chamber coincidence counting. The signal-to-noise ratio is much smaller and the variation of the pulse size may be very large. The problem is further complicated with ionization chambers, since the pulses may not be of a constant shape. The original pulses being very small, high-gain linear amplifiers are necessary to amplify them to the level of a few volts, and because of the unfavourable signal-to-noise ratio there must be a discriminating stage in each amplifier in order to prevent noise from reaching the mixing stage. Again, since the pulses are in general of various shapes and sizes, a stage which converts all pulses into pulses of a standard size and shape, before injecting them into the mixing stage, must be included in each discriminator or added to it. Moreover, because of the difference in pulse size alone, full treatment of the results is not possible without the determination of a 'coincidence bias curve' using the discriminators for this purpose.

From what has been said it is clear that the minimum resolving time which can be used depends upon the speed of rise of the pulse when it enters the discriminating

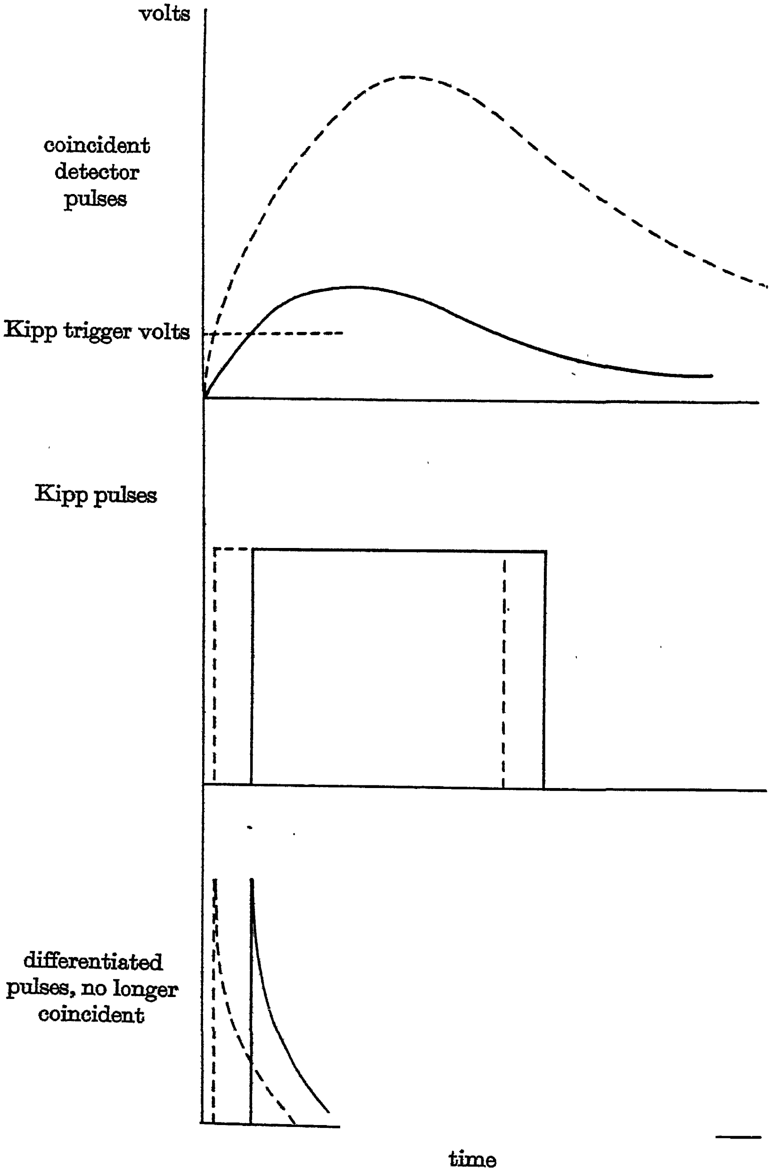
volts
coincident detector pulses
Kipp trigger volts
Kipp pulses
differentiated pulses, no longer coincident
time

Figure 1

and pulse-shaping stage (see figure 1). Also, close attention must be paid to the frequency response of all circuits, if the best results are to be obtained.

With slow pulses, such as are obtained from some types of ionization chamber, the frequency response of the circuits can—and should—be adjusted to pass the pulse undistorted, and, to maximize the signal-to-noise ratio, no frequencies above or below those necessary to transmit an undistorted pulse should be passed. Then the minimum resolving time should be roughly equal to the time of collection of the ions (of either sign) in the detector.

With a 'fast' detector of heavy particles (proportional counter or electron-collecting ionization chamber) the time of rise of the primary pulse may be a fraction of a microsecond; on the other hand, the circuits may not have a wide enough frequency response to pass such a pulse undistorted. The effective time of rise of the pulse is then determined, essentially, by the upper limit of frequency response of the circuits. In such a case it is clearly necessary to make this upper limit as high as possible. With 'fast' detectors, however, it is not generally possible to use a minimum resolving time determined only by the time of rise of the pulse at the discriminating and pulse-shaping stage. It is known that between the entry of an ionizing particle into a detector and the appearance of a voltage pulse on an electrode there is a delay due to the finite mobility of the ions (Dunworth 1939). This delay depends upon the type of detector, upon the gas filling and other factors, and, because the delay fluctuates, coincidences are missed even with resolving times as long as the average delay. For proportional counters of conventional design, which must certainly exhibit the effect, the average delay is likely to be of the order of a microsecond.

In the experiments described in this paper, particular attention was paid to this problem of 'missed' coincidences. The resolving time was carefully chosen in each experiment to suit the type of detector used and was matched with the frequency response of the circuits. In the second series of experiments, a repetition was made with a longer resolving time to check that the resolving time used was not, in fact, too short.

With attention to these details it was confidently expected that the value of η, experimentally derived by applying equation (1), would give a true indication of the number of secondary charged particles emitted per fission.

EXPERIMENTAL WORK

The experiments were performed in two different geometries; for the purpose of reference these experiments will be spoken of as experiments A and B.

In experiment A coincidences were sought between fission fragments and charged particles with ranges greater than the ranges of the fission fragments. This experiment, roughly performed, showed that the probability of emission of long-range charged particles was small, and it was not pursued in great detail. It was felt that the coincidence method was not necessarily the best way of looking for these long-range secondary charged particles which were certainly not of frequent occurrence. Photographic plate or cloud-chamber studies would obviously yield data capable of more direct interpretation.

Secondly, an experiment was performed in greater detail to look for short-range secondary charged particles. This experiment (B) occupied the major part of the time of this research. It will be seen later that it showed a small positive effect.

Experiment A

The apparatus used in the attempt to detect the long-range secondary charged particles is illustrated in figure 2. The cylindrical proportional counter consisted of an outer brass cathode, with most of the wall cut away, and a central tungsten wire sealed into pyrex supports. A platinum foil, of 21 mg./cm.^{2} thickness, with a uranium oxide (U_3O_8) layer approximately 1 mg./cm.^{2} thick deposited on the outside, was wrapped round the skeleton cathode of the counter. The platinum foil was just thick enough to stop the natural α-particles (and, therefore, also the fission fragments) from the U layer. The counter, 5 cm. long and 2 cm. diameter, was placed inside and coaxial with an insulated brass cylinder 4·5 cm. in diameter. This brass cylinder was

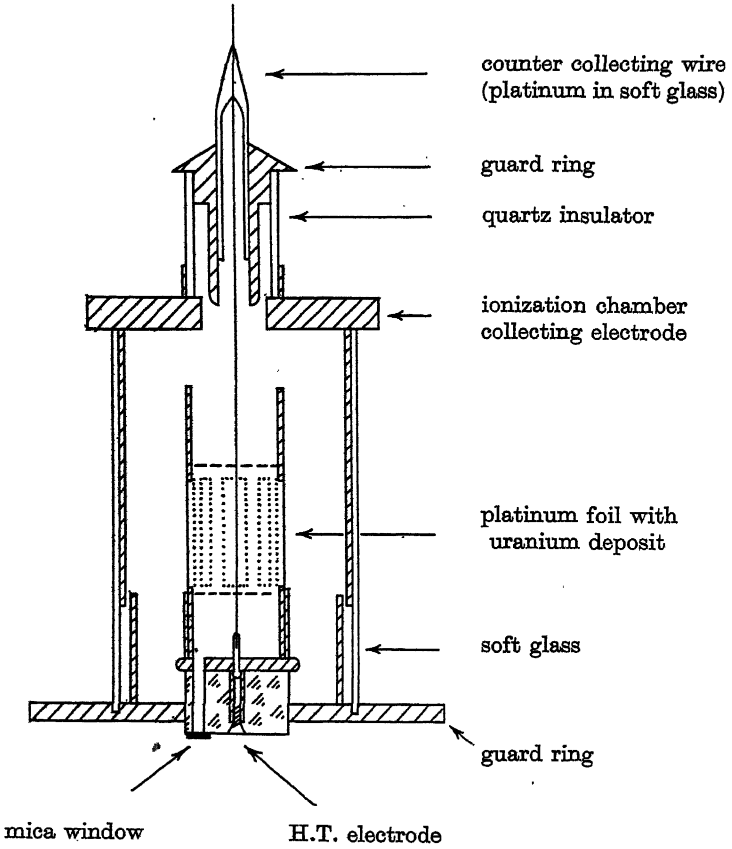
counter collecting wire (platinum in soft glass)
guard ring
quartz insulator
ionization chamber collecting electrode
platinum foil with uranium deposit
soft glass
guard ring
mica window
H.T. electrode

FIGURE 2. Counter used for experiment A.

the collecting plate of an ionization chamber whose high-voltage electrode was the cathode of the counter. The assembly was filled with argon at 20 cm. pressure. There was a small, thin (approximately 2 cm. air equivalent) mica window at one end of the counter. This was used to allow the natural α-particles of Th C and Th C′ to enter the counter, for test and calibration purposes. The apparatus was put in a screening brass cylinder and irradiated with a mixture of fast and slow neutrons. The primary fast neutrons, which had an energy of approximately 0·5 MeV, were produced by bombarding a target of lithium hydroxide with 2·5 MeV protons from the cyclotron. Paraffin wax placed round the apparatus provided the slowing-down material.

The experimental procedure was to count coincidences between fission fragments, as recorded by the ionization chamber, and all pulses above a certain size from the proportional counter. By comparison with the pulses produced by Th C and Th C′ α-particles, this size was estimated to correspond to an energy loss of roughly 50 keV in the counter, assuming counter proportionality.

A block diagram of the experimental arrangement is shown in figure 3. The head amplifiers were mounted near the cyclotron, connexions to the detectors being short lengths of screened polythene-insulated cable. The rest of the apparatus was placed in a screened cabin, connexions from head to main amplifiers being made by means of about 5 m. of screened flex. The main amplifiers were of a conventional resistance-capacity coupled type with an approximately uniform frequency response from 10^3 to 10^5 cyc./sec. In the coincidence unit there were discriminating and pulse-shaping circuits followed by a simple Rossi circuit.

The single rates P, F and the coincidence rate C were determined for various intensities of cyclotron beam. (It was assumed that the slow neutron flux was proportional to the proton current.) Counting was continued for a time sufficient to make the standard error in C less than or equal to 10 %. C/F was plotted against P and the intercept on the $P = 0$ axis determined. Two runs were made, the results of one being shown in figure 4, in which standard deviations are indicated by the vertical lines. Only a rough determination of the resolving time was made in this experiment. This gave $\tau = 2 \times 10^{-4}$ sec., approximately. From the geometry of the chamber and the frequency response of the amplifiers it seemed unlikely that any large fraction of genuine coincidences can have been missed.

From figure 4 it can be seen that the most probable value of the intercept is 6×10^{-3}. The value obtained from the other run was 2×10^{-3}. The standard errors were approximately 2×10^{-3}; thus the mean of these results gives $\eta\epsilon = (4 \pm 1{\cdot}4) \times 10^{-3}$. Now ϵ is certainly less than $\frac{1}{3}$ and greater than $\frac{1}{6}$ for protons with original energies from 1·5 to 3 MeV, and for α-particles of from 5 MeV to greater than 20 MeV.* The corresponding value of η is therefore approximately $\frac{1}{60}$ with an uncertainty of, roughly, a factor of 2; it applies, of course, only to particles with energies between the above limits.

---

* Not more than two-thirds of the uranium oxide layer was 'in view' of the proportional counter through the windows cut in the cylindrical cathode.

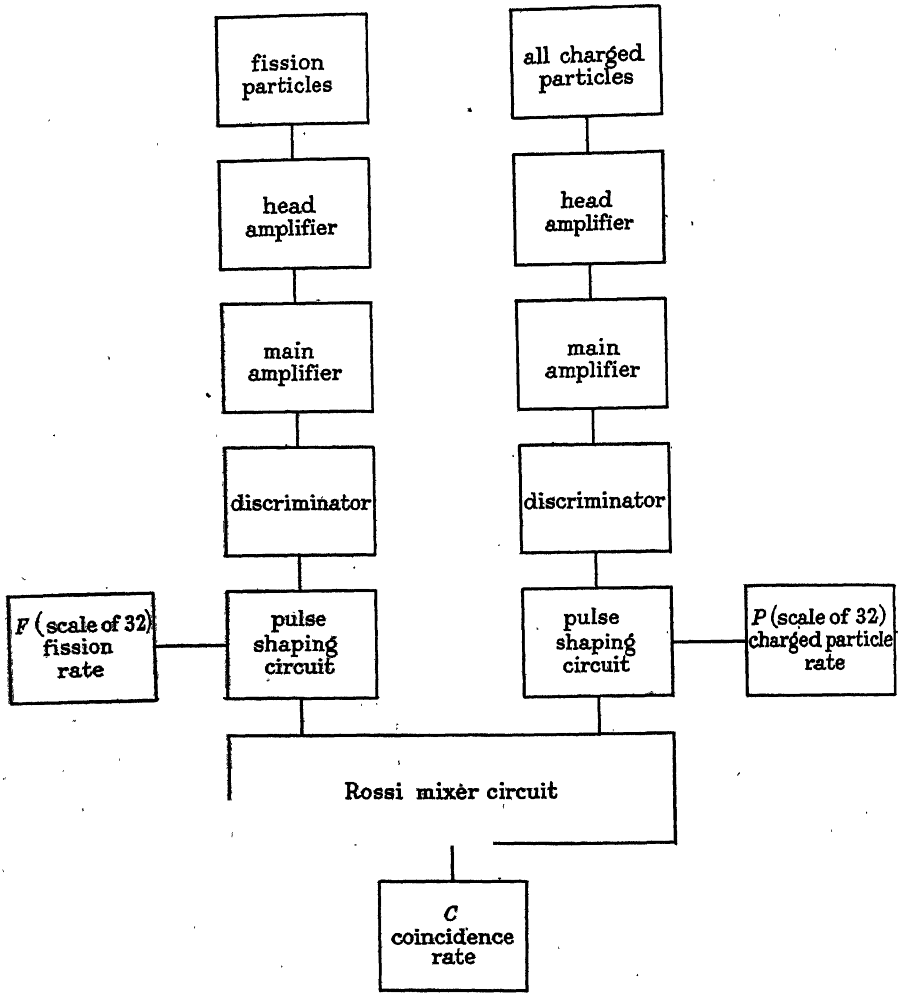

FIGURE 3. Block diagram of the electronic apparatus.

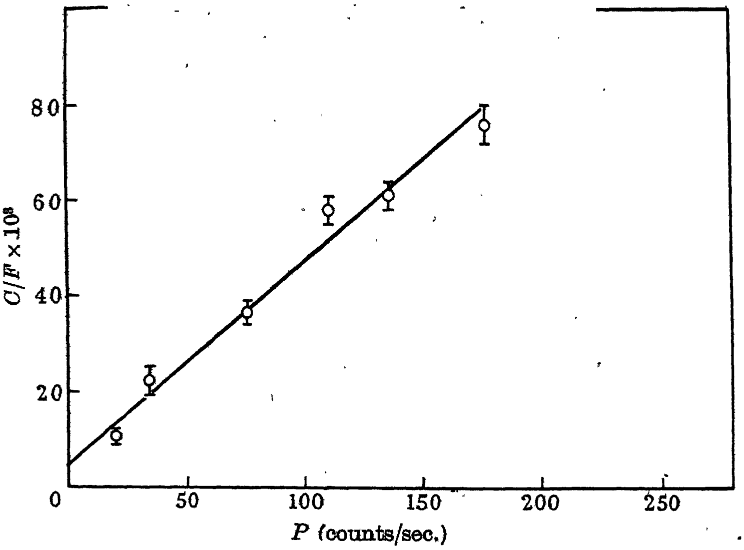

FIGURE 4. Experiment A. Second run. $\epsilon\eta = 6 \pm 2 \times 10^{-3}$.

The result shows that the emission of charged particles of range greater than that of the fission fragments is not an important process in which mass and charge may be 'lost' in fission. Once this was established, experiment A was not continued any further. It had served its purpose of showing that the number of secondary charged particles was small, and, as stated above, it is now considered that the emission of such long-range particles can with more certainty be established by other means (Livesey & Green 1946; Green & Livesey 1947).

Experiment B

The object of this experiment was to search for secondary charged particles, the range of which might be shorter than the maximum range of the fission fragments.

Figure 5 shows the apparatus used. This consisted of two open-ended counters P_1 and F, and a 'blind' counter P_2 which was used for control experiments. Two thin (~ 1 mg./cm.^{2}) uranium sources, enriched in their ^{235}U content and deposited on platinum foils, were placed in the apparatus, one at 45° both to P_1 and to F, the other within P_2, at one end, as shown in figure 5. A very thin gold foil (0·2 mg./cm.^{2}) was placed in front of F in order to prevent possible capacitative pick-up between the wires of F and P_1. The whole apparatus was surrounded by a screening box embedded in paraffin wax. Irradiation with neutrons was carried out as in experiment A.

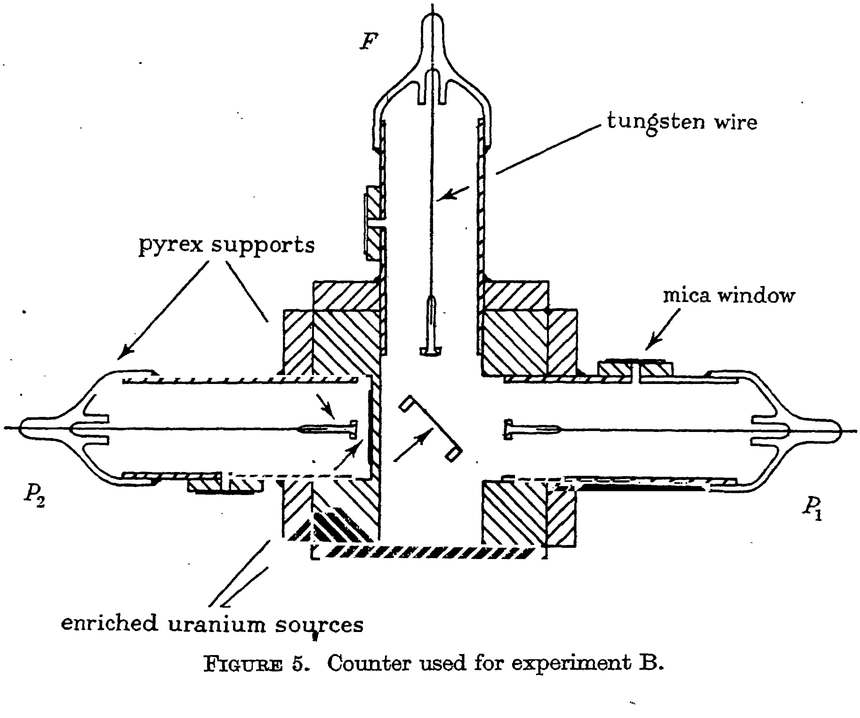

FIGURE 5. Counter used for experiment B.

The electronic equipment had the same block diagram and general arrangement as before, but the high-frequency limit of the circuits was raised to about a Mcyc./sec.

to take advantage of the fact that proportional counters only were being used. The resolving time could probably have been set lower than the value of about 6 μsec. used throughout most of the experiment, but it was considered important to make certain that no true coincidences were being lost. The 'charged particle' line was attached to P_1 or P_2 as required.

Using P_1, the amplification in this line was adjusted so that the noise at the discriminator stage was about 3 V. The voltage on the counter was then raised until the size of the pulses obtained by bringing up a polonium source to the window of the counter was 20 V at the same stage. These calibration pulses represented a calculated energy loss of 160 keV in the counter. The energy loss corresponding to a range of pulse sizes was then known, since the amplifier was linear up to pulse sizes of about 60 V. The counter itself was assumed to be 'proportional' over the range of ionizations in question.

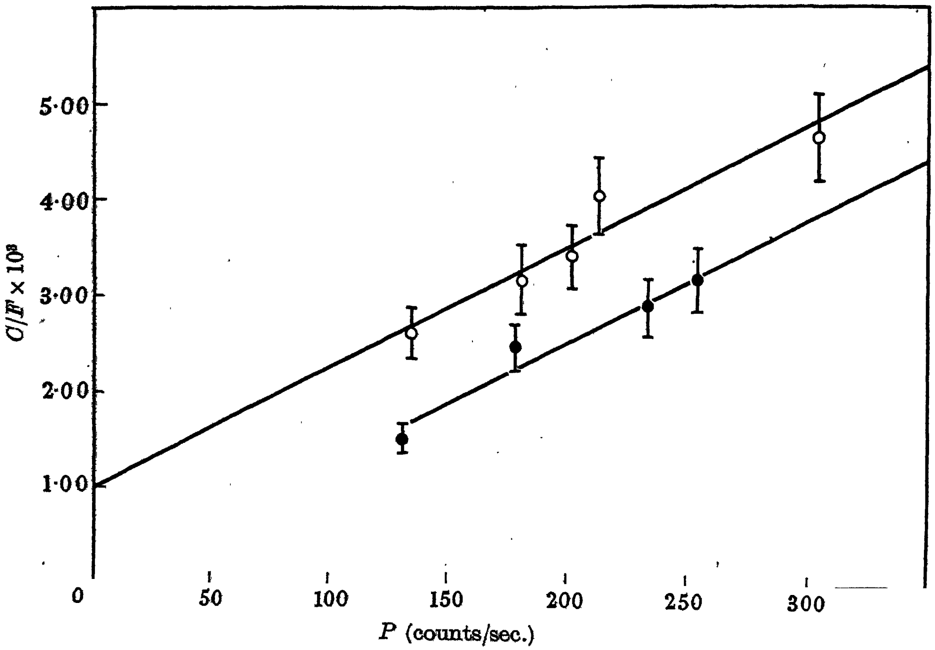

FIGURE 6. Experiment B at $\tau = 6\cdot31 \pm 0\cdot24\,\mu$sec., $e\eta = 0\cdot99 \pm 0\cdot11 \times 10^{-3}$. ○ from P_1, ● from P_2.

Throughout the runs recorded on figures 6, 7 and 8, the bias on the 'charged particle' discriminator was held at 4 V, so that all particles losing more than 32 keV energy in P_1 could be detected. These particles would obviously include the natural α-particles from the uranium and all heavy charged particles produced in the fission process. The amplification on the fission line was adjusted so that no pulses other than those due to fission particles were larger than 7 V at the discriminator stage. The bias was then set at 10 V. Most of the runs were continued until a statistical accuracy of 10 % in C had been attained. Standard deviations are shown in the diagrams.

Figures 6 and 7 show the results obtained at resolving times equal to 6·31 ± 0·24 and 13·37 ± 0·36 μsec. respectively. The points represented by full circles refer to coincidences between fissions in F and charged particles in P_2; those represented by open circles were obtained using F and P_1. It will be seen that the full circles lie on straight lines through the origin, as would be expected from the relation

$$C/F = 2P\tau.$$

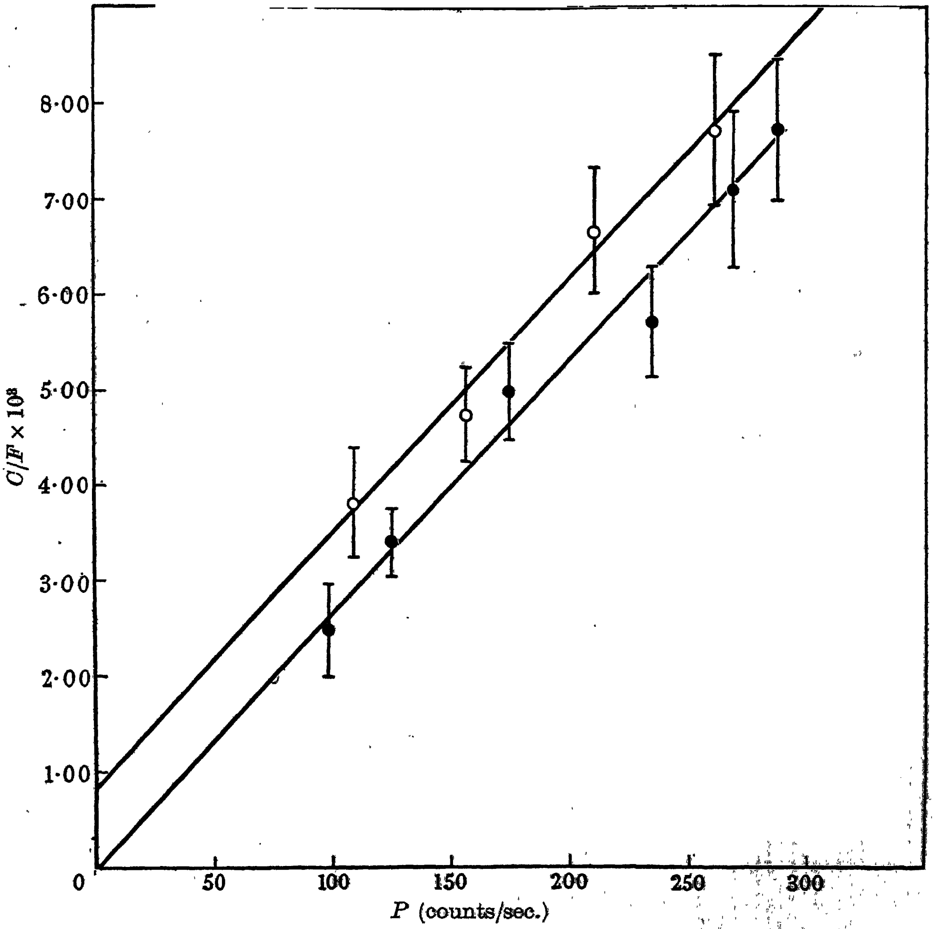

FIGURE 7. Experiment B at $\tau = 13{\cdot}37 \pm 0{\cdot}36$ μsec., $e\eta = 0{\cdot}85 \pm 0{\cdot}15 \times 10^{-3}$.
○ from P_1, ● from P_2.

In this arrangement there was no possibility of genuine coincidences occurring, and the 'best straight line' gave the value of τ. This method of measuring τ was chosen because it was feared that spurious effects might arise from the very large fission pulses on the 'charged particle line'. By using a similar pulse distribution for the control experiment correction was made for any such effect. It is now realized that it would probably have been better to have taken control counts between fissions in P_2 and charged particles in P_1, thus preserving throughout more nearly the same distribution of pulses in the charged particle line. One point was, in fact, taken in this way and gave a normal result, but, statistically, this single observation does not carry much weight.

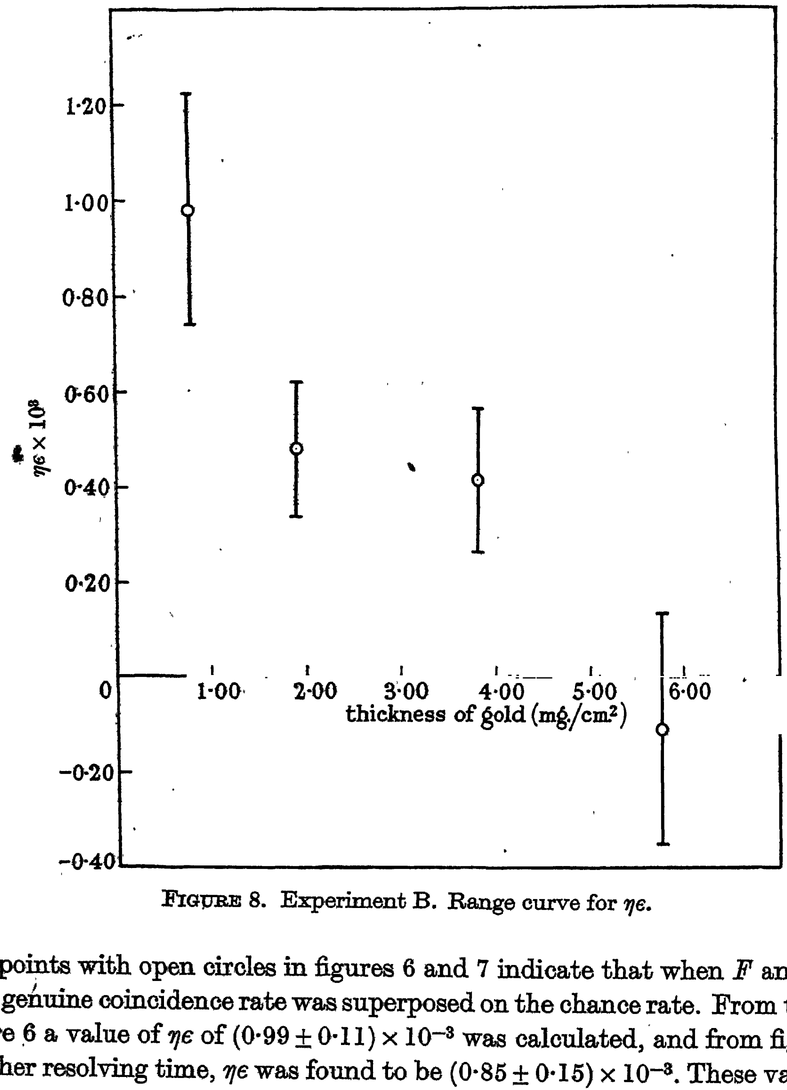

FIGURE 8. Experiment B. Range curve for $\eta\epsilon$.

The points with open circles in figures 6 and 7 indicate that when F and P_1 were used, a genuine coincidence rate was superposed on the chance rate. From the points of figure 6 a value of $\eta\epsilon$ of $(0·99 \pm 0·11) \times 10^{-3}$ was calculated, and from figure 7, at the higher resolving time, $\eta\epsilon$ was found to be $(0·85 \pm 0·15) \times 10^{-3}$. These values were considered to be in agreement.

After the resolving time had been fixed at $5·93 \pm 0·18\,\mu$sec., an attempt was made to investigate the properties of the secondary particles giving rise to this genuine coincidence rate. Figure 8 shows a range curve obtained by placing gold foils of different thickness in front of P_1, and figure 9 the variation of $\eta\epsilon$ with the bias on the 'charged particle' line, no gold foil being present. The statistical accuracy of the points was very poor owing to the low rate of counting which had to be accepted in order to obtain a reasonable ratio of genuine to chance coincidences. It was not thought justifiable to draw definite curves through the points of figures 8 and 9 because of this fact. However, it seems likely that the 'average' range of the particles is about 1 cm. of air (~ 4 mg./cm.^{2} of gold), and that the upper limit to the pulse size in the arrangement used was about 40 V, corresponding to an energy loss of 320 keV in the counter.

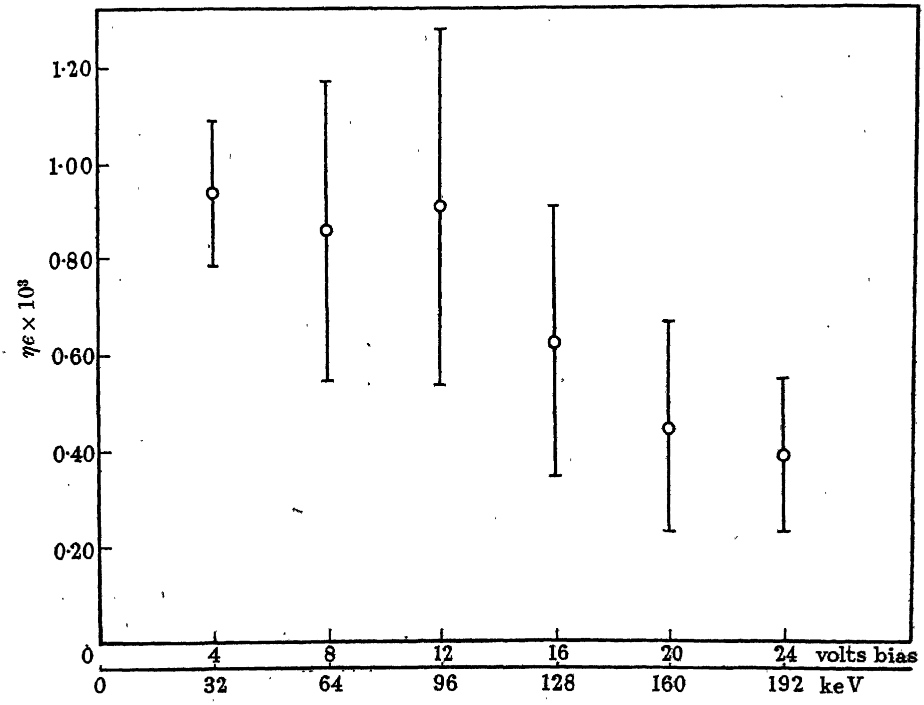

FIGURE 9. Experiment B. Bias curve for $\eta\epsilon$.

Two points were also taken with biases 'normal' and no foils in front of P_1, but with 10·5 cm. pressure of argon in the counter instead of 5 cm., as previously used. These gave $\eta\epsilon = (0{\cdot}81 \pm 0{\cdot}22) \times 10^{-3}$, in agreement with the values obtained above.

DISCUSSION OF RESULTS

There seem to be three possible explanations for the genuine coincidence rate found in experiment B:

(i) Particles were being projected into P_1 either from the source material or supporting foil, or from the gas in the apparatus, by collision of fission fragments.

(ii) Coincidences between two fission fragments were being observed, either because of 'reflexion' of fission fragments in the material of the source or its supports, or because of the occurrence of true ternary fission in a small proportion of cases.

(iii) Secondary light charged particles (protons or α-particles) emitted at the instant of fission, or with inappreciable delay, were being detected.

The table below shows the approximate maximum energy in keV which would be lost in the counter by protons, α-particles and 'average' (binary) fission fragments of various 'air' ranges. The first range given is just sufficient to enable a particle from the centre of the source to traverse the counter completely. Values refer throughout to 5 cm. pressure of argon in the counter. Considering the value for the maximum energy loss deduced from the rather uncertain data of figure 9, the particle fitting in best with the facts is the α-particle. The rough value for the maximum range deduced from figure 8 tends to confirm this conclusion.

range (cm.) ...	0·39	1	2	3
particle:				
proton	165	110	70	70
α-particle	300	490	320	240
fission fragment	3,000	3,900	14,000	—

Now α-particles could only have been present as secondary particles emitted in the fission process, since the particles to be expected from process (i) are protons, or atoms of mass greater than that of carbon with ionizing powers intermediate between those of α-particles and fission fragments. That argon recoil atoms, in particular, were not being projected into P_1 in significant numbers by collisions of fission fragments in the gas in the immediate neighbourhood of the source was clear from the fact that $\eta\epsilon$ did not increase when the counter pressure was doubled.

Provisionally, therefore, the experiment indicates that secondary α-particles of ranges up to about 1 cm. of air are emitted in the fission process to the extent of about 1 secondary α-particle in 30 fissions—assuming ϵ to be $\sim\frac{1}{38}$. An accuracy of about 50 % should be assigned to this figure, to take account of statistical errors and uncertainties in ϵ. It is hoped shortly to repeat the investigation under improved conditions in respect of fast neutron background, resolving time, and counter geometry. Apart from the question of uncertainties introduced by the assumption of isotropic emission, the value of 1 ($\pm$ 0·5) secondary charged particle in 30 fissions does, however, constitute an upper limit to any genuine effect (range >3 mm. of air). This is further definite evidence against the emission of light charged particles being a major feature of the fission process.

The work described in this paper was carried out at the Cavendish Laboratory, Cambridge, at various times during the period March 1943 to April 1945, and is now published by permission of the Ministry of Supply (Department of Atomic Energy).

Note added 27 *May* 1947. Since the above paper was written, a publication has appeared (Farwell, Segrè & Wiegand (1947), *Phys. Rev.* 71, 327) giving a preliminary account of the results of an experiment very similar in design to our experiment A, but carried out under much more favourable conditions than we were able to command. These authors conclude that the secondary charged particles are α-particles and estimate their number as about 1 in 250 fissions with ^{235}U, with ranges significantly greater than the range of the natural α-particles from this body. It will be seen that our overall results are readily reconcilable with this estimate, based, like our own, on the assumption of isotropic secondary emission.

REFERENCES

Broda, Feather & Wilkinson 1947 *Report of Cambridge Conference, July* 1946. In course of publication.
Dunworth 1939 *Nature*, **144**, 152.
Green & Livesey 1947 *Nature*, **159**, 332.
Livesey & Green 1946 *Nature*, **158**, 272.

A connexion between the criterion of yield and the strain ratio relationship in plastic solids

BY SIR GEOFFREY TAYLOR, F.R.S.

(*Received* 5 *March* 1947)

The assumption that the work done during a small plastic strain is a maximum as the yield-stress criterion is varied is shown to give rise to a connexion between the yield-stress and the strain-ratio relationship. The strain-ratio relationship is that which exists between the ratios of principal stress differences and the ratios of the corresponding strain differences. It is common to assume that this relationship is one of simple proportionality. Experiments, however, show that this assumption is not true in metals. The observed strain-ratio relationship is used in conjunction with the assumption of maximum work during a given strain to calculate the criterion of yield. It is found that this is very close to, but not identical with, the Mises-Hencky criterion.

INTRODUCTION

The three principal properties which define the plastic behaviour of an isotropic material and must be known or assumed before the solution of any problem in plastic flow can be attempted are:

(*a*) The criterion of yield (Mises-Hencky, maximum stress difference, etc.).

(*b*) The relationship between the ratios of small strains parallel to the principal axes and the ratios of principal stress differences. This relationship may be called the strain-ratio relationship.

(*c*) The amount of strain hardening after yielding.

When problems concerning small strains are considered it is frequently a good enough approximation to assume that there is no strain hardening, so that the criterion of yield is independent of the amount of small strain considered. On the other hand, both (*a*) and (*b*) must be known before any problems in which the stress depends on the strain can be solved.

It has usually been considered that (*a*) and (*b*) are quite unrelated, and from the purely mathematical point of view this is true. Problems are solvable mathematically, for instance, if either the Mises-Hencky or the maximum-stress difference hypothesis is assumed in conjunction either with the strain-ratio relationship observed with viscous fluids or with other strain-ratio assumptions. When the physical nature of a plastic material is considered, however, it seems that a certain relationship between (*a*) and (*b*) must exist. A relationship is here deduced using an assumption that the energy dissipation for a given strain is a maximum. The theoretical result is compared with available observations.

REPRESENTATION OF PLASTICITY CONDITIONS

(*a*) *Criterion of yield*

If σ_1, σ_2 and σ_3 are the three principal stresses it may be assumed that the yield criterion depends only on the stress differences $\sigma_1-\sigma_2$, $\sigma_2-\sigma_3$, $\sigma_3-\sigma_1$ and is independent of the mean pressure $\overline{p} = -\frac{1}{3}(\sigma_1+\sigma_2+\sigma_3)$. It is convenient to express results in terms of the three residual stresses σ_1', σ_2', σ_3', which result from subtracting the mean pressure from the principal stress, so that

$$\sigma_1' = \tfrac{2}{3}\sigma_1-\tfrac{1}{3}\sigma_2-\tfrac{1}{3}\sigma_3, \text{ etc.,} \quad \text{and} \quad \sigma_1'+\sigma_2'+\sigma_3' = 0. \tag{1}$$

In these co-ordinates the Mises-Hencky criterion of yield is

$$(\sigma_1')^2+(\sigma_2')^2+(\sigma_3')^2 = \tfrac{2}{3}Y^2, \tag{2}$$

and the maximum shear stress criterion is

$$\sigma_1'-\sigma_3' = Y, \tag{3}$$

where Y is the yield stress in direct tensile loading and

$$\sigma_1' \geqslant \sigma_2' \geqslant \sigma_3'. \tag{4}$$

(*b*) *Strain-ratio relationship*

It will be assumed that the compressibility of the material is unchanged when plastic flow sets in. If e_1, e_2, e_3 are the principal strains (assumed small) it is convenient to use the residual principal strains

$$e_1' = e_1-\tfrac{1}{3}(e_1+e_2+e_3), \text{ etc.,} \tag{5}$$

because

$$e_1'+e_2'+e_3' = 0, \tag{6}$$

so that if

$$e_1' \geqslant e_2' \geqslant e_3', \tag{7}$$

all possible strain ratios have been considered when e_3'/e_1' varies from $-\frac{1}{2}$ to -2.

In considering all possible relationships between stress ratios and strain ratios it is clear that any one of them could be represented by a curve in a diagram with σ_3'/σ_1' as abscissa and e_3'/e_1' as ordinate, the full range extending from $-\frac{1}{2}$ to -2 in each case. This diagram is unsymmetrical in the sense that if the yield is the same in compression as in tension the symmetrical diagram would show the compression part of the curve as similar to the part representing extension. The former extends from $\sigma_3'/\sigma_1' = -\frac{1}{2}$ to -1, while the latter extends from -1 to -2, so that the diagram is unsymmetrical. To avoid this difficulty Lode (1926) introduced the symmetrical variables

$$\left.\begin{aligned} \mu &= \frac{2\sigma_2'-\sigma_1'-\sigma_3'}{\sigma_1'-\sigma_3'} \quad \text{or} \quad -3\frac{\sigma_1'+\sigma_3'}{\sigma_1'-\sigma_3'}, \\ \nu &= \frac{2e_2'-e_1'-e_3'}{e_1'-e_3'} \quad \text{or} \quad -3\frac{e_1'+e_3'}{e_1'-e_3'}. \end{aligned}\right\} \tag{8}$$

The results of experiments on all possible combinations of σ_1', σ_2', σ_3', e_1', e_2', e_3' can be represented on a square diagram (2) showing μ as abscissa and ν as ordinate and covering the range $-1 < \mu < +1$, $-1 < \nu < +1$. It will be seen that when ν is positive, e_2' is positive. This corresponds with cases where the residual principal strain which has the greatest absolute value is compressive; the point $\nu = +1$ for instance corresponds with a uniaxial compressive load parallel to e_3'. When e_2' is negative the residual strain which has the greatest absolute value is positive and $\nu = -1$ corresponds with uniaxial extension parallel to e_1'. In an isotropic medium the μ, ν curve must pass through the points $\mu = \nu = -1$, $\mu = \nu = 0$, $\mu = \nu = +1$. Otherwise no limitations on the form of the μ, ν curve are imposed by considerations of symmetry alone. The results of experiments in which complex stresses were produced in a tube (*a*) by simultaneous end-load and internal pressure (Lode 1926), and (*b*) by simultaneous end-load and torque are given in a paper (Taylor & Quinney 1931) by the present author and the late Mr H. Quinney. It was found that with most of the metals used, namely, mild steel, decarburized mild steel, copper, nickel and aluminium, the μ, ν curve lies below the line $\mu = \nu$ when μ and ν are positive (i.e. $\mu > \nu > 0$), and above this line when μ and ν are negative (i.e. $\mu < \nu < 0$). With very soft metals like lead and cadmium this was still true, but the experimental μ, ν curves lie nearer to the line $\mu = \nu$ than with the above-mentioned metals. Experiments made with glass heated till it began to flow gave points lying very closely on the line $\mu = \nu$. This is to be expected in view of the fact that $\mu = \nu$ for viscous fluids.

Values of μ and ν found in experiments with annealed tubes of pure copper are given in columns 1 and 2 of table 1, and the corresponding values of $\sigma_3'/\sigma_1' = (\mu+3)/(\mu-3)$ are given in column 3.

TABLE 1

1 μ	2 ν	3 $-\sigma_3'/\sigma_1'$	4 χ	5 $\dfrac{1}{\chi-\sigma_3'/\sigma_1'}$	6 m	7 $\dfrac{\frac{1}{2}m}{1+\sigma_3'/\sigma_1'}$
−0·021	−0·011	0·9860	1·022	0·498	0·025	0·907
−0·242	−0·171	0·8507	1·412	0·442	0·280	0·885
−0·471	−0·393	0·7286	2·295	0·331	0·515	0·946
−0·597	−0·502	0·6680	3·016	0·271	0·68	0·978
−0·652	−0·554	0·6429	3·484	0·240	0·70	0·980
−0·773	−0·659	0·5902	4·865	0·183	0·80	0·978
−0·874	−0·775	0·5487	7·889	0·118	0·90	0·997
−0·954	−0·876	0·5174	15·13	0·064	0·95	0·983

POSSIBLE MAXIMUM ENERGY DISSIPATION ASSUMPTION

In a paper published recently (Hill, Lee & Tupper 1947) it is shown that if the strain-ratio relationship expressed by the equation

$$\mu = \nu \tag{9}$$

holds, the work done during a given small strain is a maximum if the Mises-Hencky criterion of flow applies. Since experiments with most metals reveal a marked divergence from the ideal relationship (9), it is of interest to find out what criterion of flow would correspond with the maximum of work during a small strain when the experimentally observed relationship between μ and ν is used instead of (9). The work done during a small strain is

$$W = \sigma_1' e_1' + \sigma_2' e_2' + \sigma_3' e_3'$$

or

$$W = \sigma_1'(2e_1' + e_3') + \ldots + \sigma_3'(e_1' + 2e_3'). \tag{10}$$

A stationary value of W for a given strain occurs when

$$\frac{d\sigma_3'}{d\sigma_1'} = -\frac{2e_1' + e_3'}{e_1' + 2e_3'}. \tag{11}$$

It has been seen that experiments on the strain-ratio relationship give σ_3'/σ_1' in terms of e_3'/e_1', so that (11) will enable the criterion of yield to be determined by numerical integration. Alternatively, if the relationship between σ_3' and σ_1' is known by experiment, (11) gives directly the strain-ratio relationship. To determine the criterion of yield from the observed relationship between σ_3'/σ_1' and e_3'/e_1' (11) may be written

$$\frac{d\sigma_3'}{d\sigma_1'} = \sigma_1' \frac{d}{d\sigma_1'}\left(\frac{\sigma_3'}{d_1'}\right) + \frac{\sigma_3'}{\sigma_1'} = -\frac{(2 + e_3'/e_1')}{(1 + 2e_3'/e_1')}. \tag{12}$$

Taking the experimental value of e_3'/e_1' corresponding with each value of σ_3'/σ_1', the corresponding experimental value of $-\dfrac{2 + (e_3'/e_1')}{1 + (2e_3'/e_1')}$ can be found. Calling this χ, (11) can be integrated, giving

$$\text{constant} + \log_e \sigma_1' = \int \frac{d(\sigma_3'/\sigma_1')}{\chi - (\sigma_3'/\sigma_1')} = I. \tag{13}$$

Expressed in terms of ν, $\chi = \dfrac{1-\nu}{1+\nu}$. Values of this for copper are given in column 4, table 1, and values of the integrand of (12) in column 5. To perform the integration the values given in column 5, table 1, were plotted against σ_3'/σ_1'. The values of the integral I were then determined from this diagram for values of σ_3'/σ_1' ranging from -1 to $-0{\cdot}5$. These are given in column 2, table 2. The value of the constant in (13) is determined by the fact that when $\sigma_3'/\sigma_1' = -0{\cdot}5$, $\sigma_1' = \frac{2}{3}Y$. In this way the values given in column 3 of table 2 were found for $3\sigma_1'/2Y$.

TABLE 2

1	2	3	4 (Mises-Hencky)	5 (Mohr)
σ_3'/σ_1'	I	$\frac{3\sigma_1'}{2Y}$	$\frac{\sqrt{3}}{2}\left\{1+\frac{\sigma_3'}{\sigma_1'}+\left(\frac{\sigma_3'}{\sigma_1'}\right)^2\right\}^{-\frac{1}{2}}$	$\frac{3}{2}\left(1-\frac{\sigma_3'}{\sigma_1'}\right)$
−1	0	0·849	0·866	0·750
−0·95	0·0247	0·870	0·888	0·770
−0·90	0·0487	0·891	0·908	0·789
−0·85	0·0716	0·912	0·927	0·810
−0·80	0·0926	0·931	0·945	0·834
−0·75	0·1114	0·949	0·960	0·856
−0·70	0·1278	0·964	0·974	0·882
−0·65	0·1416	0·978	0·985	0·909
−0·60	0·1526	0·989	0·992	0·938
−0·55	0·1605	0·996	0·997	0·969
−0·525	0·1629	0·999	0·999	0·985
−0·50	0·1640	1·00	1·00	1·00

COMPARISON WITH MISES-HENCKY AND MAXIMUM STRESS DIFFERENCE CRITERIA

The Mises-Hencky criterion (2) may be written

$$\sigma_1'^2+\sigma_1'\sigma_3'+\sigma_3'^2 = \tfrac{1}{3}Y^2, \tag{14}$$

so that

$$\frac{3}{2}\frac{\sigma_1'}{Y}=\frac{\sqrt{3}}{2}\left\{1+\frac{\sigma_3'}{\sigma_1'}+\left(\frac{\sigma_3'}{\sigma_1'}\right)^2\right\}^{-\frac{1}{2}}. \tag{15}$$

Values of this function are given in column 4 of table 2.

The maximum stress difference criterion is

$$\sigma_1'-\sigma_3' = Y \quad \text{or} \quad \frac{\sigma_1'}{Y}=\frac{1}{1-\sigma_3'/\sigma_1'}. \tag{16}$$

For comparison the values of $\frac{3}{2(1-\sigma_3'/\sigma_1')}$ are shown in column 5 of table 2. The values given in columns 3, 4, and 5 are shown graphically in figure 1.

COMPARISON WITH OBSERVED CRITERION

The observations made with copper tubes subjected to combined end-load and torsion (Taylor & Quinney 1931) were carried out by first loading the tube till it stretched, say, 0·5 %.

If the longitudinal stress for this pure extension was Y the load was reduced to $P = mY$ $(0<m<1)$ and torque applied till plastic flow occurred. It was found that though the beginning of inelastic displacement was not easy to measure the torque at which steady plastic flow occurred was definite. The shear stress corresponding with this condition being S, the angle θ between the axis of the tube and the axis of the greatest principal stress is given by

$$\tan 2\theta = \frac{2S}{P}. \tag{17}$$

The principal stresses are

$$\sigma_1 = \tfrac{1}{2}P(1+\sec 2\theta), \quad \sigma_2 = 0, \quad \sigma_3 = \tfrac{1}{2}P(1-\sec 2\theta), \tag{18}$$

so that

$$\sigma_1'/Y = \tfrac{1}{2}m(1+\sec 2\theta) = \tfrac{1}{3}m, \tag{19}$$

and

$$\frac{\sigma_1'}{\sigma_3'} = \frac{\frac{1}{3}-\sec 2\theta}{\frac{1}{3}+\sec 2\theta} \quad \text{or} \quad \cos 2\theta = 3\frac{\sigma_3'+\sigma_1'}{\sigma_3'-\sigma_1'}. \tag{20}$$

Hence

$$\frac{3}{2}\frac{\sigma_1'}{Y} = \frac{1}{2}\frac{m}{1+(\sigma_3'/\sigma_1')}. \tag{21}$$

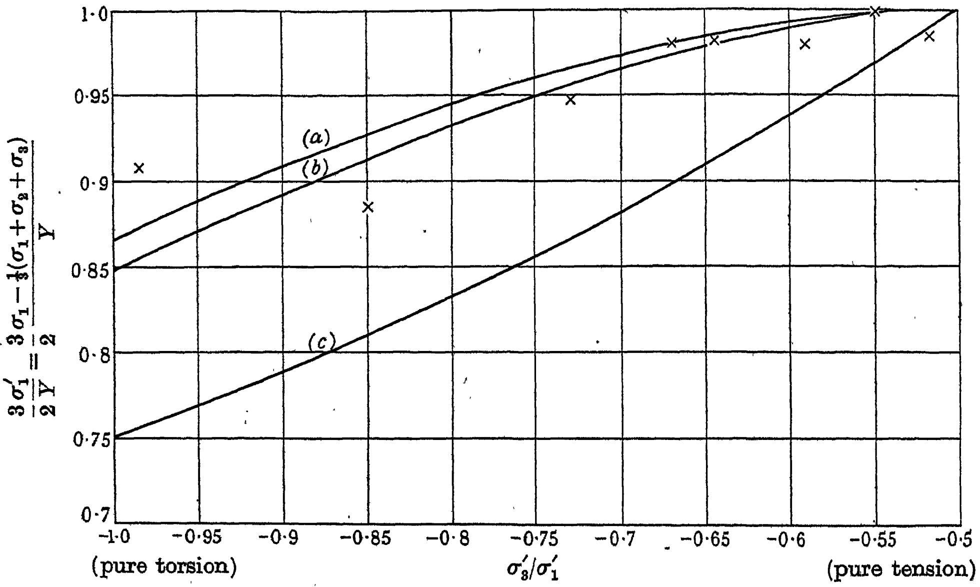

FIGURE 1. (*a*) Mises-Hencky. (*b*) Calculated by stationary energy dissipation hypothesis. (*c*) Maximum stress difference (Mohr). × × Observed points (Taylor & Quinney 1931).

The experimental values of m and σ_3'/σ_1' are given in columns 6 and 3 of table 1. The values of $3\sigma_1'/2Y$ found by inserting those in (21) for values of $m > 0\cdot28$ are given in column 7 of table 1. When m is very small (21) tends to the form 0/0, so that another expression for σ_1' is more accurate. The form used when $m = 0\cdot025$ and $m = 0\cdot28$ was

$$\frac{3\sigma_1'}{2Y} = \frac{P}{Y}\left\{\frac{1}{4}+\frac{3}{4}\sqrt{\left(1+\frac{4S^2}{P^2}\right)}\right\}. \tag{22}$$

The experimental points are plotted in figure 1, where it will be seen that the material behaves very nearly in accordance with the prediction based on the assumed stationary energy principle and the measured strain ratio relationship. Both the observed points and those calculated by the minimum energy relationship lie close to the Mises-Hencky line.

REFERENCES

Hill, R., Lee, E. H. & Tupper, S. J. 1947 *Proc. Roy. Soc.* A, **191**, 278.
Lode, W. 1926 *Z. Phys.* **36**, 913.
Taylor, G. I. & Quinney, H. 1931 *Phil. Trans.* A, **230**, 364.

The method of the hypercircle in function-space for boundary-value problems

By J. L. Synge, F.R.S., *Carnegie Institute of Technology*

(*Received* 19 *March* 1947)

For certain boundary-value problems, the conditions to be satisfied are split into two parts, so that the solution of a given problem is the common solution of two relaxed problems. Solutions of the two relaxed problems are easy to obtain, and such solutions give information regarding the solution of the original problem. This information is interpreted by a function-space representation. If the scalar product in function-space is suitably defined, solutions of the relaxed problems locate the solution of the original problem on, or inside, a hypercircle in function-space. The approximation may be improved by introducing further solutions of the relaxed problems. If the centre of the hypercircle is regarded as an approximate solution to the original problem, its error in a mean-square sense is immediately known.

The method has been applied to problems of the Dirichlet and Neumann types in Riemannian N-space, and to elastostatic boundary-value problems. In these cases, the metric of function-space is positive-definite, and the hypercircle on which the solution is located is bounded in the mean-square sense. Applications are also made to vibration problems (membrane and electromagnetic), but here the metric of function-space is indefinite, and the hypercircle becomes an unbounded pseudo-hypercircle.

1. INTRODUCTION

Many inequalities are known in connexion with the boundary-value problems of mathematical physics, such as the Dirichlet integral inequality in potential theory and the principle of minimum energy in elastostatics. Such inequalities are, however, scalar in character. This is no defect if the goal is a scalar, such as electrostatic capacity or torsional rigidity. But if further information is desired regarding the solution, a more powerful method is needed; as frequently happens, the more powerful method at the same time illuminates the question of scalar inequalities.

The method of the hypercircle has already been used for the elastostatic problem by Prager & Synge (1947). The elastostatic problem is discussed below in a slightly more general way, but the principal aim of the present paper is to explore the range of applicability of the method. For the sake of generality, some of the results are stated for a Riemannian N-space. This generalization is, however, not very significant. For, if the results are developed for Euclidean 3-space in a manner which does not essentially involve the dimensionality, the transition to Euclidean N-space is immediate. Then the passage to Riemannian N-space requires only the replacement of partial differentiation by covariant differentiation, and an examination of the validity of the integration procedures.

When we consider the problems in their simplest forms (e.g. Dirichlet and Neumann problems in a plane or in Euclidean 3-space), it is natural to expect anticipation on account of the amount of consideration which has been given to those problems. However, the explicit anticipation appears to be slight, because mathematicians have not exploited the simple geometry of function-space which provides a common approach to apparently diverse problems. In the work of Trefftz (1926) on the Dirichlet problem, the connexion with the hypercircle is particularly close.

The pattern of the method is as follows. We deal with a linear partial differential equation, or a set of such equations, with boundary conditions. We are not concerned with homogeneous (or eigenvalue) problems. We shall suppose that the differential equations are homogeneous, and the boundary-values non-homogeneous. There is no loss of generality here, since a problem with non-homogeneous differential equations can be brought to this form by use of a particular solution.

We split the boundary-value problem into two relaxed problems, such that a common solution of the two relaxed problems is a solution of the original problem. Next, we decide what function, or set of functions, shall correspond to a vector, or point, in function-space. Finally, we decide on a suitable definition of the scalar product in function-space; this gives a metric in function-space. From this point on, the procedure, once set up, is automatic, or nearly so, for most of the cases considered. The solution of the original problem is located in function-space on, or inside, a hypercircle of known centre and radius.

In an illustration, the detailed work is given for the Neumann problem, and the conclusions stated for similar problems. Mixed boundary-value problems and elastostatic problems are also discussed.

It is highly desirable to have a positive-definite metric in function-space, for only then is a hypercircle bounded in the mean-square sense. In the case of vibration problems (membrane and electromagnetic) no suitable positive-definite metric has been found. The metric which naturally suggests itself is indefinite, and the solution is located on a hypercircle of imaginary radius, i.e. on a pseudo-hypercircle.

In the case of a positive-definite metric, the location of the solution on a hypercircle gives upper and lower bounds for the solution in the neighbourhood of any prescribed point of the domain.

2. THE NEUMANN PROBLEM

Consider a Riemannian N-space R with positive-definite metric, metric tensor a_{ij} and co-ordinates x^i. Covariant differentiation will be denoted by a stroke: $T^{i}_{.|j}$, $T_{i|j}$. Let V be an open domain of N-dimensions, bounded by a surface, or $(N-1)$-space, B; V may be simply or multiply connected.

Our problem is to find a single-valued function w harmonic in V with $\partial w/\partial n$ assigned on B. These conditions may be written

$$\varDelta w = 0, \quad (\partial w/\partial n)_B = f, \tag{1}$$

where $\varDelta$ is the Laplace differential operator, and f a piecewise continuous function assigned on B, and satisfying $\int f\,dB = 0$, where dB is an $(N-1)$-dimensional volume element of B, and the integral is taken over B. More explicitly, we may write (1) as

$$w|^{i}_{.i} = 0, \quad (w^{|i} n_i)_B = f, \tag{2}$$

where n_i is the covariant unit normal to B, drawn outward. With regard to the smoothness of B, we shall assume n_i to be piecewise continuous, so that a solution w exists.

Consider now two relaxed problems. First, to find a vector field p^{*i} satisfying

$$p^{*i}_{\cdot|i} = 0, \quad (p^{*i}n_i)_B = f. \tag{3}$$

Secondly, to find a vector field p''_i satisfying

$$p''_i = w''_{|i}, \tag{4}$$

and no boundary conditions, where w'' is a single-valued function. We note that (4) implies

$$p''_{i|j} - p''_{j|i} = 0, \tag{5}$$

and this is in fact equivalent to (4) if V is simply connected.

Suppose now that we have a common solution of the two relaxed problems. (The transition from contravariant to covariant is, of course, carried out in the usual way: $p^*_i = a_{ij}p^{*j}$.) Then, omitting the star and primes, we have

$$w_{|i} = p_i, \quad p^i_{\cdot|i} = 0, \quad (p^i n_i)_B = f, \tag{6}$$

which imply that w satisfies the original problem (2).

Now we introduce the idea of function-space, which we shall denote by F. Naturally, we must be careful to distinguish between vectors in the Riemannian space R, and vectors in the function-space F. The latter will be denoted by heavy type, **S**.

We define a vector **S** in F to be any vector field p^i in $V+B$, subject to certain conditions of smoothness, namely, that V can be divided into a finite number of subregions such that p^i has continuous first derivatives in each such subregion, and the normal component $(p^i n_i)$ is continuous across the $(N-1)$-dimensional division between two subregions.

The scalar product of two vectors, **S** and **S**′, in F will be denoted by **S**.**S**′. It is defined by

$$\mathbf{S}.\mathbf{S}' = \int p^i p'_i \, dV = \int a_{ij} p^i p'^j \, dV, \tag{7}$$

where p^i and p'^i are the vectors in R corresponding to **S** and **S**′ respectively; dV is a volume-element of V, and the integration extends throughout V. Obviously, $\mathbf{S}.\mathbf{S}' = \mathbf{S}'.\mathbf{S}$. On putting $\mathbf{S}' = \mathbf{S}$, we get

$$|\mathbf{S}|^2 = \mathbf{S}^2 = \mathbf{S}.\mathbf{S} = \int p^i p_i \, dV = \int a_{ij} p^i p^j \, dV. \tag{8}$$

This gives the metric in F; it is positive-definite, since $a_{ij}p^i p^j$ is positive-definite. In fact, $|\mathbf{S}| = 0$ implies $p^i = 0$ throughout V.

The vectors $\mathbf{S}^*$, corresponding to p^{*i} satisfying (3), will be called *completely associated* vectors. Their extremities define a subspace F^* of F. The vectors $\mathbf{S}''$, corresponding to p''_i satisfying (4), will be called *complementary* vectors. Their extremities define a subspace F'' of F. The solution vector **S** corresponds to $p_i = w_{|i}$, where w is the solution of (1) or (2); the extremity of $\mathbf{S}$ is on the intersection of F^* and F''—a single point, since the solution of the Neumann problem is unique to within an additive constant.

So far, the definitions employed have been, to some extent, specific to the Neumann problem. Now we embark on a general procedure, by evaluating $\mathbf{S}^*.\mathbf{S}''$. We have

$$
\begin{aligned}
.\mathbf{S}'' &= \int p^{*i} p''_i \, dV \\
&= \int p^{*i} w''_{|i} \, dV \\
&= \int (p^{*i} w'')_{|i} \, dV - \int p^{*i}_{.|i} w'' \, dV.
\end{aligned}
\tag{9}
$$

The last integral vanishes, by (3), and Green's theorem may be applied to the first integral. This gives

$$\mathbf{S}^*.\mathbf{S}'' = \int w'' p^{*i} n_i \, dB. \tag{10}$$

Now $\mathbf{S}$ (the solution) is certainly a completely associated vector (i.e. it belongs to F^*), and so we may replace S^* in (10) by $\mathbf{S}$, obtaining

$$\mathbf{S}.\mathbf{S}'' = \int w'' p^{i} n_i \, dB. \tag{11}$$

But

$$(p^{*i} n_i)_B = (p^i n_i)_B = f, \tag{12}$$

and so subtraction of (10) from (11) gives our first basic equation

$$(\mathbf{S} - \mathbf{S}^*).\mathbf{S}'' = 0. \tag{13}$$

Remembering that $\mathbf{S}^*$ and $\mathbf{S}''$ are supposed to be known vectors (corresponding to solutions of the relaxed problems), it is clear that (13) locates the extremity of the solution vector $\mathbf{S}$ on a hyperplane Π in F, Π being orthogonal to $\mathbf{S}''$ and passing through the extremity of $\mathbf{S}^*$.

Since (13) is homogeneous in $\mathbf{S}''$, we may replace it by

$$\mathbf{S}.\mathbf{I}'' = \mathbf{S}^*.\mathbf{I}'', \tag{14}$$

where $\mathbf{I}''$ is the unit vector codirectional with $\mathbf{S}''$, i.e. $\mathbf{I}'' = \mathbf{S}''/|\,\mathbf{S}''\,|$.

The geometry of the linear 3-space in F defined by $\mathbf{S}$, $\mathbf{S}^*$, $\mathbf{I}''$ is Euclidean with metric (8), and (14) tells us that $\mathbf{S}$ and $\mathbf{S}^*$ have equal orthogonal projections on $\mathbf{I}''$; this projection is $\mathbf{S}^*.\mathbf{I}''$. Since $\mathbf{S}$ cannot be less than its projection, we get the scalar inequality

$$|\,\mathbf{S}\,| \geqslant |\,\mathbf{S}^*.\mathbf{I}''\,| = |\,\mathbf{S}^*.\mathbf{S}''\,|/|\,\mathbf{S}''\,|. \tag{15}$$

The first equality sign holds if, and only if, $\mathbf{S}$ and $\mathbf{S}''$ are codirectional or opposed, i.e. $\mathbf{S} = k\mathbf{S}''$ or $p_i = kp''_i$.

Let us return to (13). Since $\mathbf{S}$ is a complementary vector (i.e. it belongs to F''), we may replace $\mathbf{S}''$ in (13) by $\mathbf{S}$, and obtain

$$(\mathbf{S} - \mathbf{S}^*).\mathbf{S} = 0. \tag{16}$$

This equation may also be written

$$(\mathbf{S}-\tfrac{1}{2}\mathbf{S}^*)^2 = \tfrac{1}{4}\mathbf{S}^{*2}. \tag{17}$$

This shows that the extremity of S lies on a hypersphere in F with centre at the extremity of the vector $\frac{1}{2}\mathbf{S}^*$ and radius $\frac{1}{2}|\mathbf{S}^*|$. In fact, this hypersphere is the hypersphere described on the vector S* as diameter.

The equations (14) and (16) are the two basic equations which are found to hold in a number of problems to which the present method has been applied. Taken together, they confine the extremity of the (unknown) solution vector S to a hypercircle Γ in F, which has its centre at the extremity of the vector C, where

$$\mathbf{C} = \tfrac{1}{2}[\mathbf{S}^*+\mathbf{I}''(\mathbf{S}^*.\mathbf{I}'')]; \tag{18}$$

the radius R of Γ is given by

$$R^2 = \tfrac{1}{4}[\mathbf{S}^{*2}-(\mathbf{S}^*.\mathbf{I}'')^2]. \tag{19}$$

The solution vector S satisfies

$$(\mathbf{S}-\mathbf{C})^2 = R^2, \quad (\mathbf{S}-\mathbf{C}).\mathbf{I}'' = 0, \tag{20}$$

as is easily verified directly. We can also express the fact that S lies on Γ by writing

$$\mathbf{S} = \mathbf{C}+R\mathbf{J}, \tag{21}$$

where J is some unit vector satisfying the orthogonality condition

$$\mathbf{J}.\mathbf{I}'' = 0. \tag{22}$$

It is suggested by a simple diagram in F that the extremity of S* is the point of Γ farthest from the origin and that the extremity of $\mathbf{I}''(\mathbf{S}^*.\mathbf{I}'')$ is the point of Γ nearest to the origin. Hence we have the inequalities

$$(\mathbf{S}^*.\mathbf{I}'')^2 \leqslant \mathbf{S}^2 \leqslant \mathbf{S}^{*2}, \tag{23}$$

of which the former has already been given in (15). They are easy to verify directly. Noting that, by (14),

$$\mathbf{I}''.(\mathbf{S}-\mathbf{I}''(\mathbf{S}^*.\mathbf{I}'')) = 0,$$

we have

$$\begin{aligned}\mathbf{S}^2 &= [\mathbf{I}''(\mathbf{S}^*.\mathbf{I}'')+\mathbf{S}-\mathbf{I}''(\mathbf{S}^*.\mathbf{I}'')]^2\\ &= (\mathbf{S}^*.\mathbf{I}'')^2+[\mathbf{S}-\mathbf{I}''(\mathbf{S}^*.\mathbf{I}'')]^2\\ &\geqslant (\mathbf{S}^*.\mathbf{I}'')^2,\end{aligned}$$

on account of the positive-definite character of the metric in F. Also, using (16), we have

$$\begin{aligned}\mathbf{S}^2 &= (\mathbf{S}-\mathbf{S}^*+\mathbf{S}^*)^2\\ &= (\mathbf{S}-\mathbf{S}^*)^2+2\mathbf{S}^*.(\mathbf{S}-\mathbf{S}^*)+\mathbf{S}^{*2}\\ &= (\mathbf{S}-\mathbf{S}^*)^2-2(\mathbf{S}-\mathbf{S}^*)^2+2\mathbf{S}.(\mathbf{S}-\mathbf{S}^*)+\mathbf{S}^{*2}\\ &= -(\mathbf{S}-\mathbf{S}^*)^2+\mathbf{S}^{*2}\\ &\leqslant \mathbf{S}^{*2}.\end{aligned}$$

To see what the results obtained amount to, let us state them, first, in terms of the geometry of the function space F, and, secondly, without reference to function-space.

THEOREM I. *If* S* *is a completely associated vector* (*class* F^*), *and* S″ *a complementary vector* (*class* F''), *then the extremity of the solution vector* S *lies on a hypercircle* Γ *defined by* (20), *or equivalently by* (21) *and* (22), *and its magnitude is bounded below and above by the inequalities* (23).

The above theorem has been proved for the Neumann problem. But it is stated in a form valid for a wider class of problems.

We now state our result without reference to function-space.

THEOREM II. *The* (*single-valued*) *solution* w *of the Neumann problem defined by* (2) *satisfies*

$$\int (w^{|i} - c^i)(w_{|i} - c_i)\, dV = R^2, \tag{24}$$

$$\int (w^{|i} - c^i)\, w''_{|i} dV = 0, \tag{25}$$

where

$$c_i = \frac{1}{2}\left[p^*_i + w''_{|i}\left(\int p^{*j} w''_{|j} dV\right) \Big/ \left(\int w''^{|k} w''_{|k} dV\right)\right], \tag{26}$$

$$R^2 = \frac{1}{4}\left[\int p^{*i} p^*_i dV - \left(\int p^{*i} w''_{|i} dV\right)^2 \Big/ \left(\int w''^{|k} w''_{|k} dV\right)\right]. \tag{27}$$

Further

$$\left(\int p^{*i} w''_{|i} dV\right)^2 \Big/ \left(\int w''^{|j} w''_{|j} dV\right) \leqslant \int w^{|i} w_{|i} dV \leqslant \int p^{*i} p^*_i dV. \tag{28}$$

Here p^*_i is any vector field satisfying (3) and w'' an arbitrary scalar field; p^*_i and $w''_{|i}$ are subject to conditions of smoothness given earlier.

The second inequality of (28) is an immediate generalization of Kelvin's theorem (Lamb 1932), to the effect that, when the normal velocity is prescribed, the irrotational motion of an incompressible fluid (with zero circulation in irreducible circuits) has minimum kinetic energy.

The basic idea behind the above procedure, regarded as a method of approximation, is that C, the centre of the hypercircle Γ, should be regarded as an approximation to the solution S. Unless $R = 0$, C cannot coincide with S, because, by (20), the extremity of S lies at a distance R from the extremity of C. But, if C is accepted as an approximate solution, we have the satisfaction of knowing that its error $|\mathrm{S} - \mathrm{C}|$ is precisely known; it is R, as given by (19) or (27). It should be noted that C gives an approximation to $w_{|i}$, not to w. However, once a good approximation to $w_{|i}$ has been obtained, we can get an approximation to w by integrating $w_{|i}dx^i$ along a family of curves in V.

We now consider the improvement of the approximation. To this end, we introduce an orthonormal set of vectors $\mathrm{I}'_{(p)}$ ($p = 1, 2, \ldots, m$), which we shall call *homogeneous associated* vectors. Any such vector corresponds to a vector field p'^i in $V + B$ satisfying

$$p'^i_{|i} = 0, \quad (p'^i n_i)_B = 0, \tag{29}$$

and the smoothness conditions described earlier. The conditions of orthonormality give

$$\mathbf{I}'_{(p)} \cdot \mathbf{I}'_{(q)} = \delta_{(pq)} \quad (p, q = 1, 2, \ldots, m), \tag{30}$$

$\delta_{(pq)}$ being the usual Kronecker delta.

It is easy to see that the solution $\mathbf{S}$ is orthogonal to every homogeneous associated vector, so that

$$\mathbf{S} \cdot \mathbf{I}'_{(p)} = 0 \quad (p = 1, 2, \ldots, m). \tag{31}$$

Now we introduce an orthonormal set of complementary vectors $\mathbf{I}''_{(q)}$ $(q = 1, 2, \ldots, n)$ so that

$$\mathbf{I}''_{(p)} \cdot \mathbf{I}''_{(q)} = \delta_{(pq)} \quad (p, q = 1, 2, \ldots, n). \tag{32}$$

It is easy to show that every homogeneous associated vector is orthogonal to every complementary vector, so that

$$\mathbf{I}'_{(p)} \cdot \mathbf{I}''_{(q)} = 0 \quad (p = 1, 2, \ldots, m;\ q = 1, 2, \ldots, n). \tag{33}$$

In fact, the homogeneous associated vectors $\mathbf{I}'_{(p)}$ and the complementary vectors $\mathbf{I}''_{(q)}$ together form an orthogonal set of $(m+n)$ unit vectors.

By (14), we have
$$\mathbf{S} \cdot \mathbf{I}''_{(q)} = \mathbf{S}^* \cdot \mathbf{I}''_{(q)} \quad (q = 1, 2, \ldots, n). \tag{34}$$

Thus, by (31) and (34), the extremity of $\mathbf{S}$ is located on a hyperplane which is the intersection of $(m+n)$ hyperplanes defined by those equations. But the extremity of $\mathbf{S}$ lies also on the hypersphere (16). Hence the extremity of $\mathbf{S}$ lies on a hypercircle Γ. The centre $\mathbf{C}$ and radius R of Γ are easily found; they are given by

$$\mathbf{C} = \frac{1}{2}\left[\mathbf{S}^* - \sum_{p=1}^{m} \mathbf{I}'_{(p)}(\mathbf{S}^* \cdot \mathbf{I}'_{(p)}) + \sum_{q=1}^{n} \mathbf{I}''_{(q)}(\mathbf{S}^* \cdot \mathbf{I}''_{(q)})\right], \tag{35}$$

$$R^2 = \frac{1}{4}\left[\mathbf{S}^{*2} - \sum_{p=1}^{m} (\mathbf{S}^* \cdot \mathbf{I}'_{(p)})^2 - \sum_{q=1}^{n} (\mathbf{S}^* \cdot \mathbf{I}''_{(q)})^2\right]. \tag{36}$$

We note that R decreases with each addition of a vector to either of the sets $\mathbf{I}'_{(p)}$, $\mathbf{I}''_{(q)}$, provided it is not orthogonal to $\mathbf{S}^*$.

We may write the equation of the hypercircle Γ in the form

$$\mathbf{S} = \mathbf{C} + R\mathbf{J}, \tag{37}$$

where $\mathbf{J}$ is a vector subject only to the conditions

$$\begin{aligned} \mathbf{J}^2 = 1, \quad \mathbf{J} \cdot \mathbf{I}'_{(p)} &= 0 \quad (p = 1, 2, \ldots, m), \\ \mathbf{J} \cdot \mathbf{I}''_{(q)} &= 0 \quad (q = 1, 2, \ldots, n). \end{aligned} \tag{38}$$

As in Prager & Synge (1947), we can establish the inequalities

$$\mathbf{V}''^2 \leqslant \mathbf{S}^2 \leqslant \mathbf{V}^{*2}, \tag{39}$$

where
$$\mathbf{V}'' = \sum_{q=1}^{n} \mathbf{I}''_{(q)}(\mathbf{S}^* \cdot \mathbf{I}''_{(q)}), \quad \mathbf{V}^* = \mathbf{S}^* - \sum_{p=1}^{m} \mathbf{I}'_{(p)}(\mathbf{S}^* \cdot \mathbf{I}'_{(p)}). \tag{40}$$

We shall end this section with some remarks on the exterior Neumann problem, confining our attention to a Euclidean space of N dimensions ($N \geqslant 2$). The conditions (1) are now supplemented by a condition at infinity. We shall take this to be that w tends to zero at infinity and that the derivatives of w with respect to rectangular Cartesian co-ordinates shall be bounded like R^{-N}, where R is the distance from a fixed point. The argument proceeds along the same lines as before, provided we supplement the conditions (3), (4), and (29) with conditions at infinity, namely, that p_i^*, p_i'', p_i' shall be bounded like R^{-N}, and that w'' in (4) shall tend to zero at infinity. Under these conditions, all scalar products in function-space converge. If $N > 2$, we can replace the bound R^{-N} by R^{-N+1}.

3. SOME PROBLEMS LEADING TO THE HYPERCIRCLE

As mentioned in § 1, there are three essential steps in the treatment of any problem which lends itself to the method of the hypercircle in function-space. Stated in the order best suited to present purposes, these steps involve answering the following questions:

(*a*) What function, or set of functions, shall correspond to a vector, or point, in function-space?

(*b*) What is the scalar product in function-space?

(*c*) How are the relaxed problems defined, or, equivalently, what are the completely associated, complementary, and homogeneous associated vectors in function-space?

Once these questions have been answered, the passage to the basic equations (13) and (16) is direct; from those, equations (18) to (23) inclusive, follow, and also theorem I. Equations (30) to (40) inclusive also follow. It seems sufficient, therefore, to answer the questions (*a*), (*b*), (*c*) above in tabular form, and leave the verification to the reader. The results are set out in table 1.

4. THE DIRICHLET-NEUMANN MIXED BOUNDARY-VALUE PROBLEM

In a region V of Riemannian N-space, with positive-definite metric, bounded by an $(N-1)$-space B, consider the problem

$$\Delta w = 0, \quad (\alpha w + \beta \partial w/\partial n)_B = f, \tag{41}$$

where α, β, f are assigned functions on B.

Here the relaxed problems are not distinct; they are combined in the boundary conditions. We consider vector fields p^{*i} satisfying

$$p^{*i}_{.|i} = 0, \tag{42}$$

and vector fields p_i'' satisfying

$$p_i'' = w''_{|i}, \tag{43}$$

where w'' is a single-valued function of position in V. But we link these problems together by the boundary condition

$$(\alpha w'' + \beta p^{*i} n_i)_B = f. \tag{44}$$

It is clear that if $p^{*i} = p''^i$, we have a solution of (41) in the form $w = w''$.

TABLE 1. BOUNDARY-VALUE PROBLEMS IN RIEMANNIAN N-SPACE WITH POSITIVE-DEFINITE METRIC ($T_{ij\dots} = a_{im}a_{jn}\dots T^{mn\dots}$)

Solution **S** located on hypercircle specified by equations (21) and (22), or (35) to (38).

problem	vector in function-space	scalar product $\mathbf{S}.\mathbf{S}'$	completely associated vector $\mathbf{S}^*$	complementary vector $\mathbf{S}''$, normalized to $\mathbf{I}''$	homogeneous associated vector $\mathbf{S}'$, normalized to $\mathbf{I}'$
Dirichlet $w\|^{i}_{.i} \equiv \Delta w = 0$, $(w)_B = f$	p^i	$\int p^i p'_i \, dV$	$p^*_i = w^*_{\|i}$, $(w^*)_B = f$	$p''^{i}_{.\|i} = 0$	$p'_i = w'_{\|i}$, $(w')_B = 0$
Neumann $w\|^{i}_{.i} \equiv \Delta w = 0$, $(\partial w/\partial n)_B = f$	p^i	$\int p^i p'_i \, dV$	$p^{*i}_{.\|i} = 0$, $(p^{*i} n_i)_B = f$	$p''_i = w''_{\|i}$	$p'^{i}_{.\|i} = 0$, $(p'^{i} n_i)_B = 0$
biharmonic $w\|^{ij}_{..ji} \equiv \Delta\Delta w = 0$, $(w)_B = f$, $(w_{\|i})_B = g_i$	p^{ij}	$\int p^{ij} p'_{ij} \, dV$	$p^*_{ij} = w^*_{\|ij}$, $(w^*)_B = f$, $(w^*_{\|i})_B = g_i$	$p''^{ij}_{..\|ji} = 0$	$p'_{ij} = w'_{\|ij}$, $(w')_B = 0$, $(w'_{\|i})_B = 0$
triharmonic $w\|^{ijk}_{...kji} = 0$, $(w)_B = f$, $(w_{\|i})_B = g_i$, $(w_{\|ij})_B = h_{ij}$	p^{ijk}	$\int p^{ijk} p'_{ijk} \, dV$	$p^*_{ijk} = w^*_{\|ijk}$, $(w^*)_B = f$, $(w^*_{\|i})_B = g_i$, $(w^*_{\|ij})_B = h_{ij}$	$p''^{ijk}_{...\|kji} = 0$	$p'_{ijk} = w'_{\|ijk}$, $(w')_B = 0$, $(w'_{\|i})_B = 0$, $(w'_{\|ij})_B = 0$
generalized Dirichlet $(\rho w^{\|i})_{\|i} = 0$, $\rho > 0$, $(w)_B = f$	p^i	$\int \rho^{-1} p^i p'_i \, dV$	$p^*_i = \rho w^*_{\|i}$, $(w^*)_B = f$	$p''^{i}_{.\|i} = 0$	$p'_i = \rho w'_{\|i}$, $(w')_B = 0$
generalized Neumann $(\rho w^{\|i})_{\|i} = 0$, $\rho > 0$, $(\partial w/\partial n)_B = f$	p^i	$\int \rho^{-1} p^i p'_i \, dV$	$p^{*i}_{.\|i} = 0$, $(p^{*i} n_i)_B = \rho f$	$p''_i = \rho w''_{\|i}$	$p'^{i}_{.\|i} = 0$, $(p'^{i} n_i)_B = 0$
modified wave equation I $\Delta w - \lambda w = 0$, $\lambda > 0$, $(w)_B = f$	p^i, w	$\int (p^i p'_i + \lambda w w') \, dV$	$p^*_i = w^*_{\|i}$, $(w^*)_B = f$	$p''^{i}_{.\|i} - \lambda w'' = 0$	$p'_i = w'_{\|i}$, $(w')_B = 0$
modified wave equation II $\Delta w - \lambda w = 0$, $\lambda > 0$, $(\partial w/\partial n)_B = f$	p^i, w	$\int (p^i p'_i + \lambda w w') \, dV$	$p^{*i}_{.\|i} - \lambda w^* = 0$, $(p^{*i} n_i)_B = f$	$p''_i = w''_{\|i}$	$p'^{i}_{.\|i} - \lambda w' = 0$, $(p'^{i} n_i)_B = 0$

A vector in function-space will correspond to a vector field p^i in $V+B$. The scalar product is defined as in (7). Consider a class of F-vectors $\mathbf{S}^*$ satisfying (42) and a class $\mathbf{S}''$ satisfying (43). Then

$$\begin{aligned} \mathbf{S}^*.\mathbf{S}'' &= \int p^{*i}p''_i\,dV = \int p^{*i}w''_{|i}\,dV \\ &= \int w''p^{*i}n_i\,dB - \int w''p^{*i}_{.|i}\,dV; \end{aligned} \tag{45}$$

the last integral vanishes, by (42). Also, if $\mathbf{S}$ is a solution of (41), with $p_i = w_{|i}$, then $\mathbf{S}$ belongs to the class of $\mathbf{S}^*$, and so (45) gives

$$\mathbf{S}.\mathbf{S}'' = \int w''p^in_i\,dB. \tag{46}$$

Also, since $\mathbf{S}$ belongs to the class of $\mathbf{S}''$, we have, from (45) and (46),

$$\mathbf{S}^*.\mathbf{S} = \int wp^{*i}n_i\,dB, \quad \mathbf{S}.\mathbf{S} = \int wp^in_i\,dB. \tag{47}$$

By combination of (45), (46), (47), we have

$$\mathbf{S}.\mathbf{S}-\mathbf{S}.\mathbf{S}^*-\mathbf{S}.\mathbf{S}''+\mathbf{S}^*.\mathbf{S}'' = \int (w-w'')\,(p^in_i-p^{*i}n_i)\,dB. \tag{48}$$

So far (44) has not been used. We now subject $\mathbf{S}^*$ and $\mathbf{S}''$ to this condition, and use also the fact that $\mathbf{S}$ satisfies

$$(\alpha w+\beta p^in_i)_B = f. \tag{49}$$

Subtraction of (44) from (49) gives, on B,

$$\alpha(w-w'')+\beta(p^in_i-p^{*i}n_i) = 0, \tag{50}$$

and hence

$$2\alpha\beta(w-w'')\,(p^in_i-p^{*i}n_i) = -\alpha^2(w-w'')^2-\beta^2(p^in_i-p^{*i}n_i)^2. \tag{51}$$

Let us now subject α, β to the condition *that $\alpha\beta$ is not negative on B, and that at no point do we have $\alpha = 0$ and $\beta = 0$*. We have then to consider three possibilities at any point of B:

(i) $\alpha \neq 0,\ \beta \neq 0,\ \alpha\beta > 0$; (ii) $\alpha \neq 0,\ \beta = 0$; (iii) $\alpha = 0,\ \beta \neq 0$.

At a point where (i) holds, the integrand in (48) is not positive, by (51). At a point where (ii) holds, $w-w'' = 0$ by (50), and so the integrand in (48) vanishes. At a point where (iii) holds, we have $p^in_i-p^{*i}n_i = 0$, and so the integrand again vanishes. Hence, under the stated condition, we may write (48) in the form

$$\mathbf{S}.\mathbf{S}-\mathbf{S}.\mathbf{S}^*-\mathbf{S}.\mathbf{S}''+\mathbf{S}^*.\mathbf{S}'' \leqslant 0, \tag{52}$$

or, equivalently,

$$[\mathbf{S}-\tfrac{1}{2}(\mathbf{S}^*+\mathbf{S}'')]^2 \leqslant \tfrac{1}{4}(\mathbf{S}^*-\mathbf{S}'')^2. \tag{53}$$

This inequality locates the extremity of the solution vector $\mathbf{S}$ inside, or on, a hypersphere with centre at the extremity of $\tfrac{1}{2}(\mathbf{S}^*+\mathbf{S}'')$ and with radius $\tfrac{1}{2}\,|\,\mathbf{S}^*-\mathbf{S}''\,|$.

We now introduce orthonormal F-vectors $\mathbf{I}'_{(p)}$ $(p = 1, 2, \ldots, m)$ corresponding to vector fields p'^i satisfying

$$p'^i_{.|i} = 0, \quad (p'^i n_i)_B = 0, \tag{54}$$

and orthonormal F-vectors $\mathbf{I}'''_{(q)}$ $(q = 1, 2, \ldots, n)$ corresponding to vector fields p'''_i satisfying

$$p'''_i = w'''_{|i}, \quad (w''')_B = 0. \tag{55}$$

We find

$$\mathbf{I}'_{(p)} . \mathbf{I}'''_{(q)} = \int p'^i p'''_i \, dV = 0, \tag{56}$$

so that $\mathbf{I}'_{(p)}$, $\mathbf{I}'''_{(q)}$ form an orthonormal set of $m+n$ vectors. Further

$$\mathbf{S} . \mathbf{I}'_{(p)} = \int p'^i p_i \, dV = 0, \quad \mathbf{S} . \mathbf{I}'''_{(q)} = \int p'''_i p^i \, dV = 0, \tag{57}$$

so that we have

$$\mathbf{S} . \mathbf{I}_{(r)} = 0 \quad (r = 1, 2, \ldots, m+n). \tag{58}$$

This expresses the orthogonality of $\mathbf{S}$ to the orthonormal set of $(m+n)$ vectors $\mathbf{I}'_{(p)}$, $\mathbf{I}'''_{(q)}$, if we use $\mathbf{I}_{(r)}$ to refer to any one of these vectors.

By (53), we located the extremity of $\mathbf{S}$ inside, or on, a hypersphere. But (58) we located it on $(m+n)$ hyperplanes. Hence the extremity of $\mathbf{S}$ lies on the hyperplane which is the intersection of (58), and inside the hypercircle Γ which is the intersection of (58) with the hypersphere

$$[\mathbf{S} - \tfrac{1}{2}(\mathbf{S}^* + \mathbf{S}'')]^2 = \tfrac{1}{4}(\mathbf{S}^* - \mathbf{S}'')^2. \tag{59}$$

The centre $\mathbf{C}$ of Γ is given by

$$\mathbf{C} = \frac{1}{2}\left[\mathbf{S}^* + \mathbf{S}'' - \sum_{r=1}^{m+n} \mathbf{I}_{(r)}\{(\mathbf{S}^* + \mathbf{S}'') . \mathbf{I}_{(r)}\}\right], \tag{60}$$

and its radius R by

$$R^2 = \frac{1}{4}\left[(\mathbf{S}^* - \mathbf{S}'')^2 - \sum_{r=1}^{m+n} \{(\mathbf{S}^* + \mathbf{S}'') . \mathbf{I}_{(r)}\}^2\right]. \tag{61}$$

However, it is easy to verify that

$$\mathbf{S}^* . \mathbf{I}'''_{(q)} = 0, \quad \mathbf{S}'' . \mathbf{I}'_{(p)} = 0, \tag{62}$$

and so (60) and (61) may be written

$$\mathbf{C} = \frac{1}{2}\left[\mathbf{S}^* + \mathbf{S}'' - \sum_{p=1}^{m} \mathbf{I}'_{(p)}(\mathbf{S}^* . \mathbf{I}'_{(p)}) - \sum_{q=1}^{n} \mathbf{I}'''_{(q)}(\mathbf{S}'' . \mathbf{I}'''_{(q)})\right], \tag{63}$$

and

$$R^2 = \frac{1}{4}\left[(\mathbf{S}^* - \mathbf{S}'')^2 - \sum_{p=1}^{m} (\mathbf{S}^* . \mathbf{I}'_{(p)})^2 - \sum_{q=1}^{n} (\mathbf{S}'' . \mathbf{I}'''_{(q)})^2\right]. \tag{64}$$

Since we do not change the value of this expression (cf. (62)) if we substitute $\mathbf{S}^* - \mathbf{S}''$ for $\mathbf{S}^*$ in the first summation and for $\mathbf{S}''$ in the second summation, we have

$$R^2 = \frac{1}{4}\left[(\mathbf{S}^* - \mathbf{S}'' - \sum_{p=1}^{m} \mathbf{I}'_{(p)}\{(\mathbf{S}^* - \mathbf{S}'') . \mathbf{I}'_{(p)}\} - \sum_{q=1}^{n} \mathbf{I}'''_{(q)}\{(\mathbf{S}^* - \mathbf{S}'') . \mathbf{I}'''_{(q)}\}\right]^2, \tag{65}$$

which verifies that R is real.

We can easily use the hypercircle Γ to obtain lower and upper bounds for $\mathbf{S}^2$.

5. ELASTOSTATIC PROBLEMS

We shall discuss elastostatic problems here in a slightly more general way than was done by Prager & Synge (1947). We treat the problem in Euclidean 3-space, with rectangular Cartesian co-ordinates x_i; partial derivatives will be denoted by commas ($V_{,i} = \partial V/\partial x_i$). All suffixes will be written as subscripts, but the summation convention is understood.

A vector S in function-space F corresponds to a state of stress E_{ij} ($= E_{ji}$) throughout a body V, bounded by a surface B. The strain components e_{ij} ($= e_{ji}$) are given by the generalized Hooke's Law, so that anisotropic bodies are included. A strain energy function ($\frac{1}{2}e_{ij}E_{ij}$) is assumed, so that we have the 21-constant theory, and the reciprocity relation $e_{ij}E'_{ij} = e'_{ij}E_{ij}$ holds. In general, a state S does not satisfy the equations of compatibility; in such cases, no displacement u_i exists.

The scalar product of two vectors in function-space is defined by

$$\mathrm{S}.\mathrm{S}' = \int e_{ij}E'_{ij}\,dV = \int e'_{ij}E_{ij}\,dV = \mathrm{S}'.\mathrm{S}. \tag{66}$$

We shall make the usual assumption that strain-energy is positive-definite. Then

$$\mathrm{S}^2 = \int e_{ij}E_{ij}\,dV \geqslant 0, \tag{67}$$

the sign of equality holding if, and only if, the stress vanishes throughout. Thus our function-space has a positive-definite metric.

We shall consider only the case where there are no body forces.

Before we introduce any boundary-values, we define a class F^* of vectors S^* satisfying the equations of equilibrium

$$E^*_{ij,j} = 0. \tag{68}$$

Also we define a class F'' of vectors S'' satisfying the equations of compatibility; for such states, a displacement u''_i exists, satisfying

$$u''_{i,j} + u''_{j,i} = 2e''_{ij}. \tag{69}$$

Then

$$\begin{aligned}\mathrm{S}^*.\mathrm{S}'' &= \int e''_{ij}E^*_{ij}\,dV \\ &= \int u''_{i,j}E^*_{ij}\,dV \\ &= \int u''_i E^*_{ij}n_j\,dB - \int u''_i E^*_{ij,j}\,dV,\end{aligned} \tag{70}$$

where n_i is the unit outward normal to B. The last integral vanishes, by (68). Let us denote surface stress by T_i, so that $T_i = E_{ij}n_j$ for any state. Then (70) reads

$$\mathrm{S}^*.\mathrm{S}'' = \int u''_i T^*_i\,dB. \tag{71}$$

Suppose now that S lies in the intersection of the classes F^* and F'', i.e. it corresponds to a state which satisfies the equations of equilibrium and compatibility. Then we obtain at once from (71)

$$\mathbf{S}.\mathbf{S}'' = \int u_i'' T_i \, dB, \quad \mathbf{S}^*.\mathbf{S} = \int u_i T_i^* \, dB, \quad \mathbf{S}.\mathbf{S} = \int u_i T_i \, dB. \tag{72}$$

Combining (71) and (72), we get

$$(\mathbf{S}-\mathbf{S}^*).(\mathbf{S}-\mathbf{S}'') = \int (u_i - u_i'')(T_i - T_i^*) \, dB. \tag{73}$$

Let us now suppose that boundary conditions are assigned, and let S be the solution of the elastostatic problem for the body V under these boundary conditions on B. The boundary conditions may be the assignment of displacement u_i or surface stress T_i, or a mixture of these conditions. Our plan is to subject S* and S″ to boundary conditions connected with the assigned boundary conditions in such a way as to make the integral in (73) zero or negative.

Suppose that the assigned boundary condition is $(u_i)_B = f_i$, where f_i is a given vector field on B. Then we subject S″ to $(u_i'')_B = f_i$, but place no boundary condition on S*. This makes the integral in (73) vanish.

On the other hand, suppose that the assigned boundary condition is $(T_i)_B = g_i$, where g_i is a given vector field on B. Then we subject S* to $(T_i^*)_B = g_i$, but place no boundary condition on S″. Again the integral in (73) vanishes.

Finally, we consider a more general type of assigned boundary condition in which neither the complete vector field u_i, nor the complete vector field T_i, is given over B. We shall, in fact, assume as boundary conditions on B

$$A_{ij} u_j + B_{ij} T_j = C_i, \tag{74}$$

where A_{ij}, B_{ij}, C_i are given functions on B. In this case, we subject S* and S″ to the mixed condition

$$A_{ij} u_j'' + B_{ij} T_j^* = C_i, \tag{75}$$

so that, by subtraction from (74),

$$A_{ij}(u_j - u_j'') + B_{ij}(T_j - T_j^*) = 0. \tag{76}$$

We shall now make two assumptions about the matrices A_{ij}, B_{ij}:

(i) There exist positive numbers l, m such that

$$l A_{ij} A_{ik} + m B_{ij} B_{ik} = \delta_{jk}. \tag{77}$$

(ii) $$A_{ij} B_{ik} X_j X_k \geqslant 0 \quad \text{for all } X_i. \tag{78}$$

In matrix notation, using the tilda to denote the transpose, these conditions read

$$l\tilde{\mathbf{A}}\mathbf{A} + m\tilde{\mathbf{B}}\mathbf{B} = 1, \quad \mathbf{X}\tilde{\mathbf{A}}\mathbf{B}\mathbf{X} \geqslant 0. \tag{79}$$

We now multiply (76) by $A_{ik}(T_k - T_k^*)$, obtaining

$$A_{ij} A_{ik} (u_j - u_j'')(T_k - T_k^*) = -A_{ik} B_{ij} (T_j - T_j^*)(T_k - T_k^*).$$

Similarly, multiplying (76) by $B_{ik}(u_k - u''_k)$, we obtain

$$B_{ij}B_{ik}(u_k - u''_k)(T_j - T^*_j) = -A_{ij}B_{ik}(u_j - u''_j)(u_k - u''_k).$$

We multiply these two equations by l, m respectively, and add. Then by (77), (78), we have, at all points of B,

$$(u_j - u''_j)(T_j - T^*_j) \leqslant 0. \tag{80}$$

It follows from (73) that
$$(\mathbf{S} - \mathbf{S}^*) . (\mathbf{S} - \mathbf{S}'') \leqslant 0, \tag{81}$$

so that the vectors drawn from the extremities of $\mathbf{S}^*$ and $\mathbf{S}''$ to the extremity of $\mathbf{S}$ make an obtuse angle with one another. Equivalently,

$$[\mathbf{S} - \tfrac{1}{2}(\mathbf{S}^* + \mathbf{S}'')]^2 \leqslant \tfrac{1}{4}(\mathbf{S}^* - \mathbf{S}'')^2, \tag{82}$$

showing that the extremity of $\mathbf{S}$ lies inside, or on, a hypersphere with centre at $\tfrac{1}{2}(\mathbf{S}^* + \mathbf{S}'')$ and with radius $\tfrac{1}{2}|\mathbf{S}^* - \mathbf{S}''|$. The equality sign holds in the particular cases where $(u_i)_B$ is completely assigned, or where $(T_i)_B$ is completely assigned, and $\mathbf{S}^*$ and $\mathbf{S}''$ subjected to the boundary conditions as stated earlier. In these cases, the extremity of $\mathbf{S}$ lies *on* the hypersphere. These cases are particular cases of (74). The case where $(u_i)_B$ is assigned corresponds to $A_{ij} = \delta_{ij}$, $B_{ij} = 0$, and the case where $(T_i)_B$ is assigned corresponds to $A_{ij} = 0$, $B_{ij} = \delta_{ij}$. Obviously, in each case (77) and (78) are satisfied.

It is clear from inspection of the equations preceding (80) that the extremity of $\mathbf{S}$ will fall on the hypersphere, rather than inside, if the condition

$$A_{ij}B_{ik} = 0 \tag{83}$$

is satisfied over B. We verify that this is the case where either $(u_i)_B$ or $(T_i)_B$ is assigned.

The conditions (77), (78) are satisfied when at each point of B the normal component of one of the vectors u_i, T_i and the tangential component of the other are assigned. This case has been considered by Prager & Synge (1947), in a rather different way. To verify the above statement, take axes such that, at a given point, the axis of x_1 is normal to B, and the axes of x_2, x_3 tangential. Suppose that the normal component of u_i and the tangential component of T_i are assigned. Then our boundary conditions at this point are: u_1, T_2, T_3 assigned. Comparing this statement with (74), we have

$$\mathbf{A} = \begin{pmatrix} 1 & 0 & 0 \\ 0 & 0 & 0 \\ 0 & 0 & 0 \end{pmatrix}, \quad \mathbf{B} = \begin{pmatrix} 0 & 0 & 0 \\ 0 & 1 & 0 \\ 0 & 0 & 1 \end{pmatrix},$$

and it is easily verified that (77) and (78) hold. Indeed, (83) holds, so that (78) is an equality, and the extremity of $\mathbf{S}$ lies *on* the hypersphere.

Once the inequality (82) has been established, further approximations may be made along the same lines as in § 4. We may introduce an orthonormal set of vectors $\mathbf{I}'_{(p)}$ satisfying the equations of equilibrium and making $(T'_i)_B = 0$, and an orthonormal set of vectors $\mathbf{I}'''_{(q)}$ satisfying the equations of compatibility, and making $(u'''_i)_B = 0$. We then obtain

$$\mathbf{S}.\mathbf{I}'_{(p)} = 0, \quad \mathbf{S}.\mathbf{I}'''_{(q)} = 0, \quad \mathbf{I}'_{(p)}.\mathbf{I}'''_{(q)} = 0, \tag{84}$$

and thus locate $\mathbf{S}$ inside, or on, a hypercircle Γ with centre and radius given by (63) and (64) respectively.

6. Bounds for the solution in the neighbourhood of a point

So far, we have located solutions on, or inside, hypercircles. If the centre of the hypercircle is taken as an approximate solution, we know its error in a mean-square sense, i.e. in terms of an integral taken over the domain V in which the solution exists. But this gives us no information regarding the solution at a given point P of V.

It will be sufficient to consider only the case where the extremity of the solution vector $\mathbf{S}$ lies *on* a hypercircle Γ, since if it lies inside the same bounds hold. Consider, then, the case where $\mathbf{S}$ satisfies

$$\mathbf{S} = \mathbf{C} + R\mathbf{J}, \tag{85}$$

where $\mathbf{C}$ is a given vector, R a given positive number, and $\mathbf{J}$ is a unit vector subject to conditions

$$\mathbf{J}.\mathbf{I}_{(r)} = 0 \quad (r = 1, \ldots, m), \tag{86}$$

where $\mathbf{I}_{(r)}$ form a set of orthonormal vectors.

Let $\mathbf{K}$ be any unit vector. Consider the orthogonal projection $\mathbf{S}.\mathbf{K}$ of $\mathbf{S}$ on $\mathbf{K}$. It appears obvious geometrically that, as the extremity of $\mathbf{S}$ ranges over the hypercircle Γ, $\mathbf{S}.\mathbf{K}$ will have lower and upper bounds. Let us find them. We have, by (85),

$$\mathbf{S}.\mathbf{K} = \mathbf{C}.\mathbf{K} + R\mathbf{J}.\mathbf{K}. \tag{87}$$

Here $\mathbf{J}$ is arbitrary, except for $\mathbf{J}.\mathbf{J} = 1$ and (86). The stationary values of $\mathbf{S}.\mathbf{K}$ correspond to stationary values of $\mathbf{J}.\mathbf{K}$, and hence by variation

$$\mathbf{K} = \sum_{r=1}^{m} c_{(r)}\mathbf{I}_{(r)} + b\mathbf{J}, \tag{88}$$

where $c_{(r)}$ and b are undetermined multipliers. Multiplication of (88) by $\mathbf{I}_{(s)}$ gives, in view of (86),

$$c_{(s)} = \mathbf{K}.\mathbf{I}_{(s)} \quad (s = 1, 2, \ldots, m), \tag{89}$$

and then $\mathbf{J}^2 = 1$ gives, from (88),

$$b^2 = 1 - \sum_{r=1}^{m} (\mathbf{K}.\mathbf{I}_{(r)})^2. \tag{90}$$

This value is, of course, always positive, so that b is real. We shall understand by b the positive root of (90). The minimum and maximum values of $\mathbf{J}.\mathbf{K}$ are $-b$ and b, by (88); substituting these values in (87) we have

$$\mathbf{C}.\mathbf{K} - bR \leqslant \mathbf{S}.\mathbf{K} \leqslant \mathbf{C}.\mathbf{K} + bR. \tag{91}$$

These are the desired lower and upper bounds to $\mathbf{S}.\mathbf{K}$.

So far we have used only a general argument in function-space. At this point it is necessary to consider the actual boundary-value problem. If this problem is stated in Riemannian space, complications are introduced, and so we shall confine ourselves to an Euclidean space of N dimensions ($N \geqslant 2$). It is necessary to describe the functions in the domain V which correspond to a vector in function-space. In the case of the Neumann problem, we had p^i; in the case of the elastostatic problem we had E_{ij}. Since we are dealing with Euclidean space, we can use subscripts only, and we shall designate by $T_{i\ldots}$ the set of functions corresponding to a vector in function-space, the dots indicating that the order of the tensor may be 1, 2, ...

Let P be any point of the domain V. We seek bounds for the solution $T_{i\ldots}$ in the neighbourhood of P. We enclose P in a small volume $V^{(0)}$, contained entirely in V, and we define the unit vector **K** of (91) to be the F-vector corresponding to $T^{(0)}_{i\ldots}$, where $T^{(0)}_{i\ldots}$ vanishes outside V^0 and is constant inside V^0. Let us denote by $T^{(c)}_{i\ldots}$ the functions corresponding to **C**, and by $T^{(r)}_{i\ldots}$ the functions corresponding to the orthonormal vectors $\mathbf{I}_{(r)}$. Since **K** is a unit vector, we have

$$V^{(0)} T^{(0)}_{i\ldots} T^{(0)}_{i\ldots} = 1. \tag{92}$$

We have also

$$\mathbf{S}.\mathbf{K} = T^{(0)}_{i\ldots}\int T_{i\ldots}\,dV^{(0)}, \quad \mathbf{C}.\mathbf{K} = T^{(0)}_{i\ldots}\int T^{(c)}_{i\ldots}\,dV^{(0)}, \quad \mathbf{K}.\mathbf{I}_{(r)} = T^{(0)}_{i\ldots}\int T^{(r)}_{i\ldots}\,dV^{(0)}, \tag{93}$$

these integrals being taken through $V^{(0)}$. Let us use a bar to indicate mean values in $V^{(0)}$, so that generally

$$\bar{\phi} V^{(0)} = \int \phi\, dV^{(0)}, \tag{94}$$

and in particular

$$\mathbf{S}.\mathbf{K} = T^{(0)}_{i\ldots}\bar{T}_{i\ldots}V^{(0)}, \quad \mathbf{C}.\mathbf{K} = T^{(0)}_{i\ldots}\bar{T}^{(c)}_{i\ldots}V^{(0)}, \quad \mathbf{K}.\mathbf{I}_{(r)} = T^{(0)}_{i\ldots}\bar{T}^{(r)}_{i\ldots}V^{(0)}. \tag{95}$$

The constants $T^{(0)}_{i\ldots}$ are at our disposal, subject only to (92). Let us make them all zero save one; by (92) its value is $(V^{(0)})^{-\frac{1}{2}}$. Let $i\ldots$ now denote that set of suffixes for which $T^{(0)}_{i\ldots}$ does not vanish. Then (95) read, for that set of subscripts, and hence for all,

$$\mathbf{S}.\mathbf{K} = \bar{T}_{i\ldots}(V^{(0)})^{\frac{1}{2}}, \quad \mathbf{C}.\mathbf{K} = \bar{T}^{(c)}_{i\ldots}(V^{(0)})^{\frac{1}{2}}, \quad \mathbf{K}.\mathbf{I}_{(r)} = \bar{T}^{(r)}_{i\ldots}(V^{(0)})^{\frac{1}{2}}. \tag{96}$$

Let us substitute in (91) and divide by $(V^{(0)})^{\frac{1}{2}}$; this gives

$$\bar{T}^{(c)}_{i\ldots} - bR(V^{(0)})^{-\frac{1}{2}} \leqslant \bar{T}_{i\ldots} \leqslant \bar{T}^{(c)}_{i\ldots} + bR(V^{(0)})^{-\frac{1}{2}}, \tag{97}$$

where b is the positive root of

$$b^2 = 1 - V^{(0)} \sum_{r=1}^{m} (\bar{T}^{(r)}_{i\ldots})^2. \tag{98}$$

Since everything in (97) is known except $\bar{T}_{i\ldots}$, *these inequalities set lower and upper bounds for the mean values of the components of the solution tensor* $T_{i\ldots}$ *in the region* $V^{(0)}$ *enclosing the point* P.

The presence of the factor $(V^{(0)})^{-\frac{1}{2}}$ is embarrassing. For, naturally, we would like to know the mean value of $T_{i\ldots}$ in a *small* region enclosing P, but if (for fixed R) we let $V^{(0)}$ approach zero, the bounds draw apart to $-\infty$ and $+\infty$. Obviously, we must exercise discretion in the choice of $V^{(0)}$, and as good a choice as any seems to be

$$V^{(0)} = R/k^2, \tag{99}$$

where k is any constant, which we regard as fixed (i.e. not dependent on R). We have then the inequalities

$$\bar{T}^{(c)}_{i\ldots} - kR^{\frac{1}{2}}\left[1-k^{-2}R\sum_{r=1}^{m}(\bar{T}^{(r)}_{i\ldots})^2\right]^{\frac{1}{2}} \leqslant \bar{T}_{i\ldots} \leqslant \bar{T}^{(c)}_{i\ldots} + kR^{\frac{1}{2}}\left[1-k^{-2}R\sum_{r=1}^{m}(\bar{T}^{(r)}_{i\ldots})^2\right]^{\frac{1}{2}}. \quad (100)$$

Simpler, but weaker, inequalities are

$$\bar{T}^{(c)}_{i\ldots} - kR^{\frac{1}{2}} \leqslant \bar{T}_{i\ldots} \leqslant \bar{T}^{(c)}_{i\ldots} + kR^{\frac{1}{2}}, \quad (101)$$

in which we might, for example, put $k = 1$. If we try to draw the bounds together by decreasing k, we automatically increase $V^{(0)}$, and hence reduce the significance of our result.

If we are interested only in mean values over the whole domain V, we go back to (97) and put $V^{(0)} = V$. This draws the bounds together as far as possible, the difference between them being then

$$2RV^{-\frac{1}{2}}\left[1-V\sum_{r=1}^{m}(\bar{T}^{(r)}_{i\ldots})^2\right]^{\frac{1}{2}}. \quad (102)$$

The method given above bears a resemblance to that given by Diaz & Greenberg (1946). The present method has an advantage of generality, but their method gives bounds precisely at a point, by means of the appropriate Green's function.

7. VIBRATION PROBLEMS

So far we have considered cases in which the metric assigned to function-space F is positive-definite. In some other important problems we can carry through the same type of formal technique, but the metric is indefinite, so that instead of locating the solution on a (bounded) hypercircle, we locate it on an (unbounded) pseudo-hypercircle. In such cases, the method cannot, in its present form, be regarded as a practical method of approximation, but the results appear worth recording.

Consider the vibrations of a membrane under assigned periodic displacement of the boundary. When a time-factor is taken out, we have the equations

$$\Delta w + k^2 w = 0, \quad (w)_B = f, \quad (103)$$

where k is an assigned constant, and f an assigned function on the boundary B. This is, of course, essentially the same mathematical problem as that of the forced vibrations of a membrane with fixed boundary. It should be emphasized that we are *not* here concerned with eigen-value problems: k is assigned and f is not identically zero.

Mathematically, there is no advantage in remaining in two dimensions, so we shall take the problem (103) in a domain V of Euclidean N-space. Generalization to Riemannian space with positive-definite metric is immediate.

A vector $\mathbf{S}$ in F corresponds to the $(N+1)$ functions (p_i, w) in V, and the scalar product is defined by

$$\mathbf{S}.\mathbf{S}' = \int (p_i p'_i - k^2 w w')\, dV. \quad (104)$$

Thus
$$\mathbf{S}^2 = \int (p_i p_i - k^2 w^2)\, dV, \tag{105}$$
which is not positive-definite.

We define the class F^* of vectors $\mathbf{S}^*$ by
$$p_i^* = w_{,i}^*, \quad (w^*)_B = f, \tag{106}$$
the comma denoting partial differentiation, and the class F'' of vectors $\mathbf{S}''$ by
$$p''_{i,i} + k^2 w'' = 0. \tag{107}$$
Obviously, the solution $\mathbf{S}$ is the intersection of F^* and F''.

Now
$$\begin{aligned}\mathbf{S}^* . \mathbf{S}'' &= \int (p_i^* p_i'' - k^2 w^* w'')\, dV \\ &= \int w^* n_i p_i'' dB - \int w^* p''_{i,i} dV - \int k^2 w^* w'' dV \\ &= \int w^* n_i p_i'' dB,\end{aligned} \tag{108}$$
by (107). Since $\mathbf{S}$ lies both in F^* and in F'', we deduce from (108)
$$\mathbf{S} . \mathbf{S}'' = \mathbf{S}^* . \mathbf{S}'', \quad \mathbf{S} . (\mathbf{S} - \mathbf{S}^*) = 0. \tag{109}$$
The first of (109) locates the extremity of $\mathbf{S}$ on a hyperplane in F; the second may be written
$$(\mathbf{S} - \tfrac{1}{2}\mathbf{S}^*)^2 = \tfrac{1}{4}\mathbf{S}^{*2}, \tag{110}$$
which is (formally) the equation of a hypersphere. But since $\mathbf{S}^{*2}$ is not necessarily positive, we must describe this region in F as a *pseudo-hypersphere*. The equations (109) together locate the extremity of $\mathbf{S}$ on a *pseudo-hypercircle* Γ.

Further approximations are obtained by introducing a class F' of orthonormal vectors $\mathbf{I}'_{(p)}$ $(p = 1, 2, \ldots, m)$ satisfying
$$p_i' = w'_{,i}, \quad (w')_B = 0, \tag{111}$$
and an orthonormal set of vectors $\mathbf{I}''_{(q)}$ $(q = 1, 2, \ldots, n)$ of the class F'', already defined by (107). However, normalization requires care on account of the indefinite character of the metric. A vector $\mathbf{I}'_{(p)}$ is normalized by the condition $|\mathbf{I}'_{(p)} . \mathbf{I}'_{(p)}| = 1$, and so we write
$$\mathbf{I}'_{(p)} . \mathbf{I}'_{(p)} = \int (p_i' p_i' - k^2 w'^2)\, dV = \epsilon'_{(p)} = \pm 1, \tag{112}$$
and call $\epsilon'_{(p)}$ the *indicator* of the vector $\mathbf{I}'_{(p)}$.

It is easy to verify the results:
$$\begin{aligned}&\mathbf{S} . \mathbf{I}'_{(p)} = 0 \quad (p = 1, 2, \ldots, m), \\ &\mathbf{S} . \mathbf{I}''_{(q)} = \mathbf{S}^* . \mathbf{I}''_{(q)} \quad (q = 1, 2, \ldots, n).\end{aligned} \tag{113}$$
With the second of (109), or (110), these equations locate the extremity of $\mathbf{S}$ on a pseudo-hypercircle Γ. Its centre $\mathbf{C}$ is found by starting at the centre $\tfrac{1}{2}\mathbf{S}^*$ of the

hypersphere (110), and then travelling in a direction in the linear space of $\mathbf{I}'_{(p)}$, $\mathbf{I}''_{(q)}$ until we arrive at the hyperplane (113). Thus we write

$$\mathbf{C} = \frac{1}{2}\left[\mathbf{S}^* + \sum_{p=1}^{m} c'_{(p)}\mathbf{I}'_{(p)} + \sum_{q=1}^{n} c''_{(q)}\mathbf{I}''_{(q)}\right], \tag{114}$$

and determine the coefficients by the conditions (113), with $\mathbf{C}$ substituted for $\mathbf{S}$. We use the obvious relations

$$\mathbf{I}'_{(p)}.\mathbf{I}''_{(q)} = 0 \quad (p = 1, 2, \ldots, m;\ q = 1, 2, \ldots, n), \tag{115}$$

and obtain
$$c'_{(p)} = -\epsilon'_{(p)}\mathbf{S}^*.\mathbf{I}'_{(p)}, \quad c''_{(q)} = \epsilon''_{(q)}\mathbf{S}^*.\mathbf{I}''_{(q)}, \tag{116}$$

so that
$$\mathbf{C} = \frac{1}{2}\left[\mathbf{S}^* - \sum_{p=1}^{m} \epsilon'_{(p)}\mathbf{I}'_{(p)}(\mathbf{S}^*.\mathbf{I}'_{(p)}) + \sum_{q=1}^{n} \epsilon''_{(q)}\mathbf{I}''_{(q)}(\mathbf{S}.\mathbf{I}''_{(q)})\right]. \tag{117}$$

Using the second of (109), we have

$$\begin{aligned}(\mathbf{S}-\mathbf{C})^2 &= \mathbf{S}^2 - 2\mathbf{S}.\mathbf{C} + \mathbf{C}^2\\ &= \mathbf{S}.(\mathbf{S}^* - 2\mathbf{C}) + \mathbf{C}^2.\end{aligned} \tag{118}$$

By (117) and (113),

$$\begin{aligned}\mathbf{S}.(\mathbf{S}^* - 2\mathbf{C}) &= \mathbf{S}.\left[\sum_{p=1}^{m} \epsilon'_{(p)}\mathbf{I}'_{(p)}(\mathbf{S}^*.\mathbf{I}'_{(p)}) - \sum_{q=1}^{n} \epsilon''_{(q)}\mathbf{I}''_{(q)}(\mathbf{S}^*.\mathbf{I}''_{(q)})\right]\\ &= -\sum_{q=1}^{n} \epsilon''_{(q)}(\mathbf{S}^*.\mathbf{I}''_{(q)})^2,\end{aligned} \tag{119}$$

and, by (117),
$$\mathbf{C}^2 = \frac{1}{4}\left[\mathbf{S}^{*2} - \sum_{p=1}^{m} \epsilon'_{(p)}(\mathbf{S}^*.\mathbf{I}'_{(p)})^2 + 3\sum_{q=1}^{n} \epsilon''_{(q)}(\mathbf{S}^*.\mathbf{I}''_{(q)})^2\right]. \tag{120}$$

Substitution from (119) and (120) in (118) gives

$$(\mathbf{S}-\mathbf{C})^2 = \eta R^2, \tag{121}$$

where
$$R^2 = \frac{\eta}{4}\left[\mathbf{S}^{*2} - \sum_{p=1}^{m} \epsilon'_{(p)}(\mathbf{S}^*.\mathbf{I}'_{(p)})^2 - \sum_{q=1}^{n} \epsilon''_{(q)}(\mathbf{S}^*.\mathbf{I}''_{(q)})^2\right], \tag{122}$$

and $\eta = \pm 1$, the value being chosen to make R^2 positive; we shall understand R to be the positive root of (122).

With the above values of $\mathbf{C}$ and R, we may write the equation of the pseudo-hypercircle Γ in the form
$$\mathbf{S} = \mathbf{C} + R\mathbf{J}, \tag{123}$$

where $\mathbf{J}$ is a vector which is arbitrary except for the following conditions:

$$\left.\begin{aligned}\mathbf{J}^2 &= \eta,\\ \mathbf{J}.\mathbf{I}'_{(p)} &= 0 \quad (p = 1, 2, \ldots, m),\\ \mathbf{J}.\mathbf{I}''_{(q)} &= 0 \quad (q = 1, 2, \ldots, n).\end{aligned}\right\} \tag{124}$$

Finally, let us study electromagnetic radiation in a vacuum of finite volume V of Euclidean 3-space. We suppose the radiation simple harmonic with respect to t, with given frequency; the tangential component of the electric vector is assigned over B, the bounding surface of V, but does not vanish all over B. Thus we are studying forced oscillations, not free cavity oscillations (eigen-modes).

The time factor $\exp(-ikct)$ being taken out, the electric vector E_i satisfies the differential equations

$$(\Delta + k^2) E_i = 0, \quad E_{i,i} = 0, \tag{125}$$

i.e. the wave equation and the divergence condition, with the boundary condition that the tangential vector component of E_i is assigned on B. (We assume that k is not an eigenvalue of the problem with the tangential component of E_i vanishing on B.)

A vector $\mathbf{S}$ in function-space F will correspond to a vector field E_i in V; the scalar product in F is defined by

$$\mathbf{S}.\mathbf{S}' = \int (\operatorname{curl}\mathbf{E}.\operatorname{curl}\mathbf{E}' - k^2\mathbf{E}.\mathbf{E}')\, dV, \tag{126}$$

in ordinary vector notation: in indicial notation this reads

$$\mathbf{S}.\mathbf{S}' = \int (E_{i,j}E'_{i,j} - E_{i,j}E'_{j,i} - k^2 E_i E'_i)\, dV. \tag{127}$$

We define a class F^* of vectors $\mathbf{S}^*$ by the condition that the tangential component of E^*_i takes the assigned value on B, and we define a class F'' of vectors $\mathbf{S}''$ by the conditions

$$(\Delta + k^2) E''_i = 0, \quad E''_{i,i} = 0. \tag{128}$$

Obviously, the solution $\mathbf{S}$ is the intersection of the classes F^* and F''.

Now, by (127),

$$\begin{aligned} \mathbf{S}^*.\mathbf{S}'' &= \int (E^*_{i,j}E''_{i,j} - E^*_{i,j}E''_{j,i} - k^2 E^*_i E''_i)\, dV \\ &= \int E^*_i n_j (E''_{i,j} - E''_{j,i})\, dB - \int E^*_i (E''_{i,jj} - E''_{j,ij} + k^2 E''_i)\, dV, \end{aligned} \tag{129}$$

where n_j is the unit normal to B, drawn outwards. By virtue of (128), the last integral in (129) vanishes.

Now $\mathbf{S}$ (the solution) belongs to the class F^*, and so we may replace $\mathbf{S}^*$ in (129) by $\mathbf{S}$. If we do this, and subtract (129) from the result, we get

$$(\mathbf{S} - \mathbf{S}^*).\mathbf{S}'' = \int (E_i - E^*_i)\, n_j (E''_{i,j} - E''_{j,i})\, dB. \tag{130}$$

But E_i and E^*_i have the same tangential component, and so the vector $(E_i - E^*_i)$ is normal to B, i.e.

$$E_i - E^*_i = \theta n_i, \tag{131}$$

where θ is some scalar factor. Substitution in (130) gives

$$(\mathbf{S} - \mathbf{S}^*).\mathbf{S}'' = 0. \tag{132}$$

But $\mathbf{S}$ belongs to the class F'', and so we may substitute $\mathbf{S}$ for $\mathbf{S}''$, obtaining

$$(\mathbf{S} - \mathbf{S}^*).\mathbf{S} = 0. \tag{133}$$

By (132) and (133), the extremity of the solution vector S is located on a pseudo-hypercircle in function-space. From here on, we may proceed in the same manner as we proceeded from (109) in the case of the membrane problem.

I wish to thank my colleague, Professor A. Weinstein, for valuable discussions on the material of this paper.

REFERENCES

Diaz, J. B. & Greenberg, H. J. 1946 Restricted Report.
Lamb, H. 1932 *Hydrodynamics*, p. 47. Camb. Univ. Press.
Prager, W. & Synge, J. L. 1947 *Quart. App. Math.* (in the Press).
Trefftz, L. 1926 *Proc. 2nd Int. Congr. Appl. Mech.* pp. 131–137.

Photoelectric measurements of the seasonal variations in daylight at Plymouth, from 1938 to March 1941, compared with the years 1930 to 1937

BY W. R. G. ATKINS, F.R.S. AND M. A. ELLISON, SC.D.

(*Received* 2 *April* 1947)

INTRODUCTION

The objects of this paper are: (1) to reconsider the methods used in the light of experience extending over more than eleven years; (2) to present the observations made since 1937 and to compare them with those already published; (3) to consider the observations on illumination in relation to those ordinarily recorded by the Meteorological Office for sunshine, cloud, rainfall, etc.; (4) to compare the variations found with those obtainable from the examination of records made elsewhere.

THE PHOTOELECTRIC MEASUREMENT OF DAYLIGHT

The use of a Burt (number 299) vacuum sodium cell and Cambridge Instrument Co. 'thread recorder' for the measurement of daylight has already been described (Atkins & Poole 1930, 1936), and an account has been given of the standardization of the cells (Poole & Atkins 1935). It was shown that the measurements relate to the ultra-violet, violet and blue, but are chiefly an indication of the changes in light of wave-length about 0·41μ, at which the sodium cell exhibits a sharp maximum of sensitivity in a mean noon sunshine spectrum. The selection of the cell was governed mainly by two considerations: first, that it should remain constant in sensitivity over a long period, and secondly, that the current should suffice to operate the thread recorder which has, unshunted, a full-scale deflexion for 5 μA. The cell is mounted in a heavy gun-metal case with thick glass window. Over this is placed a flashed opal glass surface set horizontally so as to have full sky exposure; it gave nearly 5 μA on clear days around 21 December and required × 2, × 5 and × 10 shunts subsequently. The surface of the flashed glass is smooth, because the properties of a rough surface alter when wet. The first records were obtained in December 1929, and daily recordings continued (with a gap of three months in 1933) till interrupted by enemy action on the night of 20 March 1941. The photocell lost some sensitivity, due apparently to the heat from the fire which destroyed the other end of the block, where the recorder was located. The latter was put out of action by salt water from a hose, but it was overhauled almost at once and used elsewhere till recordings were begun again in Plymouth. A similar cell mounted without adequate precautions against the sun's radiation reaching the sides of the photometer lost most of its sensitivity in about three years at Wad Medani, Sudan. The cell surface appeared to have taken on a yellow tint, just as had the Plymouth cell—to a lesser extent—after the fire. Acting on the suggestion of Dr Burt's associate, Professor D. H. Loughridge, the cell aperture was cautiously heated with a small Bunsen flame. As a result the sensitivity was increased about eighteen times, being restored to something near its original value. The volatilization of the sodium film showed that the film deposited on the glass by electrolysis was still silvery. But the thin internal coating on all parts of the bulb led to a definite, though unimportant, dark current. The Plymouth cell was only reduced in sensitivity by about one-quarter as compared with previous mid-winter readings.

Evidence was adduced (Atkins 1938) to show that the sodium cell had remained constant up to the end of 1937. Since much of the value of the records depends upon this, further results are shown in table 1. These comparisons on windy March days appear specially reliable. It was not possible to restandardize against the electric arc without interrupting the readings, but a comparison was made against a similar Burt cell, B 188, which had been exposed but little since its arc standardization. This check, overlooked when the 1930–7 results were published, was undertaken in connexion with tests on cells being sent abroad. Observations of 18 October 1937 showed that at noon, with 41 kilolux illumination, the ratio of B 299/B 188 was down to 91 % of that found in June 1934 and at 15 hr. 20 min., with 19 kl., the value was 90 %. But these cells, apparently identical in preparation, have nevertheless appreciable differences in colour sensitivity, and the weakness of the October light in the shorter waves appears adequately to account for the apparent loss of sensitivity. According to Selényi, traces of oxygen introduced electrolytically give sodium cells an unstable red sensitivity. This probably accounts for the differences in colour sensitivity found to exist in the Burt cells, among which those with a more marked sensitivity to longer wave-lengths exhibit a greater sensitivity to daylight as might be expected; this apparently persists with high stability long after the red sensitivity —if any—has gone.

In general, it may be said that comparisons of these apparently identical cells may give different ratios under different atmospheric conditions. But we have found the behaviour of our exposed photometer to be constant when its records have been compared at the same time of the year in different years. March, on account of its bright, windy weather, has proved favourable for such comparisons, as may be seen in table 1. These results give no indication of any alteration in sensitivity, whether due to a change in the cell or to 'solarization' of the protecting window. As this glass did not transmit the extreme ultra-violet, such alterations as occur in glasses specially transparent to this region do not concern us here.

TABLE 1. DAILY MAXIMUM CURRENT IN MICROAMPERES, FROM BURT SODIUM CELL NUMBER 299, AS MOUNTED ON FRONT PARAPET OF LABORATORY ROOF. BRIGHT DAYS IN MARCH ARE COMPARED

March	1930	1933	1937	1938	1939	1940
18	23·85	23·90	24·10*	17·95	17·95	17·75
21	23·90	22·75	10·70	23·20	21·30	24·20*
22	22·60	22·40	23·90*	20·55	22·45	21·00
23	9·60	23·50	23·00	16·40	24·80*	19·40
24	22·85	21·00	25·30*	20·40	25·20	10·90
27	9·11	18·50	24·1	19·70	22·90	24·30*
28	12·00	17·55	17·7	14·80	17·70	26·40*
29	26·00	17·55	22·1	9·10	27·20*	26·20
30	26·00	26·70*	26·70*	24·40	17·70	20·00

* Highest for date in the 6 years.

VERTICAL COMPONENT OF THE ILLUMINATION IN THE YEARS 1930–41

Tables 2 and 3 show results for 1938 onwards, and comparisons with the earlier years are in figures 1 and 5. Yearly maxima have an asterisk. The daily values of the maximum vertical illumination in kilolux and of the total vertical illumination in kilolux-hours have been filed for reference. In the tables which follow only the least, greatest and mean monthly values of the vertical and integrated illumination are shown.

Comparing table 2 with its fellow of 1938, it may be seen in the first section that the least values of the daily maxima occurred in December 1939, but several of the other months had no low maximum; for example, in May 1940 the value was 73 kl. In the second section the greatest values of the daily maxima appear to be low, but one cannot accept loss of cell sensitivity as an explanation, for the March 1939 value, 103 kl., ranks third in the 11-year series; also May 1938, with 147 kl., ranks sixth.

The monthly means of the daily maxima show yearly maxima in May for 1939 and 1940 and in June for 1938. These figures bring May's total up to seven and June's to three, out of the 11 years, with one record, 1930, for July. Thus June does not necessarily have the brightest moments of the year, though it has the maximum solar elevation.

In this series of papers the term 'vertical illumination integral' has been used for the quantity 'light intensity multiplied by duration', expressed in kilolux-hours and tabulated for each day. It is obtained by measuring the daily records with a planimeter. It was not possible to use 'total light', as this was required to express the light reaching a point from all angles, as measured by the globe photometer (Atkins & Poole 1936).

TABLE 2. DAILY MAXIMUM VERTICAL ILLUMINATION IN KILOLUX, AT PLYMOUTH, LATITUDE 51° 5′ N. TOP SECTION, LEAST VALUES; MIDDLE SECTION, GREATEST VALUES; AND BOTTOM SECTION, MONTHLY MEAN OF DAILY MAXIMA. YEARLY MAXIMA HAVE ASTERISK

year	Jan.	Feb.	Mar.	Apr.	May	June	July	Aug.	Sept.	Oct.	Nov.	Dec.
1938	6·6	8·9	16·7	47·1	35·7	28·5	22·0	24·7	28·3	14·8	7·2	5·1
1939	5·3	4·5	15·4	45·2	41·0	27·4	25·8	47·5	30·4	17·1	3·7	1·4
1940	7·6	6·6	31·7	30·8	73·0	54·3	34·2	54·0	40·8	11·0	5·7	3·4
1941	3·0	8·8	—	—	—	—	—	—	—	—	—	—
1938	33·1	56·0	92·7	117	147*	144	136	106	96·5	65·9	42·4	25·8
1939	28·8	61·9	103	114	135*	123	130	109	83·2	72·4	47·5	23·0
1940	32·7	64·2	100	118	128*	117	122	96·1	83·3	64·0	44·8	23·7
1941	33·8	59·6	—	—	—	—	—	—	—	—	—	—
1938	18·3	33·4	60·3	85·6	95·0	108·2*	97·3	79·3	72·9	45·2	21·2	14·9
1939	18·1	35·0	64·0	89·9	97·3*	93·0	96·7†	77·2	64·7	44·5	22·0	13·9
1940	18·1	33·0	66·0	91·3	94·3*	87·6	93·1	76·6	65·5	42·9	23·7	18·1
1941	19·2	34·9	—	—	—	—	—	—	—	—	—	—

† Mean of 24 days (17th to 23rd missing).

TABLE 3. VERTICAL ILLUMINATION INTEGRAL IN KILOLUX-HOURS A DAY, AT PLYMOUTH. THE SECTIONS SHOW LEAST, GREATEST AND MONTHLY MEAN VALUES

year	Jan.	Feb.	Mar.	Apr.	May	June	July	Aug.	Sept.	Oct.	Nov.	Dec.
1938	18·3	38·5	77·7	204	144	206	164	123	108	45·9	25·8	16·0
1939	19·5	19·8	63·6	164	166	109	147	160	139	56·3	14·2	6·2
1940	21·6	17·0	91·7	132	262	226	180	195	161	42·2	25·2	14·7
1941	11·5	28·7	77·7	—	—	—	—	—	—	—	—	—
1938	126	266	470	733	860	957*	842	590	553	269	186	81·1
1939	128	270	460	668	884*	775	748	616	429	332	184	83·5
1940	128	214	475	738	753*	723	699	602	451	319	123	75·8
1941	118	272	—	—	—	—	—	—	—	—	—	—
1938	61·0	129	285	486	472	567*	477	383	330	178	71·5	51·0
1939	65·9	130	251	431	563*	531	408†	395	322	180	72·0	47·1
1940	65·8	113	274	411	557*	548	487	413	327	172	73·6	44·1
1941	63·2	128	—	—	—	—	—	—	—	—	—	—

† Mean of 31 days but 17th to 23rd, 7 days, have had approximate values assigned from sunshine and rainfall data. The 7 days were undoubtedly low with average 1·9 hr. sunshine. Mean of 24 days = 448.

On comparing table 3 with its 1938 counterpart, it may be seen in the top section that the darkest day was in December 1939 with 6·2 kl.hr., followed by one in January 1941 with 11·5. The January minima for 1938–40 were remarkably similar, lying between 18·3 and 21·6. The darkest June day was also in 1939, with 109, followed by 1931 with 124 kl.hr.

The middle section shows the greatest daily values for which (1938 paper) 1930 comes first with 1323 in July, with April, June, May and August all over 1000, also May 1931 and June 1936. With 957 kl.hr. 1938 tops the list in table 3. The factors which combine to give these exceptionally bright days are complex and will be considered later.

The bottom section records the mean monthly values, which for plant growth are the most important ones. The January results for 1938–41 vary but little, and the same holds for February, but all four are low, the 1940 value being the minimum for twelve years, as is also March 1939, and May 1938 for eleven years. The Septembers from 1937 to 1940 gave almost identical values as did the Octobers from 1934 onwards. November 1937 was by far the brightest of the series and December 1940 was by a little the darkest.

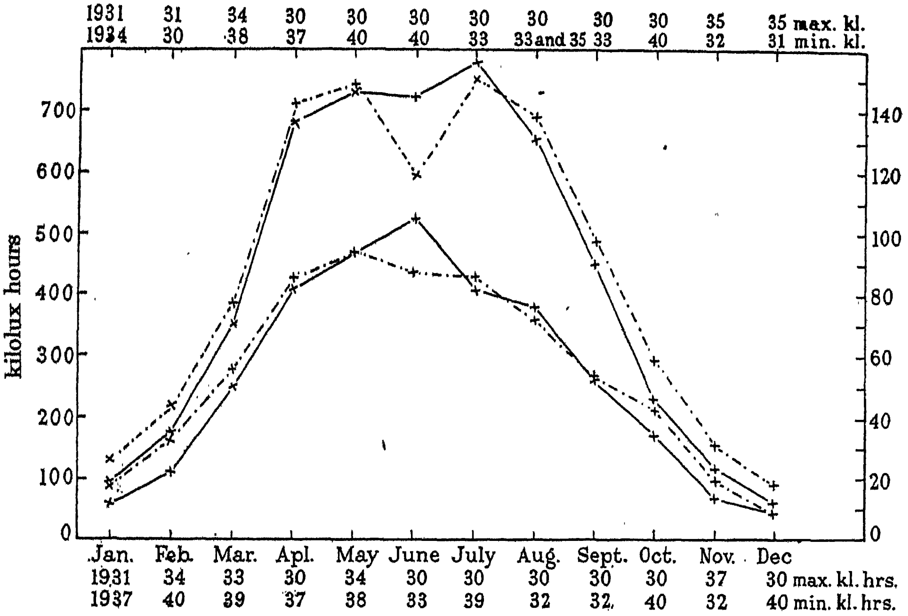

Figure 1. The ordinates on the left denote mean monthly illumination, in kilolux-hours. The months are shown on the abscissae, and these values are related by the full lines; of these the upper shows the maximum value and the lower the minimum in the years 1930–40 inclusive. The year of occurrence is shown underneath the figure, maximum upper, minimum lower. The century figures are inserted once in each line. The lines with dot and dash are similar mean monthly maxima and minima for maximum daily brightness in kilolux, shown on the right-hand ordinate. The two rows of figures on top give the years of occurrence. Thus 1930 had the greatest values of the mean daily maximum from April to October inclusive.

The extremes in the monthly values, both for vertical illumination integral and for vertical illumination, are shown in figure 1 as explained in the legend. It may be seen that 1930 came first in the integral for 7 months and for 7 consecutive months in maximum illumination. The integral maxima fell in 1934 for February and May, which year also had the brightest March day. It is to be noted that the 1930 values are below other years for the first 3 months. The brightest day recorded, 7 July 1930, was noted as being specially clear and gave exceptionally high values for the ratio of sunlight plus skylight to skylight alone, when the direct rays were screened by a small disk. This was done several times as the day appeared exceptional. Figure 1 may be compared with table 4 of the 1938 paper which tabulates also the year ranking second and the excess percentage. It is very remarkable that the latter should amount to 31·1, 32·1 and 37·8 for the months of April, July and August 1930, these being the percentage excess over the months ranking next in brightness and occurring respectively in the years 1933, 1934 and 1934. May 1934 had 1·5 % excess over 1930 and June 1930 had 8·2 % over June 1934. The brightest November, 1937, had 18·8 % excess over the next in brightness, 1930. It seems impossible to reconcile figures such as these with any deterioration in cell sensitivity from that obtaining in 1930. Aurén (1934) found that of the 5 years 1928–32, 1930 was the brightest in March, April, May, June and November, with July ranking second. April 1930 was much brighter than the others. 1928 was brightest in January, February, July and September; 1929 in August and December, and 1931 in October.

COMPARISON WITH SUNSHINE RECORDS

The brightness of a month is usually assessed by its hours of sunshine. Figure 2 shows for 1930 and for an average year, 1936 (full line), the quantity of light (kilolux-hours) on the brightest days of each month divided by the number of hours of sunshine. This gives the kilolux-hours per hour of sunshine, neglecting the amount contributed by the sky light on these same days when the sun was not out. The conclusion is that from March to October inclusive the vertical component of 1930 sunshine seems particularly bright, especially in April, May, July and August.

ILLUMINATION ON SUNNY AND SUNLESS DAYS

Figure 3 shows for 1930 and 1936 the ratio of the light on sunless days to that on the brightest days as explained in the legend. It may appear remarkable that the means for the monthly sets agree so closely, the values being respectively 0·33 and 0·30. This agreement is indirect evidence that the cloud during 1930 merely diffused the light in the normal manner, and was not specially transparent. The difference in the years must lie either in the sun's radiation or in the reflecting or absorbing properties of the atmosphere other than the cloud droplets. One would *a priori* consider it most unlikely that there should be any considerable variation in the radiation, though such as is observed is more likely to be found in the short-wave end. This has been discussed in the 1938 paper. It should be remembered that we are measuring the vertical component, not the total radiation, so that the angular distribution of the scattered light may in itself account for a certain variability,

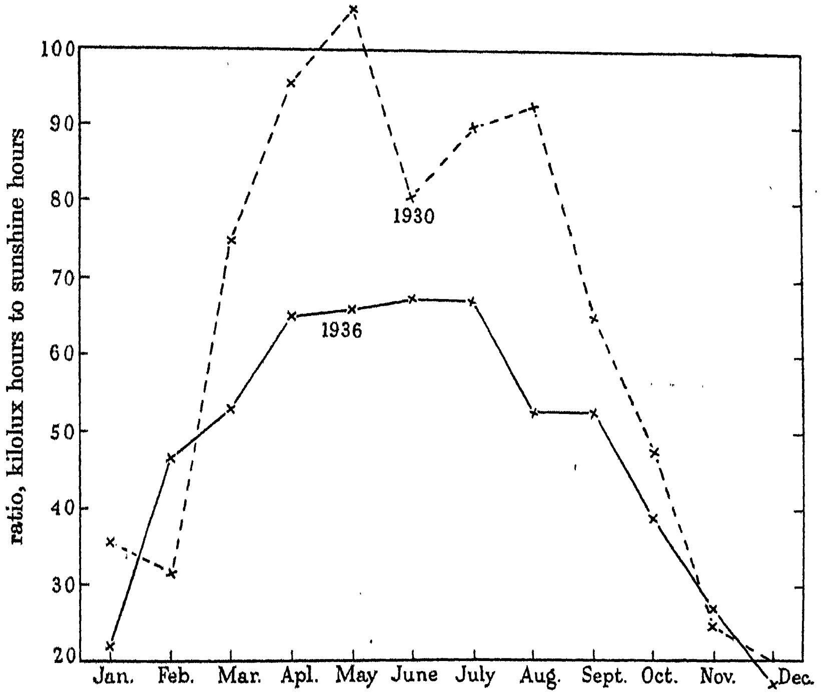

FIGURE 2. The ordinates show the ratio of the kilolux-hours on the brightest days in each month to the number of hours of sunshine on the same days. The abscissae show the months. The full line relates to an average year, 1936; the broken line to the very bright, 1930.

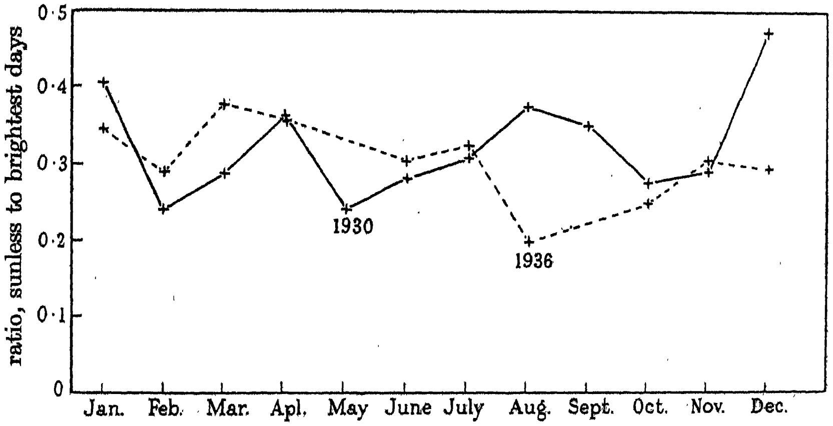

FIGURE 3. Light, in kilolux-hours. The ordinates show the ratio of the amount of light on sunless days to the amount on the brightest days in each month, taking averages which included all the sunless days and a variable number of very bright days. Results for 1930 are shown by a full line, for 1936 by a broken line. There were no sunless days in May or September 1936, so no ratio could be determined. The abscissae show months.

though the close agreement in the ratios 0·33 and 0·30 suggests that this factor is small. The brightness of the sky at various altitudes and for various azimuths with respect to the sun has been discussed by Poole & Atkins (1933).

Figure 4 affords additional evidence that the clouds were not responsible for the peculiar characteristics of 1930. It shows the illumination on sunless days during 1930 and 1936. While closely the same in January, February and March, the sunless days of 1930 were later on much the brighter. The figure also shows the number of sunless days per month. It may be seen that sunless days from March to August inclusive, with 200 to 250 kl.hr., provide about four times the illumination of the average midwinter day, and considerably more than the October average.

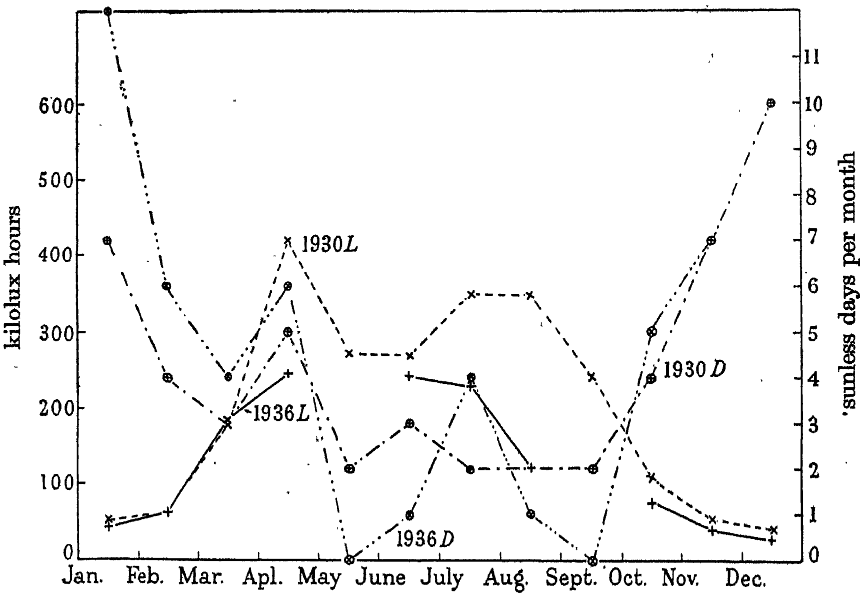

Figure 4. The light graphs, *L*, show the illumination in kilolux-hours on sunless days during the years 1930, dashes, and 1936, full line. The left-hand ordinates show illumination, the abscissae give the months. As there were no sunless days in May and September 1936 the *L* curve has two breaks. The graphs *D* show for the same years the number of sunless days in each month, 1930 having dash and dot, while 1936 has dash and three dots.

DISTRIBUTION OF ILLUMINATION THROUGHOUT THE YEAR

Table 4 gives the percentage of the yearly light received in each month, with the 11-year mean value, etc., as in heading. The average percentages for May and June are identical. Though there is no shift in the position of the months with respect to radiation there is yet a remarkably large range, as shown in the penultimate column. Thus for November the range is 59 % and is even as much as 20 % for June. The monthly percentages of the earlier years are given in table 6 of the 1938 paper. The last column gives the mean monthly illumination integral for an 11-year period.

TABLE 4. VERTICAL ILLUMINATION INTEGRALS FOR EACH CALENDAR MONTH AS A PERCENTAGE OF THE TOTAL FOR THE INDIVIDUAL YEAR WITH CORRESPONDING VALUES FOR WINTER AND SUMMER; ALSO MEAN PERCENTAGE VALUES FOR 1930–40 AND MAXIMUM AND MINIMUM VALUES WITH YEAR OF OCCURRENCE, TOGETHER WITH THE PERCENTAGE RANGE OF VARIATION CALCULATED ON THE MEAN VALUE. THIS TABLE COMPARES DISTRIBUTION OF ILLUMINATION WITHIN THE YEAR, NOT ACTUAL QUANTITIES OF LIGHT, EXCEPT IN THE LAST COLUMN

	1938	1939	1940	11-year mean	year of max.	max.	year of min.	min.	range % of mean	11-year mean, kilolux-hours a day for each month
Jan.	1·78	1·89	1·92	1·86	1933	2·50	1934	1·47	55	70·9
Feb.	3·40	3·55	3·08	3·68	1934	3·87	1930	2·60	34	140·1
Mar.	8·31	7·56	7·99	8·01	1933	9·60	1930	6·47	39	304·8
Apr.	13·70	12·56	11·58	12·76	1933	13·81	1937	10·92	23	485·9
May	13·74	16·94	16·20	15·61	1934	17·72	1938	13·74	26	595·5
June	16·00	15·50	15·44	15·59	1932	17·17	1933	13·98	20	594·1
July	13·90	12·29	14·18	13·72	1930	16·03	1939	12·29	27	522·5
Aug.	11·16	11·39	12·02	11·62	1930	13·38	1932	10·42	26	442·7
Sept.	9·30	9·38	9·22	8·60	1939	9·38	1932	6·87	29	327·1
Oct.	5·20	5·42	5·02	4·92*	1932	5·45	1934	4·20	25	187·3*
Nov.	2·02	2·10	2·07	2·26*	1937	3·12	1934	1·80	59	86·3*
Dec.	1·48	1·42	1·28	1·37*	1937	1·67	1934	1·11	41	52·3*
Winter	22·19	21·94	21·36	22·10	1932	23·53	1930	18·96	16	140·3
Summer	77·80	78·06	78·64	77·90	1930	81·04	1932	76·47	6	494·6

* Ten-year mean, omitting October, November, December 1933.

TABLE 5. ELEVEN ANNUAL TOTALS OF THE VERTICAL ILLUMINATION INTEGRAL, IN KILOLUX-HOURS, WITH THE CORRESPONDING MEAN DAILY VALUE; MEAN DAILY SUNSHINE IN HOURS; RAINFALL IN MILLIMETRES AND NUMBER OF DAYS WITH RAIN, AS RECORDED FOR PLYMOUTH HOE

	1930	1931	1932*	1933	1934	1935	1936*	1937	1938	1939	1940*
kilolux-hours, Jan.–Sept.	138,570	108,573	103,126	102,653	118,592	103,067	103,334	101,143	97,082	93,730	97,482
kilolux-hours, year	150,160	118,948	113,175	[113,000]†	127,666	113,353	113,013	112,037	106,326	102,932	106,388
kilolux-hours a day	412	326	309	310	350	311	309	307	291	282	290
sunshine hours a day	4·38	4·03	4·28	5·17	4·88	4·51	4·27	4·25	4·25	4·69	4·92
total rainfall	1,115	983	1,075	782	1,002	1,075	928	1,050	945	1,024	945
days with rain	209	193	184	169	192	193	183	184	182	197	159
ratio of daily kilolux-hours to value for 1936, mean of 1932, 1933, 1935, 1936, 1937	1·33	1·055	1·00	1·00	1·13	1·005	1·00	0·99	0·94	0·91	0·94
ratio of daily hours of sunshine to value for 1936	1·03	0·945	1·00	1·21	1·14	1·055	1·00	0·995	0·995	1·10	1·16

* Leap year.

† This value has been taken as an approximation, since for 9 months 1933 and 1936 were much alike and the last three months of 1933 were sunny. This approximate total has been used to calculate the 1933 percentages shown in table 4.

COMPARISON OF ILLUMINATION AND OTHER METEOROLOGICAL OBSERVATIONS

(a) *Sunshine, rainfall, days with rain*

In table 5 the illumination integrals for the 11 years are shown together with the usual meteorological observations and certain ratios. The remarkable uniformity of the yearly totals is broken by an outstandingly high value for 1930, a high one for 1934 and a low for 1939. There is agreement with a high sunshine record for 1934, but not for 1930, and the high sunshine of 1933 and of 1940 is not reflected in high illumination integrals, nor can one trace any connexion with the rainfall. The latter is active in removing industrial pollution from the air, though high humidity may lead to droplet formation on the normal salt nuclei and so decrease transmission. The lack of correlation of the vertical illumination integral and the other observations is evident from figure 5.

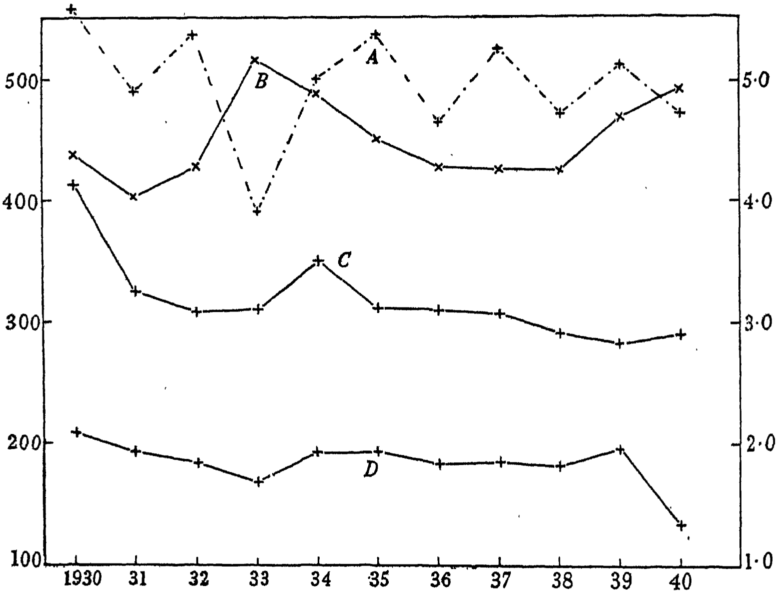

FIGURE 5. The left-hand ordinates represent one-half of the annual rainfall in millimetres, curve *A*, and the number of days with rain for each year, curve *D*; also the amount of light in kilolux-hours per day, curve *C*. The corresponding values for sunshine in hours per day are represented by curve *B*, as marked on the right-hand ordinate. The abscissae show the 11 years.

On checking over the illumination integrals obtained from the daily records and comparing them with the daily sunshine observations an impossible juxtaposition was discovered at the end of October 1930. An error had been made in the date of changing the shunt of the recording galvanometer from × 5 to × 2, so that the last two entries for October and the first three for November are, as shown in table 4 (Atkins & Poole 1936), too high in that proportion. This brings the mean for October to 217·1 kl.hr. and for November to 95·3 and lowers the November maximum to 207, so that this month no longer ranks as the highest in the 11-year series. The necessary corrections in the 1936 paper and also in that of 1938 have been made in the authors' bound copies now in the Society's library. For this unfortunate error the senior author expresses his regret and acknowledges sole responsibility.

(*b*) *Wind direction*

In view of the fact that Plymouth Hoe receives clean sea air when the wind is in the south-west or thereabouts, but may get the city's smoke (including that of Devonport on the west) and industrial pollution from the rest of England when the wind is in the north and east, it appeared advisable to compare the records with those of the Borough Meteorologist for wind direction made at the adjacent observatory during the 11 years. For wind direction, three daily observations at 9, 15 and 21 hr. were used, as most nearly coinciding in time with the light measurements. The number of monthly observations was tabulated for each of the sixteen cardinal points, together with the number of calms. Against these values was set the mean vertical illumination integral for the month, expressed as a percentage of the average mean monthly value for 1930–40, which may be calculated back from table 4 if required.

A plot was made in which wind-direction frequencies were represented by horizontal rows of dots, the ordinates being the corresponding monthly vertical illumination integrals. The distribution of points on this 11-year diagram showed no preference whatever for any special wind direction. For example, the greatest asymmetry from a uniform distribution of the points amounted to a deficiency of only 3·3 % from the mean, 100 %, in the direction west-north-west. No special significance could be attached to this, since the values for the directions west and north-west were 100·0 and 100·3 % respectively.

Taking the years month by month there is thus no correlation with the wind direction. The possibility remains that specially bright days might be related to wind direction.

In this further work comparisons were limited to the typical year 1936 and the abnormal 1930, on account of the great labour of the 11-year comparison. Tables were prepared for the brightest days in each month, as judged by the number of kilolux-hours. The selection was somewhat arbitrary, but was governed in each month by the position of a well-defined gap between days classed as bright and the others. With the illumination integral was tabulated the hours of sunshine, solar altitude at noon, relative humidity, wind direction and force at 15 hr., also visual range, state of sky and cloud tenths, the latter being tabulated also for the mean of the day. It appears unnecessary to reproduce these, but it was obvious from inspection that there was no connexion with wind direction.

(*c*) *Wind force*

It seemed possible, however, that wind force, Beaufort scale, might be a factor, as strong winds increase the vertical mixing of the air and drive away smoke and dust. The bright days in 1930 gave mean values for the months which when averaged showed force 3·00 as against 3·33 for the average of the monthly means. But 1936 gave respectively 3·86 and 3·75. The two years together yielded for bright days 3·43 and for monthly averages 3·54. One must conclude that the mixing is normally adequate. But none of the bright days were calms and force 1 occurred four times only in 1930, out of 62 bright days and not at all in 1936; force 2 occurred nine times in 1930 and eight out of fifty-four in 1936. In 1930 a bright day had force 5 three times only and there was nothing higher; whereas in 1936 the record was fourteen for force 5 and four for force 6. It has been pointed out by Fleming (1943) that measurements of the electrical conductivity of the air show on smoky days a value constant for wind velocity below about 5 miles per hour, force 2, but increase with wind velocities above this point. This is consonant with the idea, that, for wind velocities above 5 miles per hour, turbulence is sufficient to dilute the lower layer with air from higher layers having greater conductivities. This supports the conclusion previously reached that vertical mixing is normally adequate.

(*d*) *Visual range and relative humidity*

Since, according to Wright (1939, 1940), salt nuclei become droplets increasing in size as relative humidity rises above 72, the mean monthly values for 9, 15 and 21 hr. were tabulated for the 2 years. This table has been omitted, as once more there was no important difference bearing on the horizontal visual range, which is of possible interest in the absence of observations on the vertical range.

Values for 15 hr. should have more effect upon the brightness of the day than those at 9 and 21 hr. The 15 hr. observations of visual-range frequencies are accordingly given in table 6, and using Koschmieder's equation the horizontal extinction coefficients of the air were calculated for each of the range limits corresponding to the meteorological code numbers B to M. The Plymouth Hoe records are dual, range over land and over sea, which differ greatly. Over-land records for poor visibility or worse were twice as frequent in 1930 as in 1936, 128 as against 68; over sea they were identical, 17. Over land moderate visibility had 9 in 1930 and 17 in 1936; over sea the figures were 153 and 134. Good visibility and upwards occurred over land 228 times in 1930, 281 in 1936; over sea 195 times in 1930 and 215 in 1936. The visibility records are thus in favour of 1936. Even taking the six outstandingly bright months of 1930, April and June to October, the frequency of visibility poor or worse was 46 over land as against 18 for 1936 and 7 over sea as against 9. Though for suitable objects one cannot always rely on distinctions such as between K and L, there should in Plymouth be no doubt about records of below 4 miles, classed as poor.

(*e*) *Cloud*

The values for cloud tenths are given in table 7. There is no definite indication that this factor bears any relation to the excess of 1930 over 1936, the ratio for which is given in the last column. But the monthly mean, averaged for the year, was 6 % less in 1930 than in 1936. It is obvious, however, that specially bright days have less cloud than the average. Broken cloud often increases the vertical illumination, particularly with low-altitude sun. With cloud tenths 1·9 and 2·9 respectively April and July bright days, 1930, had unusually low values.

TABLE 6. VISUAL-RANGE FREQUENCIES AT 15 HR. OVER LAND AND OVER SEA AT PLYMOUTH DURING 1930 AND 1936. WITH THE RANGES ARE GIVEN THE CORRESPONDING EXTINCTION COEFFICIENTS PER KILOMETRE, TO BASE *e*, ATMOSPHERIC CONDITIONS AND CODE LETTERS

range	0·05		0·2		0·5		1		2		4		7		10		20		30		50	
to	0·1		0·5		1·0		2		4		7		10		20		30		50		on	
extinction	78		19·5		7·82		3·91		1·95		0·98		0·56		0·39		0·19		0·13		0·08	
to	39		7·8		3·91		1·95		0·98		0·56		0·39		0·19		0·13		0·08		—	
condition	fog		fog		mod. fog		haze		poor vis.		mod. vis.		mod. vis.		good		v.g. vis.		v.g. vis.		ex. vis.	
code	B		D		E		F		G		H		I		J		K		L		M	
	frequencies: left over land, right over sea																					
1930																						
Jan.	.	.	.	1	1	.	.	.	12	1	.	1	1	16	.	1	6	10	11	1	.	.
Feb.	.	.	.	.	.	.	.	.	11	.	.	3	.	15	.	1	5	9	12	.	.	.
Mar.	.	.	.	.	.	.	.	.	11	1	.	1	.	15	.	.	5	14	15	.	.	.
Apr.	.	.	.	.	.	.	.	.	9	.	.	.	.	14	4	2	3	13	14	1	.	.
May	.	.	.	.	.	.	.	.	10	.	.	.	.	16	.	1	5	13	16	1	.	.
June	.	.	.	2	1	.	.	.	10	.	1	1	.	9	.	1	2	15	16	2	.	.
July	.	.	.	.	.	.	.	.	3	.	.	.	1	2	1	2	4	27	22	.	.	.
Aug.	.	.	1	1	.	.	.	.	2	2	1	.	3	7	2	3	3	16	19	1	.	.
Sept.	.	.	.	.	1	.	.	.	6	2	.	1	.	9	2	.	8	18	13	.	.	.
Oct.	.	.	.	.	.	.	.	.	13	.	.	1	.	11	.	.	8	17	9	1	1	1
Nov.	.	.	.	.	1	1	1	.	18	3	.	3	.	14	1	.	5	8	4	.	.	.
Dec.	1	.	.	1	6	.	.	.	10	2	.	2	2	12	4	1	3	13	5	1	.	.
Year	1	0	1	5	10	1	1	0	115	11	2	13	7	140	14	12	57	173	156	8	1	1
1936																						
Jan.	.	.	.	.	1	.	1	.	15	2	1	3	1	14	.	.	7	12	5	.	.	.
Feb.	.	.	.	.	1	1	.	.	13	2	.	1	.	13	.	.	1	12	14	.	.	.
Mar.	.	.	.	.	.	1	1	.	6	.	.	.	.	17	8	.	3	13	13	.	.	.
Apr.	.	.	.	.	.	.	1	.	2	2	.	.	.	5	4	.	5	22	18	1	.	.
May	.	.	.	.	.	.	.	.	.	.	.	.	2	11	2	.	5	20	22	.	.	.
June	.	.	.	.	.	.	.	.	3	.	.	.	.	9	3	.	1	21	23	.	.	.
July	.	.	.	.	.	.	1	.	4	2	.	1	.	5	1	.	3	23	22	.	.	.
Aug.	1	.	.	1	.	.	.	.	1	1	.	.	.	6	2	.	1	23	26	.	.	.
Sept.	.	.	.	.	.	1	.	.	2	1	.	.	3	12	4	.	3	16	18	.	.	.
Oct.	.	.	.	.	.	.	1	.	1	1	.	.	2	7	.	.	4	23	23	.	.	.
Nov.	.	.	.	.	.	.	1	1	4	.	.	2	5	12	1	.	2	15	17	.	.	.
Dec.	.	.	.	.	1	.	2	.	5	1	1	4	2	12	6	.	4	14	10	.	.	.
Year	1	0	0	1	3	3	8	1	56	12	2	11	15	123	31	.	39	214	211	1	.	.

Table 7. Cloud tenths, monthly means for 1930 and 1936, also values for bright days only

	cloud 1930	number of bright days	bright day cloud 1930	cloud 1936	number of bright days	bright day cloud 1936	kl.hr. ratio, months 1930/36
Jan.	7·5	3	5·0	8·2	3	5·0	1·20
Feb.	6·0	3	3·0	7·2	3	5·3	1·01
Mar.	6·9	3	5·0	7·2	4	3·5	1·10
Apr.	5·9	7	1·9	6·3	4	4·5	1·48
May	7·0	5	5·4	5·5	4	2·5	1·12
June	5·6	9	3·5	7·5	5	4·8	1·28
July	6·5	7	2·9	7·7	6	6·3	1·61
Aug.	6·7	6	5·2	5·2	4	3·5	1·46
Sept.	6·0	5	3·0	7·3	4	7·2	1·54
Oct.	7·2	3	4·3	6·1	5	3·6	1·27
Nov.	6·9	4	3·0	7·5	5	5·4	1·41
Dec.	7·5	7	6·7	7·7	7	4·1	1·16

Comparison with similar records obtained elsewhere

Aurén obtained a long series of records in Stocksund, a suburb of Stockholm, 59° 23·2′ N. and 18° 3·2′ E. This constitutes the only series, comparable with the Plymouth observations, which we have been able to find (Aurén 1930, 1933, 1934, 1939, 1942, 1943, 1944). Aurén's records were obtained using a potassium vacuum cell mounted under an opal glass plate with, owing to the low sensitivity of the cell, sensitive galvanometers (about $3{\cdot}4 \times 10^{-11}$ A per scale division) and photographic recording of the light spot. Below the glass cover, ground on both faces, a yellow filter 5 mm. thick was placed, the Schott (Jena) GG 11. This cuts off fairly sharply at $0{\cdot}50\mu$. The combination therefore registers blue-green and green only, since the cell is insensitive to the yellow and longer wave-lengths. It is accordingly rather less disturbed by atmospheric pollution than is our own cell. Aurén's work has already been discussed by Atkins & Poole (1936). His records extended from 1928 to 1937. These and the Plymouth results were tabulated as percentages of their respective mean monthly and yearly values for 10 and 11 years. This table was used to construct table 8 which shows the percentage differences from the mean values, also the percentage range and the series S or P in which maxima or minima occur. The maximum monthly range was for S 70 and for P 72, with mean monthly ranges S 43·3, P 48·5. When one considers that the Plymouth records relate to $0{\cdot}41\mu$ and the Stockholm records to over $0{\cdot}50\mu$, it is only to be expected that the swing should be slightly greater for the former. But there is nothing to suggest that the Plymouth ranges are incredibly great, a conclusion against which we have struggled all along, since we had a mental bias in favour of a more even monthly and annual illumination.

At the bottom of table 8 the numbers of months with minus signs are given for each year, namely, those with illumination below the average for the years. Thus in 1931 Stockholm had 10 months each below the average; similarly, 1933 had 9 months;

Table 8. Vertical illumination integrals Stocksund and Plymouth. The percentage differences are given, calculated on the mean monthly and yearly values for ten and eleven years respectively, also the percentage range from maximum positive to negative. An * signifies that the figure occurs again in the same horizontal line

Year		1928	1929	1930	1931	1932	1933	1934	1935	1936	1937	1938	1939	1940	range		max.	min.
Jan.	S	24·0	5·0	1·7	*−14·9*	−9·1	−6·6	−5·0	11·6	−4·1	−5·0	—	—	—	39	S	—	—
	P	—	—	16	34	−1	28	−14	−9	−4	*−21*	−14	−7	−7	55	P	P	P
Feb.	S	42·7	5·3	10·0	*−25·6*	8·7	−16·5	5·9	−10·6	−3·4	−15·6	—	—	—	68	S	S	S
	P	—	—	−1	16	−4	10	25	−5	−1	−7	−8	−7	*−22*	47	P	—	—
Mar.	S	4·5	18·6	26·3	9·2	5·1	−7·7	*−39·0*	5·4	−7·7	−13·8	—	—	—	65	S	S	S
	P	—	—	3	4	11	15	9	−7	−6	5	−7	*−18*	−10	33	P	—	—
Apr.	S	0·2	5·8	14·5	*−35·7*	−2·3	10·6	7·0	6·6	−14·4	7·6	—	—	—	50	S	—	S
	P	—	—	40	−2	4	7	2	−4	−5	*−16*	0	−11	−15	56	P	P	—
May	S	0·4	3·8	8·1	*−9·4*	−4·7	−8·1	8·1	−5·0	4·6	2·3	—	—	—	17·5	S	—	—
	P	—	—	21	5	−7	−5	22	−7	7	−5	*−21*	−5	−7	43	P	P	P
June	S	*−10·2*	−4·3	7·6	−8·8	−1·6	7·0	−2·9	3·8	14·3	−4·8	—	—	—	24·5	S	—	—
	P	—	—	22	−1	9	*−11**	13	−3	−5	−1	−5	*−11**	−8	33	P	P	P
July	S	7·7	−4·3	6·3	*−17·3*	6·2	−5·3	−6·8	3·5	6·0	3·5	—	—	—	25	S	—	—
	P	—	—	50	2	−6	−5	13	2	−7	−11	−9	*−22*	−7	72	P	P	P
Aug.	S	−5·0	−1·0	−5·5	*−13·7*	−3·1	−0·9	20·7	2·7	−3·0	8·7	—	—	—	34	S	—	—
	P	—	—	47	6	−14	*−17*	7	−5	1	2	−14	−11	−7	64	P	P	P
Sept.	S	18·2	−7·2	−10·4	*−16·3*	−2·1	−6·7	10·6	−9·0	23·0	−0·2	—	—	—	39	S	—	—
	P	—	—	38	−8	*−21*	−16	10	7	−10	1	1	−1	0	59	P	P	P
Oct.	S	8·5	*−19·9*	4·2	15·2	1·1	−13·6	6·4	−5·3	−1·3	3·6	—	—	—	35	S	—	S
	P	—	—	23	3	6	—	*−8**	0	−2	−5	−5	−4	*−8**	31	P	P	—
Nov.	S	4·9	8·5	32·2	*−38·0*	11·3	−4·2	−16·9	−24·0	2·8	24·0	—	—	—	70	S	—	S
	P	—	—	30	14	−20	—	−11	8	−8	36	*−17**	*−17**	−15	56	P	P	—
Dec.	S	−2·9	10·3	*−23·5*	−1·5	−13·2	29·4	0·0	−14·7	−2·9	17·7	—	—	—	53	S	S	S
	P	—	—	17	−11	11	—	−13	7	0	15	−3	−10	*−16*	33	P	—	—
Year	S	2·2	−0·3	6·1	−12·9	−0·2	−1·8	1·6	0·4	4·0	4·3	—	—	—	19	S	—	S
	P	—	—	30·0	2·5	−2·8	−2·4	10·0	−2·1	−2·8	−3·4	−8·5	−11·4	−8·5	41·4	P	P	—

Maximum monthly range S 70, P 72; mean monthly range S 43·3, P 48·5

no. of																		
minus	S	3	5	3	10	7	9	5	6	7	5	—	—	—	—	—	—	—
months	P	—	—	1	4	7	—	4	7	9	7	10	12	11	—	—	—	—

1929, 1934 and 1937 had 5 such months. One may regard this as evidence against any serious deterioration in the sensitivity of the cell. In the Plymouth series one has to go to 1938 to find 10 minus months, but then one finds 12 and 11 in 1939 and 1940. Table 1 is definitely against any deterioration in the cell, and there was European war, with additional atmospheric pollution from both factories and warfare, during part of 1939 and all 1940. It seems difficult to avoid the suspicion that there may have been a little loss of sensitivity, but the evidence is conflicting.

We are indebted to Dr A. H. R. Goldie, Assistant Director, Meteorological Office (Climatology, Instruments and Research), for pointing out that 1930 had not only (as tabulated) more rain and more days with rain (209 as against 199 for second place) but also a greater number of 'wet days' (170 as against 146 for second place) than any other year in the period 1930–40 inclusive. A 'wet day' is defined as one having at least 0·04 in., 0·9 mm. of rain. So he considers it quite likely that 1930 had a greater number of days with clear transparent turbulent air from the Atlantic and fewer days with turbid air of continental origin than the other years concerned. Dr J. M. Stagg, Superintendent of the Kew Observatory, has also pointed out that for Kew the annual mean values for atmospheric pollution, in milligrams per cubic metre of air, are from 1928 to 1937 respectively 0·15, 0·18, 0·14, 0·18, 0·19, 0·21, 0·20, 0·13, 0·17, 0·12. Certainly 1930 is here one of the low values though not the only one. Furthermore, Gloucester (the nearest recording place to Plymouth though about 133 miles away) had in 1930 its lowest value of the period 1926–36. Dr G. M. B. Dobson, Chairman of the Atmospheric Pollution Research Committee, called attention to this as possibly connected with the industrial depression of 1930–3. Dr Goldie, however, considers that the major cause (both of the greater daylight and of the low pollution of 1930) was the character of the air supply. This would not *necessarily* show up in local wind direction statistics, since wind direction is not always a reliable guide to the origin of the air.

We are indebted to Dr Stagg for revised values of the direct solar radiation (normal incidence) in gram-calories per square centimetre at Kew. The monthly totals for the 17 years, 1930–46 were tabulated for 7 months during which runs had been obtained which were unbroken save that 22 days only were recorded for October and 13 days for November 1931. Considering the totals for the 5 months July to November each year, 1933, 1934, 1935 and 1940 are all bigger than 1930. July 1933, 1934, 1935 and 1940 are all greater than the exceptionally bright Plymouth July 1930. There is, in fact, no relation between the two sets of measurements, for at Kew normally incident sunlight was measured by its heating effect, at Plymouth blue light from the sun and sky as received on a horizontal surface. The Kew observations do however bring out the very great variation in the solar radiation from year to year, even in the summer months. Table 9 shows the mean, maximum and minimum values for the months, June to December, for which an almost complete series had been obtained during seventeen years. Below are given the corresponding percentage values and at the bottom the percentage range. Thus even in June and July the range is 60 to 94 %, with a minimum range of 50 in October and a maximum of 147·5 in December. Our climate is, in fact, very variable, and that this variation should extend to the light received, direct and diffused, is not perhaps so very surprising.

TABLE 9. DIRECT SOLAR RADIATION (NORMAL INCIDENCE), MONTHLY TOTALS FOR KEW, IN GRAM-CALORIES PER SQ. CENTIMETRE PER DAY FOR 1930 TO 1946 INCLUSIVE. THE VALUES SHOWN ARE THE MEAN, MAXIMUM AND MINIMUM, TOGETHER WITH THE CORRESPONDING PERCENTAGES AND RANGE

month	June	July	Aug.	Sept.	Oct.	Nov.	Dec.
mean	8,778	7,308	7,211	5,108	3,356	1,487	1,094
max.	12,141	11,224	9,684	7,433	4,239	2,324	1,941
min.	6,884	4,308	4,958	2,334	2,561	761	329
max. %	138·4	153·4	134·2	145·4	126·4	156·4	177·6
min. %	78·5	59·0	68·7	45·7	76·4	51·2	30·1
range	59·9	94·4	65·5	99·7	50·0	105·2	147·5

SUMMARY

The measurement of daylight using a vacuum sodium photoelectric cell and a Cambridge 'thread recorder' have been continued for 11 years and confirm the previous conclusions as to suitability of the method.

The illumination during the last 3 years was rather below the average, but the three were closely similar. Of the 11 years 1930 was much the brightest, followed by 1934. The remainder were rather uniform.

June was the brightest month in 1938, May in 1939 and 1940. But of the 11 years May came first in six, June in four and July once, in 1930. This refers to the measurements of the illumination integral, as do also the following paragraphs.

The dullest months were as follows: January, February, April 1937; March and July 1939; May 1938; June 1933; August, September, November 1932; October 1934 and 1940 almost equal; December 1940. The brightest months were: January 1931; February and May 1934; March 1933; April, June, July, August, September, October and December 1930; November 1937.

Within each year the mean value of the December illumination is 1·37 %, with May 15·61 % and June 15·59 %. The range of the monthly means lies between 20 % for June and 59 % for November.

There is no simple relation between the illumination integral and the number of hours of sunshine, rainfall, number of days with rain or wind direction. Calm days are never exceptionally bright, and few days with wind force 1 or 2 are so; wind force about 3 is usual for the brightest days.

The illumination on days showing complete cloud throughout was, during 1930 and 1936, 0·326 and 0·304 respectively of that on the brightest days, calculating on a month by month basis, or weighted for the number of bright days in each month, 0·348 and 0·320 respectively.

The illumination on the sunless days of 1930 was considerably above that of similar days in 1936, a year of average illumination.

On comparing the Plymouth records with Aurén's, obtained near Stockholm, it is seen that the wide range in light intensity (kilolux-hours) within the same month, as found at Plymouth, was also found near Stockholm, where the wave-length concerned was a little over 0·50μ, as against 0·41μ at Plymouth. The mean monthly range was Plymouth 48·5 %, Stockholm 43·3 %. The maximum range was Plymouth 72 %, in July, followed by Stockholm 70 % in November, 68 % in February, 65 % in March, with Plymouth 64 % in September.

We desire to acknowledge our indebtedness and to express our thanks to the Government Grant Committee of the Royal Society for defraying the cost of the thread recorder, photocells and other apparatus; to Dr H. H. Poole of the Royal Dublin Society for standardizations of certain photocells as in the work already published and to Dr A. H. R. Goldie and Dr J. M. Stagg of the Meteorological Office, Air Ministry, for the benefit of their helpful criticism from the standpoint of climatology. Our thanks are also due to the Director, Meteorological Office, to various members of his staff and to the Borough Meteorologist, Plymouth, for their help in giving us access to the climatological observations. We are also indebted to Mr F. J. Warren and other members of the staff of the Department of General Physiology, Marine Biological Laboratory, Plymouth for attention to the thread recorder and general assistance.

REFERENCES

Atkins, W. R. G. 1938 *Proc. Roy. Soc.* A, **165**, 453–465.
Atkins, W. R. G. & Poole, H. H. 1930 *Nature*, **125**, 305.
Atkins, W. R. G. & Poole, H. H. 1936 *Phil. Trans.* A, **235**, 245–272.
Aurén, T. E. 1930 *Medd. met.-hydr. Anst. Uppsala*, **5**, no. 4.
Aurén, T. E. 1933 *Ark. Mat. Astr. Fys.* **24** A, no. 4.
Aurén, T. E. 1934 *Met. Z.* **51**, 173.
Aurén, T. E. 1939 *Ark. Mat. Astr. Fys.* **26** A, no. 20.
Aurén, T. E. 1942 *Ark. Mat. Astr. Fys.* **28** A, no. 11.
Aurén, T. E. 1943 *Ark. Bot.* **30** A, no. 15.
Aurén, T. E. 1944 *Ark. Mat. Astr. Fys.* **31** A, no. 11.
Fleming, J. A. 1943 *Trans. Amer. Geophys. Un.* p. 229–234.
Koschmieder, H. 1924 *Beitr. Phys. frei. Atmos.* **12**, 33–53 and 171–181.
Poole, H. H. & Atkins, W. R. G. 1933 *Sci. Proc. Roy. Dub. Soc.* **21**, no. 1, 1.
Poole, H. H. & Atkins, W. R. G. 1935 *Phil. Trans.* A, **235**, 1–27.
Wright, H. L. 1939 *Quart. J. Roy. Met. Soc.* **65**, 411–442; **66**, 3–11.
Wright, H. L. 1940 *Quart. J. Roy. Met. Soc.* **66**, 66–77.

Progressive lightning. VII
Directly-correlated photographic and electrical studies of lightning from near thunderstorms

By D. J. Malan, D.ès.Sc. and B. F. J. Schonland, F.R.S.
Bernard Price Institute for Geophysical Research, Johannesburg

(*Received* 23 *April* 1947)

[Plates 21 and 22]

An analysis has been made of the direct correlation of luminous and electrical field-changes produced by thirty-seven lightning discharges to ground. These discharges comprised 199 separate strokes, most of which were within a distance of 6 km.

A new form of drum camera and a camera shutter operated by the first leader were employed, and many records were obtained in daylight.

When compared with results previously reported for flashes at distances of 10 km. or more, the following major differences are found: negative field-changes from near leaders, absence of electrical effects of first leader steps and hook-shaped field-changes during the period immediately following the return stroke.

The hook field-changes are shown to be associated with components in the continuing luminosity of the channel of the type investigated by Malan & Collens and to be due to subsidiary discharges in this channel. These '*M*' components carry negative charge to ground in quantities between one-fifth and one-hundredth of those carried by main strokes.

The height of the lower negative charge in these thunderclouds is found to be from 4 to 9 km.

During a discharge to ground, no rapid discharges occur within the cloud or elsewhere than in the cloud-ground channel. A fairly slow discharge of the upper positive charge in the thundercloud appears to occur to the upper air immediately after the lower negative pole has discharged to ground.

1. Introduction

In a previous paper (Schonland, Hodges & Collens 1938)* a discussion has been given of the results of correlating the electrical field-changes accompanying lightning discharges with the details of luminosity recorded by the Boys camera. Most of the correlations were indirect and in only a few cases were simultaneous records of camera and oscillograph available. Although the indirect correlation of many others enabled progress to be made in the interpretation of the discharge process, it was clear that certain questions could be answered only by the collection of a large number of direct correlations, such as are analyzed and reported on here.

The first question which prompted the work to be described was whether, during the time interval occupied by the several strokes of a discharge to ground, there occur other field-changes which are not due to, or associated with, changes in the discharge channel to ground. It is conceivable that discharges, fast or slow, within the cloud itself, or upwards into the upper air, frequently occur during the period occupied by discharges to ground. Glows from the tops of distant clouds have been reported (Malan 1937) which appear to show this association, and it has remained an open question whether the discharge to ground is not often part of a more complex discharge process:

---

* Referred to subsequently as P.L. V.

A second subject for further inquiry was the nature of the correlation which would be obtained when the discharge was nearly overhead. The pioneer work of Appleton & Chapman (1937) in England on electrical field-changes, like that in South Africa, has been carried out on storms which were usually more than 10 km. away. It was to be expected that new and interesting information would be obtained from much nearer discharges since the interpretation of their field-changes would be very much simplified by the predominance of the electrostatic over the induction and radiation fields which complicate records at 10 km. and beyond.

To obtain a large number of correlated discharge records from near storms is a difficult task. The present results were made possible by the special facilities available in the Bernard Price Institute, which included, apart from technical services, a special balcony with large glass windows providing wide openings shielded from rain and an uninterrupted view of all storms to the south, east and west. A further factor in securing results in sufficient number was the use of an automatic leader-operated camera trigger (Schonland & Elder, 1941) with which good photographic records of the discharges could be obtained on a fast-moving drum camera at any hour of the day.

With these and other aids it has proved possible in two years to secure directly-correlated records of thirty-seven separate discharges, comprising 199 strokes to ground. The observations were made in the summers of 1937 and 1938 by the last-named author. Their analysis has had to be deferred until after the war and has been assisted by a study of the advance results of a new series of observations with improved technique.

2. Equipment

(*a*) *The camera.* The main camera used in this work consisted essentially of a fixed lens (focal length 5 cm., aperture $f/0{\cdot}8$), and a horizontal motor-driven drum with photographic film on its outer circumference.

The drum was of aluminium, 56·6 cm. in diameter and 7·2 cm. wide. The difficulty of keeping the film taut at the high speeds employed was solved by making use in the following way of an ingenious device described by Whipple (1936). The circumference of the drum carried three narrow slots, 2 mm. wide, parallel to the axis and arranged to pass the ends of the film. Two were placed 1 mm. apart, and the third was diametrically opposite their centre. Slotted cylinders, which could be turned and locked in position from outside, were mounted inside the drum and close to these slots. The ends of two films of standard length were passed through the single slot and wound tightly on one cylinder. The films were then passed around the drum in opposite directions, and their free ends wound up on separate cylinders after passing through the appropriate slots. The films remained taut at the highest speeds used and it was easy to remove and replace them.

The field of the lens was less than half the width of the film and so the lens mounting was arranged to slide vertically to enable two separate records to be obtained on each set of films.

For daylight operation the lens was fitted with a Compur shutter actuated by the daylight trigger. This trigger operates on the electromagnetic radiation from the first stepped-leader process. The shutter always opened in time to record the first return stroke and it was possible in several instances to record the lower end of the stepped-leader which itself actuated the trigger.

(*b*) *Recording of electrical field-changes.* Some modifications were made in the technique of recording the electrical field-changes. To avoid the possibility of brush discharge from the aerial system in strong fields, this aerial took the form of a copper ball 15 cm. in radius. The ball, which was insulated and mounted in the manner described by Wilson (1921), was at a height of 1·0 m. above the flat roof of the building, and a screened lead from it ran through the roof to the equipment below.

The damping resistance of 5000 ohms, the battery of mica condensers and the shunt resistance of 10 megohms were as described in P.L. V. A paraphase amplifier (Cossor 3355) provided a balanced output to a hard cathode-ray tube (Cossor 3278) with 6 kV on the final anode.

Since the screen of the tube would have been badly burnt by long exposure to the bright cathode-ray spot, spot brilliancy was controlled by an automatic brilliancy unit (Cossor 3365).

The recording film was carried on an axially traversed drum driven by a motor with a constant speed regulator. The angular velocity of this drum was kept at one of three selected values with the aid of a stroboscopic disk.

Some sacrifice of resolution in the oscillograph records had to be made to secure correlations. To catch a lightning flash on both camera and oscillograph in the time occupied by a run of the drum requires considerable experience and skill and if the run is made too short the opportunity may be missed. For this reason the peripheral velocity of the drum was usually set at 250 cm./sec., giving a run duration of 5 min. A few successful runs were made at twice this velocity.

Both sets of equipment, the outside camera and the oscillograph, could be controlled by one person operating the former. As soon as a satisfactory photograph had been obtained, the oscillograph spot was switched off by remote control, producing a gap on the field-change record which served to mark the field-changes of the flash which had been photographed.

3. GENERAL DISCUSSION

The general results of this analysis of the correlated records obtained from near discharges are shown in figure 1A for a flash at a distance of 3 to 4 km. For convenience of comparison the corresponding field-changes which would be observed at

10 to 15 km. are shown in figure 1B. This figure is based upon the work already reported in P.L. V. The figures refer to an unbranched vertical discharge. Complications introduced into the field record by branching in both the leader, or *a*, and return, or *b*, processes have been ignored, as have been the effects of a channel inclined to the vertical.

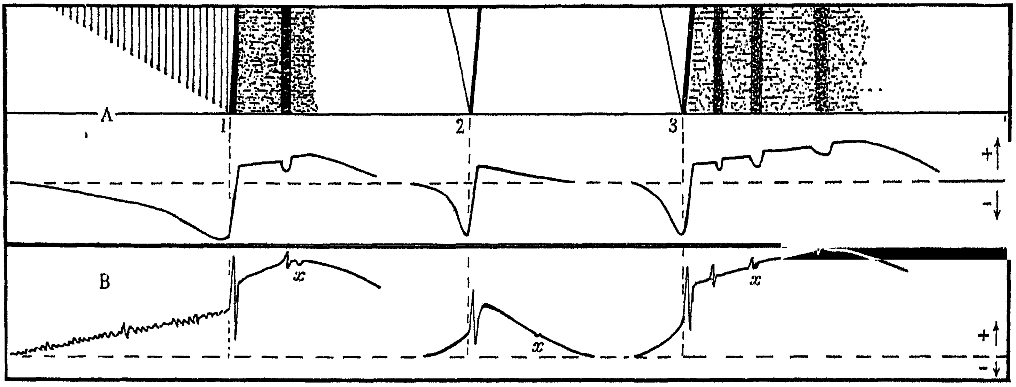

FIGURE 1

The durations of both *a* and *b* field-changes are shown as longer than those of the corresponding luminous changes, since the camera cannot record streamers when they are above the base of the cloud. No attempt has been made to show the detailed electrical structure of the *b* process, as this requires further study with faster recording equipment.

The small depressions marked as *x* on figure 1B occur with remarkable consistency of form and time on practically all our distant discharge records. Since their separation from the start of the *b* process is always very close to 600 μsec., they must owe their appearance to the ionosphere. Many examples of these '*x* bumps' are to be seen in figures 5 and 6 of P.L. V. They are not found on records of near discharges, presumably because their amplitude is too small to be recorded with the reduced sensitivity then employed. They will not be further discussed here.

Figures 1A and B illustrate some very marked differences in the form of the field-changes from the same flash at distances of 3 and 15 km.

In the first place it will be seen that in figure 1A the leader field-change is negative (i.e. increasing an existing negative field) and with the positive *b* portion takes the shape of a hook, whereas in figure 1B it is positive. Since the leader process lowers negative charge into the channel, such a field-change reversal effect with distance is to be expected and has already been indicated in observations by Wormell (1939).

The second difference is the general absence of marked 'step' effects on the *a* portion of near first strokes. It was to be expected that radiation effects, which produce the leader ripple on records of more distant strokes, should be absent when the discharge is nearly overhead, and, in fact, radiation pulses are also absent on the near records of the rapid *b* portion. But the absence of any appreciable electrostatic field-change corresponding to the intensely luminous steps is a little surprising. It establishes that the main electrical process in the first leader is the continuously moving pilot-streamer (Schonland 1938), and that the abrupt changes in luminosity provided by the steps are secondary from an electrical point of view. Observations by Chapman (1939) have indicated a similar conclusion.

The third difference between the near and distant field-change records concerns the *c*, or continuing, portion of the field-change. For near strokes it is often absent, as in the second stroke of figure 1 A and when present, as in the first and third strokes, it is of much smaller magnitude than would be expected from the distant records. When the *c* change is present on near records it is always associated with small hook-shaped subsequent field-changes, which on the distant records change to radiation pulses or oscillations of a complex type.

These hook components, as indicated in figure 1 A, have been found to correspond in time with faint components in the continuing luminosity of the channel. Malan & Collens (1937) have discussed two types of such components of luminosity. The first is associated with branching in the first return stroke, and will be referred to as the branch component type; the second occurs in the continuing luminosity after the main return stroke process reached the cloud and has previously been observed up to 900μsec. after the start of this process. This type will be referred to as an *M* component of a continuing discharge. As it is usually weak in intensity and ill-defined, it is generally impossible to record an *M* component at distances of 10 km. or more. For this reason in earlier work (P.L. V) on the complexities occurring in the *c* portion of the field-change no luminous effects could be found to correspond with the minor radiation pulses now suggested in figure 1 B to be directly connected with *M* components. It was stated in P.L. V (§2 (*d*)) that 'in the majority of cases examined this complexity increases progressively from stroke to stroke of the series which makes up a flash'. A similar tendency towards an increase in the number of *M* components, and of the corresponding hooks on near field-change records has been observed in the course of the present work though it does not show anything like a regular progression, only a tendency for *M* components and hooks to become more numerous in the continuing discharges of later strokes. It has not yet been possible to establish by observation the actual form of the radiation pulses shown in figure 1 B and the evidence for their correspondence with *M* components is at present circumstantial only.

4. SOME ILLUSTRATIVE RECORDS

Drawings of the correlated records of twenty-seven strokes from ten different flashes are reproduced in figure 2. On the left of each separate panel is given the code name of the flash, its distance and a drawing of the form taken by the discharge. The camera records are placed below the field-change records, but for the sake of clarity each separate stroke and *M* component is represented as if the channel had been vertical. These representations of the channel each carry figures on the left indicating the number of the stroke in the series making up the discharge and figures in the horizontal section below indicating the number of the *M* component. Thus BAU 2, 2, 2 is the second *M* component observed in the continuing luminosity of the second stroke of flash BAU 2. Successive strokes of a series have been separated by a short gap from one another and no information is given in the diagram about the continuous field-changes in the comparatively long interval between them. The time-scale, which runs from left to right, is not linear since, to show full details of the field-changes of short duration without using excessive space for the leaders and other effects of long duration, it is necessary to compress these last very considerably. Full details of the time-measurements are given in table 1, which also lists the values of the time-constant of the recording system in each case. The records have not been corrected for this time-constant. Corrected records, together with more recent observations with a different technique, have been used in preparing the diagrams of figure 1A.

The zero of the oscillograph record is shown by a horizontal dashed line; positive field-changes are upwards. The off-scale limits of the recording system are indicated where necessary by horizontal full lines. Such off-scale movements occurred frequently, because it is extremely difficult in practice to estimate the amplitude of the field-change to be expected from a flash to ground at an unpredictable distance. The result has been to produce in many cases a limit to the amplitudes of the *a* and *b* processes and so to exaggerate the smaller hook components in comparison with these. Flash BV 2 is an outstanding example.

The photographic intensities of the various *M* components are given in column 5 of table 1; the symbols s., m., f. and v.f. correspond to 'strong', 'medium', 'faint' and 'very faint'. The flashes selected for figure 2 do not show many examples of photographed leaders as most of them were taken in daylight. Where leaders have been photographed, they are shown in correct time-relation to their field-changes, (BAU 1, BV 2, 2 and BAU 2, 2).

The correspondence in time between *M* components and hook field-changes is shown in columns 6 to 9 of table 1. The times of start and end of each are measured from the end of the *b* process. *M* components are often very difficult to place exactly and where the measurements are subject to large error they are either placed in brackets or the limits of error are given.

Table 1 shows that the correlation of *M* components and hook field-changes is satisfactory, but it will be clear from an examination of the data that it is not at present possible to determine whether the times of start and end correspond exactly.

Some general points not covered by table 1 may be noted in connexion with figure 2.

BDB. The hook on BDB 1, which occurs 200 μsec. after the *b* change, shows no corresponding *M* component because the continuing luminosity is very dense.

BCI 5. This flash is of interest because the first stroke shows a positive-going, and the second a negative-going, leader. The explanation is probably to be found (see § 8) in the fact that this flash occurred at about the reversal distance for the sign of the

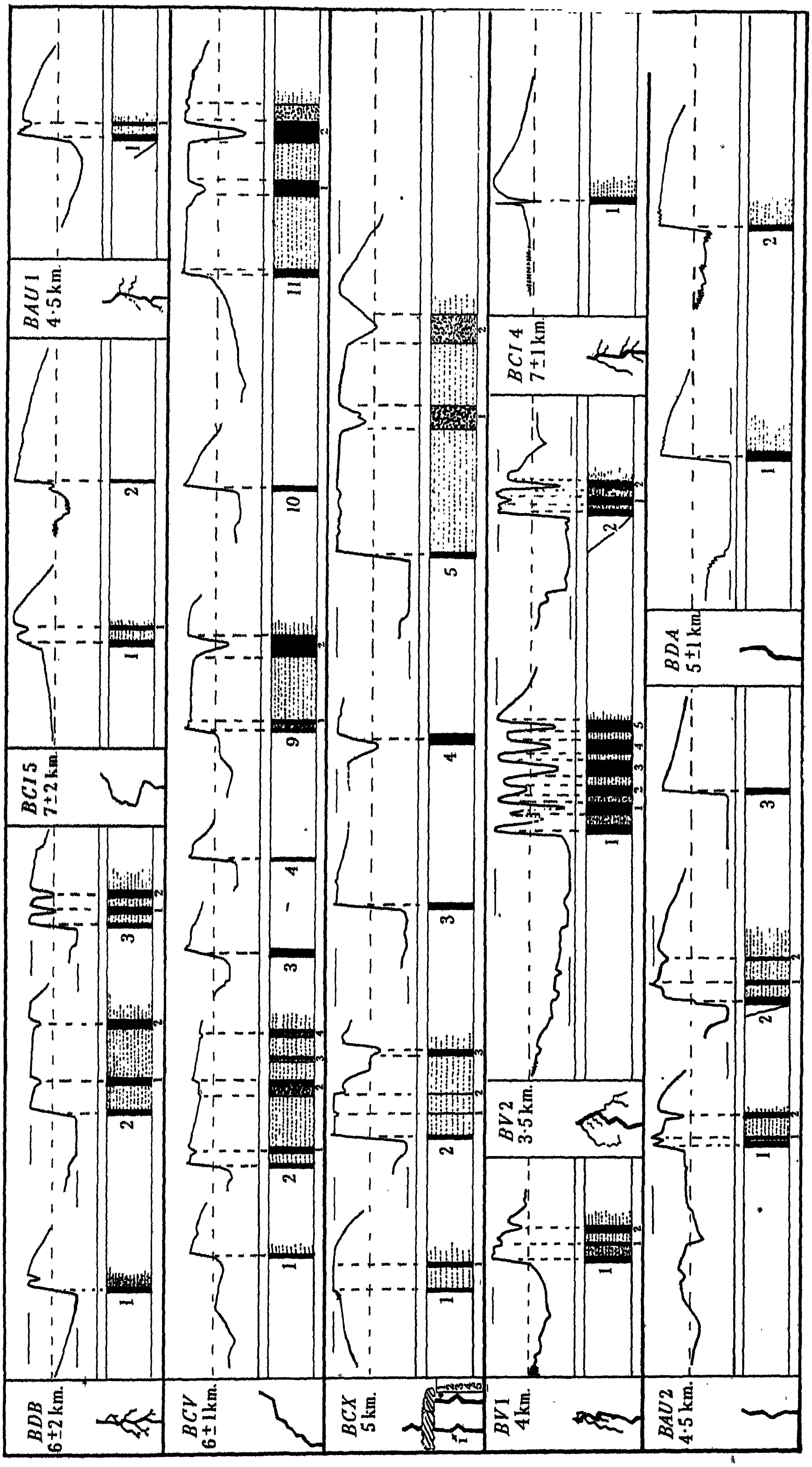
BDB
6±2 km.
BCI 5
7±2 km.
BAU 1
4·5 km.
BCV
6±1 km.
BCX
5 km.
BV1
4 km.
BV2
3·5 km.
BCI 4
7±1 km.
BAU2
4·5 km.
BDA
5±1 km.

FIGURE 2

TABLE 1. (Data for figure 2)

flash	time-constant (sec.)	stroke number	'M' components		times of 'M' components (μsec.)		times of 'hook' field-changes (μsec.)		remarks
			number	intensity	start	end	start	end	
BDB	0·0035	1	absent	—	—	—	200	240	*M* obscured by main discharge
		2	1	m.	980	(1200)	900	1020	
		2	2	s.	2200 ± 100	(2400)	2100	2180	
		3	1	v.f.	(400)	—	340	480	
		3	2	f.	800	—	740	880	
BCI 5	0·0035	1	1	v.f.	—	300	200	280	
BAU 1	0·021	1	1	f.	300	400	(200)	400	
BCV	0·001	2	1	m.	300	400	280	380	
		2	2	m.	2800 ± 300	3000 ± 200	2400	2600	
		2	3	v.f.	4000	—	—	—	very faint *M*; no hook
		2	4	f.	(6700)	7300 ± 200	6400 ± 100	6600 ± 100	
		9	1	m.	—	600	—	600	both *M* and hook continuous from main stroke
		9	2	s.	3200 ± 300	3700 ± 200	3000	3500	edge of *M* fuzzy
		11	1	v.f.	1600 ± 200	1900 ± 200	1400	1760	
		11	2	m.	2700	3500 ± 200	2400	3200	
BCX	0·005	1	1	m.	400	(500)	—	—	off-scale; no hook shown
		2	1	f.	500 ± 50	(700)	480	680	
		2	2	s.	1000 ± 100	1300	1080	(1200)	
		2	3	m.	2000 ± 200	2300	2000	2400	
		5	1	f.	(4500)	(5500)	5200	5600	
		5	2	v.f.	(7500)	—	6000	7200	
BV 1	0·021	1	1	f.	810	(1150)	800	1200	
		1	2	v.f.	(1620)	—	1600	2000	
BV 2	0·021	1	1	s.	540	800	500	800	slow c.r.o. recording; all figures ± 75 μsec.
		1	2	f.	920	1000	900	1000	
		1	3	m.	1200	1300	1100	1300	
		1	4	v.f.	1400	1600	1400	1550	
		1	5	m.	1800	2070	1700	2000	
		2	1	s.	250	400	200	400	
		2	2	v.f.	(600)	—	600	860	
BAU 2	0·021	1	1	s.	200	270	(180)	270	
		1	2	f.	(3000)	(3100)	2200	2500	
		2	1	v.f.	280	—	280	400	
		2	2	v.f.	1150	—	900	1200	

leader process and the two strokes came from different parts of the cloud. Leader ripple is evident on stroke 2.

BAU 1. This single-stroke flash shows a portion of the stepped-leader which triggered the camera. The whole *a* process lasted 0·032 sec., and the leader was first recorded 0·016 sec. after the start of the *a* process. The leader field-change was preceded by other slow field-changes lasting 0·06 sec.

BCV. Strokes 5 to 8 inclusive have been omitted from the figure, since they show only simple *b* process correlations and are too faint for *M* component correlation. The actual records for strokes 9 and 11 are reproduced in figure 6, plate 21 to the same time-scale. The figure carries a fixed photograph of the whole flash at the top right-hand corner.

BCX. This flash is an example of several we have obtained in which the first stroke to ground has come from a portion of the cloud higher or nearer than the others. This is illustrated in the left-hand panel. The leader field-change for BCX 1 is positive-going while for the remaining strokes it is negative-going. A reasonable explanation is that the first track ran initially from the front of the cloud away from the observer before passing almost vertically to ground. The smallness of the *b* field-change shown on BCX 1 is due to the record going off-scale.

BV 1. The records for this single-stroke flash are reproduced in figure 7, plate 21. The leader process lasted for 0·16 sec. and began with a short set of step effects.

BV 2. This flash, which like the previous one was photographed in daylight, is reproduced in figure 8, plate 22. At the left of each half of the figure is the complete drum camera picture for a stroke. Enlargements of parts of these, showing the *M* components, have been mounted above the field-change records, both on the time-scale shown in the figure. It also began with an indication of stepped-leader processes, but for the rest of its 0·03 sec. the leader shows no ripple. The sudden irregularities shown on the *a* portion correspond, in most cases, with points of change of direction and branching in the leader channel.

BV 2, 1 shows five *M* components associated with hooks in the field-change record.

BV 2, 2 shows a good dart leader of total duration 800 μsec. between cloud-base and ground. The corresponding *a* field-change is strongly negative and lasts for 2200 μsec. The last two irregularities in the *a* field-change are again found to correspond in time with major changes in the direction of the channel.

BV 2, 2 carries two hooks for the second and larger of which the *M* component can only just be distinguished, since the photograph is heavily fogged by the excessive intensity of the main stroke and its first component. As the trace of the c.r.o. had fallen below the off-scale line by the time it occurred, this hook is exaggerated in comparison with that corresponding to BV 2, 2, 1 which occurred when the spot was off-scale. This second hook is an example of several whose nett effect is apparently a negative field-change but is actually positive when account is taken of the slope of the trace on which it is superimposed.

BCI 4. This record is introduced to show a simple example of the more distant type of field-change record with a radiation field. It was taken a few minutes before

BCI 5, which has already been discussed, and was probably a few kilometres farther away. The positive-going leader shows stepped-leader radiation ripple on the a portion. The b portion with its strong radiation oscillation occupied 40μsec. and the c portion 160μsec. The whole flash consisted of the single stroke shown.

BAU 2. The first stroke of BAU 2 shows a leader field-change lasting for 0·058 sec. with several large irregular changes. From other records for which the first leader luminosity has been directly correlated with such irregularities, we are able to identify these with multiple dart streamers forming type $\beta 2$ leaders (Schonland, Malan & Collens 1938). BAU 2, 2 has a visible leader which took 1000μsec. to pass from cloud-base to ground. The corresponding a field-change occupied 1350μsec.

BAU 2, 3 shows a simple recovery field-change of the type already described in § 3 and shown also by BCV 10 and BDA 1.

BDA. The first two of a series of five strokes are shown. The a portions of both show radiation effects of the type to be expected from stepped-leader processes. They occur at the start of both BDA 1 and 2 and at the end of the a portion of BDA 2. The interval of time between these two strokes was long (0·072 sec.), and the leader to the second stroke probably reverted to the stepped process in approaching the ground (Schonland, Malan & Collens 1935). The durations of the a portions are 1600 and 1160μsec. respectively.

5. CORRELATION OF LUMINOUS CHANGES IN THE CHANNEL FROM CLOUD-BASE TO GROUND WITH RAPID ELECTRICAL FIELD-CHANGES

As one object of this investigation was to find out whether discharges occur elsewhere than in the cloud-ground channel during the time occupied by a flash to ground, the correlated records have been examined to determine whether they include any rapid field-changes which do not correspond to luminous changes in the channel. A total of thirty-seven correlated discharges is available for study. These show 189 separate strokes on the camera records and 199 rapid field-changes on the oscillograph records. Each of the 189 photographed strokes can be correlated accurately in time with a rapid field-change of the type shown in figure 1A. Of the ten rapid field-changes for which no corresponding strokes can be found on the camera records, eight were of characteristic flash to ground type but recorded under conditions such that weak strokes, either owing to distance or to poor visibility, would not have been sufficiently luminous to be photographed. The remaining two are of the same type and may have arisen from flashes from other thunderclouds in the neighbourhood which were not caught by the camera. No records of the kind characteristic of flashes within the cloud were ever obtained during the time occupied by a flash to ground, though they were plentiful at other times. It must therefore be concluded that a flash to ground is rarely, if ever, accompanied by any other rapid type of discharge in some other part of the cloud.

An analysis has also been made of the correspondence between M components in the channel and hook field-changes. Fewer camera records are available for this purpose, for *M* components are not always present and when present they form part of the continuous afterglow and are difficult to detect. Sixteen discharges which were photographed under reasonably good conditions have been selected as suitable for comparison with field-change records taken at the same time. The photographs contain twenty-five strokes with one or more *M* components and the total number of *M* components is forty-one.

Of these, thirty-nine correspond in time, usually within 30 μsec., with hooks in the field-change records. The remaining two *M* components occurred within 200 μsecs. of the start of the *b* change and the corresponding hooks could have been missed owing to off-scale movement of the recording system.

It is more difficult to prove the converse, that every hook corresponds to an *M* component in the channel. The field-change records of these sixteen discharges show a further nineteen hook field-changes which cannot be fitted to *M* components in the photographs. These come from ten of the twenty-five strokes in six of the sixteen discharges and are found in each case to have been recorded under conditions of distance or obscuration by rain which would have hampered the photography of weak *M* components.

From the examinations described, it is reasonable to conclude that all the sudden field-changes, of both *b* and hook type, observed by us are associated with sudden changes of luminosity, and hence with discharges, in the cloud-ground channel itself. There is thus no evidence to support the view that *rapid* discharges between different parts of the cloud, or from the top of the cloud upwards, accompany a discharge to ground or occur during the intervals between strokes. The possibility remains that much slower discharges in these regions may take place during, and as a result of, a discharge to ground. This question is discussed in §9.

6. THE '*c*' FIELD-CHANGE

Many records of the fields associated with near strokes to ground show no *c* field-change at all, for the oscillograph record, even when corrected for the time-constant of the recording system, slopes downwards towards the zero line. (Appleton & Chapman (1937) have also reported that the *c* change is frequently absent in more distant discharges.) The approximate form of the near field-change in such cases is shown on the second stroke of figure 1A; actual examples are BCV 10, BAU 2, 3 and BDA 1 of figure 2. It must be concluded that strokes of this type are effectively terminated by the passage of charge to ground in the *b* process and that any subsequent continuing current in the channel is very small, if it exists at all. Such '*type* 1' strokes, which for the same reason show no *M* components, constitute 60 % of the near strokes examined by us.

On strokes of the kind exemplified by the first and third strokes of figure 1A, however, the record of the field-change slopes upwards after the *b* portion and indicates a current discharge continuing after the main return process. Figure 2 shows many cases of such '*type* 2' strokes, uncorrected for time-constant. The time occupied by this c process ranges from 150 to 2000 μsec. with a most frequent value of 300 μsec. In exceptional cases it has been found to be as long as 17 msec. In stroke BCX 5 of figure 2 (table 1) it is 7 msec.

It is of interest that these records are further differentiated from those of type 1 by the fact that they alone carry the superimposed hook-shaped field-changes, and that the corresponding discharge-channel photographs show simultaneous M components. The obvious interpretation of this difference is that the continuing current in type 2 strokes is subject to sudden increases which give rise to the M components and the 'hooks'.

In earlier work on the magnitude of the total c field-change, carried out on more distant flashes, it was found to constitute from one-third to one-half of the entire field-change due to all processes in the stroke (P.L. V, § 2 (*c*) and (*d*)). On the records of these much nearer flashes its contribution is only about half as much. One reason for this difference can be stated as follows:

Let the charges conveyed to ground in the b and c processes be Q_b and Q_c. These are both originally at height H above the ground and Q_c is conveyed from this height to earth in the continuing current of the c process. Q_b is lowered by the leader process into the air to fill the leader channel and to a first approximation it is held at an equivalent height $\frac{1}{2}H$ at the start of the b process (P.L. V, § 3 (*b*)). If ΔE_b and ΔE_c are the field-changes from the b and c processes and D is the horizontal distance involved:

$$\Delta E_b = \frac{2Q_b\frac{1}{2}H}{[(\frac{1}{2}H)^2+D^2]^{\frac{3}{2}}} \quad \text{and} \quad \Delta E_c = \frac{2Q_cH}{[H^2+D^2]^{\frac{3}{2}}}.$$

A reasonable lower limit for H (see § 8) is 4 km. Substituting this in the above equations, then

$$\left.\begin{aligned} \Delta E_b/\Delta E_c &= 0{\cdot}56\, Q_b/Q_c \quad \text{for} \quad D = 12\,\text{km.} \\ \text{and} \qquad \Delta E_b/\Delta E_c &= 1{\cdot}01\, Q_b/Q_c \quad \text{for} \quad D = 4\,\text{km.} \end{aligned}\right\} \qquad (1)$$

Thus the ratio of the c to the b field-change falls for the same stroke by a factor of 1·8 when the distance changes from 12 to 4 km. A more exact calculation, involving integration of the field due to the leader-charge Q_b uniformly distributed along a vertical channel from cloud to ground makes this factor 1·6. If H is taken as 6 km. (see § 8) these factors become 2·3 and 2·0 respectively.

Measurements on records free from off-scale effects and corrected for time-constant, give values of $\Delta E_b/\Delta E_c$ for strokes at about 4 km., which range from 10 to 5. From equation (1) it follows that Q_c/Q_b lies between 0·10 and 0·20. The hook components contribute further in a variable and irregular manner to the total c field-change and on occasion they may raise Q_c/Q_b effectively to 0·5. These values are significantly less than those derived from field-change studies of more distant flashes (P.L. V, § 3 (*e*)), which gave values of Q_c/Q_b ranging from 1·0 to 0·5. One explanation of the difference is discussed in § 9.

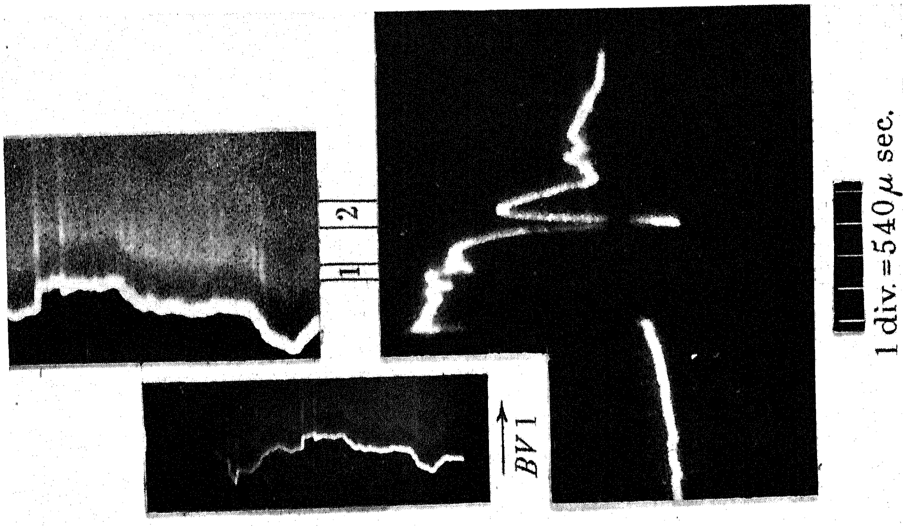

FIGURE 7

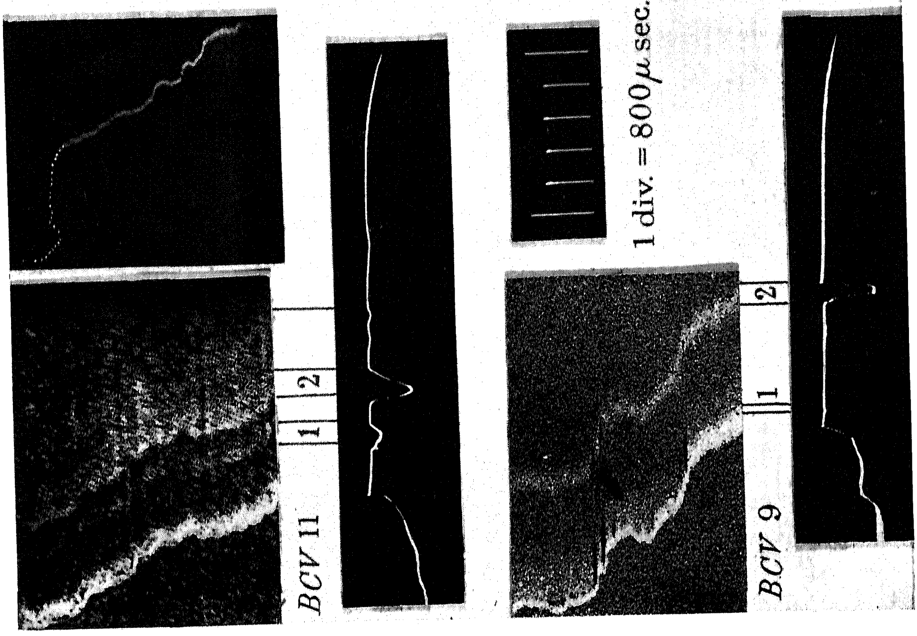

FIGURE 6

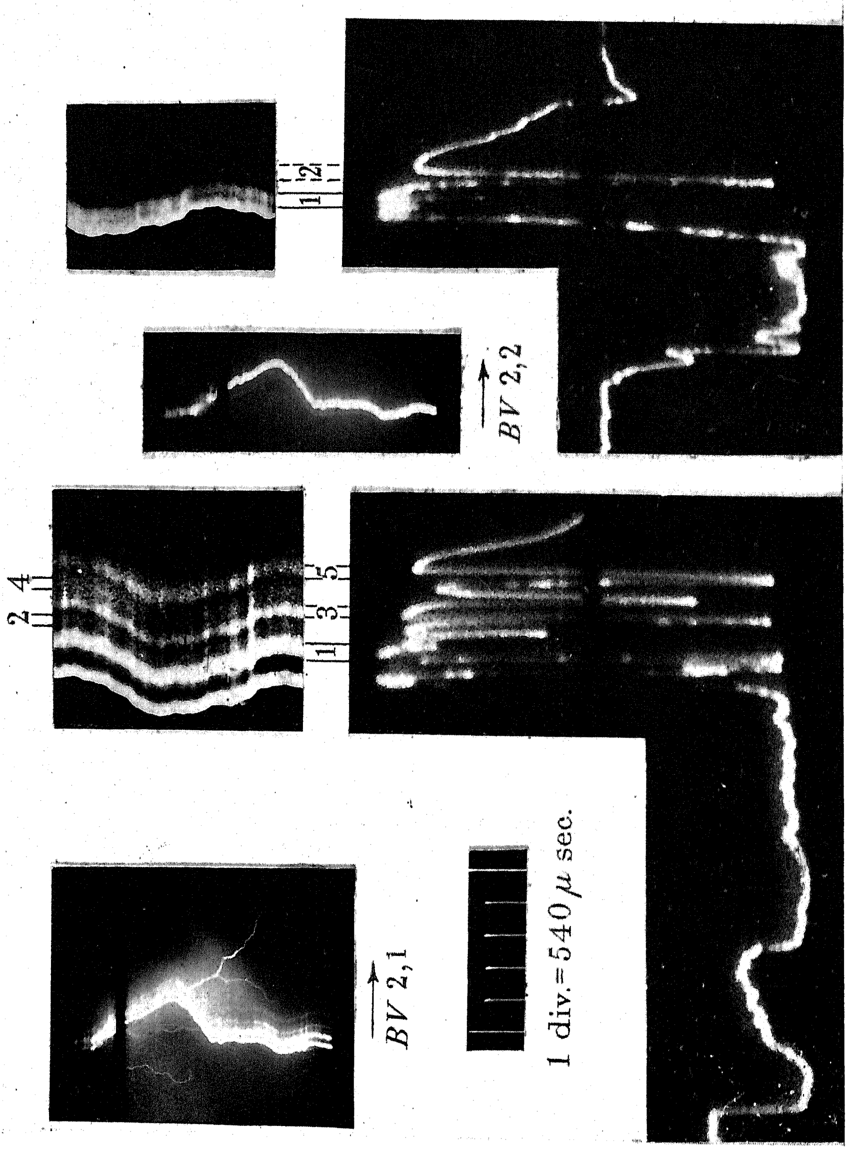

FIGURE 8

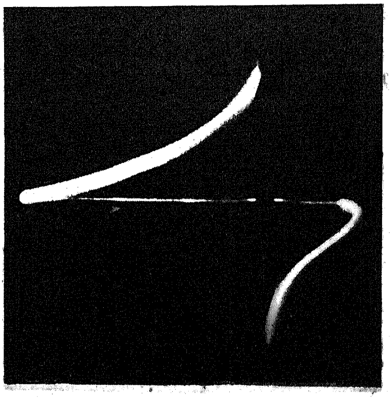

FIGURE 9

7. THE HOOK PROCESS

The hook components of the *c* field-change are always similar in general form. Each begins with a negative field-change, ΔE_1, followed without any pause by a larger positive field-change, ΔE_2, so that the nett field-change, ΔE_h, is always positive. ΔE_h is usually from one-fifth to one-hundredth of the *b* field-change preceding it.

The whole hook process generally occupies between 200 and 800 μsec. though values as high as 1600 μsec. have been observed; see BCX 5, 2 of table 1 and figure 2, (1200 μsec.). In such cases a long time-interval has elapsed since the *b* process. BCP 2, 2, 3 of figure 3 shows what is probably, but not certainly, a hook of duration 2400 μsec., starting 3600 μsec. after the *b* change. When there is more than one hook component to a stroke, it is found that the durations of successive hooks increase with the time which has elapsed since the *b* change. Some examples are shown in figure 3 where the times are marked in units of 100 μsec.

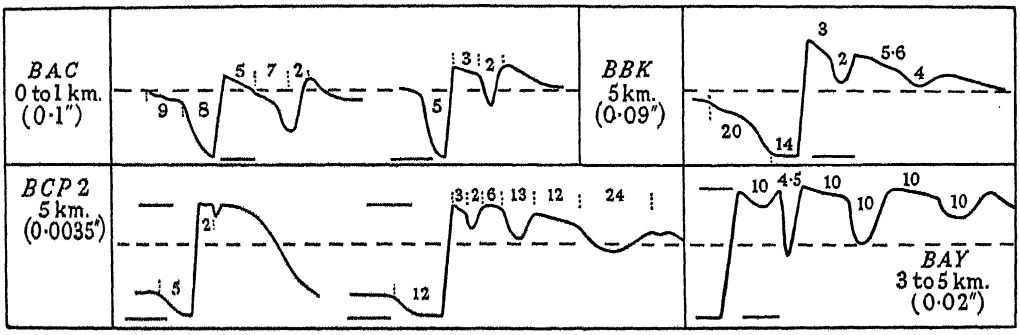

FIGURE 3

In order to show this significant feature, the data from all available strokes with more than one hook are given in figure 4, where hook durations are plotted against time-intervals measured from the end of the *b* change. There are fifteen such strokes in our records, of which one, BAA 3, has four hooks and five others have three each.

The duration in a few cases remains constant and in one it decreases with time but the general tendency for it to increase with time and hence with the age of the channel is evident. The actual durations vary considerably from stroke to stroke. A rough estimate of most frequent values is given in table 2.

TABLE 2. DURATION (T) OF HOOK PROCESSES

interval since '*b*' process (μsec.)	most frequent value of T (μsec.)
500	275
1000	320
2000	400
(3000)	(600)

The dependence of hook duration upon the age of the channel, together with the close connexion already established between hook field-changes and M components in luminosity, provides strong evidence that the hook process is a discharge in the channel between cloud and ground, that it is in fact a minor form of subsequent stroke.

This conclusion gains support from the similarity in form of all hook components and from the resemblance of the hook field-change to the a and b processes of the main discharge. The first part, ΔE_1, is of the same form as, but usually more rapid than, the leader field-change from a near stroke and the second, ΔE_2, is similar to, though generally slower than the b and c field-changes. Several examples of this parallelism in form are shown in figure 3 in flashes BAC and BBK. The former was a very close discharge and the latter took place at 5 km. Both these records are free from the off-scale effects mentioned earlier.

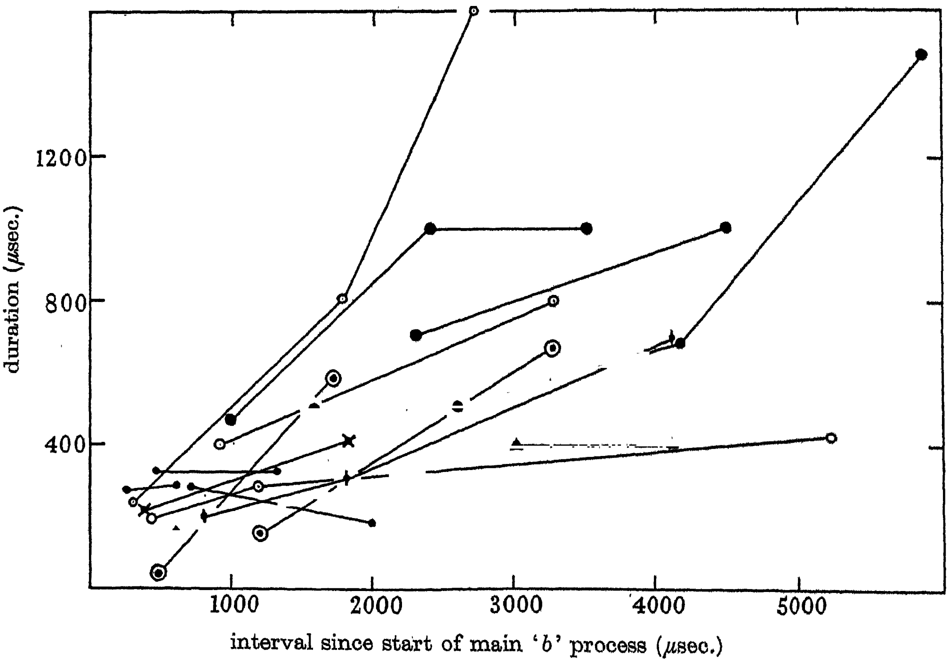

FIGURE 4

A full discussion of the details and the mechanism of the hook process is postponed until further work now in progress has been completed. The information at present available suggests that it takes place in two stages. In the first stage a small negative cloud charge passes down and fills the already ionized channel at a rate depending upon the age of this channel, giving rise to ΔE_1. In the second stage this charge passes to ground. The charge is usually not large enough, and the other conditions are not always such as, to give rise to a return stroke from the ground.

The process is a continuous one and the size of ΔE_h is a measure of the smallness of the charge involved, from 0·2 to 0·01 of that in the b process.

It is significant that our data show no certain case of a hook with a negative value of ΔE_h. These subsidiary discharges, according to our observations, always carry negative charge to ground.

8. THE FORM AND MAGNITUDE OF THE FIELD-CHANGE DUE TO THE LEADER PROCESS

In this section an examination is made of the dependence of the form of the a field-change on the height of the cloud charge (H) and the horizontal distance from the point of observation (D). It will be assumed for simplicity that the discharge channel is vertical and that the leader streamer as it comes down distributes a charge of uniform density, $-q$, per unit length, along the channel. These assumptions are adequate for the general purpose in hand and can easily be modified to deal with special cases.

Consider an element dx of a streamer of length x with origin at the centre of the cloud charge. The field due to the element of charge $-q\,dx$ at height $H-x$ is given by

$$dE = \frac{-2q\,dx(H-x)}{[(H-x)^2+D^2]^{\frac{3}{2}}},$$

and by integration the total field due to the leader streamer when it has extended to a length x is

$$E_x = -2q\left[\frac{1}{[(H-x)^2+D^2]^{\frac{1}{2}}} - \frac{1}{[H^2+D^2]^{\frac{1}{2}}}\right]. \tag{2}$$

Since the original field, due to the charge $-qx$ in the cloud before the streamer started, was

$$\frac{-2qxH}{[H^2+D^2]^{\frac{3}{2}}},$$

the total field-change when the leader has extended to x is algebraically given by

$$E_x = 2q\left[\frac{1}{[(H-x)^2+D^2]^{\frac{1}{2}}} - \frac{1}{(H^2+D^2)^{\frac{1}{2}}} - \frac{Hx}{(H^2+D^2)^{\frac{3}{2}}}\right]. \tag{3}$$

The form of this field-change as x passes from zero to its final value H is shown in figure 5. It is convenient to draw the curves for different values of $\alpha = D/H$. For a given height H the curves refer, therefore, to different values of D. If the velocity of the leader is uniform, which is approximately true for the dart leaders of strokes subsequent to the first, but not for the leaders to first strokes, these curves should represent a fair approximation to the shape of the a field-change records at various distances.

Comparison of figure 5 with figures 1 A and 1 B shows that the correspondence of theory with observation is qualitatively good. For small values of α, or D, the leader field-change is completely negative; for large values it is completely positive. At intermediate distances the leader begins with an increase in negative field, passes through zero and finally causes a positive field-change. A good example of a leader at a distance of 3 km. which shows an initial negative-going field-change becoming positive-going just before the *b* change is given in figure 9 of plate 22. This was recently recorded by one of us (D.J.M.) on a slow-moving oscillograph.

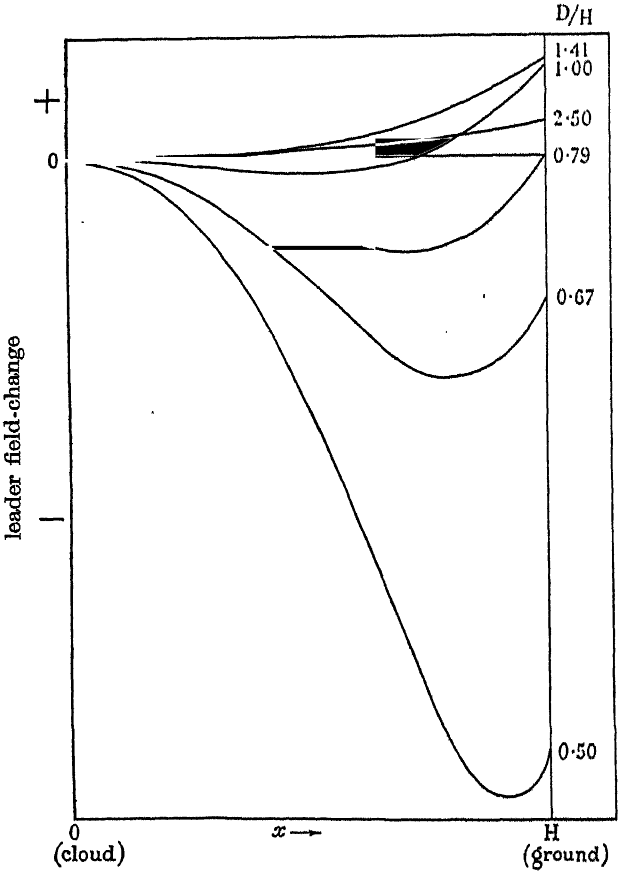

FIGURE 5

By putting $x = H$ in equation (3) it is found that the final field-change at the moment the leader reaches the ground is zero for $D/H = 0{\cdot}79$. On our records this condition is observed for values of D ranging from 4 to 7 km., the range being due mainly to the departure of discharge channels from the vertical. Hence H in these discharges may be estimated as from 5 to 9 km.

This estimate agrees with one made in an entirely different way. Our present records contain a number of instances in which the time spent by leader streamers in passing from cloud-base to ground can be compared with the total time occupied by the leader streamer in passing from the charge-centre in the cloud to the ground. Examples are BAU 2, 2 and BV 2, 2 in figure 2, and others have already been reported in P.L. V (§ 2 (*b*)). The duration of the whole leader process is roughly twice that of the portion photographed after emergence from the cloud-base. From direct measurements the vertical length of this visible portion is from 2 to 2·5 km. and hence H is of the order of 4 to 5 km. Since this assumes that the velocity of the streamer in the cloud is equal to that in the air, and it is likely to be higher, the above estimate is probably on the low side.

More satisfactory methods of determining H would be to apply equation (3) to the shape of the records of leader field-change and to compare the nett leader field-change with the b field-change. Preliminary applications of these methods give results in agreement with those quoted above.

9. THE UPPER POSITIVE CHARGE ON THE THUNDERCLOUD

As was the case in the series of observations previously reported (P.L. V, § 2 (e)), the correlations studied here show that separate strokes to ground almost always carry negative charge to the earth in the b and c processes. They have added the additional information that practically all the minor M components of the main discharge do the same.

The exceptions which we have found to these statements are few and their rarity has led us to withhold discussion of them until a sufficient number has been observed.

It is possible, therefore, to say that in general the upper positive charge on these thunderclouds does not discharge to ground at all. As a thundercloud is a bipolar generator (Wilson 1921), this positive charge must discharge, or otherwise be removed, to the conducting layers of the upper air. Such a process is most likely to occur immediately after the return stroke (b) portion of a stroke to ground, when the field above the cloud is suddenly increased. Since the observations show no sign of a field-change due to a rapid discharge at this time, it is necessary to examine the c field-change to see whether it exhibits any evidence of a slow discharge.

We begin by seeing what effect an upward movement of positive charge, or its equivalent, a downward flow of negative charge from the upper air, would have upon the field immediately after the b change. In either case the positive cloud charge is to be completely removed, or neutralized, so that the final field-change at all distances must be negative.

If H_1 is the height of the charge and D its horizontal distance, its upward movement will produce an initial positive or negative field-change according as D is $>$ or $< D_0$, where $D_0 = \sqrt{2} \times H_1$. For $D > D_0$ the growth of the initial positive field-change ceases when the charge reaches an effective height $D/\sqrt{2}$. Thereafter the field goes negative and the final nett field-change is negative. For $D < D_0$ the field-change is negative at all times.

If H_1 lies in the region 6 to 10 km., D_0 is 8·4 to 14·1 km., say 11 km. for purposes of discussion.

If, therefore, a slow discharge of this kind follows the b change, one would expect to find the following effects on our records of strokes to ground.

(a) *Strokes of type* 1

These strokes, which have no appreciable continuing current, should show negative-going field-changes at distances less than 11 km. and these changes should be more rapid than can be explained by the return of the recording system to zero.

Evidence of effects of this kind are shown on a great many of our records when the instrumental time-constant is large. For example, when it is as great as 0·021 sec., the trace often returns to zero at a rate about seven times faster than could be accounted for on instrumental grounds. Such tests as we have so far made suggest that the effect is real and not due to an unsuspected decrease in the instrumental time-constant such as might be caused by point-discharge from the ball aerial.

Beyond 11 km., strokes of type 1 should show an initial positive rise in the field after the *b* change. Since it is not easy to distinguish this from a true *c* change due to a continuing current, many of the distant records which show apparent *c* changes may in fact have been from strokes with little or no continuing current.

(b) *Strokes of type* 2 (*showing continuing current and c field-change*)

Within 11 km., the effect described under (*a*) will in this case oppose and reduce that due to the continuing current. The nett *c* field-change will, therefore, be smaller, and its rate of rise slower, than if no effect was present. Beyond 11 km., on the other hand, the effect will initially be added to the *c* field-change and only later will it oppose it and cut it down. It would, therefore, be expected that analyses of *c* field-changes on the supposition that they are solely due to continuing current would show inconsistencies between records of near and of distant flashes. This has already been found in § 6.

It is clear that further work is needed before these observations and arguments can be regarded as fully establishing the existence of a regular upward discharge of the upper positive pole of a thundercloud immediately after the return stroke to ground has occurred. At this stage it can only be said that it seems highly probable.

Discharges of this type have been reported as having been seen by two experienced observers of thunderstorms, Boys (1926) and Malan (1937). Malan's observations were made under very favourable circumstances, with the discharges to ground hidden by a hill. He describes the discharge as 'une longue et faible bande d'une lueur rougeâtre' and gives to it an extension to a height of about 50 km. and a width of several hundred metres. 'Deux fois le phenomène se présente comme un rideau auroral composé de cinq ou six de ces bandes.' He also reports that the bands were slightly curved in the direction to be anticipated if the discharge carried positive charge upwards to, or negative downwards from, the upper air.

The discharges observed by Boys were of feeble intensity but otherwise similar to ordinary flashes. They took place at the same time as discharges to ground.

It is a pleasure to express our gratitude to Mr J. A. Keiller for his ingenuity and assistance in the construction of the equipment used in this work. We are further indebted to him, to other members of the staff of the Institute and to Mr D. Schonland for help with the observations.

REFERENCES

Appleton, E. W. & Chapman, F. W. 1937 *Proc. Roy. Soc.* A, **158**, 1.
Boys, C. V. 1926 *Nature*, **118**, 749.
Chapman, F. W. 1939 *Proc. Phys. Soc.* **51**, 876.
Malan, D. J. 1937 *C.R. Acad. Sci., Paris*, **205**, 812.
Malan, D. J. & Collens, H. 1937 *Proc. Roy. Soc.* A, **162**, 175.
Schonland, B. F. J. 1938 *Proc. Roy. Soc.* A, **164**, 132.
Schonland, B. F. J. & Elder, J. S. 1941 *J. Franklin Inst.* **231**, 39.
Schonland, B. F. J., Hodges, D. B. & Collens, H. 1938 *Proc. Roy. Soc.* A, **166**, 56.
Schonland, B. F. J., Malan, D. J. & Collens, H. 1935 *Proc. Roy. Soc.* A, **152**, 595.
Schonland, B. F. J., Malan, D. J. & Collens, H. 1938 *Proc. Roy. Soc.* A, **168**, 455.
Whipple, G. A. 1936 *J. Instn. Elect. Engrs*, **78**, 497.
Wilson, C. T. R. 1921 *Phil. Trans.* A, **221**, 73.
Wormell, T. W. 1939 *Phil. Trans.* A, **238**, 249.

A note on a problem of Mahler

BY C. A. ROGERS

(*Communicated by H. Davenport, F.R.S.—Received* 4 *March* 1947)

The author answers one of the questions proposed by Mahler in a recent paper on the critical lattices of star bodies.

1. In a recent paper Mahler (1946) has developed a general theory of the critical lattices of star bodies. Let $F(X) = F(x_1, x_2, \ldots, x_n)$ be a continuous function of the co-ordinates $(x_1, x_2, \ldots, x_n)$ of the point X and suppose that:

(*a*) $F(X) \geqslant 0$ for all points X.

(*b*) $F(tX) = |t| F(X)$ for all points X and real numbers t.

Then the set S of the points X, for which

$$F(X) \leqslant 1,$$

is a star body. A lattice Λ is said to be admissible for S if the origin O is the only point of the lattice in the interior of S. The star body S is said to be of the finite type, if there is at least one lattice which is admissible for S. In this case, as Mahler proves, the determinants of the lattices admissible for S have a lower bound, $\Delta(S)$, which is attained for one or more of the lattices admissible for S. Such an admissible lattice with determinant $\Delta(S)$ is said to be a critical lattice of S. It is almost immediate (see Mahler's theorem 13) that, if Λ is a critical lattice of S, then, for any $\epsilon > 0$, there exists a point P of Λ such that

$$1 \leqslant F(P) < 1 + \epsilon.$$

Mahler proposes the following

PROBLEM. *Let $S: F(X) \leqslant 1$ be any star body of the finite type, Λ a critical lattice of S, and $\epsilon > 0$ any arbitrarily small number. Do there exist n independent points $P_1, P_2, \ldots, P_n$ of Λ such that*

$$1 \leqslant F(P_r) < 1 + \epsilon,$$

where $r = 1, 2, \ldots, n$?

It is well known that such points always exist if the star body is bounded. I prove the following result, which shows that it is not always possible to find such points if the star body is unbounded.

THEOREM 3. *For any λ, satisfying $1 < \lambda < \sqrt{(1\cdot 6)}$, there exists an n-dimensional star body S, such that the inequalities*

$$1 \leqslant F(P) < \lambda^{1/n}$$

are satisfied only by one pair P and $-P$ of points of the unique critical lattice of S.

The existence of such a star body will be shown to be an immediate consequence of the following result.

THEOREM 2. *For any λ, satisfying $1 < \lambda < \sqrt{(1\cdot 6)}$, there exists an n-dimensional star body S, such that*

(*a*) *S has a unique critical lattice with determinant* 1,

(*b*) *if Λ is any lattice, with determinant less than λ, which is admissible for S, then Λ can be obtained from the critical lattice by a magnification.*

This theorem will also be used to show that, if S is a variable star body, then $\Delta(S)$ may be in a certain sense a discontinuous function of S. This is discussed in § 6, where I shall prove

THEOREM 4. *For any λ, satisfying $1 < \lambda < \sqrt{(1\cdot 6)}$, there exists an n-dimensional star body S and a star body S_θ, depending on a positive parameter θ, such that*

(*a*) *for every $\theta > 0$, the body S_θ contains S,*

(*b*) $$\lim_{\theta \to +0} V(S_\theta - S) = 0,$$

where $V(S_\theta - S)$ is the volume of the set of points in S_θ but not in S,

(*c*) $$\lim_{\theta \to +0} \Delta(S_\theta) = \lambda \Delta(S).$$

I am grateful to Professor Davenport who has advised me, during the construction of these star bodies. In particular, one of his suggestions enabled me to simplify very considerably my treatment of the two-dimensional case.

2. We first prove the results in the two-dimensional case.

THEOREM 1. *Let S be the two-dimensional star body defined by*

$$\min\{|x^2-xy-y^2|, |y^2-yx-x^2|\} \leqslant 1.$$

Then:

(*a*) *The lattice of points with integral co-ordinates is the unique critical lattice of S.*

(*b*) *If Λ is any lattice, with determinant $\Delta < \sqrt{(1\cdot 6)}$, which is admissible for S, then Λ is the lattice of points whose co-ordinates are integral multiples of $\sqrt{\Delta}$.*

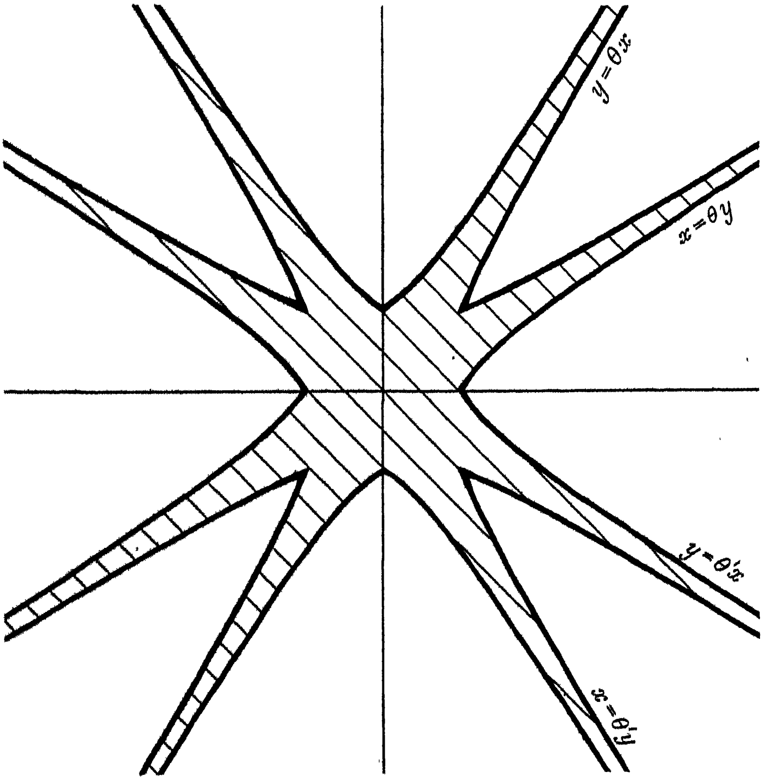

FIGURE 1. The star body S of Theorem 1.

Proof. We first prove (*b*). The set S is the set of points for which either

$$|(x-\theta y)(x-\theta' y)| \leqslant 1,$$

or

$$|(y-\theta x)(y-\theta' x)| \leqslant 1,$$

where

$$\theta = \tfrac{1}{2}\{1+\sqrt{5}\} \quad \text{and} \quad \theta' = \tfrac{1}{2}\{1-\sqrt{5}\}.$$

Suppose Λ is any lattice, admissible for S, with determinant

$$\Delta < \sqrt{(1\cdot 6)} = \sqrt{8}/\sqrt{5}.$$

Suppose Λ is generated by the points with co-ordinates (a_1, b_1) and (a_2, b_2). Then for all integers u and v not both zero

$$\begin{aligned} 1 \leqslant & \left| \{ua_1 + va_2 - \theta(ub_1 + vb_2)\}\{ua_1 + va_2 - \theta'(ub_1 + vb_2)\} \right| \\ & = \left| \{(a_1 - \theta b_1)u + (a_2 - \theta b_2)v\}\{(a_1 - \theta' b_1)u + (a_2 - \theta' b_2)v\} \right|. \end{aligned} \tag{1}$$

The discriminant of this indefinite quadratic form is

$$\begin{aligned} \begin{vmatrix} a_1 - \theta b_1, & a_2 - \theta b_2 \\ a_1 - \theta' b_1, & a_2 - \theta' b_2 \end{vmatrix}^2 &= \begin{vmatrix} -(\theta - \theta')b_1, & -(\theta - \theta')b_2 \\ a_1, & a_2 \end{vmatrix}^2 \\ &= 5\Delta^2 < 8. \end{aligned} \tag{2}$$

It follows from (1) and (2) and Markoff's theory of the minimum of an indefinite binary quadratic form (Dickson 1930, theorem 62) that $\Delta \geqslant 1$, and that the quadratic form can be transformed by an integral unimodular transformation into the form

$$\Delta(u - \theta v)(u - \theta' v).$$

So, if the points (a_1, b_1) and (a_2, b_2) generating the lattice are chosen suitably, either

$$\left.\begin{aligned} (a_1 - \theta b_1)u + (a_2 - \theta b_2)v &\equiv \mu(u - \theta v) \\ (a_1 - \theta' b_1)u + (a_2 - \theta' b_2)v &\equiv \nu(u - \theta' v) \end{aligned}\right\}, \quad \text{where} \quad |\mu\nu| = \Delta \geqslant 1,$$

or

$$\left.\begin{aligned} (a_1 - \theta b_1)u + (a_2 - \theta b_2)v &\equiv \mu'(u - \theta' v) \\ (a_1 - \theta' b_1)u + (a_2 - \theta' b_2)v &\equiv \nu'(u - \theta v) \end{aligned}\right\}, \quad \text{where} \quad |\mu'\nu'| = \Delta \geqslant 1.$$

In the first case write

$$\alpha_1 = a_1, \quad \beta_1 = b_1, \quad \alpha_2 = -a_2, \quad \beta_2 = -b_2,$$

and in the second case write $\mu' = \theta\mu, \quad \nu' = \theta'\nu,$

and $$\alpha_1 = a_2, \quad \beta_1 = b_2, \quad \alpha_2 = a_1, \quad \beta_2 = b_1.$$

Then either

$$\left.\begin{aligned} (\alpha_1 - \theta\beta_1)u - (\alpha_2 - \theta\beta_2)v &\equiv \mu(u - \theta v) \\ (\alpha_1 - \theta'\beta_1)u - (\alpha_2 - \theta'\beta_2)v &\equiv \nu(u - \theta' v) \end{aligned}\right\}, \quad \text{where} \quad |\mu\nu| = \Delta \geqslant 1,$$

or

$$\left.\begin{aligned} (\alpha_2 - \theta\beta_2)u + (\alpha_1 - \theta\beta_1)v &\equiv \mu(\theta u + v) \\ (\alpha_2 - \theta'\beta_2)u + (\alpha_1 - \theta'\beta_1)v &\equiv \nu(\theta' u + v) \end{aligned}\right\}, \quad \text{where} \quad |\mu\nu| = \Delta \geqslant 1.$$

In either case Λ is generated by the points with co-ordinates (α_1, β_1) and (α_2, β_2), where

$$\alpha_1 - \theta\beta_1 = \mu, \quad \alpha_1 - \theta'\beta_1 = \nu,$$

$$\alpha_2 - \theta\beta_2 = \theta\mu, \quad \alpha_2 - \theta'\beta_2 = \theta'\nu,$$

and $$|\mu\nu| = \Delta \geqslant 1.$$

By a similar consideration of the quadratic form

$$\{(ub_1+vb_2)-\theta(ua_1+va_2)\}\{(ub_1+vb_2)-\theta'(ua_1+va_2)\}$$

we can prove that Λ is also generated by the points with co-ordinates (γ_1, δ_1) and (γ_2, δ_2), where

$$\delta_1-\theta\gamma_1 = \rho, \quad \delta_1-\theta'\gamma_1 = \sigma,$$
$$\delta_2-\theta\gamma_2 = \theta\rho, \quad \delta_2-\theta'\gamma_2 = \theta'\sigma,$$

and
$$|\rho\sigma| = \Delta.$$

Consider now the rectangle defined by

$$|x| < \sqrt{(1\cdot 6)}, \quad |y| < 1, \tag{3}$$

of area
$$4\sqrt{(1\cdot 6)} > 4\Delta.$$

This rectangle must contain, besides O, another point of Λ; the point with co-ordinates (ξ, η), say. We may suppose that

$$\xi = u\alpha_1+v\alpha_2 = w\gamma_1+t\gamma_2,$$
$$\eta = u\beta_1+v\beta_2 = w\delta_1+t\delta_2,$$

where u, v, w and t are integers. Then

$$\begin{aligned}|\xi^2-\xi\eta-\eta^2| &= |(\xi-\theta\eta)(\xi-\theta'\eta)|\\ &= |\{(\alpha_1-\theta\beta_1)u+(\alpha_2-\theta\beta_2)v\}\{(\alpha_1-\theta'\beta_1)u+(\alpha_2-\theta'\beta_2)v\}|\\ &= |\mu\nu|.|(u+\theta v)(u+\theta' v)|\\ &= \Delta|u^2+uv-v^2|,\end{aligned}$$

and similarly
$$|\eta^2-\eta\xi-\xi^2| = \Delta|w^2+wt-t^2|.$$

But
$$-\tfrac54\eta^2 \leqslant (\xi-\tfrac12\eta)^2-\tfrac54\eta^2 = \xi^2-\xi\eta-\eta^2 = \tfrac54\xi^2-(\eta+\tfrac12\xi)^2 \leqslant \tfrac54\xi^2,$$

so that, as the point (ξ, η) is in the rectangle (3) but is not inside S,

$$1 \leqslant |\xi^2-\xi\eta-\eta^2| < \tfrac54\cdot\tfrac85 = 2.$$

Since $\Delta \geqslant 1$ this implies
$$0 < |u^2+uv-v^2| < 2.$$

Similarly
$$0 < |w^2+wt-t^2| < 2.$$

As u, v, w and t are integers, we must have

$$|u^2+uv-v^2| = |w^2+wt-t^2| = 1,$$

so that
$$|\xi^2-\xi\eta-\eta^2| = |\eta^2-\eta\xi-\xi^2| = \Delta.$$

This implies that either $\xi\eta = 0$ and $|\xi^2-\eta^2| = \Delta$,

or $\xi^2-\eta^2 = 0$ and $|\xi\eta| = \Delta$.

As $\Delta \geqslant 1$ and $|\eta| < 1$ the conclusion is that

$$\eta = 0 \quad \text{and} \quad |\xi| = \sqrt{\Delta}.$$

Thus the point with co-ordinates $(\sqrt{\Delta}, 0)$ is a point of Λ. A similar consideration of the points of Λ in the rectangle defined by

$$|x| < 1, \quad |y| < \sqrt{(1\cdot 6)},$$

shows that the point with co-ordinates $(0, \sqrt{\Delta})$ is a point of Λ. So all points of the lattice of points, whose co-ordinates are integral multiples of $\sqrt{\Delta}$, are points of the lattice Λ. Since these two lattices have the same determinant Δ they must be identical. This proves (*b*) and also shows that every lattice which is admissible for S has a determinant greater than or equal to 1.

Now to prove (*a*) we have only to prove that the lattice of points with integral co-ordinates is admissible for S. But this is obvious, as, if x and y are integers, (x^2-xy-y^2) and (y^2-yx-x^2) are integers and neither is numerically less than 1, unless $x = y = 0$.

Corollary I. *For all* λ, *satisfying* $1 < \lambda < \sqrt{(1\cdot 6)}$, *and all positive* $\theta < 1$, *let* S_θ *be the star body obtained by adding to* S *the points outside* S *in the rectangle given by*

$$|x| \leqslant \sqrt{\lambda}, \quad |y| \leqslant \theta. \tag{4}$$

Then the unique critical lattice of S_θ *is the lattice of points whose co-ordinates are integral multiples of* $\sqrt{\lambda}$. *Further the only points of this lattice in the interior of the body* $\sqrt{\lambda} \,.\, S_\theta$ *are the points with co-ordinates*

$$(-\sqrt{\lambda}, 0), \quad (0,0) \quad \text{and} \quad (\sqrt{\lambda}, 0).$$

Proof. The only points with integral co-ordinates, which are in the interior of S_θ are the points with co-ordinates

$$(-1, 0), \quad (0,0) \quad \text{and} \quad (1,0).$$

Thus the lattice of points, whose co-ordinates are integral multiples of $\sqrt{\lambda}$, is admissible for S_θ and the only points of this lattice which are in the interior of $\sqrt{\lambda} \,.\, S_\theta$ are the points with co-ordinates

$$(-\sqrt{\lambda}, 0), \quad (0,0) \quad \text{and} \quad (\sqrt{\lambda}, 0).$$

We have only to prove that this lattice with determinant λ is the unique critical lattice of S_θ. If Λ is any lattice with determinant $\Delta \leqslant \lambda$, which is admissible for S_θ, then Λ is admissible for S. Consequently Λ is generated by the points with the co-ordinates

$$(\sqrt{\Delta}, 0) \quad \text{and} \quad (0, \sqrt{\Delta}).$$

As the first of these points is not in the interior of the rectangle (4), we must have $\Delta \geqslant \lambda$. Thus $\Delta = \lambda$ and Λ is the lattice of points whose co-ordinates are integral multiples of $\sqrt{\lambda}$. This completes the proof of the corollary.

Corollary II. *The star bodies* S *and* S_θ *of theorem* 1 *and corollary* I *satisfy the conditions* (*a*), (*b*) *and* (*c*) *of theorem* 4.

3. To prove the results in the n-dimensional case we need three lemmas.

LEMMA 1. *Suppose K is a closed convex n-dimensional body symmetrical about the origin and with volume $V(K)$. Let $|X|$ denote the least value of λ for which the point X is in the body λK. Suppose Λ is any lattice of determinant Δ. Then Λ can be generated by points $P_1, P_2, \ldots, P_n$ such that*

$$|P_1|.|P_2|.\ldots.|P_n|V(K) \leqslant k_n \Delta,$$

where k_n is a constant independent of K and Λ. Further P_1 can be taken to be any point of Λ for which the function $|X|$ assumes its minimum positive value.

This result is proved by Mahler (1938, theorem 1), and also by Weyl (1942, theorem VI). In particular Weyl shows that the result is true when

$$k_n = 2(n!).$$

Neither of these authors state the last clause of the lemma explicitly; but its truth is obvious from their proofs.

LEMMA 2. *Let $A_1, A_2, \ldots, A_n$ be points, generating a lattice of determinant Δ, in the sphere given by*

$$x_1^2 + x_2^2 + \ldots + x_n^2 < R^2. \tag{5}$$

Suppose A_n is in the cone C given by

$$x_1^2 + x_2^2 + \ldots + x_{n-1}^2 \leqslant \left(\frac{\Delta}{2R^n}\right)^2 x_n^2.$$

Then no point, other than O, of the $(n-1)$-dimensional space α defined by $O, A_1, A_2, \ldots, A_{n-1}$ is in the cone C.

Proof. As the points $A_1, A_2, \ldots, A_{n-1}$ are in the sphere given by (5), the determinant Δ' of the lattice in α generated by these points satisfies

$$\Delta' < R^{n-1}.$$

So, if d is the perpendicular distance from A_n to α,

$$d\Delta' = \Delta$$

and

$$d > \Delta / R^{n-1}.$$

Suppose A_n has co-ordinates $(a_1, a_2, \ldots, a_n)$ and let B be the point with co-ordinates $(0, 0, \ldots, 0, a_n)$. Then the square of the distance between A_n and B is

$$a_1^2 + a_2^2 + \ldots + a_{n-1}^2 \leqslant \left(\frac{\Delta}{2R^n}\right)^2 a_n^2 < \left(\frac{\Delta}{2R^{n-1}}\right)^2,$$

as A_n is in the cone C and the sphere given by (5). So the perpendicular distance from B to α is greater than

$$d - \frac{\Delta}{2R^{n-1}} \geqslant \frac{\Delta}{2R^{n-1}}. \tag{6}$$

Let the point X with co-ordinates $(x_1, x_2, \ldots, x_n)$ be any point other than O of the space α. If $x_n = 0$ then clearly X is not in the cone C. If $x_n \neq 0$ then the point X' with co-ordinates

$$\left(\frac{x_1}{x_n} a_n, \frac{x_2}{x_n} a_n, \ldots, a_n\right)$$

is also in α, and so the distance

$$\left\{\left(\frac{x_1}{x_n} a_n\right)^2 + \left(\frac{x_2}{x_n} a_n\right)^2 + \ldots + \left(\frac{x_{n-1}}{x_n} a_n\right)^2\right\}^{\frac{1}{2}}$$

from B to X' is greater than or equal to the perpendicular distance from B to α. Thus, using (6) and the fact that A_n is in the sphere given by (5),

$$x_1^2 + x_2^2 + \ldots + x_{n-1}^2 > \left(\frac{\Delta}{2R^{n-1}}\right)^2 \frac{x_n^2}{a_n^2} > \left(\frac{\Delta}{2R^n}\right)^2 x_n^2,$$

and so X is not in the cone C.

Lemma 3. *Suppose, for some* λ *satisfying* $1 < \lambda < \sqrt{(1 \cdot 6)}$ *and for some positive integer* n, *there exists a star body* S *which satisfies the conditions* (*a*) *and* (*b*) *of theorem* 2. *Then there exists a star body* S, *which satisfies these conditions, and which also satisfies*

(*c*) *The critical lattice of* S *is the lattice of points with integral co-ordinates.*

(*d*) *The set* S *contains the cube defined by*

$$|x_1| \leq 1, \; |x_2| \leq 1, \; \ldots, \; |x_n| \leq 1. \tag{7}$$

Proof. If there is a star body S satisfying the conditions (*a*) and (*b*) of theorem 2 then there is a linear transformation which transforms the critical lattice of S into the lattice of points with integral co-ordinates. The star body obtained from S by use of this transformation satisfies the conditions (*a*), (*b*) and (*c*). If S is any star body satisfying the conditions (*a*), (*b*) and (*c*), then the star body obtained from S by adding to it the points of the cube given by (7), satisfies the conditions (*a*), (*b*), (*c*) and (*d*).

4. Proof of theorem 2. The theorem is trivial when $n = 1$. We have proved the theorem when $n = 2$. We assume that the theorem is true when $n = r \geq 2$ and prove that it is true when $n = r + 1$. The result will then follow by induction.

We may suppose that S_r is an r-dimensional star body, symmetrical about O, which satisfies the conditions obtained from (*a*) and (*b*) by replacing λ by $\frac{1}{2}(\lambda + \sqrt{(1 \cdot 6)})$. By lemma 3 we may suppose that S_r satisfies the conditions obtained from (*c*) and (*d*) by replacing n by r. Further we may suppose that S_r is the set of points given by

$$F(x_1, x_2, \ldots, x_r) \leq 1,$$

for some continuous non-negative function $F(x_1, x_2, \ldots, x_r)$ with the property that

$$F(tx_1, tx_2, \ldots, tx_r) = |t| \, F(x_1, x_2, \ldots, x_r)$$

for all real numbers t.

Let T be the $(r+1)$-dimensional set of all points for which both

(*a*) $F(x_1, x_2, \ldots, x_r) \leqslant 1$ and

(*b*) $x_1^2 + x_2^2 + \ldots + x_r^2 - \epsilon^2 x_{r+1}^2 \geqslant -\epsilon^2$,

where $\epsilon = \epsilon(\lambda, r)$ is a sufficiently small positive number. Then, as S_r satisfies the conditions (*c*) and (*d*) of lemma 3, with n replaced by r, the star body T contains the cube given by

$$|x_1| \leqslant 1, \ |x_2| \leqslant 1, \ \ldots, \ |x_{r+1}| \leqslant 1,$$

but does not contain in its interior any point with integral co-ordinates, apart from the origin O. Let T' be the $(r+1)$-dimensional set of all points for which both

(*a*) $F(x_1, x_2, \ldots, x_r) \leqslant 1$, and

(*b*) either $|x_{r+1}| \leqslant 1$ or $x_1^2 + x_2^2 + \ldots + x_r^2 \geqslant \epsilon^2 x_{r+1}^2$.

Clearly every point of T' is in T. We prove that if Λ is any lattice, admissible for T' (and a fortiori if Λ is admissible for T), with determinant $\Delta < \lambda$, then Λ can be generated by a set of points with co-ordinates of the form

$$\begin{array}{l} (\mu, 0, 0, \ldots, 0, d_1), \\ (0, \mu, 0, \ldots, 0, d_2), \\ \ldots\ldots\ldots\ldots\ldots\ldots\ldots \\ (0, 0, 0, \ldots, \mu, d_r), \\ (0, 0, 0, \ldots, 0, \nu\ ), \end{array}$$

where

$$1 \leqslant \mu < \sqrt{(1{\cdot}6)}, \ 1 \leqslant \nu < \sqrt{(1{\cdot}6)}, \ \mu^r \nu = \Delta \quad \text{and} \quad |d_s| \leqslant \tfrac{1}{2}\nu, \quad \text{for} \quad s = 1, 2, \ldots, r.$$

In the first place T' contains all the points of the rectangular parallelepiped

$$|x_1| \leqslant 1, \ |x_2| \leqslant 1, \ \ldots, \ |x_r| \leqslant 1, \ |x_{r+1}| \leqslant \lambda,$$

except the points for which

$$1 < |x_{r+1}| \leqslant \lambda, \quad \text{and} \quad x_1^2 + x_2^2 + \ldots + x_r^2 < \epsilon^2 x_{r+1}^2.$$

The volume of the parallelepiped is

$$2^{r+1}\lambda > 2^{r+1}\Delta,$$

so there is a point A_{r+1}, with co-ordinates $(a_{r+1,1}, a_{r+1,2}, \ldots, a_{r+1,r+1})$, say, of Λ inside this parallelepiped and different from the origin O. As Λ is admissible for T', we must have

$$1 \leqslant |a_{r+1,r+1}| < \lambda \quad \text{and} \quad a_{r+1,1}^2 + a_{r+1,2}^2 + \ldots + a_{r+1,r}^2 \leqslant \epsilon^2 a_{r+1,r+1}^2. \tag{8}$$

We may clearly choose A_{r+1} so that

$$1 \leqslant a_{r+1,r+1} < \lambda$$

and also so that there is no point of Λ, other than O, inside the rectangular parallelepiped K given by

$$|x_1| \leqslant 1, \ |x_2| \leqslant 1, \ \ldots, \ |x_r| \leqslant 1, \ |x_{r+1}| \leqslant a_{r+1,r+1}.$$

Applying lemma 1 to this convex body K, it follows that Λ is generated by points $A_{r+1}, A_1, A_2, \ldots, A_r$ such that

$$|A_{r+1}|\cdot|A_1|\cdot|A_2|\cdot\ldots\cdot|A_r|\, 2^{r+1}a_{r+1,r+1} \leqslant k_{r+1}\Delta.$$

Here
$$|X| = \max\left(|x_1|, |x_2|, \ldots, |x_r|, \frac{|x_{r+1}|}{a_{r+1,r+1}}\right).$$

Since $|A_s| \geqslant 1$ for $s = 1, 2, \ldots, r+1$ and $a_{r+1,r+1} \geqslant 1$, we have

$$1 \leqslant |A_s| \leqslant 2^{-r-1}\sqrt{(1\cdot 6)}\,.\,k_{r+1}, \quad \text{for} \quad s = 1, 2, \ldots, r+1.$$

If the co-ordinates of A_s are $(a_{s,1}, a_{s,2}, \ldots, a_{s,r+1})$ then this implies that

$$\begin{aligned}|a_{s,t}| &\leqslant 2^{-r-1}\sqrt{(1\cdot 6)}\,.\,k_{r+1}\,a_{r+1,r+1}\\ &\leqslant 2^{-r-1}(1\cdot 6)\,k_{r+1}, \quad \text{for} \quad s, t = 1, 2, \ldots, r+1. \qquad (9)\end{aligned}$$

The determinant Δ of Λ is the absolute value of the determinant

$$\begin{vmatrix} a_{1,1}, & a_{1,2}, & \ldots, & a_{1,r+1}\\ a_{2,1}, & a_{2,2}, & \ldots, & a_{2,r+1}\\ \multicolumn{4}{c}{\cdots\cdots\cdots\cdots\cdots\cdots}\\ a_{r+1,1}, & a_{r+1,2}, & \ldots, & a_{r+1,r+1}\end{vmatrix}.$$

Let Δ' denote the absolute value of the determinant

$$\begin{vmatrix} a_{1,1}, & a_{1,2}, & \ldots, & a_{1,r}\\ a_{2,1}, & a_{2,2}, & \ldots, & a_{2,r}\\ \multicolumn{4}{c}{\cdots\cdots\cdots\cdots\cdots\cdots}\\ a_{r,1}, & a_{r,2}, & \ldots, & a_{r,r}\end{vmatrix}.$$

Then using (8) and (9), either for the plus sign or for the minus sign

$$\begin{aligned}&|\Delta \pm a_{r+1,r+1}\Delta'|\\ &\quad\leqslant r!\,\{2^{-r}k_{r+1}\}^r\{|a_{r+1,1}| + |a_{r+1,2}| + \ldots + |a_{r+1,r}|\}\\ &\quad\leqslant r!\,\{2^{-r}k_{r+1}\}^r(\sqrt{r})\,\epsilon a_{r+1,r+1}\\ &\quad< \lambda(r!)\,(\sqrt{r})\,\{2^{-r}k_{r+1}\}^r\,\epsilon.\end{aligned}$$

So, provided $\quad \epsilon < [\lambda(r!)\,(\sqrt{r})\,\{2^{-r}k_{r+1}\}^r]^{-1}\,.\,\tfrac{1}{2}(\sqrt{(1\cdot 6)} - \lambda),$

we have, in either case, $\quad |\Delta - a_{r+1,r+1}\Delta'| < \tfrac{1}{2}(\sqrt{(1\cdot 6)} - \lambda),$

and, as $a_{r+1,r+1} \geqslant 1$, $\quad \Delta' < \Delta + \tfrac{1}{2}(\sqrt{(1\cdot 6)} - \lambda) < \tfrac{1}{2}(\lambda + \sqrt{(1\cdot 6)}). \qquad (10)$

Now, by (9), the points $A_1, A_2, \ldots, A_{r+1}$ are in the $(r+1)$-dimensional sphere with centre O and radius

$$R = 2^{-r-1}(1\cdot 6)\,k_{r+1}\sqrt{(r+1)}. \qquad (11)$$

Also, by (8), provided
$$\epsilon < \tfrac{1}{2}\Delta R^{-r-1}, \tag{12}$$
the point A_{r+1} is in the cone given by
$$x_1^2 + x_2^2 + \ldots + x_r^2 < (\tfrac{1}{2}\Delta R^{-r-1})^2 x_{r+1}^2. \tag{13}$$
So, by lemma 2, no point, other than O, of the r-dimensional space α defined by $O, A_1, A_2, \ldots, A_r$ is in the cone defined by (13). By (12), no point of α other than O lies in the cone given by
$$x_1^2 + x_2^2 + \ldots + x_r^2 < \epsilon^2 x_{r+1}^2.$$

Since no point other than O of the r-dimensional lattice generated in α by the points $A_1, A_2, \ldots, A_r$ lies inside T', this implies that for all points, other than O, of this lattice, we have
$$F(x_1, x_2, \ldots, x_r) \geqslant 1.$$
Consider the r-dimensional lattice generated by the points with co-ordinates
$$(a_{s,1}, a_{s,2}, \ldots, a_{s,r}), \quad s = 1, 2, \ldots, r.$$
This lattice has a determinant Δ' satisfying (10), and none of its points, apart from O, lie inside the star body S_r. As S_r satisfies condition (*b*) of theorem 2 with $\frac{1}{2}(\lambda + \sqrt{(1\cdot 6)})$ in place of λ and also satisfies condition (*c*) of lemma 3, this r-dimensional lattice can be obtained from the r-dimensional lattice of points with integral co-ordinates by a magnification. Thus the lattice of points of Λ in α is generated by points $B_1, B_2, \ldots, B_r$ with co-ordinates of the form
$$\begin{gathered}(\mu, 0, 0, \ldots, 0, b_1),\\ (0, \mu, 0, \ldots, 0, b_2),\\ \cdots\cdots\cdots\cdots\cdots\cdots\\ (0, 0, 0, \ldots, \mu, b_r),\end{gathered}$$
where $1 \leqslant \mu$ and $\mu^r = \Delta'$. As $\Delta' < \sqrt{(1\cdot 6)}$, clearly $\mu < \sqrt{(1\cdot 6)}$.

Now as the points $B_1, B_2, \ldots, B_r$ are in α, they are not in the cone given by (13). Consequently,
$$\mu^2 \geqslant (\tfrac{1}{2}\Delta R^{-r-1})^2 b_s^2,$$
and
$$|b_s| < 4\Delta^{-1}R^{r+1}, \quad \text{for } s = 1, 2, \ldots, r.$$
Since T' contains the cube given by
$$|x_1| \leqslant 1, \ |x_2| \leqslant 1, \ \ldots, \ |x_{r+1}| \leqslant 1,$$
and Λ is admissible for T', we have $\Delta \geqslant 1$. Thus
$$|b_s| < 4R^{r+1}, \quad \text{for } s = 1, 2, \ldots, r.$$
This implies that the points $B_1, B_2, \ldots, B_r$ all lie inside the sphere with radius
$$2 + 4R^{r+1},$$
and further the point $B_1 + A_{r+1}$ lies in the sphere with radius
$$R_1 = \sqrt{(r+2)} + 2 + 4R^{r+1}.$$

Consider the points $B_1 + A_{r+1}, B_2, B_3, \ldots, B_r, A_{r+1}$. These points generate the lattice Λ with determinant Δ, and lie in the sphere with centre O and radius R_1.

So, as above, it follows by use of lemma 2, that if ϵ is sufficiently small, no point, other than O, of the r-dimensional space β defined by O, B_1+A_{r+1}, B_2, B_3, ..., B_r lies in or on the cone

$$x_1^2+x_2^2+\ldots+x_r^2 \leqslant \epsilon^2 x_{r+1}^2.$$

Also, as above, provided ϵ is sufficiently small, the determinant Δ'' of the lattice generated by the projections of the points B_1+A_{r+1}, B_2, B_3, ..., B_r upon the space $x_{r+1}=0$, satisfies

$$\Delta'' < \tfrac{1}{2}(\lambda+\sqrt{(1\cdot 6)}).$$

As before it follows that, provided ϵ is sufficiently small, the lattice of points of Λ in β is generated by points $C_1, C_2, \ldots, C_r$ with co-ordinates of the form

$$\begin{array}{c}(\nu, 0, 0, \ldots, 0, c_1),\\(0, \nu, 0, \ldots, 0, c_2),\\\cdots\cdots\cdots\cdots\cdots\cdots\\(0, 0, 0, \ldots, \nu, c_r),\end{array}$$

where $1 \leqslant \nu < \sqrt{(1\cdot 6)}$ and $\nu^r = \Delta''$.

Consider the point $B_1+A_{r+1}-C_1$ with co-ordinates

$$(a_{r+1,1}+\mu-\nu, a_{r+1,2}, \ldots, a_{r+1,r}, a_{r+1,r+1}+b_1-c_1).$$

This is a point of Λ in β. As

$$1 \leqslant \mu < \sqrt{(1\cdot 6)}, \quad 1 \leqslant \nu < \sqrt{(1\cdot 6)}$$

and the co-ordinates of A_{r+1} satisfy (8), provided ϵ is sufficiently small, the co-ordinates of $B_1+A_{r+1}-C_1$ satisfy

$$|x_1|<1, \; |x_2|<1, \; \ldots, \; |x_r|<1. \tag{14}$$

But as the point is in β its co-ordinates satisfy

$$x_1^2+x_2^2+\ldots+x_r^2 \geqslant \epsilon^2 x_{r+1}^2. \tag{15}$$

Now all points satisfying (14) and (15) lie in T', as S_r contains the r-dimensional cube given by (14). Consequently the point $B_1+A_{r+1}-C_1$ of Λ must coincide with O, and

$$a_{r+1,1}+\mu-\nu = a_{r+1,2} = \ldots = a_{r+1,r} = 0.$$

As $r \geqslant 2$ we have $$a_{r+1,2} = a_{r+1,3} = \ldots = a_{r+1,r} = 0.$$

Similarly $$a_{r+1,1} = 0.$$

Thus Λ is generated by a set of points with co-ordinates of the form

$$\left.\begin{array}{c}(\mu, 0, 0, \ldots, 0, d_1),\\(0, \mu, 0, \ldots, 0, d_2),\\\cdots\cdots\cdots\cdots\cdots\cdots\\(0, 0, 0, \ldots, \mu, d_r),\\(0, 0, 0, \ldots, 0, \nu),\end{array}\right\} \tag{16}$$

where $$1 \leqslant \mu < \sqrt{(1\cdot 6)}, \quad 1 \leqslant \nu < \sqrt{(1\cdot 6)} \quad \text{and} \quad \mu^r \nu = \Delta.$$

By adding or subtracting some multiple of the last point from each of the first r points we can always arrange that

$$|d_s| \leqslant \tfrac{1}{2}\nu < \sqrt{(0\cdot 4)}, \quad \text{for} \quad s = 1, 2, \ldots, r. \tag{17}$$

Let T^* be the $(r+1)$-dimensional set of all points X for which both

(*a*) $F(x_{r+1}, x_1, x_2, \ldots, x_{r-1}) \leqslant 1$, and

(*b*) $x_{r+1}^2 + x_1^2 + x_2^2 + \ldots + x_{r-1}^2 - \epsilon^2 x_r^2 \geqslant -\epsilon^2$,

where ϵ is the number used in the definition of T. Let S_{r+1} be the set of all points which belong to either T or T^*. Then S_{r+1} is a star body and the set of points with integral co-ordinates is admissible for S_{r+1}.

Suppose Λ is any lattice with determinant $\Delta < \lambda$, which is admissible for S_{r+1}. Then, provided $\epsilon = \epsilon(\lambda, r)$ has been chosen to be a sufficiently small positive number, as Λ is admissible for T it is generated by points $D_1, D_2, \ldots, D_{r+1}$ with co-ordinates of the form (16), where $1 \leqslant \mu < \sqrt{(1\cdot 6)}$, $1 \leqslant \nu < \sqrt{(1\cdot 6)}$, $\mu^r \nu = \Delta$ and $d_1, d_2, \ldots, d_r$ satisfy (17). Similarly as Λ is admissible for T^*, it is generated by points $E_1, E_2, \ldots, E_{r+1}$ with co-ordinates of the form

$$\begin{gathered}
(\rho, 0, 0, \ldots, e_1, 0), \\
(0, \rho, 0, \ldots, e_2, 0), \\
\cdots\cdots\cdots\cdots\cdots\cdots \\
(0, 0, 0, \ldots, \sigma, 0), \\
(0, 0, 0, \ldots, e_{r+1}, \rho),
\end{gathered}$$

where $$1 \leqslant \rho < \sqrt{(1\cdot 6)}, \quad 1 \leqslant \sigma < \sqrt{(1\cdot 6)}, \quad \rho^r \sigma = \Delta,$$

and $$|e_s| < \sqrt{(0\cdot 4)}, \quad \text{for} \quad s = 1, 2, \ldots, r-1, r+1.$$

But, for $s = 1, 2, \ldots, r+1$ the point $D_s - E_s$ lies in the cube given by

$$|x_1| < 1, \ |x_2| < 1, \ \ldots, \ |x_{r+1}| < 1,$$

and so coincides with the origin. Thus

$$d_1 = d_2 = \ldots = d_r = e_1 = e_2 = \ldots = e_{r-1} = e_{r+1} = 0,$$

and $$\mu = \rho, \quad \mu = \sigma \quad \text{and} \quad \nu = \rho.$$

Consequently Λ is generated by the points with co-ordinates

$$\begin{gathered}
(\mu, 0, 0, \ldots, 0), \\
(0, \mu, 0, \ldots, 0), \\
\cdots\cdots\cdots\cdots \\
(0, 0, 0, \ldots, \mu),
\end{gathered}$$

where $\mu^{r+1} = \Delta$, and so is the lattice of all points whose co-ordinates are integral multiples of $\Delta^{1/(r+1)}$. As the lattice of points with integral co-ordinates is admissible for S_{r+1}, and no lattice with a smaller determinant is admissible, this proves that the lattice of points with integral co-ordinates is the unique critical lattice of S_{r+1} and conditions (*a*) and (*b*) of the theorem are satisfied by S_{r+1}. The result now follows by induction.

5. PROOF OF THEOREM 3. Suppose λ is any number satisfying $1 < \lambda < \sqrt{(1 \cdot 6)}$ and θ is any positive number less than 1. Then there exists an n-dimensional star body S satisfying the conditions obtained from conditions (*a*) and (*b*) of theorem 2 by replacing λ by $\frac{1}{2}(\lambda + \sqrt{(1 \cdot 6)})$. By lemma 3 we may suppose that S satisfies also the conditions (*c*) and (*d*) of that lemma. Let S_θ be the star body obtained by adding to S the points outside S in the rectangular parallelepiped given by

$$|x_1| \leqslant \lambda^{1/n}, \ |x_2| \leqslant \theta, \ |x_3| \leqslant \theta, \ \ldots, \ |x_n| \leqslant \theta.$$

It follows, just as in the proof of corollary I to theorem 1 that S_θ satisfies the conditions of theorem 3.

6. If A and B are two star bodies we use $V(A, B)$ to denote the volume of the set of all points X which are in just one of the bodies A and B. It is easy to verify that for all star bodies A, B and C:

(*a*) $V(A,B) = V(B,A) \geqslant 0$, and $V(A,B) = 0$ if and only if $A = B$.

(*b*) $V(A,C) \leqslant V(A,B) + V(B,C)$.

So the function $V(A,B)$ defines a metric in the space $\mathscr{S}$ of all star bodies. The set $\mathscr{K}$ of all convex star bodies K forms a subspace of $\mathscr{S}$. It is not difficult to prove that the functional $\Delta(K)$ is, under this metric, continuous relative to $\mathscr{K}$ for all points K of $\mathscr{K}$. It is easy to show that $\Delta(S)$ is not continuous under this metric. For example take S to be the square

$$|x| \leqslant 1, \quad |y| \leqslant 1,$$

and S_θ to be the set of points such that

$$|x| \leqslant 1, \quad |y| \leqslant 1 \quad \text{and} \quad \theta x^2 - y^2 \leqslant \tfrac{1}{4}\theta.$$

Clearly

$$\lim_{\theta \to +0} V(S, S_\theta) = 0,$$

while

$$\lim_{\theta \to +0} \Delta(S_\theta) < \Delta(S).$$

I have found that, for the set of bounded star bodies it is still possible, but not easy, to prove a result of a one-sided character. If S is a bounded star body and S_θ is a star body, uniformly bounded for all positive θ, and such that

$$\lim_{\theta \to +0} V(S, S_\theta) = 0,$$

then it is possible to prove that

$$\lim_{\theta \to +0} \Delta(S_\theta) \leqslant \Delta(S).$$

It is clear that the star bodies S and S_0, defined in the proof of theorem 3, satisfy the conditions of theorem 4. This proves theorem 4, and shows that even this one-sided result is false for unbounded star bodies.

The results of this section should be compared with the results obtained by Mahler (1946) using a different definition of *limit* in the space $\mathscr{S}$.

REFERENCES

Dickson, L. E. 1930 *Studies in the theory of numbers*. Chicago.

Mahler, K. 1938 *Proc. Acad. Sci. Amst.* **41**, 634.

Mahler, K. 1946 *Proc. Roy. Soc.* A, **187**, 151; *Proc. Acad. Sci. Amst.* **49**, 331–343, 444–454, 524–532, 622–631.

Weyl, H. 1942 *Proc. Lond. Math. Soc.* (2), **47**, 268.

Extensive penetrating cosmic ray showers

BY D. BROADBENT AND L. JÁNOSSY

The Physical Laboratories, The University, Manchester

(*Communicated by P. M. S. Blackett, F.R.S.—Received* 19 *April* 1947)

Extensive penetrating cosmic-ray showers were recorded with an arrangement consisting of a penetrating shower set P and an extension E containing shielded and unshielded counters. The following results were obtained: (1) The effective density integral spectrum of the showers observed is given by $D(x) = Ax^{-0\cdot5}$, where x is the number of particles per m.^{2}. (2) The rate of shower coincidences decreases only slightly when the extension is moved from a distance of 0·5 m. to a distance of 9 m. from the main set P. (3) The ratio of the coincidences obtained with shielded and unshielded extension counters does not change noticeably with increasing separation between E and P. The results are based on approximately 10,000 hr. of recording.

1. INTRODUCTION

In a former paper (Broadbent & Jánossy 1947, referred to as I) it has been shown that penetrating showers are of two distinct types: (*a*) local penetrating showers, which probably consist of groups of mesons produced by fast nucleons, and (*b*) extensive penetrating showers, which are large air showers containing some penetrating particles.

It has been inferred by Cocconi, Loverdo & Tongiorgi (1942, 1943, 1946) that *all* extensive showers contain penetrating particles; the penetrating extensive showers under investigation will thus be assumed to be ordinary extensive showers, that is, large cascade showers containing some penetrating particles (see also Daudin 1942; and Clay 1943).

The present investigation deals with the production of penetrating particles in extensive air showers.

2. The experimental arrangement

The arrangement consisted of the penetrating shower set P, described in I, together with an extension shown in detail in figure 1. The extension consisted of two counter trays, an unshielded tray E of twelve counters in parallel of area 2500 cm.^{2}, and the tray S of area 1000 cm.^{2} covered on the top and sides by 15 cm. of lead and with 10 cm. of lead below. The tray S consisted of eight counters in two groups S_1 and S_2 of four counters each, alternate counters being in the same group as shown in figure 1 (see also figure 2).

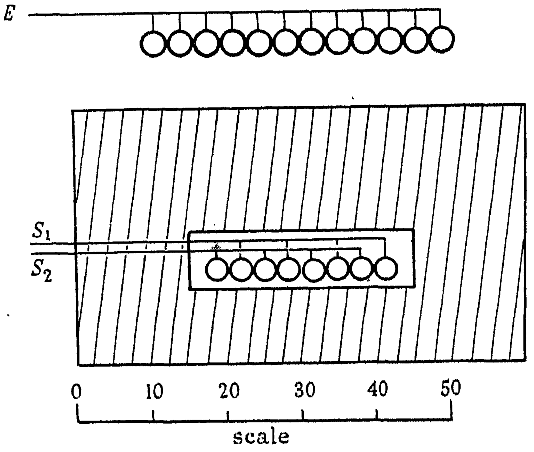

Figure 1. The extension.

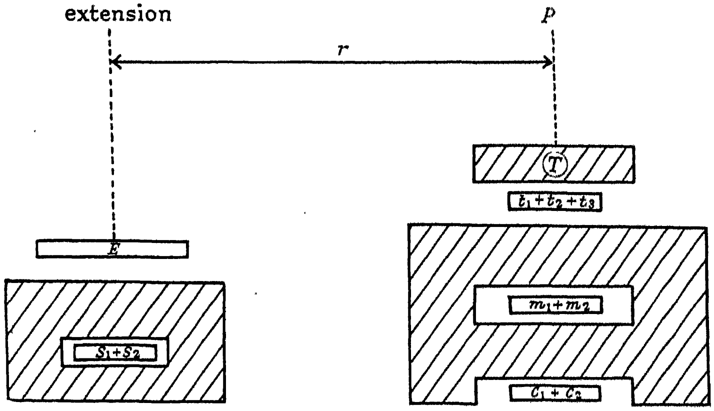

Figure 2. Scheme of the experimental lay-out.

Coincidences of the following types were recorded:

(1) Coincidences between P and at least one of the counters of the tray E; designated (P, E).

(2) Coincidences between P and at least one of the counters S; designated (P, S). The coincidences (P, S) were caused by extensive showers containing at least one penetrating particle at S.

(3) Coincidences between P and at least one counter in each of the trays S_1 and S_2, designated (P, S_1, S_2). The coincidences (P, S_1, S_2) were due to extensive showers containing at least two penetrating particles at P and at least two particles penetrating the extension.

During part of the experiment, an additional tray E' of eight counters in parallel covering an area of 1000 cm.^{2} was used and the coincidences (P, E') were recorded simultaneously with the coincidences (P, E).

Various absorbers T of lead and paraffin were placed close above the top tray of counters of the set P during some of the observations. The values of T are attached to the tables of results given below.

3. The experimental results

(a) *The density distribution of the showers*

The density distribution of penetrating showers was derived from counter observations, using a method somewhat similar to that used by Cocconi and also by Daudin (1942). In the present experiment the size F of a counter tray was varied and a record of the coincidences (P, F) as a function of the area F was taken.

In Cocconi's experiments the areas of *several* trays are changed *simultaneously* and the rate of coincidences is measured as a function of the simultaneous change of area of all trays.

In our experiments the area of the extension F is changed but P remains unchanged. Thus the interpretation of our results is different from the interpretation of the Cocconi type of experiment, and is as follows.

The set P introduces a certain bias towards the showers of higher densities, and therefore those showers capable of setting off P have a certain density spectrum $D(x)$ different from the *unbiased* density spectrum $C(x)$ of all showers. By varying only the area F of the extension the biased spectrum $D(x)$ is measured, while changing the areas of all trays of the set simultaneously would give the unbiased spectrum $C(x)$.

The actual bias introduced by the set P was found to differ according to the thickness and material of the absorber T.

In the actual experiment, instead of changing the area of one extension, the simultaneous coincidences with two extensions of areas E and E' were observed.

Thus we observed simultaneously: (1) coincidences (P, E); (2) coincidences (P, E'); (3) coincidences $(P, E+E')$. The last type of coincidences are effectively the coincidences between P and a tray $E+E'$, containing in parallel all the counters of the trays E and of E'. The three coincidence rates thus represented the variation of the coincidence rate as a function of the size of the extension.

The coincidence rates obtained with $T = 5$ cm. Pb and $T = 10$ cm. Pb and the average of the two rates are collected in table 1.

TABLE 1. COINCIDENCE RATE AS FUNCTION OF THE AREA F OF THE EXTENSION TRAY. $T = 5$ cm. Pb AND $T = 10$ cm. Pb

T/cm. Pb	time hr.	$F = 1000$ cm.^{2} (P, E')	$F = 2500$ cm.^{2} (P, E)	$F = 3500$ cm.^{2} $(P, E+E')$
5·0	280	26	46	51
	rate	$0{\cdot}093 \pm 0{\cdot}018$	$0{\cdot}164 \pm 0{\cdot}024$	$0{\cdot}182 \pm 0{\cdot}026$
10·0	308	17	27	33
	rate	$0{\cdot}055 \pm 0{\cdot}013$	$0{\cdot}088 \pm 0{\cdot}017$	$0{\cdot}107 \pm 0{\cdot}019$
average rate		$0{\cdot}073 \pm 0{\cdot}011$	$0{\cdot}124 \pm 0{\cdot}015$	$0{\cdot}143 \pm 0{\cdot}016$

Note that the rate of coincidences increases noticeably with increasing area of the extension tray. It must be emphasized that the three types of coincidences are recorded simultaneously, and that therefore the comparatively small difference between the rates obtained for different values of F are still statistically significant. The relative difference rates between the various extensions have the following numerical values.

TABLE 2

$\dfrac{(P,E)-P,E')}{(P,E)+(P,E')}$	$\dfrac{(P,E+E')-(P,E)}{(P,E+E')+(P,E)}$
$0{\cdot}259 \pm 0{\cdot}053$	$0{\cdot}070 \pm 0{\cdot}021$

Assuming that the coincidence rates vary as the γth power of the area F, the comparison of E and E' gives $\gamma = 0{\cdot}62 \pm 0{\cdot}12$. The comparison of E and $E+E'$ gives $\gamma = 0{\cdot}42 \pm 0{\cdot}13$. These two values for γ do not differ significantly (their difference is equal to the standard error of their difference). The average of the two γ-values is therefore significant, and the best value obtained comparing all three areas is thus

$$\gamma = 0{\cdot}56 \pm 0{\cdot}10, \tag{1}$$

assuming

$$(P, F) \propto F^{\gamma}. \tag{2}$$

The above equations refer to observations with thick lead absorbers (5 to 10 cm.)' of lead above P.

Independent evidence for the density spectrum of the showers was obtained by Miss B. Choudhuri. An unshielded cloud chamber was controlled by coincidences (P, E'), and it was found that the numbers of photographs containing n or more tracks was proportional to $n^{-0{\cdot}5}$, confirming equation (2).

(b) *Soft and penetrating particles*

(1) Observations have also been made with various separations r between the extension E and the main set P, and with no absorber T placed above the set P. The results are collected in table 3.

TABLE 3. RATES OF COINCIDENCES AS FUNCTION OF THE SEPARATION r BETWEEN P AND THE EXTENSION. $T = 0$

	$r = 0{\cdot}5$ m.		2·5 m.		9 m.	
coincidences	time	rate per hour	time	rate per hour	time	rate per hour
(P, E)	2934·7	$0{\cdot}109 \pm 0{\cdot}006$	1518·3	$0{\cdot}100 \pm 0{\cdot}008$	1405·7	$0{\cdot}075 \pm 0{\cdot}008$
(P, S)	—	—	3877·2	$0{\cdot}027 \pm 0{\cdot}003$	3178·7	$0{\cdot}015 \pm 0{\cdot}002$
(P, S_1, S_2)	—	—		$0{\cdot}013 \pm 0{\cdot}002$		$0{\cdot}005 \pm 0{\cdot}001$

Note from table 3 that the rates of coincidences (P, S) are much smaller than the rates (P, E). The difference between the two rates is partly due to the fact that the tray S is smaller than the tray E, but this cannot account completely for the difference and the comparatively small (P, S) rate must therefore be due to the lead absorber shielding the tray S.

Assuming that most of the shower particles are capable of penetrating the lead above the counters S, then one would expect the rates of coincidences to increase with the size of the extension tray not more than is given by equation (2). But

$$(E/S)^{\gamma} = 1{\cdot}6 \quad (\gamma = 0{\cdot}5),$$

when E and S are the areas of the respective trays, while

$$(P, E)/(P, S) = 4 \text{ (observed).}$$

Thus the coincidence rate is reduced more strongly than one would expect in terms of a mere change of area of the extension. It must be concluded therefore that the showers contain many soft particles which are incapable of discharging the shielded counters. The actual fraction of penetrating particles will be estimated in a subsequent paper where a detailed analysis of the present data will be given. It will be seen that this fraction is of the order $\frac{1}{50}$.

(2) On the suggestion of Dr Ferretti, we have carried out observations with lead and iron shields above the counters S. These experiments are analogous to experiments carried out by Cocconi & Festa.* Coincidences (P, S) with $T = 0$, $r = 9$ m. were observed, the counters S being shielded either with 16 cm. Pb or with 15 cm. Fe placed *above* 11 cm. Pb. The results of the observations are given in table 4.

TABLE 4

material over the counters S	rate of coincidences (P, S)
16 cm. Pb	$0{\cdot}013 \pm 0{\cdot}004$
15 cm. Fe + 11 cm. Pb	$0{\cdot}016 \pm 0{\cdot}003$
	difference $= 0{\cdot}003 \pm 0{\cdot}005$

---

* We are indebted to Professor Cocconi for communicating unpublished results.

The ratio Q of the two coincidence rates is thus

$$Q = (P, S)_{\mathrm{Fe}}/(P, S)_{\mathrm{Pb}} = 1{\cdot}23 \pm 0{\cdot}38. \tag{3}$$

The ratio is not significantly different from 1, so there is no indication of a variation of the coincidence rate with shielding material.

A similar result was obtained by Mura, Salvini & Tagliaferri (1947). Comparing their data referring to 20 cm. Pb and to 36 cm. Fe + 5 cm. Pb, the corresponding Q value is found to be

$$Q = 1{\cdot}37 \pm 0{\cdot}27.$$

The statistical significance of the results is greatly enhanced when they are taken together.

We discuss briefly the interpretation of the ratio Q.

(c) *Significance of the iron-lead ratio Q*

The physical significance of the ratio Q depends on the mechanism by which the penetrating particles are produced in air showers. There are two main possibilities which can be considered.

(i) It may be assumed that the penetrating particles are mainly produced in the air. In this case one is led to expect $Q = 1$; indeed, the number of penetrating particles with ranges exceeding 16 cm. of lead must be almost equal to the number of penetrating particles with ranges exceeding 15 cm. Fe + 11 cm. Pb.

Thus the observed value of Q is compatible with the assumption that the penetrating particles are produced in the air.

(ii) Alternatively, it may be assumed that the penetrating particles are produced in the absorber covering the counters S. In this case the material of the absorber might be of importance. Denote by $\Phi_p(Z)$ the cross-section for production of the penetrating particles and by $\Phi_A(Z)$ the cross-section for the absorption of the primaries of the penetrating particles by other processes. The probability of a penetrating particle being produced by a suitable primary is thus proportional to $\alpha(Z) = \Phi_p(Z)/\Phi_A(Z)$. Assuming that the primaries producing the penetrating particles are electrons, we may put

$$\Phi_A \propto (Z^2/A)\log(183Z^{-\frac{1}{3}}) \text{ per nucleon}$$

and thus

$$\Phi_A(\mathrm{Pb})/\Phi_A(\mathrm{Fe}) = 2{\cdot}5.$$

Assuming further $\alpha(\mathrm{Fe})/\alpha(\mathrm{Pb}) = Q$, we find with help of the observed value of Q

$$\frac{\Phi_p(\mathrm{Fe})}{\Phi_p(\mathrm{Pb})} = 0{\cdot}49 \pm 0{\cdot}15.$$

Thus, if we reject fluctuations exceeding three times the standard error as improbable, we conclude

$$\Phi_p(\mathrm{Pb}) > \Phi_p(\mathrm{Fe}).$$

This is very strongly supported by the results of the Italian school, as their results are statistically independent and have about the same weight as our own.

Thus, assuming that the penetrating particles are produced in the local absorbers by electrons or photons, the cross-section $\Phi_p(Z)$ for production must increase with Z. The observations would be in agreement with the assumption of a cross-section $\Phi_p(Z)$ proportional to Z^2/A.

The possibility of the penetrating particles being produced, not by electrons, but by nucleons present in the shower, will be discussed in detail in a subsequent paper.

(*d*) *The lateral spread of shower particles*

It is seen from table 3 that the rate of coincidences (P, E) decreases only slightly as the distance between P and E is increased from 0·5 to 9 m. The rate of coincidences (P, S), which is due to showers containing penetrating particles at the extension, was only observed from 2·5 to 9 m., but the ratio between soft and penetrating particles does not change greatly between these separations as can be inferred from the values of the ratio $(P, S)/(P, E)$ for the two separations obtained from table 3. Table 5 shows the values of this ratio.

TABLE 5

	$r = 2{\cdot}5$ m.	9 m.
$(P, S)/(P, E)$	$0{\cdot}27 \pm 0{\cdot}03$	$0{\cdot}20 \pm 0{\cdot}03$

These results are compatible with the assumption that the density of the penetrating particles is proportional to the density of the soft particles throughout the shower, although a slow change of this ratio throughout the shower is not excluded.

A detailed discussion of the physical significance of the above results will be given in a subsequent publication.

We are greatly indebted to Miss B. Choudhuri for communicating unpublished results. We are also indebted to Dr B. Ferretti for valuable discussion.

REFERENCES

Broadbent, D. & Jánossy, L. 1947 *Proc. Roy. Soc.* A, **190**, 497.
Clay, J. 1942 *Physica*, **9**, 897.
Cocconi, G., Loverdo, A. & Tongiorgi, V. 1943 *Nuovo Cim.* **1**, 314.
Cocconi, G., Loverdo, A. & Tongiorgi, V. 1946 *Phys. Rev.* **70**, 841, 846, 852.
Daudin, J. 1942 Thesis, University of Paris.
Mura, A., Salvini, G. & Tagliaferri, G. 1947 *Nature*, **159**, 368.

An investigation, by the method of characteristics, of the lateral expansion of the gases behind a detonating slab of explosive*

BY R. HILL AND D. C. PACK

Branch for Theoretical Research, Armament Research Department, Ministry of Supply

(*Communicated by W. G. Penney, F.R.S.—Received* 28 *April* 1947)

The phenomena occurring when an uncased explosive charge is detonated in a fluid medium are examined by hydrodynamical methods.

Attention is focused chiefly on the pressure and velocity distributions in the gaseous products of the explosion, which expand laterally behind the detonation wave as it travels down the charge, the results being shown in graphical form. To simplify the problem, the charge, and the gas and fluid fields, were treated as two-dimensional.

The hydrodynamical equations were solved numerically using the method of characteristics. This dates back to Monge, but it is only recently that it has been applied to the numerical solution of hyperbolic equations. The methods of numerical integration used in this paper are similar to those developed early in the war by the Research Section of the External Ballistics Department, Ordnance Board, for determining the velocity distributions around projectiles moving at supersonic speeds.

The nature of the boundary conditions made it necessary to find explicit theoretical formulae for the gas field near the charge, and the analysis involved is given at length.

For the problem in which the surrounding medium is air, the shape and position of the shock waves set up by the explosion are calculated. The shock waves are found to be straight to the nominal accuracy of the calculations (1 in 5000) for six charge widths from their intersections with the block of explosive.

1. INTRODUCTION

When a block of explosive is detonated, the gaseous products expand laterally behind the detonation wave. At the wave front their velocity relative to the wave is taken equal to the local velocity of sound, in accordance with the Chapman-Jouguet condition; but elsewhere in the gas field this relative flow is supersonic, and the expansion is so rapid that the pressure along the axis of the charge falls to one-tenth of its value at the face, in a distance comparable with the thickness of the charge. The velocity of detonation, being far greater than the sonic velocity in the outer medium, causes a shock wave to be formed. For normal conditions in air, the shock wave meets the detonation wave on the surface of the charge, but it is possible, for certain initial conditions of the outer medium, to have the shock wave travelling ahead of the detonation wave, the possibilities being analogous to those for a projectile in flight.

The boundary between the gas and the outer medium is curved, and across it the stream velocities are discontinuous. In general, too, the shock wave is curved, and vorticity, resulting from the variation of entropy along and immediately behind the wave, spreads into the high-pressure region. Along each streamline when the outer medium is a perfect gas, the vorticity is, in fact, proportional to the pressure. Only when the shock wave is straight, the initial conditions in the medium being uniform, is the motion irrotational. This has been the case, however, over all the field covered by the present investigation, since the shock wave was found to be straight for a considerable distance behind the detonation wave.

---

* Originally published as a Ministry of Supply report, January 1944.

The treatment of these phenomena by hydrodynamical means presents, therefore, a complicated mathematical problem, and it does not seem possible to obtain an analytical solution in finite terms; thus recourse must be had to numerical integration of the equations involved. To make the problem more tractable the block of explosive and the gas and fluid fields are considered to be two-dimensional.

Certain difficulties are inherent in the numerical integration of the equations, on account of the sonic velocity of relative flow immediately behind the detonation wave. It was clear that the problem could only be begun by obtaining analytical solutions which would enable boundary conditions to be stipulated along a line away from the face. The various types of analytical solution which it was necessary to seek are given in §§ 5, 6 and 7, and in a subsequent section the question of accuracy achieved in the fitting of the boundary conditions is discussed.

In § 8 is to be found a general account of the way in which perturbations of the flow are carried through the gas field. It shows how the conditions at a considerable distance from the corner are dependent upon conditions very close to the face on the axis of the charge, and demonstrates that a simple Meyer expansion provides a remarkably accurate solution over a large part of the gas field.

2. INITIAL CONDITIONS

Throughout the present paper c.g.s. units are used. The block of explosive is taken to be T.N.T., of which the unexploded density is 1·5 g./c.c., for which the observed velocity of detonation is 6790 m./sec. The thickness of the block is taken to be 2 cm. The velocity of the gases just behind the detonation wave, relative to the wave itself, is equal to the local velocity of sound a_0 (§ 1). a_0 is taken to be 4697 m./sec. corresponding to a gas density of 1·895 g./c.c. Tables of pressure-density relations and of density—gas velocity—velocity of sound relations were supplied by Mr C. R. Illingworth, who obtained them by using the results of two papers by Dr H. Jones (unpublished). In calculating the densities, the solid carbon was separated from the detonation products, in preparation for the application of the hydrodynamical equations for the flow of a compressible fluid.

The initial conditions in the outer medium were taken for half-saturated air at 60° F, with γ, the ratio of specific heats, taken equal to 1·405, the velocity of sound 341·359 m./sec., and the pressure 1015·9 mb. The Mach number for the incident air, moving with a velocity equal to the velocity of detonation, is 19·8911.

3. MATHEMATICAL FORMULATION OF THE PROBLEM

The problem is considered to be two-dimensional, a section of the block normal to its surface and to the detonation wave (considered plane) being a rectangle. For the purposes of mathematical treatment, the rectangle is taken to be semi-infinite in length, although finite in breadth.

Except where otherwise stated, Cartesian axes moving with the detonation wave are used. The ordinates are measured parallel to the wave, and the abscissae parallel to the axis of symmetry. The origin is at the centre of the block face.

The detonation wave is supposed to travel steadily down the block, thus enabling the equations for steady motion in conjunction with the moving axes, to be applied to the field behind the wave.

The general features of the gas and fluid fields are shown in figure 1. *OD* marks the line of separation between the gas and the outer medium and is a streamline for both media. The gas and fluid velocities are, in general, not equal along *OD*, but the pressure is continuous across *OD*.

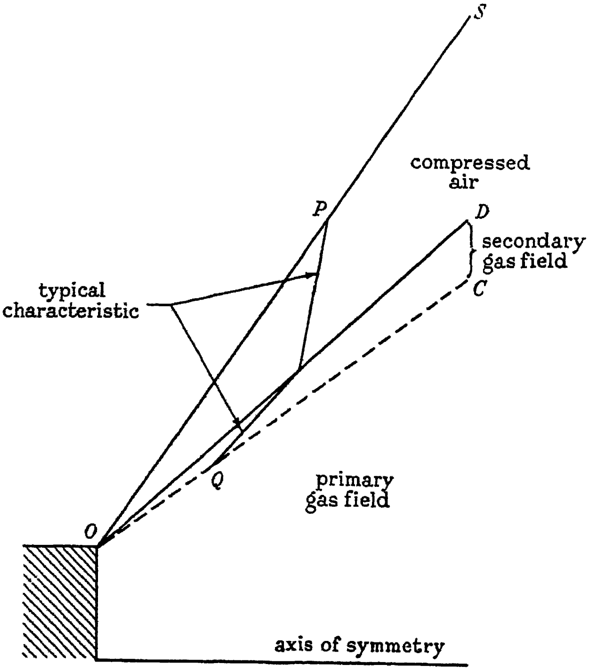

FIGURE 1. The subdivisions of the fields of product gases and air. *OS* is a shock wave in air, and *OD* is the boundary between air and product gases.

The gas region is divided into the primary field and the secondary field, *OC* marking the boundary between them. The distinction between these two fields is chiefly of mathematical significance. In the primary gas field, defined by the singularity at the corner and the boundary conditions along the detonation wave and axis of symmetry, all streamlines originate from the charge face and there is no streamline from the corner. But the line of separation of the gas and the outer medium must be a streamline from the corner in both fluids. Mathematically, the reconciliation is effected by the possibility of adjoining a secondary gas field to the primary field. The line of separation *OC* must be a characteristic (Goursat 1922) from the corner in the primary field, and the velocity and pressure must be continuous across it. The actual characteristic and the velocity and pressure distribution throughout the secondary field are then uniquely determined by the initial conditions in the outer medium (in contradistinction to the distribution in the primary field which is independent of the outer medium). It is important to notice that there is no singularity at the corner in the secondary field, so allowing the existence of a streamline from the corner. In the case of the semi-infinite block, where characteristics from the corner are radii and conditions in the primary field are constant along radii, the secondary region is one of uniformity of velocity and pressure. For the finite block, OC is the characteristic whose initial direction is that of the line of separation in the semi-infinite block solution (for the same conditions in the outer medium). The hydrodynamical equations of motion (§ 4) for the secondary region are exactly those for the primary region.

Referring again to figure 1, OS is the shock wave in the surrounding fluid and the region bounded by OS and OD is filled with fluid which has passed through the shock wave and which will, in general, be in vortex motion. Irrotational motion implies a straight shock wave (with uniform initial conditions in the outer medium).

4. GENERAL THEORY OF GAS FIELD

Referred to the axes described in § 3, the equation satisfied by the velocity potential ϕ of the relative motion is

$$(u^2-a^2)\frac{\partial^2\phi}{\partial x^2}+2uv\frac{\partial^2\phi}{\partial x\,\partial y}+(v^2-a^2)\frac{\partial^2\phi}{\partial y^2}=0. \tag{4·1}$$

(u, v) are the components of relative stream velocity in the x and y directions. a is the local velocity of sound, given in terms of the total velocity by Bernoulli's equation

$$u^2+v^2=a_0^2-2\int_{\rho_0}^{\rho}\frac{a^2\,d\rho}{\rho}, \tag{4·2}$$

where the suffix zero denotes values on the face. Equation (4·1) is integrated using the method of characteristics (Goursat 1922). The equations of the two sets of characteristics are

$$dy=\mu_1 dx \quad \text{and} \quad dy=\mu_2 dx, \tag{4·3}$$

where μ_1, μ_2 are the roots of

$$(u^2-a^2)\mu^2-2uv\mu+(v^2-a^2)=0,$$

and are real since the flow is everywhere supersonic.

Along $dy=\mu_1 dx$, u and v satisfy the relation

$$du+\mu_2 dv=0, \tag{4·4}$$

and along $dy=\mu_2 dx$, $\qquad du+\mu_1 dv=0.$

These equations are converted into difference relations, using mean values, and then integrated numerically. The details of this process are given in § 9.

A general picture of the characteristics is given in figure 2. The two sets radiate from the corners of the block, one set from each corner. This may be compared with the case of the semi-infinite block where one set of characteristics are simply radius vectors from the corner. The values of (u, v) at any point of the field are obtained by integrating along the two characteristics through the point using the known boundary values. The boundary conditions in this problem are the given velocity on the face, the vanishing of v along the axis of symmetry and the singularities expressing the existence of the corner. No difficulty arises from the axis condition, nor from the singularities, since the velocities immediately at the corners are provided by the Meyer solution. But a serious difficulty presents itself in the conditions near to and on the face, for the gradients of the characteristics tend to infinity as the face is approached, and in the limit the characteristics initially making a zero angle with the face coincide entirely with it. It is, therefore, impossible to use

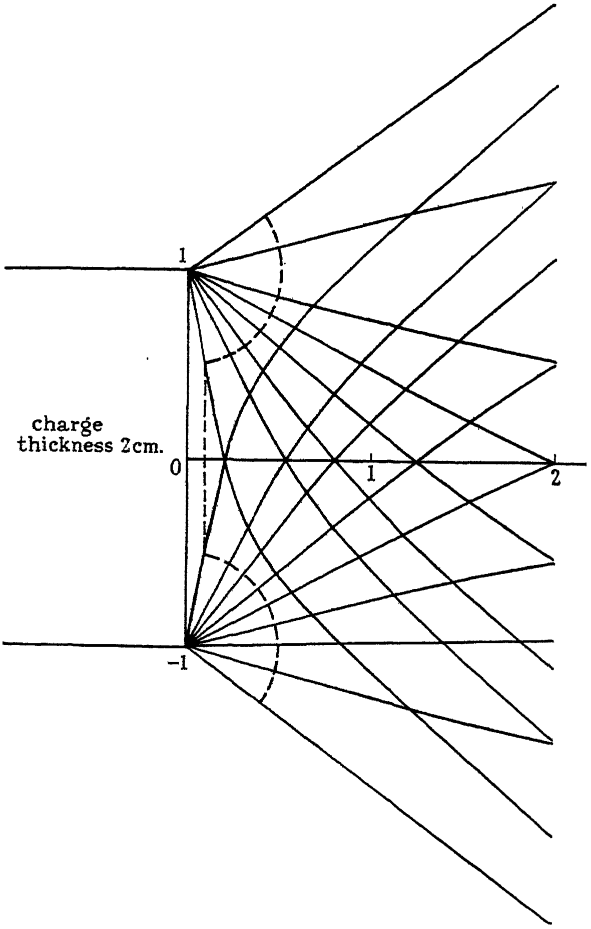

Figure 2. Typical characteristics in the primary gas field. The broken lines represent the limit to which the analytical solutions were taken.

equations (4·3) and (4·4), and in order to start on the problem at all, recourse must be had to some other means. The method adopted here is to obtain analytical solutions in series form, valid near to the face and close to the corners. Effectively, this substitutes for the boundary conditions on $x = 0$ boundary conditions some distance out into the field where the gradients of the characteristics are sufficiently small to permit using equations (4·3) and (4·4) to the degree of accuracy required.

Three different types of series solutions are used:

(*a*) A solution in powers of x, covering the field near the face (§ 5).

(*b*) A solution in powers of θ (the angular distance between the face and a radius from the corner), the necessary boundary conditions being given by (*a*) (§ 6).

(*c*) A solution in powers of r, using boundary conditions given by (*b*) (§ 7).

Finally, in § 8, a more general method of approach is used to indicate the extent of the region of validity of the solutions, and the way in which the existence of an axis of symmetry modifies the Meyer expansion near the block.

5. SOLUTION NEAR THE FACE

(u, v) denote Cartesian components of velocity referred to the axes described in § 4.

The equation of continuity is

$$\frac{\partial}{\partial x}(\rho u)+\frac{\partial}{\partial y}(\rho v) = 0. \tag{5·1}$$

Bernoulli's equation is
$$u^2+v^2 = a_0^2-2\int_{\rho_0}^{\rho}\frac{a^2\,d\rho}{\rho}, \tag{5·2}$$

where suffix zero refers to values on the face.

It is required to find a solution in the form of a power series in x, valid in some region near the face. Assume the velocity potential ϕ is expressible as

$$\phi(x,y) = a_0 x+P_2(y)\,x^2+P_3(y)\,x^3+\dots, \tag{5·3}$$

where
$$u=\frac{\partial\phi}{\partial x},\quad v=\frac{\partial\phi}{\partial y}.$$

The axis condition gives

$$P_2'(0)=0,\quad P_3'(0)=0,\quad \text{etc.} \tag{5·4}$$

If
$$\rho(x,y) = \rho_0+F_1(y)\,x+F_2(y)\,x^2+\dots,$$

then
$$\int_{\rho_0}^{\rho}\frac{a^2\,d\rho}{\rho} = \frac{a_0^2}{\rho_0}(F_1x+F_2x^2+\dots)+\alpha_2(F_1x+F_2x^2+\dots)^2+\dots,$$

where
$$\alpha_2=\frac{1}{2!}\frac{d}{d\rho_0}\left(\frac{a_0^2}{\rho_0}\right),\quad \text{etc.}$$

Substituting the series into (5·1) and (5·2) and equating coefficients of powers of x, we obtain successively:

From the coefficients of x^0 in (5·1) and x in (5·2), the same relation, viz.

$$a_0F_1+2\rho_0P_2=0.$$

From the coefficients of x in (5·1) and x^2 in (5·2), on elimination of P_3

$$\left(3+\frac{2\alpha_2\rho_0^2}{a_0^2}\right)F_1^2=0.$$

The dimensionless quantity $$\frac{2\alpha_2\rho_0^2}{a_0^2}$$

will, in future, be denoted by β. Its value, obtained from the data described in § 3, is 4·8496. Since $3+\beta\neq 0$, $F_1=0$, and so

$$P_2\equiv 0. \tag{5·5}$$

Hence $$a_0F_2+3\rho_0P_3=0.$$

From the coefficients of x^2 in (5·1) and x^3 in (5·3), two equations are obtained from which P_5 and F_4 can be simultaneously eliminated to give a differential equation for P_3, viz.

$$P_3''=P_3^2\frac{18}{a_0}(3+\beta). \tag{5·6}$$

Integrating and using (5·4)

$$(P_3')^2=\frac{12(3+\beta)}{a_0}[P_3^3(y)-P_3^3(0)],$$

therefore $$y\left[\frac{12(3+\beta)}{a_0}P_3(0)\right]^{\frac{1}{2}}=\int_1^t\frac{dt}{(t^3-1)^{\frac{1}{2}}},$$

where $t=P_3(y)/P_3(0)$. $P_3(0)$ is determined by the singularity at $y=L$ (taking L to be half the width of the face). This is expressed mathematically by making the pole of the elliptic function involved in the solution of (5·6) correspond to $y=L$. The justification of the assumption that $P_3(y)$ has a singularity at $y=L$ is given in § 6.

The equation for $P_3(0)$ then becomes

$$\left[\frac{12(3+\beta)}{a_0}L^2P_3(0)\right]^{\frac{1}{2}}=\int_1^\infty\frac{dt}{(t^3-1)^{\frac{1}{2}}}=\tfrac{1}{3}\pi^{\frac{1}{2}}\frac{\Gamma(\frac{1}{6})}{\Gamma(\frac{2}{3})} \tag{5·7}$$

(Whittaker & Watson 1927). Taking $L=1$, it is found that $P_3(0)=0{\cdot}294$.

In the usual notation, if $\wp(z)$ denotes the Weierstrassian elliptic function with invariants

$$g_2=0 \quad\text{and}\quad g_3=4P_3^3(0),$$

it is not difficult to show that

$$P_3(1-r)=\wp\left[\left\{\frac{3(3+\beta)}{a_0}\right\}^{\frac{1}{2}}r\right]. \tag{5·8}$$

The asymptotic expansion of $P_3(1-r)$ for small r is

$$P_3(1-r)\sim\frac{1}{Ar^2}+\frac{P_3^3(0)}{7}(Ar^2)^2+\frac{1}{13}\frac{P_3^3(0)^2}{7^2}(Ar^2)^5+\dots, \tag{5·9}$$

where $A = 3(3+\beta)/a_0$. Putting in numerical values, with $L = 1$,

$$P_3(1-r) \sim \frac{0{\cdot}19946}{r^2} + 0{\cdot}0913r^4 + 0{\cdot}0032r^{10} + \dots.$$

This expression serves to calculate P_3 as far as $r = 1$ to the accuracy required here.

It was not found necessary to continue the series for ϕ beyond the x^3 term, and so the actual approximations used take the form

$$u = a_0 + 3P_3(y)\,x^2, \quad v = P_3'(y)\,x^3. \tag{5·10}$$

The region over which these formulae were taken to hold will be described in § 9.

6. SOLUTION FOR SMALL θ WITH ORIGIN AT A CORNER

Taking a corner as origin, and measuring θ from the face of the block, it is required to find a solution of the equations, valid for small θ.

Using polar co-ordinates, let u be the component velocity along the radius vector, and v the transverse component. Assume the expansion for the velocity potential ϕ to be

$$\phi = \sum_1^\infty Q_n(r)\,\theta^n, \tag{6·1}$$

giving

$$u = \frac{\partial\phi}{\partial r} = \sum_1^\infty Q_n(r)\,\theta^n \tag{6·2}$$

and

$$v = \frac{\partial\phi}{r\partial\theta} = \sum_0^\infty (n+1)\frac{Q_{n+1}(r)}{r}\,\theta^n. \tag{6·3}$$

Further, assume

$$\rho = \sum_0^\infty G_n(r)\,\theta^n. \tag{6·4}$$

Then if a_0 = velocity of sound at the block face, and ρ_0 is the density of the gases there,

$$G_0(r) \equiv \rho_0, \quad Q_1(r) \equiv a_0 r. \tag{6·5}$$

Bernoulli's equation, giving relations between Q's and G's, is, as before,

$$u^2+v^2 = a_0^2 - \frac{2a_0^2}{\rho_0}(\rho-\rho_0) - 2\alpha_2(\rho-\rho_0)^2 - 2\alpha_3(\rho-\rho_0)^3. \tag{6·6}$$

The equation of continuity is

$$\frac{\partial}{\partial r}(\rho r u) + \frac{\partial}{\partial\theta}(\rho v) = 0. \tag{6·7}$$

On substitution of equations (6·2), (6·3) and (6·5) in (6·7) and equating coefficients of θ^0, θ,

$$G_1 a_0 r + 2\rho_0 Q_2 = 0, \tag{6·8}$$

$$\rho_0 a_0 + 4G_1\frac{Q_2}{r} + 2G_2 a_0 + 6\rho_0\frac{Q_3}{r} = 0, \tag{6·9}$$

and from equation (6·6), by equating coefficients of θ, θ^2,

$$4a_0\frac{Q_2}{r} = -\frac{2a_0^2}{\rho_0}G_1, \tag{6·10}$$

$$a_0^2+\frac{6a_0}{r}Q_3+\frac{4Q_2^2}{r^2} = -\frac{2a_0^2}{\rho_0}G_2-2\alpha_2 G_1^2. \tag{6·11}$$

Equations (6·8) and (6·10) are the same, but combining with equations (6·9) and (6·11) it follows that

$$Q_2^2\left(3+2\alpha_2\frac{\rho_0^2}{a_0^2}\right) = 0.$$

The expression in brackets is non-zero (§ 5). It follows, therefore, that

$$Q_2(r)\equiv 0$$

and hence

$$G_1(r)\equiv 0. \tag{6·12}$$

Equating coefficients of θ^2 in equation (6·7) and of θ^3 in equation (6·6) supplies only one new equation, namely,

$$4\frac{Q_4}{r}+\frac{a_0}{\rho_0}G_3 = 0. \tag{6·13}$$

Equating coefficients of θ^3 in the continuity equation and of θ^4 in Bernoulli's equation, and eliminating the G functions, it follows eventually that

$$rQ_3''(r)-6Q_3'(r) = \frac{a_0}{2}(1+\beta)+6(1+\beta)\frac{Q_3(r)}{r}+\frac{18(3+\beta)}{a_0}\frac{\{Q_3(r)\}^2}{r^2}, \tag{6·14}$$

where β is equal to $2\alpha_2(\rho_0^2/a_0^2)$ as in § 5. Two particular integrals of this equation can be seen at once to be $Q_3 = \alpha r$, where

$$\alpha = -\tfrac{1}{6}a_0 \text{ or } -\tfrac{1}{6}a_0\lambda \text{ with } \lambda = (1+\beta)/(3+\beta) = 0{\cdot}7452.$$

It can be shown that the former value of α contributes a term towards a solution representing steady flow with velocity a_0, and that the latter contributes a term towards the expansion of Meyer's solution in which the velocities are constant along a radius vector.

If α is allowed to be a function of r in order to get a more general solution the following alternative forms of solution are obtained:

$$Q_3(r)\equiv -\frac{a_0\lambda}{6}r+A_1r^7+A_2r^{13}+\dots \tag{6·15}$$

ascending in powers of r^6 with A_1 arbitrary and A_n $(n>1)$ a function of A_1,

$$Q_3(r)\equiv -\frac{a_0r}{6}+B_1r^3+B_2r^5+\dots$$

ascending in powers of r^2 with B_1 arbitrary and B_n $(n>1)$ a function of B_1,

$$Q_3(r)\equiv -\frac{a_0r}{6}+C_1r^4+C_2r^7+\dots$$

ascending in powers of r^3 with C_1 arbitrary and C_n $(n > 1)$ a function of C_1. Of these solutions the last two are discarded, since they do not tend to Meyer's solution near the corner.

Equation (6·15) is now used to justify the assumption in § 5 that $P_3(y)$ has a singularity at $y = 1$. $P_3(y)$ is expanded in a series of positive and negative powers of $(1-y)$, and then the substitution $y = 1-r(1-\frac{1}{2}\theta^2+\ldots)$, $x = r(\theta-\frac{1}{6}\theta^3+\ldots)$ is made in the expression for the velocity potential in powers of x. The coefficients of θ, θ^3 are compared with the corresponding coefficients in the expression for the velocity potential in powers of θ, viz.

$$\phi = a_0 r\theta - \left[\frac{a_0\lambda}{6} r - A_1 r^7 - A_2 r^{13} - \ldots\right]\theta^3 + \ldots. \tag{6·16}$$

It is easily deduced that $P_3(y)$ has a pole of the second order at $y = 1$.

The series for $P_3(1-r)$ in the neighbourhood of $r = 0$, found in equation (5·9), may now be used to obtain A_1, A_2, etc., by further equating of coefficients above. It is found that $A_1 = 0·0913$, $A_2 = 0·0032$, since $A_1 = \frac{A^2}{7} P_3^3(0)$, $A_2 = \frac{1}{13}\frac{A^5}{7^2} P_3^6(0)$, using the notation of (5·9).

The components of velocity in the θ expansion are

$$u_r = a_0\theta - \left[\frac{a_0\lambda}{6} - A^2 P_3^3(0)\, r^6 - \frac{A^5}{7^2} P_3^6(0)\, r^{12} \ldots\right]\theta^3 + \ldots,$$

$$v_\theta = a_0 - 3\left[\frac{a_0\lambda}{6} - \frac{A^2}{7} P_3^3(0)\, r^6 - \frac{A^5}{13.7^2} P_3^6(0)\, r^{12} - \ldots\right]\theta^2 + \ldots.$$

7. SOLUTION NEAR THE CORNER

$u(r, \theta)$ and $v(r, \theta)$ denote (r, θ) components of velocity, where r is the distance from one corner and θ the angular distance from the face. $u(\theta)$, $v(\theta)$, $\rho(\theta)$, $a(\theta)$, denote quantities in the semi-infinite block solution, constant along radius vectors. A solution is sought for the field near to and around a corner. The expansion in powers of r assumed for the velocity potential is

$$\phi(r, \theta) = ru(\theta) + r^n R_n(\theta) + \text{higher powers of } r, \tag{7·1}$$

where n is some integer $\geqslant 2$ to be determined. The velocities are given by

$$u(r, \theta) = u(\theta) + nr^{n-1} R_n(\theta) + \ldots, \tag{7·2}$$

$$v(r, \theta) = v(\theta) + r^{n-1} R_n'(\theta) + \ldots, \tag{7·3}$$

remembering that $v(\theta) = du/d\theta$.

The corner condition is automatically satisfied since in the limit as $r \to 0$, $u(r, \theta)$ and $v(r, \theta)$ tend to the semi-infinite block solution. For the density it is assumed that

$$\rho(r, \theta) = \rho(\theta) + r^{n-1} H_n(\theta) + \ldots. \tag{7·4}$$

Bernoulli's equation is

$$u^2(r,\theta)+v^2(r,\theta) = u^2(\theta)+v^2(\theta)-2\int_{\rho(\theta)}^{\rho(r,\theta)}\frac{a^2\,d\rho}{\rho}. \tag{7·5}$$

On substituting the series in equation (7·5) and equating to zero the coefficient of r^{n-1}, there results

$$nuR_n+vR_n' = -\frac{a^2}{\rho}H_n, \tag{7·6}$$

where all variable quantities are functions of θ only.

The r^{n-1} term in the continuity equation

$$\rho u+\frac{r\partial}{\partial r}(\rho u)+\frac{\partial}{\partial\theta}(\rho v) = 0$$

gives
$$\rho R_n''+\rho' R_n'+n^2\rho R_n+vH_n'+(nu+v')H_n = 0. \tag{7·7}$$

The elimination of H_n between equations (7·6) and (7·7) leads, after some reduction, to

$$-2R_n'+R_n\left[\frac{v'}{v}-\frac{nu}{v}+(n-1)\frac{u'}{u}-\frac{\rho'}{\rho}\right] = 0.$$

R_n'' has disappeared during the elimination, due to the relation $v = a$.

Integrating
$$R_n(\theta) = C\frac{u^{\frac{1}{2}(n-1)}v^{\frac{1}{2}}}{\rho^{\frac{1}{2}}}\exp\left[-\frac{n}{2}\int_0^\theta\frac{u\,d\theta}{v}\right], \tag{7·8}$$

where C is a constant to be determined by the remaining boundary condition, viz. the equivalence of this expansion when θ is small with that of § 6 when r is small. To order of θ^3,

$$R_n(\theta) = \frac{Ca_0^{\frac{1}{2}n}}{\rho_0^{\frac{1}{2}}}\theta^3+\dots.$$

When the solution in § 6 is expanded for small r, it is found that the first term of type θ^3r^n, where $n\geqslant 2$, is

$$\frac{P_3^3(0)}{7}A^2\theta^3r^7 \quad \left(A = \frac{3(3+\beta)}{a_0}\text{ as in equation (5·9)}\right).$$

It follows that $n = 7$,
$$\frac{Ca_0^{\frac{7}{2}}}{\rho_0^{\frac{1}{2}}} = \frac{P_3^3(0)}{7}A^2,$$

and so
$$R_7(\theta) = \frac{P_3^3(0)}{7}A^2\frac{[u/a_0]^3\,[v/a_0]^{\frac{1}{2}}}{[\rho/\rho_0]^{\frac{1}{2}}}\exp\left[-\frac{7}{2}\int_0^\theta\frac{u\,d\theta}{v}\right]. \tag{7·9}$$

In the case considered in the present paper, when the block has a thickness of 2 cm., $R_7(\theta)$ increases from zero on $\theta = 0$ to a maximum value of 0·0117 when θ is about 48·4°, and thereafter decreases asymptotically to zero. $R_7'(\theta)$ attains a maximum positive value of 0·025 when θ is 30° and a maximum negative value of $-0·020$ when θ is 72° and then decreases numerically to zero. Thus the second terms of equations (7·2) and (7·3) are always very small compared with the first terms whenever r is $<\frac{1}{2}$, say.

Equations (7·2), (7·3) and (7·4) make it possible to assess the accuracy to which the solution for a semi-infinite block holds in the case of a finite block in a region near a corner.

Since the perturbation terms depend on r^6, the accuracy will be very good, certainly for $r < \frac{1}{2}$. As might be expected on physical grounds alone, the accuracy is least in the region $30° < \theta < 75°$, and highest in the region round the corner away from the axis of symmetry.

8. General method of approximate solution

It is possible to give a more general treatment of the way in which the solution in the gas field for a finite block differs from the solution for a semi-infinite block. Taking (r, θ) co-ordinates from one corner, let $\phi(r, \theta)$ be the velocity potential in the first case, and, as in § 7, let $u(\theta)$, $v(\theta)$, $\rho(\theta)$, $a(\theta)$ denote the known quantities occurring in the second case.

Writing
$$\phi(r,\theta) = ru(\theta) + \epsilon(r,\theta) \tag{8·1}$$
and
$$\rho(r,\theta) = \rho(\theta) + \zeta(r,\theta), \tag{8·2}$$

ϵ and ζ are determined over any region in which the two solutions differ by small quantities of the first order. From Bernoulli's equation

$$\frac{u\,\partial\epsilon}{\partial r} + \frac{v}{r}\frac{\partial\epsilon}{\partial\theta} = -\frac{v^2}{\rho}\zeta. \tag{8·3}$$

From the equation of continuity

$$(u+v')\,\zeta + ru\frac{\partial\zeta}{\partial r} + v\frac{\partial\zeta}{\partial\theta} + \rho\left[r\frac{\partial^2\epsilon}{\partial r^2} + \frac{\partial\epsilon}{\partial r} + \frac{1}{r}\frac{\partial^2\epsilon}{\partial\theta^2} + \frac{\rho'}{\rho}\frac{1}{r}\frac{\partial\epsilon}{\partial\theta}\right] = 0. \tag{8·4}$$

Eliminating ζ from equations (8·3) and (8·4)

$$\left[-\frac{u}{v} + \frac{v'}{v} - \frac{\rho'}{\rho}\right]\frac{\partial\epsilon}{\partial r} + \left[\frac{v}{u} - \frac{u}{v}\right]r\frac{\partial^2\epsilon}{\partial r^2} - \frac{2\partial^2\epsilon}{\partial r\,\partial\theta} = 0, \tag{8·5}$$

using the relation $v = u'$.

Integrating equation (8·5) with respect to r

$$\left[-\frac{u'}{u} + \frac{v'}{v} - \frac{\rho'}{\rho}\right]\epsilon + r\left[\frac{v}{u} - \frac{u}{v}\right]\frac{\partial\epsilon}{\partial r} - 2\frac{\partial\epsilon}{\partial\theta} = 0, \tag{8·6}$$

since $\qquad \epsilon,\ \dfrac{\partial\epsilon}{\partial r}$ and $\dfrac{1}{r}\dfrac{\partial\epsilon}{\partial\theta} \to 0$ as $r \to 0$ for all θ.

The general integral of equation (8·6) is

$$\frac{\rho u}{v}\epsilon^2 = F\left[ur^2\exp\left\{-\int_0^\theta \frac{u\,d\theta}{v}\right\}\right], \tag{8·7}$$

where F is a function to be determined by the size of the block.

Now the curves $\qquad r^2u\exp\left[-\int_0^\theta \frac{u\,d\theta}{v}\right] = \text{constant},$

constitute the family of curved characteristics in the semi-infinite block solution, and equation (8·7) shows that $\rho u\epsilon^2/v$ is constant along each member of the set. The value of this constant is determined from the intersection of the characteristic with known boundary conditions. For example, the solution in § 5 could be used. It may be noted in passing that by taking $F(z) \sim z^7$ the solution in § 7 is found.

Returning to equation (8·7) the factor $\rho u/v$ is itself constant along the other set of characteristics in the case of a semi-infinite block, i.e. along radius vectors from the corner. Thus ϵ at any point of the field is determined by the product of two factors which parametrically specify the characteristics through the point. Theoretically it would be possible to use equation (8·7) to replace the individual solutions in §§ 5, 6 and 7, but in practice the latter were found to be more convenient. Equation (8·7), apart from indicating in a general way how the presence of an axis modifies the Meyer solution, makes it possible to assess the extent of the regions over which the individual solutions may safely be used. The curved set of characteristics in the Meyer solution bend away rapidly from the corner in a manner closely resembling that illustrated in figure 2. Since ϵ^2 varies like $v/\rho u$ along such a characteristic and $v/\rho u$ does not vary much for $\theta > 5°$, the size of ϵ is of the same order all over the region between a given characteristic and the corner. This explains, for example, why the solution § 7 holds so much further out from the corner than solution § 5 does from the face, and also, in the case of a surrounding medium of air, why the shock wave is straight for a considerable distance from the corner.

9. Details of the numerical integration

In the numerical integration of the equations it was hoped to obtain values accurate to within 1 in 500. In order to achieve this it was necessary to work to a much higher nominal accuracy, since an error in (u, v) at any point causes a much larger percentage error in the evaluation of the co-ordinates of the point, and since errors accumulate as the field is developed.

The chief difficulty in obtaining the accuracy required is caused by the gradients of the characteristics tending to infinity as the block face is approached. In substituting conditions at a distance from the face, by means of the series solutions, a new source of error is introduced, namely, the terms omitted from the expansions. A balance had to be struck between the two cases. It was decided to take the series near the axis as valid for boundary conditions on $x = 0{\cdot}1$ from the axis of $y = \pm 0{\cdot}5$. The rest of the boundary conditions were supplied by the expansion near the corner in powers of r over a circular arc of radius 0·5, and by the vanishing of v on the axis of symmetry. The gas field was covered by the network of characteristics from the points taken on the boundary chosen above.

The values of the velocity components at a point P of the field were obtained from nearby points on the two characteristics passing through P. The two points were called 'top' or 'bottom', according as they lay on the characteristic through P emanating from the upper or lower corner of the block, respectively, and the suffixes

T and B were used to distinguish them. The gradients of the characteristics were denoted by $\overset{-}{\mu}$, $\overset{+}{\mu}$ respectively, with the appropriate suffixes.

In the equations which follow, quantities without suffixes refer to the point P for which (u, v, x, y) are to be found.

In the approximate integration of the differential relations in §4, arithmetic mean values of the gradients are taken, and hence the differential relations are replaced by the following difference equations

$$u-u_T+\tfrac{1}{2}[\overset{+}{\mu}+\overset{+}{\mu}_T]\,[v-v_T]=0,\quad u-u_B+\tfrac{1}{2}[\overset{-}{\mu}+\overset{-}{\mu}_B]\,[v-v_B]=0, \tag{9·1}$$

$$y-y_T=\tfrac{1}{2}[\overset{-}{\mu}+\overset{-}{\mu}_T]\,[x-x_T],\quad y-y_B=\tfrac{1}{2}[\overset{+}{\mu}+\overset{+}{\mu}_B]\,[x-x_B]. \tag{9·2}$$

If the quantities $\overset{+}{\Sigma}=\overset{+}{\mu}+\overset{+}{\mu}_T$, $\overset{-}{\Sigma}=\overset{-}{\mu}+\overset{-}{\mu}_B$, $\overset{+}{\Sigma}{}'=\overset{+}{\mu}+\overset{+}{\mu}_B$, $\overset{-}{\Sigma}{}'=\overset{-}{\mu}+\overset{-}{\mu}_T$ are defined, then, by solving the simultaneous equations (9·1), u and v may be obtained in the useful computing form

$$\left.\begin{aligned}(\overset{+}{\Sigma}-\overset{-}{\Sigma})\,u&=\overset{+}{\Sigma}u_B+(-\overset{-}{\Sigma})\,u_T+(-\overset{+}{\Sigma}\overset{-}{\Sigma})\left[\frac{v_T-v_B}{2}\right],\\(\overset{+}{\Sigma}-\overset{-}{\Sigma})\,v&=\overset{+}{\Sigma}v_T+(-\overset{-}{\Sigma})\,v_B+2(u_T-u_B),\end{aligned}\right\} \tag{9·3}$$

and (x, y) are obtaining similarly from equations (9·2) in the form

$$\left.\begin{aligned}(\overset{+}{\Sigma}-\overset{-}{\Sigma}{}')\,y&=\overset{+}{\Sigma}{}'y_T+(-\overset{-}{\Sigma}{}')\,y_B+(-\overset{+}{\Sigma}{}'\overset{-}{\Sigma}{}')\left[\frac{x_T-x_B}{2}\right],\\(\overset{+}{\Sigma}-\overset{-}{\Sigma}{}')\,x&=\overset{+}{\Sigma}{}'x_B+(-\overset{-}{\Sigma}{}')\,x_T+2(y_T-y_B).\end{aligned}\right\} \tag{9·4}$$

The actual method of use of the equations involves successive approximations to (u, v). Values of u, v having been guessed, the corresponding values of $\overset{+}{\mu}$ and $\overset{-}{\mu}$ are calculated, and then used in equations (9·3) to obtain more accurate values. When this process ends, the values of x, y are immediately obtainable from equations (9·4).

When the point P lies on the axis of symmetry, only one integration has to be performed, and the equations reduce to the simpler form

$$\left.\begin{aligned}&u=u_T+\tfrac{1}{2}(\overset{+}{\mu}+\overset{+}{\mu}_T)\,v_T,\\\text{with}\quad&\overset{+}{\mu}=\left[\frac{u^2}{a^2}-1\right]^{-\frac{1}{2}}\\\text{and}\quad&x=x_T+\frac{2y_T}{(-\overset{-}{\Sigma}{}')}.\end{aligned}\right\} \tag{9·5}$$

Diagrams based on the results obtained by the above methods are shown in figures 3 to 7 showing the distributions of the velocity components and the pressure at given distances from the block face, and the manner in which the velocity increases and the pressure drops, outwardly along the axis of the charge. The solution was carried out to a distance approximately equal to the thickness of the charge, where the pressure on the axis is already less than 10 % of its value just behind the detonation wave.

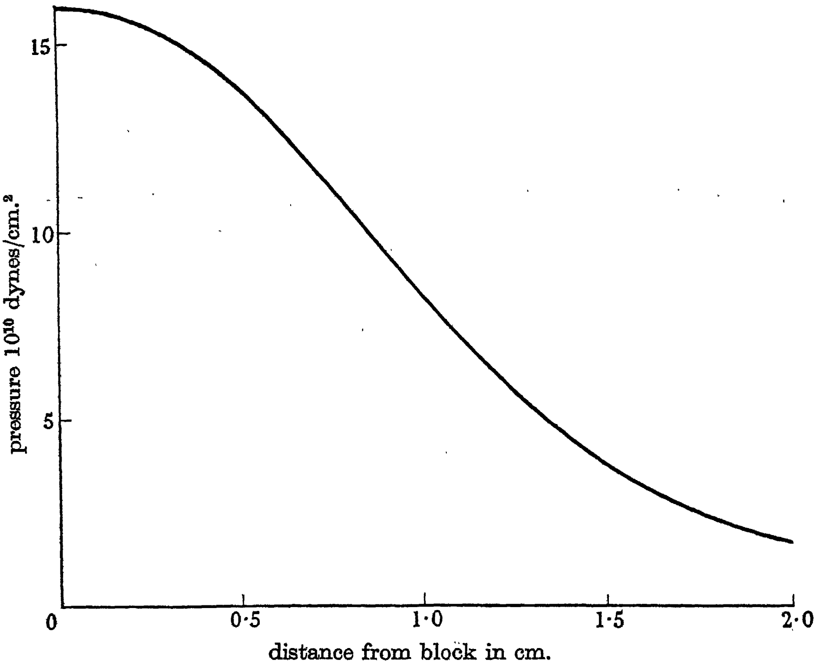

FIGURE 3. The pressure distribution along the axis of symmetry.

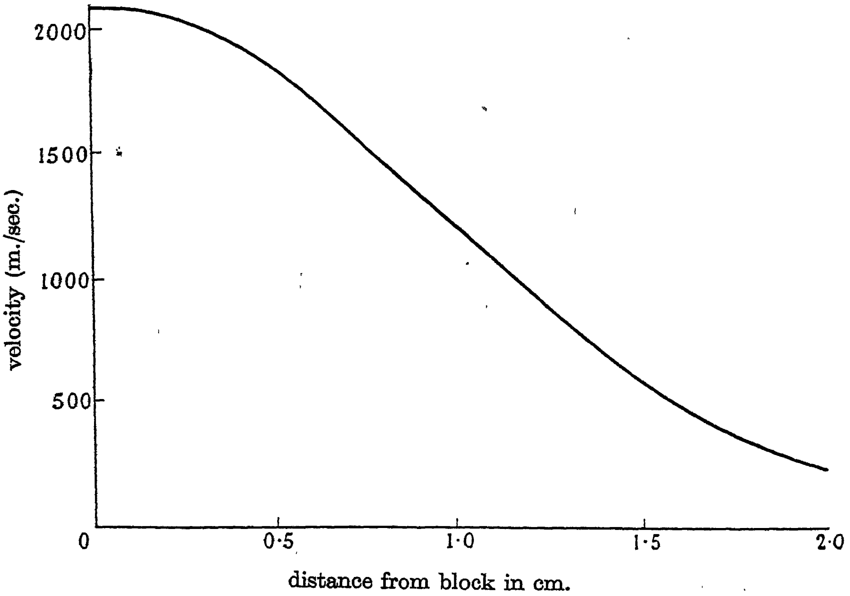

FIGURE 4. The gas velocity along the axis.

Figure 5 shows clearly one interesting feature of the pressure distribution. The crossing of the curves implies a local, temporary, increase in pressure behind the detonation wave in regions farther from the axis of symmetry than 1 cm. (i.e. farther from the axis than the corner of the charge). At greater distances from the detonation wave the pressure falls again. An allied phenomenon can be seen in figure 7, where the transverse-velocity curves also cross.

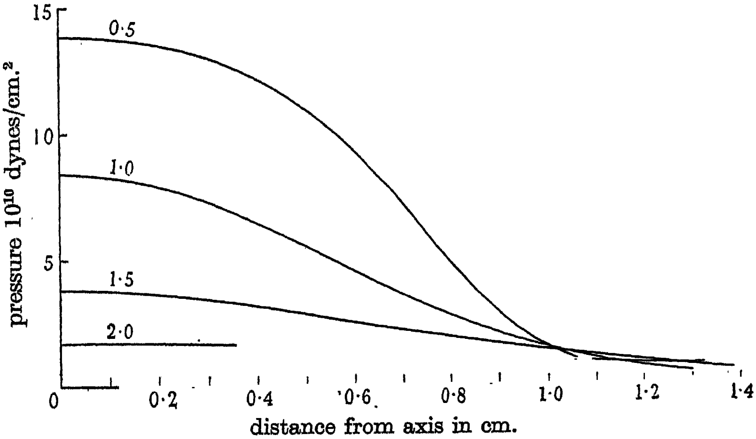

FIGURE 5. The pressure distribution along lines perpendicular to the axis. The number attached to each curve denotes the distance from the block in centimetres.

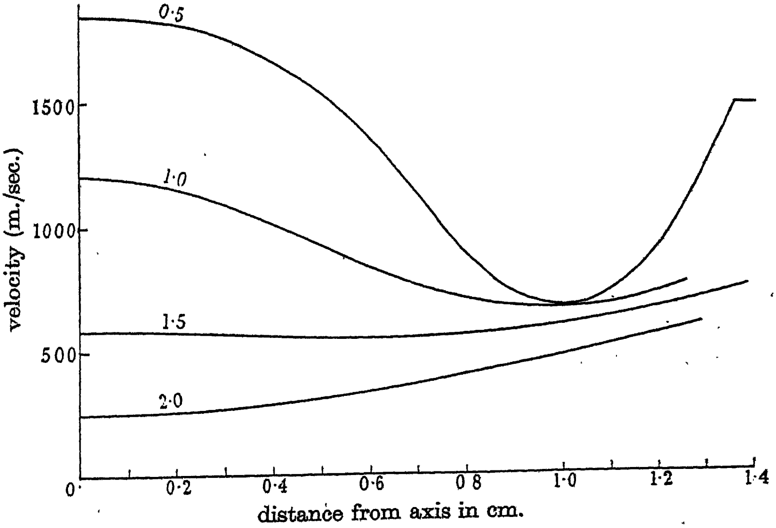

FIGURE 6. Distribution of the axial component of velocity along lines perpendicular to the axis. The number attached to each curve denotes the distance from the block in centimetres. The discontinuity in gradient on the 0·5 cm. curve occurs at the boundary between the primary and secondary gas fields.

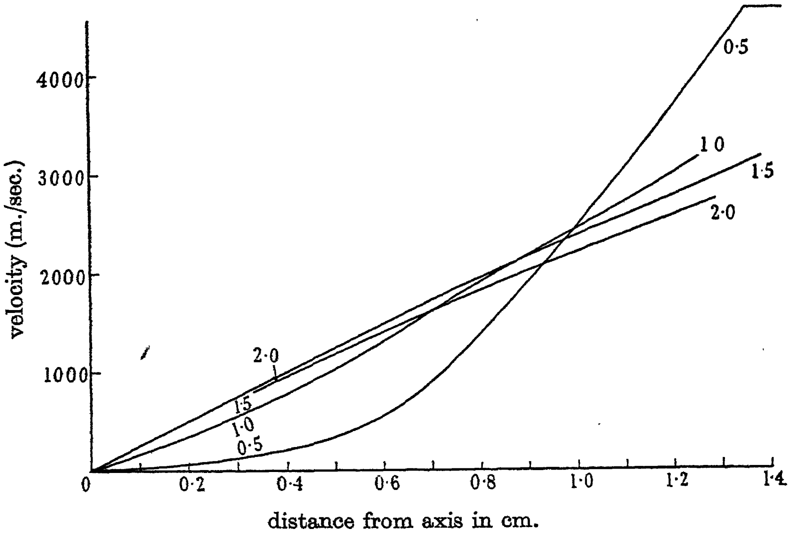

FIGURE 7. Distribution of the transverse component of velocity along lines perpendicular to the axis. The number attached to each curve denotes the distance from the block in centimetres. The discontinuity in gradient on the 0·5 cm. curve occurs at the boundary between the primary and secondary gas fields.

10. CALCULATION OF THE POSITION OF THE SHOCK WAVE

The discussion in § 3 shows that the initial direction of OC (figure 1) is found from the semi-infinite block solution, and that it depends on the conditions in the outer medium. The position of OC and velocity distribution along it then follow from the primary field solution. The velocity and pressure distributions in the secondary field are defined by the boundary conditions along OC and the initial conditions in the outer medium. The most convenient method to be adopted in numerical calculation seems to be that of successive approximation, in which the position of an elementary segment of OD or OS is guessed. Each guess entails solving the field equations in the secondary region. In the vortex region behind the shock wave the field equations are analogous to those derived by Crocco (1936) with the appropriate generalizations when the surrounding medium cannot be treated as a perfect gas. The leading feature of vortex flow of a compressible fluid is that each streamline is an adiabatic.

Along the streamline boundary OD, the vorticity in the outer medium is zero; this follows since the vorticity vanishes at the corner and is elsewhere proportional to the product of density and absolute temperature along a streamline. When the vorticity is everywhere small, it is sufficiently accurate to proceed from OS to OD along a characteristic in one step, and the numerical integration is then greatly simplified. This case occurs when the curvature of OC is small.

When the outer medium is air (as in the present paper), the position of OC is such that it lies in the part of the primary field closely approximating to the Meyer expansion and so OC is found to be straight for two charge widths (4 cm.) from the corner to the nominal accuracy of the calculations (1 in 5000). To this accuracy the shock wave is therefore straight up to the point where it is met by the characteristic from the point on OC distant 4 cm. from O. A calculation shows that the shock wave is straight for nearly 12 cm. from O. The shock wave then gradually bends round towards the axis of symmetry, until at a great distance from the charge it makes an angle with the axis equal to the Mach angle corresponding to air streaming with the detonation velocity under the given initial conditions of pressure and density.

The angles made with the axis by OC, OD and OS are found (from the Meyer expansion) to be

$$OC,\quad 35{\cdot}45^\circ;\qquad OD,\quad 40{\cdot}98^\circ;\qquad OS,\quad 54{\cdot}52^\circ$$

Relatively to the detonation wave the air streams along OD with a velocity of 4054 m./sec. and the gas with a velocity of 7021 m./sec. The pressure behind the shock wave is 306·4 atm.

The authors are indebted to Mr C. R. Illingworth, who kindly supplied the tables of gas relationships referred to in § 2, and the numerical values quoted at the end of § 10; and to the Chief Scientific Officer, Ministry of Supply, for permission to publish this paper.

REFERENCES

Crocco, L. 1936 *R.C. Accad. Lincei*, **23**, 115.
Goursat, E. 1922 *Cours d'Analyse Mathématique*, **2**. Paris.
Whittaker, E. T. & Watson, G. N. 1927 *Modern analysis*, 4th ed. p. 526. Camb. Univ. Press.

The interaction of radiation and matter

By P. M. Davidson, *University College, Swansea*

(*Communicated by Sir Owen Richardson, F.R.S.—Received* 23 *May* 1947)

This paper is based on the idea that wave mechanics is primarily suitable for giving an indirect description of nature. The world to which the equations of the theory here proposed are directly applicable is an unnatural one, containing sources and sinks of matter which give to its radiational laws a symmetry lacking in nature. The theory may be regarded as consisting of two postulates. The first (which may, if desired, be regarded as a definition) specifies the character and properties of an unnatural assembly of systems, each consisting of an electron in a static potential field U. It states that, of the energy radiated in an elementary solid angle of standard magnitude, the part which will pass through an analyzer which transmits the component of electric field in a given direction (perpendicular to the line of observation) is determined by applying the usual Schrödinger interpretations (of density, current and material energy) to a Schrödinger equation perturbed by a term which is a certain constant multiplied by the electric field, in that direction, acting on the electron, due to the potential field U. (For comparison with classical radiation theory, it will be noted that the perturbation term vanishes in any region in which, from the classical standpoint, the electron is not accelerated, in that direction, by the field U.) In the process of specifying the radiation from the assembly, the Schrödinger interpretations will have specified also the nature and magnitude of the sources and sinks of electrons (each in a field U). Their presence is due, mathematically speaking, to the multiplying constant mentioned above being a complex quantity. From these results the properties of a natural assembly are specified by means of the second postulate, which states that when the sources and sinks are removed, any process which in their absence is meaningless or physically inconceivable will cease, and all other processes will remain unaffected. The calculation is readily extended to include the effect of an external field of radiation. The theory requires no representation of radiation other than the Maxwellian wave, and will be free from the difficulties encountered in other theories.

1. The starting-point in the setting up of the Schrödinger equation was the classical Hamiltonian for an electron moving in a stationary electric field, under the influence of no external radiation, and with the force exerted on the electron by its own radiation neglected. It was soon found that to explain Einstein's induced transitions it was only necessary to start from a classical Hamiltonian which took account of the applied electromagnetic field, while still neglecting the force on the electron due to its own radiation. The calculation naturally predicted no spontaneous transitions; and an attempt to calculate them from the radiational field which the electron set up at a distance led to the impossible conclusion that the rate of spontaneous transition from one level to another depends on the number present in both levels. If an attempt is made to obtain the spontaneous transitions by adding a simple perturbing term to the Schrödinger equation, it is found that no simple equation and interpretations can give the radiational law which is found in nature; the expressions obtained are always too symmetrical. In the theories now current, the law results from the introduction of certain non-commuting quantities (associated, in most theories, with the radiation); but their introduction leads at once to some puzzling physical conceptions, giving the impression that the mathe-

matics has been forced to describe certain characteristics of a system, for a general description of which it is unsuitable. And when it is found that, after many years, it is still a matter of discussion whether the expressions of infinite magnitude which arise in a detailed study of the most widely used of these theories constitute a fundamental defect, or are due in all cases to the erroneous use of an expansion process, it may be felt that such theories, even if not actually wrong, probably do not give the simplest possible approach to the subject. I propose, therefore, to consider whether it is possible to develop a theory from which the fundamental cause of these difficulties is absent. The theory will postulate a simple wave equation and interpretations, and will therefore, as remarked above, not be directly applicable to the world of nature. Use will thus be made of the general idea, due to Dirac, that it may be possible to specify some unnatural world which lends itself more readily to mathematical representation than does the real world, but which is nevertheless so simply related to the real world that the properties of the latter may be derived, by some simple and general rule, from those of the former. To anticipate somewhat, it may be said that in the unnatural world which will be proposed in the present paper there are sources and sinks of matter, but light requires no representation other than the Maxwellian wave.

2. Taking first the (entirely academic) one-dimensional case, and writing $'$ for $\partial/\partial x$, we will start from the Schrödinger equation for *an electron of charge* $-e$ *and mass* m, *moving in the* x *direction in an electric field of intensity* $E(x)$, *constant in time.* We write U for the potential energy of the electron; thus $eE = U'$. In visualizing the solutions we may think of the potential curve as a hollow; and, to avoid a trivial complication, we may suppose that at infinite distances U is infinitely greater than at the minimum. We will now develop the mathematical properties of a differential equation, to which at present we assign no physical significance, obtained from this Schrödinger equation by adding a perturbation term $H_1 = \lambda U'$, thus changing the equation to

$$\left(H_0 + H_1 - \frac{h}{2\pi i}\frac{\partial}{\partial t}\right)\psi = 0, \tag{1}$$

where $$H_0 = -\frac{h^2}{8\pi^2 m}\frac{\partial^2}{\partial x^2} + U \quad \text{and} \quad H_1 = \lambda U' = \lambda eE = ME, \quad \text{say.}$$

All we can say at this stage is that H_1 must have the dimensions of energy, and hence that M must have the dimensions of an electric or magnetic moment. Let us consider how an M having these dimensions can be formed from fundamental quantities. First, the Bohr magneton $he/4\pi mc$, say M_1, is a magnetic moment. Again, if we multiply the electron's charge by its 'electromagnetic diameter', $4e^2/3c^2m$, say a, we obtain a quantity which evidently has the dimensions of an electric moment; and since in wave mechanics we are not unaccustomed to encounter electric moments with imaginary values, we need not hesitate to consider a moment, say M_2, defined as iae. To the M in H_1 we will give the value $\sqrt{(2M_1M_2)}$. It is $\sqrt{(2iaeM_1)}$, so that $H_1 = ME = \sqrt{i}\,\beta U'$, where $\beta = \sqrt{(2aM_1/e)}$. By the definition of a, we may write

H_1 as $\sqrt{(32\pi i e^2/3hc)}\,M_1 E$, in which it will be noted that the dimensionless quantity under the root depends on the fine structure constant $2\pi e^2/hc$.

Let $\psi_n = \phi_n(x)\exp(2\pi i W_n t/h)$ be a solution of (1) reducing, as $\beta \to 0$, to a normalized solution $\psi_n^0 = \phi_n^0(x)\exp(2\pi i W_n^0 t/h)$ of the unperturbed equation. Writing $U'_{nm} = \int \phi_n^{0*}\, U' \phi_m^0\, dx$, it is readily shown that

$$U'_{nn} = 0, \quad U'_{nm} = 4\pi^2 m \nu_{nm}^2 x_{nm},$$

where $$\nu_{nm} = (W_n^0 - W_m^0)/h \quad \text{and} \quad x_{nm} = \int \phi_n^{0*}\, x \phi_m^0\, dx.$$

The well-known general formulae of the perturbation theory reduce, on account of $U'_{nn} = 0$, to

$$\phi_n = \phi_n^0 + \sqrt{i}\,\beta \sum_m{}' \frac{U'_{mn}\phi_m^0}{W_n^0 - W_m^0} + \text{terms in } \beta^2 + \dots, \tag{1a}$$

$$W_n = W_n^0 + i\beta^2 \sum_m{}' \frac{|U'_{nm}|^2}{W_n^0 - W_m^0} + \dots = W_n^0 + i\beta^2 k_n + \dots, \tag{1b}$$

where $\sum_m{}'$ means a summation over all m's for which $W_m^0 \neq W_n^0$. Thus

$$\psi_n = \phi_n(x)\exp(-2\pi\beta^2 k_n t/h)\exp(2\pi i W_n^0 t/h). \tag{2}$$

Writing $$A_{nm} = \frac{64\pi^4 e^2}{3c^3 h}\nu_{nm}^3 |x_{nm}|^2,$$

then $$(W_n^0 - W_m^0) A_{nm} = \frac{2\pi\beta^2}{h}|U'_{nm}|^2 \quad \text{and} \quad \frac{2\pi\beta^2 k_n}{h} = \sum_m{}' A_{nm}.$$

The ϕ_n's, like the ϕ_n^0's, are normalized, but the orthogonality is perturbed. It will be noted that $\nu_{mn} = -\nu_{nm}$, and hence $A_{mn} = -A_{nm}$. When $n > m$, A_{nm} is positive and equal to the Einstein coefficient of spontaneous transition.

2*a*. Besides specifying these solutions, we will note some general properties of equation (1). From that equation and its conjugate we readily obtain

$$\frac{\partial \rho}{\partial t} = -\frac{\partial j}{\partial x} - \frac{2\sqrt{2}\,\pi\beta}{h}U'\rho, \tag{3}$$

where $$\rho = \psi\psi^* \quad \text{and} \quad j = \frac{ih}{4\pi m}(\psi^*\psi' - \psi\psi^{*\prime})$$

$$\frac{\partial \epsilon}{\partial t} = -\frac{\partial F}{\partial x} - \frac{2\sqrt{2}\,\pi\beta}{h}U'w - \frac{2\pi\beta^2}{h}U'^2\rho, \tag{4}$$

where $$2\epsilon = \psi^* H\psi + \psi H^*\psi^* = \frac{h}{2\pi i}(\psi^*\dot{\psi} - \psi\dot{\psi}^*), \quad H \text{ being } H_0 + H_1.$$

$$2w = \psi^* H_0 \psi + \psi H_0 \psi^*$$
$$= 2\epsilon - \sqrt{2}\,\beta U'\rho,$$

and F is a quantity which may be written in several ways, one of which is

$$\frac{ih^3}{32\pi^3m^2}(\psi^{*\prime}\psi'' - \psi'\psi^{*\prime\prime}) - \frac{h^2}{16\pi^2m}j'' + \left(U + \frac{\beta U'}{\sqrt{2}}\right)j - \frac{\sqrt{2}\,\beta h}{8\pi^2m}U''\rho.$$

We are not much interested in the expression for F, except to note that for a linear sum of our ψ_n's (and we shall consider no other type of solution) it goes to zero at great distances. We note also that the last term in (4) is a positive quantity preceded by a negative sign; we shall be particularly concerned with the integral

$$\int 2\pi\beta^2 U'^2 \rho\, dx/h. \tag{5}$$

One further point may be mentioned; for a solution $\psi = \Sigma c_n \psi_n$ the integral $\int \frac{\partial \epsilon}{\partial t} dx$ only differs from $\int \frac{\partial w}{\partial t} dx$ by terms which are either of smaller order than (5) or are purely oscillatory in time.

3. After this purely mathematical introduction we proceed to physical considerations.

The setting up of a quantum-mechanical wave theory may be thought of as conducted in the following manner. We propose a differential equation (and interpretations) which we hope will prove applicable to a certain system. Certain immediate consequences of the equation and interpretations, such as the presence or absence of sources and sinks, in the hydrodynamical sense of the terms,* must, of course, be incorporated in our specifications of the system to which we hope the theory will apply. If the system is one which can occur in nature, and if on working out the detailed consequences of the equation and interpretations we obtain results in agreement with the experimental properties of that system, then we may say that the calculation constitutes a satisfactory wave theory of that system. If, on the other hand, the system to which we hope the equation and interpretations are applicable is an unnatural one (if, for example, it contains sources and sinks), then our list of interpretations must conclude with one which specifies the effect of removing the unnatural features of the system; for it is only when that has been done that we can make the comparison with experiment which decides whether the theory is satisfactory.

Before proceeding to a theory which takes account of radiational processes the above remarks will be illustrated by a simple example, in which will be constructed a wave theory of a certain system, first by a natural, or direct, method, and secondly by an unnatural, or indirect, method. (It happens that the system considered is one in which there is an emission process; but it is an emission of particles, and it is not wished to draw any comparison between that emission and the emission of light, of which the present theories do not yet take account.) The leakage of particles from a spherical region through a high potential barrier surrounding it is considered, the number of particles inside the barrier not being maintained by an artificial (unnatural) generation of matter inside the barrier, or by bombardment from outside. In the well-known treatment the Schrödinger equation is proposed, with the usual interpretations of density, current and so forth. (The equation of continuity thus holds.) Solutions are found which are in satisfactory agreement with the experimental facts concerning the emission of α-particles from radioactive nuclei, to which the system considered is regarded as approximating. The W in a solution contains a small imaginary part; in other words, the number of particles inside the barrier, or inside a surface drawn round the barrier, progressively diminishes, and there is an outward current through such a surface.

---

* In hydrodynamics a fluid in which the equation of continuity does not hold (and which could thus only exist if we had the power of creating and annihilating matter continuously when and where we chose), is described as containing sources and sinks. The use of the term will serve to remind us that, from a classical standpoint, there is nothing new or objectionable in considering such systems. The properties of fluids having this unnatural character were, of course, worked out in detail at an early stage in the development of hydrodynamical theory, and are employed as a powerful mathematical device.

In the artificial or indirect theory we will begin by proposing an equation and interpretations which we hope will apply to a system which differs from the above in that the decay is prevented by an artificial generation of particles inside the barrier, to replace those which escape by leakage. The equation which is proposed is obtained from the previous one by adding to the potential inside the barrier a quantity, say $-i\gamma$, where γ is a real constant. The interpretations of density, current and so forth will be retained; thus inside the barrier $\partial\rho/\partial t = -\operatorname{div}\mathbf{j} + 4\pi\gamma\rho/h$, where ρ is the density and $\mathbf{j}$ the vectorial current. By adjusting the strength of the internal source specified by this last equation, that is, by adjusting the value of γ, we obtain, for comparison with each of the decaying states described above, a slightly different state, in which W has a slightly different value and is real; that is, there is no decay. There is still, of course, an outward current, and the rate of leakage, as measured by the emission coefficient, is, as would be expected, practically the same as in the previous calculation.* In this indirect theory, the final step which we have now to take, in order to compare the predictions with experiment, will, as stated above, be regarded as an interpretation (though it may appear somewhat pedantic to do so, since it is fairly obvious on physical grounds that the artificial maintenance would merely prevent the decay, and would not appreciably affect such quantities as the emission coefficient). This interpretation, to be employed in all such cases, will be formulated as follows. Processes whose existence is directly dependent on the artificial generation or destruction of matter will be absent in the natural system; all other processes will be the same as in the artificial system.

We have seen, then, that in the example cited the direct and the indirect theory (which begins by considering a system containing an artificial source) lead to the same predictions and are thus equally satisfactory. The example is merely intended to show that there is nothing unsatisfactory in the idea of employing an artificial, or indirect, theory of this kind. In the example, the actual calculations in the indirect theory are only slightly neater than those in the direct theory, and this is what we should expect, considering the simplicity of the phenomena involved. But if, now, we wish to construct a theory in which the dissipation of energy as light is no longer neglected the situation is different; for in a system such as that described in italics in the first sentence of § 2 (or in any atomic system), the natural spontaneous transitions cannot be represented by expressions which have algebraic symmetry (in a sense to be explained in the following section); thus it will not be surprising if, associated with the natural system, there is an artificial system which has more symmetrical properties, and can thus be represented by a much simpler equation and interpretations (giving rise to simpler and more symmetrical calculations) than would be possible in a natural treatment. It will now be shown that to such an artificial system equation (1), with simple interpretations, applies.

---

* Strictly speaking, the system to which wave-mechanical calculations refer is, of course, an assembly. It does not matter whether we think of the artificial generation of α-particles, which keeps the total radioactive power of the assembly constant, as a generation of α-particles inside existing nuclei, to make up for those which have escaped, or as a continual addition of new, undissociated, atoms to the assembly.

4. We will first choose our interpretations, for as we have said, they determine in some measure the system to which we may hope the calculations will apply.

We will retain the Schrödinger interpretations. That is, for the density and current we will retain the usual interpretations, while for the total energy of matter, or material energy (which we now define as an energy any diminution of which in a system, in excess of that attributable to an actual removal of particles from the system, indicates the emission of an equal quantity of light energy), we retain the Schrödinger expression $\int w dx$. We will go further and attribute a material energy w to the matter in unit length. (3) asserts that on these interpretations the system to which we may hope the calculations will apply is not a natural one, but is one in which, in every elementary region of x, we are annihilating, in unit time, a fraction $2\sqrt{2}\,\pi\beta U'/h$ of the matter there present; while (4), integrated over the whole range of x, asserts that if, in annihilating this fraction of the matter in each region, we have annihilated the same fraction of the material energy, then light energy is being radiated from the system at a rate given by the expression (5), as is seen on noting the mathematical property mentioned in the last sentence of § 2*a*.

Inserting the solution $\psi = \Sigma c_n \psi_n$ in (5), we may, in evaluating that expression, replace ϕ_n by ϕ_n^0 for the accuracy considered; then (using $U'\phi_n^0 = \sum_m{}' U'_{mn}\phi_m^0$) we readily find that its value, apart from smaller or oscillating terms, is

$$\sum_n \exp\left(-4\pi\beta^2 k_n t/h\right) c_n c_n^* \sum_m \left(W_n^0 - W_m^0\right) A_{nm}.$$

As usual in wave mechanics, the complete system whose statistical properties the wave equation and interpretations will be regarded as specifying is best thought of as an assembly of separate systems, each consisting, in our case, of an electron in a potential field U. The sources and sinks indicate an addition, or abstraction, of these separate systems to, or from, the complete system, or assembly (or, otherwise expressed, a generation or annihilation of separate systems in the assembly).

There is no question of varying e and m. It is easily shown that the expressions obtained above for the rate of radiation of light energy, and rates of annihilation of matter and material energy, indicate that the statistical processes occurring in the assembly represented by ψ_n may be expressed in words thus.

In unit time, two simultaneous processes have (with our assistance) taken place: (1) a transition, to each m level, of a fraction A_{nm} of the particles in the n level, with emission† of light, and (2) an annihilation of this number of particles in the m level, and also in the n level. (The processes are symmetrical in the sense that these statements are true for all m's, whether greater or less than n.) It need hardly be said that the annihilation of a negative number of particles can equally well be described as the creation of a positive number, and the transition of a negative number of particles from a level X to a level Y can equally well be described as the transition of a positive number from the level Y to the level X.

As a result of the two processes (1) and (2), we have the exponential change in the number of particles in the n level (represented by the time factor $\exp\{-2\sum_m{}' A_{nm}t\}$ in $\int\psi_n\psi_n^* dx$), all the other levels remaining empty.

The process (2) is, of course, entirely due to our own activities, and will be absent in the natural system. We have to apply the interpretation formulated in § 3 to decide whether the process (1) will be altered by the absence of the annihilations (2). When $m > n$, A_{nm} is negative, so that in the absence of process (2) process (1) is physically impossible (it would consist of the transition of a negative number of particles to an unoccupied level). But when $m < n$, A_{nm} is positive, and the transitions to the m level are not made impossible by the mere fact that we are no longer annihilating the particles as fast as they arrive in the m level; thus our interpretation requires that these transitions shall continue. They are, of course, the familiar Einstein A transitions. The result may then be extended to the case $\psi = \sum_n c_n\psi_n$.

As regards the term H_1, it will be noted that our factor $\sqrt{i}$ makes the real and imaginary parts of the electric moment M equal in magnitude; but this equality is not essential to the theory.

5. As might be expected there are other ways in which the processes may be made symmetrical. In particular we may take H as

$$-\frac{h^2}{8\pi^2 m}\frac{\partial^2}{\partial x^2}+U(x+\sqrt{i}\beta), \tag{6}$$

so that to the accuracy of the expressions corresponding to (1a) and (1b) we have changed H_1 from $\sqrt{i}\beta U'$ to $\sqrt{i}\beta U'+\frac{1}{2}i\beta^2 U''$. Then since it is readily shown that

$$\tfrac{1}{2}i\beta^2 U''_{nn} = -i\beta^2 \sum_m{}'\{|U'_{nm}|^2/(W_n^0-W_m^0)\},$$

---

† It will be noted that whether m is greater or less than n, the radiated energy $(W_n^0 - W_m^0)\,A_{nm}$ is a positive quantity.

we see that, owing to the extra term in H_1, W_n will now be equal to W_n^0; and if we retain the Schrödinger interpretations we find that in the system to which we may hope the equation will apply we are still generating matter artificially, even though the total rate of generation is evidently zero; we find, in fact, that the processes taking place are just as before, except that in process (2) the rate of annihilation in the n level is of the same magnitude as before, but of opposite sign; that is why there is no decay. On applying our interpretation of the effect of removing the artificial characteristics of the system we find the same predictions as before; thus the treatment is equally satisfactory.

It will be noted that if we write $X = x+\sqrt{i}\,\beta$, equation (1), to the accuracy considered, is

$$\left(-\frac{h^2}{8\pi^2 m}\frac{\partial^2}{\partial X^2}+U(X)-\tfrac{1}{2}i\beta^2\frac{\partial^2 U(X)}{\partial X^2}-\frac{h}{2\pi i}\frac{\partial}{\partial t}\right)\psi = 0, \tag{7}$$

or if we prefer to use (6) the equation is

$$\left(-\frac{h^2}{8\pi^2 m}\frac{\partial^2}{\partial X^2}+U(X)-\frac{h}{2\pi i}\frac{\partial}{\partial t}\right)\psi = 0. \tag{8}$$

Writing the equations in this form makes it very clear why W_n is W_n^0 in the second case and $W_n^0-\frac{1}{2}i\beta^2 U''_{nn}$ in the first case.

6. In the one-dimensional case the potential field U may be thought of as due to a fixed cloud of electricity (arranged in infinite sheets, each of uniform electrification). If now we imagine the cloud concentrated into a small region, or nucleus, preferably not too symmetrical, we obtain a typical three-dimensional case. Using the treatment based on (1) or the equivalent equation (7), the generalized equation which may be proposed in a three-dimensional case is obvious from (7), and it is easily shown that the expressions for the transition coefficients will assume their familiar three-dimensional form. Also it is easily shown that $W_n - W_n^0$ is $-\frac{1}{2}i\beta^2 4\pi N e^2 \rho_n^0$ (where Ne is the nuclear charge and ρ_n^0 is the value of $\phi_n^0\phi_n^{0*}$ in the region of the nucleus). Its value is small compared with a fine structure interval. This expression for it is, however, of less interest than the summational expression for it in terms of the A_{nm}'s.

7. However, we do not wish to dwell on a mere three-dimensional generalization of the previous theory, for in making the extension to three dimensions it is convenient at the same time to modify the theory so as to specify not only the rate of energy radiation but also its angular distribution and polarization. The mathematics is, in fact, actually simplified by so doing.

Considering the radiation emitted in an element of solid angle (of standard magnitude Δ) around a given line drawn from the atom, we fix our attention on the part of this radiation which emerges from an analyzer (through which the atom is observed) which transmits only the component of electric field in the direction of a unit vector $\mathbf{d}$ (perpendicular, of course, to the line of emission). Starting from the three-dimensional Schrödinger equation, we postulate that the processes which give rise to this part of the radiation are determined by adding to the Schrödinger equation a perturbation term which is simply a constant multiplied by the electric field, in the same direction, acting on the electron, due to the static potential U. A simpler postulate cannot be imagined. Since this perturbation term is $\sqrt{i}\,\beta_1(\mathbf{d}\,\mathrm{grad}\,U)$, where β_1 is a constant, it will readily be seen that §§ 2, 2*a* and 4, rewritten in three-dimensional form and with this perturbation term instead of the original H_1, will give the desired results* if β_1^2 is given the value $3\beta^2\Delta/8\pi$. §§ 5 and 6 are now superfluous.

It must be remembered that the characteristic of our unperturbed equation is that it neglects only the force on the electron due to its own radiation, and that the radiation processes to which the above perturbation procedure refers are those not revealed by such an unperturbed equation. Thus if we now consider how our calculation is modified by the presence of an external field of radiation, we see that we have to apply the perturbation, not to the simple Schrödinger equation, but to the Schrödinger equation modified so as to include the external field, regarded as an oscillating field of electric potential (or alternatively we may generalize the treatment so as to take as the unperturbed equation the Schrödinger equation in the form which takes account of the vector potential field which more accurately represents a light wave). It has always been recognized that, with a general radiational field, the solutions of this equation (our new unperturbed equation) are not purely oscillatory, and give a full account of the Einstein B transitions. But if, for example, we wish to calculate the Raman transitions which arise when the radiation does not contain resonance frequencies, we have, as solutions of the new unperturbed equation, a set of purely oscillatory functions (an expansion as far as the first power in the amplitude of the external field is sufficient for this purpose), reducing as the amplitude of the external field is reduced, to the eigenfunctions of the original unperturbed equation. On applying our perturbation we find, in addition to the A transitions, a set of transitions some of which depend entirely on the artificial generation of matter, and are physically meaningless in its absence; in accordance with our rule we delete them in passing over to the natural system, and the set which remain are the well-known expressions specifying in detail the intensities of the Raman radiation.

Further details are added to the results by introducing the refinement which was mentioned in the footnote, and which is dictated by consideration of the finite velocity of light; and by setting the nucleus free, so that we now have six co-ordinates. We then obtain very detailed results, employing the Schrödinger equation in the form which takes account of a vector potential $\mathbf{a}$, not forgetting, in the perturbation term, that the electric field now contains a contribution from the vector potential, so that the term is $\sqrt{i}\,\beta_1\left(\mathbf{d}\left\{\mathrm{grad}\,U-\frac{e}{c}\dot{\mathbf{a}}\right\}\right)$. The calculations are straightforward, and from the solutions we see that in all the changes in the atom's state, whether spontaneous or under the influence of light, there is a change in its translational motion (specified by a vector equation which, remembering the classical expression for the momentum contained in a light wave, is seen to express the conservation of momentum), the emitted frequencies being slightly different from what they would be if the nucleus were held fixed. The solutions give us the familiar intensity expressions for all these processes (they actually arise as expressions involving, of course, the matrix elements of ($\mathbf{d}$ grad U), but they are easily transformed into the familiar expressions). One point may be mentioned, concerning the intensity in the scattering transitions (which differ from Raman transitions in that the atom's electronic state does not change); if we transform our expression for the scattered intensity into the Dirac expression (rather than the equivalent Kramers-Heisenberg expression), we see that the part of it which is usually referred to as the $\cos\theta$ term has arisen from the $\dot{\mathbf{a}}$ part of our perturbation term, and the rest of the expression from the grad U part. If we carry out our calculations using a free electron instead of the atom (the perturbation term thus reducing to the $\dot{\mathbf{a}}$ part), we find that the scattered intensity expression reduces, as it should, to the $\cos\theta$ term.

---

* As a refinement of the theory, the perturbation term has to be modified if the results are to remain correct when the wave-lengths of the emitted light are so small as to be comparable with the linear dimensions of the atom.

8. For relativistic calculations we must write the perturbation term in a more general form, dictated by the following considerations. Taking an equation $\left(H_0-\frac{h}{2\pi i}\frac{\partial}{\partial t}\right)\psi_0=0$, which may be the Schrödinger equation for an electron in a general field $\mathbf{E}$ and $\mathbf{H}$, or the corresponding Dirac equation, and defining the time-dependent matrix elements of an operator in the usual way, a well-known expression, usually written $\frac{d\mathbf{F}}{dt}=\frac{\partial\mathbf{F}}{\partial t}+\frac{2\pi i}{h}\{\mathbf{F}H_0-H_0\mathbf{F}\}$, enables us to specify an operator whose matrix elements are the time differentials of those of a given operator $\mathbf{F}$. Thus we can specify an operator, say $\mathbf{v}$, which we will call the velocity, whose matrix elements are the time differentials of those of $\mathbf{r}$, and an operator, say $\mathbf{f}$, which we will call the acceleration, whose matrix elements are the time differentials of those of $\mathbf{v}$. In the non-relativistic case we find that $\mathbf{f}$ is simply $\mathbf{P}/m$, where $\mathbf{P}$ is $-e\left\{\mathbf{E}+\frac{1}{c}\mathbf{v}\times\mathbf{H}\right\}$, which is the usual expression for the force exerted on the electron by the field. (This, of course, is just the result which we should expect to find in non-relativistic mechanics.) Now in this non-relativistic case, the perturbation term which we employed was a constant times the component (in the direction of $\mathbf{d}$) of a force which differed from $\mathbf{P}$ by the omission of the $\mathbf{v}\times\mathbf{H}$ term; and though the difference is trivial for the cases which we considered it is evident on logical grounds that we should not have omitted one part of the total force on the electron (we should, in fact, have included also the force exerted on the electron by its own radiation; but this may conveniently be assigned to a higher approximation). Inserting the value of β_1^2 we see that *the perturbation term was* $\sqrt{i}B$ $(\mathbf{d}.\mathbf{f})$ *where* B^2 *is* $e^2h\Delta/4\pi^2c^3$, *and* $\mathbf{f}$ *is an operator whose matrix elements are the time differentials of those of the velocity.*

Now since we are formulating a perturbation term which is to specify a rate of emission of electromagnetic radiation, we may expect it to depend on the time differentials of the velocity; the definition given above in italics will therefore be proposed as the general form, to be used also in relativistic calculations. (As remarked above, there will be no difficulty in finding an explicit expression for **f** but for many purposes we are only concerned with its matrix elements.) As the simplest application of the relativistic theory, the Klein-Nishina formula is readily derived.

Without going further into the detailed applications of radiation theory, it seems safe to conclude that a theory of this kind, suitably generalized and extended, would give all the results obtained by existing theories, in so far as they are correct, and from its nature it would never encounter their characteristic difficulties, such as those which arise from their non-convergent integrals. In conclusion, brief consideration will be given to one other matter—the width of the energy levels in a natural system—which illustrates a rather different aspect of the theory.

In our expressions for the ψ's of artificial systems, the real exponential time factors have a simple interpretation in terms of the transition rates of the artificial systems, and are, of course, characteristics of the artificial systems; they do not indicate the widths of energy levels in a real system. As a typical example of a real system used in spectroscopy we may take the atoms in a discharge tube. The total number of atoms in each energy level does not change progressively with time, but in every instant the level is gaining and losing atoms, in equal statistical number, by uncorrelated (incoherent) processes. An atom after entering the n level only remains there during a finite mean lifetime whose reciprocal, say γ_n, consists of a term $\sum\limits_{m<n} A_{nm}$ due to the atom's spontaneous transitions from the n level, together with other terms, often of negligible magnitude, which are due to other causes and depend on the experimental conditions. By our fundamental postulate a wave representation of the real system is not to be regarded as a solution of a differential equation, but it must evidently incorporate the properties which we have found for the real system. Only in the case of non-interacting and unexcited atoms permanently in the ground state would an expression with time factor $\exp(2\pi i W_n^0 t/h)$ be an adequate representation; a sum of such terms with the various W_n^0's is not adequate to represent the atoms in a discharge tube, since it contains no indication of the finite mean lifetime of an atom in a given level. When the expressions are modified to indicate this departure from a strictly harmonic character, a Fourier analysis gives the familiar quantum-mechanical expression (with half width $h\gamma_n$) for the broadening of the n level.

INDEX TO VOLUME 191 (A)

Absorption spectra of benzene derivatives in the vacuum ultra-violet, I (Price & Walsh), 22.

Absorption spectra of benzene derivatives in the vacuum ultra-violet, II (Walsh), 32.

Application of quaternions to rotations in hyperbolic space of four dimensions (Conway), 137.

Atkins, W. R. G. & Ellison, M. A. Photoelectric measurements of the seasonal variations in daylight at Plymouth, from 1938 to March 1941, compared with the years 1930 to 1937, 467.

Attempts to detect the emission of secondary charged particles in the fission of ^{235}U by slow neutrons (Cassels, Dainty, Feather & Green), 428.

Binding energies of very light nuclei (Fröhlich, Kun Huang & Sneddon), 61.

Born, M. & Green, H. S. A general kinetic theory of liquids. IV. Quantum mechanics of fluids, 168.

Boyes-Watson, J., Davidson, E. & Perutz, M. F. An X-ray study of horse methaemoglobin, I, 83.

Broadbent, D. & Jánossy, L. Extensive penetrating cosmic ray showers, 517.

Brummage, K. G. An electron-diffraction study of the heating of straight-chain organic films and its application to lubrication, 243.

Cassels, J. M., Dainty, J., Feather, N. & Green, L. L. Attempts to detect the emission of secondary charged particles in the fission of ^{235}U by slow neutrons, 428.

Champion, F. C. & Roy, R. R. The ejection of protons from nitrogen on bombardment with α-particles of short range, 269.

Connexion between the criterion of yield and the strain ratio relationship in plastic solids (Taylor), 441.

Conway, A. W. Application of quaternions to rotations in hyperbolic space of four dimensions, 137.

Coulson, C. A. & Longuet-Higgins, H. C. The electronic structure of conjugated systems. I. General theory, 39.

Dainty, J. *See* Cassels, Dainty, Feather & Green.

Davidson, E. *See* Boyes-Watson, Davidson & Perutz.

Davidson, P. M. The interaction of radiation and matter, 542.

Davis, R. & Standring, W. G. Discharge currents associated with kite balloons, 304.

Discharge currents associated with kite balloons (Davis & Standring), 304.

Egerton, Sir Alfred & Minkoff, G. J. The formation of hydrogen peroxide in the combustion of hydrogen at low pressures, 145.

Ejection of protons from nitrogen on bombardment with α-particles of short range (Champion & Roy), 269.

Electron-diffraction study of the heating of straight-chain organic films and its application to lubrication (Brummage), 243.

Electronic structure of conjugated systems. I. General theory (Coulson & Longuet-Higgins), 39.

Eliezer, C. Jayaratnam. Quantum electrodynamics and low-energy photons, 133.

Ellison, M. A. *See* Atkins & Ellison.

Extensive penetrating cosmic-ray showers (Broadbent & Jánossy), 517.

Feather, N. *See* Cassels, Dainty, Feather & Green.
First order wave equations for elementary particles without subsidiary conditions (Wild), 253.
Formation of hydrogen peroxide in the combustion of hydrogen at low pressures (Egerton & Minkoff), 145.
Fröhlich, H., Kun Huang & Sneddon, I. N. The binding energies of very light nuclei, 61.

General kinetic theory of liquids. IV. Quantum mechanics of fluids (Born & Green), 168.
Green, H. S. *See* Born & Green.
Green, L. L. *See* Cassels, Dainty, Feather & Green.

Hall, T. A. & Tsao, P. H. Heat transfer at low temperatures between tube walls and gases in turbulent flow, 6.
Heat transfer at low temperatures between tube walls and gases in turbulent flow (Hall & Tsao), 6.
Hill, R., Lee, E. H. & Tupper, S. J. The theory of combined plastic and elastic deformation with particular reference to a thick tube under internal pressure, 278.
Hill, R. & Pack, D. C. An investigation, by the method of characteristics, of the lateral expansion of the gases behind a detonating slab of explosive, 524.
Hodograph transformation in trans-sonic flow. I, II & III (Lighthill), 323, 341, 352.

Initial stages of explosion in nitroglycerine (Mulcahy & Vines), 210.
Interaction of radiation and matter (Davidson), 542.
Interference microscopy (Merton), 1.
Interference studies of diamond faces. A crossed-fringe technique (Tolansky & Wilcock), 182.
Investigation, by the method of characteristics, of the lateral expansion of the gases behind a detonating slab of explosive (Hill & Pack), 524.

Jánossy, L. *See* Broadbent & Jánossy.

Kun Huang. *See* Fröhlich, Kun Huang & Sneddon.

Lee, E. H. *See* Hill, Lee & Tupper.
Lighthill, M. J. The hodograph transformation in trans-sonic flow. I. Symmetric channels, 323.
Lighthill, M. J. The hodograph transformation in trans-sonic flow. II. Auxiliary theorems on the hypergeometric functions $\psi_n(r)$, 341.
Lighthill, M. J. The hodograph transformation in trans-sonic flow. III. Flow round a body, 352.
Longuet-Higgins, H. C. *See* Coulson & Longuet-Higgins.

Malan, D. J. & Schonland, B. F. J. Progressive lightning. VII. Directly-correlated photographic and electrical studies of lightning from near thunderstorms, 485.
Merton, Sir Thomas. On interference microscopy, 1.
Methaemoglobin, X-ray study (Boyes-Watson, Davidson & Perutz), 83.
Method of the hypercircle in function-space for boundary-value problems (Synge), 447.
Minkoff, G. J. *See* Egerton & Minkoff.

Mulcahy, M. F. R. & Vines, R. G. The initial stages of explosion in nitroglycerine, 210.
Mulcahy, M. F. R. & Vines, R. G. The propagation of detonation in thin layers of nitroglycerine, 226.

Note on a problem of Mahler (Rogers), 503.

Pack, D. C. *See* Hill & Pack.
Paterson, Sir Clifford. The Research Laboratories of the General Electric Company, 417.
Perutz, M. F. *See* Boyes-Watson, Davidson & Perutz.
Photoelectric measurements of the seasonal variations in daylight at Plymouth, from 1938 to March 1941, compared with the years 1930 to 1937 (Atkins & Ellison), 467.
Pippard, A. B. The surface impedance of superconductors and normal metals at high frequencies. I. Resistance of superconducting tin and mercury at 1200 Mcyc./sec., 370.
Pippard, A. B. The surface impedance of superconductors and normal metals at high frequencies. II. The anomalous skin effect in normal metals, 385.
Pippard, A. B. The surface impedance of superconductors and normal metals at high frequencies. III. The relation between impedance and superconducting penetration depth, 399.
Price, W. C. & Walsh, A. D. The absorption spectra of benzene derivatives in the vacuum ultra-violet. I, 22.
Progressive lightning. VII. Directly correlated photographic and electrical studies of lightning from near thunderstorms (Malan & Schonland), 485.
Propagation of detonation in thin layers of nitroglycerine (Mulcahy & Vines), 226.

Quantum electrodynamics and low-energy photons (Eliezer), 133.

Ramsey, W. H. On the scattering of fast neutrons by protons, 195.
Research Laboratories of the General Electric Company (Paterson), 417.
Rogers, C. A. A note on a problem of Mahler, 503.
Roy, R. R. *See* Champion & Roy.

Scattering of fast neutrons by protons (Ramsey), 195.
Schonland, B. F. J. *See* Malan & Schonland.
Sneddon, I. N. *See* Fröhlich, Kun Huang & Sneddon.
Standring, W. G. *See* Davis & Standring.
Surface impedance of superconductors and normal metals at high frequencies, I, II & III (Pippard), 370, 385, 399.
Synge, J. L. The method of the hypercircle in function-space for boundary-value problems, 447.

Taylor, Sir Geoffrey. A connexion between the criterion of yield and the strain-ratio relationship in plastic solids, 441.
Theory of combined plastic and elastic deformation with particular reference to a thick tube under internal pressure (Hill, Lee & Tupper), 278.
Tolansky, S. & Wilcock, W. L. Interference studies of diamond faces. A crossed-fringe technique, 182.
Tsao, P. H. *See* Hall & Tsao.
Tupper, S. J. *See* Hill, Lee & Tupper.

Vines, R. G. *See* Mulcahy & Vines.

Walsh, A. D. *See* Price & Walsh.
Walsh, A. D. The absorption spectra of benzene derivatives in the vacuum ultra-violet, II, 32.
Wilcock, W. L. *See* Tolansky & Wilcock.
Wild, E. On first order wave equations for elementary particles without subsidiary conditions, 253.

X-ray study of horse methaemoglobin, I (Boyes-Watson, Davidson & Perutz), 83.

END OF THE ONE HUNDRED AND NINETY-FIRST VOLUME (SERIES A)

IARI 75

INDIAN AGRICULTURAL RESEARCH
INSTITUTE LIBRARY, NEW DELHI

Date of Issue	Date of Issue	Date of Issue

GIPNLK—H-40 I.A.R.I.—29-4- 5—15,000